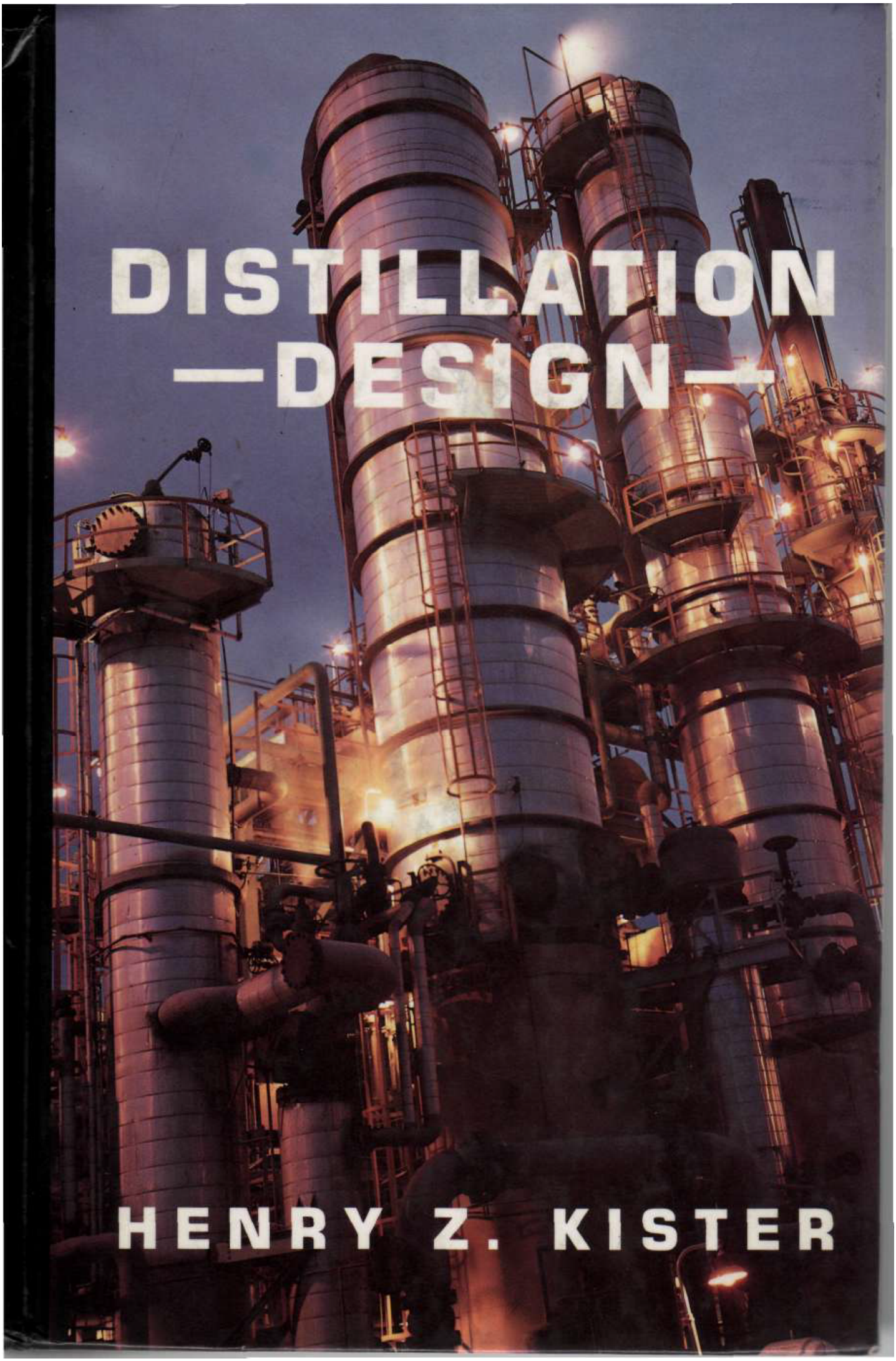
DISTILLATION
—DESIGN—
HENRY Z. KISTER

Distillation Design

Henry Z. Kister
Engineering Advisor
Brown & Root Braun, Alhambra, California

Chapter 4 Rigorous Distillation Calculations

Joe R. Haas, *UOP, Des Plaines, Illinois*

Chapter 5 Batch Distillation

David R. Hart, *RUST Engineering, Birmingham, Alabama*

Chapter 10 Packing Capacity and Pressure Drop GPDC Interpolation Charts Atlas

Henry Z. Kister, *Brown & Root Braun, Alhambra, California*

David R. Gill, *Simulation Sciences, Inc., Brea, California*

McGraw-Hill, Inc.

New York St. Louis San Francisco Auckland Bogotá
Caracas Lisbon London Madrid Mexico Milan
Montreal New Delhi Paris San Juan São Paulo
Singapore Sydney Tokyo Toronto

Library of Congress Cataloging-in-Publication Data

Kister, Henry Z.
Distillation design / Henry Z. Kister.
p. cm.
Includes bibliographical references.
ISBN 0-07-034909-6
1. Distillation. I. Title.
TP156.D5K555 1992
660'.28425—dc20 91-25976
CIP

1 2 3 4 5 6 7 8 9 0 DOC/DOC 9 8 7 6 5 4 3 2

ISBN 0-07-034909-6

The sponsoring editor for this book was Gail F. Nalven, the editing supervisor was Peggy Lamb, and the production supervisor was Donald F. Schmidt. This book was set in Century Schoolbook by McGraw-Hill's Professional Book Group composition unit.

Printed and bound by R. R. Donnelley & Sons Company.

To My Mum
Who contributed so much to my work over the years; inspired, encouraged and helped in preparing this book, but did not live to see it. Your memory will live forever in this book.

Contents

Preface

People believe 50 percent of what they hear, 75 percent of what they see, and 100 percent of what the computer tells them.

SOURCE UNKNOWN

In the past, mass production of mathematical models and column design correlations was hindered by the extensive calculations involved. With the event of high-speed and personal computers, this bottleneck has been eliminated. Flood gates have opened, and new mathematical models are pouring into the published literature at a record pace. Further growth in mathematical model production appears to be restricted only by the availability of persons willing to punch buttons on computer keyboards.

One would expect this state of art to be the heaven that column designers always dreamt of. Instead, it turned out to be the hell they always feared. Few could keep up with the large influx of mass produced mathematical models. Little is known about the limitations of each new correlation or design method. Our prediction methods turned into black boxes: key in numbers, print out results. But how reliable are these results?

About fifteen years ago I was applying a leading and very well known literature correlation as part of my graduate thesis. I punched in keys and the computer printed out results. For some reason the results did not look right. Upon investigation, I discovered the unbelievable: the correlation just did not work for my case. Not that the correlation was bad; over many years, it gained a very healthy reputation. It just happened that it had limitations, just like every other correlation. The limitations of this correlation were fairly well explored, but a quarter of a century after it was derived, I found the hard way that it had one more limitation which remained hidden over all these years.

Fortunately, I was only doing a graduate thesis and not basing a column design on this prediction. Fortunately, the correlation was simple enough to permit a person to identify the limitation. And fortunately, some gut feeling saved me from falling into the trap.

As we head into the twenty-first century, the above type of anecdote is becoming ancient history. The black box in the computer has taken

over. Looking for correlation limitations today becomes like looking for a needle in an ever-growing haystack.

With the busy life style and the pressure to publish papers, the problem is becoming more acute. There are deadlines to meet, technical papers need to be produced, and there is no time to explore correlation limitations. Besides, who needs to look for limitations when a computerized regression analysis (performed, of course, by one of the best regression packages in the business) shows an excellent data fit? Does it really matter if a handful of points do not fit the correlation—even if this handful includes all the points for systems above atmospheric pressures? In real life, no one will know, unless the designer ends up with a column that does not work. And if the error is on the conservative side, no one will ever find out, because the column will work.

Data collection is another neglected child of the late twentieth century. There are so many data around that collecting them all (or even most of them) for the sake of deriving a correlation becomes painful, mundane, and an extremely unattractive exercise. Not to mention the labor involved in reading data off plots and in the arithmetic involved in ensuring that all the data points have been correctly entered. I challenge anyone to cite a more boring task than this. An economical way of dealing with the excess data problem is by using the "ignore it and hope it goes away" principle. It will suffice that the new correlation will fit a handful of data thrown at it. And if data from other sources do not agree, that just means there is something wrong with the other data.

What hope has the designer who sits at the other end of the rainbow and attempts to make use of the mathematical models and design correlations?

The purpose of this book is to bridge the gap between developers of design procedures and those who ultimately use them. Correlations and design methods are recommended only when their data base is wide, and their range of application and limitations are well understood. Rules of thumb are recommended over theoretical models provided they have been shown to be more reliable in predicting commercial column performance. Sound theoretical models that give unreliable or sparsely tested predictions were left outside the covers of this book.

Contrary to a popular belief, some distillation characteristics still cannot be satisfactorily predicted by correlation, regardless of the number of correlations available for their prediction. Data interpolation with the aid of an empirical procedure is probably the most reliable means of estimating these characteristics. The last two chapters of this book provide the designer with the data needed.

Throughout, the book emphasizes designing columns that "look right," and techniques that can help distinguish a design that makes sense from one that does not. Computers have provided distillation designers with speed, accuracy, and flexibility. Computers, however, still have a long way to go before—if ever—they are capable of replacing good engineering judgment.

Henry Z. Kister

Acknowledgments

The author wishes to express his gratitude to Brown & Root Braun, particularly to Walt Stupin and to Jim Gosnell, for their strong backing and support for this effort. Special thanks are also due to my parents for their warm encouragement and inspiration throughout and for the German translations. The author is also grateful to his coauthors—Joe Haas, David Hart, and David Gill—for producing outstanding chapters while keeping ahead of all the deadlines. Appreciation is also due to my mentors over the years, particularly Ian Doig, Dick Harris, Trevor Whalley, Reno Zack, Tom Hower, Walt Stupin, and Jack Hull, for their immense encouragement of my work; much of their teaching found its way into the following pages.

The author is grateful to the many contributors that willingly shared experiences with him, provided unpublished data for developing the charts in Chapter 10, and supplied advice on applying their correlations. Special thanks are due to McGraw-Hill's editorial and production staff, in particular to Peggy Lamb, for outstanding quality, efficiency, and cooperation. Finally, the author gratefully acknowledges the efforts of Sherlyn Severson who tirelessly and flawlessly typed this manuscript.

The author will be pleased to hear any comments or experiences any readers may wish to share for possible inclusion in a future edition. Write to H. Z. Kister, Brown & Root Braun, 1000 South Fremont Avenue, Alhambra, CA, 91802, USA. All communications will be answered.

Chapter

1

Introduction to Distillation

Distillation, King in separations, will remain as the workhorse separations device of the process industries. Even though it is old in the art, with a relatively mature technology support base, it attracts research and professional interest. Without question, distillation will sail into the future with clear skies and a strong wind. It will remain the key separation method against which alternate methods must be judged.

DR. JAMES R. FAIR, 1990

Distillation is the most important and most visible separation technology. The skyline of many refineries and chemical plants is dominated by tall distillation towers, and it cannot be denied that their spatial arrangements often amounts to architectural beauty. Less spectacular, but also visible are the smoke stacks of these industrial complexes; they represent the energy used in processing, the major part of which is consumed by distillation processes.

DR. FRITS J. ZUIDERWEG, 1988

As we move through the 1980's, with full recognition of the energy intensiveness of distillation, we can expect to see relatively little displacement of distillation by alternative separation methods, at least for the large scale process throughputs. Thus, development of distillation devices will continue. The result will be improved separation efficiency at lower pressure drop and lower cost.

DR. JAMES R. FAIR, 1983

1.1 Distillation Background

1.1.1 What is distillation?

Distillation is an ancient unit operation, and has been widely practiced for thousands of years. Early applications used crude vaporization and condensation equipment, often for concentrating the alcoholic content of beverages. The first vertical columnar continuous distillation still was developed by Cellier-Blumenthal in France in 1813. Perrier introduced an early version of the bubble-cap tray in England in 1822. Packings were used as early as 1820 by a technologist named Clement who used glass balls in an alcohol still. Coffey developed the first sieve tray column in 1830. The first book on fundamentals of distillation was *La Rectification de l'alcohol* by Ernest Sorel in 1893.

During the first quarter of the twentieth century, the application of distillation expanded from a tool for enhancing the alcohol content of beverages into the prime separation technique in the chemical industry. This expansion accelerated once distillation was recognized as an effective means of separating crude oil into various products. From there, the application of distillation spread into the majority of chemical processes. Detailed descriptions of the history of distillation, including illustrations of historic exhibits, are given by Fair (1), Underwood (2), and Forbes (3).

Distillation is a process of physically separating a mixture into two or more products that have different boiling points, by preferentially boiling the more volatile components out of the mixture. When a liquid mixture of two volatile materials is heated, the vapor that comes off will have a higher concentration of the more volatile (i.e., lower-boiling-point) material than the liquid from which it was evolved. Conversely, if a vapor is cooled, the less volatile (i.e., higher-boiling-point) material has a tendency to condense in a greater proportion than the more volatile material.

1.1.2 Why distillation?

Distillation is a unit operation that has been around for a long time and continues to be the primary method of separation in processing plants, in spite of its inherently low thermodynamic efficiency. The preeminence of distillation for the separation of fluid mixtures is not accidental, but fundamental, and therefore unlikely to be displaced. The reasons are both kinetic and thermodynamic.

From a kinetic standpoint (4), mass transfer per unit volume in distillation is limited only by the diffusional resistances on either side of the vapor-liquid interface in turbulent phases, with no inerts present. In almost every other separation process, there are inert solvents or

solid matrices present, and these lower mass fluxes. Distillation, therefore, has the potential for high mass transfer rates (low capital costs).

From a thermodynamic viewpoint, a typical thermodynamic efficiency of a distillation system is about 10 percent (4). This can be enhanced if intercondensers and interreboilers are used. In fact, it has been shown that conceptually, a distillation system can be devised which requires only the minimum work of separation. Although a thermodynamic efficiency of 10 percent appears low, not many other processes are more efficient (4).

Distillation in general provides the cheapest and best method for separating a liquid mixture to its components (4–8), except when (4):

1. The difference of volatility between the components is small.
2. A small quantity of high-boiling-point component is to be recovered from the feed. Distillation requires that the whole feed be vaporized in order to recover this small quantity.
3. A compound is thermally unstable even under vacuum conditions.
4. The mixture is extremely corrosive or highly fouling.

1.2 Vapor-Liquid Equilibrium (VLE)

It is difficult, perhaps altogether impossible, to do justice to the wide topic of vapor-liquid equilibrium (VLE) in a modest amount of space. Many texts are devoted entirely to this topic, or even to fractions of it. The numerous published texts and reviews (e.g., Refs. 9 through 24) can testify to the large volume of information available.

It is also difficult to discuss distillation without addressing some of the implications of VLE to distillation design. For this reason, some discussion of VLE is included in this text. This discussion focuses on those VLE principles that in the author's opinion must be understood by distillation practitioners. Extensive theoretical discussions and data presentation are excluded, and left to the thermodynamic texts. Discussions on predictive models and procedures are far too bulky and have also been excluded. The author recommends Refs. 9 to 26 to those seeking further information. References 25 and 26 are brief, practical, and very useful state-of-the-art reviews.

1.2.1 *K*-value and relative volatility

$$K_i = \frac{\text{Mole of fraction of component } i \text{ in vapor phase}}{\text{Mole of fraction of component } i \text{ in liquid phase}} \qquad (1.1)$$

The K-value is a measure of the tendency of component i to vaporize.

If the K-value is high, the component tends to concentrate in the vapor; if low, it tends to concentrate in the liquid. If the K-value is unity, the component will split equally between the vapor and the liquid.

The K-value is a function of temperature, pressure, and composition. At equilibrium, whenever two of these three variables are fixed, so is the third. The K-value can therefore be regarded as a function of pressure and composition, or temperature and composition (or temperature and pressure).

The *relative volatility* of components i and j is defined as

$$\alpha_{i,j} = \frac{K\text{-value of component } i}{K\text{-value of component } j} \tag{1.2}$$

Distillation is a technique of separating components according to their relative volatility. The relative volatility is a measure of the ease of separation. This definition makes the relative volatility the ratio between the tendency to vaporize of the two components. If relative volatility is high, one component has a much greater tendency to vaporize (i.e., is more volatile) than the other, and it will be easy to separate the two by vaporizing one from the other (i.e., by distillation). On the other hand, when one component has as high a tendency to vaporize (i.e., is as volatile) as the other, relative volatility will approach unity, and the components will be difficult to separate from each other by distillation. If relative volatility is unity, each component is as volatile as the other, and they cannot be separated by distillation.

By convention, relative volatility is defined as the K-value ratio of the more-volatile to the less-volatile component, and therefore, relative volatility is always greater or equal to unity.

For binary system, Eqs. (1.1) and (1.2) can be combined to give

$$\alpha_{1,2} = \frac{K_1}{K_2} = \frac{y_1}{x_1}\frac{(1 - x_1)}{(1 - y_1)} \tag{1.3}$$

This equation can be rearranged to give

$$y_1 = \frac{\alpha_{1,2}x_1}{1 + (\alpha_{1,2} - 1)x_1} \tag{1.4}$$

Equation (1.4) expresses the more-volatile component (MVC) mole fraction in the vapor as a function of the mole fraction of the MVC in the liquid and the relative volatility. This relationship is plotted in Fig. 1.1.

Figure 1.1*a* is a plot called an *x-y diagram*. The x and y axes show the concentration of the MVC in the liquid and in the vapor, respectively. The 45° diagonal represents points at which vapor and liquid

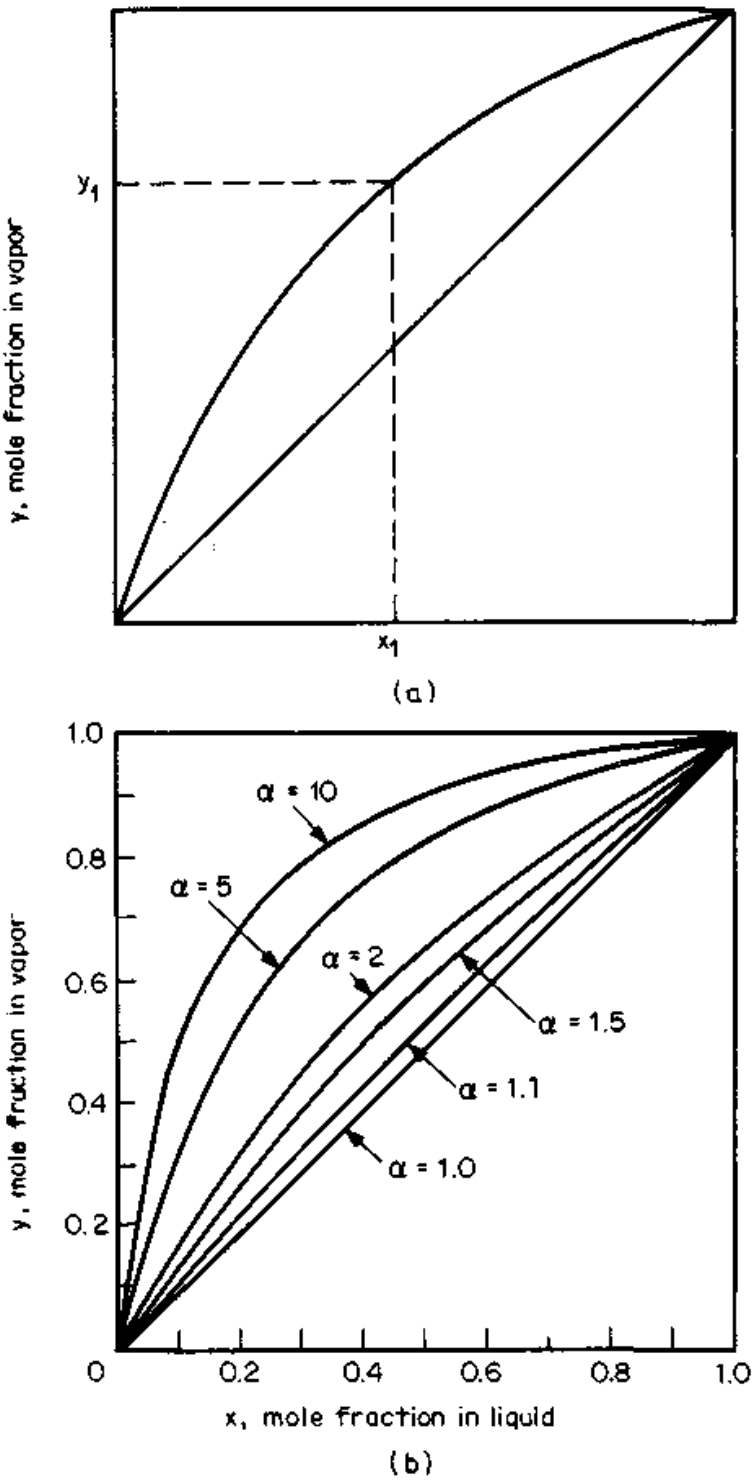

Figure 1.1 The relative volatility concept. (*a*) Concentration of the more-volatile component (MVC) in the vapor. (*b*) Effect of relative volatility on the concentration of the MVC in the vapor.

compositions are the same. The curve on Fig. 1.1*a* is an equilibrium relationship. Figure 1.1*a* illustrates how the MVC concentrates in the vapor. A liquid mixture containing x_1 mole fraction MVC ($x_1 = 0.45$ in Fig. 1.1*a*) is in equilibrium with vapor containing y_1 mole fraction MVC ($y_1 = 0.71$ in Fig. 1.1*a*). If this vapor is collected and condensed, one will end up with a mixture in which the MVC mole fraction has been enriched from 0.45 to 0.71.

Figure 1.1*b* illustrates the effect of relative volatility on the tendency of the MVC to concentrate in the vapor. When volatility is high, the enrichment is large. For instance, when relative volatility is 10, a liquid mixture containing 0.45 mole fraction MVC is in equilibrium with vapor containing 0.88 mole fraction of MVC; it would take only a few steps to convert the liquid mixture into pure components. Conversely, when relative volatility is very low, say 1.1, a liquid mixture containing 0.45 mole fraction MVC is in equilibrium with vapor containing 0.47 mole fraction MVC. Under these conditions, it will take a very large number of steps to separate the mixture into the pure components.

1.2.2 Ideal and nonideal systems

An ideal system is one where the vapor obeys the ideal gas law and the liquid obeys Raoult's law.

An ideal gas mixture obeys Dalton's law, i.e.,

$$p_i = y_i P \tag{1.5}$$

An ideal solution obeys Raoult's law, which states that the partial pressure of a component in solution is equal to the product of its mole fraction and of the vapor pressure of the pure component; thus,

$$p_i = x_i p_i^\circ \tag{1.6}$$

From Eqs. (1.5) and (1.6) and the definition of K-value (Sec. 1.2.1), one obtains

$$K_i = \frac{y_i}{x_i} = \frac{p_i^\circ}{P} \tag{1.7}$$

For nonideal systems, the fugacities of component i in the vapor and in the liquid play the same role as the component partial pressure in the vapor and the component vapor pressure in the liquid. The fugacity can be regarded as a thermodynamic pressure. For equilibrium, vapor fugacity is equal to liquid fugacity, i.e.,

$$f_i^V = f_i^L \tag{1.8}$$

The vapor fugacity can be regarded as a corrected partial pressure, given by the equation

$$f_i^V = \phi_i^V (P y_i) \tag{1.9}$$

Similarly, the liquid fugacity can be regarded as a corrected vapor pressure, given by

$$f_i^L = \phi_i^L \gamma_i \psi_i (x_i p_i^\circ) \tag{1.10}$$

A detailed derivation of these equations from the thermodynamic relationships is presented in most thermodynamics texts (e.g., Refs. 9–12, 15). The various coefficients in Eqs. (1.9) and (1.10) are discussed below.

ϕ_i^V The vapor fugacity coefficient. It accounts for the effect of vapor nonideality on vapor fugacity. It is usually estimated from an equation of state and is based on system temperature, pressure, and vapor mole fraction.

ϕ_i^L The liquid fugacity coefficient. It accounts for the effect of vapor nonideality on liquid fugacity. This coefficient is estimated in a similar manner to the vapor fugacity coefficient, but it is based on the system temperature and the pure component vapor pressure.

ψ_i The Poynting correction factor. It accounts for the effect of pressure on liquid fugacity. Since ϕ_i^L is evaluated at the vapor pressure of the pure component, ψ_i is used to account for the difference between the pure component vapor pressure and the mixture pressure. This effect is small and can be neglected at low pressures (11,27), but is important at high pressures.

γ_i The liquid activity coefficient. It corrects the liquid fugacity for the effect of composition. Its value depends on how similar the components are. For two similar components, such as an isobutane–normal butane mixture, the liquid activity coefficient is close to unity. If the components are different, activity coefficients deviate from unit.

Combining Eqs. (1.1), (1.8), (1.9), and (1.10) one gets

$$K_i = \frac{y_i}{x_i} = \frac{\phi_i^L}{\phi_i^V} \gamma_i \psi_i \frac{p_i^\circ}{P} \tag{1.11}$$

1.2.3 Effect of temperature, pressure, and composition on *K*-values and volatility

For the purpose of this discussion, Eq. (1.11) is simplified by omitting the Poynting correction, which is usually small at low pressures. Combining Eq. (1.11) with the definition of relative volatility, Eq. (1.2) gives

$$\alpha_{ij} = \frac{K_i}{K_j} = \phi_r \gamma_r p_r^\circ \tag{1.12}$$

where

$$p_r^\circ = \frac{p_i^\circ}{p_j^\circ} \tag{1.13a}$$

$$\gamma_r = \frac{\gamma_i}{\gamma_j} \tag{1.13b}$$

$$\phi_r = \frac{\phi_i^L}{\phi_j^L} \frac{\phi_j^V}{\phi_i^V} \tag{1.13c}$$

The most important term in the equations both for K-values and relative volatility is the vapor pressure term.

Effect of temperature or pressure. This effect can be illustrated with the aid of a Cox chart (Fig. 1.2*a*). This chart shows a steep increase of vapor pressure with temperature. For this reason, the K-value for each component increases steeply with temperature.

The Cox chart also shows that in general, for members of a homologous series, vapor pressure of the less-volatile component increases faster with temperature than the vapor pressure of the more-volatile components. This causes p_r° in Eq. (1.13*a*) to diminish as temperature is raised. As the critical point is approached, the ratio p_r° approaches unity. Applying Eq. (1.12), relative volatility decreases as temperature is raised, until it approaches unity as the critical point is approached.

The above trend is valid for members of a homologous series. For components which are not members of a homologous series, the reverse trend may occur over a limited temperature range, causing relative volatility to increase as the equilibrium temperature is raised [Eq. (1.12)]. However, as temperature is raised further and approaches the critical point, relative volatility eventually diminishes and will reach unity at the pseudocritical point of the mixture.

At a given composition, the higher the saturation temperature, the higher the saturation pressure. For this reason, the effect of saturation temperature discussed above can be considered as the effect of saturation pressure. A study of boiling point data in the pressure range of 1 to 10 atmospheres and a wide temperature range (28) led to a simple and rough approximation of the relationship between saturation pressure and saturation temperature for common substances:

$$T \propto P^q \tag{1.14}$$

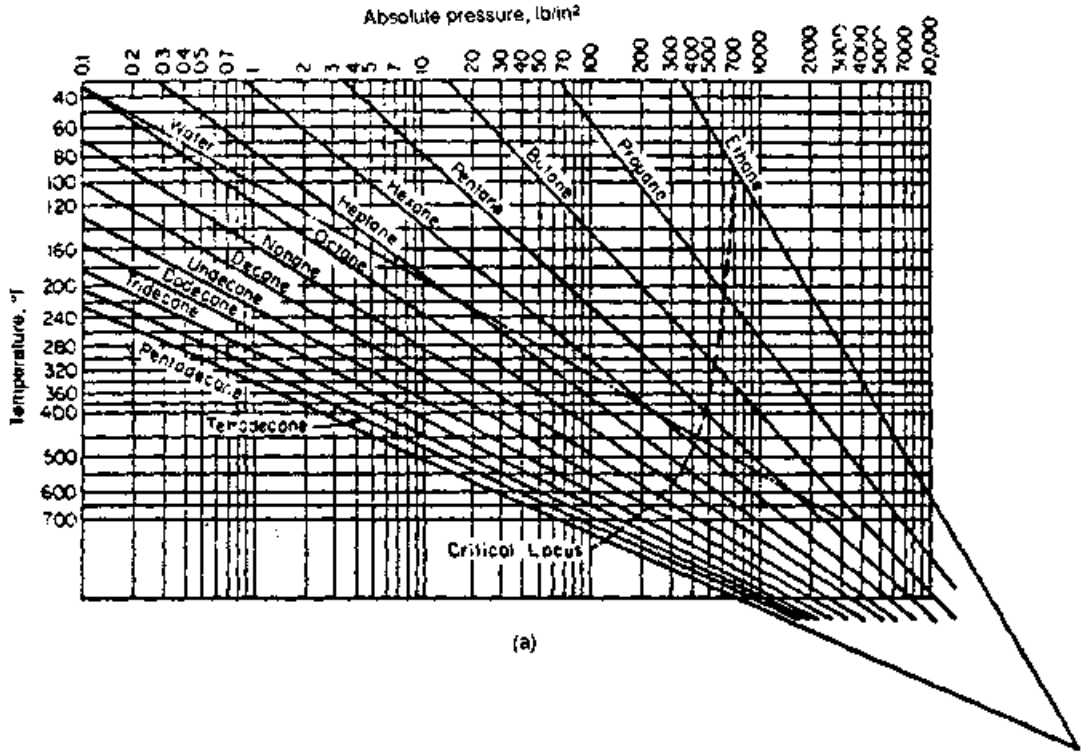

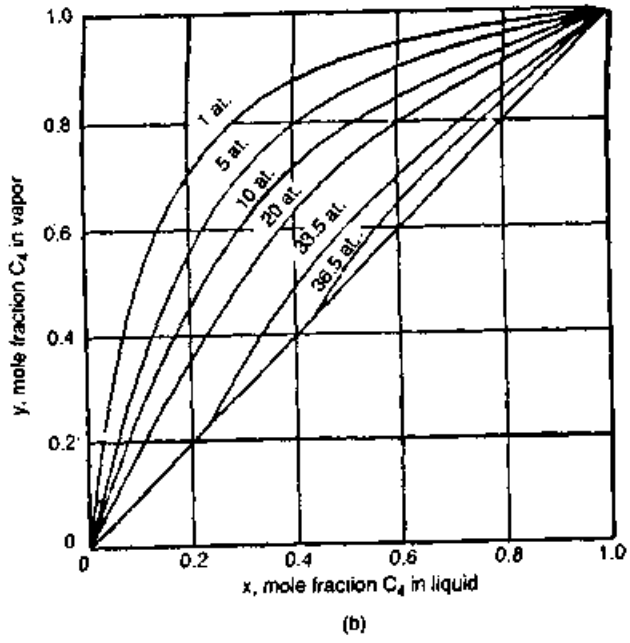

Figure 1.2 Effect of temperature and pressure on K-values and volatilities. (a) A Cox chart; (b) an x-y diagram for separation of C_4 from C_5 hydrocarbons, showing a reduction in relative volatility with an increase in pressure. (Part a, Sage and Lacey, "Volumetric and Phase Behavior of Hydrocarbons," Stanford University Press, Stanford, Calif., 1939. Part b C. S. Robinson and E. R. Gilliland, "Elements of Fractional Distillation," 4th ed., 1950. *Copyright © by McGraw-Hill, Inc. Reprinted by permission.*)

where $0.08 < q < 0.11$ with a mean value of 0.09.

The effect of temperature (or pressure) on relative volatility is further illustrated in Fig. 1.2*b* (29). The diagram clearly shows a reduction in relative volatility as pressure is raised and illustrates that relative volatility approaches unity as the pseudocritical point of the mixture is approached.

Effect of composition. The main effect of composition on K-values and relative volatilities is a result of the effect of composition on the liquid activity coefficient. Composition also has an effect on the fugacity coefficient. The latter effect is generally small at low pressures.

Activity coefficients are classified according to the nature of their deviation from Raoult's law. This depends on the heat of mixing of the components. If heat needs to be added to the mixture to achieve solution, i.e., the components "prefer to be alone" than in solution, the deviations are positive (Fig. 1.3*a*). Positive deviations give activity coefficients greater than unity and higher K-values than those predicted from Raoult's law. If heat is evolved on solution, the reverse applies

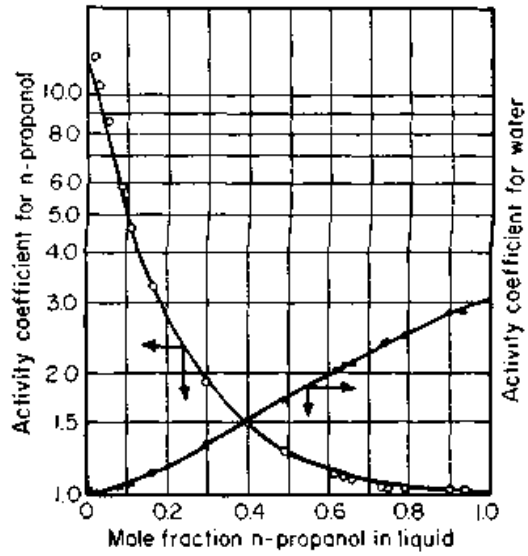

(a)

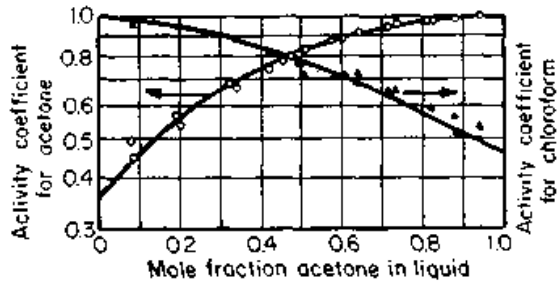

(b)

Figure 1.3 Effect of composition on liquid activity coefficients. (*a*) For the positive-deviation system *n*-propanol-water at 1 atm; (*b*) for the negative-deviation system acetone-chloroform at 1 atm. (From R. H. Perry, *Chemical Engineer's Handbook*, 5th ed., 1973. Copyright © by McGraw-Hill, Inc. Reprinted by permission.)

(Fig. 1.3*b*); the deviations are negative and K-values are lower than those obtained from Raoult's law.

The magnitude of the deviations from Raoult's law increases with the difference in nature between the components. For instance, the normal propanol-water system (Fig. 1.3*a*) and the acetone-chloroform system (Fig. 1.3*b*) show large activity coefficients, the highest being 13. On the other hand, the highest-activity coefficient in a mixture of isobutane–normal butane, which are similar to each other, is smaller than 1.1 (at about 100 psia).

Figure 1.4*a* and *b* shows the effect of composition on the activity coefficient ratio. According to Eq. (1.12), this ratio represents the main effect of composition on relative volatility. When a system shows positive deviations, relative volatility decreases as the concentration of the MVC increases. The reverse applies for negative-deviation systems.

1.2.4 Phase diagrams

Phase diagrams are used to describe binary systems by plotting two out of the three variables—composition, temperature, and pressure, at a constant value of the remaining one. The most popular of these plots are the T-x plot and the x-y plot. The x-y plot was described earlier (Sec. 1.2.1, Fig. 1.1).

Temperature-composition (T-x) diagrams (Fig. 1.5). Curve ABC shows the composition-temperature relationship for the saturated liquid. At temperature T_1 and liquid composition x_1, point B is the condition at which the liquid is ready to start boiling. Point B is termed the *bubble point.*

When the liquid starts to boil at temperature T_1 (point B), the first vapor formed has a composition y_1 and is therefore at its dew point. At this point, the vapor is as rich in the light component as it will ever be. As temperature is further raised, more of the heavier component is boiled off. The quantity of vapor formed increases, but the mole fraction of the light component in both vapor and liquid drops. At temperature T_2, the liquid composition is x_2 and the vapor composition is y_2. Some of the initial charge is now vapor and some is liquid. A further increase in temperature to T_3 will vaporize the rest of the liquid. The vapor composition will now be x_1, and the last drop of liquid vaporized has a composition x_3. The liquid always travels along its bubble-point curve (*BEH*) while the vapor always travels along the dew-point curve (*DFG*). Therefore, in distillation, bubble-point liquid is always in equilibrium with dew-point vapor.

The concept of dew point and bubble point is useful in the construc-

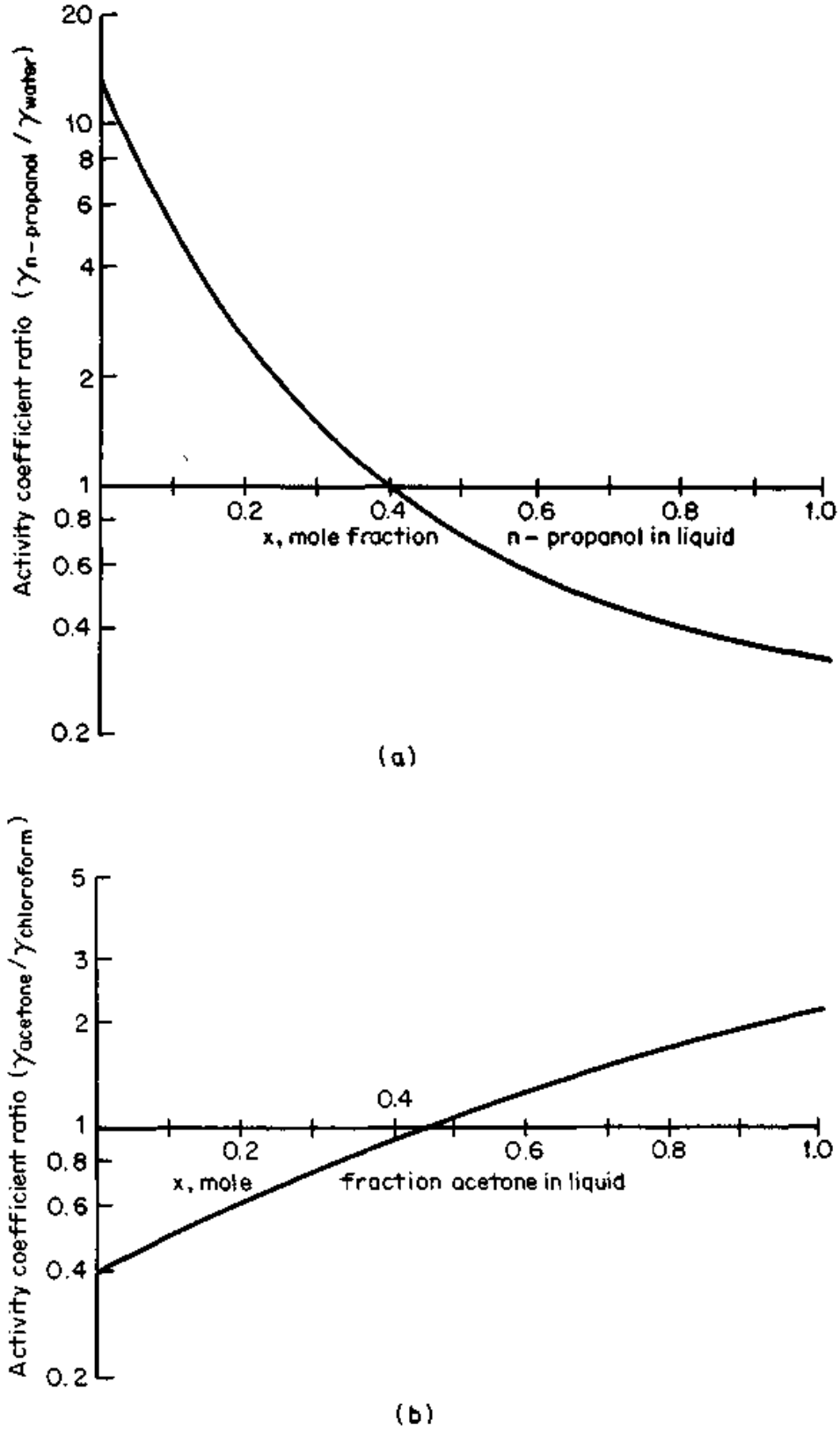

Figure 1.4 Activity coefficient ratios (*a*) in the positive-deviation system, *n*-propanol–water; (*b*) in the negative-deviation system, acetone–chloroform.

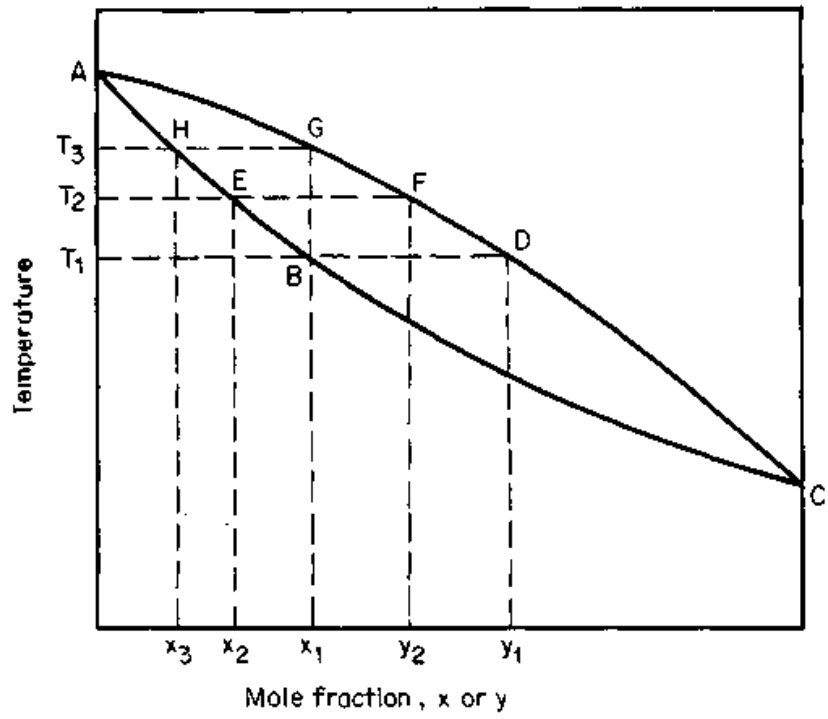

Figure 1.5 T-x diagram.

tion of x-y diagrams (Fig. 1.1). When bubble points and dew points can be readily calculated for a mixture of components, the saturated liquid and saturated vapor curves can be plotted for the system as in Fig. 1.5. From these data, values of x and y can be obtained for a number of temperatures and used to construct the x-y diagram. Similarly, bubble-point calculations yield the equilibrium vapor compositions, giving the values of both x and y. These can also be derived from dew-point calculations in a similar manner.

1.2.5 Calculation of bubble points and dew points

The bubble point of a mixture is calculated from

$$\sum_{i=1}^{c} K_i x_i = 1.0 \tag{1.15}$$

The dew point of a mixture is calculated from

$$\sum_{i=1}^{c} \frac{y_i}{K_i} = 1.0 \tag{1.16}$$

The calculation method is as follows (at constant pressure):

1. Guess a temperature.

2. Calculate K-values.
3. Calculate the sum on the lefthand side of Eq. (1.15) for bubble-point calculation. If smaller than unity, increase temperature. If greater than unity, decrease temperature. Repeat steps 2 and 3 until converged.

   Alternatively, obtain the lefthand side of Eq. (1.16) for dew-point calculation. If smaller than unity, decrease temperature. If greater than unity, increase temperature. Repeat steps 2 and 3 until converged.

1.2.6 Azeotropes

Figures 1.1 and 1.5 are phase diagrams for "normal" systems. In such systems, as the concentration of the less-volatile component increases, so do the dew point and the bubble point.

If the components exhibit strong physical or chemical interaction, the phase diagrams may be different from those shown in Figs. 1.1 and 1.5, and more like those shown in Fig. 1.6. In such systems there is a critical composition (the point of intersection of the equilibrium curve with the 45° diagonal) for which the vapor and liquid compositions are identical. Once this vapor and liquid composition is reached, the components cannot be separated at the given pressure. Such mixtures are called *azeotropes*.

A minimum-boiling azeotrope boils at a temperature lower than either of the pure components. When distilling a system made up of these components, the top product is the azeotrope. The bottom product is the high-boiling-point component when the MVC is present at low concentrations. On the other hand, when the low-boiling-point component is present at high concentrations, the bottom product is the MVC.

A maximum-boiling azeotrope boils at a temperature higher than either of the pure components and therefore always leaves at the bottom of the column. The top product is the high-boiling-point component when the MVC is present at low concentrations. The top product is the MVC when it is present at high concentrations.

If liquid phase separation occurs, the boiling temperature of the mixture as well as the vapor phase composition remain constant until one of the liquid phases disappears. Under such conditions, a mixture of the two liquids will leave the top of the column while either of the components will leave at the bottom, depending on the composition.

1.3 Nomenclature

1.3.1 English letters

c	Number of components
f	Fugacity, psia

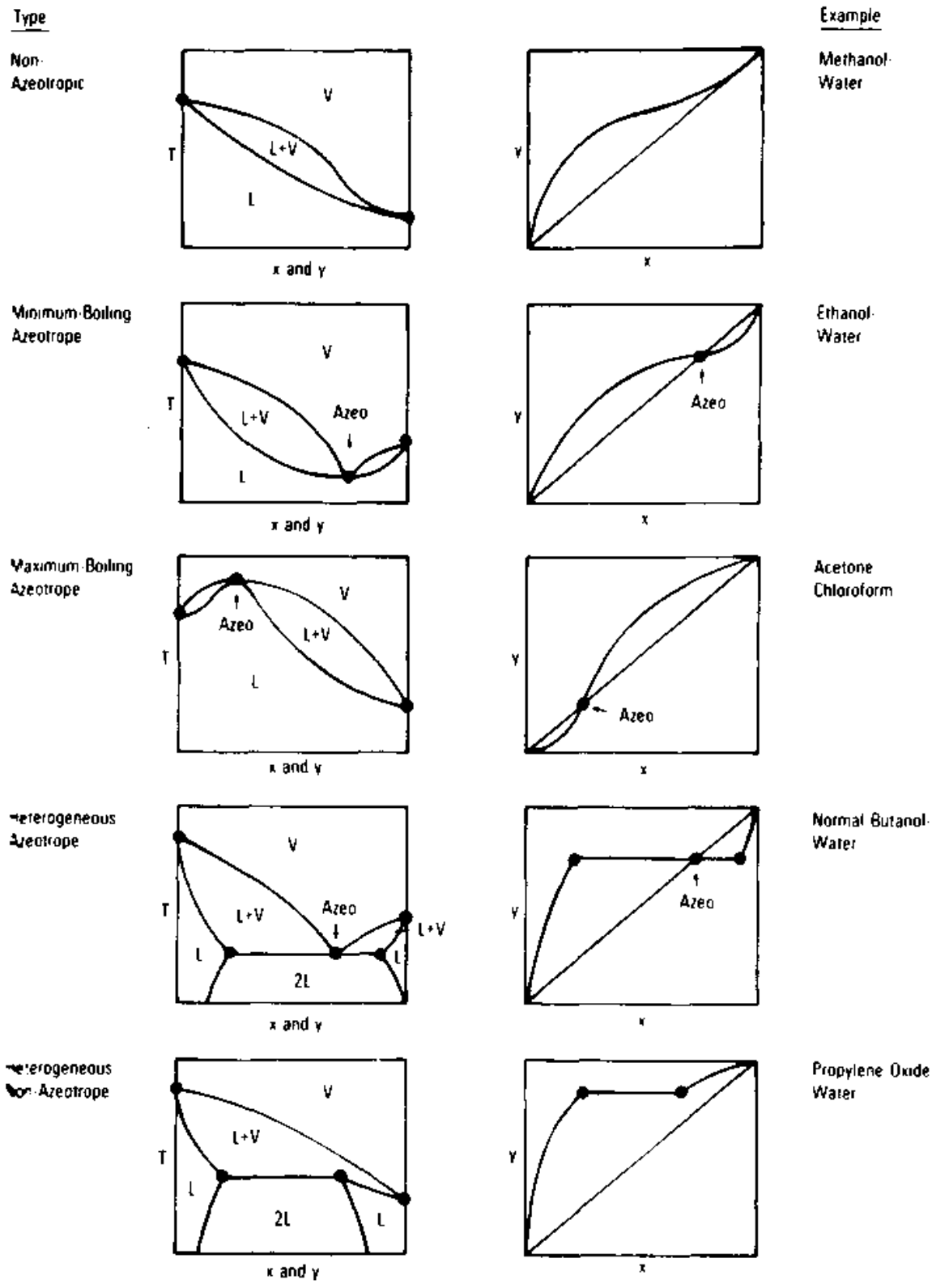

Figure 1.6 Common types of equilibrium diagrams for binary systems. (From J. R. Fair, "Distillation," in R. W. Rousseau, *Handbook of Separation Process Technology*, copyright © 1987 by John Wiley & Sons, New York. Reprinted by permission of John Wiley & Sons Inc.)

K	K-value (defined in Sec. 1.2.1)
MVC	More-volatile component
P	Pressure, psia
p	Partial pressure, psia
p°	Vapor pressure, psia
q	Exponent in Eq. (1.14)
T	Temperature, °R
x	Mole fraction of MVC in liquid
y	Mole fraction of MVC in vapor

1.3.2 Greek letters

α	Relative volatility
γ	Activity coefficient
ϕ	Fugacity coefficient
ψ	Poynting pressure correction term

1.3.3 Subscripts

1,2	Component number. In a binary system, 1 signifies the more-volatile component, 2 the less-volatile component.
i,j	Components in mixture
r	Ratio

1.3.4 Superscripts

L	Liquid
V	Vapor

1.4 References

1. Fair, J. R., *AIChE Symp. Ser. 79,* 235, 1, 1983.
2. Underwood, A. J. V., *Trans. Inst. Chem. Engrs. 13,* 34, 1935.
3. Forbes, R. J., *Short History of the Art of Distillation,* E. J. Brill, Leiden, 1948.
4. Haselden, G. G., in P. N. Snowden, *Practical Distillation—A Post Experience Course,* University of Leeds, 1981.
5. Rush, F. E., *I. Chem. E. Symp. Ser. 56,* p. 4.1.1, 1979.
6. Zuiderweg, F. J., *Chem. Engr. Centenary Supplement,* p. 44, Dec. 1988.
7. Fair, J. R., *Chem. Proc.* p. 23, Sept. 1990.
8. Ellis, S. R. M., and A. P. Boyes, *Trans. Inst. Chem. Engrs.* (London), *52,* 202, 1974.
9. Prausnitz, J. M., C. A. Eckert, R. V. Orye, and J. P. O'Connell, *Computer Calculation for Multicomponent Vapor-Liquid Equilibrium,* Prentice-Hall, Englewood Cliffs, N.J., 1967.
10. Prausnitz, J. M., T. Anderson, E. Grens, C. Eckert, R. Hsieh, and J. O'Connell, *Computer Calculations for Multicomponent Vapor-Liquid and Liquid-Liquid Equilibria,* Prentice-Hall, Englewood Cliffs, N.J., 1980.

11. Reid, R. C., J. M. Prausnitz, and T. K. Sherwood, *The Properties of Gases and Liquids,* 3d ed., McGraw-Hill, New York, 1977.
12. Edimister, W. C., *Applied Hydrocarbon Thermodynamics,* vol. 1, 2d ed., Gulf Publishing, Houston, Texas, 1984.
13. American Petroleum Institute, *Technical Data Book—Petroleum Refining,* 3d ed., API, Division of Refining, Washington, 1976.
14. *GPA Engineering Data Book,* 9th ed., Tulsa, 1981.
15. Null, H. R., *Phase Equilibrium in Process Design,* Wiley-Interscience, New York, 1970.
16. Hala, E., J. Pick, V. Fried, and O. Vilim, *Vapor-Liquid Equilibrium,* 2d ed., Pergamon Press, London, 1968.
17. Hala, E., I. Wichterle, J. Polak, and T. Boublik, *Vapor-Liquid Equilibrium Data at Normal Pressures,* Pergamon Press, Oxford, 1968.
18. Wichterle, I., J. Linek, and E. Hala, *Vapor-Liquid Equilibrium Data Bibliography,* Elsevier, Amsterdam, 1973; *Vapor-Liquid Equilibrium Data Bibliography—Supplement I,* Elsevier, Amsterdam, 1976.
19. Gmehling, J., and U. Onken, *Vapor-Liquid Equilibrium Data Collection,* DECHEMA Chemistry Data Series, Frankfurt, 1977.
20. Hiza, M. J., A. J. Kidnay, and R. C. Miller, *Equilibrium Properties of Fluid Mixtures—A Bibliography of Data on Fluids of Cryogenic Interest,* NSRDS Bibliography Series, Plenum, New York, 1975.
21. Hicks, C. P., "Bibliography of Thermodynamic Quantities for Binary Fluid Mixtures," in M. L. McGlashan (ed.), *Chemical Thermodynamics,* vol. 2, Chem. Soc., London, 1978.
22. Hirata, M., S. Ohe, and K. Nagahama, *Computer Aided Data Book of Vapor-Liquid Equilibria,* Elsevier, Amsterdam, 1975.
23. Palmer, D. A., *Handbook of Applied Thermodynamics,* CRC Press, Boca Raton, Fla., 1987.
24. Fredenslund, A., J. Gmehling, and P. Rasmussen, *Vapor-Liquid Equilibria Using UNIFAC,* Elsevier, Amsterdam, 1977.
25. Roy, P., and G. K. Hobson, *I. Chem. E. Symp. Ser. 104,* p. A273, 1987.
26. Heidemann, R. A., and A. Fredenslund, *I. Chem. E. Symp. Ser. 104,* p. A291, 1987.
27. Mathur, G. P., and M. B. Powley in E. J. Henley (ed.), *Stagewise and Mass Transfer Operations,* vol. 1, A.I.Ch.E. Modular Instruction, 1980.
28. Doig, I. D., *Aust. Chem. Eng., 12*(7), 5, 1971.
29. Robinson, C. S., and E. R. Gilliland, *Elements of Fractional Distillation,* McGraw-Hill, New York, 1950.

Chapter

2

Key Fractionation Concepts

The concepts described in this chapter are the foundations of distillation engineering. A thorough understanding of these concepts is essential for distillation practitioner. This is one chapter that the novice can ill-afford to skip.

The author stresses and applies the visual approach (i.e., graphical methods) when introducing these concepts. This approach was deemphasized when computers began to make rapid inroads into distillation design. For some time, graphical techniques were considered a tool of the past, never to be used again. An undesirable by-product was that the distillation column became a "black box," and the engineers' understanding of distillation suffered.

The last decade saw the pendulum swing the other way. It was appreciated that there is no conflict between computer and graphical techniques, and that the two can coexist. It was realized that the graphical techniques themselves can be programmed and used side by side with computer simulation. This hybrid approach combined the speed and accuracy of the computer with the analytical and visual value of the graphical techniques.

This chapter first discusses the stage concept, and how stages are put together in a column. It then presents the principles of the x-y diagram, which is the main graphical tool for distillation analysis. It applies this graphical technique to define and illustrate several key distillation concepts: pinching, minimum and total reflux, minimum stripping, effects of the thermal state of the feed, and column complexities (e.g., multifeed columns). The chapter then reviews the basic concepts of multicomponent distillation, and the application of graphical techniques to such systems. Finally, the chapter describes the use of graphical techniques in analyzing computer simulation results.

2.1 Theoretical Stages

2.1.1 Ideal and nonideal stages

The *ideal distillation stage* is a device that meets these criteria:

1. It operates in steady state and has a liquid product and a vapor product.
2. All vapor and liquid entering the stage are intimately contacted and perfectly mixed.
3. Total vapor leaving the stage is in equilibrium with total liquid leaving the stage.

Examples. Figure 2.1 illustrates the first criterion. The system in Fig. 2.1*a* has a vapor product and a liquid product and therefore obeys this criterion. The systems in Fig. 2.1*b* and *c* have no vapor products and therefore are not equilibrium stages. Generating a vapor phase in these systems (Fig. 2.1*d* and *e*) renders them equilibrium stages. Figure 2.1*c* and *e* depict a total and a partial condenser, respectively. The total condenser is not a distillation stage, whereas the partial condenser is.

Figure 2.2 illustrates common distillation stage arrangements. All satisfy criterion 1. Criteria 2 and 3 determine which arrangements are ideal stages. Nonideal stages can still be modeled using the ideal stage model, but the nonideality must be accounted for.

Figure 2.2*a* and *b* shows thermosiphon reboiler arrangements. The system in Fig. 2.2*a* is not an ideal stage. The liquid product is made up from liquid leaving the reboiler and liquid descending from the bottom tray. Although the former is perfectly mixed with the leaving vapor, the latter does not contact the vapor and is not in equilibrium with it. The system in Fig. 2.2*b* is an ideal stage. Here the liquid product is made up from the liquid leaving the reboiler only. This liquid is in equilibrium with vapor leaving the reboiler, which is the vapor product from the stage.

Figure 2.2*c* and *d* shows distillation tray arrangements. The system in Fig. 2.2*c* is typical. It does not satisfy criterion 2, and therefore, is not an ideal stage. Further, only the vapor leaving the stage at point *B* can be in equilibrium with the liquid leaving the tray. Vapor leaving the tray at point *A* can only be in equilibrium with the tray inlet liquid, but not with liquid leaving the tray. The system in Fig. 2.2*d* is rarely encountered, but it satisfies criterion 2. Here liquid composition across the tray is uniform and equals the composition of liquid leaving the tray. Vapor at both points *A* and *B* is in contact with the liquid product stream. Providing there is sufficient time and area for

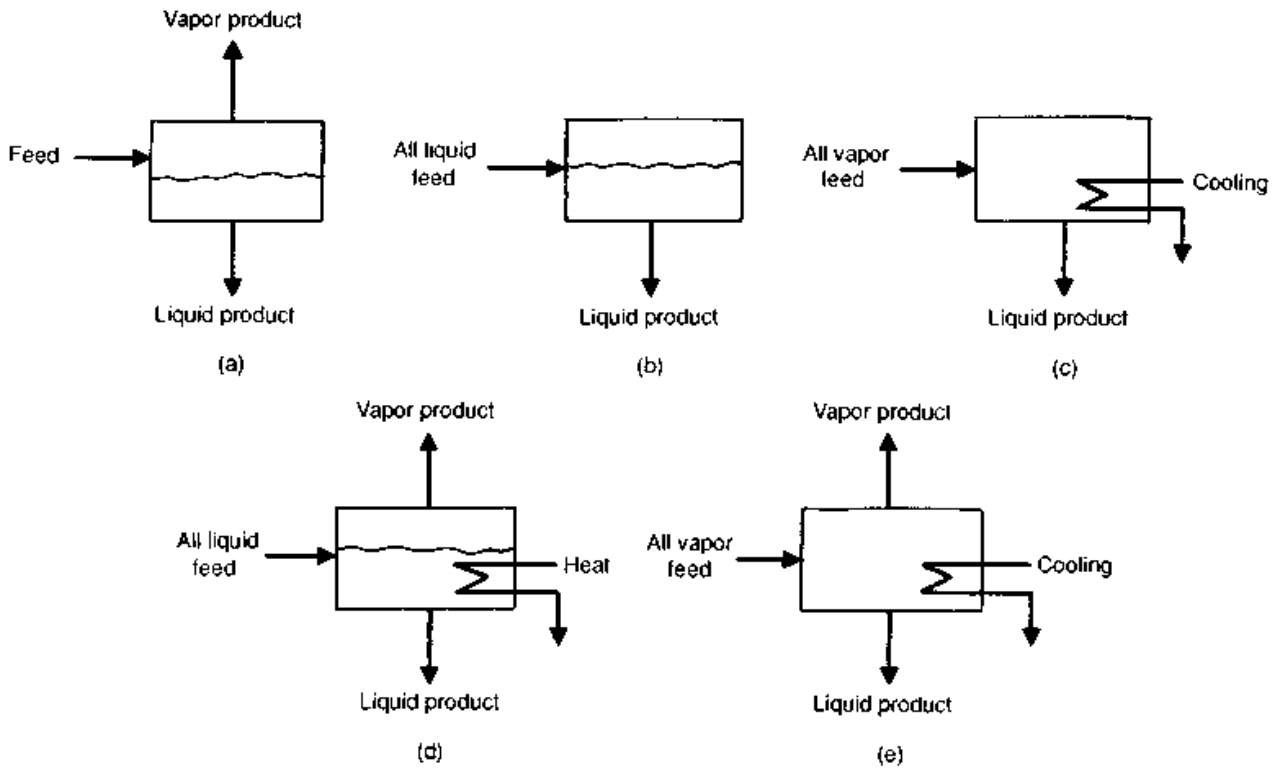

Figure 2.1 The distillation stage concept. (*a*) General presentation of an ideal distillation stage; (*b*) and (*c*) single-phase product (these are not ideal distillation stages); (*d*) and (*e*) two-phase product (these are ideal distillation stages).

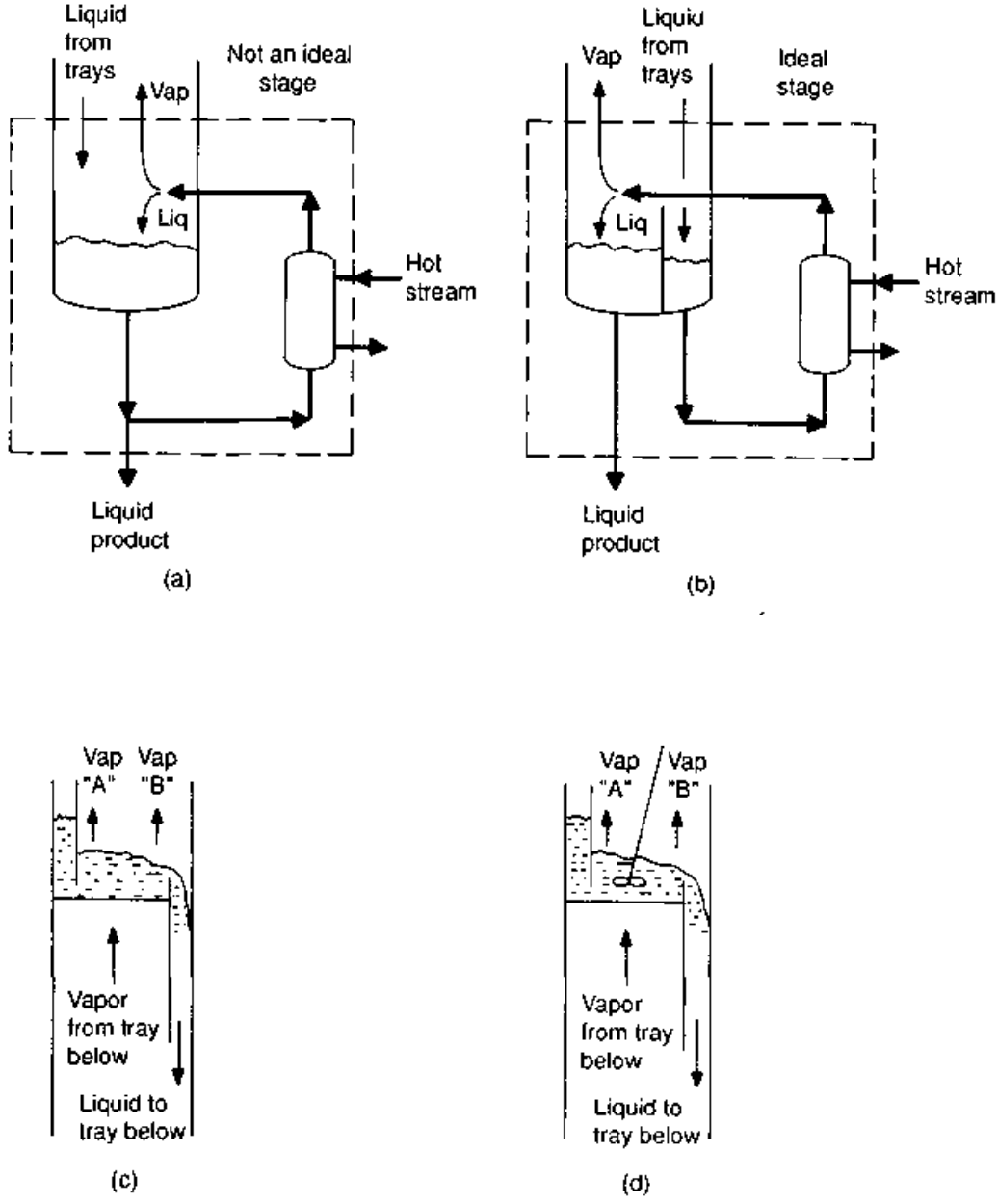

Figure 2.2 Ideal and nonideal stages in distillation systems. (*a*), (*b*) Thermosiphon reboiler arrangements; (*c*), (*d*) fractionation tray arrangements; (*e*), (*f*) intercondenser arrangements. Arrangements (*b*), (*d*), and (*f*) are ideal stages. Arrangements (*a*), (*c*), and (*e*) are nonideal stages.

vapor-liquid contact, equilibrium will be established. Criterion 3 will be satisfied, making arrangement 2.2*d* an ideal stage.

Figure 2.2*e* and *f* shows intercondenser arrangements. The system in Fig. 2.2*e* is not an ideal stage. Liquid leaving the stage is made up from liquid condensed in the intercondenser and liquid from the top column. While the condensate is in equilibrium with vapor leaving the stage, the liquid from the column does not mix with this vapor and is not in equilibrium with it. Mixing the column liquid with the vapor-

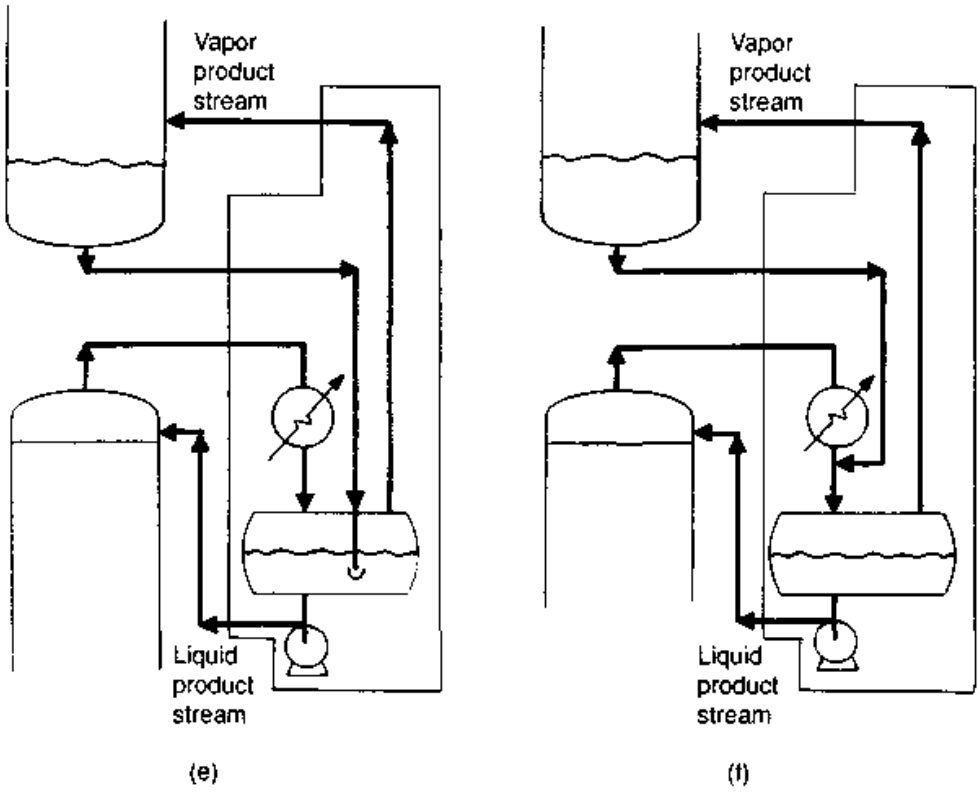

Figure 2.2 (*Continued*)

liquid mixture leaving the condenser (Fig. 2.2*f*) converts the nonideal into an ideal stage, provided the line downstream of the mixing point is sufficiently long.

Stage efficiency. This accounts for the nonideality of a stage. The number of ideal stages is equal to the number of nonideal stages multiplied by the stage efficiency. The nonideality may lower or enhance the separation; if it enhances the separation, the stage efficiency can exceed 100 percent. Stage efficiencies are discussed in Chaps. 7 and 9.

2.1.2 Stripping, rectification, and fractionation

Vapor leaving a distillation stage is richer than the feed in the more-volatile components. Liquid leaving the stage is richer than the feed in the less-volatile components. In order to improve the separation, multiple stages are used.

Stripping stages (Fig. 2.3*a*) concentrate the less-volatile components in a liquid stream. A vapor recycle vaporizes ("strips") the more-volatile components from the liquid. To generate the vapor recycle, heat is supplied to vaporize a portion of the bottom-stage liquid. This vapor recycle is termed *boilup*.

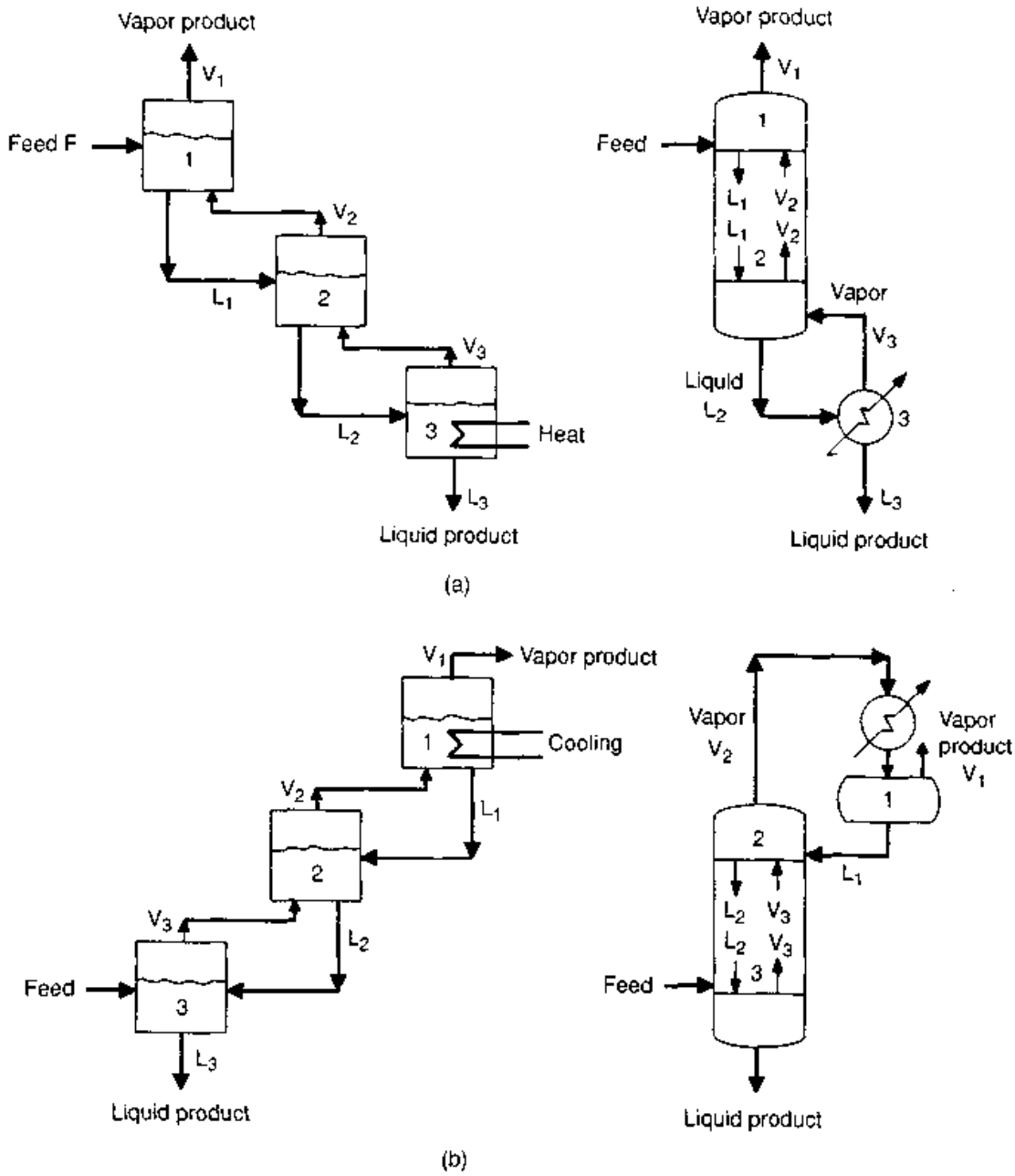

Figure 2.3 Multiple-stage arrangements. (*a*) Stripping; (*b*) rectifying; (*c*) fractionator.

Rectifying stages (Fig. 2.3*b*) concentrate the more-volatile components in a vapor stream. A liquid recycle condenses the less-volatile components from the rising vapor. To generate the liquid recycle, cooling is applied to condense a portion of the overhead vapor. The liquid recycle is termed *reflux.*

The stripping and rectifying stages shown in Fig. 2.3*a* and *b* can be combined into a single separation process with internal recycle (Fig. 2.3*c*). This process is termed *fractionation.*

In a single-feed fractionator, stages above the feed are rectifying

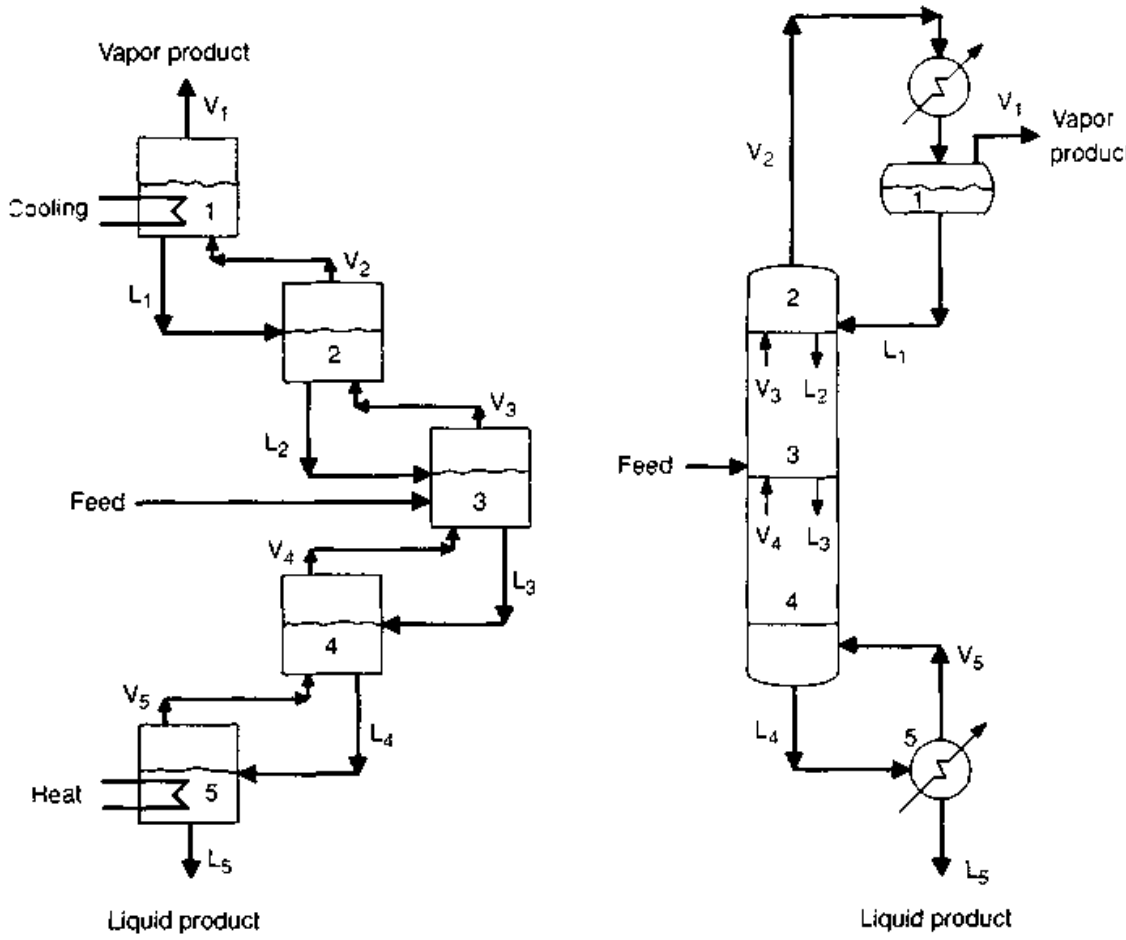

Figure 2.3 *(Continued)*

and those below it are stripping (Fig. 2.3c). In multifeed fractionators, the more precise functional criterion below is used to distinguish the rectifying from stripping sections.

The stripping section has a net downflow of material. The vapor serves only as a recycle stream to remove lights from the liquid. Therefore, the quantity of liquid exceeds the quantity of vapor in the stripping section. The converse applies in the rectifying section. This section has a net upflow of material, and the quantity of vapor exceeds the quantity of liquid.

Figure 2.4 shows a multifeed fractionator. The top three sections have a net upflow of material and are therefore rectifying. The bottom three sections have a net downflow of material, and are therefore stripping.

2.1.3 Material and energy balances

For a single binary distillation stage (Fig. 2.5*a*) the following equations apply:

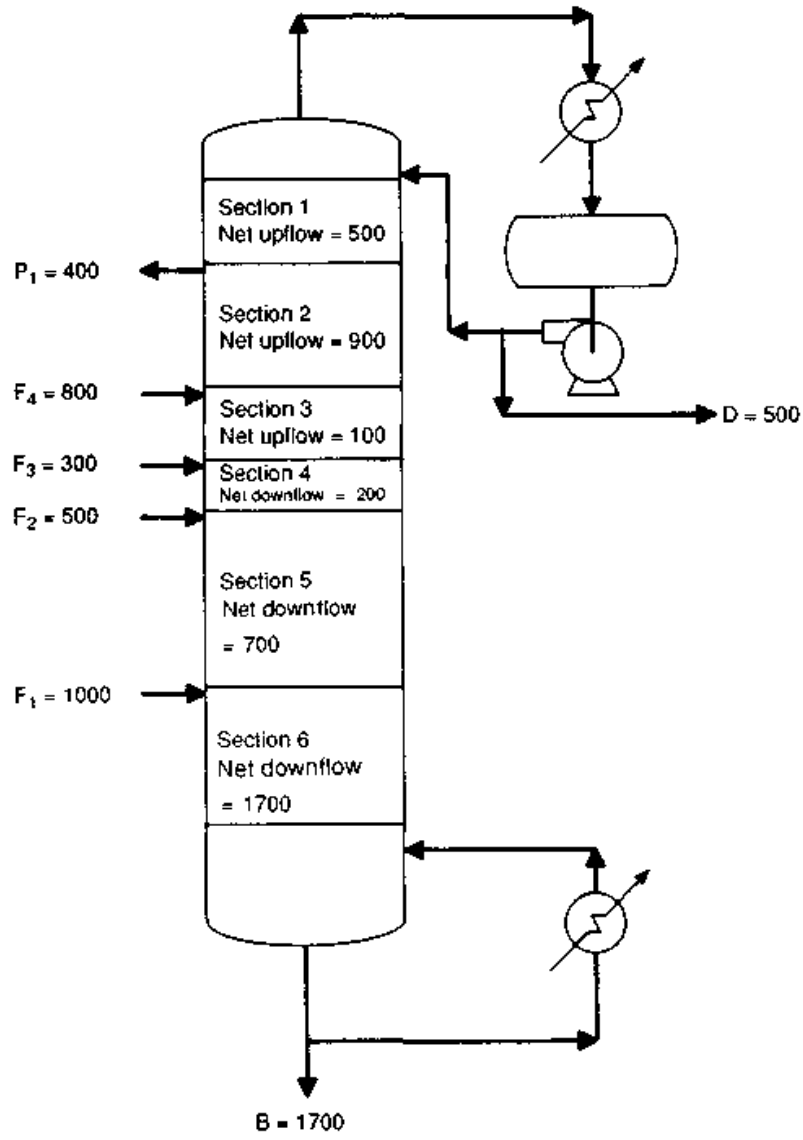

Figure 2.4 Stripping and rectifying sections.

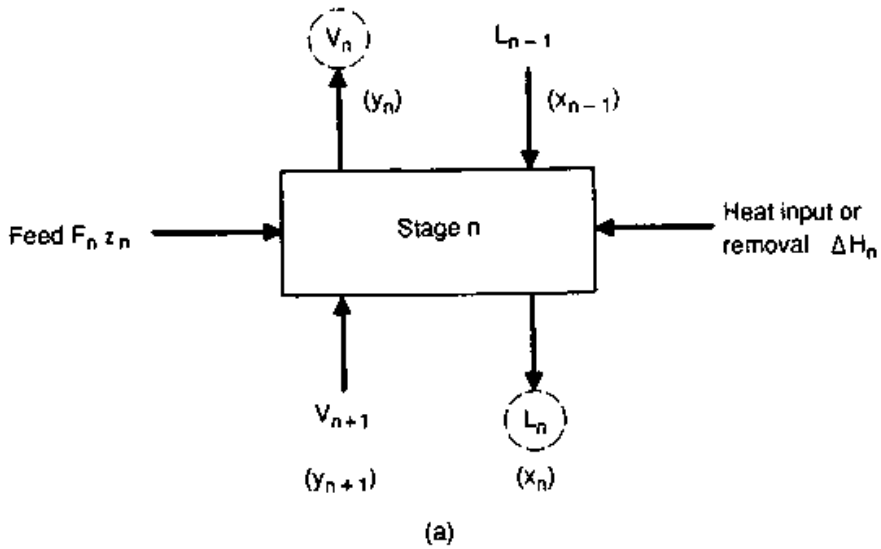

(a)

Figure 2.5 Fractionation-stage model nomenclature. (*a*) Each stage; (*b*) fractionator.

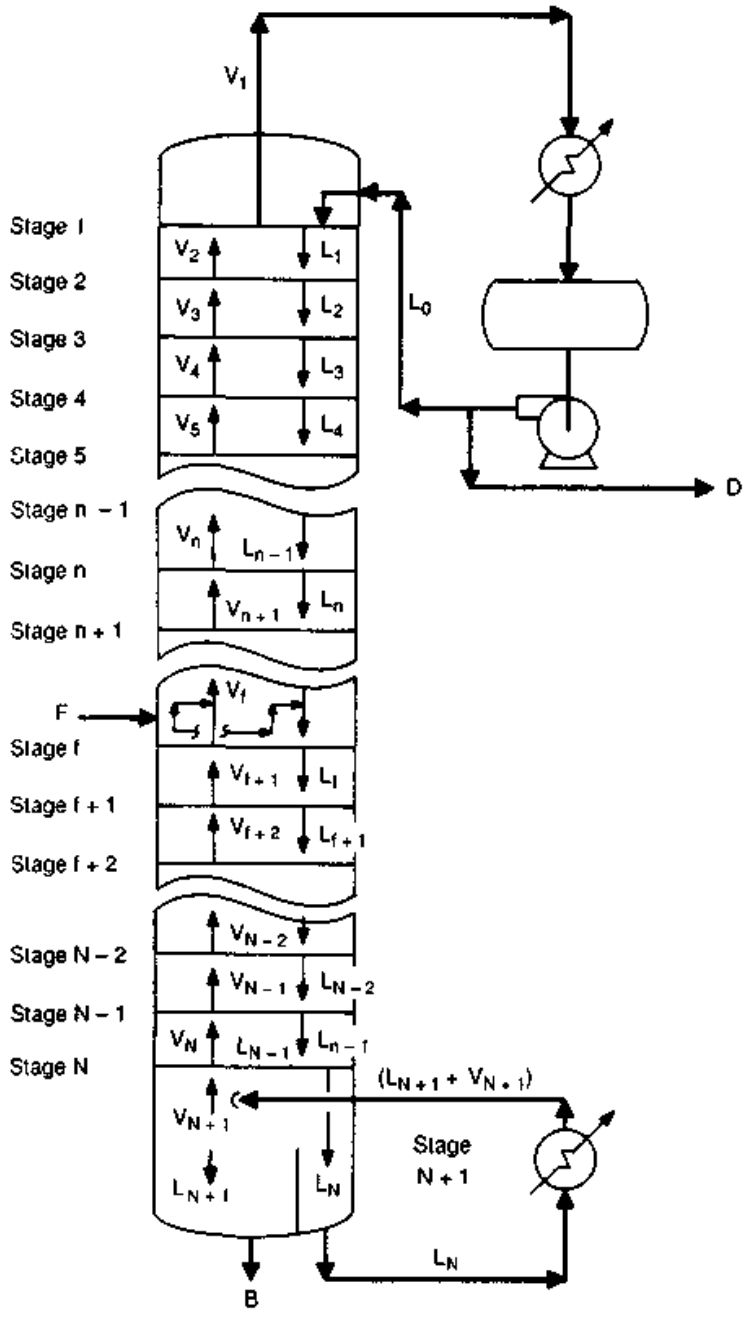

Figure 2.5 (*Continued*)

Mass Balance

$$F_n + V_{n+1} + L_{n-1} = V_n + L_n \tag{2.1}$$

Component Balance

$$F_n z_n + V_{n+1} y_{n+1} + L_{n-1} x_{n-1} = V_n y_n + L_n x_n \tag{2.2}$$

Energy Balance

$$\Delta H_n + F_n H_{f,n} + V_{n+1} H_{V,n+1} + L_{n-1} H_{L,n-1} = V_n H_{V,n} + L_n H_{L,n} \qquad (2.3)$$

Equilibrium Relationship

$$y_n = K x_n \qquad (2.4)$$

In multicomponent distillation of j components, there are $j - 1$ component balances and $j - 1$ equations describing the equilibrium relationship.

Multiple stages (Fig. 2.5*b*). Equations (2.1) to (2.4) apply to each stage. A rigorous solution (Chap. 4) simultaneously solves these equations for each stage and each component. The equations can be simplified and solved by analytical shortcut procedures (Chap. 3) or graphically. The rest of this chapter focuses on the graphical procedures, which are applied to introduce and illustrate several key fractionation concepts.

2.2 *x-y* Diagrams

Computers have superseded graphical techniques as the main distillation design and performance evaluation tool. Nevertheless, graphical techniques are still widely used in modern distillation technology. Their prime application is as an analytical tool. They provide a means of visualizing the process and enable spotting pinched conditions, excessive reflux, incorrect feed points, and a nonoptimum thermal condition of the feed. They are powerful for analyzing computer solutions (Sec. 2.4.1). Other applications are screening and optimization of design options, providing initial estimates for computer calculations and engineer training.

The graphical technique most frequently used in distillation is the *x-y* or McCabe-Thiele diagram (1). The *H-x*, or Ponchon-Savarit diagram (2,3), is harder to visualize and cannot be readily extended to multicomponent distillation. Due to their limited application, *H-x* diagrams were excluded from this book, and are discussed elsewhere (4–6).

2.2.1 McCabe-Thiele diagrams: fundamentals

A mass balance for the "envelope" shown in Fig. 2.6*a*, cutting below any plate n in the rectifying section, gives

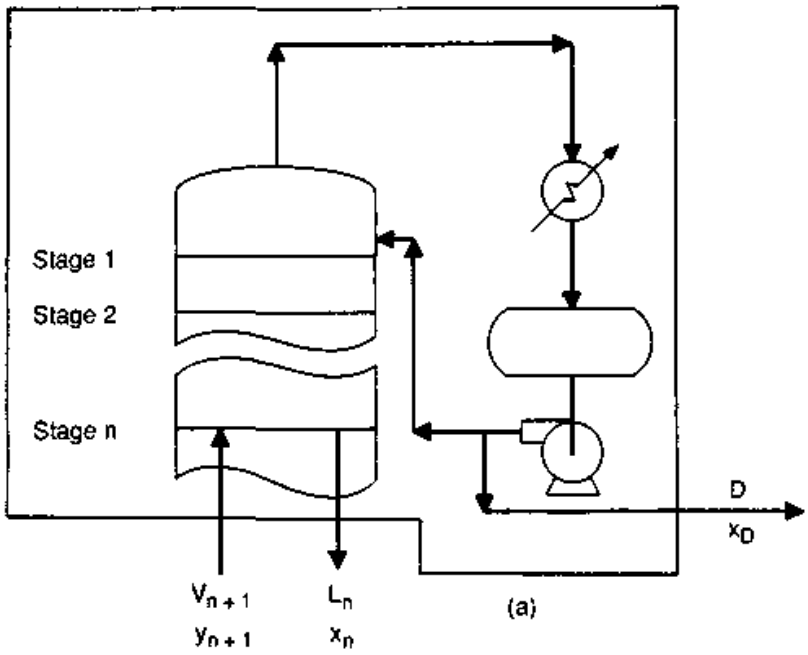

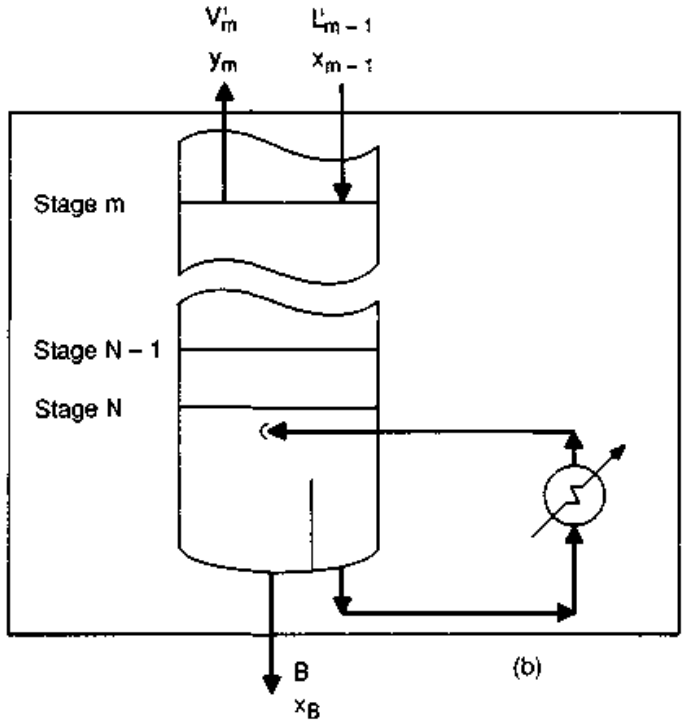

Figure 2.6 Material balances. (*a*) Rectifying section; (*b*) stripping section; (*c*) overall.

$$V_{n+1} = L_n + D \tag{2.5}$$

Similarly, a component balance gives

$$V_{n+1}y_{n+1} = L_n x_n + Dx_D \tag{2.6}$$

Instead of an energy balance, the McCabe-Thiele method assumes

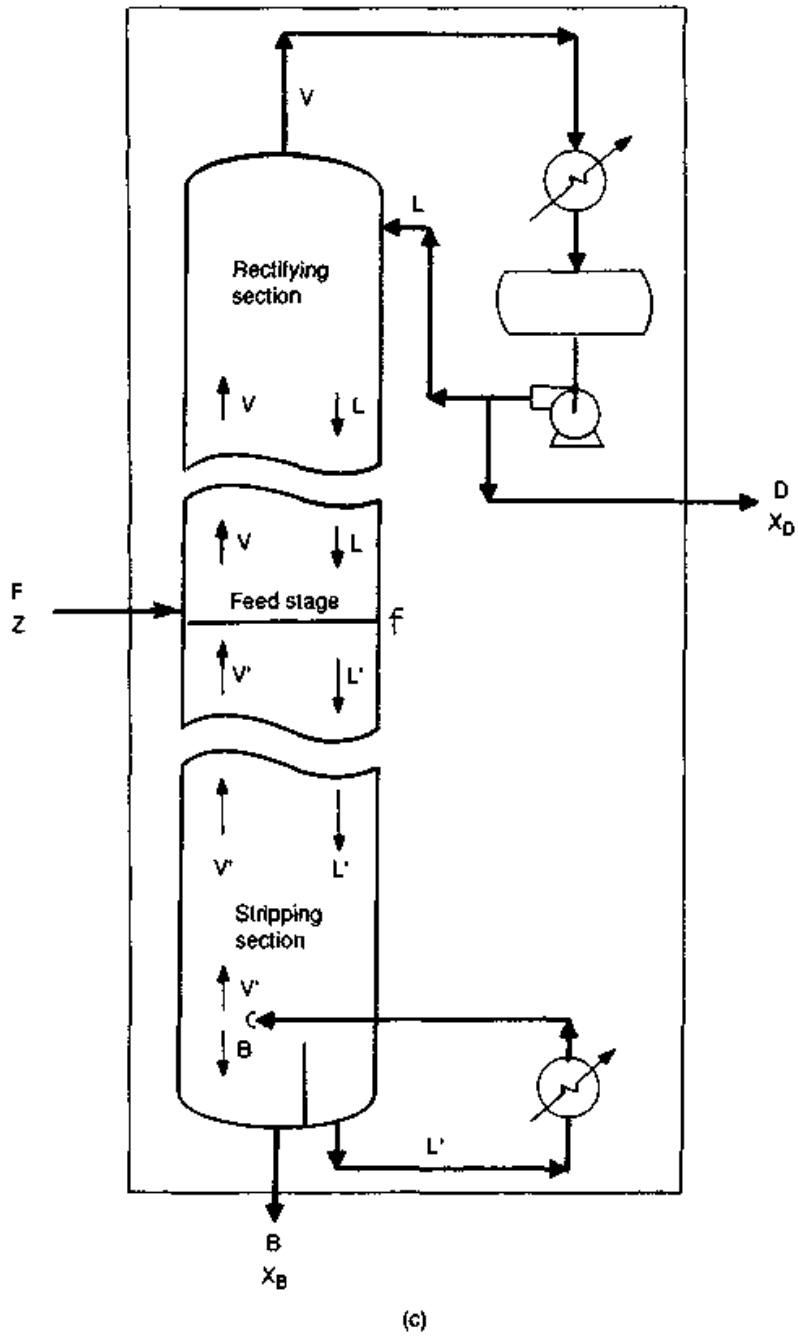

(c)

Figure 2.6 (*Continued*)

constant molar overflow (Sec. 2.2.2). Mathematically, this assumption means

$$L_0 = L_1 = L_2 = L_3 = \ldots = L_n = L \tag{2.7}$$

From Eqs. (2.5) and (2.7) it follows that

$$V_1 = V_2 = V_3 = \ldots = V_n = V_{n+1} = V \tag{2.8}$$

These equations simplify Eq. (2.6) to

$$y_{n+1} = \frac{L}{V}x_n + \frac{D}{V}x_D \tag{2.9}$$

A similar derivation for the stripping section (Fig. 2.6*b*) gives

$$y_m = \frac{L'}{V'}x_{m-1} - \frac{B}{V'}x_B \tag{2.10}$$

Equations (2.9) and (2.10) are basic building blocks for McCabe-Thiele diagrams. They are discussed further in Sec. 2.2.3. Equations (2.7) and (2.8) also simplify Eq. (2.5) to

$$V = L + D \tag{2.11}$$

A similar derivation for the stripping section gives

$$V' = L' - B \tag{2.12}$$

An overall column mass balance (Fig. 2.6*c*) gives

$$F = B + D \tag{2.13}$$

Combining Eqs. (2.11), (2.12), and (2.13) gives a relationship that can also be derived from a feed stage mass balance (Fig. 2.6*c*)

$$V' - V = (L' - L) - F \tag{2.14}$$

An overall column component balance gives

$$Dx_D + Bx_B = Fz \tag{2.15}$$

The definition of reflux ratio is

$$R = \frac{L}{D} \tag{2.16}$$

Similarly, the stripping ratio is

$$S = \frac{V'}{B} \tag{2.17}$$

2.2.2 Constant molar overflow and other assumptions

Constant molar overflow. This assumption is a substitute for the energy balances. It states that the mixture has a constant heat of vaporization and that sensible heat and heat of mixing effects are negligible. Equations (2.7) and (2.8) give a mathematical expression of this assumption. Detailed thermodynamic implications of this assumption are described elsewhere (e.g., Refs. 6–8).

Generally, constant molar overflow holds well for systems where the components are similar in nature and molecular weights, and

where heat-of-solution effects are not significant. When heat-of-solution effects are small, the ratio of the molar latent heats of the pure components provides insight into the suitability of the assumption (Table 2.1). The assumption holds well for the benzene-toluene, isobutane–normal butane, propane–normal butane, and normal heptane–ethylbenzene systems, where the latent heat ratios are close to unity. The assumption is less satisfactory for the acetone-water and methane-ethylene systems, where this ratio is higher. The assumption is poor for the ammonia-water system where the latent heat ratio is close to 2.

When in doubt, it is best to adjust the x-y diagram for heat effects. This can be achieved by one of the following techniques.

- When a computer simulation is available, the component balance lines (Sec. 2.2.3) can be constructed from compositions printed out by the simulation. The simulation energy balances adjust the component balance lines for heat effects. These heat effects convert each component balance line thus constructed into a curve (Sec. 2.4.1).
- Using an H-x diagram to adjust Eqs. (2.9) and (2.10) for latent heat effects. This approach also converts each component balance line into a curve, but the curve is constructed using an H-x diagram instead of a computer simulation. Further details are described by Fisher (10).
- Using an H-x diagram to derive pseudo molecular weights and pseudo latent heats of vaporization for the components. These pseudo properties are then applied to construct an x-y diagram. This method is described in detail by Robinson and Gilliland (6).

Other assumptions. Two additional assumptions are inherent in the x-y diagram method:

1. The separation is at constant pressure. This assumption is usually good unless the column operates under vacuum. For vacuum systems, the equilibrium curve needs adjustment for pressure variations.
2. The feed stream mixes with the feed-stage fluids prior to any separation. This assumption is good for a single-phase feed, but less satisfactory for a partially vaporized feed (11). A partially vaporized feed splits prior to mixing; the feed liquid then mixes with liquid of the tray below, while vapor mixes with vapor of the tray above. Ledanois and Olivera-Fuentes (11) derived a simple correction to the x-y diagram construction to alleviate the inaccuracy. Their correction is valid where tray efficiency is high (i.e., above 60 to 70 percent); at lower tray efficiencies, the inaccuracy is more difficult to quantify.

TABLE 2.1 Using Latent Heat Ratio as a Guide to the Application of Constant Molar Overflow

Component no. 1	Component no. 2	Pressure, psia	Boiling points, °F		Latent heat, Btu/lb-mole		Latent heat ratio, (comp. 2)/(comp. 1)	Note
			Component no. 1	Component no. 2	Component no. 1	Component no. 2		
Benzene	Toluene	14.7	176	231	13300	14500	1.09	1
Isobutane	*n*-butane	75	100	122	7900	8300	1.05	1
Propane	*n*-butane	200	100	201	5900	6700	1.13	1
n-heptane	Ethylbenzene	14.7	210	277	13600	15500	1.14	3
Acetone	Water	14.7	133	212	12800	17500	1.37	1
Methane	Ethylene	470	−140	10	2200	3100	1.41	1
Ammonia	Water	295	120	413	7700	15200	1.97	2

NOTES: (1) Data from Gallant, Ref. 9; (2) data from Robinson and Gilliland, Ref. 6; (3) data from Van Winkle, Ref. 4.

The inaccuracy due to this assumption is usually minor. It is substantial (11) only where the feed split significantly affects the separation; typically with very few stages (about five or fewer) and very high relative volatility (>3).

2.2.3 McCabe-Thiele diagrams: line equations

Equilibrium curve (Figs. 1.1*a*, 2.9*b*). This curve is the locus of all equilibrium points. For a given liquid composition x_n, it gives the equilibrium vapor composition, y_n, and vice versa. An equilibrium stage n is represented as a point (x_n,y_n) on the equilibrium curve where x_n and y_n are the liquid and vapor compositions leaving the stage.

45° diagonal line (Fig. 2.9*b*). This line is the locus of all the points where

$$y_{n+1} = x_n \tag{2.18}$$

Component balance (operating) lines (Fig. 2.9*b*). The component balance equations, Eqs. (2.9) and (2.10), can be represented as straight lines on an x-y diagram. The rectifying section component balance line is the locus of points that obey the rectifying section component balance, Eq. (2.9). Similarly, the stripping section component balance line is the locus of points that obey the stripping section component balance, Eq. (2.10).

Unfortunately, component balance lines are referred to as "operating lines." The author believes that *operating lines* is a poor choice of words, since it states little about the physical nature of these lines. The term *component balance lines* is far more descriptive and appropriate, and will be used in this book.

Slopes of component balance (operating) lines. Equations (2.9) and (2.10) indicate that the slopes of the component balance lines are L/V and L'/V' for the rectifying and stripping sections, respectively. As $L < V$ [Eq. (2.11)] and $L' > V'$ [Eq. (2.12)], the slope of the rectifying section component balance line is smaller than unity, while that of the stripping section component balance line is greater than unity.

When latent heat varies from stage to stage, so do the L/V and L'/V' ratios. For this reason, when the constant molar overflow assumption (Sec. 2.2.2) does not apply, the component balance relationship becomes a curve instead of a straight line.

Intersection of component balance (operating) lines with diagonal. The point where the rectifying section component balance line intersects

the 45° diagonal line satisfies both Eqs. (2.9) and (2.18). Solving these simultaneously and then using Eq. (2.11) gives

$$y_{n+1} = x_n = \frac{Dx_D}{V - L} = x_D \tag{2.19}$$

Both Eqs. (2.9) and (2.19) are for a column equipped with a total condenser (Fig. 2.7*a*). Since a total condenser is not an equilibrium stage (Sec. 2.1.1), the first equilibrium stage is inside the column. If the condenser is partial (Fig. 2.7*b*), then it is the first equilibrium stage. In this case, y_D replaces x_D in Eq. (2.9), D is identical to V_1, and L_0 is zero. Substituting in Eq. (2.9) gives

$$y_{n+1} = y_D \tag{2.20}$$

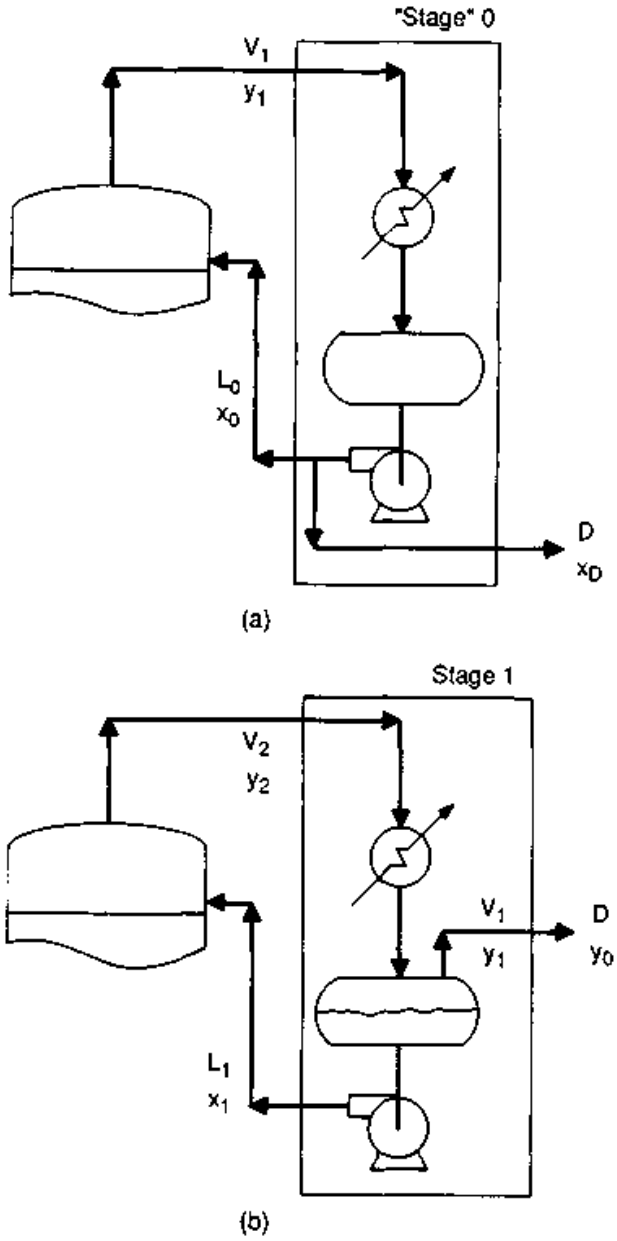

Figure 2.7 Condenser component balances. (*a*) Total condenser; (*b*) partial condenser.

Therefore, the rectifying section component balance line intersects the 45° diagonal line at the point $x = x_D$ and $x = y_D$ for a total and partial condenser, respectively. The intersection point can be expressed as

$$x = y = \text{product composition} \tag{2.21}$$

A similar derivation for the stripping section shows that the stripping section component balance line intersects the 45° diagonal line at the point

$$x = y = \text{bottom product composition} \tag{2.22}$$

Intersection of the two-component balance (operating) lines. Intersection takes place at a point (x_i,y_i) that satisfies both Eqs. (2.9) and (2.10). Multiplying both sides of Eq. (2.9) by V and both sides of (2.10) by V' and subtracting one from the other yields

$$(V - V')y_i = (L - L')x_i + Dx_D + Bx_B \tag{2.23}$$

Using Eq. (2.15), this simplifies to

$$(V - V')y_i = (L - L')x_i + Fz \tag{2.24}$$

Let

$$\frac{L' - L}{F} = q \tag{2.25}$$

Dividing both sides of Eq. (2.14) by F, and substituting Eq. (2.25), gives

$$\frac{V' - V}{F} = q - 1 \tag{2.26}$$

Substituting Eqs. (2.25) and (2.26) in Eq. (2.24), and dividing both sides by $(q - 1)F$

$$y_i = \frac{q}{q - 1}x_i - \frac{z}{q - 1} \tag{2.27}$$

Equation (2.27) represents the locus of the points at which the rectifying section component balance line intersects the stripping section component balance line. This equation is called the *q-line equation.* The q-line is illustrated later in Fig. 2.9*b*.

Intersection of the q-line with the 45° diagonal. If $x_i = z$, then Eq. (2.27) gives $y_i = x_i = z$. Therefore, the q-line intersects the 45° diagonal line at the point (z,z).

Slope of the q-line. The slope is $q/(q - 1)$, per Eq. (2.27). Equation (2.25), which defines q, can be rewritten as

$$L' - L = qF \tag{2.28}$$

From this equation, the quantity q is the fraction of the feed that is liquid. The product qF is the quantity of liquid contained in the feed. This quantity joins the liquid descending from the rectifying section to provide the liquid for the stripping section. Similarly, $(1 - q)F$ is the quantity of vapor in the feed; this vapor joins the vapor ascending from the stripping section to provide the rectifying section vapor flow. Table 2.2 summarizes the relationship between q, the thermal condition of the feed, slope of the q-line, and column flows. Figure 2.8*a* illustrates the slope of the q-line for each of these conditions. Figure 2.8*b* illustrates the effect of the slope on the component balance line, assuming the rectifying section component balance line (and therefore the reflux ratio) is fixed.

Summary. In order to draw a straight line on an x-y diagram, the slope of the line and one point on the line need to be determined. The derivations above enable the determination of the slope and one point on the following lines:

1. The rectifying section component balance (operating) line.
2. The stripping section component balance (operating) line.
3. The q-line.

In each case the point defined is the intersection of the line with the 45° diagonal line. The slopes and intersection points of each of these lines are summarized in Table 2.3. In addition, it has been shown that the rectifying section component balance line and the stripping section component balance line meet on the q-line.

2.2.4 McCabe-Thiele diagrams: construction

Example 2.1 It is required to separate 200 lb-mole/h of a 40% benzene and 60% toluene mixture into a top product containing 95% benzene and a bottom stream containing 90% toluene. The feed mixture is 25 percent vaporized. The reflux ratio is 3:1, and a total condenser is to be used. (*a*) How many theoretical stages are required? (*b*) At what stage should the feed be introduced?

solution STEP 1 Obtain an overall material balance for the column. (Refer to Figs. 2.6*c* and 2.9*a*.)

1. Given $F = 200$ lb-mole/h, $x_F = 0.4$, $x_D = 0.95$, $x_B = 0.1$
2. Overall mass balance, Eq. (2.13)

$$200 = B + D$$

3. Overall component balance on benzene, Eq. (2.15)

$$200 \times 0.4 = 0.1B + 0.95D$$

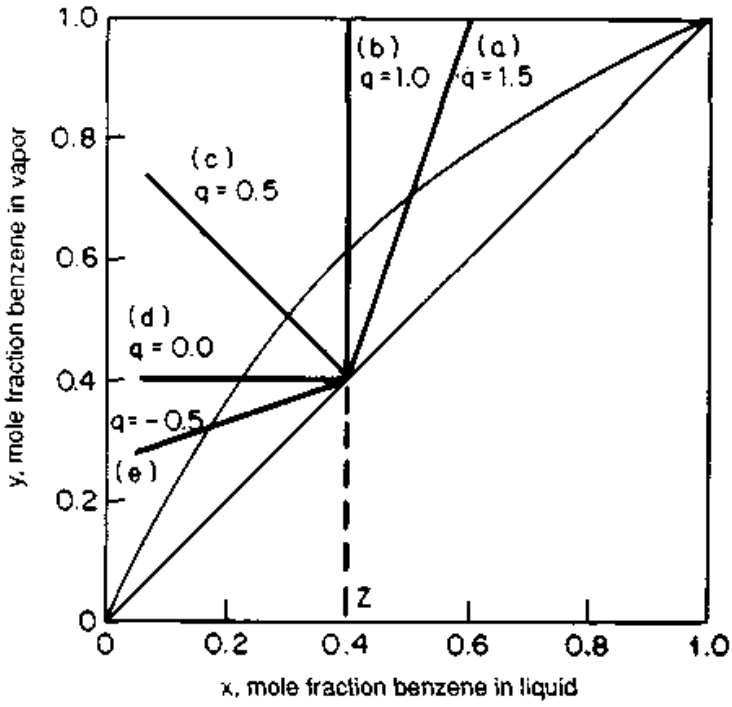

(a)

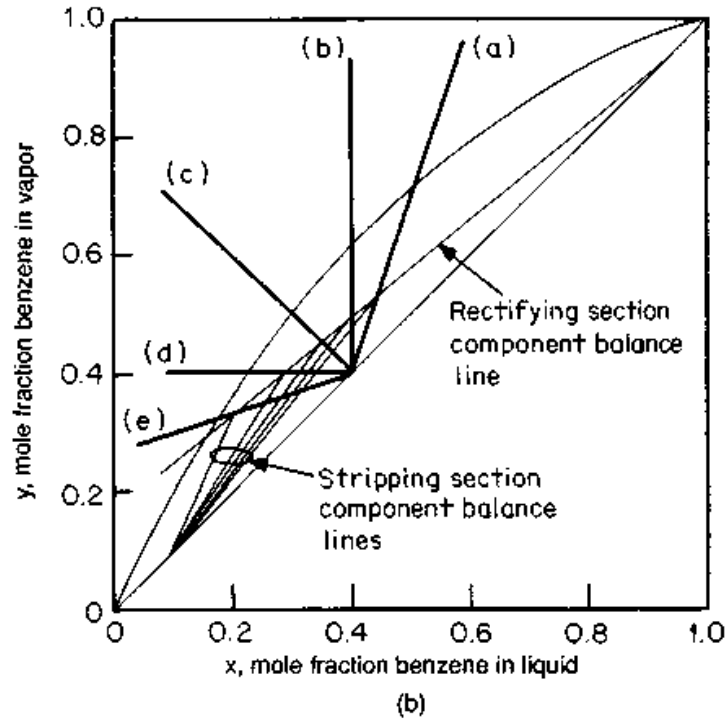

(b)

Figure 2.8 The q-line and its implications. (*a*) The q-line as a function of the thermal state of the feed; (*b*) effect of q on stripping section component balance line at constant reflux ratio.

TABLE 2.2 Relationship between q, q-Line, and Column Flows

Feed condition	q	How to calculate q	Slope of q line	Relationship between L and L'	Relationship between V and V'	Line in Fig. 2.8a
Subcooled liquid	> 1	$q = 1 + \dfrac{C_{pL}(T_{BP} - T_f)}{H_V}$	$+ve$	$L' > L$	$V' > V$	(a)
Saturated liquid	1	$q = 1$	∞	$L' > L$	$V' = V$	(b)
Vapor-liquid mixture	$0 < q < 1$	q = molar liquid fraction of feed	$-ve$	$L' > L$	$V' < V$	(c)
Saturated vapor	0	$q = 0$	0	$L' = L$	$V' < V$	(d)
Superheated vapor	< 0	$q = \dfrac{-C_{pV}(T_f - T_{DP})}{H_V}$	$+ve$	$L' < L$	$V' < V$	(e)

TABLE 2.3 McCabe-Thiele Diagram Lines

Line	What the line describes	Slope	Point through which line passes
1. Rectifying section component balance (operating) line	Rectifying section component balances	L/V	(x_D,x_D) if total condenser (y_D,y_D) if partial condenser
2. Stripping section component balance (operating) line	Stripping section component balances	L'/V'	(x_B,x_B)
3. q-line	Locus of points of intersection of rectifying and stripping component balance lines	$\dfrac{q}{q-1}$	(z,z)
4. 45° diagonal line	1. Locus of points where $x = y$ 2. At total reflux it represents the component balance lines	1.0	(0,0) and (1.0,1.0)

4. Solving the equations simultaneously, $D = 71$, $B = 129$.

STEP 2 Set vapor and liquid flow in the column.

1. Find L from the definition of reflux [Eq. (2.16)]

$$L = 3 \times D = 213 \text{ lb-mole/h}$$

2. Find V from Eq. (2.11).

$$V = L + D = 213 + 71 = 284 \text{ lb-mole/h}$$

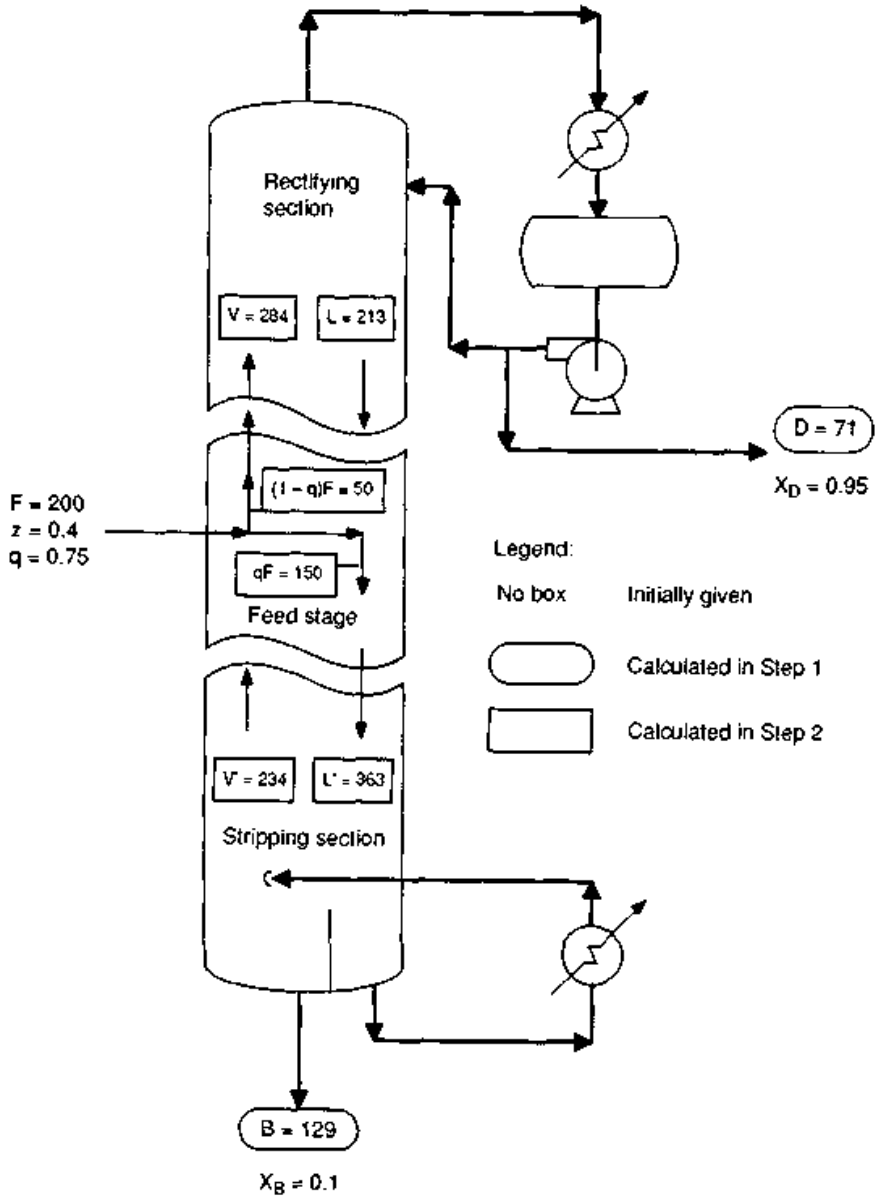

Figure 2.9 Solution to Example 2.1. (*a*) Steps 1, 2; (*b*) step 3; (*c*) step 4.

3. Since 25 percent of the feed is vaporized, $q = 0.75$. Find L' from the definition of q, Eq. (2.28)

$$L' = L + qF = 213 + 0.75 \times 200 = 363 \text{ lb-mole/h}$$

4. Find V' from Eq. (2.12).

$$V' = L' - B = 363 - 129 = 234 \text{ lb-mole/h}$$

The material balances and flows are shown in Fig. 2.9*a*.

STEP 3 Establish component balance and q-lines. Use the equations in Table 2.3.

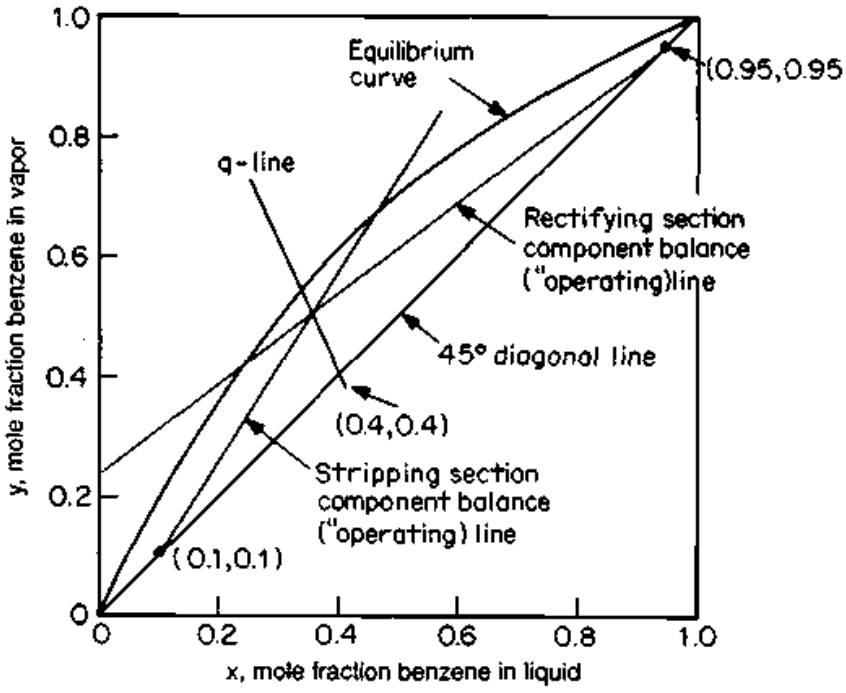

(b)

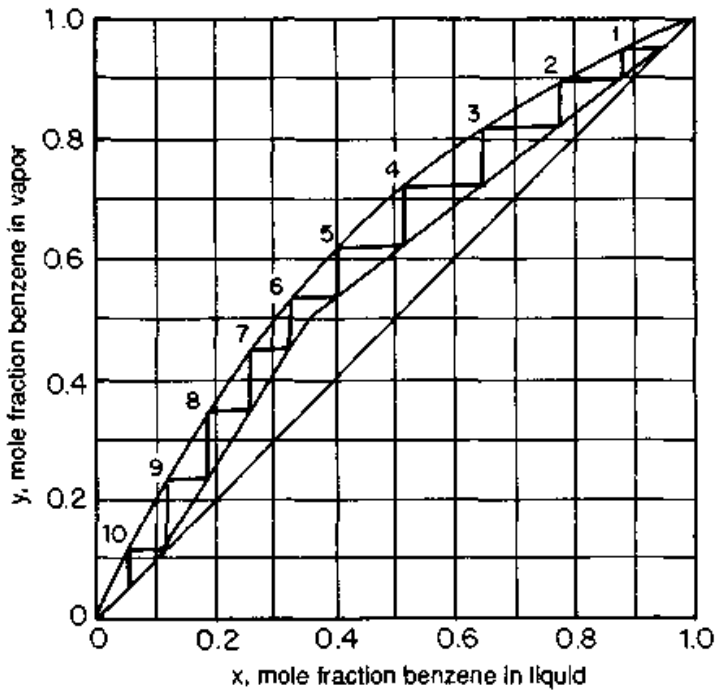

(c)

Figure 2.9 (*Continued*)

Line	Slope	Point through which it passes
1. Rectifying section component balance (operating) line	$\frac{L}{V} = \frac{213}{284} = 0.75$	(0.95, 0.95)
2. Stripping section component balance (operating) line	$\frac{L'}{V'} = \frac{363}{234} = 1.55$	(0.10, 0.10)
3. q-line	$\frac{q}{q-1} = \frac{0.75}{-0.25} = -3.0$	(0.40, 0.40)

These lines are shown in Fig. 2.9*b*. Note that the *q*-line passes through the intersection of the two component balance lines.

STEP 4 Step off the stages. Start off at the point (x_D,x_D). Move horizontally to the left until you meet the equilibrium curve. The point of intersection with the equilibrium curve represents the vapor and liquid compositions of stage 1 (x_1, y_1). Then move vertically down to the point (x_1,y_2), which is located on the component balance line [Eq. (2.9)]. Move horizontally to the left until you meet the equilibrium curve at point (x_2,y_2). Continue stepping off stages until reaching the bottom composition x_B. The number of times the equilibrium curve is met is the number of stages. Note that the optimum feed point is where the component balance lines intersect. The number of stages above the intersection point is the number of rectifying stages. The number of stages below is the number of stripping stages.

This procedure is illustrated in Fig. 2.9*c*. For this example, just over 9 stages are required; 10 stages will ensure that the separation is achieved. The best feed point is stage 6, giving 5 rectifying and 5 stripping stages.

If the condenser were a partial condenser, the condenser would have been stage 1. In this case, the number of stages in the column would have been reduced from 10 to 9.

2.2.5 Optimum feed stage and pinching

In Sec. 2.2.4, it was assumed that the feed enters the column at the optimum feed stage, which is located at the intersection of the component balance lines. At that point, the construction was switched from the rectifying section component balance line to the stripping section component balance line.

This switch could have been made earlier or later, depending on the location of the *actual* feed point. Figure 2.10*a* shows a switch taking place earlier, because the column feed point is located between stages 4 and 5 (compared to stage 5 and 6 in Sec. 2.2.4). Figure 2.10*b* shows a switch taking place later, because the column feed point is located between stage 8 and 9. In either case, more stages are required (11 and 12 stages in Fig. 2.10*a* and *b*, respectively, compared to 10 stages in Fig. 2.9*c*).

The reason for the greater number of stages is that steps become smaller as the component balance line moves closer to the equilibrium curve, and therefore more steps are required. The optimum feed point is therefore achieved when the "active" component balance line is as far as possible from the equilibrium curve.

Pinching. As the component balance line approaches the equilibrium curve, the steps become smaller. An infinite number of stages is required to reach the intersection of the component balance line and the equilibrium curve. This intersection is termed the *pinch point*. The bottom pinch point is (0.22, 0.4) in Fig. 2.10*b*, and the top pinch point

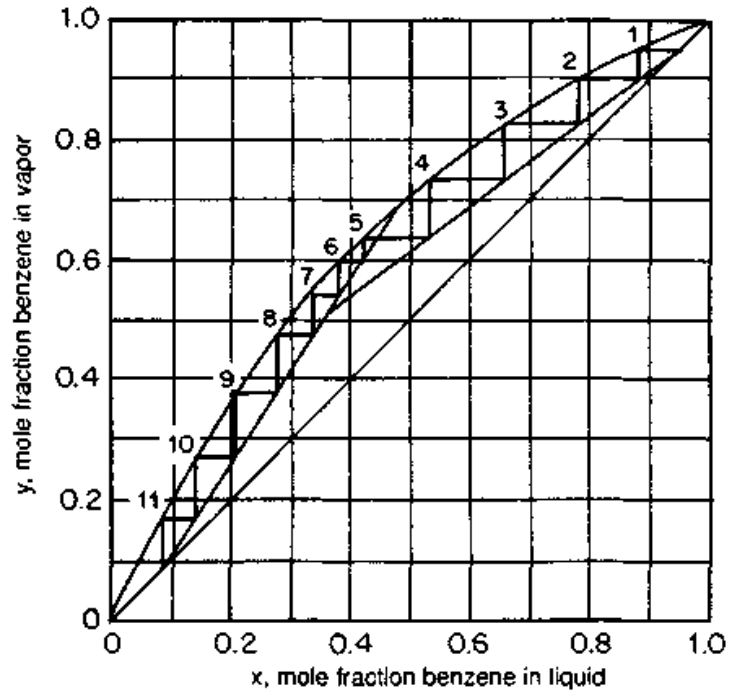

(a)

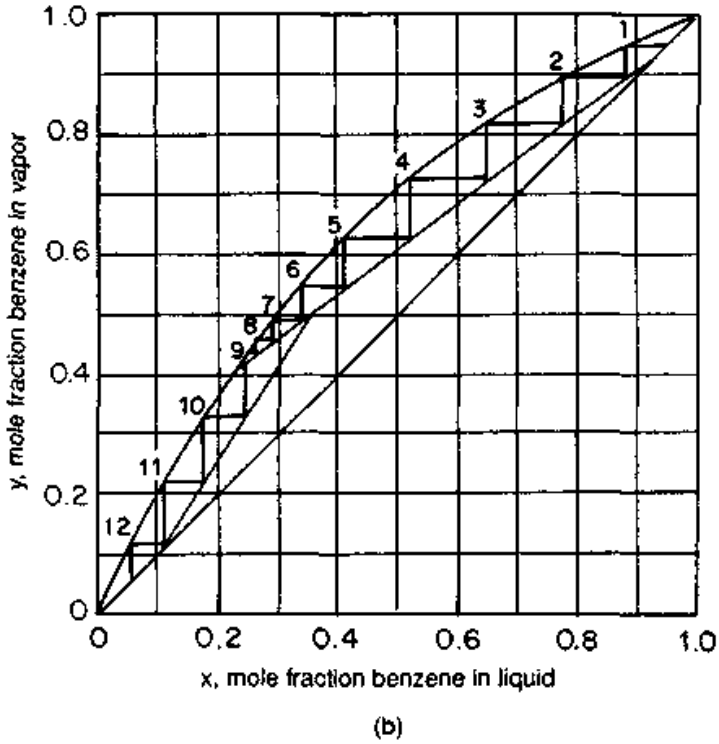

(b)

Figure 2.10 Nonoptimum feed points. (*a*) Feed point located too high; (*b*) feed point located too low; (*c*) increasing reflux and reboil in order to accommodate for a feed point located too high.

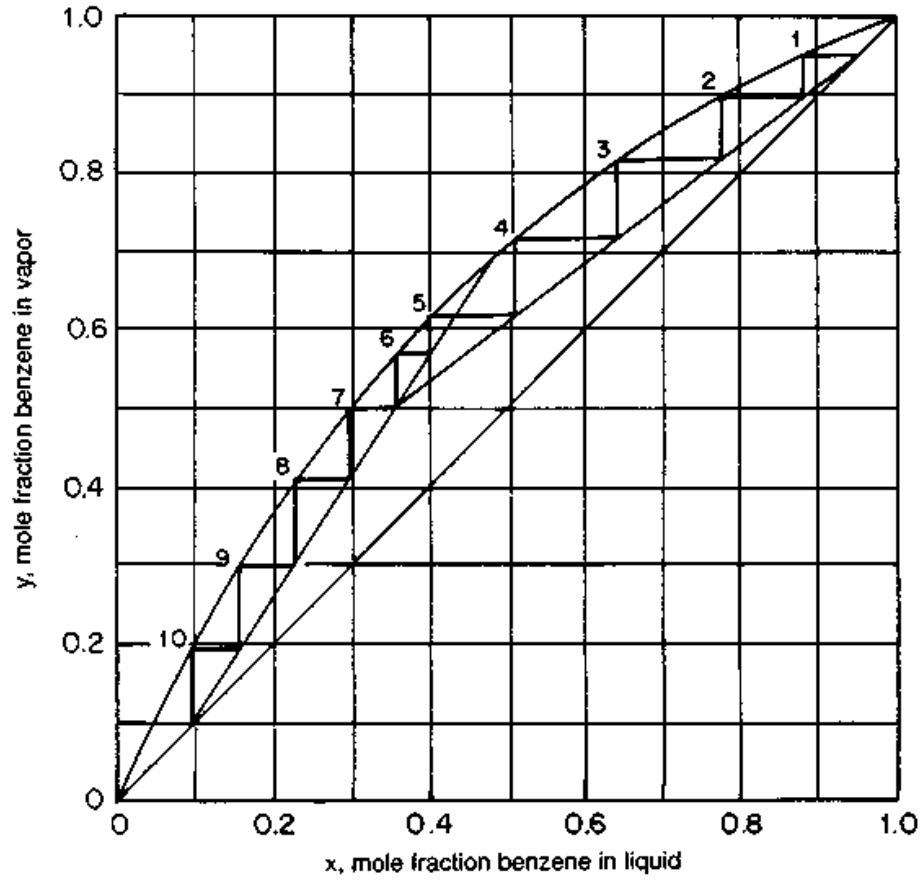

(c)

Figure 2.10 (*Continued*)

is (0.47, 0.69) in Fig. 2.10*a*. These points change when the component balance lines do.

A column is said to be "pinching" when the component balance line is too close to the equilibrium curve. Physically, this represents a situation where several stages are doing very little separation and are practically wasted.

Pinching in a column design does not only waste stages, thereby leading to an oversized column, but is also risky. Even minor inaccuracies in relative volatilities and enthalpies may bring the component balance line and the equilibrium curve closer, or even to cross, earlier than anticipated. This exponentially escalates the stage requirement. If the additional stages required are unavailable, the column will not accomplish the desired separation. It is therefore imperative to design a column away from the pinched region.

In an existing column, mechanical reasons often make it difficult to change feed location. A pinch can then be remedied by increasing reflux and reboil. This draws the component balance line and the equilibrium curve further apart, enlarging the steps, and thereby per-

mitting the required separation to be achieved with the existing feed location. Example 2.2 illustrates this. Increasing reflux and reboil in order to overcome a pinch, however, is achieved at the penalty of greater energy consumption, higher operating costs, and greater vapor and liquid traffic through the column. When the column or its heat exchangers are close to a capacity limit, the greater vapor and liquid traffic may reduce column feed-handling capacity.

In the field, a symptom of pinching is a very small temperature difference across many trays, particularly near the feed. This symptom can also suggest flooding, dry, or otherwise inefficient trays. A distinguishing feature of pinching is that as reboil and reflux ratios are increased, the temperature difference becomes larger and operation returns to normal. Note that "dry trays" is a specific case of pinching. When $L = 0$, the slope of the component balance line is 0, and it will become horizontal until it meets the equilibrium curve. A field test to check whether a column is pinching is described elsewhere (12).

Example 2.2 A 10-stage column, with feed entering between stage 4 and 5, was used to separate a benzene-toluene mixture similar to that described in Example 2.1. The composition of feedstock has changed, and the new feedstock contains 40% benzene. Relocating the feed nozzle requires column shutdown, which is costly. Is it necessary? (Product composition specifications are as given in Example 2.1.)

solution A McCabe-Thiele diagram is shown in Fig. 2.10*a*. With 10 stages, the overhead product can be kept on-spec, but the bottoms product will contain 17% benzene, compared to the 10% specification. If this can be tolerated, a shutdown to change column feed nozzle is unnecessary.

If 17% benzene is unacceptable in the bottom product, reflux and reboil can be raised to achieve the required separation in 10 stages. The slope of the rectifying section component balance line is increased, and that of the stripping section component balance line is lowered. This is a trial-and-error calculation, which ends when 10 theoretical stages are accommodated between the component balance line and the equilibrium curve, the top and bottom products are at their desired specifications, and the feed enters between stages 4 and 5. The slopes of the component balance lines will determine the new required reflux and boilup rate. The final result is shown in Fig. 2.10*c*. From this diagram,

$$\frac{L}{V} = 0.758 \text{ (slope of rectifying section component balance line)}$$

$$\frac{L'}{V'} = 1.54 \text{ (slope of stripping section component balance line)}$$

To calculate the actual vapor and liquid rates, proceed as follows:

1. From Eq. (2.11), and since $D = 71$ lb-mole/h (Example 2.1) and $L = 0.758V$ (above)

$$V = 0.758V + 71$$

$$V = 293 \; lb\text{-}mole/h$$

$$L = 0.758 \times 293 = 222 \; lb\text{-}mole/h$$

2. Find L' from Eq. (2.28), and since $q = 0.75$ and $F = 200$ lb-mole/h (Example 2.1)

$$L' = qF + L = 0.75 \times 200 + 222 = 372 \text{ lb-mole/h}$$

Find V' from Eq. (2.12), and since $B = 129$ lb-mole/h (Example 2.1)

$$V' = L' - B = 372 - 129 = 243 \; lb\text{-}mole/h$$

3. Check that L'/V' is the same as that determined from the slope of the component balance line.

$$\frac{L'}{V'} = \frac{372}{243} = 1.53$$

Comparison of Examples 2.1 and 2.2. Table 2.4 gives a measure of the effect of nonoptimum feed point on the column in this example. Table 2.4 shows that V' and V, and therefore reboiler and condenser duties, increase by about 3 to 4 percent in Example 2.2. This roughly corresponds to a 3 to 4 percent increase in energy consumption and operating costs. If the column or its heat exchangers are at a maximum capacity limit, the column feed rate will need to be reduced by 3 to 4 percent. If these consequences can be tolerated, a shutdown to change the column feed nozzle will be unnecessary. Note that in this example, the effect of nonoptimum feed was quite mild. In other cases, it may be far more detrimental.

TABLE 2.4 Comparison of Examples 2.1 and 2.2

Variable	This variable gives a measure of	Example 2.1, lb-mole/h	Example 2.2, lb-mole/h	Effect of nonoptimum feed in Example 2.2
L	Rectifying section liquid load	213	222	4% greater
V	1. Rectifying section vapor load 2. Condenser duty	284	293	3% greater
L'	Stripping section liquid load	363	372	2.5% greater
V'	1. Stripping section vapor load 2. Reboiler duty	234	243	4% greater

2.2.6 Minimum reflux ratio

Using Eqs. (2.11) and (2.16), Eq. (2.9) for the rectifying section component balance line can be expressed in terms of the reflux ratio

$$y_{n+1} = \frac{R}{R+1}x_n + \frac{x_D}{R+1} \tag{2.29}$$

As the reflux ratio decreases, so does the slope of the upper component balance line. The effect of reflux ratio on the component balance lines is illustrated in Fig. 2.11, using the benzene-toluene system in Example 2.1.

Any practical separation requires that the component balance lines intersect below the equilibrium curve, as for a reflux ratio of 3.0 in Fig. 2.11*a*. The McCabe-Thiele construction corresponding to this ratio is shown in Fig. 2.9*c*. If insufficient reflux is provided, the component balance lines intersect above the equilibrium curve, as for a reflux ratio of 1.0 in Fig. 2.11*a*. The McCabe-Thiele construction (Fig. 2.11*b*) for these conditions shows that even with an infinite number of stages, the separation cannot be achieved.

The separation is theoretically possible if the component balance lines intersect at a point just below the equilibrium curve. The corresponding reflux ratio is termed *minimum reflux*. The separation at minimum reflux requires an infinite number of stages. In Fig. 2.11, the minimum reflux ratio is 2.0. The McCabe-Thiele construction for this ratio is shown in Fig. 2.11*c*.

At minimum reflux, the pinch occurs at the intersection of the component balance line and the q-line when the equilibrium curve has no inflection points (Fig. 2.11*c*). This would be expected because the component balance lines intersect on the q-line. When the equilibrium curve has a point of inflection (Fig. 2.12), the pinch between the equilibrium curve and the component balance line may occur at the point of tangency instead of the intersection of the q-line and the component balance line. This condition is termed *tangent pinch*.

To determine minimum reflux, construct the q-line and identify its point of intersection with the equilibrium curve. Then draw a line from the product composition point on the 45° diagonal line to this intersection point. From Eq. (2.29), the slope of the line is $R_{\min}/(R_{\min}+1)$, and the intercept of this line on the y axis is $x_D/(R_{\min}+1)$. Minimum reflux can be determined from either of these. If minimum reflux occurs at a tangent pinch, the minimum reflux is independent of the q-line and the feed composition. It can then be determined from the equilibrium curve alone (13).

Neither minimum reflux nor a tangent pinch is an operable condition. Either will require an infinite number of stages in the column, and this is physically impossible. Nevertheless, operation can some-

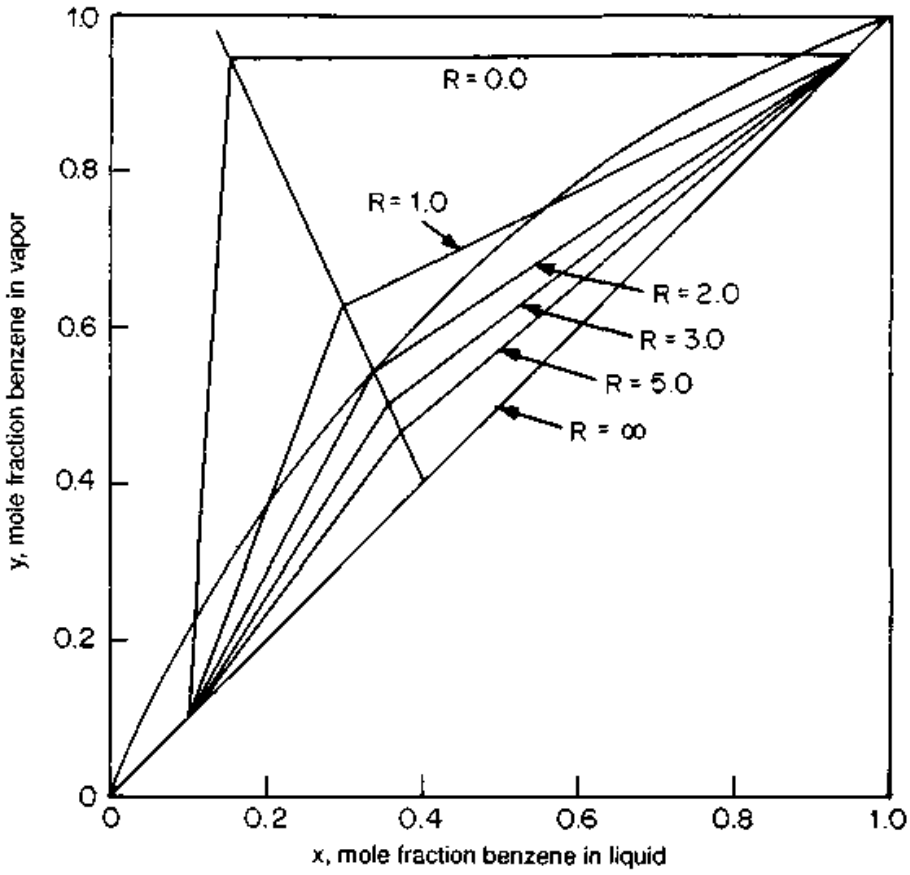

(a)

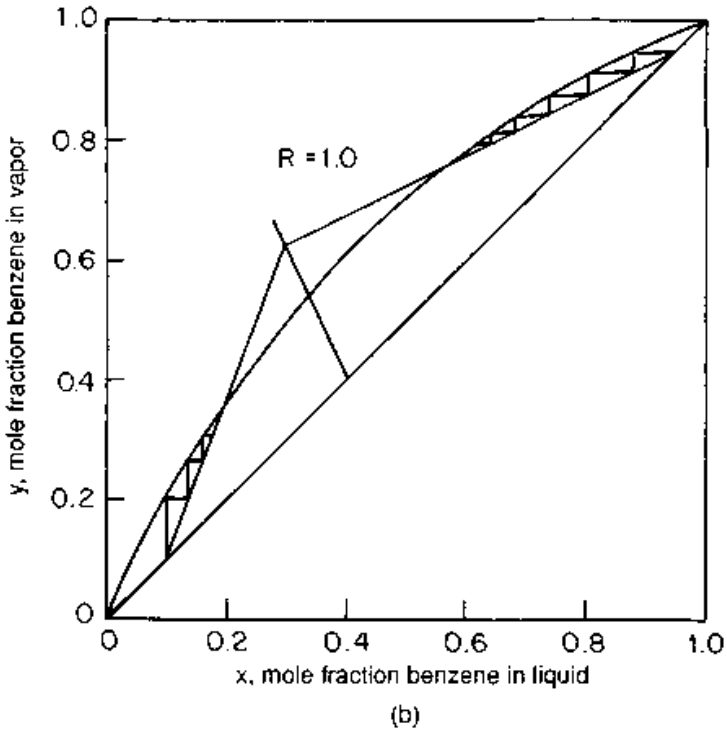

(b)

Figure 2.11 Effect of reflux ratio on component balance lines. (*a*) Overall; (*b*) $R < R_{min}$, impossible operation; (*c*) $R = R_{min}$, minimum reflux; (*d*) $R = \infty$, total reflux.

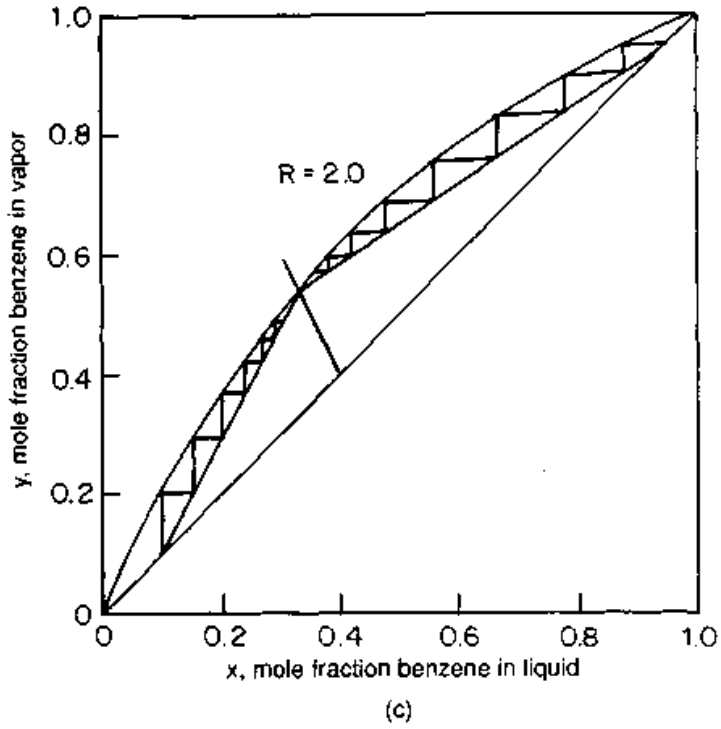

(c)

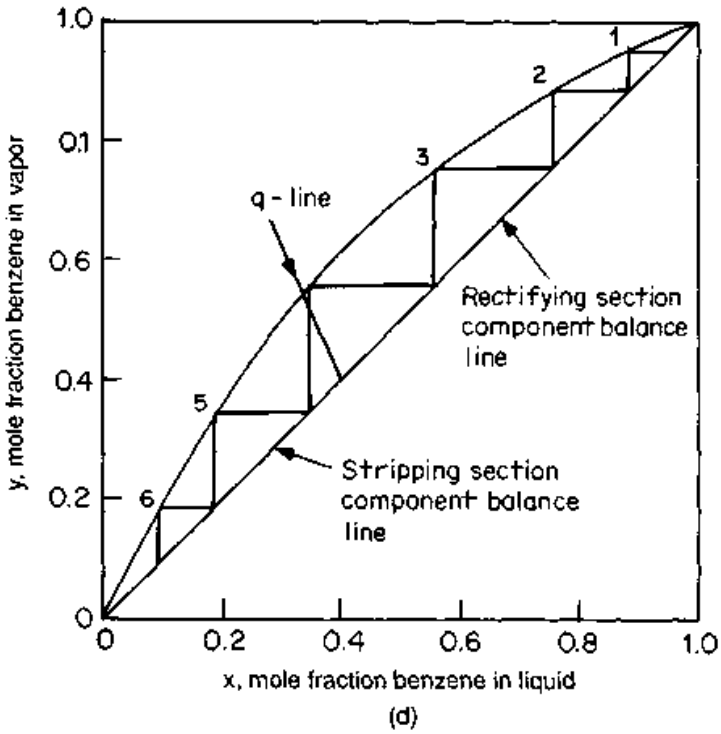

(d)

Figure 2.11 (*Continued*)

times approach minimum reflux when a column contains a large excess of stages.

2.2.7 Minimum stripping

Using Eqs. (2.12) and (2.17), the stripping section component balance line [Eq. (2.10)] can be expressed in terms of the stripping ratio

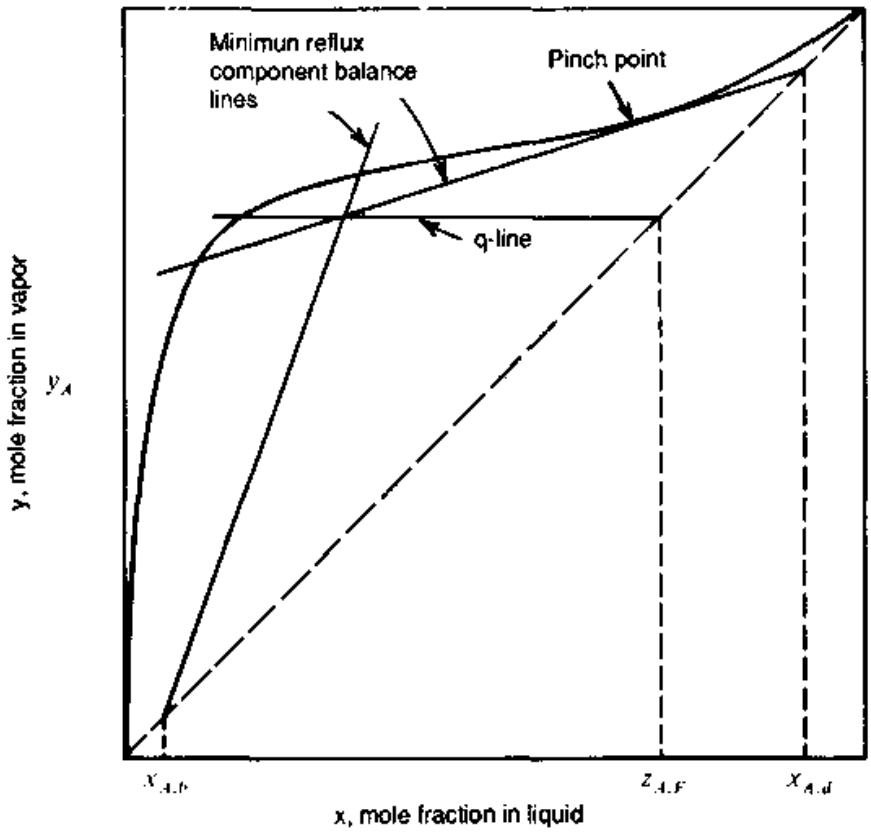

Figure 2.12 Tangent pinch. (From C. J. King, *Separation Processes*, 2d ed., Copyright © by McGraw-Hill, Inc. Reprinted by permission.)

$$y_m = \frac{1 + S}{S} x_{m-1} - \frac{x_B}{S} \tag{2.30}$$

Minimum stripping is analogous to minimum reflux. The discussion in Sec. 2.2.6 is also valid to minimum stripping. To determine minimum stripping, draw a line from the bottom composition point on the 45° diagonal line to the intersection of the q-line with the equilibrium curve. From Eq. (2.30), the slope of this line is $(1 + S_{\min})/S_{\min}$ and its intercept on the y axis is $-x_B/S_{\min}$.

2.2.8 Total reflux and minimum stages

As reflux ratio increases, so does the slope of the upper component balance line. The effect of increasing reflux ratio on the component balance lines is illustrated in Fig. 2.11, using the benzene-toluene system of Example 2.1. At the limit, where reflux ratio approaches infinity, the rectifying section component balance line [Eq. (2.29)] reduces to

$$y_{n+1} = x_n \tag{2.31}$$

and the component balance line becomes the 45° diagonal line. The reflux ratio [Eq. (2.16)] can approach infinity only if the product rate

D approaches zero. Similarly, when the stripping ratio approaches infinity, the stripping section component balance line [Eq. (2.30)] reduces to

$$y_m = x_{m-1} \tag{2.32}$$

and the component balance line becomes the 45° diagonal. The stripping ratio [Eq. (2.17)] can approach infinity only when the bottoms rate B approaches zero.

The condition where the reflux and stripping ratios approach infinity is termed *total reflux*. No feed enters the column and no product leaves. Both component balance lines coincide with the 45° diagonal line and are therefore furthest away from the equilibrium curve. Total reflux sets the minimum number of stages required for the separation. For Example 2.1, Fig. 3.11*d* shows that the minimum number of stages required for the separation is 6.

2.2.9 Allowance for stage efficiencies

Distillation stage calculations are usually performed with ideal stages. The number of ideal stages required for the separation is divided by the overall column efficiency (Sec. 7.1.1) to obtain the required number of trays. In packed towers, the number of stages in the column is multiplied by the HETP (Height Equivalent of a Theoretical Plate, see Sec. 9.1.2) to obtain the packed height.

For tray columns, an alternative approach uses Murphree tray efficiencies (Sec. 7.1.1). This efficiency is easy to incorporate into an x-y diagram, and the diagram construction can be performed using actual rather than ideal stages. The Murphree tray efficiency is defined as

$$E_{MV} = \frac{y_n - y_{n-1}}{y^*_n - y_{n-1}} \tag{2.33}$$

On an x-y diagram, the denominator equals the spacing between the equilibrium curve and the component balance line (Fig. 2.13). y_n is given by

$$y_n = E_{MV}\left[\begin{array}{l}\text{spacing between equilibrium curve} \\ \text{and component balance line}\end{array}\right] + y_{n-1} \tag{2.34}$$

2.2.10 Extension to complex columns

Extension of the x-y diagram to columns containing a second feed or a side product has been discussed by numerous authors (7, 8, 14–17). Yaws et al. (18) extended the McCabe-Thiele diagram to three-feed columns. Kister (19) extended the McCabe-Thiele diagram to columns

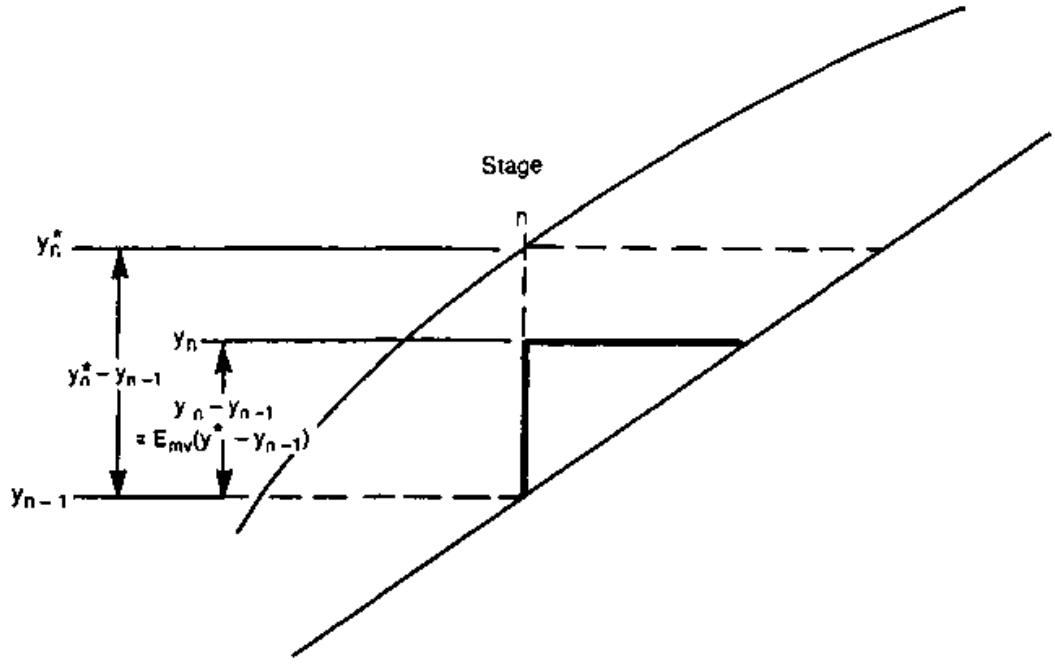

(a)

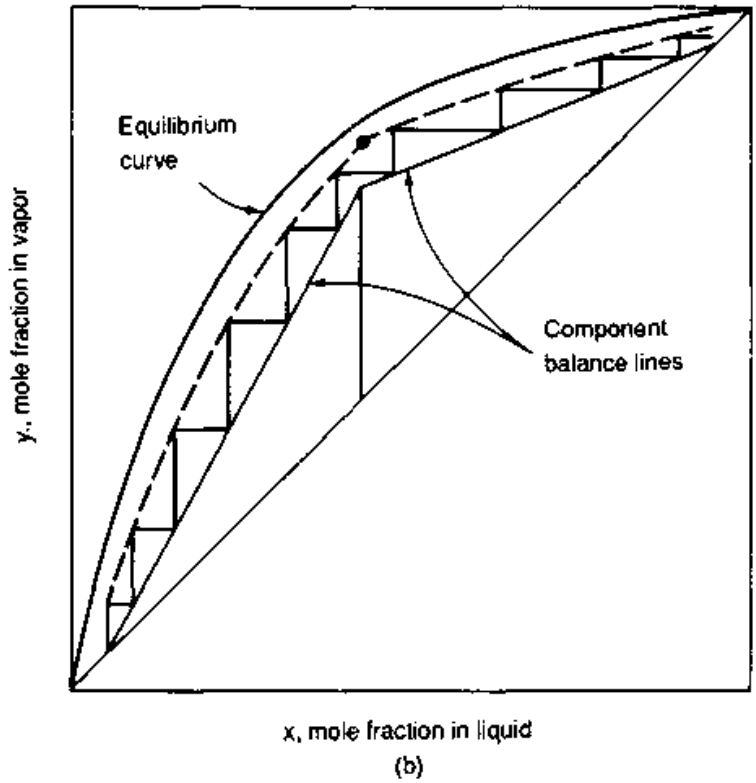

(b)

Figure 2.13 Use of Murphree tray efficiency in *x-y* diagram construction. (*a*) An enlarged section of the diagram; (*b*) an *x-y* diagram incorporating Murphree efficiencies. (Part *b* from C. J. King, *Separation Processes*, 2d ed., Copyright © by McGraw-Hill, Inc. Reprinted by permission.)

having multiple feeds, multiple side products, multiple points of heat removal or addition, and any combination of these.

A complex fractionator is divided into $N + 1$ sections (Fig. 2.14). The partition between each two adjacent sections occurs either at a feed point, or a sidedraw point, or a heat removal point, or a heat addition point (Fig. 2.14). Table 2.5 shows the equations applying to each section of a complex fractionator (19).

Two other useful relationships derived from applying Eq. (2.35) to L_J and L_{J-1} and Eq. (2.36) to V_J and V_{J-1} are (19)

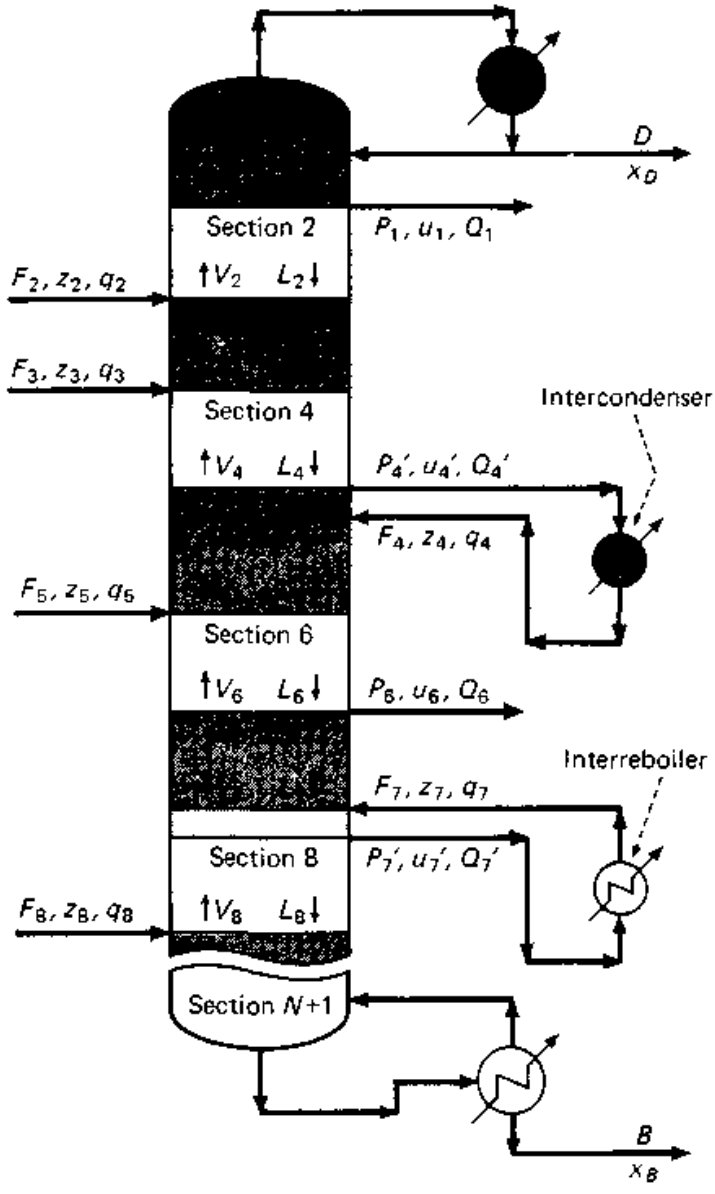

(a)

Figure 2.14 Dividing a complex fractionator into $N + 1$ sections at points of feed entry, sidedraw removal, and heat removal and addition. (From Henry Z. Kister, *Chemical Engineering*, January 21, 1985, pp. 97–104. Reprinted courtesy of *Chemical Engineering*.)

TABLE 2.5 Equations Applying to Each Section "J" of a Complex Fractionator

The following equations have been derived for a complex fractionator. For each Section J, these equations apply:

Liquid flowrate:

$$L_J = RD + \sum_{k=1}^{J-1} q_k F_k \tag{2.35}$$

Vapor flowrate:

$$V_J = (R + 1)D + \sum_{k=1}^{J-1} (q_k - 1)F_k \tag{2.36}$$

Component balance line:

$$y_{n+1} = (L_J/V_J)x_n + \left(Dx_D - \sum_{k=1}^{J-1} F_k z_k\right)/V_J \tag{2.37}$$

Point of intersection of the component balance line with the 45 deg diagonal line:

$$x_{int} = \left[\left(\sum_{k-1}^{J-1} F_k z_k\right) - Dx_D\right] / \left[\left(\sum_{k=1}^{J-1} F_k\right) - D\right] \tag{2.38}$$

The q-line:

$$y = \left(\frac{q_J}{q_J - 1}\right)x - \frac{z_J}{q_J - 1} \tag{2.39}$$

Intercept of component balance line on the y-axis

$$y(o) = \frac{x_D - \sum_{k=1}^{J-1} (F_k/D)z_k}{(R + 1) + \sum_{k=1}^{J-1} (F_k/D)(q_k - 1)} \tag{2.40}$$

The foregoing equations can be directly applied to a column having several feeds and no side-products. They

$$L_J = L_{J-1} + q_{J-1}F_{J-1} \tag{2.44}$$

and

$$V_J = V_{J-1} + (q_{J-1} - 1)F_{J-1} \tag{2.45}$$

A simple column can be regarded as a two-section complex column. Section 1 is the rectifying section, while section 2 is the stripping section. Table 2.6 draws an analogy between the simple and the complex

TABLE 2.5 Equations Applying to Each Section "J" of a Complex Fractionator (*Continued*)

also apply if side-products exist and the following values are used for point k of each side-product:

$$\left.\begin{aligned} F_k &= -P_k \\ z_k &= u_k \\ q_k &= Q_k \end{aligned}\right\} \quad (2.41)$$

If heat is removed (e.g., via an intercondenser) or added (e.g., via an interreboiler), the foregoing equations still apply when each source of heat removal or addition is treated as two simultaneous partitions, one from which a stream leaves the column and one to which a stream of the same composition reenters. The two partitions are denoted k' and k, respectively. For heat removal, the stream leaving the column is saturated vapor, and the stream reentering is condensed liquid; the reverse applies for heat addition. The following equations are used:

$$\left.\begin{aligned} F_k &= \Delta H/H_V \\ q_k &= 1 \text{ for heat removal} \\ q_k &= 0 \text{ for heat addition} \\ z_k &= \text{composition of stream leaving (or reentering) the column} \end{aligned}\right\} \quad (2.42)$$

$$\left.\begin{aligned} P_{k'} &= -F_k \\ Q_{k'} &= 0 \text{ for heat removal} \\ Q_{k'} &= 1 \text{ for heat addition} \\ u_{k'} &= z_k \end{aligned}\right\} \quad (2.43)$$

Note that there is no net inflow or outflow of material at the point of heat removal or addition; therefore, the "q-line," Eq.(2.39), cannot be used to determine minimum reflux for the section directly above these points.

SOURCE: From Henry Z. Kister, *Chemical Engineering*, January 21, 1985, pp. 97–104. Reprinted courtesy of *Chemical Engineering*.

column equations. It is apparent that the complex column equations are merely a series expansion of the simple column equations. Detailed derivation is elsewhere (19).

Minimum reflux. The minimum reflux in a simple fractionator is calculated by drawing a straight line between the product composition on

TABLE 2.6 Analogy Between Simple Column Equations and Complex Column Equations

Equation for	Simple column		Complex column
	Rectifying section	Stripping section	
L	RD	$RD + qF$	$RD + q_1F_1 + q_2F_2 + \cdots$
V	$(R + 1)D$	$(R + 1)D + (q - 1)F$	$(R + 1)D + (q_1 - 1)F_1 + (q_2 - 1)F_2 + \cdots$
y	$\frac{L}{V}x + \frac{D}{V}x_D$	$\frac{L'}{V'}x + \frac{Dx_D - Fz}{V'}$	$\frac{L_J}{V_J}x + \frac{Dx_D - F_1z_1 - F_2z_2 - \cdots}{V_J}$
x_{int}	x_D	$x_B = \frac{Fz - Dx_D}{F - D}$	$\frac{F_1z_1 + F_2z_2 + \cdots - Dx_D}{F_1 + F_2 + \cdots - D}$

the 45° diagonal and the intersection of the feed q-line with the equilibrium curve. The line drawn is the minimum reflux component balance line; the minimum reflux ratio can be determined from the intercept of this line on the y axis (Sec. 2.2.6).

The procedure for finding minimum reflux in each section of a complex fractionator is similar. First, the point of intersection of the component balance line with the 45° diagonal is found by using Eq. (2.38). Second, the point of intersection of the q-line for the feed or side product with the equilibrium curve is graphically determined. A straight line is then drawn between the two points. This line is the minimum reflux component balance line. The minimum reflux is found from the intercept of this line on the y axis, using Eq. (2.40).

In case of heat removal or addition, there is no q-line. In such a case, the second point that is used to construct the minimum-reflux component balance line is the point on the equilibrium curve representing the compositions of the liquid and vapor stream leaving the heat-addition or heat-removal stage.

Design procedure. The minimum refluxes computed for each section are compared with each other. The highest value is the minimum reflux for the column. From Eq. (2.35) the corresponding minimum liquid flow in the section is calculated. This flow can be multiplied by a certain factor, commonly between 1.05 and 1.3 to give the optimum flow. Guidelines for selecting factors are given in Sec. 3.1.6. The liquid flow can now be resubstituted into Eq. (2.35) and the actual reflux ratio calculated.

The intercept of each component balance line on the y axis can now be calculated from Eq. (2.40), using the actual reflux ratio. Each com-

ponent balance line is drawn by connecting this intercept with the point of intersection of the component balance line with the 45° diagonal line, already determined during the minimum reflux calculation.

This procedure can be simplified if there are no points of heat addition or removal, and q-lines exist between all adjacent sections. In this case, the only intercept on the y axis that is actually required is that of the first section. Once the component balance line for this section is drawn, its points of intersection with the first q-line are used, instead of the intercept on the y axis, to construct the second component balance line, etc.

After the component balance lines have been determined, stages can be stepped off in the usual manner.

Example 2.3 (from H. Z. Kister, *Chemical Engineering*, January 21, 1985, pp. 97–104. Reproduced courtesy of *Chemical Engineering*) illustrates the extension of the x-y diagram to complex columns:

Example 2.3 Benzene is to be separated from toluene in a distillation column. Three feed streams are available, having the following characteristics:

Stream number	1	2	3
Lb-mol/h	200	500	300
Benzene mole fraction	0.7	0.5	0.2
Fraction vaporized	0.25	0.0	0.5
q	0.75	1.0	0.5

A high-purity product containing 98-mol% benzene is required at the rate of 200 lb-mol/h. The balance of the benzene is to be recovered as a liquid at a purity of 90 mol%. Toluene is to be recovered at 95 mol% purity. A total overhead condenser is to be used.

Cooling water is at a premium in the plant, but a warmer process stream is available for intercondensing. This stream's available heat is 2.8 million Btu/h, and its temperature is such that it is best for condensing vapor containing 0.7 mole-fraction benzene.

The column is designed to operate at an L/V ratio 25 percent above the minimum.

How many stages are required, and where should the feed streams, the product stream and the intercondenser be located?

solution The column is shown in Fig. 2.15*a*.

1. An overall mass and component balance for determining P_1 (which is equal to $-F_1$) and B yields $P_1 = 252$ and $B = 548$.
2. Via Eq. (2.42) and assuming the latent heat is 14,000 Btu/lb-mol, F_3 (which is equal to $-P_3$) = $(2.8 \times 10^6)/14{,}000 = 200$ lb-mol/h.
3. Construct the equilibrium curve. Construct all q-lines by drawing a line of slope $q/(q - 1)$ through the composition point of each feed (Fig. 2.15*b*).

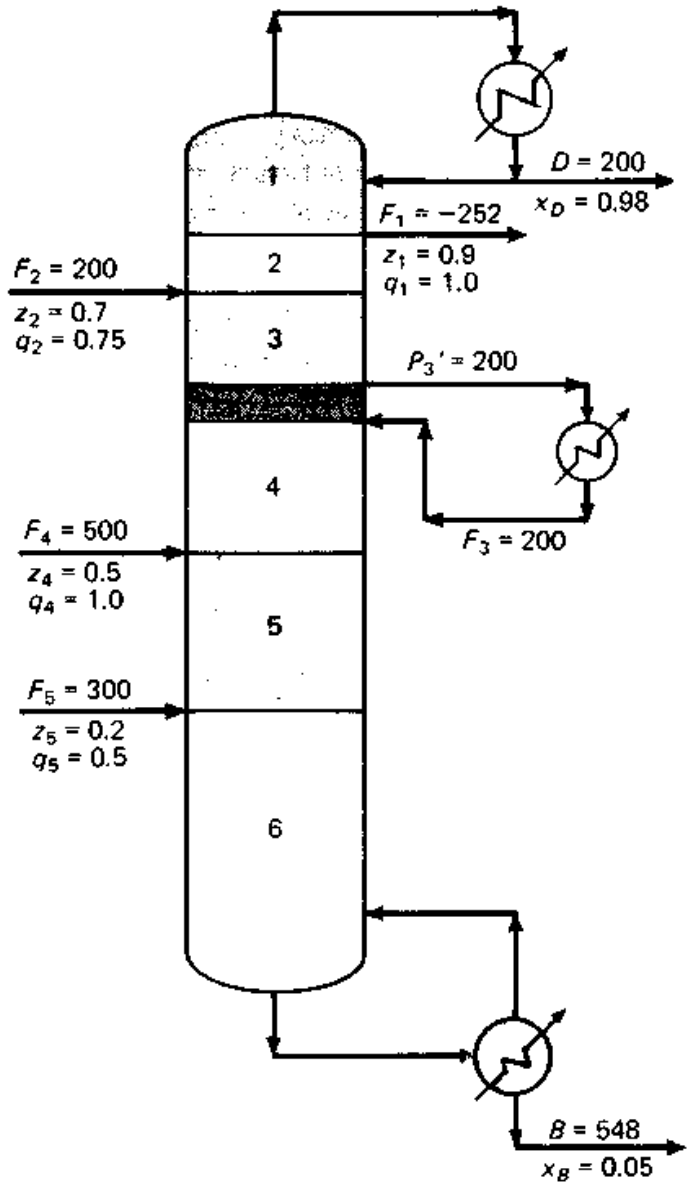

Figure 2.15 Example 2.3—Complex benzene-toluene separation. (*a*) The example column, divided into sections; (*b*) minimum reflux determination; (*c*) determining theoretical stages and feed and drawoff points. (From Henry Z. Kister, *Chemical Engineering*, January 21, 1985, pp. 97–104. Reprinted courtesy of *Chemical Engineering*.)

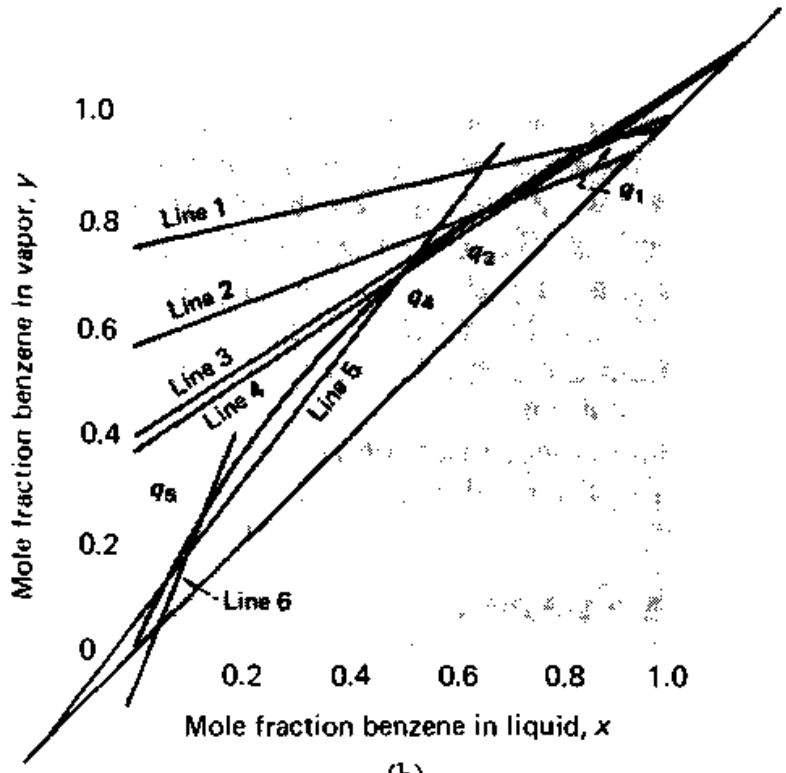

(b)

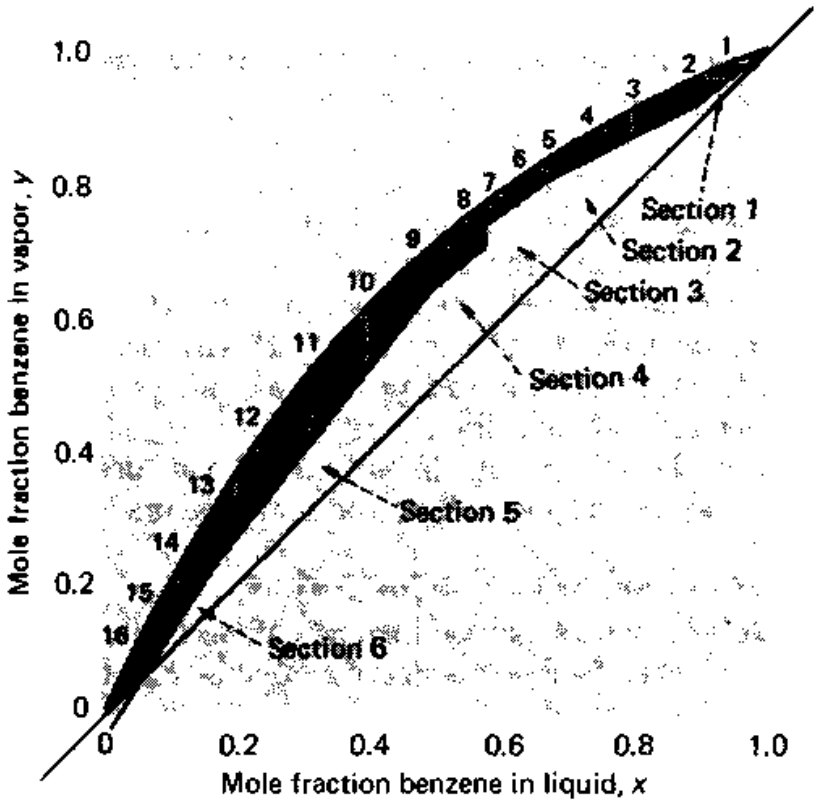

(c)

Figure 2.15 (*Continued*)

4. Via Eq. (2.38), determine x_{int} for each feed:

J	x_{int}
1	$x_D = 0.98$
2	$[(-252)(0.9) - (200)(0.98)]/(-252 - 200) = (-422.8)/(-452) = 0.935$
3,4	$[(200 \times 0.7) - 422.8]/(200 - 452) = (-282.8)/(-252) = 1.122$
5	$[(500 \times 0.5) - 282.8]/(500 - 252) = (-32.8)/248 = -0.132$
6	$[(300 \times 0.2 - 32.8)]/(300 + 248) = 0.05$

5. Connect the x_{int} points with the intersections of the q-line and equilibrium line. Via Eq. (2.40), determine minimum reflux for each stream (Fig. 2.15*b*).

$$J = 1: R = 0.98/0.755 - 1 = 0.30$$

$$J = 2: R = [0.98 - (0.9)(-252/200)]/0.58 - 0 - 1 = 2.114/0.58 - 1 = 2.64$$

$$J = 3: R = [2.114 - 0.7(200/200)]/0.395 - (0.75 - 1)200/200 - 1 = 1.414/0.395 + 0.25 - 1 = 2.83$$

$$J = 4: R = 1.414/0.365 + 0.25 - [(-1)(-200)/200] - 1 = 1.414/0.365 - 0.75 - 1 = 2.12$$

$$J = 5: R = [1.414 - 0.5(500/200)]/0.05 - 0.75 - 1 = 0.164/0.05 - 0.75 - 1 = 1.53$$

$$J = 6: R = [0.164 - 0.2(300/200)]/(-0.08) - 0.75 - (-0.5)300/200 - 1 = -0.136/(-0.08) - 0.75 + 0.75 - 1 = 0.7$$

A comparison of the minimum reflux ratio for each section shows the highest value to be 2.83 for section $J = 3$. Therefore, the minimum for the column is 2.83, or $2.83 \times 200 = 566$ lb-mol/h.

6. For operation at 25 percent above minimum L/D, find L for $J = 3$ from Eq. (2.35) at a minimum reflux: $L_3 = 2.83 \times 200 + (-252 \times 1) + (200 \times 0.75) = 464$ lb-mol/h.

   To operate at 25 percent above minimum L/D, the reflux rate required = $(464 \times 0.25) + (2.83 \times 200) = 682$ lb-mol/h. And the reflux ratio = 682/200 = 3.41.

7. Find the number of stages by means of the McCabe-Thiele diagram. The component balance lines are constructed using the x_{int} (Step 4) and the $y(o)$ coordinate [from Eq. (2.40)], using the operating reflux ratio, as shown by the following relationships:

$$J = 1: y(o) = \frac{0.98}{3.41 + 1} = 0.22$$

$$J = 2: y(o) = \frac{0.98 - 0.9(-252/200)}{3.41 + 1 + 0} = \frac{2.114}{4.41} = 0.48$$

$$J = 3: y(o) = \frac{2.114 - 0.7(200/200)}{3.41 + 1 + (-0.25)(200/200)}$$

$$= \frac{1.414}{4.16} = 0.34$$

$$J = 4: y(o) = \frac{1.414}{3.41 + 1 - 0.25 + (-1)(-200/200)}$$

$$= \frac{1.414}{5.16} = 0.27$$

$$J = 5: y(o) = \frac{1.414 - 0.5(500/200)}{3.41 + 1 + 0.75} = \frac{0.164}{5.16} = 0.03$$

$$J = 6: y(o) = \frac{0.164 - 0.2(300/200)}{3.41 + 1 + 0.75 + (-0.5)(300/200)}$$

$$= \frac{-0.136}{4.41} = -0.03$$

8. From the McCabe-Thiele diagram (Fig. 2.15c), 16 theoretical stages are required. The product drawoff is at stage 2. Feeds should enter stages 5, 9, and 13. The intercondenser should be located at stage 7.

2.3 Key Concepts of Multicomponent Distillation

2.3.1 Key and nonkey components

This topic is best illustrated using an example. The example used here is the depropanizer described by King (7), which has previously been analyzed by Jenny (20), Hengstebeck (21), and Edmister (22).

Example 2.4 A material balance for the column is shown in Table 2.7. The column operates at a pressure of 315 psia. The feed is 66 percent vapor at the column inlet. The relative volatilities of the components at 205°F (feed plate temperature) are shown in Table 2.8. The column is equipped with a partial condenser, and the reflux ratio is 1.5. It is required to determine the number of theoretical stages.

TABLE 2.7 Material Balance for Example 2.4

		Mole %			Moles per 100 moles of feed	
		Feed	Distillate	Bottoms	Distillate	Bottoms
Methane	(C_1)	26	43.5		26	
Ethane	(C_2)	9	15.0		9	
Propane	(C_3)	25	41.0	1.0	24.6	0.4
n-Butane	(C_4)	17	0.5	41.7	0.3	16.7
n-Pentane	(C_5)	11		27.4		11.0
n-Hexane	(C_6)	12		29.9		12.0
		100	100	100	59.9	40.1

TABLE 2.8 *K*-Values for Example 2.4 (at 205°F, Feed Plate Temperatures)

Component	K
Methane	15.0
Ethane	3.8
Propane	1.55
n-Butane	0.80
n-Pentane	0.38
n-Hexane	0.19

Key components are the two components in the feed mixture whose separation is specified. The more volatile of these components is the *light key*, and the less volatile is the *heavy key*. In Example 2.4, propane is the light key and *n*-butane the heavy key. Other components are termed *nonkeys*. The nonkeys which are more volatile than the keys are termed *light nonkeys* (methane and ethane in Example 2.4), and those less volatile are *heavy nonkeys* (pentane and hexane in Example 2.4).

The key components appear to a significant extent in both overhead and bottom products. Light nonkeys end up almost exclusively in the overhead product, and heavy nonkeys end up almost exclusively in the bottom product.

In many separations, components are present whose relative volatilities are intermediate between the light key and the heavy key. These components are termed *intermediate keys* or *distributed keys*. Intermediate keys are split between the top and bottom products.

2.3.2 Column composition and temperature profiles

King (7) discusses highlights from Edmister's (22) rigorous solution to Example 2.4. The separation requires 17 theoretical stages (including reboiler and condenser), with feed entering on stage 9 (reboiler being stage 0, condenser stage 16). Figure 2.16 shows the liquid and vapor composition profiles in the column. The following observations are made:

- There is a significant concentration of all components at the feed stage. The heavy nonkeys, C_5 and C_6, die out rapidly in both the liquid and vapor above the feed because of their low volatilities. Pentane persists longer than hexane because it is more volatile. A similar behavior is exhibited by the light nonkeys (methane and ethane) below the feed.
- The heavy nonkeys, C_5 and C_6, have relatively constant mole fractions in the liquid and vapor below the feed until about three or four stages above the bottom. These heavy nonkeys are merely trans-

ported from the feed to the bottom. In this region, the nonkeys are diluted with keys, and the main separation taking place is that of the light key from the heavy key. A similar behavior is apparent for the light nonkeys in the rectifying section.

- About three or four stages above the bottom, the concentration of heavy nonkeys starts to rapidly climb, with C_6 rising faster than C_5. The climb begins roughly where most of the light key is depleted from the mixture. Below that point, the mixture consists mainly of heavy key and heavy nonkeys. The heavy nonkeys regard the heavy key as a "light," and fractionate it up. In this bottom region, both keys are fractionated up against the nonkeys, resulting in a rapid growth of the concentration of the heavy nonkeys at the expense of the keys (particularly the heavy key, which is the more plentiful of the keys in this region). A similar behavior is apparent for the light nonkeys in the rectifying section.
- The heavy key mole fraction increases down the column, until about three to four stages from the bottom. This behavior is similar (except near the bottom) to the behavior of a binary system. About three to four stages from the bottom, the column begins fractionating the heavy key from the heavy nonkeys (see above); therefore, the mole fraction of the heavy key diminishes down the column. This is the reason for the maximum in the C_4 concentration near the bottom. Again, a similar behavior is apparent for the light key in the rectifying section.

Physically, between the composition peaks of Fig. 2.16, the main terms on the left-hand side of the bubble-point equation, Eq. (1.15), belong to the keys. Since the light key K-value is greater than unity, it concentrates upward (Sec. 1.2.1), while the heavy key, whose K-value is below unity, concentrates downward. Moving down the tower, a point is reached where the light key concentration is depleted to the extent where it makes little contribution to Eq. (1.15). Mixture temperature rises to generate K-values high enough to satisfy Eq. (1.15). Since the K-values of the heavy nonkeys are low and the lights are gone, Eq. (1.15) can only be satisfied when the K-value of the heavy key rises above unity. Once it does, the heavy key begins concentrating upward like a light. The heavy key concentration will therefore peak when its K-value passes through unity. Again, an analogous behavior is apparent for the light key in the top section.

Figure 2.17 is a temperature profile for the column. The temperature changes most rapidly at the very top, the very bottom, and near the feed points. These are the regions where nonkey concentrations are changing fastest. At the top, and just below the feed, the light nonkeys concentrations in the liquid change rapidly, and the bubble-point

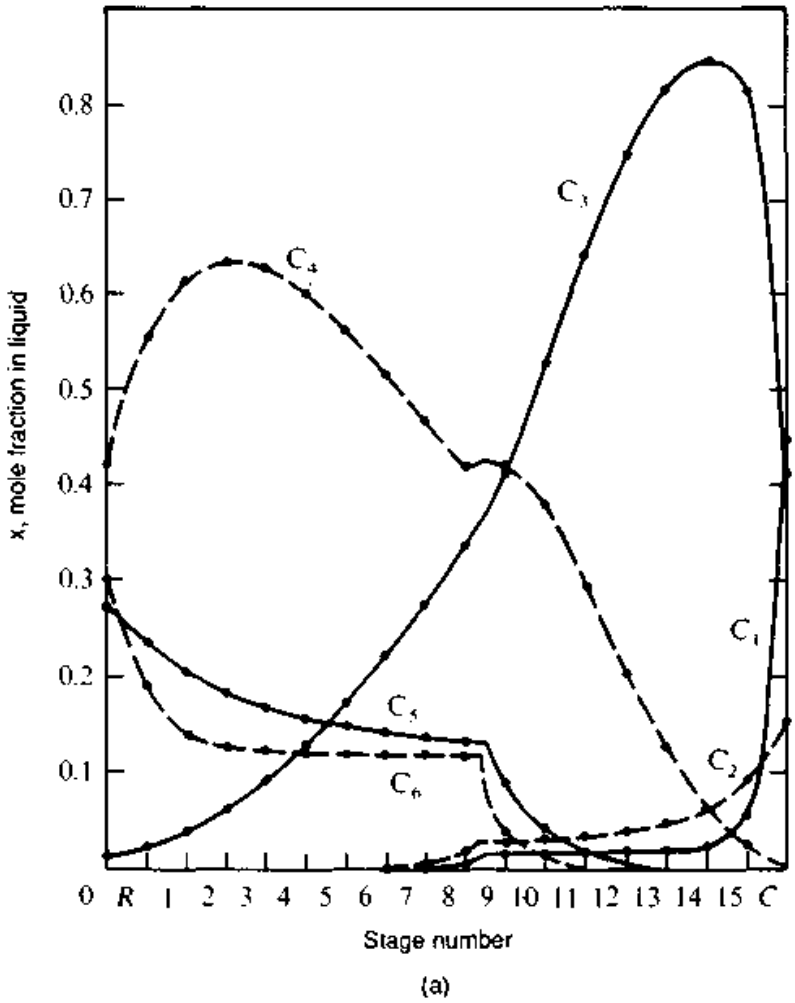

Figure 2.16 Composition profiles in multicomponent distillation, Example 2.4. (*a*) Liquid; (*b*) vapor. (From C. J. King, *Separation Processes*, 2d ed., Copyright © by McGraw-Hill, Inc. Reprinted by permission.)

temperatures are highly sensitive to the amount of lights present. At the bottom, and just above the feed, the heavy nonkeys concentrations in the liquid change rapidly, and the bubble-point temperature is sensitive to the amount of heavies present.

2.3.3 Hengstebeck diagrams: principles

Hengstebeck's (15) procedure extends the *x-y* diagram to multicomponent distillation. A multicomponent separation is treated as a binary separation between the keys. Flows and compositions are based on the two keys alone, that is,

$$x_{e,\mathrm{LK}} = x_{\mathrm{LK}}/(x_{\mathrm{LK}} + x_{\mathrm{HK}}) \tag{2.46}$$

$$y_{e,\mathrm{LK}} = y_{\mathrm{LK}}/(y_{\mathrm{LK}} + y_{\mathrm{HK}}) \tag{2.47}$$

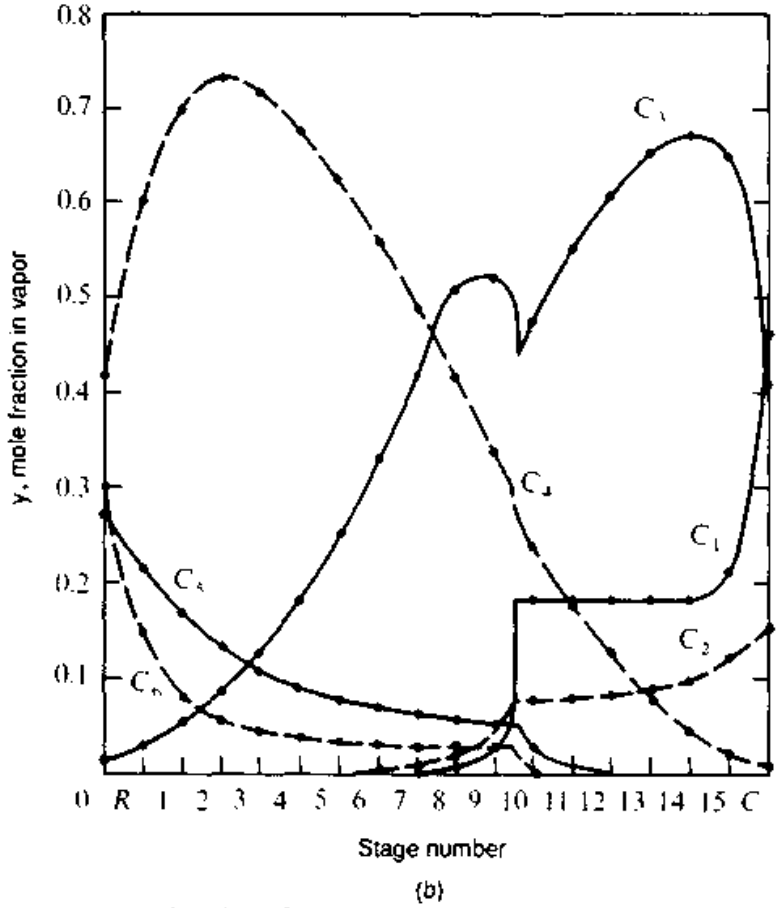

Figure 2.16 *(Continued)*

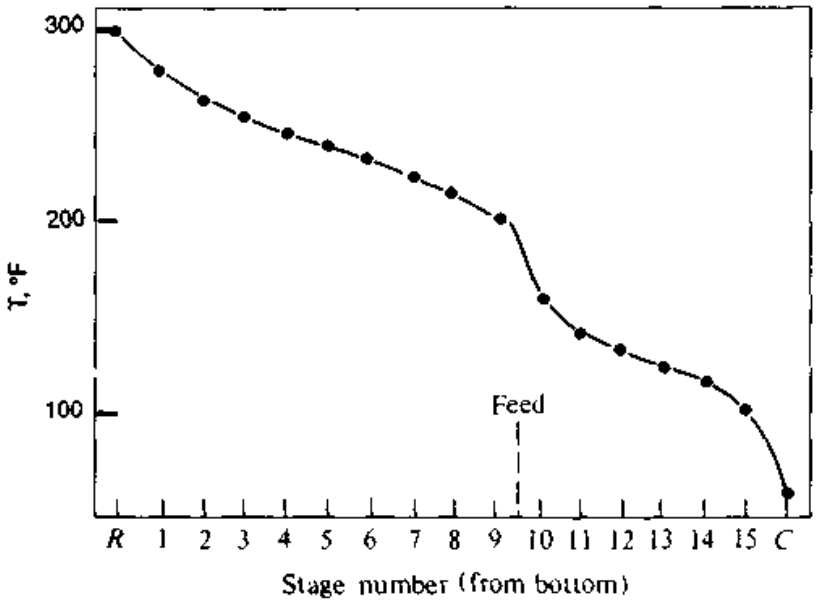

Figure 2.17 Temperature profile in multicomponent distillation, Example 2.4. (From C. J. King, *Separation Processes*, 2d ed., Copyright © by McGraw-Hill, Inc. Reprinted by permission.)

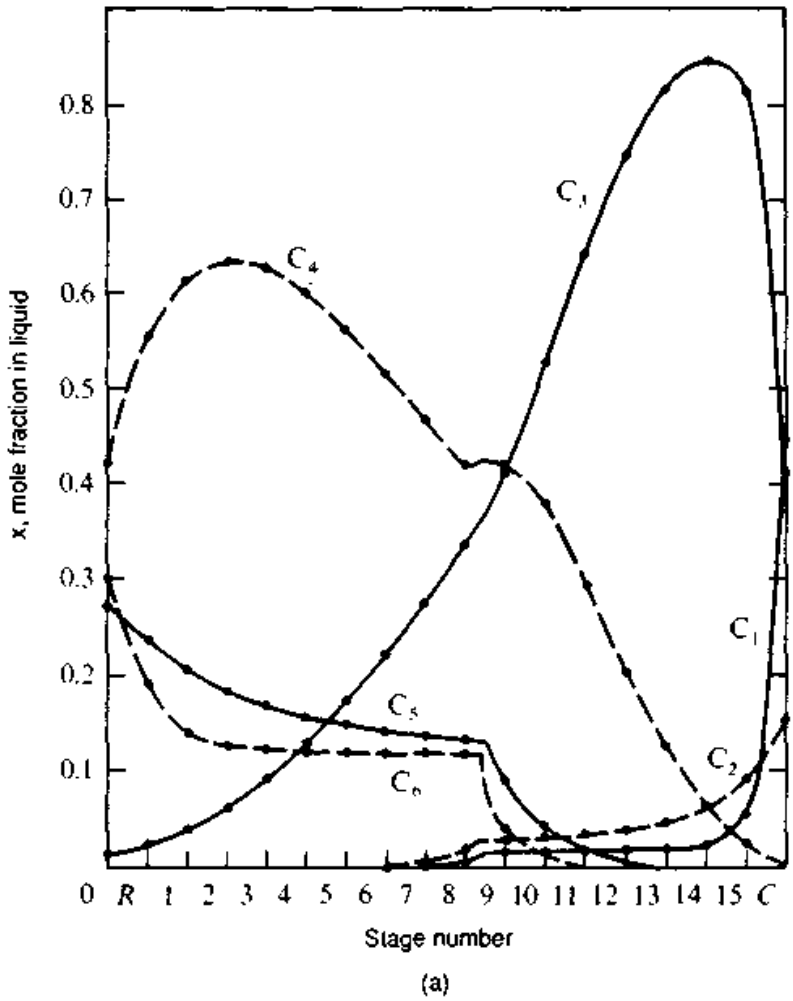

Figure 2.16 Composition profiles in multicomponent distillation, Example 2.4. (*a*) Liquid; (*b*) vapor. (From C. J. King, *Separation Processes*, 2d ed., Copyright © by McGraw-Hill, Inc. Reprinted by permission.)

temperatures are highly sensitive to the amount of lights present. At the bottom, and just above the feed, the heavy nonkeys concentrations in the liquid change rapidly, and the bubble-point temperature is sensitive to the amount of heavies present.

2.3.3 Hengstebeck diagrams: principles

Hengstebeck's (15) procedure extends the x-y diagram to multicomponent distillation. A multicomponent separation is treated as a binary separation between the keys. Flows and compositions are based on the two keys alone, that is,

$$x_{e,\mathrm{LK}} = x_{\mathrm{LK}}/(x_{\mathrm{LK}} + x_{\mathrm{HK}}) \tag{2.46}$$

$$y_{e,\mathrm{LK}} = y_{\mathrm{LK}}/(y_{\mathrm{LK}} + y_{\mathrm{HK}}) \tag{2.47}$$

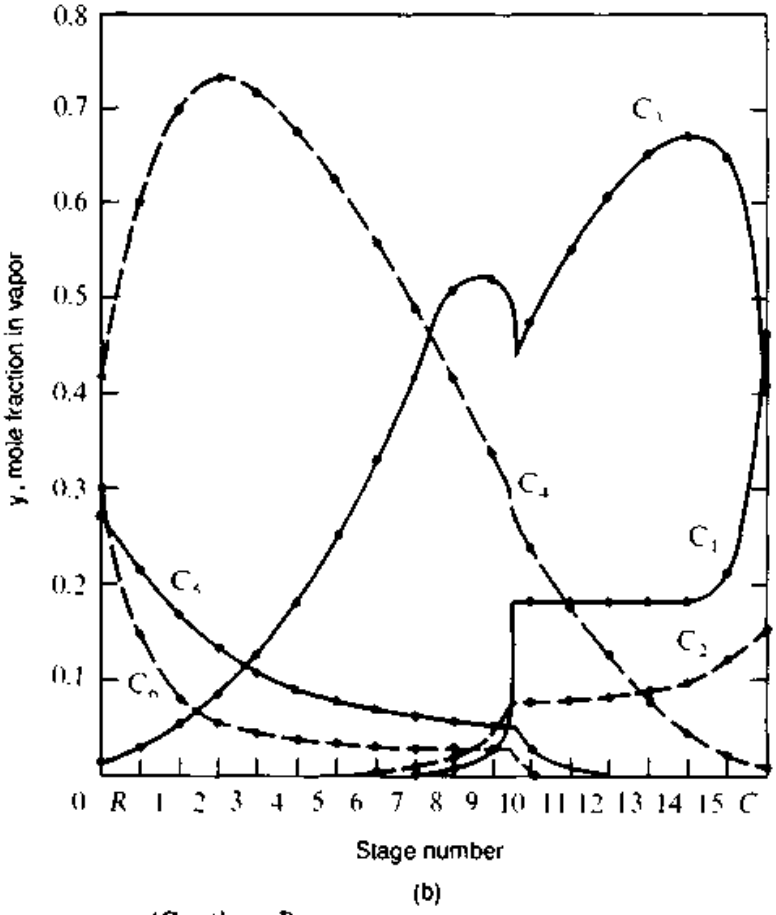

(b)

Figure 2.16 (*Continued*)

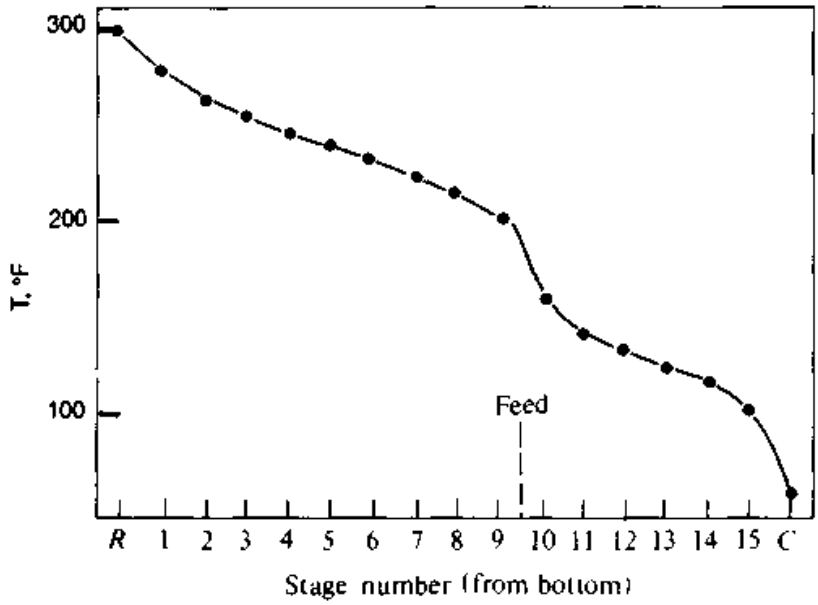

Figure 2.17 Temperature profile in multicomponent distillation, Example 2.4. (From C. J. King, *Separation Processes*, 2d ed., Copyright © by McGraw-Hill, Inc. Reprinted by permission.)

$$L_e = L(x_{LK} + x_{HK}) \tag{2.48}$$

$$V_e = V(y_{LK} + y_{HK}) \tag{2.49}$$

Limiting compositions. In order to apply Eqs. (2.46) to (2.49), the limiting compositions of the nonkeys are determined. The limiting composition of each nonkey is the composition of the component in the zone where it has constant mole fraction.

Estimation of the limiting nonkey composition is based on Jenny's approximation (20). Accordingly, K_{LK}, the equilibrium ratio of the light key, is equal to L'/V' in the stripping section zone of constant heavy nonkey mole fraction. Similarly, K_{HK}, the equilibrium ratio of the heavy key, is equal to L/V in the rectifying section zone of constant light nonkey mole fraction. Based on this approximation, the limiting compositions of each nonkey are [detailed derivation is elsewhere (7,15)].

$$x_{HNK,\,lim} = \frac{x_{HNK,B}(B/L')}{1.0 - K_{HNK}/K_{LK}} \tag{2.50}$$

$$x_{LNK,\,lim} = \frac{y_{LNK,D}(D/L)}{K_{LNK}/K_{HK} - 1.0} \tag{2.51}$$

and

$$y_{HNK,\,lim} = \frac{x_{HNK,B}(B/V')}{K_{LK}/K_{HNK} - 1.0} \tag{2.52}$$

$$y_{LNK,\,lim} = \frac{y_{LNK,D}(D/V)}{1.0 - K_{HK}/K_{LNK}} \tag{2.53}$$

For the rectifying section, it is assumed that light nonkeys are at their limiting compositions and that heavy nonkeys are absent. For the stripping section, it is assumed that heavy nonkeys are at their limiting composition and that light nonkeys are absent.

Equations (2.46) to (2.49) can therefore be written for the zone of constant nonkey mole fraction in the rectifying section as follows:

$$x_{e,LK} = x_{LK}/(1.0 - \Sigma x_{LNK,lim}) \tag{2.54a}$$

$$y_{e,LK} = y_{LK}/(1.0 - \Sigma y_{LNK,lim}) \tag{2.54b}$$

$$L_e = L(1.0 - \Sigma x_{LNK,lim}) \tag{2.54c}$$

$$V_e = V(1.0 - \Sigma y_{LNK,lim}) \tag{2.54d}$$

Similarly, Eqs. (2.46) to (2.49) can be written for the zone of constant nonkey mole fraction in the stripping section as follows:

$$x_{e,\mathrm{LK}} = x_{\mathrm{LK}}/(1.0 - \Sigma x_{\mathrm{HNK,lim}}) \tag{2.55a}$$

$$y_{e,\mathrm{LK}} = y_{\mathrm{LK}}/(1.0 - \Sigma y_{\mathrm{HNK,lim}}) \tag{2.55b}$$

$$L_e' = L'(1.0 - \Sigma x_{\mathrm{HNK,lim}}) \tag{2.55c}$$

$$V_e' = V'(1.0 - \Sigma y_{\mathrm{HNK,lim}}) \tag{2.55d}$$

2.3.4 Hengstebeck diagrams: construction

End points. These can be calculated from the overhead and bottom compositions using Eqs. (2.46) and (2.47).

Slopes of component balance lines. These can be calculated from Eqs. (2.54*c*), (2.54*d*), (2.55*c*), and (2.55*d*).

Example Calculate the end points and the slope of the operating line for Example 2.4.

1. *End points:* Using the data in Table 2.7, the end points are calculated using Eqs. (2.46) and (2.47)

$$(y_D)_e = \frac{y_{D,\mathrm{C_3}}}{y_{D,\mathrm{C3}} + y_{D,\mathrm{C4}}} = \frac{0.41}{0.41 + 0.005} = 0.988$$

$$(x_B)_e = \frac{x_{B,\mathrm{C3}}}{x_{B,\mathrm{C3}} + x_{B,\mathrm{C4}}} = \frac{0.01}{0.01 + 0.417} = 0.023$$

2. Vapor and liquid flow rates are set in a manner similar to the binary calculation (Sec. 2.2.4), that is,

$$D = 59.9 \text{ (Table 2.7)}$$

$$B = 40.1 \text{ (Table 2.7)}$$

$$L = RD = 1.5 \times 59.9 = 89.9$$

$$V = (R + 1)D = 2.5 \times 59.9 = 149.8$$

$$L' = L + qF = 89.9 + 0.34 \times 100 = 123.9$$

$$V' = L' - B = 123.9 - 40.1 = 83.8$$

3. *Find the limiting compositions:* The limiting nonkey composition is relatively a weak function of the nonkey K-value ratios. Because of this, the K-ratios (i.e., volatilities) used in the limiting nonkey composition calculation can be approximate. Hengstebeck (14) recommends the use of K-ratios at an intermediate temperature. Inspection of Fig. 2.17 shows that the feed temperature of 205°F is close enough to being an intermediate temperature. Therefore, the K-values shown in Table 2.8 are satisfactory for limiting composition calculation.

   From Eqs. (2.50) to (2.53)

$$x_{\mathrm{C5,lim}} = \frac{0.274(40.1/123.9)}{1.0 - (0.38/1.55)} = 0.12$$

$$x_{C6,lim} = \frac{0.299(40.1/123.9)}{1.0 - (0.19/1.55)} = 0.11 \qquad \Sigma x_{HNK,lim} = 0.23$$

$$x_{C1,lim} = \frac{0.435(59.9/89.9)}{(15/0.8 - 1.0)} = 0.016$$

$$x_{C2,lim} = \frac{0.15(59.9/89.9)}{(3.8/0.8 - 1.0)} = 0.027 \qquad \Sigma x_{LNK,lim} = 0.043$$

$$y_{C6,lim} = \frac{0.274(40.1/83.8)}{(1.55/0.38 - 1.0)} = 0.043$$

$$y_{C6,lim} = \frac{0.299(40.1/83.8)}{(1.55/0.19 - 1.0)} = 0.020 \qquad \Sigma y_{HNK,lim} = 0.063$$

$$y_{C1,lim} = \frac{0.435(59.9/149.8)}{(1.0 - 0.8/15.0)} = 0.18$$

$$y_{C2,lim} = \frac{0.15(59.9/149.8)}{(1.0 - 0.8/3.8)} = 0.08 \qquad \Sigma y_{LNK,lim} = 0.26$$

4. Calculate the limiting vapor and liquid flows for each section using Eqs. (2.54*c*), (2.54*d*), (2.55*c*), and (2.55*d*). Use these to determine the slopes of the component balance lines.

$$L_e = 89.9(1.0 - 0.043) = 86.0$$

$$V_e = 149.8(1.0 - 0.26) = 110.9$$

$$L'_e = 123.9(1.0 - 0.23) = 95.4$$

$$V'_e = 83.8(1.0 - 0.063) = 78.5$$

$$\text{Rectifying section slope} = L_e/V_e = 86.0/110.9 = 0.776$$

$$\text{Stripping section slope} = L'_e/V'_e = 95.4/78.5 = 1.215$$

Equilibrium curves. To establish the equilibrium curve for the key components, Hengstebeck (15) recommends that the relative volatilities of the key components be determined at the bottom product bubble-point temperature and at the overhead product dew-point temperature. If these top and bottom values differ by less than 10 percent, the equilibrium curve is drawn from Eq. (1.4), that is,

$$y_{LK} = \frac{\alpha x_{LK}}{1 + (\alpha - 1)x_{LK}} \tag{2.56}$$

where

$$\alpha = \frac{K_{LK}}{K_{HK}} \tag{2.57}$$

When relative volatilities vary, the equilibrium curve is a weak function of the reflux ratio because the operating temperature shows some dependence on the reflux ratio. In order to draw the equilibrium curve, first set the reflux ratio. Set vapor and liquid flow rates. Calculate the limiting compositions of the nonkeys using Eqs. (2.50) to (2.53). Determine the relative volatilities of the keys at several values of x_e in the rectifying and stripping sections, by carrying out bubble-point calculations using the limiting nonkeys compositions. Plot points (x_e, y_e) to give the equilibrium curve.

Figure 2.18*a* is the equilibrium curve for Example 2.4. There are two equilibrium curves, one for the rectifying section and one for the stripping section. The discontinuity at the feed is due to the sudden change in composition, and therefore temperature, when passing from one section to another. Also, some heavy nonkeys are present above the feed and some light nonkeys below it. Hengstebeck (14,15) recommends drawing the equilibrium curve arbitrarily in the feed region (Fig. 2.18*a*).

q-line. Hengstebeck (15) recommends the following equation to calculate q:

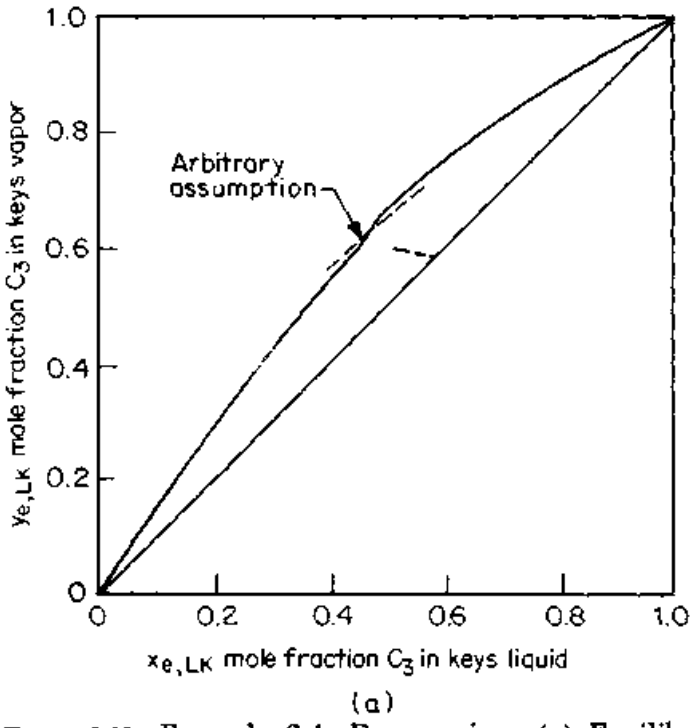

Figure 2.18 Example 2.4—Depropanizer. (*a*) Equilibrium curve; (*b*) Hengstebeck diagram; (*c*) minimum reflux determination. (Part *b*, from C. J. King, *Separation Processes*, 2d ed., Copyright © by McGraw-Hill, Inc. Reprinted by permission. Parts a and c based on C. J. King, loc. cit.)

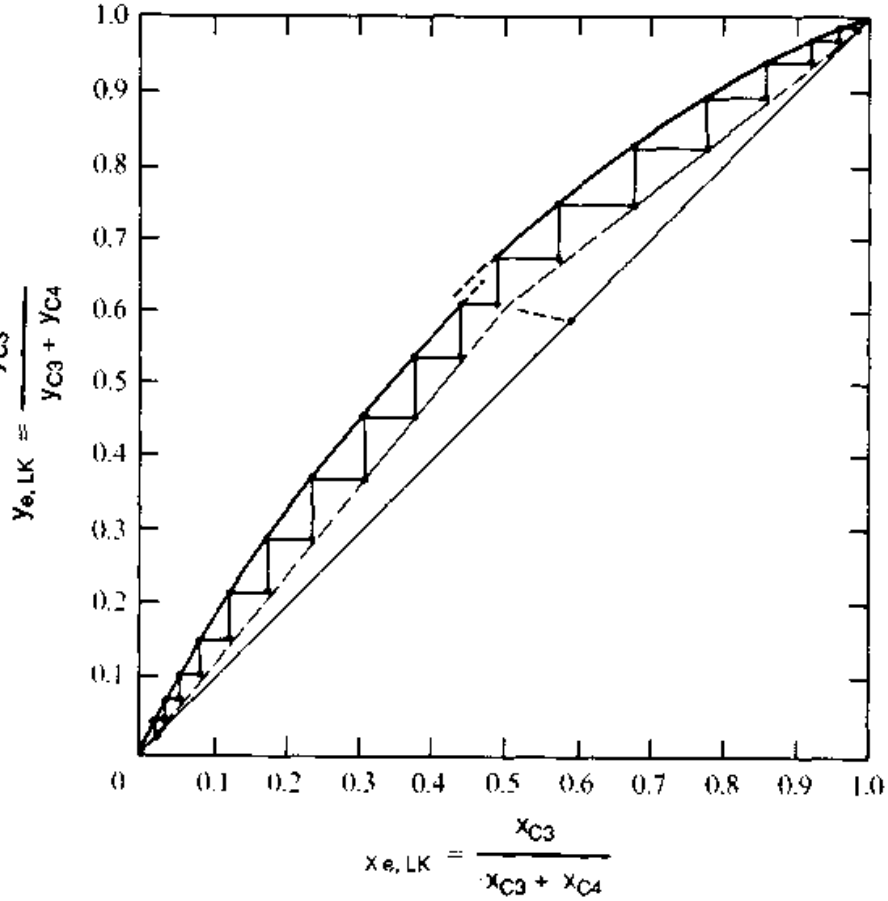

(b)

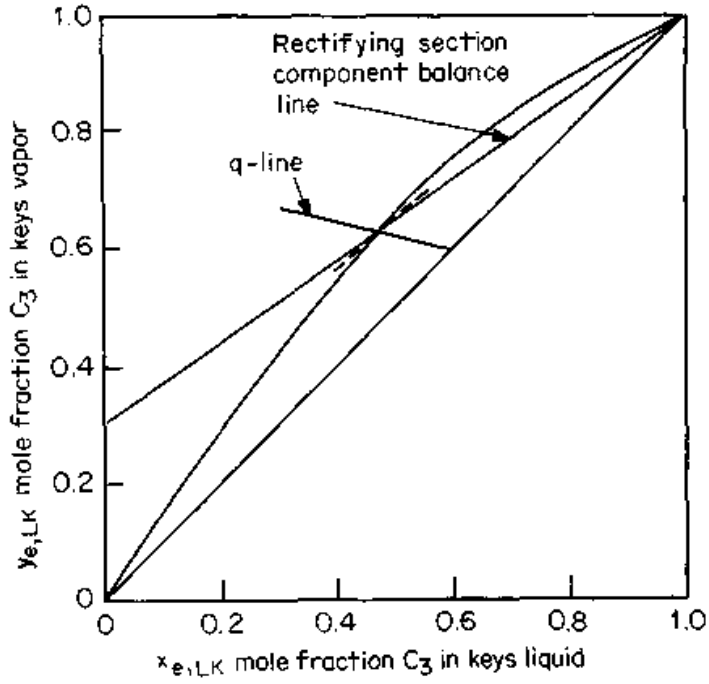

(c)

Figure 2.18 (*Continued*)

$$q = \frac{F_L + L\Sigma x_{\text{LNK,lim}} - L'\Sigma x_{\text{HNK,lim}}}{F_e} \tag{2.58}$$

The q-line for Example 2.4 can therefore be calculated from

$$q = \frac{34 + 89.9 \times 0.043 - 123.9 \times 0.23}{42} = 0.22$$

$$\text{Slope of the } q\text{-line} = \frac{q}{q - 1} = \frac{0.22}{0.22 - 1} = -0.282$$

Equivalent feed composition is obtained from Eq. (2.46)

$$x_{e,\text{LK(feed)}} = \frac{0.25}{0.25 + 0.17} = 0.60$$

Number of stages. Once the equilibrium curve, q-line, end points, and slopes of the component balance lines are established, stages can be stepped off. Figure 2.18*b* (for Example 2.4) gives a total of 15 theoretical stages (not including the reboiler and condenser) with the feed entering at stage 9 (reboiler being stage 0).

Complex columns. The Hengstebeck diagram can be extended to complex columns using the concepts described in Sec. 2.2.10. The derivation, equations, and a worked example are elsewhere (23).

2.3.5 Minimum reflux by Hengstebeck diagram

Hengstebeck (15) recommends the following procedure for minimum reflux:

1. Calculate the limiting flow rate of the light nonkeys in the rectifying section and the limiting flow rate of the heavy nonkeys in the stripping section. These limiting flow rates for each nonkey can be calculated from Eqs. (2.50) and (2.51) as follows:

$$l_{\text{HNK,lim}} = L'x_{\text{HNK,lim}} = \frac{x_{\text{HNK},B}B}{1.0 - K_{\text{HNK}}/K_{\text{LK}}} \tag{2.59}$$

$$l_{\text{LNK,lim}} = Lx_{\text{LNK,lim}} = \frac{y_{\text{LNK},D}D}{K_{\text{LNK}}/K_{\text{HK}} - 1.0} \tag{2.60}$$

2. Construct the equilibrium curve for the key components and the q-line (Sec. 2.3.4).
3. Draw a line from the product composition point to the intersection of the q-line with the equilibrium curve. This line has a slope of

$[L_e/(L_e + D_e)]_{min}$. With D_e (flow rate of keys in the top product) known, L_e can be calculated.

4. The minimum reflux can be calculated as the sum of L_e and the limiting flows of the light nonkeys, $l_{LNK,lim}$.

Example Calculate the minimum reflux ratio for Example 2.4.

solution The q-line is not affected by the reflux ratio [see Eq. (2.58)], and therefore there is no need to calculate the limiting flow of the heavy nonkey. The limiting flow of the light nonkeys is given by Eq. (2.60)

$$l_{C1,lim} = \frac{0.435 \times 59.9}{(15/0.8 - 1)} = 1.5$$

$$l_{C2,lim} = \frac{0.15 \times 59.9}{(3.8/0.8 - 1)} = 2.4$$

The slope of the component balance line is determined graphically from Fig. 2.18*c* to be equal to 0.70

$$\left[\frac{L_e}{L_e + D_e}\right]_{min} = 0.70$$

D_e = 24.9 and therefore $L_{e,min}$ = 58.1. Adding the limiting flows of the nonkeys

$$L_{min} = 58.1 + 1.5 + 2.4 = 62.0$$

Therefore, minimum reflux ratio is

$$R_{min} = \frac{L_{min}}{D} = \frac{62.0}{59.9} = 1.035$$

WARNING: Minimum reflux ratios calculated by this method are somewhat lower than true values. This is because the method neglects the presence of light nonkeys just below the feed and heavy nonkeys just above it (see Sec. 2.3.6).

2.3.6 Key ratio plots and retrograde distillation

Key ratio is the mole fraction ratio of the light key to the heavy key.

Key ratio plots (Figs. 2.19, 2.20) plot key ratio in the liquid (x_{LK}/x_{HK}) against stage number on a semilog scale. The slope of each curve gives a measure of the relative fractionation accomplished per stage in various locations along the fractionator. Fenske's equation (Sec. 3.2.1) implies that at total reflux and constant relative volatility, the logarithm of the key ratio is a linear function of the stage number. This is approached in the key ratio plot for the high reflux ratio (Fig. 2.19*a*). At lower reflux, this proportionality usually applies near the two ends of the column (24), but the curve flattens as the pinch zone near the feed is approached (Fig. 2.19*b–d*).

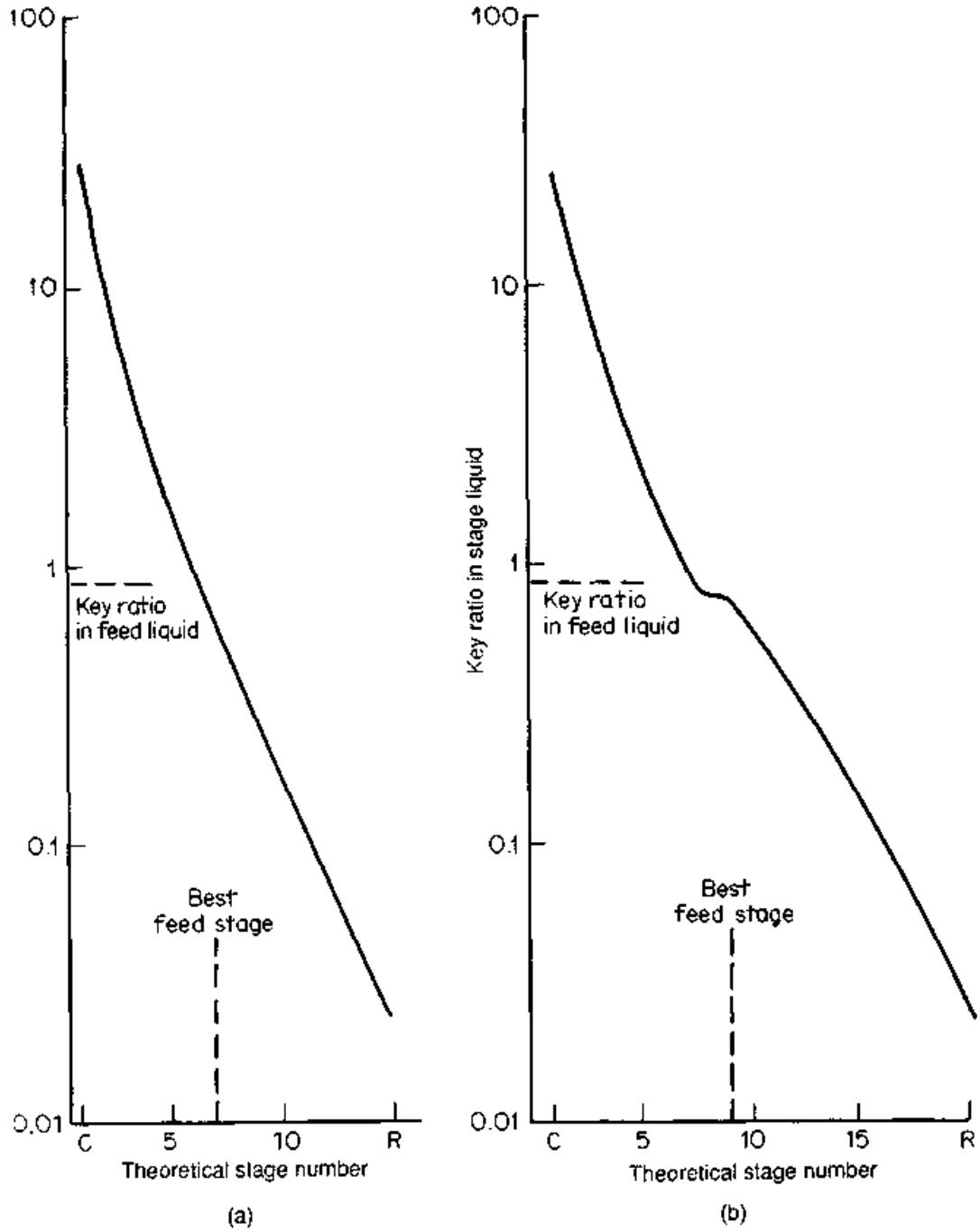

Figure 2.19 Key ratio plots, depropanizer example. Feed and products compositions identical to Example 2.4. (*a*) 15 theoretical stages, $R/R_{min} = 2.66$; (*b*) 20 theoretical stages, $R/R_{min} = 1.40$; (*c*) 25 theoretical stages, $R/R_{min} = 1.19$; (*d*) 33 theoretical stages, $R/R_{min} = 1.094$.

As reflux ratio is reduced, the key ratio profile develops an inflection point. As minimum reflux is approached, the profile develops a maximum below the feed point and a minimum above the feed point. Between the maximum and the minimum, there is a region in which the key ratio actually decreases as one moves up the column. This be-

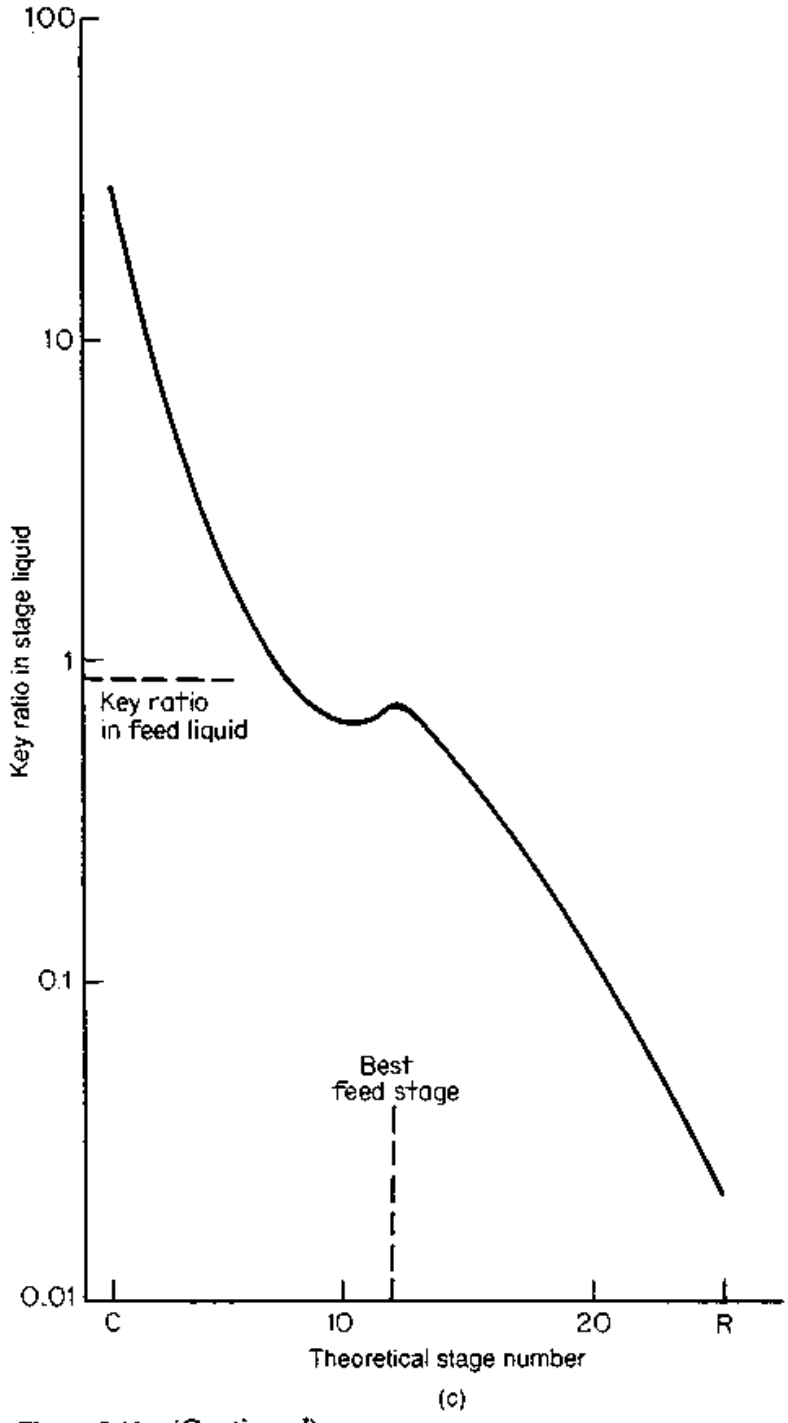

Figure 2.19 (*Continued*)

havior is unique to multicomponent distillation near minimum reflux or when the keys make up a small part of the feed, and is termed *retrograde distillation* or *reverse distillation.* Figure 2.20 shows a similar behavior when the feed points are nonoptimum.

This behavior results from the presence of light nonkeys below the feed and heavy nonkeys above it. The pinch zones in multicomponent

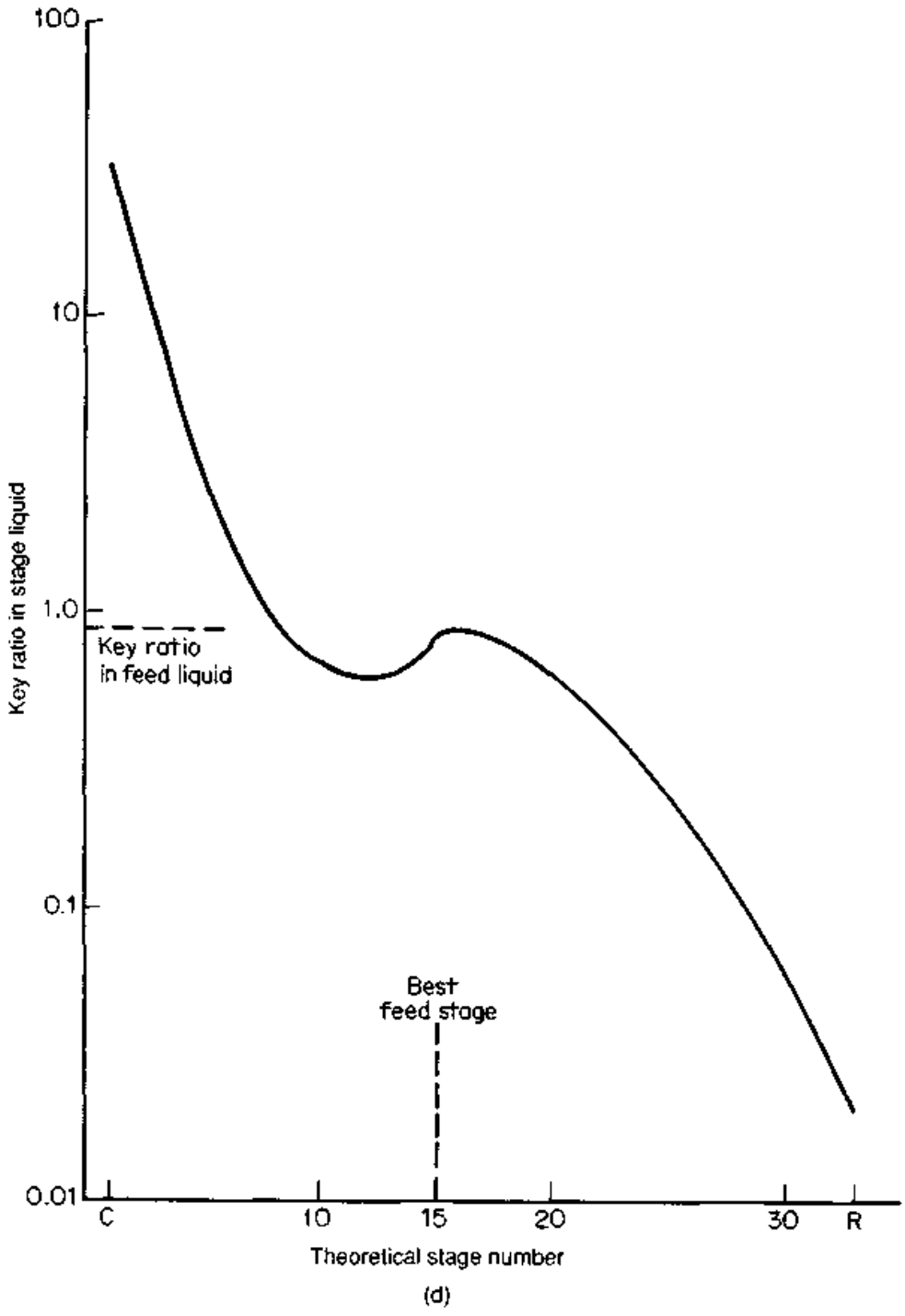

Figure 2-19 (*Continued*)

distillation do not occur at the feed points, as they do in binary distillation, but above and below the feed points. The stages between the lower pinch zone and the feed point fractionate the light nonkeys from the bottom section liquid, and those between the upper pinch zone and the feed fractionate the heavy nonkeys from the rectifying section liquid.

2.3.7 Best feed stage location

Due to the presence of nonkeys near the feed, determination of the best feed point in multicomponent distillation is difficult. King (7) surveyed published criteria and their shortcomings. The following rules of thumb are often used:

1. The key ratio in the feed stage liquid should be as close as possible to the key ratio in the liquid portion of the feed (flashed to tower pressure).
2. The binary equivalent composition of the light key in the feed should correspond to the intersection of the component balance lines on a Hengstebeck diagram (e.g., Fig. 2.18*b*).
3. The feed point should give the most equal slopes on both sides of the feed stage in a key ratio plot (Fig. 2.20). Too high a feed causes excessive retrograde distillation below the feed, and too low a feed causes excessive retrograde distillation above it. In order to reach the optimum feed point, the feed stage should be moved from the "sharp" maximum (or minimum) toward the flat one (Fig. 2.20).
4. Applying an analytical technique, shortcut (Sec. 3.2.6) or rigorous.

Hanson and Newman (25) demonstrated the following shortcomings of the first two rules of thumb:

1. Although rules 1 and 2 often work well, there are many instances where they give poor feed locations. The rules become less reliable as minimum reflux is approached.
2. Light nonkeys raise the optimum key ratio at the feed stage, while heavy nonkeys lower it. Rules 1 and 2 therefore become less reliable when there are a lot more light than heavy nonkeys or vice versa, or when the amount of nonkeys exceeds the amount of keys.
3. Nonkeys whose volatility is either close to the keys or far removed from the keys tend to shift the optimum key ratio (or light key concentration) at the feed stage to a lesser degree than nonkeys whose volatility is moderately removed from the keys.
4. The first rule of thumb tends to work better when there are more light than heavy nonkeys, while the second tends to work better when there are more heavy than light nonkeys.

Shortcut analytical techniques tend to be just as unreliable as the rules above. The third rule of thumb accounts for the nonkeys and is a favored shortcut method by the author and others (7). While a rigorous analytical technique (Sec. 3.1.7) is generally the most reliable pro-

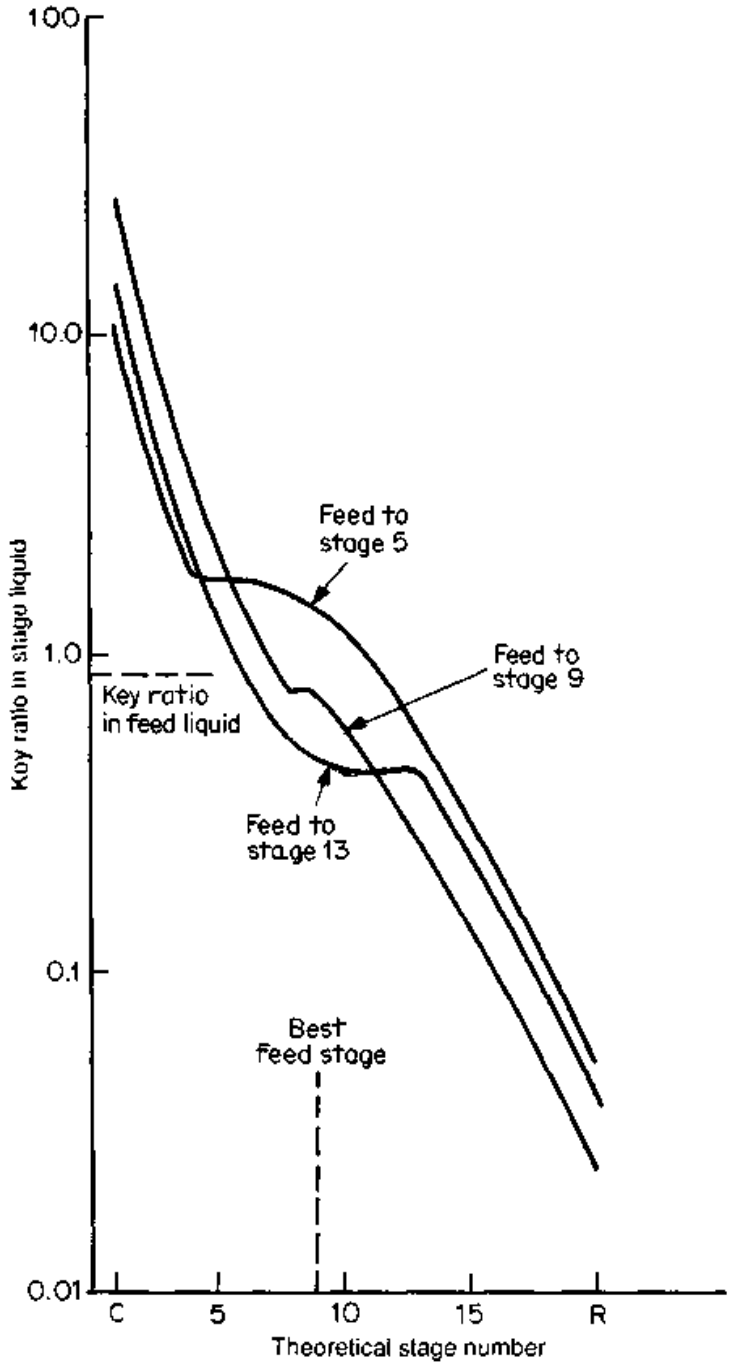

Figure 2.20 Effect of feed stage on key ratio plot. Depropanizer example, feed composition same as Example 2.4, 20 theoretical stages, $R/R_{min} = 1.40$.

cedure for predicting the best feed point, the third rule of thumb provides an invaluable check.

2.3.8 Distribution of nonkeys (*d/b* plots)

The *d/b* plot provides a useful estimate of the distribution of nonkeys and intermediate keys in the products. Hengstebeck (14) and Geddes

(26) noted that at total reflux, application of Fenske's equation (Sec. 3.2.1) for each component gives

$$\log\left(\frac{x_d}{x_b}\right)_i = N_{\min} \log \alpha_i + C \tag{2.61}$$

Thus at total reflux, a log-log plot of x_d/x_b (or d/b) for each component against relative volatility gives a straight line with a slope equal to the minimum number of stages (Fig. 2.21). Stupin and Lockhart (27) noted that this relationship is nonlinear at minimum reflux and at finite reflux ratios (Fig. 2.21). At minimum reflux, the curve becomes asymptotic to the dashed lines at the relative volatilities of the light and heavy keys, corresponding to a total recovery of light nonkeys and heavy nonkeys in the distillate and bottoms, respectively. On the other hand, intermediate keys are separated to a better degree at total reflux than at minimum reflux.

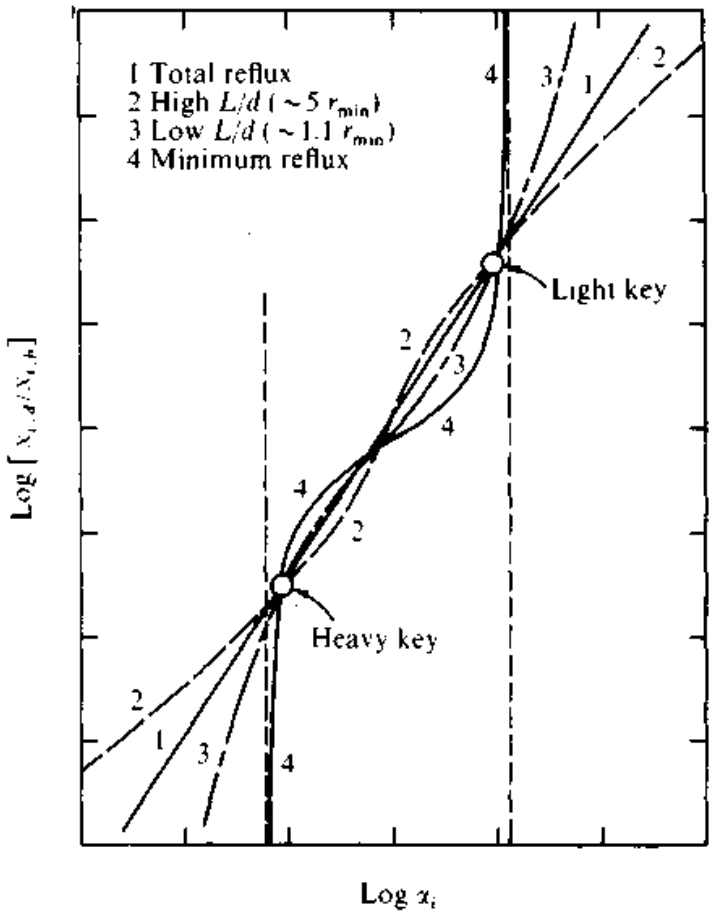

Figure 2.21 Distribution of components at various reflux ratios. (Reproduced from W. J. Stupin and F. J. Lockhart, paper presented at the annual meeting of the AIChE, Los Angeles, 1968. Reprinted courtesy of Dr. W. J. Stupin.)

Stupin and Lockhart (27) also noted that as reflux is lowered from total to minimum, the separation of nonkeys first worsens (curve 2, Fig. 2.21), then improves (curve 3, Fig. 2.21). The intermediate keys follow the converse pattern. At a reflux ratio of about 1.2 to 1.5 times the minimum, component distribution resembles that of the total reflux component distribution. Detailed discussion is elsewhere (7,27). Figure 2.16 demonstrates that light nonkeys are fractionated out in the stripping section and heavy nonkeys in the rectifying section. The *d/b* plot depicts this behavior (Sec. 2.4.2).

2.4 Analyzing Computer Simulation Results by Graphical Techniques

A prime application of graphical methods in modern distillation technology is for analyzing the results of computer simulations. Several of the graphical construction rules can be bent in order to benefit from computer accuracy and to reduce effort. Johnson and Morgan (28) described several key considerations; their work is expanded here using the author's experience.

2.4.1 Use of *x-y* diagrams (McCabe-Thiele and Hengstebeck)

It has been the author's experience that an *x-y* diagram is the most useful graphical technique for analyzing computer simulation results. The *x-y* diagram is capable of

1. *Detecting pinched regions (Sec. 2.2.5):* Pinching and its cause (minimum reflux, mislocated feed, tangent pinch, etc.) are readily visible on an *x-y* diagram. Figure 2.22 compares a well-located feed point in the depropanizer example with a mislocated feed point. The pinch is clearly seen in Fig. 2.22*b*, while no pinch exists in Fig. 2.22*a*.

   The *x-y* diagram should be examined for pinching both for design conditions and for some deviations (variation in feed temperature, feed composition, errors in relative volatility, etc.). For deviations, a simple construction (e.g., a *q*-line with a slightly different slope) on the design conditions *x-y* diagram is usually sufficient. When the threat of a pinched region is detected, a more detailed analysis (e.g., a computer run for the deviated conditions) is warranted.
2. *Identifying mislocated feed points:* The feed point should be where the *q*-line intersects the equilibrium curve. This rule works well for binary distillation (Sec. 2.2.5), but not so well for multicomponent distillation (Sec. 2.3.7). In Fig. 2.22 it works well; the *x-y* diagram

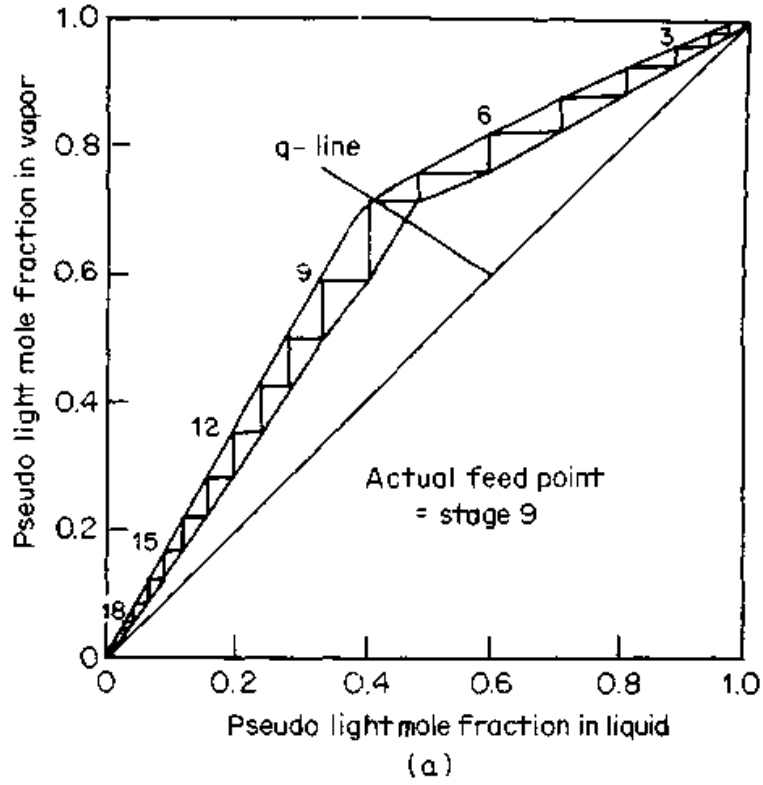

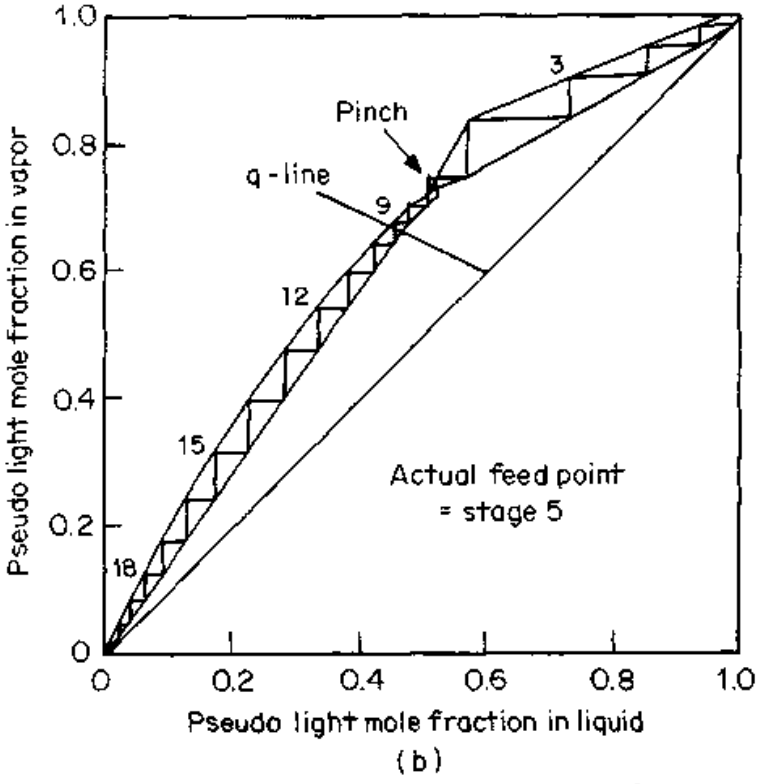

Figure 2.22 Application of x-y diagrams to analyze a computer simulation. Diagrams were prepared using computer composition printouts. Depropanizer example, 20 theoretical stages, $R/R_{min} = 1.4$. (*a*) Correct feed point. (*b*) Feed point too high.

suggests stage 8 is the best feed point. Simulation showed that stage 9 is slightly better, but stage 8 is adequate. However, the author has encountered many multicomponent distillations where the simulated optimum feed point did not match the intersection of the q-line with the equilibrium curve.

3. *Identifying excessive reflux and reboil:* This can be recognized by too wide a gap between the component balance line and the equilibrium curve throughout the column. Errors in estimating minimum reflux and/or convergence difficulties in the computer simulation are often the culprit. The author has experienced a case where the design reflux rate was lowered by 30 percent after an x-y diagram identified excess reflux. Figure 2.22 suggests that there is some room for reducing reflux and reboil in this example. Simulation confirmed that adding five stages can reduce reflux and reboil by 15 percent while still maintaining adequate margin from pinching.
4. *Identifying cases where feed or intermediate heat exchangers are attractive:* A wide gap between the component balance line and the equilibrium curve in the bottom section indicates a potential for a preheater or interreboiler; a wide gap in the top section suggests a potential for a precooler or intercondenser. In Fig. 2.22, the gaps are wide in both sections, suggesting excessive reflux and reboil rather than a potential for adding an intermediate heat exchanger.
5. *Guiding column optimization,* and showing the effects of changing feed or product composition, thermal state of the feed, use of side draws, multifeed arrangements, etc.

Construction. Once a converged computer simulation is available, construction of an x-y diagram is far easier than constructing one from scratch. Many computer simulations provide the option of plotting an x-y diagram. If this option is unavailable, the following sequence of steps can be followed:

1. *Find the key components:* If any components have similar volatilities to one of the keys, and end up in the same product, lump them with the keys. Convert all mole fractions to the equivalent binary [Eqs. (2.46) and (2.47)]. An alternative, simpler procedure is to lump all light keys and light nonkeys into a single light pseudocomponent, and all heavy keys and heavy nonkeys into a single heavy pseudocomponent. This procedure (used in Fig. 2.22) is preferred by the author and others (28). Whichever method is preferred, it must be consistently applied.

2. *Plot the equilibrium curve, using compositions printed out by the computer*

   In multicomponent systems, these compositions must first be converted to the appropriate binary equivalent or pseudo-light-component as per item 1 above. Since vapor and liquid leaving each stage are in equilibrium, plotting the composition of the vapor leaving a stage against the composition of liquid leaving the same stage will give a point on the equilibrium curve. Repeating for several stages will define the equilibrium curve.

3. *Plot the component balance lines, using compositions printed out by the computer (expressed as the appropriate binary equivalents or pseudo-light-component compositions as per item 1 above)*

   Equation (2.9) states that the component balance line can be obtained by plotting the vapor composition entering a stage against liquid composition leaving the same stage. The plotted component balance "line" may turn out to be a curve. The computer accounts for enthalpy variations and does not assume constant molar overflow (Sec. 2.2.2). The resulting component balance curves overcome the greatest accuracy problem (Sec. 2.2.2) of conventional x-y diagrams. Figure 2.22 shows some curvature of the component balance lines.

4. *Draw the 45° diagonal line*

   Plot the feed composition on the diagonal (expressed as the appropriate binary equivalent or pseudo-light-component composition as per item 1 above).

5. *Calculate* q

   If using the equivalent binary method, use Eq. (2.58). For $x_{\mathrm{LNK,lim}}$ obtain an average value from near the middle of the rectifying section; for $x_{\mathrm{HNK,lim}}$ obtain an average value from near the middle of the stripping section. If using the pseudo-light key component method, take q as the liquid leaving the feed stage minus liquid entering the feed stage from the stage above, and the difference divided by the feed rate. Note that this is slightly different from and more appropriate than the normal definition of q. Construct the q-line using Eq. (2.27).

6. *Step the stages off in the normal manner.*

2.4.2 Use of key ratio and *d/b* plots

Key ratio plots are primarily for identifying mislocated feed stages in multicomponent distillation. For this purpose, they are superior to x-y diagrams. Key ratio plots are easy to construct; all it takes is calculating the key ratio in the liquid for a few stages in the feed region

and plotting these against stage number on semilog paper. Figures 2.19 and 2.20 are key ratio plots prepared from compositions calculated by a computer simulation.

d/b plots (Sec. 2.3.8) are primarily used when there is a tight spec on a nonkey component or a concern about the distribution of an intermediate key component. *d/b* plots are easy to construct. One component (say the heavy key) is selected as the reference component, and the relative volatility of each of the other components is calculated in relation to it. Then the mole fraction of each component in the top product is divided by its mole fraction in the bottom product, and the quotient is plotted against its relative volatility on log-log scales. Often, the ratio of number of moles in the top to number of moles in the bottom is used instead of the mole fraction ratio. In other cases (28), recovery is plotted on an inverse log scale [(100%/overhead recovery) − 1] instead of the mole fraction ratio.

The *d/b* ratio plot is frequently non-linear, but should be smooth (Sec. 2.3.8). The prime cause of bumps is a poor estimate of relative volatility. If a refined estimate (see Sec. 3.2.1 for estimating guidelines) does not improve things, the bump may reflect anomalies or a need to relocate a feed. The *d/b* plot gives a measure of how relocating the feed point affects the nonkey component split.

Figure 2.23 shows *d/b* plots for the depropanizer example, based on compositions calculated by the computer. The diagram shows that for a

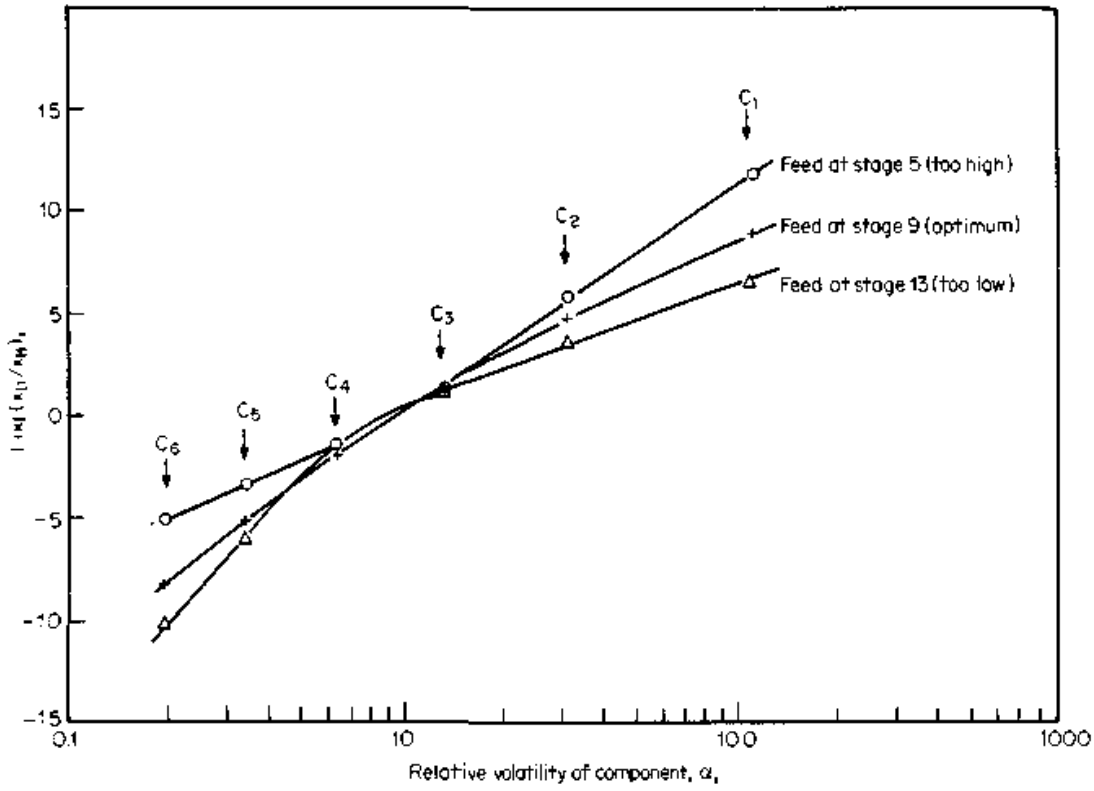

Figure 2.23 Application of *d/b* plots to examine nonkey component distribution in products. Depropanizer example, 20 theoretical stages, R/R_{min} = 1.40.

given C_3/C_4 split, feeding the column higher than the ideal feed point improves the light nonkey split at the expense of a worse heavy nonkey split. Conversely, feeding the column lower than the ideal feed point improves the heavy nonkey split at the expense of a worse light nonkey split.

2.5 Nomenclature

2.5.1 English Letters

B	Bottom flow rate, lb-mole/h
b	Flow rate of a component in bottom product, lb-mole/h
C	Constant in Eq. (2.61)
C	Condenser stage (Figs. 2.16, 2.19, 2.20)
C_p	Molar heat capacity, Btu/(lb-mole) (°F)
D	Overhead product flow rate, lb-mole/h
d	Flow rate of a component in top product, lb-mole/h
E_{MV}	Murphree tray efficiency, Eq. (2.33), fractional
F	Feed rate, lb-mole/h
H	Enthalpy, Btu/lb-mole
ΔH	Heat added or removed, Btu/h
H_L	Liquid enthalpy, Btu/lb-mole, Eq. (2.3)
H_V	Latent heat of vaporization, Btu/lb-mole. In Eq. (2.3) only, H_V is vapor enthalpy, Btu/lb-mole
i,j	Counter of the number of components
J	A section identifier in a complex column
K	Equilibrium K-value, Eq. (1.1)
k	Section counter in a complex column
k'	Section counter for second simultaneous stream at the point of heat addition or removal in a complex column
L	Liquid flow rate, lb-mole/h. In Secs. 2.2.1 to 2.2.5 and 2.3.3 to 2.3.5, L specifically denotes liquid flow rate in rectifying section
l	Flow rate of nonkeys in the liquid, lb-mole/h
L'	Stripping section liquid flow rate, lb-mole/h
$N + 1$	Number of sections in a complex column
N,n	Stage number
P	Flow rate of side product, lb-mole/h
P'	Flow rate of stream going to interboiler or intercondenser, lb-mole/h
q	Pound-moles of liquid introduced with the introduction of 1 lb-mole of feed
Q	Heat added, Btu/h
Q	Pound-moles of liquid withdrawn with the withdrawal of 1 lb-mole of side product

Q'	Pound-moles of liquid per 1 lb-mole of stream going to intercondenser or interreboiler
R,r	Reflux ratio, Eq. (2.16)
R	Reboiler stage (Figs. 2.16, 2.19, 2.20)
S	Stripping ratio, V′/B
T	Temperature, °F
u	Mole fraction of the more volatile component in a side product
u'	Mole fraction of the more volatile component in stream going to intercondenser or interreboiler
V	Vapor flow rate, lb-mole/h. In Secs. 2.2.1 to 2.2.5 and 2.3.3 to 2.3.5, V specifically denotes vapor flow rate in rectifying section
V'	Stripping section vapor flow rate, lb-mole/h
x	Mole fraction of the more volatile component in the liquid (binary distillation); mole fraction of a component in the liquid (multicomponent distillation)
y	Mole fraction of the more volatile component in the vapor (binary distillation); mole fraction of a component in the vapor (multicomponent distillation)
y^*	Equilibrium mole fraction of the more volatile component in the vapor
$y(0)$	Intercept of the component balance line on the y axis of an x-y diagram
z	Mole fraction of the light key in the feed

2.5.2 Greek letters

α	Relative volatility

2.5.3 Subscripts

0,1,2,...	Stage number
$1,2,\ldots,J$	Section number in a complex column
B,b	Column bottom
BP	Bubble point
$C_1,\ldots,C_6$	Refers to each hydrocarbon in the worked example
D,d	Column overhead product
DP	Dew point
e	Equivalent binary of the keys
F,f	Feed
HK	Heavy key
HNK	Heavy nonkey
i,j	Counter of the number of components
i	Component balance lines intersection point
int	Point of intersection of the component balance line with the 45° diagonal

J	A section of identifier in a complex column
k	Section counter in a complex column
k'	Section counter for second simultaneous stream at the point of heat addition or removal in a complex column
L,l	Liquid
lim	Limiting composition of a nonkey component
LK	Light key
LNK	Light nonkey
m	Stripping stage
min	Minimum
n,N	Stage number
$N + 1$	Number of sections in a complex column
V	Vapor

2.6 References

1. McCabe, W. L., and E. W. Thiele, *Ind. Eng. Chem. 17,* 605, 1925.
2. Ponchon, M., *Tech. Moderne 13,* 20, 1921.
3. Savarit, R., *Arts et metiers,* pp. 65, 142, 178, 241, 266, 307, 1922.
4. Van Winkle, M., *Distillation,* McGraw-Hill, New York, 1967.
5. Henley, E. J., ed., *Stagewise and Mass Transfer Operations,* Vols. 1 and 2, A.I.Ch.E., New York, 1980.
6. Robinson, C. S. R., and E. R. Gilliland, *Elements of Fractional Distillation,* 4th ed., McGraw-Hill, New York, 1950.
7. King, C. J., *Separation Processes,* 2d ed., McGraw-Hill, New York, 1980.
8. Brian, P. L. T., *Staged Cascades in Chemical Processing,* Prentice-Hall, Englewood Cliffs, N.J., 1972.
9. Gallant, R. W., *Physical Properties of Hydrocarbons,* Vols. 1 and 2, Gulf Publishing, Houston, Texas, 1968 and 1984.
10. Fisher, G. T., *Ind. Eng. Chem. Proc. Des. Dev. 2*(4), 284, 1963.
11. Ledanois, J., and C. Olivera-Fuentes, *Ind. Eng. Chem. Proc. Des. Dev. 23,* 1, 1982.
12. Kister, H. Z., *Distillation Operation,* McGraw-Hill, New York, 1990.
13. Arnold, V. E., *Chem. Eng.,* February 4, p. 59, 1985.
14. Hengstebeck, R. J., *The Refining Engineer,* p. C-6, November, 1957.
15. Hengstebeck, R. J., *Distillation—Principles and Design Procedures,* Reinhold Publishing, 1961.
16. Eduljee, H. E., *Br. Chem. Eng. 9*(10), 668, 1964.
17. Granville, W. H., *Br. Chem. Eng. 9*(2), 89, 1964.
18. Yaws, C. L., K. Y. Li, and C. S. Fang, *Chem. Eng.,* May 18, p. 153, 1981.
19. Kister, H. Z., *Chem. Eng.,* January 21, p. 97, 1985.
20. Jenny, P. J., *Trans. Am. Inst. Chem. Engrs., 35,* 635, 1939.
21. Hengstebeck, R. J., *Trans. Am. Inst. Chem. Engrs., 42,* 309, 1946.
22. Edmister, W. C., *Petrol. Engr.,* p. 47, June 1948.
23. Kister, H. Z., *Chem. Eng.,* May 13, p. 71, 1985.
24. Hengstebeck, R. J., *Chem. Eng.,* July 29, p. 145, 1968.
25. Hanson, D. N., and J. S. Newman, *Ind. Eng. Chem. Proc. Des. Dev. 16,* 223, 1977.
26. Geddes, R. L., *AIChEJ.* 4, 389, 1958.
27. Stupin, W. J., and F. J. Lockhart, Paper presented at the AIChE annual meeting, Los Angeles, December, 1968.
28. Johnson, J. E., and D. J. Morgan, *Chem. Eng.,* July 8, p. 72, 1985.

Chapter

3

Column Process Design, Optimization, and Shortcut Calculations

Column process design specifies the separation, and sets column pressure, reflux, stages, and feed point. These in turn yield internal flows and reboiler and condenser duties. This chapter addresses the main column process design considerations. The column is optimized during the process design, and many times later during operation. Computer control continuously optimizes the column on-line. Both design and on-line optimization are also addressed in this chapter.

Column process design proceeds stepwise. The shortcut step eliminates the least-desirable options and provides a starting point for the rigorous step. The rigorous step fine-tunes the design and completes the column optimization. This chapter addresses the shortcut step. Graphical shortcut techniques were covered in the previous chapter. Rigorous simulation is addressed in detail in the next chapter.

3.1 Process Design and Optimization

3.1.1 Separation specification: requirements and options

Columns that have no side products are bound by two overall equations: a mass balance and a component balance, that is,

$$F = B + D \tag{3.1}$$

and

$$Fz = Bx_B + Dx_D \tag{3.2}$$

At a given feed flow rate and feed composition, there are two equations [Eqs. (3.1) and (3.2)] and four unknowns: B, D, x_B, and x_D. There-

fore, only two variables can be specified for the separation. Further, at least one of the two specified variables must be a composition. Usually, either two purities or a purity and a product rate are specified.

Product rate specification. The product rate specification can be expressed simply as a flow rate. Alternatively, it can be expressed as a "recovery." Some examples of the use of recovery specification are

1. "60 percent (say) of the feed is to be recovered as the distillate." This is equivalent to setting the distillate rate to $0.6F$.
2. "95 percent (say) of the light key component in the feed is to be recovered in the distillate." This is equivalent to setting the distillate rate to ($0.95Fz_{LK}$ + impurities + light nonkeys).
3. A double-recovery specification is equivalent to specifying one product rate and one product purity. For instance, "95 percent of the light key in the feed is to be recovered in the distillate, and 90 percent of the heavy key in the feed is to be recovered in the bottom." This sets both the distillate rate to $(z_{LNK} + 0.95z_{LK} + 0.10z_{HK})F$, and the heavy key concentration of the distillate at

$$\frac{0.10z_{HK}}{0.95z_{LK} + 0.10z_{HK} + z_{LNK}}$$

Example 3.3 in Sec. 3.2.3 uses a double-recovery specification.

Composition specification. If one recovery or one product flow is specified, the concentration of one component either in the distillate or in the bottom (but not both) can be specified. If neither a recovery nor a product rate is specified, the concentration of one component in the distillate and one component in the bottom can be specified.

The above applies to both binary and multicomponent distillation. In multicomponent distillation, once the above are specified, other components will distribute according to the equilibrium relationship. Frequently, a product spec sets the maximum concentration of impurities that can be tolerated in the product. Product specs are "less than" specifications. The one impurity which is dependent on the column separation and is most difficult to achieve sets the composition specification in the column. This is illustrated in Table 3.1 for a propylene-propane separation (C_3 splitter). Since the light nonkeys (hydrogen, methane, ethylene, ethane, and oxygen) end up in the distillate, their concentration in the distillate is independent of the column. Of the others, the most difficult purity to achieve sets the composition specification. Similarly, the heavy nonkeys (MAPD, C_4 and

TABLE 3.1 Typical Product Specs for a C_3 Splitter

Component	Top product—polymer grade propylene	Bottom product—propane
Hydrogen	< 10 ppmv	< 100 ppmv
Methane	< 4000 ppmv	< 0.5%
Ethylene	< 50 ppmv	< 1%
Ethane	< 4000 ppmv	< 1%
Propylene	> 99.5 mole	< 5% mole
Propane	< 5000 ppmv	> 90% mole
MAPD (methyl acetylene/propadiene)	< 5 ppmv	< 5% mole
Butadiene	< 1 ppmv	< 1% mole
Butenes	< 50 ppmv	< 1% mole
Butanes	< 4000 ppmv	< 10% mole
C_5+	< 1 ppmv	< 2% mole
Oxygen	< 1 ppmv	< 5 ppmv
Sulfur	< 2 ppmw	< 10 ppmw

heavier, and sulfur) end up in the bottom product; their concentration in the bottom product is independent of the column. Of the others, the most difficult purity to achieve sets the composition specification.

Sometimes, column design has a bearing on which spec is most difficult to achieve. For instance, in some C_3 splitters, the feed point location has a greater effect on MAPD than on the propane concentration in the top product. With a low feed point, the propane spec may be the most difficult to achieve; with a high feed point, the MAPD spec may be more difficult to achieve. The nonkey content of the feed also has an effect. For instance, if the methane plus ethane in the product is 500 ppmv, then up to 4500 ppm propane can be tolerated. This may be easier to achieve than the MAPD spec. On the other hand, if methane plus ethane is 3000 ppm, then no more than 2000 ppm of propane can be tolerated. This may be more difficult to achieve than the MAPD spec.

Physical property specification. A product composition can often be specified in terms of a physical property that is a direct function of composition. For instance, the vapor pressure of a bottom product is often a good measure of the concentration of lights in the bottoms, and may be specified instead. Other physical properties include the Reid vapor pressure (RVP), viscosity, refractive index, freezing point, mo-

lecular weight, and others. A physical property specification is often preferred either when it is easy to monitor (e.g., refractive index), or when it provides a good functional spec of product purity.

Heat duty (or internal flow) specification. A composition or product rate specification may be substituted by a heat duty or internal flow (e.g., reflux) specification. This is done either to improve convergence in a computer simulation (especially if compositions are in the part per million levels), or in a revamp when the column or its exchangers are at a capacity limit. The mass, component, and energy balance equations translate this specification into a composition or product rate specification. Sections 4.2.3 and 4.3.1 have some further discussion.

Side product. For each side product, one additional specification is required. This specification is either a product rate (e.g., the side product rate) or a product composition.

Heat addition or removal. For each point of heat addition or removal, an additional specification is required. This specification is usually a heat duty or an internal product flow.

3.1.2 Optimizing product recovery (material balance optimization)

The previous section assumed that product composition (or product flow) requirements are fixed. In this very common situation, the optimum design minimizes the costs of achieving these requirements. Often, product specs are not fixed, but depend on economics. Even when a product must obey a "less than" purity spec, better purity may fetch a better price. The better price may justify additional investment in equipment and/or a higher operating cost. Here, a design must optimize product purity value versus distillation cost. This optimization is also important in an operating column and is commonly performed by on-line computer control. It is outlined below, and discussed in detail elsewhere (1,2).

Material balance optimization. Figure 3.1*a* shows the concentration of the light key at the distillate and bottoms at a fixed separation S, where

$$S = (x_{LK}/x_{HK})_D\,(x_{HK}/x_{LK})_B \tag{3.3}$$

The x axis of Fig. 3.1*a* is D/F, or the distillate recovery. When D/F approaches zero, almost all the material entering the column leaves in the bottoms. The bottom composition approaches the feed composition,

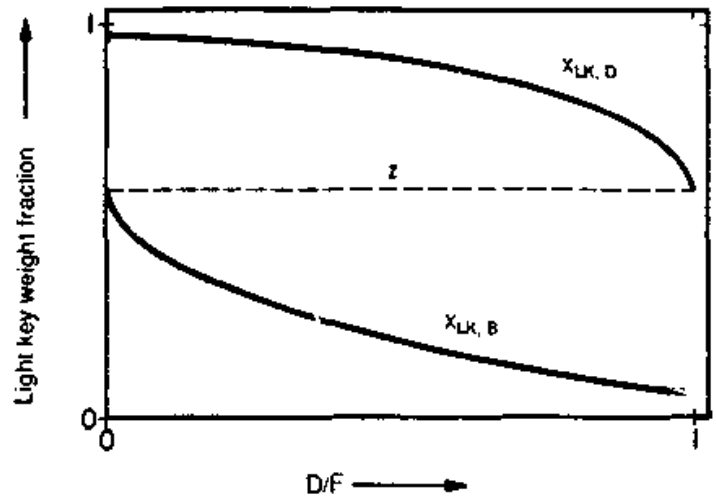

(a)

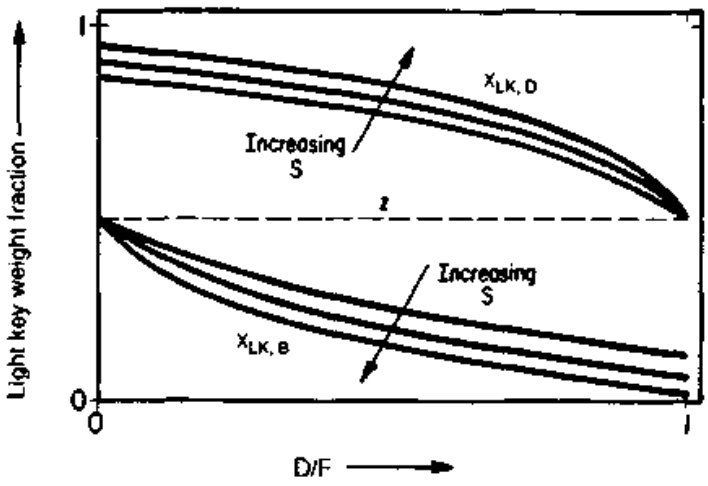

(b)

Figure 3.1 Concentration of the light key component at the distillate and bottom products. (*a*) At a single separation, S (or at a single reflux ratio); (*b*) effect of S (or of reflux ratio). (Reprinted by permission. Copyright © Instrument Society of America, 1978, from P. R. Latour, *Instrumentation Technology*, July 1978).

while the distillate contains the highest possible fraction of light key. The converse applies when D/F approaches unity.

Fixing S is equivalent to setting a composition specification. At a fixed S, each D/F in Fig. 3.1*a* specifies a recovery and a composition. These specifications are sufficient for setting all product flows and purities (Sec. 3.1.1). Since D/F fixes distillate and bottoms flows and purities, each D/F also fixes the total product value. The total (distillate plus bottom product) values can therefore be calculated and plotted against D/F at fixed S (Fig. 3.2).

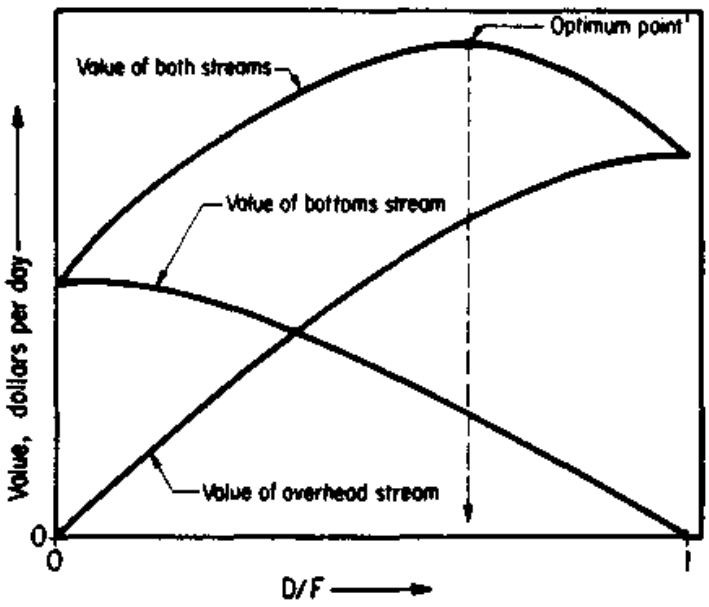

Figure 3.2 Material balance optimization at a fixed separation S (or reflux ratio). (Reprinted by permission. Copyright © Instrument Society of America, 1978, from P. R. Latour, *Instrumentation Technology*, July 1978).

The optimum in Fig. 3.2, termed the *optimum recovery value,* gives the highest total aggregate value of the top and bottom products. At lower recovery (D/F), more bottoms are produced, but at a lower purity (and, therefore, at a lesser value). At higher recovery, more distillate is produced, but at a lower purity (and therefore at a lesser value).

Not shown on Fig. 3.2 are constraints. Each product usually has a maximum impurity level, beyond which it cannot be sold or utilized. Each constraint can be marked on the diagram either as a vertical line at the D/F value corresponding to this maximum impurity level, or as a drop of product value to zero (or even negative) at that point. A constraint precludes operation at the optimum recovery value when the optimum coincides with one of the products being "off-spec." The best product value is then realized where the vertical constraint line meets the aggregate value curve.

In the above discussion, the optimization was described as a function of the recovery D/F. This was done for convenience only. The same optimization can also be described in terms of any other variable. Figure 3.3 shows a similar optimization (2), where product losses are described as an annual cost on the y axis, and the bottoms concentration is the x axis. As in Fig. 3.2, the curve in Figure 3.3 is for a fixed separation S.

The optimization described so far is referred to as *material balance optimization,* or *D versus B optimization.* At a fixed separation, the capital and utility costs of the column are relatively insensitive to the

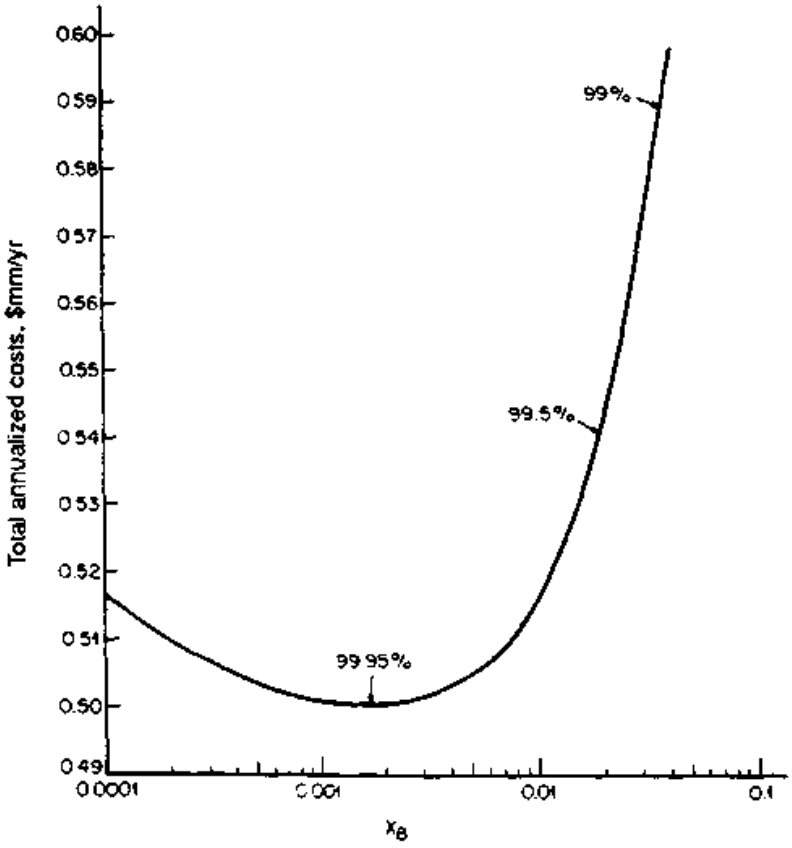

Figure 3.3 Material balance optimization at a fixed separation S. Numbers marked on curve show the percent recovery of light component in the distillate stream. (Reprinted with permission from W. R. Fisher, M. F. Doherty, and J. H. Douglas, *Ind. Eng. and Chem. Proc. Des. and Devel.*, Vol. 24, p. 955, Copyright © (1985), American Chemical Society.)

location of the optimum. This is because the costs are primarily dependent on the separation S, which is assumed to be fixed.

In an operating column, a symptom of nonoptimum material balance is one product far purer than needed, and the other experiencing excessive impurity levels. The culprit is usually a deficiency in the control system or a constraint in the column.

3.1.3 Optimizing separation (energy balance optimization)

Figure 3.1*b* shows the effect of changing separation on Fig. 3.1*a*. For a fixed recovery (D/F), the greater the separation, the better the purity of both products.

Unlike the material balance optimization, which has a relatively small impact on the column capital and utility costs, the energy balance optimization is the prime factor setting these costs. Reflux and stage requirements strongly depend on the separation S. The greater S, the higher the reflux and stage requirements, and the greater the

capital and utility costs. For an existing column, the capital costs are fixed, but the utility costs increase with S.

Diagrams similar to Fig. 3.2 can be drawn for several different values of S. Constraints should be marked on each. Each diagram determines the best product value within the constraints. The best product values are plotted against S, normally showing a monotonous increase with S. On the same plot, a cost curve is required. A rough column design, therefore, needs to be performed separately for several values of S. Each design should be performed at the best achievable recovery for the given S (i.e., from Fig. 3.2, taking constraints into account). The capital cost needs to be expressed as dollars per day; this can be obtained by dividing the total capital cost by the life (or equivalent life based on discounted cash flow) of the column. The capital cost for a given value of S is then added to the corresponding operating cost, and the total is plotted as a point against S. The costs should include the column auxiliaries (e.g., reboiler reflux pumps) and allow for effects on other equipment (e.g., cooling tower, vent header). The total costs would normally monotonously increase with S.

The difference between the product value and the total costs can now be determined for each value of S. This difference is the profit from the separation as a function of S. The profit curve will normally show a maximum (unless restricted by constraints). The highest profit will set the optimum value of S. Going back to the Fig. 3.2 diagram for the optimum value of S, the optimum D/F value can be determined. This procedure sets the optimum product purity and recovery values.

Figure 3.4 illustrates this type of analysis for an existing column. Since the number of stages is fixed, S becomes a function of the reflux

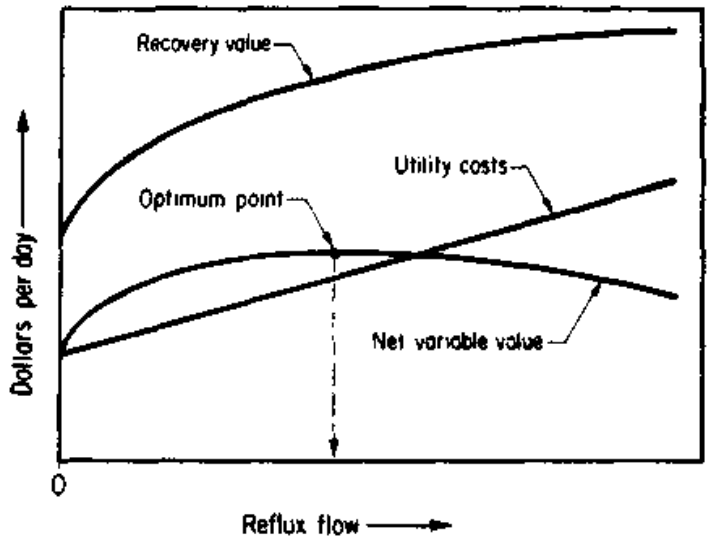

Figure 3.4 Reflux rate optimization for an existing column. (Reprinted by permission. Copyright © Instrument Society of America, 1978, from P. R. Latour, *Instrumentation Technology*, July 1978.)

only. For simplicity, the reflux rate can be used instead of S. Further, since the column is existing, there is no capital cost, and all the costs involved are utility costs. Therefore, the total costs curve becomes the utility costs curve. The "net variable value" is the difference between the recovery value (or product value) curve and the utility costs curve, and features an optimum. Not shown on Figure 3.4, but extremely important for existing columns, are constraints on reflux flow. For instance, the boilup is a function of reflux flow; as reflux flow is raised, the reboiler may reach its maximum capacity. This needs to be expressed as a limiting reflux flow, and is shown as a vertical constraint line on Fig. 3.4. Similarly, constraints related to column flooding, condenser capacity, minimum liquid flow, etc., need also to be shown as vertical constraint lines on Fig. 3.4. Often, such constraints may prohibit operation at the optimum.

3.1.4 Application of recovery and separation optimization

The analysis in Secs. 3.1.2 and 3.1.3 is important whenever product specs are not well defined, or whenever there may be an incentive to generate a product better than the specs. The analysis applies both to new and existing columns. In existing columns, this optimization is often incorporated in a computer control strategy and performed on-line. When computer control is unavailable, the optimization can be performed off-line and translated into operating procedures.

In the above analysis, it was assumed that product prices and the value of products as a function of their impurity content are well defined. Often, this is not so, for example, when one of the products is recycled to a reactor. In this case, the product value needs to be calculated as a function of its impurity content from data on the expected effect of impurity and recycle on the reactor performance. This analysis can become complicated.

One variable not considered in the analysis is fluctuations in feed composition. Such fluctuations may have an effect on product values and on the separation, and need to be considered in the optimization. Where significant fluctuations are expected, it may be worthwhile to work with component recoveries (Dx_{LK}/Fz_{LK}) rather than D/F.

The analysis also did not take into account the thermal state of the feed. In most situations, the thermal state can be optimized separately before the product recovery and separation are optimized. If the thermal state optimization leads to the conclusion that preheating or precooling is unjustified, and the thermal state is likely to vary (e.g., feed coming in from a reactor), fluctuations in this thermal state need to be taken into account in the product specs and recovery optimization.

Finally, it should be noted that the optimization described above is of a shortcut nature. The author is yet to encounter a practical situation where the recovery and separation optimization is performed more rigorously. In the majority of new designs experienced by the author, the optimization did not even go that far. Procedures for more rigorous optimization are available (e.g., Ref. 3), but uncertainties in product values, project life, and costs often makes further fine-tuning difficult to justify.

3.1.5 Setting column pressure

Raising column pressure

Unfavorable effects

1. Lowers relative volatility and increases separation difficulty. This raises reflux and stage requirements and reboiler and condenser duties.
2. Raises column bottom temperature. This increases chemical degradation, polymerization, and fouling.
3. Above about 100 psig, increases column shell thickness (4,5) and, therefore, capital cost. This is not a significant factor at pressures lower than about 100 psig (4).
4. Raises reboiler temperature, thereby requiring an unavailable or a more expensive heating medium. For the same heating medium, it increases the reboiler area requirement.
5. For superatmospheric separations, it increases leakage, and if process materials are inflammable or toxic, also the hazard potential.

Favorable effects

1. Increases the distillate boiling point and permits using a cheaper cooling medium. For the same cooling medium it reduces the condenser area requirements.
2. Below 1 atm, reduces the costs of creating and maintaining a vacuum (e.g., ejector energy consumption and capital costs).
3. Increases vapor density and therefore vapor-handling capacity. This leads to major reductions in column diameter and capital costs under vacuum, and to smaller reductions up to pressures of 50 to 150 psia (6).
4. In distillation of liquefied gases, raises boiling points of the column liquid. This allows cheaper construction materials to be used.
5. Reduces the size of vapor pipes and valves.

6. Below 1 atm, reduces air leakage into the system. In case of flammable materials, this also reduces the associated hazards.

Setting the pressure. Either the second or the fourth consideration on the "unfavorable" list is almost always the sole reason for going to vacuum. When chemical degradation, polymerization, or fouling are not significant, and when an adequate heating medium is available, separation is carried out at or above atmospheric pressure. For vacuum separations, it is desirable to set the pressure as high as possible, due to the third, and to a lesser degree also the second, favorable factors. The pressure is therefore set at the highest possible pressure that provides a bubble-point temperature sufficiently low to prevent significant degradation of the bottom materials and to be satisfactorily reboiled with the available heating medium.

For pressure separations, the controlling factors are usually the first favorable and first unfavorable effects. The pressure is usually set at the lowest possible pressure that permits satisfactory condensation using cooling water or air. A satisfactory temperature approach between the coolant and distillate is normally 10 to 20°F with cooling water, and 30 to 50°F with air.

For separation of liquefied gases, the critical temperature of the distillate may be lower than the cooling water temperature, and refrigeration is needed. The economic balance is still primarily between the first favorable and first unfavorable effects, but the refrigeration complicates the analysis. Optimization is required for selecting the best pressure, and can be lengthy and tedious if correctly performed. Shortcuts often lead to nonoptimum conclusions. Each case must be considered on its own merits. An example of such an optimization for an ethylene-ethane separation column, as well as of some optimization pitfalls, is described elsewhere (7).

3.1.6 Optimum reflux ratio

As reflux ratio is raised,

- Condensing and reboiling duties rise. Since these make up the bulk of the column operating costs, operating costs also rise.
- The number of stages decreases (Fig. 3.5), making the column shorter, but column diameter increases. Near minimum reflux, small increases in reflux ratio considerably shorten the column, but only marginally increase its diameter. Capital cost declines. Upon further increases in reflux, the height reduction slows down while the diameter increases accelerate. Eventually, the savings from the shorter column become less than the cost of increasing

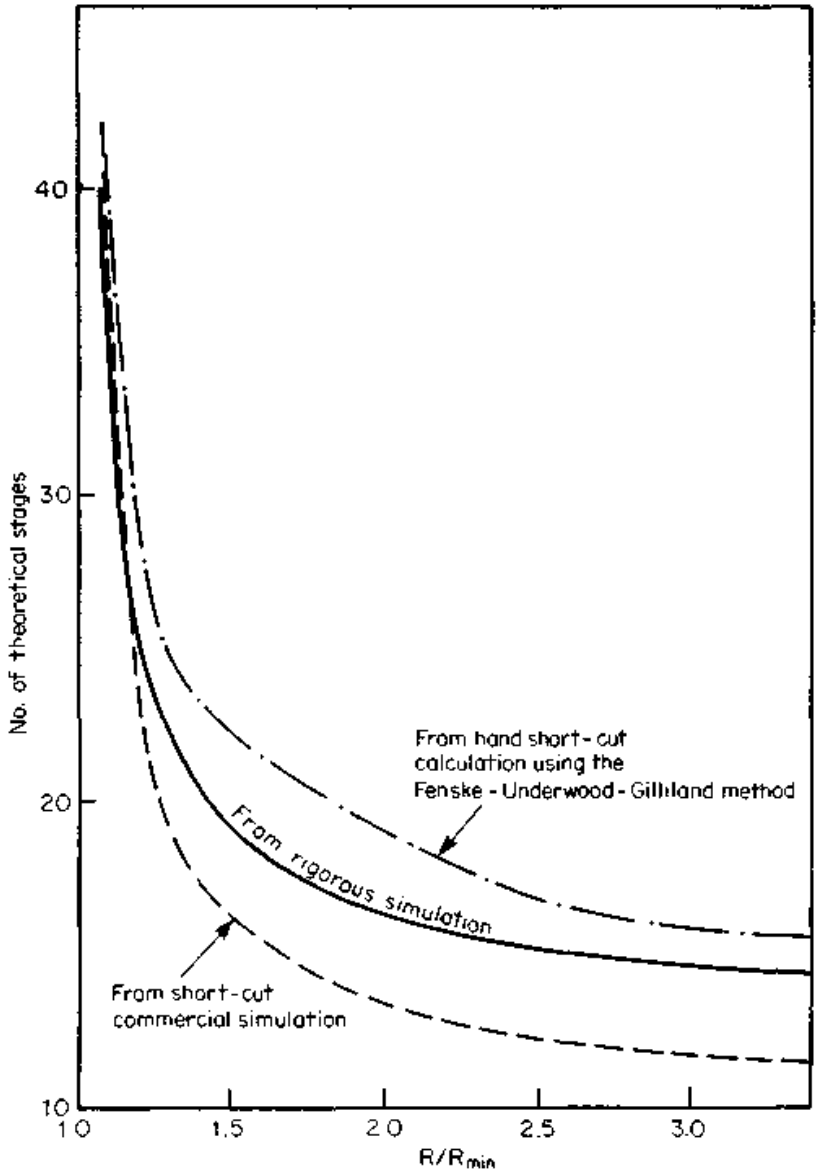

Figure 3.5 Stages-reflux relationship for the depropanizer in Example 3.4.

the diameter, and capital costs begin to escalate as reflux ratio is raised.

Figure 3.6*a* shows how costs for a new distillation system vary with the reflux ratio. It expresses the capital cost as an annual cost. This can be achieved by dividing the capital cost by the expected payout period. A discounted cash flow (DCF) analysis is used for estimating this payout period. The capital cost should include the costs of auxiliaries (reboiler, condenser, vacuum equipment, pumps, piping; in many cases, costs of vent systems, coolant, and heating medium handling equipment are also affected). The operating costs should include reboiler

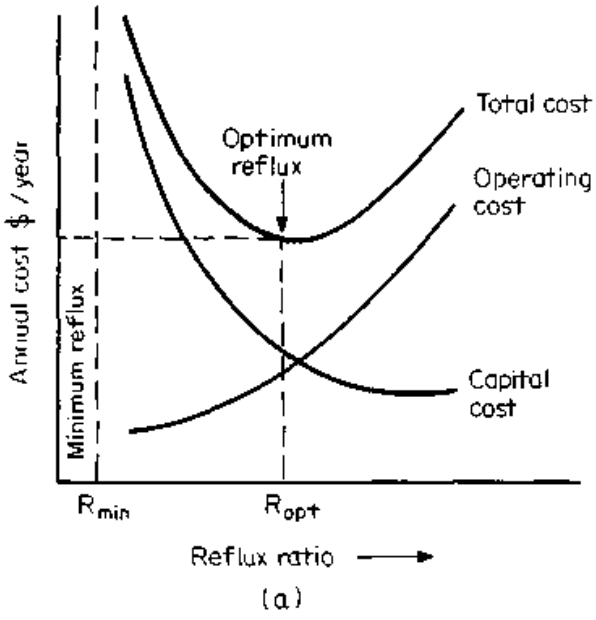

Figure 3.6 Optimum reflux ratio. (*a*) Capital and operating cost curves; (*b*) effect of using expensive materials of construction on the optimum; (*c*) effect of high energy costs on the optimum; (*d*) optimum reflux, toluene-benzene separation, show a flat total cost curve near the optimum. (Part *d* reprinted with permission from W. R. Fisher, M. F. Doherty, and J. M. Douglas, *Ind. Eng. and Chem. Proc. Des. and Devel.*, Vol. 24, p. 955, Copyright © (1985) American Chemical Society).

heat, coolant, reflux pumping, and utility pumping. In most water-cooled and air-cooled columns, the cost of reboiler heat is the dominant operating cost.

Figure 3.6*a* shows that there is an optimum reflux ratio. Using expensive materials of construction (ALLOY curves in Fig. 3.6*b*) shifts the optimum to the right, and favors high-reflux designs. High energy cost (HEC curves in Fig. 3.6*c*) shifts the optimum to the left, favoring operation closer to minimum reflux.

With energy-saving designs, optimum reflux is often near minimum reflux. Here small errors in relative volatilities and enthalpies lead to large errors in the number of trays. In addition, any maldistribution will cause part of the column to operate below minimum reflux, and the separation will not be achieved. It is customary to leave a safety margin from minimum reflux. An excellent alternative practice for towers whose optimum reflux is close to minimum is (8) to leave this safety margin only in the design of the reflux system and utilities. The number of trays is designed to the optimum reflux. This practice permits approaching minimum reflux while safeguarding against potential disasters arising from volatility and enthalpy errors or maldistribution near minimum reflux.

The total cost curve tends to flatten near the optimum. Figure 3.6*d*, based on a benzene-toluene separation case study (2), shows a total cost within 2 percent of the optimum for reflux ranging from 1.15 to 1.5 times the minimum. King (9) reached an identical conclusion and demonstrates it with an entirely different case study. The author observed this flatness in many actual designs.

Rules of thumb are often used by designers to shortcut reflux opti-

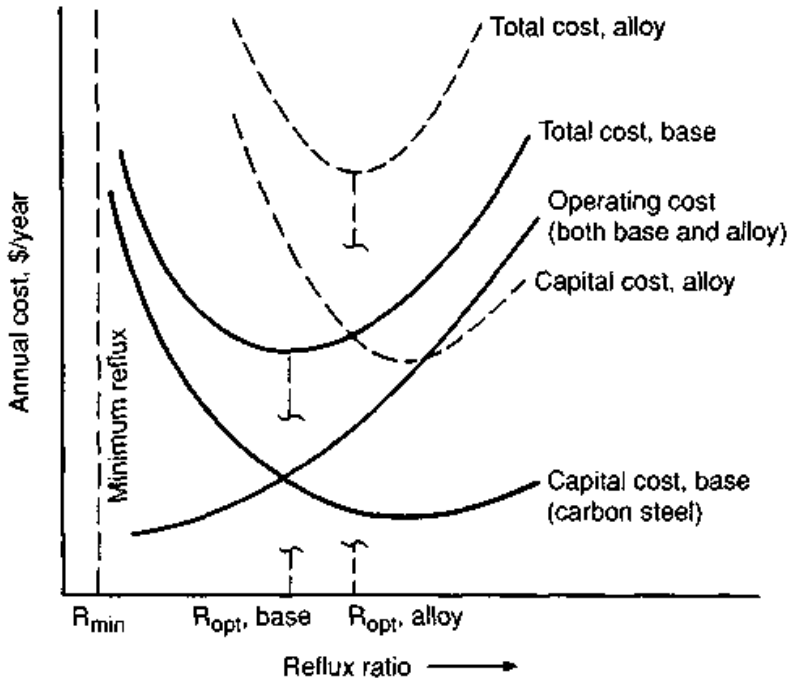

(b)

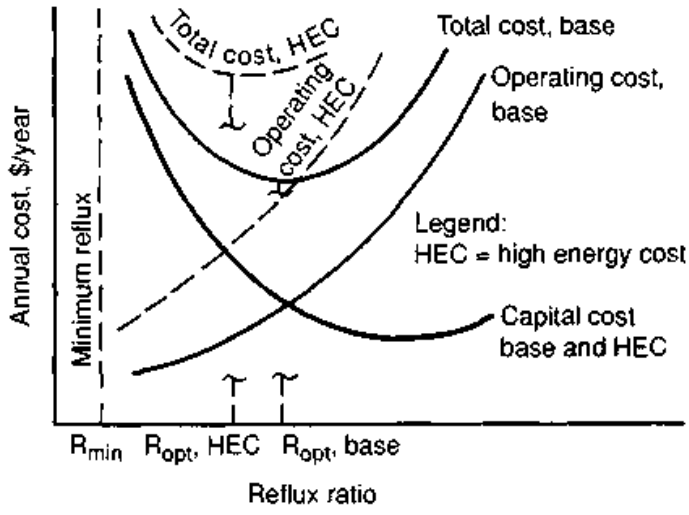

(c)

Figure 3.6 (*Continued*) Optimum reflux ratio. (*b*) effect of using expensive materials of construction on the optimum; (*c*) effect of high energy costs on the optimum;

mization. Due to the flatness of the total cost curves near the optimum, this shortcut usually incurs no more than a minor economic penalty. The rules of thumb are expressed as the optimum ratio of reflux to minimum reflux R_{opt}/R_{min}.

During the 1960s, when energy was cheap, R_{opt}/R_{min} ratios were high. An extensive survey by King (9), however, shows that even with cheap energy, these "high" ratios were generally very close (1.1 to

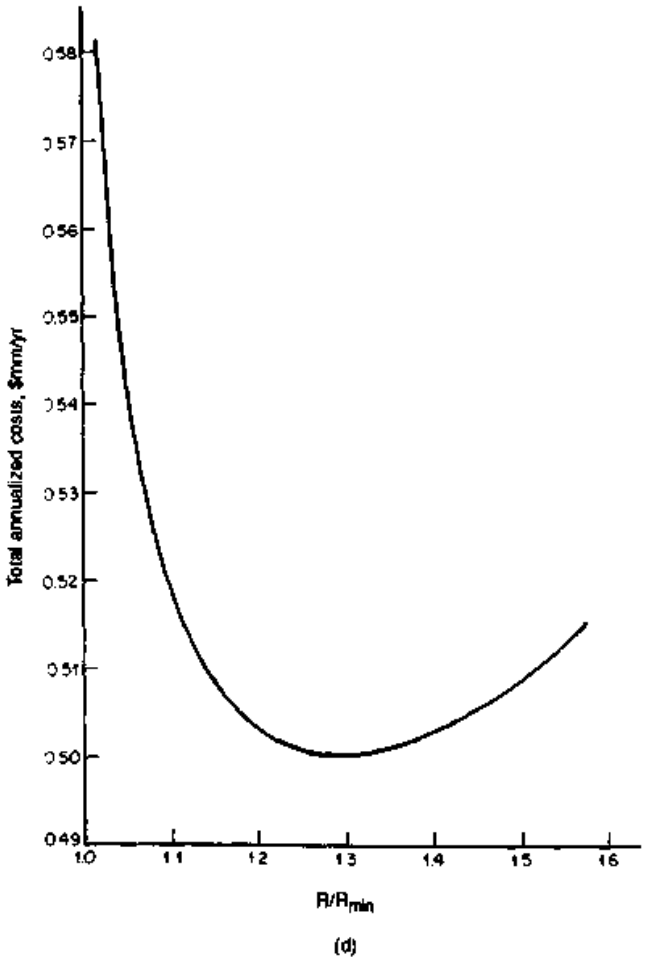

Figure 3.6 *(Continued)* Optimum reflux ratio. (*d*) optimum reflux, toluene-benzene separation, showing a flat total cost curve near the optimum. (Part *d* reprinted with permission from W. R. Fisher, M. F. Doherty, and J. M. Douglas, *Ind. Eng. and Chem. Proc. Des. and Devel.*, Vol. 24, p. 955, Copyright © (1985) American Chemical Society).

1.25 times) to the minimum. The optimum ratio dropped when the cost of energy sharply escalated in 1973. Although energy prices have declined since, the awareness of the high cost of energy remained, and so has the practice of using low R_{opt}/R_{min} ratios. Pre-1973 rules of thumb for optimum reflux are therefore not recommended. Rules of thumb proposed for R_{opt}/R_{min} in recent years are summarized in Table 3.2.

3.1.7 Feed stage optimization by computer

The ideal feed point can be determined by graphical (Sec. 2.3.7), shortcut (Sec. 3.2.6), or rigorous techniques. Commercial simulations often incorporate search techniques (e.g., Ref. 15) for seeking the optimum

TABLE 3.2 Rules of Thumb for R_{opt}/R_{min} Ratio

	R_{opt}/R_{min}	Ref.	Note
Water-cooled or air-cooled condensers (Note 1, 2)	1.2–1.3	10,11	
	1.2	2,12	
	1.1	9	3
	1.2–1.5	13	
High-level refrigeration condensers (Note 1)	1.1–1.2	10,13,14	
	< 1.1	9	
Low-level refrigeration condensers (< −150°F)	1.05–1.1	10,13	1,4

[1]Presumably, the rules are based on carbon and stainless steel. For columns constructed out of more expensive materials, R_{opt}/R_{min} is higher (Fig. 3.6*b*).

[2]Presumably, these rules are based on steam, hot oil, or a similar heating medium. For columns reboiled with waste heat, R_{opt}/R_{min} ratios as high as 1.4 to 1.5, and even larger, are often optimum.

[3]Author of this rule presents a thorough survey to back it up.

[4]Due to uncertainty in the vicinity of minimum reflux (see text), the author does not recommend designing for R_{opt}/R_{min} lower than 1.1.

feed stage. These are usually based on minimizing an objective function. Small variations are introduced to the feed point, and their effect on top and bottom compositions is estimated by a rigorous or shortcut method. The results are substituted into the objective function, and the next trial begins with the feed entering a stage for which the objective function is lower.

Alternatively, results from a computer simulation can be plotted to determine the optimum feed stage. Simulation runs are performed at several different feed points, keeping the material balance, reflux ratio, and total number of stages constant. Key component concentrations in the product streams are plotted against the feed stage number (Fig. 3.7). The minimum is at the optimum feed stage.

Generally, the ratio of optimum feed stage to total number of stages is independent of the number of stages. This is predicted from Fenske's feed point relationship (Sec. 3.2.6). In Fig. 3.7*a*, optimum N_S/N is between 0.44 and 0.47 for N between 15 and 25. On the other hand, the optimum N_S/N is a strong function of the material balance (Fig. 3.7*b*). Reducing the distillate rate shifts the ideal feed stage down the column, while reducing the bottoms rate shifts it up the column. In Fig. 3.7*b*, a product rate shift of less than 2 percent shifts the optimum feed by more than 3 stages out of 20.

The minima are usually flat, but steepen as a pinch or as minimum reflux is approached. They appear quite flat in Fig. 3.7 even though reflux declines from 2.6 times to 1.2 times the minimum (as the number of stages rises from 15 to 25). The steepening of the minima as reflux is lowered would have been apparent had the x-axis of Fig. 3.7*a* been the ratio of rectifying (or stripping) stages to total stages.

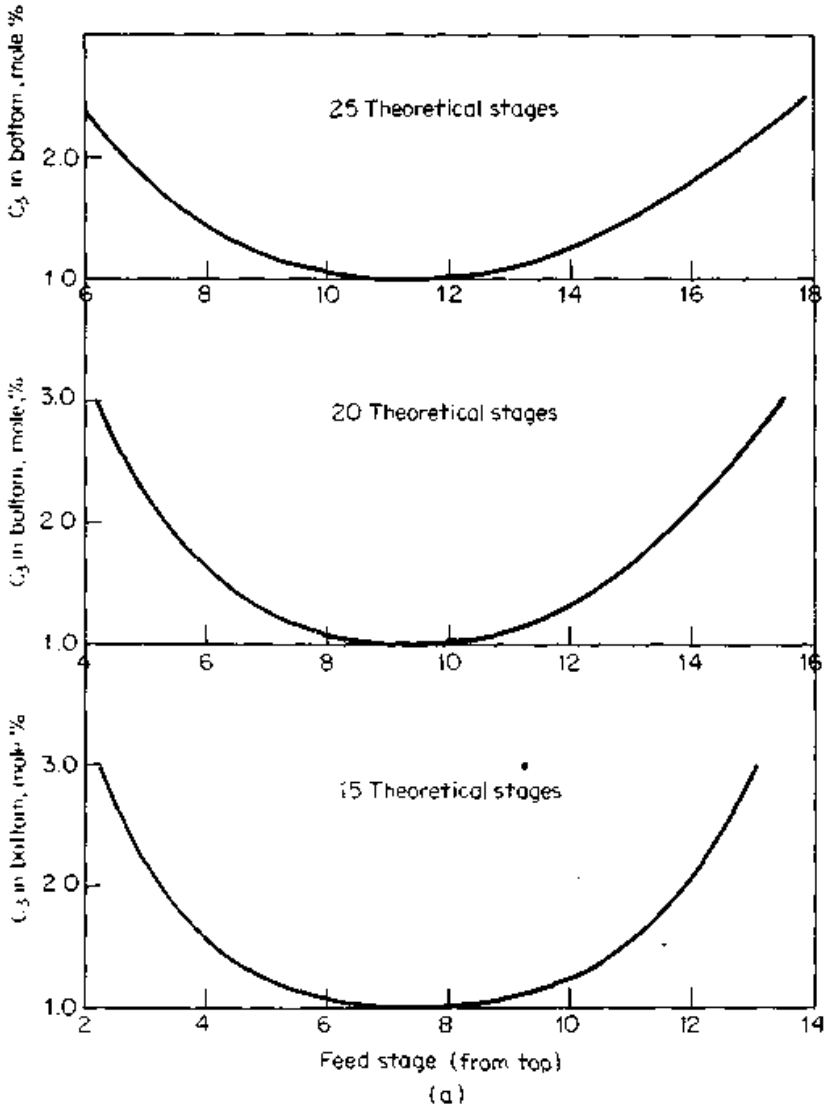

Figure 3.7 Feed point optimization by plotting results of computer simulation, depropanizer in Example 3.4. (*a*) Effect of the total number of stages $F = 100$, $D = 59.9$

3.1.8 Minimum reflux by computer

Minimum reflux can be determined by graphical (Secs. 2.3.5, 2.4.1), shortcut (Secs. 3.2.2 to 3.2.4), or rigorous techniques. Most graphical and shortcut methods give good results either when constant molar overflow (Sec. 2.2.2) applies, or when the method is corrected for energy balance. Unfortunately, shortcut methods in most commercial simulations apply no energy balance correction, and wild minimum reflux predictions are not uncommon.

Rigorous procedures (e.g., Refs. 15 to 20) accurately predict minimum reflux. Since convergence of rigorous calculations near minimum reflux is extremely difficult, these methods often fail to converge. Bolles (21) reported that Chien's rigorous method (20) works extremely well for practically all systems, even the highly nonideal,

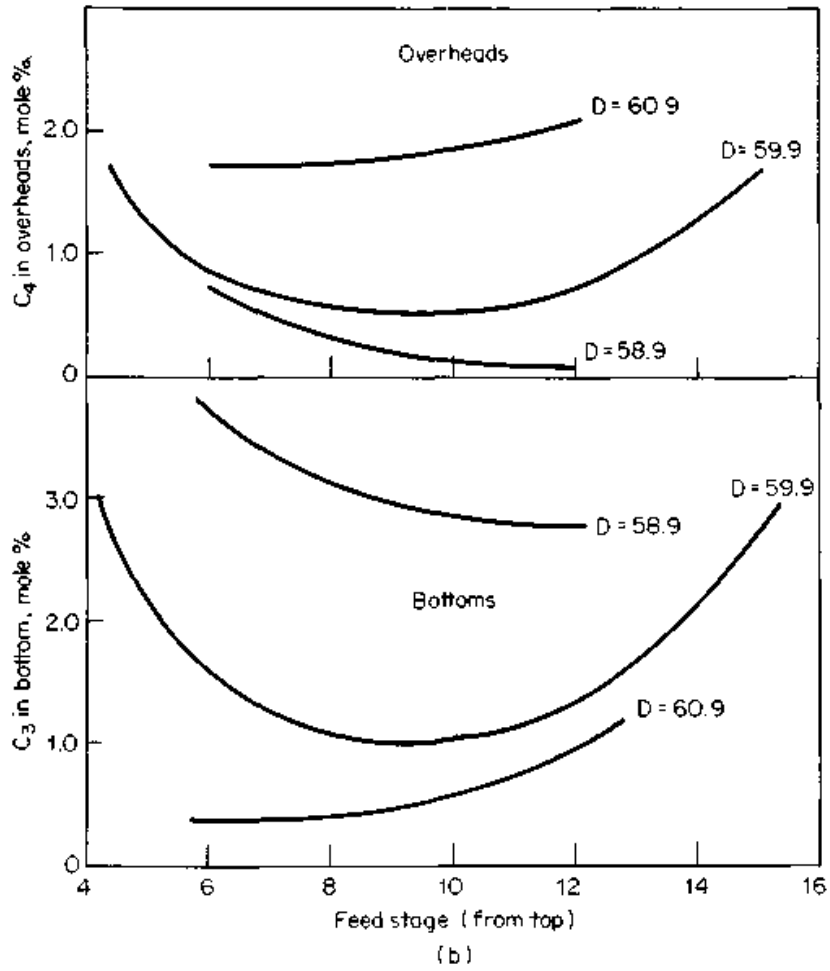

Figure 3.7 (*Continued*) Feed point optimization by plotting results of computer simulation, depropanizer in Example 3.4. (*b*) effect of column material balance $N = 20$.

with no convergence difficulties. Chien (20) stated that his method experiences convergence problems only when a tangent pinch is encountered (Fig. 2.12). Chien's method is incorporated in Monsanto's FLOWTRAN simulator.

A simple method (22) which rigorously calculates minimum reflux without convergence problems is extrapolation of the reflux-stages plot (Fig. 3.8). Simulation runs are performed at different numbers of stages, keeping the material balance, product compositions, and N_S/N constant, while letting reflux rate vary. For each run, the number of stages is plotted against reflux, and the curve is extrapolated asymptotically to an infinite number of stages.

An alternative method proposed by Rose (23) is to plot $1/R$ versus $1/N$, extrapolating to $1/N$ of zero to obtain minimum reflux. The author found this extrapolation to be far more difficult, and also this plot to be a curve and not the straight line shown by Rose (23).

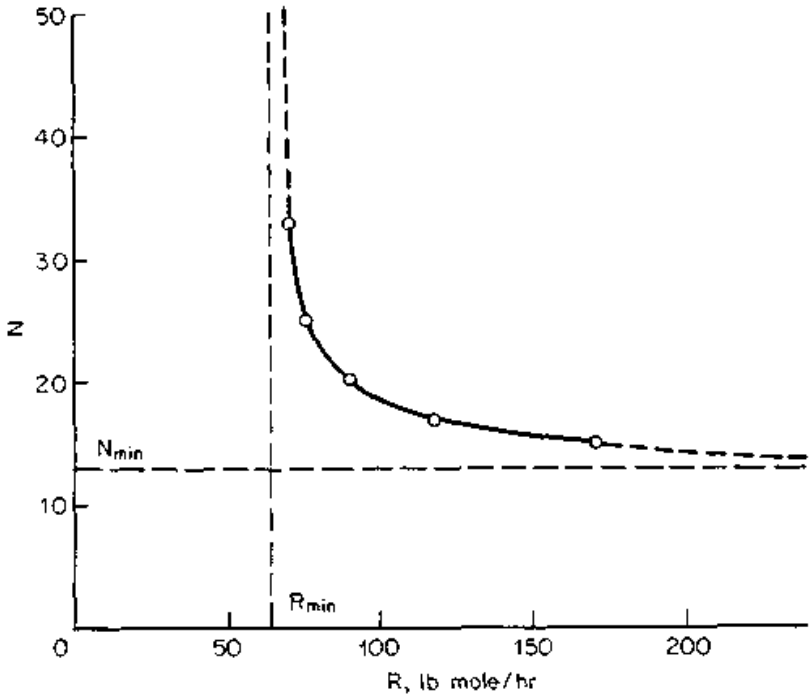

Figure 3.8 Calculating minimum reflux and minimum stages by extrapolating the reflux stages curve obtained by computer simulation. Depropanizer in Example 3.4, D = 59.9 lb-mole/h.

3.1.9 Minimum stages by computer

Minimum stages can be determined by graphical (Sec. 2.2.8), shortcut (Sec. 3.2.1), or rigorous techniques. Usually, shortcut techniques are satisfactory, providing a good approximation is applied for relative volatility. For systems where relative volatility varies widely from column top to bottom, a more rigorous method may be desired. Chien (24) presented such a method, and Bolles (21) reported favorable experiences with it. Alternatively, extrapolation of a reflux-stages plot (Fig. 3.8) to infinite reflux gives a rigorous approximation of the minimum number of stages, as outlined in Sec. 3.1.8.

3.1.10 Process design procedure

Process design proceeds in the following steps:

1. Specify separation. If product composition or product flow requirements are not defined, determine them by material and energy balance optimization.
2. Set column pressure.
3. Determine the minimum reflux and minimum number of stages.
4. Find the optimum feed stage.

5. Select three ratios of actual to minimum reflux. For each, calculate a number of stages and size the column and auxiliaries. Determine which is the most economical. This optimization procedure can be bypassed by selecting a single ratio of reflux to minimum reflux.
6. The calculations so far can be shortcut or rigorous. If a rigorous (tray-by-tray) calculation has not been performed yet, now is the time.
7. Reexamine steps 3 and 4, refining earlier estimates as necessary. If the refinements are large, steps 5 and 6 may need repeating.
8. Analyze the design graphically (Sec. 2.4) to ensure optimum design and absence of pinched regions.

3.2 Reflux and Stages: Shortcut Methods

3.2.1 Minimum stages

The minimum number of stages is given by Fenske's equation (25)

$$N_{\min} = \ln S / \ln (\alpha_{LK/HK})_{av} \tag{3.4}$$

where S was given earlier by Eq. (3.3)

$$S = (x_{LK}/x_{HK})_D (x_{HK}/x_{LK})_B \tag{3.5}$$

The Fenske equation was shown to be rigorous (25) if

$$(\alpha_{LK/HK})_{av} = \sqrt[N]{\alpha_{LK/HK,1}\alpha_{LK/HK,2}\cdots\alpha_{LK/HK,N}} \tag{3.6}$$

However, $(\alpha_{LK,HK})_{av}$ is usually obtained from one of the following approximations:

1. Evaluate α_{av} at $T_{av} = (T_{top} + T_{bot})/2$
2. $\alpha_{av} = (\alpha_{top} + \alpha_{bot})/2$
3. $\alpha_{av} = \alpha$ at feed tray temperature
4. $\alpha_{av} = \sqrt{\alpha_{top}\alpha_{bot}}$
5. $\alpha_{av} = \sqrt[3]{\alpha_{top}\alpha_{mid}\alpha_{bot}}$

(3.7)

Method 1 was recommended by Maddox (26,27); method 2 was recommended by Van Winkle (28), method 4 or 5 was recommended by Fair (29), Seader and Kurtyka (30), and McCormick and Roche (13), method 3 or 4 was preferred by King (9), while method 4 was preferred by a number of designers (11,31–33). Douglas (34) proposed a criterion for testing the relative volatility approximation.

$$\frac{\alpha_{top} - \alpha_{bot}}{\alpha_{top} + \alpha_{bot}} \leq 0.1 \ln \frac{\alpha_{top} + \alpha_{bot}}{2}$$

When the above inequality is obeyed, relative volatility is reasonably constant throughout the column, and the simpler approximations such as 2 or 4 are appropriate.

The Fenske equation applies not only to the light key and heavy key components. It can also be applied to any pair of components.

Winn's modification. In an attempt to account for temperature variation of the relative volatility, Winn (35) proposed the equation

$$N_{min} = \frac{\ln \left[\dfrac{x_{LK,D}}{x_{LK,B}} \left(\dfrac{x_{HK,B}}{x_{HK,D}} \right)^{\theta_{LK}} \right]}{\ln \beta_{LK/HK}} \tag{3.8}$$

$\beta_{LK/HK}$ and θ_{LK} are constants at a fixed pressure, evaluated from the K-values for the light key and heavy key at the top and bottom temperatures. $\beta_{LK/HK}$ and θ_{LK} are related to each other by (35)

$$\beta_{LK/HK} = K_{LK}/(K_{HK})^{\theta_{LK}} \tag{3.9}$$

The Winn equation reduces to Fenske's equation when $\theta_{LK} = 1.0$ and $\beta_{LK/HK} = \alpha_{LK/HK}$.

Example 3.1 Evaluate the minimum number of stages for the depropanizer in Example 2.4 using each of the methods described above. Use the following data:

	Top	Middle	Bottom	@ T_{av}
K_{LK} (propane)	0.514	1.584	2.146	1.381
K_{HK} (n-butane)	0.177	0.847	1.359	0.710
α	2.904	1.870	1.579	1.945

solution The separation parameter S is determined from Eq. (3.5)

$$\ln S = \ln \left(\frac{0.41}{0.005} \frac{0.417}{0.01} \right) = 8.137$$

Calculate α_{av} according to Eqs. (3.7)

1. $\alpha_{av} = 1.945$ $N_{min} = 8.137/\ln 1.945 = 12.2$
2. $\alpha_{av} = (2.904 + 1.579)/2 = 2.242$ $N_{min} = 8.137/\ln 2.242 = 10.1$
3. $\alpha_{av} = 1.870$ $N_{min} = 8.137/\ln 1.870 = 13.0$
4. $\alpha_{av} = \sqrt{2.904 \times 1.579} = 2.141$ $N_{min} = 8.137/\ln 2.141 = 10.7$
5. $\alpha_{av} = (2.904 \times 1.870 \times 1.579)^{1/3} = 2.047$

   $N_{min} = 8.137/\ln 2.047 = 11.4$
6. Using Winn's methods, find $\beta_{LK/HK}$ and θ_{LK} at the top and bottom [Eq. (3.9)]

$$\text{Top } \beta_{LK/HK} = 0.514/(0.177)^{\theta_{LK}}$$

$$\text{Bottom } \beta_{LK/HK} = 2.146/(1.359)^{\theta_{LK}}$$

Solving gives $\beta_{LK/HK} = 1.731$, $\theta_{LK} = 0.7011$

$$N_{min} = \frac{\ln\left[\dfrac{0.41}{0.01}\left(\dfrac{0.417}{0.005}\right)^{0.7011}\right]}{\ln 1.731} = 12.4$$

For comparison, extrapolation of rigorous computer simulation runs (Fig. 3.8) gives $N_{min} = 13$. Also, from the simulation and Eq. (3.6), $(\alpha_{LK/HK})_{av}$ was calculated to be 1.956. This gives

$$N_{min} = 8.137/\ln 1.956 = 12.1$$

In this example, α_{av} approximations 1 and 3 and Winn's method gave close estimates of N_{min}. Two of the less rigorous approximations of α_{av}, (2 and 4), gave poor estimates. A check using Douglas's inequality gives

$$\frac{\alpha_{top} - \alpha_{bot}}{\alpha_{top} + \alpha_{bot}} = \frac{2.904 - 1.579}{2.904 + 1.579} = 0.296$$

$$0.1 \ln \frac{\alpha_{top} + \alpha_{bot}}{2} = 0.1 \ln \frac{2.904 + 1.579}{2} = 0.081 < 0.296$$

Douglas's inequality is not obeyed; therefore, the simpler approximations of α_{av} (such as 2, 3, and 4) can be expected to be inaccurate.

3.2.2 Minimum reflux

Underwood's method (36). This method solves an equation which relates feed composition, thermal condition of the feed, and relative volatility at the average temperature of the column for a factor θ which lies numerically between the relative volatilities of the keys. This factor is substituted in a second equation which relates minimum reflux to relative volatility and distillate composition. The method assumes constant relative volatility at the mean column temperature and constant molar overflow (Sec. 2.2.2). This method gives reasonable engineering accuracy for systems approaching ideality (28). The Underwood method has traditionally been the most popular for minimum reflux determination. When no distributed key components are present, the method is

1. Find θ (which must lie between the relative volatilities of the keys) by trial and error from

$$\sum_{j=1}^{n} \frac{\alpha_j z_j}{\alpha_j - \theta} = 1 - q \tag{3.10}$$

2. Substitute θ in the following equation to calculate $(L/D)_{min}$:

$$\left(\frac{L}{D}\right)_{min} + 1 = \sum_{j=1}^{n} \frac{\alpha_j x_{Dj}}{\alpha_j - \theta} \tag{3.11}$$

Example 3.2 Calculate the minimum reflux for the depropanizer in Example 2.4 using Underwood's method.

solution Since the feed is 66 percent vapor, $1 - q = 0.66$.

To obtain relative volatilities, use the heavy key as reference such that $\alpha_{HK} = 1.0$. For all other components j $\alpha_j = K_j/K_{HK}$.

			$\alpha z/(\alpha - \theta)$				
			Trial 1	Trial 2	Trial 3		
Component	α	z	$\theta = 1.4$	$\theta = 1.37$	$\theta = 1.352$	x_D	$\frac{\alpha x_D}{\alpha - \theta}$
Methane	18.75	0.26	0.281	0.280	0.280	0.435	0.469
Ethane	4.75	0.09	0.128	0.126	0.126	0.15	0.210
Propane	1.94	0.25	0.898	0.851	0.825	0.41	1.353
Butane	1.00	0.17	−0.425	−0.459	−0.483	0.005	−0.014
Pentane	0.48	0.11	−0.057	−0.059	−0.061		
Hexane	0.24	0.12	−0.025	−0.025	−0.026		
			0.800	0.714	0.661 OK		2.018

$$\left(\frac{L}{D}\right)_{min} = 2.018 - 1 = 1.018, \text{ say } 1.02$$

This compares well with the value of 1.04 obtained from the Hengstebeck diagram (Sec. 2.3.5), and with a value of 1.07 obtained either from the Underwood method, corrected for nonconstant molar overflow (Sec. 3.2.4), or from extrapolation of computer simulation results (Fig. 3.8).

Graphical Underwood method. To eliminate the trial and error involved, Van Winkle and Todd (37) developed a graphical solution technique for obtaining θ. This technique is only applicable to bubble-point liquid feeds.

Other shortcut methods. Other methods are also available for minimum reflux calculations. Van Winkle (28) surveyed them and recommended Underwood's and two others:

1. *The Brown-Martin method (38):* This method is based on the observation that at the feed pinch point, the ratio of key components is essentially equal to their ratio in the liquid feed. This method is the least complicated and gives conservative estimates. Suitable mainly for hydrocarbons in situations where great accuracy is not required (28).

2. *The Colburn method (39):* This method calculates the minimum reflux ratio of the key components as if they formed a binary system, then corrects this value for light and heavy nonkeys. The Colburn method assumes constant molar overflow and constant relative volatility in each zone of constant composition in the column. This method is more elaborate, but has been recommended (28) as probably the most accurate shortcut method for minimum reflux.

3.2.3 Minimum reflux for systems containing distributed nonkeys

A component is said to be *distributed* (or distributing) at minimum reflux if it appears both in the distillate and the bottoms at minimum reflux. Usually, nonkeys are nondistributed (or nondistributing), that is, at minimum reflux the heavy nonkeys are totally contained in the bottoms and the light nonkeys in the distillate. A nonkey component may be distributed if

- It has a volatility very close to that of one of the keys, or
- If the specified separation of the keys is sloppy (i.e., not sharp), or
- If the nonkey has a volatility intermediate between the keys.

Shiras et al. (40) developed an equation to determine whether or not a component is distributed at minimum reflux

$$D_R = \frac{Dx_{D,i}}{Fz_i} = \frac{\alpha_i - 1}{\alpha_{LK} - 1}\frac{Dx_{D,LK}}{Fz_{LK}} + \frac{\alpha_{LK} - \alpha_i}{\alpha_{LK} - 1}\frac{Dx_{D,HK}}{Fz_{HK}} \qquad (3.12)$$

The relative volatilities are based on a reference value of 1.0 for the heavy key component. The Shiras et al. criterion applies at minimum reflux as follows:

$D_R > 1$	Component is nondistributed; contained entirely in distillate.
$0 < D_R < 1$	Component distributed, D_R is the recovery of the component in the distillate.
$D_R < 0$	Component is nondistributed; contained entirely in bottoms.

Hines and Maddox (26) stated that they solved literally hundreds of minimum reflux cases and are yet to find a case in which predictions from Eq. (3.12) are not correct.

Application of Underwood's equation to systems containing distributed nonkey components is as follows:

1. Find which components are distributed using Eq. (3.12).
2. For n distributed components (including the keys) solve Eq. (3.10) for $n - 1$ values of θ, so that each value of θ is between the relative

volatilities of adjacent components. For instance, if a system contains four distributed nonkey components, plus two key components, Eq. (3.10) needs to be solved for five values of θ. If $\alpha_{DK1} > \alpha_{LK} > \alpha_{DK2} > \alpha_{DK3} > \alpha_{HK} > \alpha_{DK4}$, then $\alpha_{LK} < \theta_1 < \alpha_{DK1}$; $\alpha_{DK2} < \theta_2 < \alpha_{LK}$; $\alpha_{DK3} < \theta_3 < \alpha_{DK2}$; $\alpha_{HK} < \theta_4 < \alpha_{DK3}$; $\alpha_{DK4} < \theta_5 < \alpha_{HK}$.

3. Treat the mole fraction of each distributed nonkey component in the distillate as an unknown. Write Eq. (3.11) for each value of θ calculated above. $(L/D)_{min}$ is also unknown. Solve the equations simultaneously to get the mole fraction of each distributed component in the distillate and $(L/D)_{min}$. In the above example, there are five values of θ and therefore five equations. There are also five unknowns—the mole fractions of DK1, DK2, DK3, and DK4 in the distillate, and $(L/D)_{min}$.

Example 3.3 Calculate the minimum reflux for a depropanizer similar to that of Example 2.4 using Underwood's method. In this case, butane is acceptable both in the top and bottom product, but it is required that 98 percent of the propane in the feed is recovered in the top product, and 99 percent of the pentane is to be recovered in the bottom product.

solution In this case, propane and *n*-pentane are the light key and heavy key, respectively. It is apparent that *n*-butane is a distributed key, while other components (methane, ethane, and *n*-hexane) are nondistributed nonkeys. However, for the sake of the exercise, we will check this using Eq. (3.12). Relative volatilities based on a reference value of 1.0 for the heavy key are shown in the table below. From the statement of the problem,

$$\frac{Dx_{D,LK}}{Fz_{LK}} = 0.98 \quad \text{and} \quad \frac{Dx_{D,HK}}{Fz_{HK}} = 0.01$$

For methane

$$D_R = \frac{39.47 - 1}{4.08 - 1} 0.98 + \frac{4.08 - 39.47}{4.08 - 1} 0.01 = 12.13 > 1$$

For ethane

$$D_R = \frac{10.00 - 1}{4.08 - 1} 0.98 + \frac{4.08 - 10.00}{4.08 - 1} 0.01 = 2.84 > 1$$

For butane

$$D_R = \frac{2.11 - 1}{4.08 - 1} 0.98 + \frac{4.08 - 2.11}{4.08 - 1} \quad 0.01 = 0.36$$

For hexane

$$D_R = \frac{0.5 - 1}{4.08 - 1} 0.98 + \frac{4.08 - 0.5}{4.08 - 1} \quad 0.01 = -0.15 < 0$$

This confirms the apparent observation that n-butane is the only distributed component. Equation (3.10) is now solved for two values of θ such that $1.0 < \theta_1 < 2.11$ and $2.11 < \theta_2 < 4.08$. Since the feed is 66 percent vapor, $1 - q = 0.66$. The calculations are in Table 3.3, and give $\theta_1 = 1.264$, $\theta_2 = 2.847$.

Equation (3.11) can be written as

$$L_{\min} + D = \sum_{j=1}^{n} \frac{\alpha_j Dx_{Dj}}{\alpha_j - \theta} \tag{3.13}$$

where

$$D = \sum_{j=1}^{n} Dx_{Dj} \tag{3.14}$$

Now

$$Dx_{D,\text{ methane}} = 26 \text{ (nondistributed light nonkey)}$$

$$Dx_{D,\text{ ethane}} = 9 \text{ (as for methane)}$$

$$Dx_{D,\text{ propane}} = 0.98 \times 25 = 24.5 \text{ (Specified in the problem)}$$

$$Dx_{D,\ n\text{-butane}} = \text{Unknown, denoted } (Dx_D)_{C4}$$

$$Dx_{D,\ n\text{-pentane}} = 0.01 \times 11 = 0.11 \text{ (Specified in the problem)}$$

$$Dx_{D,\ n\text{-hexane}} = 0 \text{ (nondistributed heavy nonkey)}$$

Applying Eq. (3.13) for each value of θ,

$$L_{\min} + D = \frac{39.47 \times 26}{39.47 - 1.264} + \frac{10.00 \times 9}{10.00 - 1.264} + \frac{4.08 \times 24.5}{4.08 - 1.264} + \frac{2.11(Dx_D)_{C4}}{2.11 - 1.264} + \frac{0.11}{1.00 - 1.264}$$

TABLE 3.3 Calculation for Example 3.3

			$\alpha z/(\alpha - \theta_1)$ $1.0 < \theta_1 < 2.11$			$\alpha z/(\alpha - \theta_2)$ $2.11 < \theta_2 < 4.08$		
			Trial 1	Trial 2	Trial 3	Trial 1	Trial 2	Trial 3
Component	α	z	$\theta_1 = 1.3$	$\theta_1 = 1.25$	$\theta_1 = 1.264$	$\theta_2 = 2.8$	$\theta_2 = 2.85$	$\theta_2 = 2.847$
Methane	39.47	0.26	0.269	0.269	0.269	0.280	0.280	0.280
Ethane	10.00	0.09	0.103	0.103	0.103	0.125	0.126	0.126
Propane	4.08	0.25	0.367	0.360	0.362	0.797	0.829	0.827
Butane	2.11	0.17	0.443	0.417	0.424	−0.520	−0.485	−0.487
Pentane	1.00	0.11	−0.367	−0.440	−0.417	−0.061	−0.060	−0.060
Hexane	0.50	0.12	−0.075	−0.080	−0.079	−0.026	−0.026	−0.026
			0.740	0.629	0.662	0.595	0.664	0.660

$$L_{\min} + D = \frac{39.47 \times 26}{39.47 - 2.847} + \frac{10.00 \times 9}{10.00 - 2.847} + \frac{4.08 \times 24.5}{4.08 - 2.847} + \frac{2.11(Dx_D)_{C4}}{2.11 - 2.847} + \frac{0.11}{1.00 - 2.847}$$

or

$$L_{\min} + D = 72.243 + 2.494(Dx_D)_{C4}$$

$$L_{\min} + D = 121.614 - 2.863(Dx_D)_{C4}$$

Eliminating $(L_{\min} + D)$ and solving gives $(Dx_D)_{C4} = 9.22$
Now

$$D = \Sigma(Dx_D)_i = 26 + 9 + 24.5 + 9.22 + 0.11 = 68.83 \text{ lb mole/h}$$

$$\frac{L_{\min}}{D} = \frac{72.243}{68.83} + 2.494\frac{9.22}{68.83} - 1 = 0.384$$

3.2.4 Extension of the minimum reflux equations

Varying relative volatilities. When relative volatility varies throughout the column, the average relative volatility is estimated by one of the criteria in Sec. 3.2.1.

Nonconstant molar overflow. When the assumption of constant molar overflow (Sec. 2.2.2) does not apply, the Underwood method still gives a good estimate of the minimum liquid flow in the zones above and below the feed, assuming that constant molar overflow applies in these regions (9). The minimum reflux flow to the top stage can then be obtained by solving combined enthalpy and mass balances written for an envelope cut by the flows above the feed and those at the top of the column. A more accurate method involves using modified molecular weights and modified mole fractions; the method is described in detail elsewhere (9).

Complex columns. A number of distinct approaches have been used for calculating minimum reflux in complex columns. Barnés et al. (41) extended the Underwood equation to multifeed columns. The minimum reflux in each section between two adjacent feeds is considered separately. The light key in the vapor leaving each section is used in Eq. (3.10), and can be calculated by subtracting the amount of light keys entering in the feed above a section from the light key in the total overhead product. A complicating factor here is the presence of distributed components (41).

Yaws et al. (42–44) proposed an alternative "factor" method for extending the Underwood equation to columns containing multiple feeds or side products. This method calculates an apparent minimum reflux for one feed as if no other feed is present and assigns a factor to convert each other feed (or side product) to an add-on minimum reflux term.

3.2.5 Reflux-stages relationships

The most popular reflux-stages relationships are by Gilliland (45) and Erbar and Maddox (46). Many designers (9,11,29,47) recommend both, some (10,23,28,30,32,33,48) prefer Gilliland's, while others (13,49) prefer Erbar and Maddox's. The Erbar and Maddox correlation is considered more accurate (22,26,29,33,49), especially at low reflux ratios (49); however, the accuracy of Gilliland's equation for shortcut calculations is usually satisfactory. The single curve in Gilliland's correlation is easier to computerize.

It is important to use a consistent set of minimum reflux/minimum stages/reflux-stages correlation (27). Both the Gilliland and the Erbar and Maddox methods are consistent with the popular Fenske (Sec. 3.2.1) and Underwood (Sec. 3.2.2) methods.

Gilliland plot (45; Fig. 3.9*a*). This plot correlates reflux and stages by

$$X = \frac{R - R_{min}}{R + 1} \tag{3.15}$$

and

$$Y = \frac{N - N_{min}}{N + 1} \tag{3.16}$$

When $R = R_{min}$, $X = 0$, and Y approaches unity. When $N = N_{min}$, $Y = 0$, and X approaches unity. The curve therefore stretches from the coordinates (0,1) at minimum reflux to (1,0) at total reflux.

Gilliland (45) used the Fenske method (Sec. 3.2.1) to compute minimum stages, and his own method for computing minimum reflux. However, it was shown (11,48) that the Underwood method (Sec. 3.2.2) for minimum reflux can also be used.

Numerical Gilliland equations. Since Gilliland derived his original plot (45), several authors (5,37,48,50–53) developed numerical equations to represent it. Chang (52) shows that Hengstebeck's equation (5) gives the best fit to the Gilliland plot. However, there is some scatter in the fit of data to the Gilliland plot, and the expression that best fits the plot is not necessarily the best reflux-stages correlation (48,52).

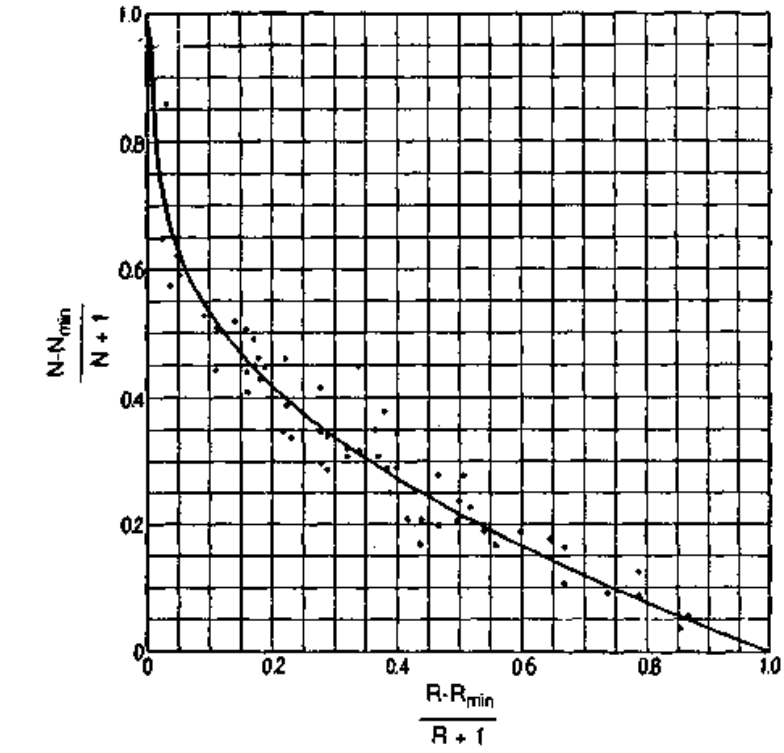

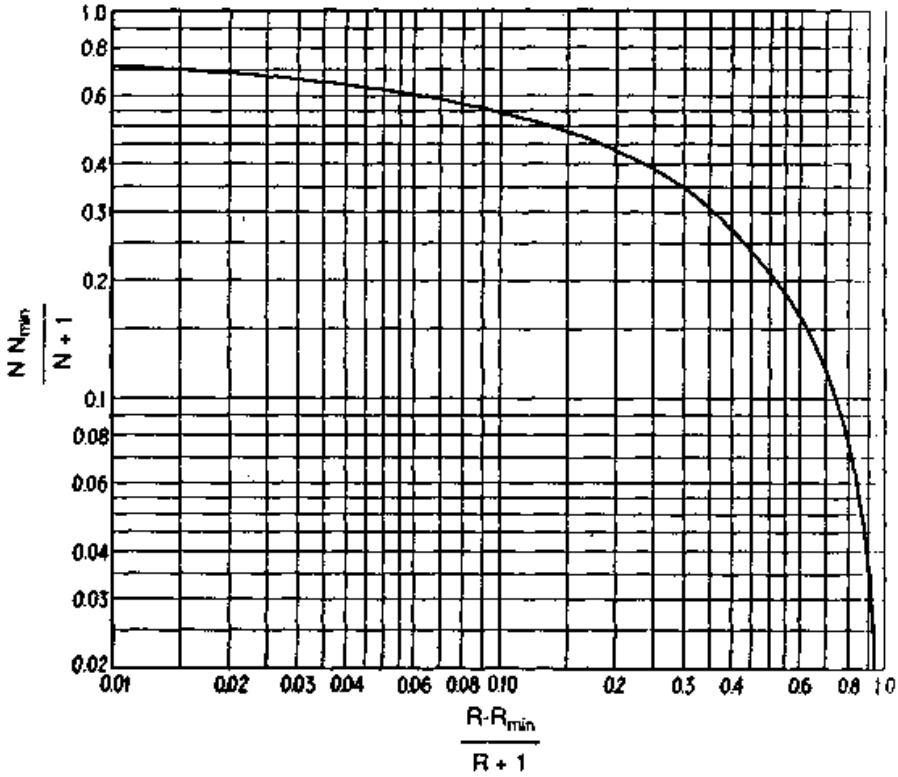

(a)

Figure 3.9 Reflux-stages correlations. (a) The Gilliland correlation

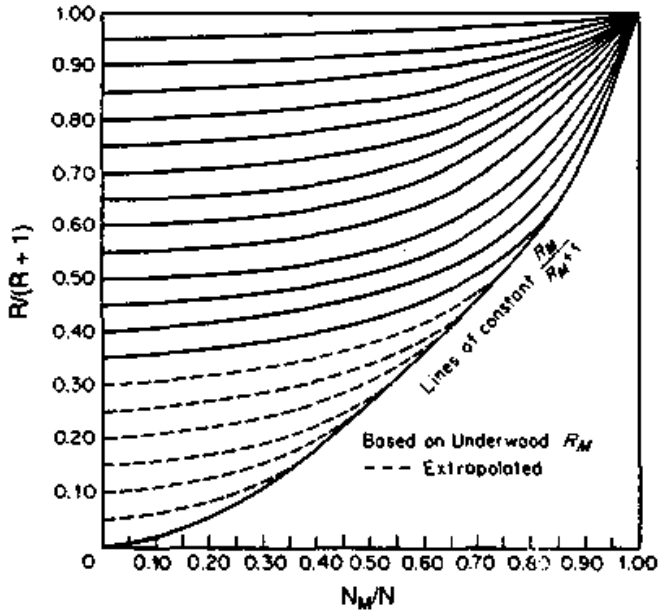

(b)

Figure 3.9 (*Continued*) Reflux-stages correlations. (*b*) the Erbar-Maddox correlation. (Part *a* from C. S. Robinson and E. R. Gilliland. Copyright © by McGraw-Hill, Inc. Reprinted by permission. Part *b* from J. H. Erbar and R. N. Maddox, *Pet. Ref.*, vol. 40, no. 5, p. 183, 1961. Reprinted courtesy of *Hydrocarbon Processing*.)

Further, as seen in Example 3.1, choice of the volatility estimation method affects the agreement between the data and the correlation. Of the various numerical methods, that of Molokanov et al. (51) was preferred by some authors (30,54) and that by Eduljee (48) by others (11,23,29,49,55). Eduljee's equation has a simplicity advantage. King (9) suggests using Eduljee's equation where high accuracy is not required and Molokanov's when better accuracy is desired. Eduljee's equation is given by

$$Y = 0.75(1 - X^{0.5668}) \tag{3.17}$$

This equation applies in the range of $0.01 < X < 1$. Values of X lower than 0.01 are of little practical importance.

Erbar-Maddox method (Fig. 3.9*b*). This method uses a plot of $R/(R + 1)$ against N_{min}/N, with $R_{min}/(R_{min} + 1)$ as the parameter. When $R = R_{min}$, the x axis becomes zero. Therefore, the y axis of the diagram represents minimum reflux conditions. When $N = N_{min}$, both x and y coordinates become unity.

Figure 3.9*b* is based on a bubble-point feed. For other types of feed, the following correlation is used (46).

$$V_u = V_K + \frac{(1 - D/F)(H_{F,u} - H_{F,K})}{Q_c/L_o} \tag{3.18}$$

In the Erbar-Maddox correlation, minimum stages are calculated by the Winn method (Sec. 3.2.1) and minimum reflux by the Underwood method (Sec. 3.2.2), but the Fenske minimum stages method (Sec. 3.2.1) can also be used (11,26).

Example 3.4 Calculate the number of theoretical stages for the depropanizer in Example 2.4.

solution In Example 3.1, the minimum number of stages was estimated using several variations of the Fenske equation. We will select the estimate by the Winn equation, so that $N_{min} = 12.4$. Similarly, in Example 3.2 minimum reflux was estimated using the Underwood equation. This calculation gave $R_{min} = 1.02$. From the problem statement of Example 2.4, $R = 1.5$.

1. Using the Gilliland method

$$X = \frac{1.5 - 1.02}{1.5 + 1} = 0.192 \tag{3.15}$$

From Fig. 3.9*a*, $Y = 0.42$ (based on linear curve)

$$\frac{N - 12.4}{N + 1} = 0.42, N = 22.1$$

2. Using the Eduljee method

$$X = 0.192 \text{ (as in part 1)}$$

$$Y = 0.75(1 - 0.192^{0.5668}) = 0.456 \tag{3.17}$$

$$\frac{N - 12.4}{N + 1} = 0.456, N = 23.6 \tag{3.16}$$

3. Using the Erbar and Maddox correlation

$$\frac{R}{R + 1} = 0.60$$

$$\frac{R_{min}}{R_{min} + 1} = 0.505$$

From Fig. 3.9*b*, $N_{min}/N = 0.60$

$$N = 12.4/0.60 = 20.7$$

Correcting the result of Erbar and Maddox with Eq. (3.18) is not performed here.

For the same problem, the Hengstebeck diagram (Sec. 2.3.4) gave 16 theoretical stages, while a rigorous computer simulation (for a reflux ratio of 1.5, as specified in Example 2.4) gave 20 theoretical stages. Figure 3.5 compares results from a Fenske-Underwood-Gilliland (step 1 in Ex-

ample 3.4 above) hand calculation with a rigorous simulation and a shortcut commercial simulation. The comparison is based on the depropanizer, but extends from minimum to total reflux. Figure 3.5 shows that the shortcut methods approximate the depropanizer reason ably well.

3.2.6 Feed stage location

The most popular shortcut relationships for best feed location are the Fenske equation (25) and the Kirkbridge equation (56). The former is recommended by Refs. 11 and 33, and the latter is recommended by Refs. 11, 28, and 37. Both methods are only approximations. Additional feed location criteria are in Sec. 2.3.7.

Fenske equation (25)

$$N_{\min,S} = \ln S_S / \ln \alpha_S \tag{3.19}$$

where

$$S_S = \frac{z_{\mathrm{LK}}}{z_{\mathrm{HK}}} \frac{x_{B,\mathrm{HK}}}{x_{B,\mathrm{LK}}} \tag{3.20}$$

where α_s is the average relative volatility of the light key in the bottom section. The number of actual trays in the bottom section is estimated from

$$\frac{N_S}{N_{\min,S}} = \frac{N}{N_{\min}} \tag{3.21}$$

Kirkbridge equation (56)

$$\frac{N_R}{N_S} = \left[\frac{z_{\mathrm{HK}}}{z_{\mathrm{LK}}} \left(\frac{x_{B,\mathrm{LK}}}{x_{D,\mathrm{HK}}} \right)^2 \frac{B}{D} \right]^{0.206} \tag{3.22}$$

Akashah et al. (57) presented a modified version of Eq. (3.22), which gives

$$N_R = N_R \text{ [calculated from Eq. (3.22)]} - 0.5 \log N \tag{3.23}$$

Example 3.5 Calculate the ideal feed plate location for the depropanizer in Example 3.4.

solution

1. Using Fenske's equation, Eq. (3.19)

$$z_{\mathrm{LK}} = 0.25 \qquad z_{\mathrm{HK}} = 0.17 \qquad x_{B,\mathrm{HK}} = 0.417 \qquad x_{B,\mathrm{LK}} = 0.01$$

$$S_S = \ln \left(\frac{0.25}{0.17} \frac{0.417}{0.01} \right) = 4.12$$

Using the relative volatility values in Example 3.1,

$$\alpha_{\mathrm{av,bot}} = \sqrt{\alpha_{\mathrm{mid}} \alpha_{\mathrm{bot}}} = \sqrt{1.870\ 1.579} = 1.718$$

$$N_{\min,S} = 4.12/\ln 1.718 = 7.61$$

Assuming 20 theoretical stages (Example 3.4), and 12.4 to be the minimum number of stages (Example 3.1),

$$N_S = (7.61/12.4) \times 20 = 12.3$$

$$N_R = 20 - 12.3 = 7.7$$

2. Using Kirkbridge's equation, Eq. (3.22)

$$\frac{N_R}{N_S} = \left[\frac{0.17}{0.25}\left(\frac{0.01}{0.005}\right)^2 \frac{40.1}{59.9}\right]^{0.206} = 1.13$$

Assuming 20 theoretical stages,

$$N_S = (1/2.13) \times 20 = 9.4 \qquad N_R = 20 - 9.4 = 10.6$$

3. Applying Akashah et al.'s correction, Eq. (3.23),

$$N_R = 10.6 - 0.5 \log 20 = 9.9$$

$$N_S = 20 - 9.9 = 10.1$$

4. From the Hengstebeck diagram (Sec. 2.3.4), prorating to 20 stages

$$N_S = \frac{9+1}{17} \times 20 = 11.8 \qquad N_R = 20 - 11.8 = 8.2$$

5. A rigorous computer calculation gave $N_S = 11$, $N_R = 9$.

3.2.7 Analysis of existing columns: the Smith-Brinkley method

The Smith and Brinkley (58) method is more convenient for the analysis of existing columns than for the design of new ones. This method applies to absorption and extraction as well as distillation. For distillation, this method gives

$$f_i = \frac{(1 - S_{n,i}^{N-M}) + R(1 - S_{n,i})}{(1 - S_{n,i}^{N-M}) + R(1 - S_{n,i}) + h_i S_{n,i}^{N-M}(1 - S_{m,i}^{M+1})} \tag{3.24}$$

where

$$f_i = (Bx_B/Fz)_i \tag{3.25}$$

$$S_{n,i} = K_i(V/L) \tag{3.26}$$

$$S_{m,i} = K_i'(V'/L') \tag{3.27}$$

h_i is a correlating factor, defined by Eqs. (3.28a) and (3.28b). If the feed is mostly liquid,

$$h_i = \frac{K_i'}{K_i}\frac{L}{L'}\frac{(1 - S_{n,i})}{(1 - S_{m,i})} \tag{3.28a}$$

If the feed is mostly vapor

$$h_i = \frac{L}{L'} \frac{(1 - S_{n,i})}{(1 - S_{m,i})} \tag{3.28b}$$

K_i and K_i' are determined at the effective top and bottom section temperatures. If the temperature profile is available (e.g., from a computer simulation), the effective temperature is the arithmetic average of all tray temperatures in the column section. Alternatively, an arithmetic average of the feed-stage and end-stage temperatures is often used:

$$t_n = \frac{t_{\text{top}} + t_{\text{above feed}}}{2} \tag{3.29a}$$

$$t_m = \frac{t_{\text{below feed}} + t_{\text{bot}}}{2} \tag{3.29b}$$

Strictly speaking, Eq. (3.24) does not apply to a column with a partial condenser, since it ignores any difference between the overhead and reflux compositions. However, a partial condenser can be closely approximated by increasing N by 1 (58).

Application. Previous methods (Secs. 3.2.1 to 3.2.6) produce a design. They take product compositions and deliver the number of stages, reflux, and optimum feed stage. The Smith-Brinkley method rates a column using the reverse sequence of steps. It takes the number of stages, reflux ratio, and actual feed location, and yields the product compositions.

Once a base case is available, small changes in variables can be easily made. For instance, for a change in feed temperature, half the change is added to t_n and the other half to t_m. For a change in reflux rate, the extra liquid is added to S_m and S_n. If the changes are large, some trial-and-error solution is required in which t_m and t_n are varied. This is analogous to an operator who adjusts the control temperature by trial and error until the desired end products are obtained.

The above features make the Smith-Brinkley method valuable for on-line optimization (e.g., using microprocessor or computer control). It can be beneficial for assessing the effects of perturbations on column performance and driving the control point toward an optimum. It is also valuable for off-line optimization and for revamp studies. Rice (58a) extended the Smith-Brinkley method to yield individual stage temperatures and compositions and successfully applied it for control.

Example 3.6 A depropanizer capable of providing 20 theoretical stages, with a feed point on the 9th stage from the top, is available to separate the mixture in Example 2.4. The reflux ratio is 1.5.

(*a*) Would the column achieve the separation?

(*b*) What effect would raising the reflux ratio by 13 percent have on the product purity?

Data: Dew point at top of column = 70°F
Bubble point at bottom of column = 308°F
Temperature at feed stage (approx.) = 211°F

***K*-values (for typical tray mixture)**

	140.5°F	259.5°F
Methane	6.72	6.42
Ethane	2.26	3.15
Propane	1.00	1.85
n-Butane	0.44	1.085
n-Pentane	0.20	0.650
n-Hexane	0.092	0.394

solution (*a*) First estimate t_n and t_m using Eq. (3.29)

$$t_n = (70 + 211)/2 = 140.5°\text{F}$$

$$t_m(308 + 211)/2 = 259.5°\text{F}$$

Using the material balance in Example 2.4

$$D = 59.9, B = 40.1 \text{ lb-mole/h}$$

Assuming constant molar overflow,

$$L = RD = 1.5 \times 59.9 = 89.9 \text{ lb-mole/h}$$

$$V = (R + 1)D = 2.5 \times 59.9 = 149.8 \text{ lb-mole/h}$$

$$L' = L + qF = 89.9 + 0.34 \times 100 = 123.9 \text{ lb-mole/h}$$

$$V' = L' - B = 123.9 - 40.1 = 83.8 \text{ lb-mole/h}$$

From the problem definition, $N = 20$, $M = 12$. Due to the partial condenser, $N = 20 + 1 = 21$. Since the feed is mostly vapor, h_i is calculated using Eq. (3.28*b*).

Calculations for the first trial are shown in Table 3.4. The calculated value of B is 40.2, which approximates the specified value of 40.1 in the material balance in Example 2.4. The propane in the bottoms is 0.73/40.2 = 1.8 percent, while the *n*-butane in the distillate is (17 − 16.46)/59.8 = 0.9 percent. These values are higher than those used in Examples 2.4 and 3.4.

Depending on the initial guesses, the calculated value of B may not equal the specified B. A calculated B higher than specified indicates that t_m and t_n are too low, and that the bottom product contains excessive lights. An additional trial is then needed, at higher t_n and/or t_m. Usually, the estimated feed temperature is raised; this raises both t_n and t_m. Since the top and bottom temperatures are fixed by the products dew and bubble points, they are best maintained constant until Bx_B adds up to the specified amount. Conversely, if the calculated Bx_B is lower than specified, the estimated feed temperature should be lowered. The above is analogous to an operator adjusting the control temperature to obtain a desired split.

TABLE 3.4 Calculation for Example 3.6

Part *a*

Component	K_i	$S_{n,i}$	K_i'	$S_{m,i}$	h_i	$S_{n,i}^9$	Numerator	$h_i S_{n,i}^9$	$S_{m,i}^{13}$	Denominator, 3d term	Denominator	f_i	Bx_B
Methane	6.72	11.2	6.42	4.34	2.22	2.8×10^9	-2.8×10^9	6.2×10^9	0.194×10^9	-1.2×10^{18}	-1.2×10^{18}	2.3×10^{-9}	—
Ethane	2.26	3.77	3.15	2.13	1.78	0.15×10^6	-0.15×10^6	0.27×10^6	18.6×10^3	-5.1×10^9	-5.1×10^9	29×10^{-6}	—
Propane	1.00	1.666	1.85	1.25	1.933	98.9	−98.9	191.1	18.2	−3287	−3386	0.029	0.73
n-Butane	0.44	0.733	1.085	0.734	0.728	0.0611	1.339	0.0445	0.0179	0.0437	1.383	0.968	16.46
n-Pentane	0.20	0.333	0.650	0.440	0.864	0.050×10^{-3}	2.00	0.44×10^{-4}	2.32×10^{-5}	0.44×10^{-4}	2.00	1.0	11.0
n-Hexane	0.092	0.153	0.394	0.267	0.838	46×10^{-9}	2.27	39×10^{-9}	3.5×10^{-8}	39×10^{-9}	2.27	1.0	12.0
												$B = \Sigma Bx_B =$	40.2

Part *b*

Propane	1.00	1.588	1.85	1.304	1.45	64.2	−64.2	93.1	31.4	−2831	−2895	0.022	0.55
n-Butane	0.44	0.699	1.085	0.765	0.96	0.0398	1.472	0.0382	0.0305	0.0371	1.509	0.976	16.58
Others													23.0
												$B = \Sigma Bx_B =$	40.1

(*b*) Since the light nonkeys appear to all go to the distillate, and the heavy nonkeys all to the bottom, only the keys needs to be considered. In addition

$$R = 1.13 \times 1.5 = 1.7$$

$$L = RD = 1.7 \times 59.9 = 101.8 \text{ lb-mole/h}$$

$$V = (R + 1)D = 2.7 \times 59.9 = 161.7 \text{ lb-mole/h}$$

$$L' = L + qF = 101.8 + 0.34 \times 100 = 135.8 \text{lb-mole/h}$$

$$V' = L' - B = 135.8 - 40.1 = 95.7 \text{ lb-mole/h}$$

Calculations are shown in Table 3.4. The propane in the bottom diminishes to 0.55/40.1 = 1.4 percent, while the butane in the distillate diminishes to (17 − 16.57)/59.9 = 0.7 percent. The calculated value of B is 40.1, which equals the specified 40.1; a second trial is not necessary.

3.2.8 The analytical *x-y* diagram: Smoker's equation

The Smoker equation (59) is convenient to use in binary separations with a large number of stages. The equation assumes constant relative volatility and constant molar overflow. The main application is in superfractionators such as ethylene-ethane and isobutane-*n*-butane separations. The Smoker equation is essentially an analytical solution of the *x-y* diagram. The Smoker equation is

$$N = \frac{\log \dfrac{x_0'\{1 - [mc(\alpha - 1)x_n'/(\alpha - mc^2)]\}}{x_n'\{1 - [mc(\alpha - 1)x_0'/(\alpha - mc^2)]\}}}{\log[\alpha/(mc^2)]} \tag{3.30}$$

where

$$x_o' = x_o - k \tag{3.31}$$

$$x_n' = x_n - k \tag{3.32}$$

$$c = 1 + (\alpha - 1)k \tag{3.33}$$

$$x_{\text{int}} = [(R + 1)z + (q - 1)x_D]/(R + q) \tag{3.34}$$

and k is the root of the quadratic equation $(0 < k < 1)$

$$m(\alpha - 1)k^2 + [m + b(\alpha - 1) - \alpha]k + b = 0 \tag{3.35}$$

The Smoker equation must be applied individually for the rectifying and stripping sections. The values used for the rectifying section are

$$m = R/(R + 1) \tag{3.36a}$$

$$b = x_D/(R + 1) \tag{3.37a}$$

$$x_o = x_D \tag{3.38a}$$

$$x_n = x_{\text{int}} \tag{3.39a}$$

Similarly, for the stripping section

$$m = \frac{L'}{V'} = \frac{R + q + q(B/D)}{R + q - (1 - q)(B/D)} \tag{3.36b}$$

$$b = \frac{(z - x_D)x_B}{(R + 1)z + (q - 1)x_D - (R + q)x_B} \tag{3.37b}$$

$$x_o = x_{\text{int}} \tag{3.38b}$$

$$x_n = x_B \tag{3.39b}$$

Hohmann (60) presents an extension of the Smoker equation to complex columns.

Example 3.7 Solve Example 2.1 using Smoker's method. Assume an average relative volatility of 2.49.

solution (*a*) Rectifying section:

$$m = 3/(3 + 1) = 0.75 \tag{3.36a}$$

$$b = 0.95/(3 + 1) = 0.2375 \tag{3.37a}$$

$$x_o = 0.95 \tag{3.38a}$$

$$x_{\text{int}} = [(3 + 1)0.4 + (0.75 - 1)0.95]/(3 + 0.75) = 0.363 \tag{3.34}$$

$$x_n = 0.363 \tag{3.39a}$$

$$0.75(2.49 - 1)k^2 + [0.75 + 0.2375(2.49 - 1) - 2.49]k + 0.2375 = 0 \tag{3.35}$$

Solving $1.1175k^2 - 1.3861k + 0.2375 = 0$,

$$k = \frac{1.3861 \pm \sqrt{(1.3861)^2 - 4 \times 1.1175 \times 0.2375}}{2 \times 1.1175} = 1.035 \text{ or } 0.2053$$

Since $0 < k < 1$, use $k = 0.2053$,

$$x_o' = 0.95 - 0.2053 = 0.7447 \tag{3.31}$$

$$x_n' = 0.363 - 0.2053 = 0.1577 \tag{3.32}$$

$$c = 1 + (2.49 - 1)0.2053 = 1.3060 \tag{3.33}$$

Numerator of the top log term in Eq. (3.30) is

$$0.7447\{1 - [0.75 \times 1.3060(2.49 - 1)0.1577/(2.49 - 0.75 \times 1.3060^2)]\} = 0.6031$$

Denominator of the top log term in Eq. (3.30) is

$$0.1577\{1 - [0.75 \times 1.3060(2.49 - 1)0.7447/(2.49 - 0.75 \times 1.3060^2)]\} = 0.0161$$

Bottom term in Eq. (3.30) is $2.49/(0.75 \times 1.306^2) = 1.9465$

$$N_R = [\log (0.6031/0.0161)]/\log 1.9465 = 5.44$$

(*b*) Similarly for the stripping section

$$m = \frac{3 + 0.75 + 0.75(129/71)}{3 + 0.75 - 0.25(129/71)} = 1.5514 \tag{3.36b}$$

$$b = \frac{(0.4 - 0.95)0.1}{(3 + 1)0.4 + (0.75 - 1)0.95 - (3 + 0.75)0.10} = -0.0557 \tag{3.37b}$$

$$x_0 = 0.3633 \tag{3.38b}$$

$$x_n = 0.10 \tag{3.39b}$$

$$1.5514(2.49 - 1)k^2 + [1.5514 - 0.0557(2.49 - 1) - 2.49]k - 0.0557 = 0 \tag{3.35}$$

$$2.3116k^2 - 1.0216k - 0.0557 = 0$$

$$k = \frac{1.0216 \pm \sqrt{(1.0216)^2 + 4 \times 2.3116 \times 0.0557}}{2 \times 2.3116} = 0.491 \text{ or } -0.0491$$

Since $0 < k < 1$, use $k = 0.491$.

$$x_0' = 0.3633 - 0.491 = -0.1277 \tag{3.31}$$

$$x_n' = 0.10 - 0.491 = -0.391 \tag{3.32}$$

$$c = 1 + (2.49 - 1)0.491 = 1.7316 \tag{3.33}$$

Numerator of the top by term in Eq. (3.30) is

$$-0.1277\{1 - [1.5514 \times 1.7316(2.49 - 1)(-0.3910)/(2.49 - 1.5514\ 1.7316^2)]\} = -0.0352$$

Denominator of the top log term in Eq. (3.30) is

$$-0.391\{1 - [1.5514 \times 1.7316(2.49 - 1)(-0.1277)/(2.49 - 1.5514\ 1.7316^2)]\} = -0.2985$$

Bottom term of Eq. (3.30) is $2.49/(1.5514\ 1.7316^2) = 0.5353$

$$N_S = [\log [(-0.0352)/(-0.2985)]/\log 0.5353 = 3.42$$

Total number of stages is therefore

$$N_R + N_S = 5.44 + 3.42 = 8.86 \qquad \text{say } 9$$

This checks with the graphical solution of Example 2.1 which gave just above 9 stages.

3.2.9 The Jafarey, Douglas, and McAvoy equation: design and control

Jafarey et al. (61) derived a simple, approximate equation for binary distillation by simplifying the solution to Smoker's equation. Their equation is powerful for predicting the effect of disturbances on column performance. This makes their equation particularly useful in computer and microprocessor control, where it can be applied to estimate the effect of disturbances and the control action needed to compensate for them. This application is highlighted in Examples 3.8 and 3.9. The Jafarey et al. equation is

$$N = \frac{\ln S}{\ln\left[\alpha\sqrt{1 - \dfrac{R + q}{(R + 1)(Rz + q)}}\right]} \tag{3.40}$$

S is given by Eq. (3.3). Equation (3.40) is stated (61) to predict N within plus or minus two to three stages. The effect of disturbances on column performance can be evaluated by combining Eq. (3.40) with the column overall mass and component balance equations [Eqs. (3.1), (3.2)]. Douglas et al. (62) illustrate several applications. Example 3.8 illustrates this for binary distillation.

Extension to multicomponent separations. Douglas et al. (62) extended Eq. (3.40) to multicomponent distillation. Their procedure lumps the light key and light nonkeys into a pseudo-light-key component and the heavy key and heavy nonkeys into a pseudo-heavy-key component according to Hengstebeck's method (63). The Douglas et al. (62) procedure is complex but was shown to give accurate results. Douglas et al. (62) also describe a simple, but less accurate approach. The author proposes an alternative variation of the simple procedure, illustrated in Example 3.9.

Example 3.8 A benzene-toluene column normally operates as described in Example 2.1. The column is computer-controlled, using the Jafarey et al. algorithm. The algorithm manipulates boilup flow to control toluene purity. If the

toluene purity is to be temporarily increased from 90 to 95 percent, and the benzene purity to remain unaffected, what would the controller set the boilup flow rate at? Assume that any boilup changes will be compensated by reflux and distillate rate changes, such that the benzene purity remains unaffected. Also assume a relative volatility of 2.49.

solution First, determine N for normal operation from Eq. (3.40)

$$\ln S = \ln [(0.95/0.05)(0.90/0.10)] = 5.142 \qquad \text{[Eq. (3.3)]}$$

The denominator of Eq. (3.40) is

$$\ln \left[2.49 \sqrt{1 - \frac{3 + 0.75}{(3 + 1)(3 \times 0.4 + 0.75)}} \right] = 0.5846$$

$$N = 5.889/0.5846 = 8.80$$

This checks with the x-y diagram (Example 2.1) and with Smoker's method (Example 3.7).

Solve the material and component balances for the new conditions:

$$200 = B + D \qquad \text{[Eq. (3.1)]}$$

$$200 \times 0.4 = 0.05B + 0.95D \qquad \text{[Eq. (3.2)]}$$

Solving these simultaneously gives $B = 122$ and $D = 78$ lb-mole/h.

Recalculate S for the new conditions

$$\ln S = \ln [(0.95/0.05)(0.95/0.05)] = 5.889$$

The denominator of Eq. (3.40) will be equal to $(\ln S)/N$, i.e., $5.889/8.80 = 0.6692$. The term inside the square root will be equal to $(\exp 0.6692/2.49)^2$, i.e., 0.6150. Therefore,

$$\frac{R + 0.75}{(R + 1)(0.4R + 0.75)} = 1 - 0.6150 = 0.3850$$

This gives the quadratic equation

$$0.1540R^2 - 0.5572R - 0.4612 = 0$$

Solving

$$R = \frac{0.5572 \pm \sqrt{0.5572^2 + 4 \times 0.1540 \times 0.4612}}{2 \times 0.1540} = 4.314$$

Since $D = 78$, $L = 78 \times 4.314 = 336$ lb-mole/h.

$$L' = 336 + 0.75 \times 200 = 486 \text{ lb-mole/h}$$

$$V' = L' - B = 486 - 122 = 364 \text{ lb-mole/h}$$

The computer control will therefore increase the boilup rate from 234 lb-mole/h (Example 2.1) to 364 lb-mole/h.

Example 3.9 A depropanizer normally operates as described in Example 2.4. The column is computer-controlled, using the Jafarey et al. algorithm. The algorithm manipulates reflux flow to control top product purity. Distillate flow rate must remain fixed, but bottom purity is allowed to vary. The top product purity spec is temporarily relaxed from 0.5 mole percent to 0.9 mole percent. What would the controller set the reflux flow at?

solution First, lump all the light nonkeys into a pseudo light key (PLK), and all the heavy nonkeys into a pseudo heavy key (PHK). The material balance of Example 2.4 can now be written in terms of the pseudo nonkeys.

Component	Feed	Mole % distillate	Bottoms	Moles per 100 moles of feed	
				Distillate	Bottoms
PLK	60	99.5	1.0	59.6	0.4
PHK	40	0.5	99.0	0.3	39.7
				59.9	40.1

The separation parameter is calculated using Eq. (3.3).

$$\ln S = \ln [(99.5/0.5)(99/1)] = 9.888$$

To estimate the relative volatility, one can use the volatility between the key components. This may provide a good approximation when the fraction of nonkeys is small, but a less satisfactory approximation when the fraction of nonkeys is large. In this case, this approximation will give an N of 44 stages, which compares unfavorably with previous calculations (Example 3.4).

An alternative approach is to use a pseudo relative volatility, which can be obtained if the number of theoretical stages is known. This number of stages can be computed using a rigorous simulation of the column. A pseudo relative volatility is then calculated using Eq. (3.40), and can be applied for control purposes. A rigorous computer simulation gave 20 theoretical stages for this calculation (Example 3.4). The pseudo relative volatility is therefore back-calculated from

$$20 = \frac{9.888}{\ln\left[\alpha_{\text{pseudo}}\sqrt{1 - \dfrac{1.5 + 0.34}{(1.5 + 1)(1.5 \times 0.6 + 0.34)}}\right]}$$

Solving give $\alpha_{\text{pseudo}} = 2.572$

A material balance for the new conditions gives

Component	Feed	Distillate	Bottoms	Distillate	Bottoms
PLK	60	99.1	1.6	59.36	0.64
PHK	40	0.9	98.4	0.54	39.46
				59.9	40.1

The new separation parameter is obtained using Eq. (3.3)

$$\ln S = [(99.1/0.9)(98.4/1.6)] = 8.821$$

The denominator of Eq. (3.40) will be equal to $(\ln S)/N$, i.e., 8.821/20 = 0.441. The term inside the square root will be equal to $(\exp 0.441/2.572)^2$, i.e., 0.3652. Therefore,

$$\frac{R + 0.34}{(R + 1)(0.6R + 0.34)} = 1 - 0.3652 = 0.6348$$

This gives the quadratic equation

$$0.3809R^2 - 0.4033R - 0.1242 = 0$$

Solving

$$R = \frac{0.4033 \pm \sqrt{0.4033^2 + 4 \times 0.3809 \times 0.1242}}{2 \times 0.3809} = 1.31$$

The new reflux flow will be 78.4 lb-mole/h.

A rigorous simulation gave the value $R = 1.27$ and a reflux flow of 76.0 lb-mole/h.

CAUTION: The procedure for applying the Jafarey et al. equation (61,62) in this example was empirically developed by the author. It worked in a few examples attempted by the author, but may not work in other cases.

The author strongly recommends that before this algorithm is used for computer control of a multicomponent column, it is first thoroughly tested against the results of a rigorous computer simulation for the column considered. Alternative procedures for extending the Jafarey et al. algorithm for multicomponent distillation are discussed elsewhere (62).

3.3 Nomenclature

3.2.1 English letters

B	Bottom flow rate, lb-mole/h
b	Intercept parameter in Smoker's equation, defined by Eqs. (3.37*a* and *b*)
c	Parameter in Smoker's equation, defined by Eq. (3.33)
D	Distillate flow rate, lb-mole/h
D_R	Recovery of a component in the distillate product, given by Eq. (3.12)
F	Feed flow rate, lb-mole/h
f_i	Ratio of component flow rate in the bottom to component flow rate in the feed, Eq. (3.25)
H	Enthalpy, Btu/h
h	Factor in the Smith-Brinkley method, given by Eqs. (3.28*a* and *b*)

j	Component counter
K	Equilibrium constant Eq. (1.1). In Sec. 3.2.7 only, it is the equilibrium constant in the rectifying section
K'	Equilibrium constant in the stripping section
k	Parameter in Smoker's equation, given by Eq. (3.35)
L	Liquid flow rate in the rectifying section, lb-mole/h
L'	Liquid flow rate in the stripping section, lb-mole/h
L_o	Liquid condensed at the condenser, lb-mole/h
M	Number of stages below the feed
m	Slope of the component balance line, given by Eqs. (3.36*a* and *b*)
N	Number of stages
n	Number of components
PHK	Pseudo heavy key
PLK	Pseudo light key
q	Number of pound-moles of liquid formed on the feed stage when introducing 1 lb-mole of feed
Q_c	Condenser duty, Btu/h
R	Reflux ratio
S	Separation parameter, defined by Eq. (3.3)
S_m,S_n	Factors in the Smith-Brinkley equation, defined by Eqs. (3.26) and (3.27)
T,t	Temperature, °F
t_m	Average temperature in the stripping section, °F, estimated by Eq. (3.29*b*)
t_n	Average temperature in the rectifying section, °F, estimated by Eq. (3.29*a*)
V	Vapor flow rate in the rectifying section, lb-mole/h
V'	Vapor flow rate in the stripping section, lb-mole/h
X	Gilliland's correlation reflux parameter, given by Eq. (3.15)
x	Mole fraction in the liquid
x_o,x'_o	Parameters in Smoker's equation, defined by Eqs. (3.31) and (3.38*a* and *b*)
x_{int}	Liquid mole fraction at the intersection of the component balance line and the q-line, given by Eq. (3.34)
x_n,x'_n	Parameters in Smoker's equation, defined by Eqs. (3.32) and (3.39*a* and *b*)
Y	Gilliland's correlation parameter, given by Eq. (3.16)
y	Mole fraction in the vapor
z	Mole fraction in the feed

3.3.2 Greek letters

α	Relative volatility
$\beta_{LK/HK}$	Parameter in the Winn equation [Eq. (3.8)]
θ	Parameter in the Underwood equation [Eq. (3.10)]
θ_{LK}	Exponent in the Winn equation [Eq. (3.8)]
Σ	Sum of

3.3.3 Subscripts

av	Average
B,bot	Bottom
D	Distillate
DK	Distributed key component
DK1,DK2...	Distributed key component 1, 2...
F	Feed
HK	Heavy key component
i	Component *i*
j	Component *j*
K	At the bubble point [Eq. (3.18)]
LK	Light key component
LNK	Light nonkey component(s)
M	Minimum
mid	Middle of the column
min	Minimum
opt	Optimum
pseudo	Pseudo component
R	Rectifying
S	Stripping
top	At the top of the column
u	At the conditions differing from bubble point [Eq. (3.18)]

3.4 References

1. Latour, P. R., *Instrumentation Technology 25*(7), 67, 1978.
2. Fisher, W. R., M. F. Doherty, and J. M. Douglas, *Ind. Eng. Chem. Proc. Des. Dev. 24*, 955, 1985.
3. Beveridge, G. S. G., and R. S. Schechter, *Optimization: Theory and Practice*, McGraw-Hill, New York, 1970.
4. Doig, I. D., *Aust. Chem. Eng. 12*(7), 5, 1971.
5. Hengstebeck, R. J., *Distillation*, Reinhold, New York, 1961.
6. Kister, H. Z., and I. D. Doig, *Hydrocarb. Proc. 56*(7), 132, 1977.

7. Kister, H. Z., and R. W. Townsend, *Hydrocarb. Proc. 63*(1), 105, 1984.
8. Ducote, D. J., and R. Ragsdale, *Hydrocarb. Proc. 60*(9), 149, 1981.
9. King, C. J., *Separation Processes*, 2d ed., McGraw-Hill, New York, 1980.
10. Frank, O., *Chem. Eng.* March 14, p. 110, 1977.
11. Thompson, R. E., in Calo, J. M., and E. J. Henley, *Stagewise and Mass Transfer Operations*, vol. 2, AIChE Modular Instruction, 1981.
12. Walas, S. M., *Chem. Eng.* March 16, p. 75, 1987.
13. McCormick, J. E., and E. C. Roche, in P. A. Schweitzer (ed.) *Handbook of Separation Techniques for Chemical Engineers*, McGraw-Hill, New York, 1979, pp. 1–59.
14. Zdonik, S. B., *Chem. Eng.* July 4, p. 99, 1977.
15. Holland, C. D., *Fundamentals of Multicomponent Distillation*, McGraw-Hill, New York, 1981.
16. Bachelor, J. B., *Pet. Ref. 36*(6), 161, 1957.
17. Erbar, R. C., and R. N. Maddox, *Can. J. Chem. Engrs. 40*(1), 25, 1962.
18. Yamada, I., T. Iwata, Y. Nishi, and S. Hiraoka, *J. Chem. Eng.* (Japan) *10*(6), 440, 1977.
19. Tavana, M., and D. N. Hanson, *Ind. Eng. Chem. Proc. Des. Dev. 18*(1) 154, 1979.
20. Chien, H. Y., *AIChEJ. 24*(4), 606, 1978.
21. Bolles, W. L. (Monsanto Company, St. Louis), private communication, May 1991.
22. Fair, J. R., and W. L. Bolles, *Chem. Eng.* April 22, p. 156, 1968.
23. Rose, L. M., *Distillation Design in Practice*, Elsevier, Amsterdam, 1985.
24. Chien, H. Y., *Chem. Eng. Sci. 28*, 1967, 1973.
25. Fenske, M. R., *Ind. Eng. Chem. 24*, 482, 1932.
26. Hines, A. L., and R. N. Maddox, *Mass Transfer*, Prentice-Hall, Englewood Cliffs, N.J., 1985.
27. Maddox, R. N., *Chem. Eng.* December 11, p. 127, 1961.
28. Van Winkle, M., *Distillation*, McGraw-Hill, New York, 1967.
29. Fair, J. R., "Distillation," in Rousseau, R. W., *Handbook of Separation Process Technology*, Chap. 5, Wiley, New York, 1987.
30. Seader, J. D., and Z. M. Kurtyka, "Distillation," in Perry, R. H., and D. Green (eds.), *Perry's Chemical Engineers' Handbook*, Sec. 13, 6th ed., McGraw-Hill, New York, 1984.
31. Treybal, R. E., *Mass Transfer Operations*, 3d ed., McGraw-Hill, New York, 1980.
32. Wankat, P. C., *Equilibrium Staged Separations*, Elsevier, New York, 1988.
33. Ludwig, E. E., *Applied Process Design for Chemical and Petrochemical Plants*, 2d ed., vol. 2, Gulf Publishing, Houston, Texas, 1979.
34. Douglas, J. M., *Hydroc. Proc. 57*(2), 155, 1978.
35. Winn, F. W., *Pet. Ref. 37*(5), 216, 1958.
36. Underwood, A. J. V., *Chem. Eng. Progr. 44*, 603, 1948.
37. Van Winkle, M., and W. G. Todd, *Chem. Eng.* Sept. 20, p. 136, 1971.
38. Martin, H. Z., and G. G. Brown, *Trans. Am. Inst. Chem. Eng. 35*, 679, 1939.
39. Colburn, A. P., *Trans. Am. Inst. Chem. Eng. 32*, 1220, 1940.
40. Shiras, R. N., D. N. Hanson, and C. H. Gibson, *Ind. Eng. Chem. 42*(5), 871, 1950.
41. Barnés, F. J., D. N. Hanson, and C. J. King, *Ind. Eng. Chem. Proc. Des. Dev. 11*, 136, 1972.
42. Chou, S. M., and C. L. Yaws, *Hydroc. Proc. 65*(12), 41, 1986.
43. Chou, S. M., C. L. Yaws, and J. S. Cheng, *Can. J. Chem. Engrs. 64*, 254, 1986.
44. Tsuo, F. M., C. L. Yaws, and J. S. Cheng, *Chem. Eng.* July 21, p. 49, 1986.
45. Gilliland, E. R., *Ind. Eng. Chem. 32*, 1220, 1940.
46. Erbar, J. H., and R. N. Maddox, *Pet. Ref. 40*(5), 183, 1961.
47. Branan, C., *The Fractionator Analysis Pocket Handbook*, Gulf Publishing, Houston, Texas, 1978.
48. Eduljee, H. E., *Hydrocarb. Proc. 54*(9), 120, 1975.
49. Barna, B. A., and R. F. Ginn, *Hydrocarb. Proc. 64*(5), 115, 1985.
50. Liddle, C. J., *Chem. Eng.* Oct. 21, p. 137, 1968.
51. Molokanov, Y. K., T. P. Korablina, N. I. Mazurina, and G. A. Nikiforov, *Int. Chem. Eng. 12*(2), 209, 1972.
52. Chang, H. Y., *Hydrocarb. Proc. 60*(10), 146, 1981.

53. Al-Ameeri, R. S., and A. S. Said, *Separ. Sci. Technol. 20*, 565, 1985.
54. Henley, E. J., and J. D. Seader, *Equilibrium Stage Separation Operations in Chemical Engineering*, Wiley, New York, 1981.
55. Chianese, A., H. Campana, and M. Picciotti, *Hydrocarb. Proc. 61*(1), 133, 1982.
56. Kirkbridge, C. G., *Pet. Ref. 23*(9), 321, 1944.
57. Akashah, S. A., J. H. Erbar, and R. N. Maddox, *Chem. Eng. Commun. 3*, 461, 1979.
58. Smith, B. D., *Design of Equilibrium Stage Processes*, McGraw-Hill, New York, 1963.
58a. Rice, V. L., *Hydroc. Proc. 63*(8), 83, 1984.
59. Smoker, E. H., *Trans. Am. Inst. Chem. Engrs. 34*, 165, 1938.
60. Hohmann, E. C., in E. J. Henley (ed), Stagewise and Mass Transfer Operations, vol. 1, AIChE Modular Instruction, 1980.
61. Jafarey, A., J. M. Douglas, and T. J. McAvoy, *Ind. Eng. Chem. Proc. Des. Dev. 18*(2), 197, 1979.
62. Douglas, J. M., A. Jafarey, and R. Seemann, *Ind. Eng. Chem. Proc. Des. Dev. 18*(2), 203, 1979.
63. Hengstebeck, R. J., *Chem. Eng.* June 13, p. 115, 1969.

Chapter

4

Rigorous Distillation Calculations

Joe R. Haas

UOP, Des Plaines, Illinois

Before the 1950s, column calculations were performed by hand. Although rigorous calculation procedures were available, they were difficult to apply for all but very small columns. Shortcut methods were therefore the primary design tool. Rigorous procedures were only used for small columns or for final design checks. Inaccuracies and uncertainties in the shortcut procedures were usually accommodated by overdesign.

The introduction of computers has entirely reversed the design procedure. Rigorous calculations, once taking several days, sometimes weeks, for even a relatively simple column, can now be performed quickly and efficiently using a computer. No longer is there a need to tolerate the inaccuracies and uncertainties inherent in the shortcut procedures. In modern distillation practice, rigorous methods are the primary design tool.

The use of computers also led to a rapid development of better rigorous procedures. The rigorous methods developed in the 1930s were replaced by more efficient methods. Further, developments took place to permit application of rigorous methods to many complex fractionators, some of which could not be adequately modeled by shortcut methods.

With the superior accuracy and capabilities of modern rigorous methods, a column should not be designed without them. A shortcut calculation is inferior in accuracy, and in some cases may give mis-

leading results. In most modern column design work, the role of shortcut calculations is restricted to eliminating the least-desirable design options, providing the designer with an initial estimate for the rigorous step and for troubleshooting the final design. The rigorous methods are used as the primary design and optimization tool.

4.1 Basic Concepts

4.1.1 Stage and column models

Column model. A rigorous method describes a column as a group of equations and solves these equations to calculate the operating conditions of the column. All flows are usually expressed in terms of moles/hour. Also, when a rigorous calculation is performed, the following is usually specified:

- Rate, composition, and condition of each feed
- Number of stages in the column
- The stage for each feed, product, heat exchanger, and pumparound
- Separation specifications (see Sec. 3.1.1)
- Column pressure profile (see Sec. 3.1.3)

Column design and performance calculations present the column at steady state. What enters the column matches with what exits, for example,

$$\Sigma \text{ (molar feed flow rates)} = \Sigma \text{ (molar product flow rates)}$$

$$\Sigma \text{ (moles of any component in the feeds)} = \Sigma \text{ (moles of the component in the products)}$$

$$\text{Feeds enthalpy} + \text{heat added} = \text{products enthalpy} + \text{heat removed}$$

Some definitions

MESH equations. All of the equations used to describe the steady-state operation of a distillation column (Sec. 4.1.2). MESH stands for:

*M*aterial or flow rate balance equations, both component and total.

*E*quilibrium equations including the bubble-point and dew-point equations.

*S*ummation or stoichiometric equations or composition constraints.

*H*eat or enthalpy or energy balance equations.

Rigorous method: The mathematical method used to solve the MESH equations.

Solution: A solution is reached when all of the MESH equations are satisfied.

Simple stage: An equilibrium stage that contains no feeds, side products, or heat exchangers (top condenser/receiver, bottom reboiler, interreboiler, or intercondenser).

Simple column: A column with one feed, a top product and a bottom product, and no side products. The column can have a top condenser or receiver and bottom reboiler but no interreboiler or intercondenser.

Complex column: A column with more than one feed, or having one or more of the following features: side products; interreboilers, intercondensers, or pumparounds; and sidestrippers.

Figure 4.1*a* shows a complex column with two feeds and two side products. The top stage of the column is a partial condenser, with a vapor product D and a liquid product d. The reflux is the liquid, L_1, and the reflux ratio is $L_1/(D + d)$. The bottoms product B leaves stage N, the reboiler. The stages are numbered from the top, with the condenser as stage 1 and the reboiler as stage N. Components are numbered from 1 to the last, C.

The simple stage model. The ideal or equilibrium stage was defined and discussed earlier (Sec. 2.1). The material and energy flows in and out of a simple stage, with no feeds or side products, is depicted in Fig. 4.1*b*.

In this chapter, j represents the stage number and i the component number. The enthalpy terms, H_j and h_j, are molar enthalpies of the vapor and liquid leaving the stage, respectively. These molar enthalpies are multiplied by the total flow rates, V_j and L_j, leaving the stage to give the total energy leaving the stage in each phase.

Feed stage model. Piping arrangements encountered in most commercial columns were described by Kister (14). The feed stage model of Fig. 4.1*c* simulates the mixing pattern induced by these piping arrangements at the feed region. The feed stage model assumes that the feed liquid mixes with the liquid entering the feed stage while feed vapor mixes with vapor leaving the stage. If the feed is all liquid, it is added to the liquid flow entering the stage. If the feed is all vapor, it is added to the vapor flow entering the stage. A two-phase feed is distributed between the vapor leaving the feed stage and the liquid entering the feed stage. The distribution is found by an adiabatic flash of

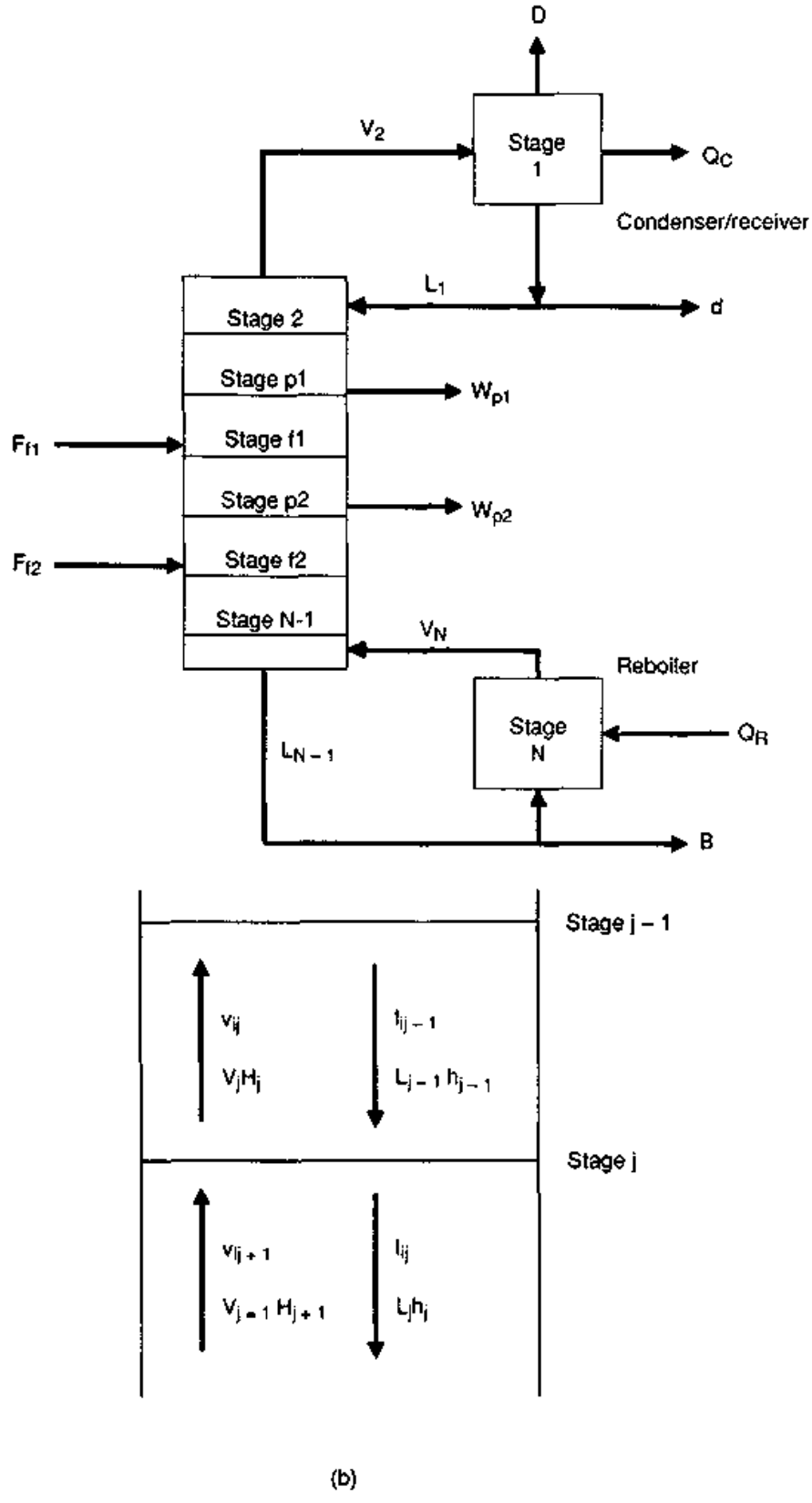

(b)

Figure 4.1 Stage and column models. (*a*) Overall column model; (*b*) simple stage model

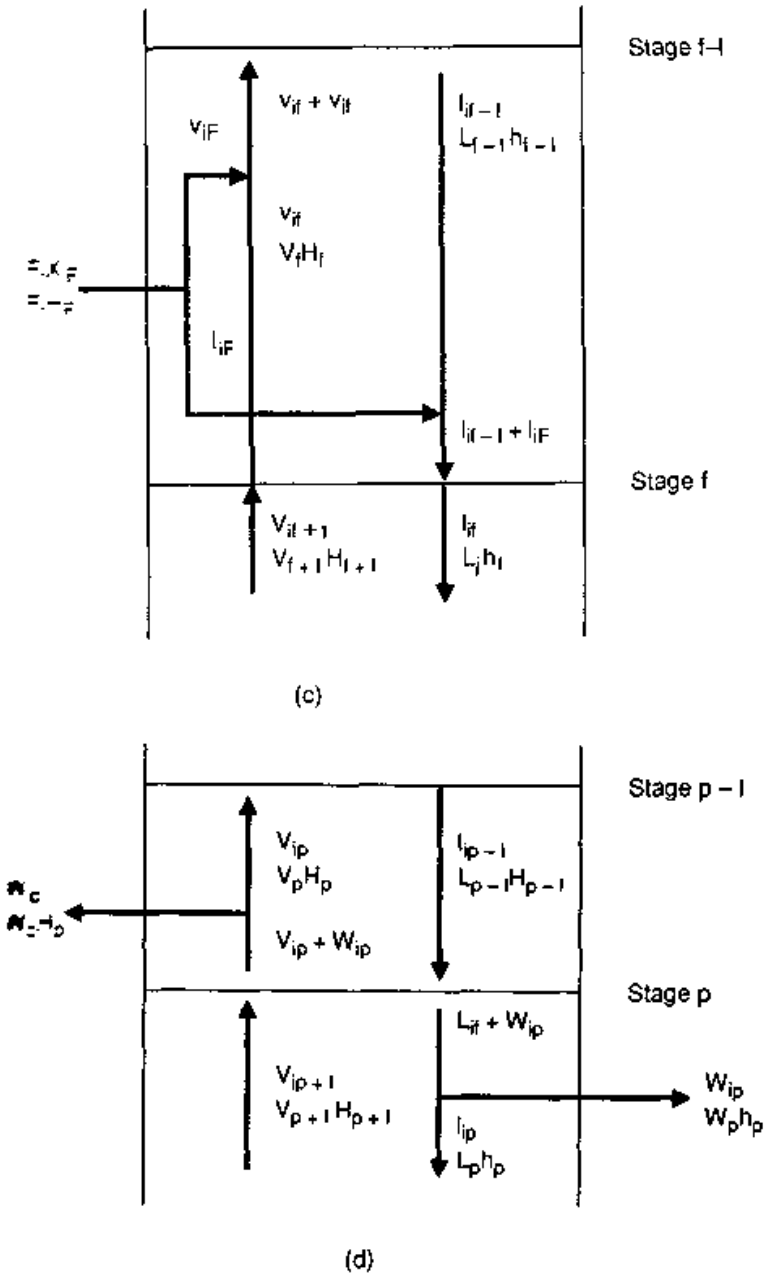

Figure 4.1 (*Continued*) Stage and column models. (*c*) feed stage model; (*d*) sidestream product withdrawal stage model.

the feed at the feed stage pressure but using the enthalpy of the feed, H_F, before the feed enters the column.

If a feed is subcooled liquid, it condenses some of the vapor ascending from the stage below the feed stage. If the feed is superheated, it vaporizes some of the liquid descending from the stage above the feed stage. For the bottom stage of a rectifier, the vapor feed substitutes the vapor entering from the reboiler. Likewise, for the top stage of a stripper, the liquid feed substitutes the reflux.

Side product stage model. For a stage with a side product, the side product, W_P, is subtracted from the material leaving the stage (i.e., W_P is drawn from the vapor leaving the stage to the stage above when W_P is a vapor product and is drawn from the liquid leaving the stage to the stage below if W_P is a liquid product). This stage is illustrated in Fig. 4.1*d*.

4.1.2 Basic (MESH) equations of rigorous distillation

The basic equations below fully describe a distillation column. They must be satisfied in any solution technique. These equations define the overall column total material balances, energy balances, and product compositions. Internal to the column, they describe equilibrium conditions, internal (stage-to-stage) component and total material balances, and internal energy balances. The independent variables of a column are the product rates and compositions, internal vapor and liquid rates and compositions, and stage temperatures. Equilibrium constants, K-values, and mixture enthalpies are dependent variables. Each stage is assumed to be at equilibrium (a theoretical stage), though an efficiency can be applied in the equations.

The rigorous methods thus convert a column to a group of variables and equations. The equations were first referred to as the MESH equations by Wang and Henke (24). The MESH variables are often referred to as *state variables*. These are

- Stage temperatures, T_j's
- Internal total vapor and liquid rates, V_j's and L_j's
- Stage compositions, y_{ij}'s and x_{ij}'s, or instead, component vapor and liquid rates, v_{ij}'s and l_{ij}'s.

The summation equation. The summation equation or composition constraint simply states that the sum of the mole fractions on each stage is equal to unity. For the liquid phase,

$$\sum_{i=1}^{C} x_{ij} - 1 = 0 \quad \text{or} \quad \sum_{i=1}^{C} l_{ij}/L_j - 1 = 0 \quad \text{or} \quad \sum_{i=1}^{C} y_{ij}/K_{ij} - 1 = 0 \qquad (4.1)$$

and for the vapor phase,

$$\sum_{i=1}^{C} y_{ij} - 1 = 0 \quad \text{or} \quad \sum_{i=1}^{C} v_{ij}/V_j - 1 = 0 \quad \text{or} \quad \sum_{i=1}^{C} K_{ij}x_{ij} - 1 = 0 \qquad (4.2)$$

The equilibrium equation. The equilibrium equation is

$$y_{ij} = K_{ij}x_{ij} \qquad \text{or} \qquad v_{ij}/V_j = K_{ij}\, l_{ij}/L_j \tag{4.3}$$

The equilibrium constant, K_{ij}, can be complex function itself, dependent on x_{ij} and y_{ij}

$$K_{ij} = K_{ij}(T_j, P_j, x_{ij}, y_{ij}) \tag{4.4}$$

as described in Chap. 1. The dependence of K_{ij} on x_{ij} and y_{ij} often appears in the MESH equations. The component rates of Eq. (4.3) can also be expressed in the terms of each other, giving

$$v_{ij} = l_{ij}\,(K_{ij}\,V_j/L_j) = l_{ij}\,S_{ij} \tag{4.5}$$

and

$$l_{ij} = v_{ij}(L_j/K_{ij}\,V_j) = v_{ij}\,A_{ij} \tag{4.6}$$

$K_{ij}\,V_j/L_j$ is termed the *stripping factor*, S_{ij}, while $L_j/K_{ij}\,V_j$ is termed the *absorption factor*, A_{ij}. The stripping and absorption factors have been used since the earliest absorber and distillation methods.

The component balances. A great effort in all rigorous methods is in solving the component balances. Proper construction of the equations and choice of numerical method is important. For a simple column (single feed, no side products), the overall component balance equation is

$$f_i - d_i - b_i = 0 \tag{4.7}$$

The component balance for the simple stage (no feed or side product), j, of Fig. 4.1*b*, is

$$v_{ij+1} + l_{ij-1} - v_{ij} - l_{ij} = 0 \tag{4.8}$$

Only the liquid portion of a feed, l_{iF}, appears in the component balance for feed stage, f, of Fig. 4.1*c*, that is,

$$v_{if+1} + l_{if-1} + l_{iF} - v_{if} - l_{if} = 0 \tag{4.9}$$

The vapor portion, v_{iF}, appears in the component balance for stage $f - 1$. For stage p of Fig. 4.1*d*, from which material is withdrawn, the component material balance is

$$v_{ip+1} + l_{ip-1} - v_{ip} - l_{ip} - w_{ip} = 0 \tag{4.10}$$

By convention, material leaving a tray has a negative value and material entering a tray has a positive value.

The total material balances. The total material balances are organized in the same manner as the component balances. The total material balance for the simple stage of Fig. 4.1*b* is

$$V_{j+1} + L_{j-1} - V_j - L_j = 0 \tag{4.11}$$

The same convention applies to feed and product trays where the total flow rate of a feed, F_f, is positive and the product, W_p, is negative.

The bubble- and dew-point equations. The equilibrium equation (Eq. 4.3) and the composition constraint [Eq. (4.1)] are combined to get the bubble-point equation,

$$\frac{1}{\sum_{i=1}^{C} l_{ij}} \sum_{i=1}^{C} K_{ij}\, l_{ij} - 1 = 0 \tag{4.12}$$

and the dew-point equation,

$$\frac{1}{\sum_{i=1}^{C} v_{ij}} \sum_{i=1}^{C} \frac{v_{ij}}{K_{ij}} - 1 = 0 \tag{4.13}$$

The bubble-point and dew-point equations are used in some of the solution methods to help determine the stage temperature.

The energy balance equations. The energy balance equations are required in any rigorous method. In narrow-boiling mixtures, they influence the internal total flow rates. In wide-boiling mixtures and in columns where there are great heat effects (e.g., oil refinery fractionators), they also strongly influence stage temperatures. The overall energy balance for a column with one feed and side product is

$$FH_F - DH_D - Bh_B - WH_W + Q_R - Q_C = 0 \tag{4.14}$$

The enthalpy terms, H and h, are per mole of mixture. Note that the enthalpies of the top and side products are written so that a vapor or liquid enthalpy can be substituted, depending on the phase of the product. The energy balance for the simple stage of Fig. 4.1*b* is

$$V_{j+1}H_{j+1} + L_{j-1}h_{j-1} - V_jH_j - L_jh_j = 0 \tag{4.15}$$

The enthalpies (energy per mole) for each phase are functions of temperature, pressure, and composition

$$H_j = H_j\,(T_j, P_j, y_{ij}) \tag{4.16}$$

$$h_j = h_j(T_j, P_j, x_{ij}) \tag{4.17}$$

For feed stages, sidestream product stages, and stages with intercondensers or interreboilers, additional terms are included in the energy balance equations [Eqs. (4.14) and (4.15)]. These terms are the same as those used in the overall column energy balance. The energy balance for the reboiler is

$$L_{N-1}h_{N-1} - V_N H_N - Bh_N + Q_R = 0 \tag{4.18}$$

and for a partial condenser with both vapor and liquid products:

$$V_2 H_2 - L_1 h_1 - dh_1 - DH_1 - Q_C = 0 \tag{4.19}$$

Subcooling is accounted for in h_1 (the enthalpy of the reflux L_1 and the liquid distillate d).

The energy balances are not solved in the same manner as the component or total material balances. With some solution methods, they are simultaneously solved with other MESH equations to get the independent column variables; in others they are used in a more limited manner to get a new set of total flow rates or stage temperatures.

Tray efficiencies. To characterize the deviation from ideality, stage efficiencies are often used (Sec. 2.1.1). Most computer simulations work with ideal stages. Once the number of ideal stages is established, the number of actual trays or packing height is calculated using stage efficiencies. Tray and packing efficiencies are discussed in detail in Chaps. 7 and 9. Some rigorous procedures incorporate tray efficiencies in the method. Commonly, a Murphree vapor efficiency (Sec. 7.1.1) is used for each component, given as

$$E_{MVij} = \frac{y_{ij} - y_{ij+1}}{y^*_{ij} - y_{ij+1}} \tag{4.20}$$

where y^*_{ij} is what the vapor composition would be if the vapor were in equilibrium with the actual liquid on the stage and y_{ij} and y_{ij-1} are actual vapor compositions. If the absorption factor is used [Eq. (4.6)], the vapor efficiency can be expressed in terms of variables already presented:

$$E_{MVij} = \frac{v_{ij} - v_{ij+1}(V_j/V_{j+1})}{(K_{ij}\, V_j/L_j)l_{ij} - v_{ij+1}(V_j/V_{j+1})} \tag{4.21}$$

The Murphree efficiency can be rearranged to form a modified equilibrium equation

$$y_{ij} = E_{MVij}\, K_{ij}\, x_{ij} + (1 - E_{MVij})\, y_{ij+1} \tag{4.22}$$

and can now appear in the absorption and stripping factors of the component balances and in the bubble-point and dew-point equations.

A vaporization efficiency E_{ij} based on the Murphree efficiency was defined by Holland and Liapis (10)

$$E_{ij} = E_{MVij} + (1 - E_{MVij}) \frac{y_{ij+1}}{K_{ij} x_{ij}} \tag{4.23}$$

This can be used in the MESH equations to account for stage nonideality. This vaporization efficiency is applied to the equilibrium constant K_{ij} and appears as the product $E_{ij}K_{ij}$. The vaporization efficiency does solve a computational problem in placing an efficiency in the MESH equations. As shown by Lockett (105), a major disadvantage of the vaporization efficiency is that it does vary with composition. Near the top of a high-purity column, as y_{ij+1} and x_{ij} approach unity, E_{ij} also approaches unity, and so a vaporization efficiency does not truly reflect stage nonidealities.

Caution then should be used in any choice of efficiency. Some limitations are outlined above; others are discussed in Chap. 7 and by Lockett (105). Both the author of the book and the author of this chapter feel that usually it is best to perform the rigorous calculation using ideal stages and then apply an overall column efficiency to account for stage nonideality.

4.2 Rigorous Computational Methods

4.2.1 The basic classification of the methods

Friday and Smith (1) and King (11) have divided the rigorous methods into four basic classes. These are

1. The bubble-point methods (BP)
2. The sum-rates methods (SR)
3. The $2N$ Newton methods
4. The global Newton or simultaneous correction (SC) methods

The original method of Wang and Henke (24) gave the name to the BP methods because the stage temperatures are found by directly solving the bubble-point equation. The SR methods use the energy balances to update the stage temperatures. The $2N$ Newton's methods calculate temperatures and total flow rates together but compositions are calculated in a separate, dependent step. These three classes are referred to as equation tearing or decoupling methods because the

MESH equations are divided and grouped or partitioned and paired with MESH variables to be solved in a series of steps. The SC methods attempt to solve all of the MESH equations and variables together. Additional classes are

5. Inside-out methods
6. Relaxation methods
7. Homotopy-continuation methods
8. Nonequilibrium models

The relaxation, inside-out, and homotopy-continuation methods are extensions of whole or part of the first four methods in order to solve difficult systems or columns. The nonequilibrium models are rate- or transport phenomena–based methods that altogether do away with the ideal-stage concept and eliminate any use of efficiencies. They are best suited for columns where a theoretical stage is difficult to define and efficiencies are difficult to predict or apply.

4.2.2 Precomputer methods

The Thiele-Geddes (15) and Lewis-Matheson (16) methods are rigorous methods referred to as stage-to-stage methods. Both preceded the computer and suit manual calculations.

The Thiele-Geddes method. This method is one of the first (1933) rigorous methods for distillation and is the basis of most modern rigorous methods. A key point of the Thiele-Geddes method is the use of the absorption and stripping factors. These will appear in the computer methods. It is known as the rating method because it requires the specification of all feed conditions, feed-stage locations, reflux rate, total product rates, and number of stages. Product compositions and exchanger duties are calculated.

The original form of the Thiele-Geddes method uses the stripping and absorption factors to calculate liquid and vapor compositions. The compositions for the rectifying section are calculated stage to stage by successive substitution, beginning with the distillate product, until the feed stage is reached.

$$y_{ij} = X_{Di}\,(A_{ij}A_{ij-1}\cdots A_{i1} + A_{ij-1}\cdots A_{i1} + \cdots + A_{i2}A_{i1} + A_{i1} + 1) \qquad (4.24)$$

Compositions for the stripping section are found by the same procedure, but beginning with the reboiler and calculating up to the feed. With these compositions, the temperatures are updated, usually by a trial-and-error bubble-point technique. With the new temperatures,

the total flow rates are calculated from the energy balances. A test is then made of the overall total and component balances. If the column is out of balance, the top and bottom compositions are adjusted and the calculation is repeated.

The Lewis-Matheson method. This method, published in 1932, is the converse of the Thiele-Geddes method. Here, the product light-key and heavy-key component distributions are specified, while the number of stages above or below the feed stage are changed. Stage-to-stage calculations are made from the top stage down to the feed stage and from the reboiler up to the feed stage. A comparison is made between the feed stage compositions from the top-down and from the bottom-up calculations. If the two do not match, stages are added to or removed from either the rectifying or stripping sections and the procedure is repeated. Temperatures and total flow rates can be found as in the Thiele-Geddes method. Because the number of stages is adjusted, the Lewis-Matheson method is called the design method.

The Lewis-Matheson method does not work well for wide-boiling mixtures because of the required component distribution. There is also the difficulty of deciding what is a good match at the feed stage.

The Lewis-Matheson method can be modified so that the number of stages is fixed and instead the product compositions or the reflux ratio is adjusted. The criterion of a match at the feed stage is preserved.

4.2.3 The strategy of solution using a rigorous method

A rigorous method proceeds in the following steps:

1. Problem setup
2. Initialization of the MESH variables
3. Actual calculation
4. Solution test
5. Output and engineer's evaluation

Problem setup. Section 4.1.1 describes the variables that are usually specified. All of these, except the separation specification, are straightforward.

Section 3.1.1 states that in a process design, a separation is specified in terms of purities and product flows. For a simple column, two specifications are made and at least one must be a purity. Section 3.1.1 also states that the purity specification can be substituted by a physical property which is a function of the purity or composition, while a product flow can be substituted by a recovery specification.

In a computer simulation, the number of stages and the feed point location are fixed (Sec. 4.1.1) for a given solution. Once these are fixed, distillate (or bottom) composition becomes a function of reflux rate, and the purity specification is met through a reflux rate specification. Since the reflux is only one of the internal flows in the column, a similar argument will apply to any other internal stage flow. It follows that the purity specification can be met by specifying any internal stage flow, either vapor or liquid. Similarly, other variables that can be specified include reflux-to-distillate ratio, boilup-to-bottoms ratio, reboiler heat duty, and temperature of a given stage.

The option of specifying an internal flow instead of a purity specification is particularly useful with some of the methods described below that do not permit direct purity specifications. However, the larger number of options available to the user also increases the pitfalls of inconsistent specifications. These pitfalls are discussed in Secs. 4.3.1 and 4.3.2.

For a column with side products, the number of specified variables increases with each side product. In most methods, the product flow rate is specified for each side product, but sometimes it is possible to specify the purity of a side product. For columns with interreboilers or intercondensers, the number of specified variables increases by the number of these exchangers. Usually, the interreboilers or intercondenser duties are specified, but in some methods, these duties may be allowed to vary to meet a product specification. With these complex columns, inconsistent specifications are a major pitfall and simpler specifications are preferred.

Initial values. Before a trial is begun, stage temperatures, T_j's, and total flow rates, V_j's and L_j's, have to be given initial values. The stage component rates, v_{ij}'s and l_{ij}'s, do not have to be estimated since these can be calculated from the component balances. The component balances are dependent on the K-values and for the first component balances, composition-independent K-values must be used. A composition-independent K-value can be found from the pure component fugacities calculated from an equation of state:

$$K_{ij} \text{ (composition independent)} = f_{ijL}(\text{pure})/f_{ijV}(\text{pure}) \qquad (4.25)$$

For the rest of the first column trial and for succeeding trials, the composition-dependent K-values are used.

The initial total flow rate and temperature profiles can make the difference between success and failure of a rigorous method. Usually for distillation columns, the condenser and reboiler temperatures are estimated and a calculation that assumes constant molal overflow (Sec. 2.2.2) is used to initialize the internal vapor and liquid flow

rates. These carry down through the column to any feed or side product stage. The problem at these stages is that there is an abrupt change in the internal vapor and/or liquid rates when the feed is added or the product subtracted. At the feed stage, the feed is flashed at the stage pressure to give its distribution (Sec. 4.1.1). Also, a product rate can be defined as a ratio to the remaining vapor or liquid to keep from starving a stage.

Any program should permit the user to initialize the internal flow rates and temperatures. The best way is to have the user initialize a few internal flow rates and temperatures and have the program calculate the others by linear interpolation. User-provided internal flows and temperatures are especially important for

- Wide-boiling mixtures and energy-coupled systems where the profiles may shift drastically from linear.
- Where constant molar overflow does not work well, such as with nonideal systems or where there is a drastic difference between internal vapor and liquid rates. Section 2.2.2 discusses the applicability of constant molal overflow.
- Complex columns—e.g., multiple feeds, side products, interreboilers and intercondensers, pumparounds and side strippers—at or near the stages where these appear. See Sec. 4.1.1 for other examples.
- The stage below a subcooled receiver where the temperature difference between the two may be great.
- The overhead vapor and overhead liquid products of a partial condenser. In a column with a high amount of noncondensables, the split between these two products is very sharp and wrong estimates can prevent a solution.
- Reflux in high-purity or narrow-boiling columns.

For some systems, the initial values have to be near the expected solution results. For superfractionators, and columns with purity specifications and highly nonideal systems, the initial temperature profile should be near the expected results. For narrow-boiling systems, an accurate reflux estimate is necessary.

Solution criteria. With any rigorous method it is imperative to set criteria to determine when a solution is reached. Each rigorous method has its own unique criteria, but they all must conform to some physical criteria. Section 4.1.1 states that at solution, overall mass, component, and energy balances are achieved. There are other criteria a method should meet. If there are specifications such as product flow

rates, heat duties, or product compositions, these must be matched within some tolerance. At the solution, the temperature and total flow rate profiles should not change between iterations; i.e., the accumulated fractional change in stage temperatures and in stage vapor rates between trials k and $k + 1$ should be very small:

$$\sum_{j=1}^{N} \frac{|T_{j,k+1} - T_{j,k}|}{T_{j,k}} \to 0 \tag{4.26}$$

$$\sum_{j=1}^{N} \frac{|V_{j,k+1} - V_{j,k}|}{V_{j,k}} \to 0 \tag{4.27}$$

Errors in the MESH equations of Sec. 4.1.2 should be small, including the stage energy; total material and component balances and summation equation should be small. The physical solution criteria above should take precedence over any mathematical criteria, such as having Newton-Raphson functions approach zero (Sec. 4.2.6).

4.2.4 Tridiagonal matrix method for the material balances

Calculating the component flow rates. The tridiagonal matrix method introduced by Wang and Henke (24), is a fast and accurate technique for calculating the component and total flow rates. This method for calculating the component flow rates is used in most of the following rigorous methods.

The component liquid rates are eliminated from Eq. (4.10) using the absorption factors [Eq. (4.6)] to leave only the component vapor rates. Any feed rates are moved to the right of the equal sign. The terms that multiply the component vapor rates are the factors in the diagonals of the tridiagonal matrix:

$$L_{j-1}/K_{ij-1}\, V_{j-1}(1 + L_j/K_{ij}V_j)\, v_{ij} + v_{ij+1} = -f_{ij} \tag{4.28}$$

or

$$A_{ij-1}\, v_{ij-1} - (1 + A_{ij})\, v_{ij} + v_{ij+1} = -f_{ij} \tag{4.29}$$

This equation expresses both the component liquid and vapor rates for the stage in terms of vapor rates only. In matrix terms, the system of equations is expressed as

$$\underline{\mathbf{r}}_i\, \underline{\mathbf{v}}_i = -\underline{\mathbf{f}}_i \tag{4.30}$$

where the transposed vapor rate vector is

$$\underline{\mathbf{v}}_i = (d_i, v_{i1}, v_{i2}, \cdots, v_{iN-1}, v_{iN})^T \tag{4.31}$$

and the transposed feed rate vector is:

$$\underline{\mathbf{f}}_i = (0, 0, \cdots, v_{if}, l_{if}, \cdots, 0, 0)^{\mathrm{T}} \tag{4.32}$$

The feed to a stage is split into the two phases of an adiabatic flash as v_{iF} for the vapor portion and l_{iF} for the liquid portion. The coefficients of the component vapor rates in Eq. (4.29) form the elements of the tridiagonal matrix

$$\underline{\mathbf{r}}_i = \begin{vmatrix} m_{i1} & 1 & 0 & & \cdots & \cdot\cdot & \cdot\cdot & \cdot\cdot & \cdots & \cdots \\ A_{i1} & m_{i2} & 1 & 0 & \cdots & \cdot\cdot & \cdot\cdot & \cdot\cdot & \cdots & \cdots \\ 0 & A_{i2} & m_{i3} & 0 & \cdots & \cdot\cdot & \cdot\cdot & \cdot\cdot & \cdots & \cdots \\ \cdot\cdot & 0 & A_{i3} & \cdot\cdot & \cdots & \cdot\cdot & \cdot\cdot & \cdot\cdot & \cdots & \cdots \\ \cdot\cdot & \cdot\cdot & \cdot\cdot & \cdot\cdot & \cdots & 0 & \cdot\cdot & \cdot\cdot & \cdots & \cdots \\ \cdot\cdot & \cdot\cdot & \cdot\cdot & \cdot\cdot & m_{ij-1} & 1 & 0 & \cdot & \cdots & \cdots \\ \cdot\cdot & \cdot\cdot & \cdot\cdot & \cdot\cdot & A_{ij-1} & m_{ij} & 1 & \cdot & \cdots & \cdots \\ \cdot\cdot & \cdot\cdot & \cdot\cdot & \cdot\cdot & 0 & A_{ij} & m_{ij+1} & \cdot & \cdots & \cdots \\ \cdot\cdot & \cdot\cdot & \cdot\cdot & \cdot\cdot & \cdots & 0 & \cdot\cdot & \cdot\cdot & \cdots & \cdots \\ \cdot\cdot & \cdot\cdot & \cdot\cdot & \cdot\cdot & \cdots & \cdot\cdot & \cdot\cdot & \cdot\cdot & 0 & \cdot\cdot \\ \cdot\cdot & \cdot\cdot & \cdot\cdot & \cdot\cdot & \cdots & \cdot\cdot & \cdot\cdot & \cdots & 1 & 0 \\ \cdot\cdot & \cdot\cdot & \cdot\cdot & \cdot\cdot & \cdots & \cdot\cdot & \cdot\cdot & A_{iN-2} & m_{iN-1} & 1 \\ \cdot\cdot & \cdot\cdot & \cdot\cdot & \cdot\cdot & \cdots & \cdot\cdot & \cdot\cdot & 0 & A_{iN-1} & m_{iN} \end{vmatrix} \tag{4.33}$$

where for any stage j, the term for the main diagonal is

$$m_{ij} = -(1 + L_j/K_{ij}\, V_j) = -(1 + A_{ij}) \tag{4.34}$$

for the lower diagonal, the term for stage j is the absorption factor A_{ij}, given by Eq. (4.6), and for the upper diagonal, the terms for all stages are unity.

For a stage with a side product, the term for the main diagonal is modified to include the ratio of the side product total flow rate to the stage flow rate corresponding to its phase (see Sec. 4.1.1). For a stage p with a vapor side product, W_{V_p}, the term is

$$m_{ip} = -(1 + L_p/K_{ip}\, V_p + W_{V_p}/V_p) \tag{4.35}$$

For a stage p with a liquid side product, W_{L_p}, the term for the main diagonal, is

$$m_{ip} = -[1 + L_p/K_{ip}\, V_p\,(1 + W_{LP}/L_p)] \tag{4.36}$$

The total distillate rate replaces the vapor rate in the terms for a condenser. For a partial condenser, the terms for the middle and lower diagonals are

$$m_{i1} = -(1 + L_1/K_{i1}\, D) \tag{4.37}$$

$$A_{i1} = L_1/K_{i1}\, D \tag{4.38}$$

For a total condenser, the terms include just the reflux ratio:

$$m_{i1} = -(1 + L_1/D) \tag{4.39}$$

$$A_{i1} = L_1/D \tag{4.40}$$

For a reboiler, as stage N, the term for the middle diagonal is

$$m_{iN} = -(1 + B/K_{iN}\, V_N) \tag{4.41}$$

The absorption factor in Eq. (4.6) is used to get the liquid rates after the vapor rates are calculated in the solution of the component balances described above. The equations can just as well be rearranged to calculate the component liquid rates with the component vapor rates found from Eq. (4.5).

Calculating the total flow rates. Rearrangement of the total material balance equations parallels that of the component balance equations above. To create the tridiagonal matrix, the equations are rearranged to allow for the total vapor rates to be used as the independent variables. Ratios of the total liquid and vapor rates become the coefficients of the vapor rate terms that go into the tridiagonal matrix.

$$(L_{j-1}/V_{j-1})V_{j-1} - (1 + L_j/V_j)\, V_j + V_{j+1} = 0 \tag{4.42}$$

In matrix form, the total material balance equations are expressed as:

$$\underline{\mathbf{R}}\,\underline{\mathbf{V}} = -\underline{\mathbf{F}} \tag{4.43}$$

The new liquid rates are found by multiplying the new total vapor rate by the ratio of the old liquid and vapor rates:

$$L_{j\text{new}} = (L_j/V_j)V_{j\text{new}} \tag{4.44}$$

Few of the rigorous methods use this means to calculate the total flow rates. The tridiagonal total material balance matrix [Eqs. (4.42) to (4.44)] can still be used to bring the column back into a good material balance before the next calculation of the component material balances. It can also be used to get a complete initial column flow rate profile once some initial estimates have been entered.

The numerical method for solving the tridiagonal matrix. There are solution techniques geared specifically for tridiagonal matrices. One method commonly used is the recurrence formulas of the Thomas algorithm. In recurrence formulas, the calculation (forward elimination) will begin at the upper left corner (top stage) of the tridiagonal and proceed down the main diagonal. A set of factors will be generated for

each row of the matrix. Then a calculation (back substitution) is made starting at the lower right corner (last stage) of the matrix and proceeding up the diagonal to get the values of the independent variables (component or total vapor rates).

In calculation methods like the original Thomas algorithm, where the factors of a stage are calculated from the factors of a previous stage, a buildup of computer truncation errors can occur (from subtraction operations). Boston and Sullivan (25) presented a modified Thomas algorithm with the subtraction steps eliminated. This modified version has been shown to help some columns that have difficulty in solving the component balances, especially those with multiple feeds and side streams. The modified version has also been shown to help wide-boiling mixtures that have components with K-values greater than unity in one part of the column and less than unity in another part of the column.

When the component balances are solved by recurrence formulas, the flow rate of a component on the extremes of the mixture boiling range often approaches zero. This leads to computer underflow and divide-by-zero errors. Protection against such errors should be included in the recurrence calculations to trap such errors and set the component flow rate to zero on that stage.

The shape of a tridiagonal matrix permits easy storage in three vectors instead of one large $N \times N$ matrix. Since this storage is consistent for all tridiagonal matrices, they can all be handled in the same manner and there are a number of subroutines available specifically for these. Press et al. (121), the IMSL package from IMSL, in Houston, Texas, and others have tridiagonal matrix solution routines.

4.2.5 Bubble-point (BP) methods

The BP methods use a form of the equilibrium equation and summation equation to calculate the stage temperatures. The first BP method, by Wang and Henke (24), included the first presentation of the tridiagonal method to calculate the component flow rates or compositions. These are used to calculate the temperatures by solving the bubble-point equation but this temperature calculation can be prone to failure.

An alternative is to use the tridiagonal method for calculating compositions, but to calculate the new temperatures directly, without iterating on the bubble-point equation. These new temperatures are approximate but as long as the internal compositions are properly corrected during each column trial, the temperature profile will continue to move toward the solution. This is the basis of the theta method of Holland (7, 9, 26). With either alternative, the energy balances are used to find the total flow rates.

The BP methods generally work best for narrow-boiling, ideal or nearly ideal systems, where composition has a greater effect on temperature than the latent heat of vaporization.

The theta method. This method has been primarily applied to the Thiele-Geddes equations but a form of the theta method equation has also been applied to the equations of the Lewis-Matheson method. The main independent variable of the method is a convergence promoter, theta (or θ). The convergence promoter θ is used to force an overall component and total material balance and to adjust the compositions on each stage. These new compositions are then used to calculate new stage temperatures by an approximation of the dew- or bubble-point equation called the K_b method. The power of the K_b method is that it directly calculates a new temperature without the sort of failures that occur when iteratively solving the bubble- or dew-point equations.

The theta function. This function begins with the component balance for a conventional column:

$$\Sigma FX_{iF} = d_i + b_i \qquad \text{or} \qquad \frac{\Sigma FX_{iF}}{d_i} = 1 + (b_i/d_i) \tag{4.45}$$

where ΣFX_i represents the molar flow rate of the component in all feeds. The theta multiplier is defined as a corrector to the ratio of the component product rates calculated by the tridiagonal matrix method

$$\left|\frac{b_i}{d_i}\right|_{co} = \theta \left|\frac{b_i}{d_i}\right|_{ca} \tag{4.46}$$

The corrected distillate and bottoms component product rates are

$$(d_i)_{co} = (d_i)_{ca}\, p_i \tag{4.47}$$

$$(b_i)_{co} = \theta\, (b_i)_{ca}\, p_i \tag{4.48}$$

where p_i is a corrector created by combining the overall component balance [Eq. (4.45)] with the definition of θ [Eq. (4.46)]:

$$p_i = \frac{FX_i}{(d_i)_{ca} + \theta\, (b_i)_{ca}} \tag{4.49}$$

In the theta method, the total distillate rate and reflux ratio are all that can be specified and the theta function [Eq. (4.50)] is written to find a value of theta such that the sum of the corrected component distillate rates equals the total distillate rate:

$$\frac{1}{D_{\text{spec}}} \sum_{i=1}^{C} (d_i)_{co} - 1 = 0 \tag{4.50}$$

For complex columns, an additional theta multiplier is defined for each side product W. The p_i correction factor is expanded to include in the denominator a term for each additional product and the total flow for each side product is specified. The final values of all of the θ's will be unity.

To continue with the column trial, the p_i factors are used to correct the stage-to-stage component flow rates:

$$(v_{ij})_{co} = (v_{ij})_{ca}\, p_i \qquad (l_{ij})_{co} = (l_{ij})_{ca}\, p_i \tag{4.51}$$

and the compositions

$$(y_{ij})_{co} = \frac{(v_{ij})_{co}}{\sum_{i=1}^{C} (v_{ij})_{co}} \qquad (x_{ij})_{co} = \frac{(l_{ij})_{co}}{\sum_{i=1}^{C} (l_{ij})_{co}} \tag{4.52}$$

These new compositions are used to find a new set of stage temperatures.

The K_b method. For updating the tray temperatures, the theta method relies on the K_b method. The K_b method takes advantage of the near-linear dependence of the logarithm of the K-values and the relative volatilities on temperature over short temperature spans. Relative volatilities ($\alpha_{ij,k}$'s) are calculated with respect to a base component K-value, $K_{bj,k}$, at the stage temperature of the current column trial, $T_{j,k}$. The base component is usually a middle boiler or a hypothetical component. The K-value of the base component for the next trial, $K_{bj,k+1}$, is calculated using a form of the bubble-point equation unique to the K_b method:

$$K_{bj,k+1} = \sum_{i=1}^{C} (x_{ij})_{co}\, (\alpha_{ij})_k \tag{4.53}$$

where $\alpha_{ij} = K_{ij,k}/K_{bj,k}$. The stage temperature for the next trial $(k + 1)$ is calculated from

$$T_{j,k+1} = B_{j,k}/(A_{j,k} - \ln K_{bj,k+1}) \tag{4.54}$$

$A_{j,k}$ and $B_{j,k}$ are the constants for a pseudo-Clausius-Clapeyron equation for the base component K-value. These constants are unique for every stage and are updated at every trial in the calculation. They are calculated as follows. Using the K-value method chosen for the simu-

lation, two K-values are calculated for the base component at the corrected compositions, $(x_{ij})_{co}$ and $(y_{ij})_{co}$, one at temperature $T_{j,k} + \Delta T_k$ and the other at $T_{j,k} - \Delta T_k$. $A_{j,k}$ and $B_{j,k}$ are then calculated using Eq. 4.54). The ΔT_k should be no more than 25 to 50°F for the first trial and reduced in size for succeeding trials (as the final temperature profile is approached). Billingsley (30), Boston and Sullivan (69), Lo (31), and Jelinek (73) have proposed modifications to the K_b method.

The constant-composition method. Since in the theta method temperatures are found using the equilibrium and summation equations, the next set of stage-to-stage total flow rates is calculated through the energy balances. The liquid rate leaving a stage, L_j, can be found by rearranging the energy balance for that stage. The vapor entering from the stage below, V_{j+1}, is still unknown but can be eliminated using the component balances for the stage. The liquid rate is found by

$$L_j = \frac{V_j[H(T_{j+1},y_{ij}) - H(T_j,y_{ij})] - L_{j-1}[H(T_{j+1},x_{ij-1}) - h(T_{j-1},x_{ij-1})]}{H(T_{j+1},x_{ij}) - h(T_j,x_{ij})} \quad (4.55)$$

Because of the rearrangement, the constant-composition method requires calculating an enthalpy of a phase at the temperature of one stage but using the composition of a different phase and stage. As stated by Holland (8), this "may be represented by a thermodynamic process which occurs at constant composition." The enthalpy per mole terms above are specifically:

$H(T_{j+1},y_{ij})$ = vapor enthalpy at T_{j+1} and vapor composition y_{ij}.

$H(T_j,y_{ij})$ = vapor enthalpy at T_j and vapor composition y_{ij}.

$H(T_{j+1},x_{ij-1})$ = vapor enthalpy at T_{j+1} and liquid composition x_{ij-1}.

$h(T_{j-1},x_{ij-1})$ = liquid enthalpy at T_{j-1} and liquid composition x_{ij-1}.

$H(T_{j+1},x_{ij})$ = vapor enthalpy at T_{j+1} and liquid composition x_{ij}.

$h(T_j,x_{ij})$ = liquid enthalpy at T_j and liquid composition x_{ij}.

The total vapor rate entering from the stage below is found from the total material balance:

$$V_{j+1} = V_j + L_j - L_{j-1} \quad (4.56)$$

The total vapor entering the condenser is calculated using the reflux ratio:

$$V_2 = (1 + L_1/D)D \quad (4.57)$$

The calculation begins with the energy balance of the condenser to get its duty and continues stage to stage down through the column.

Next trial. With these new total flow rates and using the new temperatures, the component flow rates can be recalculated using the tridiagonal method and a new column trial can be initiated. Note again that the theta method is different from other methods in that the total product rates and reflux ratio are specified while the condenser and reboiler duties are calculated.

Summary of the theta method procedure

1. Set initial stage temperatures, T_j's, and vapor rates, V_j's. Initial liquid rates are found using the tridiagonal method for the total material balances. The theta method requires the distillate rate, sidestream product rates, and reflux ratio to be specified.
2. Based on the most recent set of temperatures and total flow rates, calculate the component vapor rates using the tridiagonal matrix method. Find the component liquid rates by $l_{ij} = A_{ij}\, v_{ij}$.
3. Calculate the θ (or θ's for a complex column) and p_i's such that the theta function (or functions) is very nearly zero.
4. Correct the component flow rates and the compositions for each stage using the p_i's developed in step 3.
5. With these corrected compositions, calculate new stage temperatures, T_j's, using the K_b method.
6. Calculate the total liquid rates from the constant composition method, using the most recent set of compositions and temperatures. Total vapor rates are found from the material balance for each stage.
7. Convergence is achieved when the θ's are very nearly unity and all other solution criteria (see Sec. 4.2.3) have been met. If not solved, return to the component balances of step 2.

The theta method has found many applications. The FRAKB routines of FLOWTRAN use the theta method. Portions of the theta method, such as the K_b method for temperatures, appear in other rigorous methods. Poor initial temperature and flow rate estimates do not greatly hinder the approach to solution and the calculation is relatively rapid. It has been shown to work well for the systems that the BP methods are meant for, i.e., narrow- and middle-boiling ranges, ideal or nearly ideal mixtures. It has solved columns with as many as 200 stages without great difficulty.

4.2.6 Numerical methods—the Newton-Raphson technique

The MESH equations can be regarded as a large system of interrelated, nonlinear algebraic equations. The mathematical method used to solve these equations as a group is the Newton-Raphson method. The solution gives the steady-state values of the column variables: temperatures, flow rates, compositions, etc. A particular rigorous method may not make use of all of the MESH equations in the Newton-Raphson portion of the method. Instead, it may solve the remaining MESH equations by some other means. The methods in Secs. 4.2.7 to 4.2.13 make some use of the Newton-Raphson method. This section reviews the Newton-Raphson technique itself. Detailed discussion of the Newton-Raphson method and its variations can be found in Holland's text (8).

Each MESH equation is dependent on more than one MESH variable. The MESH equations are represented as a set of functions, f_1, $f_2, \ldots, f_n$, with a corresponding set of independent variables, $x_1, x_2, \ldots, x_n$. The Newton-Raphson method is a matrix method in which the partial derivatives or change of each function with respect to each variable are placed in a square $n \times n$ matrix called the *Jacobian.*

$$\underline{\mathbf{J}}_k = \begin{vmatrix} \frac{\delta f_1}{\delta x_1} & \frac{\delta f_1}{\delta x_2} & \cdots & \frac{\delta f_1}{\delta x_n} \\ \frac{\delta f_2}{\delta x_1} & \frac{\delta f_2}{\delta x_2} & \cdots & \frac{\delta f_2}{\delta x_n} \\ \cdot & \cdot & & \cdot \\ \cdot & \cdot & & \cdot \\ \cdot & \cdot & & \cdot \\ \frac{\delta f_n}{\delta x_1} & \frac{\delta f_n}{\delta x_2} & \cdots & \frac{\delta f_n}{\delta x_n} \end{vmatrix} \tag{4.58}$$

In matrix language, the Newton-Raphson equation is

$$\underline{\mathbf{J}}_k \, \Delta \underline{\mathbf{x}}_k = -\underline{\mathbf{f}}_k \tag{4.59}$$

where $\underline{\mathbf{f}}_k$ is a vector of the independent functions at column trial k:

$$\underline{\mathbf{f}}_k = [f_1 f_2 \ldots f_n]^T \tag{4.60}$$

The $\Delta \underline{\mathbf{x}}_k$ represents a vector of the changes in the independent variables that bring an improvement in the functions, $\underline{\mathbf{f}}_k$, from trial k to trial $k + 1$:

$$\Delta \underline{\mathbf{x}}_k = [\Delta x_1 \, \Delta x_2 \ldots \Delta x_n]^T \tag{4.61}$$

where for any $x_{k+1} = x_k + \Delta x_k$. The objective in the Newton-Raphson is to find a set of independent variables

$$\underline{\mathbf{x}}_k = [x_1 x_2 \ldots x_n]^T \tag{4.62}$$

so that all of the independent functions are very nearly zero. The MESH equations presented earlier were written so that they all equal zero in order to fulfill this requirement of the Newton-Raphson method.

Generating the derivatives is the most difficult part of the method. Writing analytical derivatives of composition-dependent K-values and enthalpies can be very difficult, especially if a method such as UNIQUAC and NRTL is being used. The alternative is numerical derivatives. For any independent variable, these can be found by:

$$\frac{\delta f}{\delta x} = \frac{[f(x + e) - f(x - e)]}{2e} \tag{4.63}$$

where e is a perturbed value for x, e.g., $e = 0.001x$. Numerical derivatives also have inherent problems. If the perturbed value e is too small, the derivative will be meaningless. If it is too large, the derivative may actually cause the Newton-Raphson to move away from the solution. After all, the Newton-Raphson is an approximation technique. In the derivatives, it assumes that the nonlinear MESH equations are linear over short distances. If too large a distance is used, the convergence will be very coarse.

If analytical derivatives for the K-values and enthalpies are available, they should be used. More effort will be needed when developing analytical derivatives but once tested and error-free, the rigorous method will be more reliable. Lucia and Westman (52) used a hybrid method that included a mixture of analytical and numerical derivatives and found it improved convergence.

In addition to the solution criteria in Sec. 4.2.3, the Newton-Raphson method requires an additional check on convergence. This check, termed the *norm* or the *square root of the sum of the squares,* tests that all of the functions are driven nearly to zero:

$$\text{norm} = \frac{\left|\sum_1^n f(x)^2\right|^{1/2}}{n} \tag{4.64}$$

When the norm is small (i.e., $<10^{-4}$), the Newton-Raphson method has found a set of variables that reasonably satisfies the independent equations. If the norm is at a small value but the other solution crite-

ria have not been reached, the calculation should continue with the norm driven increasingly smaller.

Produced from the manipulation of the Jacobian are the changes in the variables, i.e., the $\Delta \mathbf{x}_k$ vector. The variables for the next trial are calculated from $\underline{\mathbf{x}}_{k+1} = \underline{\mathbf{x}}_k + s_k \Delta \underline{\mathbf{x}}_k$ (i.e., $x_{1,k+1} = x_{1,k} + s_k \Delta x_{1,k}$, etc.). The s_k scalar is generated to ensure that the norm of functions improve between trial $k + 1$ and trial k. Usually, $s_k = 1$ but may have to be smaller on some trials. The Newton-Raphson method assumes that the curves of the independent functions are close to linear and the slopes will point toward the answers. The MESH equations can be far from linear and the full predicted steps, $\Delta \underline{\mathbf{x}}_k$, can take the next trial well off the curves. The s_k scaler helps give an improved step search or prevents overstepping the solution. Holland (8) and Broyden (119) present formulas for getting s_k.

There should also be a restriction in the Newton-Raphson so that the independent variables calculated in a trial are within a tolerance. When the independent variables are temperatures, they should be in a range, $T_{\min} < T_j < T_{\max}$. Also, all flow rates must be greater than zero. If any variable is not within the tolerances, all steps, $\Delta \underline{\mathbf{x}}_k$, should be halved.

Holland (8) recommends LU (lower-upper) factorization for calculating the $\Delta \underline{\mathbf{x}}_k$ vector. Older methods such as a Gauss-Jordan elimination should be avoided because they build excessive computer error. In LU factorization, the Jacobian is rearranged into two matrices; $\underline{\mathbf{J}}_k = \underline{\mathbf{L}}_k \underline{\mathbf{U}}_k$ where the $\underline{\mathbf{L}}_k$ matrix or lower triangle has elements on the diagonal and below and the $\underline{\mathbf{U}}_k$ matrix or upper triangle has elements on the diagonal and above. LU factorization has similar characteristics of the forward and back substitution of the Thomas algorithm for tridiagonal matrices. There are many LU factorization routines available. Press et al. (121) and Kahaner et al. (122) have well-documented routines in their texts. Commercial packages such as from IMSL, Inc., in Houston, Texas, the Harwell Subroutine Library from AERE Harwell in Oxford, England, and the LINPACK system from the National Energy Software Center, Argonne National Laboratory, Argonne, Illinois, all have a more than one LU factorization and matrix solution routine.

A basic Newton-Raphson iterative calculation proceeds as follows:

1. Assume a set of independent variables $\underline{\mathbf{x}}_k$, where $k = 0$ for the first trial.
2. Using $\underline{\mathbf{x}}_k$, calculate the values for the independent functions $\underline{\mathbf{f}}_k$. Test if a solution has been reached by calculating the norm.

3. Calculate the partial derivatives for the Jacobian matrix $\underline{\mathbf{J}}_k$ [Eq. (4.58)].
4. Using LU factorization, solve the Jacobian for the $\Delta\underline{\mathbf{x}}_k$ vector. Add this to the existing set of independent variables, $\underline{\mathbf{x}}_k$, to get a new set of independent variables, $\underline{\mathbf{x}}_{k+1}$. Continue through the rigorous method. The next pass through the Newton-Raphson begins at step 2.

In some Newton-Raphson-based rigorous methods, a poor set of starting values can cause the calculation to never approach a solution. Occasionally, the calculation oscillates, with values swinging to either side of the solution. A good simulation program should include means for detecting and preventing this, e.g., by damping or limiting the change to the next set of variables. A Newton-Raphson method will normally take even steps toward the solution.

The quasi-Newton methods. In the Newton-Raphson method, the Jacobian is filled and then solved to get a new set of independent variables in every trial. The computer time consumed in doing this can be very high and increases dramatically with the number of stages and components. In quasi-Newton methods, recalculation of the Jacobian and its inverse or LU factors is avoided. Instead, these are updated using a formula based on the current values of the independent functions and variables. Broyden's (119) method for updating the Jacobian and its inverse is most commonly used. For LU factorization, Bennett's (120) method can be used to update the LU factors. The Bennett formula is

$$\underline{\mathbf{J}}_{k+1} = \underline{\mathbf{L}}_{k+1}\,\underline{\mathbf{U}}_{k+1} = \underline{\mathbf{L}}_k\,\underline{\mathbf{U}}_k + [\underline{\mathbf{f}}_{k+1} - (1 - s_k\,\underline{\mathbf{f}}_k)]\,C\,\Delta\mathbf{x}_k \qquad (4.65)$$

where s_k is the scalar found above such that $\text{norm}_{k+1} < \text{norm}_k$ and C is a scalar found by

$$C = \frac{1}{s_k\,\Delta\underline{\mathbf{x}}_k T\,\Delta\underline{\mathbf{x}}_k} \qquad (4.66)$$

Just as LU factorization is more efficient and more accurate than calculating the inverse, the use of the Bennett method is less time consuming than the Broyden method.

The quasi-Newton methods reduce the computer time spent per trial by reevaluating the Jacobian but at the expense of a greater number of trials. The total computer time sometimes exceeds that of the conventional Newton-Raphson method. The quasi-Newton methods also are more sensitive to how close the initial values are to a final solution and tend to fail more readily. They may have to be avoided

altogether for difficult problems or where the number of independent variables exceeds 100.

Quasi-Newton methods like Broyden's and Bennett's do work well when the curves are almost linear across the entire range. To have independent functions nearly linear, they need to be designed so that they are quite simple. The inside-out method (Sec. 4.2.10) is one of the methods that do this.

4.2.7 Sum-rates (SR) method

The SR method is suitable for modeling absorbers and strippers. For some extremely wide boiling systems, especially those with noncondensables, it is the best method. It has been found to work very well for the side strippers of a refinery fractionator. Absorbers typically have a rich gas bottom stage feed and a lean oil top stage feed. The equations of the SR method do not allow its direct use for reboiled absorbers, absorbers with condensers, or distillation columns. For these columns, other methods like that of Tomich (Sec. 4.2.8) or Russell (Sec. 4.2.10) can be used.

The SR method was first presented by Sujata (35) and McNeese (36), and was given its name by Friday and Smith (1). The application of the tridiagonal method for solving the material balances was added by Burningham and Otto (34).

In the SR method, temperatures are the dominant variables and are found by a Newton-Raphson solution of the stage energy balances. Compositions do not have as great an influence in calculating the temperatures as do heat effects or latent heats of vaporization. The component flow rates are found by the tridiagonal matrix method. These are summed to get the total rates, hence the name sum rates.

The single independent equation for each stage is its energy balance. The equation should be written in terms of the ratio of the energy entering the stage to that leaving the stage, i.e.,

$$\frac{V_{j+1}H_{j+1} + L_{j-1}h_{j-1}}{V_jH_j + L_jh_j} - 1 = 0 \tag{4.67}$$

The enthalpy of a feed, such as the lean oil feed, L_o, on the top stage or the rich gas feed, V_{N+1}, on the bottom stage will appear in the numerator. An interreboiler duty also appears in the numerator of the stage. The enthalpy for a side product or an intercondenser duty appears in the denominator of the stage.

The number of independent functions is equal to the number of stages:

$$\underline{f}_k = [E_1\, E_2 \ldots E_{N-1}\, E_N] \tag{4.68}$$

The independent variables of the Newton-Raphson method are the stage temperatures:

$$\underline{\mathbf{x}}_t = [T_1\ T_2 \ldots T_{N-1}\ T_N] \tag{4.69}$$

The SR method requires that the total molal flow rate, composition, location, and thermal condition of all feeds be specified, including the lean oil, L_o, to the top stage and the rich gas, V_{N+1}, to the bottom stage. The steps of the algorithm are as follows:

1. Set initial temperatures and total vapor rates for each stage. Initial liquid rates can be found by total material balances.
2. Based on the most recent set of temperatures and total flow rates, calculate the component vapor rates using the tridiagonal matrix method. Calculate the component liquid rates by applying the absorption factor [Eq. (4.6)].
3. Calculate the total flow rates by summing the component flow rates.

$$V_j = \sum_{i=1}^{C} v_{ij} \qquad \text{and} \qquad L_j = \sum_{i=1}^{C} l_{ij} \tag{4.70}$$

4. Calculate all of the independent functions and their norm. Get a new set of temperatures T_j's by solving the independent equations during one pass through the Newton-Raphson procedure.
5. The norm of the independent functions must be very small at the solution (see Sec. 4.2.6 for criteria). This should be tested in step 4 before proceeding through the calculation and solution of the Jacobian. If the norm is not small or other criteria (Sec. 4.2.3) have not been met, return to step 2.

Whenever the stage temperatures are varied, such as in the calculation of the derivatives for the Jacobian, steps 2 and 3 must be included in the calculation of the independent functions. The temperatures affect the K-values and therefore compositions, and these changes cascade through the column. Because of this, there are no zero elements in the Jacobian and a tridiagonal matrix technique cannot be used in its solution.

The test of the summation of the vapor component rates to see if a solution has been reached should be based on the total vapor flow rate of the previous trial and the component rates of the current trial. If the solution is based on the independent functions alone, the SR

method may not calculate through enough trials and the solution may not material balance.

The SR method can be applied to distillation columns, but the equations of the algorithm do not allow the solution of the condenser and the reboiler with the other stages in the column. Because only the energy balances are used as independent functions, reboiler and condenser duties, reflux ratio, and the boilup ratio have to be specified. This overspecifies the column and the solution cannot be found. The condenser and the reboiler can be solved as separate unit operations in a flowsheet as demonstrated by Fonyo et al. (39). The SR method is used in the ABSBR step of FLOWTRAN of Monsanto, St. Louis, Missouri, and also in both the public release version of ASPEN and in ASPENPlus of AspenTech, Cambridge, Massachusetts.

4.2.8 2*N* Newton methods

In both the BP and SR methods (Secs. 4.2.5 and 4.2.7) the temperatures and the total flow rates are calculated separate of each other. An alternative is to calculate the temperatures and total flow rates together in a Newton-Raphson technique. The name 2*N* Newton comes from that there are two equations per stage for a total of $2 \times N$ functions and variables per column for the Newton-Raphson. In all three of these approaches, the component flow rates are still calculated in an intermediate step.

The best-known presentations are by Tomich (32), Holland (8), and Orbach et al. (33). These vary in their choice of Newton-Raphson equations and independent variables and each may solve a different range of columns. These methods have been shown to work well for wide-boiling mixtures including refinery fractionators, absorber-stripper columns, and reboiled absorbers.

The Tomich method. This method has the summation equations for the vapor and liquid compositions are merged for the first independent equation:

$$\sum_{i=1}^{C} y_{ij} - \sum_{i=1}^{C} x_{ij} = 0 \tag{4.71}$$

The x_{ij}'s and y_{ij}'s are found from the component balances and the equilibrium equation.

The other independent function is the stage energy balance and is the same as Eq. (4.67) of the SR method above.

In the original statement of the Tomich method, condenser and

reboiler duties must be specified, but the equations can be readily adjusted to make these variable. The independent functions are then

$$\underline{\mathbf{f}}_k = [S_1\, S_2 \ldots S_{N-1}\, S_N\, E_1\, E_2 \ldots E_{N-1}\, E_N]^T \tag{4.72}$$

The independent variables are the stage temperatures and total vapor flow rates

$$\underline{\mathbf{x}}_k = [T_1\, T_2 \ldots T_{N-1}\, T_N\, V_1\, V_2 \ldots V_{N-1}\, V_N]^T \tag{4.73}$$

The calculation sequence of the Tomich method is as follows:

1. Set initial temperatures and total vapor for each stage.
2. Find total liquid rates by stage-to-stage material balance.
3. Based on the most recent set of temperatures and total flow rates, calculate the liquid compositions using the tridiagonal matrix method and find the vapor compositions by the equilibrium equation.
4. Get a new set of temperatures and vapor rates by solving the independent equations during one pass through the Newton-Raphson procedure.
5. The norm of the independent functions must be very small at the solution (Sec. 4.2.6). If this or the other criteria (Sec. 4.2.3) have not been met, return to step 2.

Though the summation equations and the energy balances are the independent functions for the Newton-Raphson, the component and total material balances must be recalculated whenever the T_j's and V_j's vary. This includes when the functions are evaluated during the filling of the Jacobian and so there is a full Jacobian, i.e., no zero elements. While the derivatives well off the diagonal of the Jacobian are small, they cannot be ignored. Ignoring these is likely to cause the method to fail or to converge to the wrong answer.

Tomich recommends filling and inverting the Jacobian only once and using the Broyden method (Sec. 4.2.6) to update the inverse. This reduces computer time per trial but increases the number of column trials or passes through the procedure and for some columns may also decrease reliability of the method. It is the author's experience that for many columns, solution is easier to reach when the Jacobian is filled and inverted in each trial and Broyden's method is not used.

The 2*N* Newton-Raphson method. This method of Holland (8) is similar to the Tomich method but adds two innovations. The summation equa-

tion for each stage is replaced by either a dew-point or bubble-point equation as an independent function and the total vapor rate is replaced by a multiplier θ_j on the ratio of the total vapor to liquid rates L_j/V_j. Since the dew- and bubble-point equations are combinations of both the summation equation and equilibrium equation, both now directly come into play in the independent functions. The other independent functions are still the stage energy balances. The independent functions are represented by

$$\underline{\mathbf{f}}_k = [D_1\, D_2 \ldots D_{N-1}\, D_N\, E_1\, E_2 \ldots E_{N-1}\, E_N] \tag{4.74}$$

The independent variables are the temperatures and the θ_j multipliers:

$$\underline{\mathbf{x}}_k = [T_1\, T_2 \ldots T_{N-1}\, T_N\, \theta_1\, \theta_2 \ldots \theta_{N-1}\, \theta_N] \tag{4.75}$$

The multiplier θ_j is defined as follows:

$$\left|\frac{L_j}{V_j}\right|_{\text{co}} = \theta_j \left|\frac{L_j}{V_j}\right|_{\text{ca}} \tag{4.76}$$

where $(L_j/V_j)_{\text{ca}}$ uses the most recent value of the total flow rates. The corrected L_j/V_j ratio is used in the absorption and stripping factors of the component balances and in the total material balances.

The θ_j multiplier, by being a correction to the ratio of total flow rates, adds a measure of stability to the solution by preventing the existence of negative flow rates. The steps of the $2N$ Newton-Raphson method follow those of Tomich.

Application. Both the Tomich and the $2N$ Newton-Raphson methods are proven methods and have been applied often. The Tomich method was part of the GMB system of The Badger Company, Cambridge, Massachusetts, and is in many in-house simulators. Both methods are best for wide- or middle-boiling separations. Because one of the equations in the $2N$ Newton-Raphson method is a dew- or bubble-point equation, it may work better for middle or more narrow-boiling mixtures than the Tomich method. Both methods have also been applied to absorber-strippers, though an SR method is still the best method for the most wide-boiling absorber-strippers. Because of the full Jacobian more numbers to manipulate), for columns over 50 stages these methods will use excessive computer time and memory. Also, the solution of the Jacobian is prone to failure when the number of stages is high, and so these methods are not recommended for tall columns.

4.2.9 Global Newton methods

One group of methods that is very popular are the global Newton methods, also called the simultaneous correction (SC) methods. The most applied of these are that of Naphtali and Sandholm (42) and Goldstein and Stanfield (45). Other global Newton methods have been presented by Ishii and Otto (47) and Gallun and Holland (40). The general principles of a global Newton method are common to all these methods. The Naphtali and Sandholm method will be discussed first to gain an understanding of the global Newton methods. Advantages and differences of the others listed above will follow. Other methods of merit but not presented here are that of Ferraris (41), Ricker and Grens (57), and Kubicek, Hlavacek, and Prochaska (46). Global Newton methods have been extended to include additional equations and variables for solving three-phase distillation columns as done by Block and Hegner (50), Wu and Bishnoi (51) and Bondy (59), and for reactive distillation columns by Holland (8) and Rafal et al. (58).

In the global Newton methods, all of the equations are solved together in a Newton-Raphson technique. The methods vary in their choice of variables and MESH equations for the Newton-Raphson calculation, but none of the MESH equations is solved in any separate step outside of the Newton-Raphson calculation (e.g., the component balances in the $2N$ Newton methods). In the BP, SR, and $2N$ Newton methods, the compositions lag the other MESH calculations (since K-values and enthalpies are generated using the compositions from the previous trial) and compositions of each component are calculated independently of the others (due to the use of the tridiagonal matrix). These are major disadvantages with highly nonideal systems, where K-values (especially activity coefficients) and enthalpies are highly composition dependent and where the composition of one component cannot be readily decoupled from those of others. The global Newton method includes the component balances among the Newton-Raphson independent functions and compositions join other MESH variables as the independent variables.

The global Newton methods are the most sensitive of the rigorous methods to the quality of the initial values and often require initial values near the answer. While they are the most powerful in solving nonideal mixtures, it may be necessary to use another rigorous method, such as a BP or SR method, to develop initial values approaching the solution before the global Newton method takes over the calculation.

The Naphtali-Sandholm (42) method. This method chooses the stage temperatures and component vapor and liquid rates from the MESH variables as the independent variables of the Newton-Raphson calcu-

lation. The MESH equations serving as independent functions and grouped by stage are the energy balance, a component balance for each component and an equilibrium equation for each component. There are $2C + 1$ equations per stage with $N(2C + 1)$ equations for the whole column. The energy balance is the normalized version presented for the SR or Tomich methods [Eq. (4.67)] except that the total flow rates are not independent variables. Instead, they are calculated by summing the component flow rates to give

$$\frac{H_{j+1}\sum_{i=1}^{C} v_{ij+1} + h_{j-1}\sum_{i=1}^{C} l_{ij-1}}{H_j\sum_{i=1}^{C} v_{ij} + h_j\sum_{i=1}^{C} l_{ij}} - 1 = 0 \tag{4.77}$$

The normalized form of the component balance is

$$\frac{v_{ij+1} + l_{ij-1}}{v_{ij} + l_{ij}} - 1 = 0 \tag{4.78}$$

As in the energy balance, what enters is divided by what leaves. Any component in a feed is added to the numerator and a sidestream product is added to the denominator. The equilibrium equation for each component is of the form

$$\frac{K_{ij}\, l_{ij}}{\sum_{i=1}^{C} l_{ij}} - \frac{v_{ij}}{\sum_{i=1}^{C} v_{ij}} = 0 \tag{4.79}$$

The equations are normalized to keep the numerical values in the same order of magnitude. Since Naphtali-Sandholm equations are grouped by stage and for a system with C components, the independent functions for any stage j are

$$\underline{\mathbf{f}}_{j,k} = [E_j\, m_{1j}\, m_{2j} \ldots m_{ij} \ldots m_{cj}\, e_{1j}\, e_{2j} \ldots e_{ij} \ldots e_{cj}]^{-T} \tag{4.80}$$

The independent variables for the stage are

$$\underline{\mathbf{x}}_{j,k} = [T_j\, l_{1j}\, l_{2j} \ldots l_{c-1j}\, l_{cj}\, v_{1j}\, v_{2j} \ldots v_{c-1j}\, v_{cj}]^{T} \tag{4.81}$$

The functions and variables are solved together using a large Jacobian of size $N(2C + 1) \times N(2C + 1)$. When originally presented, the Naphtali-Sandholm method used derivatives of K-values and enthalpies with respect to composition and temperature, but it was not stated whether these are analytical or numerical derivatives.

As in the $2N$ Newton methods, the condenser duty Q_C and reboiler

duty Q_R are specified, while the reflux ratio and product rates are calculated. If some other specification is required such as product purity, the energy balance for that stage can be replaced with a specification function and the duty is calculated outside of the Newton-Raphson in a separate energy balance.

One characteristic of the global Newton methods is that large numbers of the derivatives are zero. In the Tomich method, all the component balances are solved in the tridiagonal matrix when evaluating every function and this gives the full Jacobian. In the global Newton methods, the component balances are left in native form and not rearranged using absorption and stripping factors. When one flow or temperature is varied, it usually has little effect on functions more than two stages away. The derivatives (except for the K-values and enthalpies) are easy to calculate. Those of the component balances, for example, will be either 1, −1, or 0. Because functions and variables are grouped by stage in the Naphtali-Sandholm method, its sparse Jacobian will be a block-banded matrix with the derivatives grouped as blocks along main, upper, and lower diagonals, giving

	$\underline{X}_1$	$\underline{X}_2$	...	$\underline{X}_j$	...	$\underline{X}_{N-1}$	$\underline{X}_N$
$\underline{f}_1$	$\frac{\partial \underline{f}_1}{\partial \underline{x}_1}$	$\frac{\partial \underline{f}_1}{\partial \underline{x}_2}$	O's	...		O's	
$\underline{f}_2$	$\frac{\partial \underline{f}_2}{\partial \underline{x}_1}$	$\frac{\partial \underline{f}_2}{\partial \underline{x}_2}$	O's		...	O's	
⋮							
$\underline{f}_{j-1}$	O's		$\frac{\partial \underline{f}_{j-1}}{\partial \underline{x}_{j-1}}$	$\frac{\partial \underline{f}_{j-1}}{\partial \underline{x}_j}$	O's	...	O's
$\underline{f}_j$			$\frac{\partial \underline{f}_j}{\partial \underline{x}_{j-1}}$	$\frac{\partial \underline{f}_j}{\partial \underline{x}_j}$	$\frac{\partial \underline{f}_j}{\partial \underline{x}_{j+1}}$	...	O's
$\underline{f}_{j+1}$	O's			$\frac{\partial \underline{f}_{j+1}}{\partial \underline{x}_j}$	$\frac{\partial \underline{f}_{j+1}}{\partial \underline{x}_{j+1}}$		O's
⋮							
$\underline{f}_{N-1}$	O's					$\frac{\partial \underline{f}_{N-1}}{\partial \underline{x}_{N-1}}$	$\frac{\partial \underline{f}_{N-1}}{\partial \underline{x}_N}$
$\underline{f}_N$	O's	...	O's			$\frac{\partial \underline{f}_N}{\partial \underline{x}_{N-1}}$	$\frac{\partial \underline{f}_N}{\partial \underline{x}_N}$

where $\underline{\mathbf{x}}_j$ represents all of the variables of stage j and $\underline{\mathbf{f}}_j$ represents all of the functions of stage j. Because of this block form of the Jacobian, the computer time and storage is not great, possibly less than that required by a Tomich method. All of the global Newton methods have a sparse Jacobian matrix. About 95 percent of the matrix is zero's and it is quite simple to store only the nonzero elements. There are many numerical methods routines available specifically for solving sparse Jacobians.

The Naphtali-Sandholm procedure is as follows

1. Set initial temperatures and total vapor and liquid rates for each stage. Calculate initial component vapor rates using the tridiagonal matrix method and find the component liquid rates by applying the absorption factor, $l_{ij} = A_{ij}\, v_{ij}$.
2. Calculate all of the independent functions and the norm.
3. Fill and solve the sparse Jacobian for a new set of temperatures, T_j's, and component vapor and liquid rates, v_{ij}'s and l_{ij}'s, by solving the independent equations during one pass through the Newton-Raphson procedure.
4. The norm of the independent functions must be very small at the solution (see Sec. 4.2.6 for criteria). If it is not small or other solution criteria (Sec. 4.2.3) have not been met, return to step 2.

Note that there are no other side calculations between passes through the Newton-Raphson procedure. Total flow rates and duties are calculated after a solution of the column is found.

Christiansen et al. (54) applied the Naphtali-Sandholm method to natural gas mixtures. They replaced the equilibrium relationships and component vapor rates with the bubble-point equation and total liquid rate to get practically half the number of functions and variables [to $N(C + 2)$]. By exclusively using the Soave-Redlich-Kwong equation of state, they were able to use analytical derivatives of K-values and enthalpies with respect to composition and temperature. To improve stability in the calculation, they limited the changes in the independent variables between trials to where each change did not exceed a preset maximum. There is a Naphtali-Sandholm method in the FraChem program of OLI Systems, Florham Park, New Jersey; CHEMCAD of Coade Inc. of Houston, Texas; PRO/II of Simulation Sciences of Fullerton, California; and Distil-R of TECS Software, Houston, Texas. Variations of the Naphtali-Sandholm method are used in other methods such as the homotopy methods (Sec. 4.2.12) and the nonequilibrium methods (Sec. 4.2.13).

The Goldstein-Stanfield (45) method. This method chooses the stage temperatures, total vapor rates, total liquid rates, and liquid compo-

sitions of each stage as the independent variables. Different from Naphtali-Sandholm, vapor compositions are not among the independent variables. Like Naphtali-Sandholm, the independent functions include normalized energy and component balances [Eqs. (4.77) and (4.78)]. In addition, a summation equation [Eq. (4.71)] and a normalized total material balance are used, giving a total of $N(C + 3)$ equations for the column. Also, Goldstein and Stanfield arranged the functions by equation type with the component material balances arranged by component and not by stage. Vector of independent functions is of the form:

$$\underline{\mathbf{f}}_k = [m_{11} \ldots m_{1N} \ldots m_{C1} \ldots m_{CN} H_1 \ldots H_N S_1 \ldots S_N M_1 \ldots M_N]^T \qquad (4.83)$$

with the corresponding set of independent variables:

$$\underline{\mathbf{x}}_k = [x_{11} \ldots x_{1N} \ldots x_{C1} \ldots x_{CN} T_1 \ldots T_N V_1 \ldots V_N L_1 \ldots L_N]^T \qquad (4.84)$$

Like the Naphtali-Sandholm, the Jacobian is mostly zeros, although it is not a block-banded matrix. The Goldstein-Stanfield method uses a series of matrix manipulations to first find the changes in the temperatures and total vapor rates, the ΔT_j's and ΔV_j's. These are then used to find the changes in the liquid rates, ΔL_j's, and the actual liquid compositions, the x_j's. The steps of the Goldstein-Stanfield method follow those of Naphtali-Sandholm, except there are these unique matrix manipulations in solving the independent equations. Like Naphtali-Sandholm, the condenser and reboiler duties and side-product rates are specified. The Goldstein-Stanfield method is included in the COPE simulation program of Exxon, the MAXPLUS program of Kesler Engineering, Highland Park, New Jersey, and the DS03 program of Paul Oleson and Associates, Laguna Beach, California. Bondy (59) extended the Goldstein-Stanfield method to nonideal three-phase systems for the CHEMDIST method in the PRO/II program of Simulation Sciences of Fullerton, California.

While Goldstein and Stanfield (45) did not include derivatives for K-values and enthalpies in their original formulation, these can be readily included. This can improve the speed of the method with reasonably ideal mixtures. Goldstein and Stanfield (45) and Boston (75) stated that the Naphtali-Sandholm approach of grouping the functions by stage is more suitable for columns with many stages and few components. Because both the component vapor and liquid rates are among the independent variables, the Naphtali-Sandholm approach should also work better for highly nonideal mixtures. The Goldstein-Stanfield approach of arranging functions by component, the tendency to ignore derivatives of K-values and enthalpies with respect to composition, the choice of independent variables, and the matrix manipu-

lations should be better for columns with few stages and many components, and has been shown to work well for refinery fractionators.

The Ishii and Otto method. The method of Ishii and Otto (47) follows an approach similar to the Goldstein-Stanfield method. The energy balance, summation equation for the liquid compositions, and the component balances are the independent functions. These equations are grouped by type, and as in the Goldstein-Stanfield method, adjustments to the temperatures and total vapor rates, ΔT_j's and ΔV_j's, are found first after the series of matrix manipulations. The liquid compositions for each stage are then found using the total rates and temperatures. While Ishii and Otto did include derivatives of K-values and enthalpies, they were based only on the simple Chao-Seader correlation and with several approximations in the derivatives. The method may reduce computer resource needs, but since the compositions calculation is split from the temperatures and total rates calculations, and due to the approximations in the derivatives, it may have difficulty solving nonideal systems. Holmes et al. (109) successfully applied the Ishii-Otto method to amine strippers in the program TSWEET of Bryan Research and Engineering, Bryan, Texas. The Ishii-Otto method is also used by the AMSYM program of D. W. Robinson and Associates of Edmonton, Alberta.

The almost band algorithm. This method of Gallun and Holland (40) and Holland (8) is unique in its flexibility, wide combination of equations for solving different types of columns, and for the strong effort in developing sparse Jacobian matrix solution techniques. It follows the Naphtali-Sandholm approach of grouping the equations by stage in a block-banded form. It allows for mixing and matching, adding and eliminating variables and equations to fit the application, and solves for all variables simultaneously without the matrix manipulations of Goldstein-Stanfield.

Gallun and Holland bring activity coefficients into the independent functions to separate them from the calculation of the ideal mixture K-values. Presenting the activity coefficients directly in the equilibrium equation emphasizes how they and their derivatives cannot be and are not ignored when considering nonideal mixtures.

The method of Gallun and Holland is the broadest application of the MESH equations in a global Newton method and may solve the widest range of columns. Formulations by Gallun and Holland (40) for distillation columns included adding the total material balance to give freedom in specifications or to substitute these for the equilibrium equations for more ideal mixtures.

Gallun and Holland (40) also presented solution techniques for the sparse matrices of the global Newton method. There are many other

solution techniques available. The Jacobian matrix of these methods contain values in only 3 to 10 percent of the elements. To save storage and allow the solution of tall columns and mixtures with many components, none of the zero elements should have to be stored or manipulated.

The matrix solution techniques of the block-banded formulations of Naphtali and Sandholm (42) and of Holland (8) are generally simpler than that of the other global Newton methods. Also, the Naphtali-Sandholm and almost band methods are better suited for nonideal mixtures than other global Newton methods.

4.2.10 *Inside-out methods*

The inside-out algorithm has become one of the most popular methods because of its robustness and its ability to solve a wide variety of columns. The inside-out concept was developed by Boston and Sullivan (69) and Boston (70). Russell (72) presented an inside-out method that works well for many refinery fractionators. Jelinek (73) presented a simplified Russell method.

In the previous four groups of methods (Secs. 4.2.5 and 4.2.7 to 4.2.9), the MESH variables of temperatures, total flow rates, and component flow rates are the primary solution variables and are used to generate the K-values and enthalpies from complex correlations. These methods update the MESH variables in an outer, though sometimes partitioned, loop with the K-values and enthalpies updated whenever the MESH variables change. The inside-out concept reverses this by using the complex K-value and enthalpy correlations to generate parameters for simple K-value and enthalpy models. These parameters are unique for each stage and become the variables for the outside loop. The inside loop consists of the MESH equations and is a variation on the BP, SR, and $2N$ Newton methods. Since the K-values and enthalpies are simple, the inside loop works well for a wide range of mixtures and is little affected by the nonideality of mixtures. In every step through the outside loop, the simple models are updated using MESH variables (mostly temperatures and compositions) from the inside loop. This sets up the next pass through the inside loop.

The Boston method. The original Boston and Sullivan (69) inside-out algorithm has evolved to that presented by Boston and Britt (71), Boston (70), and Trevino-Lozano et al. (74). There have been more advances to the Boston method which were not reported in the literature. The concepts of outside loop K-value and enthalpy models with the inside-loop column solution is preserved throughout.

The outer-loop K-value model is based on the K_b method (Sec. 4.2.5):

$$\ln K_{bj} = A_j + B_j\,(1/T_j - 1/T^*) \tag{4.85}$$

where T^* is a reference temperature for the K-value correlation. Outer-loop variables, A_j and B_j, are generated for each stage from a reference $K_{bj,\mathrm{Ref}}$ of a composite component:

$$\ln K_{bj,\mathrm{Ref}} = \sum_{i=1}^{C} w_i \ln K_{ij,\mathrm{actual}} \tag{4.86}$$

where the w_i's are weight factors found by a method in Boston and Britt (71). The temperatures and compositions used to get the $K_{ij,\mathrm{actual}}$ are the latest from the inside loop. Simple relative volatilities are among the outside-loop variables, and are used in the K_b method to calculate the temperatures and whenever K-values are needed in the inside loop

$$\alpha_{ij} = K_{ij,\mathrm{actual}}/K_{bj,\mathrm{Ref}} \tag{4.87}$$

These simple relative volatilities change little over the range of temperatures that is seen on a given stage and greatly simplify temperature and composition calculations in the inside loop. For nonideal mixtures, an activity coefficient for each component accounts for composition effects in the inside loop. This activity coefficient has a simple model, similar to the K_b model:

$$\ln \gamma^*_{ij} = a_{ij} + b_{ij}\,x_{ij} \tag{4.88}$$

where the new outer-loop variables, a_{ij} and b_{ij}, for each component are determined from the actual activity coefficient model at the current stage temperature and stage composition.

The simple K-values used in the inside loop are easily determined from

$$K_{ij,\mathrm{simple}} = K_{bj}\,\alpha_{ij}\,\gamma^*_{ij} \tag{4.89}$$

The activity coefficient model is dropped for ideal or nearly ideal mixtures.

The enthalpy models are actually for the enthalpy departure function. Normally, the molar enthalpy of a phase is found from the ideal gas enthalpy and the enthalpy departure

$$H_j = H^\circ_j + \Delta H_{Vj} \tag{4.90}$$

$$h_j = h^\circ_j + \Delta H_{Lj} \tag{4.91}$$

where H°_j and h°_j are the ideal gas enthalpies based on the vapor- and liquid-phase compositions and ΔH_{Vj} and ΔH_{Lj} are the enthalpy departures calculated by the enthalpy correlation. The simple enthalpy departure used in the inside loop is a straight-line function:

$$\Delta H_{Vj} = C_j - D_j\,(T_j - T^*) \tag{4.92}$$

$$\Delta H_{Lj} = E_j - F_j\,(T_j - T^*) \tag{4.93}$$

where T^* is a base temperature. Thus, the outside-loop calculation consists of updating the terms of the simple K-value, activity, and enthalpy models. In some systems, such as ammonia-water, the enthalpy model gives too crude an approximation and is therefore inappropriate. In those systems, the enthalpy model is not used and enthalpies of the inside loop are calculated directly by the enthalpy correlations.

The inside loop consists of the actual calculation of the MESH variables and is similar to one of the BP or SR methods. For the inside loop, Boston defines two new variables, R_j and p_{ij}:

$$R_j = K_{bj,\mathrm{Ref}}\,V_j/(K_{bj,\mathrm{Ref}}\,V_j + L_j) \tag{4.94}$$

$$p_{ij} = FX_i/(1 + R_j + R_j\,\alpha_{ij}) \tag{4.95}$$

where FX_i is for component i in all feeds. The term R_j is a combination of temperature (through K_b) and the ratio of the total vapor and liquid rates. This combination frees the method from some sensitivity to wide- or narrow-boiling mixtures. From R_j and p_{ij}, the compositions can be calculated directly:

$$x_{ij} = \frac{p_{ij}}{\sum_{i=1}^{C} p_{ij}} \quad \text{and} \quad y_{ij} = \frac{\alpha_{ij}\,p_{ij}}{\sum_{i=1}^{C} \alpha_{ij}\,p_{ij}} \tag{4.96}$$

The temperatures are calculated from a K_b method:

$$K_{bj} = \frac{p_{ij}}{\sum_{i=1}^{C} \alpha_{ij}\,p_{ij}} \tag{4.97}$$

with the new temperature calculated using the K-value model:

$$T_j = \frac{1}{(\ln K_{bj} - A_j)/B_j + 1/T^*} \tag{4.98}$$

Total liquid rates are also found using the R_j's:

$$L_j = (1 - R_j)\sum_{i=1}^{C} p_{ij} \tag{4.99}$$

and total vapor rates are found by total material balances. The energy balances, using the temperatures and compositions found in the pre-

vious steps, form the equations of a Broyden's method (Sec. 4.2.6). Their solution is used to update the R_j's.

The outer-loop variables, the α_{ij}'s A_j's, B_j's, a_{ij}'s, b_{ij}'s, C_j's, D_j's, E_j's, and F_j's, are updated after each inside-loop solution using the latest temperatures and compositions from the inside loop. Using the new $K_{bj,\text{Ref}}$'s, the inside-loop variables, the R_j's, are reinitialized and the inside-loop calculation begins again.

One major problem with all column methods is the initial values. Boston uses a set of scale factors that force a component and total flow rate distribution throughout the tower that conform to product specifications. The distribution is forced by multiplying the component flow rates by a base stripping factor for each stage:

$$S_{ij} = (K_{bj,\text{Ref}}\, L_j/V_j)\, S_b\, \alpha_{ij} \tag{4.100}$$

where S_b is a scalar multiplier on the base stripping factors that is changed before the start of every column trial. This scalar forces the distribution of components and flows up or down the column in order to prevent negative or zero flow rates and to have the sum of the component flow rates approach a specified or estimated total flow rate. Once the flow rates are adjusted, the temperature profile can be smoothed or generated by using the flow rates to calculate dew or bubble points on selected stages.

Boston (75) added a middle loop to allow for column specifications and constraints. The arrangement of equations in the inner loop, where the solution of the MESH variables occurs, allows for only a few control or specified variables, such as fixed reflux ratio and product rates. The middle loop adjusts the control variables to meet the specifications. The middle loop can be built as an optimization method with process specification equations and economic objectives and constraints.

The calculation sequence of the Boston method is as follows:

1. Set initial temperatures and total rates for each stage.
2. Initialize the outside-loop variables; the reference base K-value, $K_{bj,\text{Ref}}$; the relative volatilities, α_{ij}; and parameters A_j and B_j of the K-value model, parameters a_{ij} and b_{ij} of the activity coefficient model and parameters C_j, D_j, E_j, and F_j of the enthalpy models, using the actual K-value and enthalpy correlations and the estimated set of temperatures and compositions.
3. Adjust the component flow rates using the base stripping factor of Eq. (4.96). Update the total flow rates and temperatures with these adjusted component flows.
4. Initialize the inside-loop variables, R_j's, based on the current set of flow rates and reference $K_{bj,\text{Ref}}$'s.

The inside loop consists of steps 5, 6, 7, 8, and 9.

5. Calculate the inside loop p_{ij}'s, K_{bj}'s, x_{ij}'s, and y_{ij}'s.
6. Get new stage temperatures by the K_b method.
7. Calculate the total liquid rates using the R_j's.
8. Get a new set of R_j's by solving the energy balances as the independent functions of the quasi-Newton technique of Broyden (Sec. 4.2.6). The derivatives of the Jacobian matrix are generated numerically and must include steps 5, 6, and 7 each time the independent variables are perturbed. The Jacobian is not recalculated after the first trial in the loop.
9. Any calculation of the independent functions of step 8 must include a pass through steps 5, 6, and 7. The norm of the functions with the new R_j's should be small to leave the loop (see Sec. 4.2.6 for criteria). If not, return to step 5.
10. Update the outside-loop variables; the reference base K-value, $K_{bj,\text{Ref}}$; the relative volatilities, α_{ij}; and parameters A_j and B_j of the K-value model, parameters a_{ij} and b_{ij} of the activity coefficient model and parameters C_j, D_j, E_j, and F_j of the enthalpy models, using the complex K-value and enthalpy correlations and the current set of temperatures and compositions.
11. The test for solution is that the relative volatilities and the parameters of the K-value and enthalpy models generated in the outer loop using the complex correlations have not changed greatly between outer-loop trials. If this or other solution criteria (Sec. 4.2.3) have not been met, return to step 3.

From the equations, it may appear that the Boston method is most appropriate for narrow-boiling mixtures. However, the forcing style of the method allows it to also work well for wide-boiling mixtures. The Boston method has been found to be the better inside-out method for tall, high-purity (superfractionator) types of columns. The Boston method was extended to absorbers by Trevino-Lozano et al. (74). There, the inside loop was changed to have a base stripping factor as the independent variables in a Broyden's method solution of the energy balances. These base stripping factors were also used in a tridiagonal matrix solution of the component balances, while the K_b method for calculating the temperatures remained the same. These modifications to the inside-out method can and have been extended to distillation columns. In later variations of the Boston method, the tridiagonal matrix method of Boston and Sullivan (25) replaces Eq. (4.96) to calculate the compositions. Also, for better solution of absorb-

ers and strippers, a sum-rates method can replace the inside loop. Boston's method was extended to three-phase distillation by Boston and Shah (76) and to reactive distillation by Venkataraman et al. (77). A well-supported Boston method with a wide variety of features, options, and power to solve a wide range of columns is in the RADFRAC and the MULTIFRAC methods in ASPENPlus of ASPENTech of Cambridge, Massachusetts.

The Russell method. Russell (72) follows the same structure in the outer loop as the Boston method except the base temperature in the K-value model is removed from the equation:

$$\ln K_{bj} = A_j - (B_j/T_j) \tag{4.101}$$

The reference K_{bj} is generated as in the Boston method [Eq. (4.86)] but the weight factors, w_i's, have been simplified to be based on the change in the K-values with respect to temperature:

$$w_i = \frac{t_i}{\sum_{i=1}^{C} t_i} \quad \text{and} \quad t_i = y_{ij} \frac{d(\ln K_{ij,\text{actual}})}{d(1/T_j)} \tag{4.102}$$

where the y_{ij}'s, temperatures, and compositions used to get the $K_{ij,\text{actual}}$'s are the latest available in the calculation. The relative volatilities are still found from Eq. (4.87) and the α_{ij}'s, A_j's, and B_j's are among the outer-loop variables. Russell also has an activity coefficient model similar to Boston, and Russell's method uses Boston's simple enthalpy models.

Russell's method differs from Boston's in the inside loop by calculating the component flow rates by the tridiagonal matrix method and the total flow rates by summing the component rates. The temperatures are calculated by Russell's version of the K_b method. As in Boston's method, one energy balance is drawn per stage, for a total of N equations per column, and these are the independent functions of a Broyden's method solution. Additional equations can join the independent functions to support specifications for product quality, stage temperatures, internal flow rates, etc. Independent variables of Russell's inside loop matrix are logarithms of base stripping and withdrawal factors:

$$\ln S_{bj} = \ln(K_{bj} L_j/V_j) \tag{4.103}$$

$$\ln R_{vj} = \ln(W_{vj}/V_j) \qquad \text{for a vapor side product} \tag{4.104}$$

$$\ln R_{Lj} = \ln(W_{Lj}/L_j) \qquad \text{for a liquid side product} \tag{4.105}$$

For every side product, a withdrawal factor is added to the independent variables. With it, a specification function joins the energy balances in the independent functions. These and the energy balances are the functions of a Newton-Raphson method, and whenever they are calculated (as in filling the Jacobian), a pass must be made through the calculations of the compositions and temperatures.

The outside-loop variables; the relative volatilities, α_{ij}'s; the constants of the K_b model, A_j's and B_j's; and the constants of the enthalpy models, C_j and D_j and E_j and F_j are not updated except in the outer loop. The factors, S_{bj}'s, R_{vj}'s, and R_{vj}s, are initialized at the start of each inside loop. The base stripping factors enter in inside-loop solution where they are needed to get the stripping factors of the component material balances:

$$S_{ij} = \alpha_{ij} S_{bj} \tag{4.106}$$

Russell organizes the tridiagonal matrix method to calculate the component liquid rates instead of the vapor rates (as in Sec. 4.2.3) but either can be used. The component vapor rates are found by $v_{ij} = S_{ij} l_{ij}$. The total flow rates are found by summing the component flow rates:

$$\sum_{i=1}^{C} l_{ij} = L_j \qquad \text{and} \qquad \sum_{i=1}^{C} v_{ij} = V_j \tag{4.107}$$

The inside loop K_{bj} is found using the outside-loop relative volatilities:

$$K_{bj} = \sum_{i=1}^{C} \frac{v_{ij}/V_j}{\alpha_{ij}} \qquad \text{or} \qquad K_{bj} = \frac{1}{\sum_{i=1}^{C} \alpha_{ij} l_{ij}/L_j} \tag{4.108}$$

with the new temperatures calculated using the outside-loop K model constants of the composite base component and Eq. (4.101)

The calculation sequence of the Russell method is as follows:

1. Set initial temperatures and total rates for each stage.
2. Initialize the outside-loop variables; the reference $K_{bj,\text{Ref}}$'s; the relative volatilities, α_{ij}'s; and parameters A_j's and B_j's of the K-value model and parameters C_j's, D_j's, E_j's, and F_j's of the enthalpy models, using the complex K-value and enthalpy correlations and the estimated set of temperatures and compositions.
3. Initialize the base stripping factors, S_{bj}'s, based on the current set of flow rates and reference $K_{bj,\text{Ref}}$'s.

The inside loop consists of steps 4, 5, 6, 7, and 8.

4. Calculate the component liquid rates by the tridiagonal matrix method. Component vapor rates are found by the component (not the base) stripping factors, $v_{ij} = S_{ij}\, l_{ij}$.
5. Get the total flow rates by summing the component flow rates.
6. Get new stage temperatures by the K_b-method.
7. Get a new set of stripping factors by solving the energy balances and specification equations as the independent functions of the quasi-Newton technique of Broyden (Sec. 4.2.6). The derivatives of the Jacobian matrix are generated numerically and must include steps 4, 5, and 6 each time the independent variables are perturbed. The Jacobian is not recalculated after the first trial in the loop but is instead updated by Broyden's equation.
8. Any calculation of the independent functions must include a pass through steps 4, 5, and 6. The norm of the functions with the new stripping factors should be small (see Sec. 4.2.6 for criteria) to leave the loop. If not, return to step 4.
9. Update the outside-loop variables; the reference $K_{bj,\mathrm{Ref}}$'s; the relative volatilities, α_{ij}'s; and parameters A_j's and B_j's of the K-value model and parameters C_j's, D_j's, E_j's, and F_j's of the enthalpy models, using the complex K-value and enthalpy correlations and the current set of temperatures and compositions.
10. The test for solution is that the relative volatilities and the parameters of the K-value and enthalpy models generated in the outer loop using the complex correlations have not changed greatly between outer-loop trials. If this and the other solution criteria (Sec. 4.2.3) have not been met, return to step 3.

Russell's method is insensitive to the quality of initial values. The user does not have to provide additional stage temperatures and flow rates beyond what might be estimated by the method. The scaling factor of Eq. (4.100) in Boston's method is used only in the first trial to force a better material distribution in the column.

Russell's method is one of the methods used in the MULTIFRAC option for multiple columns in ASPENPlus and is the column method in HYSIM of Hyprotech of Calgary, Alberta. Russell's method as written by Richard Russell is in the PD+Plus system available from Deerhaven Technical Software in Deerhaven, Massachusetts. The HYSIM and PD+Plus versions of Russell's method have been found to work well for refinery fractionators with sidestrippers and other similar columns including columns for which a version of Boston's method failed.

Outlook. The inside-out methods are now the methods of choice for mainstream column simulation. While other methods still have their

place, the inside-out methods have displaced the BP, SR, and 2*N* Newton methods and their application should continue to grow. Other products that have inside-out methods include PRO/II of Simulation Sciences of Fullerton, California, and ChemStation of COADE of Houston, Texas.

4.2.11 Relaxation methods

One of the earliest successful solution methods was the relaxation method. The first statement of this method was by Rose, Sweeny, and Schrodt (60). Others have been by Ball (63); Jelinek, Hlavacek, and Kubicek (61); Ketchum (64); and Mori et al. (62).

A relaxation method finds a steady-state solution of a column as if it were an operating column changing with time. The column is initialized using some realistic condition such as startup, with the liquid on every stage having the feed composition at its bubble point. The column is carried to the steady-state conditions by successive approximations of the unsteady-state distillation equations. These unsteady-state equations are modifications to the MESH equations to include changes in the MESH variables with respect to time. This process could be said to be mimicking the physical startup of the column, but the objective is not to follow the dynamic operation but to seek the steady-state solution. The earliest relaxation methods used an unsteady-state, time-dependent form of the component balances to get the compositions instead of the tridiagonal matrix method presented earlier. Later methods added calculating changes in temperature with respect to time.

The unsteady-state form of the component balance for a conventional tray written with respect to time t is

$$(V_{j+1}y_{ij+1} + L_{j-1}x_{ij-1} - V_j y_{ij} - L_j x_{ij})/U_j = \frac{dx_{ij}}{dt} \qquad (4.109)$$

The term U_j is the material holdup on the tray. The vapor holdup is very small and the liquid holdup here is assumed not to change with time. The composition for the next trial, $k + 1$, is calculated using Euler's equation:

$$x_{ij,k+1} = x_{ij,k} + \Delta t \frac{dx_{ij}}{dt} \qquad (4.110)$$

Euler's equation will suffice as long as the time step, Δt, is kept small. Jelinek et al. (61) and Mori et al. (62) developed techniques for calculating the time step and the composition derivative and restated the component balance equations accordingly.

In relaxation equations, the total flow rates and K-values do not change from one time step to the next. Once the compositions are

found for a step, the K-values can be updated and the remaining MESH equations can be solved by a conventional column solution method. Since the relaxation equations yield a calculated set of product compositions, Ball (63) uses the theta method (Sec. 4.2.5) to correct these when initiating a new trial. As in the theta method, temperatures are updated by the K_b method and total flow rates by energy balance. Jelinek et al. (61) use the theta method for distillation columns and a sum-rates method (Sec. 4.2.7) for absorbers.

The success of relaxation is dependent on a choice of the step size, Δt. The method can fail if too large a step is chosen or be very slow if too small a step is chosen. Since computers are getting faster, a small step size, unless excessive, should not be a great problem. Mori et al. (62) used the inverse of an internal vapor rate, such as the reboiler boilup, V_N, as a step size in order to take into account both feed rate and reflux rate.

A relaxation method will make a stable, stepwise movement toward the steady-state values. Problems arising from poor initial values are absent. A BP or SR method (Secs. 4.2.5 and 4.2.7) can be converted to a relaxation method by substituting the relaxation composition calculation for the one used in the method. Brierley and Smith (106) found the relaxation method to be reliable for a wide range of columns, including stripper-absorbers, and their method is part of DISTPACK of ICI. Jelinek et al. (61) also applied their method to nonideal systems and extended BP and SR methods outside of their normal range of systems. Since global Newton methods (Sec. 4.2.9) need good initial values, a relaxation method can be used to bring the column near the solution before switching to the global Newton method. Such a technique, using a Naphtali-Sandholm–like method, should work well for solving nonideal systems. This is the method of Ketchum (64) and Brierley and Smith (106).

The Ketchum method. Ketchum (64), in his review of relaxation methods, pointed out three inherent weaknesses:

1. The compositions, x_{ij}'s, are corrected separate of the temperatures and total flow rates, which are calculated by a more conventional BP or SR method. The temperature calculation can be unstable or sluggish.
2. There is no estimate of the change of temperature with time. This could be especially important for wide-boiling mixtures. All of the rigorous methods are a balance between the composition and temperature calculations but K-values and enthalpies are assumed to be constant with respect to time.
3. All relaxation methods tend to move slowly, especially near the solution.

Any of the global Newton methods can be converted to a relaxation form in Ketchum's method by making both the temperatures and the liquid compositions time dependent and by having the time step increase as the solution is approached. The relaxation technique should be applied to difficult-to-solve systems and the method of Naphtali and Sandholm (42) is best-suited for nonideal mixtures since both the liquid and vapor compositions are included in the independent variables. Drew and Franks (65) presented a Naphtali-Sandholm method for the dynamic simulation of a reactive distillation column but also stated that this method could be used for finding a steady-state solution.

The change in the temperature with time is expressed as

$$T_{j,k+1} = T_{j,k} + \Delta t \frac{dT_j}{dt} \tag{4.111}$$

The independent functions are transient versions of the Naphtali-Sandholm functions, including the component balances [Eq. (4.109)] and the energy balance of each stage:

$$\frac{1}{\mathrm{Cpu}_j U_j} \frac{H_{j+1} \sum_{i=1}^{C} v_{ij+1} + h_{j-1} \sum_{i=1}^{C} l_{ij-1}}{H_j \sum_{i=1}^{C} v_{ij} + h_j \sum_{i=1}^{C} l_j} - 1 = \frac{dT_j}{dt} \tag{4.112}$$

where change in the enthalpy of the holdup, U_j, with respect to temperature is the heat capacity of the liquid phase, Cpu_j. The equilibrium equation [Eq. (4.79)] does not have a time-dependent form and remains the same.

The time step, Δt, is used to switch the method from being a relaxation method to a global Newton method. When the time step is small, e.g., $\Delta t = 0.1$, then the changes in the independent variables are small. The method performs like a damped Newton-Raphson method, where the steps are small but in the direction of the solution and without any oscillation. When the value of Δt is large, i.e., $\Delta t = 1000$, the method performs like a Newton-Raphson method. The value of Δt at each column trial determines the speed and stability of the method. The units of the time step are the same as the flows to and from the column. The calculation sequence of the Ketchum method is as follows:

1. Develop a set of initial total flow rates and temperatures. Also set liquid compositions for trial $k = 1$ and the time step size, Δt.
2. Calculate all of the independent functions and their norm. Get a

new set of all of the independent variables, including the temperatures, T_j's, and liquid composition, x_{ij}'s by solving the independent equations during one pass through the Newton-Raphson procedure.

3. Besides the usual solution criteria, there is one additional criterion for the relaxation method. The maximum difference between a composition and temperature on any stage calculated in the last trial and the previous should be very small, i.e.,

$$\max_{ij} |x_{ij,k+1} - x_{ij,k}| < 10^{-4}$$

and (4.113)

$$\max_{j} |T_{j,k+1} - T_{j,k}| < 10^{-4}$$

If the criteria have not been met, return to step 2.

The equations will still form the same block-banded sparse matrix as in the Naphtali-Sandholm method. No matter what size the time step, the same matrix solution technique can be used to calculate the next set of independent variables.

Ketchum's relaxation method is stable and fast because the time step, Δt, acts as switch to a global Newton method. The time step can be increased as changes in the temperatures and liquid compositions become slight, i.e., the above solution criterion is within the same magnitude as the convergence limit. The global Newton methods may be the only choice for solving nonideal systems, but they suffer from needing very good starting values. A Ketchum relaxation technique applied to a global Newton method can bring the composition and temperature profiles to a point where a solution can be found. For very nonlinear, nonideal K-value and enthalpy curves, the relaxation form will step slowly along the curves of the MESH equations and not make large changes in independent variables that could place the calculation well off. The method has proved highly reliable for difficult problems such as reactive distillation [Komatsu (67)] and extractive distillation [Ishikawa and Hirata (68)]. Many dynamic simulation methods can be adapted as relaxation methods. Agreda et al. (112) used the dynamic methods in the DYFLOW system from DuPont to find the steady-state solution of a reactive distillation column. A complete study of dynamic simulation methods was presented by Holland and Liapis (10) and the DYFLOW system is described by Franks (66).

4.2.12 Homotopy-continuation methods

Homotopy or continuation methods have recently been applied to difficult-to-solve columns. The beauty of these methods is that they are a simple means of forcing a solution. Tom Wayburn's analogy is

"They are like a blind man using a rope to cross a room." The MESH equations can be difficult to solve, either due to the nature of the column (many feeds or side draws, side strippers, near-minimum reflux, etc.) or due to the nonidealities of the K-values or enthalpies. K-values and enthalpy methods for nonideal mixtures, dependent on both temperature and composition, are far from linear, can have discontinuities, and may even change slope. With global Newton methods like the Naphtali-Sandholm (Sec. 4.2.9), there are problems in estimating initial values for the column from which the desired solution can be reached. For three-phase systems, azeotropic systems, or systems of columns with two or more feed-recycle stream combinations, there may be more than one calculated solution. The method must be forced to reach the desired solution. Homotopy methods begin with a known solution of the column and from there follow a path (or integrate) to the desired solution. The known solution can be at different conditions or with much simpler K-value and enthalpy methods and stepped changes are made from there, solving the column at each step, until the final solution is reached.

The homotopy methods can be divided into two general classes, mathematical homotopies and physical or parametric homotopies. The mathematical homotopies are conventions without a physical relationship to the MESH equations and this occasionally causes problems. The physical homotopies have a basis in the MESH equations and these will be emphasized. Taylor, Wayburn, and Vickery (80) state that the physical homotopies should outperform the mathematical homotopies and are easier to implement.

The homotopy principle. A homotopy function is a continuous blending of two other functions so that

$$\underline{\mathbf{H}}(\underline{\mathbf{x}},t) = t\,\underline{\mathbf{F}}(\underline{\mathbf{x}}) + (1 - t)\,\underline{\mathbf{G}}(\underline{\mathbf{x}}) \tag{4.114}$$

where $\underline{\mathbf{F}}(\underline{\mathbf{x}})$ is the difficult solution of a column and $\underline{\mathbf{G}}(\underline{\mathbf{x}})$ is a simpler problem or the column at known conditions. The homotopy parameter t travels between values of 0 and 1 and is the term shown in Fig. 4.2

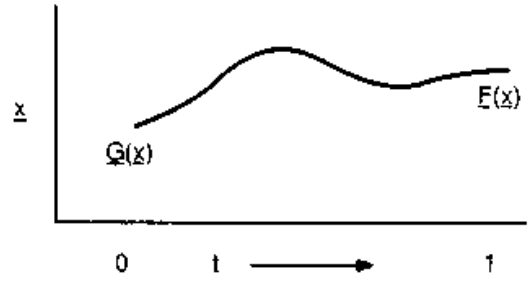

Figure 4.2 The homotopy path.

used to travel the path from $\underline{\mathbf{G}}(\underline{\mathbf{x}})$ to $\underline{\mathbf{F}}(\underline{\mathbf{x}})$. At each value of t, a new set of independent variables $\underline{\mathbf{x}}$ is found.

The converged solution is where $\underline{\mathbf{F}}(\underline{\mathbf{x}}) = 0$ and so at $t = 1$, $\underline{\mathbf{H}}(\underline{\mathbf{x}},t) = 0$. The integration shows the effect on $\underline{\mathbf{H}}(\underline{\mathbf{x}},t)$ as t changes. Differentiation of $\underline{\mathbf{H}}(\underline{\mathbf{x}},t)$ with respect to t gives

$$\underline{\mathbf{H}}_x \frac{d\underline{\mathbf{x}}}{dt} + \underline{\mathbf{H}}_t = 0 \tag{4.115}$$

Vickery and Taylor (81) used a Naphtali-Sandholm method containing all of the MESH equations and variables [$N(2C + 3)$ equations] with the variables represented by $\underline{\mathbf{x}}$. $\underline{\mathbf{H}}_x$ is the Jacobian from the Naphtali-Sandholm method solution of the known problem, $\underline{\mathbf{G}}(\underline{\mathbf{x}}) = 0$. This is numerically integrated from $t = 0$ to $t = 1$, finding a $\underline{\mathbf{H}}_t$ at each step and updating $\underline{\mathbf{H}}_x$ when the solution is reached at each step. With $\underline{\mathbf{H}}_x$ and $\underline{\mathbf{H}}_t$ known, $d\underline{\mathbf{x}}/dt$ is solved, and with step size Δt, a new set of values for the independent variables $\underline{\mathbf{x}}$ is found by Euler's rule

$$\underline{\mathbf{x}}_{n+1} = \underline{\mathbf{x}}_n + \Delta t\,(d\underline{\mathbf{x}}/dt)_n \tag{4.116}$$

At $t = 1$, the values of $\underline{\mathbf{x}}$ should yield the difficult solution $\underline{\mathbf{F}}(\underline{\mathbf{x}}) = 0$. This technique resembles the relaxation method, but only requires modifying the independent MESH functions to get the derivatives with respect to one term t. This is a purely mathematical approach and Ellis et al. (78) state that it can give negative flow rates at intermediate values of t, something that K-value and enthalpy routines may not tolerate. An alternative is a homotopy function that is rooted in the MESH equations themselves.

The homotopy procedure is as follows:

1. Set initial temperatures and total vapor and liquid rates for each stage. Solve the column for the known solution.
2. The results from step 1 form the initial values $\underline{\mathbf{x}}$ of the global Newton's method. Set $t = 0$.
3. Solve $\underline{\mathbf{H}}(\underline{\mathbf{x}},t) = 0$ using the global Newton's method (Sec. 4.2.9). The K-values and enthalpies used are determined by the current value of t.
4. If $t < 1$, solve Eq. (4.115) for $d\underline{\mathbf{x}}/dt$.
5. Use Euler's rule to get a new set of variables $\underline{\mathbf{x}}$, and return to step 3.

The efficiency homotopy. Taylor, Wayburn, and Vickery (80) propose a physical homotopy based on a pseudo-Murphree efficiency. As stated earlier, the efficiency can be entered into the MESH by modifying the

equilibrium equation [see Eq. (4.23)]. The pseudo-efficiency homotopy takes the column from little separation, such as $E_{MVij} = 0.1$, with little difference in composition between the top and bottom of the column, to maximum pseudo-efficiency, where $E_{MVij} = 1.0$, at the final solution. The pseudo-efficiency, E_{MVij}, represents the homotopy parameter t applied in the Naphtali-Sandholm method. The calculation sequence is as follows:

1. Initialize the MESH variables of the column with $E_{MVij} = 0.0$. Taylor et al. (80) present suggestions for the initialization. Since $E_{MVij} = 0.0$, all stages have the same temperature and constant molal overflow. Taylor et al. (80) also use a four-diagonal matrix method to solve for the initial-stage liquid compositions. These are normalized and used to find a better set of stage temperatures by solving for the bubble points. With $E_{MVij} = 0.1$, the compositions and temperatures are recalculated until a satisfactory initial temperature profile is reached.
2. With $E_{MVij} = 0.1$, solve the Naphtali-Sandholm method for the column. The solution criteria for intermediate values of E_{MVij} (0.1, 0.4, and 0.7) should be looser than for the final value of $E_{MVij} = 1.0$, i.e., a norm of the functions less than 10^{-1} instead of 10^{-4}.
3. When the solution is reached at an intermediate value of E_{MVij} (0.1, 0.4, and 0.7), increase E_{MVij} to the next value and restart the problem. The solution results from one value of E_{MVij} are used to initialize the next. When $E_{MVij} = 1.0$, the criteria of solution should be much more strict than that of other values of E_{MVij}.

The examples tested by Taylor et al. (80) for the efficiency homotopy were for moderate- or narrow-boiling mixtures. No wide-boiling mixtures were tested. Since the temperature profiles at the intermediate values of E_{MVij} will be flat and not broad, the homotopy may be best for the moderate- and narrow-boiling systems. Most of the mixtures were nonideal and the efficiency homotopy should lessen the effect of nonideal K-values where E_{MVij} acts as a damper on the K-values. The efficiency homotopy does not work for purity specifications because the purity will not be satisfied in solutions of early values of E_{MVij}.

Vickery and Taylor (81) presented a thermodynamic homotopy where ideal K-values and enthalpies were used for the initial solution of the global Newton method and then slowly converted to the actual K-values and enthalpies using the homotopy parameter t. The homotopy functions were embedded in the K-value and enthalpy routines, freeing from having to modify the MESH equations. The K-values and enthalpies used are the homotopy functions:

$$K_{ij} = (K_{ij,\text{simple}})^{1-t} + (K_{ij,\text{actual}})^{t} \tag{4.117}$$

$$H_j = (H_{j,\text{simple}})(1 - t) + (H_{j,\text{actual}})t \tag{4.118}$$

$$h_j = (h_{j,\text{simple}})(1 - t) + (h_{j,\text{actual}})t \tag{4.119}$$

where composition-independent K-values can be used. The thermodynamic homotopy is easier to implement and faster than those based on mathematics alone. This should be true for other physically based homotopies such as the above efficiency-based homotopy.

You may have at times come up with homotopy-like techniques for reaching a solution; what some engineers call "sneaking up on the answer." For instance, water often causes nonideal behavior and can make the solution difficult. One can first solve the column with water absent from the feed, then slowly increase the amount of water, solving the column at each increase, with all of the profiles from one solution used to initialize the next. Methods like these are described by Brierley and Smith (106).

The global Newton methods, such as the Naphtali-Sandholm method (Sec. 4.2.9), are often used to solve highly nonideal systems. These are frequently prone to failure. Good explanations of the theory of homotopy methods are provided by Seader (86) and Wayburn (83). A homotopy method can greatly expand the global Newton method ability to solve difficult nonideal systems. Homotopy methods have been associated with the Naphtali-Sandholm method, where the derivatives of the K-values and enthalpies with respect to all compositions directly appear within the Jacobian. Using a thermodynamic homotopy for another method such as a Tomich has not been presented in the literature.

ASPENPlus of AspenTech, Cambridge, Massachusetts; PROCHEM of OLI Systems, Florham Park, New Jersey; and other programs use homotopies in their solution methods. The HOMDIS program, available from Dr. Warren Seider of the University of Pennsylvania, uses a homotopy in the solution of azeotropic and three-phase distillation columns.

4.2.13 Nonequilibrium or rate-based methods

Chapters 7 and 9 present that stage efficiency prediction and scaleup can be difficult and unreliable. Section 4.1.2 points out that the computational form in which stage efficiencies are often applied, as multipliers to the equilibrium K-values, may inadequately reflect actual equilibrium or column operation. For highly nonideal, polar, and reactive systems, such as amine absorbers and strippers, prediction and

use of efficiencies is particularly difficult. In such mixtures, it is the mass transfer and not the equilibrium that often limits the separation.

Nonequilibrium methods attempt to get around the difficulty of predicting efficiencies by doing away with the equilibrium-stage concept. Instead, they apply a transport phenomena approach for predicting mass transfer rates. The mass transfer rates are calculated continuously along the column length and not in discrete equilibrium stages. This process is similar to the transfer unit concept (Sec. 10.3.1).

While the bulk vapor and liquid phases are not at equilibrium with each other, there is equilibrium at the interface between phases with a movement from the bulk phase through the interface (Fig. 4.3). The net loss or gain for a component at the interface is expressed in a rate form (hence the alternate name, rate-based methods):

$$N_{ij}^{V^*} = N_{ij}^{V}\, da_j \qquad \text{for the net gain by the vapor} \tag{4.120}$$

$$N_{ij}^{L^*} = N_{ij}^{L}\, da_j \qquad \text{for the net loss by the liquid} \tag{4.121}$$

where N_{ij}^{V} and N_{ij}^{L} are vapor and liquid molar fluxes of the component at some point through the interface and da_j is the small interface area through which the flux passes. There is also an energy rate equation between the two phases:

$$E_j^{V^*} = e_j^{V}\, da_j \qquad \text{for the net energy gain by the vapor} \tag{4.122}$$

$$E_j^{L^*} = e_j^{L}\, da_j \qquad \text{for the net energy loss by the liquid} \tag{4.123}$$

where e_j^{V} and e_j^{L} are energy fluxes through interfacial area da_j.

In nonequilibrium models, as in the other models, the subscript j is for the stage. In a trayed column, it is the actual tray. In a packed column, j is a section of packing. By convention, transfer is to be from the liquid to the vapor with the mass transfer rate to the vapor, $N_{ij}^{V^*}$, taken as positive.

The movement of mass and energy from one phase through the interface to the other phase is illustrated in Fig. 4.3. One mass transfer rate is shown to the vapor from the liquid and one rate from the liquid to the vapor, but there is strictly only one independent rate, N_{ij}^{*}, where $N_{ij}^{*} = N_{ij}^{V^*} = N_{ij}^{L^*}$. The mass transfer rates are dependent on the mass transfer coefficients for each phase. The coefficients are dependent on the composition in the bulk phase and at the interface; the temperature in the bulk phase and at the interface; the area of the interface, a_j; and the mass transfer rates and coefficients of the other components.

The total energy transfer rates for each phase are dependent on heat transfer coefficients and the mass transfer rates of each compo-

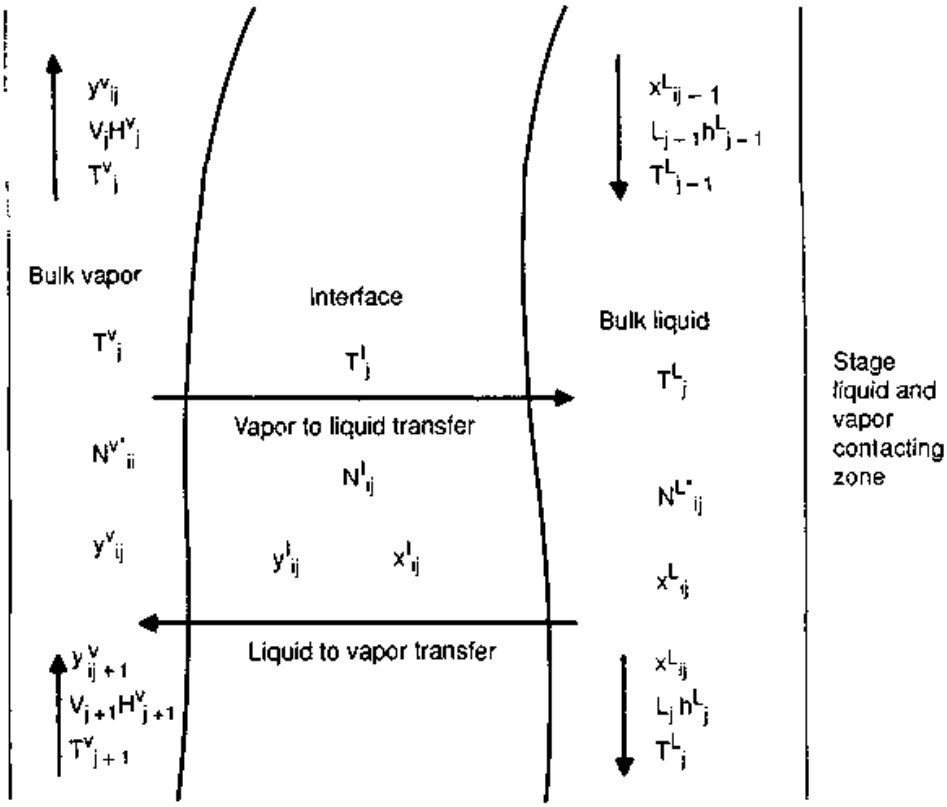

Figure 4.3 Model of nonequilibrium stage.

nent along with the compositions in the bulk phase, the temperature in the bulk phase, and at the interface and the area of the interface, a_j.

The correlations for the mass and heat transfer coefficients and interfacial also take into account packing or tray geometries for the actual column. The total mass and energy rates are calculated from intergrating the mass and energy fluxes across the total surface area, a_j.

The Taylor method. Krishnamurthy and Taylor (88, 89) present and test a nonequilibrium model which includes rate equations for mass transfer, and sometimes reaction, among the traditional MESH equations. These include individual mass and energy balances in the vapor and the liquid and across the interface. An equilibrium equation exists for the interface only. The solution method for these equations is the same as that of the block-banded matrices of the global Newton methods and the style of the method is similar to the Naphtali-Sandholm (Sec. 4.2.9).

The total mass transfer rates are added to an expanded set of the MESH equations called the *MERQ equations*. The new MERQ acronym stands for

Material balances for each component; one for the bulk vapor, one for the bulk liquid, and one across the interface.

Energy balance equations; one for the bulk vapor, one for the bulk liquid, and one across the interface.

Rate equations for mass transfer for all but one component; one from the interface to the bulk vapor and one from the bulk liquid to the interface, plus one energy transfer rate equation from the liquid to the vapor.

eQuilibrium equation at the interface only.

In component balances, feed and side product streams are considered in the bulk phases only. The component balance for the bulk vapor is

$$v_{ij+1} - v_{ij} + (f_{ij}^V) - (w_{ij}^V) + N_{ij}^{V^*} = 0 \tag{4.124}$$

and the component balance for the bulk liquid is

$$l_{ij-1} - l_{ij} + (f_{ij}^L) - (w_{ij}^L) - N_{ij}^{L^*} = 0 \tag{4.125}$$

Material transfer across the interface should cancel.

$$N_{ij}^{V^*} - N_{ij}^{L^*} = 0 \tag{4.126}$$

As in the component balances, a separate energy transfer equation is written for each bulk phase and all energy transfer between the two phases is at the interface. The energy balance for the bulk vapor is

$$V_{j+1}H_{j+1}^V - V_jH_j^V + (F_j^V H_j^{FV}) - (W_j^V H_j^{WV}) + (-)(Q_j^V) + E_j^{V^*} = 0 \tag{4.127}$$

and the energy balance for the bulk liquid is

$$L_{j-1}h_{j-1}^L - L_jh_j^L + (F_j^L h_j^{FL}) - (W_j^L h_j^{WL}) + (-)(Q_j^L) - E_j^{L^*} = 0 \tag{4.128}$$

Net energy gained or lost by each phase from the transfer between the two phases will cancel at the interface:

$$E_j^{V^*} - E_j^{L^*} = 0 \tag{4.129}$$

The mass transfer rate equations force values of the mass transfer coefficients such that the rates of each phase, $N_{ij}V^*$ and $N_{ij}L^*$, are equal. The above equations for material and energy balance across the interface are used to form these rate equations and are excluded from the final set of equations. Since the vapor and liquid are only at equilibrium at the interface, one equilibrium equation per component is drawn there:

$$K_{ij}^I x_{ij}^I - y_{ij}^I = 0 \tag{4.130}$$

There are $(5C + 1)$ equations per section of packing or per tray. The $N(5C + 1)$ equations of a complete column are arranged to have the block-banded form of a global Newton method and can be solved by the same numerical methods. The independent equations for a tray or a section of packing are

$$\begin{aligned}\underline{\mathbf{F}}_j = [&m_{1j}^V\, m_{2j}^V \cdots m_{Cj}^V\, m_{1j}^L\, m_{2j}^L \cdots m_{Cj}^L \\ &R_{1j}^V\, R_{2j}^V \cdots R_{C-1j}^V\, R_{1j}^L\, R_{2j}^L \cdots R_{C-1j}^L\, Q_{1j}^I\, Q_{2j}^I \cdots Q_{Cj}^I \\ &E_j^V\, E_j^L\, R_{Ej}^I]\end{aligned} \tag{4.131}$$

The independent variables for this global Newton method will be the bulk component vapor and liquid flow rates; compositions at the interface for each component less one; a mass transfer rate for each component and the temperatures of the bulk vapor, bulk liquid, and the interface:

$$\begin{aligned}\underline{\mathbf{X}}_j = [&v_{1j}\, v_{2j} \cdots v_{Cj}\, l_{1j}\, l_{2j} \cdots l_{Cj} \\ &y_{1j}^I\, y_{2j}^I \cdots y_{C-1j}^I\, x_{1j}^I\, x_{2j}^I \cdots x_{C-1j}^I\, N_{1j}^*\, N_{2j}^* \cdots N_{Cj}^* \\ &T_j^V\, T_j^L\, T_j^I]\end{aligned} \tag{4.132}$$

The number of equations, $N(5C + 1)$, for a large number of trays and components, can be excessive. The global Newton method will suffer from the same problem of requiring initial values near the answer. This problem is aggravated with nonequilibrium models because of difficulties due to nonideal K-values and enthalpies then compounded by the addition of mass transfer coefficients to the thermodynamic properties and by the large number of equations. Taylor et al. (80) found that the number of sections of packing does not have to be great to properly model the column, and so the number of equations can be reduced. Also, since a system is seldom mass-transfer-limited in the vapor phase, the rate equations for the vapor can be eliminated. To force a solution, a combination of this technique with a homotopy method may be required.

The methods based on the equilibrium stage model have existed for over 30 years and refinements continue, but serious development of nonequilibrium models has begun only recently. These methods are an alternative means to the stage model for predicting column performance. They are expected to make inroads, especially for systems for which stage efficiency prediction is very difficult, such as reactive distillation, chemical absorption, and three-phase distillation. However, their progress into systems where efficiency prediction is well-established is likely to be slower. Their complexity due to the restriction to

a global Newton method can be overcome, but the ability to reliably predict mass transfer coefficients, interfacial areas, and diffusion coefficients must also be resolved.

For development of nonequilibrium methods to continue, the calculations for mass transfer coefficients and interfacial areas required by these models will have to be added to physical property packages. Krishnamurthy and Taylor (89) present methods and recommendations for calculating the mass and energy transfer coefficients and rates. Help may be available from published manuals or supplier literature.

There are commercially available programs that use nonequilibrium models or consider mass transfer rates when calculating K-values or efficiencies. A rate-based method can include both mass transfer and reaction rate equations. Programs with such a method are the Gasplant-Plus system of Taylor, Weiland and Associates of Potsdam, New York, and the RATEFRAC method in ASPENPlus from AspenTech of Cambridge, Massachusetts. Other programs that contain attributes of a rate-based system are TSWEET from Bryan Research and Engineering of Bryan, Texas, and the AMSYM program from D. W. Robinson and Associates of Edmonton, Alberta, which also can be installed in HYSIM from Hyprotech of Calgary, Alberta. The FraChem program of OLI Systems, Florham Park, New Jersey, supports both mass transfer and reaction equations in its global Newton method.

4.3 How to Use and Which to Use

Section 4.2.3 discusses the importance of problem setup, selecting specifications, and of initial profiles. Tools used in problem setup include x-y diagrams (Chap. 2) and shortcut methods such as Smoker and Fenske-Underwood-Gilliland (Chap. 3). These are useful for providing initial estimates, for troubleshooting failure to reach a converged solution, and for analyzing the rigorous solution. The global Newton methods are the most sensitive to the quality of initial estimates, but the guidelines in Sec. 4.2.3 also apply to other methods. The sections below provide additional guidelines on how to reach a good converged solution.

4.3.1 Hints for setting separation specifications

For the first four rigorous methods (Secs. 4.2.5 and 4.2.7 to 4.2.9) and most of their variations, there is only a limited set of compatible column specifications. Usually a reflux ratio (or reflux rate) specification

and a product rate specification with possibly substituting the condenser and reboiler duties are compatible. These are inherent in the MESH equations, and any method begins with these specifications. While these are the easiest specifications to solve, designers often prefer to set purity specifications [including specifications such as a true boiling point (TBP), cut point, vapor pressure, or top tray temperature] or recovery of some component. Some of the above methods allow for their equations to be modified for these and other specifications.

For a product purity specification for some component C in the distillate, the purity specification equation is

$$\frac{X_{CD,\,\text{calc}}}{X_{CD,\,\text{spec}}} - 1 = 0 \tag{4.133}$$

In methods such as the $2N$ Newton or global Newton methods (Secs. 4.2.8 and 4.2.9), Eq. (4.133) can substitute for the energy balance of the top stage. A purity specification for the bottoms product replaces the energy balance of the bottom stage. On the other hand, a specification made on the reflux ratio, condenser duty, or reboiler duty does not require replacing the energy balance equation. Other purity specification equations, such as one based on the product temperature, will also replace the energy balance.

$$\frac{T_{D,\,\text{calc}}}{T_{D,\,\text{spec}}} - 1 = 0 \tag{4.134}$$

For some methods, many specifications may not be used simultaneously and there is little freedom in setting specifications. In the $2N$ Newton or global Newton methods, there can usually be only one specification equation, such as Eqs. (4.133) or (4.134). The new equation will be sensitive to only a few of the independent variables, and if a second equation is added, any attempt to manipulate the Jacobian matrix will fail. For this reason, specifying both top and bottom purities often fails when using such methods.

When setting a column specification, some other variable must be allowed to change in order to meet the specification, and it and other variables should be particularly sensitive to the specification. For instance, in a complex column, the bottoms purity can be more sensitive to an interreboiler duty rather than that of the reboiler, especially if the interreboiler duty is large. In a simple column with a small condenser duty relative to the reboiler duty, the distillate purity will be more sensitive to reboiler duty.

Often these variables are something that can be manipulated in the column operation and control to meet the specification such as reboiler duty (or steam), reflux rate, or a stripper steam rate. Both the speci-

fications and the variables should have some physical significance in column operation. The philosophy in matching specification to floating variable is the same as matching controlled parameter to manipulated variable in process control of a column.

If the specified component concentration is small (e.g., in the part-per-million range) there may not be any variables that are sensitive to Eq. (4.133). In this concentration range, temperature is insensitive to composition and a temperature specification is therefore unsuitable [Eq. (4.134)]. In these cases, another set of specifications and floating variables must be used.

In a simple column, with only two products and a condenser and a reboiler, there are only two degrees of freedom and there can only be two specifications and two floating variables. For complex columns, a degree of freedom is added with each intercondenser, interreboiler, side product, and so on.

How the MESH equations are arranged in the method should not have to restrict the number and combination of specifications and corresponding floating variables but can in the bubble-point (Sec. 4.2.5), sum-rates (Sec. 4.2.7), $2N$ Newton (Sec. 4.2.8), and global Newton (Sec. 4.2.9) methods. The best methods for invoking numerous column specifications are the inside-out methods (Sec. 4.2.10). There, the handling of specifications is inherent in the methods and they provide the greatest number and freedom in column specifications and floating variables. The inside-out methods allow a more natural way of mixing specifications and variables to where specifications and variables do not have to be paired at points in the column and can be well spread across the column.

Further discussion of separation specifications is in Secs. 4.1.1, 4.2.3, and 3.1.1.

4.3.2 Problems when setting simulation input

- *Feed stage location:* Locating the feed stage far above or below the optimum will cause a composition pinch. The pinch represents a column that as specified cannot be solved. A pinch can best be detected with an x-y diagram (Sec. 2.4.1).
- *Feed temperature:* Too cold or too hot a feed may disturb one or more stages and may also cause a composition pinch. The temperature of the lean oil to an absorber will affect the removal of the heavies from the vapor along with losses of the lean oil overhead. Convergence problems in the simulation may represent actual physical problems, suggesting that a feed exchanger is needed.
- *Reflux ratio or vapor boilup:* These should be above the minimum

for the separation. An x-y diagram (Sec. 2.4.1) is the most effective way to detect if the calculation is below the minimum. Also an Underwood minimum reflux calculation (Sec. 3.2.2) can show if the reflux or boilup is below the minimum. However, an Underwood calculation may be inaccurate if constant molal overflow (Sec. 2.2.2) cannot be assumed for the column.

It is common to design and operate reasonably close to the minimum reflux or minimum boilup (Sec. 3.1.4). A computer solution at such low reflux ratios can be unstable and fail. A solution may only be reached if very good initial values are available. The technique of "sneaking up on an answer" is powerful in these cases. Initially, the column is solved at a higher reflux ratio. This solution is used as the initial value for the subsequent calculation, in which the reflux ratio is slightly lowered. This process is continued until the desired reflux ratio is reached. Other examples of how to use the solution of one simulation to initialize another simulation are described by Brierley and Smith (106). The "sneaking-up" technique is part of the basis of the homotopy methods (Sec. 4.2.12) and these and other forcing techniques may also be used.

- *More than one product purity or recovery specification:* Not all methods will accept or solve. Replace one purity specification with some other such as reflux rate or a product rate. The methods best suited to solve multiple purity specifications are the inside-out methods (Sec. 4.3.1).
- *Two purities or recoveries for the same product:* In a simple column, two purity specifications may be impossible. Once a purity is set, the concentrations of all other components become dependent variables. In a complex column, the degrees of freedom increase and just as there can be more than one purity specification across the column, there may be two specifications on the same product. This can be solved but only if the relative volatilities between the components of the specifications are high enough to make this feasible. The solution will also be difficult if the concentrations of both components are small and therefore insensitive to the floating variables.
- *Two purities or recoveries of the same component in different products:* While this is a feasible separation, it is difficult for a method to solve. Directly specifying the purity of a component in different products will not give the program needed freedom in calculating the component balance.
- *Extreme purity or recovery specifications (e.g., 99.8 percent):* The

alternative is an impurity specification of all other components in the product or a loss specification of the component in the other product. Impurity specifications give the solution more freedom and are inherently easier to solve.

- *Combining purity or recovery and product flow specifications:* These may clash, especially on binary systems. Free one and find something else to specify.
- *Specifying all product flow rates:* This will not give the program freedom in establishing the overall material balance. At least one product flow rate must be allowed to float.
- *Specifying overhead vapor product in a system with noncondensables:* Since the split in the condenser can be very sharp, there will be little freedom of movement. It may be better to specify a variable such as reflux rate, condenser temperature, or any specification on the liquid overhead product (if it exists).
- *Specifying stage temperatures:* These are effective only where temperature is sensitive to composition, e.g., where composition changes significantly. They should not be used at a high-purity product location. Section 4.3.1 has additional discussion.
- *Product rates:* A simple way to either specify or estimate the products is to examine the feed and using boiling point splits, decide what components will be in what products.
- *Specifying duties and reboiler boilup or reflux:* Energy input and internal flows directly affect each other, and specifying both may not be possible.
- *Both the temperature and the product on a stage:* There is only a narrow range of solution for this combination.

4.3.3 Recovering from failures and analyzing results

- *Negative flow rates:* Some methods have safeguards that prevent negative flow rates or techniques to recover from them. A method that uses a Newton-Raphson procedure can reduce the step in the independent variables (Sec. 4.2.6). The inside-out methods apply a stripping factor to adjust the flow rates. Often the cause is poor estimates of the internal and product flows and the user may need to modify the estimates. In complex columns, negative flows can be caused by high (or excessive) interreboiler or intercondenser duties or side product flow rate specifications. The negative flows may be removed by increasing reflux, reducing interreboiler or intercondenser duties and side product flow rates, or by refining the initial estimates.

- *Oscillation in the column variables:* This occurs where the temperature and flow rate profiles swing widely either side of what should be the final answer, often in the Newton-Raphson–based methods. Oscillation is caused by too large a step in the profiles from one column trial to the next. This oscillation is prevented by limiting the step or percentage change in the MESH variables to below the amount generated by the Newton-Raphson technique.
- *"Bad actor" components:* Components such as water can seriously upset the VLE method and prevent solution without very good initial values. If the water is not a steam feed, use the sneaking-up technique by solving the column first without water in the feed to establish the initial profiles. Then slowly increase the water during the succeeding runs.
- *Systems with highly nonideal VLE suffer from requiring very good initial profiles:* The sneaking-up technique can be used by first solving the column with a simple approximation of the VLE and then slowly introducing the nonideal VLE. This is described by Brierley and Smith (106) and is also the thermodynamic homotopy of Vickery and Taylor (81). As stated in Secs. 4.2.9 and 4.2.12, this can occur in the global Newton methods. The inside-out methods avoid these problems in their use of simple VLE models.
- *Initial estimates can also be generated using simpler solution methods:* The 2*N* Newton (Sec. 4.2.8) and global Newton (Sec. 4.2.9) methods require good initial estimates and the more complex the method, the greater the need for good estimates. A relaxation method (Sec. 4.2.11) or a BP method (with a simple VLE method) (Sec. 4.2.5) are far less sensitive to initial estimates. These can be used to bring the profile close to the solution from where the preferred method can complete the calculation.
- *It is helpful for programs to be able to plot temperature, flow rate, composition, and stripping factor profiles plus x-y diagrams and key ratio plots:* These are powerful in detecting composition pinches. They also help in analyzing a column's performance, such as when rating an operating column to understand why it fails to meet the required products. Section 3.4 discusses the use of these graphical techniques in analyzing simulation results.

Flat profiles or hardly any change in composition or temperature over a large range of stages can indicate the location of a pinch. If the range is above or below the feed, move the feed stage in the direction of the range. If the range spans the feed stage, increase reflux or remove some stages.

A reversed temperature profile (or temperature increasing up the

column) may indicate a problem with the feed temperature. It may also be caused by a shift in the concentration of an inert component in the vapor phase.

Composition profile plots often show the buildup of some middle components in the column, forced there by lighter or heavier components. The profiles plots may not show the relative separation between components and there the x-y diagrams are better suited.

Using these plots in preliminary computer runs with simple specifications such as product rates and reflux or boilup will also help to determine if more or fewer stages are needed or if the feed stage is properly located. These simple runs will also help establish initial profiles and even whether the separation is feasible at all. Once such problems are conquered, the column can be simulated at the desired conditions and with the required specifications.

4.3.4 Which method to use

Friday and Smith (1) were the first to classify the methods and present recommendations on which method to use for different columns. A good recent source with recommendations on most of the types of methods is King (11). He presents a decision diagram to show which family of methods is best for a column. Figure 4.4 is an updated diagram. Table 4.1 summarizes the strengths and weaknesses of many common methods. The choice of method is based on the type of mixture and type of column. The diagram and table are intended to provide general guidelines only; favorable or unfavorable experience with a specific application may override these guidelines.

The inside-out methods (Sec. 4.2.10) can be used for most columns. The Russell method is simple to implement and does work well for a wide variety of refinery and hydrocarbon columns. The Boston method also works well for a wide range of columns and has been shown to work for superfractionators or tall, high-purity columns. Since the outer loops of the two methods are similar, they can be combined with a choice between the two methods, depending on the type of column. as part of the inside loop.

The global Newton method (Sec. 4.2.9) can be used for highly nonideal systems or reactive distillation systems with a homotopy forcing (Sec. 4.2.12) or relaxation technique (Sec. 4.2.11).

Nonequilibrium methods (Sec. 4.2.13) tend to be global Newton methods extended to solve mass-transfer-inhibited systems. Nonequilibrium methods are not yet completely extended to more common systems, but these methods should see the greatest amount of development in distillation modeling.

Alternates (marked as the entries in parentheses in Fig. 4.4) could

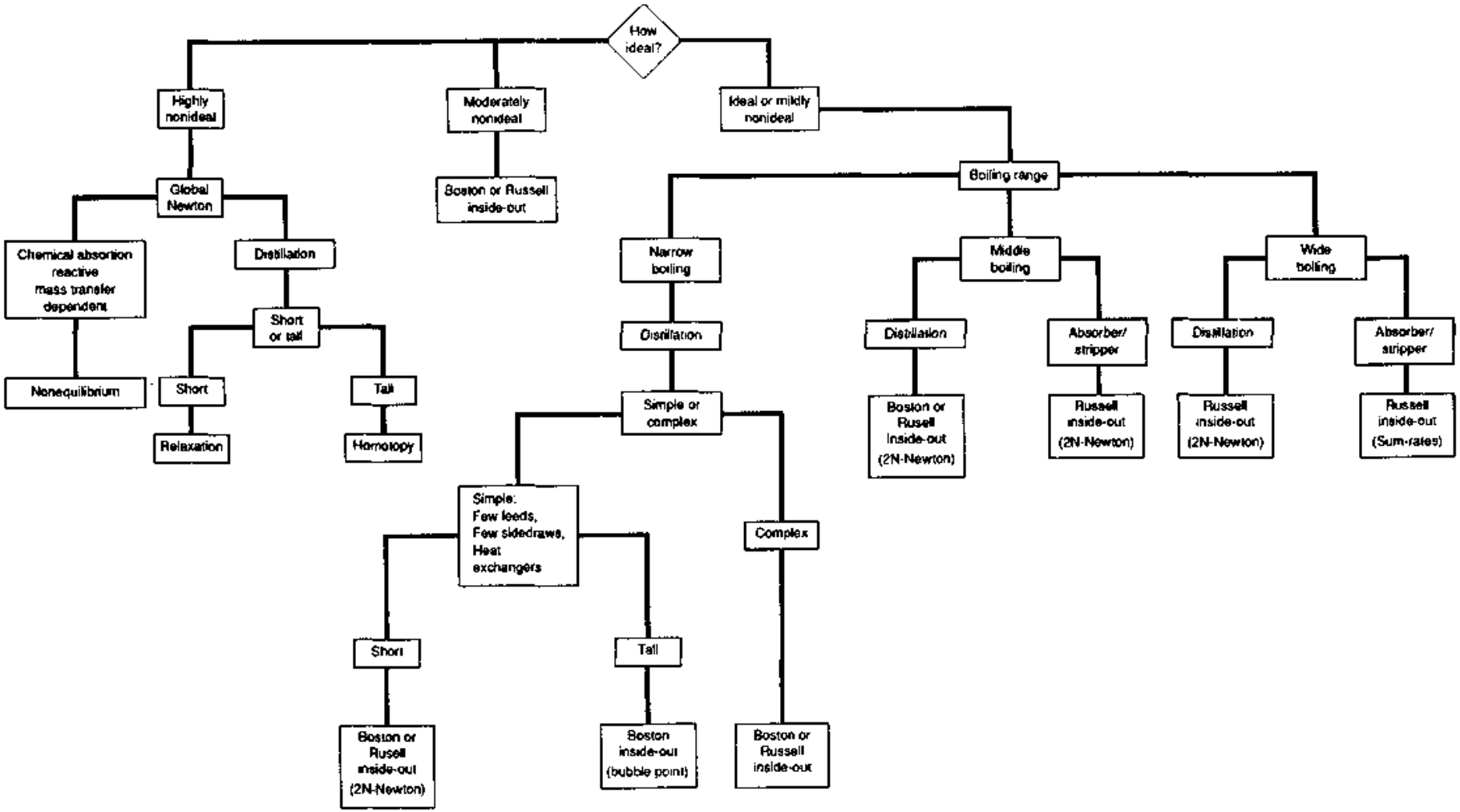

Figure 4.4 Method decision diagram.

TABLE 4.1 Methods Summary

Method	Source	Best applications	Range of specifications
Boiling point	Wang and Henke (24) Holland (8)	Narrow-boiling systems Ideal or nearly ideal systems Best if few feeds and sidedraws, superfractionators, isostrippers	Product rates and reflux; or two of condenser duty, reboiler duty, reflux ratio, and boilup
Sum rates	Sujata (35) McNeese (36) Burningham and Otto (34)	Absorbers and strippers, especially the widest-boiling systems Steam strippers	All side products flows and duties must be specified
2*N* Newton	Tomich (32) Holland (8)	Narrow- or middle-boiling systems Nearly ideal, many trays a problem Debutanizers, demethanizers	Two of condenser duty, reboiler duty, reflux, and boilup plus all side product flows, one purity allowed
Global Newton	Naphtali and Sandholm (42) Holland (8)	High number of trays, few components All type mixtures including nonideal Requires good starting values Chemical and reactive systems	Two of condenser duty, reboiler duty, reflux, and boilup plus all side product flows, one purity allowed
Global Newton	Goldstein and Stanfield (45)	Few trays and many components, mildly nonideal to nonideal Refinery columns	Variety but may allow only one purity
Global Newton	Ishii and Otto (47)	Ideal to nonideal systems Has been applied to amine systems	Variety but may allow only one purity
Relaxation	Rose, Sweeny, and Schrodt (60)	Wide range of difficult to solve columns	
Relaxation	Ketchum (64) Drew and Franks (65)	Nonideal and reactive systems	Same as Naphtali-Sandholm
Inside-out	Boston (70)	Wide variety of boiling-point ranges, columns and specifications Ideal to nonideal systems Superfractionators, petrochemical, chemical columns	Wide variety, multiple purity, allows for broad mix including least squares solution when overspecified
Inside-out	Russell (72)	Wide variety of boiling-point ranges, columns, and specifications Ideal to nonideal systems Refinery columns, complex columns	Wide variety, multiple purity must have balance between number of specifications and variables
Nonequilibrium	Krishnamurthy and Taylor (88, 89)	Mass-transfer-inhibited systems, replacement for use of efficiencies Highly nonideal and reactive systems	Same as Naphtali-Sandholm

be the BP method (Sec. 4.2.5) for simple, tall, nearly ideal columns distilling narrow-boiling mixtures, the 2*N* Newton (Sec. 4.2.8) for shorter columns with wider boiling ranges, and the SR method (Sec. 4.2.7) for very wide boiling absorber-strippers. If you have a very specific problem, you may be able to tune any of the methods to solve your problem.

4.3.5 What to look for in choosing a package or a method

The conditions listed below are somewhat ordered from most important to least important. Chan et al. (5) provide a detailed overview in selecting distillation software.

1. The accuracy of the final results is the most important test of a rigorous method. At the solution, these are usually dependent on the *K*-value and enthalpy methods rather than the rigorous method itself. If the method converges on the wrong answer, the whole effort is worthless. The program should then allow the user to adjust, tune, or add his or her own *K*-value or enthalpy methods to fit the specific system and to interpolate basic VLE data.
2. The reliability or stability of a method covers its ability to reach a solution for a wide group of problems in a general range of mixtures, such as wide or narrow boiling, and if it can solve columns across the whole spectrum of boiling point ranges. It also covers the ability of the method to solve the same column with variations in some of the specifications such as number of trays, reflux ratio, or feed conditions.
3. Whether a method is robust is found by testing it for a variety of columns. Being robust also covers whether a program can still solve when starting with a minimum amount or poor initial values. The quality of the initial values can be very important for certain methods but usually an experienced engineer will know what conditions his or her column will run at. You should consider how much effort has been placed in producing the program. Most methods require a set of conditional tests, heuristics, or "tricks" that improve the method's initial profiles or ability to converge; these things are not always stated in the literature and do take time to develop. In spite of what some salespeople may tell you, a method does not yet exist that solves all columns and works every time.
4. The flexibility and ease of input can make a major difference in encouraging an engineer to use the program. Covered within this is how difficult is the input to learn, the quality of any manual supporting the program, interactive power, how the program catches

input mistakes, and how it responds when the program fails to reach a solution.

5. A variety of features and accepted column specifications are necessary. The specifications are not just product rates or duties but also product compositions or properties and someone will always stretch the limits on stages and components in a program.
6. The ease of implementation of any method is important only if the program is being written rather than purchased complete. After studying these methods, though, you may find that differences in understanding each method may not be great.
7. The amount of computer time used by a method is overrated. Very overrated. As very fast computers become more available, the computer time used will hardly be noticeable.

4.4 Nomenclature

4.4.1 English letters

A_j Term of simple K-value model in the inside-out methods, defined by Eq. (4.85).

$A_{j,k}$ Term in the pseudo-Clausius-Clapeyron equation of the K_b method, defined by Eq. (4.54).

A_{ij} Absorption factor, component i, stage j, defined by Eq. (4.6).

a_j Mass transfer surface area between two phases, stage j, Sec. 4.2.13.

a_{ij} Term of simple liquid activity model in inside-out methods, Eq. (4.88).

B Total bottoms rate.

B_j Term of simple K-value model in the inside-out methods, defined by Eq. (4.85).

$B_{j,k}$ Term in the pseudo-Clausius-Clapeyron equation of the K_b method, defined by Eq. (4.54).

b_i Component bottoms rate, component i.

b_{ij} Term of simple liquid activity model in inside-out methods, defined by Eq. (4.88).

C Last or total number of components.

C Scalar used in a quasi-Newton update of a Jacobian, Sec. 4.2.6.

C_j Term of simple vapor enthalpy model in the inside-out methods, defined by Eq. (4.92).

Cpu_j Heat capacity of the liquid holdup in the column, stage j, Sec. 4.2.11.

D_j Dew-point equation as an independent function for a stage in Sec. 4.2.8.

D Total vapor distillate rate.

D_j Term of simple vapor enthalpy model in the inside-out methods, defined by Eq. (4.92).

d Total liquid distillate rate.

d_i Component distillate rate, component i.

E_j Energy balance as a function for a stage in Secs. 4.2.7 to 4.2.9.

E_j Term of simple liquid enthalpy model in the inside-out methods, defined by Eq. (4.93).

E_{MVij} Murphree efficiency, component i, stage j, defined by Eq. (4.20).

E_{ij} Vaporization efficiency, component i, stage j, defined by Eq. (4.23).

E^*_j Net energy gain by a phase in a nonequilibrium method, stage j, Sec. 4.2.13.

e Perturbed value for x_k in a derivative of a Newton-Raphson solution, Sec. 4.2.6.

e_j Energy flux for energy transfer between two phases, stage j, Sec. 4.2.13.

e_{ij} Equilibrium equation in a global Newton method, Sec. 4.2.9.

F_f Total feed rate, stage f.

F_j Term of simple liquid enthalpy model in the inside-out methods, defined by Eq. (4.93).

$\underline{\mathbf{F}}_j$ Vector of independent functions of stage j, for a Newton-Raphson solution in a Naphtali-Sandholm or nonequilibrium method.

$\underline{\mathbf{F}}(\underline{\mathbf{x}})$ Vector representing the difficult, desired solution in a homotopy method, Sec. 4.2.12.

$\underline{\mathbf{F}}$ Vector of total feed rates to a column in the total material balances.

f_i Rate of component in the feed to a column.

f_k Independent function of a Newton-Raphson solution, Sec. 4.2.6.

f_{ijL} Fugacity of the liquid, K-value, component i, stage j.

f_{ijV} Fugacity of the vapor, K-value, component i, stage j.

$\underline{\mathbf{f}}_i$ Vector of component feed rates to a column, component i, Sec. 4.2.4.

$\underline{\mathbf{f}}_k$ Vector of values for the independent functions in a Newton-Raphson method, trial k, Sec. 4.2.6.

$\underline{\mathbf{G}}(\underline{\mathbf{x}})$ Vector of function values for the easier solution in a homotopy method, Sec. 4.2.12.

h_B Molar enthalpy of bottoms product.

H_D Molar enthalpy of distillate product, liquid or vapor phase.

H_W Molar enthalpy of side product, liquid or vapor phase.

H_J Molar enthalpy of vapor phase, stage j.

H°_j Molar ideal gas enthalpy of vapor phase, stage j.

H_F Enthalpy of a feed, encompassing all phases, feed F.

$\underline{\mathbf{H}}_t$ Jacobian at each homotopy step t, Sec. 4.2.12.

$\underline{\mathbf{H}}_x$ Jacobian of the known solution in a homotopy method, Sec. 4.2.12.

$\underline{\mathbf{H}}(\underline{\mathbf{x}},t)$ Jacobian of derivatives of the homotopy matrix, Sec. 4.2.12.

h_j Molar enthalpy of liquid phase, stage j.

h°_j Molar ideal has enthalpy of liquid phase, stage j.

$\underline{\mathbf{J}}_k$ Jacobian of partial derivatives in Newton-Raphson method, trial k, Sec. 4.2.6.

K_{ij} Equilibrium constant, K-value, component i, stage j.

K_{bj} K-value for base component of the K_b method and the simple K-value model of the inside-out methods, stage j, Sec. 4.2.10.

L_j Internal total liquid rate, stage j.

L_0 Lean oil feed rate to the top stage of an absorber.

L_1 External total reflux rate; internal total liquid rate, stage 1.

$\underline{\mathbf{L}}_k$ Lower triangular matrix of LU factorization, trial k, Sec. 4.2.6.

l_{iF} Component liquid rate in the feed, component i.

l_{ij} Internal component liquid rate, component i, stage j.

M_j Total material balance as a function for a stage in Sec. 4.2.9.

m_{ij} Element of middle diagonal in tridiagonal matrix, component i, stage j, Eq. (4.33).

m_{ij} Component balance in a global Newton method, Sec. 4.2.9.

N Last or total number of stages.

N_{ij} Molar flux for mass transfer between two phases, component i, stage j, Sec. 4.2.13.

N^*_j Net material gain by a bulk phase in a nonequilibrium method, stage j, Sec. 4.2.13.

norm_k Square root of the sum of the squares of the functions, trial k, Sec. 4.2.6.

n Number of independent equations and variables in a Newton-Raphson method, Sec. 4.2.6.

P_j Stage pressure, stage j.

p_i Correction factor for stage compositions in the θ method, component i, defined by Eq. (4.49).

p_{ij} Variable of the Boston inside-out method, defined by Eq. (4.95).

Q_C Condenser duty.

Q_R Reboiler duty.

Q_S Duty of intercondenser or interreboiler of some stage.

Q_j Duty to a bulk phase in a nonequilibrium method, stage j, Sec. 4.2.13.

R_j Variable of the Boston inside-out method, defined by Eq. (4.94).

R_{Lj} Withdrawal factor for a liquid side product in the Russell method, Sec. 4.2.10.

R_{Vj} Withdrawal factor for a vapor side product in the Russell method, Sec. 4.2.10.

R_{ij} Component mass transfer rate equation a nonequilibrium method, stage j, Sec. 4.2.13.

$\underline{\mathbf{r}}_i$ Tridiagonal matrix of the component balances, component i, Eq. (4.33).

$\underline{\mathbf{R}}$ Tridiagonal matrix of the total material balances, Sec. 4.2.4.

S_b Base stripping factor in Eq. (4.100) of inside-out methods.

S_j Summation equation as a function for a stage in Secs. 4.2.8 and 4.2.9.

S_{ij} Stripping factor, component i, stage j, defined by Eq. (4.5), and an adjustment term in the inside-out methods, Eq. (4.100).

s_k Scalar to control step in a Newton-Raphson method, trial k, Sec. 4.2.6.

T_j Stage temperature, stage j.

T^* Reference temperature of the simple K-value model of an inside-out method, Eq. (4.85).

t Time value used in a relaxation method, Sec. 4.2.11.

t Homotopy parameter defined by Eq. (4.114).

t_i Term used in the weighting factors of an inside-out method, defined by Eq. (4.102).

U_j Liquid holdup in the column, stage j, Sec. 4.2.11.

$\underline{\mathbf{U}}_k$ Upper triangular matrix of LU factorization, trial k, Sec. 4.2.6.

V_j Internal total vapor rate, stage j.

V_N Reboiler boilup; internal total vapor rate, stage N.

V_{N+1} Rich gas feed to the bottom stage of an absorber.

v_{iF} Component vapor rate in the feed, component i.

v_{ij} Internal component vapor rate, component i, stage j.

$\underline{\mathbf{V}}$ Vector of total vapor rates in the column used in the total material balances, Sec. 4.2.4.

$\underline{\mathbf{v}}_i$ Vector of component vapor rates in the column, component i, Sec. 4.2.4.

W_p Total side product withdrawal rate, stage p.

W_{Lj} Total liquid side product rate used in the withdrawal factors of the Russell method, Sec. 4.2.10.

W_{Vj} Total vapor side product rate used in the withdrawal factors of the Russell method, Sec. 4.2.10.

w_i Weighting factor in Sec. 4.2.10, component i.

w_{ij} Rate of component i in the side product of stage j.

X_{Di} Composition of top product, covering all phases, of component i.

X_{iF} Composition in feed, covering all phases, component i, feed F.

$\underline{\mathbf{X}}_j$ Vector of independent variables of stage j, for a Newton-Raphson solution in a Naphtali-Sandholm or nonequilibrium method, Sec. 4.2.9 and 4.2.13.

x_{ij} Liquid composition, component i, stage j.

x_k Independent variable in a Newton-Raphson solution, Sec. 4.2.5 only.

$\underline{\mathbf{x}}_k$ Vector of independent variables in Newton-Raphson method, trial k, Sec. 4.2.6.

$\underline{\mathbf{x}}$ Vector of independent variables in a homotopy solution, Sec. 4.2.12.

y_{ij} Vapor composition, component i, stage j.

y^*_{ij} Equilibrium composition of the vapor for the Murphree vaporization efficiency, component i, stage j, defined by Eq. (4.20).

4.4.2 Greek letters

α_{ij} Relative volatility, used in the K_b method and in the simple K-value model of the inside-out methods, component i, stage j.

ΔH_{Lj} Liquid-phase enthalpy departure, stage j.

ΔH_{Vj} Vapor-phase enthalpy departure, stage j.

ΔT_k Temperature span used to generate constants of K_b method, Eq. (4.54).

Δt Time step in the relaxation methods of Sec. 4.2.11.

Δx_k Change in the independent variable x_k to move it toward solution in a Newton-Raphson method, trial k, Sec. 4.2.6.

$\Delta \underline{\mathbf{x}}_k$ Vector of the changes in the independent variables in a Newton-Raphson method, trial k, Sec. 4.2.6.

γ^*_{ij} Simple activity coefficient used in the inside-out methods component i, stage j, Sec. 4.2.10.

θ Theta convergence promoter as defined by Eq. (4.46).

θ_j Independent variable used as a multiplier on the ratio of total liquid rate to total vapor rate in the $2N$ Newton-Raphson method, defined by Eq. (4.76).

4.4.3 Subscripts

actual Rigorously calculated K-value or enthalpy for any component, in the inside-out or homotopy methods, Secs. 4.2.10 and 4.2.12.

ca Compositions or flows calculated by component material balances in the theta method and $2N$ Newton-Raphson method, Secs. 4.2.5 and 4.2.8.

co Corrected composition or flows by theta in the theta method and $2N$ Newton-Raphson method, Secs. 4.2.5 and 4.2.8.

F Column feed stream.

f Feed stage.

i Component index, $i = 1 \ldots C$.

j Stage index or number, $j = 1, 2 \ldots f \ldots N$.

k Trial number of the solution in any method.

min Minimum value limit on a MESH variable.

max	Maximum value limit on a MESH variable.
n	Number of independent functions and variables in a Newton-Raphson method, Sec. 4.2.6.
new	Updated or most recent values of the internal flows.
P	Side withdrawal product stream.
p	Sidestream withdrawal stage.
Ref	Reference or base component in Sec. 4.2.10.
simple	K-value or enthalpy generated by the simple models of an inside-out method or a homotopy method, Sec. 4.2.10 and 4.2.12.
spec	Specified value.

4.4.4 Superscripts

F	Bulk feed to a phase in a nonequilibrium method, Sec. 4.2.13.
I	Interface in a nonequilibrium method, Sec. 4.2.13.
T	Transpose, mathematical representation of a vector.
L	Bulk liquid in a nonequilibrium method, Sec. 4.2.13.
V	Bulk vapor in a nonequilibrium method, Sec. 4.2.13.
W	Bulk side product from a phase in a nonequilibrium method, Sec. 4.2.13.
*	Net energy or mass transferred between bulk phases in a nonequilibrium method, Sec. 4.2.13.

4.5 References

4.5.1 General reviews and surveys

1. Friday, J. R., and B. D. Smith, *Am. Inst. Chem. Engrs. J., 10,* p. 689, 1964.
2. Holland C. D., *Am. Inst. Chem. Engrs. Symp. Ser., 80,* p. 15, 1983.
3. Seader, J. D., and Z. M. Kurtyka in R. H. Perry and D. W. Green (eds.), *Chemical Engineers' Handbook,* 6th ed., McGraw-Hill, New York, 1984.
4. Wang, J. C., and Y. L. Wang, in R. S. H. Mah and W. D. Seider (eds.), *Foundations of Computer-Aided Chemical Process Design,* vol. II, p. 121, Engineering Foundation, 1981.
5. Chan, W. K., J. F. Boston, and L. B. Evans, Paper presented at AIChE National Meeting, Chicago, Ill., November, 1990.
6. Humphrey, J. L., R. A. Koort, and A. F. Seibert, Paper presented at AIChE National Meeting, Chicago, Ill., November, 1990.

4.5.2 General sources used throughout

7. Holland, C. D., *Fundamentals and Modeling of Separation Processes,* Prentice-Hall, New York, 1975.
8. Holland, C. D., *Fundamentals of Multicomponent Distillation,* McGraw-Hill, New York, 1981.
9. Holland, C. D., *Unsteady State Processes with Applications in Multicomponent Distillation,* Prentice-Hall, New York, 1966.
10. Holland, C. D., and A. I. Liapis, *Computer Methods for Solving Dynamic Separation Problems,* McGraw-Hill, New York, 1983.

11. King, C. J., *Separation Processes,* McGraw-Hill, New York, 1980.
12. Rose, L. M., *Distillation Design in Practice,* Elsevier, New York, 1985.
13. Henley, E. J., and J. D. Seader, *Equilibrium-Stage Separation Operations in Chemical Engineering,* Wiley, New York, 1981.
14. Kister, H. Z., *Distillation Operation,* McGraw-Hill, New York, 1990.

4.5.3 First statement of the general methods

15. Thiele, E. W., and R. L. Geddes, *Ind. Eng. Chem., 25,* p. 289, 1933.
16. Lewis, W. K., and G. L. Matheson, *Ind. Eng. Chem., 24,* p. 494, 1932.

4.5.4 Early methods for computers

17. Edmister, W. C., *Am. Inst. Chem. Engrs. J., 3,* p. 165, 1957.
18. Smith, B. D. *Design of Equilibrium Stage Processes,* McGraw-Hill, 1963.
19. Amundson, N. R., and A. J. Pontinen, *Ind. Eng. Chem., 50,* p. 730, 1958.
20. Bonner, J. S., *Am. Pet. Inst., Div. of Refining, 36*(3), p. 23, 1956.
21. Donnell, J. W., and K. Turbin, *Chem. Eng., 56*(7), p. 112, 1951.
22. Rea, H. E., Jr., and D. N. Hanson, *Pet. Refiner, 31*(11), p. 139, 1952.
23. Greenstadt, J. Y., Y. Bard, and B. Morse, *Ind. Eng. Chem., 50,* p. 1944, 1958.

4.5.5 Material balance methods

24. Wang, J. C., and G. E., Henke, *Hydrocarb. Proc., 45*(8), p. 155, 1966.
25. Boston, J. F., and S. L. Sullivan, Jr., *Can. J. Chem. Eng., 50,* p. 663, 1972.

4.5.6 Theile-Geddes oriented (including bubble-point) methods

26. Holland, C. D., *Multicomponent Distillation,* Prentice-Hall, New York, 1963.
27. Holland, C. D., and G. P. Pendon, *Hydrocarb. Proc., 53*(7), p. 148, 1974.
28. Hess, F. E., S. E. Gallun, G. W. Bentzen, C. D. Holland, R. McDaniel, and N. J. Tetlow, *Hydrocarb. Proc., 56*(6), p. 181, 1977.
29. Haas, J. R., M. A. Gomez, and C. D. Holland, *Separation Sci. Tech., 16*(1), p. 1, 1981.
30. Billingsley, D. S., *Am. Inst. Chem. Engrs. J., 16,* p. 441, 1970.
31. Lo, C. T., *Am. Inst. Chem. Engrs. J., 21,* p. 1223, 1975.
32. Tomich, J. F., *Am. Inst. Chem. Engrs. J., 16,* p. 229, 1970.
33. Orbach, O., C. M. Crowe, and A. I. Johnson, *Chem. Eng. J., 3,* p. 176, 1971.

4.5.7 Sum-rates or absorber-oriented methods

34. Burningham, D. W., and F. D. Otto, *Hydrocarb. Proc., 46*(10), p. 163, 1967.
35. Sujata, A. D., *Hydrocarb. Proc. Pet. Refiner, 40*(12), p. 137, 1961.
36. McNeese, C. R., *Chem. Eng. Prog. Sym. Series, 37*(58), p. 43, 1962.
37. Boynton, G. W., *Hydrocarb. Proc., 49*(1), p. 153, 1970.
38. Holland, C. D., G. P. Pendon, and S. E. Gallun, *Hydrocarb. Proc., 54*(1), p. 101, 1975.
39. Fonyo, Z., H. Nishimura, and Y. Yamashita, *Am. Inst. Chem. Engrs. J., 29,* p. 538, 1983.

4.5.8 Global Newton methods

Also called simultaneous-correction methods; both original presentations of a method and variations of that method.

40. Gallun, S. E., and C. D. Holland, *Hydrocarb. Proc., 55*(1), p. 137, 1976.
41. Ferraris, G. B., *Comp. Chem. Eng., 7,* p. 73, 1983.
42. Naphtali, L., and D. S. Sandholm, *Am. Inst. Chem. Engrs. J., 17,* p. 148, 1971.
43. Fredenslund, A., J. Gmehling, and P. Rasmussen, *Vapor-Liquid Equilibrium Using UNIFAC,* Elsevier, New York, 1977.
44. Hofeling, B. S., and J. D. Seader, *Am. Inst. Chem. Engrs. J., 24,* p. 1131, 1978.
45. Goldstein, R. P., and R. B. Stanfield, *Ind. Eng. Chem. Proc. Des. Dev., 9,* p. 78, 1970.
46. Kubicek, M., V. Hlavacek, and F. Prochaska, *Chem. Eng. Sci., 31,* p. 277, 1976.
47. Ishii, Y., and F. D. Otto, *Can. J. Chem. Eng., 51,* p. 601, 1973.
48. Browne, D. W., Y. Ishii, and F. D. Otto, *Can. J. Chem. Eng., 55,* p. 307, 1977.
49. Ferraris, G. B., and M. Morbidelli, *Am. Inst. Chem. Engrs. J., 27,* p. 881, 1981.
50. Block, U., and B. Hegner, *Am. Inst. Chem. Engrs. J., 22,* p. 583, 1976.
51. Wu, J.-S., and P. R. Bishnoi, *Comp. Chem. Eng., 10,* p. 343, 1986.
52. Lucia, A., and K. R. Westman, in A. W. Westerberg and H. H. Chien (eds.), *Foundations of Computer-Aided Process Design,* 741, CACHE, 1983.
53. Westman, K. R., A. Lucia, and D. C. Miller, *Comp. Chem. Eng., 8,* p. 219, 1984.
54. Christiansen, L. J., M. L. Michelsen, and A. Fredenslund, *Comp. Chem. Eng., 3,* p. 535, 1979.
55. Shah, M. K., and P. R. Bishnoi, *Can. J. Chem. Eng., 56,* p. 478, 1978.
56. Billingsley, D. S., and G. W. Boynton, *Am. Inst. Chem. Engrs. J., 17,* p. 65, 1971.
57. Ricker, N. L., and E. A. Grens, *Am. Inst. Chem. Engrs. J., 20,* p. 238, 1974.
58. Rafal, M., S. J. Sanders, and R. D. Young, Paper presented at AIChE National Meeting, Washington, D.C., November, 1988.
59. Bondy, R. W., Paper presented at AIChE National Meeting, Chicago, Ill., November, 1990.

4.5.9 Relaxation methods

60. Rose, A., R. F. Sweeny, and V. N. Schrodt, *Ind. Eng. Chem., 50,* p. 737, 1958.
61. Jelinek, J., V. Hlavacek, and M. Kubicek, *Chem. Eng. Sci., 28,* p. 1825, 1973.
62. Mori, H., I. Yamada, T. Tsuiki, and S. Hiraoka, *J. Chem. Eng. Japan, 20,* p. 460, 1987.
63. Ball, W. E., Paper presented at AIChE National Meeting, New Orleans, Louisiana, February, 1961.
64. Ketchum, R. G., *Chem. Eng. Sci., 34,* p. 387, 1979.
65. Drew, D., and R. G. E. Franks, Class notes from MIT course "Modeling, Simulation and Optimization of Chemical Processes," 1988.
66. Franks, R. G. E., *Modeling and Simulation in Chemical Engineering,* Wiley, New York, 1972.
67. Komatsu, H., *J. Chem. Eng. Japan, 10,* p. 200, 1977.
68. Ishikawa, T., and M. Hirata, *J. Chem. Eng. Japan, 5,* p. 125, 1972.

4.5.10 Inside-out algorithms

69. Boston, J. F., and S. L. Sullivan, Jr., *Can. J. Chem. Eng., 52,* p. 52, 1974.
70. Boston, J. F., *ACS Symp. Ser.* No. *124,* p. 135, 1980.
71. Boston, J. F., and H. I. Britt, *Comp. Chem. Eng., 2,* p. 109, 1978.
72. Russell, R. A., *Chem. Eng., 90*(20), p. 53, 1983.
73. Jelinek, J., *Comp. Chem. Eng., 12,* p. 195, 1988.
74. Trevino-Lozano, R. A., T. P. Kisala, and J. F. Boston, *Comp. Chem. Eng., 8,* p. 105, 1984.
75. Boston, J. R., Paper presented at AIChE National Meeting, Houston, Texas, April, 1979.
76. Boston, J. R., and V. B. Shah, Paper presented at AIChE National Meeting, Houston, Texas, April, 1979.
77. Venkataraman, S., W. K. Chan, and J. F. Boston, *Chem. Eng. Prog., 86,* p. 8, 1990.

4.5.11 Homotopy methods

78. Ellis, M. F., R. Koshy, G. Mijares, A. Gomez-Munoz, and C. D. Holland, *Comp. Chem. Eng., 10,* p. 433, 1986.
79. Byrne, G. D., and L. A. Baird, *Comp. Chem. Eng., 9,* p. 593, 1985.
80. Taylor, R., T. L. Wayburn, and D. J. Vickery, *I. Chem. E. Symp. Ser.* No. *104,* p. B305, 1987.
81. Vickery, D. J., and R. Taylor, *Am. Inst. Chem. Engrs. J., 32,* p. 547, 1986.
82. Vickery, D. J., J. J. Ferrari, and R. Taylor, *Comp. Chem. Eng., 12,* p. 99, 1988.
83. Wayburn, T. L., *Am. Inst. Chem. Engrs. CAST Comm., 11,* p. 8, 1988.
84. Wayburn, T. L., and J. D. Seader, in A. W. Westerberg and H. H. Chien (eds.), *Foundations of Computer-Aided Process Design,* 765, CACHE, 1983.
85. Seader, J. D., Class notes from MIT course "Modeling, Simulation and Optimization of Chemical Processes," 1988.
86. Seader, J. D., *Am. Inst. Chem. Engrs. Monogr. Ser.* No. *15,* Vol. 81, 1985.

4.5.12 Nonequilibrium models

87. Taylor, R., M. F. Power, M. Lao, and A. Arehole, *I. Chem. E. Symp. Ser.* No. *104,* p. B321, 1987.
88. Krishnamurthy, R., and R. Taylor, *Am. Inst. Chem. Engrs. J., 31,* p. 449, 1985.
89. Krishnamurthy, R., and R. Taylor, *Am. Inst. Chem. Engrs. J., 31,* p. 456, 1985.
90. Sivasubramanian, M. S., R. Taylor and R. Krishnamurthy, *Am. Inst. Chem. Engrs. J., 33,* p. 325, 1987.
91. Billingsley, D. S., and A. Chirachavala, *Am. Inst. Chem. Engrs. J., 27,* p. 968, 1981.
92. Biardi, G., and Grottoli, M. G., *Comp. Chem. Eng., 13,* p. 441, 1989.
93. Sivasubramanian, M. S., and J. F. Boston, Paper presented at AIChE National Meeting, Washington, D.C., November, 1989.
94. Seader, J. D., *Chem. Eng. Prog., 85,* p. 10, 1989.
95. Ponter, A. B., and P. H. Au-Yeung, Paper presented at AIChE National Meeting, Orlando, Florida, March, 1990.
96. Young, T. C., and W. E. Stewart, Paper presented at AIChE National Meeting, Chicago, Ill., November, 1990.

4.5.13 Incorporation of efficiencies in rigorous distillation calculations

97. Standart, G., *Chem. Eng. Sci., 20,* p. 611, 1965.
98. Toor, H. L. Am. Inst. Chem. Engrs. J., 10, 545, 1964.
99. Economopoulos, A. P., *Chem. Eng., 85*(53), p. 109, 1978.
100. Graham, J. P., J. W. Fulton, M. S. Kuk, and C. D. Holland, *Chem. Sci. Eng., 28,* p. 473, 1973.
101. Fletcher, J. P., *I. Chem. E. Symp. Ser.* No. *104,* p. A437, 1987.
102. Krishnamurthy, R., and R. Taylor, in N. P. Cheremisinoff (ed.), *Handbook of Heat and Mass Transfer,* Gulf Publishing, Houston, Texas, 1986.
103. Huber, W. F., *Hydrocarb. Proc., 56*(8), p. 121, 1977.
104. Muhrer, C. A., M. A. Collura, and W. L. Luyben, *Ind. Eng. Chem. Res., 27,* p. 716, 1988.
105. Lockett, M. J., *Distillation Tray Fundamentals,* Cambridge University Press, Cambridge, U.K., 1986.

4.5.14 Applications of convergence methods and comparisons

106. Brierley, R. J. P., and R. Smith, *I. Chem. E. Symp. Ser.* No. *56,* 89, 1979.
107. Pierucci, S., F. Troiani, E. Ranzi, and G. Biardi, *Comp. Chem. Eng., 6,* p. 39, 1982.

108. Petryschuk, W. F., and A. I. Johnson, *Can. J. Chem. Eng., 44,* p. 241, 1986.
109. Holmes, J. W., M. L. Spears, and J. A. Bullin, *Chem. Eng. Prog., 79,* p. 5, 1984.
110. Russell, R. A., *Comp Chem. Eng., 4,* p. 167, 1980.
111. Morris, C. G., W. D. Sim, T. Vysniauskas, and W. Y. Svrcek, *Chem. Eng. Prog., 84,* 11, 1988.
112. Agreda, V. H., L. R. Partin, and W. H. Heise, *Chem. Eng. Prog., 86,* p. 2, 1990.

4.5.15 Program reference manuals

113. *ASPEN Technical Reference Manual,* Massachusetts Institute of Technology, May 1982.
114. *HYSIM User's Guide, Version C1.0,* Hyprotech Ltd., Calgary, Alberta, 1989.
115. *Professional Distillation and PD + Plus,* Deerhaven Technical Software, Burlington, Mass., 1987.
116. *PROCESS Reference Manual,* Simulation Sciences Inc., Fullerton, Calif., 1988.
117. *DESIGN II User's Guide,* Chemshare Corporation, Houston, Texas, 1988.
118. *TSWEET User's Manual,* Bryan Research & Engineering, Inc., Bryan, Texas, 1987.

4.5.16 Numerical methods

119. Broyden, C. G., *Math. Comp., 19,* p. 577, 1965.
120. Bennett, J. N., *Numerische Mathematik, 7,* p. 217, 1965.
121. Press, W. H., B. P. Flannery, S. A. Teukolsky, and W. T. Vetterling, *Numerical Recipes,* Cambridge Press, Cambridge, U.K., 1986.
122. Kahaner, D., C. Moler, and S. Nash, *Numerical Methods and Software,* Prentice-Hall, New York, 1988.
123. Orbach, O., and C. M. Crowe, *Can. J. Chem. Eng., 49,* p. 509, 1971.

4.5.17 Personal communications

124. Dr. John T. Baldwin, The M. W. Kellogg Co., 1988.
125. Mr. Dale L. Embry, Phillips Petroleum Co., 1988.
126. Mr. Richard A. Russell, Deerhaven Technical Software, 1989.
127. Mr. Willie Chan, AspenTech Inc., 1988.
128. Dr. Ross Taylor, Clarkson University, 1989, 1990.
129. Dr. Tom Wayburn, ChemShare Corp., 1989.

Chapter

5

Batch Distillation

David R. Hart

RUST International Corporation
Birmingham, Alabama

Although neither as widely used nor as sophisticated as their continuous counterparts, batch stills play an important role in the chemical process industries. Batch stills are typically used

1. Where the compositions of the materials to be separated vary over wide ranges
2. Where the separation only needs to be performed infrequently, such as in pilot-plant operations
3. Where the materials to be separated are produced in relatively small quantities, such as in semiworks or small-scale commercial facilities
4. Where the main product contains only relatively small amounts of light and/or heavy impurities

Selection of a batch still usually involves evaluating the performance of an existing distillation system to determine whether its performance is acceptable. However, it may be necessary to design a new system for the specific separation to be performed.

With an existing system, the following are common concerns:

1. What product compositions would be obtained
   a. without reflux, or

b. with reflux when using,
   (1) a constant reflux ratio, or
   (2) a varying reflux ratio?

2. How much time would be required to obtain some specific product composition at some constant boil-up rate, or what boil-up rate would be required to obtain some specific product composition within some specified time under conditions of,
   a. constant reflux ratio,
   b. varying reflux ratio?

The design of a new system for a specific separation involves determining a minimum reflux ratio and selecting a control protocol (fixed or variable reflux ratio) and an amount of time to be allowed for distilling a batch of some given size.

This chapter addresses each of these concerns in order. Before passing on to that discussion, however, the distillation nomenclature will be briefly restated, both because batch stills are analyzed after the same fashion as continuous stills, and for completeness within this chapter. The overall material balance is

$$F = D + B \tag{5.1}$$

where F = feed, moles
D = distillate, moles
B = bottoms, moles

(in the case of batch stills, the bottoms are generally called *residue*). A material balance on the "light" (lower boiling) component in a binary mixture, or the light "key" component in a more complex mixture is

$$Fx_F = Dx_D + Bx_B \tag{5.2}$$

where $x_{\text{subscript}}$ = mole fraction in the liquid phase

A material balance around a total condenser gives

$$V = L + D \tag{5.3}$$

where V = vapor from column
L = liquid returning to column (equals zero in "simple" distillation)

By definition

$L/D = R$ = reflux ratio (sometimes called *external reflux ratio*)

$$V = D(R + 1) \tag{5.4}$$

From Eq. (5.3),

$$V = L + D$$

$$\frac{V}{L} = 1 + \frac{D}{L}$$

but from the definition of reflux ratio

$$\frac{D}{L} = \frac{1}{R}$$

$$\frac{V}{L} = 1 + \frac{1}{R}$$

$$= \frac{R + 1}{R}$$

or

$$L/V = \frac{R}{R + 1} \tag{5.5}$$

Relative volatility, α, which describes the equilibrium relationship between vapor and liquid compositions, is defined as

$$\alpha = \frac{y/x}{(1 - y)/(1 - x)} \tag{5.6}$$

where α = relative volatility
y = mole fraction of light component or key in vapor phase

This relationship is usually rearranged into

$$y = \frac{\alpha x}{1 + (\alpha - 1)x} \tag{5.7}$$

and used to calculate vapor-phase compositions in equilibrium with a particular liquid-phase composition (see Chap. 1).

Refer to Chap. 3 for a more detailed discussion of this nomenclature and its usage.

5.1 Existing Systems

5.1.1 Simple distillation

In simple distillation, the vapor leaving the still passes into a total condenser, and the liquid leaving the condenser passes into a product receiver. No reflux is returned to the still.

The first vapor which leaves the still is richer in the lighter compo-

nent than the liquid originally present because the still acts as a single theoretical separation stage. As the process continues, the material remaining in the still becomes increasingly depleted in the lighter component, so the vapor leaving the still progressively contains larger amounts of the "heavy" component. Thus, the "product" in the receiver gets diluted with material which continuously becomes heavier.

Lord Rayleigh (15) first analyzed such a system mathematically. With no reflux returning to the still, the rate at which the more-volatile component leaves the still is equal to the rate of change of composition in the still.

$$-y\,dV = d(xW) \tag{5.8}$$

where dV = vapor rate, moles/h
W = total moles in still

Differentiating Eq. (5.8),

$$-y\,dV = x\,dW + W\,dx \tag{5.9}$$

but

$$dV = -dW$$

so

$$y\,dW = x\,dW + W\,dx$$

Rearranging

$$(y - x)dW = W\,dx \tag{5.10}$$

$$\frac{dW}{W} = \frac{dx}{(y - x)} \tag{5.11}$$

Integrating this equation gives

$$\ln \frac{W_f}{W_0} = \int_{x_0}^{x_f} \frac{dx}{(y - x)} \tag{5.12}$$

where W_f = moles in still at end
W_0 = moles originally changed to still

Typically the right-hand side of Eq. (5.12) is evaluated by graphical integration, using the assumption that the vapor and liquid phases are in equilibrium.

If the system to be separated is ideal or can be assumed to be ideal. relative volatility [Eq. (5.6)] is constant, and Eq. (5.7) can be used di-

rectly to compute equilibrium compositions. If the system is not ideal, experimental vapor-liquid equilibrium data must be available (see Chap. 2).

Assuming the relative volatility of a benzene-toluene mixture is 2.90, the vapor-liquid equilibrium compositions can be calculated as shown in Table 5.1. The resultant curve is plotted in Fig. 5.1*a*.

TABLE 5.1 Equilibrium Vapor-Liquid Compositions, Benzene-Toluene System, 14.7 psia

x	αx	$(\alpha - 1)x$	$1 + (\alpha - 1)x$	y
0.000	0.000	0.000	1.00	0.000
0.100	0.290	0.190	1.19	0.244
0.200	0.580	0.380	1.38	0.420
0.300	0.870	0.570	1.57	0.554
0.400	1.16	0.760	1.76	0.659
0.500	1.45	0.950	1.95	0.744
0.600	1.74	1.14	2.14	0.813
0.700	2.03	1.33	2.33	0.871
0.800	2.32	1.52	2.52	0.921
0.900	2.61	1.71	2.71	0.963
1.00	2.90	1.90	2.90	1.00

Figure 5.1 Equilibrium and $1/(y\text{-}x)$ plots, Example 5.1. (*a*) Equilibrium vapor-liquid compositions, benzene-toluene system, 14.7 psia, $\alpha = 2.90$.

Example 5.1 A benzene-toluene mixture consists of 50 moles of benzene and 50 moles of toluene. It is desired to reduce the residual benzene concentration to 0.1 mole fraction. Calculate the overall material balance for this distillation.

solution Note that in this and all subsequent examples, vapor ("boil-up") rate is considered constant, and the effect of column holdup is ignored.

From Fig. 5.1*a*

x	y	$y - x$	$\frac{1}{(y - x)}$
0.500	0.744	0.244	4.10
0.400	0.659	0.259	3.86
0.300	0.554	0.254	3.94
0.200	0.420	0.220	4.55
0.100	0.244	0.144	6.94

The values of $1/(y - x)$ are plotted versus x in Fig. 5.1*b*.

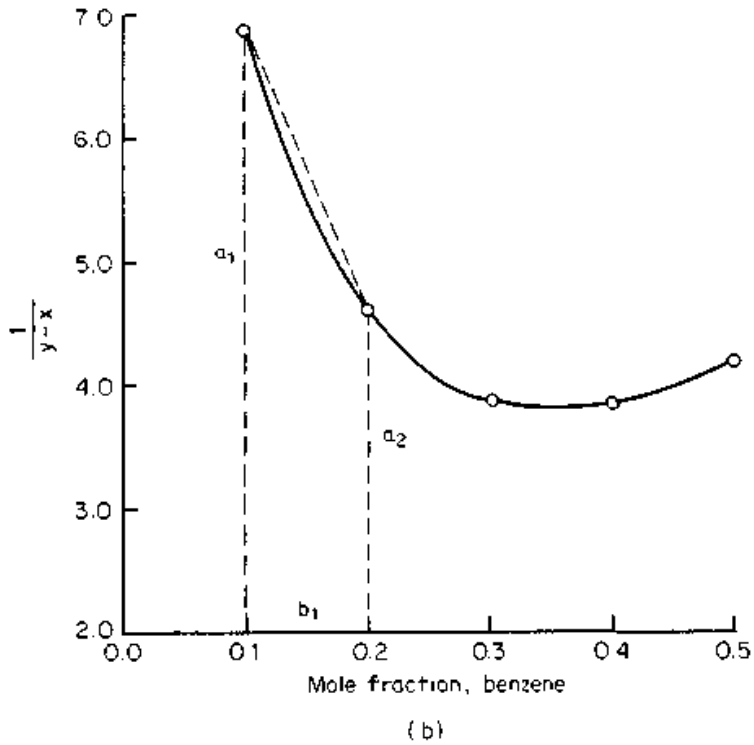

Figure 5.1 (*Continued*) Equilibrium and $1/(y\text{-}x)$ plots, Example 5.1. (*b*) Simple fractionation of benzene-toluene, $1/(y\text{-}x)$ vs. x.

Assuming the individual values of $1/(y - x)$ can be joined by a straight line, the area under the curve may be approximated:

$$\text{Area} = ba$$

$$= (b_1 a_{1\to 2} + b_2 a_{2\to 3} \ldots)$$

but

$$b_1 = b_2 = b_3, etc.$$

$$\text{Area} = b(a_{1\to 2} + a_{2\to 3}\ldots)$$

but

$$a_{1\to 2} = \frac{a_1 + a_2}{2}$$

$$\text{Area} = b\left(\frac{a_1 + a_2}{2} + \frac{a_2 + a_3}{2}\ldots\right)$$

$$= \tfrac{1}{2}\, b\,(a_1 + 2a_2 + 2a_3 + 2a_4 + a_5)$$

$$= \tfrac{1}{2}\, b\,[a_1 + 2(a_2 + a_3 + a_4) + a_5]$$

$$= \tfrac{1}{2}\,(0.1)\,[4.10 + 2(3.86 + 3.94 + 4.55) + 6.94]$$

$$= 1.79$$

Because the still is being depleted, the value of this integral must be negative.

$$\ln \frac{W_f}{100} = -1.79$$

$$W_f = 100\,(0.167)$$

$$= 16.7$$

So, the material balance is

	Still		
	Start	End	Receiver
Benzene	50	1.67	48.3
Toluene	50	15.0	35.0
	100	16.7	83.3
Mole-fraction benzene	0.50	0.10	0.58

A more universal and accurate way of evaluating $1/(y - x)$ is through the use of Simpson's rule

$$\text{Area} = \tfrac{1}{3}\, h\,[y_0 + y_n + 4(y_1 + y_3\ldots) + 2(y_2 + y_4\ldots)]$$

where h = width of an *even* number of *equally spaced* segments
y = height

Using this method,

$$\text{Area} = \tfrac{1}{3}\,(0.1)[4.10 + 4(3.86 + 4.55) + 2(3.94) + 6.94]$$

$$= 1.75$$

$$\ln \frac{W_f}{100} = -1.75$$

$$W_f = 100(0.173)$$

$$= 17.3$$

	Still		
	Start	End	Receiver
Benzene	50	1.73	48.27
Toluene	50	15.57	34.43
	100	17.3	82.7
Mole-fraction benzene	0.500	0.100	0.584

which produces results essentially identical to the previous calculation. (In the interest of conciseness, Simpson's rule will be used in all subsequent examples.) Clearly, simple distillation is not a good method for either removing or concentrating the benzene. Of the original 100 moles, 82.7 moles had to be distilled off to reduce the original benzene concentration to 10 mole percent, and the concentration of the recovered benzene only increased from 50 to 58 mole percent.

When relative volatility is constant, Eq. (5.6) can be substituted for y in Eq. (5.12), and the Rayleigh equation can be integrated to obtain

$$\ln \frac{W_f}{W_0} = \frac{1}{(\alpha - 1)} \ln \frac{x_f(1 - x_0)}{x_0(1 - x_f)} + \ln \frac{(1 - x_0)}{(1 - x_f)} \tag{5.13}$$

Example 5.2 The initial concentration of benzene in a benzene-toluene mixture is 5 mole percent. Calculate the material balance for the separation when the residual benzene concentration is 1 mole percent, again using an original charge of 100 moles of mixture.

solution

$$\ln \frac{W_f}{W_0} = \frac{1}{(\alpha - 1)} \ln \frac{x_f(1 - x_0)}{x_0(1 - x_f)} + \ln \frac{(1 - x_0)}{(1 - x_f)}$$

$$\ln \frac{W_f}{100} = \frac{1}{(2.90 - 1)} \ln \frac{[0.01(1 - 0.05)]}{[0.05(1 - 0.01)]} + \ln \frac{(1 - 0.05)}{(1 - 0.01)}$$

$$= \frac{1}{1.90} \ln \frac{0.0095}{0.0495} + \ln \frac{0.95}{0.99}$$

$$= \frac{1}{1.90} \ln 0.192 + \ln 0.960$$

$$= -0.869 - 0.0412$$

$$= -0.910$$

$$\frac{W_f}{100} = 0.402$$

$$W_f = 40.2$$

Material Balance

	Still		
	Start	End	Receiver
Benzene	5	0.402	4.60
Toluene	95	39.8	55.2
	100	40.2	59.8
Mole fraction benzene	0.050	0.010	0.077

Thus, even when starting with the relatively dilute concentration of 5 mole percent benzene, 60 percent of the mixture has to be boiled off in order to reduce the residual benzene concentration to 1 mole percent. Furthermore, the concentration of the recovered benzene is not a dramatic improvement over the starting mixture.

As shown by the two examples above, simple distillation produces only poor separations, with either high or low concentrations of the light component, even with large energy expenditures. This performance led to the development in which a fractionating column, with a reflux stream from the condenser fed back to it, was incorporated into the distillation system.

5.1.2 Constant reflux ratio

Batch distillation under conditions of constant reflux is similar to simple distillation inasmuch as the distillate and still compositions continuously vary with time. Again, the initial distillate contains the highest concentration of the light component, and distillate composition continuously gets heavier as the distillation proceeds. However, because of the interaction between the liquid reflux falling down through the column and the vapor rising up through the column, the rate of change of the distillate composition is much slower.

Batch distillation under constant reflux ratio is analyzed mathematically by considering that the moles lost from the still represent moles of distillate collected in the product receiver. Thus,

$$-dW = dD \tag{5.14}$$

where W = moles in still
D = moles of distillate

Taking a material balance on the light component,

$$-d\,(x_w\,W) = x_D\,dD \tag{5.15}$$

where x_w = mole fraction in still
x_D = mole fraction in receiver

Differentiating,

$$-(x_x\,dW + W\,dx_w) = x_D\,dD \tag{5.16}$$

and substituting Eq. (5.14) into Eq. (5.16),

$$x_w\,dW + W\,dx_w = x_D\,dW \tag{5.17}$$

Rearranging,

$$(x_w - x_D)\,dW = -W\,dx_w \tag{5.18}$$

$$\frac{dW}{W} = -\frac{dx_w}{(x_W - x_D)}$$

or

$$\frac{dW}{W} = \frac{dx_w}{(x_D - x_w)}$$

Integrating,

$$\ln \frac{W_f}{W_0} = \int_{x_{W_0}}^{x_{W_f}} \frac{dx_W}{(x_D - x_W)} \tag{5.19}$$

and, again, it is typical to evaluate the integral graphically. [Note the similarity between Eqs. (5.19) and (5.12).]

Example 5.3 A mixture containing 50 moles each of benzene and toluene is to be distilled under conditions of constant reflux ratio until mole fraction of the residual benzene is less than 0.20. The column contains three theoretical stages. Calculate the material balance for this separation.

solution By trial and error, a reflux ratio is determined which allows the construction of four theoretical stages (three in the column and one for the still) between the composition in the still and the $x = y$ line. See Fig. 5.2*a*. Then, other lines are drawn parallel to this component balance (see Chap. 2) line, and four theoretical stages are stepped off (Figs. 5.2*b* to *e*). This process is continued until the residual benzene concentration reaches the desired value.

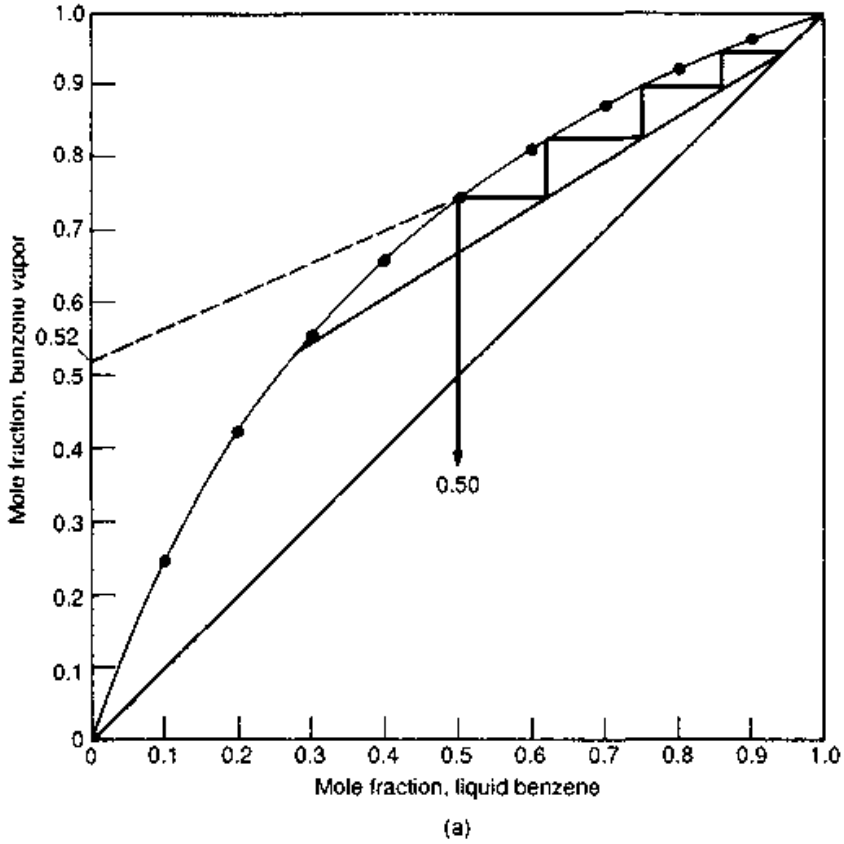

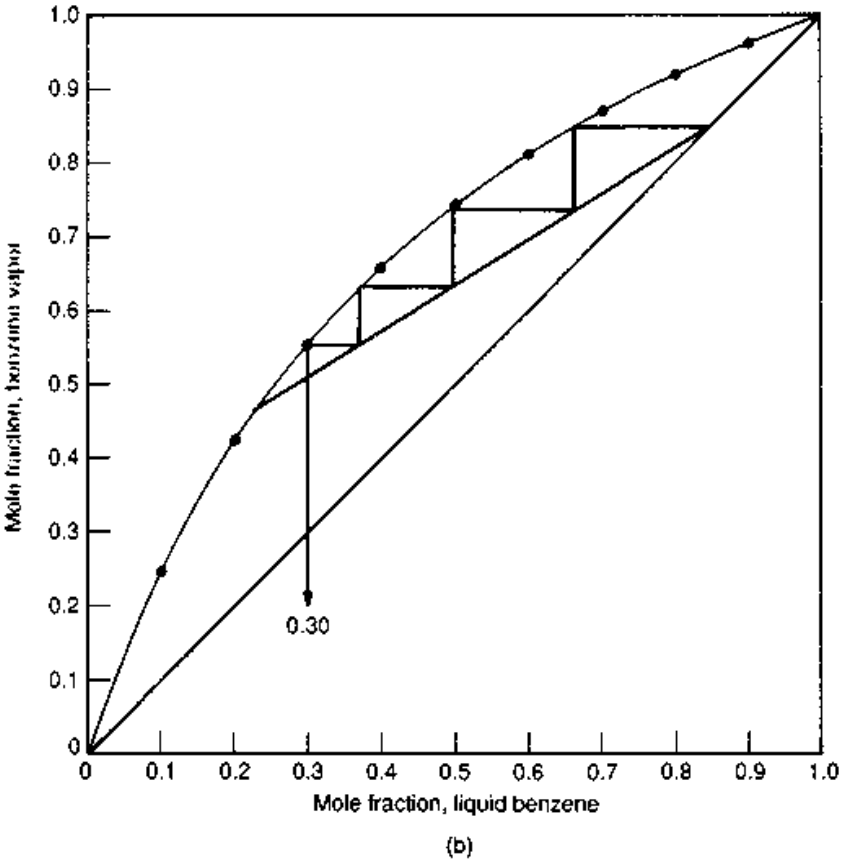

Figure 5.2 Batch distillation of benzene-toluene at constant reflux ratio, Example 5.3. (*a–e*) McCabe-Thiele diagram for progressively reducing still concentration to 0.13 mole fraction benzene.

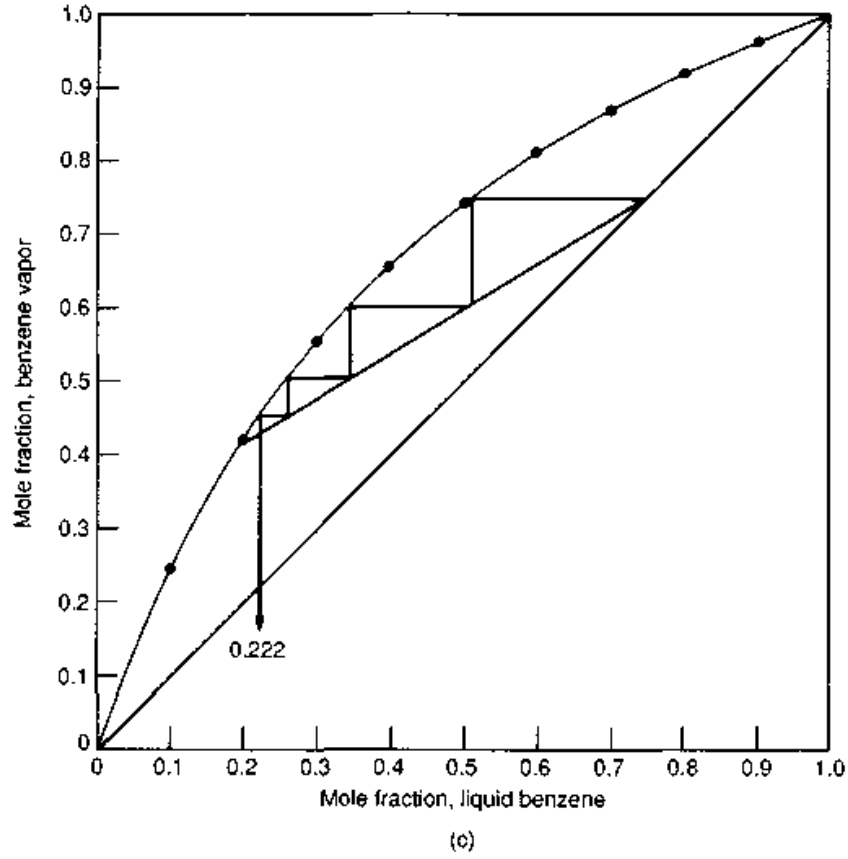

(c)

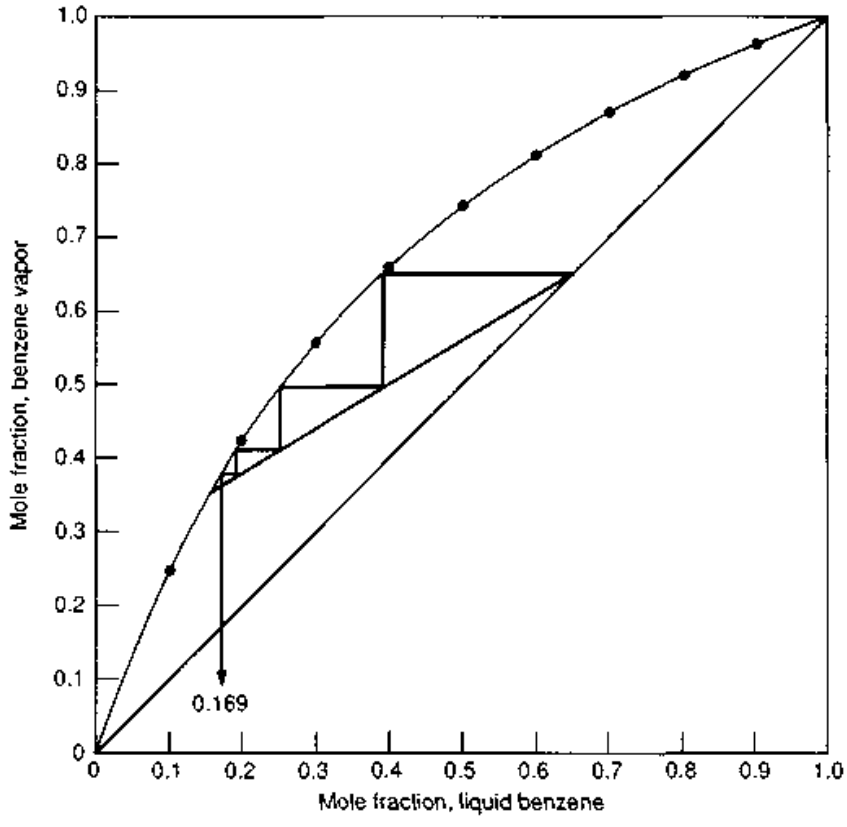

(d)

Figure 5.2 (*Continued*) Batch distillation of benzene-toluene at constant reflux ratio, Example 5.3. (*a–e*) McCabe-Thiele diagram for progressively reducing still concentration to 0.13 mole fraction benzene.

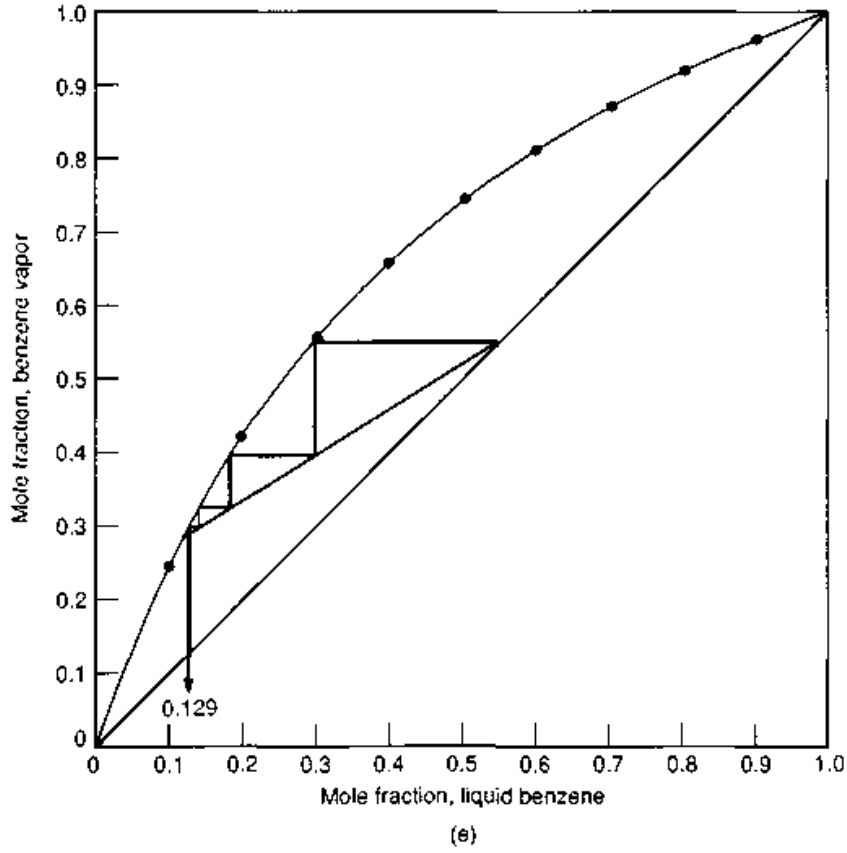

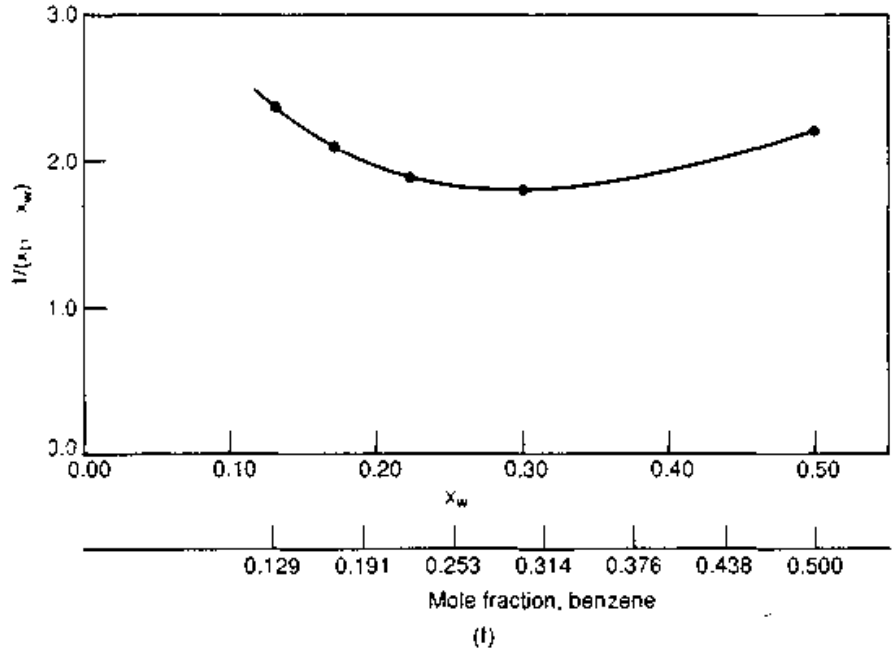

Figure 5.2 (*Continued*) Batch distillation of benzene-toluene at constant reflux ratio, Example 5.3. (*a–e*) McCabe-Thiele diagram for progressively reducing still concentration to 0.13 mole fraction benzene. (*f*) $1/(x_D - x_W)$ vs. x_W plot.

NOTE: The x_W values are divided into segments of equal size for application of Simpson's rule.

Values from Figs. 5.2*a* to *e* are plotted in Fig. 5.2*f* as follows:

x_D	x_w	$x_D - x_w$	$\frac{1}{x_D - x_w}$
0.950	0.500	0.450	2.22
0.850	0.300	0.550	1.82
0.750	0.222	0.528	1.89
0.650	0.169	0.481	2.08
0.550	0.129	0.421	2.38

Reading values from Fig. 5.2*f* for numerical integration

x_w	$\frac{1}{x_D - x_w}$
0.129	2.38
0.191	2.00
0.253	1.85
0.314	1.83
0.376	1.90
0.438	2.04
0.500	2.22

By Simpson's rule,

$$\text{Area} = \frac{0.0618}{3}[2.38 + 4(2.00 + 1.83 + 2.04) + 2(1.85 + 2.04) + 2.22]$$

$$= 0.739$$

$$\ln \frac{W_f}{W_0} = -0.739 \qquad W_f = 100\,(0.478) \qquad = 47.8$$

Material Balance

	Still		
	Start	End	Receiver
Benzene	50	6.2	43.8
Toluene	50	41.6	8.4
	100	47.8	52.2
Mole fraction benzene	0.50	0.13	0.84

So, by returning reflux to the column at a constant rate, the mole fraction of benzene was increased to 0.84 in the receiver and decreased to 0.13 in the still pot. (Remember, the simple still only concentrated the product to 0.58 mole fraction while reducing still concentration to 0.10 mole fraction.)

Other useful information can be developed by further consideration of Fig. 5.2*a* through *e*.

1. Because the column has only a rectifying section, the concentration of the light component in the still can never be reduced to zero (except in the trivial extreme of evaporating all the liquid). Note that as overhead composition regularly reduces by increments of 0.100 mole fraction, the residual still composition changes by decreasing increments.
2. Once the initial overhead composition has been determined in the trial-and-error process, both minimum and actual reflux ratios can be determined from the relationship.

$$y_{\text{int}} = \frac{x_D}{R + 1} \tag{5.20}$$

where y_{int} = value of y at $x = 0$

Minimum reflux ratio is obtained by extending a line connecting overhead composition with that of the vapor composition that is in equilibrium with the feed (in this case, $y = 0.744$). From the dashed line in Fig. 5.2*a*

$$y_{\text{int}} = 0.52 \qquad \text{so } R_{\text{min}} = 0.83$$

Also from Fig. 5.2*a*, the value of y_{int} corresponding to the use of four theoretical separation stages is 0.36, so $R_{\text{act}} = 1.64$. Therefore, for this particular separation,

$$R_{\text{act}} = 2.0R_{\text{min}}$$

In the event that some specific distillate composition is desired rather than the reduction of residual composition to some low acceptable value), the procedure outlined above is followed, but trial-and-error is required to determine when the distillation must be stopped. The result of stopping the distillation process shown in Example 5.3 before the benzene concentration in the still reached 13 mole percent, for example, would be a distillate with a benzene concentration greater than 84 mole percent. Continuing the distillation further than shown in the example would produce a more dilute distillate ("overhead") concentration.

5.1.3 Varying reflux ratio

By continuously varying the reflux ratio during the course of the distillation, an essentially constant overhead concentration can be obtained. The boil-up rate is constant in this case, too, but as reflux ratio increases, the amount of liquid returned to the column increases.

Therefore, the L/V ratio increases as the distillation proceeds.

The varying-reflux-ratio case is analyzed mathematically in exactly the same manner as was the constant-reflux case.

Example 5.4 A mixture containing equal molar quantities of benzene and toluene is to be distilled under conditions of varying reflux ratio to maintain a constant overhead composition of 95 mole percent, using the column specified in Example 5.3.

Calculate the material balance for this case if the final reflux ratio is 13:1.

solution Beginning with an overhead concentration of 95 mole percent, a reflux ratio is selected such that the four theoretical separation stages will produce a bottoms composition which essentially conforms to that of the feed. Then, different reflux ratios are selected, and four theoretical stages are stepped off, with the corresponding still compositions noted. See Figs. 5.3*a* to *e*.

This process can be simplified by recalling the previously discussed relationship:

$$y_{\text{int}} = \frac{x_D}{R + 1}$$

Inserting various reflux ratios into this relationship produces values of y_{int} which simplify plotting of the corresponding component balance lines.

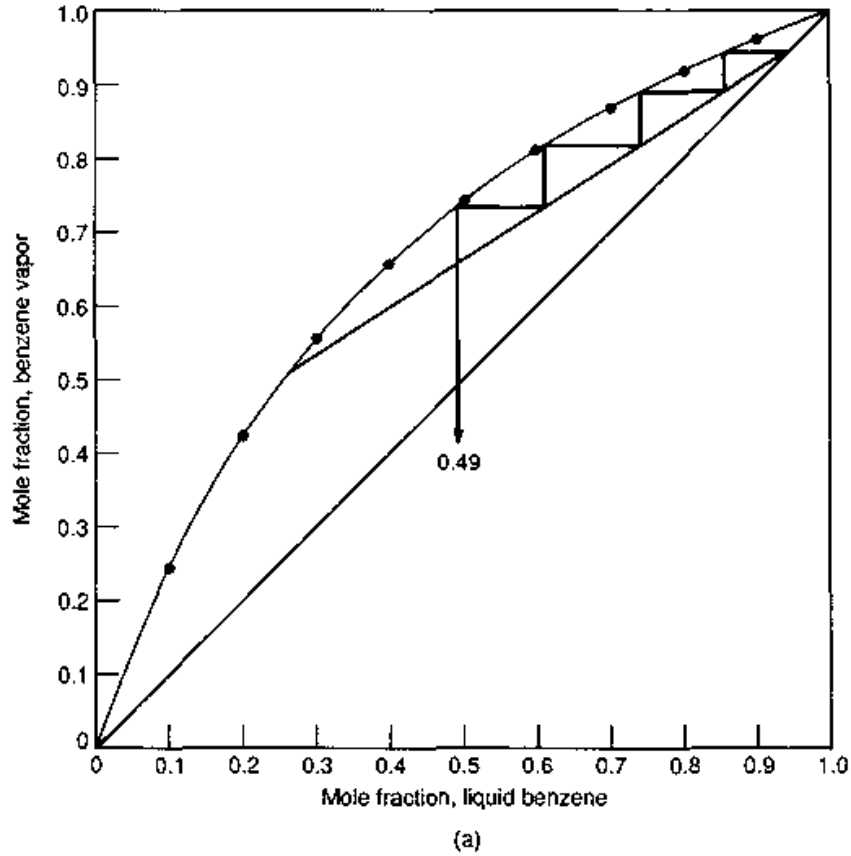

Figure 5.3 Batch distillation of benzene-toluene with variable reflux ratio, Example 5.4. (*a–e*) McCabe-Thiele diagram for progressively increasing reflux ratio to 13:1.

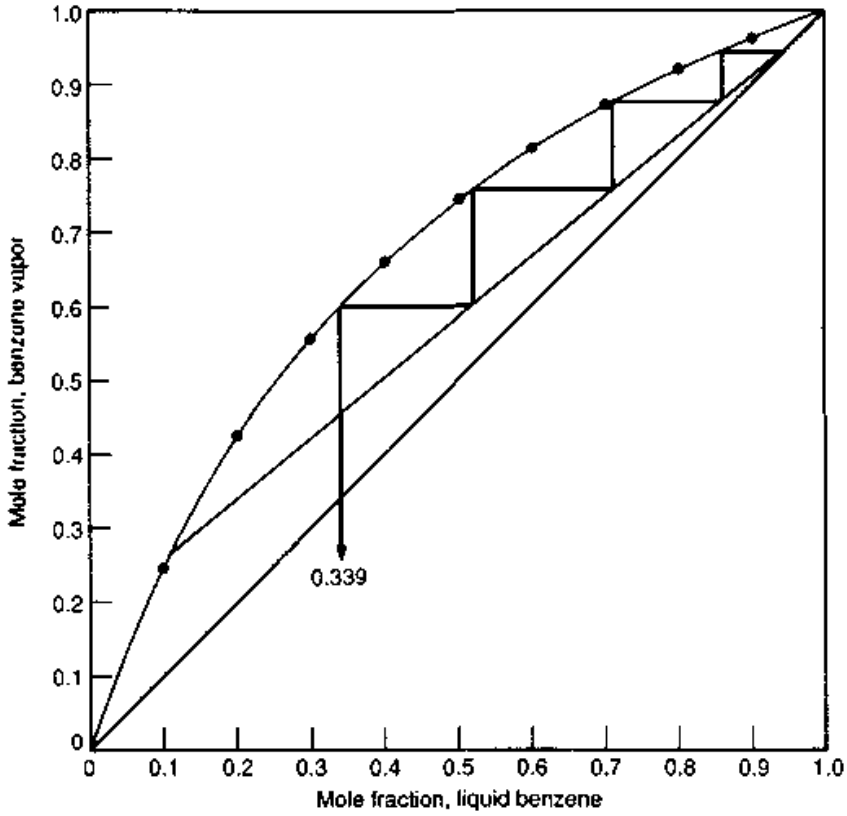

(b)

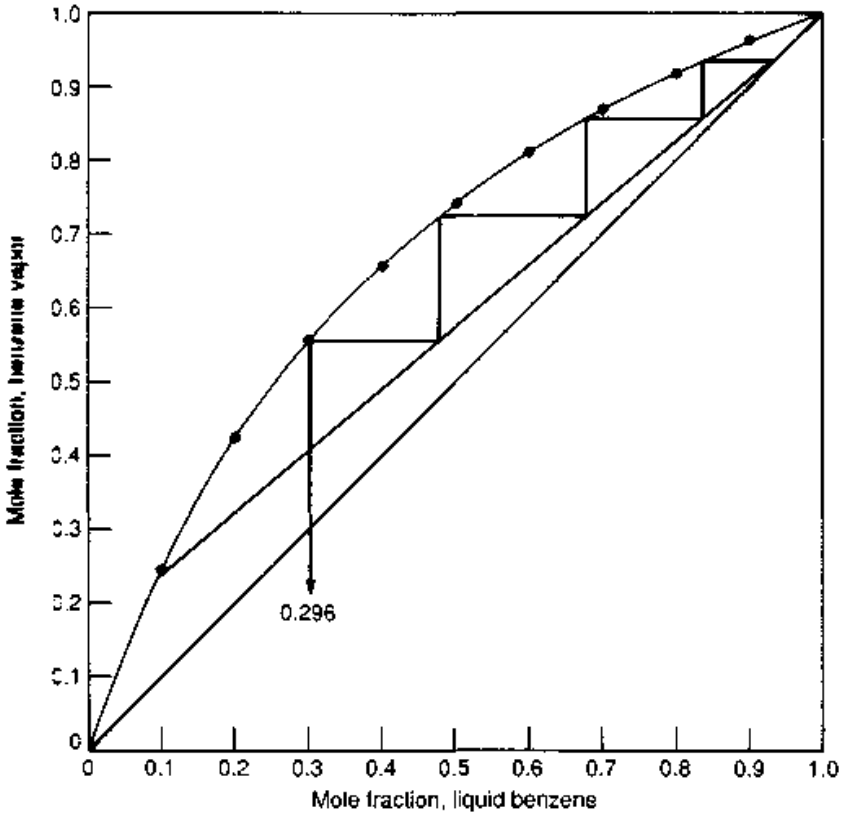

(c)

Figure 5.3 (*Continued*) Batch distillation of benzene-toluene with variable reflux ratio, Example 5.4. (*a–e*) McCabe-Thiele diagram for progressively increasing reflux ratio to 13:1.

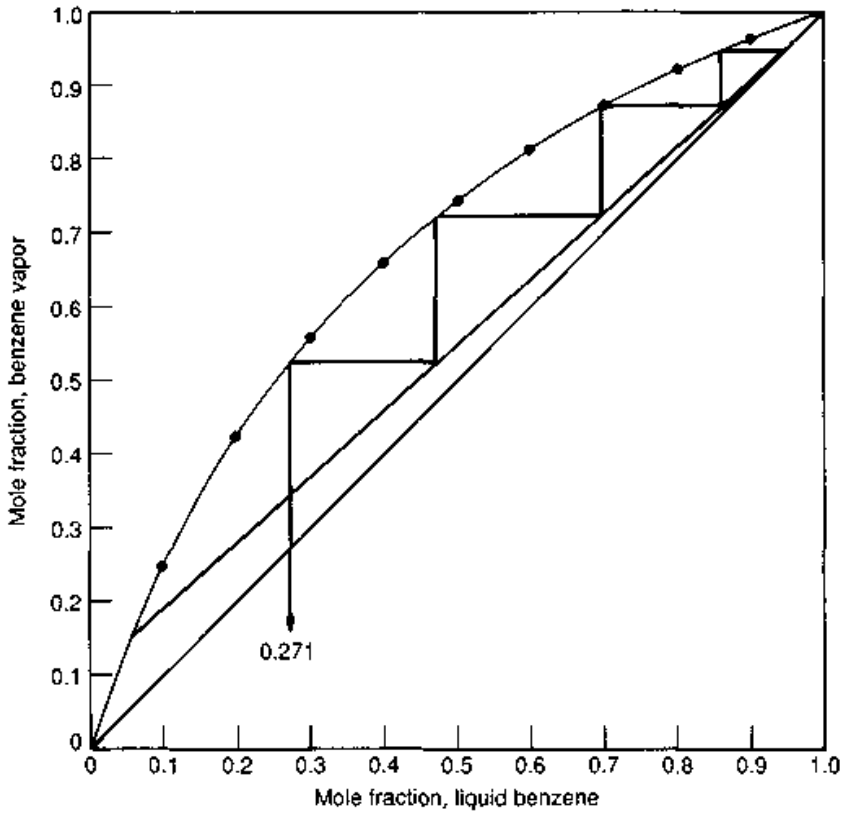

(d)

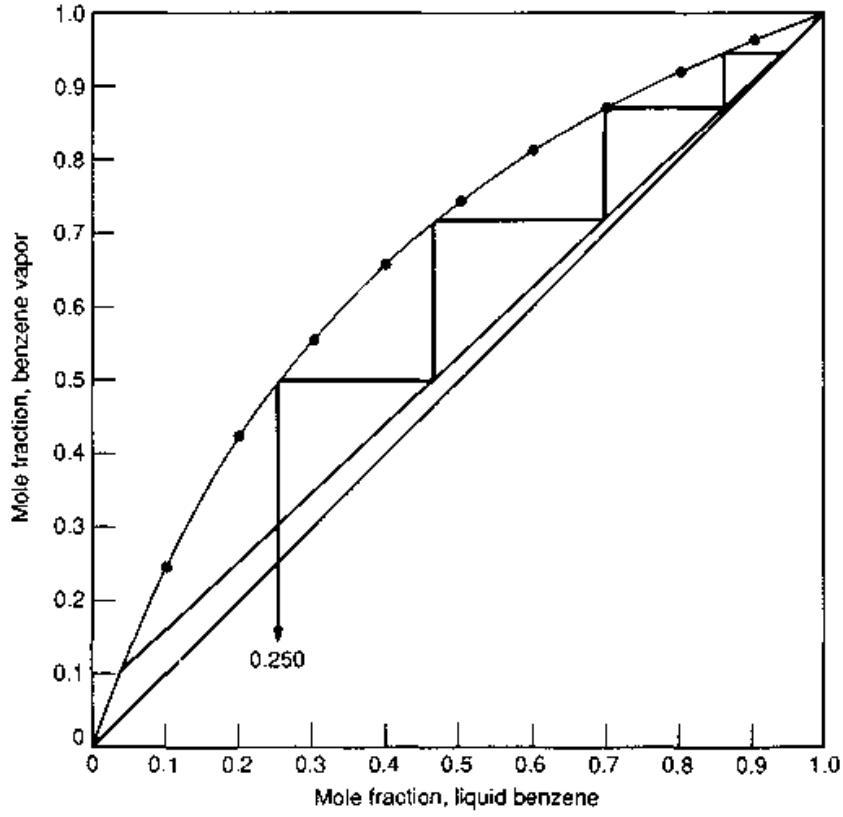

(e)

Figure 5.3 (*Continued*) Batch distillation of benzene-toluene with variable reflux ratio, Example 5.4. (*a–e*) McCabe-Thiele diagram for progressively increasing reflux ratio to 13:1.

The values of the still composition from Figs. 5.3*a* to *e* are plotted in Fig. 5.3*f* as follows:

R	x_W	$x_D - x_W$	$\frac{1}{x_D - x_W}$
1.59	0.490	0.460	2.17
3.59	0.339	0.611	1.64
4.86	0.296	0.654	1.53
7.48	0.271	0.679	1.47
10.00	0.250	0.700	1.43

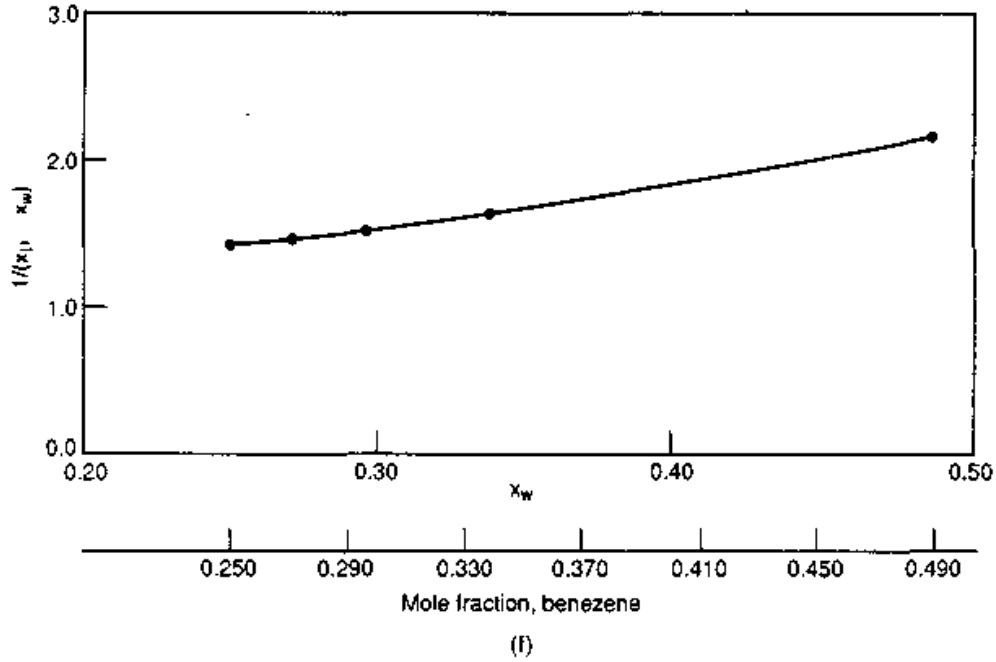

(f)

Figure 5.3 *(Continued)* Batch distillation of benzene-toluene with variable reflux ratio, Example 5.4. (*f*) $1/(x_D - x_W)$ vs. x_W plot.

Reading values from Fig. 5.3*f* for numerical integration

x_W	$\frac{1}{x_D - x_W}$
0.250	1.43
0.290	1.50
0.330	1.62
0.370	1.75
0.410	1.88
0.450	2.02
0.490	2.17

$$\text{Area} = \frac{0.04}{3}[1.43 + 4(1.50 + 1.75 + 2.02) + 2(1.62 + 1.88) + 2.17]$$

$$= 0.422$$

$$\ln \frac{W_f}{W_0} = -0.422$$

$$W_f = 100\,(0.656)$$

$$= 65.6$$

So, by adopting a varying reflux ratio, the mole fraction of the benzene in the receiver was maintained constant at 0.95, higher than in either of the two cases already considered. However, the mole fraction of the benzene remaining in the still was also higher than in either of the two previous cases.

Material Balance

	Still		
	Start	End	Receiver
Benzene	50	17.3	32.7
Toluene	50	48.3	1.7
	100	65.6	34.4
Mole fraction benzene	0.50	0.26	0.95

Because the overhead composition is constant, the integral of

$$\int \frac{dx_W}{(x_D - x_W)}$$

can be obtained analytically.

Integration of

$$\int \frac{dx}{a + bx}$$

produces $1/b \ln (a + bx)$.

Using the values from above

$$\int \frac{dx}{(x_D - x_W)} = -1 \ln (0.950 - x_W)\Big|_{x_{W_0}}^{x_{W_f}}$$

$$= -[\ln (0.950 - 0.250) - \ln (0.950 - 0.490)]$$

$$= -\ln \frac{(0.950 - 0.250)}{(0.950 - 0.490)}$$

$$\ln \frac{W_f}{W_0} = \ln \frac{0.950 - 0.490}{0.950 - 0.250}$$

$$\frac{W_f}{100} = \frac{0.46}{0.70}$$

$$W_f = 65.7$$

which gives the same result as obtained by graphical integration.

Note in Figs. 5.3*a* to *e* (deliberately stopped at a reflux ratio of 13:1 for clarity of illustration) that increases in reflux ratio produce an ever-diminishing increment in reduction of the concentration of the light component in the still. Increasing reflux ratio to 20:1, for example, would only decrease the residual mole fraction of the benzene to 0.23 (from 0.25 for 13:1).

5.1.4 Time and boil-up requirements

Constant reflux ratio. With a constant reflux ratio and a constant vapor rate in the distillation system, the moles of vapor that must be produced during the distillation can be simply calculated from Eq. (5.4). In Example 5.3, it was calculated that 52.2 moles of distillate were produced when a reflux ratio of 1.64 was used.

Therefore

$$V = D(R + 1)$$

$$= 52.2 \text{ moles } (1.64 + 1)$$

$$= 138 \text{ moles of vapor}$$

Because the boil-up rate associated with a specific distillation system should be known from past experience with the system, this calculation of total vapor load immediately produces a time required for the new separation.

Conversely, in the design of a new system, the time available for the distillation can be divided into the vapor load to determine the boil-up rate required.

Varying reflux ratio. The amount of material which must be vaporized to achieve some specified separation under conditions of varying reflux ratio may be developed from Eq. (5.3).

$$V = L + D$$

Differentiating

$$dV = dL + dD$$

Multiplying dL by dV/dV

$$dV = \frac{dL}{dV}dV + dD \tag{5.21}$$

Substituting from Eq. (5.5)

$$dV = \frac{R}{R+1}dV + dD$$

(where R is variable).

Rearranging

$$dV\left(1 - \frac{R}{R+1}\right) = dD$$

$$dV = dD/[1 - R/(R+1)]$$

Integrating

$$\int_0^V dV = \int_0^D \frac{dD}{1 - R/(R+1)} \tag{5.22}$$

From Eqs. (5.1) and (5.2)

$$F = D + B \qquad \text{and} \qquad Fx_F = Dx_D + Bx_F$$

but in batch distillation

$$F = W_0$$

$$B = W$$

$$D = W_0 - W$$

Multiplying the third of these by x_D

$$Dx_D = W_0x_D - Wx_D$$

and

$$Dx_D = W_0x_0 - Wx_W$$

Setting equals to Dx_D equal to each other.

$$W_0x_0 - Wx_W = W_0x_D - Wx_D$$

$$W_0(x_0 - x_D) = W(x_W - x_D)$$

or

$$W = \frac{W_0(x_0 - x_D)}{x_W - x_D} \tag{5.23}$$

Differentiating (remembering that W_0, x_0, and x_D are all constant when reflux ratio varies) and rearranging,

$$dW = -\frac{W_0(x_D - x_0)}{(x_D - x_W)^2}\,dx_W$$

As in simple distillation $dD = -dW$. Therefore, inserting Eq. (5.22)

$$\int_0^V dV = \int_{x_0}^{x_W} \frac{W_0(x_D - x_0)\,dx_W}{[1 - R/(R + 1)](x_D - x_W)^2}$$

$$V = W_0(x_D - x_0)\int_{x_0}^{x_W} \frac{dx_W}{[1 - R/(R + 1)](x_D - x_W)^2} \tag{5.24}$$

And again the right-hand side must be evaluated by graphical integration.

Example 5.5 Using the values generated in the solution of Example 5.4, calculate the moles of vapor produced during the separation.

R	$R + 1$	$\frac{R}{R+1}$	$1 - R/(R + 1)$
1.79	2.79	0.642	0.358
4.46	5.46	0.817	0.183
5.13	6.13	0.837	0.163
7.96	8.96	0.888	0.112
13.0	14.0	0.929	0.0714

x_W	$(x_D - x_W)^2$	$\left(1 - \frac{R}{R+1}\right)(x_D - x_W)^2$	$\frac{1}{\left(1 - \frac{R}{R+1}\right)(x_D - x_W)^2}$
0.490	0.212	0.0759	12.2
0.339	0.373	0.0683	12.3
0.296	0.428	0.0698	13.7
0.271	0.461	0.0516	18.4
0.250	0.490	0.0350	22.4

These values of $1/[1 - R/(R + 1)](x_D - x_W)^2$ are plotted versus x_W in Fig. 5.4.

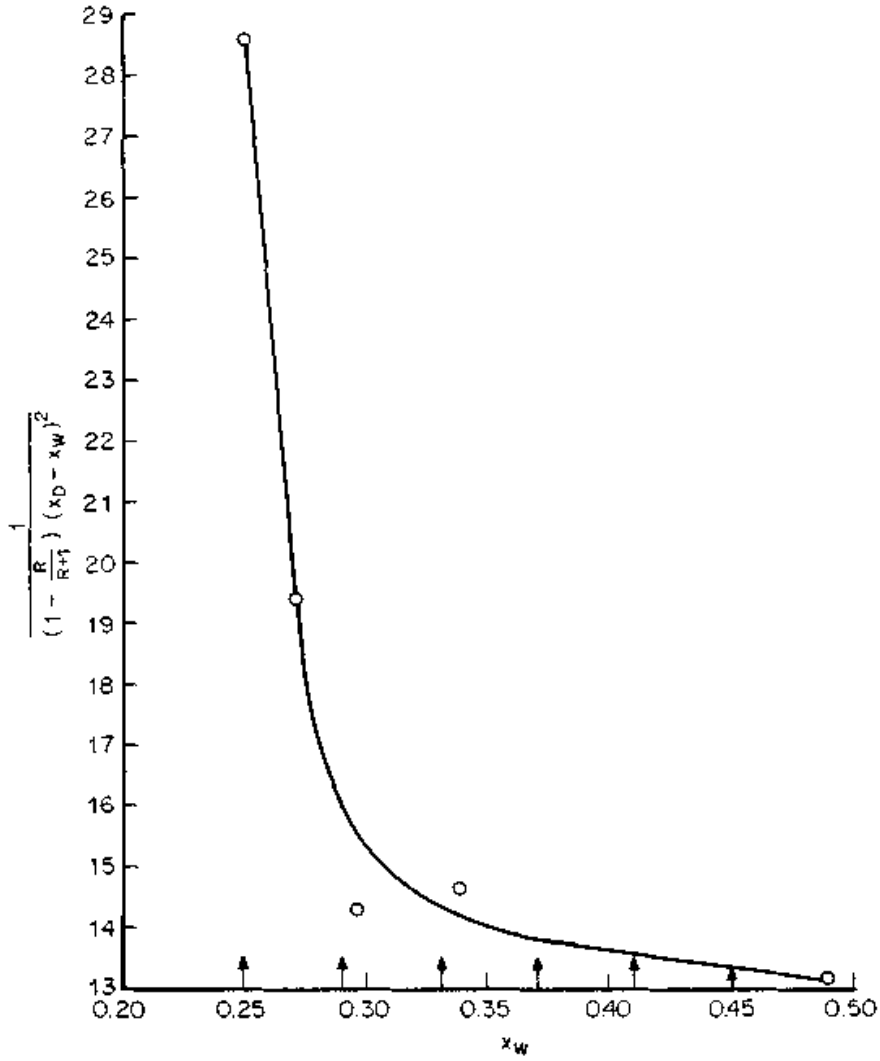

Figure 5.4 Batch distillation of benzene-toluene at variable reflux, calculation of the moles of vapor produced.

Note: In Fig. 5.4, the x_W values are divided into segments of equal size for application of Simpson's rule.

Reading values from Fig. 5.4 for numerical integration

x_W	$\dfrac{1}{\left(1 - \dfrac{R}{R+1}\right)(x_D - x_W)^2}$
0.250	28.6
0.290	16.0
0.330	14.3
0.370	13.8
0.410	13.6
0.450	13.4
0.490	13.2

Applying Simpson's rule

$$\text{Area} = \frac{0.04}{3}[28.6 + 4(16.0 + 13.8 + 13.4) + 2(14.3 + 13.6) + 13.2]$$

$$= 3.61$$

$$V = W_0(x_D - x_0)(\text{Area})$$

$$= 100\,(0.95 - 0.50)(3.61)$$

$$= 162 \text{ moles vapor}$$

As noted under the discussion of the constant reflux ratio case, the boil-up rate of an existing distillation system should be well known, so use of that boil-up rate with the vapor quantity just calculated will yield the time required for the separation of the new system. Note that this value of time refers only to the distillation itself: charging time, heat-up time, cooling time and clean-out time are not included.

The results obtained in all of the examples except 5.2 are summarized in Table 5.2. Table 5.2 also contains the results of other calculations, the percentage of the benzene originally in the still which was recovered in the overhead and the heat required to obtain the separation.

Even a brief review of Table 5.2 suggests a number of conclusions:

1. Simple distillation
   a. Gives highest percentage recovery of benzene in the product,

TABLE 5.2 Comparing Results for Simple Distillation, Constant Reflux Ratio, and Varying Reflux Ratio Batch Distillation, Examples 5.1, 5.3, 5.4

	Still residue		Receiver		Benzene recovery (receiver), %	Benzene recovery, lb	Vapor required, moles	Heat required, Btu
	Moles	Mol. frac.	Moles	Mol. frac.				
Simple distillation								
Benzene	1.67	0.10	48.3	0.58	96.6	3770	83.3	1.14×10^6
Toluene	15.0	0.90	35.0	0.42				
Constant reflux ratio								
Benzene	6.2	0.13	43.8	0.84	87.6	3420	131	1.75×10^6
Toluene	41.6	0.87	8.4	0.16				
Varying reflux ratio								
Benzene	17.3	0.26	32.7	0.95	65.4	2550	162	2.15×10^6
Toluene	48.3	0.74	1.7	0.05				

b. But the concentration of benzene obtained is only 58 mole percent, and
c. The concentration of benzene in the still only drops to 10 mole percent (not a very pure toluene).

2. Constant reflux ratio
   a. Requires about 50 percent more heat input than simple distillation to achieve approximately the same distribution of benzene, but
   b. The benzene concentration in the product is much better than that obtained by simple distillation (84 percent vs 58 mole percent).
3. Varying reflux ratio
   a. Permits specification of the purity of the overhead product, but
   b. Requires the most heat input of the three methods, and
   c. Leaves the highest benzene concentration in the still.

Although these last two points seem significant, the heat requirements for the separation actually achieved in the variable reflux ratio case is only about 20 percent greater than the heat requirement of the constant reflux case. The benzene concentration in the still residue can be reduced by decreasing reflux ratio to some intermediate point (say 2:1 or 3:1) and continuing the distillation until the residual concentration is reduced to some acceptable value. Of course, the concentration of the benzene recovered in the overhead would be less than 95 mole percent, but this material would not be combined with the product. Instead, this so-called "slop" cut or "tailings" cut would be collected in a different receiver and be recycled to the still during recharging for the next distillation.

Thus, as so frequently is the case, the chemical engineer must choose between alternatives: should high product recoveries with low energy expenditures and low product concentrations, or modest product recoveries with high energy inputs to achieve high product purities be chosen, or is some intermediate case best? Such questions can only be answered on an *ad hoc* basis.

Several final points remain to be considered. First, all of the discussions above ignored the effect of liquid holdup in the column and condenser, but because the combined volumes of these two are quite small as compared to the volumes in the still and receiver (particularly because so many batch stills include packed sections rather than trays), this assumption does not seem unwarranted, particularly for binary mixtures.

When column holdup is significant, and especially when multicomponent mixtures must be considered, the analysis of the effect of holdup is extremely complex. This problem has been addressed by a number of investigators (11,14, 16, 17), however, and it has been concluded the column holdups on the order of 10 to 15 percent actually are beneficial in obtaining better separation. The interested reader should consult the references cited.

Second, analysis of the effect of holdup is so complex that large computers are invariably involved in the process (7, 12, 13). Perhaps the most versatile program is the one developed by Boston et al. (5). The basic problem involved in the computer analysis is that the differential equations describing holdup in the column have small time constants, while the variation in the still content varies over a period of hours. Thus, the combination of equations is "stiff," i.e., difficult to integrate numerically. Because the equations are stiff, small time increments must be used, and the software must contain built-in stability controls. Therefore, in the simulation of batch distillation, "...computer time hundreds of times longer than the time for steady state distillations are obtained and design costs are inappropriate to the size of the equipment being designed" (19).

Third, the examples developed above were presented on the basis of a small number of theoretical stages, primarily for clarity of the figures illustrating the calculation methods, and no mention was made of the effect of some other number of theoretical stages. However, it should be obvious that more stages will give sharper separations—just as one would expect in a continuous still.

Last, the point was made early on that the separation could be calculated on the basis of a light "key," but all of the examples were based on a binary mixture. Simple distillation of a multicomponent mixture is analyzed on the basis of the light key as follows.

By material balance, the moles of liquid leaving the still at any time are equal to the moles of liquid entering the receiver (6).

For component A (using the symbol l for liquid)

$$-dl_A = y_A\,dV \tag{5.25}$$

For component B

$$-dl_B = y_B\,dV \tag{5.26}$$

Dividing 5.26 into 5.23

$$\frac{dl_A}{dl_B} = \frac{y_A}{y_B} \tag{5.27}$$

Recalling the definition of relative volatility, Eq. (5.6)

$$\alpha = \frac{y_A(1 - x_A)}{x_A(1 - y_A)}$$

Substituting $1 - x_B$ and $1 - y_B$ for x_A and y_A

$$\alpha = \frac{y_A[1 - (1 - x_B)]}{x_A[1 - (1 - y_B)]}$$

$$= \frac{y_A x_B}{x_A y_B} \tag{5.28}$$

Rearranging

$$\alpha \frac{x_A}{x_B} = \frac{y_A}{y_B} \tag{5.29}$$

But, at any particular time during the distillation

$$l_A = x_A W$$

$$l_B = x_B W$$

or

$$\frac{l_A}{l_B} = \frac{x_A}{x_B} \tag{5.30}$$

Substituting Eq. (5.29) into (5.27)

$$\frac{dl_A}{dl_B} = \alpha \frac{l_A}{l_B}$$

Rearranging and integrating (assuming relative relativity is constant)

$$\ln \frac{l_{A_f}}{l_{A_0}} = \alpha \ln \frac{l_{B_f}}{l_{B_0}} \tag{5.31}$$

And, of course, a similar relationship can be developed for components A and C.

Example 5.5 A quantity of 100 moles of a mixture containing 50 mole percent benzene, 25 mole percent toluene, and 25 mole percent *p*-xylene is to be simply distilled until the residual benzene content in the still is reduced to 1.73 moles. Calculate the material balance for the separation.

From Eq. (5.31) with $\alpha = 2.90$ for the benzene-toluene system and $\alpha = 6.94$ for the benzene–*p*-xylene system,

$$\ln \frac{1.73}{50} = 2.90 \ln \frac{l_{B_f}}{25}$$

$$\ln \frac{l_{B_f}}{25} = -1.16$$

$$l_{B_f} = 25(0.313)$$

$$= 7.84$$

$$\ln \frac{1.73}{50} = 6.94 \ln \frac{l_{C_f}}{25}$$

$$\ln \frac{l_{C_f}}{25} = -0.485$$

$$l_{C_f} = 25(0.616)$$

$$= 15.4$$

Comparing this result with the results of Example 5.1 shows the effect of adding a higher boiling material to the still (while holding benzene distribution constant). The high boiler permits the benzene concentration to be reduced below that achieved with the binary mixture. The benzene concentration in the product receiver is also increased, but the product is now a ternary mixture instead of a binary.

Material Balance

	Still		
	Start	End	Receiver
Benzene	50.0	1.7	48.3
Toluene	25.0	7.8	17.2
p-Xylene	25.0	15.4	9.6
	100	24.9	75.1
Mole fraction benzene		0.0683	0.643

The ternary mixture can be separated into three relatively pure fractions by the use of varying reflux to obtain high overhead concentrations, with intermediate slop cuts being taken during the transition between components.

5.2 New Design—A Case History

Most of the concepts discussed to this point are also used in the design of new distillation systems. The material that follows is based on the design of such a system that operated successfully over the life of the plant in which it was situated.

The XYZ Chemical Company is designing a plant to produce 3,300,000 lb per year of a new product called "R." R is to be purified by separating it from light and heavy impurities by vacuum distillation in a batch still. Because the new plant is expected to be able to operate 330 days per year, the distillation system must be able to separate 10,000 lb per day of R from its impurities. As received from the upstream processing facilities, crude R contains impurities C, P, and W.

The XYZ research department has thoroughly investigated the manufacture of R, and the final report on their investigation presents the following information on R, C, P, and W.

The molecular weights, freezing points, and normal boiling points of pure R, C, P, and W have been determined, as have the constants for vapor pressure (VP), expressed as

$$\ln \text{VP} = A - B/T$$

where VP is in mmHg, and T is in kelvin. This information is summarized below.

Compound	MW	Freezing point, °C	Normal BP, °C	Vapor pressure constants	
				A	*B*
R	110.1	110.7*	276.5	21.65	−8239
C	110.1	105.0	244.9	20.02	−6936
P	94.1		181.9	21.36	−6631
W	18.0		100.0	21.03	−5341

*For pure R; commercial-grade R freezes at 109.6°C (min).

The density of crude R is 8 lb/gal, and the density of commercial-grade R is 10.6 lb/gal.

R, C, and P are members of a homologous series, so it is reasonable to assume that their mixtures are ideal and, therefore, may be represented by constant relative volatilities. W is not a member of the homologous series, but its vapor pressure is so high compared to the other compounds that it will have been totally distilled off before the real separation process begins.

Unfortunately, C is only produced during the manufacture of R by

some side reaction whose mechanism is not understood, and the amount of C present in any particular still charge cannot be predicted. Therefore, the design will have to be based on the relative volatilities of R and P, and the capabilities of the design for removing C acceptably will have to be checked later. (Fortunately, the quality of R can be easily assessed during the course of the distillation by observing product color and measuring product freezing point. When freezing point has attained a particular minimum value, and the product is essentially colorless, product quality is acceptable.)

Specification-grade R has been obtained from crude R in a number of laboratory distillations. The research chemists have decided that the distillations should be performed at 10 mmHg absolute in order to minimize the thermal degradation of R. The results obtained in the research work have been averaged, and the following values have been obtained.

R	4250
Tailings	75.2
Foreruns	212.5
P	317.8
W	36.1
Loss	108.4
	5000 g

Thus, the problem resolves itself into the following assignment: "Using the data provided by the research department, design and specify a complete distillation system for a plant which must produce 10,000 lb per day of specification-grade R while operating 330 days per year. The design should be based on recovering P, which has a purity high enough to be commercially attractive. C has no known commercial uses at this time."

Because 10,000 lb of R must be produced daily to meet plant capacity requirements, the laboratory distillation results must be scaled up to this basis. Doing so produces the following values:

Products	Quantity, lb	Moles	Mole fraction
R	10,000	90.8	0.829
Tailings	177	1.61	0.015
Foreruns	500	4.54	0.041
P	748	7.95	0.072
W	85	4.72	0.043
		109.6	1.000
Loss	255		
	11,765		

Because the research work has indicated that R should be recovered at an absolute pressure of 10 mmHg, the relative volatility of P to R should be evaluated at this pressure.

	Vapor pressure, mmHg		
Temperature, °C	R	P	$\alpha_{P \to R}$
138.0	5	178.6	34.7
152.1	10	305.4	30.5
168.0	20	536.6	26.8

$$\alpha = (35.7 \times 30.5 \times 26.8)^{1/3} \qquad \alpha = 30.8$$

(As will be discussed later, it is not essential that the separation system be operated at the design pressure throughout the distillation. Therefore, the relative volatility was averaged over three pressures in the vicinity of the design point.) The equilibrium vapor-liquid compositions were calculated using this value for relative volatility:

x	y	x	y
0.000	0.000	0.600	0.979
0.100	0.774	0.700	0.986
0.200	0.885	0.800	0.992
0.300	0.930	0.900	0.996
0.400	0.954	1.00	1.00
0.500	0.969		

These values are plotted in Fig. 5.5*a*.

As discussed in the problem statement, it is possible that the P recovered from the distillation could be sold, thus it is desirable to recover P in a state of reasonably high purity (say, 0.98 mole fraction). Therefore, drawing a line joining 0.98 distillate composition and the vapor composition in equilibrium with the feed in Fig. 5.5*a* produces a y intercept of 0.647. Therefore, minimum reflux ratio is, from Eq. (5.20)

$$R = \frac{x_D}{y_{\text{int}}} - 1 = \frac{0.98}{0.647} - 1 = 0.515$$

Selecting a reasonable actual reflux ratio (say, $1.3 \times R_{\min}$) ≅ 0.7

$$y_{\text{int}} = \frac{0.98}{1.3(0.515) + 1} = 0.587$$

Drawing a line connecting this point with x_D in Fig. 5.5*b* and stepping off theoretical stages shows that only three stages are required.

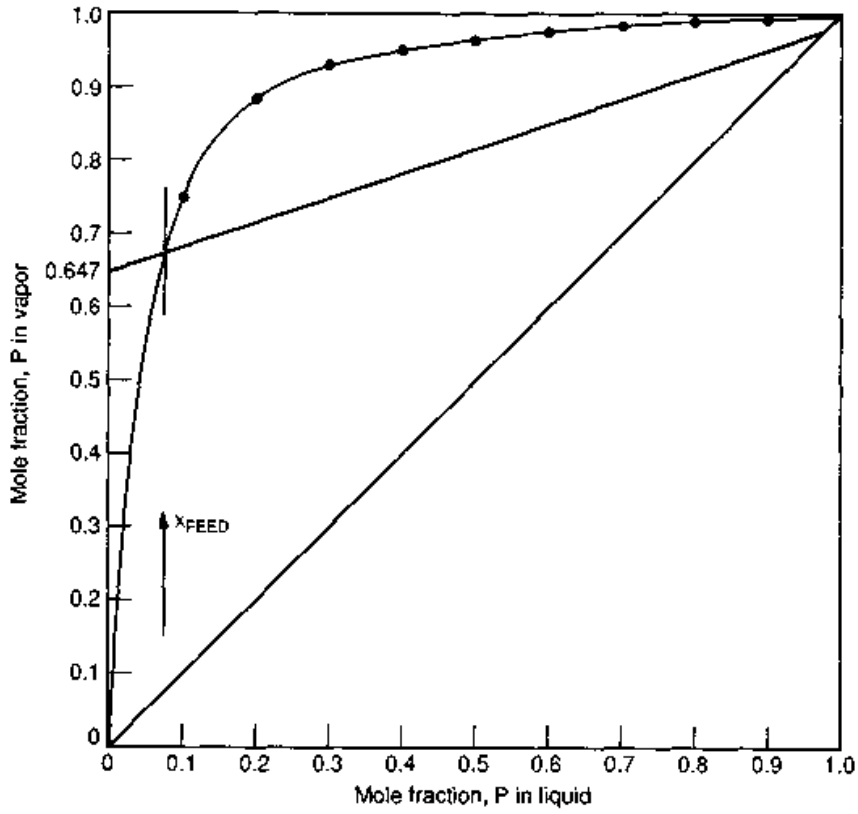

(a)

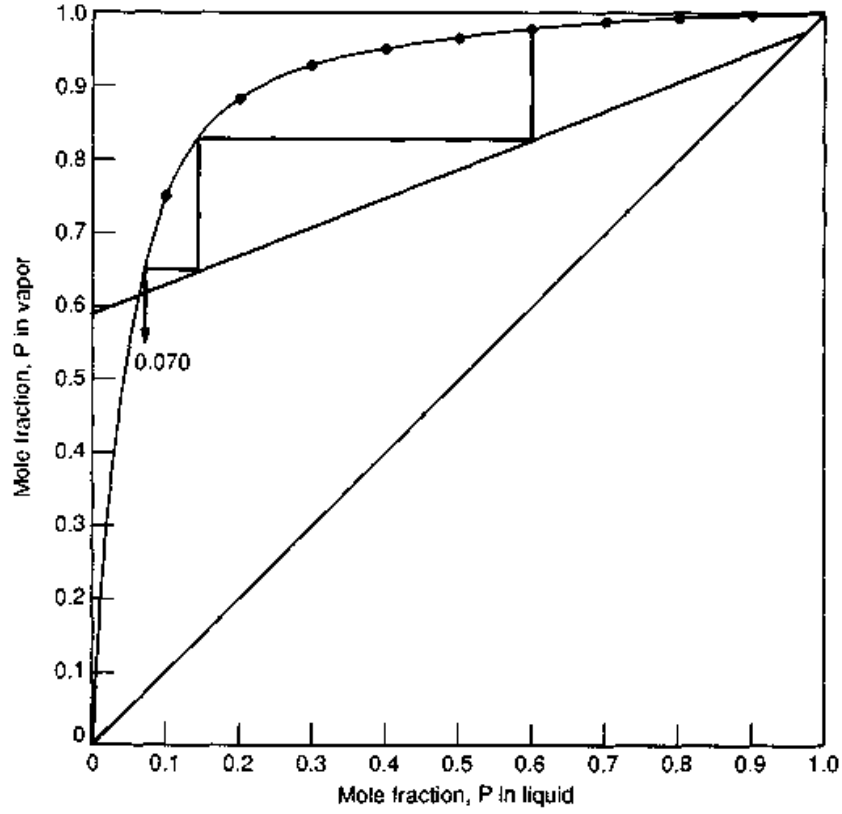

(b)

Figure 5.5 Separation of P from R in case history. (*a–f*) McCabe-Thiele diagram, α = 30.8, for separation at progressively higher reflux ratios.

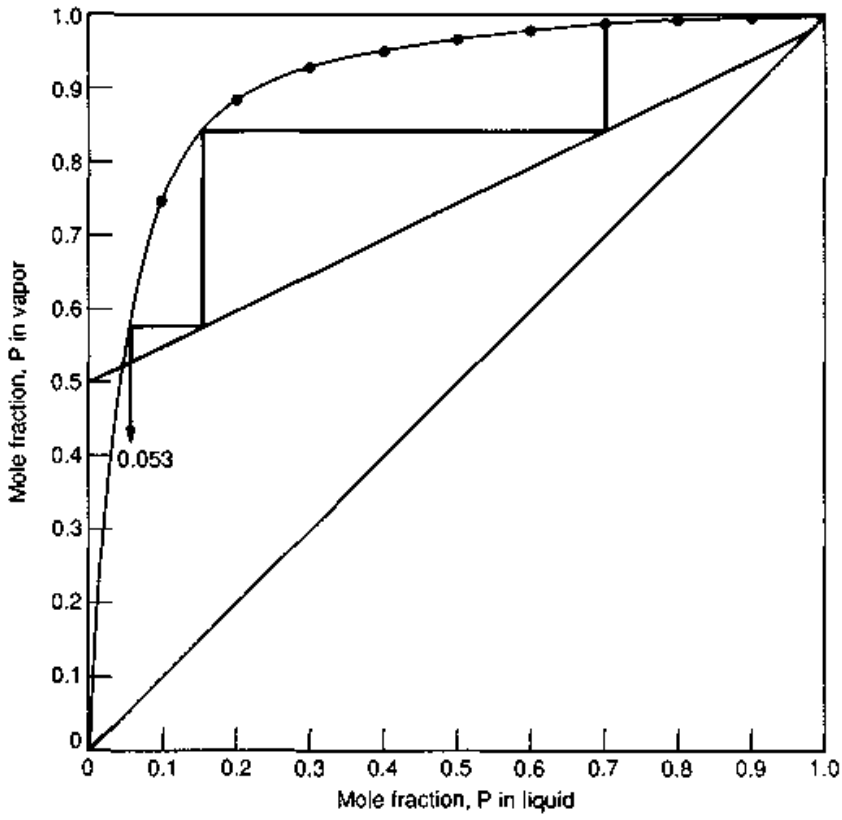

(c)

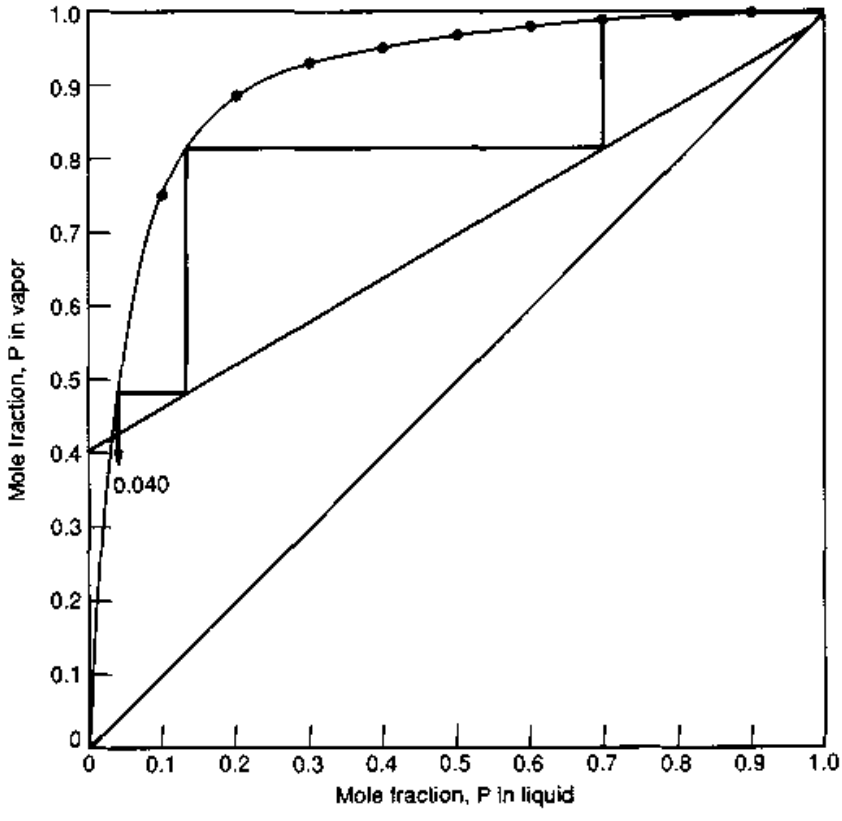

(d)

Figure 5.5 (*Continued*) Separation of P from R in case history. (*a–f*) McCabe-Thiele diagram, $\alpha = 30.8$, for separation at progressively higher reflux ratios.

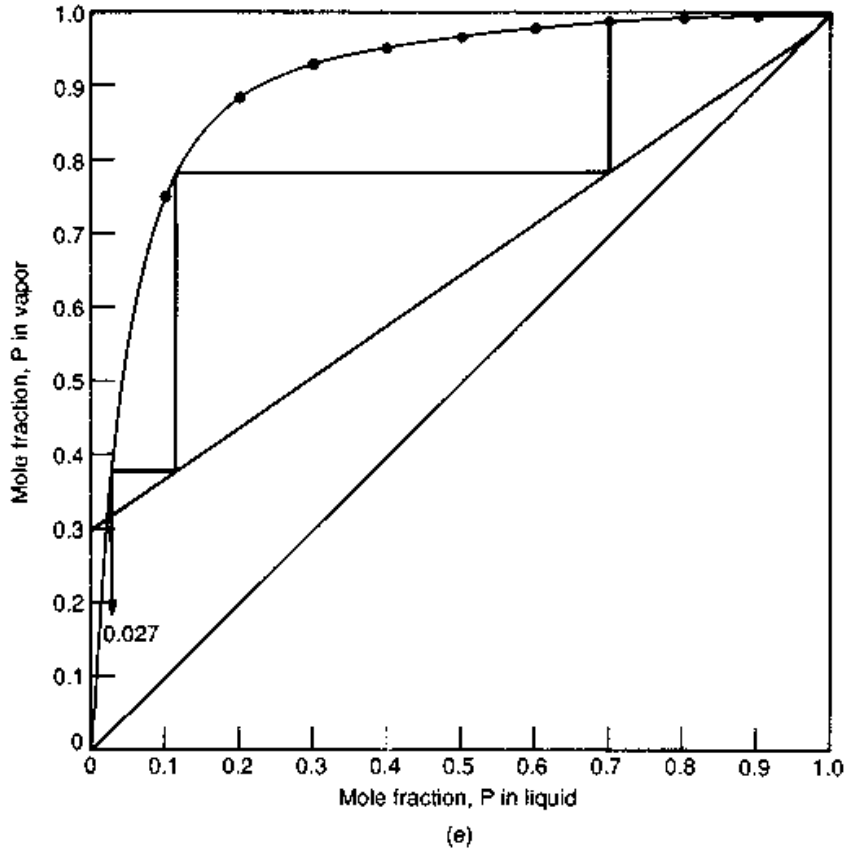

(e)

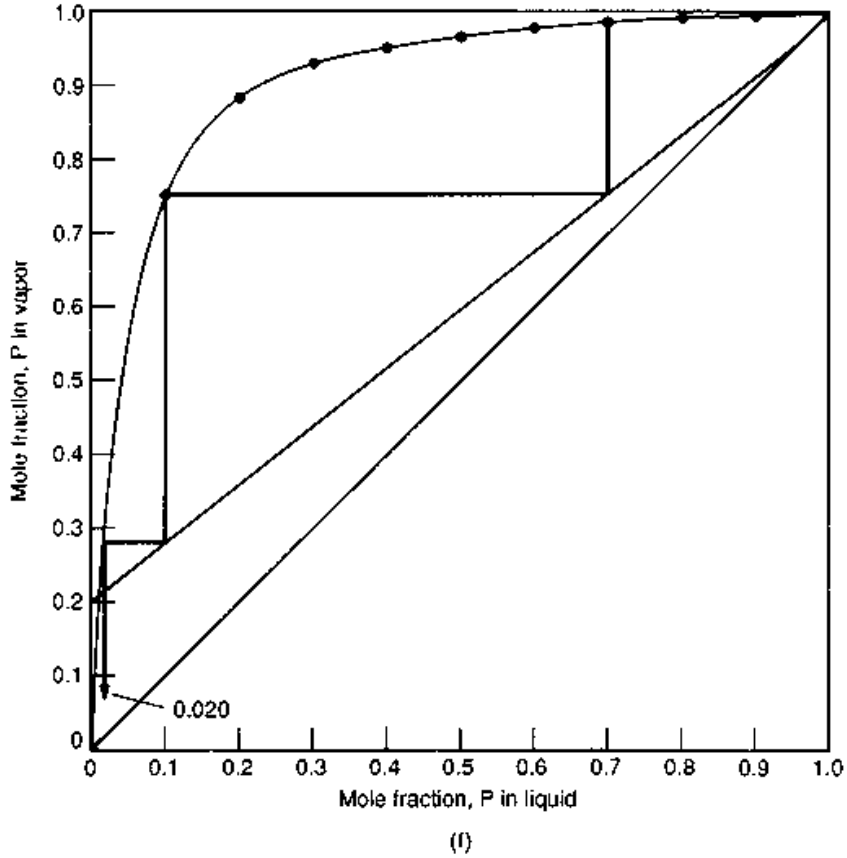

(f)

Figure 5.5 (*Continued*) Separation of P from R in case history. (*a–f*) McCabe-Thiele diagram, $\alpha = 30.8$, for separation at progressively higher reflux ratios.

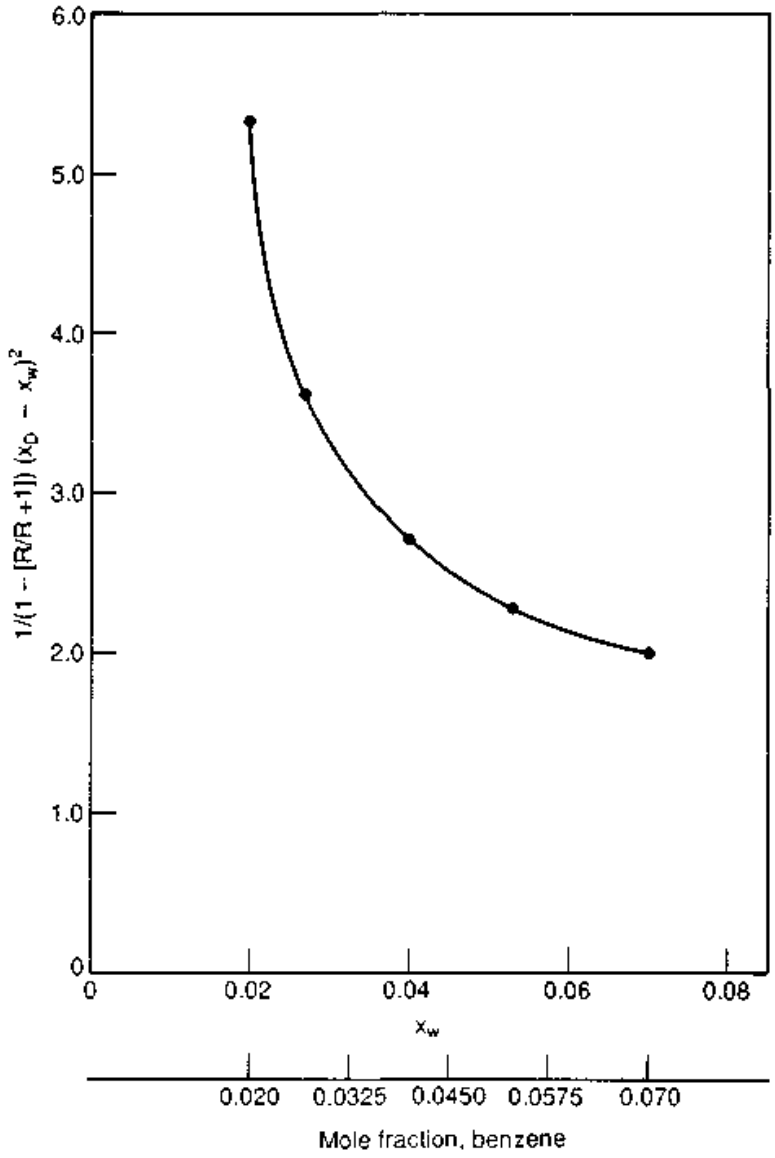

(g)

Figure 5.5 (*Continued*) Separation of P from R in case history. (*g*) Calculation of moles vapor produced.

Drawing lines corresponding to other reflux ratios and stepping off three theoretical stages in Fig. 5.5*c* to *f* produces the following information:

x_W	y_{int}	R
0.070	0.59	0.66
0.053	0.50	0.96
0.040	0.40	1.4
0.027	0.30	2.3
0.020	0.20	3.9

Following Example 5.5,

x_W	$\frac{1}{[1 - R/(R+1)](x_D - x_W)^2}$
0.070	2.01
0.053	2.28
0.040	2.71
0.027	3.63
0.020	5.32

These values are plotted on Fig. 5.5*g*.

Using Simpson's rule:

$$\text{Area} = \frac{0.0125}{3}[2.01 + 4(2.17 + 3.12) + 2(2.50) + 5.32]$$

$$= 0.140$$

$$V = W_0(x_D - x_W)(\text{Area})$$

$$= 109.6\,(0.98 - 0.020)(0.140)$$

$$= 15 \text{ moles vapor}$$

Having determined that three theoretical stages are required for the separation of P from R, attention can be redirected to the problem of C. As has been stated, there is no assurance that C will be present in any still charge, but any C which is present must be effectively removed (to at least fairly low levels).

Considering that the freezing point of commercial-grade R is 109.6°C and those of pure R and C are 110.7 and 105.0°C, the composition of a mixture of pure R and pure C which has a freezing point of 109.6°C can be calculated by assuming a linear relationship. Let x = moles C and $1 - x$ = moles R

$$(1 - x)(110.7) + x(105.0) = 109.6 \qquad x = 0.193$$

Therefore, any C present must be removed down to a mole fraction of 0.193 if the linear assumption is appropriate. To be conservative, it is assumed that a residual mole fraction of 0.100 is an acceptable concentration of C. The relative volatility of C to R can be calculated from vapor pressure values.

	Vapor pressure, mmHg		
Temperature, °C	R	C	α_{C-R}
138.0	5	23.4	4.68
152.1	10	41.0	4.10
168.0	20	73.8	3.69

$$\alpha = (4.68 \times 4.10 \times 3.69)^{1/3} = 4.14$$

Using this value of relative volatility, the following vapor-liquid equilibrium compositions can be calculated:

x	y	x	y
0.000	0.000	0.600	0.861
0.100	0.315	0.700	0.906
0.200	0.505	0.800	0.943
0.300	0.640	0.900	0.974
0.400	0.734	1.00	1.00
0.500	0.805		

These values are plotted in Fig. 5.6*a* to *c*. Using a bottoms mole fraction of 0.100 and three theoretical stages in Fig. 5.6*a* it is only possible to achieve an overheads mole fraction of C of approximately 0.883 at total reflux. Thus, it may be concluded that essentially pure C cannot be recovered with this particular distillation system. Therefore, C will be removed in the foreruns cut until the distillation produces an acceptable R.

Selecting a reflux ratio of 5:1 (based on the maximum of 3.9 encountered in the removal of P), the corresponding y intercept is computed using the overhead mole fraction of 0.883

$$y_{\text{int}} = \frac{x_D}{R + 1} = 0.147$$

Connecting 0.147 with $x_D = 0.883$ in Fig. 5.6*b* and stepping off three theoretical stages shows residual mole fraction of C is 0.160.

Continuing this process in Fig. 5.6*c* an overhead mole fraction of 0.800 corresponds to a residual mole fraction in the still of 0.100. The area represented by this change can be calculated as a square of average height

$$[(0.883 - 0.160) + (0.800 - 0.100)]/2 = 0.712$$

and base (0.160 − 0.100) with area = 0.0427. Assuming that all W and P have been distilled by this time—and that all distillation losses have occurred—there are 97.0 (109.6 − 7.95 − 4.72) moles of crude remaining in the still.

$$\ln \frac{W}{97.0} = -0.0427$$

$$W = 97.0\,(0.958)$$

$$= 92.9$$

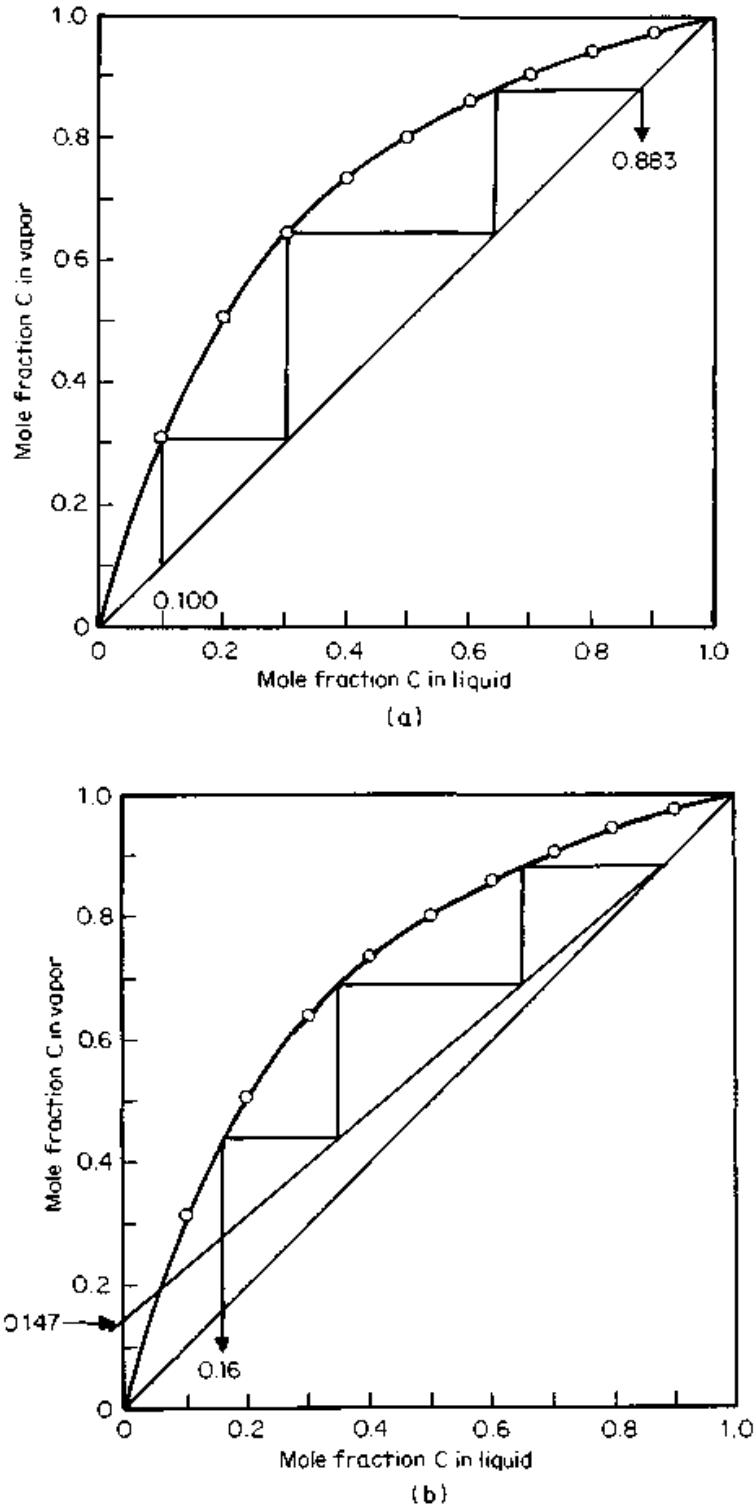

Figure 5.6 Separation of C from R in case history; McCabe-Thiele diagram, $\alpha = 4.14$. (*a*) Total reflux; (*b*) 5:1 reflux, 0.883 top purity.

Thus, 4.1 moles of material are distilled to remove any C presumed to be present.

However, the research department report indicates that 4.54 moles

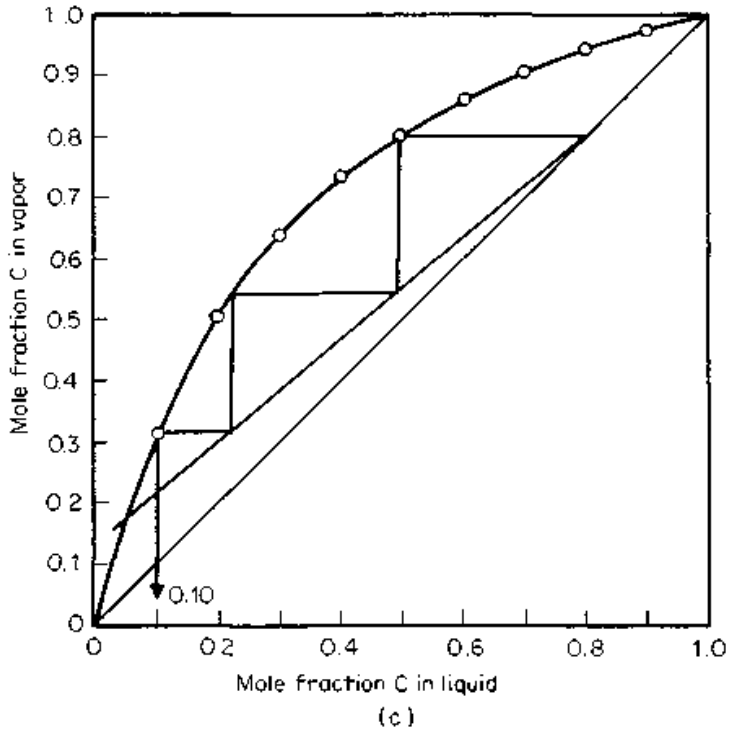

Figure 5.6 (*Continued*) Separation of C from R in case history; McCabe-Thiele diagram, $\alpha = 4.14$. (*c*) 5:1 reflux, 0.8 top purity.

may be expected to be removed as a foreruns cut. Maintaining the 5:1 reflux ratio, the amount of vapor removed during the foreruns cut is

$$V = D(R + 1) = 4.54(6) = 27.2 \text{ moles}$$

(Of course, the end of the foreruns cut is determined by the quality of the product being obtained—not because some amount of foreruns have been collected.)

The material remaining in the still at this point is a mixture of R and some heavy impurities, mainly off-color materials that tend to boil at the same temperature as R. The research department report indicates that 90 percent of the product can be removed at a reflux ratio of 1:1 while the remaining product should be removed at a ratio of 5:1 to obtain the best possible separation of product and tailings. The tailings may be recovered at a reflux ratio of 2:1.

$$\text{Moles vapor} = 0.9(90.8)(1 + 1) = 163$$
$$\text{Moles vapor} = 0.1(90.8)(5 + 1) = 54.5$$
$$\text{Moles vapor} = 1.61(2 + 1) = 4.8$$

Thus, the total moles of vapor to be generated during the distillation are:

W	4.7*
P	15
Foreruns	27.2
Product	217.4
Tailings	4.8
	269.1

The heat duties associated with these fractions can be estimated by the Clausius-Clapeyron equation (20)

$$\ln \frac{P_2}{P_1} = \frac{\Delta H}{R}\left(\frac{1}{T_1} - \frac{1}{T_2}\right)$$

For R, for example, vapor pressure is 5, 10, and 20 mmHg at temperatures of 411.2, 425.3, and 441.2°

$$\ln \frac{10}{5} = \Delta H_{vap}\left[\frac{\text{lb mole °R}}{1.987\ \text{Btu}}\right]\left[\frac{1}{(411.2 \times 1.8)} - \frac{1}{(425.3 \times 1.8)}\right]\frac{1}{\text{°R}}$$

$$0.6931 \times 1.987 = \Delta H_{vap}\,(0.00004465)$$

$$\Delta H_{vap} = 30{,}750\ \text{Btu/lb-mole}$$

Also,

$$\ln \frac{20}{10} = \frac{\Delta H_{vap}}{1.987}\left[\frac{1}{(425.3 \times 1.8)} - \frac{1}{(441.3 \times 1.8)}\right]$$

$$0.6931 \times 1.987 = \Delta H_{vap}\,(0.00004733)$$

$$\Delta H_{vap} = 29{,}100\ \text{btu/lb-mole}$$

$$\Delta H_{vap,ave} = 29{,}900\ \text{Btu/lb-mole}$$

Similarly for P,

$$\Delta H_{vap,ave} = 25{,}540\ \text{Btu/lb-mole}$$

and *W*

$$\Delta H_{vap} = 18{,}180\ \text{Btu/lb-mole}$$

Total heat required (*Note:* For distillation duty only)

*The relative volatility of W with respect to P is so large that it can be considered to be capable of being separated without reflux.

W	4.7 × 18180 =	85,500
P	15 × 25540 =	383,000
$(F + R + T)$	249.4 × 29900 =	7,460,000
		7,930,000

With these calculations and the time allowable for the distillation, the still system can be specified. A batch must be distilled every day to meet plant capacity requirements, so a reasonable schedule might be

Charge still	0.5–1 h
Empty still	0.5–2 h
Heatup	2 h
Distillation	18 h
Total	say 22 h

Therefore, distillation heat duty = 7,930,000/22 = 360,000 Btu/h. Of course, the condenser must be capable of removing this amount of heat.

Because a still pot for such a system should only be filled to about 70 percent of its capacity, the still volume should be

$$\frac{11{,}765 \text{ lb}}{8 \text{ lb/gal} \times 0.70} = 2100 \text{ gal}$$

The 18-h distillation time means that the rectifying column must be designed for a vapor loading of

$$\frac{269.1 \text{ lb-mole}}{18 \text{ h}} = 15.0 \text{ lb-mole/h}$$

The most drastic condition which will exist in the column will occur during the foreruns cut and during the finishing of the product cut when reflux ratio will be 5:1. At these points, the L/V ratio will be at its maximum value, and the column must be capable of adequately handling such a loading (see Chap. 12).

The still system will consist of a receiver for W, a receiver for P, a foreruns-tailing receiver, and a product receiver.

The method of operation of the system will be:

1. Charge system
2. Start heat to still
3. Start vacuum system
4. Divert product to W receiver

5. Observe temperature profiles in the column to change delivery from
   a. W receiver to P receiver (increase reflux ratio)
   b. P receiver to foreruns-tailings receiver (increase reflux ratio)
6. Based on product appearance and freezing point, divert to product receiver (decrease reflux ratio)
7. Based on product appearance (mainly) and freezing point, divert to foreruns-tailings receiver
8. Cut off heat, break vacuum.

The discussion above leaves many things unsaid. It would be extremely unlikely that a competent research department that had "thoroughly investigated the manufacture of R" would not have developed better information about C than is shown. Of course, better information, and consequent better understanding, would make the process engineer's task easier, but the real point is to show how some otherwise-clumsy materials can be accounted for.

The suggestion to start the heating system and vacuum-producing system and to begin removing W immediately is a departure from the conventional idea of operating a batch system at total reflux "to equilibrate" it before starting product removal. If the first material to come out of the distillation system is a valuable product, the system should be equilibrated. In a case like the one discussed above, where W, P, and foreruns are distilled off before the product cut is started, equilibration is unnecessary. After all, batch distillation is always a transient process, so why worry about achieving equilibrium before starting a strictly nonequilibrium process?

"Observing temperature profiles" in the column is a clear recommendation of installing thermocouples in at least the bottom, middle, and top of the column. Further, use of the vapor pressure regressions and a little imagination permits the construction of graphs which allow the operators to infer product composition from temperature and pressure readings.

The material collected in the foreruns-tailings receiver would normally be recharged to the still as part of the next cycle. One should not be surprised to observe that the amount of foreruns and tailings separated (and returned) tends to become a fairly stable quantity, even though "logic" would dictate otherwise.

Product quality was easy to assess in the example inasmuch as color is easy to detect and freezing points are easy to measure—even by relatively unskilled operators. For operation with other systems, product quality needs to be easily assessable to aid operator decisions—finding the exact analytical tool required for such assessment might not be so easy.

Neither trays nor packing have been discussed in any of the above. If trays are used, tray efficiency must be considered, and if packing is specified, the HETP of the packing must be known. The vendors of column internals can be most helpful here, but also see Chaps. 10 and 12.

"Safety factors" have not been discussed inasmuch as these factors should reflect the engineer's confidence in the data he or she has, the distillation system performance deduced in manipulating these data, the reliability the equipment must demonstrate, etc., in short, "engineering judgment." There is never anything better than reliable experimental data on the system which is to be distilled, of course. In other, less-well-defined circumstances, conservatism is advised (9). Batch stills are usually (at least relatively) low-cost items, and increased capabilities represent small incremental costs.

5.3 Special Note to Readers

As stated earlier, the development above is based on a "real-life" design, but does not reflect that design identically. The crude actually had a nondistillable residue associated with it, and it was necessary to remove this material from the still after each distillation. However, the residue had no other effect on the distillation and, for this reason, was not included in the discussion above. The reflux ratio actually used between foreruns and product cuts was 10:1, and for reasons that are now nonretrievable, the column contained about 15 feet of Intalox® saddles—equivalent to five to eight theoretical stages. The operating procedures which evolved with practice were those recommended above, and the quantities of foreruns and tailings recovered and recycled leveled out fairly well. The only really serious problem not anticipated in the design was the gradual increase in viscosity in the still residue to the point where it was no longer transferable by the centrifugal pump provided. Substitution of a positive-displacement pump remedied this problem.

5.4 References

1. Barb, D. K., and C. D. Holland, 7th World Congress, Mexico City, April 1967.
2. Block, B., *Chem. Eng.*, *68*(3), pp. 87–98, 1961.
3. Block, B., in Perry, R. H., and C. H. Chilton (eds.), *Chemical Engineers' Handbook*, 5th ed., McGraw-Hill, New York, 1973.
4. Bogart, M. J. P., Trans. AIChE, *33*, pp. 139–151, 1937.
5. Boston, J. F., in R. S. Mah, and W. D. Seider (eds.), *Foundations of Computer-Aided Chemical Process Design*, Vol. 2, American Institute of Chemical Engineers, New York, 1981.
6. Coates, J. A., and B. S. Pressburg, *Chem. Eng.*, *68*(2), pp. 131–136, 1961.
7. Distefano, G. P., *Am. Inst. Chem. Engrs. J.*, *14*(1), pp. 190–199, 1968.
8. Ellerbee, R. W., *Chem. Eng.*, *80*(12), pp. 110–116, 1973.

9. Ellerbee, R. W., in P. A. Schweitzer (ed.), *Handbook of Separation Techniques for Chemical Engineers*, McGraw-Hill, New York, 1979.
10. Frank, O., *Chem. Eng., 84*(6), pp. 110–128, 1977.
11. Houtman, J. P. W., and A. Husain, Chem. Eng. Sci., *5*, pp. 178–187, 1956.
12. Huckaba, C. E., and D. E. Danly, *Am. Inst. Chem. Eng. J., 6*, pp. 335–342, 1960.
13. Meadows, E. L., *Chem. Eng. Prog. Sym. Ser. 46, 59*(46), pp. 48–55, 1963.
14. Pigford, R. L., J. B. Tepe, and C. J. Garrahan, *Ind. Eng. Chem., 43*, pp. 2592–2602, 1951.
15. Rayleigh, Lord, *Phil. Mag.*, 6th series, *4*, pp. 521–537, 1902.
16. Robinson, C. S., and E. H. Gilliland, *Elements of Fractional Distillation*, 4th ed., McGraw-Hill, New York, 1950.
17. Rose, A., Chem. Eng. Prog, *48*, p. 549, 1952.
18. Rose, A., Chem. Eng. Prog, *49*, p. 15, 1953.
19. Rose, L. M., *Distillation Design in Practice*, Elsevier, Amsterdam, 1985.
20. Smith, J. M., and H. C. Van Ness, *Introduction to Chemical Engineering Thermodynamics*, 4th ed., McGraw-Hill, New York, 1987.
21. Smoker, E. H., and A. Rose, *Trans. Am. Inst. Chem. Engrs., 36*(2), pp. 285–293, 1940.

Chapter

6

Tray Design and Operation

Once the process design is completed, the equipment design begins. This phase of the design translates the process requirements (i.e., the vapor and liquid loads in each section of the column) into actual hardware.

The hardware design proceeds in two phases: primary (basic) and secondary (detailed layout). The primary phase sets column diameter, type of tray, and split of tray area into bubbling and downcomer areas. This phase also provides a preliminary (and usually close) estimate of tray spacing, number of passes, and other features of tray and downcomer layout such as weir height, fractional hole area, hole diameter, and clearance under the downcomer. These estimates are later firmed up in the secondary phase.

Functionally, the primary phase sets the major equipment requirements, while the secondary phase engineers the finer details. The primary phase has a major impact on column costs, but a relatively small influence on achieving trouble-free operation. These roles are reversed in the secondary phase: it has a relatively small impact on column costs, but a major impact on achieving trouble-free operation.

This chapter deals with the primary phase of hardware design. The secondary phase is outside the scope of this book, and occupies several chapters of a companion book (1).* This chapter describes the physical processes that constrain equipment design, including flooding, entrainment, weeping, pressure drop, clear liquid height, and flow regimes. This chapter then describes how knowledge of these physical processes is harnessed to set hardware design.

The discussions in this chapter emphasize sieve and valve trays, as these trays are most frequently encountered in industrial practice. Several of the considerations also apply to other tray types (e.g., bubble-cap trays). Considerations unique to bubble-cap trays were excluded from this chapter. The infrequent application of this type of tray in modern distillation practice argues against a detailed discus-

*References for Chap. 6 appear at the end of Chap. 7.

sion here. A large amount of information on bubble-cap trays is documented in several texts (2–5).

6.1 The Common Tray Types

6.1.1 Description of the common tray types

The *bubble-cap tray* was the workhorse of distillation before the 1960s. It was superseded by the sieve and valve trays. Presently, bubble-cap trays are specified only for special applications, while sieve and valve trays are the most popular types.

The bubble-cap tray (Fig. 6.1*a*) is a flat perforated plate with risers (chimneylike pipes) around the holes, and caps in the form of inverted cups over the risers. Several cap designs are shown in Fig. 6.1*b*. The caps are usually (but not always) equipped with slots or holes through which the vapor comes out (Fig. 6.2*a*). Liquid and froth are trapped on the tray to a depth at least equal to the weir height or riser height, giving the bubble-cap tray a unique ability to operate at low vapor and liquid rates.

The *sieve tray* (Fig. 6.1*c*) is a flat perforated plate. Vapor issues from the holes to give a multiorifice effect (Fig. 6.2*b*). The vapor velocity keeps the liquid from flowing down through the holes (weeping). At low velocities, liquid weeps through the holes, bypassing some of the tray and reducing efficiency, giving sieve trays relatively poor turndown. Sieve trays are simple and easy to fabricate, and are therefore relatively inexpensive.

A *dual-flow tray* (Fig. 6.1*d*) is a sieve tray with no downcomers. This tray operates with liquid continuously weeping through the holes, hence its low efficiency. Tray froth height diminishes rapidly when vapor velocity is reduced, causing further efficiency deterioration upon turndown. Turndown of a dual-flow tray is even poorer than that of a sieve tray with downcomers. Large-diameter (>8 ft) dual-flow trays are known to sometimes experience instability. Insight into the nature of this instability can be inferred from Yanagi's thorough description of dual flow hydraulics (6). Dual flow trays are prone to channeling, and are therefore sensitive to out of levelness and to liquid distribution.

Due to the absence of downcomers, dual-flow trays give more tray area, and therefore have a greater capacity than any of the common tray types. This makes them an ideal revamp tool if some efficiency can be sacrificed. The absence of downcomers, and the larger open areas, renders dual-flow trays the most suitable to handle highly fouling services, slurries, and corrosive services. Dual-flow trays are also the least expensive to make, and easiest to install and maintain.

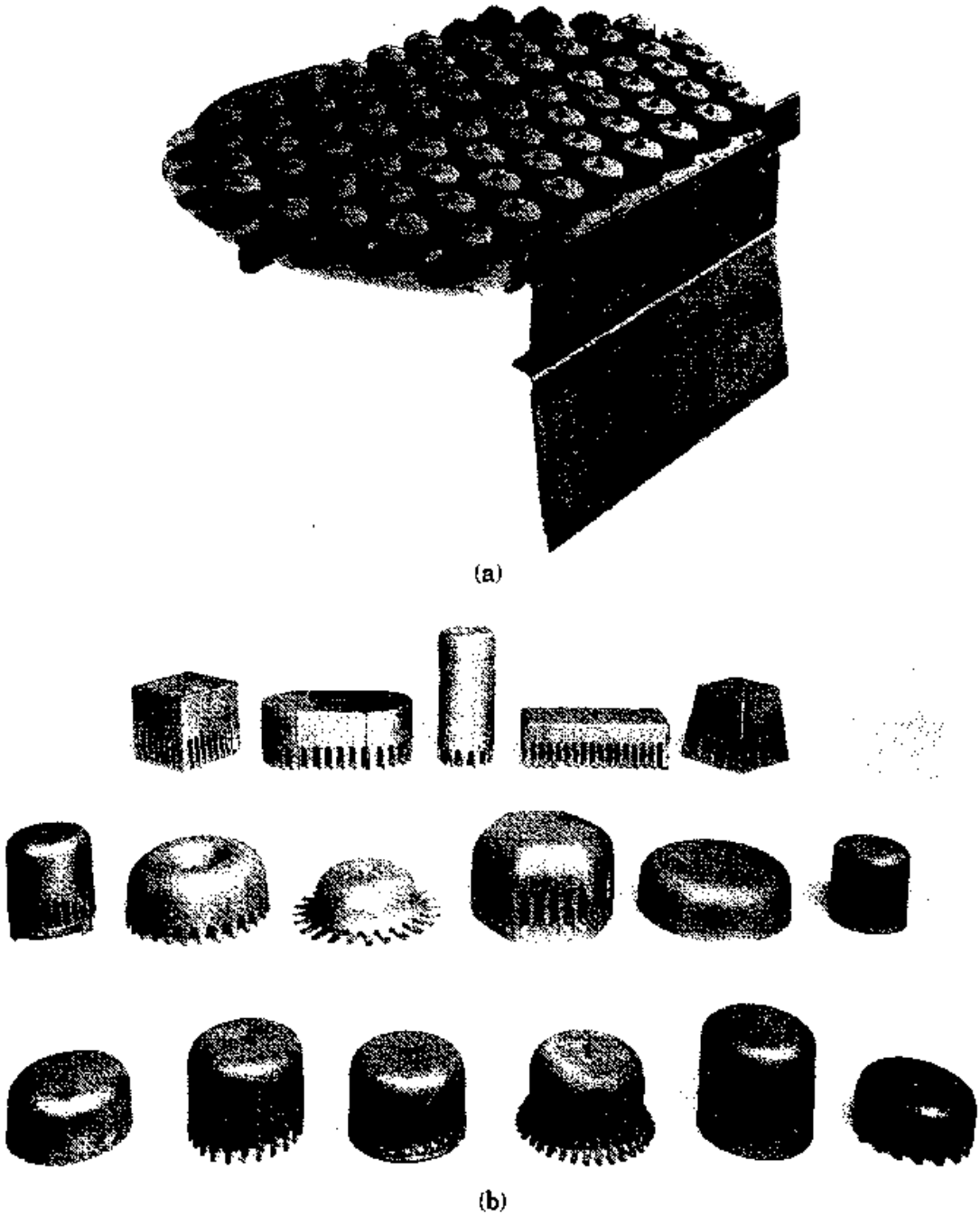

(a)

(b)

Figure 6.1 Common tray types. (*a*) Bubble-cap tray; (*b*) different types of bubble-cap designs [*Parts a and b courtesy of Glitsch, Inc.*]

Figures 6.3 and 6.4 show different types of *valve trays* and valve units. Valves can be round or rectangular, with or without a caging structure. A detailed description is available elsewhere (1), and in manufacturers' literature (7–9). The valve disks rise as vapor rate is increased (Fig. 6.2*c*). The upper limit of opening is controlled by a caging structure or by restrictive legs at the bottom of the valve unit. As vapor rate falls, the disk openings are reduced, or they may settle intermittently over the holes. This stops the liquid from

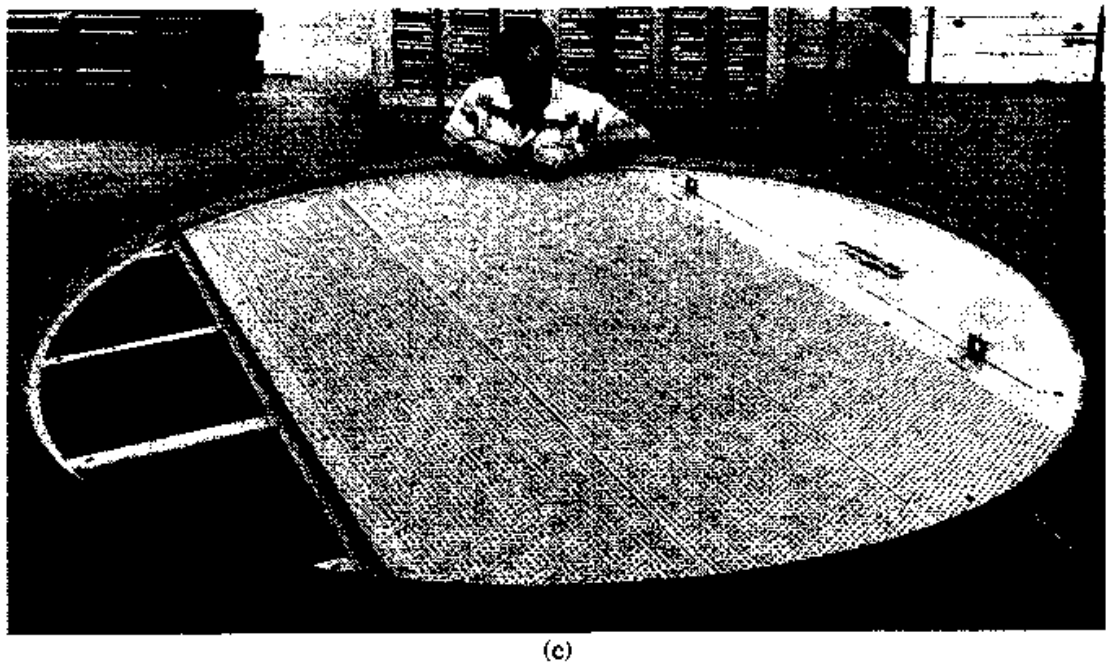

(c)

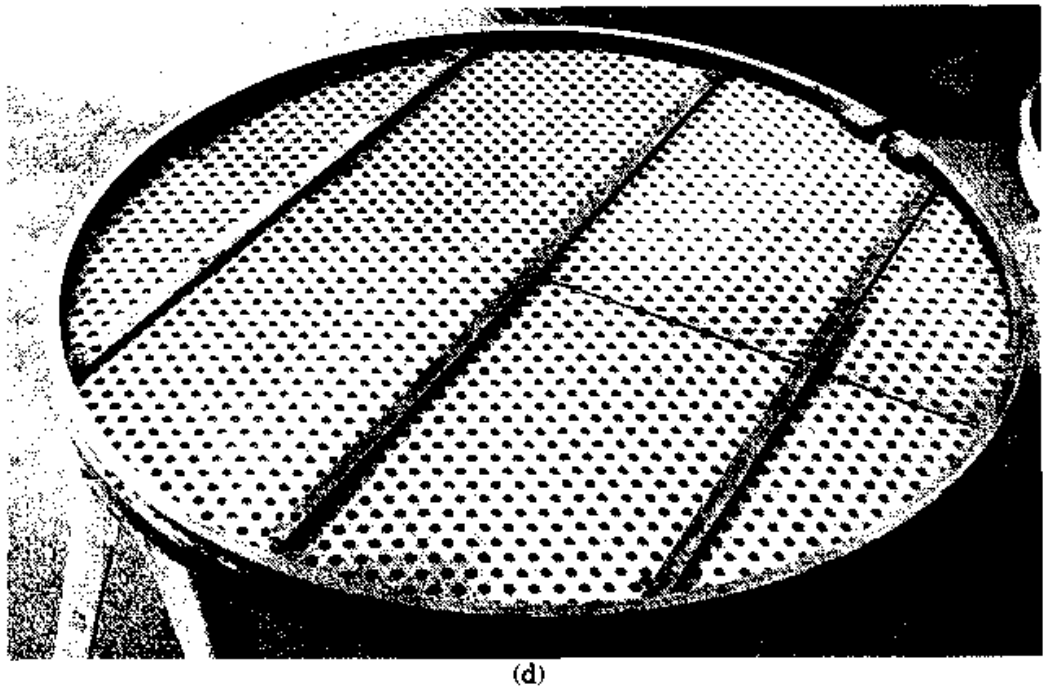

(d)

Figure 6.1 (*Continued*) Common tray types. (*c*) Sieve tray; (*d*) dual-flow tray. [*Part c courtesy of Glitsch, Inc.*] [*Part d courtesy of Fractionation Research Inc. (FRI).*]

weeping and gives the valve tray its main advantage—good operation at low flow rates, and therefore, a high turndown.

6.1.2 Comparison of the common tray types

Table 6.1 compares the main tray types. The comparison is general and assumes the trays are properly designed, installed, and operated. Sieve and valve trays have comparable capacity, efficiency, entrain-

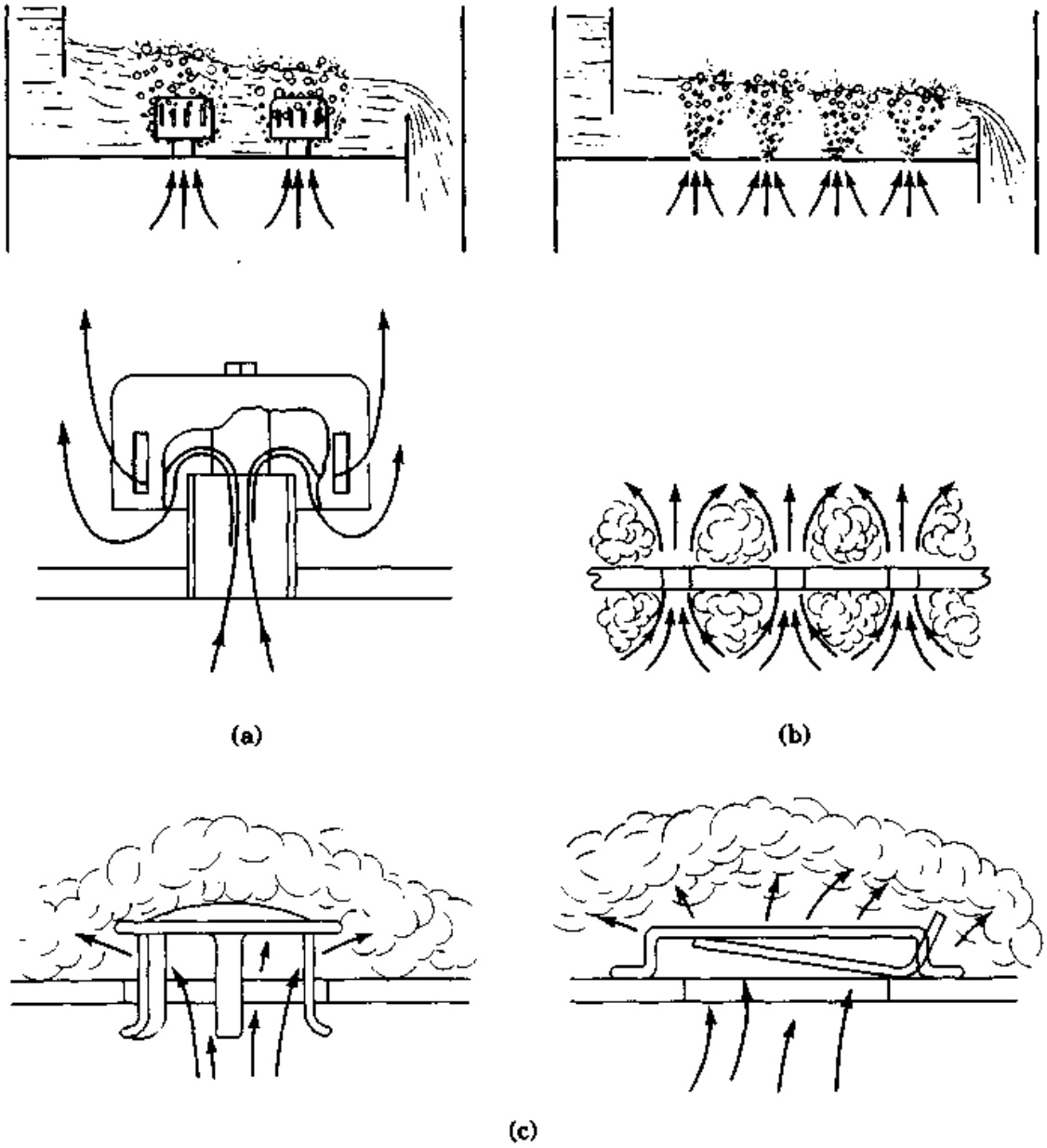

Figure 6.2 Flow-through tray vapor passages. (*a*) Bubble-cap tray, (*b*) sieve tray (*c*) valve tray. (*M. Van Winkle,* Distillation, *Copyright © 1967 by McGraw-Hill Inc., reprinted by permission.*)

ment, and pressure drop. Bubble-cap trays have lower capacity and efficiency and higher entrainment and pressure drop than sieve and valve trays. Dual-flow trays show better capacity but inferior efficiency than other types.

The turndown of valve trays is much better than sieve trays, but not as good as bubble-cap trays. Bubble-cap trays are the most suitable to handle extremely low liquid rate applications [less than 2 gpm per foot of average flow width (10)].

The cost of bubble-cap trays is by far the highest. Sieve trays are the least expensive, but valve trays are only slightly more expensive.

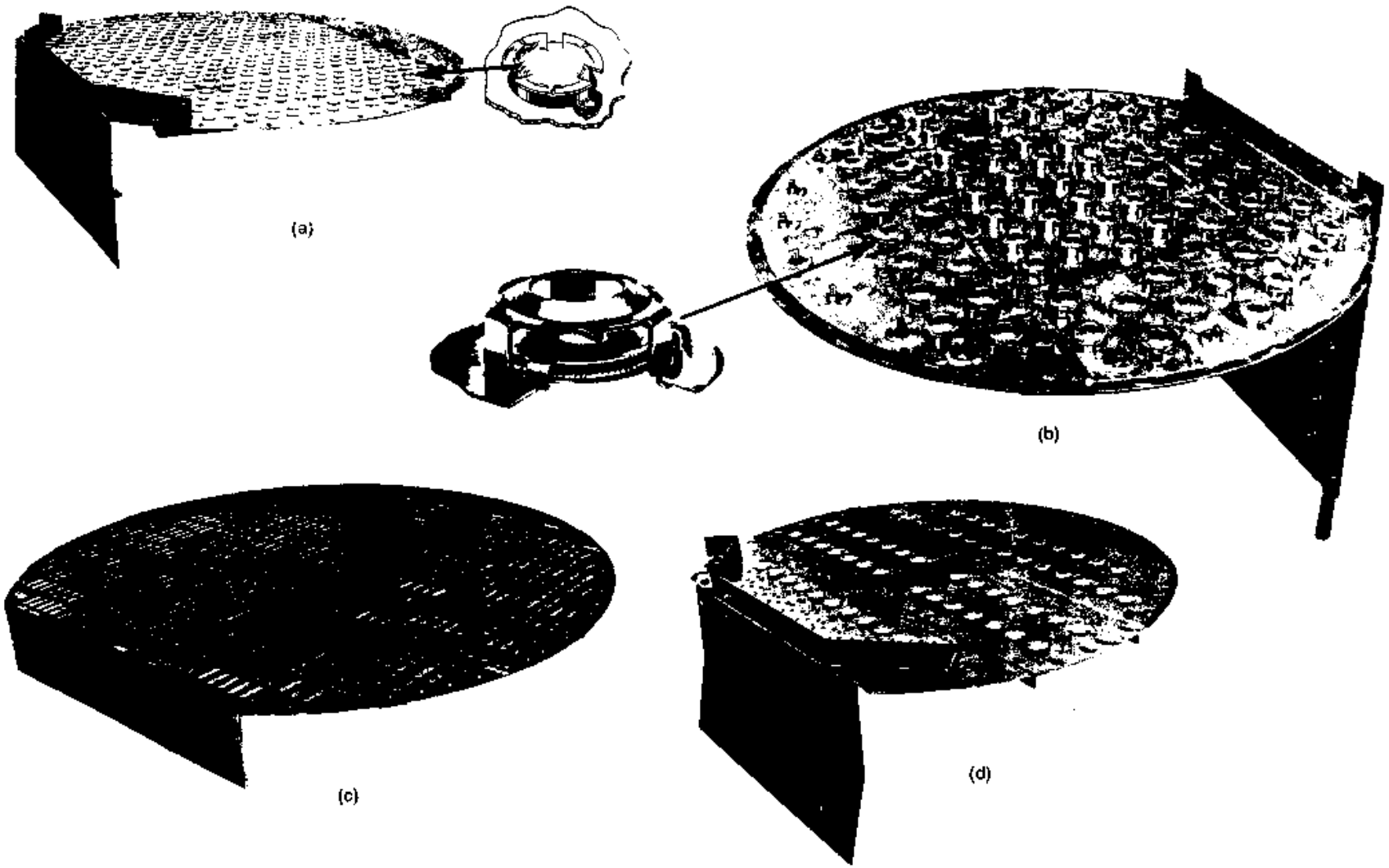

Figure 6.3 Valve trays. (*a*) A valve tray equipped with round, uncaged valves. (*b*) A valve tray equipped with round, caged valves. (*c*) A valve tray equipped with rectangular valves. (*d*) A valve tray containing both round, uncaged valves and perforations. (*Parts a and d courtesy of Koch Engineering Company Inc; part b courtesy of Glitsch, Inc; part c courtesy of Nutter Engineering*)

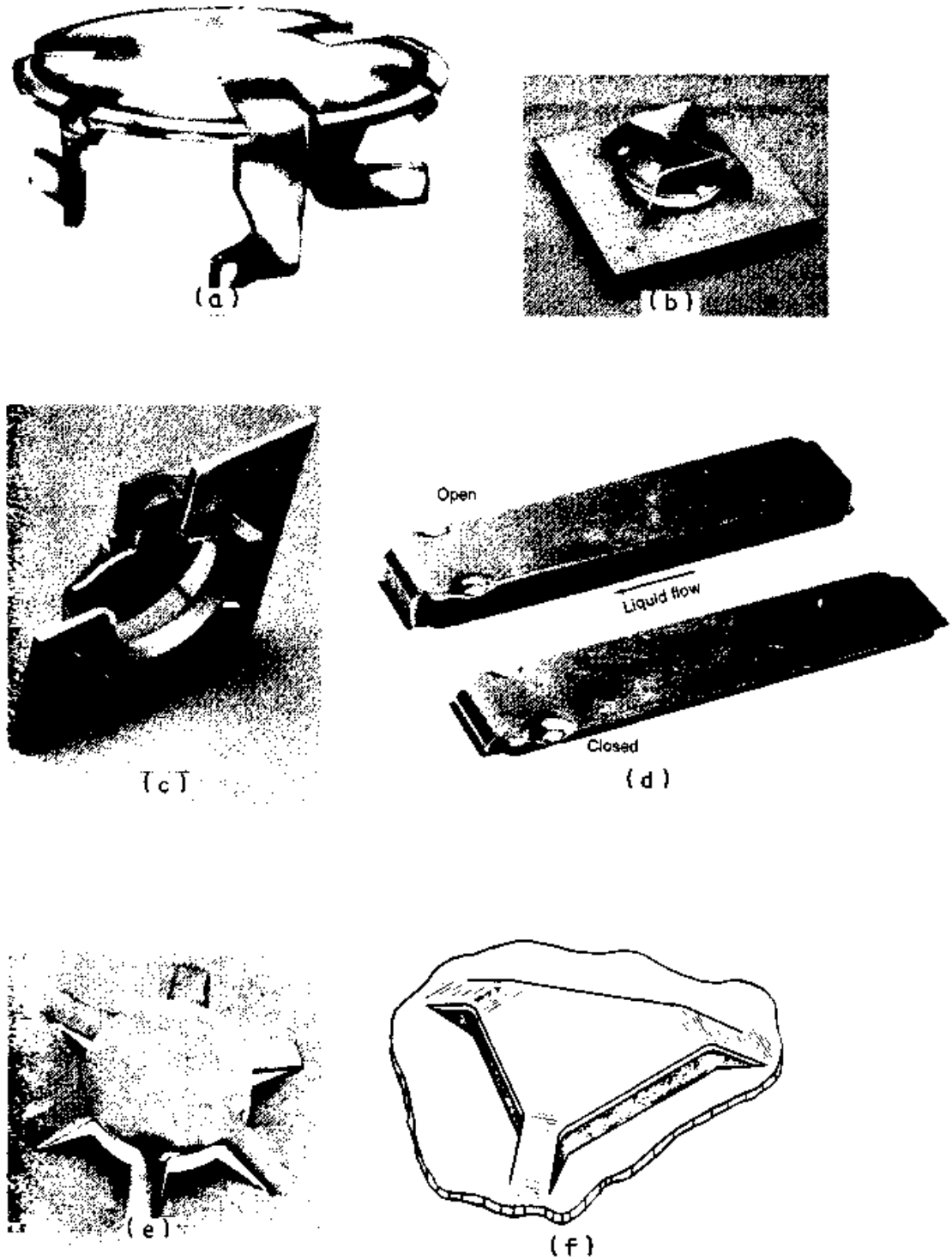

Figure 6.4 Types of valve units. (*a*) An uncaged, round valve unit. (*b*) A caged, round valve unit. (*c*) A caged, round valve unit featuring a contoured orifice. (*d*) A rectangular valve unit. (*e*) A fixed, round valve unit. (*f*) A fixed, triangular valve unit. (*Parts a and e courtesy of Glitsch Inc.; parts b, c and f courtesy of Koch Engineering Company, Inc. part d courtesy of Nutter Engineering.*)

TABLE 6.1 Comparison of the Common Tray Types

Type	Sieve tray	Valve tray	Bubble-cap tray	Dual-flow tray
Diagram	6.1*c*	6.3, 6.4	6.1*a*,*b*	6.1*d*
Tray action diagram	6.2*b*	6.2*c*	6.2*a*	
Capacity	High	High to very high	Moderately high	Very high
Efficiency	High	High	Moderately high	Lower than other types
Turndown	About 2:1. Not generally suitable for operation under variable loads	About 4-5:1. Some special designs achieve (or claim) 10:1 or more	Excellent, better than valve trays. Good at extremely low liquid rates	Low, even lower than sieve trays (10). Unsuitable for variable load operation
Entrainment	Moderate	Moderate	High, about 3 times higher than sieve trays (4)	Low to moderate
Pressure drop	Moderate	Moderate. Early designs somewhat higher. Recent designs same as sieve trays	High	Low to moderate
Cost	Low	About 20 percent higher than sieve trays (11)	High. About 2–3 times the cost of sieve trays (10,11)	Low

Maintenance, fouling tendency, and effects of corrosion are least in sieve trays, although these are not much greater for valve trays.

In general, bubble-cap trays and dual-flow trays are mainly used in special applications. Bubble caps are preferred either when extremely high turndown is required or when leakage must be eliminated. Dual-flow trays are preferred for handling slurries, highly corrosive and highly fouling services, or when a column is revamped for high capacity.

For most other services, either sieve or valve trays are the best choice. Sieve trays are at an advantage when the service is fouling, or corrosive, or when turndown is unimportant, while valve trays are preferred when turndown is important. With high energy costs, the energy saved during even short turndown periods usually justifies the relatively low cost difference between valve and sieve trays. This has made valve trays most popular.

TABLE 6.1 Comparison of the Common Tray Types (*Continued*)

Type	Sieve tray	Valve tray	Bubble-cap tray	Dual-flow tray
Maintenance	Low	Low to moderate	Relatively high	Low
Fouling tendency	Low	Low to moderate	High. Tends to collect solids	Extremely low. Suitable where fouling is extensive and for slurry handling.
Effects of corrosion	Low	Low to moderate	High	Very low
Availability of design information	Well known	Proprietary, but information readily available	Well known	Some information available
Other				Instability sometimes occurs in large diameter (>8 feet) columns
Main applications	Most columns when turndown is not critical	1. Most columns, 2. Services where turndown is important	1. Extremely low flow conditions 2. Where leakage must be minimized	1. Capacity revamps where efficiency and turndown can be sacrificed 2. Highly fouling and corrosive services
Share of the market (11)	25%	70%	5%	No information

6.2 Tray Capacity Limits

6.2.1 The classical hydraulic model

Figure 6.5 illustrates the classical hydraulic model of a fractionation tray. Liquid enters the tray from the downcomer of the tray above. The liquid entering the tray is aerated with vapor rising from the tray below to form froth on the tray. The froth flows across the tray until it reaches the outlet weir. The froth then flows over the weir into the downcomer, where the vapor is disengaged from the liquid.

Recent work (Sec. 6.4.1) has shown that this model is an oversimplification of the processes occurring on a distillation plate. Nevertheless, many of the modern design procedures are based on this model and are expressed in terms of this model.

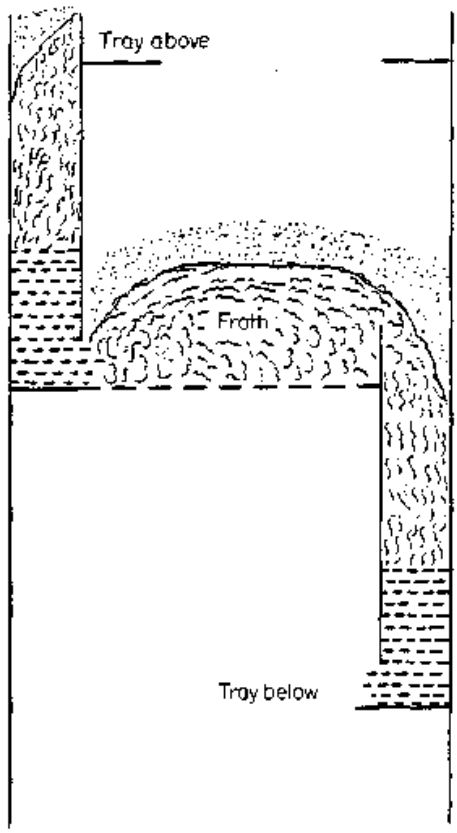

Figure 6.5 The classical tray hydraulic model.

6.2.2 Tray stability diagram

Figure 6.6 is a typical tray stability diagram. The area of satisfactory operation (shaded) is bound by the tray stability limits. These limits are discussed in the following sections. The upper capacity limit is the onset of flooding. At moderate and high liquid flow rates, the entrainment (jet) flooding limit is normally reached when vapor flow is raised, while the downcomer flooding limit is normally reached when liquid flow is raised. When flows are raised while the column operates at constant L/V (i.e., constant reflux ratio), either limit can be reached. At very low liquid rates, as vapor rate is raised, the limit of excessive entrainment is often reached.

As vapor rate is lowered, either at constant liquid rate or at a constant L/V ratio, the limit of excessive weeping is reached. This limit is not identical with the weep point, as some weeping can usually be tolerated.

6.2.3 Definitions of tray area, vapor load, and liquid load

Area definitions. Areas used for defining tray velocity are:

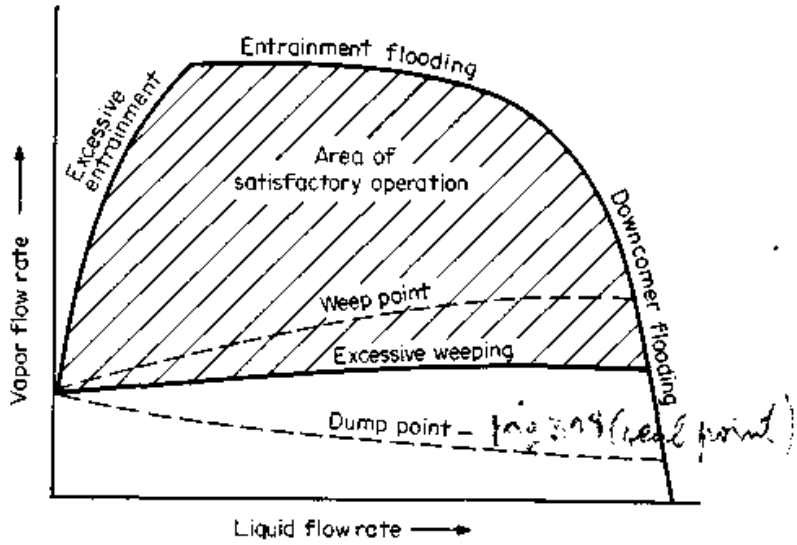

Figure 6.6 Sieve tray performance diagram.

Total tower cross-section area, A_T: the inside cross-section area of the empty tower (without downcomers or trays).

Net area, A_N: the total tower cross-section area A_T less the area at the top of the downcomer (sometimes referred to as *free area*; the term free area has been used inconsistently in the literature). The net area represents the smallest area available for vapor flow in the intertray spacing.

Bubbling area, A_B: the total tower cross-section area less the total of downcomer area, downcomer seal area, and any other nonperforated regions (often referred to as *active area, A_a*). In practice, nonperforated regions less than 4 in wide are counted as perforated areas, while regions wider than 4 in are counted as nonperforated areas. The bubbling area represents the area available to vapor flow near the tray floor.

Hole area, A_h: the total area of perforations on the tray. The hole area is the smallest area available for vapor passage.

Slot area, A_S: the total (i.e., of all the valves) vertical curtain area through which vapor passes in a horizontal direction as it leaves the valves. It is based on the narrowest opening of each valve. The slot area is a function of the number of valves that are open. The slot area is usually the smallest area available for vapor flow on a valve tray.

Open slot area, A_{So} (valve trays): the slot area when all the valve units are fully open.

Fractional hole area, A_f: the ratio of hole area to bubbling area (sieve trays) or slot area to bubbling area (valve trays).

Vapor load definitions. One vapor load term is VLOAD

$$\text{VLOAD} = \text{CFS}\sqrt{\frac{\rho_V}{\rho_L - \rho_V}} \tag{6.1}$$

This term is inconvenient because it is based on CFS and not on a velocity. A more convenient vapor load term is the *F-factor,*

$$F_S = u_S\sqrt{\rho_V} \tag{6.2}$$

The F-factor is the square root of the kinetic energy of the vapor. The velocity in Eq. (6.2) is usually (but not always) based either on the bubbling area A_B or on the net area A_N. The user must beware of any data for which the area basis is not clearly defined. In some cases, the *hole F-factor,* F_h, is used. This parameter is based on the hole velocity, u_h, and is given by

$$F_h = u_h\sqrt{\rho_V} \tag{6.3}$$

A term even more suitable for describing vapor loads than the F-factor is the *C-factor,* C_S, defined as

$$C_S = u_S\sqrt{\frac{\rho_V}{\rho_L - \rho_V}} \tag{6.4}$$

The C-factor is related to VLOAD and to the F-factor by

$$C_S = \frac{\text{VLOAD}}{A} = \frac{F_S}{\sqrt{\rho_L - \rho_V}} \tag{6.5}$$

The C-factor, C_S, is also usually based either on the bubbling or the net area. The inconsistency regarding the area basis of the F-factor extends to the C-factor. The user must beware of any data for which the area basis is not clearly defined. The C-factor has the same units as velocity (feet per second) and directly relates to droplet entrainment (Sec. 6.2.6). In the author's experience, the C-factor is by far the best vapor load term for comparing capacities of systems of different physical properties.

Tray liquid load definitions. For tray (as distinct from downcomer) design the liquid load is usually defined as

$$Q_L = \frac{\text{GPM of liquid}}{\text{length of outlet weir, in}} = \frac{\text{GPM}}{L_W} \tag{6.6}$$

In concept, this definition describes the flux of liquid across the tray. An alternative definition sometimes used for describing liquid load is the flow parameter, F_{lv}

$$F_{lv} = \frac{L}{V}\sqrt{\frac{\rho_V}{\rho_L}} = \frac{1}{448.8}\frac{Q_L}{u_B}\frac{L_W}{A_B}\sqrt{\frac{\rho_L}{\rho_V}} \tag{6.7}$$

The flow parameter is more suitable for packed columns (12), where vapor-liquid counterflow exists, but has also been used in tray columns. For tray columns the author prefers Q_L [Eq. (6.6)] to the flow parameter.

Downcomer liquid load definitions. For downcomer design, the liquid load is usually defined as

$$Q_D = \frac{\text{GPM of liquid}}{\text{Downcomer entrance area, ft}^2} = \frac{\text{GPM}}{A_D} \tag{6.8}$$

Q_D is the velocity of clear liquid at the downcomer entrance, expressed in gpm per square foot. In some cases, this liquid load is expressed in feet per second instead of gpm per square foot.

6.2.4 Tray flooding mechanisms

Flooding is excessive accumulation of liquid inside the column. This accumulation is generally caused by one of the following mechanisms.

Spray entrainment flooding (Fig. 6.7*a*). At low liquid flow rates, trays operate in the spray regime, where most of the liquid on the tray is in the form of liquid drops (Figs. 6.25*d* and 6.27*b*). As vapor velocity is raised, a condition is reached where the bulk of these drops are entrained into the tray above. The liquid accumulates on the tray above instead of flowing to the tray below.

Froth entrainment flooding (Fig. 6.7*b*). At higher liquid flow rates, the dispersion on the tray is in the form of a froth (Figs. 6.25*c* and 6.27*a*). When vapor velocity is raised, froth height increases. When tray spacing is small, the froth envelope approaches the tray above. As this surface approaches the tray above, entrainment rapidly increases, causing liquid accumulation on the tray above.

When the tray spacing is large (>18 to 24 in), the froth envelope seldom approaches the tray above. As vapor velocity is raised, a con-

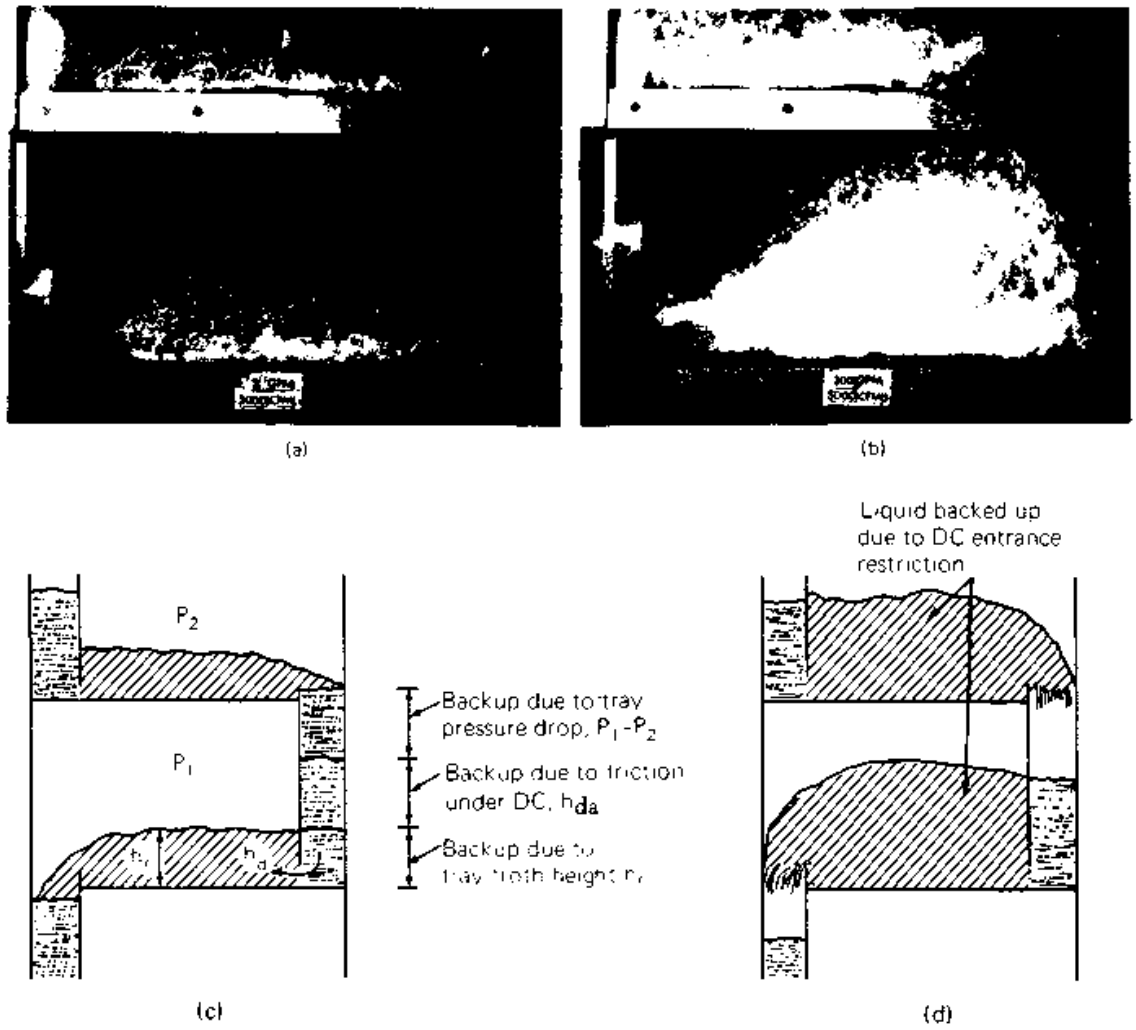

Figure 6.7 Common flooding mechanisms in tray columns. (*a*) Spray entrainment flood; (*b*) froth entrainment flood; (*c*) downcomer backup flood; (*d*) downcomer choke flood. (*Parts a and b reproduced from Dr. D. C. Hausch,* Discussion of Papers Presented in the Fifth Session, *Proceedings of the International Symposium on Distillation, the Institution of Chemical Engineers (London), 1960, reprinted courtesy of the Institution of Chemical Engineers, UK. Parts c and d from H. Z. Kister,* Distillation Operation. *Copyright © 1990 by McGraw-Hill, Inc.; reprinted by permission.*)

dition is reached when some of the froth inverts into spray. Flooding will then take place by the previously described spray entrainment mechanism.

At high liquid rates (>6 gpm/in of outlet weir), high ratio (>2.5) of flow-path length to tray spacing, and a high fractional hole area (>11 percent), cross flow of vapor in opposite direction to the liquid can build up froth near tray inlet and center. The froth buildup raises the liquid head in the tray inlet and center. This channels more vapor to the tray outlet region, thus accelerating the cross flow. The inlet froth keeps rising until it reaches the tray above.

Downcomer backup flooding (Fig. 6.7*c*). Aerated liquid is backed up into the downcomer because of tray pressure drop, liquid height on the tray, and frictional losses in the downcomer apron. All of these increase when liquid flow rate is raised, while tray pressure drop also increases when vapor flow rate is raised. When the backup of aerated liquid in the downcomer exceeds the tray spacing, liquid accumulates on the tray above, causing downcomer backup flooding.

Downcomer choke flooding (Fig. 6.7*d*). As liquid flow rate increases, so does the velocity of aerated liquid in the downcomer. When this velocity exceeds a certain limit, friction losses in the downcomer and downcomer entrance become excessive, and the frothy mixture cannot be transported to the tray below. This causes liquid accumulation on the tray above.

6.2.5 Factors affecting flooding

Effect of pressure and *L/V*. Figure 6.8 is a rough application chart showing the effect of pressure and L/V on the mechanism of flooding. This chart does not take into account the tray and downcomer geometry, type of system, and operating conditions, all of which strongly influence the flooding mechanism. For this reason, the chart is suitable for defining general guidelines only.

Low pressures favor high vapor velocities and low liquid flow rates and, therefore, spray regime dispersions. Flooding in vacuum columns and in columns operating at a low liquid-to-vapor ratio is usually caused by the spray entrainment mechanism.

At high pressures, the difference between vapor and liquid density

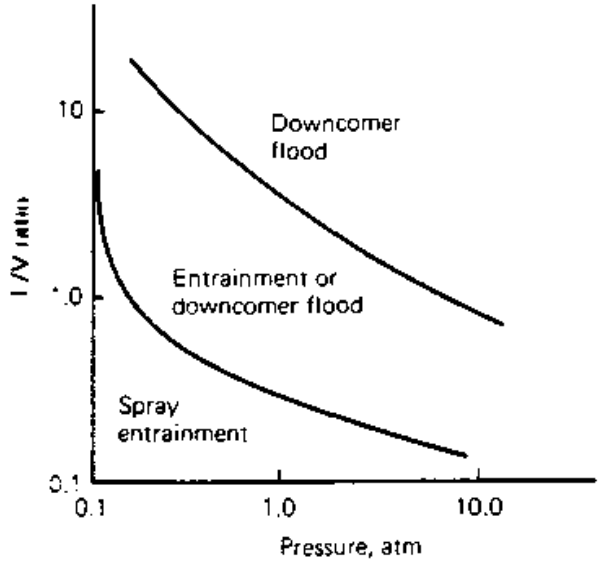

Figure 6.8 A rough flooding mechanism application chart. (*From H. Z. Kister,* Distillation Operation, *Copyright © 1990 by McGraw-Hill, Inc.; reprinted by permission.*)

becomes smaller, and separation of vapor from liquid in the downcomer becomes difficult. Because of the more difficult separation, downcomer aeration increases, raising both downcomer frictional losses and froth backup in the downcomer. High liquid flow rates also increase tray pressure drop, tray liquid level, and frictional losses in the downcomer. For these reasons, downcomer flooding is favored at high pressures and high liquid flow rates.

At moderate pressures and moderate L/V ratios, the dispersion on the tray tends to be in the froth regime, and any of the above mechanisms can dominate. Generally, at low tray spacing (<12 to 15 in) froth entrainment flooding is favored. At higher tray spacing, and when conditions do not favor vapor cross flow (see above), the froth regime will turn into a spray as vapor velocity increases, and spray entrainment flooding is favored. Finally, when downcomers are small or downcomer backups are high, downcomer flooding is favored.

Effect of design parameters. A number of design parameters have a far greater effect on one flooding mechanism than on others. These parameters are listed in Table 6.2.

Low bubbling areas or low fractional hole areas enhance the flooding tendency of all types of flooding except downcomer choke. Low bubbling areas and low fractional hole areas generate high vapor velocities, thus enhancing entrainment, pressure drop, and downcomer backup. These parameters have little effect on downcomer liquid velocity or downcomer froth density, and therefore, on downcomer choke flooding.

TABLE 6.2 Effect of Tray Geometry on Various Types of Flooding

Design parameters that lower the flooding point	Spray entrainment flooding	Froth entrainment flooding	Downcomer backup flooding	Downcomer choke flooding
Low bubbling area	X	X	X	
Low fractional hole area (<8%)	X	X	X	
Low tray spacing	X	X	X	
High weirs (> 4 in)		X	X	
Small weir length		X	X	
Small clearance under downcomer			X	
Small downcomer top area				X

SOURCE: From H. Z. Kister, *Distillation Operation*, Copyright © 1990 by McGraw-Hill Inc. Reprinted by permission.

Low tray spacing also enhances the tendency of all types of flooding other than downcomer choke flooding. As tray spacing diminishes, drops have to travel a shorter distance to be entrained (spray entrainment flooding), the froth envelope becomes closer to the tray above (froth entrainment flooding), and a lower downcomer backup is sufficient to cause flooding. Tray spacing has little effect on either downcomer liquid velocity or downcomer froth density, and therefore, on downcomer choke flooding.

High weirs and small weir lengths reduce spray action and therefore slightly decrease the tendency for spray entrainment flooding, but they increase the height of the froth envelope and therefore increase the tendency for froth entrainment flooding. They also increase liquid height on the tray and tray pressure drop and, therefore, downcomer backup. Weir height and length have little effect on either downcomer liquid velocity or downcomer froth density, and therefore, on downcomer choke flooding.

The other two parameters, small clearance under the downcomer and small downcomer top area, have little effect on entrainment flooding, as they are associated with the downcomer only. Downcomer clearance affects downcomer backup, but not downcomer liquid velocity, while downcomer area affects the velocity, but has little effect on downcomer backup.

6.2.6 Entrainment (jet) flooding

Entrainment flooding can be classified into spray entrainment flooding and froth entrainment flooding. Spray entrainment flooding is far more common. Froth entrainment flooding is only encountered when ‹Sec. 6.2.4)

- *Tray spacing is small:* At tray spacing lower than 18 in, either spray entrainment flooding or froth entrainment flooding can restrict tray capacity, with froth entrainment flooding becoming the more likely mechanism as tray spacing diminishes and/or liquid load increases.
- *Conditions favor vapor cross flow:* These are the only conditions under which froth entrainment flooding is likely to be encountered when tray spacing exceeds 18 in.

The entrainment flooding prediction methods described below are based primarily on the spray entrainment flooding mechanism. Considerations unique to froth entrainment flooding prediction are presented later in the section.

Spray entrainment flooding prediction. Most available entrainment flooding prediction methods derive from the original work of Souders and Brown (13). Souders and Brown theoretically analyzed entrainment flooding in terms of droplet settling velocity. Flooding occurs when the upward vapor velocity is high enough to suspend a liquid droplet, giving Eq. (6.9)

$$u_{S,\text{flood}} = C_{\text{SB}} \sqrt{\frac{\rho_L - \rho_V}{\rho_V}} \tag{6.9}$$

From Eq. (6.9) the Souders and Brown flooding constant, C_{SB}, can be defined

$$C_{\text{SB}} = u_{S,\text{flood}} \sqrt{\frac{\rho_V}{\rho_L - \rho_V}} \tag{6.10}$$

The Souders and Brown constant, C_{SB}, is the C-factor [Eq. (6.4)] at the flood point. Most modern entrainment flooding correlations retain the Souders and Brown equation (6.10) as the correlation basis, but depart from the notion that C_{SB} is a constant. Instead, they express C_{SB} as a function of several variables (below), which differ from one correlation to another. Depending on the correlation, C_{SB} and $u_{S,\text{flood}}$ are based either on the net area A_N or on the bubbling area A_B.

Variables affecting the capacity factor C_{SB}

- *Tray spacing:* C_{SB} rises with tray spacing. Roughly, C_{SB} is proportional to the tray spacing to a power of 0.5 to 0.6 (7,8,14–17). At low tray spacing (<15 in), the power may be somewhat higher due to the proximity of the froth envelope and/or excessive splashing from the dispersion at the tray.
- *Liquid load:* Figure 6.9*a* is a plot of flood F-factor against liquid load. From Eq. (6.5), it also illustrates the effect of liquid load on the flood C-factor, or C_{SB}. As liquid load increases, C_{SB} first rises, then declines. The decline is slow, as illustrated by the cyclohexane-*n*-heptane curves in Fig. 6.9*a*. Some of the earlier flood correlations (18–20) predict that C_{SB} rapidly diminishes at high liquid loads (as illustrated for the butane curves in Fig. 6.9*a*). Later work, first reported by Gerster et al. (21) and then by many others (15,22–26), however, showed that the rapid decline (such as that for the butane system) is associated with downcomer flooding, and not with entrainment flooding.

  The increase in C_{SB} with liquid loads at very low liquid loads co-

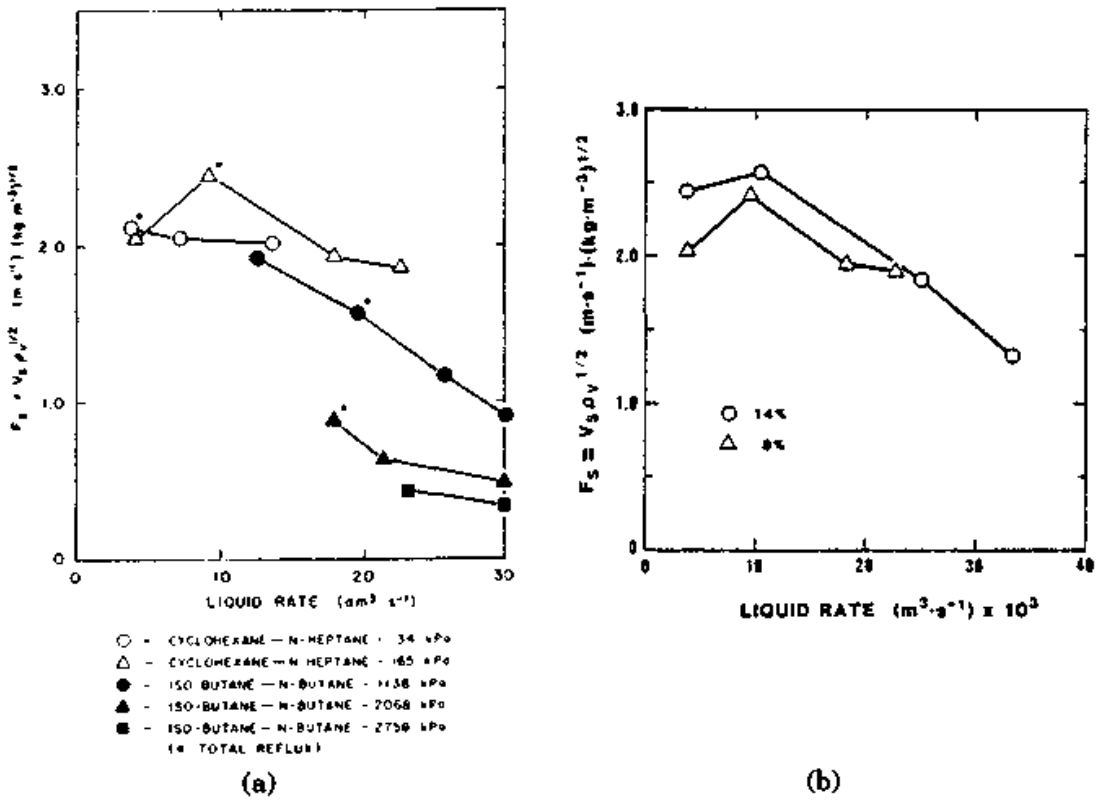

Figure 6.9 Factors affecting the flood capacity factor. FRI sieve tray test data, D_T = 4 ft, S = 24 in, h_w = 2 in, d_H = 0.5 in, straight downcomers, A_D/A_T = 0.13. (*a*) Effect of liquid rate, A_f = 0.08. (*b*) Effect of fractional hole area. Cyclohexane-*N*-heptane, 24 psia. For the cyclohexane-*N*-heptane data, the likely flooding mechanism was spray entrainment flooding. For the butane data, the likely flooding mechanism was downcomer flooding. (Part *a* from M. Sakata and T. Yanagi, *I. Chem. E. Symp. Ser.* 56, p. 3.2/21, 1979. Reprinted courtesy of The Institution of Chemical Engineers, UK. Part *b* reprinted with permission from T. Yanagi and M. Sakata, *Ind. Eng. Chem. Proc. Des. Dev.*, Vol. 21, p. 712, copyright (1982) *American Chemical Society*.)

incides to the decline of entrainment as liquid load is increased, which occurs in the spray regime (15,22–24,27; see Sec. 6.2.11). There is, however, some uncertainty as to whether the limit in this region is that of actual entrainment flooding, or that of excessive entrainment ("blowing").

- *Fractional hole area:* C_{SB} increases with fractional hole area (Fig. 6.9*b*). Roughly, when fractional hole area is between 0.05 and 0.08, an increase in fractional hole area of the order of 0.01 will enhance C_{SB} by about 5 percent (1,18,19,26,28,29). When fractional hole area exceeds 0.1, the rate of increase of C_{SB} with hole area is substantially lower (1,18,19,23,28,29).
- *Hole diameter:* C_{SB} increases as hole diameter is reduced. Roughly, C_{SB} increases with the reciprocal of hole diameter to a power of 0.1 to 0.2 (14,15,26,28).

- C_{SB} is practically independent of pressure in distillation systems (21,25; see also cyclohexane-*n*-heptane curves on Fig. 6.9*a*). This suggests that C_{SB} is, at the most, only a very weak function of physical properties. Further, it suggests that any physical property variations that accompany a change in distillation pressure (and, therefore, also in the equilibrium temperature), do not affect C_{SB}. This contradicts trends predicted by some of the earlier flood correlations (18–20).

Fair's correlation (19, Fig. 6.10). The Fair flood has been the standard of the industry for entrainment flood prediction and was recommended by most designers (5,11,18,30–33). C_{SB} is a function of the flow parameter F_{lv} [Eq. (6.7)], tray spacing, surface tension, and fractional hole area. C_{SB} is based on the net area A_N, and is evaluated from Fig. 6.10. The flooding vapor velocity is calculated from

$$u_{N,\text{flood}} = C_{SB}\left(\frac{\sigma}{20}\right)^{0.2}\sqrt{\frac{\rho_L - \rho_V}{\rho_V}} \tag{6.11}$$

Figure 6.10 applies to a fractional hole area of 0.10 or greater. For fractional hole areas of 0.08 and 0.06, C_{SB} from Fig. 6.10 should be multiplied by 0.9 and 0.8, respectively (18).

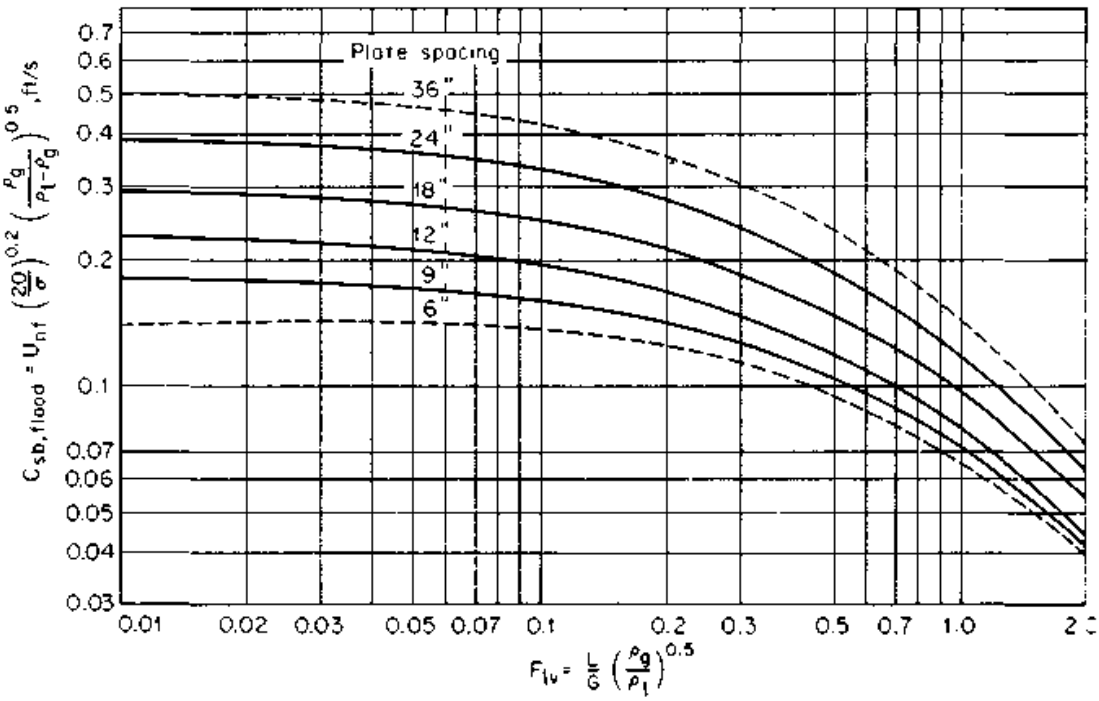

Figure 6.10 Fair's entrainment flooding correlation. (*J. R. Fair, Petro/Chem Eng.* 33 (*10*), *p. 45, 1961, reprinted courtesy of Petroleum Engineer International, Dallas, Texas.*

Fair's correlation applies to nonfoaming or low-foaming systems. For highly foaming systems, the capacity is lower. The correlation applies to sieve trays with holes ½-in or smaller and where weir height does not exceed 15 percent of the tray spacing (18). Fair's correlation also applies to bubble-cap and valve trays (3,18,34). For bubble-cap and valve trays, the fractional hole areas used in the correction term are the ratio of the slot area to bubbling area, and the ratio of full valve-opening area to bubbling area, respectively (18). The correlation can also be used for dual-flow trays with fractional hole area greater than 0.2 (18).

When Fair's correlation was developed, little was known about the difference between spray and froth entrainment flooding, and the data base used was small and included both types. The author compared predictions from Fair's correlation to a much wider data bank available at present. The correlation predicted most of these data well, perhaps somewhat on the conservative side. However, the correlation has been less successful in reliably predicting some of the effects (described above) of physical properties, operating variables, and tray geometry on entrainment flooding.

The Smith et al. correlation (20, Fig. 6.11). This is another early entrainment flooding prediction method that has sometimes been recommended (11). Compared to Fair's correlation, the Smith et al. correlation is claimed (20) to be less conservative. It was derived from a small base of field data for sieve, valve, and bubble-cap trays. Similar to Fair's correlation, Smith's correlation uses C_{SB} versus a flow parameter plot, but here the dependence of C_{SB} on the flow parameter is weaker, and there is no surface tension correction factor. C_{SB} and u_{flood} are both based on the net area A_N, and are evaluated from Fig. 6.11 and Eq. (6.9), respectively. The height over the weir, h_{ow}, is obtained from Eq. (6.49).

The Kister and Haas correlation (15). This is a recent correlation for entrainment flooding

$$C_{SB} = 0.144 \left[\frac{d_H^2\,\sigma}{\rho_L}\right]^{0.125} \left[\frac{\rho_G}{\rho_L}\right]^{0.1} \left[\frac{S}{h_{ct}}\right]^{0.5} \tag{6.12}$$

h_{ct} is the clear liquid height at the transition from the froth to spray regime, based on the Jeronimo and Sawistowski (35) correlation as modified for physical properties by Kister and Haas (36). h_{ct} is calculated using Eqs. (6.68) to (6.70) (15,36).

For surface tensions greater than 25 dynes/cm, the authors recom-

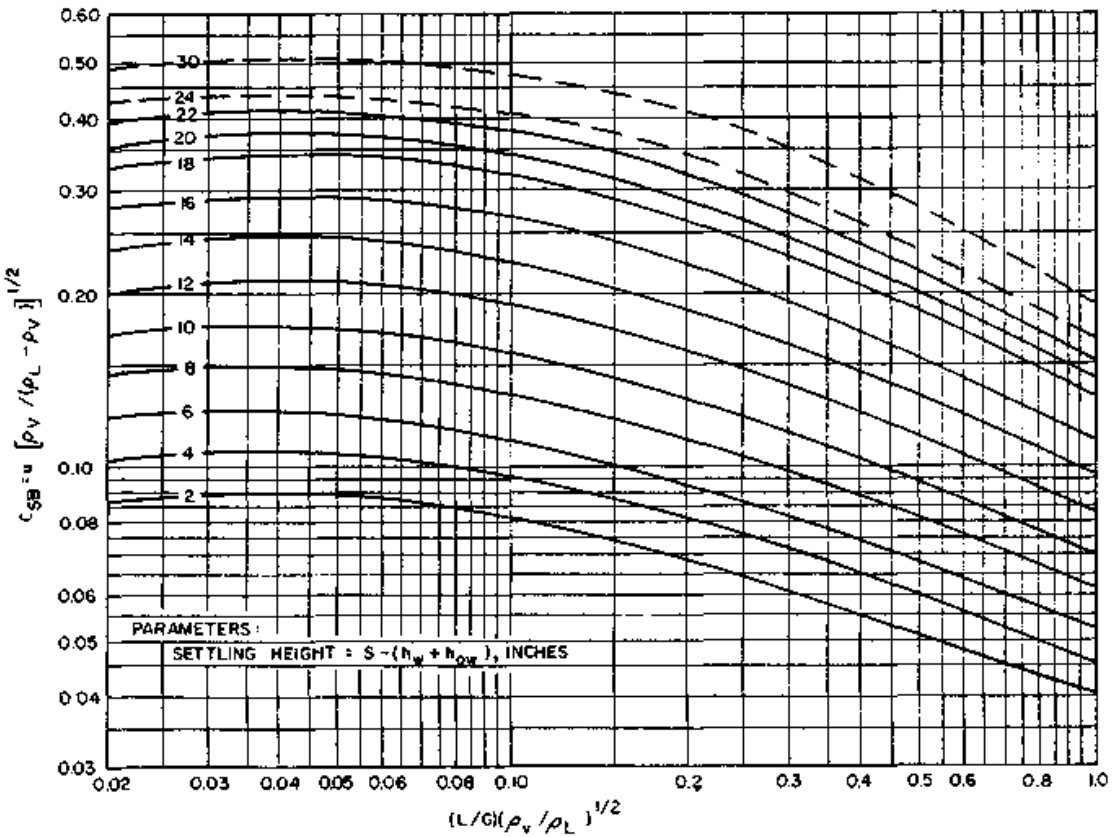

Figure 6.11 The Smith, Dresser, and Ohlswager entrainment flooding correlation. (*R. B. Smith, T. Dresser and S. Ohlswager, Hydrocarb. Proc. & Pet. Ref.*, 40 (5), *p. 183, 1963, reprinted courtesy of Hydrocarbon Processing.*)

mend using the value of 25 dyne/cm in Eq. (6.12). Both C_{SB} and u_{flood} are based on the net area A_N and are calculated from Eqs. (6.12) and (6.9), respectively. The correlation applies for nonfoaming systems at tray spacing greater than 14 in. Other restrictions are listed in Table 6.3. There are four advantages that make this correlation superior to those described above:

- It gives a close approximation to the effects of physical properties, operating variables, and tray geometry on the flood point. This is a major improvement compared to the previous correlations above.
- It was shown to predict most of the presently published sieve-tray and valve-tray entrainment flood data to within ±15 and ±20 percent, respectively. This is an improvement compared to the previous correlations above.
- It can be expressed in terms of dimensionless groups that describe

TABLE 6.3 Recommended Range of Application. The Kister and Haas (15) Entrainment Flood Correlation

Flooding mechanism: Entrainment (jet) flood only
Tray types: Sieve or valve trays only
Pressure: 1.5–500 psia (Note 1)
Gas velocity: 1.5–13 ft/s
Liquid load: 0.5–12 gpm/in of outlet weir (Notes 2, 3, 5)
Gas density: 0.03–10 lb/ft^3 (Note 1)
Liquid density: 20–75 lb/ft^3
Surface tension: 5–80 dyne/cm
Liquid viscosity: 0.05–2.0 cP
Tray spacing: 14–36 in (Notes 4, 5)
Hole diameter: ⅛–1 in
Fractional hole area: 0.06–0.20 (Note 5)
Weir height: 0–3 in

NOTES:

1. At pressures above 150 psia, downcomer flood is often the capacity limitation. This limitation is not predicted by the correlation. Caution is required.
2. At high liquid loads (above 7–10 gpm/in), downcomer flood is often the capacity limitation. This limitation is not predicted by the correlation. Caution is required.
3. Equation (6.70) does not apply for liquid loads lower than 0.5 gpm/in of weir (35). For this reason, this correlation must not be extended to lower liquid rates.
4. At lower tray spacing, entrainment flooding may be related to lifting of the froth envelope and to froth rather than spray height. This correlation must not be extended to lower tray spacing.
5. The correlation does not apply when the following three conditions occur simultaneously. (*a*) Ratio of flow path length to tray spacing is high (>3); (*b*) liquid rate is high (>6 gpm/in of weir); and (*c*) fractional hole area is high (>11%). Under these conditions, entrainment flooding is related to vapor channeling and vapor cross flow rather than spray height.

spray regime entrainment. It therefore has stronger theoretical basis compared to the previous correlations above.

- It was derived from a much wider data base of commercial- and pilot-scale columns data.

Valve trays. Manufacturer literature contains correlations for entrainment flooding (7–9). The three sieve tray correlations above are also applicable to valve trays. Of the three, the author recommends the Kister and Haas (15) correlation because it was specifically extended for valve trays and because it possesses the advantages listed above. When applying this correlation to valve trays, A_f is the fractional hole area when all valves are open, i.e.,

$$A_f = (\text{Total area of opening of all valves when fully open})/A_B = A_{So}/A_B \quad (6.13)$$

while d_H is taken as the equivalent hydraulic diameter of a fully open valve opening given by

$$d_H = \frac{4\,(\text{Area of opening of one fully open valve})}{(\text{Wetted perimeter of opening of one fully open valve})} \quad (6.14)$$

For a round valve with a diameter d_v at the narrowest opening, the expressions for A_f and d_H are

$$A_f = \frac{N_v \pi d_v h_v}{144 A_B} \quad (6.15)$$

and

$$d_H = \frac{2\pi d_v h_v}{\pi d_v + h_v} \quad (6.16)$$

Froth entrainment flooding. Most of the work reported in the literature lumps spray and froth regime entrainment flooding together. Froth entrainment flooding is far less common than spray entrainment flooding, and occurs mainly at close (<18 in.) tray spacing, when the froth envelope can approach the tray above. Some flood data at close tray spacing that pertains to froth entrainment flooding were reported (14,20,37,38). Froth regime entrainment work (37–41) is also relevant to froth entrainment flooding.

The factors affecting froth entrainment flooding differ from those affecting spray entrainment flooding. The critical variable is the distance between the top of the froth and the tray above (20,39,41). This

implies that the flood velocity strongly increases as tray spacing is raised, liquid load is lowered and weir height is lowered. Some flood and entrainment data (37–40) confirm this trend. On the other hand, tray geometry variables such as hole diameter and fractional hole area can be expected to have a lesser effect (if any) on froth entrainment flooding. This was confirmed by entrainment data (38–40) but not by flood data.

Froth entrainment flood can be predicted using the Fair or the Smith et al. correlations. Both included froth entrainment flood data in their data base. Testing of Fair's correlation (20,41) against a handful of more recent data suggests that it gives conservative froth entrainment flood predictions. The Smith et al. correlation is claimed (20) to be less conservative. The Kister and Haas correlation is unsuitable for froth entrainment flood prediction.

Froth entrainment flooding is only encountered at close tray spacing. It can be excluded from any capacity checks when tray spacing exceeds 18 in (except when conditions are conducive to vapor cross flow, Sec. 6.2.4). Note that at low tray spacing (< 18 in), either spray or froth entrainment flooding can restrict capacity.

6.2.7 Downcomer backup flooding.

Downcomer backup flooding occurs when the backup of aerated liquid in the downcomer exceeds the tray spacing, i.e.,

$$h'_{dc} = S + h_w \tag{6.17}$$

where

$$h'_{dc} = h_{dc}/\phi_{dc} \tag{6.18}$$

Downcomer backup. The factors that resist liquid flow from the downcomer onto the tray below are the froth height on the tray, the pressure drop on the tray, and the friction loss under the downcomer apron. These factors cause liquid to back up in the downcomer. Each of these factors can be expressed in terms of clear liquid heads. A tray pressure balance gives

$$h_{dc} = h_c + h_t + h_{da} \tag{6.19}$$

The clear liquid height is equal to the sum of the weir height, the height over the weir, and half the hydraulic gradient, giving

$$h_c = h_w + h_{ow} + h_{hg}/2 \tag{6.20}$$

and Eq. (6.19) becomes

$$h_{dc} = h_t + h_w + h_{ow} + \frac{h_{hg}}{2} + h_{da} \tag{6.21}$$

Calculation of each of the individual terms in Eq. (6.21) is described in Secs. 6.3.1 to 6.3.4.

6.2.8 Downcomer aeration

The downcomer aeration factor ϕ_{dc} is defined by Eq. (6.18). It describes the fractional volumetric liquid holdup in the downcomer.

Mechanism. Vapor enters the downcomer with the froth that flows over the outlet weir. Additional vapor is entrained into the liquid due to the impact of the falling liquid on the liquid surface in the downcomer, in the same manner as a waterfall induces air entrainment into the pool below it. Inside the downcomer, vapor disengages from the liquid due to its higher buoyancy. The driving force for vapor disengagement is the density difference between the liquid and the vapor.

Figure 6.12*a* shows the structure of the fluid mixture in a downcomer operated at low liquid rates with a nonfoaming mixture. At the upper (froth) zone of the downcomer, the vapor fraction is high and of the same order as in the tray froth. As the mixture travels downward, much of the vapor is disengaged. The froth zone transforms into an aerated liquid zone where vapor bubbles rise through a liquid pool. Upon further vapor disengagement, the aerated liquid zone transforms into a clear liquid zone.

Factors affecting downcomer aeration

- *Foaming tendency:* Vapor disengagement is easy in nonfoaming low-pressure systems. Vapor disengagement from downcomer liquid in foaming systems is difficult as the liquid hangs on to the entrained vapor. At high pressure, vapor disengagement from liquid is difficult because of the smaller vapor-liquid density difference (i.e., lower vapor buoyancy). In distillation systems, the decrease in surface tension as pressure (and, therefore, equilibrium temperature) rises promotes foaminess, and further retards vapor disengagement.
- *Liquid flow rate:* At low liquid flow rates, with nonfoaming systems, the line of demarcation between zones in Fig. 6.12*a* is fairly sharp (42). As liquid rate increases, so does the fractional gas holdup in the downcomer liquid. Lockett and Gharani (43) found

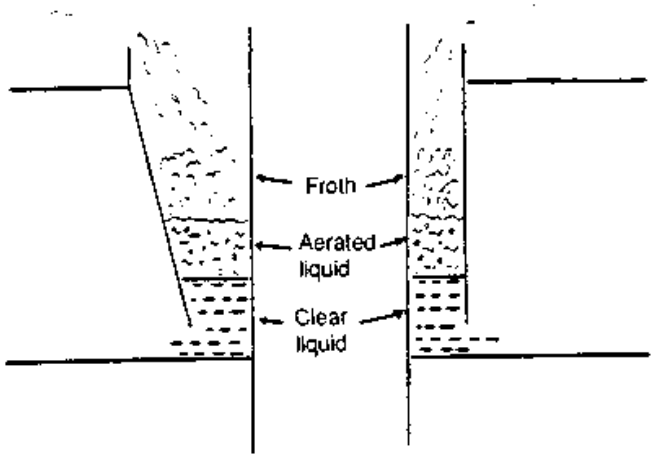

(a)

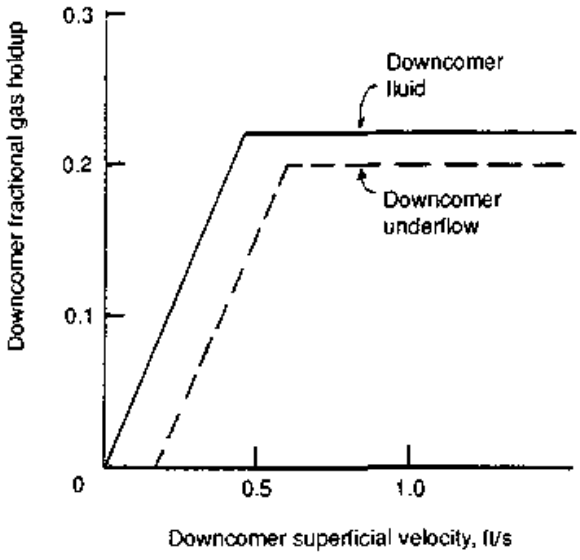

(b)

Figure 6.12 Downcomer aeration. (*a*) Structure of two-phase mixture in the downcomer; (*b*) dependence of downcomer and downcomer underflow gas fraction on downcomer liquid velocity, air-water tests. (*Data for part b based on M. J. Lockett and A. A. W. Gharani, I. Chem. E. Symp. Ser. 56, p. 2.3/43, The Institution of Chemical Engineers UK, 1979.*)

that this continues up to a certain critical velocity, beyond which the fractional gas holdup (and therefore downcomer aeration) becomes constant and independent of the liquid load (Fig. 6.12*b*). They also observed that when this point was reached, pressure drop on

the tray started increasing rapidly suggesting downcomer-choke flooding (Sec. 6.2.9).

Downcomer vapor underflow. In the past, it was thought that downcomer velocity needed to be kept small to avoid vapor being carried under the downcomer apron to the tray below. Thomas (42) and Lockett and Gharani (43), however, showed that some vapor underflow exists even at velocities considered "safe." The latter authors showed that the gas fraction in the downcomer underflow depends on downcomer superficial liquid velocity in a manner similar to downcomer gas fraction (Fig. 6.12*b*).

Downcomer vapor underflow ("vapor entrainment" or "gas recycle") is analogous to liquid entrainment. It reduces both tray capacity and efficiency (17,44,45). In low- and medium-pressure distillation systems, where gas density is significantly lower than liquid density, it takes only a small quantity of gas to generate volumes comparable to the liquid volumetric flow rate. The quantity of gas recycle is therefore small, and it has little effect on tray performance. At high pressures, the quantity of gas recycled is significant. An analysis of some FRI data (44) for iC_4–nC_4 distillation showed vapor entrainment increases from about 7 percent at 165 psia to about 50 to 60 percent at 400 psia on a molar basis.

Downcomer aeration factor prediction. The fractional liquid holdup varies from about 0.3 in the froth zone to close to unity in the clear liquid zone (Fig. 6.12*a*). The height of each zone is a complex function of system properties, operating conditions, and downcomer geometry. This makes it practically impossible to theoretically predict the average downcomer aeration factor ϕ_{dc}. Correlations in the literature (e.g., 46) are based on limited data obtained in atmospheric pressure simulator work with small downcomers. It is therefore difficult to recommend them for commercial-size applications. Zuiderweg (17) presented a plot of downcomer aeration factors derived theoretically from commercial-scale high-pressure flood data. However, the plot is based on a handful of data and is therefore difficult to recommend for general aeration factor prediction.

Popular aeration factor prediction criteria are rules of thumb based on the foaming tendency of the system (Table 6.4). The three criteria listed are supplementary, with one criterion adding examples not listed by the others. The author recommends applying the criteria accordingly. For instance, an aeration factor of 0.4 is appropriate to either mineral oil absorbers or for systems whose vapor density exceeds 3 lb/ft^3. The criterion of Fair et al. (18) is perhaps a little conservative compared to the others.

TABLE 6.4 Criteria for Downcomer Aeration Factors

Foaming tendency	Bolles' criterion (47)		Glitsch's criterion (7)		Fair et al's criterion (18)	
	Examples	ϕ_{dc}	Examples	ϕ_{dc}	Examples	ϕ_{dc}
Low	Low-molecular-weight hydrocarbons* and alcohols	0.6	$\rho_G < 1.0$ lb/ft^3	0.6	Cases favoring rapid bubble rise such as low gas density, low liquid viscosity	0.5
Moderate	Distillation of medium-molecular-weight hydrocarbons	0.5	$1.0 < \rho_G < 3.0$ lb/ft^3	0.5		
High	Mineral oil absorbers	0.4	$\rho_G > 3.0$ lb/ft^3	0.4		
Very high	Amines, glycols	0.3			Cases favoring slow bubble rise, such as high gas density, high liquid viscosity, foaming systems	0.2–0.3

*The author believes that "low-molecular-weight hydrocarbons" refers to light hydrocarbons at near atmospheric pressure or under vacuum. The foam stability of light hydrocarbon distillation at medium and high pressure is best inferred from the Glitsch criterion.

6.2.9 Downcomer choke flooding

A downcomer must be sufficiently large to transport all of the liquid downflow without choking. If the friction losses in the downcomer and/or downcomer entrance are excessive, liquid will back up onto the tray and eventually flood the column. This is termed *downcomer choke*. The prime design parameter is the downcomer top area, where friction losses are highest. Further down the downcomer, vapor disengages and the aerated liquid downflow is greatly reduced. With sloped downcomers, the downcomer bottom area is normally set at about 1.7 to 2 times less than the area at the top of the downcomer (1,8,9,10,48). This taper is small enough to keep the downcomer top area the prime downcomer choke variable.

Criteria for determining downcomer area are described below. The author recommends that the downcomer area is set large enough to satisfy all of these criteria. A more detailed discussion is available elsewhere (1).

Downcomer velocity. The most popular criteria for maximum velocity of clear liquid at the downcomer entrance are the Glitsch (7), Koch (8), and Nutter (9) correlations. Lockett (12) noted large differences between the predictions of these correlations, but made no recommendations on which correlation to use. Lockett's analysis shows that generally the Glitsch correlation tends to predict the highest downcomer velocities, while the Koch correlation tends to predict the lowest downcomer velocities, with the Nutter correlation giving intermediate values. The Glitsch correlation (7) is

$$(Q_{D,\max})_1 = 250 \tag{6.22}$$

$$(Q_{D,\max})_2 = 41\sqrt{\rho_L - \rho_G} \tag{6.23}$$

$$(Q_{D,\max})_3 = 7.5\sqrt{S\,(\rho_L - \rho_G)} \tag{6.24}$$

$$Q_{D,\max} = [(Q_{D,\max})_1 \text{ or } (Q_{D,\max})_2 \text{ or } (Q_{D,\max})_3, \text{ whichever is lowest}] \times \text{SF} \tag{6.25}$$

SF is the derating factor (Sec. 6.2.10); if no derating, SF = 1.0.

The Koch correlation (8) and Nutter correlation (9) are maximum residence time criteria (see below) which were converted into downcomer velocity criteria. The maximum downcomer velocity is calculated from

$$Q_{D,\max} = 448.8\left(\frac{S}{12\,t_R}\right)\text{SF} \qquad S \le 30 \tag{6.26}$$

The values of t_R to be used in Eq. (6.26) are given by Fig. 6.13.

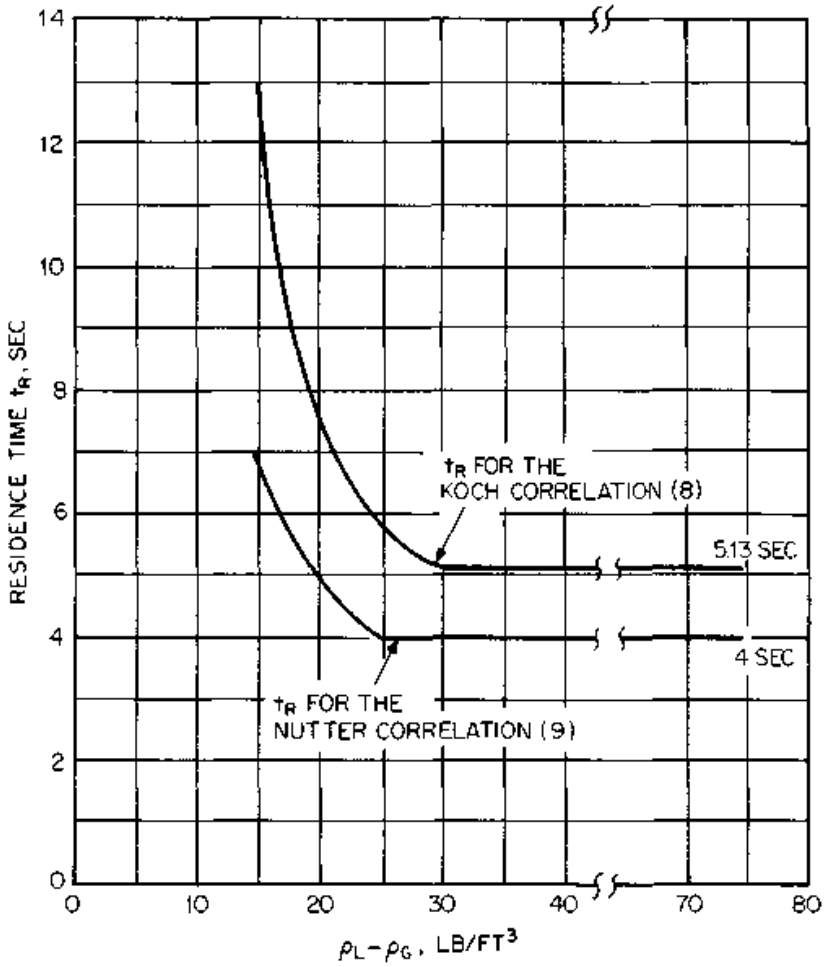

Figure 6.13 Values of downcomer residence time t_R to be used in the Koch correlation and in the Nutter correlation for maximum downcomer velocity [Eq. (6.26)]. Data based on Koch Engineering Co. Inc. *Design Manual-Flexitray*, Bulletin 960-1, Wichita, Kansas, 1982 and on Nutter Engineering *Float Valve Design Manual*, Tulsa, Oklahoma, 1976.

Kister (1) surveyed the multitude of published criteria for maximum downcomer velocity. He pointed at the poor accuracy and inconsistency of these criteria, then incorporated them together with his own experience into the single set of guidelines shown in Table 6.5. The values in Table 6.5 are not conservative, and some may even be slightly optimistic. For a conservative design, a value from Table 6.5 can be multiplied by a safety factor of 0.75.

Residence time in downcomers. Sufficient residence time must be provided in the downcomer to allow adequate disengagement of vapor from the descending liquid, so that the liquid is relatively vapor free by the time it enters the tray below. Inadequate removal of vapor from the liquid may choke the downcomer.

Two different definitions are used for downcomer residence time (3).

TABLE 6.5 Maximum Downcomer Velocities

Foaming tendency	Example	Clear liquid velocity in downcomer, ft/s		
		18-in spacing	24-in spacing	30-in spacing
Low	Low-pressure (<100-psia) light hydrocarbons, stabilizers, air-water simulators	0.4–0.5	0.5–0.6	0.6–0.7
Medium	Oil systems, crude oil distillation, absorbers, midpressure (100–300 psia) hydrocarbons	0.3–0.4	0.4–0.5	0.5–0.6
High	Amine, glycerine, glycols, high-pressure (>300-psi) light hydrocarbons	0.2–0.25	0.2–0.25	0.2–0.3

SOURCE: From H. Z. Kister, *Distillation Operation*, Copyright © 1990 McGraw-Hill, Inc. Reprinted by permission.

The *apparent residence time* is the ratio of the downcomer volume to the clear liquid flow in the downcomer. The downcomer volume is the tray spacing times the average downcomer cross-section area. The *true residence time* is the ratio of froth volume in the downcomer to the frothy liquid flow in the downcomer. The true residence time can alternatively be expressed as the ratio of the clear liquid volume in the downcomer to the clear liquid flow. The definition adopted here is that of the apparent downcomer residence time. The author found this definition to be better and to be consistent with published criteria for downcomer residence times (1).

Kister (1) reviewed various published criteria available for downcomer residence times, and recommended those by Bolles (47) and Erbar and Maddox (49). Both sets of guidelines are similar, and express downcomer residence time as a function of the system's tendency to foam (Table 6.6).

Minimum downcomer width and minimum downcomer area. As the downcomer becomes smaller, its width decreases faster than its length, turning the downcomer into a long and narrow slot. This geometry increases the resistance to liquid downflow and to upflow of disengaging vapor. Small downcomers are also extremely sensitive to foaming, fouling, construction tolerances, and introduction of debris. Smaller weirs associated with small downcomers distort the liquid flow pattern as it approaches the weir ("weir constriction effect"), which in-

TABLE 6.6 Recommended Minimum Residence Time in the Downcomer

Foaming tendency	Example	Residence Time, s
Low	Low-molecular-weight hydrocarbons,* alcohols	3
Medium	Medium-molecular-weight hydrocarbons	4
High	Mineral-oil absorbers	5
Very high	Amines and glycols	7

*The author believes that "low-molecular-weight hydrocarbons" refers to light hydrocarbons at atmospheric conditions or under vacuum. The foaming tendency of light hydrocarbon distillation at medium pressure (> 100 psia) is medium; at high pressure (>300 psia) is high.
SOURCE: Bolles, W. L. (Monsanto Company), private communication, 1977.

creases tray pressure drop (2–4,18) and promotes the formation of stagnant regions near the tray periphery. Such stagnant regions may be detrimental to column efficiency (Sec. 7.3.3).

Generally, downcomers smaller than 5 to 8 percent of the column cross-section area should therefore be avoided (1,5,10,12,30,43,50). This rule is often expressed as a minimum ratio of weir length or downcomer width to column diameter. An alternative rule for small (<10 percent of column area) downcomers (7,51) is to set the minimum downcomer area to either twice the area calculated using the normal downcomer area criteria or 10 percent of the column cross-section area (whichever is smaller). Additional discussion on small downcomers is elsewhere (1).

If liquid flows are extremely small, and the system is nonfoaming, circular or envelope downcomers may be installed within the area subtended by a segmental weir (1,10). These should have twice the area calculated using the normal design procedure.

6.2.10 Derating ("system") factors

With certain systems, traditional flooding equations (e.g., Secs. 6.2.6 to 6.2.9) consistently predict higher flood points than those actually experienced. To allow for this discrepancy, an empirical *derating* or *system factor* SF (such that SF <1.0) is applied. To obtain the actual or derated flood load for a given system, the predicted flood vapor load (entrainment flooding) or liquid load (downcomer choke) obtained from the traditional equation is multiplied by the derating factor. In case of downcomer backup flood, the froth height predicted from the correlation is divided by the derating factor.

Derating factors are often vaguely related to the foaming tendency

TABLE 6.7 Derating Factors

System	Factor	Reference	Notes
Nonfoaming regular systems	1.0	7,8,9,12	
High pressure ($\rho_G > 1.8$)	$1.21/\rho_G^{0.32}$	8	Do not double-derate.
	Low-foaming		
Depropanizers	0.9	12	
H_2S strippers	0.9	9,12	
	0.85	8	
Fluorine systems (Freons, BF_3)	0.9	7,12	
Hot carbonate regenerators	0.9	8,12	
	Moderate-foaming		
Deethanizers			
Absorbing type, top section	0.85	7,8,9,12	
Absorbing type, bottom section	1.0	9	
	0.85	7,8,12	
Refrigerated type, top section	0.85	12	
	0.8	9	
Refrigerated type, bottom section	1.0	7,9	
	0.85	12	
Demethanizers			
Absorbing type, top section	0.85	7,8,9	
Absorbing type, bottom section	1.0	9	
	0.85	7,8	
Refrigerated type, top section	0.8	9	
Refrigerated type, bottom section	1.0	9	
Oil absorbers			
Above 0°F	0.85	7,8,9,12	Ref. 8 proposes these
Below 0°F	0.95	9	for "absorbers" rather
	0.85	7,12	than "oil absorbers."
	0.8	8	
Crude towers	1.0	9	
	0.85	12	
Crude vacuum towers	1.0	9	
	0.85	8	

of the system. The higher the foaming tendency, the lower the derating factor. Derating factors are not unique to foaming systems. They are applied to nonfoaming systems where experience has consistently shown that standard flooding equations predict too high. Sometimes derating factors are used solely as overdesign factors. Typical derating factors found in the literature are listed in Table 6.7.

The application of derating factors is fraught with confusion. Caution is required, especially when communicating with an outside company whose derating practices may differ. The following need to be carefully specified.

TABLE 6.7 Derating factors (*Continued*)

System	Factor	Reference	Notes
Furfural refining towers	0.85	8	
	0.80	12	
Sulfolane systems	1.0	9	
	0.85	12	
Amine regenerators	0.85	7,8,9,12	
Glycol regenerators	0.85	7,12	
	0.8	9	
	0.65	8	
Hot carbonate absorbers	0.85	8,12	
Caustic wash	0.65	8	The author suspects that this low factor refers only to some caustic wash applications but not to others.
	Heavy-foaming		
Amine-absorbers	0.8	8	
	0.75	9,12	
	0.73	7	
Glycol contactors	0.73	7	Ref. 8 recommends 0.65 for glycol contactors in glycol synthesis gas service, 0.5 for others.
	0.65	9,12	
	0.50	8	
Sour water strippers	0.5–0.7	9	
	0.6	8	
Oil reclaimer	0.7	8	
MEK units	0.6	7,12	
	Stable foam		
Caustic regenerators	0.6	8	
	0.3	7,12	
Alcohol synthesis absorbers	0.35	8,12	

1. The flooding mechanism to which the derating factor applies (entrainment flood, downcomer backup, downcomer choke, or all).
2. Avoiding double derating. For instance, the values in Table 6.7 apply with the equations in Sec. 6.2.6, since these do not take foaminess into account. However, they will double-derate the flood calculation if applied jointly with a correlation or criterion that

already takes foaminess into account (e.g., the criteria for downcomer backup flooding or downcomer choke in Tables 6.4 to 6.6). Similarly, two different factors from Table 6.7 may apply to a single system; only one of them should be used.

3. Choosing the appropriate value for the derating factor. Derating factors vary from source to source, and may depend on the correlation used as well as the application. For instance, some caustic wash applications have a track record of foaming more severely than other caustic wash applications (see note in Table 6.7). The derating factors in Table 6.7 are useful as a guide, but are not absolute.

6.2.11 Entrainment

Entrainment (Figure 6.14) is liquid transported by the gas to the tray above. This liquid contains more of the less-volatile material than the tray above, and therefore it counteracts the mass transfer process and reduces tray efficiency. Other undesirable effects of entrainment are carryover of nonvolatile impurities upward to contaminate the overhead product and the possibility of damage to rotating machinery located in the path of the column overhead vapor.

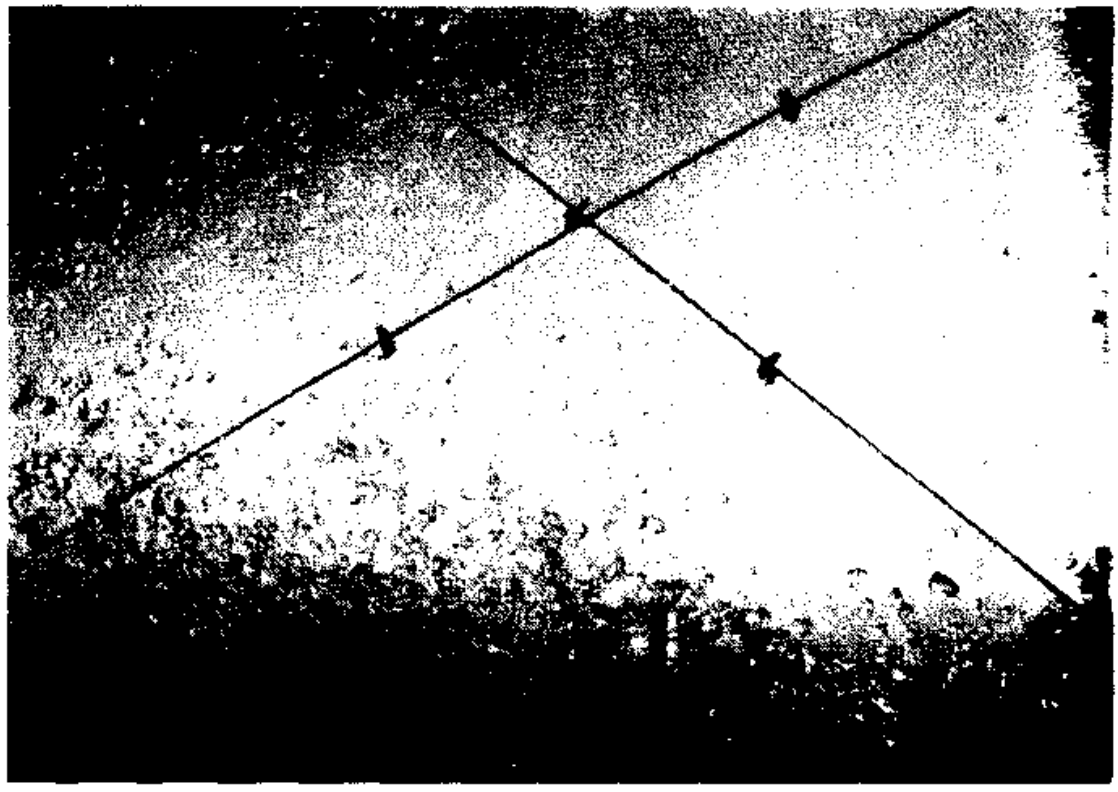

Figure 6.14 Entrainment. [*Reprinted courtesy of Fractionation Research Inc. (FRI).*]

Mechanism. In the froth regime, most tray holes are bubbling; entrainment is produced by breakup of liquid sheets defining emergent bubble. The mechanism forms small drops (typically <200 μm) at low projection velocities (52), resulting in low entrainment. In the fully developed spray regime, most holes are continuously jetting; entrainment is produced by atomization of liquid by gas jets passing through the tray holes. This mechanism forms large drops (typically >1000 μm) at high projection velocities, resulting in high entrainment. When the spray regime is only partially developed on the tray, both bubbling and jetting occur simultaneously at adjacent tray holes. Entrainment produced by the holes undergoing jetting far outweighs that from holes which are bubbling. Entrainment in the partially developed spray region is therefore similar to entrainment in the fully developed spray regime (40).

Effect of vapor velocity. Entrainment increases with vapor velocity to a high power (19,22,23,26,27,36,38–40,53,54). Most investigations report a power between 2 and 5, but in some cases as little as a 10 percent change in vapor rate results in a tenfold change in entrainment (22,36). Generally, smaller powers, indicative of a relatively gradual change, are typical of low-pressure systems, while high powers, which indicate a steep change, are typical of high-pressure systems.

At high pressure, the vapor velocity at which entrainment becomes significant tends to coincide with the flood point. Due to the rapid rise of entrainment with vapor velocity, it only takes a small additional velocity rise to escalate entrainment past the point of flooding initiation. Conversely, a small vapor velocity reduction lowers entrainment to a negligible extent. At low pressure, the rate of change of entrainment with vapor velocity is much slower, and entrainment can be significant even when the tray operates well below the flood point. For this reason, excessive entrainment is a common problem in low-pressure and vacuum systems, but is seldom troublesome with high-pressure systems (unless operated right near the flood point).

Effect of liquid rate. At low liquid rates, entrainment diminishes with higher liquid loads, while at high liquid rates entrainment increases with liquid loads (22,24,26,38,40,53–55; Fig. 6.15). When most of the dispersion is in the form of a spray, entrainment diminishes with higher liquid loads (22,24,27). The point at which the trend reverses, and entrainment begins to increase with liquid rate, has been interpreted either as the point where the dispersion changes from partially developed spray to froth (40,53), or where the dispersion changes from the spray to froth regime (22–24,45,55).

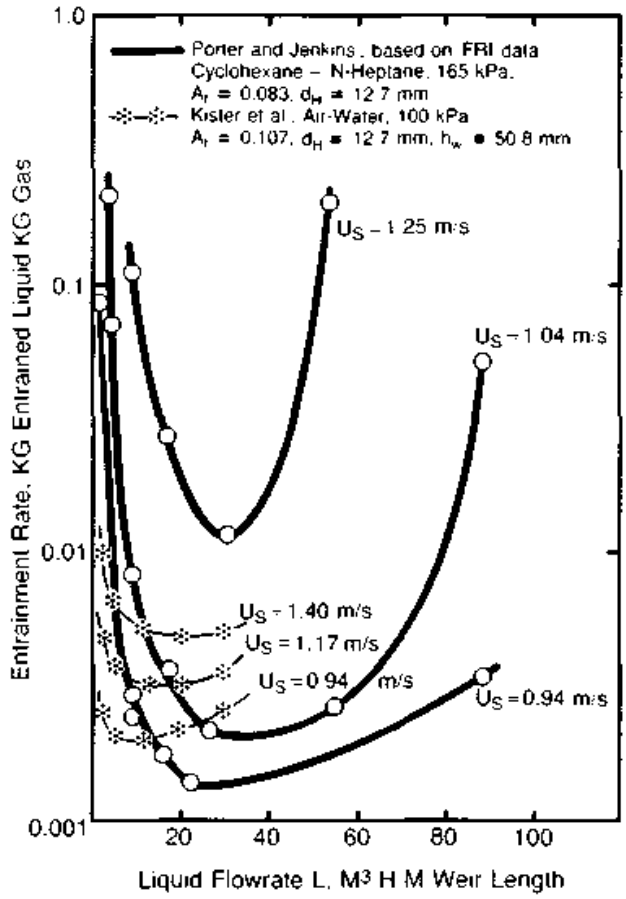

Figure 6.15 Plots of entrainment versus liquid flow rate featuring entrainment minima. (*H. Z. Kister and J. R. Haas, I. Chem. E. Symp. Ser. 104, p. A483, 1987, reprinted courtesy of the Institution of Chemical Engineers, UK.*)

Effect of other variables. Entrainment diminishes with an increase in tray spacing (27,36,39,40,54) and increases with hole diameter (26,27,36,40,52–54). This hole diameter effect is large in the spray regime, and small in the froth regime (40). Entrainment generally increases as the fractional hole area is reduced, particularly when the dispersion is essentially in the form of a spray (23,27,36,38,52,53); however, when the dispersion is essentially frothy and the fractional hole area exceeds 10 percent, fractional hole area has little effect on entrainment (23,38,40,53). Entrainment shows a small dependence on weir height, with low weirs tending to cause more entrainment in the spray type of dispersions (38,40,53) and high weirs tending to cause more entrainment in the frothy type of dispersions (38,40,53,54). Entrainment diminishes with higher surface tension (39). A detailed analysis of the effects of tray geometry on entrainment is presented elsewhere (27,36,40).

Entrainment prediction. For spray regime entrainment, the Kister and Haas correlation (36) was shown to give good predictions to a wide commercial- and pilot-scale data bank. This correlation is

$$E_S = 4.742^{(10/\sqrt{\sigma})^{-1.64}} \chi^{(10/\sqrt{\sigma})} \tag{6.27}$$

where

$$\chi = 1.684\left(\frac{u_B h_L}{\sqrt{d_H S}}\right)^4 \left(\frac{\rho_G}{Q_L \rho_L}\right)\left(\frac{\rho_L - \rho_G}{\sigma}\right)^{0.25} \tag{6.28}$$

and

$$h_L = \frac{h_{ct}}{1 + 0.0665 h_w} \tag{6.29}$$

The clear liquid height at the froth-to-spray transition, h_{ct}, is calculated using the Jeronimo and Sawistowski (35) correlation, as modified for physical properties by Kister and Haas (36). The relevant equations are Eqs. (6.68) to (6.70). The recommended range of application of the correlation is shown in Table 6.8.

Koziol and Mackowiak (55*a*) found the Kister and Haas correlation to give good agreement with experimental data. They developed a new dimensionless correlation [thus overcoming the need for a dimensional exponent in Eq. (6.27)] for spray regime entrainment at very low liquid rates (0.1–1.5 gpm/in). Their correlation, however, postulates that entrainment rises with tower diameter at the same steep rate at which it rises with hole diameter. This postulate conflicts with the industry's experience that entrainment does not increase upon tower diameter scale-up.

An early entrainment correlation by Fair (19,34) was recommended by many design publications (5,18,30–33). In the spray regime, Fair's correlation gives reasonable predictions (36), but is less accurate than the Kister and Haas correlation. The same conclusion was reached in-

TABLE 6.8 Recommended Range of Application for the Kister and Haas (36) Spray Regime Entrainment Correlation

Flow regime	Spray only
Pressure	3–180 psia
Gas velocity	1.3–15 ft/s
Liquid flow rate	0.5–4.5 gpm/in
Gas density	0.03–2 lb/ft^3
Liquid density	30–90 lb/ft^3
Surface tension	5–80 dyne/cm
Liquid viscosity	0.05–2 cP
Tray spacing	15–36 in
Hole diameter	⅛–¾ in
Fractional hole area	0.07–0.16
Weir height	½–3 in

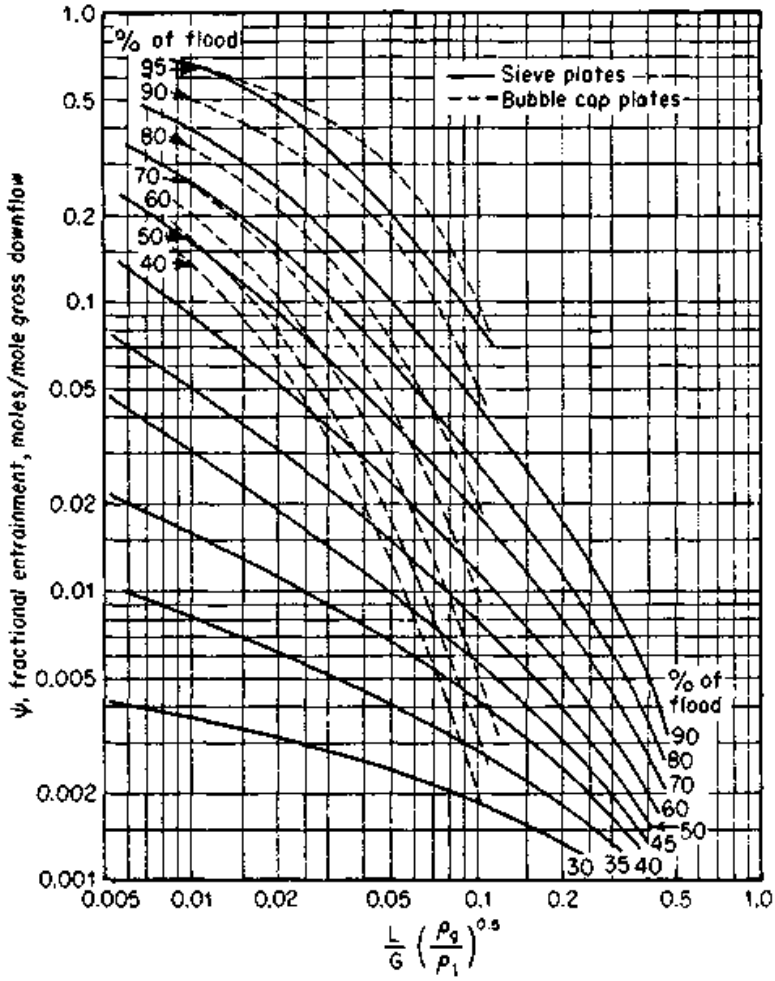

Figure 6.16 Fair's entrainment correlation. (*J. R. Fair, Petro/Chem Engr.* 33 (*10*), *p. 45, 1961, reprinted courtesy of Petroleum Engineer International, Dallas, Texas.*)

dependently by the extensive data analysis of Koziol and Mackowiak (55*a*). In the froth regime, the Kister and Haas correlation does not apply, and Fair's correlation has little competition. Fair's correlation (Fig. 6.16) predicts entrainment in terms of the flow parameter [Eq. (6.7)], and the ratio of gas velocity to flooding gas velocity. Fractional entrainment is defined as

$$\psi = \frac{e}{L_o + e} \tag{6.30}$$

The restrictions applying to the use of Fair's flooding correlation (Sec. 6.2.6) also apply to the use of Fair's entrainment correlation (5).

Several other entrainment correlations have been reported in the literature (17,27,29,39,40,54). Some of their limitations were described elsewhere (12,36,40). In the spray regime, Koziol and Mackowiak

(55*a*) described the agreement between two of these correlations (17,29) and experimental data as "rather poor."

6.2.12 Sieve tray weeping

Weeping is liquid descending through the tray perforations. Under weeping conditions, part of the liquid flows over the outlet weir while the rest descends through the perforations. The liquid descending through the perforations short-circuits the primary contacting zone, causing a reduction in tray efficiency.

At the tray floor, the static liquid head tends to force liquid down through the perforations. The vapor pressure drop counteracts the downward force and acts to keep liquid on the tray. Weeping takes place when the liquid head on the tray exceeds the pressure drop that is holding the liquid on the tray.

For most systems and tray designs, weeping takes place to some extent under practically all conditions. Sloshing and oscillation of liquid on the tray cause the liquid depth to vary instantaneously at different locations on the tray. With the pressure essentially constant in the vapor space below, weeping occurs at those locations where the liquid head is temporarily high, even when the average head on the plate does not exceed the tray vapor pressure drop.

Weeping may not be uniform across the tray. Tests by Banik and Lockett (56,57) in a 4 ft × 2 ft rectangular simulator showed fairly uniform weeping at low weir heights. With higher weirs (2 in and more), most of the weep issued from the inlet half of the tray at low liquid rates (<3 gpm/in of outlet weir), while at high liquid rates (>6 gpm/in of outlet weir) most of the weep issued from the exit half of the tray. A tray with high fractional hole area was observed to weep mostly from the inlet region even at high liquid flow rates. When weeping was nonuniform, some areas appeared to be totally bubbling while others totally weeping.

Some weep can be tolerated without appreciably affecting tray efficiency (4,58,59). Some mass transfer to and from the weeping liquid occurs, and this reduces the impact of bypassing on efficiency (60). Weep from the exit half of the tray is far less detrimental to tray efficiency than weep from the inlet half of the tray (57), and can be tolerated to a much greater degree.

The weep point is defined as the vapor rate when weeping first becomes noticeable. At that point, little efficiency is lost. As vapor rate is reduced below the weep point, the fraction of tray liquid falling through the holes increases, and the reduction in efficiency becomes more noticeable. When this fraction is sufficiently large to effect a sig-

nificant reduction in tray efficiency, the actual lower tray operating limit is reached.

The mechanism of weeping is not well understood. Lockett and Banik (56) observed the weeping mechanism to vary with hole diameter and with the weep rate (Fig. 6.17). In one mechanism, weeping liquid bridged into a layer that covered the underside of the tray, sometimes extending over holes (⅛-in holes), at other times not (½-in holes, slight weep). Liquid disengaged as streams from this layer. In another mechanism, liquid jets disengaged directly from the holes. The jets sometimes filled the hole (¼-in holes; heavy weep from ½-in holes), at other times did not (½-in holes, moderate weep).

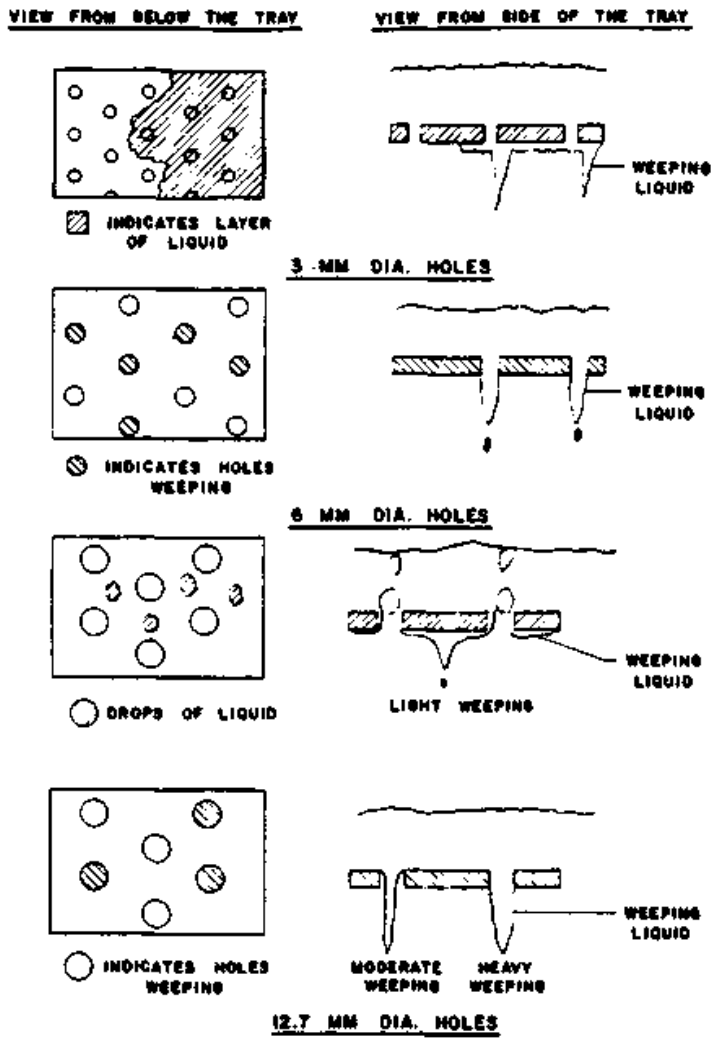

Figure 6.17 Sieve tray weeping mechanisms. [*Reprinted with permission from M. J. Lockett and S. Banik, Ind. Eng. Chem. Proc. Des. Dev., vol. 25, p. 561, Copyright (1986) American Chemical Society.*]

Factors affecting weeping. Weeping tendency increases with

- Larger fractional hole area (4,39,56–63).
- Larger liquid rate (26,56,63–65).
- Taller weirs (28,48,63). Lockett and Banik (56) observed that taller weirs increased the weeping tendency, except (1) at high liquid rates and high weirs (2) at high vapor rates, low liquid rates, and low weirs. In both of these exceptions, weir height had little effect on weeping.
- The effect of hole diameter varies, possibly due to the variation of the weeping mechanism with hole size (Fig. 6.17). Lemieux and Scotti (26) noted that the weep tendency is greater for large holes at low liquid rates, but for small holes at high liquid rates. Kreis and Raab (28) noted that the weeping tendency increases with hole diameter for holes smaller than 3/16 in at low liquid rates, and for holes smaller than ½ in at high liquid rates. For larger holes, they observed no effect of hole diameter on the weeping tendency. Lockett and Banik (56) observed that over a wide range of liquid flows, the weeping tendencies for ⅛-in and ½-in holes were comparable and lower than the weeping tendency of ¼-in holes. On the basis of proprietary data, Hsieh and McNulty (63) concluded that an increase in hole diameter decreases weeping tendency. Others noted an increase in weeping tendency with an increase in hole diameter (4,39,49,61–63,66).
- Lower surface tension (4,28,39,61,62,66). For hole sizes commonly used in commercial practice (> ⅛ in), however, experimental data (28,56,63) suggest a negligible surface tension effect.
- Increasing plate thickness (48). Another source (62), however, states that decreasing plate thickness increases weeping tendency.

Weep point prediction. Until recently, there was no reliable means of predicting weep rates. Trays were designed (4,26,67) to operate above the weep point, which could be predicted with confidence. This practice forfeited the portion of area on the stability diagram (Fig. 6.6) between the "weep point" and "excessive weeping" curves. The recent appearance of reliable weep rate correlations (below) is likely to strip the weep point of most of its practical significance for tray design.

Most weep point correlations are based on a pressure balance between the static head of the clear liquid, and the tray pressure drop. Lockett (12) reviewed the performance of several weep point correlations, and noted that their success often depends on how the clear liquid height is estimated. Lockett (12) also presents Mayfield's (37),

Fair's (31), and Zuiderweg's (17) correlations as those that are generally more reliable. Other design publications (4,18,64) recommended the use of Fair's correlation (31). The author has also had favorable experience with it. According to Fair's model (31), the force balance defining the weep point is

$$h_d + h_\sigma = h_w + h_{ow} \tag{6.31a}$$

If the left-hand side is larger than the right-hand side, the vapor will keep the liquid on the tray; if the converse occurs, liquid will weep. h_σ is given by (18)

$$h_\sigma = \frac{0.04}{\rho_L d_H}\sigma \tag{6.31b}$$

h_d and h_{ow} can be calculated from the equations in Sec. 6.3. Equation (6.31*a*) is the theoretical curve in Fig. 6.18. This equation gave poor agreement with experimental data, and Fair modified it empirically to give

$$h_d + h_\sigma = f(h_w + h_{ow}) \tag{6.31c}$$

Equation (6.31*c*) is shown in Fig. 6.19. No weeping is predicted for points above the correlating curve, while weeping is predicted below it.

Weep rate prediction. Lockett and Banik (56) and Hsieh and McNulty (63) proposed correlations for predicting weep rates from sieve trays. Both correlations are based on pilot scale data, mainly with the air-water system. The Hsieh and McNulty correlation is based on a broader data bank, which includes the experimental data by Lockett and Banik. Hsieh and McNulty used an even wider, non-air-water, proprietary data bank for testing some of their predicted trends.

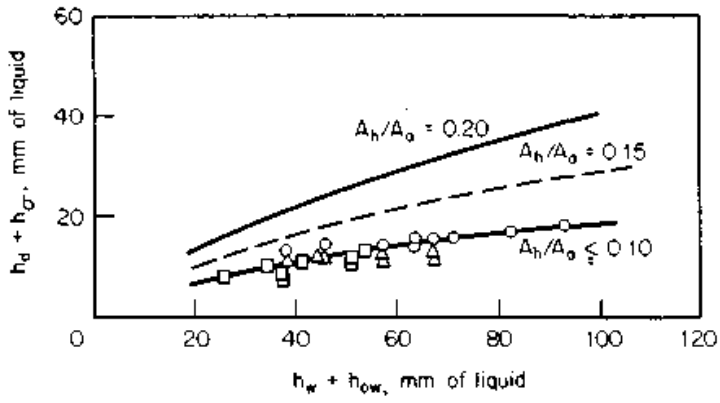

Figure 6.18 Fair's weep point correlation. (*From B. D. Smith,* Design of Equilibrium Stage Processes. *Copyright © 1963 by McGraw-Hill, Inc., reprinted by permission.*)

Colwell and O'Bara (58) applied both the Lockett and Banik and the Hsieh and McNulty correlations for estimating tray efficiency under weeping conditions. At low pressures, use of the Lockett and Banik correlation gave good efficiency predictions, while use of the Hsieh and McNulty correlation gave optimistic efficiency predictions. At high pressures, use of the Hsieh and McNulty correlation gave good efficiency predictions, while use of the Lockett and Banik correlation gave conservative efficiency predictions. Colwell and O'Bara (58) recommended the Lockett and Banik correlation for low-pressure (<165 psia) systems, and the Hsieh and McNulty correlation for high-pressure (>165 psia) systems.

The Lockett and Banik correlation (56) is

$$\frac{W}{A_h} = \frac{29.45}{\sqrt{Fr_h}} - 44.18 \tag{6.32}$$

where

$$Fr_h = 0.373 \frac{u_h^2}{h_c} \frac{\rho_V}{\rho_L - \rho_V} \tag{6.33}$$

It was recommended (12,56) that the clear liquid height h_c in Eq. (6.33) be calculated using Colwell's (68) clear liquid height correlation (Sec. 6.3.3). The denominator of Eq. (6.33) contains the difference between liquid and vapor densities instead of the liquid density in the original Lockett and Banik correlation (56). This modification, incorporated by Colwell and O'Bara (58), has negligible effect at low pressure, but makes the correlation less conservative at high pressure.

Colwell and O'Bara (58) show that the Lockett and Banik correlation tends to give optimistic weep rate predictions near the weep point. They therefore recommended Eq. (6.32) only for hole Froude numbers smaller than 0.2. For larger Froude numbers, they proposed an alternative equation

$$\frac{W}{A_h} = \frac{1.841}{\mathrm{Fr}_h^{1.533}} \tag{6.34}$$

Correlation limitations cited by Lockett and Banik (56) are

- With large-diameter trays and low liquid loads, a small ratio of W/A_h corresponds to a large fractional weep. Under these conditions, the correlation is inaccurate.

- The correlation is unsuitable for trays with very small (< ⅛ in) holes.
- The correlation appears to fit most data points to an accuracy of ±15 to ±30 percent.

The Hsieh and McNulty correlation (63,69)

$$\sqrt{J_G^*} + m\sqrt{J_L^*} = C_w \tag{6.35}$$

where

$$J_G^* = u_h \left[\frac{\rho_G}{gZ\,(\rho_L - \rho_G)}\right]^{0.5} \tag{6.36}$$

and

$$J_L^* = \frac{W}{448.83A_h}\left[\frac{\rho_L}{gZ\,(\rho_L - \rho_G)}\right]^{0.5} \tag{6.37}$$

$$Z = h_c^{1.5}/(12d_H^{0.5}) \tag{6.38}$$

For sieve trays, $m = 1.94$, $C_w = 0.79$. Note that the constants (69) are a slight revision of those presented in the original paper (63). Clear liquid height h_c is calculated from Colwell's correlation (Sec. 6.3.5). The Hsieh and McNulty correlation applies to trays with 9 percent and larger hole area. For trays with smaller hole area, Hsieh and McNulty (63) expect the weeping rate to be smaller than predicted.

Weep fraction. f_w is the ratio of weep rate from the tray to the total liquid flow rate entering the tray, i.e.,

$$f_w = W/\text{GPM} \tag{6.40}$$

Above the weep point, $W = 0$ and $f_w = 0$. At the dump point (Sec. 6.2.14), all liquid weeps from the tray, and $f_w = 1.0$. It was stated (50,70) that when weeping across the tray is uniform, the decrease in tray efficiency is usually considered acceptable with a weep fraction of up to 0.1.

6.2.13 Valve tray weeping

Bolles (71) extended Fair's sieve tray weep point correlation (31; Fig. 6.18) to investigate weeping in valve trays. Some results are depicted in Fig. 6.19. The axes of Fig. 6.19 are identical to those of Fig. 6.18. Each dashed line is the locus of weep points predicted from Bolles' extended Fair correlation. The heavy lines are the "operating lines," i.e.,

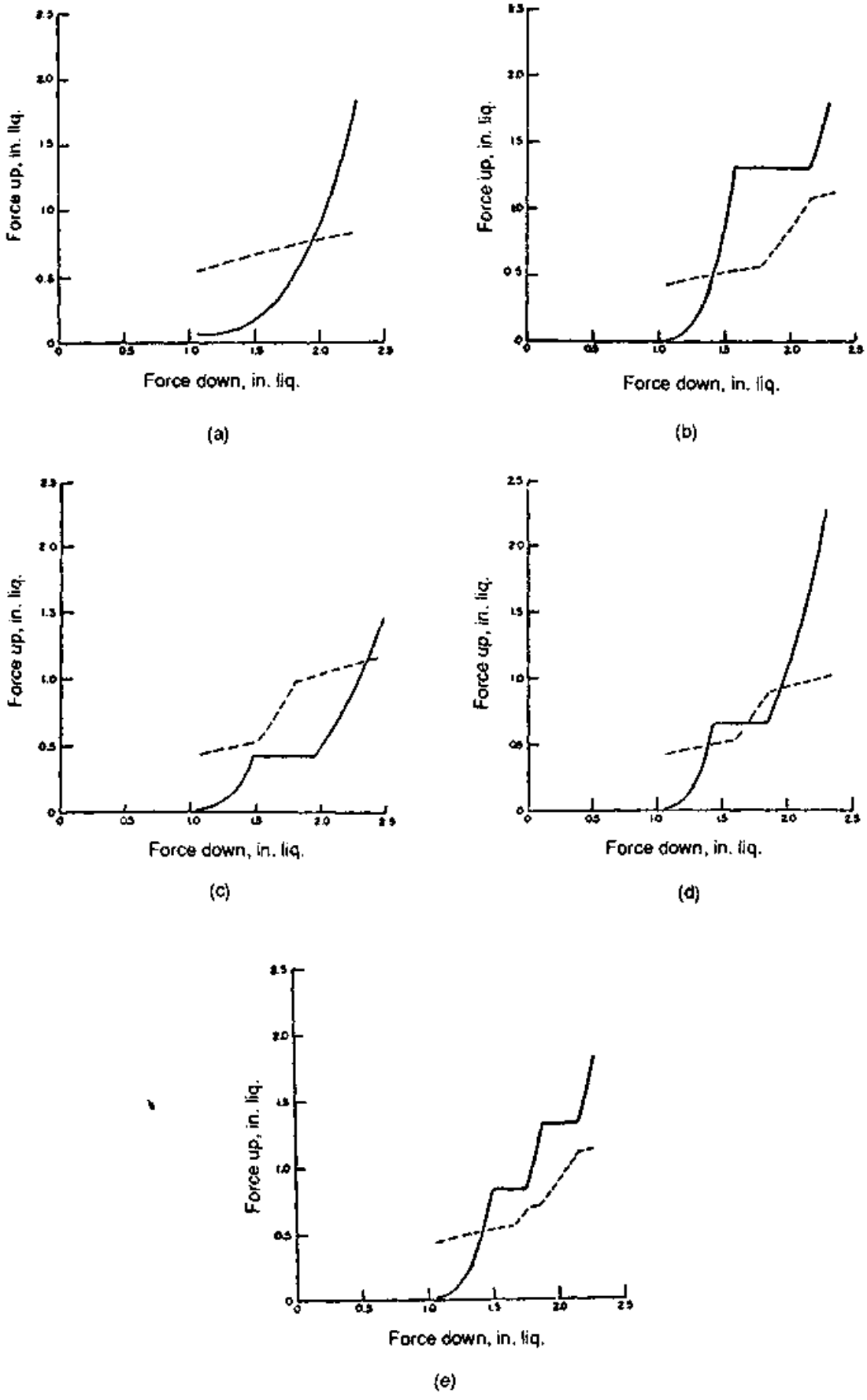

Figure 6.19 Weep point pressure balance for sieve and valve trays. (*a*) Sieve tray; (*b*) well-designed valve tray; (*c*) valve tray with too many valves or with valves that are too light; (*d*) valve tray with too many valves, but fewer than in *c*; (*e*) well-designed valve tray with two valve weights. (*From W. L. Bolles, Chem. Eng. Prog.*, 72 (9), p. 43 (September 1976), reprinted courtesy of the American Institute of Chemical Engineers.)

the relationship between the upward force [left-hand side of Eq. (6.31*c*)] and downward force [right-hand side of Eq. (6.31*c*)] as column loadings increase. When the heavy line is below the dashed line, the force up is lower than the force up at the weep point, and weeping occurs. When the heavy line is above the dashed line, no weeping occurs. The point of intersection of the heavy and dashed line is the weep point.

In a well-designed valve tray (Fig. 6.19*b*), the weep point is below the vapor load at which the valves open. Throughout the valve-opening process (flat portion of the heavy curve in Fig. 6.19*b*), the operating curve remains above the weep point. The weep point of a sieve tray (Fig. 6.19*a*) is shown for comparison. Figure 6.19*c* shows a tray with too many valves, or one with valves that are too light. Here the weep point is high, and the turndown may be even worse than that of a sieve tray. Figure 6.19*d* shows a tray with fewer valves (or heavier valves) than those in Fig. 6.19*c*. Here the tray will stop weeping as the vapor load rises, but will resume weeping as valves open up. Turndown again will be poor, but performance will be better than the valve in Fig. 6.19*c*. Figure 6.19*e* illustrates a well-designed valve tray with two valve weights. The diagram illustrates how this design overcomes the problem depicted in Fig. 6.19*d*.

Several experiences of severe weeping from valve trays have been reported (1,71,75). A well-designed valve tray is unlikely to have too many valves, but trays with light valves are common in an effort to reduce pressure drop. To avoid the turndown problems, manufacturers often specify a valve tray with two valve weights (Fig. 6.19*e*). When the light valves open, the heavy ones are still shut, which reduces the ratio of slot to active area and avoids weeping. This practice is discussed in detail elsewhere (1,71).

Weep mechanism. Banik (72) made some observations on the mode of weeping from valve trays. At high vapor loads (low weep rates), weeping takes place through the valve openings, is induced by the horizontal liquid velocity, and the weeping liquid descends at an angle. At low vapor loads (high weep rates), liquid weeps through the opening between the valve legs and the hole edge and through the peripheral openings of the valve.

Tests by Banik (72) and Zhang et al. (70) show that weeping from valve trays is nonuniform. In Banik's 4 ft × 2 ft rectangular simulator, most of the weep issued from the inlet half of the tray at low liquid rates (< 3 gpm/in of outlet weir) and from the outlet half of the tray at high liquid rates (> 10 gpm/in of outlet weir). The nonuniformity appeared to escalate as weir height increased. This pattern of nonuniformity is similar to that observed by Banik and Lockett (56) on sieve trays. In Zhang et al.'s (70) 5 ft × 1 ft rectangular simulator.

weeping was uniform before valves started to open. Opening of the valves began from the outlet end of the tray, and was accompanied by weeping mostly from the inlet half of the tray.

Unlike sieve trays, valve trays were observed to experience substantial weeping from the inlet row of valves (72). An inlet weir about 1 in tall was shown (72) to roughly half this inlet weep at higher liquid rates (>5 gpm/in) but to be less effective at lower liquid rates. The installation of such an inlet weir ("interrupter" or "breaker" bar) is a common design practice on valve trays.

Factors affecting weep. The mechanical design of the valves has a large impact on the weeping tendency. This is discussed elsewhere (1). In addition, most of the factors that increase weeping tendency in sieve trays also increase weeping tendency in valve trays. These include

- Increasing valve slot area (1,71)
- Increasing liquid rate (63,65,71,72)
- Increasing weir height (71,72)
- Reducing valve weight (1,71)
- Contouring valve orifices

Weep prediction. The weep point of valve trays can be calculated from the Bolles extension (71) of Fair's weep point correlation (31). The same correlation (Fig. 6.18) is used, except that the sieve fractional hole area is substituted by the ratio of valve slot area to tray active area. An alternative weep point correlation for valve trays was presented by Klein (73). Hsieh and McNulty (63) extended their sieve tray weep rate correlation (Sec. 6.2.12) to valve trays. The extension is complex, and discussed elsewhere (63).

Vapor channeling. The turndown of valve trays may be restricted by channeling (poor vapor distribution) or by pulsation at low vapor rates rather than by excessive weeping. Zhang's simulator study, and motion pictures discussed by Lieberman (74), suggest that at low throughputs, valves at the low-liquid level regions (near the outlet weirs) open first, while those near the tray inlet remain shut, causing vapor channeling at the tray outlet. On the other hand, tests by Zuiderweg et al. (75) and a case study by Reay (1), both in large-diameter (>13 ft) columns at relatively low liquid rates, suggests that vapor channels through a small aerated zone located in some intermediate position on the tray, with the remaining valves completely shut. On two-pass trays, one panel sometimes tends to be active and the other panel inactive (1). In any of the above cases, vapor channeling induces

nonuniform weeping, a reduction in tray efficiency, and possibly other adverse effects (e.g., Ref. 1).

To minimize vapor channeling, valve trays are designed to exceed a minimum unit reference (50). A unit reference is the ratio of the vapor rate to the vapor rate at which all the valves are open (Sec. 6.3.2). A minimum unit reference of 40, 60, and 80 percent is recommended for one-, two-, and four-pass trays, respectively (50). If the unit reference falls below the minimum, selected valves can be blanked, valve density can be reduced, or the ratio of light to heavy valves can be varied (7,50).

6.2.14 Dumping

As vapor rate is lowered below the weep point, the fraction of liquid falling through the holes increases until a condition is reached where all liquid fed onto a tray weeps through the holes and none reaches the downcomer. This condition is referred to as *dump point* or *seal point.*

Below the dump point (100 percent weep), tray efficiency is a small fraction of its normal value, and mass transfer is extremely poor. Since no liquid enters the downcomers, they lose the liquid seal that prevents vapor from rising through them. Operation below the dump point can be accompanied by severe hydraulic instability due to unsealing of downcomers, as was demonstrated by field experience (76). The startup stability diagram (1), which defines the range of vapor and liquid rates needed for satisfactory startup, has the dump point as the lower limit. The tendency of dumping increases when (77–79)

- Liquid rate decreases (*Note:* This is the reverse of the effect of liquid rate on the weeping tendency. The effect of liquid rate on weeping and dumping is depicted in Fig. 6.6.)
- Fractional hole area increases.
- Weir height increases.

The most extensive studies on dumping were reported by Prince and Chan (77–79). The Chan and Prince dump-point correlation (Fig. 6.20) was recommended by Chase (30). The author has also had favorable experience with the correlation under conditions widely different from those used in its derivation. Alternatively, the dump point can be predicted from a weep rate correlation by setting the weep rate equal to 100 percent of the liquid entering the tray. However, little has been reported by either Lockett and Banik (56) or Hsieh and McNulty (63) about the reliability of dump-point predictions from their correlation.

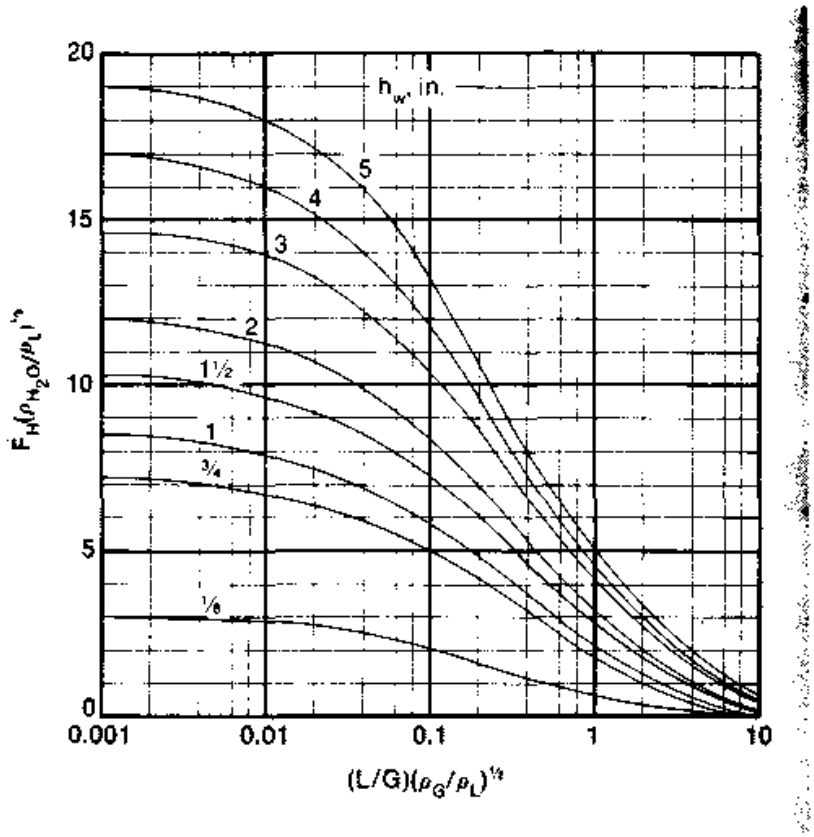

Figure 6.20 The Chan and Prince dump point correlation. *B. K. C. Chan, Ph.D. Thesis, University of Sydney, Australia, 1965; courtesy of Professor Prince.)*

6.3 Tray Hydraulic Parameters

6.3.1 Pressure drop

The total pressure drop across a tray is the sum of the pressure drop across the disperser unit, h_d (dry hole for sieve trays; dry valve for valve trays), and the pressure drop through the aerated mass h_l, i.e.,

$$h_t = h_d + h_l \tag{6.41}$$

6.3.2 Dry pressure drop

The dry pressure drop across the disperser unit [h_d in Eq. (6.41)] is given by a variation of the orifice equation

$$h_d = K \frac{\rho_G}{\rho_L} u_h^2 \tag{6.42}$$

Sieve trays. K in Eq. (6.42) is given by (4,5,18,30,31)

$$K = 0.186/C_v^2 \tag{6.43}$$

The prime variables affecting the orifice coefficient, C_v, are the fractional hole area and the ratio of tray thickness to hole diameter. More than 20 published correlations are available for evaluating C_v (12). Fair et al. (18) and Van Winkle (5) recommend the correlation by Liebson et al. (48; Fig. 6.21*a*). The Hughmark and O'Connell correlation (66) is preferred by Ludwig (4) and Chase (30).

Valve trays. Figure 6.21*b* illustrates the dry pressure drop of a typical valve tray as a function of vapor velocity. At low vapor velocities, all valves are closed (i.e., seated on the tray deck). Vapor rises through the crevices between the valves and the tray deck, and friction losses through these crevices constitute the dry pressure drop. Once the closed balance point (CBP) is reached, there is sufficient force in the rising vapor to open some valves. A further increase in vapor velocity opens more valves. Since vapor flow area increases as valves open, pressure drop remains constant until all valves open. This occurs at the open balance point (OBP). Further increases of vapor velocity cause the dry pressure drop to escalate in a similar manner to a sieve tray. When two weights of valves are used in alternate rows on the tray, a similar behavior applies to each valve type. The result is the pressure drop–vapor velocity relationship in Fig. 6.19*e*.

K in Eq. (6.42) depends on whether the valves are fully open and also on the shape and weight of the valves. These are best obtained from manufacturer literature (7–9), but can also be calculated from Bolles' (71), Lockett's (12), or Klein's (80) methods. Klein's method was derived from and fine-tunes the Bolles' model, was tested against a wide data base, and gives

- For all valves fully closed (below the closed balance point)

$$K = K_c \tag{6.44a}$$

- For all valves fully open (above the open balance point)

$$K = K_o \tag{6.44b}$$

- Between the closed and open balance points, the dry pressure drop is constant (Fig. 6.21*b*), and equals the pressure drop at either the closed or open balance points. Therefore, Eq. (6.44*a*) can be used, with u_h in Eq. (6.42) set equal to the velocity at the closed balance point, $u_{vh,CBP}$. Alternatively, Eq. (6.44*b*) can be used with u_h in Eq. (6.42) set equal to the velocity at the open balance point, $u_{vh,OBP}$. Note that between the open and closed balance points the hole velocity at the relevant balance point, and not the actual gas velocity of gas through the holes, is used as u_h in Eq. (6.42).

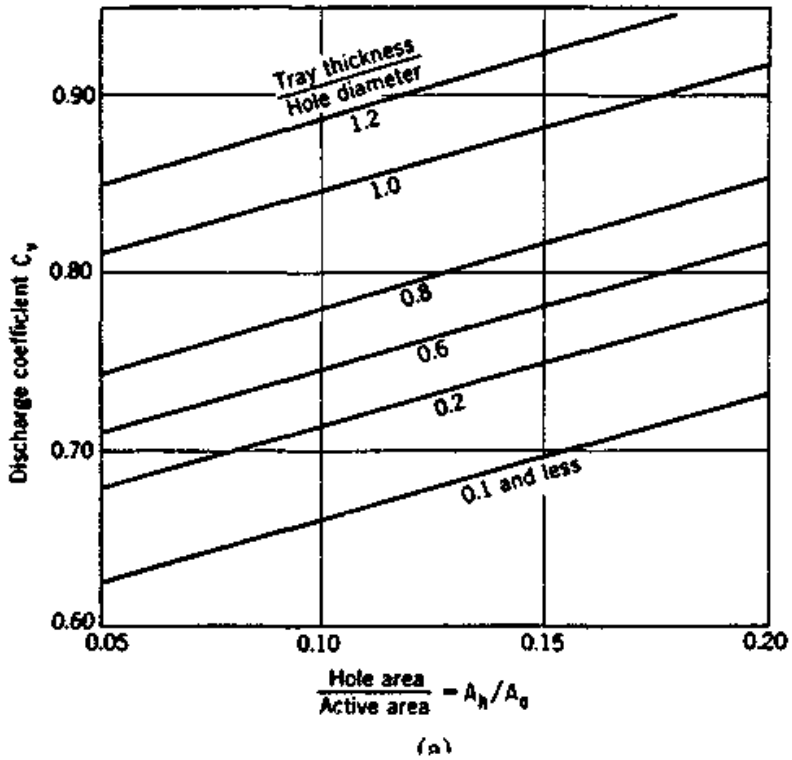

(a)

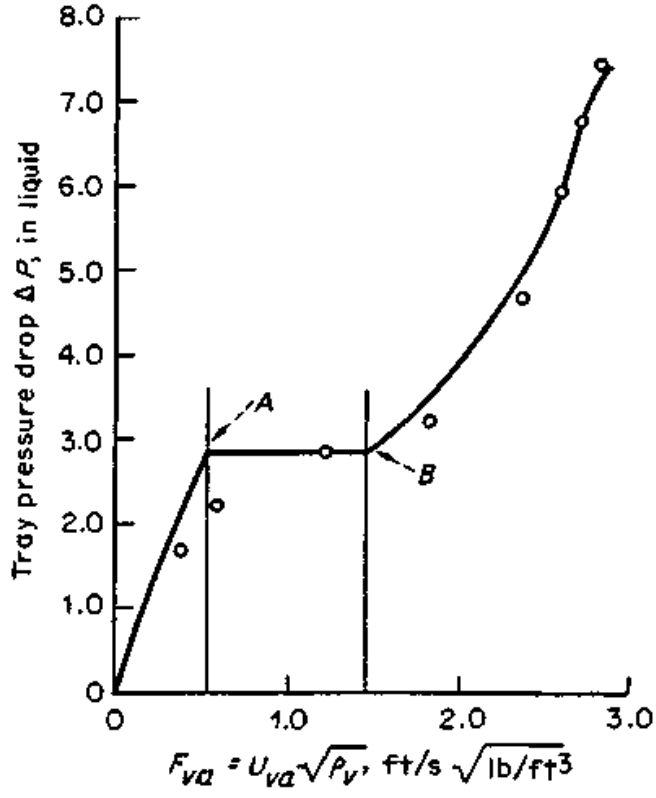

Figure 6.21 Dry pressure drop. (*a*) Discharge coefficients for gas flow in sieve trays. (*b*) Typical valve tray pressure drop profile. Valves start to open at point *A* (the closed balance point) and are fully open at point *B* (the open balance point). (*Part a from I. Leibson, R. E. Kelley, and L. A. Bullington, Pet. Ref., February 1957, p. 127, reprinted courtesy of Hydrocarbon Processing. Part b from George F. Klein, Chemical Engineering, May 3, p. 81, 1982, reprinted courtesy of Chemical Engineering.*)

TABLE 6.9 Coefficients for Valve Tray Dry Pressure Drop Equations

Coefficient	Meaning	Condition	Flat valve	Venturi orifice valve
R_{vw}	Ratio of valve weight with legs to valve weight without legs	Uncaged, 3 legs	1.23	1.29
		4 legs	1.34	1.45
		Caged (no legs)	1.0	1.0
K_c	Loss coefficient, valve closed		6.154	3.077
K_o	Loss coefficient, valve open	t = 10 gage (0.134 in)	0.821	0.448
		12 gage (0.104 in)	0.931	0.448
		14 gage (0.074 in)	1.104	0.448
C_{vw}	Eddy loss coefficient		1.3	
ρ_{vm}	Valve material density, lb/ft^3	Carbon steel	490	
		Stainless steel, 400 series	484	
		Stainless steel, 304 or 316	501	
		Monel 400	551	
		Aluminum	169	
		Titanium	282	

SOURCE: George F. Klein, *Chemical Engineering*, May 3, p.81, 1982, reprinted courtesy of *Chemical Engineering*.

Klein's method requires that in the dry pressure drop equation, Eq. (6.42), the vapor hole velocity u_h is based on the area of holes on the deck of a valve tray (A_{do}), and not on the slot area. In many valve trays, the orifice diameter is standardized at 1 17/32 in. Values of K_c and K_o are listed in Table 6.9. K_o is listed as a function of the tray deck thickness t, not the valve thickness. When the tray deck thickness is not listed in Table 6.9, K_o can be evaluated from

$$K_o \propto 1/\sqrt{t} \tag{6.45}$$

In order to determine whether the valves are fully open, fully closed, or in between, and in order to apply the pressure drop equation between the open and closed balance points, the vapor hole velocities at each balance point must be evaluated. The balance-point hole velocities are evaluated from a balance between the vapor force pushing the valve open and the gravity force tending to close it. This force balance gives (71,80)

$$u_{vh,\mathrm{CBP}} = \sqrt{H_v R_{vw} (C_{vw}/K_c) (\rho_{vm}/\rho_v)} \tag{6.46a}$$

$$u_{vh,\mathrm{OBP}} = u_{v,\mathrm{CBP}} \sqrt{K_c/K_o} \tag{6.46b}$$

Values of R_{vw}, K_c, K_o, C_{vw}, and ρ_{vm} are listed in Table 6.9. The hole vapor velocities, $u_{vh,\mathrm{CBP}}$ and $u_{vh,\mathrm{OBP}}$ are based on the area of holes in the tray deck, A_{do}.

6.3.3 Pressure drop through the aerated liquid

For sieve trays, most designers (3–5,18,31) have been recommending Fair's pressure drop correlation (18,31). A recent correlation by Bennett et al. (81) was recommended (18,81) for accurate pressure drop prediction. For valve trays, a slight modification of Fair's sieve tray correlation (80) is described.

The pressure drop through the aerated liquid [h_l in Eq. (6.41)] is calculated from (3–5,18,30,31,77)

$$h_l = \beta h_c \tag{6.47a}$$

An alternative, more fundamental relationship sometimes used is (12)

$$h_l = h_c + h_R \tag{6.47b}$$

where the residual pressure drop h_R is often interpreted as the excess pressure required to overcome surface tension when bubbles are formed at the orifice (12).

The relationship in Eq. (6.47*a*) is more popular and will be adopted here. The tray aeration factor, β, is obtained from Fig. 6.22*a* for sieve trays (18,31) and Fig. 6.22*b* for valve trays (5,80). For sieve and valve trays, h_c is calculated from (2–5,18,30)

$$h_c = h_w + h_{ow} + h_{hg}/2 \tag{6.48}$$

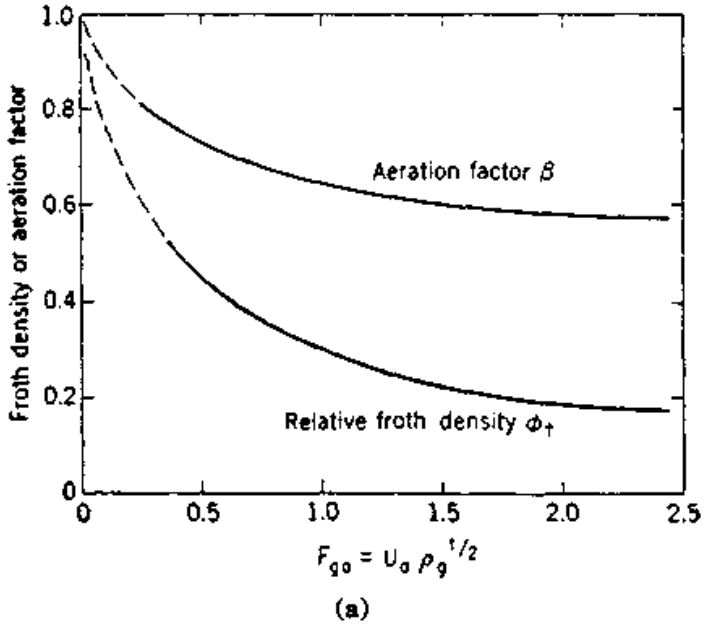

(a)

Figure 6.22 Tray aeration factor prediction for pressure drop calculations. (*a*) Aeration factor for sieve and bubble-cap trays. (*Part a from B. D. Smith,* Design of Equilibrium Stage Processes, *Copyright © 1963, by McGraw-Hill, Inc., reprinted by permission.*)

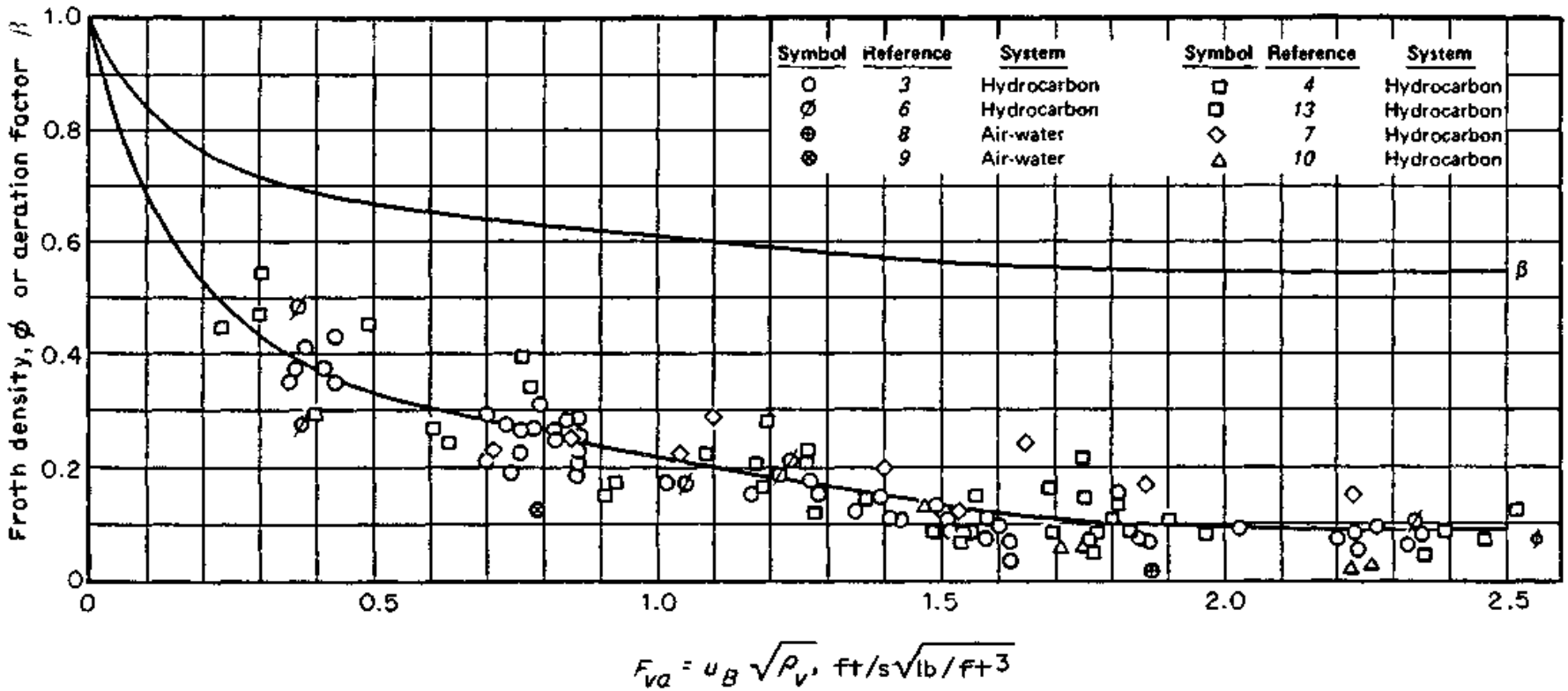

Figure 6.22 (*Continued*) Tray aeration factor prediction for pressure drop calculations. (*b*) A modified version of the correlation in *a*, suitable for valve trays. (*Part b from George F. Klein, Chemical Engineering, May 3, p. 81, 1982, reprinted courtesy of Chemical Engineering*)

Liquid height over the weir. h_{ow} is calculated from a corrected Francis weir formula (2–5,18,31). For segmental weirs

$$h_{ow} = 0.48F_w\,(Q_L)^{2/3} \tag{6.49}$$

The correction term F_w (2–5,9,18,31) corrects the equation for the distortion of the liquid flow pattern as it approaches the weir, and is shown in Fig. 6.23 (18). Some variations of Eq. (6.49) for unique weir designs are

- For picket-fence weirs and for rectangular notched weirs, and tray liquid level below the top of the teeth, Q_L in Eq. (6.49) is based on the weir length less the total weir length occupied by the teeth. F_w is based on the total weir length (including the length of the teeth).
- For weirs with triangular notches, notches not fully covered by liquid (2,67):

$$h_{ow} = 0.96\,(Q_L h_n)^{0.4} \tag{6.49a}$$

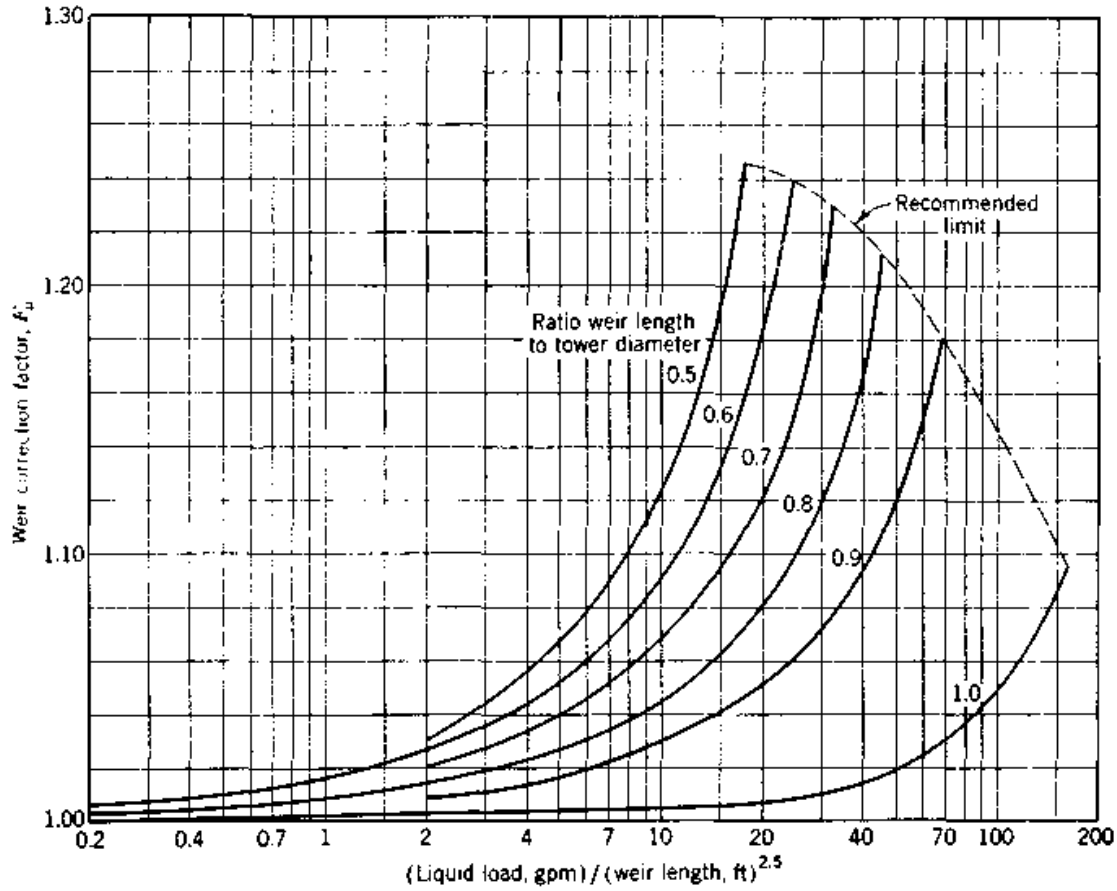

Figure 6.23 Weir correction factor for segmental downcomers in calculation of liquid head over the weir. (*From W. L. Bolles, Pet. Ref., 25, p. 613, 1946, reprinted courtesy of Hydrocarbon Processing.*)

- For weirs with triangular notches, notches fully covered by liquid (2,67).

$$Q_L = 1.19\,[h_{ow}^{2.5} - (h_{ow} - h_n)^{2.5}]/h_n \tag{6.49b}$$

- For circular weirs (18)

$$h_{ow} = 0.20\,(\mathrm{GPM}/d_w)^{0.704} \tag{6.49c}$$

Hydraulic gradient. The hydraulic gradient, h_{hg} is the head of liquid necessary to overcome the frictional forces in the path of the liquid on the tray. If the gradient is excessive, most of the vapor tends to issue near the outlet weir, where liquid level is low, whereas liquid tends to weep near the liquid inlet to the tray, where the liquid level is high. It has been recommended (18) to avoid hydraulic gradients greater than 40 percent of the dry pressure drop. Hydraulic gradients are negligible for most sieve trays, and the usual practice is to omit this term from the pressure drop calculation (4,18,67). In cases of a long flow path of liquid on the tray, it should be checked using the correlation of Hughmark and O'Connell (66), as recommended by most designers (4,5,18,30,31). The author recommends caution with this equation. On a couple of occasions when he applied it, it appeared to predict very low. The correlation is

$$h_{\mathrm{hg}} = \frac{12 f U_f^2 L_f}{g R_h} \tag{6.50}$$

R_h is the hydraulic radius of the aerated mass, estimated from

$$R_h = \frac{\text{cross section}}{\text{wetted perimeter}} = \frac{h_f D_f}{2h_f + 12D_f} \tag{6.51}$$

U_f is the velocity of the aerated mass across the tray (which is also equal to the clear liquid velocity across the tray), given by

$$U_f = \frac{1}{37.4}\frac{Q_L}{h_l}\frac{L_w}{D_f} \tag{6.52}$$

h_f is the froth density, and is estimated from

$$h_f = h_l/\phi_t \tag{6.53}$$

h_l is estimated from Eq. (6.47*a*) and ϕ_t is estimated from Fig. 6.22*a*. As h_l is a weak function of the hydraulic gradient, only a small amount of trial and error is necessary. The friction factor f in Eq. (6.50) is correlated in terms of the Reynolds number, $N_{\mathrm{Re},h}$

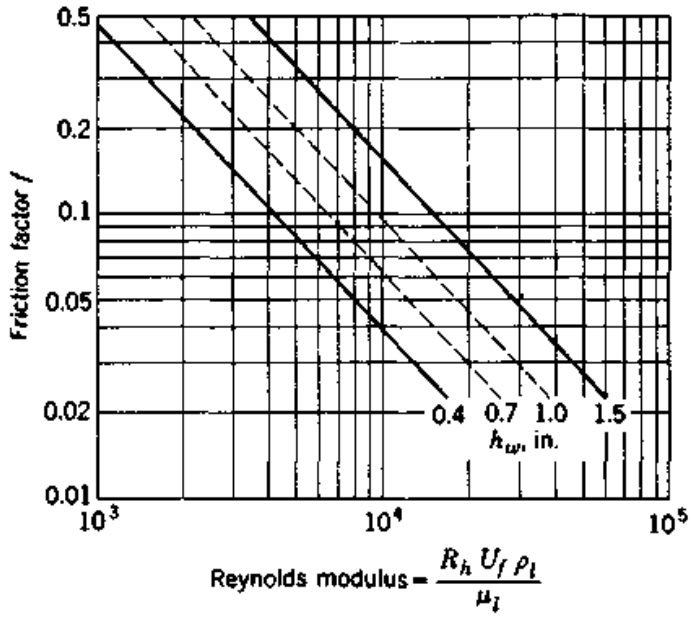

Figure 6.24 Friction factor for froth cross-flow on sieve trays. (*From B. D. Smith* Design of Equilibrium Stage Processes. *Copyright © 1963 by McGraw-Hill, Inc., reprinted by permission.*)

$$N_{\mathrm{Re},h} = \frac{R_h U_f \rho_L}{\mu_l} \tag{6.54}$$

The friction factor is obtained from Fig. 6.24 (18).

For valve trays, the hydraulic gradient is somewhat larger than that of sieve trays, probably not by much (18). In a similar manner to sieve trays, it is often neglected in the pressure drop calculation (7–9,71,80). In cases of a long flow path of liquid, it should be checked using the Hughmark and O'Connell correlation above.

The Bennett et al. correlation. This correlation was shown (81) to predict experimental sieve tray pressure drop data more accurately than Fair's correlation. The correlation is based on froth regime considerations and is not applicable to the spray regime. The Bennett et al. calculation of dry pressure drop is identical to Fair's, using Eqs. (6.42) and (6.43) and the Liebson et al. correlation (Fig. 6.21*a*). To calculate the h_l term in Eq. (6.41), Bennett et al. depart from the concept of clear liquid flow corrected for aeration effects [Eq. (6.47*a*)]. Instead, they use Eq. (6.47*b*) and a model of froth flow across the weir. Their residual pressure drop, h_R, is a surface tension head loss term, which is important for trays with very small holes (< ⅛ in. diameter). The Bennett et al. correlation is

$$h_R = \frac{0.2165}{\rho_L}\left[\frac{\sigma^2 (\rho_L - \rho_G)}{d_H}\right]^{1/3} \tag{6.55}$$

The effective clear liquid height is given by

$$h_c = \phi\left[h_w + 11.07C\left(\frac{Q_L}{\phi}\right)^{2/3}\right] \tag{6.56}$$

The factor C is analogous to the Francis weir constant in Eq. (6.49) and is given by

$$C = 0.0327 + 0.0286 \exp(-3.5\, h_w) \tag{6.57}$$

The froth density ϕ is estimated by an expression analogous to Fig. 6.22*a*

$$\phi = \exp(-4.2570\, C_S^{0.91}) \tag{6.58}$$

where C_S is the C-factor, given by Eq. (6.4), with C_S and u_S based on the tray bubbling area.

6.3.4 Head loss under downcomer apron

This head loss, required for downcomer backup calculation (Sec. 6.2.7), is calculated for segmental downcomers from (2–5,18,31,32)

$$h_{da} = 0.03\left(\frac{\text{GPM}}{100\, A_{da}}\right)^2 \tag{6.59}$$

A_{da} should be taken as the most restrictive area in the downcomer outlet region. For instance, if an inlet weir is used and the area open for liquid flow between the segmental downcomer and the inlet weir is smaller than the area under the downcomer apron, the smaller area should be used in Eq. (6.59).

Equation (6.59) was derived from the orifice equation with an orifice coefficient of 0.6 (3), and assuming pure liquid is passing under the downcomer. Tests by Lockett and Gharani (43) showed that Eq. (6.59) gives conservative predictions, even under conditions of significant vapor entrainment in the downcomer underflow (Sec. 6.2.8).

6.3.5 Clear liquid height and froth density

The clear liquid height, or the liquid holdup, is the height to which the aerated mass would collapse in the absence of vapor flow. The clear liquid height gives a measure of the liquid level on the tray, and is used in efficiency, flooding, pressure drop, downcomer backup, weep-

ing, and entrainment calculations. The term h_1 in Eq. (6.41) is the clear liquid height derived from pressure drop data. It has, however, been shown (82,83) that an estimate of clear liquid height from pressure drop data is unsatisfactory for other purposes. The clear liquid height is related to the froth density and froth height by

$$h_c = \phi_f h_f \tag{6.60}$$

Sieve trays, froth regime. Most clear liquid height and froth density correlations (35,68,81–86) are based on the Francis weir formula. A correlation by Colwell (68), based on a model of froth flow over the weir, was demonstrated to agree with experimental data better than other published correlations. Colwell's correlation is recommended by the author and by Lockett (12), and was successfully used as a building block in weeping correlations (56,63,69) and in froth regime entrainment correlation (40). Colwell's correlation is

$$h_c = \phi_f\left[0.527\left(\frac{Q_L(1 - f_w)}{C_d\phi_f}\right)^{2/3} + h_w\right] \tag{6.61}$$

where ϕ_f is given by Eq. (6.60), and C_d is given by Eq. (6.62)

$$\left.\begin{aligned} C_d &= 0.61 + 0.08\frac{h_{\text{fow}}}{h_w} \qquad \frac{h_{\text{fow}}}{h_w} < 8.135 \\ C_d &= 1.06\left(1 + \frac{h_w}{h_{\text{fow}}}\right)^{1.5} \qquad \frac{h_{\text{fow}}}{h_w} > 8.135 \end{aligned}\right\} \tag{6.62}$$

$$h_{\text{fow}} = h_f - h_w \tag{6.63}$$

The froth density, ϕ_f, is calculated from

$$\eta = 12.6\text{Fr}^{0.4}\left(\frac{A_B}{A_h}\right)^{0.25} \tag{6.64}$$

$$\phi_f = \frac{1}{\eta + 1} \tag{6.65}$$

$$\text{Fr} = 0.37\frac{\rho_V u_B^2}{h_c(\rho_L - \rho_G)} \tag{6.66}$$

f_w in Eq. (6.61) is calculated from the correlations in Sec. 6.2.12. Usually, the weeping fraction is small, and f_w can be set to zero. The original Colwell correlation (68) did not contain the $1 - f_w$ correction term; this term was added while adopting the correlation to perform

weeping studies (56,58). This correction term must be applied when weeping is significant.

Some trial and error is required in this calculation, because the clear liquid height [Eq. (6.61)] and the froth density [Eqs. (6.64) to (6.66)] depend on each other. Under weeping conditions, additional trial and error is required because the weep fraction f_w depends on the clear liquid height (Sec. 6.2.12).

Hofhuis and Zuiderweg (85) presented an alternative correlation for predicting clear liquid height in the froth regime. It was shown (68) to be less accurate than Colwell's, and incorrectly predicts zero clear liquid height if either weir height or liquid flow rate drops to zero. Nevertheless, this correlation has been successful as a building block for the correlation for froth to emulsion regime transition (Sec. 6.4.3). This correlation is

$$h_c = 2.08 \left(F_{lv} \frac{N_p A_B}{L_w} p \right)^{0.25} h_w^{0.5} \tag{6.67}$$

Sieve trays, spray regime. Several correlations for clear liquid height in the spray regime were proposed (29,35,85,87–91). Lockett (12) recommended Stichlmair's (29) correlation. Since then Kister and Haas (36) modified an earlier correlation by Jeronimo and Sawistowski (35) and used it successfully as a building block for correlating entrainment flooding and spray regime entrainment. The modified Jeronimo and Sawistowski correlation is

$$h_{ct} = (h_{ct})_{H_2O} \left(\frac{62.2}{\rho_L} \right)^{0.5(1-n)} \tag{6.68}$$

$$n = 0.0231 d_H / A_f \tag{6.69}$$

$$(h_{ct})_{H_2O} = \frac{0.29 A_f^{-0.791} d_H^{0.833}}{1 + 0.0036 Q_L^{-0.59} A_f^{-1.79}} \tag{6.70}$$

Strictly, the Jeronimo and Sawistowski correlation predicts clear liquid heights at the froth to spray regime transition. However, it has been shown (27,92) that clear liquid height in the spray regime is much the same as clear liquid height at that transition.

Valve trays. Development of a clear liquid height correlation for valve trays has been inhibited by difficulties in measurement of clear liquid heights on these trays. A number of correlations have been proposed (86,93–95), but questions have been raised about their applicability (12,86,87). None has been tested against a sufficiently large data base

to be recommended for general use. Lockett (12) prefers Dhulesia's (86) and Brambilla's (95) correlations to the others.

6.3.6 Turndown

The turndown ratio is the ratio of the normal operating (or design) vapor throughput to the minimum allowable vapor throughput. The minimum allowable throughput is usually at the excessive weeping limit, while the normal operating throughput is a safe margin away from the relevant flooding limit.

Sieve trays have a poor turndown (about 2:1). The minimum operating throughput in sieve trays is almost always restricted by excessive weeping. Turndown of sieve trays can be improved by

- *Blanking some tray holes:* Blanking reduces the fractional hole area on the tray, thus decreasing weeping. However, reducing fractional hole area also decreases maximum capacity. A shutdown in which the blanking strips are removed is necessary before full capacity is reestablished. Blanking practices are discussed elsewhere (1).
- *Using low fractional hole areas:* A fractional hole area reduction to about 5 percent of the bubbling area typically boosts sieve tray turndown to about 3 to 4:1 at the expense of a lower maximum capacity, i.e., of a larger column diameter. This technique is not recommended because traying the column with valve trays is normally a cheaper alternative.

Valve tray turndown is normally about 4 to 5:1. The minimum operating rate in valve trays is usually restricted by excessive weeping, but it may also be restricted by the onset of vapor channeling (Sec. 6.2.13).

Special valve designs achieve higher turndown. One design (7,74,96; Fig. 6.3*b*) has a light orifice coverplate contained within a heavier cap. The cap can move vertically within a cage. At low vapor rates, the light orifice coverplate is lifted. At its maximum travel, it is pushed against the heavier cap. At high flow rates, both the plate and the heavier cap travel upward until reaching the cage. FRI data (96) demonstrate a turndown better than 6:1 to 10:1 with this design.

Another high-turndown valve design (Figs. 6.3*c* and 6.4*d*) has rectangular valves oriented with their long edge parallel to the liquid flow so that the slot opening facing the approaching liquid flow is minimized. Data by FRI and by Van Winkle et al. (9,97) demonstrate a turndown better than 7:1 to 9:1 with this design.

A third design (98) has a caged vertically moving plate with an or-

ifice drilled in the plate. At low rates, vapor issues only from the orifice; at higher rates, the plate itself moves. Turndown of up to 12:1 (98) was claimed with this design.

6.4 Flow Regimes on Trays

6.4.1 The common flow regimes

The classic hydraulic model (Sec. 6.2.1) oversimplifies tray action. There are five main flow regimes on distillation trays (12,99). These regimes (Figs. 6.25 to 6.28) may all occur on the same tray under different liquid and vapor flow rates (Fig. 6.29). An excellent overview of the fundamentals and modeling of these flow regimes is presented by Lockett (12).

Bubble regime (Fig. 6.25*a*) or "deep pool" occurs at low vapor velocities. Discrete noncoalescing bubble swarms rise through quiescent liquid, which has a very clear surface. For the air-water system, Wallis (100) showed that this regime is unlikely to occur when vapor velocities exceed 0.15 ft/sec, and therefore, in industrial columns. It may occur in bench-scale and pilot columns where outlet weirs are tall. If this regime occurs in a test unit, caution is required in data scale-up.

Cellular foam (Figs. 6.25*b*, 6.26*a*) is a wall-stabilized foam. Bubbles grow to an extent which limits the liquid to thin films between the

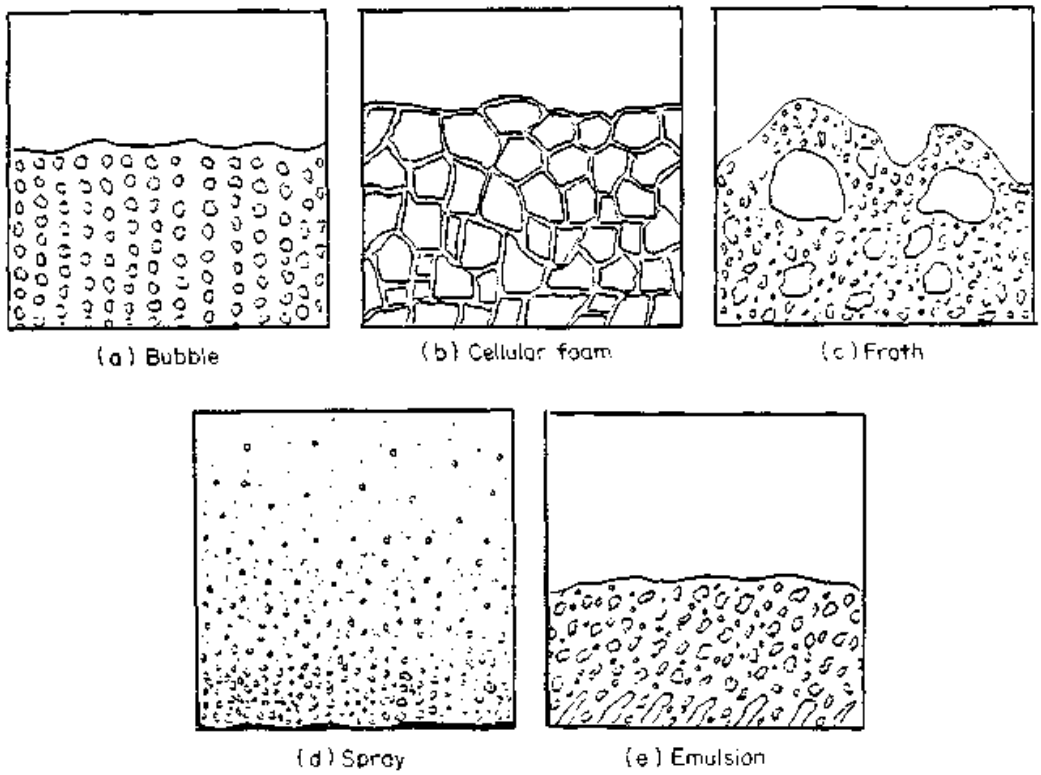

Figure 6.25 Common flow regimes on distillation trays.

bubbles, still with a very definite top or surface to the dispersion. Bubbles formed at the tray perforations rise unbroken to the top of the foam, and little bulk circulation occurs. The bubbles are distorted to polyhedra. This model is described in detail elsewhere (101,102).

Cellular foam occurs at low vapor velocities in small columns, where the wall provides foam stabilization. It occurs with some systems or tray designs but not with others and is promoted by surface tension effects such as the Marangoni effect (99). Cellular foam is uncommon in industrial columns. The foam that causes problems in industrial installations is mobile foam, where the bubbles are in turbulent motion. Mobile foam is associated with the froth and emulsion regimes. Cellular foam is encountered in bench-scale and pilot-scale columns. If cellular foam occurs in the test unit, caution is required when scaling up the results.

Froth (Figs. 6.25*c*, 6.26*b*, and 6.27*a*; sometimes referred to as the "mixed" regime). As vapor rates are increased in the bubble and cellular foam regimes, the dispersion changes to froth. In this regime each perforation bubbles vigorously, with chain bubbling common; the bubbles circulate rapidly through the liquid, are of a wide size range, of nonuniform shapes, and travel at varying velocities. The froth surface is mobile and not level, and generally covered by droplets. Often, waves or oscillations are present. Bubbles are formed at the tray perforations and are swept away by the froth.

At low liquid depths (i.e., very low liquid loads), bubbles break the liquid surface before detaching from the tray orifices, causing nonuniformity and some unique performance characteristics (40). This region (low vapor loads and very low liquid loads), however, is infrequently encountered in industrial practice.

As vapor load increases in the froth regime, jetting begins to replace bubbling in some holes. The fraction of holes that are jetting increases with vapor velocity. When jetting becomes the dominant mechanism, the dispersion changes from froth to spray. Prado and Fair (103) showed that this change is gradual and that the transition from froth to spray takes place as jetting replaces bubbling in 45 to 70 percent of the tray holes.

The froth regime is the most common operating regime in distillation practice, and its hydraulics is reasonably well approximated by the classical hydraulic model (Sec. 6.2.1; Fig. 6.5).

Spray (Figs. 6.25*d*, 6.26*c*, and 6.27*b*; sometimes referred to as the "drop" regime). As vapor load is increased at relatively low liquid rates, the spray regime is reached. While in the previous three regimes (and also

(a)

(b)

Figure 6.26 Tray action closeups in various flow regimes. (*a*) Cellular foam; (*b*) froth (*Part a from P. H. Calderbank and M. B. Moo-Young, International Symposium on Distillation, p. 59, the Institution of Chemical Engineers, UK, 1960; part b from M. J. Lockett,* Distillation Tray Fundamentals, *Cambridge University Press, Cambridge, 1986. Part a reprinted courtesy of the Institution of Chemical Engineers, UK. Part b reprinted courtesy of Cambridge University Press, Cambridge, UK.*)

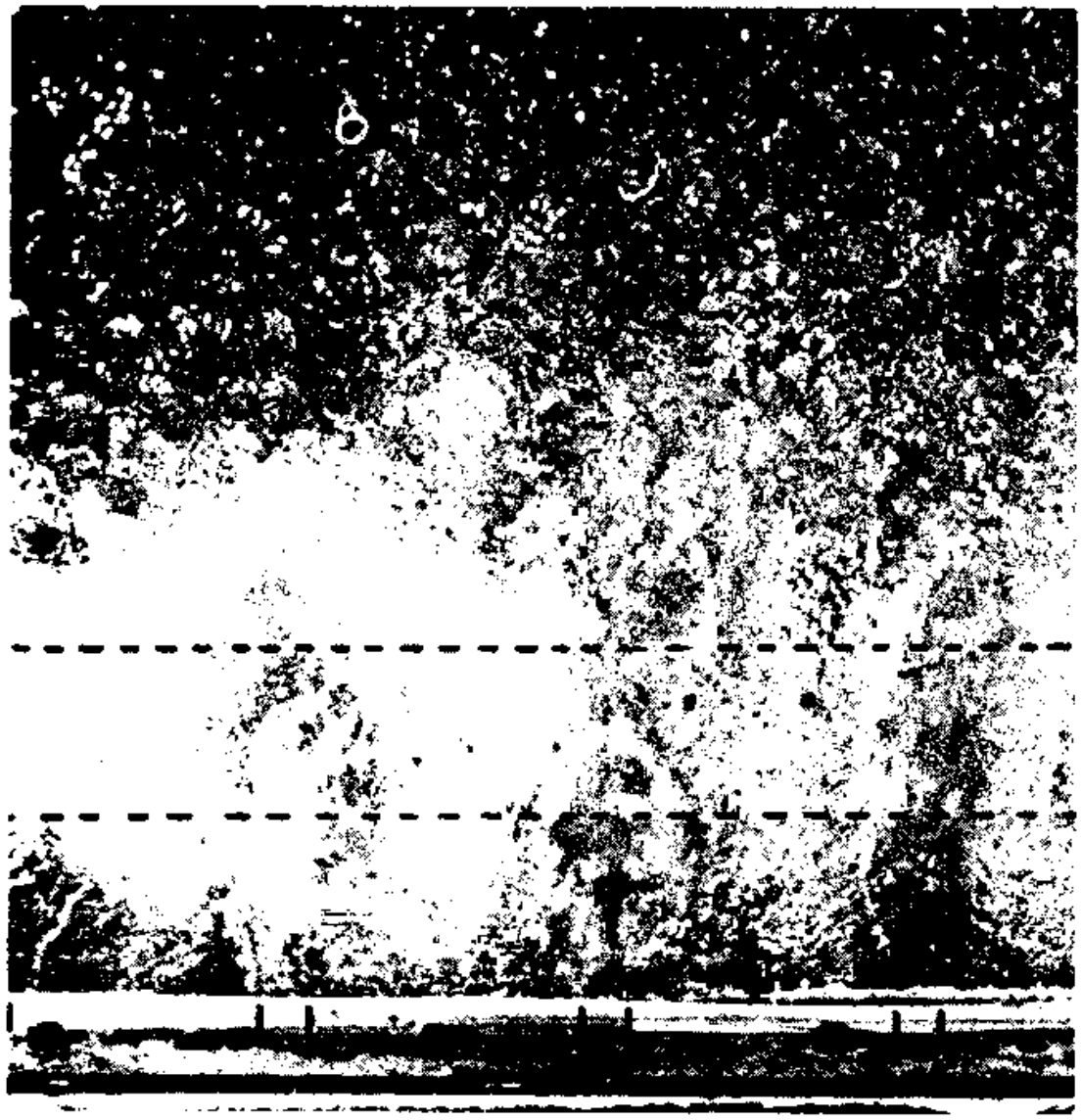

(c)

(d)

Figure 6.26 (*Continued*) Tray action closeups in various flow regimes. (c) spray. Note the existence of gas jets at tray orifices (orifice positions are marked). Dotted horizontal lines indicate positions of minimum and maximum in the vertical dispersion sensitivity profiles (such as the spray profile shown in Fig. 6.28*b*). (*d*) Inclined gas bubbling under influence of a horizontal liquid flow, typical of the emulsion regime. (*part c from W. V. Pinczewski and C. J. D. Fell, Trans. Inst. Chem. Engrs. (London), 52, p. 294, 1974; part d from F. J. Zuiderweg, P. A. M. Hofhuis, and J. Kuzniar, Chem. Eng. Res. Des., 62, p. 39, 1984. Parts c and d reprinted courtesy of the Institution of Chemical Engineers, UK.*)

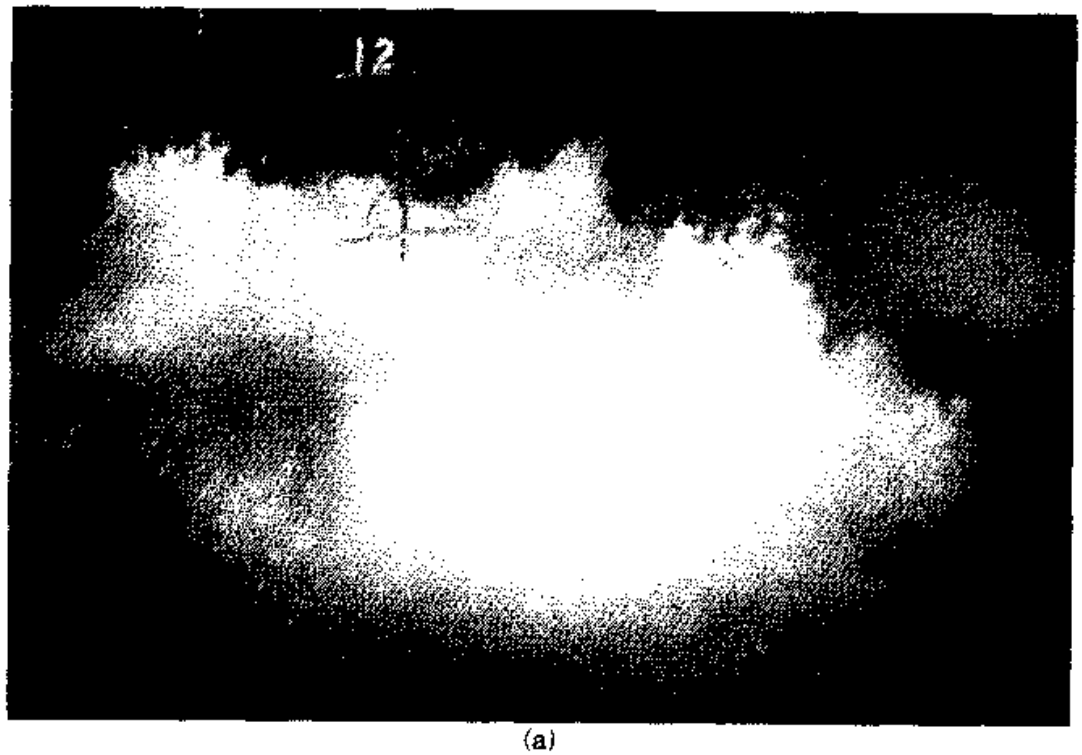

(a)

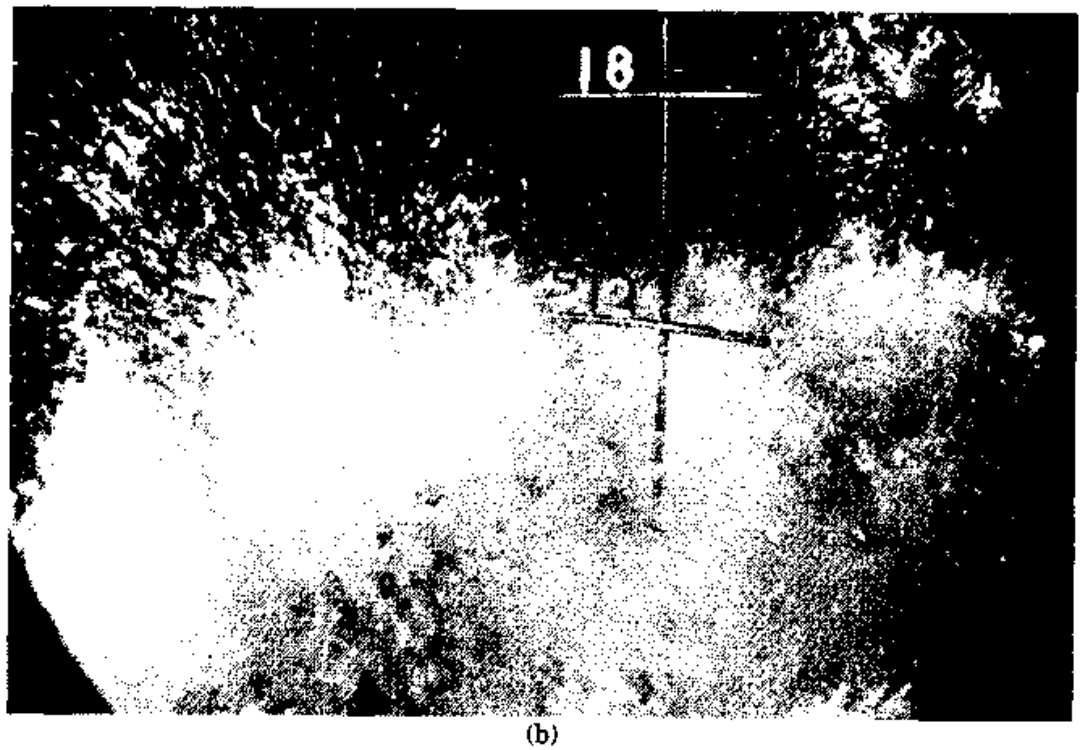

(b)

Figure 6.27 Tray action in the froth, spray, and emulsion regimes. Horizontal bars indicate height above tray floor in inches. (*a*) Froth regime; (*b*) Spray regime. [*All parts courtesy of Fractionation Research Inc. (FRI).*]

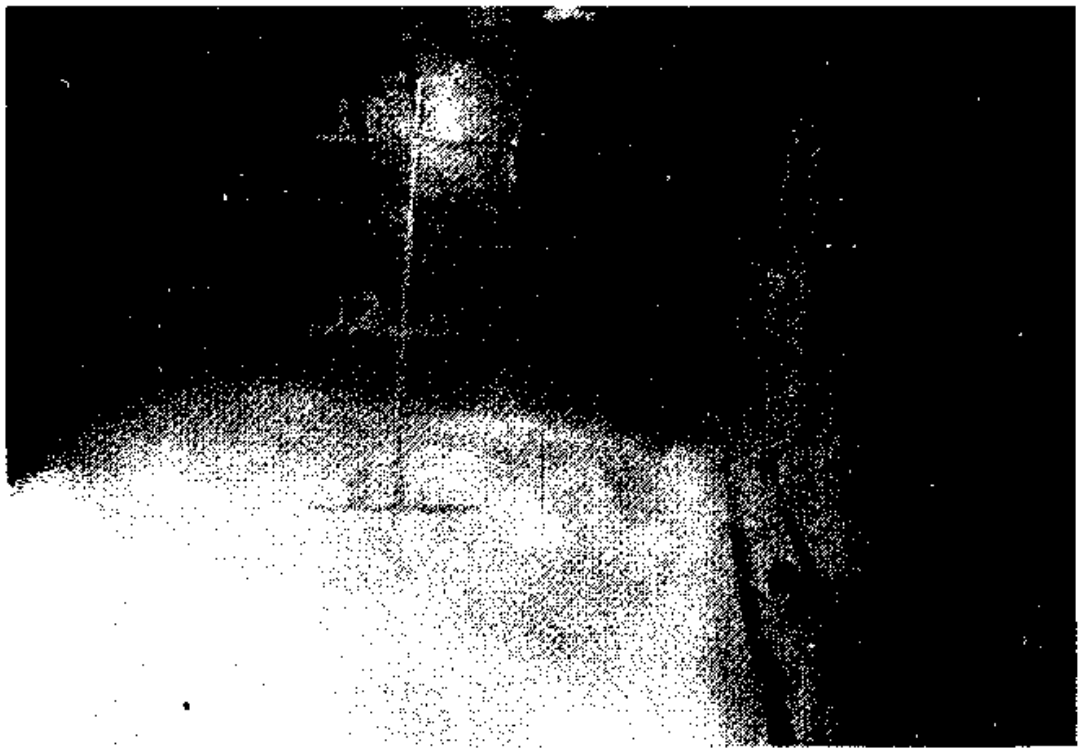

(c)

Figure 6.27 (*Continued*) Tray action in the froth, spray, and emulsion regimes. Horizontal bars indicate height above tray floor in inches. (*c*) Emulsion regime. Wall on right is downcomer from tray above. [*All parts courtesy of Fractionation Research Inc. (FRI).*]

in the emulsion regime below) vapor is distributed as bubbles in continuous liquid, in the spray regime the phases are reversed. In this regime, vapor is the continuous phase, while the liquid, which is present in the form of drops of various sizes, is the dispersed phase. The dispersion has the appearance of a highly turbulent cloud of liquid droplets. A jet is formed at each perforation, which atomizes liquid in its path. A small pool of liquid or froth exists near the tray floor, through which the gas passes as high-velocity jets. As the gas passes through, it draws up liquid into ligaments and tears them up into drops (Fig. 6.28*a*). The bulk of the liquid is present as drops that reside at high elevations above the tray (Fig. 6.28*b*) and follow free trajectories (Fig. 6.28*c*). Some may be entrained to the tray above, while others may fall back into the liquid pool, and the process repeats itself.

The spray regime frequently occurs in industrial practice, particularly where vapor velocities are high and liquid loads are low (e.g., vacuum). The classical hydraulic model (Sec. 6.2.1; Fig. 6.5) provides a poor approximation for the spray regime.

Emulsion (Figs. 6.25*e*, 6.26*d*, and 6.27*c*). At high liquid loads and relatively low vapor loads, the shearing action of the high-velocity liquid bends the vapor bubbles and jets leaving the orifices, and "tears off"

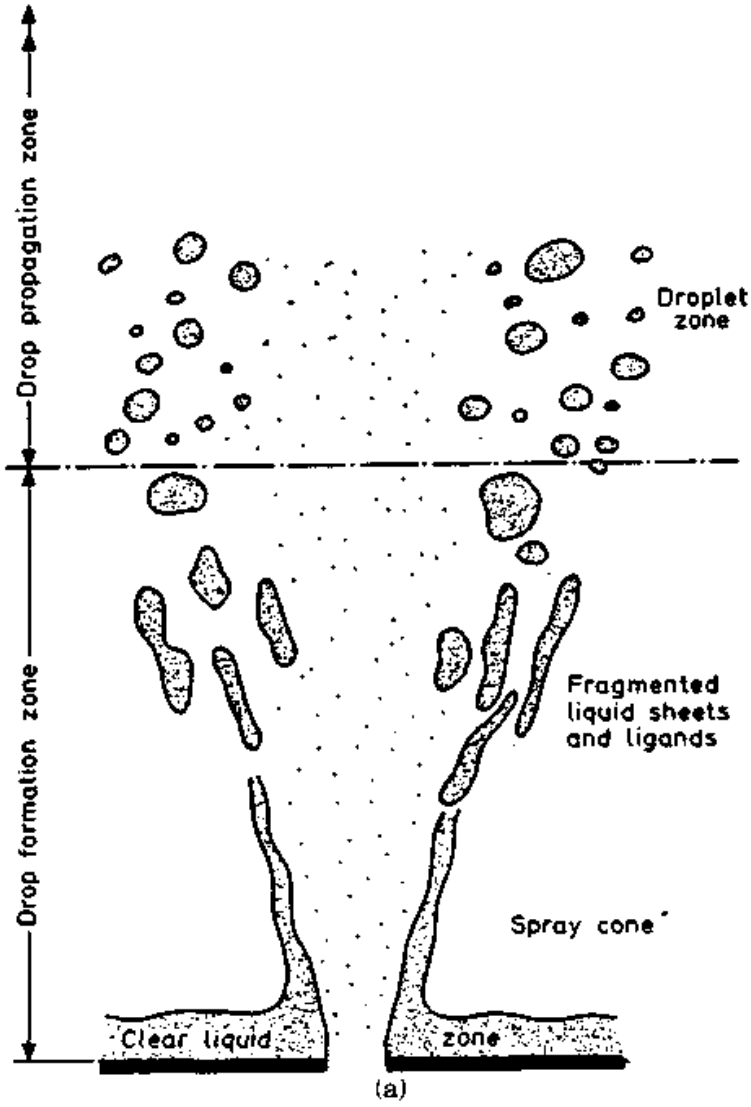

Figure 6.28 Characteristic features of the spray regime. (*a*) Generation of drops by tearing liquid sheets at tray orifices (*Part a from W. V. Pinczewski and C. J. D. Fell, Trans. Inst. Chem. Eng. (London), 52, p. 294, 1974. All parts reprinted courtesy of the Institution of Chemical Engineers, UK.*)

the vapor bubbles. In this regime, most of the gas is emulsified as small bubbles within the liquid. In the emulsion regime, the mixture behaves as a uniform two-phase fluid, which obeys the Francis weir formula (17,85,104,105). In industrial practice, the emulsion regime often occurs in high-pressure and high-liquid-rate operation. This regime is well-approximated by the classical hydraulic model (Sec. 6.2.1).

6.4.2 The flow regime likely to exist on industrial trays

Figure 6.29 suggests guidelines for the occurrence of each flow regime on commercial distillation trays. As stated earlier, the bubble and cel-

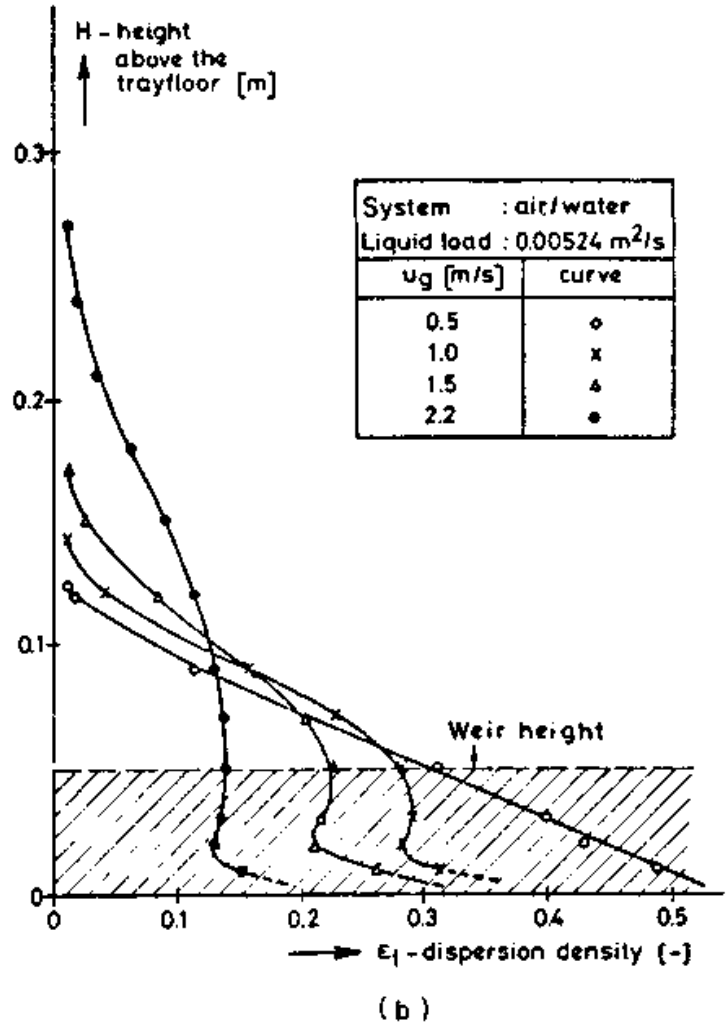

Figure 6.28 (*Continued*) Characteristic features of the spray regime. (*b*) Vertical dispersion density profiles. x axis is liquid fraction (test tray, d_H = 0.25 inches, A_f = 0.07, Q_L = 2 gpm/in. o, x froth regime; Δ froth regime, close to froth to spray transition; • spray regime. (*Part b from F. J. Zuiderweg, P. A. M. Hofhuis, and J. Kuzniar, Chem. Eng. Res. Des., 62, p. 39, 1984. All parts reprinted courtesy of the Institution of Chemical Engineers, UK.*)

lular foam regimes are not common in industrial applications, and will not be discussed further.

Effect of pressure. In vacuum columns, vapor velocities are generally high and liquid flow rates are low, which coincides with an operating point in the spray regime. If the column operates at high liquid loads, it may operate in the froth regime. The emulsion regime is unlikely to occur in vacuum columns.

In high-pressure (>200-psi) distillation, vapor velocity is low and liquid flow rate is relatively high, which coincides with an operating point in the emulsion regime. If the column operates at low liquid

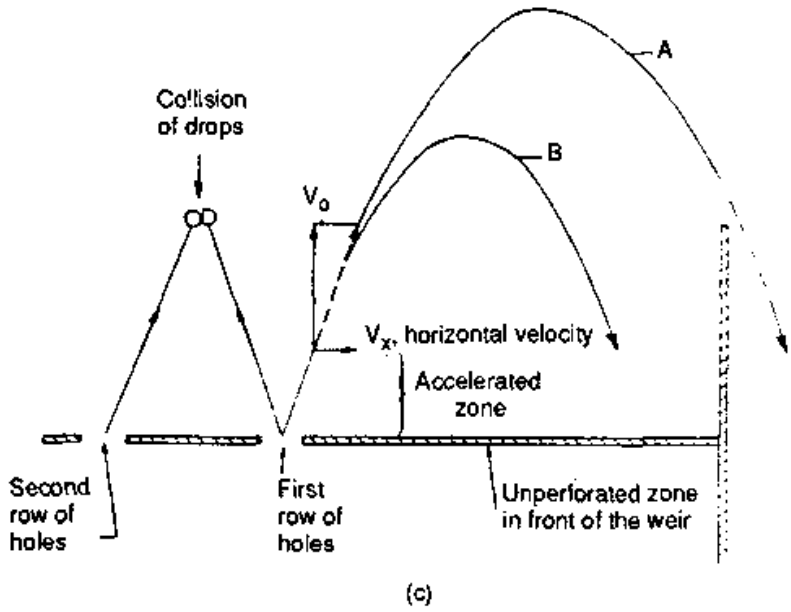

(c)

Figure 6.28 (*Continued*) Characteristic features of the spray regime. (c) Liquid transport mechanism by trajectory ("jumping") over the outlet weir. (*Part c from F. J. Zuiderweg, P. A. M. Hofhuis, and J. Kuzniar, Chem. Eng. Res. Des., 62, p. 39, 1984. All parts reprinted courtesy of the Institution of Chemical Engineers, UK.*)

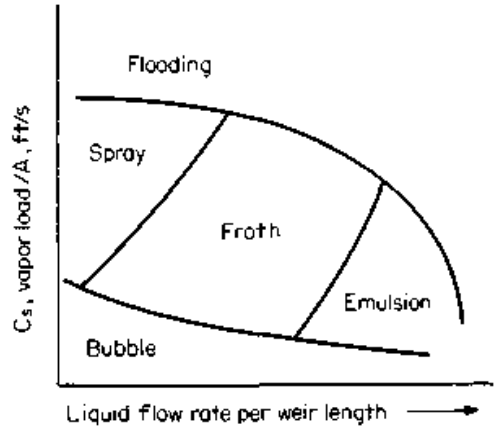

Figure 6.29 The flow regime likely to exist on a distillation tray, as a function of vapor and liquid loads.

loads, it may operate in the froth regime. The spray regime is unlikely to occur.

In atmospheric and low-pressure (<100-psi) distillation, the column is likely to operate in the froth regime, but depending on the liquid and vapor rates, it may also operate in either the spray or emulsion regime.

Effect of *L/V* ratio. In the rectifying section, the liquid load is often lower and the vapor load higher than in the stripping section. Therefore the rectifying section tends toward the spray regime, while the stripping section tends toward the emulsion regime. Similarly, a high-

liquid-load absorber or stripper tends toward the emulsion regime, while a low-liquid-load wash section tends toward the spray regime.

Effect of column diameter (at constant *L/V* and percent of flood). As column diameter increases, both the liquid and vapor flow rates increase as the square of the diameter. The area for vapor flow also increases as the square of the diameter, so the vapor load remains unaffected. On the other hand, the area available for liquid flow only increases in proportion to the diameter. Therefore, the liquid rate per unit of weir length increases, the increase being proportional to the column diameter. The operating point on Fig. 6.29 will therefore shift horizontally to the right, toward the emulsion regime. Increasing the number of liquid passes on the tray reverses the above action, and shifts the operating point back to the left.

Effect of tray spacing (at constant *L/V* and percent of flood). Lower tray spacing reduces flooding vapor rate, and therefore, the operating vapor velocity. This reduction in vapor velocity shifts the operating point on Fig. 6.29 toward the froth or emulsion regime. Conversely, an increase in tray spacing shifts the operating point toward the spray regime. Columns operating at very low (<12 in) tray spacing almost always operate in the froth regime.

Effect of fractional hole area. Low fractional hole areas increase the tendency of trays to operate in the spray regime (92,106). In terms of Fig. 6.29, lower fractional hole areas tend to shift the spray-froth boundary to the right. No effect of fractional hole area was observed (17,85) on the transition from the froth to the emulsion regime.

Effect of hole diameter. Large holes increase the tendency of trays to operate in the spray regime (88,89,92,106–108). In terms of Fig. 6.29, larger holes tend to shift the spray-froth boundary to the right. No effect of hole diameter was observed (17,85) on the transition from the froth to the emulsion regime.

Effect of weir height. Pinczewski and Fell (90,92) showed that weir height has little effect on the transition from the froth-to-spray regime. More recent work by Prado and Fair (103) and Lockett (12) suggests that the tendency of a tray to operate in the froth regime increases slightly with an increase in weir height. No effect of weir height on the transition from froth to emulsion was observed (17,85).

Effect of tray type. Most flow regime work was carried out using sieve trays. Some of the preliminary work reported for valve trays suggests

that valve trays may have the same or a somewhat greater tendency (86) to operate in the froth regime than sieve trays.

Summary. Spray regime operation is favored in vacuum and low-pressure columns, under low liquid loads, when column diameter is relatively small, and when tray spacing is relatively high. Spray regime operation is also favored by trays with large hole diameters and low fractional hole areas. Emulsion regime operation is favored in high-pressure columns and under high liquid loads.

6.4.3 Transition between flow regimes

Froth-spray. Froth-spray transition has been investigated for sieve trays using a variety of techniques (12,24,88–92,103,106–110). The gradual nature of this transition bred a large number of criteria for defining it, and made its correlation difficult. Excellent overviews of the state of art were given by Lockett (12) and Prado and Fair (103).

Porter and Jenkins (24) presented a simple correlation for the froth to spray transition.

$$F_{1v}\frac{N_p A_B}{L_w} = 0.0191 \tag{6.71}$$

This correlation is based on the premise that froth to spray transition occurs when the entrainment versus liquid load relationship passes through a minimum (Fig. 6.15, Sec. 6.2.11). This premise has been questioned, and it was argued that the minimum may represent a transition from the froth regime to a partially developed spray region (40,53). This argument implies that whenever the correlation predicts froth, it is highly unlikely that the column operates in the spray regime. If, however, it predicts spray, it may well be that the column is still operating in the froth regime.

A second correlation is by Pinczewski and Fell (52,90)

$$u_B\sqrt{\rho_G} = 2.25\left(\frac{Q_L\sqrt{\rho_L}}{100}\right)^n \tag{6.72}$$

where $n = 0.0231\, d_H/A_f$, as per Eq. (6.69).

This correlation is based on transition data obtained from orifice jetting measurements (92,106) for the air-water system and on entrainment minimum data (22) for some hydrocarbon systems.

A third recent correlation by Johnson and Fair (18,103,111) gives

$$u_B\sqrt{\rho_G} = 0.17\,\rho_L^{0.692}\,\sigma^{0.06}\,A_f^{0.25}\,Q_L^{0.05}\,d_H^{-0.1} \tag{6.73}$$

Equation (6.73) applies to 2-in weirs; for 1-in weirs, u_B should be multiplied by 0.92; for 4-in weirs it should be multiplied by 1.12 (18).

Froth-emulsion. Froth-emulsion transition occurs (17,45,85,105) when the aerated mass begins to obey the Francis weir formula. Using this criterion, the latest version of this transition correlation is

$$F_{lv}\frac{N_p A_B}{L_w h_c} = 0.0208 \tag{6.74}$$

where h_c is calculated from the Hofhuis and Zuiderweg equation [Eq. (6.67)]. A close inspection of the experimental data correlated (85) shows that this too is a gradual transition, which occurs over a range of values rather than at a sharp point.

Valve trays. The amount of work reported thus far on valve tray regime transition is small and entirely based on air-water tests. Correlations proposed to date require the knowledge of liquid holdup at transition, which is generally not available, and are therefore of limited application for commercial columns.

An early study (91) reports that a correlation derived by Barber and Wijn for sieve tray froth-to-spray transition is also applicable to valve trays. A more recent study by Dhulesia (112) disagrees, and reports that valve trays have a stronger tendency to operate in the froth regime than sieve trays. Dhulesia proposed an alternative froth-spray transition correlation for valve trays, but this correlation is based on air-water data from a single type of valve tray, and its extension to other situations has not been tested.

6.4.4 Implications of the spray regime for design and operation

While the classical hydraulic model provides a reasonable approximation for the froth and emulsion regimes, different mechanisms determine the hydraulics and mass transfer in the spray regime. The transition from froth to spray is gradual, and so is the change in the hydraulic and mass transfer behavior (110,111,113,114).

Flow across the tray. The classical hydraulic model implies that liquid flows across the tray by building up a liquid head on the tray, and when this head exceeds the weir height it overflows it. This mechanism is valid in principle when liquid is the continuous phase, but in the spray regime, vapor is the continuous phase and the liquid is present as drops in the vapor space (Figs. 6.25*d*, 6.26*c*, and 6.27*b*). In

the spray regime, liquid is transported by a "jumping" mechanism (104,113,115) (Fig. 6.28*c*).

Outlet weir. While in the classical model the weir height determines the liquid level (or the clear liquid height) on the tray, in the spray regime the weir plays a minor role. Clear liquid height shows a small, if any, dependence on weir height in the spray regime (89,90,92). Liquid enters the downcomer by jumping high over the weir and not by flowing across it (Fig. 6.28*c*). Therefore, the Francis weir formula does not apply to trays operating in the spray regime (85,104).

Close to the outlet weir, droplets that have been unsuccessful in crossing the weir form a liquid pool (113). This pool sends liquid back along the tray floor to the orifices close to the outlet weir for reatomization. When the pool is too shallow (e.g., about zero-in weirs), atomization may grow fiercer, producing more entrainment (36,40).

Pressure drop. Wet pressure drop on the tray is determined by the resistance of the aerated mass to vapor flow (Sec. 6.3.3). As the nature of the dispersion is different, one would expect a different mechanism to cause pressure drop in the spray regime. This has been confirmed by experiments (88,114). To date, not enough is known about the nature of this mechanism.

Entrainment. Different mechanisms generate entrainment in the spray and froth regimes (Sec. 6.2.11). In the spray regime much more entrainment is produced and a larger amount of liquid resides at higher elevations (Fig. 6.28*b*). Low tray spacing is not suitable for spray regime operation; generally a tray spacing of at least 18 in, and preferably 24 in or more, is recommended (108). Using high tray spacing has been a common practice in vacuum towers, which often operate in the spray regime.

Mass transfer. According to the classical model, mass transfer takes place by vapor-liquid contact in the froth. In the spray regime, mass transfer takes place on the surface of the drops (116). In order to appreciate the differences in mass transfer between the regimes, distillation systems have been classified into three types:

1. Positive-surface-tension systems ($\sigma+$) where surface tension increases as liquid flows down the column.
2. Negative-surface-tension systems ($\sigma-$) where surface tension drops as liquid flows down the column.
3. Neutral systems, where surface tension is unchanged.

It has been shown (116) that σ− gives smaller drops, thus providing more mass transfer surface in the spray regime. This is why σ− gives higher efficiency in the spray regime while σ+ gives higher efficiency in the froth regime (108,116,117). It has been proposed (108) that for negative systems, columns should be designed to operate in the spray regime in order to improve tray efficiency. However, this is seldom practical. Columns are designed to suit the required vapor and liquids loads and the process conditions, giving the tray designer very limited freedom for choosing a desired flow regime.

Some evidence has been presented to suggest that the degree of back mixing of liquid on the tray is smaller in the spray than in the froth regime (113). Much of the back mixing in the spray regime has been attributed to reatomization of the liquid from the pool near the outlet weir (113). The lower degree of back mixing tends to enhance efficiency in the spray regime.

6.4.5 Implications of the emulsion regime for design and operation

The difference in the behavior of the aerated mass between the emulsion and froth regimes is far less apparent than the difference between the froth and spray regime.

Flow across the tray. In the froth regime the liquid is thrown over as drops and slugs, and therefore the flow does not obey the Francis weir formula (85,104). In the emulsion regime a "homogeneous" dispersion flows over the weir. While in the froth regime the bubbles are of different sizes, in the emulsion regime most of the vapor is vigorously emulsified into small bubbles (Figs. 6.25*e* and 6.27*c*).

Flooding and entrainment. Entrainment represents very little problem in the emulsion regime, and is usually negligible (17,45,105). On the other hand, the quantity of vapor that enters the downcomer is much greater than in the froth regime (17,45,104). Further, emulsion flow tends to coincide with conditions where separation of liquid from vapor in the downcomer is difficult. For these reasons, the most likely flooding mechanisms in the emulsion regime are downcomer choking, downcomer backup, or both.

Vapor recycle. Because of the large quantity of vapor that enters the downcomer and the difficulty of separation in the downcomer, vapor recycle is a major consideration in the emulsion regime (Sec. 6.2.8) and can lead to reduction of both capacity and efficiency, and to an increase in pressure drop (17).

Hoek and Zuiderweg (44) described the effect of vapor entrainment on tray efficiency in terms of a theoretical model. The tray is divided into several mixing zones. Ascending vapor is split in parallel among the zones, while liquid passes in series from one zone to another. Liquid entering and leaving each zone contains the same amount of entrained vapor per mole of liquid as the downcomer underflow. In each zone, liquid is perfectly mixed while the ascending vapor is in plug flow. The model showed that the effects of vapor entrainment are most severe when liquid-phase resistance to mass transfer is controlling. When vapor-phase resistance to mass transfer controls, the effects are less severe, because the recycled vapor enhances the stripping action of the more volatile component, thus counteracting the entrainment effect.

Foaming. The emulsion flow regime is particularly sensitive to foaming (17,85). The presence of foaming impurities stabilizes the emulsion and therefore brings about a premature capacity limitation.

Mass transfer. Tray efficiency increases with pressure in the froth regime (118,119), but decreases with increased pressure in the emulsion regime (44,104,105). The efficiency decrease in the emulsion regime is caused by the greater vapor recycle (44,104,105). In general, there is otherwise little difference between mass transfer in the froth and emulsion regimes.

6.5 Column Sizing

6.5.1 General considerations

The sizing procedure is a trial-and-error calculation. A preliminary design is set, and then refined by checking against the performance correlations until an adequate design is achieved. The sizing calculations are performed at the points where column loading is expected to be highest and lowest for each section, i.e.,

- The top tray
- Above every feed, product drawoff, or point of heat addition or removal
- Below every feed, product drawoff, or point of heat addition or removal
- The bottom tray
- At any point in the column where the calculated vapor or liquid loading peaks

For a single-feed two-product column, there is generally a need to carry out the sizing calculation for the top tray, bottom tray, tray just above the feed, and tray just below the feed. The column is then designed for the more severe conditions.

6.5.2 Tray sizing example and initial steps

Example 6.1 Size the depropanizer from Examples 2.4 (Sec. 2.3.1) and 3.4 (Sec. 3.2.5). The feed rate is 2000 lb-mole/h of mixture. Minimum anticipated load is 60 percent of design.

solution The material balance based on 100 lb-mole/h feed was shown in Table 2.7. Accordingly, vapor and liquid flow rates were calculated (Sec. 2.3.4). These are prorated to 2000 lb-mole/h feed. Table 6.10 shows the column profile, loadings, and physical properties at a feed rate of 2000 lb-mole/h. The data shown in Table 6.10 are typical of data generated by commercial computer simulations.

MAXIMUM LOADS Table 6.10 shows that both the volumetric and mass vapor and liquid flow rates in the top section peak at stage 3. Stage 3 is therefore the appropriate basis for the maximum throughput calculation for the top section.

TABLE 6.10 Column Loading and Physical Properties: Depropanizer example 6.1 (Basis: 20,000 lb-mole/h feed)

	Vapor to stage				Liquid from stage					
Stage	°F	lb/h	CFS	ρ_V	°F	lb/h	GPM	ρ_L	σ	μ_L
1	108	109,728	12.705	2.399	70	73,910	310	29.820	5.31	0.136
2	119	120,812	13.559	2.475	108	84,994	378	27.979	3.37	0.129
3	126	121,184	13.584	2.478	119	85,360	380	27.944	3.30	0.128
4	134	119,412	13.451	2.466	126	83,588	370	28.187	3.35	0.128
5	144	118,186	13.378	2.454	134	82,360	360	28.498	3.44	0.129
6	157	117,122	13.339	2.439	144	81,280	352	28.816	3.53	0.130
7	172	114,732	13.246	2.406	157	78,926	336	29.208	3.66	0.131
8	199	109,310	13.060	2.325	172	73,504	304	30.122	4.44	0.133
9	225	82,856	7.629	3.017	211	139,172	598	29.029	3.40	0.123
10	235	93,602	8.347	3.115	225	149,918	656	28.457	3.60	0.124
11	242	100,406	8.751	3.187	235	156,724	694	28.159	3.41	0.126
12	249	105,908	9.049	3.251	242	162,228	724	27.934	3.28	0.126
13	255	111,198	9.332	3.310	249	167,520	754	27.735	3.16	0.125
14	261	115,806	9.560	3.365	255	172,126	778	27.574	3.07	0.123
15	266	119,144	9.705	3.410	261	175,468	796	27.454	3.00	0.121
16	272	122,464	9.863	3.449	266	178,768	816	27.344	2.94	0.119
17	280	124,948	9.954	3.487	272	181,272	828	27.268	2.90	0.117
18	291	126,714	9.963	3.533	280	183,038	838	27.225	2.87	0.115
19	309	129,112	9.924	3.614	291	185,434	850	27.191	2.84	0.113
20					309	56,324	260	26.997	2.05	0.110
Conditions selected for hydraulic calculation										
Top section										
3 (max)	126	121,184	13.584	2.478	119	85,360	380	27.944	3.30	0.128
8 (min)	199	109,310	13.060	2.325	172	73,504	304	30.122	4.44	0.133
Bottom section										
19 (max)	309	129,112	9.924	3.614	291	185,434	850	27.191	2.84	0.113
9 (min)	225	82,856	7.629	3.017	211	139,172	598	29.029	3.40	0.133

Similar reasoning selects stage 19 as the maximum throughput stage in the bottom section. Note that on this stage, the volumetric vapor flow rate is slightly lower than that of tray 18; however, the difference is about 0.4 percent, while the mass flow rate of stage 19 is 1.9 percent higher than that of stage 18, and therefore tray 19 is more appropriate. If in doubt, the C-factor [Eq. (6.4)] serves as the best indicator; here it shows that stage 19 has the greater vapor load.

$$C_S \text{ (stage 19)} = \frac{9.924}{A_N}\sqrt{\frac{3.614}{27.191 - 3.614}} = \frac{3.885}{A_N}$$

$$C_S \text{ (stage 18)} = \frac{9.963}{A_N}\sqrt{\frac{3.533}{27.225 - 3.533}} = \frac{3.847}{A_N}$$

MINIMUM LOADS Table 6.10 shows that for the bottom section, stage 9 is the apparent choice for the minimum throughput calculation. Stage 20 is ignored since it simulates the reboiler. For the top section, either stage 1 or stage 8 has the lowest vapor and liquid loads. If turndown is critical, a separate hydraulic calculation is required at each of these two stages. However, the loadings are within 2 to 3 percent of each other, and minimum throughput calculation is seldom critical. The objective of the turndown calculation is to define where efficiency begins to fall off. In stage 1, the loadings are low because of the cold entering liquid; this is a local phenomenon that affects the efficiency of one, or at most a handful, of trays. Stage 8, on the other hand, is more characteristic of the stages above it. Therefore, the minimum throughput calculation here is only performed for stage 8.

SUMMARY Stages selected for hydraulic calculations are

	Maximum throughput	Minimum throughput
Top section	3	8
Bottom section	19	9

6.5.3 Preliminary determination of tower diameter

Tray area. Using an entrainment flooding correlation is the usual method of calculation, but short-cut methods (e.g., Ref. 10) are often adequate. However, to minimize trial and error, the author prefers to perform the preliminary estimate using the flooding correlation which will eventually be used, with some simplifying assumptions. In this example, the Kister and Haas correlation [Eq. (6.12)] will be used for the preliminary determination of tray area. Make the following simplifying assumptions:

$$d_H = 0.5 \text{ in}; \qquad S = 24 \text{ in}; \qquad h_{ct} = 2.5 \text{ in}$$

Top section

$$C_{SB} = 0.144\left(\frac{0.5^2\ 3.30}{27.944}\right)^{0.125}\left(\frac{2.478}{27.944}\right)^{0.1}\left(\frac{24}{2.5}\right)^{0.5} = 0.225 \text{ ft/s}$$

Bottom section

$$C_{SB} = 0.144\left(\frac{0.5^2\,2.84}{27.191}\right)^{0.125}\left(\frac{3.614}{27.191}\right)^{0.1}\left(\frac{24}{2.5}\right)^{0.5} = 0.231 \text{ ft/s}$$

Calculate the flood velocity from Eq. (6.9)
Top section

$$u_N = 0.225\sqrt{\frac{27.944 - 2.478}{2.478}} = 0.723 \text{ ft/s}$$

Bottom section

$$u_N = 0.231\sqrt{\frac{27.191 - 3.614}{3.614}} = 0.591 \text{ ft/s}$$

To calculate the bubbling area from the flood velocity, the derating factor is needed (Table 6.7). For depropanizers, SF = 0.9 top and bottom. Also needed is a safety margin from flood; at this point, assume the column is to be designed for 80 percent of flood.

$$A_N = \frac{\text{CFS}}{(\text{SF})(0.8)u_N}$$

Top section

$$A_N = \frac{13.584}{0.9\ 0.8\ 0.723} = 26.1 \text{ ft}^2$$

Bottom section

$$A_N = \frac{9.924}{0.9\ 0.8\ 0.591} = 23.3 \text{ ft}^2$$

Downcomer area. Use Table 6.5 to obtain a preliminary estimate of downcomer top area. For a depropanizer at 315 psia, Table 6.5 recommends a velocity of 90 to 110 gpm/ft^2. Select 100 gpm/ft^2. No derating is required here, since the factors in Table 6.5 already take the foaming tendency into account.

Top section

$$A_D = 380/100 = 3.8 \text{ ft}^2$$

Bottom section

$$A_D = 850/100 = 8.5 \text{ ft}^2$$

Tower diameter. Total tower area is given by

$$A_T = A_N + A_D$$

Top section

$$A_T = 26.1 + 3.8 = 29.9 \text{ ft}^2$$

$$D_T = \sqrt{\frac{4}{\pi} 29.9} = 6.2 \text{ ft}$$

Bottom section

$$A_T = 23.3 + 8.5 = 31.8 \text{ ft}^2$$

$$D_T = \sqrt{\frac{4}{\pi} 31.8} = 6.4 \text{ ft}$$

Roughly, when the difference in calculated diameter between the top and bottom section exceeds 20 percent, different diameters for the top and bottom sections are likely to be economical (32). In the present example, the diameter difference is 3 percent, so column diameter should be uniform. The preliminary column diameter is the larger of the two, i.e., 6.4 ft. This diameter is rounded to the next highest half foot, giving 6.5 ft.

6.5.4 Preliminary tray layout

As stated in the introduction to Chapter 6, detailed tray layout is performed in the secondary phase of tray design. A preliminary layout, however, is needed at the primary phase, because the layout influences column size. In the present example, the preliminary layout will be based on tray layout guidelines detailed in a companion book (1).

Number of tray passes. Set this so that the liquid flow rate does not exceed 7 to 13 gpm/in of outlet weir (1). At this preliminary point in the calculation, assume that the weir length is 0.8 times the tower diameter, i.e.,

$$L_w = 0.8 d_T = 0.8 \times 6.5 \times 12 = 62.4 \text{ in}$$

Top section

$$Q_L = 380/62.4 = 6.1 \text{ gpm/in}$$

Bottom section

$$Q_L = 850/62.4 = 13.6 \text{ gpm/in}$$

The weir load is satisfactory for a one-pass design for the top section, but a two-pass tray is needed for the bottom section.

Tray spacing. For the bottom section, 24 in is appropriate (1). For the top section, there may be some spare capacity available, so that a smaller tray spacing (18 in) is preferred. Assume

Top section

$$S = 18 \text{ in}$$

Bottom section

$$S = 24 \text{ in}$$

Hole diameter. A good choice of size for clean services is 3/16 in, while ½ in is preferred for fouling services (1). Assuming that the depropanizer is a mildly fouling service, ½-in holes are appropriate.

Others. Based on Kister's guidelines (1), the following are appropriate preliminary choices for other tray layout parameters.

A_f = Fractional hole area = 0.1

h_w = Outlet weir height = 2.0 in

h_{cl} = 1.5 in

t = 10 gage (for carbon steel) = 0.135 in

Pitch. For an equilateral triangular arrangement, the hole pitch can be calculated from the following geometrical relationships (1).

$$p = 0.951\, d_H/\sqrt{A_f} \tag{6.75}$$

For $d_H = 0.5$, $A_f = 0.1$, $p = 0.951\ (0.5/\sqrt{0.1}) = 1.5$ in

Downcomer layout. The total tower area of a 6.5-foot tower is 33.2 ft^2. In the top section, downcomer area is 3.8 ft^2, i.e., the downcomer is about 3.8/33.2 = 11.5 percent of tower area. This is a relatively small fraction, and there is little incentive to reduce it further. On the other hand, in the bottom section the downcomer occupies 8.5/33.2 = 25.6 percent of the tower area. There is an incentive to reduce this area by using a sloped downcomer. A 2:1 top-to-bottom area ratio is appropriate (1). Therefore, downcomer top area in the bottom section is 8.5 ft^2, while downcomer bottom area is 8.5/2 = 4.25 ft^2. In summary

	Top section	Bottom section
Tower diameter, ft	6.5	6.5
Tower area, ft^2	33.2	33.2
Downcomer top area, ft^2	3.8	8.5
Downcomer bottom area, ft^2	3.8	4.25
$A_B = A_T - A_{DT} - A_{DB}$, ft^2	25.6	20.45
$A_N = A_T - A_D$, ft^2	29.4	24.7

Weir length and downcomer width. These are calculated from geometry. Bolles (2) chart expresses the geometrical relationship between downcomer area, downcomer width, and downcomer length; Fig. 6.30 is a revised version. For better accuracy, the manufacturers or Perry's tables (7,9,18) or high-accuracy charts (8) should be preferred. For the depropanizer example, using Fig. 6.30,

1. *Top section:*

$$A_D/A_T = 3.8/33.2 = 11.5 \text{ percent}$$

$$L_W/d_T = 75.5 \text{ percent (Fig. 6.30}a\text{)}$$

$$L_W = 78 \times 0.755 = 58.9 \text{ in}$$

$$w_{dc}/d_T = 17.3 \text{ percent (Fig. 6.30}a\text{)}$$

$$w_{dc} = 78 \times 0.173 = 13.5 \text{ in}$$

2. *Bottom section, side downcomer, top of downcomer:*

$A_D/(2A_T) = 8.5/(2 \times 33.2) = 12.8$ percent (*Note:* the division by 2 is because the required downcomer area is shared between two side downcomers.)

(Length of one segmental downcomer)$/d_T = 77.8$ percent (Fig. 6.30*a*)

$L_W = 2 \times 78 \times 0.778 = 121.4$ (*Note:* L_W is the total weir length, i.e., double the length of one segmental weir.)

$w_{dc}/d_T = 18.4$ percent (Fig. 6.30*a*)

$w_{dc} = 78 \times 0.184 = 14.4$ in

3. *Bottom section, side downcomer, bottom of downcomer:*

$$A_{DB}/(2A_T) = 4.25/(2 \times 33.2) = 6.4 \text{ percent}$$

(Length of one segmental downcomer)$/d_T = 64.0$ percent (Fig. 6.30*a*)

Downcomer length at bottom $= 2 \times 78 \times 0.64 = 99.8$ in

(Downcomer width at bottom)$/d_T = 11.2$ percent (Fig. 6.30*a*)

Downcomer width at bottom $= 78 \times 0.112 = 8.7$ in

4. *Bottom section, center downcomer, top downcomer:*

$$A_D/A_T = 8.5/33.2 = 25.6 \text{ percent}$$

$$L_W/d_T = 97.9 \text{ percent (Fig. 6.30}b\text{)}$$

$$L_W = 2 \times 78 \times 0.979 = 152.7$$

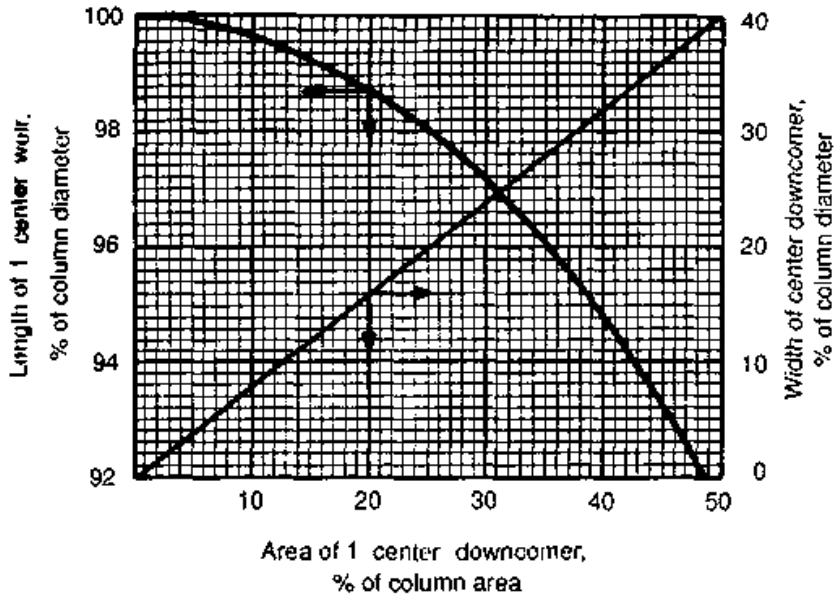

(b)

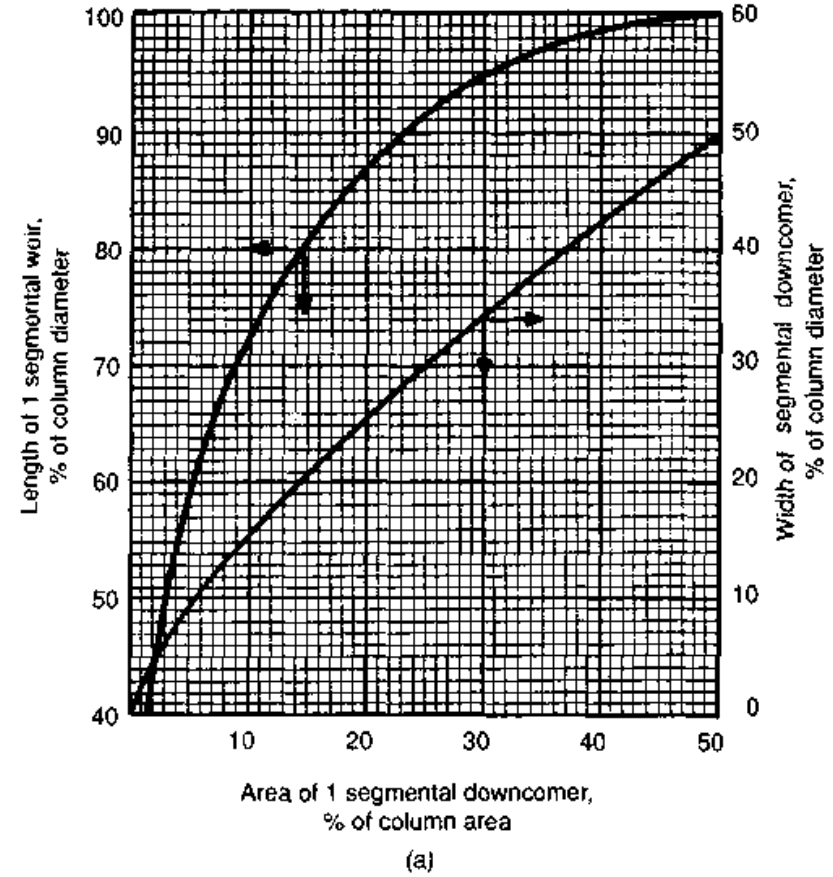

(a)

Figure 6.30 Downcomer design chart. (*a*) Side segmental downcomer; (*b*) center downcomer.

$$w_{dc}/d_T = 20.3 \text{ percent (Fig. 6.30}b\text{)}$$

$$w_{dc} = 78 \times 0.203 = 15.8 \text{ in}$$

5. *Bottom section, center downcomer, bottom of downcomer:*

$$A_{DB}/A_T = 4.25/33.2 = 12.8 \text{ percent}$$

$$\text{(Downcomer length at bottom)}/d_T = 99.5 \text{ percent (Fig. 6.30}b\text{)}$$

$$\text{Total length of downcomer at bottom} = 2 \times 78 \times 0.995 = 155.2$$

$$\text{(Downcomer width at bottom)}/d_T = 10 \text{ percent (Fig. 6.30}b\text{)}$$

$$\text{Downcomer width at bottom} = 78 \times 0.10 = 7.8 \text{ in}$$

6. *Check liquid flow path:* [Note Kister's guideline (1) of avoiding flow path lengths smaller than 16 to 18 in.]

   Top section

   $$\text{FPL} = 78 - 13.5 - 13.5 = 51 \text{ in}$$

   Bottom section, center to side flow

   $$\text{FPL} = 78/2 - 7.8/2 - 14.4 = 20.7 \text{ in}$$

   Bottom section, side-to-center flow

   $$\text{FPL} = 78/2 - 15.8/2 - 8.7 = 22.4 \text{ in}$$

   All are OK.

7. *Comment:* In the bottom section, the weir length (both at the top and bottom of the downcomer) is shorter for the side than for the center downcomers. Therefore, the liquid load (gallons per minute per inch of weir) will be higher for the center to side flow.

6.5.5 First trial

Throughout this trial, vapor and liquid loads and physical properties are taken from Table 6.10. Tray layout parameters are taken from Table 6.11.

Flooding check. It was recommended (5,30,32) to design a column to 80 to 85 percent of flood. This safety margin allows for inaccuracies in data and correlations. In addition, a drop in efficiency often occurs just before the flood point, and this practice avoids the problem region. The flooding check is performed using the Kister and Haas correlation (Sec. 6.2.6).

TABLE 6.11 Tray Layout—Example 6.1

	Top section			Bottom section			
	1st trial	2d trial	3d trial	1st trial	2d trial	3d trial	
D_T, ft	6.5	6.0	→	6.5	6.0	→	
A_T, ft^2	33.2	28.3	→	33.2	28.3	→	
A_D, top	3.8	→	→	8.5	7.73	→	
A_{DB}, bottom	3.8	→	→	4.25	3.86	→	
A_N	29.4	24.5	→	24.7	20.57	→	
A_B, ft^2	25.6	20.7	→	20.45	16.71	→	
L_W, in	58.9	56.6	→	121.4	113.4	→	(side)
				152.7	140.5	→	(center)
Length of downcomer at bottom, in	58.9	56.6	→	99.8	93.3	→	(side)
				155.2	143.2	→	(center)
Downcomer width at top, in	13.5	13.8	→	14.4	14.0	→	(side)
				15.8	15.7	→	(center)
Downcomer width at bottom, in	13.5	13.8	→	8.7	8.4	→	(side)
				7.8	7.8	→	(center)
LFP, in	51	44.4	→	20.7	18.1	→	C-S*
				22.4	19.8	→	S-C†
S, in	18	18	21	24	→	→	
d_H, in	0.5	→	→	0.5	→	→	
A_f	0.1	→	→	0.1	→	→	
h_w, in	2.0	→	→	2.0	2.0	1.5	C-S*
				2.0	2.0	2.0	S-C†
h_{cl}, in	1.5	1.5	2.0	1.5	1.5	2.0	C-S*
				1.5	1.5	2.25	S-C†
t, in	0.135	→	→	0.135	→	→	
p, in	1.5	→	→	1.5	→	→	

*Center-to-side flow.
†Side-to-center flow.

First trial flooding check (*Continued*)

	Top section	Bottom section		Note
		C-S*	S-C†	
Q_L, gpm/in	6.45	7.00	5.57	Eq. (6.6)
$(h_{ct})_{H_2O}$, in	0.937	0.940	0.931	Eq. (6.70)
n	0.115	→	→	Eq. (6.69)
h_{ct}, in	1.335	1.356	1.343	Eq. (6.68)
C_{SB}, ft/s	0.267	0.314	0.315	Eq. (6.12)
C_S, ft/s (based on A_N)	0.144	0.157	0.157	Eq. (6.4)
SF	0.9	→	→	Table 6.7
C_{SB}, derated, ft/s	0.241	0.283	0.284	SF × C_{SB}
% flood	59.9%	55.6%	55.3%	100 × C_S/(C_{SB} derated)

*Center-to-side flow.
†Side-to-center flow.

Downcomer check. Use the Koch correlation (Sec. 6.2.9), which is the more conservative correlation for downcomer design according to Lockett's analysis (12).

	Top section	Bottom section		Note
		C-S*	S-C†	
$t_{R,sec}$	5.7	6.15	6.15	Fig. 6.13 (Koch)
$Q_{D,\,max}$, gpm/ft^2	106	131	131	Eq. (6.26)
Q_D, gpm/ft^2	100	100	100	Eq. (6.8)
% $Q_{D,\,max}$	94%	76%	76%	$100 \times Q_D/Q_{D,\,max}$

*Center-to-side flow.
†Side-to-center flow.

Summary. According to the above criteria, the tower appears oversized. The next trial should be performed with a smaller tower diameter, say 6 ft.

6.5.6 Second trial

Throughout this trial, vapor and liquid loads and physical properties are taken from Table 6.10. Tray layout parameters are discussed below and shown in Table 6.11.

Layout. First, determine downcomer areas. The calculation in Sec. 6.5.5 shows that the area for the top section downcomers is about right. On the other hand, the bottom section downcomers appear somewhat oversized. Table 6.5 suggests that for the depropanizer (high foaming tendency, 18- and 24-in tray spacing) up to 110 gpm/ft^2 is an appropriate velocity. Resize the downcomer for 110 gpm/ft^2.

$$A_D = \text{GPM}/Q_D = 850/110 = 7.73 \text{ ft}^2$$

Now retain the number of passes, tray spacing, hole diameter, weir height, and clearance under the downcomer as per Sec. 6.5.5.

Recalculate weir and downcomer dimensions by the same procedure as in Sec. 6.5.4. The results are summarized in Table 6.11.

Comment. Note that the length of the flow path (LFP) will restrict any further reductions in column diameter. As stated previously (Sec. 6.5.4), flow path length smaller than about 18 in is best avoided. This limit is reached in the bottom section, center-to-side flow.

Flooding check. The calculation in Sec. 6.5.5 is now repeated.

	Top section	Bottom section C-S*	Bottom section S-C†	Note
Q_L, gpm/in	6.71	7.50	6.05	Eq. (6.6)
$(h_{ct})_{H_2O}$, in	0.938	0.942	0.934	Eq. (6.70)
n	0.115	⟶	⟶	Eq. (6.69)
h_{ct}, in	1.337	1.359	1.347	Eq. (6.68)
C_{SB}, ft/s	0.267	0.314	0.315	Eq. (6.12)
C_S, ft/s (based on net area)	0.173	0.189	⟶	Eq. (6.4)
SF	0.9	⟶	⟶	Table 6.7
C_{SB}, derated, ft/s	0.240	0.282	0.284	SF × C_{SB}
% flood	72%	67%	67%	100 × C_S/(C_{SB} derated)
$Q_{D,\,max}$, gpm/ft^2	106	131	131	Sect. 6.5.5
Q_D, gpm/ft^2	100	110	110	Eq. (6.8)
% $Q_{D,\,max}$	94%	84%	84%	100 × $Q_D/Q_{D,\,max}$

*Center-to-side flow.
†Side-to-center flow.

Comment The column still appears oversized. It is now limited by the flow path length in the bottom section. Therefore, any further reductions in diameter require going from a two-pass design back to a single-pass design in the bottom section. Going for a single-pass design will roughly double the liquid load Q_L (because the weir length will be halved). The resulting liquid load, roughly 15 gpm/in of weir, will be outside the recommended maximum of 7 to 13 gpm/in of weir (1). One way of overcoming this problem is by going to a swept-back weir (1), which in essence lengthens the weir at the expense of losing some bubbling area. This may permit reducing column diameter from 6 to 5.5 ft. For the sake of avoiding repetitious calculations this will not be done here. The reader is urged to attempt a redesign with a 5.5-ft-diameter column (based on the above) as an exercise.

Flooding check—alternative correlation. If desired, the column capacity can be checked using an alternative flooding correlation. This step is optional during column sizing. In this case, this check will be performed using Fair's correlation (Sec. 6.2.6). No derating is applied, as the surface tension correction term will automatically derate high-pressure systems such as the depropanizer.

	Top section	Bottom section C-S*	Bottom section S-C†	Note
L, lb/h (per pass)	85,360	92,717	⟶	Table 6.10
V, lb/h	121,184	129,112	⟶	Table 6.10

	Top Section	Bottom section C-S*	Bottom section S-C†	Note
F_{lv}	0.21	0.26	→	Eq. (6.7)
C_{SB} (Fair's correlation), ft/s	0.21	0.26	→	Fig 6.10
$u_{N,flood}$, ft/s	0.47	0.45	→	Eq. (6.11)
A_N, ft^2	24.5	20.6	→	Table 6.11
u_N, ft/s	0.55	0.48		CFS/A_N
% Flood	117%	107%	→	100 $u_N/u_{N,flood}$

*Center-to-side flow.
†Side-to-center flow.

Comment. This calculation predicts that the column will flood, and that a larger diameter is required. As previously stated (Sec. 6.2.6), Fair's correlation tends to be conservative, especially at high pressure and liquid rate. If a conservative design is desired, column diameter should be expanded to 6.5 ft. In normal design, this type of result for the alternate check will signal a warning against reducing the diameter any further (say to 5.5 ft, as mentioned previously), and will also suggest that it would be beneficial to carry out a flooding check with a second alternative correlation. This will be performed using the Smith et al. correlation (Sec. 6.2.6).

	Top section	Bottom section C-S*	Bottom section S-C†	Note
$\frac{GPM}{N_p}\left(\frac{12 \times N_p}{L_W}\right)^{2.5}$	7.86	8.76	5.13	
$L_W/(d_T N_p)$	0.79	0.79	0.98	
F_w	1.04	1.045	1.005	Fig. 6.23
h_{ow}, in	1.78	1.92	1.60	Eq. (6.49)
Settling height, in	14.2	20.1	20.4	Fig. 6.11
C_{SB} (Fig. 6.11), ft/s	0.185	0.26	0.265	Fig. 6.11
$u_{N,\,flood}$	0.593	0.664	0.677	Fig. 6.11
$u_{N,\,flood}$ (derated)	0.53	0.60	0.61	$u_{N,\,flood} \times$ SF
% Flood	104%	80%	79%	100 $u_N/u_{N,\,flood}$ (derated)

*Center-to-side flow.
†Side-to-center flow.

Comment. The check confirms that the bottom section is adequately sized, but it does raise concerns about the top section. With both alternate checks indicating a potential problem in the top section, it will pay to increase the tray spacing to 21 in.

Summary. Following the flooding checks, the column diameter remains at 6 ft. The tray layout remains as specified at the beginning of this section. However, the tray spacing in the top section is extended from 18 to 21 in, so that the tower has 24-in tray spacing in the bottom section and 21-in tray spacing in the top section.

6.5.7 Hydraulic checks, second trial

Flow regime. Since the trays are unlikely to operate in the spray regime (Sec. 6.4.2), it is best to first examine the froth-emulsion transition. This check requires using the Hofhuis correlation for clear liquid height (Sec. 6.3.5).

The tray flow regime is determined below.

		Bottom section		
	Top section	C-S*	S-C†	Note
F_{lv}	0.21	0.26	0.26	Sec. 6.5.6
h_c (Hofhuis)	1.71	1.71	1.62	Eq. (6.67)
Transition flow parameter	0.097	0.12	0.14	Eq. (6.74)

*Center-to-side flow.
†Side-to-center flow.

Comment. All the actual flow parameters exceed the flow parameters at the froth-to-emulsion transition. Therefore, all these checks indicate emulsion regime operation.

Entrainment. If entrainment is excessive, column diameter or tray spacing are usually increased. It has been recommended (2,67) that entrainment from the tray should not exceed about 0.10 lb liquid entrained per pound of liquid flow. At higher values, significant efficiency reduction occurs (34). Depending on the service, a lower or higher value can be set (4). For instance, if the column overhead stream is compressed and no knock-out drum is present, the entrainment that can be tolerated is smaller. Also, for trays operating at a high liquid-to-vapor ratio, 0.1 lb of liquid entrained per pound of liquid is an excessive quantity of entrained liquid, and a lower limit is set.

Section 6.2.11 recommends the use of Fair's entrainment correlation in the froth (and emulsion) regime. This section also states that entrainment in the emulsion regime is unlikely to be a problem. Fair's correlation (Fig. 6.16) predicts fractional entrainment (pound of entrained liquid per pound of liquid) of 0.011 and 0.0075 at 80 percent of flood for the top and bottom trays, respectively. Even at 90 percent of

flood the entrainment is likely to be less than 0.02 lb entrained liquid per pound of liquid at the flow parameters calculated in Sec. 6.5.6. It may therefore be concluded that entrainment is unlikely to be troublesome in the depropanizer.

Downcomer residence time. This check calculates the apparent residence time in the downcomer and ensures it is within the recommended guidelines in Sec. 6.2.9.

		Bottom section		
	Top section	C-S*	S-C†	Note
Average downcomer area, ft^2	3.8	5.8	→	$(A_{DT} + A_{DB})/2$
S, in	21	24	→	Sec. 6.5.6
Downcomer volume, ft^3	6.65	11.6	→	(Average area) × $S/12$
t_R, s	7.9	6.1	→	448.83 volume/GPM

*Center-to-side flow.
†Side-to-center flow.

Table 6.6 suggests that a residence time of 5 s is appropriate for the depropanizer. The calculated residence times exceed this figure, and are therefore okay.

Pressure drop. Pressure drop is calculated as per Secs. 6.3.1 to 6.3.3, using Fair's pressure drop correlation. Usually, it is good practice to design for a pressure drop of 3 to 5 in of liquid (approximately 0.08 to 0.12 psi) per tray. If outside this range it is best to adjust the fractional hole area (if dry pressure drop dominates) or the weir height (if wet pressure drop dominates).

1 Dry pressure drop

		Bottom section		
	Top section	C-S*	S-C†	Note
t/d_H	0.27	→		
C_v	0.72	→		Fig. 6.21*a*
K	0.359	→		Eq. (6.43)
A_h, ft^2	2.07	1.67	→	$A_f \times A_B$
u_h, ft/s	6.56	5.94	→	CFS/A_h
h_d, in	1.37	1.69	→	Eq. (6.42)

*Center-to-side flow.
†Side-to-center flow.

2 Wet pressure drop

	Top section	Bottom section C-S*	Bottom section S-C†	Note
h_{ow}, in liquid	1.78	1.92	1.60	Sec. 6.5.6
h_{hg}, in liquid	0	0	0	Sec. 6.3.3
h_c, in liquid	3.78	3.92	3.60	Eq. (6.48)
u_B, ft/s	0.656	0.594	→	$u_h \times A_f$
$u_B \rho_G^{0.5}$	1.03	1.13	→	
β	0.63	0.61	→	Fig. 6.22*a*
h_l, in liquid	2.38	2.39	2.20	Eq. (6.47*a*)

*Center-to-side flow.
†Side-to-center flow.

3 Total pressure drop

	Top Section	Bottom section C-S*	Bottom section S-C†	Note
h_r, in liq	3.75	4.08	3.89	Eq. (6.41)

*Center-to-side flow.
†Side-to-center flow.

The check shows that the pressure drop is within the desired range, and no adjustment is needed to tray layout.

Downcomer backup. For side downcomers of two-pass trays, the force balance of Eq. (6.19) makes the clear liquid height in the downcomer the sum of the pressure drop of the tray above (center-to-side flow), plus the clear liquid height of the tray below (side-to-center flow), plus the loss under the side downcomer apron. Similarly, the clear liquid height in the center downcomer is the sum of the side-to-center tray pressure drop, plus the center-to-side tray clear liquid height, plus the loss under the center downcomer apron. The aerated liquid in the downcomer must not exceed the total of the tray spacing plus weir height (Sec. 6.2.7). If downcomer backup is excessive, one must identify the cause. If it is the dry pressure drop, one can either increase column diameter, tray spacing, or fractional hole area. If it is the wet pressure drop, one can increase the number of tray passes or the weir length or reduce weir height. If it is losses in the downcomer apron, the downcomer clearance can be increased. For the depropanizer example, the downcomer backup is calculated below.

	Top section	Bottom section		Note
		Side DC	Center DC	
h_t	3.75	4.08	3.89	Above
h_c	3.78	3.60	3.92	Above
A_{da}, ft^2	0.59	0.97	1.49	Weir length at bottom × h_{cl}/144)
h_{da}, in liquid	1.25	2.29	0.97	Eq. (6.59)
h_{dc}, in liquid	8.78	9.97	8.78	Eq. (6.19)
ϕ_{dc}	0.5	0.4	——→	Table 6.4
h'_{dc}, in froth	17.6	24.9	22.0	Eq. (6.18)
S, in	21	24	——→	Sec. 6.5.6
$S + h_w$, in	23	26	——→	
% Froth in downcomer	77%	96%	84%	100 $h'_{dc}/(S + h_w)$

Comment. No derating of the downcomer backup is required, because the low aeration factor (chosen using the Glitsch and the Bolles criteria, Table 6.4) already allows for the foaminess. The calculation shows a froth height greater than 80 percent in the bottom section, and a need to reduce downcomer backup. In the top section, the froth in the downcomer is less than 80 percent, and is therefore OK. Note that the calculation also strengthens the argument expressed in Sec. 6.5.6 that a tray spacing of 21 in rather than 18 in is required in the top section. With 18-in spacing, the top section would have had 88 percent froth in the downcomer.

The froth height in the center downcomers in the bottom section is only slightly above 80 percent, and increasing the downcomer clearance will suffice to overcome the problem. However, this is unlikely to suffice for the side downcomers in the bottom section. In this example, the clearance under the downcomer will be increased to 2.0 in in the center downcomers, and to 2.25 in in the side downcomers. The weir height on the center-to-side flow trays in the bottom section will be lowered to 1.5 in to lower tray pressure drop.

Although there is no need to change the downcomer clearance in the top section, it is a good idea. The froth in the downcomer bottlenecks the top section, the head loss in the downcomer apron is quite high (1.25 in) and the tray spacing relatively low. The clearance in the top section will therefore also be increased to 2 in.

Note that in the top trays the weir height is now equal to the clearance under the downcomer (both are 2 in). In the bottom section, the outlet weirs are shorter than the clearances under the downcomers. This may raise concerns about having adequate seal on the trays. However, the practice of using outlet weirs shorter than the downcomer clearances is usually adequate for high liquid loads (1), such

as those experienced here. This practice relies on the tray pressure drop and tray liquid height to back up enough liquid in the downcomer to bridge the difference between the weir height and the clearance. In this example, there is a lot of (too much!) liquid backup in the downcomer. It was, however, recommended (1) that a check be made to ensure that at minimum vapor and liquid loads, the clear liquid height in the downcomer exceeds the downcomer clearance by at least 2 in.

Summary. The following modifications result from this check:

1. h_{cl} = 2.0 in for the top downcomers and the center bottom downcomers.
2. h_{cl} = 2.25 in for the side bottom downcomers.
3. h_w = 1.5 in for the center-to-side flow trays in the bottom section.

6.5.8 Third trial

The layout for this trial is the same for the second trial except for the above changes in weir heights and clearances. Also, the tray spacing in the top section changed from 18 to 21 in. Throughout this trial, vapor and liquid loads and physical properties are taken from Table 6.10. Tray layout parameters are shown in Table 6.11. Some variables that remain unchanged from the previous trial are

		Bottom section		
	Top section	C-S*	S-C†	Note
C_S, ft/s (based on net area)	0.173	0.189	——→	Unchanged
SF	0.9	←——	——→	Unchanged
F_{lv}	0.21	0.26	——→	Unchanged
Q_D, gpm/ft^2	100	110	——→	Unchanged
u_B, ft/s	0.656	0.594	——→	Unchanged
u_N, ft/s	0.55	0.48	——→	Unchanged
u_h, ft/s	6.56	5.94	——→	Unchanged

*Center-to-side flow.
†Side-to-center flow.

Flooding checks

1 *Kister and Haas correlation (Sec. 6.2.6)*

	Top section	Bottom section		Note
		C-S*	S-C†	
	New Calculation	Unchanged from Sec. 6.5.6	Unchanged from Sec. 6.5.6	
h_{ct}, in	1.337	↓	↓	Unchanged
C_{SB}, ft/s	0.288			Eq. (6.12)
C_{SB} (derated), ft/s	0.260			SF × C_{SB}
% Flood	67%	67%	67%	100 × C_S/C_{SB} (derated)

*Center-to-side flow.
†Side-to-center flow.

2 *Downcomer choke—Koch correlation (Sec. 8.2.9)*

	Top section	Bottom section		Note
		C-S*	S-C†	
	New calculation	Unchanged from Sec. 6.5.6	Unchanged from Sec. 6.5.6	
t_R, s	5.7	↓	↓	Fig. 6.13 (Koch)
$Q_{D,max}$, gpm/ft^2	124			Eq. (6.26)
% $Q_{D,max}$	81%	84%	84%	100 × $Q_D/Q_{D,max}$

*Center-to-side flow.
†Side-to-center flow.

3 *Fair's correlation (Sec. 6.2.6)*

	Top section	Bottom section		Note
		C-S*	S-C†	
	New calculation	Unchanged from Sec. 6.5.6	Unchanged from Sec. 6.5.6	
C_{SB} (Fair's correlation)	0.25	↓	↓	Fig. 6.10
$u_{N,flood}$	0.56			Eq. (6.11)
% Flood	98%	117%	107%	100 $u_N/u_{N,flood}$

*Center-to-side flow.
†Side-to-center flow.

4 Smith et al. correlation (Sec. 6.2.6)

	Top section	Bottom section C-S*	Bottom section S-C†	Note
	New calculation	New calculation	Unchanged from Sec. 6.5.6	
h_{ow}, in	1.78	1.92	↓	Unchanged
Settling height, in	17.2	20.6	↓	Fig. 6.11
C_{SB} (Fig. 6.11)	0.245	0.27	↓	Fig. 6.11
$u_{N,flood}$	0.785	0.69	↓	Fig. 6.11
$u_{N,flood}$ derated	0.71	0.62	↓	$u_{N,flood} \times SF$
% Flood	78%	77%	79%	$100\, u_N u_{N,flood}$ (derated)

*Center-to-side flow.
†Side-to-center flow.

Operating regime

	Top section	Bottom section C-S*	Bottom section S-C†	Note
	Unchanged from Sec. 6.5.6	New Calculation	Unchanged from Sec. 6.5.6	
h_c (Hofhuis)	↓	1.48	↓	Eq. (6.67)
Transition flow parameter	↓	0.105	↓	Eq. (6.74)
Regime	Emulsion	———	———	Eq. (6.74)

*Center-to-side flow.
†Side-to-center flow.

Entrainment

Fair's correlation (Sec. 6.2.11)

	Top section	Bottom section C-S*	Bottom section S-C†	Note
ψ, based on % flood from Kister and Haas correlation	0.0065	0.0048	0.0048	Fig. 6.16
ψ, based on % flood from Smith et al. correlation	0.0095	0.0070	0.0075	Fig. 6.16

*Center-to-side flow.
†Side-to-center flow.

Downcomer residence time

	Top section	Bottom section		Note
		C-S*	S-C†	
	Unchanged from Sec. 6.5.7	Unchanged from Sec. 6.5.7	Unchanged from Sec. 6.5.7	
t_R, s	7.9	6.1	6.1	Sec. 6.5.7
Minimum t_R,s required, s	5.0	5.0	5.0	Table 6.6

*Center-to-side flow.
†Side-to-center flow.

Pressure drop

	Top section	Bottom section		Note
		C-S*	S-C†	
1. Dry pressure drop h_d, in	1.37	1.69	1.69	Unchanged
2. Wet pressure drop	Unchanged from Sec. 6.5.7	New calculation	Unchanged from Sec. 6.5.7	
h_{bg}, in liquid	↓	0	↓	Unchanged
β		0.61		Unchanged
h_c, in liquid	3.78	3.42	3.60	Eq. (6.48)
h_l, in liquid	2.38	2.09	2.20	Eq. (6.47)
3. Total pressure drop h_t, in liquid	3.75	3.78	3.89	Eq. (6.41)

Downcomer backup

	Top section	Bottom section		Note
		Side DC	Center DC	
A_{da}, ft^2	0.79	1.46	1.99	(Weir length at bottom × h_{cl}/144)
h_t	3.75	3.78	3.89	Above
h_c	3.78	3.60	3.42	Above
h_{da}, in liquid	0.70	1.02	0.55	Eq. (6.59)
h_{dc}, in liquid	8.23	8.40	7.86	Eq. (6.19)
ϕ_{dc}	0.5	0.4	0.4	Unchanged
h_{dc}, in froth	16.5	21.0	19.7	Eq. (6.18)
$S + h_w$, in	23	25.5	26	
% froth in downcomer	72%	82%	76%	$100\, h'_{dc}/(S+h_w)$

Summary. The third trial checks well against the various hydraulic criteria. Column capacity is limited by downcomer backup flood in the bottom section center-to-side trays (i.e., side downcomers). All trays will operate in the emulsion regime.

6.5.9 Turndown checks (based on third trial)

These checks will use all the parameters in the layout summary in Sec. 6.5.8 (Table 6.11, third trial). The minimum throughput calculations will be performed for stages 8 and 9 in the depropanizer, where the loads are lowest. Since the example requires column turndown to 60 percent of the expected design loads, the vapor and liquid loads shown in Table 6.10 for stages 8 and 9 are multiplied by 0.6 for the turndown checks.

Turndown loads

		Bottom section		
	Top section	C-S*	S-C†	Note
CFS	7.836	4.577	→	0.6 × (Table 6.10)
GPM	182	359	→	0.6 × (Table 6.10)
u_B, ft/s	0.379	0.274	→	CFS/A_B
u_h, ft/s	3.79	2.74	→	CFS/A_h
L, lb/h (per pass)	44,100	41,750	→	0.6 × (Table 6.10)
V, lb/h	65,590	49,710	→	0.6 × (Table 6.10)
F_{lv}	0.19	0.27	→	Eq. (6.7)
F_H	5.78	4.76	→	Eq. (6.3)
$F_{S,B}$	0.578	0.476	→	Eq. (6.2)
Q_L, gpm/in	3.216	3.168	2.555	Eq. (6.6)

*Center-to-side flow.
†Side-to-center flow.

Weep point check. If the trays operate above their weep points at turndown conditions, checks of the fractional weep and dump point may not be needed. The weep point check will be performed using Fair's correlation (Sec. 6.2.12).

		Bottom section		
	Top section	C-S*	S-C†	Note
$\frac{\text{GPM}}{N_p}\left(\frac{12N_p}{L_w}\right)^{2.5}$	3.77	3.70	2.16	
$L_w/(12D_TN_p)$	0.79	0.79	0.98	

	Top section	Bottom section C-S*	Bottom section S-C†	Note
F_w	1.025	1.025	1.005	Fig. 6.23
h_{ow}, in	1.07	1.06	0.90	Eq. (6.49)
$h_w + h_{ow}$, in	3.07	2.56	2.90	
t/d_H	0.27	→	→	
C_v	0.72	→	→	Fig. 6.21*a*
K	0.359	→	→	Eq. (6.43)
h_d	0.40	0.28	→	Eq. (6.42)
h_σ	0.01	0.01	→	Eq. (6.31*b*)
$h_d + h_\sigma$	0.41	0.29	→	
$h_d + h_\sigma$ @ weep point	0.64	0.6	0.62	Fig. 6.18
% Weep point vapor load	80%	69%	68%	$\sqrt{h_d/(h_d \text{ @ weep point})}$

*Center-to-side flow.
†Side-to-center flow.

Comment. Figure 6.18 predicts weeping at turndown conditions in both the top and bottom sections. It is necessary to check for dumping and for fraction weep.

Dump point check. This check will be performed using the Prince and Chan correlation (Sec. 6.2.14).

	Top Section	Bottom section C-S*	Bottom section S-C†	Note
$F_H\sqrt{\rho_{H_2O}/\rho_L}$ @ dump	7.0	5.4	6.2	Fig. 6.20
Dump F_H	4.86	3.68	4.23	Above $x\sqrt{\rho_L/\rho_{H_2O}}$
% Dump	119%	129%	113%	F_H/(Dump F_H)

*Center-to-side flow.
†Side-to-center flow.

Comment. Figure 6.20 predicts that at turndown, neither top nor bottom section will dump. However, both sections will operate close to the dump point, and excessive weeping is likely. This is consistent with the prediction from Fair's weep correlation (above), which indicates that at turndown both sections operate well below the weep point.

Weep fraction calculation. For high-pressure systems (>165 psia), the Hsieh and McNulty correlation was recommended (Sec. 6.2.12) and will therefore be used here. The Hsieh and McNulty correlation requires a calculation of clear liquid height using Colwell's correlation (Sec. 6.3.5).

	Top section	Bottom section C-S*	Bottom section S-C†	Note
First trial				
h_c, in	1.5	1.5	1.5	Initial guess
Z, ft	0.217	→		Eq. (6.38)
J_G^*	0.415	0.353	→	Eq. (6.36)
J_L^*	0.0056	0.0102	→	Eq. (6.35)
W	13.21	19.14	→	Eq. (6.37)
f_w	0.073	0.053	→	Eq. (6.40)
Fr	0.00296	0.00215	→	Eq. (6.66)
η	2.182	1.919	→	Eq. (6.64)
ϕ_f	0.314	0.343	→	Eq. (6.65)
h_f, in	4.77	4.38	→	Eq. (6.60)
h_{flow}, in	2.77	2.88	2.38	Eq. (6.63)
h_{flow}/h_w	1.39	1.92	1.19	
C_d	0.72	0.76	0.71	Eq. (6.62)
h_c, in	1.55	1.44	1.52	Eq. (6.61)

*Center-to-side flow.
†Side-to-center flow.

Comment. The calculation converged on the first trial to within reasonable accuracy. The calculation showed that the weep fraction is small (<0.07). As per Sec. 6.2.12, a weep fraction of up to 0.1 can be tolerated. This small weep fraction appears inconsistent with what would be expected based on the proximity of the operating point to the predicted dump point and on the large gap between the operating point and the predicted weep point.

Colwell and O'Bara (58) imply that the Lockett and Banik (56) weep rate correlation is conservative at high pressure (Sec. 6.2.12). This correlation [as modified by Colwell and O'Bara, Eq. (6.34)] can therefore give a useful conservative check.

	Top section	Bottom section C-S*	Bottom section S-C†	Note
Fr_h	0.289	0.226	0.214	Eq. (6.33)
W	25.6	30.1	32.7	Eq. (6.34)
f_w	0.14	0.084	0.091	Eq. (6.40)

*Center-to-side flow.
†Side-to-center flow.

Comment. The Lockett and Banik correlation confirmed the prediction of the Hsieh and McNulty correlation, and as expected, gave a more conservative answer. The weep fraction is small and can be tolerated. This conclusion is further supported by the observation that

the minimum loads are about 50 percent of the maximum loads, and that a turndown of 2:1 is readily achievable by a sieve tray (Sec. 6.3.6).

Seal check. In Sec. 6.5.7, it was decided to go to clearances under the downcomers that exceed the outlet weir heights. For such designs, it has been recommended (1) that the clear liquid height in the downcomer under turndown conditions exceeds the downcomer clearance by at least 2 in. This will be checked here.

		Bottom section		
	Top section	C-S*	S-C†	Note
h_{hg}, in	0	———	———	Sec. 6.3.3
h_c, in	3.07	2.56	2.90	Eq. (6.48)
β	0.71	0.74	———	Fig. 6.22*a*
h_l, in	2.18	1.89	2.15	Eq. (6.47*a*)
h_t, in	2.58	2.17	2.43	Eq. (6.41)
	Top	Side DC	Center DC	
h_t	2.58	2.17	2.43	Above
h_c	3.07	2.90	2.56	Above
A_{da}, ft^2	0.79	1.46	1.99	(Weir length at DC bottom × h_{cl}/144)
h_{da}, in	0.16	0.18	0.10	Eq. (6.59)
h_{dc}, in	5.81	5.25	5.09	Eq. (6.19)
$h_{dc} \sim h_{cl}$, in	3.81	3.00	3.09	

*Center-to-side flow.
†Side-to-center flow.

Comment. This check indicates that at turned-down conditions, downcomer backup exceeds the clearance under the downcomer by more than 2 in. Therefore, no seal loss problem is expected.

6.5.10 Concluding comments on design philosophy

The example reflects the prime difficulty often encountered by tray designers: inconsistent predictions from different correlations. The three entrainment flood correlations used gave predictions that widely differed; the differences were up to 50 to 60 percent. Another inconsistency was in the weep-dump prediction. These inconsistencies stem from the empiricism associated with prediction methods. Our understanding of tray hydrodynamics has still a very long way to go before it can provide us with models that reliably predict tray performance from first principles.

In the meantime, we (as designers) have to make the best of the em-

pirical world we live in. The safest approach is to base the design on the most conservative prediction. At times, this is also the best approach. The decision of whether to go for a conservative prediction depends on consequences of failure, cost of conservatism, and confidence in prediction. For instance, downcomer area in this example was conservatively sized. Figure 6.8 shows that in the high-pressure region, downcomers are likely to bottleneck column throughput. Designing these too tight can lead to a premature bottleneck. The consequences of failure are too harsh, and our understanding of downcomer hydraulics is too incomplete to justify a nonconservative approach. Further, the costs of oversizing the downcomers are relatively low. Therefore, the benefits outweigh the costs, and a conservative design was justified.

In two other cases, nonconservative decisions were made, namely in weeping and entrainment flooding prediction. In the case of weeping, the correlation inconsistencies could have been resolved at relatively low cost by going to valve trays. Going to valve trays here would have been quite a reasonable design decision. The author, however, felt confident with the weep-rate predictions (both of the methods used were tested at high pressure, Sec. 6.2.12). Further, the consequences of failure can be lived with at least temporarily, and a later retray with valve trays is not too expensive. On the other hand, when it came to entrainment flooding prediction, a lot was at stake. A conservative prediction here would have grossly oversized the column, and therefore, would have had a very high price tag. Considering the limitations of the correlations used (Sec. 6.2.6) there was a good basis to believe that there was no need to go for the most conservative correlation. Noticing that capacity at high pressure is normally limited by downcomer rather than entrainment flooding (Fig. 6.8) gives one more reason for selecting a nonconservative approach.

The example reflects another philosophical aspect of the design: how to optimize sections of the column that have excess capacity. In this case, it was the top section. As a first step, the example minimized the excess capacity by cutting back on tray spacing. This shortens column height and directly saves costs. As a second step, the tray design was adjusted to give as much margin as possible from potential bottlenecks, e.g., by generously sizing downcomers and by increasing downcomer clearance. During the life of a column, feeds, loads, and capacity requirements change. A good tray design will think ahead and attempt to eliminate any future bottlenecks without incurring a substantial cost penalty. Debottlenecking at a future date is far more expensive. In practice, optimization of column sections that have excess capacity is one aspect of tray design that is often neglected. It is the author's hope that this example will help increase awareness of this aspect.

6.5.11 Tray design summary

Tower diameter, ft	6.0
Tray spacing, in	21 above feed
	24 below feed
Type of tray	Sieve
Hole diameter, in	0.5
Tray thickness	10 Ga
Number of passes	1 above feed
	2 below feed

		Bottom section	
	Top section	C-S*	S-C†
Bubbling area, ft^2	20.7	16.7	16.7
Net area, ft^2	24.5	20.6	20.6
Hole area, ft^2	2.07	1.67	1.67
Downcomer type	Straight	Sloped	Sloped
Total downcomer top/bottom area, ft^2	3.8/3.8	7.73/3.86	7.73/3.86
Side downcomer width, top/bottom, in	13.8/13.8	14.0/8.4	—
Center downcomer width, top/bottom, in	—	—	15.7/7.8
Length of one segmental weir, top/bottom, in	56.6/56.6	56.7/46.7	—
Length of one center weir, top/bottom, in	—	—	70.3/71.6
Outlet weir height, in	2	1.5	2
Clearance under side downcomers, in	2.0	—	2.25
Clearance under center downcomers, in	—	2.0	—
Length of flow path, in	44.4	18.1	19.8

*Center-to-side flow.
†Side-to-center flow.

6.5.12 Hydraulic performance summary

		Bottom section	
	Top section	C-S*	S-C†
1. Percent entrainment (jet) flood			
Kister and Haas correlation, %	67	67	67
Fair's correlation, %	98	117	107
Smith et al. correlation, %	78	77	79
2. Downcomer capacity limits			
% Froth in downcomer	72	82	76
% Maximum downcomer velocity, Koch correlation	81	84	84
Apparent downcomer residence time, s	8	6	6
3. Operating regime	Emulsion		

	Top section	Bottom section	
		C-S*	S-C†
4. Entrainment, fraction of liquid on tray	0.0065	0.0048	0.0048
5. Pressure drop			
Dry, in liquid	1.37	1.69	1.69
Wet, in liquid	2.38	2.09	2.20
Total, in liquid	3.75	3.78	3.89
6. Downcomer hydraulics			
Downcomer backup, in clear liquid	8.23	8.40	7.86
Downcomer aeration factor	0.5	0.4	0.4
Head loss under downcomer apron, in clear liquid	0.70	1.02	0.55
7. Turndown (*Note:* This is based on turndown conditions.)			
% Weep point vapor load, Fair's correlation	80	69	68
% Dump point vapor load, Prince and Chan correlation	119	129	113
Fraction of tray liquid weeping, Hsieh and McNulty correlation, %	7.3	5.3	5.3
Fraction of tray liquid weeping, Lockett and Banik correlation (as modified by Colwell and O'Bara), %	14	8.4	9.1
Downcomer seal at turned down conditions (downcomer backup less downcomer clearance, in clear liquid)	3.8	3.0	3.1

*Center-to-side flow.
†Side-to-center flow.

Chapter

7

Tray Efficiency

7.1 Tray Efficiency Fundamentals

7.1.1 Definitions

Overall column efficiency is defined by

$$E_{OC} = N_t/N_a \tag{7.1}$$

N_t is calculated by any of the methods in Chaps. 2 to 5. Once the tray efficiency is known, the number of actual trays can be obtained from Eq. (7.1).

Since efficiencies vary from one section to another, it is best (12) to apply Eq. (7.1) separately for each section (e.g., rectifying and stripping). In practice, efficiency data and prediction methods are often too crude to give a good breakdown between the efficiencies of different sections, and Eq. (7.1) is applied over the entire column.

Alternative definitions of tray efficiency are sometimes used. Lockett (12) reviewed the pros and cons of several efficiency definitions. He cited the industry's experience that the more rigorous and theoretically correct a definition is, the more difficult it is to use. For instance, the Standart efficiencies are often considered the soundest fundamentally, but apparently have never been used for a design. For the design and operation engineer, the overall column (or section) efficiency is by far the most important.

Point efficiency is defined by (Fig. 7.1*a*).

$$E_{OG} = \left(\frac{y_n - y_{n-1}}{y_n^* - y_{n-1}}\right)_{\text{point}} \tag{7.2}$$

y^* is the composition of vapor in equilibrium with the liquid at point n. y_n is the actual vapor composition at that point. The point efficiency is the ratio of the change of composition at a point to the change that would occur on a theoretical stage. As the vapor composition at a

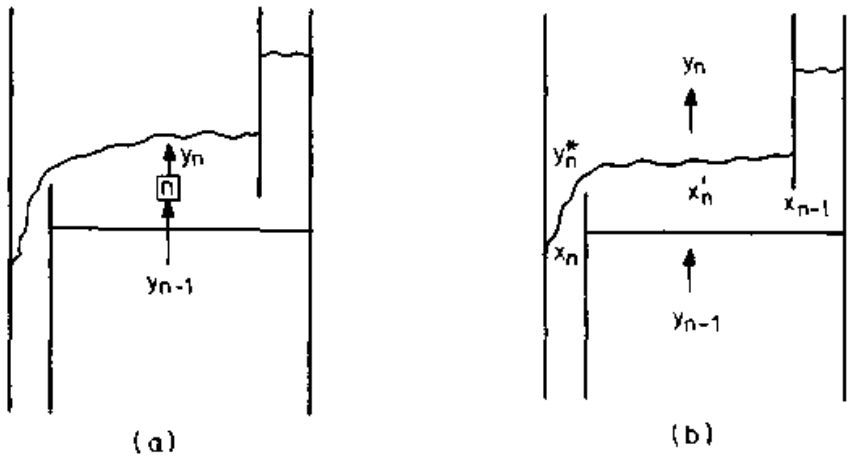

Figure 7.1 Point and Murphree efficiencies. (*a*) Point; (*b*) Murphree.

given point cannot exceed the equilibrium composition, point efficiencies are always lower than unity. If there is a concentration gradient on the tray, point efficiency will vary from point to point on the tray.

Murphree tray efficiency (120) is the same as point efficiency, except that it applies for the entire tray instead of to a single point (Fig. 7.1), i.e.,

$$E_{MV} = \left(\frac{y_n - y_{n-1}}{y_n^* - y_{n-1}}\right)_{tray} \tag{7.3}$$

y^* is the composition of vapor in equilibrium with the liquid leaving the tray. y_n is the actual composition of vapor leaving the tray. The Murphree tray efficiency is the ratio of the change of composition on the tray to the change that would occur on a theoretical stage.

If both liquid and vapor are perfectly mixed, liquid composition on the tray is uniform and so is vapor composition. The Murphree tray efficiency will then coincide with the point efficiency at any point on the tray. In practice, a concentration gradient exists in the liquid, and x_n at the tray outlet is lower than x_n' on the tray (Fig. 7.1*b*). This frequently lowers y_n^* relative to y_n, thus enhancing tray efficiency [Eq. (7.3)] compared to point efficiency. y_n^* may even drop below y_n; in this case, E_{MV} exceeds 100 percent [Eq. (7.3)].

Overall column efficiency can be calculated from the Murphree tray efficiency using the relationship developed by Lewis (121).

$$E_{OC} = \frac{\ln [1 + E_{MV}(\lambda - 1)]}{\ln \lambda} \tag{7.4}$$

where

$$\lambda = \frac{G_M}{L_M} \tag{7.5}$$

Equation (7.4) is based on the assumption of constant molar overflow (Sec. 2.2.2) and a constant value of E_{MV} from tray to tray. It needs to be applied separately to each section of column (e.g., rectifying and stripping) because G_M/L_M, and therefore λ, varies from section to section. Where molar overflows or Murphree efficiencies vary throughout a section of column, the section needs to be divided to subsections small enough to render the variations negligible. Equation (7.4) can then be applied to each subsection.

The point and Murphree efficiency definitions above are expressed in terms of vapor concentrations. Analogous efficiency definitions can be expressed in terms of liquid concentrations. Further discussion is in Refs. 12 and 122.

7.1.2 Point efficiency fundamentals

Point efficiency is usually discussed in terms of the two-film theory. The theory postulates resistances to mass transfer in both the vapor and liquid films near a vapor-liquid interface (Fig. 7.2*a*). The molar rate of diffusion, N (moles/s), is given by

$$N = k_G a_i' \rho_{M,G}(y_i - y) = k_L a_i' \rho_{M,L}(x - x_i) = K_{OG} a_i' \rho_{M,G}(y^* - y) \tag{7.6}$$

The total interfacial area, a_i', can be expressed in terms of the specific interfacial area and the froth volume

$$a_i' = a_i A_B h_f/12 \tag{7.7}$$

Combining Eqs. (7.6) and (7.7) and using a differential form over a froth element dh_f gives

$$\begin{aligned} dN &= k_G a_i \rho_{M,G}(y_i - y) A_B\, dh_f/12 = k_L a_i \rho_{M,L}(x - x_i) A_B\, dh_f/12 \\ &= K_{OG} a_i \rho_{M,G}(y^* - y) A_B\, dh_f/12 \end{aligned} \tag{7.8}$$

A material balance for the differential element shown in Fig. 7.2*b* gives

$$dN = G_M A_B\, dy = L_M A_B\, dx \tag{7.9}$$

Combining Eqs. (7.9) and (7.8), integrating, and defining transfer units N_G, N_L, and N_{OG} gives

$$N_G = \int \frac{dy}{y_i - y} = \frac{k_G a_i h_f \rho_{M,G}}{12 G_M} \tag{7.10a}$$

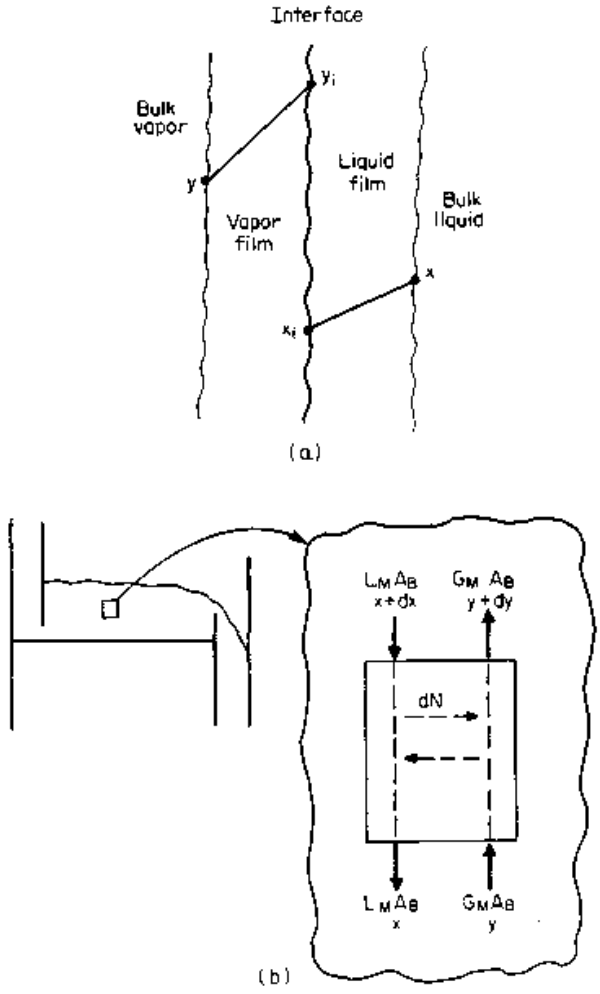

Figure 7.2 Principles of point efficiency. (*a*) Concentration profiles of the more volatile component; (*b*) component balance in a froth element.

$$N_L = \int \frac{dx}{x - x_i} = \frac{k_L a_i h_f \rho_{M,L}}{12 L_M} \tag{7.10b}$$

and

$$N_{OG} = \int \frac{dy}{y^* - y} = \frac{K_{OG} a_i h_f \rho_{M,G}}{12 G_M} \tag{7.10c}$$

y^* is the vapor composition in equilibrium with the bulk liquid composition x, and therefore

$$y^* = mx + b \tag{7.11a}$$

Equilibrium is assumed at the interface, i.e.,

$$y_i = mx_i + b \tag{7.11b}$$

Combining Eqs. (7.11) with Eq. (7.6) gives

$$\frac{1}{K_{OG}} = \frac{1}{k_G} + \frac{m}{k_L} \frac{\rho_{M,G}}{\rho_{M,L}} \tag{7.12}$$

Combining Eq. (7.12) with Eq. (7.10) gives

$$\frac{1}{N_{OG}} = \frac{1}{N_G} + \frac{\lambda}{N_L} \tag{7.13}$$

where λ is defined by Eq. (7.5). Equation (7.13) is the famous relationship used for adding vapor and liquid mass transfer resistances.

$h_f \rho_{M,G}/(12G_M)$ and $h_f \rho_{M,L}/(12L_M)$ are the residence times, t_G and t_L, respectively, of the vapor and liquid in the froth. Equations (7.10*a* and *b*) can be rewritten

$$N_G = k_G a_i t_G \tag{7.14a}$$

and

$$N_L = k_L a_i t_L \tag{7.14b}$$

The above derivation assumes that vapor flows upward in plug flow and that there is no horizontal vapor mixing, while liquid flows horizontally in plug flow and there is no vertical mixing. Lockett and Uddin (12,122) and Standart (123,124) showed that these liquid flow assumptions are poor, unnecessary, and lead to incorrect implications regarding tray efficiency. By modifying the definition of N_L, Lockett derived a fundamentally superior equation analogous to Eq. (7.13). Most theoretical models, however, use Eq. (7.13). Equation (7.13) is also the equation used for packed columns, but for packed columns, it is based on sounder assumptions (12).

For most distillation systems, the resistance to mass transfer is concentrated in the vapor phase [i.e., the $1/N_G$ term in Eq. (7.13) dominates]. Lockett (12) showed that the liquid phase mass transfer resistance increases with liquid rates. At high liquid rates, the liquid phase resistance typically constitutes 25 to 50 percent or more of the total mass transfer resistance.

In order to express the point efficiency in terms of transfer units, Eq. (7.10*c*) is integrated from point $n - 1$ to point n (Fig. 7.1*a*). The integration assumes that in the vertical direction liquid is perfectly mixed and vapor is in plug flow, and gives

$$N_{OG} = -\ln\left(\frac{y_n^* - y_n}{y_n^* - y_{n-1}}\right) \tag{7.15}$$

Combining with Eq. (7.2) gives

$$E_{OG} = 1 - \exp(-N_{OG}) \tag{7.16}$$

Standart et al. (123,124) questioned the validity of these assumptions. In one case (124), they observed a point efficiency greater than unity,

which is inconsistent with the assumptions and Eq. (7.16). They derived a model void of these assumptions, but its complexity precludes its use for design. Lockett (12) stated that the assumption of perfect liquid mixing in the vertical direction was verified to be a very good assumption, and that the assumption of no vapor backmixing is likely to be good for the spray and froth regimes but less satisfactory for the emulsion regime. An in-depth coverage of the fundamentals of point efficiency is available in several texts (12,29,84,125,126).

7.1.3 Tray efficiency fundamentals

Figure 7.3 shows the sequence of steps converting phase resistances into a tray efficiency. Gas and liquid film resistances are added to give the point efficiency (Sec. 7.1.2). Had both vapor and liquid on the tray been perfectly mixed, the Murphree tray efficiency would have equaled the point efficiency (see Sec. 7.1.1). Since the phases are not perfectly mixed, a model of the vapor- and liquid-mixing patterns is

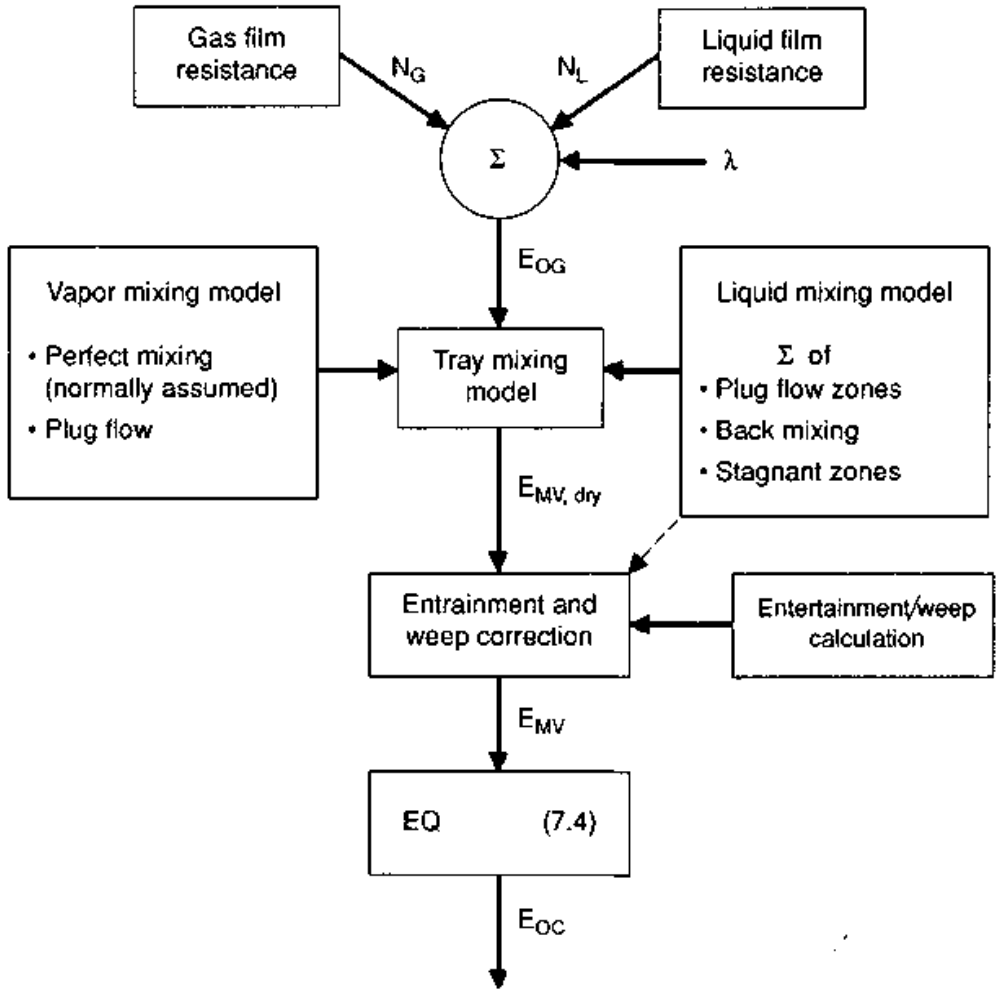

Figure 7.3 Sequence of steps for theoretical prediction of tray efficiency.

needed for converting point efficiency into tray efficiency. Liquid mixing patterns are plug flow, backmixing, and stagnant zones, while vapor-mixing patterns are perfect mixing and plug flow.

Lewis (121) was the first to derive quantitative relationships between the Murphree and the point efficiency. He defined three mixing cases, assuming plug flow of liquid in all:

Lewis case 1	Vapor perfectly mixed between trays (*Note:* in this case the direction of liquid flow on successive trays is immaterial).
Lewis case 2	Vapor unmixed between trays. Liquid flows in the same direction on successive trays.
Lewis case 3	Vapor unmixed between trays. Liquid flows in alternate direction on successive trays.

The Lewis cases give the maximum achievable tray efficiency. In practice, efficiency is lower due to liquid and vapor nonuniformities and liquid mixing. The countercurrent nature of contact is greatest in case 2 and least in case 3, causing tray efficiency to decline from case 2 to case 1 to case 3. The potential for reaching higher efficiency has enticed many specialty tray designs to use case 2 as the basis.

Most tray efficiency models are based on Lewis case 1, and fewer on case 3. Since it is uncommon to have liquid flowing in the same direction on successive trays, Lewis case 2 is seldom used. For case 1, Lewis derived the following relationship:

$$E_{MV,dry} = \frac{\exp(\lambda E_{OG}) - 1}{\lambda} \tag{7.17}$$

Most theoretical models incorporate the effects of vapor and liquid nonuniformity into the relationship between the Murphree and the point efficiency. Developing models for vapor-liquid contact on trays has been a fertile research area in the last couple of decades, with literally hundreds, maybe thousands of papers published on the subject. A thorough review is given by Lockett (12).

The "dry" Murphree efficiency calculated thus far takes into account the vapor and liquid resistances and the vapor-liquid contact patterns, but is uncorrected for the effects of entrainment and weeping. This correction converts the dry efficiency into a "wet" or actual Murphree tray efficiency. Modeling the effect of entrainment and weeping on tray efficiency is based on presumed mixing patterns of liquid on the trays (Fig. 7.3). Colburn (127) derived an equation for the effect of entrainment on efficiency, assuming perfect mixing of liquid on the tray. Although this assumption is questionable, Colburn's equation gives a reasonable approximation to the effect of entrainment on efficiency provided λ is close to unity (12,128). Colburn's equation is

$$E_{MV} = \frac{E_{MV,dry}}{1 + \frac{e}{L_o} E_{MV,dry}} \tag{7.18}$$

Lockett et al. (12,128,129) present rigorous methods for allowing for the effects of entrainment and weeping. Colwell and O'Bara (58) and Banik (57) also present rigorous methods for allowing for the effects of weeping on tray efficiency.

The Murphree tray efficiency obtained from Eq. (7.18) can be converted into a column efficiency using Eq. (7.4).

7.2 Tray Efficiency Prediction

Rigorous testing of a plant column is generally the most reliable method of obtaining tray efficiency. Test procedures are outside the scope of this book and are addressed in a companion book (1) and elsewhere (130). Alternative methods of obtaining tray efficiency are calculation and scaleup (or scale-down). Calculation is addressed in this section; scaleup in Sec. 7.3.

7.2.1 Theoretical prediction methods

Theoretical prediction methods for tray efficiency are based on the two-film theory and use the sequence of steps in Fig. 7.3. Almost all evolved from the AIChE model (84,125,132,133). This model was developed over five years in the late 1950s in three universities. Over the last few decades, several aspects of the AIChE model have been examined, criticized, corrected, and modified. State-of-the-art reviews are given by Lockett (12) and Chan and Fair (134,135). A modified version of the AIChE model that alleviated several of its shortcomings and updated its hydraulic and mass transfer relationships was produced by Chan and Fair (134,135).

The Chan and Fair correlation uses Eqs. (7.13) and (7.16) to calculate the point efficiency E_{OG}. Values of N_G and N_L in Eq. (7.13) are obtained using Eq. (7.14). Chan and Fair derived the following equation for $k_G a_i$, based on Higbie's penetration theory, observations by Calderbank et al. (136,137), and data regression.

$$k_G a_i = \frac{19.1 D_G^{0.5} (1030\text{FF} - 867\text{FF}^2)}{(h_c)^{0.5}} \tag{7.19}$$

where

$$\text{FF} = u_B / u_{B,\text{flood}} \tag{7.20}$$

The gas residence time t_G is obtained from

$$t_G = \frac{(1 - \phi)\, h_c}{12\phi\, u_B} \tag{7.21}$$

The Chan and Fair correlation uses the Bennett et al. correlation (Sec. 6.3.3) for calculating the clear liquid height h_c and the froth density ϕ [Eqs. (6.56) and (6.58)]. For calculating $k_L a_i$, Chan and Fair use a correlation by Foss and Gerster (138).

$$k_L a_i = (0.49 F_{ga} + 0.17)\,(6000 D_L^{0.5}) \tag{7.22}$$

The liquid residence time t_L is obtained from

$$t_L = \frac{h_c A_B}{0.0267 \mathrm{GPM}} \tag{7.23}$$

In order to convert point efficiencies to Murphree tray efficiencies, the Chan and Fair correlation uses the same general mixing model as the AIChE model (125). This model uses Lewis case 1 (Sec. 7.1.3), i.e., mixed vapor and plug flow of liquid. In addition, some liquid backmixing is assumed and correlated via an eddy diffusion coefficient. The model gives

$$\frac{E_{MV}}{E_{OG}} = \frac{1 - [\exp - (\eta + \mathrm{Pe})]}{(\eta + \mathrm{Pe})\left[1 + \dfrac{\eta + \mathrm{Pe}}{\eta}\right]} + \frac{\exp \eta - 1}{\eta\left(1 + \dfrac{\eta}{\eta + \mathrm{Pe}}\right)} \tag{7.24}$$

where

$$\eta = \frac{\mathrm{Pe}}{2}\left[\sqrt{1 + \frac{4\lambda E_{OG}}{\mathrm{Pe}}} - 1\right] \tag{7.25}$$

and

$$\mathrm{Pe} = \frac{(\mathrm{FPL})^2}{144 D_E\, t_L} \tag{7.26}$$

A graphical form of the above equations is shown in Fig. 7.4. The eddy diffusivity D_E is calculated from the correlation of Barker and Self (139).

$$D_E = 0.013\, u_B^{1.44} + 0.025 h_c - 0.061 \tag{7.27}$$

The Chan and Fair correlation does not include a term that per se accounts for weeping and entrainment. In principle, however, the FF

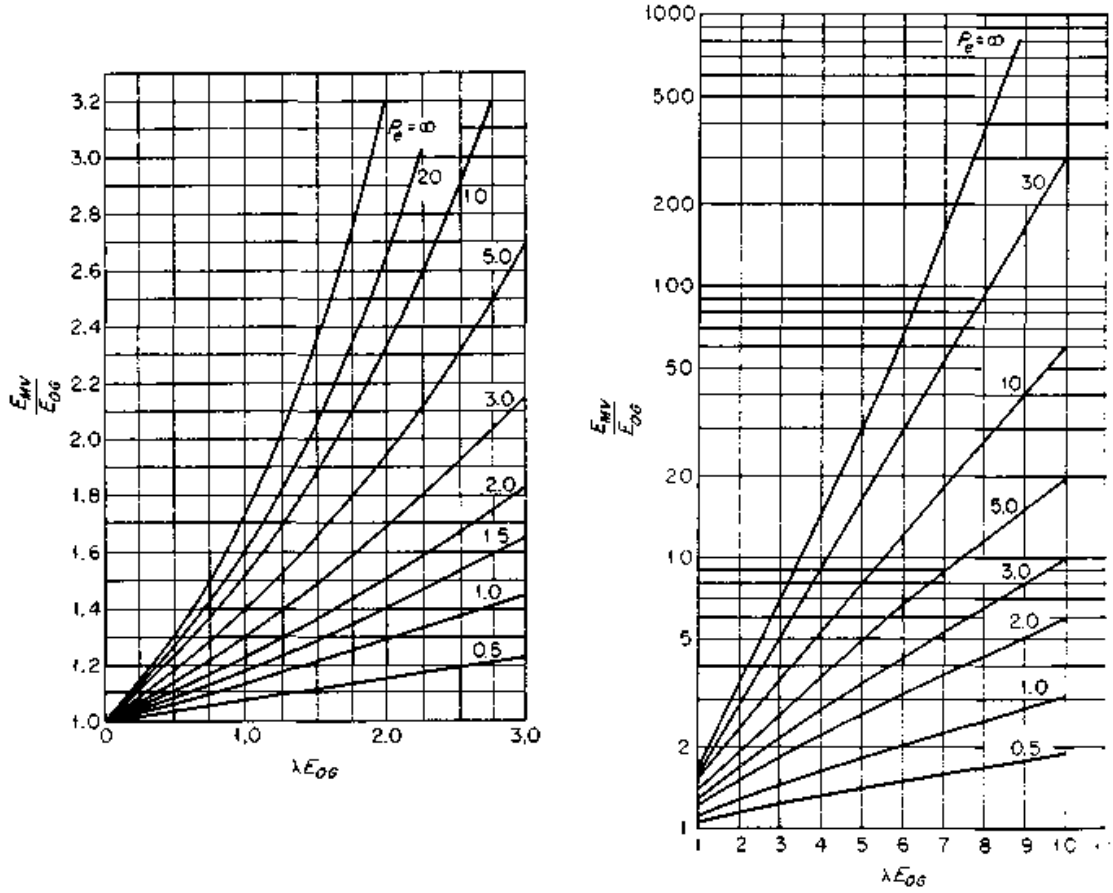

Figure 7.4 Mixing curves. (*From "Bubble Tray Design Manual," by AIChE Research Committee, Distillation Subcommittee, 1958. Reprinted courtesy of the American Institute of Chemical Engineers.*)

term in Eq. (7.19) makes an empirical correction for weeping and entrainment.

Limitations. The Chan and Fair correlation generally gave good predictions when tested against a wide data bank, but its authors also observed some deviations. Chan and Fair (134,135) describe it as "tentative until more data becomes available." Lockett (12) notes that the Chan and Fair correlation inherited the tendency to predict high point efficiencies from the AIChE correlation. Lockett also points out that the presence of the FF term in Eq. (7.19) implies that efficiency depends on tray spacing for fixed vapor and liquid loads. This implication is supported neither by theoretical nor by experimental evidence, and is considered by Lockett as "hardly reasonable."

The Chan and Fair correlation inherited several theoretical limitations from the AIChE correlation. This includes the validity of assumptions in the model for adding mass transfer resistances (Sec. 7.1.2) and the validity of plug flow plus backmixing model (Sec. 7.3.3). Chan and Fair used the Barker and Self (139) correlation for predict-

ing eddy diffusivity. Lockett (12) reviewed 11 eddy diffusivity correlations, and recommended only the Shore and Haselden (140) and Zuiderweg (17) correlations for systems other than air/water. Like the AIChE model, the Chan and Fair correlation only considers axial eddy diffusion, while transverse dispersion may also be important (141,142). Both models assume perfectly mixed vapor, an assumption valid only for small-diameter columns (12); however, Diener (143) showed that tray efficiency is insensitive to vapor-mixing pattern when efficiency is less than 80 percent.

The Chan and Fair correlation also inherited several practical limitations from the AIChE correlation. It is based on a froth regime model, and is unlikely to be valid in the spray regime. Prado and Fair (110,144) have recently proposed a fundamental model that properly accounts for the flow regime, but needs some more work before becoming simple enough to be usable for design. The rough and empirical term accounting for weeping (in terms of FF) is better than nothing (in the AIChE correlation), but is far from satisfactory. The correlation does not account for vapor entrainment, and this can be important at high pressures and high liquid flows (17,104,105). The Chan and Fair correlation is complex and requires the use of diffusivities, which are often a nightmare to obtain with reasonable accuracy.

Chan and Fair (145) extended their correlation to multicomponent systems. Unfortunately, the extension was tested only against few data points, all derived from laboratory-scale columns. However, this extension represents a large improvement over most alternative theoretical correlations.

Alternative correlations. Zuiderweg (17) presented a correlation derived from the same basic model as the AIChE model. Different equations were presented for different flow regimes. Many of the equations were derived from a small data base. In a later paper (146), Zuiderweg noted that the correlation severely underpredicts efficiencies for the methanol-water system, but claims that it should still work for hydrocarbon systems. In another paper (105) Zuiderweg states that this correlation is possibly not more reliable than alternative theoretical models, but argues that it is simpler. Additional review comments on this correlation were made by Lockett (12). Another theoretical prediction method was developed by Stichlmair (29). The basic model is also similar to that of the AIChE correlation. However, in the froth regime, it predicts a strong effect of surface tension on interfacial area, and therefore efficiency. This prediction is inconsistent with experimental work (116) that showed little effect of surface tension on efficiency in the froth regime. Additional review comments on this correlation were made by Lockett (12).

Reliability. An inspection of Eq. (7.26) indicates that for large-diameter columns the liquid is always plug flow. An inspection of Fig. 7.4 suggests therefore a significant enhancement of tray efficiency as diameter increases. This, however, is seldom observed in practice (147,148).

Plug flow tends to maximize the ratio of Murphree to point efficiency. As stated earlier, point efficiencies predicted by the Chan and Fair method tend to be high (12). Combining the two, one would expect this correlation to give optimistic efficiency estimates for large-diameter columns.

The above problem is not unique to the Chan and Fair correlation. In fact, the author feels that this is the most reliable published theoretical efficiency correlation currently available. The current correlation inherited these high efficiency predictions from the AIChE model, and the problem extends to all other theoretical tray efficiency correlations the author has experience with. When the column diameter exceeds 4 ft, one can almost count on a theoretical correlation to predict between 80 and 100 percent efficiency, regardless of the service. In the real world, most columns run closer to 60 percent efficiency. Which of the limitations listed above, and to what extent, generates the problem is unknown. The author would not trust any theoretical tray efficiency correlation for obtaining design efficiencies unless proven that it has actually overcome the above overestimating problem.

7.2.2 Empirical prediction methods

Several empirical tray efficiency correlations are available in the literature. Of these, the O'Connell correlation has been the standard of the industry for several decades.

The O'Connell correlation (149, Fig. 7.5*a*). This correlation is based on test data from 31 plant columns, including hydrocarbon, chlorinated hydrocarbon, and alcohol separation columns. It evolved from an earlier correlation by Drickamer and Bradford (150), which empirically correlated efficiency test data for 54 refinery columns. The earlier correlation was modified by O'Connell to include nonhydrocarbon and high-relative-volatility systems.

Lockett (12) and King (126) noted some theoretical sense in O'Connell's correlation. Higher viscosity usually implies lower diffusivity, and therefore, greater liquid phase resistance and lower efficiency (12). Higher relative volatility increases the significance of the liquid phase resistance [Eq. (7.13)], thus reducing efficiency (126). Lockett expressed the O'Connell plot in equation form

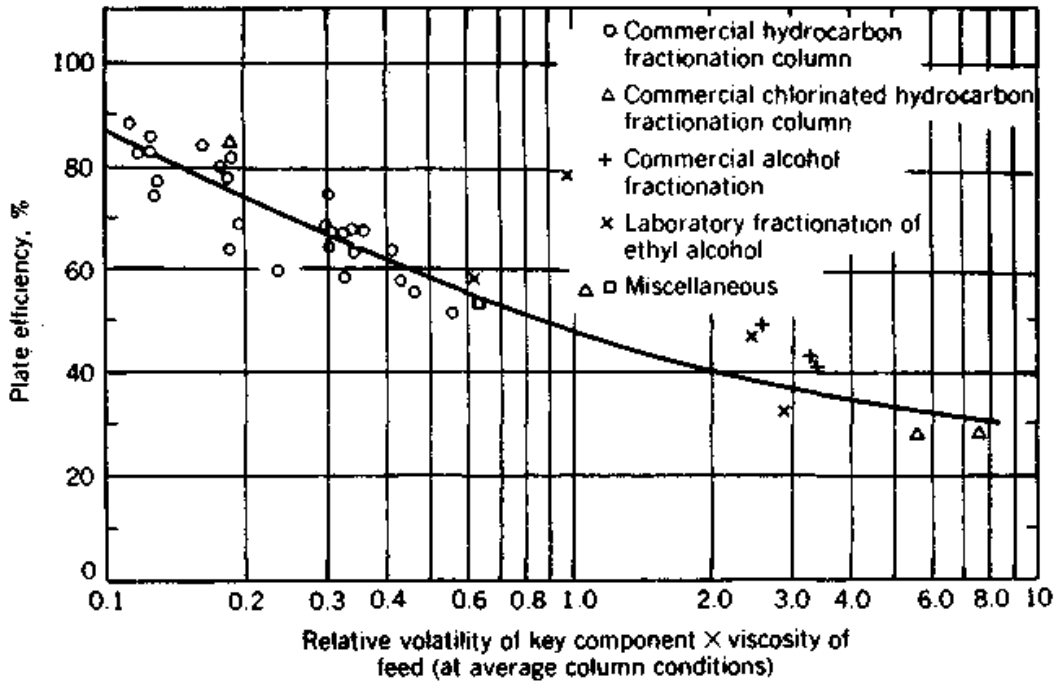

(a)

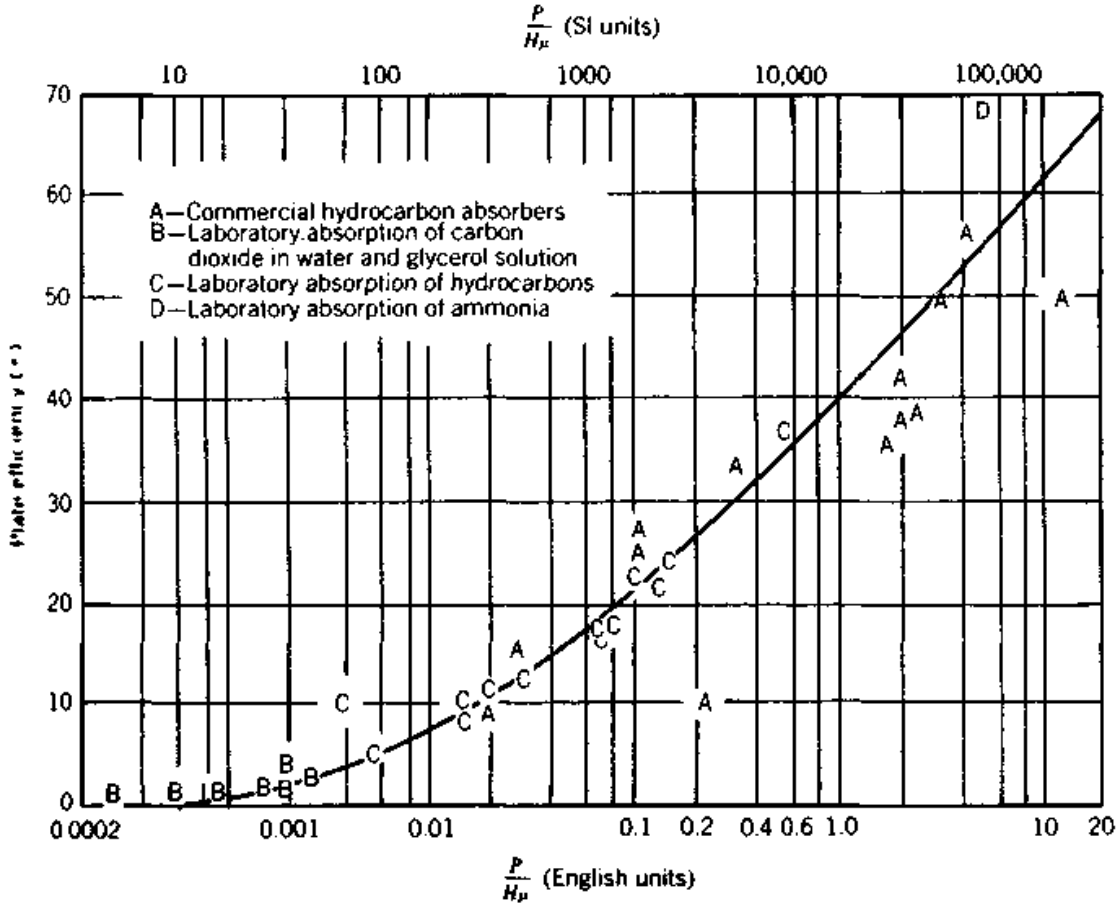

(b)

Figure 7.5 The O'Connell correlation for overall column efficiency. (*a*) Plot for distillation; (*b*) plot for absorbers. (*From H. E. O'Connell, Trans. AIChE, 42, p. 741, 1946. Reprinted courtesy of the American Institute of Chemical Engineers.*)

$$E_{OC} = 0.492(\mu_L \alpha)^{-0.245} \tag{7.28}$$

The volatility and viscosity are evaluated at the average arithmetic temperature between the column top and bottom temperatures. The relative volatility is between the key components. For absorbers, O'Connell generated a second correlation (Fig. 7.5*b*), using a solubility function instead of the relative volatility.

The O'Connell correlation was based on data for bubble-cap trays, and it was stated (131) to predict 90 percent of the efficiency data within ±10 percent, both for distillation and absorption. For sieve and valve trays, its predictions are likely to be slightly conservative (151). Ludwig (4) warns that O'Connell's *absorber* correlation (Fig. 7.5*b*) sometimes predicts efficiencies that are too high. He believes that it can be used for stripping of gases from rich oils and for absorbers provided care is exercised not to accept too high values.

The combination of reasonable accuracy, good reliability, and simplicity, together with the weakness of theoretical tray efficiency correlations, rendered the O'Connell distillation correlation (Fig. 7.5*a*) the standard of the industry. It has been recommended by most literature sources (4,10,18,33,126,131,151,152) as one of the best empirical methods available for tray efficiency prediction. The author has had extensive favorable experience with the distillation correlation (Fig. 7.5*a*), and heard the same from many others in the industry. Frank (10) and the author believe that the O'Connell plot is the best computational method for estimating distillation tray efficiency; others (4,12,33), however, prefer theoretical methods.

The MacFarland, Sigmund, and Van Winkle correlation (153). Another empirical efficiency correlation often mentioned in the literature (12,131,152), it expresses efficiency in terms of dimensionless groups. It is based on binary data for sieve and bubble-cap trays.

7.2.3 Prediction by data interpolation

Vital et al. (131) present an extensive tabulation of tray efficiency data collected from the published literature. Data interpolation is one of the more reliable methods for obtaining tray efficiency, provided the data are good and the rules recommended for data scale-up (Secs. 7.3.6 and 7.3.7) are followed.

7.2.4 Tray efficiency calculation example

Example 7.1 For the column in Examples 2.4 (Sec. 2.3.1), 3.4 (Sec. 3.2.5), and 6.1 (Sec. 6.5.2), find the tray efficiency.

solution The O'Connell correlation requires liquid viscosity and relative volatility at the average arithmetic temperature between the column top and bottom. From Table 6.10, the average temperature is (70 + 309)/2 = 190°F.This temperature is closest to stage 8. Table 6.10 gives a liquid viscosity of 0.133 cP for this stage, and shows little variation in liquid viscosity throughout the column. Also, from Example 3.1, relative volatility of the key components at the average temperature from the column is 1.945.

$$\mu_L\alpha = 0.133 \times 1.945 = 0.259$$

$$E_{OC} = 0.492 \times 0.259^{-0.245} = 0.69 \qquad (7.28)$$

Alternatively, Fig. 7.5*a* gives E_{OC} = 70 percent, which agrees well with Lockett's equation form.

Allowing for a ±10 percent error, an efficiency of 62 percent will be appropriate for design purposes. This can also be seen from Fig. 7.5*a*. The number of trays is therefore 18 stages/0.62 = 29 trays. In the rectifying section, there will be 29 × 7/18 = 11, while in the stripping section there will be 29 × 11/18 = 18 trays.

It is worth it to compare this design efficiency against data listed in the Vital et al. tabulation (131). The tabulation contains no data for depropanizers, but there are data for two related systems: a 4.7-ft ID, 264-psia stabilizer (E_{MV} = 100 percent) and a propane-butane separation (E_{OC} = 100 percent). The data suggest that the depropanizer design efficiency may be conservative. However, the data are too few and do not simulate the depropanizer closely enough to provide an adequate basis for designing for higher efficiency.

7.3 Tray Efficiency Scaleup

Prior to discussing scaleup, the factors that affect tray efficiency need to be addressed. These factors are addressed in Secs. 7.3.1 to 7.3.3. Considerations relevant to the effect of flow regime were previously discussed in Secs. 6.4.4 and 6.4.5.

7.3.1 Effect of errors in Vapor-Liquid Equilibrium (VLE) on efficiency

Errors in relative volatility are the most underrated factor that affects both tray and packing efficiency. The effects are direct when VLE errors affect separation stage requirement at a constant reflux ratio, and indirect when VLE errors affect the reflux ratio requirement (which in turn affects the stage requirement). Since higher relative volatility lowers both stage and reflux requirements (and vice versa), the direct and indirect effects complement each other and do not counteract each other. The discussion below applies to both tray and packed towers.

Direct effects. Figure 7.6 was derived (154,155) from the Fenske equation (Sec. 3.2.1) for total reflux as follows:

$$N_{\min} = S/\ln\alpha \tag{7.29}$$

where

$$S = \frac{x_D\,(1 - x_b)}{x_b(1 - x_D)} \tag{7.30}$$

Differentiating Eq. (7.29) gives

$$dN_{\min} = -S\frac{d\alpha}{\alpha}\frac{1}{(\ln\alpha)^2} \tag{7.31}$$

Using Eq. (7.29),

$$\frac{dN_{\min}}{N_{\min}} = \frac{-d\alpha}{\alpha}\frac{1}{\ln\alpha} \tag{7.32}$$

Since

$$N_{\min} = EN_a \tag{7.33}$$

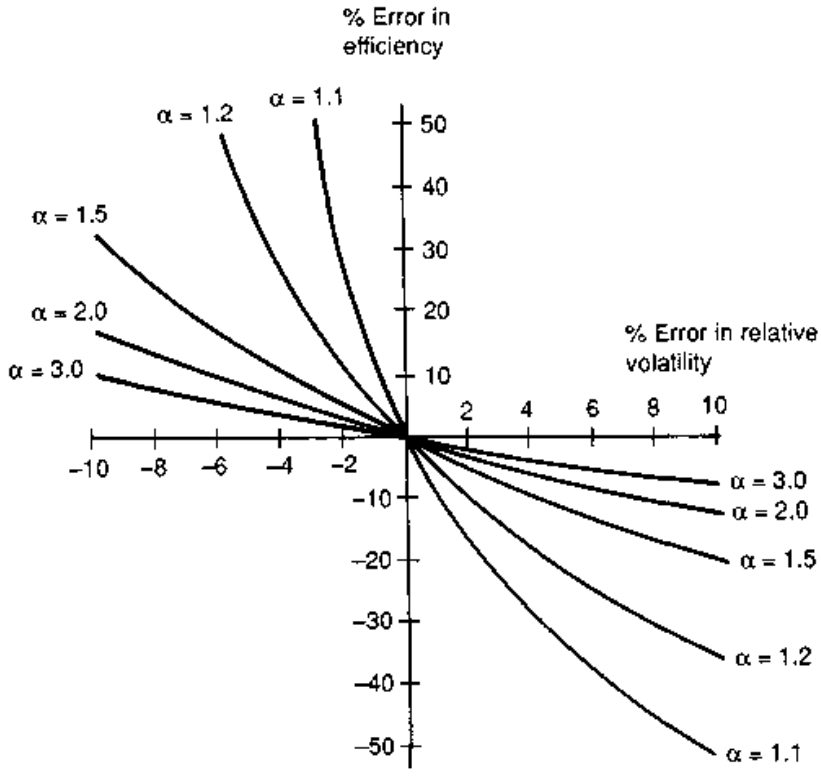

Figure 7.6 Direct effect of errors in relative volatility on error in tray efficiency.

and assuming a constant number of trays, Eq. (7.32) becomes

$$\frac{dE}{E} = \frac{-d\alpha}{\alpha}\frac{1}{\ln \alpha} \tag{7.34}$$

Now let $E = E_{true}$, $\alpha = \alpha_{true}$, $dE = E_{apparent} - E_{true}$, and $d\alpha = \alpha_{apparent} - \alpha_{true}$

$$\frac{E_{apparent} - E_{true}}{E_{true}} = \left(\frac{-\alpha_{apparent} + \alpha_{true}}{\alpha_{true}}\right)\left(\frac{1}{\ln\alpha}\right) \tag{7.35}$$

or

$$\%\ \text{Error in efficiency} = -(\%\ \text{error in volatility})/\ln\alpha \tag{7.36}$$

Figure 7.6 is a plot of Eq. (7.36). At very low relative volatilities ($\alpha < 1.2$), small errors in VLE have a huge impact on tray efficiency. For instance, at a relative volatility of 1.1, a −3 percent error in relative volatility gives a tray efficiency 40 to 50 percent higher than its true value (Fig. 7.6). Since VLE errors are seldom lower than ±2 to 3 percent, both tray efficiencies and packing HETPs of low-volatility systems become meaningless unless accompanied by VLE data. Further, for low-volatility systems, comparing efficiencies derived from different sources is misleading unless using identical VLE. In one low-relative-volatility ($\alpha = 1.1$) design check, the author used 60 percent tray efficiency. The designer used 90 percent efficiency, and came up with exactly the same number of trays. The difference was due to the designer using a relative volatility 2 to 3 percent lower than the author's.

Figure 7.6 shows that errors in relative volatility are a problem only at low relative volatilities. When relative volatility exceeds 1.5 to 2.0, VLE errors have negligible direct impact on tray efficiency.

Most efficiency data reported in the literature are obtained at total reflux. At total reflux, there are no indirect effects, and Fig. 7.6 shows the overall effect of VLE errors on column efficiency. For measurements at finite reflux ratios, the indirect effects below add to those in Fig. 7.6.

Indirect effects. Consider a case where $\alpha_{apparent} < \alpha_{true}$ and test data at a finite reflux are analyzed to calculate tray efficiency. Due to the volatility difference $R_{min,apparent} > R_{min,true}$. Since the test was conducted at a fixed reflux flow rate, $(R/R_{min})_{apparent} < (R/R_{min})_{true}$. A calculation based on the apparent R/R_{min} will give more theoretical stages than a calculation based on the true R/R_{min}. This means a higher apparent efficiency than the true value. This effect therefore supplements that of Fig. 7.6 and widens the gap between true and ap-

parent efficiency. The indirect effects are most pronounced at low relative volatility, because small errors in relative volatility lead to large errors in R/R_{min}.

The indirect effects exponentially escalate as minimum reflux is approached. Small errors in VLE or reflux ratio measurement (this includes column material balance as well as reflux rate) alter R/R_{min}. Near minimum reflux, even small R/R_{min} errors induce huge errors in the number of stages, and, therefore, in tray efficiency. Efficiency data obtained near minimum reflux are therefore meaningless.

Overall effect. A procedure for evaluating the overall effect (combining the direct and indirect effects on tray efficiency) was developed by Nelson, Olson, and Sandler (156). This method is based on the Fenske, Underwood, and Gilliland (Eduljee version) shortcut relationships (Secs. 3.2.1 to 3.2.5) and was shown to work well when comparing to a more rigorous procedure. An example (using an x-y diagram) in Sec. 7.3.6 demonstrates how differences between true and apparent volatility affect efficiencies calculated from test data.

7.3.2 Liquid flow patterns and maldistribution on large trays

Most popular theoretical models (such as the AIChE and the Chan and Fair models, Sec. 7.2.1) postulate that liquid crosses the tray in plug flow (Fig. 7.7*a*) with superimposed backmixing, and that vapor is perfectly mixed. Increasing tray diameter promotes liquid plug flow and suppresses backmixing. This should enhance efficiency in large-diameter columns, but such enhancement has not been observed (147,148). Liquid maldistribution is the common explanation to the observation.

Liquid flow patterns. Liquid entering a single-pass tray flows in a diverging channel until reaching the tray centerline, then in a converging channel as the outlet weir is approached. The liquid has little incentive to move sideways and follow the curved walls of the column. Instead, it seeks the shortest path from inlet to outlet, and channels through the tray center (Fig. 7.7*b*). This leaves stagnant zones near the curved walls on the side.

Liquid plug flow produces a horizontal (i.e., flat) flow profile (Fig. 7.7*a*). Channeling produces a U-shaped flow profile (Fig. 7.8*a*). The liquid moves fast at the tray center and slow near the walls. Wide stagnant zones, a steep U shape, and liquid recirculation in the stagnant zones (Fig. 7.8*b*) signify a highly channeled flow profile. The

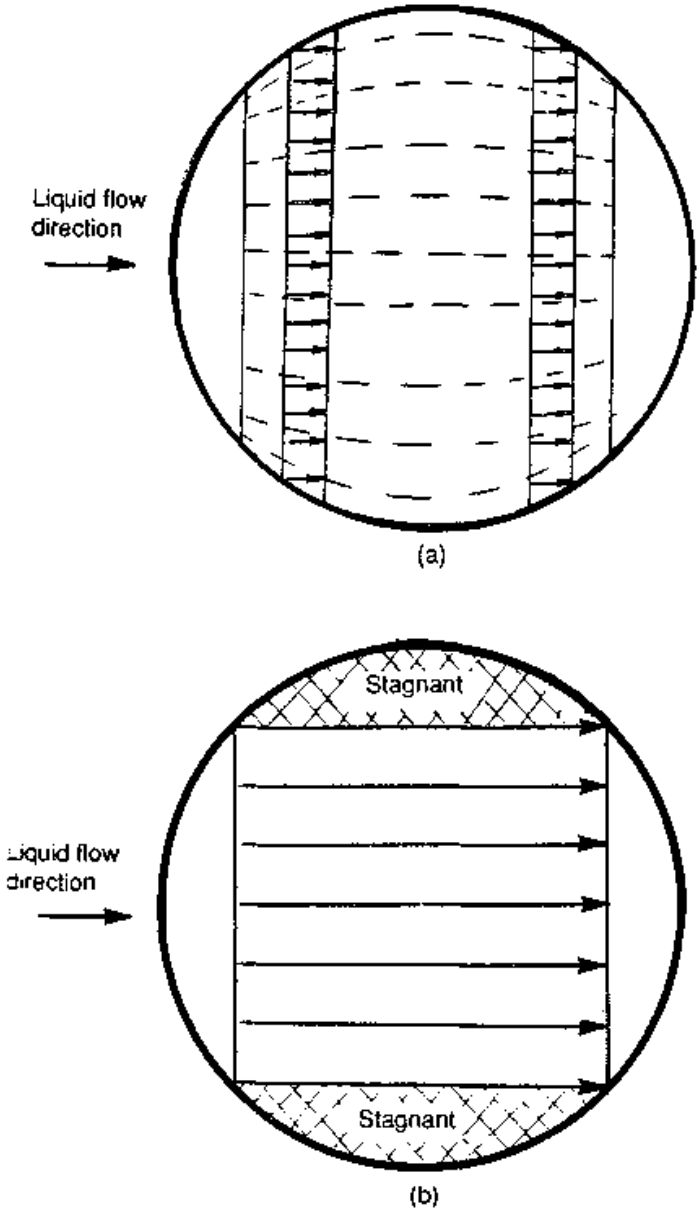

Figure 7.7 Flow patterns on distillation trays. (*a*) Plug flow; (*b*) plug flow in center, stagnant regions near wall.

stagnation point produced by the collision of liquid flow against the outlet weir wall forces liquid laterally toward the column wall. Upon collision with the column wall, this lateral flow generates backward flow in the stagnant zone. If the forward flow component is very slow, the backward component will dominate, causing recirculation.

Tray flow profiles have been investigated in large-diameter simulators using dye injection, photography, fiber optics, floating Ping-Pong balls, local temperature measurements, and other techniques. The following observations have been made:

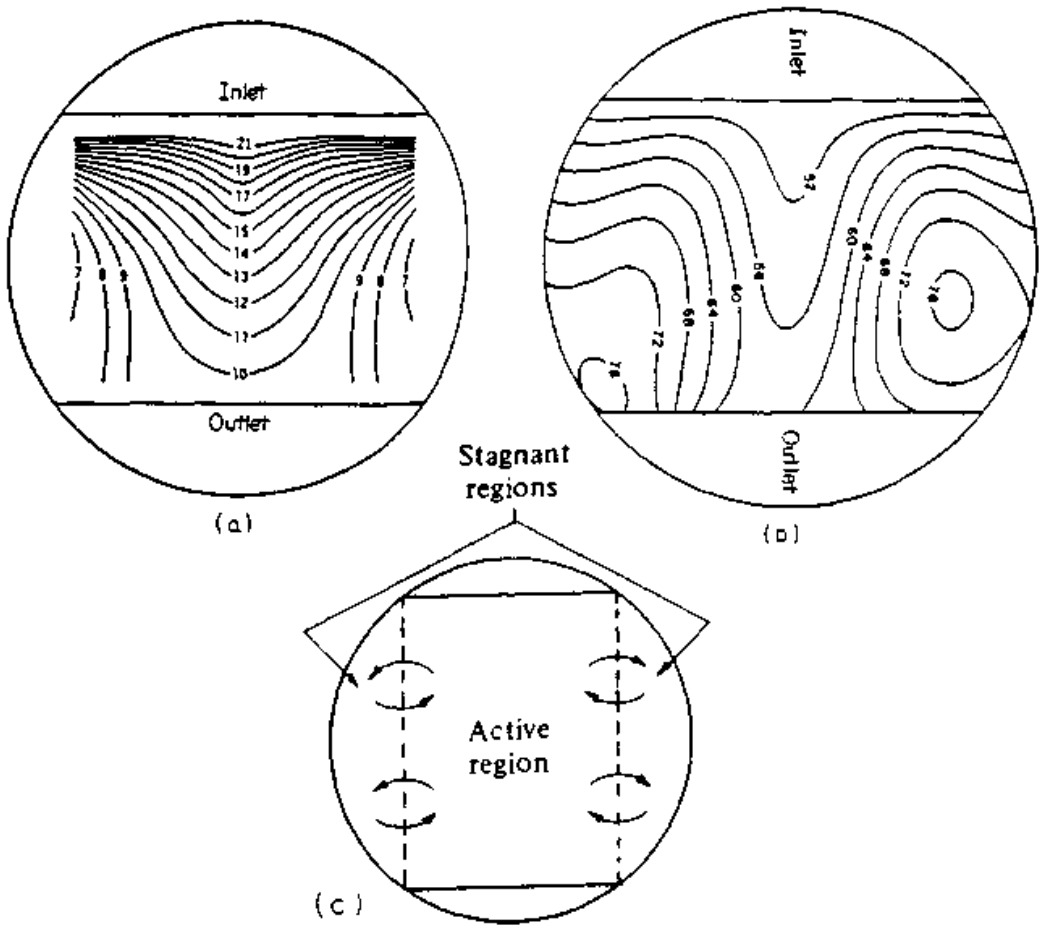

Figure 7.8 Experimentally measured residence time profiles on large distillation trays showing stagnant zones. (*a*) U-shaped flow profile with stagnant zones, 8-ft tray; (*b*) sharp U-shaped flow profile with wide stagnant zones and recirculation in stagnant zones, 8-ft tray; (*c*) replenishment of liquid in the stagnant regions by mixing from the active region. (*Part a,* from Richard L. Bell, *AIChE J. 18 (3), p. 498, May 1972. Reprinted courtesy of the American Institute of Chemical Engineers. Part b from T. Yanagi and B. D. Scott, paper presented at the AIChE National Meeting, New Orleans, Louisiana. Reprinted courtesy of Fractionation Research Inc. Part c, from M. J. Lockett,* Distillation Tray Fundamentals, *Cambridge University Press, Cambridge. Reprinted courtesy of Cambridge University Press.*)

1. Low liquid rates favor channeling (141,157,158). The following are observations on single-pass sieve trays operating at high vapor rates (about 40 to 70 percent of flood). At low liquid flow rates (<2 gpm/in of outlet weir), flow profiles are U-shaped (157–160), with regions near the wall either stagnant or having liquid recirculation (Fig. 7.8*b*). These stagnant regions widen as liquid flow rate is lowered (141,157). At higher liquid flow rates (about 3 gpm/in of outlet weir), the U shape is flattened (almost like plug flow) or is replaced by large recirculation zones. In one test series (157), there was one recirculation zone near each sidewall, another at the central tray outlet region, and another at the cen-

tral tray inlet region. At high liquid flow rates (6 to 7 gpm/in of outlet weir) the pattern turned into a multitude of recirculation zones, with a confused flow profile (157).

2. Higher gas flow rates flatten the U shape, narrow the stagnant regions, and reduce liquid recirculation in the stagnant regions (158,159,161). For single-pass sieve trays operating at liquid rates 3 to 7 gpm/in of outlet weir and at more than about 50 percent of flood, observed U shapes were quite flat (157,158). At the same liquid rates, steep U shapes were observed when vapor velocities fell below about 40 percent of flood.
3. At low and moderate gas rates, a major portion of the gas flow bubbles through the stagnant zones, contacting only a small fraction of the liquid flow. Froth formation in the central zone of the tray becomes relatively weak at low vapor rates (161). Solari et al. (158,161) estimate the stagnant zones to occupy between 5 and 60 percent of the tray bubbling area.
4. Lowering weir height flattens the U shape, narrows the stagnant regions, and reduces liquid circulation in the stagnant regions (141,161). With no outlet weir, the effects of liquid and gas flows on the flow pattern appear to be the converse of those described in items 1 and 2 above (161,162).
5. At low liquid rates (~1 gpm/in of weir), the tray liquid flow profile strongly depends on the liquid distribution at the tray inlet (e.g., inlet weir) but is practically independent even of major disturbances at the outlet weir (163). The importance of liquid distribution at tray inlet was also noted by others (159,160,164,165).
6. Small ratios of outlet weir length to column diameter (i.e., small downcomers) widen the stagnant zones and intensify recirculation in the stagnant zones (161,166).
7. Liquid channeling on two-pass trays is far less pronounced than on a single-pass tray (159,166,167). Liquid velocity profiles remain nonuniform, but stagnant regions are small, often nonexistent. At low liquid rates, the velocity profile often skews toward one wall, forming a stagnant region near the opposite wall (159). For a center-to-side (converging) flow, stagnant zones are absent (166,167) except with skewed profiles (159). For a side-to-center (diverging) flow, stagnant regions form near the corners of the outlet weirs (159) or occupy the small area near the wall (167), and are widened by skewed profiles (159).
8. Tray tilt affects the liquid flow pattern and the boundaries between the regions (148).

9. Liquid channels less when gas emerges sideways from the tray openings. Liquid-channeling on bubble-cap (163) and valve trays (168) is far smaller than on sieve trays. On sieve trays, channeling decreases as hole diameter increases, presumably due to widening of the cone angle of the gas jet (157).
10. Properly positioned baffles can improve the flow profiles (160,162–165,169,170).

7.3.3 Effect of tray maldistribution on efficiency

Liquid maldistribution. The stagnant zones (Fig. 7.7*b*; Fig. 7.8*a,b*) have a detrimental effect on efficiency in large-diameter trays. The stagnant liquid composition reaches equilibrium with the rising vapor, and from then on changes no further. Vapor rising through stagnant zones undergoes no change in composition, and tray efficiency drops. A counteracting effect is that the stagnant zones receive fresh liquid from the neighboring active region (Fig. 7.8*c*), and this reinstates mass transfer. Lockett (12) states that when the maximum width of the stagnant region is less than about 20 in, transverse mixing is sufficient to overcome the detrimental effects of stagnant regions on tray efficiency.

A far more detrimental effect of stagnant zones on tray efficiency develops in a group of trays stacked above each other (171–173). Vapor from the very bottom of the column passes from one stagnant zone to the next and remains unchanged in composition. At the top of the column, this heavy vapor contaminates the purified vapor rising from the central portion of the trays, causing a major drop in apparent efficiency. Thorogood (172) modeled this scenario as two parallel columns, with the reflux ratio in one column lower than in the other. An early pinch takes place in the column simulating the stagnant regions (lower L/V), and this reduces the purity of the overhead stream. This model is identical to the model for maldistribution in packed columns (Sec. 9.2.2).

Counteracting this highly detrimental stacking effect is mixing of both vapor and liquid. Mixing of vapor between trays is strongest at high ratios of tray spacing to column diameters, i.e., in smaller columns, but weakens as column diameter increases. Mixing of liquid occurs in the downcomers and is analogous to packed-tower redistribution (Sec. 9.2.3), but occurs far more frequently. Thorogood (172) shows that only a small amount of remixing in the downcomer—as little as 2 to 5 percent—is sufficient to mitigate the stacking effect. Weiler et al. (174) shows that at least such a limited amount of remixing occurs in the downcomer.

Modeling. Perhaps the most popular model for evaluating the effects of maldistribution on tray efficiency is the Lockett et al. stagnant region model (SRM) (12,148,167,171). This model postulates liquid plug flow at the center of the tray with stagnant zones near the wall. The stagnant zones occupy the areas enclosed by the chords joining the ends of the inlet and outlet downcomers (Fig. 7.7*b*). An alternative model by Bell and Solari (158,175) represents liquid channeling by a nonuniform velocity profile across the tray. The model can include the effect of liquid recirculation in the stagnant regions. Sohlo and Kouri (142) initially used a similar model, and later (176) attempted to account for the way nonideal flow develops. Kler and Lavin (166) and Estevez and Arreaza (177) proposed models based on two-dimensional velocity distributions.

Test data. The detrimental effects of stagnant regions on tray efficiency have never been confirmed by experiment. The only published data are by Yanagi and Scott (160,164), who measured tray efficiency in an 8-ft column with and without a flow-straightening device. They observed the severely channeled profile of Fig. 7.8*b* without their flow straighteners and plug flow with them. Despite that, they measured the same tray efficiency with and without the flow straighteners. Lockett and Safekourdi (12,169) and Bell and Solari (158) argued, based on their models, that the Scott and Yanagi test conditions were such that liquid flow maldistribution should not have had a noticeable effect on efficiency.

Case studies were reported (170,174) of large-diameter (>15-ft) towers with sieve trays not reaching the expected efficiency. Maldistribution was cited as the culprit or at least one of the causes. Improving liquid flow patterns, often among other modifications, was the fix. The only other evidence that channeling adversely affects tray efficiency comes from the above-mentioned theoretical models.

Improving liquid flow patterns. A number of special tray designs have been developed to improve liquid velocity distribution on large-diameter trays. Their main applications are vacuum distillation. In pressure distillation, liquid flows are usually high and multipass trays are used, so that stagnant zones are seldom a problem. Some means of improving the liquid flow patterns are

1. Using valve trays. Their sideways gas movement alleviates liquid channeling (Sec. 7.3.2, item 9). On the basis of eliminating the stagnant regions, Biddulph (168) expects valve tray efficiencies in

large-diameter columns to be 15 to 20 percent higher than sieve trays, but this has not been verified by experiment.

2. Using suitably directed slots and baffles to avoid channeling. Such devices (170,178) have improved efficiency in large-diameter vacuum towers with long flow paths. Use of these devices in large-diameter towers has been advocated for vacuum services (24,161) and for pressure services with tall weirs (161).
3. Using arc-shaped downcomers. Special tray designs (165,169) have arc-shaped downcomers, which direct liquid toward the column walls. These devices improve flow patterns, but their effect on efficiency has not been tested.
4. The Fractionation Research Inc. unique design for inlet downcomer baffle and outlet weir (160,164) converted a highly channeled liquid flow into plug flow. Despite that it did not improve efficiency.
5. Increasing the number of passes (167). This reduces the tendency to form stagnant zones (Sec. 7.3.2, item 7).

Vapor maldistribution. Most popular theoretical models (such as the AIChE and the Chan and Fair models, Sec. 7.2.1) postulate perfectly mixed vapor flow. In large-diameter columns, vapor is more likely to rise in plug flow. Modeling work showed (143,179,180) that in the absence of stagnant zones on the tray, vapor flow pattern has generally little effect on tray efficiency. When column efficiency exceeds 80 percent (143), or when stagnant liquid zones exist (171,173,180), vapor plug flow reduces tray efficiency.

Some theoretical work (181,182) has been done on vapor velocity maldistribution due to hydraulic gradients (Fig. 7.9). It has been

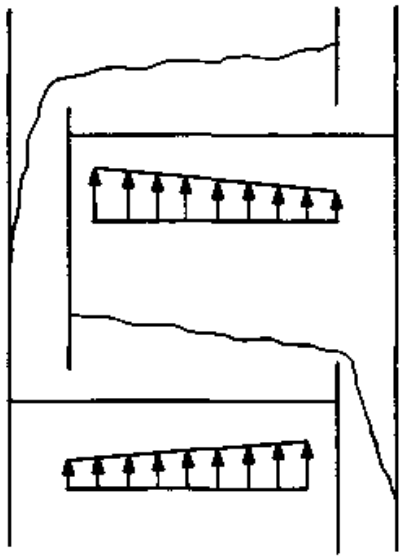

Figure 7.9 Possible nonuniform vapor flow pattern.

shown (182) that even if it occurs, it has only a minor effect on tray efficiency. A recent study suggests a more significant effect (183), but this study is based on some doubtful extensions of the AIChE correlation.

Under some conditions, vapor velocity maldistribution induced by hydraulic gradient or tray tilt can lead to excessive nonuniform weeping (183*a*; Also, see Secs. 6.2.12, 6.2.13). Such excessive weeping can be detrimental to tray efficiency.

Downcomer mixing. The AIChE model assumes that liquid along the downcomer length is perfectly mixed. A recent study using a tracer injection technique (174) showed that in large trays, the downcomer liquid is unmixed. A computational analysis (174) showed that efficiency reduction due to an unmixed downcomer is relatively small, but will intensify in the presence of liquid stagnant regions on the tray.

7.3.4 Other factors affecting tray efficiency

Weir height. Taller weirs raise liquid level on the tray in the froth and emulsion regimes. This increases interfacial area (136,137) and vapor contact time. Larger interfacial areas and contact times enhance efficiency, especially when the mass transfer resistance is concentrated in the vapor (most distillation systems). In the spray regime, weir height affects neither liquid level nor efficiency (Sec. 6.4.4).

In distillation systems, the improvement of tray efficiency due to taller weirs is small (5). Koch Engineering (8), Kreis and Raab (28), and Kalbassi et al. (184) observed little effect of weir height on distillation tray efficiency for weirs 1.5 to 3 in, 1 to 2 in, and 0.5 to 1 in tall, respectively. Finch and Van Winkle (185) reported an efficiency increase of the order of 5 to 10 percent as weir height is raised from 1 to 3 in; a similar increase was reported by Prado and Fair (110,144) in humidification and stripping tests.

A significant drop in tray efficiency was observed (184–186) when changing from a weir even as short as 0.5 in to no weir. Raising weir heights from 2 to 4 in was shown to raise froth regime efficiency by 20 to 50 percent for caustic absorption of acid gases (28), for absorption of ammonia in water (117), and for absorption of oxygen into low-viscosity water/glycerol solutions (186). In the spray regime, weir height was shown to have little effect on absorption efficiency (117,186).

Length of liquid flow path. Longer liquid flow paths enhance the liquid-vapor contact time, the significance of liquid plug flow, and, therefore, raise efficiency. However, flow-path increases are coupled with col-

umn diameter increases, and a point is reached where the tray may suffer from channeling (Sec. 7.3.3).

One experience was reported (74) where a refinery reboiled absorber was revamped by replacing single-pass trays by two-pass trays. Although the expected capacity gain was achieved, the reduction in flow-path length from 36 to 18 in caused a loss in efficiency large enough to justify reinstalling the original trays. Finch and Van Winkle (185) report an efficiency increase of the order of 0.5 percent per inch of flow-path length for flow paths 11- to 22-in long.

Fractional hole area. Efficiency increases with a reduction in fractional hole area (23,28,110,144,186). Yanagi and Sakata (23), experimenting with commercial-scale towers, show a 10 to 15 percent increase in tray efficiency when fractional hole area was lowered from 14 to 8 percent of the bubbling area (Fig. 7.10*a*). Kreis and Raab (28) show an identical increase for N_2/O_2 separation, and an even larger increase (20 to 25 percent) when fractional hole area was lowered from 8 to 5 percent of the bubbling area. Prado and Fair (110,144) showed an efficiency increase of the order of 5 percent as fractional hole area was reduced from 11 to 6 percent of the bubbling area in humidification and stripping tests. The above data were collected both in the froth and spray regimes.

Hole diameter. In the froth regime, small holes increase the interfacial area, possibly also froth height (24,62). The enhancement in efficiency is small, often negligible (5,28,136,185). Experiments by Kalbassi et al. (184) and Lopez-Bonillo et al. (187) showed that a fourfold reduction in hole diameter increased efficiency by about 15 percent or less. Prado and Fair (110,144) showed a tray efficiency rise of less than 2 percent when hole diameter was halved in humidification and stripping tests. Absorption experiments with low-viscosity systems (117,186) show a negligible to small enhancement in efficiency due to smaller holes. For high-viscosity absorption systems, efficiency significantly improved when hole diameter was reduced (186). In spray regime absorption, a threefold hole diameter reduction was shown to drop efficiency by 15 to 25 percent (117,186).

Vapor-liquid loads. A higher vapor load reduces the vapor contact time but also increases the interfacial area (136,137). These two factors have counteracting effects on tray efficiency. Usually, the contact time dominates, and efficiency decreases with higher vapor rates (185). A higher liquid load increases tray efficiency (185) because it increases tray liquid holdup, and therefore vapor contact time.

Most distillation operations are performed at constant L/V ratios.

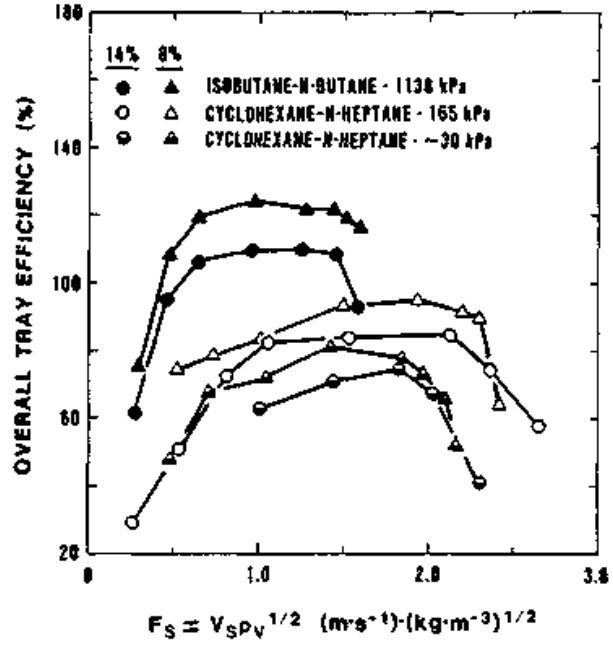

(a)

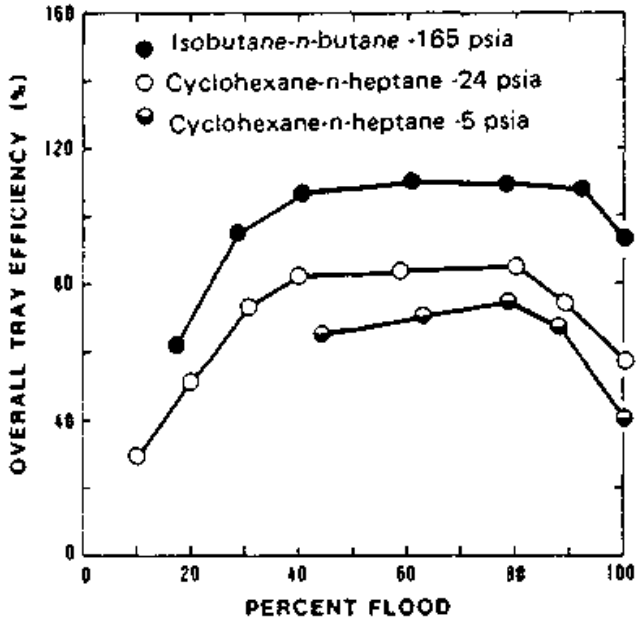

(b)

Figure 7.10 Some factors affecting sieve tray efficiency. FRI data, total reflux, D_T = 4 ft, S = 24 in, h_w = 2 in, d_H = 0.5 in. Both parts show a small efficiency rise with pressure. Both parts show little effect of vapor and liquid loads above about 40 percent of flood. (*a*) Showing efficiency reduction when fractional hole area is increased from 8 to 14 percent of the bubbling area; (*b*) emphasizing little effect of vapor and liquid loads, and an efficiency increase with pressure. A_f = 0.14 (*Both parts reprinted with permission from T. Yanagi and M. Sakata, Ind. Eng. Chem. Proc. Des. Dev. 21, p. 712, copyright 1982, American Chemical Society.*)

This means both vapor and liquid loads are raised and lowered simultaneously. Increasing vapor rate reduces efficiency, while increasing liquid rates raises efficiency. The two effects normally cancel each other, and efficiency is practically independent of load changes (assuming no excessive entrainment or weeping). Figure 7.10*b* shows a typical dependence of tray efficiency on vapor and liquid loads for a commercial-scale distillation column. Anderson et al. (97) show a similar dependence for several different valve trays.

Reflux ratio. Reflux ratio was stated to have a small effect on efficiency (5).

Viscosity. Efficiency increases as liquid viscosity diminishes (5,149, 150,186). As discussed earlier (Sec. 7.2.2), lower liquid viscosity usually implies higher liquid diffusivity, and therefore, lower resistance to mass transfer in the liquid phase. It was also argued that bubbles formed in high-viscosity liquids are larger and generate less interfacial area (186).

Relative volatility. Efficiency increases as relative volatility is lowered (5,149,150). As discussed earlier (Sec. 7.2.2), lower volatility reduces the significance of the liquid phase resistance, and therefore, raises efficiency.

Surface tension. There is uncertainty regarding the effect of surface tension on tray efficiency. Often, it is difficult to divorce the surface tension effects from those of other physical properties. For this reason, it is difficult to tell whether the effects described below are real or imaginative.

Measurements by Fane and Sawistowski (116,117) show little effect of surface tension on efficiency in the froth regime, and a rise of tray efficiency with lower surface tension in the spray regime. The surface tension gradient (Sec. 6.4.4) appears to have an effect. A positive gradient (surface tension increases down the column) enhances efficiency in the froth regime (108,116,117,146,189,190) while a negative gradient enhances efficiency in the spray regime (108,116,117). The magnitude of these enhancements is uncertain.

Surface tension effects have frequently been used to explain observed composition effects (184,187,189) or discrepancies between theory and experiment (146). Zuiderweg (146) and Dribika and Biddulph (189) argue that the Marangoni effect (Sec. 6.4.4) stabilizes the froth and therefore enhances efficiency. The enhancement is related to

$$M = (y^* - x)\frac{d\sigma}{dx} \tag{7.37}$$

The difference $y^* - x$ represents the mass transfer driving force, while $d\sigma/dx$ represents the change in surface tension with concentration. Both Zuiderweg and Dribika and Biddulph show that with large values of M (10 to 20 dynes/cm), point efficiency can be enhanced by as much as a factor of 1.5 to 2.0. However, these enhancement factors are the ratios of measured to predicted point efficiencies, and the predictions are based on the notoriously unreliable theoretical correlations (Sec. 7.2.1). Lockett (12) points out that the above enhancement factors remain high even at the froth-spray transition, and this is inconsistent with the argument. Further, experiment by Ellis and Legg (214) have demonstrated no significant effects of surface tension gradients on efficiency.

For low-viscosity absorption systems, one set of data (186) shows that in the froth regime tray efficiency increases as surface tension is reduced, while for high-viscosity absorption systems, surface tension had little effect on mass transfer (186).

Pressure. Tray efficiency slightly increases with pressure in the froth regime (17,105,119). The apparent pressure effect could be a reflection of the rise in efficiency with a reduction in liquid viscosity and in relative volatility. (*Note:* As distillation pressure rises, so does the equilibrium temperature; this in turn leads to a decrease in liquid viscosity.)

At pressures higher than 150 to 300 psia, and especially at high liquid rates, vapor entrainment in the downcomer liquid becomes important, and may lead to a reduction in tray efficiency with further raises in pressure (105).

Liquid and vapor entrainment. Both represent a recycling of lower-purity material which contaminates the tray liquid or vapor, both counteract the mass transfer process and lower efficiency. Liquid and vapor entrainment are discussed in Secs. 6.2.11 and 6.4.5, respectively.

Weeping. This represents liquid short-circuiting the stage and contaminating the tray below with more volatile material. Further discussion is in Sec. 6.2.12.

Special considerations in multipass trays. In a multipass tray, vapor distribution between the passes is largely determined by the hole area, while liquid distribution is largely a function of the weir height and length. If the geometry of the passes is perfectly identical, the distribution of vapor and liquid is the same for each pass, and tray efficiency is uniform. This is readily achievable in two-pass trays, where the design of each pass is identical to the other, but not so when a

larger number of passes is involved. For instance, in a four-pass tray, weir length of the center passes differs from that of the side passes. Unless allowed for in the design, the L/V ratio will vary from pass to pass, with a resulting reduction in tray efficiency, as demonstrated by Bolles (191).

Bolles (191) correlated the reduction in efficiency in terms of the *distribution ratio,* i.e., the maximum-pass L/V ratio divided by the minimum-pass L/V ratio. The L and V for each pass are determined from the normal pressure balance and hydraulic relationships, applied to each pass. At high distribution ratios, a substantial drop in tray efficiency occurs. Bolles shows that if this distribution ratio is kept lower than 1.2, the loss in efficiency due to maldistribution is negligible. Bolles recommends designing multipass trays for such low distribution ratios. Detailed guidelines for achieving low distribution ratios (<1.2), thus minimizing the effects of pass maldistribution on efficiency, are contained in a companion book (1) and in Bolles's paper (191).

7.3.5 Tray efficiency in multicomponent separations

Component efficiencies. In binary mixtures, the efficiencies of each of the two components are identical. In multicomponent separations, component efficiencies are all different because

1. Each component has a different diffusivity, both in the vapor and in the liquid.
2. In a multicomponent mixture, the diffusion rate of a component depends not only on its own concentration in the mixture, but also on the concentration of other components. This may lead to coupling and interaction of the mass transfer among various components. Some examples are (192)
   a. Reverse diffusion—Mass transfer opposite to the concentration driving force.
   b. Diffusion barrier—No net mass transfer even though a concentration driving force exists.
   c. Osmotic diffusion—Mass transfer in the absence of a concentration driving force.
3. The effective slope of the equilibrium curve, m, and therefore λ [Eq. (7.5)] differs for each component. Therefore, each component has a different ratio of gas-phase resistance to liquid-phase resistance [Eq. (7.13)] and a different ratio of overall column efficiency to Murphree tray efficiency [Eq. (7.4)].

Design practice. A computational case study by Toor and Burchard (192) demonstrates that accounting for the above factors can alter the

stage requirement for a multicomponent separation by 30 to 40 percent. Several other authors (12,145,193,194) also warn against assuming equal component efficiencies in multicomponent distillation design. Nonetheless, individual component efficiencies are seldom used in design practice, due to the following reasons:

- Multicomponent efficiency prediction methods are based on theoretical binary efficiency methods. As previously stated (Sec. 7.2.1), the reliability of those methods leaves a lot to be desired. This difficulty can be bypassed when reliable efficiency data are available for the binary pairs making up the multicomponent mixture. As demonstrated by Vogelpohl (193), binary efficiency data can be extended to multicomponent systems using a multicomponent computation method.
- Few commercial simulations are geared to handle rigorous multicomponent efficiency computations.
- Rigorous methods for computing multicomponent efficiencies are complex, difficult to use for design, and often of unknown reliability. The ideal method, which is simple enough, yet reliable, is still being sought. The main bottleneck here is the availability of adequate commercial-scale data that will permit proper testing of the various methods.

Pseudo binary method. The most common and generally the simplest procedure used for multicomponent efficiencies, it proceeds in the following steps (12):

1. From the column simulation in terms of theoretical stages, locate representative stages in each section of the column.
2. For each representative stage, select light key and heavy key components, and calculate the composition of the pseudo binary mixture as

$$Y_{LK} = \frac{y_{LK}}{y_{LK} + y_{HK}} \tag{7.38a}$$

$$X_{HK} = \frac{x_{LK}}{x_{LK} + x_{HK}} \tag{7.38b}$$

Some judgment is required in selecting the pseudo keys, and the two components selected are often not the same for different parts of the column. The light- and heavy-key approach can be extended to allow for multi-pair efficiencies that may be different. The choice of binary pairs depends on feed and product compositions, volatility

differences, components of major interest for design, and the components which are the majority fraction of the mixture.

3. Predict the binary diffusion coefficients of the keys in each phase at the mixture temperature and pressure.
4. Calculate Y_{LK} and X_{LK} on adjacent theoretical trays n and $n + 1$, and determine the slope of equilibrium curve m from

$$m = \frac{Y_{LK,n+1} - Y_{LK,n}}{X_{LK,n+1} - X_{LK,n}} \tag{7.39}$$

5. Use the binary correlations (Sec. 7.2.1) to predict E_{OG} and E_{MV}; possibly also E_o. The section efficiency E_o is then used to determine the number of trays in each section of column when used in conjunction with a theoretical-stage simulation.
6. There are three options for applying the efficiency:
   a. Use the section efficiency E_o in conjunction with a theoretical-stage simulation to determine the number of trays in each section. This is least accurate, but can be used with commercial theoretical-stage simulations.
   b. Assume the Murphree tray efficiency E_{MV} calculated in item 5 above is the same for all components, then apply the Murphree tray efficiency in a column simulation. This option is simple, more accurate than the previous, but requires a simulation that can use Murphree efficiencies. This option reliably predicted composition profiles both for similar (195) and dissimilar (145) components, but it is unknown whether it always works so well. Chan and Fair (145) expect it to generally work well, especially if the key components dominate the feed mixture to the column.
   c. Repeat the above steps, calculating Murphree efficiencies for many binary pairs. This requires the solution to a linear set of equations in order to obtain the component mole fractions in the mixture. Ognisty and Sakata (195) show that for systems of either similar or dissimilar components, this option predicts composition profiles practically as accurately as the rigorous diffusional interaction method below. This option, however, increases the complexity of the pseudo binary method, and also makes it difficult to use with most commercial simulations. With a large number of components, this option becomes as complex as a rigorous diffusion method (195).

Individual component efficiency method. Another simple procedure, it was recommended for the AIChE tray efficiency correlation (125). It yields individual component efficiency but takes no account of diffusional interaction. It proceeds as follows (12):

1. Predict gas phase diffusion coefficient $D_{G,i}$ for each component i in the presence of all other components, using Wilke's equation (196).

$$D_{G,i} = \frac{1 - y_i}{\sum_{j=1 \neq i} (y_j / D_{G,ij})} \tag{7.40}$$

where $D_{G,ij}$ is the gas-phase diffusion coefficient for each binary pair.

2. Predict liquid-phase diffusion coefficient $D_{L,i}$ of each component as solute through the other components as solvent.
3. Determine the slope of the equilibrium curve, m_i for each component, from the values of vapor and liquid compositions given by a theoretical stage simulation and from

$$m_i = \frac{y_{i,n+1} - y_{i,n}}{x_{i,n+1} - x_{i,n}} \tag{7.41}$$

4. Calculate $E_{OG,i}$ and $E_{MV,i}$ for each component using the equations for binary mixtures (Sec. 7.2.1).
5. $E_{MV,i}$ is used in a column simulation program that has provision to accept individual component efficiencies.

Biddulph (197–199) applied a simplified version of this method for an oxygen-nitrogen-argon column and a benzene-toluene-xylene column. In each case, the components were similar to one another, and there was experimental evidence to show that the component individual point efficiencies $E_{OG,i}$ were the same. Making the assumption of constant point efficiency in each column section permitted Biddulph to eliminate the first two steps. In a later paper, Biddulph (194) shows that this assumption, and therefore his simplification, do not always hold where components are dissimilar.

Diffusional interaction methods. These calculate component efficiencies, but account for diffusional interactions. The calculation procedure is based on the Maxwell-Stefan diffusion equations, as developed by Krishna et al. (200,201). The equations are complex and are presented in the original reference. Lockett (12) has an excellent summary. For a ternary system, the steps below are followed (12):

1. Estimate diffusion coefficients for each binary pair in each phase.
2. Calculate the number of transfer units for each of the binary pairs.
3. Using a special weighted averaging procedure, calculate the number of ternary transfer units for the gas phase. Repeat for the liquid phase.

4. Determine the slopes of the equilibrium curve.
5. Combine the number of ternary transfer units in each phase to obtain the number of ternary overall gas-phase transfer units.
6. Evaluate the elements of the ternary overall gas-phase transfer unit matrix.
7. Calculate point efficiencies based on this matrix.
8. Using the slopes of the equilibrium curve obtained in (4) above, and the appropriate mixing model, convert point to Murphree tray efficiencies.

Burghardt et al. (202), Ognisty and Sakata (195), and Chan and Fair (145) show that the diffusional interaction method gives good and reliable prediction of experimental multicomponent tray efficiency data. While Ognisty and Sakata recommend this method for precise calculations, Chan and Fair express preference for a simpler procedure if good accuracy can be assured. Burghardt et al. (202) closely examined simplifying assumptions inherent in diffusional interaction models and show that these lead to negligible errors for several cases studied.

Vogelpohl (193) and Medina et al. (203) applied the diffusional interaction method for predicting ternary distillation composition profiles using binary data. They achieved this by eliminating the first two steps and assuming that all the mass transfer resistance is in the vapor. This procedure was shown to give excellent agreement with experimental data for dissimilar components. Biddulph and Kalbassi (194), however, report some discrepancies between prediction and experiment due to this assumption.

Diffusional interaction methods have also been applied successfully to packed columns. Gorak (204) found that the Krishna-Standart model (205) is relatively simple and sufficiently accurate to predict multicomponent composition profiles. Gorak's own variation of the diffusional interaction method was also reported to predict experimental data well, while use of HETP was reported to give poor data predictions.

Multicomponent efficiency profiles. Figure 7.11 (198,199) shows typical variations of Murphree plate efficiency for a ternary system made up of a light key (LK) component, a heavy key (HK) component, and a heavy nonkey (HNK) component (benzene, toluene, and *m*-xylene, respectively). On the basis of experimental data, point efficiency was assumed the same for all components throughout the column.

Figure 7.11 shows the same Murphree tray efficiency for the binary pair of key components separated. In the upper part of the column separation is between the LK and the HK. These behave like a "bi-

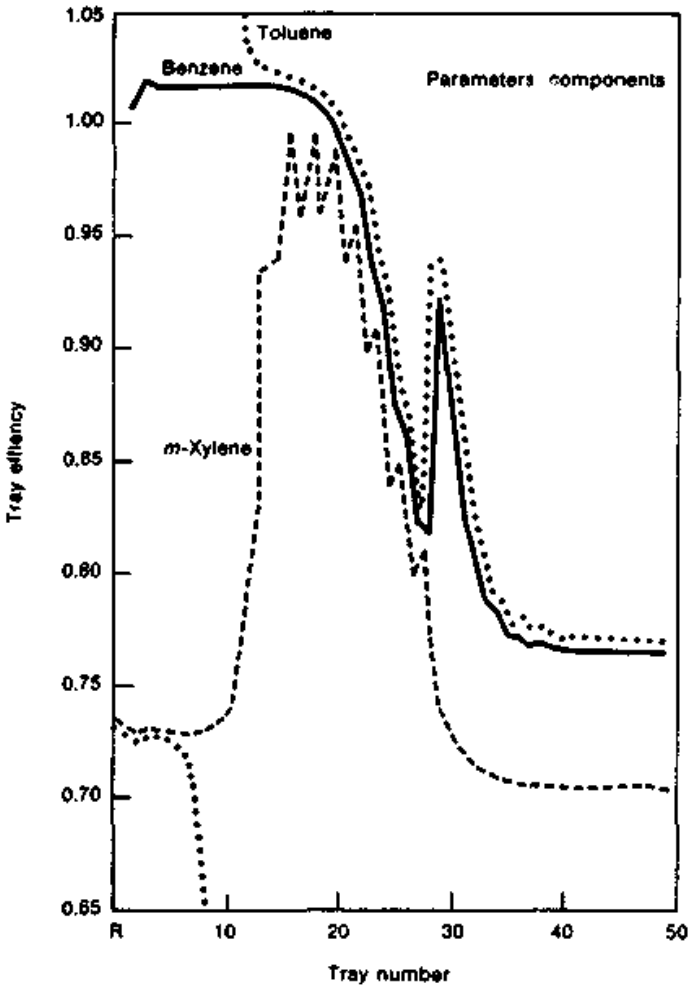

Figure 7.11 Variation of Murphree tray efficiency in multicomponent distillation. (*From M. W. Biddulph, Hydrocarb. Proc., October, p. 145, 1977, reprinted courtesy of Hydrocarbon Processing.*)

nary pair" and show the same efficiency. In the bottom few trays, separation takes places between the HK and HNK, and these components have the same efficiency. The efficiency of the LK component is higher in the region where the HK is separated from the HNK, while the efficiency of the HNK is lower in the region where the HK is separated from the LK.

The efficiency of the HK component undergoes a sharp change in the lower part of the column. This occurs when the HK component reaches its peak composition (Sec. 2.3.2). This sharp change in efficiency has no physical significance (193,203), but is a consequence of applying the Murphree efficiency concept to multicomponent systems [i.e., applying Eq. (7.3) across a concentration peak]. Sometimes, this may even lead to negative efficiencies. In this region, predictions from all multicomponent efficiency prediction methods can be in gross error (194).

The previous observations were made for the benzene-toluene-xylene system (198,199). Similar observations were made for the nitrogen-argon-oxygen system (197). In both cases, point efficiencies were assumed constant for all components throughout the column.

7.3.6 Efficiency scaleup: process factors

This section focuses only on process scaleup—i.e., scaling up from one chemical system to another, and also scaling up from one set of process conditions to another using the same system. Equipment factors such as column diameter, operating regime, and tray geometry are considered separately in the following section.

Different type of system. Sections 7.3.1 and 7.3.4 suggest that if liquid viscosity, relative volatility, surface tension, and surface tension gradients are similar, one can expect similar efficiencies. Since it is difficult to attain similarity in all these, it is best to scale up from the same chemical system. Further, in aqueous-organic systems where surface tension gradients can be steep, concentration has a marked and unpredictable effect on efficiency (116,184,187). Data collected in one concentration range may scale up poorly to another.

One type of system scaleup which can be done with confidence is extending efficiency data from one pressure to another. The small increase of efficiency with pressure (Sec. 7.3.4) can be allowed for using the O'Connell correlation (Sec. 7.2.2). Caution is required when going to high pressures (>150 psi), as vapor recycle may reduce efficiency, and this effect is difficult to predict.

Different process conditions. Here we discuss staying with the same system, but extrapolating test data to different process conditions (e.g., feed composition, reflux ratios, feed temperature, etc.). Concentration and pressure effects were discussed separately above; flow regimes are discussed separately in the next section.

In plant or pilot tests, separation data are analyzed by computer simulation that reproduces test conditions. The number of theoretical stages in the simulation is varied until the simulated product compositions and temperature profile match those measured. Tray efficiency is determined from the number of stages that give a good match to test data.

In the above procedure, errors in VLE are compensated by equivalent errors in tray efficiency. If the relative volatility calculated by the simulation is too high, fewer stages will be needed to match the measured test compositions, i.e., efficiency will be lower. Scaleup will be good as long as the VLE and efficiency errors continue to equally offset each other. This requires that process conditions (feed composition,

feed temperature, reflux ratio, etc.) remain unchanged during scaleup.

When process conditions are changed, the VLE and efficiency errors no longer offset each other equally. If the true relative volatility is higher than the simulated relative volatility, then the scaleup will be conservative. If the true volatility is lower than the simulated relative volatility, scaleup will be optimistic, and often dangerous. This is illustrated using the following example.

Example 7.2 A stripping section of a column separating propane from isobutylene needs to handle two future feeds (*a*) 72 percent propane, (*b*) 88 percent propane. Field-test data show that when column feed contained 80 percent propane, its bottoms contained 2 percent propane. Based on the test data, what will be the purity of isobutylene with the future feeds?

solution The example is solved using a McCabe-Thiele diagram (Fig. 7.12). For simplicity, the following arbitrary assumptions are made:

- The column operates at an arbitrarily fixed stripping ratio (i.e., all the operating lines on Fig. 7.12*a* to *f* have the same slopes).
- A straight component balance line (i.e., constant molar heat of vaporization, Sec. 2.2.2).
- The feed to the column is 50 percent vaporized (i.e., slopes of all the *q*-lines on Fig. 7.12*a* to *f* are -1).

The test separation data are analyzed using a McCabe-Thiele diagram (Fig. 7.12*a*), with an equilibrium curve based on experimental data (average relative volatility of about 1.7). The analysis shows that the stripping section requires 12 theoretical stages.

Consider an analysis of the same test data, but with an equilibrium curve based on a VLE prediction which gives higher relative volatilities (average of about 2.5) than the experimental data. With the calculated VLE, the McCabe-Thiele diagram (Fig. 7.12*b*) requires only eight theoretical stages.

Both Figs. 7.12*a* and *b* correctly predict the test conditions. Either Fig. 7.12*a* (using experimentally derived VLE and 12 stages) or Fig. 7.12*b* (using predicted VLE and 8 stages) will correctly predict product compositions under process conditions similar to those experienced in the test.

Consider now a propane concentration of 72 percent in the feed. The McCabe-Thiele diagram, based on the Fig. 7.12*a* interpretation of the test data, predicts that the propane concentration in the column bottoms will decline to 1 percent (Fig. 7.12*c*). On the other hand, if the McCabe-Thiele diagram were based on the Fig. 7.12*b* interpretation of the test data, it would predict 0.5 percent propane in the column bottoms (Fig. 7.12*d*). This prediction is optimistic.

Consider a propane concentration of 88 percent in the feed. The McCabe-Thiele diagram, based on the Fig. 7.12*a* interpretation of the test data, predicts a pinch just below the feed (Fig. 7.12*e*). Due to the pinch, the concentration of propane in the tower bottom will be 17 percent, i.e., much higher than the 2 percent propane in the test data. In practice, this pinch will probably be eliminated by increasing the boilup ratio (i.e., reducing the slope of the operating line). However, increasing the boilup ratio means more liquid and vapor traffic, a greater heat load on the reboiler, and possibly, a premature capacity bottleneck.

If the test data were interpreted using Fig. 7.12*b*, the pinch will not be seen. Based on the Fig. 7.12*b* interpretation, the McCabe-Thiele diagram (Fig. 7.12*f*)

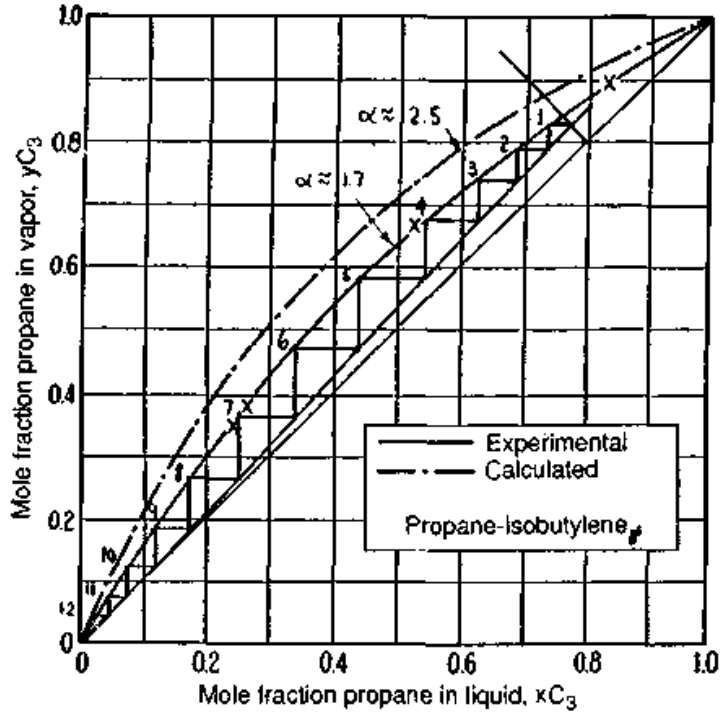

(a)

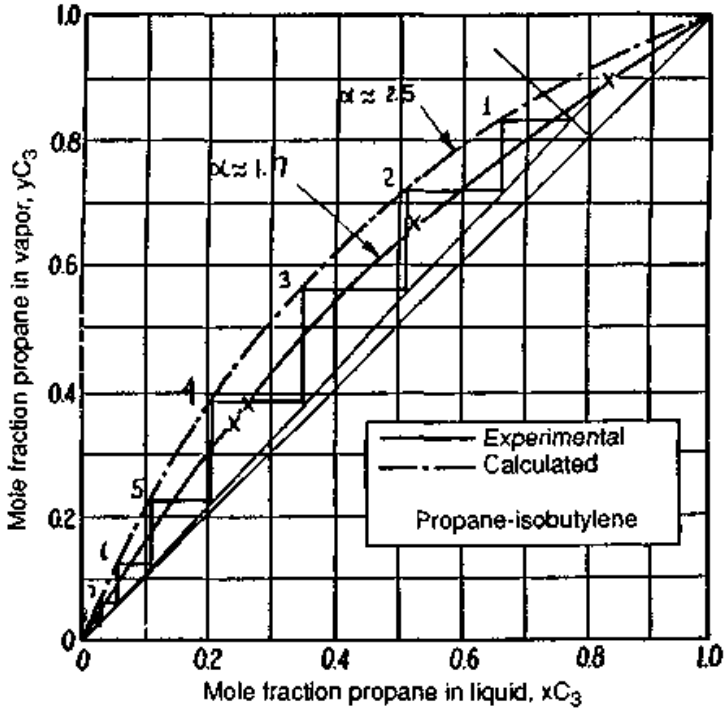

(b)

Figure 7.12 Extrapolation of test data—Example 7.2. (*a*) Test data interpretation using experimental VLE; (*b*) test data interpretation using calculated VLE

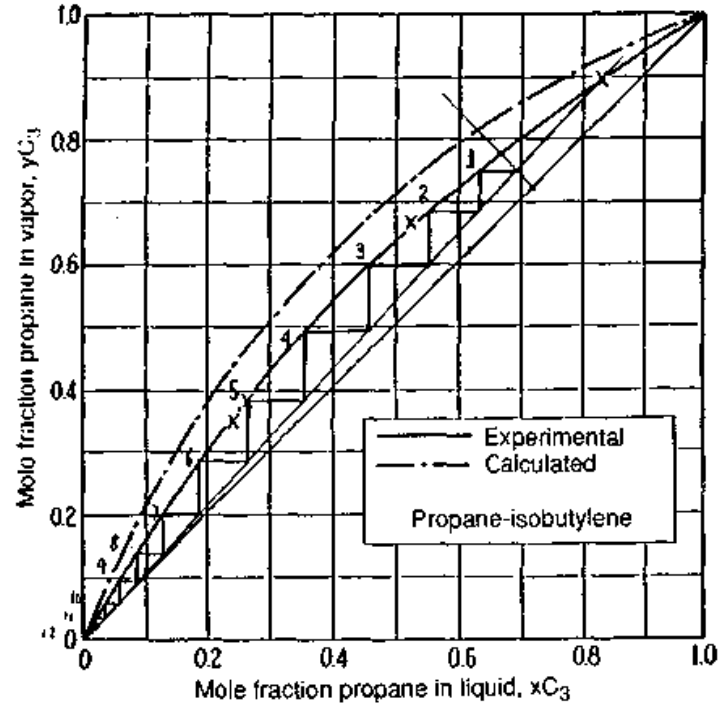

(c)

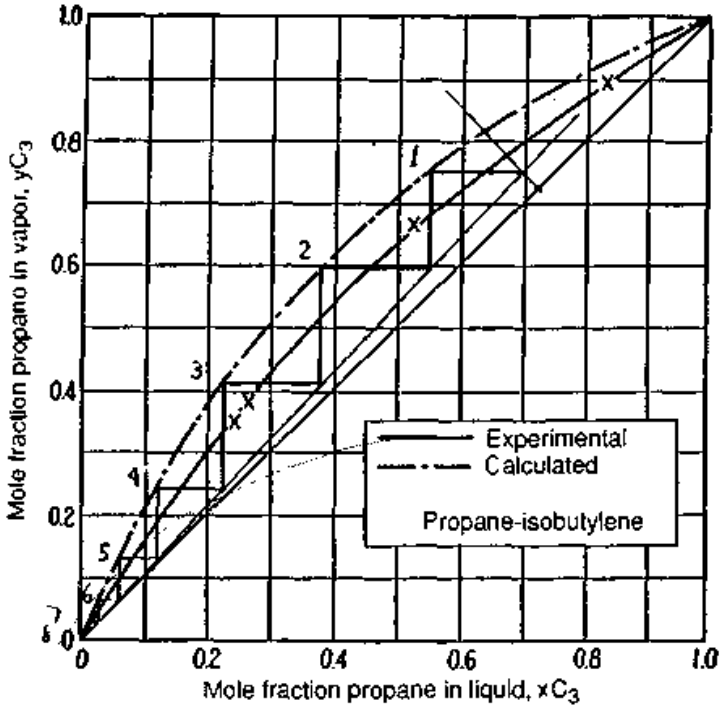

(d)

Figure 7.12 (*Continued*) Extrapolation of test data—Example 7.2. (*c*) Extrapolation to a feed leaner in propane, based on test interpretation in Fig. 7.12*a*; (*d*) extrapolation to a feed leaner in propane, based on test interpretation in Fig. 7.12*b*

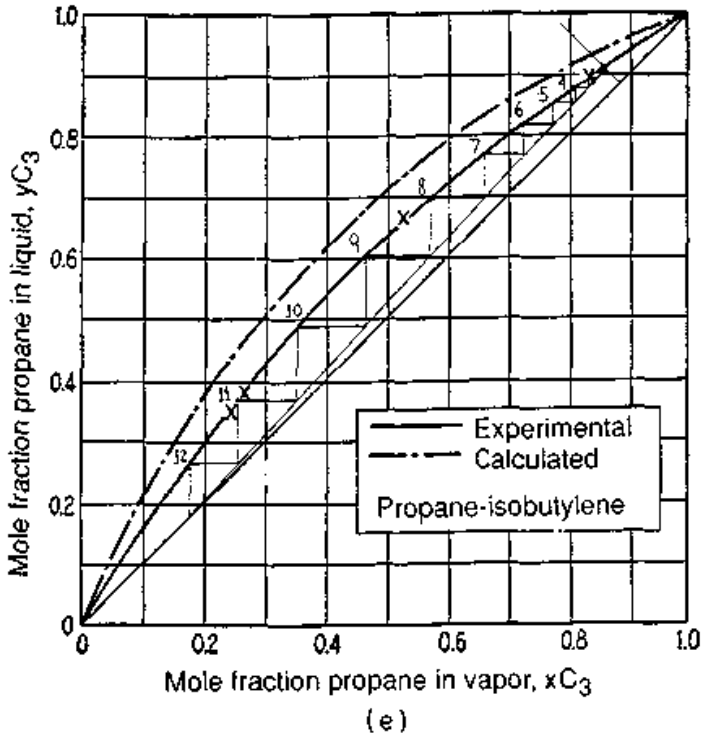

(e)

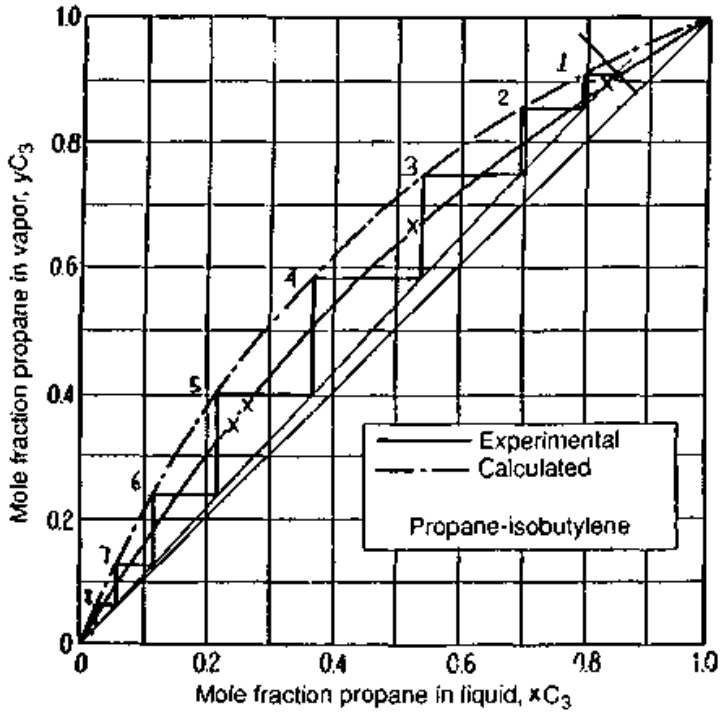

(f)

Figure 7.12 (*Continued*) Extrapolation of test data—Example 7.2. (*e*) Extrapolation to a feed richer in propane, based on test interpretation in Fig. 7.12*a*; (*f*) extrapolation to a feed richer in propane, based on test interpretation in Fig. 7.12*b*.

predicts 3 percent propane in the bottoms. This is only slightly higher than the propane concentration in the test data, and a lot lower than the 17 percent propane in the bottoms based on the Fig. 7.12*a* test data interpretation.

The above analysis demonstrates that when test data are interpreted using relative volatilities higher than actual, the resulting simulation will give optimistic predictions when extrapolated to other process conditions.

7.3.7 Efficiency scaleup: equipment factors

Different operating regimes. The operating regime on the tray governs tray efficiency (17,99,106–110,116,117,147). Scaleup of efficiency data from one regime to another is therefore dangerous and should be avoided. Further, the test data must be at similar column loading to the prototype (18,135).

Scaleup from an existing commercial column. As long as data are for the same system under similar process conditions, loadings, and operating regime, this can give excellent efficiency predictions. If both columns are about the same size, data obtained in one column directly extend to the other. Fractional hole area and the number of passes have a small but significant effect (Sec. 7.3.4), and any changes in these parameters need to be allowed for in the scaleup. The empirical information in Sec. 7.3.4 is useful for estimating the magnitude of these effects. Weir height and hole diameters also have a small effect, and these need to be considered as well.

There have been suggestions in the literature (145) to allow for tray geometry using a theoretical model. This procedure is satisfactory only if the model correctly predicts the trends of variation of tray efficiency with geometry. Considering the unreliability of current theoretical efficiency models (Sec. 7.2.1), it is doubtful whether they can be trusted for this purpose. Further, it was shown (15) that many flood correlations give good predictions but poor trends of variation of flood points with tray geometry; the same may apply to tray efficiency. Few studies compare measured to theoretically predicted trends of variation of tray efficiency with geometry.

Scaleup from pilot column. The most common scaleup is from a small column (e.g., pilot plant) to a commercial column. No reduction in efficiency on scaleup is expected (24,99) as long as

1. Both pilot and commercial columns are operated at the same approach to the flood point (18,134,135). Also, the flood point in the

pilot column must not be premature (e.g., due to foaming). This can be checked by flood testing the pilot column using a standard nonfoaming system, and comparing to the test system flood point.

2. Both pilot and commercial columns are operated in the same hydraulic regime. Larger columns, in general, tend to operate in the froth regime (Sec. 6.4.2). A parameter that can (and should) be manipulated in the pilot column to produce the desired operating regime is the tray spacing. With the pilot column running at the same percent flood as the prototype (1 above), a higher tray spacing implies higher vapor load and a tendency to generate spray, while a smaller tray spacing will promote froth regime operation.

   Both the bubble (deep pool) and the cellular foam regimes (Figs. 6.25*a*,*b*; 6.26*a*) are common in pilot and lab columns, but rare in commercial practice. Cellular foams need the small-column wall stabilization, while a deep pool forms only behind tall outlet weirs in small columns. In both these regimes, the dispersions are tall and the residence times high, leading to excellent efficiencies. Surface tension gradients further boost efficiency in the cellular foam regime (116,206). Higher efficiencies were reported in both the bubble (116) and cellular foam (116,206) regimes than in the froth or spray regimes. Pilot column data collected in the bubble or cellular foam regimes will therefore give optimistic efficiency predictions.

3. In the emulsion regime [high pressure (>150 psia) and/or high liquid rates], vapor entrainment through the downcomer (Sec. 6.4.5) is not large enough to affect efficiency.

4. Any relevant process factors (Sec. 7.3.6) are allowed for. Also, it is a good policy to pilot-test over several composition ranges engulfing all those expected in the commercial column. A pilot test is never an exact replication of a commercial column, and differences may lead to poor scaleup.

5. Pinching is avoided. It has been recommended to pilot-test at total reflux (18). At finite reflux, pinching can convert small measurement errors into major errors in efficiency estimates (130). However, finite reflux testing is useful in supplementing a total reflux test and providing information on pinch-point location.

6. Watch out for stagnant regions on the larger tray (Secs. 7.3.2, 7.3.3). A scaling-up process that failed to meet its objectives, presumably for this reason, has been described (24,170). Techniques for dealing with stagnant sections are in Sec. 7.3.3.

7. If more than two passes are used in the larger trays, watch out for possible maldistribution (Sec. 7.3.4).

8. In general, as column diameter increases, tray efficiency first increases because of the increased liquid plug flow character on the tray, and then slowly decreases because of stagnant regions and vapor plug flow. In general, it was stated that scaling up from pilot columns would be a conservative means of predicting column efficiency if the above precautions are observed (24,99).

Scaleup from Oldershaw columns. One laboratory-scale device that found wide application in supplying efficiency data is the Oldershaw column (Fig. 8.13; Ref. 207). This column is available from a number of laboratory supply houses and can be constructed from glass for atmospheric operation or from metal for superatmospheric separations. Small hole diameters and small tray spacings are used. Typical column diameters are 1 to 3 in.

Fair et al. (208) investigated scaleup of Oldershaw column data to commercial columns. Over the region of practical interest (50 to 85 percent of flood), the commercial point efficiency was either equal to or slightly higher than the Oldershaw column efficiency. Fair et al. concluded that the Oldershaw column efficiency is essentially a point efficiency measurement, and recommend this point efficiency for the design of commercial columns. A mixing model can be used to convert the point efficiency to overall column efficiency. This will enhance the commercial column efficiency. In a later paper (145), Chan and Fair include an additional correction for weir height; this correction will also enhance the commercial column efficiency. A conservative approach proposed by Fair et al. is to apply the Oldershaw column effi-

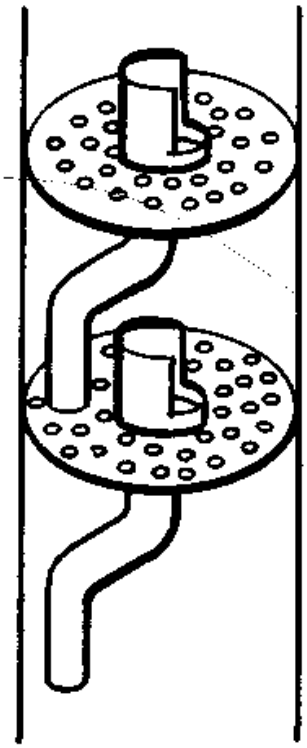

Figure 7.13 An Oldershaw column.

ciency as the overall column efficiency of the commercial column. This approach takes no credit for the greater plug-flow character and taller weir upon scaleup. The author prefers this conservative approach, considering the poor reliability of mixing models (Secs. 7.2.1 and 7.3.2).

Previous work with Oldershaw columns (209–211), however, spells a note of caution to Fair et al.'s conclusion. For a fixed system, higher Oldershaw column efficiencies were measured under cellular foam conditions than under froth conditions. For this reason, Gerster (212) warned that when cellular foam can form, scaleup from an Oldershaw column may be dangerous. The conclusions presented by Fair et al. (208) do not extend to Oldershaw columns operating in the cellular foam regime. Other considerations for scaleup from pilot columns (above) may also be important. The scaleup procedure recommended by Fair et al. (208) is

1. Run the real system in the Oldershaw column.
2. Determine the Oldershaw column flood point.
3. Establish the Oldershaw column operation at 60 percent of flood.
4. If good VLE data are available, run the Oldershaw column at total reflux and calculate efficiency. Obtain overall Oldershaw column efficiency and assume it is the same as the commercial column point efficiency. Use a mixing model to calculate the overall column efficiency for the commercial column. A conservative alternative is to assume that overall commercial column efficiency is the same as overall Oldershaw column efficiency.
5. If good VLE data are not available, vary reflux ratio and find by test the combination of reflux and stages that will give the desired separation. Assume that a commercial column with the same number of trays and operating at the same reflux ratio will give the same separation as the Oldershaw column. The number of plates thus calculated can sometimes be reduced by estimating the efficiency enhancement from point to column efficiency.

Some limitations to this procedure are mentioned above and in Ref. 208. In addition, it has been reported that reflux ratio may have a marked effect on Oldershaw column efficiency (213) and this variation must be studied carefully, especially if measurements are not conducted at total reflux. Also note that the formation of the cellular flow regime is composition-dependent (116,206), and it may occur under some conditions, but not under others.

7.4 Nomenclature (Chapters 6 and 7)

7.4.1 English letters

A	Area, ft^2.
A_a	Active area (the same as bubbling area, A_B, ft^2.
A_B	Bubbling area, i.e., column cross-section area less the total of downcomer area, downcomer seal area, and areas of any other nonperforated regions, ft^2.
A_D	Downcomer top area, ft^2. (*Note:* In multipass trays, A_D is the sum of the top areas of all downcomers transporting liquid from the tray.)
A_{DB}	Area at the bottom of the downcomer, ft^2. (*Note:* In multipass trays, A_{DB} is the sum of the bottom areas of all downcomers transporting liquid from the tray.)
A_{DT}	Same as A_D.
A_{da}	Area under the downcomer apron, ft^2.
A_{do}	Area of holes on the deck of a valve tray, ft^2.
A_f	Fractional hole area ($= A_h/A_B$).
A_h	Hole area, ft^2.
a_i	Interfacial area per unit volume of liquid and gas holdup, ft^2/ft^3.
a_i'	Interfacial area, ft^2.
A_N	Net area (column cross-section area less downcomer top area), ft^2.
A_S	Slot area, i.e., the total vertical curtain area through which vapor passes in a horizontal direction as it leaves the valves or bubble caps, ft^2.
A_{So}	Open slot area, i.e., slot area when the valve units are fully open, ft^2.
A_T	Total tower cross-section area, ft^2.
b	Intercept on linearized equilibrium relationship, Eq. (7.11).
C	Constant in Bennett et al.'s pressure drop correlation, defined by Eq. (6.57).
C_d	Coefficient in the clear liquid height correlation, defined by Eq. (6.62).
C_S	C-factor, a parameter describing vapor load, defined by Eq. (6.4), ft/s.
C_{SB}, C_{sb}	C-factor at flood, given by Eq. (6.10), ft/s.
C_v	Orifice coefficient in dry pressure drop calculation.
C_{vw}	Eddy loss coefficient through valves, dimensionless.
C_w	A constant in the weeping rate equation, Eq. (6.35), dimensionless.
CBP	Closed balance point for valve trays (Sec. 6.3.2).

CFS	Vapor flow rate, ft^3/s.
D	Diffusion coefficient, ft^2/s.
D_E	Eddy diffusion coefficient, ft^2/s.
D_f	Arithmetic average between tower diameter and weir length, ft.
d_H	Hole diameter, in.
D_T	Tower diameter, ft.
d_T	Tower diameter, in.
d_v	Diameter of valve unit at narrowest opening, in.
d_w	Diameter of circular weir, in.
E	Tray efficiency, fractional.
e	Entrainment rate, lb-mole/h.
E_{MV}	Murphree tray efficiency, fractional.
E_o	Section efficiency. Similar to E_{OC}, but taken only over a section of column, fractional.
E_{OC}	Overall column efficiency, fractional.
E_{OG}	Point efficiency, fractional.
E_S	Entrainment, lb liquid entrained/lb vapor.
f	Function of [Eq. (6.31*c*)].
f	Friction factor in hydraulic gradient correlation [Eq. (6.50)] given by Fig. 6.24, dimensionless.
F_{ga}	The active area F-factor. Same as F_S when F_S is based on the active (bubbling) area.
F_H, F_h	The hole F-factor, analogous to F_S but based on the hole area, defined by Eq. (6.3).
F_{lv}	Flow parameter, defined by Eq. (6.7).
F_S	The superficial F-factor, a parameter describing vapor load, defined by Eq. (6.2), ft/s $\sqrt{lb/ft^3}$.
F_{va}	Same as F_{ga}.
F_w	Weir constriction factor, used in Eq. (6.49).
f_w	Weep fraction, ratio of liquid weeping to liquid entering the tray [Eq. (6.40)], dimensionless.
FF	Fractional approach to flooding, defined by Eq. (7.20).
FPL	Flow-path length (distance from the inlet downcomer edge to outlet weir), in.
Fr	The Froude number, defined by Eq. (6.66) for froth regime clear liquid height calculation.
Fr_h	The Froude number, based on hole velocity, defined by Eq. (6.33), for weeping rate calculation.
G	Vapor flow rate, lb/h

g	Acceleration due to gravity, 32.2 ft/s^2.
G_M	Gas flow rate per bubbling area A_B, lb-mole/(s-ft^2).
GPM	Liquid flow rate, gpm.
H	Henry's law constant, lb-mole/(ft^3-atm).
h	Liquid head, in of liquid.
h'	Froth head, in of froth.
h_c	Clear liquid height on the tray, in of liquid.
h_{cl}	Clearance under the downcomer, in.
h_{ct}	Clear liquid height at the transition from the froth to spray regime, in of liquid.
$(h_{ct})_{H_2O}$	Clear liquid height at the transition from the froth to spray regime for the air-water system, in of water.
h_d	Dry pressure drop, in of liquid.
h_{da}	Head loss due to liquid flow under the downcomer apron, in of liquid.
h_f	Froth height on the tray, in.
h_{fow}	Froth height over the outlet weir, Eq. (6.63), in.
h_{hg}	Hydraulic gradient on the tray (high minus low clear liquid height), in of liquid.
h_i	Pressure drop through the aerated liquid on the tray, in of liquid.
h_L	Clear liquid height at the froth-to-spray transition, corrected for the effect of weir height on entrainment, given by Eq. (6.29), in of liquid.
h_n	Depth of notches in weir, in.
h_{ow}	Liquid head over the outlet weir, in of liquid.
h_R	Residual pressure drop, i.e., total tray pressure drop less dry pressure drop less clear liquid height, in of liquid.
h_t	Tray pressure drop, in of liquid.
H_v	Valve thickness, in.
h_v	Maximum vertical travel of a valve on a valve tray, in.
h_w	Outlet weir height, in.
h_σ	Head loss due to bubble formation, given by Eq. (6.31*b*), in of liquid.
J_G^*	Dimensionless vapor velocity used for correlating weeping rates, defined by Eq. (6.36).
J_L^*	Dimensionless weeping liquid velocity, defined by Eq. (6.37).
K	Dry pressure drop coefficient, defined by Eqs. (6.43) (sieve trays) and (6.44) (valve trays), in/(ft/s)^2.
k	Mass transfer coefficient, ft/s.
K_c	Pressure loss coefficient through closed valves, in/(ft/s)^2.

K_o	Pressure loss coefficient through open valves, in/(ft/s)^2.
K_{OG}	Overall mass transfer coefficient based on vapor, ft/s.
L	Liquid flow rate per tray pass, lb/h.
L_o	Liquid flow rate, lb-mole/h.
L_f	Length of flow path across the tray, ft.
L_M	Liquid flow rate per bubbling area A_B, lb-mole/(s-ft^2).
L_W,L_w	Outlet weir length, in (*Note:* In multipass trays, L_W is the total outlet weir length, i.e., the sum of lengths of all outlet weirs).
M	Marangoni effect index, or M-index, Eq. (7.37), dyne/cm.
m	A constant in the weeping rate equation, Eq. (6.35), dimensionless.
m	Slope of the equilibrium curve.
n	A parameter in the spray regime clear liquid height correlations, given by Eq. (6.69), in.
N	Rate of diffusion, lb-mole/s.
N_a	Number of actual trays in the column.
N_G	Gas film transfer units.
N_L	Liquid film transfer units.
N_{min}	Minimum number of theoretical stages for the separation.
N_{OG}	Overall gas transfer units.
N_p	Number of liquid passes per tray.
$N_{Re,h}$	Reynolds number, defined by Eq. (6.54).
N_t	Number of theoretical stages required for the separation minus the sum of theoretical stages provided by the reboiler, partial condenser, and intermediate heat exchangers.
N_v	Number of valve units on a tray.
OBP	Open balance point for valve trays, Sec. 6.3.2.
P	Pressure, atm.
p	Hole pitch (center-to-center tray hole spacing), in.
ΔP	Pressure drop, in of liquid.
Pe	Peclet number, defined by Eq. (7.26), dimensionless.
Q_D	Downcomer liquid load, defined by Eq. (6.8), gpm/ft^2.
Q_L	Liquid load, defined by Eq. (6.6), gpm/in of outlet weir length.
R	Reflux ratio (i.e., reflux rate divided by distillate rate), molar.
R_h	Hydraulic radius in hydraulic gradient calculation, defined by Eq. (6.51), ft.
R_{vw}	Ratio of valve weight with legs to valve weight without legs, dimensionless.
S	Tray spacing, in.

S	Separation parameter, defined by Eq. (7.30).
SF	Derating factor, defined in Sec. 6.2.10.
t	Tray deck thickness, in.
t_G	Residence time of vapor in froth, s.
t_L	Residence time of liquid in froth, s.
t_R	Downcomer apparent residence time, s.
u	Velocity, ft/s (in Fig. 6.11, u is $u_{\mathrm{N,flood}}$).
U_a	Same as u_B.
u_B	Superficial vapor velocity, based on bubbling area A_B, ft/s.
U_f	Velocity of the aerated mass across the tray, given by Eq. (6.52), ft/s.
u_h	Vapor hole velocity, based on the total area of the perforations, ft/s.
u_N	Superficial vapor velocity, based on the net area A_N, ft/s.
U_{nf}	Superficial vapor velocity at the flood point, based on the net area A_N, ft/s.
u_S, U_S	Superficial vapor velocity, ft/s.
U_{va}	Same as u_B.
u_{vh}	Vapor velocity through holes of valve tray, based on the area of holes on the tray deck, ft/s.
V	Vapor flow rate, lb/h.
V_S	Superficial vapor velocity (Figs. 6.9 and 7.10 only), based on total tower area, m/s.
VLOAD	A parameter describing vapor load, defined by Eq. (6.1), ft^3/s.
W	Weep rate, gpm.
w	Width, in.
X	Mole fraction of pseudo key component in the liquid.
x, x'	Mole fraction of a component in the liquid. Unless otherwise subscripted, refers to the more volatile component.
Y	Mole fraction of the pseudo key component in the vapor.
y	Mole fraction of a component in the vapor. Unless otherwise subscripted, refers to the more volatile component.
y^*	Equilibrium mole fraction of more volatile component in the vapor.
Z	Characteristic length in the weep rate equation, defined by Eq. (6.38), ft.

7.4.2 Greek letters

α	Relative volatility.
β	Tray aeration factor in pressure drop equation, Eq. (6.47a).

η	Factor used in the Chan and Fair tray efficiency correlation, defined by Eq. (7.25).
η	Factor used in froth density correlation, defined by Eq. (6.64).
λ	Ratio of the slope of the equilibrium curve to the slope of the component balance line, defined by the Eq. (7.5).
μ	Liquid viscosity, cP [*Note:* In Fig. 6.24 and in Eq. (6.54) only, viscosity has the units of lb/ft-s].
π	3.142...
ρ	Density, lb/ft^3.
ρ_{H_2O}	Density of liquid water at 60°F, 62.4 lb/ft^3.
ρ_M	Molar density, lb-mole/ft^3.
ρ_{vm}	Valve metal density, lb/ft^3.
σ	Surface tension, dyne/cm.
ϕ	Froth density.
χ	Parameter used in liquid entrainment calculation, defined by Eq. (6.28).
ψ	Entrainment, defined by Eq. (6.30), lb-mole of liquid entrained/lb-mole of liquid flow on the tray.

7.4.3 Subscripts

B	Based on bubbling area
b	Column bottom
c	Clear liquid
CBP	At closed balance point of valve tray (Sec. 6.3.2)
D	Distillate
d	Dry
da	Downcomer apron
dc	Downcomer
dry	Uncorrected for effects of weeping and entrainment (used to subscript Murphree tray efficiency).
f	Froth
flood	At the flood point
G,g	Vapor
h	Hole
HK	Heavy key component
i	At the interface
i	Component counter [Eq. (7.40)]
j	Component counter
L,l	Liquid

LK	Light key component
max	Maximum allowable
min	Minimum
N	Based on net area
n	On stage n
OBP	At open balance point of a valve tray (Sec. 6.3.2)
point	At a point on the tray
S	Superficial
t	Tray
V,v	Vapor

7.5 References (Chapters 6 and 7)

1. Kister, H. Z., *Distillation Operation,* McGraw-Hill, New York, 1990.
2. Bolles, W. L., *Pet. Process.*, Feb. 1956, p. 65; March 1956, p. 82; Apr. 1956, p. 72; May 1956, p. 109.
3. Bolles, W. L., in B. D. Smith, *Design of Equilibrium Stage Processes,* McGraw-Hill, New York, 1963.
4. Ludwig, E. E., *Applied Process Design for Chemical and Petrochemical Plants,* 2d ed., vol. 2, Gulf Publishing, Houston, 1979.
5. Van Winkle, M., *Distillation,* McGraw-Hill, New York, 1967.
6. Yanagi, T., *Chem. Eng.*, November, p. 120, 1990.
7. Glitsch, Inc., "Ballast Tray Design Manual," Bulletin 4900, 4th ed., Dallas, Texas, 1974.
8. Koch Engineering Co., Inc., "Design Manual—Flexitray," Bulletin 960-1, Wichita, Kansas, 1982.
9. Nutter Engineering, "Float Valve Design Manual," Tulsa, Oklahoma, 1976.
10. Frank, O., *Chem. Eng.,* March 14, p. 111, 1977.
11. Holland, C. D., *Fundamentals of Multicomponent Distillation,* McGraw-Hill, New York, 1981.
12. Lockett, M. J., *Distillation Tray Fundamentals,* Cambridge University Press, Cambridge, England, 1986.
13. Souders, M., Jr., and G. G. Brown, *Ind. Eng. Chem., 26*(1), p. 98, 1934.
14. Kirschbaum, E., *Destillier und Rektifiziertechnik,* 4 Aufl, Springer Verlag, Berlin, 1969.
15. Kister, H. Z., and J. R. Haas, *Chem. Eng. Prog. 86*(9), p. 63, 1990.
16. Hoppe, K., and M. Mittelstrass, *Chem. Tech. 18*(9), p. 533, 1966.
17. Zuiderweg, F. J., *Chem. Eng. Sci., 37*(10), p. 1441, 1982.
18. Fair, J. R., D. E. Steinmeyer, W. R. Penney, and B. B. Crocker in R. H. Perry and D. W. Green (eds.), *Chemical Engineers' Handbook,* 6th ed., chap. 18, McGraw-Hill, New York, 1984.
19. Fair, J. R., *Petro/Chem. Engr. 33*(10), p. 45, 1961.
20. Smith, R. B., T. Dresser, and S. Ohlswager, *Hydrocarb. Proc. & Pet. Ref. 42*(5), p. 183, 1963.
21. Gerster, J. A., W. H. Slack, Jr., and S. A. Harrison, *Ind. Eng. Chem. Proc. Des. Dev. 5*(4), p. 409, 1966.
22. Sakata, M., and T. Yanagi, *I. Chem. E. Symp. Ser.* 56, p. 3.2/21, London, 1979.
23. Yanagi T., and M. Sakata, *Ind. Eng. Chem. Proc. Des. Dev. 21,* p. 712, 1982.
24. Porter, K. E., and J. D. Jenkins, *I. Chem. E. Symp. Ser.* 56, Summary Paper, London, 1979.
25. Kister, H. Z., and I. D. Doig, *Hydrocarb. Proc., 56*(9), p. 149, 1977.
26. Lemieux, E. J., and L. J. Scotti, *Chem. Eng. Prog. 65*(3), p. 52, 1969.

27. Kister, H. Z., W. V. Pinczewski, and C. J. D. Fell, *Ind. Eng. Chem. Proc. Des. Dev. 20*, p. 528, 1981.
28. Kreis, H., and M. Raab, *I. Chem. E. Symp. Ser.* 56, p. 3.2/63, 1979.
29. Stichlmair, J., *Grundlagen der Dimensionierung des Gas/Flussigkeit-Kontaktapparates Bodenkolonne*, Verlag Chemie, Weinheim, 1978.
30. Chase, J. D., *Chem. Eng.*, July 31, p. 105, 1967 and *ibid.*, Aug. 28, p. 139, 1967.
31. Fair, J. R., in B. D. Smith, *Design of Equilibrium Stage Processes*, McGraw-Hill, New York, 1963.
32. Treybal, R. E., *Mass Transfer Operations*, 3d ed., McGraw-Hill, New York, 1980.
33. Fair, J. R., in W. C. Rousseau, *Handbook of Separation Process Technology*, Wiley, New York, 1987.
34. Fair, J. R., and R. L. Matthews, *Pet Refiner, 37*(4), p. 153, 1958.
35. Jeronimo, M. A. da S., and H. Sawistowski, *Trans. Inst. Chem. Engrs.* (London), *51*, p. 265, 1973.
36. Kister, H. Z., and J. R. Haas, *I. Chem. E. Symp. Ser.* 104, p. A483, 1987.
37. Mayfield, F. D., W. L. Church, A. C. Green, D. C. Lee, and R. W. Rasmussen, *Ind. Eng. Chem., 44*, p. 9, 2238, 1952.
38. Friend, L., E. J. Lemieux, and W. C. Schreiner, *Chem. Eng.*, Oct. 31, p. 101, 1960.
39. Hunt, C. d'A, D. N. Hanson, and C. R. Wilke, *AIChE J. 1*, p. 441, 1955.
40. Kister, H. Z., and J. R. Haas, *Ind. Eng. Chem. Res. 27*, 2331, 1988.
41. Chatterjee, N., Paper presented at the AIChE Meeting, New Orleans, March 12–15, 1973.
42. Thomas, W. J., in H. Sawistowski (ed.), *Final Report by the ABCM/BCPMA Distillation Panel*, Chem. Ind. Assoc., London, 1964.
43. Lockett, M. J., and A. A. W. Gharani, *I. Chem. E. Symp. Ser.*, 56, p. 2.3/43, 1979.
44. Hoek, P. J., and F. J. Zuiderweg, *AIChE J. 28*(4), p. 535, 1982.
45. Zuiderweg, F. J., *Proc. 2nd World Congress of Chem. Eng.*, vol. IV, p. 265, Montreal, 1981.
46. Thomas, W. J., and A. N. Shah, *Trans. Inst. Chem. Eng.* (London), *42*, T71, 1964.
47. Bolles, W. L., *Distillation Theory and Practice—Intensive Course*, University of New South Wales/University of Sydney, August 9–11, 1977.
48. Leibson, I., R. E. Kelley, and L. A. Bullington, *Pet. Ref., 36*(2), p. 127, 1957.
49. Maddox, R. N. *Process Engineer's Absorption Pocket Handbook*, Gulf Publishing, Houston, 1985.
50. Glitsch, Inc., "44 Frequently Asked Questions and Answers about Trays and Packing," Bulletin No. 681R1, Dallas, Texas, 1983.
51. Branan, C., *The Fractionator Analysis Pocket Handbook*, Gulf Publishing, Houston, 1978.
52. Fell, C. J. D., and W. V. Pinczewski, *I. Chem. E. Symp. Ser.* 73, p. D1, London, 1982.
53. Kister, H. Z., W. V. Pinczewski, and C. J. D. Fell, Paper presented in the 90th National AIChE meeting, Houston, April 1981.
54. Bain, J. L., and M. Van Winkle, *AIChE J.* 7(3), p. 363, 1961.
55. Lockett, M. J., G. T. Spiller, and K. E. Porter, *Trans. Inst. Chem. Engrs.* (London *54*, p. 202, 1976.
55a. Koziol, A., and J. Maćkowiak, *Chem. Eng. Process., 27*, p. 145, 1990.
56. Lockett, M. J., and S. Banik, *Ind. Eng. Chem. Proc. Des. Dev. 25*, p. 561, 1986.
57. Banik, S., "Non-Uniform Weeping and Its Effect on Tray Efficiency," Paper presented at the AIChE National Meeting, Houston, April 1989.
58. Colwell, C. J., and J. T. O'Bara, Paper presented at the AIChE National Spring Meeting, Houston, April 1989.
59. Smith, V. C., J. C. Upchurch, and D. W. Weiler, *Chem. Eng. Prog. 77*(9), p. 48, 1981.
60. Brambilla, A., E. Gianolio, and G. F. Nencetti, *I. Chem. E. Symp. Ser.* 56, p. 3.2/1, London, 1979.
61. Zenz, F. A., *Pet. Ref. 33*(2), p. 99. 1954.
62. Zenz, F. A. in P. A. Schweitzer (ed.), *Handbook of Separation Techniques for Chemical Engineers*, Sec. 3.2, McGraw-Hill, New York, 1979.
63. Hsieh, C. L., and K. J. McNulty, Paper presented at the annual Meeting of the AIChE, Miami Beach, Florida, November 2–7, 1986.

64. Zanelli, S., and R. Del Bianco, *Chem. Eng. J. 6*, p. 181, 1973.
65. Fasesan, S. O., *Ind. Eng. Chem. Proc. Des. Dev. 24*, p. 1073, 1985.
66. Hughmark, G. A., and H. E. O'Connell, *Chem. Eng. Prog. 53*(3), p. 127, 1957.
67. Davies, J. A., and K. F. Gordon, *Petro Chem. Eng.*, Oct. 1961, p. 230; Nov. 1961, p. 250; Dec. 1961, p. 228.
68. Colwell, C. J., *Ind. Eng. Chem. Proc. Des. Dev., 20* (2), p. 298, 1981.
69. Hsieh, C. L. (Koch Engineering Co.), Private communication, 1991.
70. Zhang, L., X. Wang, X. Xu, and F. Shen, Paper presented at the AIChE national meeting, Houston, April 1989.
71. Bolles, W. L., *Chem. Eng. Progr. 72*(9), p. 43, 1976.
72. Banik, S., "Weeping from Valve Trays," Paper presented at the AIChE National Meeting, Houston, April 1989.
73. Klein, G. F., *Chem. Eng.*, Sept. 17, p. 128, 1984.
74. Lieberman, N. P., *Process Design for Reliable Operations*, 2d ed., Gulf Publishing, Houston, 1988.
75. Zuiderweg, F. J., H. Verburg, and F. A. H. Gilissen, *International Symposium on Distillation*, p. 201, Institution of Chemical Engineers, (London), 1960.
76. Kister, H. Z., and T. C. Hower, Jr., *Plant/Operations Prog. 6* (3), p. 151, 1987.
77. Prince, R. G. H., International Symposium on Distillation, The Institution of Chemical Engineers (London), p. 177, 1960.
78. Prince, R. G. H., and B. K. C. Chan, *Trans. Inst. Chem. Engrs.* (London), *43*, p. T49, 1965.
79. Chan, B. K. C., Ph.D. thesis, University of Sydney, Australia, 1965.
80. Klein, G. F., *Chem. Eng.*, May 3, p. 81, 1982.
81. Bennett, D. L., R. Agrawal, and P. J. Cook, *AIChE J. 29*(3), p. 434, 1983.
82. Sargent, R. W. H., J. D. T. Bernard, W. P. McMillan, and R. C. Schroter, in H. Sawistowski, (ed.) *Final Report by the ABCM/BCPMA Distillation Panel*, Chem. Ind. Assoc., London, 1964.
83. Bernard, J. D. T., and R. W. H. Sargent, *Trans. Inst. Chem. Engrs.* (London), *44*, p. T314, 1966.
84. AIChE Research Committee, *Tray Efficiencies in Distillation Columns*, Final report from the University of Delaware, 1958.
85. Hofhuis, P. A. M., and F. J. Zuiderweg, *I. Chem. E. Symp. Ser.* 56, p. 2.2/1, 1979.
86. Dhulesia, H., *Chem. Eng. Res. Des. 62*, p. 321, 1984.
87. Chen, J. J. J., *Chem. Eng. Res. Des., 63*, p. 206, 1985.
88. Payne, G. J., and R. G. H. Prince, *Trans. Inst. Chem. Engrs.* (London) *55*, p. 266, 1977.
89. Lockett, M. J., *Trans. Inst. Chem. Engrs.* (London) *59*, p. 26, 1981.
90. Pinczewski, W. V., and C. J. D. Fell, *Ind. Eng. Chem. Proc. Des. Dev.* 21, p. 774, 1982.
91. Barber, A. D., and E. F. Wijn, *I. Chem. E. Symp. Ser.* 56, p. 3.1/15, 1979.
92. Pinczewski, W. V., and C. J. D. Fell, *Trans. Inst. Chem. Engrs.* (London) *50*, p. 102, 1972.
93. Todd, W. G., and M. Van Winkle, *Ind. Eng. Chem. Proc. Des. Dev., 11*(4), p. 578, 1972; and ibid., p. 589, 1972.
94. Weiss, S., and J. Langer, *I. Chem. E. Symp. Ser.* 56, p. 2.3/1, 1979.
95. Brambilla, A., G. Nardini, G. F. Nencetti, and S. Zanelli, *I. Chem. Eng. Symp. Ser.*, No. 32, p. 2:63, London, 1969.
96. Glitsch, Inc., "Glitsch Ballast Trays, A-1, V-1, V-0, Experimental Test Data," Bulletins 159/160 (revised), Dallas, 1983.
97. Anderson, R. H., G. Garrett, and M. Van Winkle, *Ind. Eng. Chem. Proc. Des. Dev. 15*(1), p. 96, 1976.
98. Stahl Apparate und Geratebau GmbH, Varioflex Valve VV16/L Bulletin, Viernheim, Germany.
99. Prince, R. G. H., *PACE*, June 1975, p. 31; July 1975, p. 18.
100. Wallis, G. B., *One-Dimensional Two-Phase Flow*, McGraw-Hill, New York, 1969.
101. Ho, G. E., R. L. Muller, and R. G. H. Prince, *I. Chem. E. Symp. Ser.* 32, p. 2:10, 1969.
102. Steiner, L., R. Hunkeler, and S. Hartland, *Trans. Inst. Chem. Engrs.* (London), *55*, p. 153, 1977.

103. Prado, M., K. J. Johnson, and J. R. Fair, *Chem. Eng. Prog. 83*(3), 32, 1987.
104. Zuiderweg, F. J., P. A. M. Hofhuis, and J. Kuzniar, *Chem. Eng. Res Des. 62,* p. 39, 1984.
105. Zuiderweg, F. J., *Int. Chem. Eng. 26*(1), p. 1, 1986.
106. Loon, R. E., W. V. Pinczewski, and C. J. D. Fell, *Trans. Inst. Chem. Engrs.* (London) 51, p. 374, 1973.
107. Porter, K. E., and P. F. Y. Wong, *I. Chem. E. Symp. Ser.* 32, p. 2:22, 1969.
108. Fell, C. J. D., and W. V. Pinczewski, *Chem. Engr.* (London), p. 45, January 1977.
109. Wong, P. F. Y., and W. K. Kwan, *Trans. Inst. Chem. Engrs.* (London) *57,* p. 205, 1979.
110. Prado, M., and J. R. Fair, *I. Chem. E. Symp. Ser.* 104, p. A529, 1987.
111. Fair, J. R., *Proceedings of the Second GRI Gas Separations Workshop,* Boulder, Colorado, October 1982.
112. Dhulesia, H., *Chem. Eng. Res. Des., 61,* p. 329, 1983.
113. Raper, J. A., W. V. Pinczewski, and C. J. D. Fell, *Chem. Eng. Res. Des., 62,* p. 111, 1984.
114. Pinczewski, W. V., N. D. Benke, and C. J. D. Fell, *AIChE J. 21,* (6), p. 1210, 1975.
115. Raper, J. A., N. T. Hai, W. V. Pinczewski, and C. J. D. Fell, *I. Chem. E. Symp. Ser.* 56, p. 2.2/57, 1979.
116. Fane, A. G., and H. Sawistowski, *I. Chem. E. Symp. Ser.* 32, p. 1:8, 1969.
117. Sawistowski, H., *Chem. Ing. Tech. 50*(10), p. 743, 1978.
118. Doig, I. D., *Aust. Chem. Eng. 12*(7), p. 5, 1971.
119. Kister, H. Z. and I. D. Doig, *Trans. Inst. Chem. Engrs.* (London), *57,* p. 43, 1979.
120. Murphree, E. V., *Ind. Eng. Chem. 17,* p. 747, 1925.
121. Lewis, W. K., Jr., *Ind. Eng. Chem. 28,* p. 399, 1936.
122. Lockett, M. J., and M. S. Uddin, *Trans. Inst. Chem. Engrs.* (London), *58,* p. 166, 1980.
123. Standart, G. L., *Chem. Engr.* (London), Nov., p. 716, 1974.
124. Standart, G. L., R. Bragg, M. S. Uddin, A. H. El Yafi, and E. Yaroson, *I. Chem. E. Symp. Ser. 56,* p. 2.1/1, London, 1979.
125. AIChE Research Committee, *Bubble Tray Design Manual,* New York, 1958.
126. King, C. J., *Separation Processes,* 2d ed., McGraw-Hill, New York, 1980.
127. Colburn, A. P., *Ind. Eng. Chem. 28,* p. 526, 1936.
128. Rahman, M. A., and M. J. Lockett, *I. Chem. E. Symp. Ser. 61,* p. 111, London, 1981.
129. Lockett, M. J., M. A. Rahman, and H. A. Dhulesia, *AIChE J. 30,*(3), p. 423, 1984.
130. AIChE Equipment Testing Procedures Committee, *AIChE Equipment Testing Procedure Tray Distillation Columns* 2d ed., 1987.
131. Vital, T. J., S. S. Grossel, and P. I. Olsen, *Hydrocarb. Proc. 63*(11), p. 147, 1984.
132. AIChE Research Committee, *Tray Efficiencies in Distillation Columns,* Final Report from University of Michigan, 1960.
133. AIChE Research Committee, *Tray Efficiencies in Distillation Columns,* Final Report from North Carolina State College, 1959.
134. Chan, H., and J. R. Fair, Paper presented at the AIChE Meeting, Anaheim, California, June 1982.
135. Chan H., and J. R. Fair, *Ind. Chem. Proc. Des. Dev. 23,* p. 814, 1984.
136. Burgess, J. M., and P. H. Calderbank, *Chem. Eng. Sci., 30,* p. 743 & 1107, 1975.
137. Calderbank, P. H., and J. Pereira, *Chem. Eng. Sci., 32,* p. 1427, 1977.
138. Foss, A. S., and J. A. Gerster, *Chem. Eng. Prog. 52*(1), p. 28-J. 1956.
139. Barker, P. E., and M. F. Self, *Chem. Eng. Sci. 17,* p. 541, 1962.
140. Shore, D., and G. G. Haselden, *I. Chem. E. Symp. Ser.* No. 32, p. 2:54, London, 1969.
141. Sohlo, J., and S. Kinnunen, *Trans. Inst. Chem. Engrs.* (London), *55,* p. 71, 1977.
142. Sohlo, J., and R. J. Kouri, *Chem. Eng. Sci. 37*(2), p. 193, 1982.
143. Diener, D. A., *Ind. Eng. Chem. Proc. Des. Dev. 6*(4), p. 499, 1967.
144. Prado, M., and J. R. Fair, *Ind. Eng. Chem. Res. 29,* p. 1031, 1990.
145. Chan, H., and J. R. Fair, *Ind. Eng. Chem. Proc. Des. Dev. 23,* p. 820, 1984.
146. Zuiderweg, F. J., *Chem. Eng. Res. Des. 61,* p. 388, 1983.

147. Zuiderweg, F. J., J. H. de Groot, B. Meeboer, and D. van der Meer, *I. Chem. E. Symp. Ser.* 32, p. 5:78, London, 1969.
148. Porter, K. E., M. J. Lockett, and C. T. Lim, *Trans. Inst. Chem. Engrs.* (London), *50*, p. 91, 1972.
149. O'Connell, H. E., *Trans. AIChE 42*, p. 741, 1946.
150. Drickamer, H. G., and J. R. Bradford, *Trans. AIChE 39*, p. 319, 1943.
151. Wankat, P. C., *Equilibrium Staged Separations*, Elsevier, New York, 1988.
152. Hines, A. L., and R. N. Maddox, *Mass Transfer*, Prentice-Hall, Englewood Cliffs, New Jersey, 1985.
153. MacFarland, S. A., P. M. Sigmund, and M. Van Winkle, *Hydrocarb. Proc. 51*(7), p. 111, 1972.
154. Kister, H. Z., *Practical Distillation Technology*, Continuing Education Seminar Sponsored by *Chemical Engineering*, 1983.
155. Roy, P., and G. K. Hobson, *I. Chem. E. Symp. Ser.* 104, p. A273, 1987.
156. Nelson, A. R., J. H. Olson, and S. I. Sandler, *Ind. Eng. Chem. Proc. Des. Dev., 22*, p. 547, 1983.
157. Porter, K. E., B. Davies, B. A. Enjugu, and C. C. Ani, *I. Chem. E. Symp. Ser.* 104, p. A569, 1987.
158. Solari, R. B., and R. L. Bell, *AIChE J., 32*(4), p. 640, 1986.
159. Bell, R. L., *AIChE J. 18*, p. 498, 1972.
160. Yanagi, T., and B. D. Scott, Paper presented at the AIChE 74th National Meeting, New Orleans, March 1973.
161. Solari, R. B., E. Saez, I. D'Apollo, and A. Bellet, *Chem. Eng. Commun.*, 13, p. 369, 1982.
162. Weiler, D. W., W. V. Delnicki, and B. L. England, *Chem. Eng. Prog. 69*(10), p. 67, 1973.
163. Stichlmair, J., and S. Ulbrich, *I. Chem. E. Symp. Ser.* 104, p. A555, 1987.
164. Yanagi, T., and B. D. Scott, *Chem. Eng. Prog. 69*(10), p. 75, 1973.
165. Müller, E. A., A. Cavero, and L. A. Estévez, *Chem. Eng. Commun.* 74, p. 195, 1988.
166. Kler, S. C., and J. T. Lavin, *Gas. Sep. Purif., 2*, March, p. 34, 1988.
167. Lim, C. T., K. E. Porter, and M. J. Lockett, *Trans. Inst. Chem. Engrs.* (London) *52*, p. 193, 1974.
168. Biddulph, M. W., *AIChE J. 23*(5), p. 770, 1977.
169. Lockett, M. J., and A. Safekourdi, *Chem. Eng. J.* 11, p. 111, 1976.
170. Smith, V. C., and W. V. Delnicki, *Chem. Eng. Prog. 71*(8), p. 68, 1975.
171. Lockett, M. J., C. T. Lim, and K. E. Porter, *Trans. Inst. Chem. Engrs.* (London) *51*, p. 61, 1973.
172. Thorogood, R. M., *I. Chem. E. Symp. Ser. 61*, p. 95, London, 1981.
173. Brambilla, A., *Chem. Eng. Sci. 31*, p. 517, 1976.
174. Weiler, D. W., R. D. Kirkpatrick, and M. J. Lockett, *Chem. Eng. Prog. 77*(1), p. 63, 1981.
175. Bell, R. L., and R. B. Solari, *AIChE J.* 20(4), p. 688, 1974.
176. Kouri, R. J., and J. J. Sohlo, *Chem. Eng. Res. Des. 63*, p. 117, 1985.
177. Estévez, L. A., and G. Arreaza, Paper presented at the AIChE annual meeting, Chicago, November 1990.
178. Winter, G. R., and K. D. Uitti, *Chem. Eng. Prog. 72*(9), p. 50, 1976.
179. Katayama, H., and T. Imoto, *Int. Chem. Eng. 13*(4), p. 728, 1973.
180. Ying, D. H. S., R. M. Thorogood, and V. G. Fox, Paper presented at the AIChE national meeting, San Francisco, November 1984.
181. Furzer, I. A., *AIChE J. 15*(2), p. 235, 1969.
182. Lockett, M. J., and H. A. Dhulesia, *Chem. Eng. J. 19*, p. 183, 1980.
183. Mohan, T., K. K. Rao, and D. P. Rao, *Ind. Eng. Chem. Proc. Des. Dev. 22*, p. 376, 1983.
183*a*. Lockett, M. J., and J. D. Augustyniak, Trans. *I. Chem. E., 69*, part A, p. 99, March 1991.
184. Kalbassi, M. A., M. M. Dribika, M. W. Biddulph, S. Kler, and J. T. Lavin, *I. Chem. E. Symp. Ser.* 104, p. A511, 1987.
185. Finch, R. N., and M. Van Winkle, *Ind. Eng. Chem. Proc. Des. Dev.* 2, 106, 1964.
186. Mahiout, S., and A. Vogelpohl, *I. Chem. E. Symp. Ser.* 104, p. A495, 1987.

187. Lopez-Bonillo, F., M. Nolla, and F. Castells, *I. Chem. E. Symp. Ser.* 104, p. B461, 1987.
188. Lockett, M. J., R. D. Kirkpatrick, and M. S. Uddin, *Trans. Inst. Chem. Engrs.* (London), *57*, p. 25, 1979.
189. Dribika, M. W., and M. W. Biddulph, *Ind. Eng. Chem. Res. 26*, p. 1489. 1987.
190. Ellis, S. R. M., and M. W. Biddulph, *Trans. Inst. Chem. Engrs.* (London), *45*, p. T223, 1967.
191. Bolles, W. L., *AIChE J. 22*(1), p. 153, 1976.
192. Toor, H. L., and J. K. Burchard, *AIChE J. 6*(2), p. 202, 1960.
193. Vogelpohl, A., *I. Chem. E. Symp. Ser.* 56, 2.1/25, London, 1979.
194. Biddulph, M. W., and M. A. Kalbassi, *Ind. Eng. Chem. Res. 27*, p. 2127, 1988.
195. Ognisty, T. P., and M. Sakata, *Chem. Eng. Prog. 83*(3), p. 60, 1987.
196. Wilke, C. R., *Chem. Eng. Prog. 46*, p. 95, 1950.
197. Biddulph, M. W., *AIChE J. 21*(2), p. 327, 1975.
198. Biddulph, M. W., and N. Ashton, *Chem. Eng. J. 14*, p. 7, 1977.
199. Biddulph, M. W., *Hydrocarb. Proc. 56*(10), p. 145, 1977.
200. Krishna, R., H. F. Martinez, R. Shreedhar, and G. L. Standart, *Trans. Inst. Chem. Engrs.* (London), *55*, p. 178, 1977.
201. Krishna, R., *Chem. Eng. Sci 32*, 1197, 1977.
202. Burghardt, A., K. Warmuzinski, J. Buzek, and A. Pytlik, *Chem. Eng. J.* 26, p. 71, 1983.
203. Medina, A. G., C. McDermott, and N. Ashton, *Chem. Eng. Sci. 34*, p. 861, 1979.
204. Gorak, A., *I. Chem. E. Symp. Ser.* 104, p. A413, 1987.
205. Krishna, R., and G. L. Standart, *AIChE J. 22*(2), p. 383, 1976.
206. Hart, D. J., and G. G. Haselden, *I. Chem. E. Symp. Ser.* 32, p. 1:19, London, 1969.
207. Oldershaw, C. F., *Ind. Eng. Chem. Anal. Ed. 13*, p. 265, 1941.
208. Fair, J. R., H. R. Null, and W. L. Bolles, *Ind. Eng. Chem. Proc. Des. Dev.* 22, p. 53, 1983.
209. Ellis, S. R. M., and R. M. Contractor, *J. Inst. Petrol., 45*(425), p. 147, 1959.
210. Ellis, S. R. M., P. E. Barker, and R. N. Contractor, *Trans. Inst. Chem. Engrs.* (London), *38*, p. 21, 1960.
211. Ellis, S. R. M., and R. J. Bennett, *J. Inst. Petrol. 46*, p. 19, 1960.
212. Gerster, J. A., *Chem. Eng. Prog., 59*(3), p. 35, 1963.
213. Ellis, S. R. M., and M. J. Hardwick, *I. Chem. E. Symp. Ser.* 32, p. 1:29, London, 1969.
214. Ellis, S. R. M., and R. J. Legg, *Can. J. Chem. Eng. 40*, p. 6, 1962.

Chapter

8

Packing Design and Operation*

8.1 Packing Types

8.1.1 Classification

Packings are generally divided into three classes:

1. *Random or dumped packings (Figs. 8.1 to 8.6):* These are discrete pieces of packing of a specific geometrical shape which are "dumped" or randomly packed into the column shell.
2. *Structured or systematically arranged packings (Figs. 8.8 to 8.11):* These are crimped layers of wire mesh or corrugated sheets. Sections of these packings are stacked in the column.
3. *Grids (Fig. 8.14):* These are also systematically arranged packings, but instead of wire-mesh or corrugated sheets these use an open-lattice structure.

Random packings are by far the most common in commercial practice. Structured packings are less common, but their share of the packing market has rapidly grown over the last decade. The application of grids is limited primarily to heat transfer and wash services and/or where a high fouling resistance is required.

8.1.2 Packing objectives

OBJECTIVES FOR MAXIMIZING EFFICIENCY

1. *To maximize the specific surface area, i.e., the surface area per unit volume:* This maximizes vapor-liquid contact area, and therefore, efficiency (see Fig. 8.12*b* and Sec. 8.1.10). A corollary is that for random packings, efficiency generally increases as the particle size is decreased (Fig. 8.7); for structured packings, efficiency generally

*Nomenclature lists and references for Chap. 8 appear at the end of Chap. 9.

increases as the space between adjacent layers is decreased, and for grid, efficiency generally increases as the lattice openings are narrowed.

2. *To spread the surface area uniformly:* This improves vapor-liquid contact, and therefore, efficiency. For instance, a Raschig ring (Fig. 8.1*a*) and a Pall® ring (Fig. 8.2*d*) of an identical size have identical surface areas per unit volume, but the Pall® ring has a superior spread of surface area and is therefore much more efficient.
3. *To promote uniform distribution of vapor and liquid throughout the packed bed:* Uniform distribution improves packing efficiency. For instance, random packing particles that "interlock" with, or "nest" inside other particles can lead to channeling and therefore to lower efficiency.
4. *To freely drain any liquid, so that stagnant liquid pockets are minimized:* Stagnant liquid contributes little to mass transfer and wastes packing surface.
5. *To maximize wetting of packing surfaces:* Dewetting of packing surfaces at low liquid rates reduces efficiency and restricts turndown. Although the wetting characteristics are primarily a function of the packing material, the size and geometry of the packing are also important.

OBJECTIVES FOR MAXIMIZING CAPACITY

1. *To maximize the void space per unit column volume:* This minimizes resistance to vapor upflow, and therefore, enhances packing capacity. A corollary is that for random packings, capacity increases with particle size (Fig. 8.7); for structured packings, capacity increases with the space between adjacent layers, and for grids, capacity increases as the lattice openings are widened. Comparing to the first objective for maximizing efficiency, this corollary states that the packing size that maximizes capacity also minimizes efficiency. A trade-off therefore exists; the ideal size of packing is a compromise between maximizing efficiency and maximizing capacity.
2. *To minimize friction:* This favors an open shape that has good aerodynamic characteristics. For instance, the Pall® ring (Fig. 8.2*d*) is far more open to gas flow compared to the Raschig ring (Fig. 8.1*a*), and therefore, has greater capacity.
3. *To ensure uniform resistance to vapor and liquid flow throughout the bed:* Concentrated pockets of aerodynamic resistance can lower the effective tower cross-section area, thus reducing capacity.
4. *To permit easy disengagement of vapor from liquid:* This is impor-

tant in high-pressure services and high-liquid-flow-rate services. Vapor disengagement is difficult when the opening available to liquid downflow is narrow (e.g., as in narrow-channel structured packings).

OTHER OBJECTIVES

1. *To maximize resistance to mechanical deformation and/or breakage and, especially, to deformation under the weight of the bed:* For instance, the partition in the center of the Lessing ring (Fig. 8.1*b*) gives it a superior resistance to deformation and breakage than that of the Raschig ring (Fig. 8.1*a*).
2. *To minimize cost:* Packing cost, as well as the requirements for packing supports and column foundations, generally rise with the weight per unit volume of packing. A corollary is that packings become cheaper as the particle size increases (random packing), as the space between layers increases (structured packing), or as the lattice openings widen (grids).
3. *To maximize fouling resistance:* Packings become more fouling resistant as the particle size increases (random packing), or the space between layers increases (structured packing) or the lattice opening widens (grids). Geometric shapes that resist trapping of sediment or polymer are advantageous.
4. *To minimize liquid holdup (where degradation or polymerization is encountered):* The more liquid is held at high temperatures, the more it degrades and polymerizes.
5. *To minimize deterioration in service:* Packing geometry and size affect the sensitivity of a packing to corrosion, erosion, chemical attack, and migration through the support grid openings.
6. *To minimize damage during abnormal operation:* Packing geometry and size affect the ability of a packed bed to weather pressure surges or to catch fire at shutdown (when containing adhered pyrophoric material or coated with hot flammable liquid).

8.1.3 Types of random packings

Historically, there were three generations of evolution in random packings. The first generation (1907 to the 1950s) produced two basic simple shapes, the Raschig ring and the Berl saddle, that became the ancestors of modern random packings. These packings have all been superseded by more modern packing and are seldom used in modern distillation practice.

The second generation (late 1950s to the early 1970s) produced two

popular geometries—the Pall® ring, which evolved from the Raschig ring, and the Intalox® saddle, which evolved from the Berl saddle. The second-generation packings are still popular and extensively used in modern distillation practice.

The third generation (the mid 1970s until present) has produced a multitude of popular geometries, most of which evolved from the Pall® ring and Intalox® saddle.

FIRST-GENERATION RANDOM PACKINGS

Raschig rings (Fig. 8.1*a*). These are the oldest, cheapest, and previously most widely used packings, first patented by Dr. Raschig in Germany in 1907. The height of the ring is equal to its diameter. The rings are cut from pipes, but in case of metal they may also be rolled from metal strips (1).

Lessing rings (Fig. 8.1*b*). These are similar to Raschig rings, but a partition is added across the center of the ring to increase the surface area. The partition strengthens the ring, but the improvement in efficiency due to the larger area is minor.

Berl saddles (Fig. 8.1*c*). These are the original type of saddle packing. They have a smaller free gas space than Raschig and Lessing rings, but their aerodynamic shape is better, giving a lower pressure drop and higher capacity than Raschig and Lessing rings.

SECOND-GENERATION RANDOM PACKINGS

Intalox® saddles (Fig. 8.2*a*). Developed by the Norton Company, they superseded the Berl saddles. The shape of the Berl saddle was modified in the Intalox® so that adjacent elements do not blank off any sig-

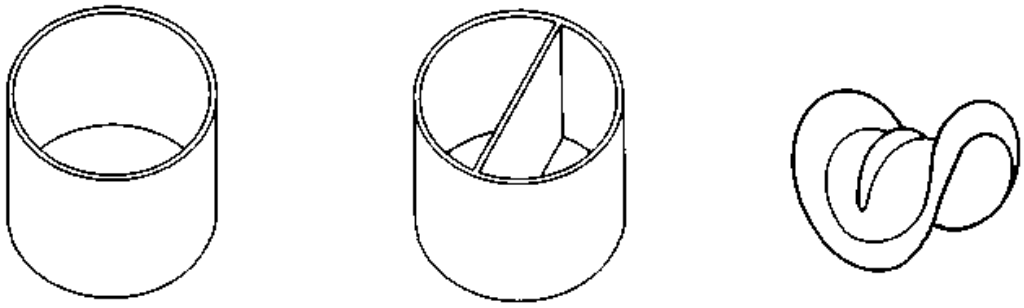

Figure 8.1 First-generation random packings. (*a*) Raschig ring, metal; (*b*) Lessing ring, metal; (*c*) Berl saddle, ceramic.

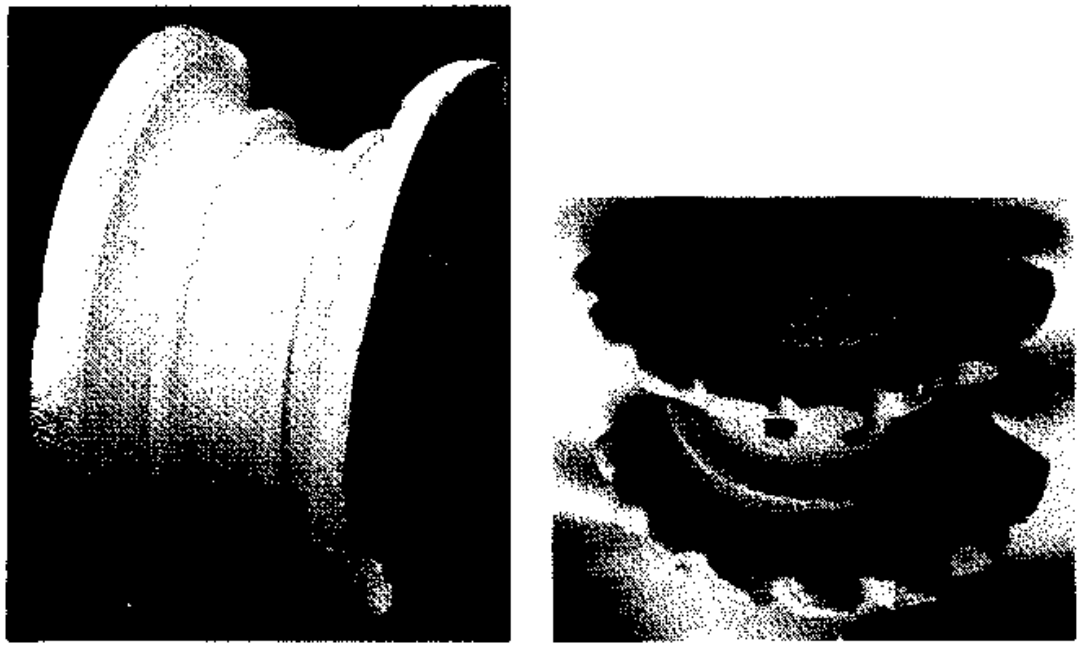

(a) (b)

Figure 8.2 Second-generation random packings. (*a*) Intalox® saddle, ceramic; (*b*) Super Intalox® saddle, ceramic (*Courtesy of Norton Company.*)

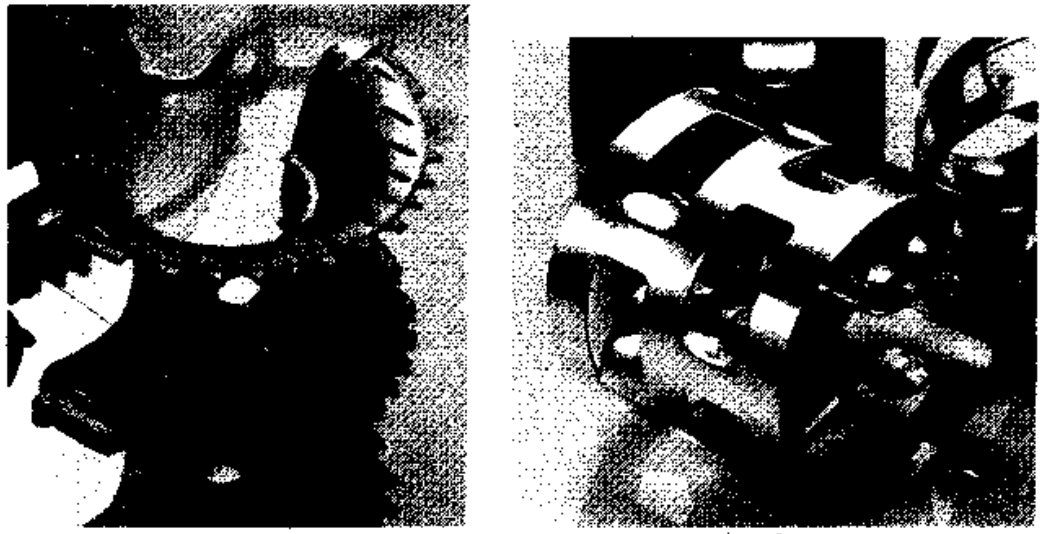

(c) (d)

Figure 8.2 (*Continued*) Second-generation random packings. (*c*) Super Intalox® saddle, plastic; (*d*) Pall® ring, metal. (*Courtesy of Norton Company.*)

nificant portion of the wetting liquid, thus avoiding stagnant pools of liquid, trapping of gas bubbles, and violent changes in the direction of the gas. These factors result in a higher capacity, higher efficiency, and lower pressure drop than Berl saddles.

Intalox® saddles are available in ceramic only from the Norton Company. Packings that are normally considered equivalent to the Intalox® saddles are marketed under the trade names of Flexisaddle™ by Koch Engineering Company, Inc.; and Novalox® saddles by Jaeger

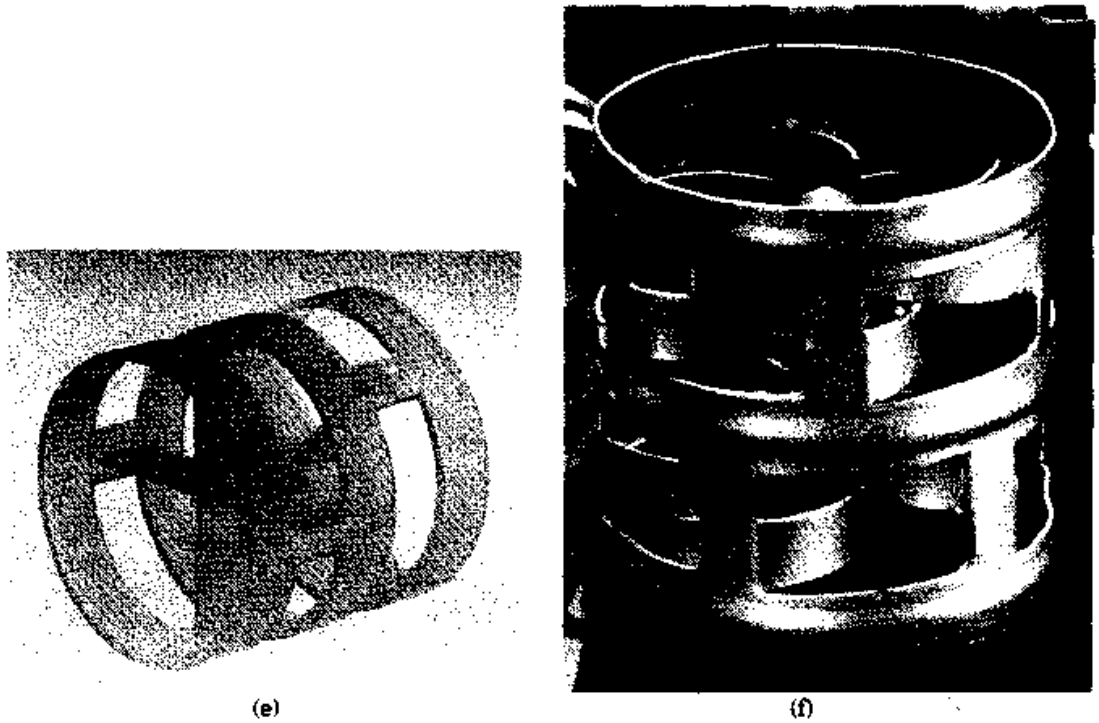

(e) (f)

Figure 8.2 (*Continued*) Second-generation random packings. (*e*) Pall® ring, plastic; (*f*) Hy-Pak® ring, metal. (*Courtesy of Norton Company.*)

Products, Inc. Rauschert Industries, Inc., also markets a packing similar to the Intalox® saddles.

Super Intalox® Tower Packing (Fig. 8.2*b,c*). This packing was developed by the Norton Company. The smooth edges of the Intalox® saddle were scalloped in the Super Intalox® and holes were inserted. These changes promote drainage of liquid, eliminate stagnant pockets, and provide more open area for vapor rise. The Super Intalox® was shown (2) to have higher capacity and higher efficiency compared to the Intalox® saddle.

Super Intalox® saddles are available in ceramic and plastic from the Norton Company. Plastic packings that are normally considered equivalent to the Super Intalox® are marketed under the trade names of Flexisaddle® by Koch Engineering Company, Inc.; Ballast® saddles by Glitsch Inc.; and Novalox® saddles by Jaeger Products, Inc.

Pall® rings (Fig. 8.2*d,e*). BASF developed the Pall® ring by cutting windows in the Raschig ring and bending the window tongues inward. This opened up the ring, lowered its friction, and improved packing area distribution, wetting, and distribution of liquid. Pall® rings have higher capacity and efficiency and lower pressure drop than the packings described so far.

Pall® rings are available in metal and plastic and are marketed by

the Norton Company; Jaeger Products, Inc.; and by Rauschert Industries, Inc. Packings that are normally considered equivalent to the Pall® rings are marketed under the trade names of Flexiring® by Koch Engineering Company, Inc., and Ballast™ ring by Glitsch, Inc.

A ceramic Pall® ring is also available and is marketed by Jaeger Products, Inc., and Rauschert Industries, Inc. The ceramic Pall® ring has not been popular, and tests by Billet (3) show that its performance is inferior to that of the ceramic Intalox® saddle.

Hy-Pak™ Tower Packing (Fig. 8.2*f*). Similar to the Pall® ring, Hy-Pak™ has more internal tongues in an effort to improve the spread of surface area. The resulting claimed efficiency improvement was traded off for greater capacity by making the ring slightly larger than the equivalent Pall® ring (4). Compared to the Pall® ring, Hy-Pak™ has been shown to give better capacity at an equivalent efficiency (4).

Hy-Pak™ is available in metals only and is marketed by the Norton Company. Packings that are normally considered equivalent to Hy-Pak™ are marketed under the trade names of K-PAC™ by Koch Engineering Co., Inc., and Ballast-plus™ by Glitsch, Inc.

THIRD-GENERATION PACKINGS

Intalox® Metal Tower Packing (IMTP®) (Fig. 8.3*a*). IMTP® combines the high void fraction and the well-distributed surface area of the Pall® ring with the low aerodynamic drag of the saddle shape. Compared to the Pall® ring, it provides a more open shape and improved liquid spread, while incorporating adequate mechanical strength and entanglement resistance (5). IMTP® is available in metals only. It is marketed exclusively by the Norton Company.

Cascade® Mini-Rings (CMR®) (Figs. 8.3*b*, 8.4*a*, 8.5*a*). These rings are similar to the Pall® ring, but have an aspect ratio (height to diameter ratio) of 1:3, compared to 1:1 in the Pall® ring. The lower aspect ratio orients the particles with their open side facing the vapor flow, thus reducing friction, and exposing more surface to mass transfer (6). CMR® is available in metal, plastic, and ceramics. It is marketed exclusively by Glitsch, Inc.

The CMR® Turbo is a metallic variation of the CMR® that has perforated walls and tongues. Compared to the normal CMR®, this variation appears to slightly improve both the capacity and the efficiency (3).

Chempak™ or Levapak (LVK®) (Fig. 8.3*c*). Cutting a Pall® ring in half creates this packing. The cutting exposes and activates the concealed

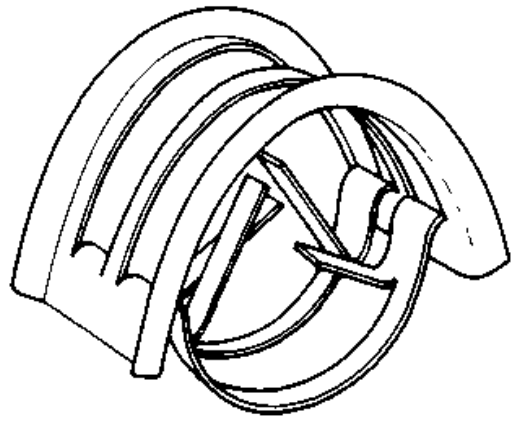

Intalox® Metal Tower Packing

(a)

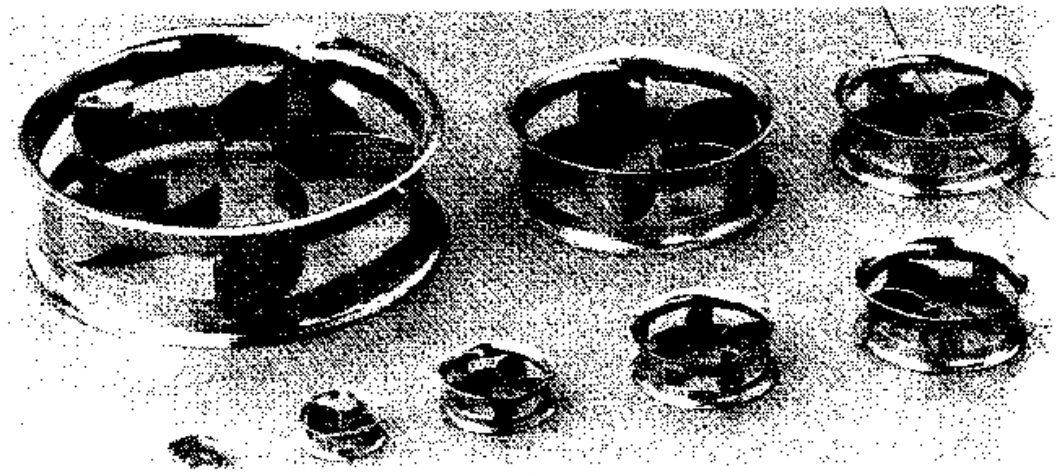

(b)

Figure 8.3 Third-generation random metal packings. (*a*) Intalox® Metal Tower Packing (IMTP®); (*b*) Cascade® MiniRing (CMR®). (*Part a, courtesy of Norton Company; part b, courtesy of Glitsch, Inc.*)

Pall® ring tongues, promoting vapor-liquid contact, mixing, and liquid spread (7). Chempak™ is available in metal from Nutter Engineering Corporation and in plastic and other nonmetals from Chemetics International.

Nutter Rings™ (Fig. 8.3*d*). Nutter Rings™ retain the low aerodynamic drag of the saddle shape, while offering a more open structure with improved liquid spread. The rib-and-hoop design minimizes nesting and interlocking and achieves adequate mechanical strength (8). Nutter Rings™ are available in metal and plastic. They are marketed exclusively by Nutter Engineering Corporation.

HcKp™ (Fig. 8.3*e*). This packing is a modified Pall® ring with a more open structure and an enhanced arrangement of internal drip tabs (8a).

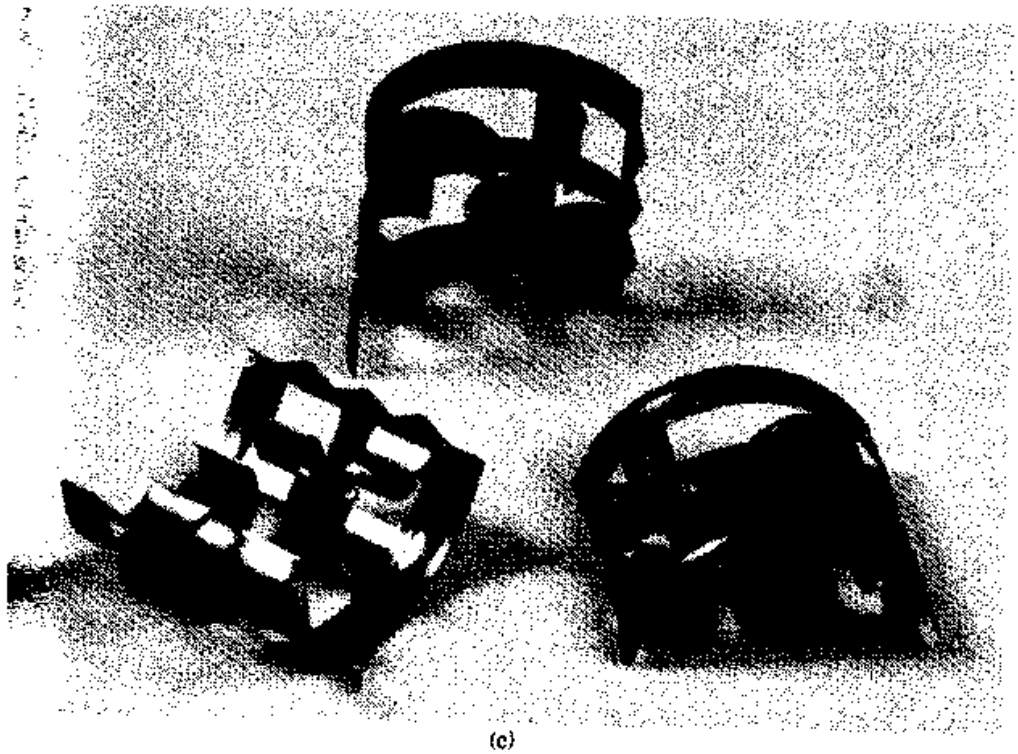

(c)

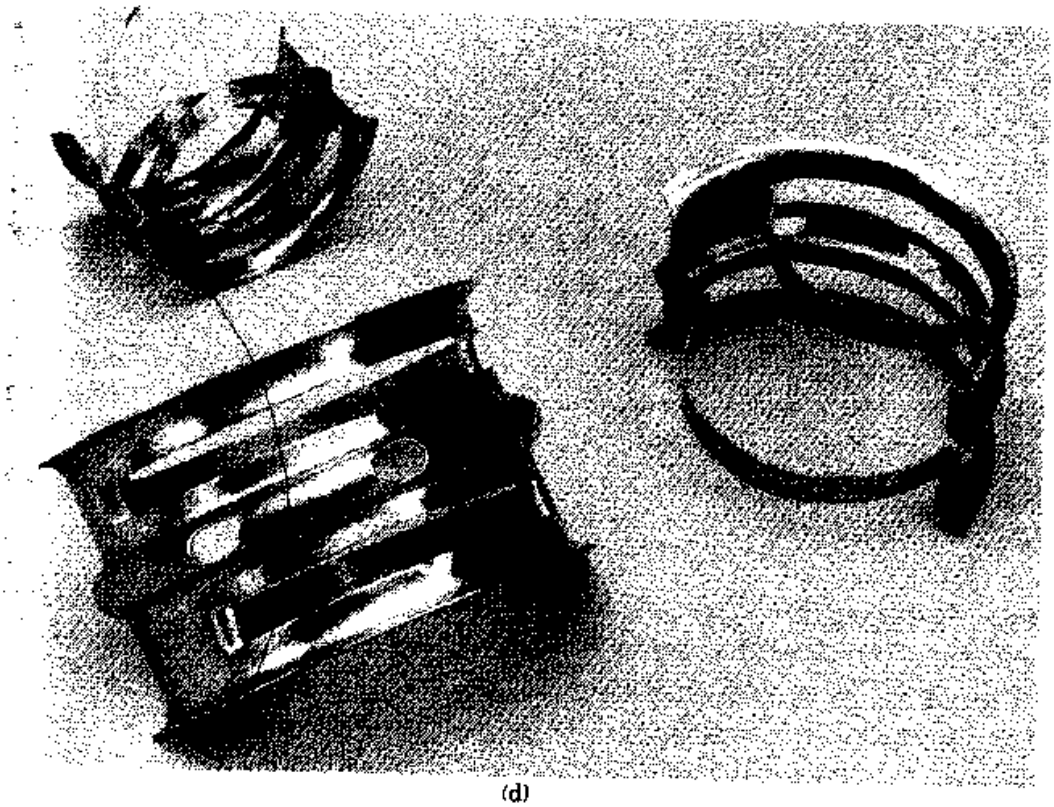

(d)

Figure 8.3 (*Continued*) Third-generation metal random packings. (*c*) Chempak®; (*d*) Nutter Ring®. (*Parts c and d, courtesy of Nutter Engineering Corp.*)

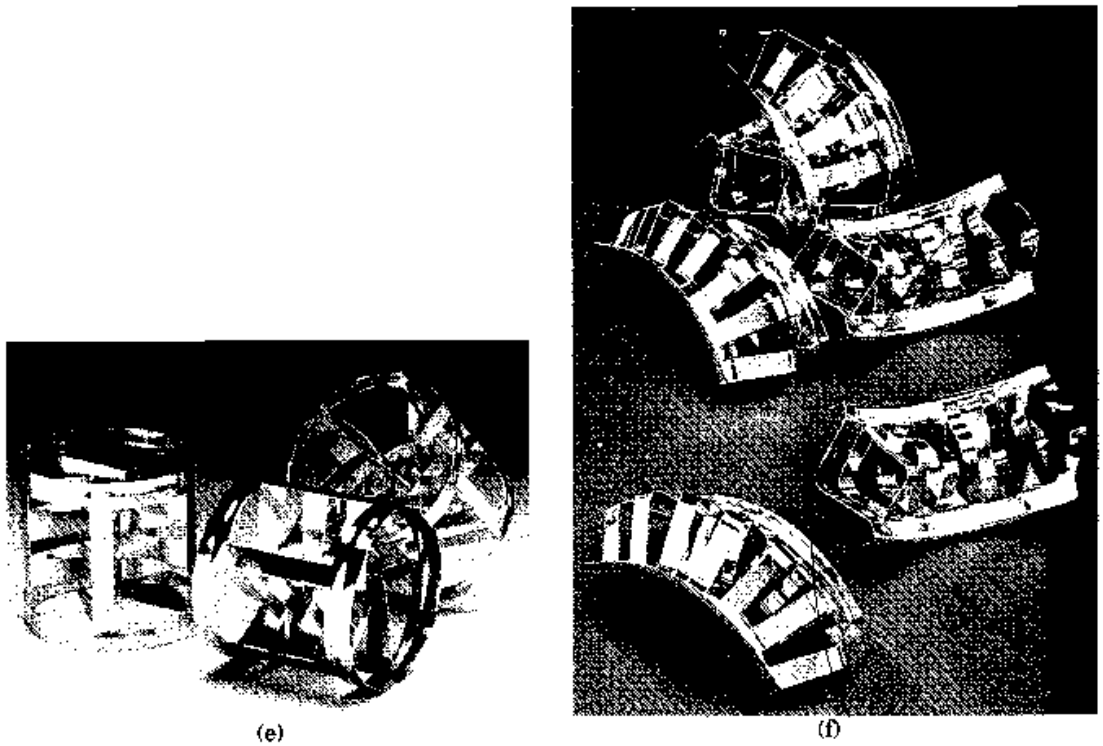

(e) (f)

Figure 8.3 (*Continued*) Third-generation metal random packings. (*e*) HcKp; (*f*) FLEXIMAX® (*Parts e and f courtesy of Koch Engineering Company, Inc.*)

It is stated to be ideal for use in high-liquid-rate systems (8*a*). HcKp® is available in metal exclusively from Koch Engineering Company, Inc.

FLEXIMAX® (Fig. 8.3*f*) This packing is an open saddle with well-spread surface area. FLEXIMAX® is available in metal exclusively from Koch Engineering Company, Inc.

Hiflow® ring (Figs. 8.3*g*, 8.4*b*, 8.5*b*). Resembling the Pall® ring but with wider openings, the Hiflow® ring shifts surface from the wall to the center of the ring and reduces resistance to vapor flow (9). The Hiflow® ring is available in metal, plastic, and ceramics from Rauschert Industries, Inc.

Jaeger Tri-Packs® (Figs. 8.3*h*, 8.4*c*). This packing replaces the cylindrical shape of the Pall® ring by a spherical shape. This provides more void space and better distribution of active surface than the Pall® ring and minimizes interlocking (10). Jaeger Tri-Packs® are available in metal (also referred to as Metal Jaeger Top-Pak®) and plastic (also referred to as Hackette®) from Jaeger Products, Inc.

NOR PAC® (NSW) rings (Fig. 8.4*d*). Replacing the solid walls of the Pall® ring by wide openings in the NOR PAC® is at the expense of losing some surface area. The result is a packing that has (3,11) high

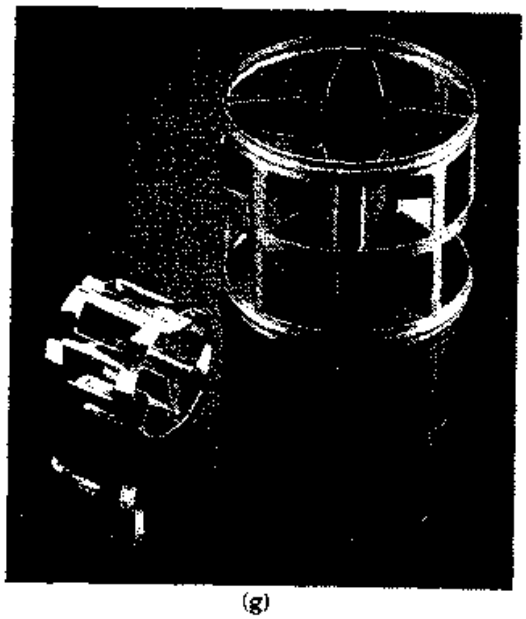

(g)

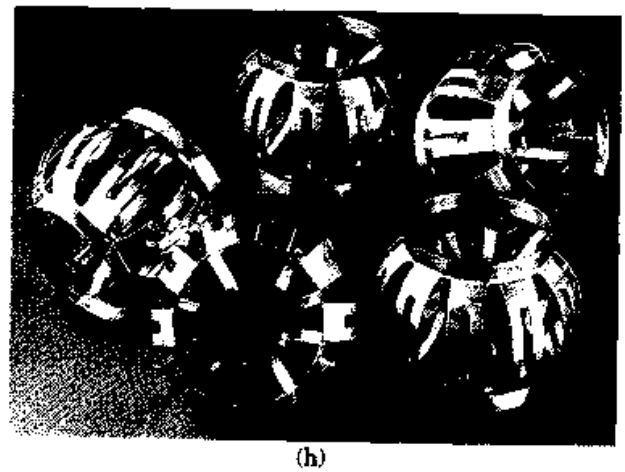

(h)

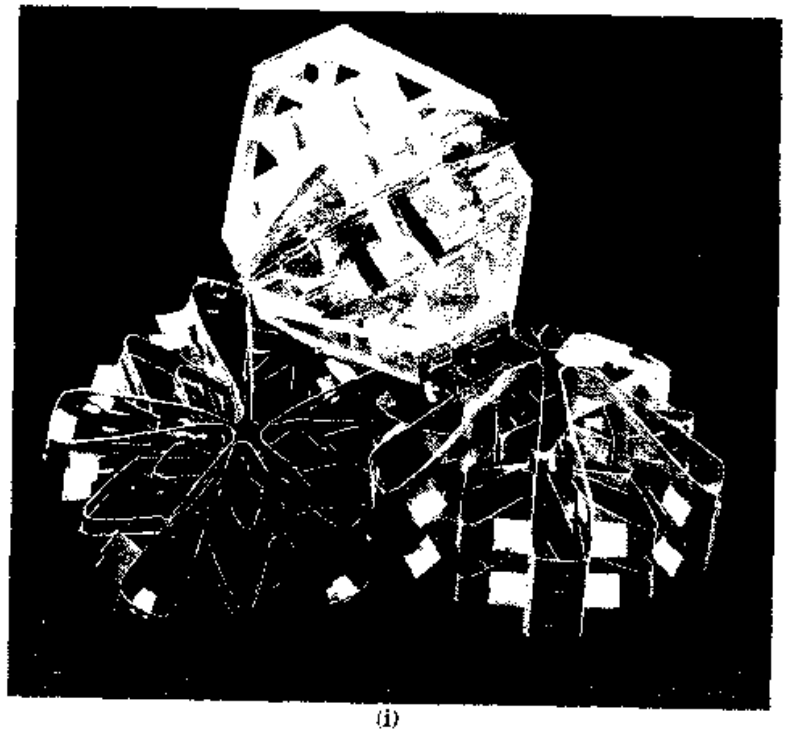

(i)

Figure 8.3 (*Continued*) Third-generation metal random packings. (*g*) Hiflow® ring; (*h*) Jaeger Tri-Packs® (Top-Pak®); (*i*) IMPAC™. (*Part g, courtesy of Rauschert Industries, Inc.; part h, courtesy of Jaeger Products, Inc.; part i, courtesy of Lantec, Inc.*)

capacity at the price of lower efficiency. NOR PAC® rings are available in plastic from Nutter Engineering Corporation and from Jaeger Products, Inc.

Intalox® Snowflake™ packing (Fig. 8.4e). The low aspect ratio (height to diameter), even lower than that of CMR®, orients the Snowflake™ par-

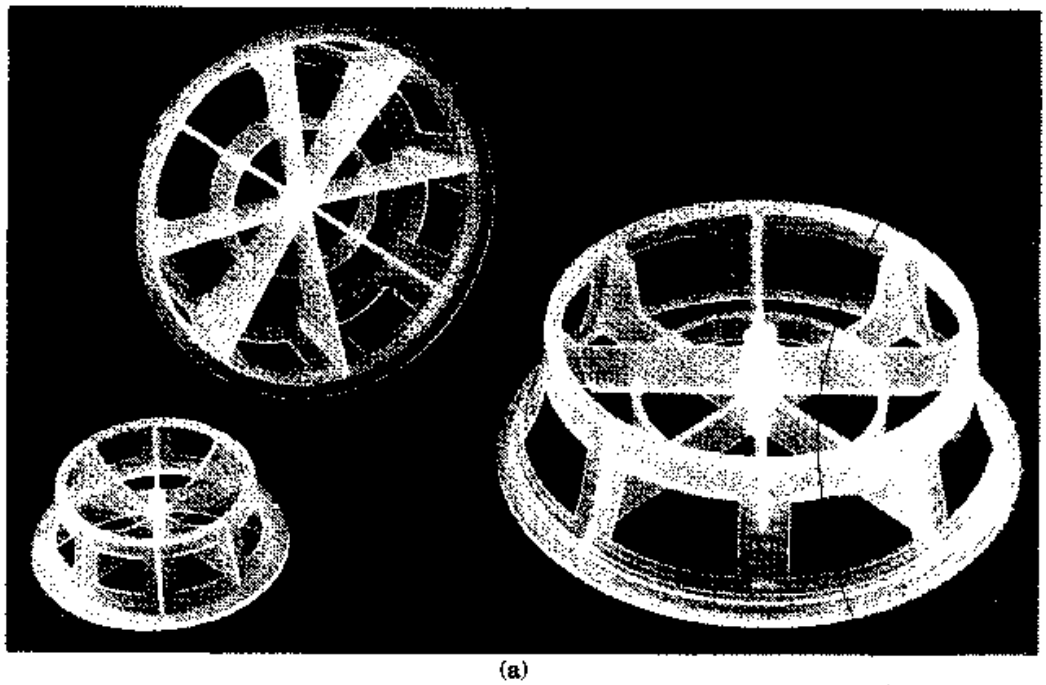

(a)

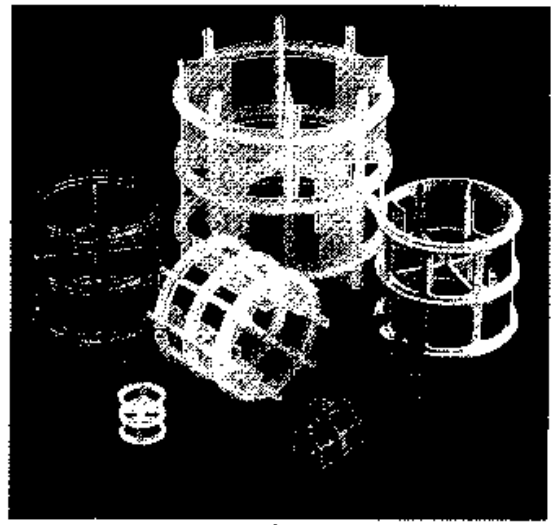

(b)

Figure 8.4 Third-generation plastic random packings. (*a*) Cascade® MiniRing (CMR®); (*b*) Hiflow® ring. (*Part a, courtesy of Glitsch, Inc.; part b, courtesy of Rauschert Industries, Inc.*)

ticles with their open side facing the vapor flow. This reduces friction and permits good liquid drainage from the ribs of the packing. Intalox® Snowflake™ packing is available in plastic from the Norton Company.

LANPAC™ (Fig. 8.4*f*). This packing has a hollow polyhedron shape, constructed on an intricate network of ribs, filaments, rods, struts, and pointed fingers, all cross-linked and uniformly spaced throughout an

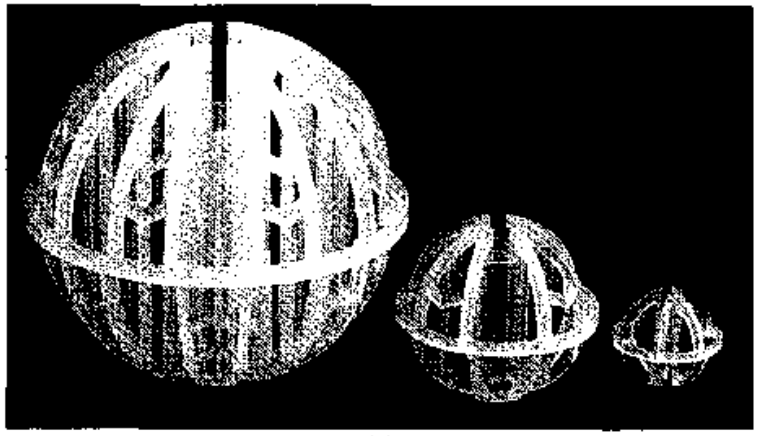

(c)

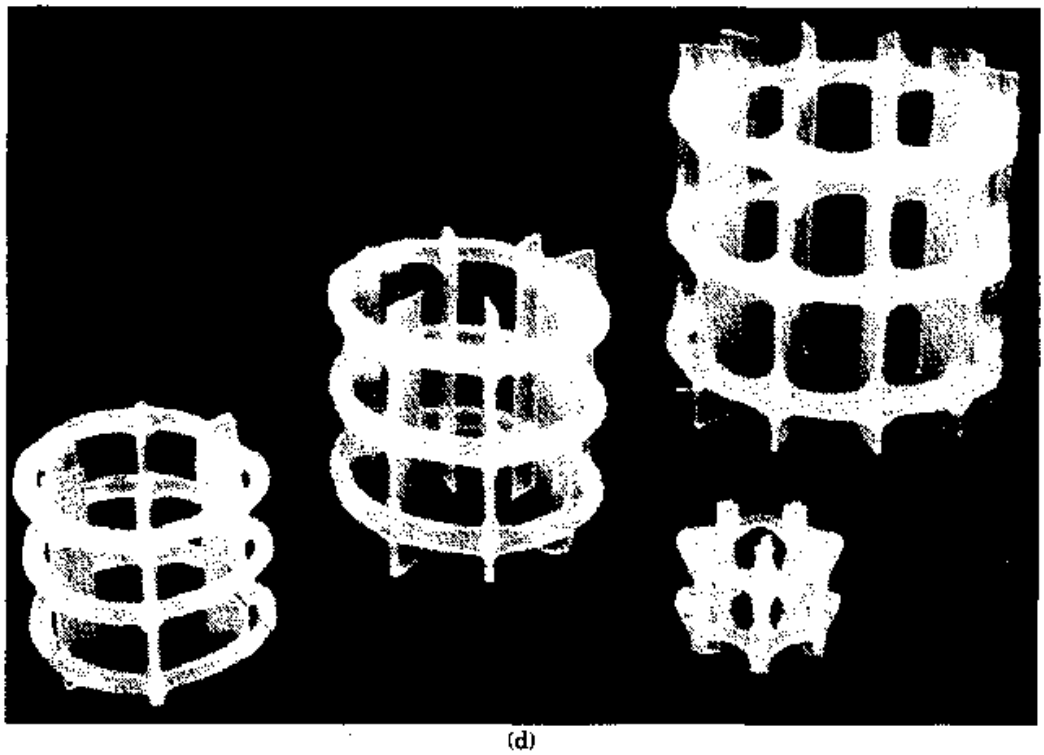

(d)

Figure 8.4 (*Continued*) Third-generation plastic random packings. (*c*) Jaeger Tri-Packs® (Hackette®); (*d*) NOR-PAC® (NSW rings). (*Part c, courtesy of Jaeger Products, Inc.; part d, courtesy of Nutter Engineering Corp.*)

open-structural framework. This design gives an open structure with a high surface area, void of nesting and interlocking. LANPAC™ is available in plastic exclusively from Lantec Products, Inc.

IMPAC™ (Figs. 8.3*i*, 8.4*g*). This is another complex-shaped packing (compared to LANPAC™). It gives as open a structure with an even higher and better distributed surface area (12). IMPAC™ is available in metal and plastic exclusively from Lantec Products, Inc.

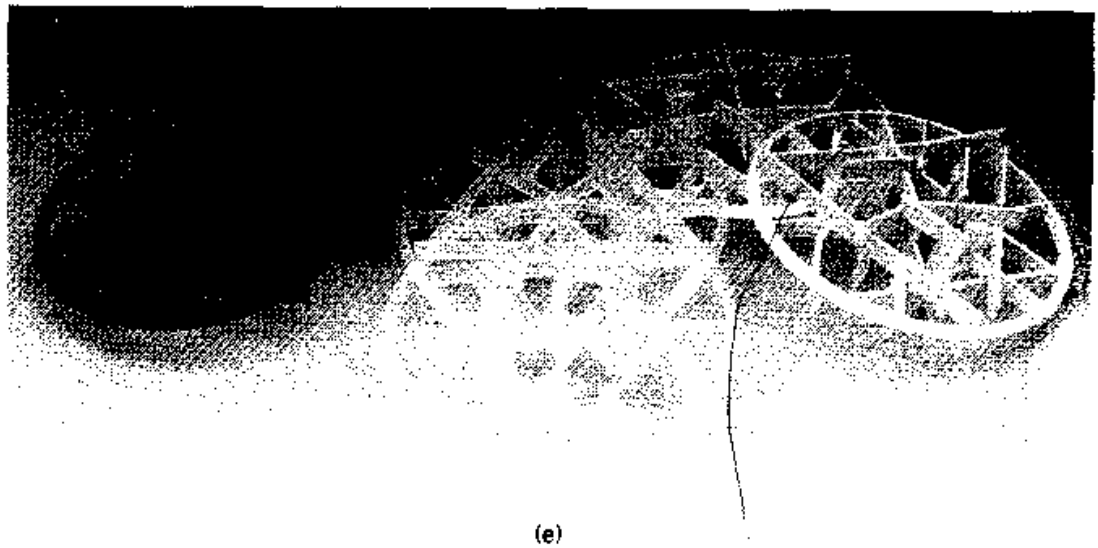

(e)

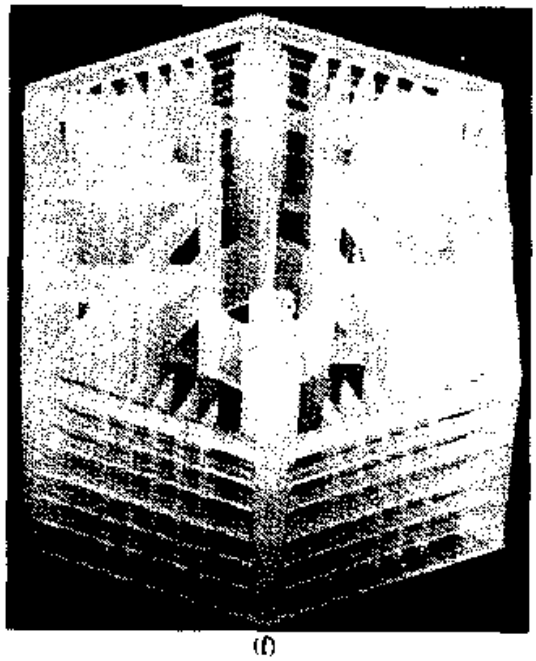

(f)

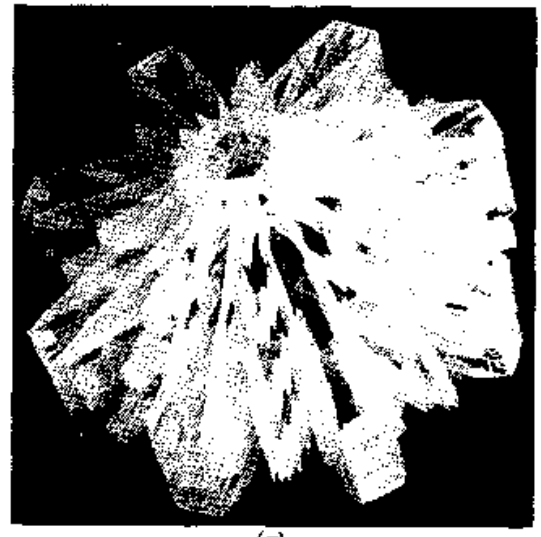

(g)

Figure 8.4 (*Continued*) Third-generation plastic random packings. (*e*) Intalox® Snowflake™ packing (*f*) LANPAC™ (*g*) IMPAC™ (*Part e, courtesy of Norton Company; parts f and g courtesy of Lantec, Inc.*)

Others. Miscellaneous random packings are shown in Fig. 8.6.

8.1.4 Comparison of random packings from different generations

Figure 8.7 is a plot of the specific surface area (surface area per unit volume) against the packing factor for metallic packings from each of the three packing generations. The specific surface area is a rough indicator of packing efficiency; the higher it is, the more efficient the packing. Packing factors are indicators of capacity; the lower the

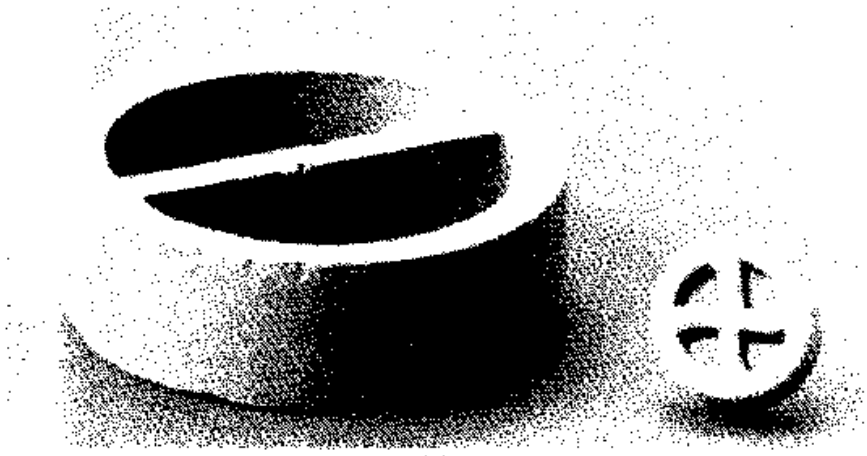

(a)

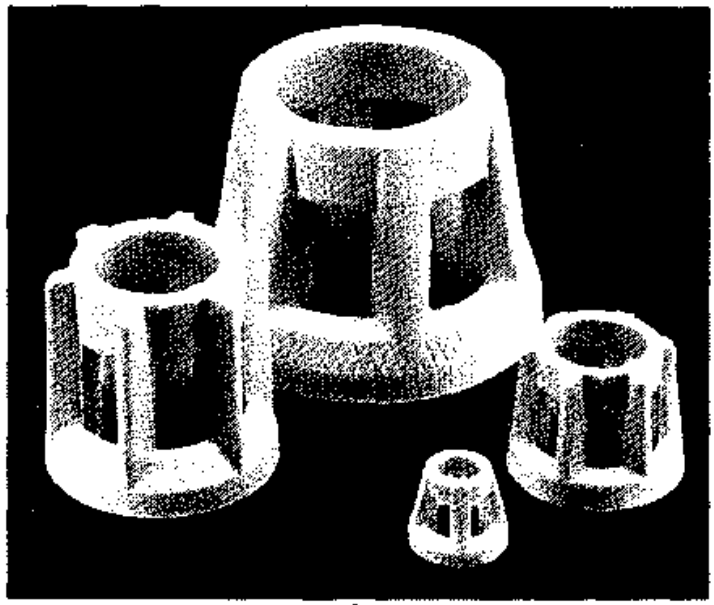

(b)

Figure 8.5 Third-generation ceramic random packings. (*a*) Cascade® MiniRing (CMR®); (*b*) Hiflow® ring. (*Part a, courtesy of Glitsch, Inc.; part b, courtesy of Rauschert Industries, Inc.*)

packing factor, the higher the capacity. Packing factors are discussed in detail later (Sec. 8.2.10). Figure 8.7 is based on the following approximations:

1. Specific surface areas were taken from Perry (14) or Strigle (15). When the value given by Perry differed from that of Strigle for the same packing, an average value was used. For most third-generation packings, specific surface areas were given neither by Perry nor by Strigle, and were obtained from the packing supplier literature.
2. For Raschig rings, packing factors were taken from Perry (14) and Strigle (15). For second- and third-generation packings, packing

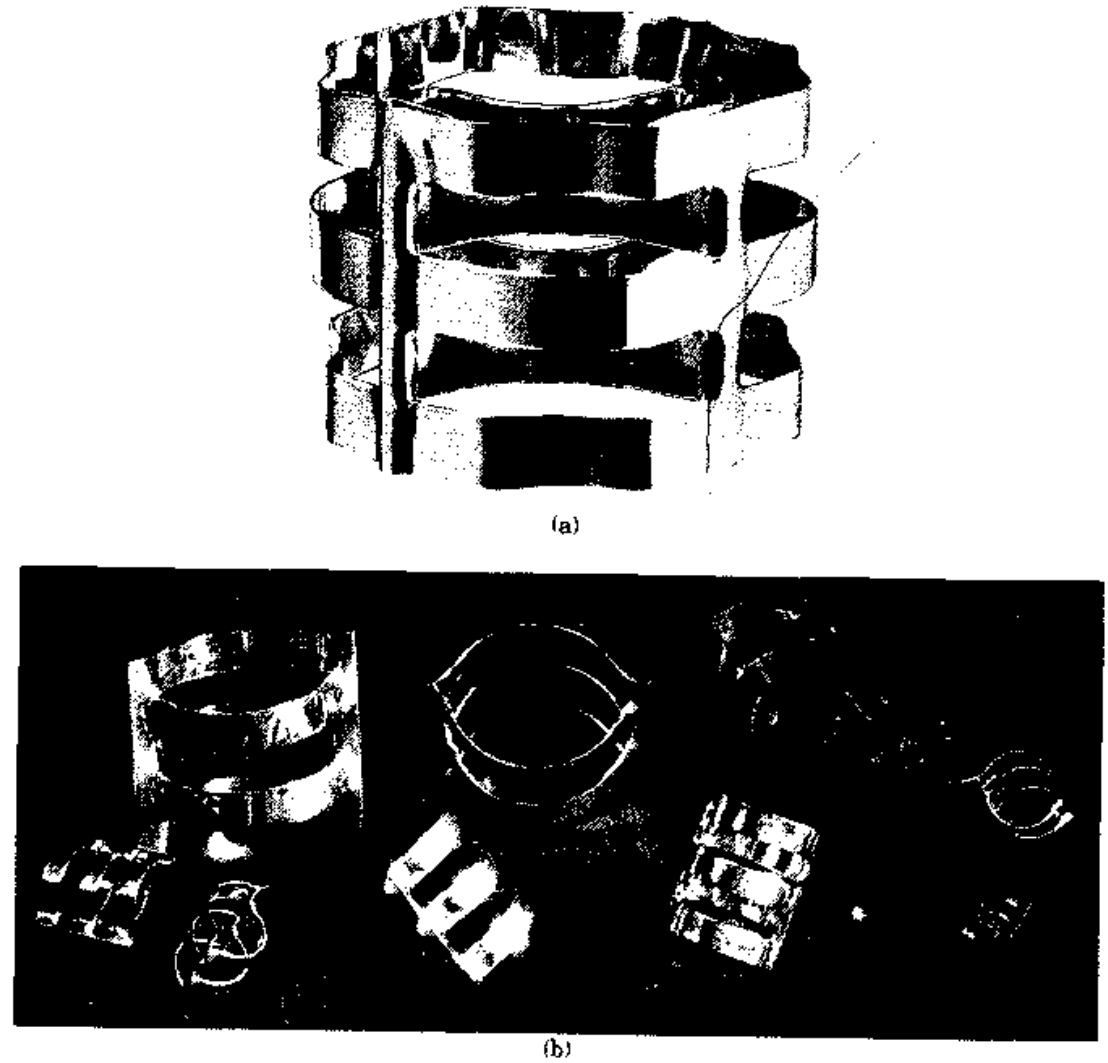

(a)

(b)

Figure 8.6 Miscellaneous random packings. (*a*) VSP®. (*b*)Interpack® (*Parts a and b courtesy of Jaeger Products, Inc.*)

factors were derived from Table 10.1. Some of the packing factors derived from Table 10.1 were modified to give better fit to experimental data shown in Chapter 10.

Due to the approximations, Fig. 8.7 is unsuitable for comparative evaluation among different third-generation packings. References to the manufacturers have therefore been omitted. The values plotted on Fig. 8.7 were arbitrarily connected by straight lines.

Figure 8.7 shows that at a constant capacity (i.e., a constant packing factor), each generation of packing enhanced the specific surface area. Similarly, at a constant specific area, packing capacity increased from generation to generation. This signifies improvements in either capacity or efficiency or both from one generation to the next. The improvements from the first to the second generation have been major.

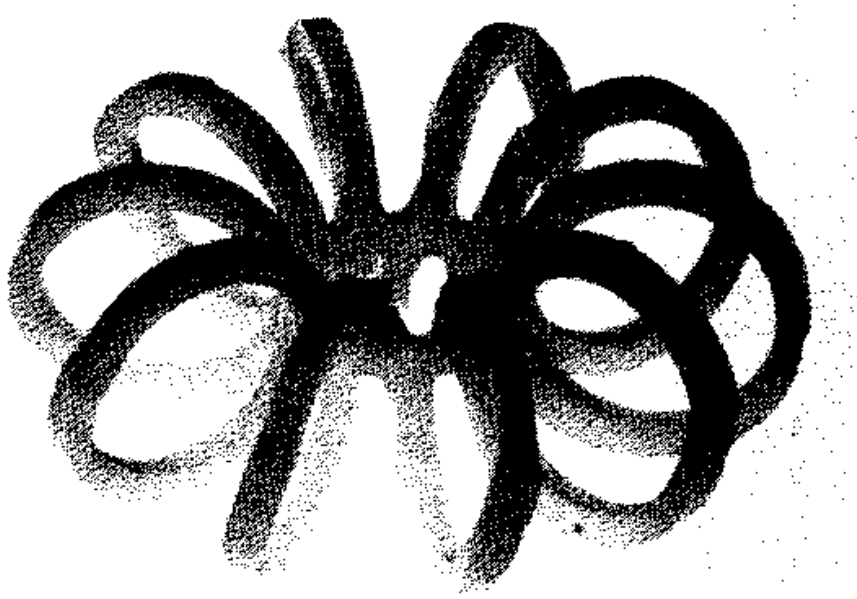

(c)

(d)

Figure 8.6 (*Continued*) Miscellaneous random packings. (c) Tellerette® packing; (*d*) Maspac® packing (*Parts c and d from* "Random Packings and Packed Towers—Design and Application," *by Ralph F. Strigle, Jr., Copyright © 1987 by Gulf Publishing Company, Houston, Texas. Used with permission. All rights reserved.*)

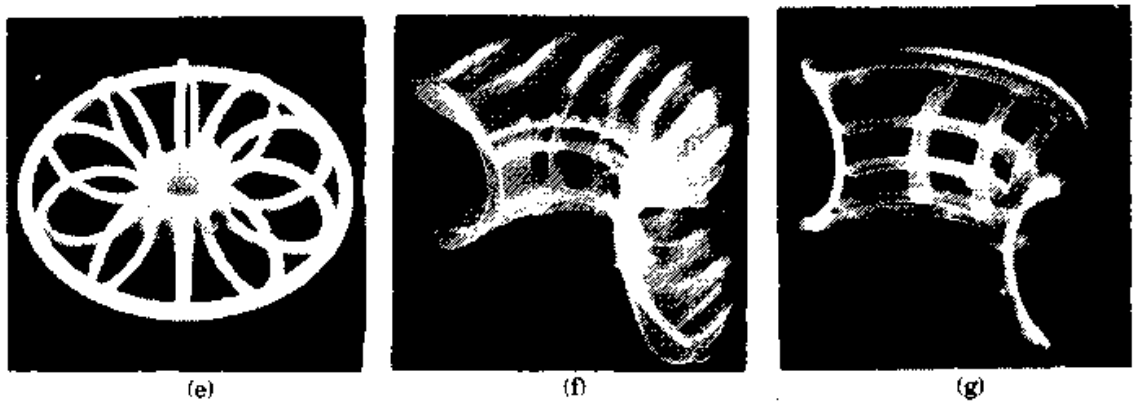

(e) (f) (g)

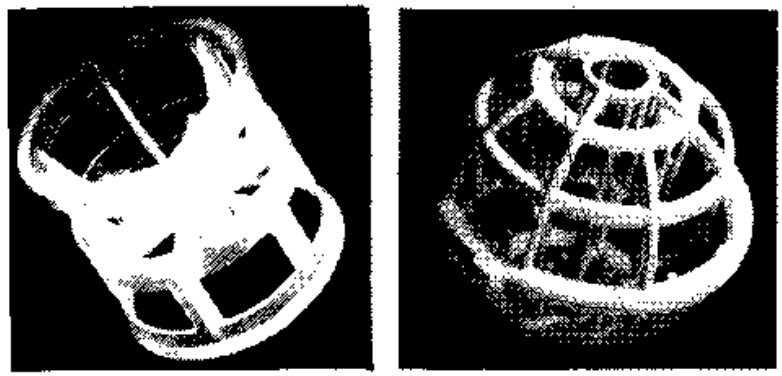

(h) (i)

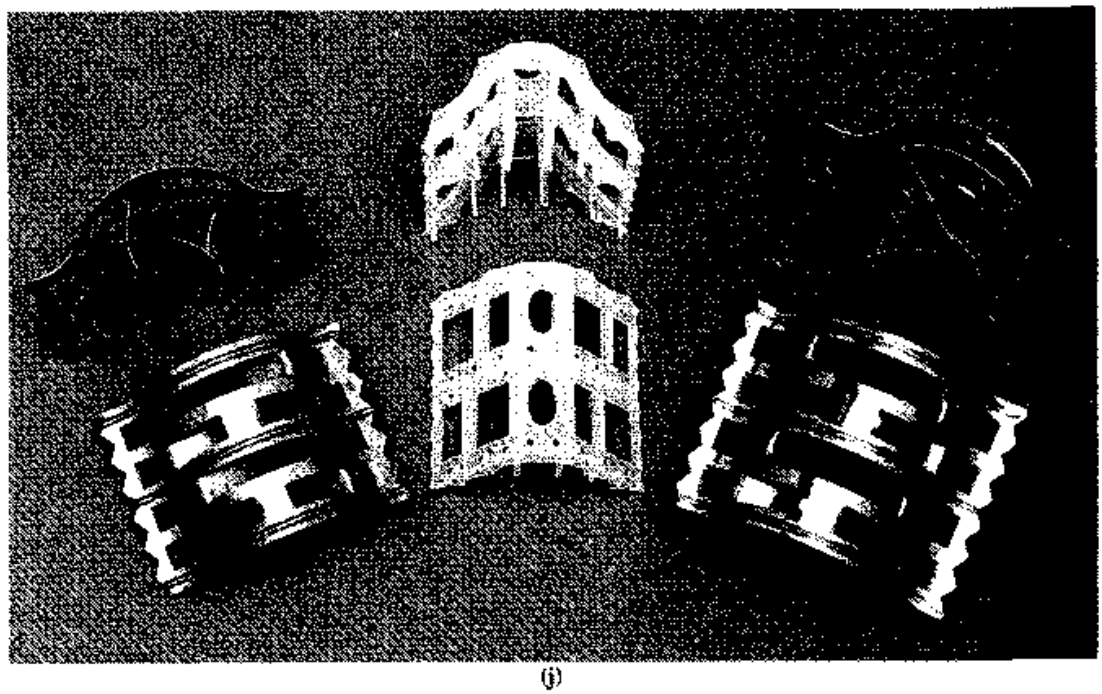

(j)

Figure 8.6 *(Continued)* Miscellaneous random packings. (*e*) Dinpak®; (*f*) SuperTorus® Saddle; (*g*) Hiflow® Saddle; (*h*) Ralu® Ring; (*i*) ENVIPAC®; (*j*) Super Levapak (S-LVK®). *(Parts f, g and h from R. Billet,* Packed Column Analysis and Design, *Ruhr University, Bochum, 1989. Reprinted courtesy of Ruhr University; parts e and i, courtesy of Enviro Engineering GmbH. Part j, courtesy of Chemetics International.)*

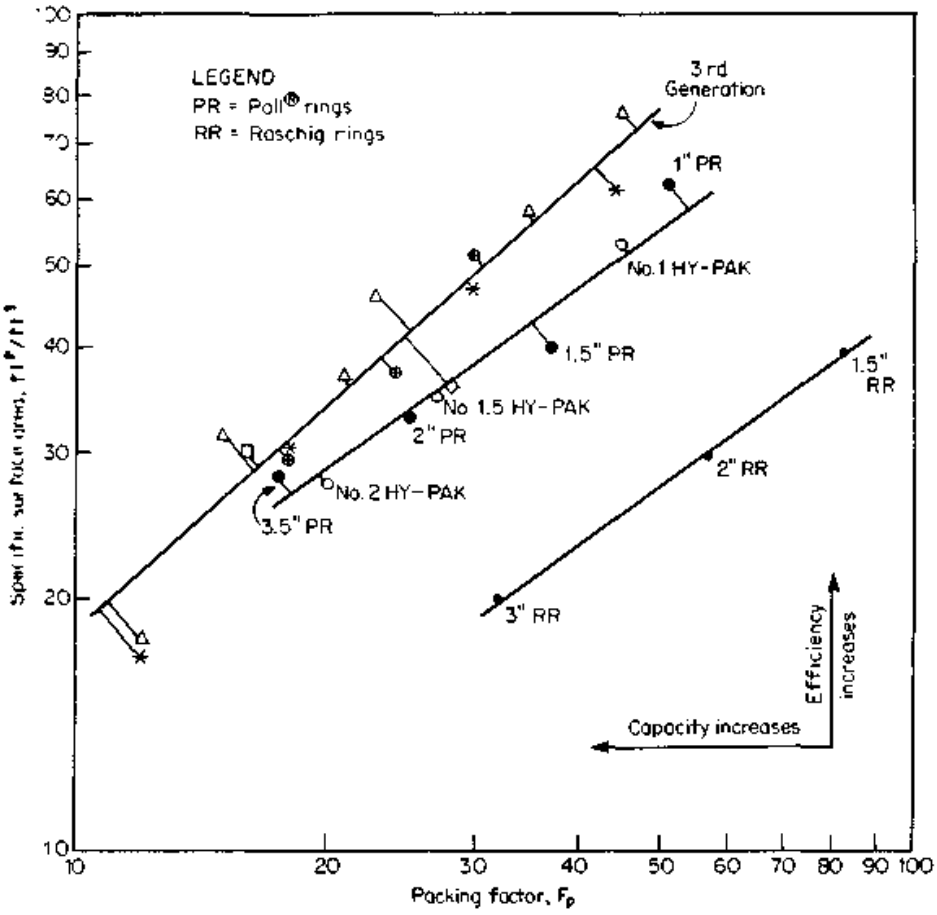

Figure 8.7 Performance comparison of the three packing generations: specific surface area versus packing factor.

those from the second to the third generation have been far less pronounced. The improvements from second to third generation appear to be more noticeable in smaller than in larger packings.

Figure 8.7 also shows that not all third-generation packings increase capacity and efficiency compared to second-generation packings. For instance, data for one third-generation packing fall right on the line for the second-generation packings. There is some uncertainty, as data reported for some third-generation packings are based on limited tests.

8.1.5 Packing material—random packings

Packing material selection is primarily based on the corrosion resistance. The factors below are also important. Reference 16 has an excellent detailed discussion.

Metals. Carbon steel packings are usually the first choice for noncorrosive services. Compared to ceramic and plastic, they normally

offer higher capacity and efficiency, a wider range of geometries, higher turndown, are unbreakable, and have a high compression resistance. Stainless steel packings cost roughly three to five times more than carbon steel (16,17); alloys are even more expensive. Generally, stainless steel and other metal packings share the same advantages as carbon steel except for the low cost. They are used in corrosive services.

Ceramics. Ceramic packings have declined in popularity ever since low-cost plastic packings became available. Compared to plastic, ceramic packings are breakable, have lower capacity, and are unavailable in many of the popular geometries. Ceramic packings are currently specified only in applications where their high chemical inertness and resistance to high temperature gives them the edge (e.g., in sulfuric acid absorption). However, despite their reputation of high chemical inertness, some grades of ceramic may chemically degrade. Case histories of ceramic packing degradation under boiling potassium carbonate solution conditions have been reported (18). A very rapid chemical degradation of ceramics takes place in the presence of hydrofluoric acid.

Plastics. Polypropylene is inexpensive and is most popular when temperatures do not exceed 250°F. Caution is required where hot spots are likely, e.g., due to heat of solution. Other plastics may be better for higher temperatures, but these tend to be more expensive. Generally, plastic Pall® rings are stiffer and resist softening more than other shapes because of their internal "arms."

Some grades of polypropylene tend to promote foaming in alkaline services (16,18). The foaming is caused by leached-off additives of the plastics; the nature of these vary with the supplier and even from batch to batch. Plastic packings tend to degrade in oxidizing atmospheres and when solvents are used, and are best avoided in such application. Plastic also degrades in ultraviolet light and becomes brittle at subfreezing temperatures; careful handling, storage, and transportation may be required. Plastic also tends to become brittle upon aging.

A disadvantage of plastic packings is their poor wettability. While the hydrophilic nature of ceramic, and to a lesser degree metal, promotes the formation of thin liquid film on the packing surfaces even at low liquid rates, the hydrophobic effect of plastic makes such a liquid film more difficult to form. Poor wettability can be particularly troublesome in the initial ("aging") period of operation (3); it may take several days to reach normal efficiency. The ease of handling of plastic packings is an advantage during startup and shutdown. Unpacking

techniques such as "sucking and blowing" can easily be used at shutdown. Repacking is easier and faster.

8.1.6 Structured packing evolution

Structured packings have been around since as early as the 1940s. Early structured packings, such as Panapak (15), never became popular. Perhaps these were not marketed aggressively enough, or perhaps they appeared before the detrimental effect of liquid maldistribution on structured packing was appreciated. First-generation structured packings are seldom used nowadays.

The second generation of structured packings began in the late 1950s with high-efficiency wire-mesh packings such as Goodloe®, Hyperfil®, and the Koch-Sulzer® (wire-mesh) packings. Extensive experimentation led by Sulzer provided insight into maldistribution, and the knowledge gained was applied for successful scaleup. By the early 1970s, these packings have made substantial inroads into vacuum distillation, where their low pressure drop per theoretical stage is a major advantage. In these services, they are extensively used today. Their high cost, high sensitivity to solids, and low capacity hindered application of these wire-mesh packings outside vacuum distillation.

The corrugated-sheet packing, first introduced by Sulzer in the late 1970s, started a third generation of structured packings. With a high capacity, lower cost, and lower sensitivity to solids, while still retaining a high efficiency, these corrugated sheet packings became competitive with conventional internals, especially for revamps. The 1980s saw an accelerated rise in popularity of structured packings, to the point of their becoming one of the most popular column internals in use today.

8.1.7 Types of Wire-Mesh Structured Packing

Sulzer® Wire Gauze Packing. This is a fabric (Fig. 8.8*a* and *b*) woven from fine-diameter wire. The packing elements consist of parallel, perforated, corrugated sheets of wire mesh. The corrugations are inclined with respect to the tower axis, and the direction of the corrugations is reversed on adjacent strips. Packing sections, which are about 7 in tall, are stacked in the shell to the required height. Adjacent sections are rotated by 90°. Three types of Sulzer® Wire Gauze packing are available: AX, BX, and CY. The BX type (Fig. 8.8*a*), by far the most common KS packing, has a mesh surface area of 150 ft^2/ft^3, a 0.35-in crimp side length, and a 60° angle of orientation to the horizontal. The CY type (Fig. 8.8*b*) has a mesh surface area of 200 ft^2/ft^3, a 0.25-in crimp side length, and a 45° angle of orientation to the horizontal (19).

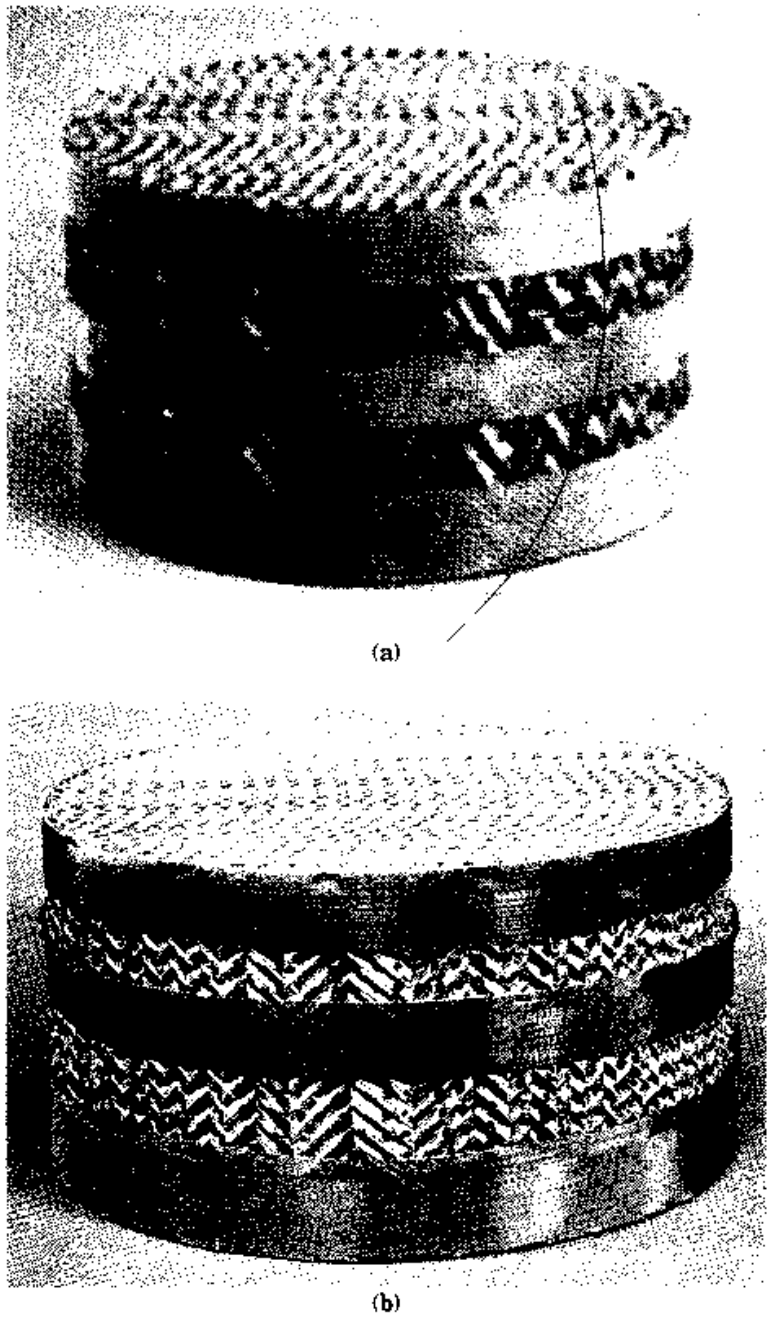

Figure 8.8 Wire-mesh structured packings. (*a*) Sulzer® wire gauze packing BX; (*b*) Sulzer® wire gauze packing CY. (*Parts a and b, courtesy of Sulzer Chemtech.*)

The Sulzer® Wire Gauze packing is available most commonly in 316 stainless steel, but also in other corrosion-resistant metals. A similar wire mesh is available in ceramics and plastics. The packing is marketed in the United States by Koch Engineering Company, Inc., and worldwide by Sulzer Chemtech. Packings that are often considered equivalent to the Sulzer® Wire Gauze BX packing are marketed by Glitsch Inc. under the trade name Gempak® 4BG, by the Norton Com-

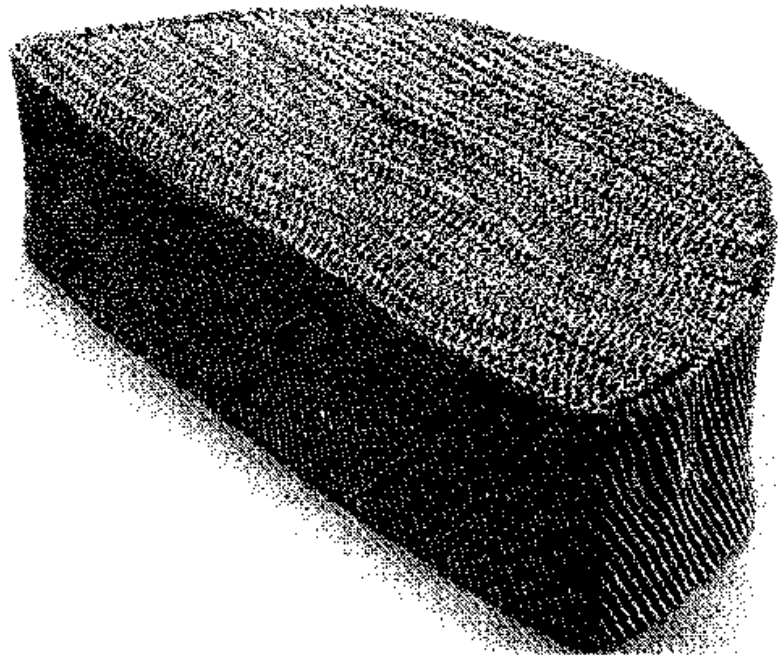

(c)

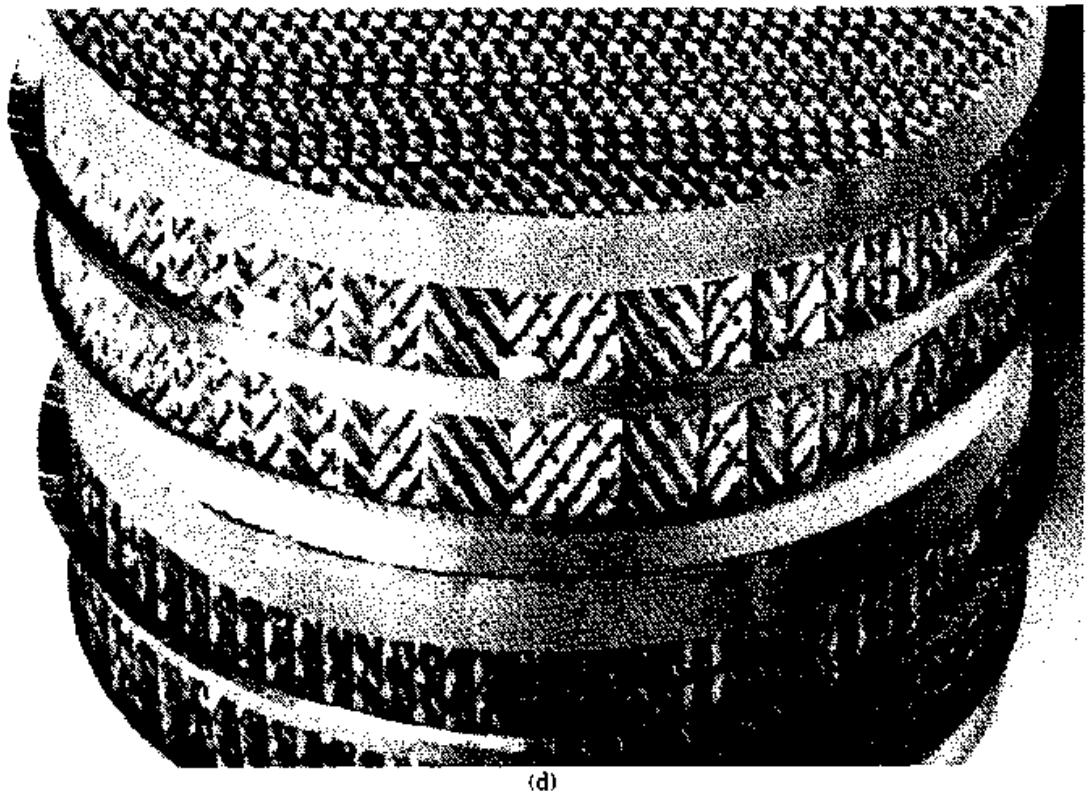

(d)

Figure 8.8 *(Continued)* Wire-mesh structured packings. (c) Goodloe®; (d) Montz A3-500®. (*Part c, courtesy of Glitsch, Inc.; part d, courtesy of Nutter Engineering Corp.*)

pany under the trade name Intalox® High-Performance Wire Gauze Packing, and by ACS under the title ST-100.

Goodloe® (Fig. 8.8*c*). This is a fabric made of a multifilament of fine-diameter wires. The wires are knitted together to form a tube, which is flattened into a ribbon, crimped, and plied. Two ribbons (one turned over so that their crimps cross each other) are then rolled together to form a cylindrical cartridge having enough layers to fit the column snugly. With larger column diameters, layering in segments is used instead of rolling. Goodloe® has a specific surface area of about 585 ft^2/ft^3 but variations of up to 1000 ft^2/ft^3 are also available (20). Goodloe® is available most commonly in 316 stainless steel, but also in carbon steel, aluminum, alloys, plastic, Kynar, and Teflon. Goodloe® is available from Glitsch Inc. and from ACS.

Hyperfil®. Like Goodloe®, Hyperfil® is a fabric made of a multifilament of fine-diameter wire. The wires knitted to form a tube, which is flattened into a ribbon, crimped, and plied. Unlike Goodloe®, a cartridge or a segment of a cartridge is then formed by folding the ribbon in parallel vertical layers, rather than rolling it into a spiral. The specific surface area of Hyperfil® is comparable to Goodloe®. Hyperfil® is available in stainless steel, copper, and corrosion-resistant alloys from ACS.

Montz A3™ (Fig. 8.8*d*). This packing is made of perforated wire mesh sheets, similar to the Sulzer® Wire Gauze Packing. The wire mesh sheets, however, are corrugated in a special contoured pattern and are arranged vertically. Adjacent sections are rotated at 90°. The Montz A3™ supersedes earlier products, Montz A2™ and Montz A1™. The surface area per unit volume of Montz A3™ is 150 ft^2/ft^3, the same as that of the Sulzer® Wire Gauze BX packing. Montz A3™ is available in stainless steel and other corrosion-resistant alloys from Nutter Engineering Corporation.

8.1.8 Geometrical features of corrugated structured packings

Corrugated structured packings are fabricated from thin, corrugated (crimped) metal sheets, arranged in parallel to each other. The surface of the corrugated sheets can be grooved, lanced, textured, or smooth. The corrugated sheets may be perforated or unperforated. The corrugated sheets are assembled into an element, typically 8 to 12 in tall. The sheets in each element are arranged at a fixed angle to the vertical. Adjacent elements are rotated so that sheets of one element are

at a fixed angle to the layer below. Table 8.1 contains geometrical data for several corrugated packings.

Crimp geometry (Fig. 8.9). The crimp size defines the opening between adjacent corrugated layers. The smaller B, h, and S are, the narrower the openings, the more sheets (and therefore, more surface area) per unit volume, and the more efficient the packing. On the other hand, narrowing of the interlayer openings reduces void space and raises resistance to gas upflow, leading to a lower capacity and to enhanced sensitivity to plugging and fouling.

The relative ratio of B to h, S to h, and the crimp angle (angle between side S and base B) define the geometry of the flow channel and of the vapor-liquid contact zone. This geometry stays relatively uniform within a single packing family, but varies from one packing family to another. Crimp angles vary from 28 to 45° and base-to-height (B-to-h) ratios range from 2:1 to 4:1. In some packings, the sides of the triangle shown on Fig. 8.9 are rounded, giving a round top apex. Rounding of the triangle apex reduces friction and prevents concentration of liquid at the corners (27).

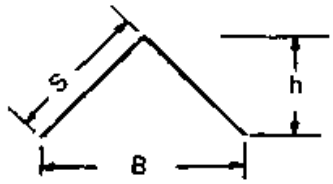

(a) Flow channel cross section

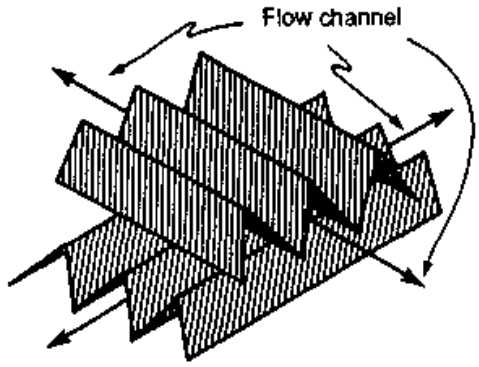

(b) Flow channel arrangement

Figure 8.9 Crimp geometry in structured packings. (*a*) Flow channel cross section; (*b*) flow channel arrangement. (*From J. R. Fair and J. L. Bravo, Chem. Eng. Progr., January 1990, p. 19, reproduced courtesy of the American Institute of Chemical Engineers.*)

TABLE 8.1 Geometric Characteristics of Common Metal Corrugated-Sheet Structured Packings

	Crimp geometry				Element geometry		
Packing	Angle deg	Height h, in	Base length B, in	Side length S, in	Height, in	Rotation angle, deg	Angle to tower axis, θ, deg
Mellapak®							
125Y	45					90	45
250Y	↓	0.47	0.95	0.67	8.27	↓	45
350Y							45
500Y							45
Flexipac® (Y-type)							
#1	45					90	45
#2	↓	0.49	1.02	0.71	10.5	↓	45
#3							45
#4							
Gempak®							
#1A	45	1.0	2.00	1.44		90	45
#1.5A	↓	0.71	1.41	1.03		↓	45
#2A		0.49	1.05	0.71	9.75		45
#2AT		0.45	1.07	0.70	9.75		45
#3A		0.37	0.75	0.53			45
#4A		0.24	0.43	0.36			45
Intalox®							
1T	28*						45
2T	↓	0.41	1.53	0.88	11.0		45
3T							45
Montz®							
B1-100	37*				8	90	45
B1-200	↓	0.59	1.57	0.98	↓	↓	45
B1-250							45
B1-300							45
MAX-PAK®	45	0.625	1.13	0.84	12	90	45
Sulzer BX® (Gauze)	45	0.25	0.5	0.35	7	90	60

*Rounded.

Element geometry. Due to the corrugations, vapor and liquid flow through a single element spreads in a series of parallel planes. In order to spread the vapor and liquid uniformly in all radial planes, each element is rotated at a certain angle with respect to the element below. The angle of rotation is the angle (in a "horizontal" plane) between the parallel layers in one element and between the parallel layers in an element above (or below).

The angle of rotation and the element height therefore affect the extent of vapor and liquid spread in a structured packing. For this reason, element height is relatively short (typically 8 to 12 in) and the angle of rotation is around 90°.

In each element, corrugated sheets are usually inclined at about 45°

TABLE 8.1 Geometric Characteristics of Common Metal Corrugated-Sheet Structured Packings (*Continued*)

Surface features		Specific surface area, ft^2/ft^3 typical	ϵ Void fraction (25,93)	Source of information (ref. no.)	Constants for the Bravo et al. pressure drop correlation (91)			
							Data range	
Surface finish	Perforation size, in				d_{eq}, in	C_5	GPM/ft^2	C_S†
Grooved		38		21				
↓		76	0.95	21,24,25				
		107		21				
↓		152		21				
Grooved			0.91		0.353	3.38	0–70	0.05–0.3
↓	5/32	68	0.93	23,25	0.707	3.08	0–70	0.1–0.6
↓			0.96		1.414	4.50	0–70	0.12–0.6
↓			0.98		2.828	7.26	0–80	0.14–0.6
Lanced		35	0.96	22	1.414	4.50	0–70	0.07–0.5
↓		49		22				
	5/32	67	0.93	22,23,25	0.707	3.08	0–70	0.06–0.45
Smooth	5/64	68		23				
Lanced		91	0.92	22	0.530	3.87	0–70	0.05–0.45
↓		138	0.91	22	0.353	3.38	0–60	0.05–0.35
Deep Embossed		67	0.97	24,25				
↓								
Shallow Embossed	None	30						
	↓	61	0.94	25,27				
		76						
↓	↓	91						
Smooth	W Shape	77	0.975	26,26a		3.0		
Gauze		150	0.90	124	0.353	3.38	0.3–5	0.03–0.33

†Defined by Eq. (8.23).

to the vertical. This angle is large enough for good drainage of liquid, avoiding stagnant pockets and regions of liquid accumulation, and small enough to prevent gas from bypassing the metal surfaces.

Surface features. The surfaces of a few structured packings are smooth (e.g., Fig. 8.10*a,g*). Most structured packings have a roughened or enhanced surface that assists the lateral spread of liquid, promotes film turbulence, and enhances the area available for mass transfer. Laboratory measurements of absorption rates showed that both mass transfer efficiency and wetted area are enhanced by texturing metal surfaces (28). The extent to which mass transfer was improved varied with the type of texturing used. Texturing employed by

common structured packings includes grooving, lancing, shallow embossing, and deep embossing (Fig. 8.10*b* to *e*). One structured packing is fabricated from expanded metal (Fig. 8.10*f*).

The surfaces of most structured packings contain perforations (an exception is Fig. 8.10*d*). The holes serve as communication channels between the upper and lower surface of each sheet. If the holes are too small, or nonexistent, both sides of a sheet will be wet only at low liquid rates. At high liquid rates, "sheeting" or "blanking" will cause liquid to run down the top surface with little liquid wetting the bottom surface (23). This may cause a reduction in efficiency as liquid flow rates are raised. A counterargument by suppliers of packings that contain no holes is that the holes impede the spread of liquid across a sheet, thus adversely affecting the surface action (27). Usually, the holes are of circular shape (Fig. 8.10*a* to *f*), but one design (Fig. 8.10*g*) employs slits in the shape of a W, with the tabs formed by the cuts bent to direct liquid to the opposite side of the sheet.

8.1.9 Types of corrugated structured packings

Mellapak® (Fig. 8.11*a*). Mellapak® has grooved and perforated surfaces. Adjacent elements are rotated 90°. The crimp angle is 45°, and the crimp apex is sharp. Mellapak® is available in several types. The Mellapak® number denotes the nominal surface area of the packing per unit volume (m^2/m^3). The suffix denotes the angle of orientation to the vertical axis; Y signifies 45°, X signifies 60°. For instance, Mellapak® 250.Y has a surface area of 250 m^2/m^3, and a 45° angle of orientation to the vertical axis. Mellapak® is available in metals and plastics from Sulzer Chemtech in Switzerland.

Flexipac® (Fig. 8.11*b*). Flexipac® is similar to Mellapak®, but not identical to it. The common Flexipac® types are Flexipac® 1 (similar to Mellapak® 500.Y), Flexipac® 2 (similar to Mellapak® 250.Y), Flexipac® 3 (similar to Mellapak® 125.Y), and Flexipac® 4. Flexipac® is marketed in the United States by Koch Engineering under a license from Sulzer. It is available in metals.

Gempak® (Fig. 8.11*c*). Gempak® has lanced and perforated surfaces. The crimp angle is 45° and the crimp apex is sharp. Gempak® is available in several types. The number denotes the inverse of the crimp height. For instance, Gempak® 4A has ¼-inch crimp height. The suffix A denotes that the packing is a standard Gempak® type with the lanced surface. A variant of Gempak® with a smooth rather than the

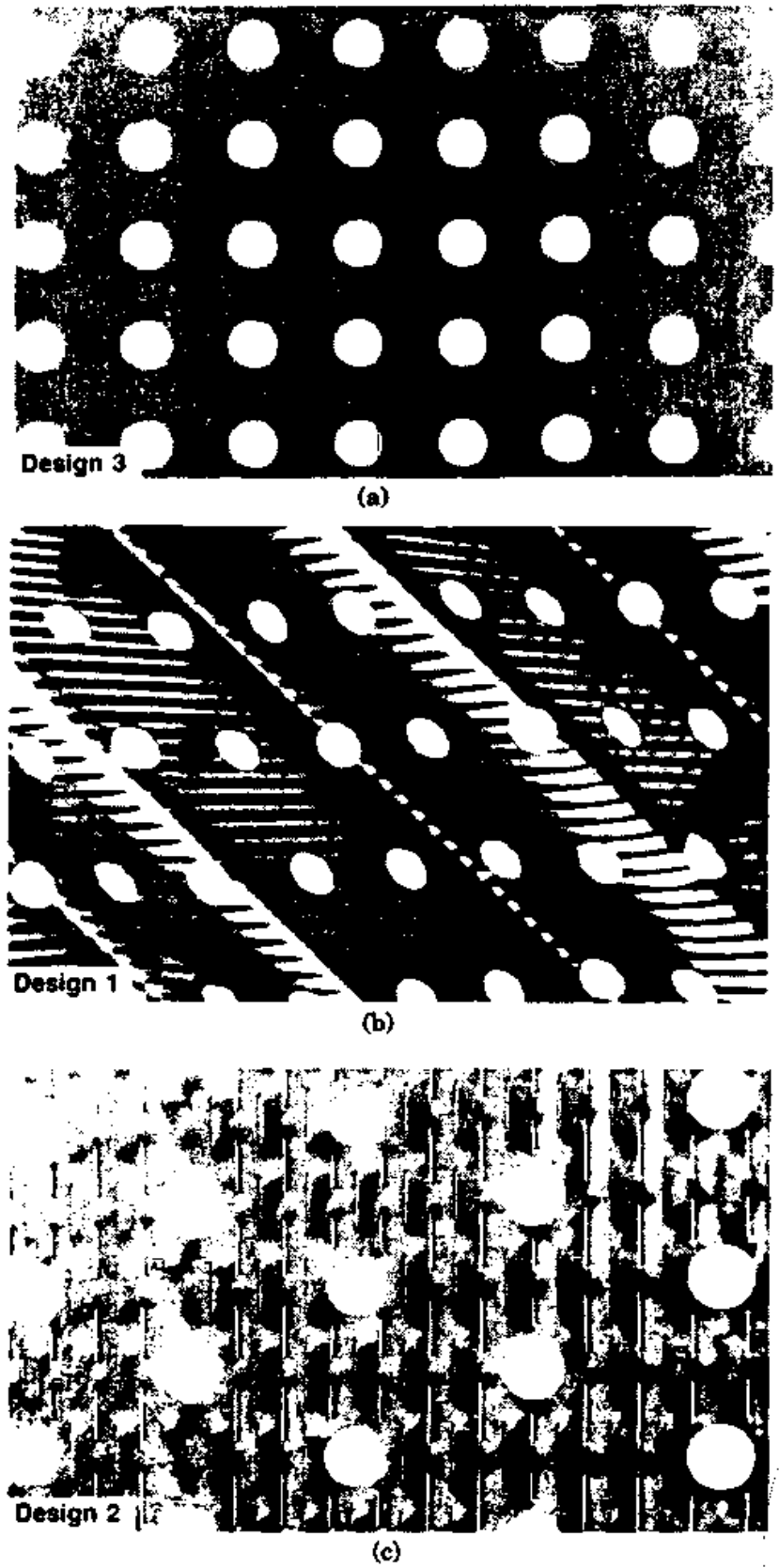

Figure 8.10 Surfaces used in commercial corrugated structured packings. (*a*) Smooth, perforated; (*b*) grooved, perforated; (*c*) lanced, perforated. (*Parts a to c, from G. K. Chen and K. T. Chuang, Hydrocarbon. Proc., February, 1989, p. 37, reproduced courtesy of Hydrocarbon Processing.*)

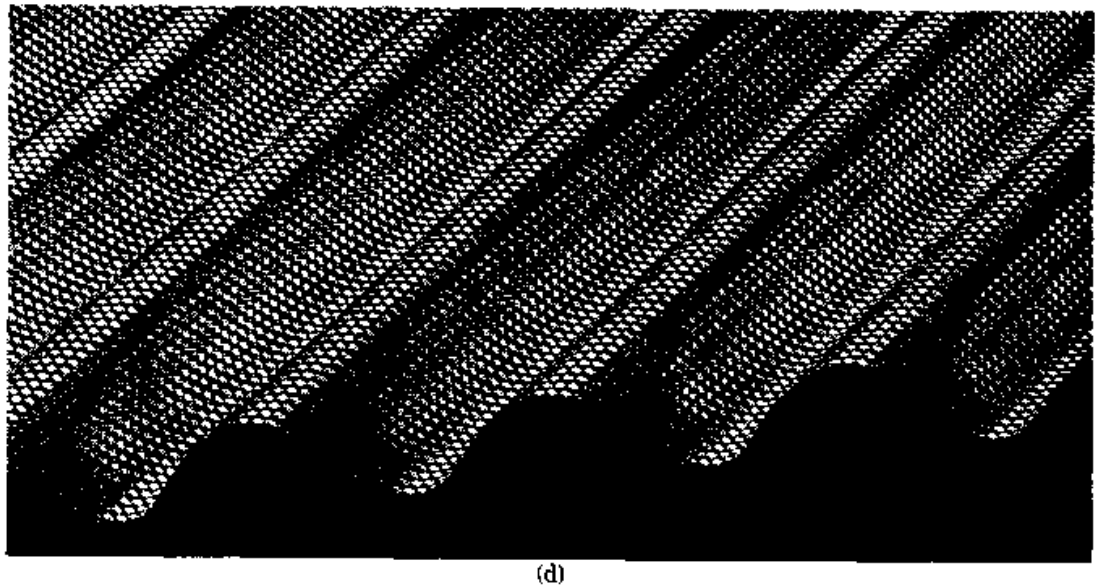

(d)

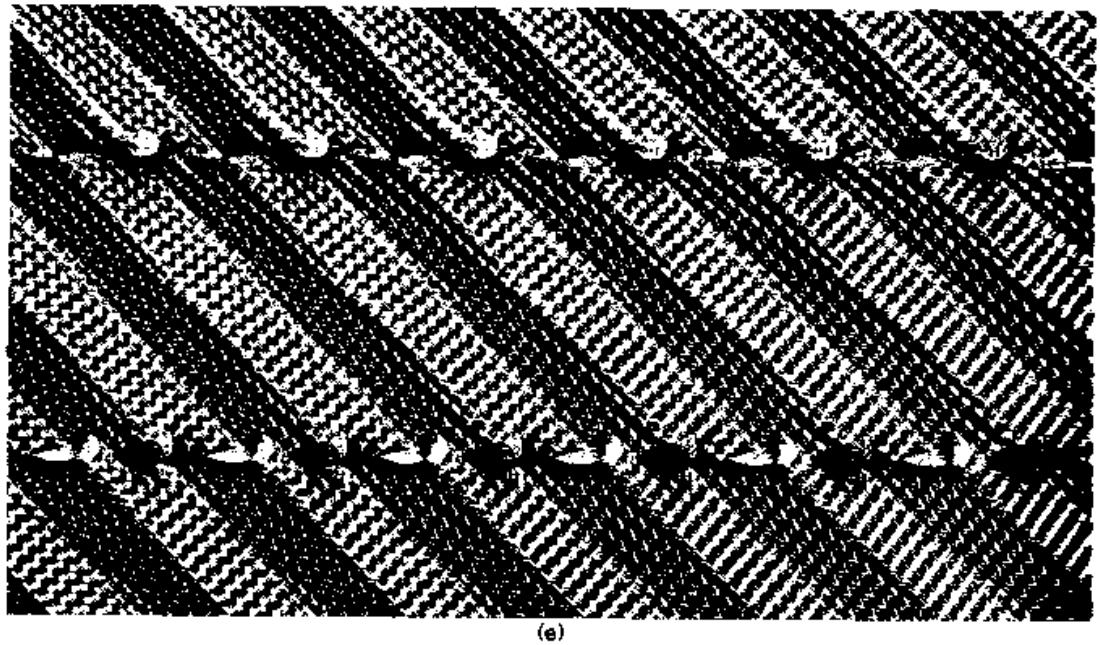

(e)

Figure 8.10 (*Continued*) Surfaces used in commercial corrugated structured packings. (*d*) Shallow embossed, unperforated; (*e*) deep embossed perforated. (*Part d, courtesy of Nutter Engineering; part e, courtesy of Norton Company.*)

lanced surface is also available, and is denoted by the suffix T after the A; for instance, Gempak® 2AT denotes a packing similar to Gempak® 2A but with a smooth surface. Another type, Gempak® 4BG is a wire-mesh packing similar to the Sulzer® Wire Gauze BX packing (Sec. 8.1.7). Gempak® is available in metals and plastics from Glitsch Inc.

Montz B1® (Fig. 8.11*d*). In contrast with Mellapak®, Flexipac®, and Gempak®, the corrugations of the Montz B1® packing are sinusoidal

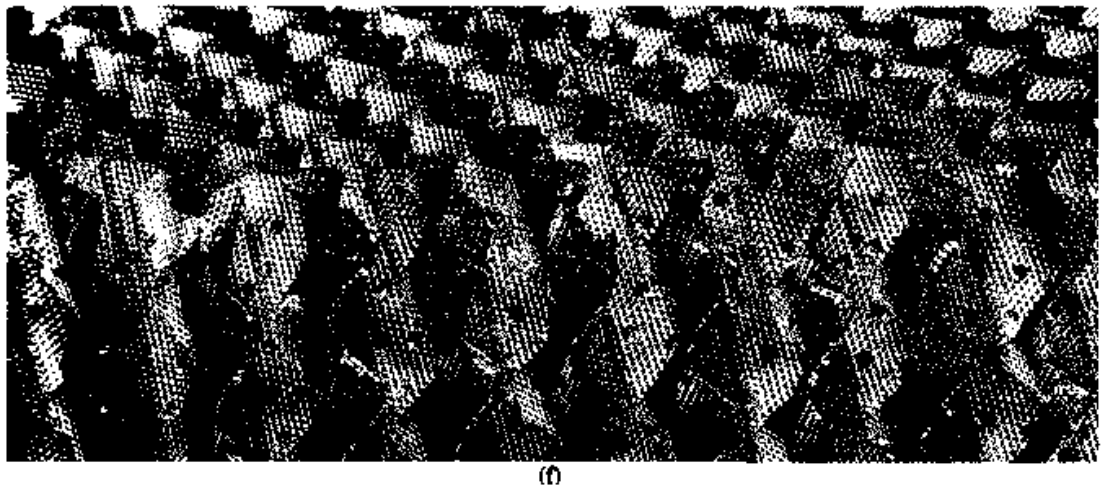

(f)

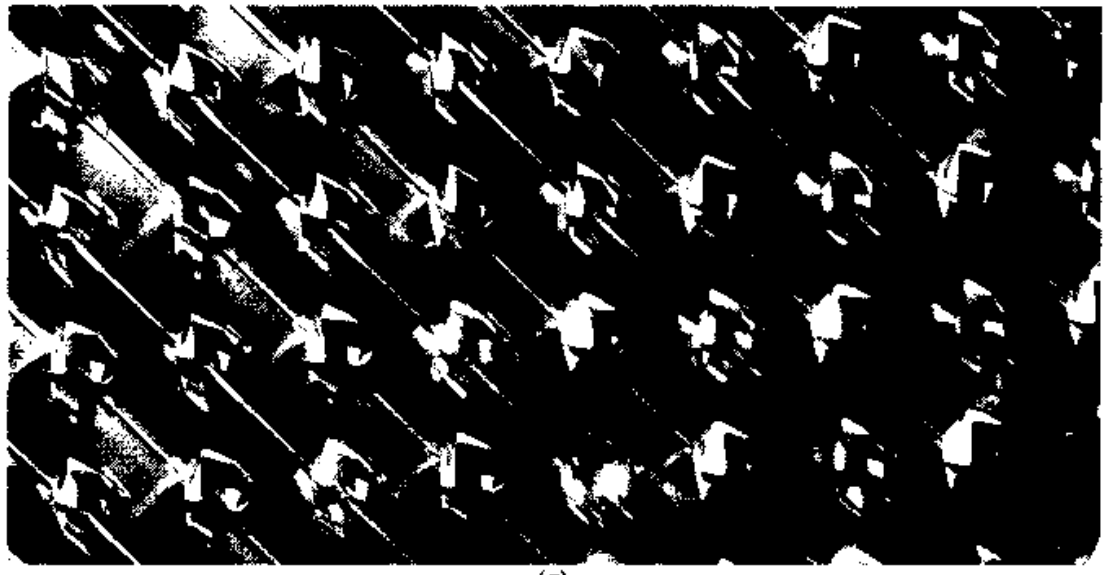

(g)

Figure 8.10 (*Continued*) Surfaces used in commercial corrugated structured packings. (*f*) Expanded metal, perforated; (*g*) smooth, with W-shape perforations. (*Part f, courtesy of Nutter Engineering; part g, courtesy of Jaeger Products, Inc.*)

rather than sharp-cornered. The surface is unperforated and embossed with small, closely spaced projections in a dot matrix pattern. The Montz B1® number indicates the nominal surface area of the packing per unit volume (m^2/m^3). For instance, Montz B1-200® has a surface area of 200 m^2/m^3. Montz B1® is available in metals from Nutter Engineering Corporation. Montz also has a C series of plastic structured packings.

Intalox® high-performance structured packing (Fig. 8.11*e*). Relatively flat crimps, somewhat rounded crimp apexes, and deeply embossed surfaces with tiny perforations distinguish Intalox® high-performance structured packing. It is available in three sizes in metals from the Norton Company.

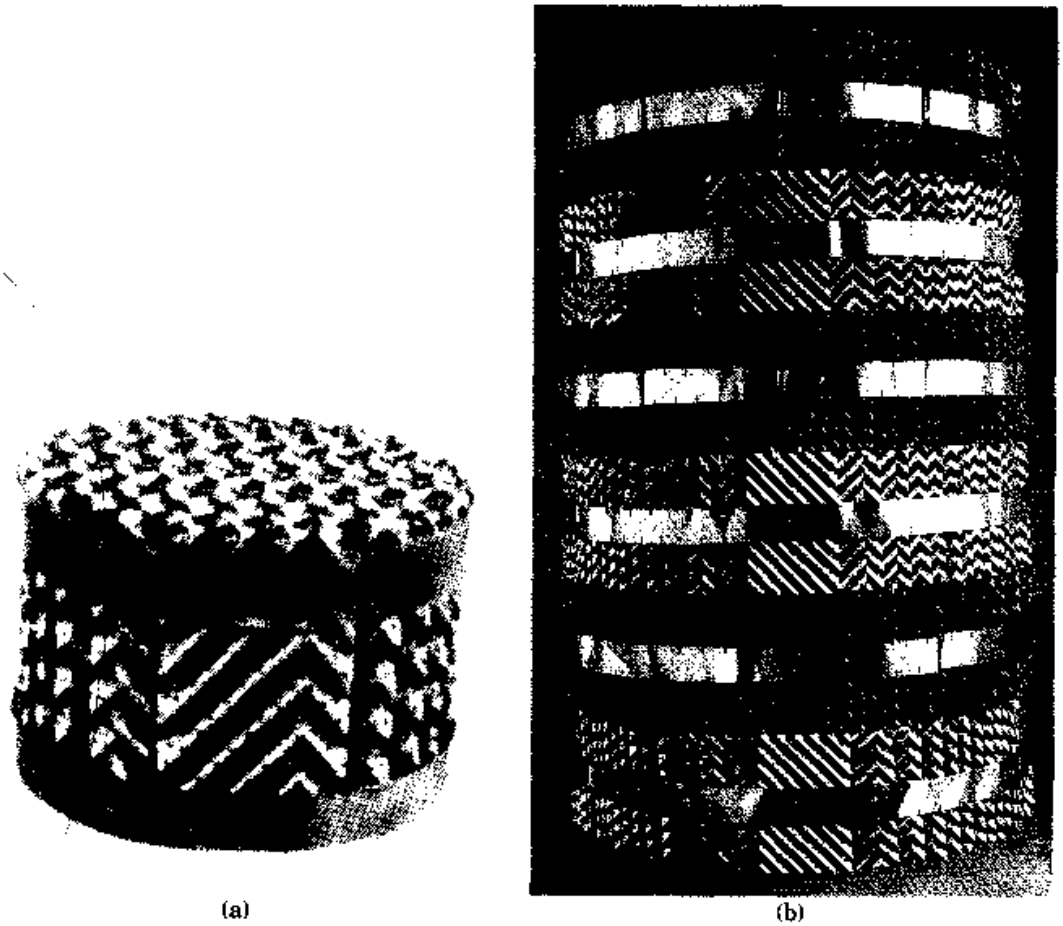

(a) (b)

Figure 8.11 Common corrugated-type structured packings. (*a*) Mellapak®; (*b*) Flexipac®. (*Part a, courtesy of Sulzer Chemtech; part b, courtesy of Koch Engineering Company, Inc.*)

MAX-PAC™ (Fig. 8.11*f*). With sharp crimp apexes and smooth surfaces, MAX-PAC™ is distinguished by surfaces that are perforated with unique W-shape perforations (Fig. 8.10*f*). MAX-PAC™ is available in metals from Jaeger Products, Inc.

Montz BSH (Fig. 8.10*f*). With sharp apexes and perforated surfaces, Montz BSH® is distinguished by its expanded metal surfaces. The see-through sheets permit liquid to easily move from one side of the sheet to the other. The numbering system and the supply information for the Montz BSH® series are identical to those described above for the B1 series.

Flexeramic™ (Fig. 8.11*g*). Flexeramic® has crimps with round apexes and smooth, unperforated surfaces. This ceramic packing is available from Koch Engineering Company, Inc.

Others. Other metal structured packings reported in the literature include Ralupak (3) and Rombopak (29). Plastic structured packing.

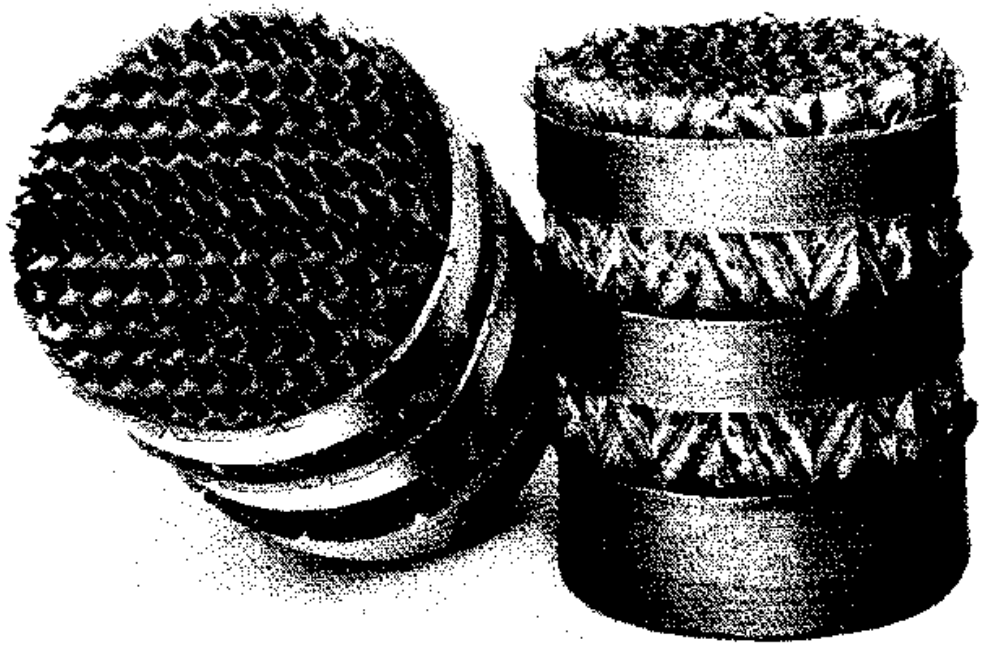

(c)

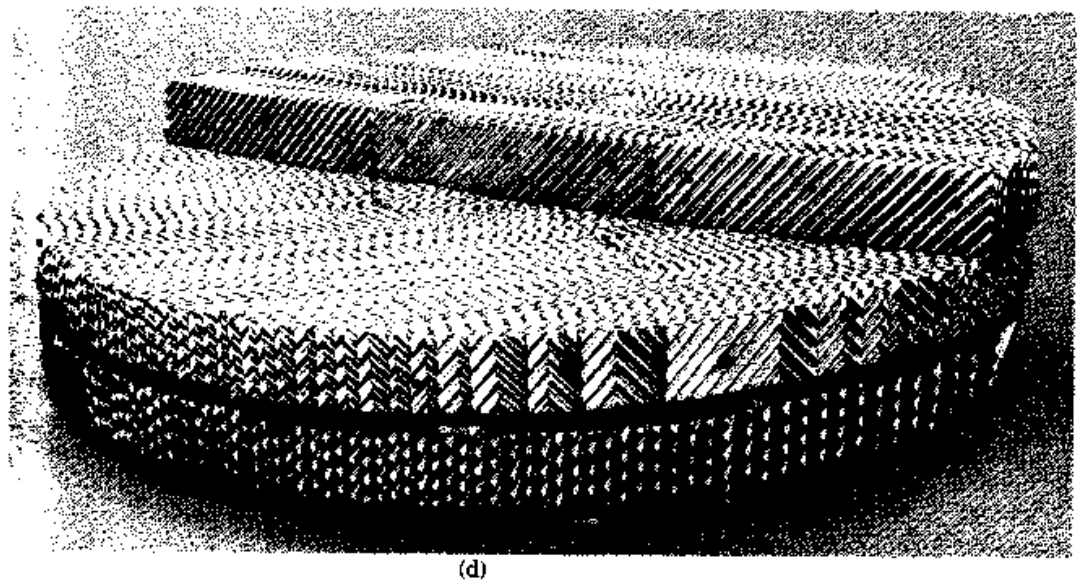

(d)

Figure 8.11 (*Continued*) Common corrugated-type structured packings. (c) Gempak®; (d) Montz B1®. (*Part c, courtesy of Glitsch, Inc.; part d, courtesy of Nutter Engineering Corp.*)

Munters and Euroform, and a ceramic structured packing, Impulse packing, have also been reported (3,41).

8.1.10 Structured packings versus random packings

Capacity and efficiency. Figure 8.12*a* compares random to corrugated sheet structured packing in terms of specific surface areas and packing factors. For random packings, the lines shown were taken from

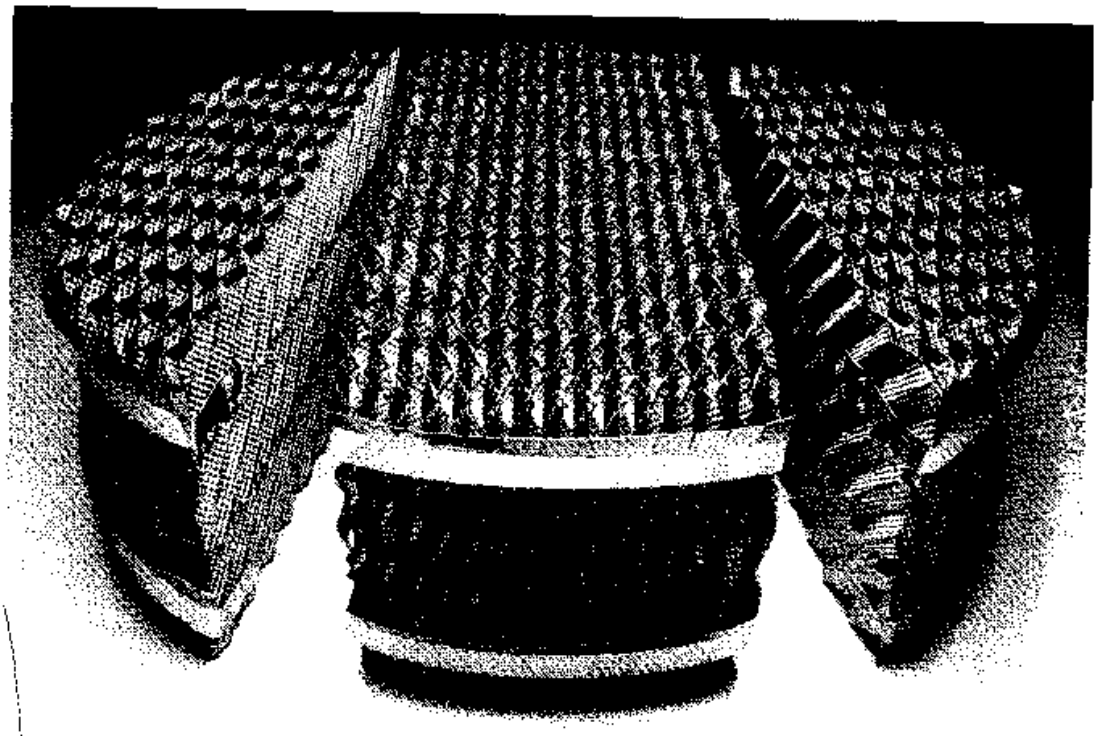

(e)

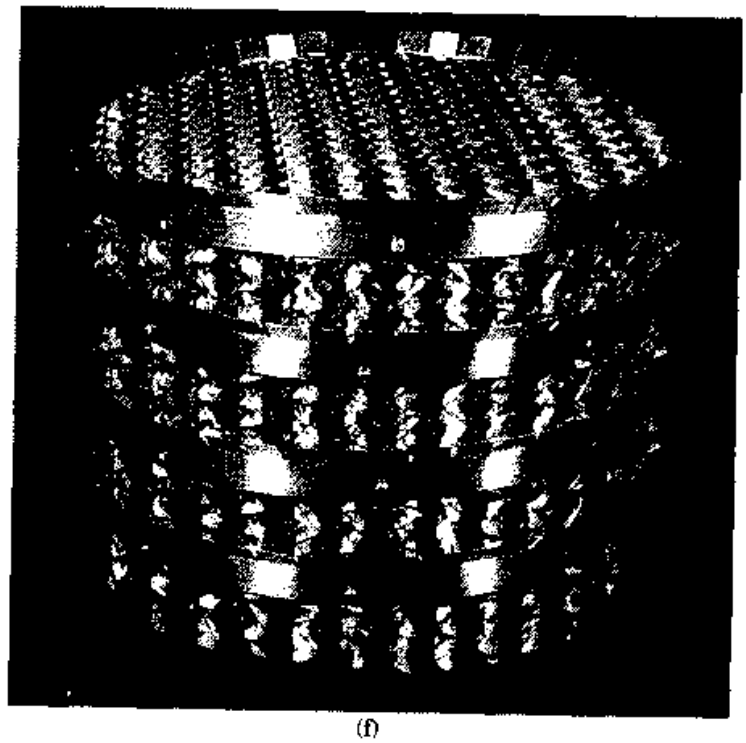

(f)

Figure 8.11 (*Continued*) Common corrugated-type structured packings. (*e*) Intalox® High-Performance structured packing; (*f*) MAX-PAC®. (*Part e, courtesy of Norton Company; part f, courtesy of Jaeger Products, Inc.*)

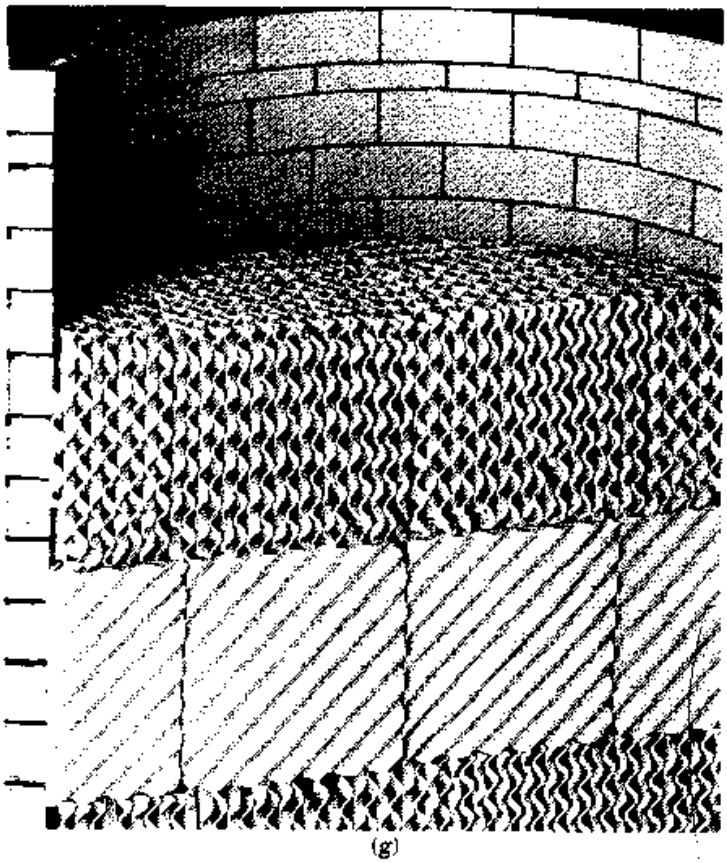

(g)

Figure 8.11 (*Continued*) Common corrugated-type structured packings. (*g*) Flexeramic®. (*Part g, courtesy of Koch Engineering Company, Inc.*)

Fig. 8.7. Specific surface areas plotted for structured packings are from Table 8.2, and the packing factors are from the manufacturers' publications (22,30,31). For structured packings, the packing factors become a function of liquid load when liquid load exceeds about 20 gpm/ft^2 (30,31). For this reason, one line (heavy) was drawn for liquid loads lower than 20 gpm/ft^2. The points for structured packings at higher liquid loads were connected by dashed lines parallel to the heavy line. Due to these approximations, Fig. 8.12*a* is unsuitable for a comparative evaluation among different structured packings.

Figure 8.12*a* shows an advantage for structured packings over random packings at low (<20 gpm/ft^2) liquid rates. At a given capacity (i.e., a constant packing factor), structured packings offer a far greater specific surface area (therefore, greater efficiency). Alternatively, for a given specific surface area, structured packings achieve a lower packing factor (therefore, greater capacity). As liquid rate increases beyond 20 gpm/ft^2, the above advantages dwindle rapidly.

Packing efficiency is not a function of the specific surface area

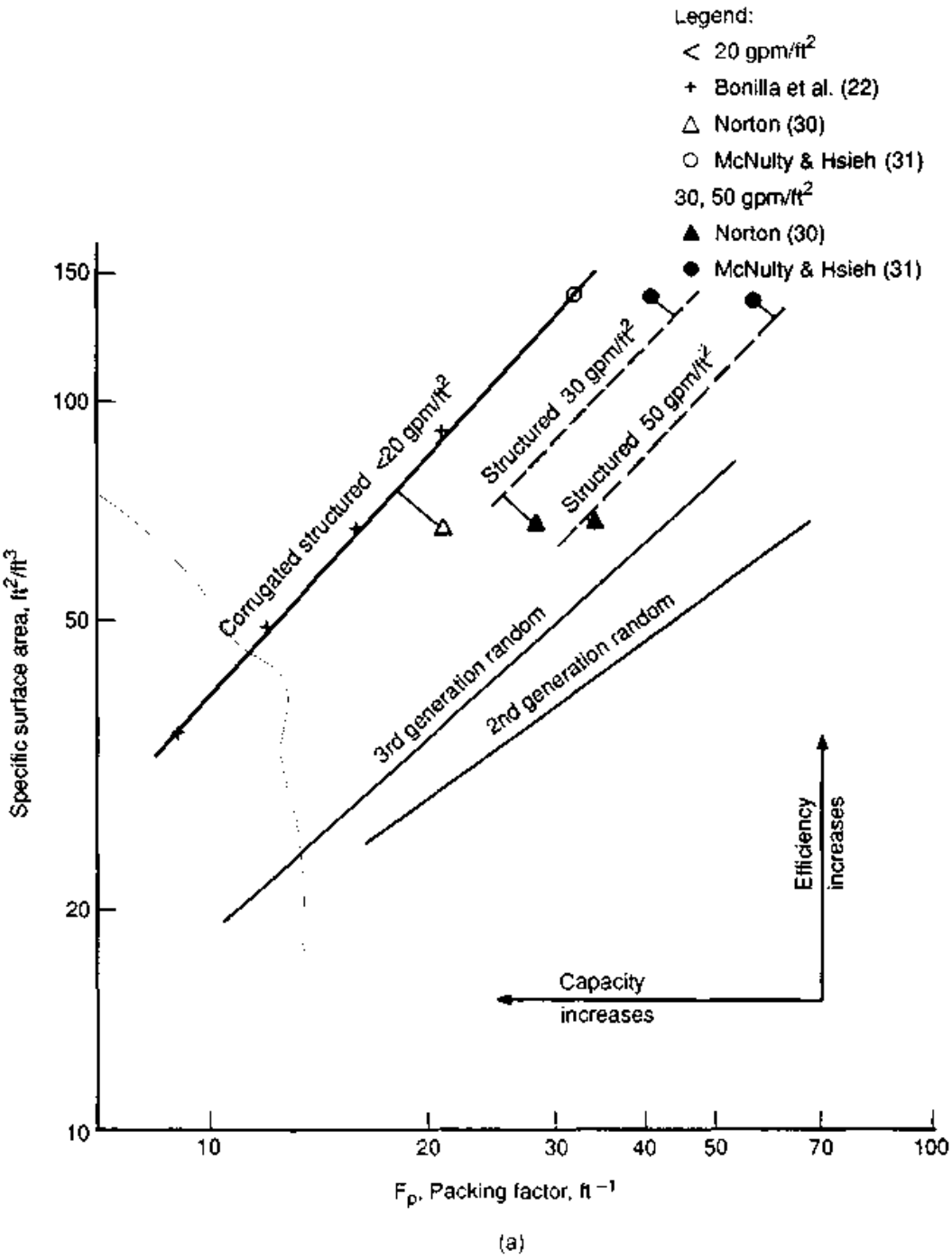

Figure 8.12 Random versus structured packings. (*a*) Specific surface area versus packing factor.

alone. Other factors (Sec. 8.1.2), such as spread of the surface area, also affect efficiency. Figure 8.12*b* suggests that at low specific surface areas (<60 ft^2/ft^3), these factors tend to favor random packings, i.e., that a second- or third-generation packing is more efficient than a structured packing of the same specific surface area. The difference in efficiency appears to widen as the specific surface area decreases. Fig-

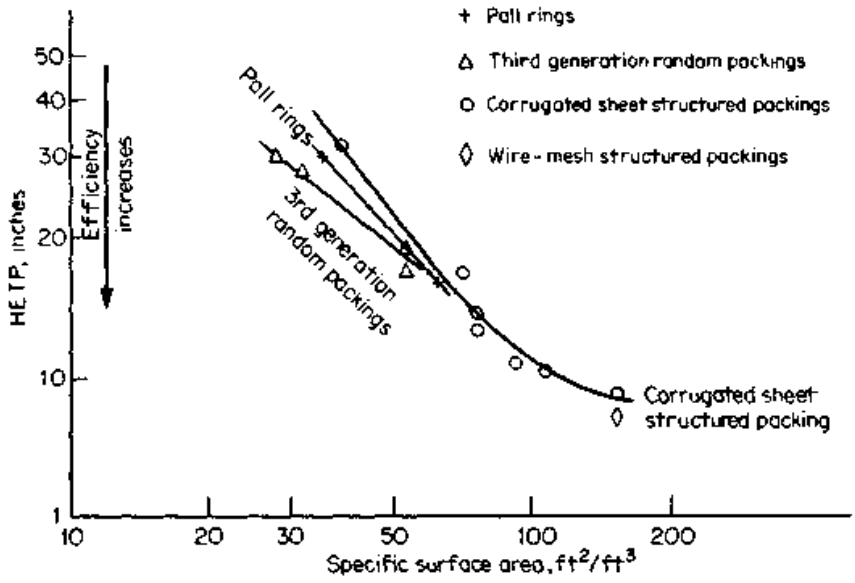

(b)

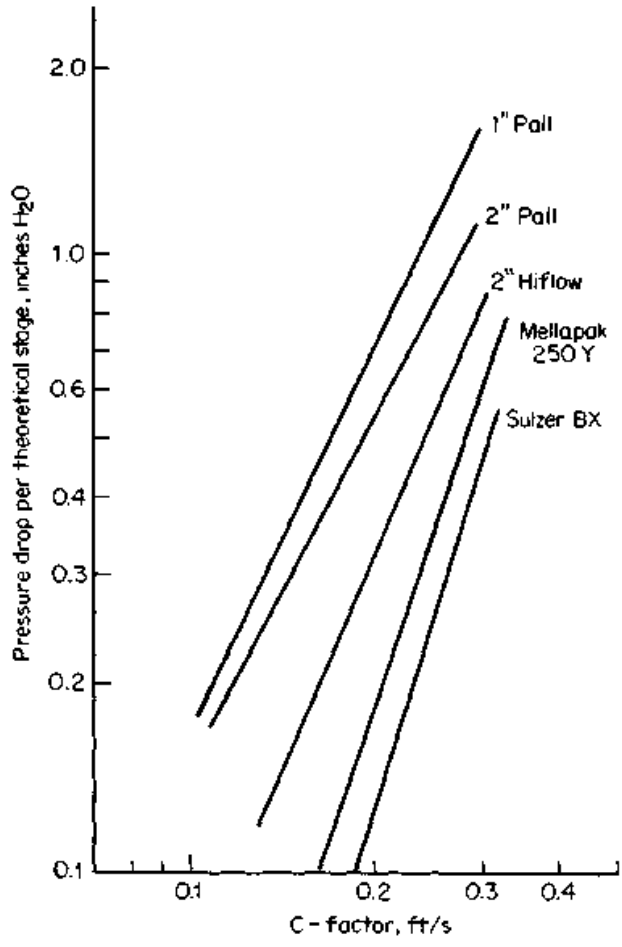

(c)

Figure 8.12 (*Continued*) Random versus structured packings. (*b*) HETP versus specific surface area, metal packings, chlorobenzene-ethylbenzene, 50 mmHg, total reflux, data by Billet (3) and Spiegel and Meier (21); (*c*) pressure drop per theoretical stage, chlorobenzene-ethylbenzene, 50 mmHg, total reflux, data by Billet (3)

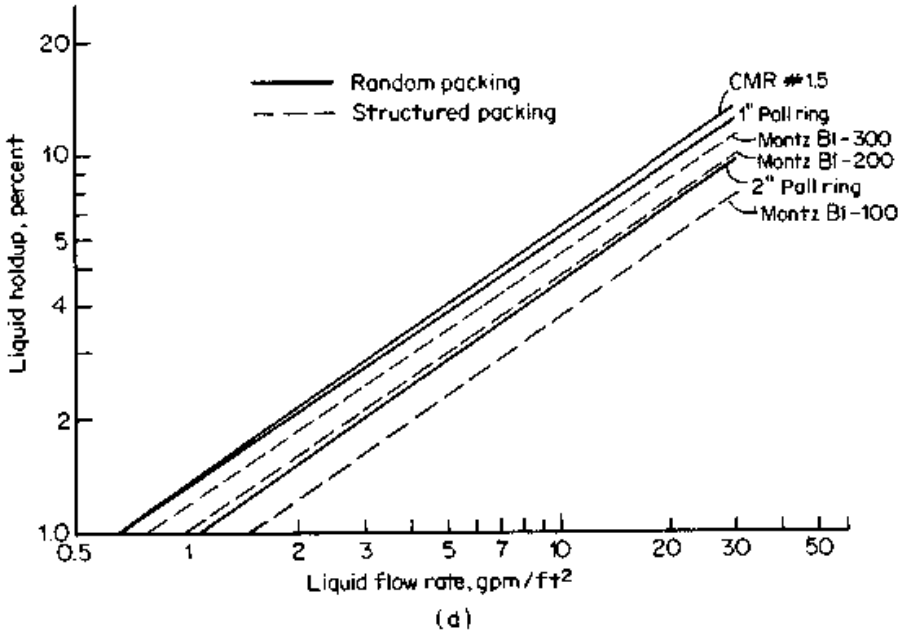

Figure 8.12 (*Continued*) Random versus structured packings. (*d*) Liquid holdup, air-water data by Billet (3), preloading regime.

ure 8.12*b* is based on test data for the chlorobenzene-ethylbenzene system at 50 mmHg (3,21).

Overall, structured packings have an efficiency and/or capacity advantage over random packings when operated at lower liquid loads (<20 gpm/ft^2). This advantage is somewhat less pronounced than one may infer from Fig. 8.12*a* alone, and is due to the nature of the resistance to vapor flow. In random packings, resistance to vapor flow is mostly due to expansion and contraction. This mechanism gives a high pressure drop. In structured packing, the regular flow channel keeps expansion and contraction to a minimum. The main friction loss mechanism becomes pressure loss through bends, which incurs a far lower resistance to vapor flow. This lower resistance permits incorporating more surface area in a bed of structured packings.

Pressure drop per theoretical stage. This parameter is of major importance at deep vacuum. For instance, a column containing 20 theoretical stages, with a packing that has a pressure drop of 0.2 in of water per theoretical stage, will have a pressure drop of 7.5 mmHg. If the column bottom pressure must not exceed 10 mmHg (e.g., to avoid excessive bottom temperatures and product degradation), the top pressure must be 2.5 mmHg or less. If the packing pressure drop were only 0.1 in of water per theoretical stage, the pressure drop will be 3.8 mmHg, and the top pressure 6.2 mmHg. This permits roughly a 20 to 30 percent reduction in column diameter and lowers the costs of generating and maintaining the vacuum.

Figure 8.12*c* shows that structured packings have a much lower pressure drop per theoretical stage than random packings. This is a major advantage in deep vacuum services.

Performance in high-pressure/high-liquid-flow services. The capacity and efficiency advantage of structured packings over random packings rapidly erodes as liquid rate or pressure increases (e.g., Fig. 8.12*a*). Numerous cases of structured packing failures have been experienced by the industry in high-pressure and/or high-liquid rate services. Successful experiences in such services have also been reported (24, 31a, 31c, 31d, 31e).

The causes of poor structured packing performance at high-pressure and/or high-liquid rate services are not well-understood. Work by Kurtz et al. (31*a*) and Kister and Gill (31*b*) identifies high-flow parameters F_{lv} and high-system frothiness as key factors. Flow parameters are high when either the pressure or the liquid rate (or both) are high. Frothiness is promoted by the low surface tensions experienced at high-pressure distillation. The high capacities and efficiencies demonstrated by Kean et al. (31*c*,31*d*) for numerous structured packings in glycol dehydrators support these statements. In these contactors, flow parameters were very low (<0.03) due to the low liquid rates. Frothiness was low due to the high glycol surface tension and the foam-prevention measures taken by Kean et al. The contactors performed well at pressures as high as 600 to 700 psia.

The above can be explained by a "downcomer choking" type of phenomenon. At higher liquid rates and/or higher pressures, disengagement of vapor from the liquid becomes more difficult. High frothiness will further retard vapor disengagement. As structured packings permit far less lateral movement of fluids than random packings, far more vapor will be carried downward, causing recycling and reduction of effective capacity and efficiency. Improved liquid distribution, and an increase in the size and number of perforations in the corrugated sheets will help spread the liquid and counteract any premature choking. Kurtz et al. (31a) report similar ideas and present two high-pressure case studies where better liquid redistribution improved both efficiency and capacity of structured packings.

Due to the poor understanding of the phenomenon, the lack of predictive methods, and the large number of failures experienced in the industry at high-pressure and/or high-liquid-rates, the author recommends extreme caution with structured packings at liquid rates exceeding 10 gpm/ft^2 and pressures higher than 100 to 200 psia. In this region, the author would use structured packings only in services where a demonstrated trouble-free track record has been established [e.g., glycol contacting (31*c*, 31*d*)].

Performance with aqueous/high-viscosity/high-surface-tension systems. Data in Chap. 11 (see Figs. 11.2 and 11.4 to 11.6) show that many aqueous systems in structured packings give HETPs roughly twice those of nonaqueous systems. This does not occur in all aqueous systems; for instance, the HETPs for methanol-water in Fig. 11.5, and for H_2O–D_2O in Figs. 11.1 and 11.3, are well in line with those of nonaqueous systems. The exceptions may be explained by arguing that the above methanol-water tests were conducted at the methanol-rich end, and that the H_2O–D_2O system, because of its very low relative volatility, achieves a high efficiency. The poor performance of structured packings with aqueous systems has been attributed to poor wettability (32,33) or underwetting (Sec. 8.2.16). Aqueous systems have high surface tension. The liquid spread on the packing, and therefore the wetting, are diminished at high surface tension. This problem is most serious with stainless steel, and the use of oxidized copper has been cited (33,34) to enhance efficiency in aqueous systems.

The poor wetting theory leaves several questions unanswered. Chen et al. (35) argued that above the minimum wetting rate, wettability and surface tension should only have a minor effect on packing efficiency. Also, high relative volatility and high liquid viscosity appear to be detrimental to efficiency, especially in aqueous systems, and this cannot be explained by poor wettability. Finally, there is uncertainty regarding the concentration at which the transition from an "organic system" HETP to an "aqueous system" HETP takes place.

These uncertainties question the validity of the above theory. Due to the poor understanding of this phenomenon, it is best to exercise caution with HETP predictions for all of the following types of systems on structured packings: aqueous, high surface tension, high liquid viscosity, and high relative volatility.

Liquid inventory. With unstable chemicals, minimizing liquid inventories at hot temperatures minimizes product loss due to degradation and decomposition reactions. In batch distillation, excessive liquid inventory lowers product recovery. With hazardous chemicals, minimizing liquid inventories lowers the hazard.

Figure 8.12*d* shows that liquid holdup (percent of packing volume) depends primarily on liquid flow rate and on packing size. Generally, liquid holdup increases as the size of packing particle (random packings) diminishes, or as the flow channel (structured packings) narrows. Figure 8.12*d* also shows that liquid holdup is comparable for random and structured packings of similar capacities.

Liquid inventory is the product of liquid holdup (percent of packing volume) and the packing volume. Since structured packings are more

efficient than random packings of approximately the same capacity (Fig. 8.12*a*), the structured packing volume needed for a given separation is lower. The total liquid inventory (cubic feet of liquid) is in turn lower for structured packings.

Wetting and minimum liquid rates. The capillary action of structured packings promotes self-wetting (Fig. 8.13). Self-wetting is strong in wire-mesh packings and weaker in corrugated-sheet packings. This self-wetting permits efficient operation at liquid rates down to 0.05 gpm/ft^2 of tower cross section with wire-mesh packings (20,37–39) and down to 0.1 gpm/ft^2 with corrugated-sheet packings (37,38). Some manufacturers (35,37) claim efficient operation even at lower liquid flow rates. These rates are 5 to 10 times lower than the minimum wetting rates of random packings, giving structured packings a major low liquid rate and turndown advantage.

8.1.11 Considerations for specifying structured packings

Solids. Wire mesh packings easily plug and are best avoided altogether in solid-containing services. Corrugated-sheet packings, especially those with wider spacings between adjacent layers, are more tolerant to solids, but their distribution equipment may not be. If a potential for fouling exists, accurate data must be gathered and com-

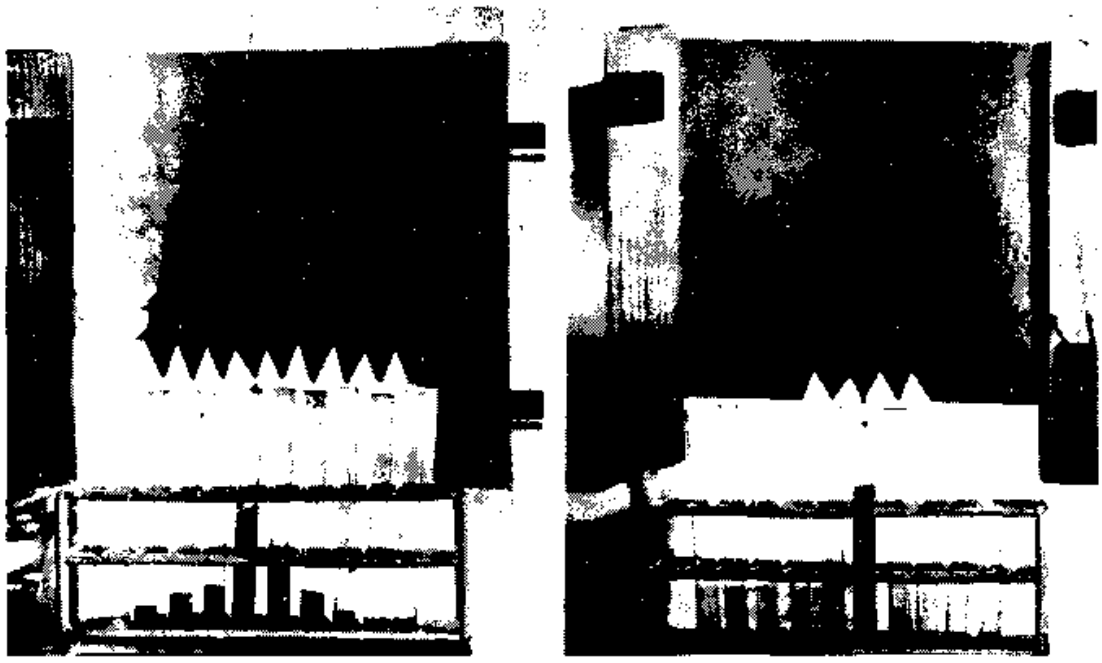

Figure 8.13 Flow of liquid over a vertical surface of Koch-Sulzer® wire mesh (*left*) and metal sheet (*right*). (*Reprinted courtesy of Koch Engineering Company, Inc.*)

municated to the manufacturer. Any economic analysis must account for the costs of plugging prevention. Several measures are described elsewhere (40).

Corrosion and oxidation. Thickness of the corrugated sheets of structured packings is typically around 30 gage (1/100 in), and seldom exceeds 20 gage (1/32 in). A 30-gage sheet is eight times thinner than a typical stainless steel tray, and several times thinner than the corrosion allowance for carbon steel trays. The thinness of the sheets makes them extremely vulnerable for attack by corrosive chemicals and oxidants. Further, the large surface area per unit volume, which is conducive to mass transfer, is also conducive for corrosion and oxidation. Thorough removal of residual liquid, wash water, air, or process gas trapped in structured packings at startup and shutdown is difficult, and the leftovers promote corrosion, oxidation, or other undesirable reactions.

It is not uncommon to find bits of corroded structured packings at the bottom of the column. There have also been several instances where a bed of structured packings caught fire when air entered the column at shutdown. These fires were initiated by small amounts of flammable or pyrophoric materials adhered to packing surfaces.

It is imperative that the packing manufacturer be supplied with accurate data on the corrosiveness of the system. Readily oxidizable metals such as carbon steel should be avoided. Generally, the metallurgy of a structured packing should be more corrosion- and oxidation-resistant than the metallurgy normally used to handle a service. Special consideration should be given to startup, shutdown, commissioning, air leakage, and vacuum relief (e.g., air entering a hot column); rapid oxidation of the packing is hazardous.

Sensitivity to upsets. Structured packings due to their lower pressure drop and bricklike structures, can weather pressure surges (such as those due to introduction of a pocket of water into a hot hydrocarbon tower) much better than random packings.

Maintenance and troubleshooting. Detecting fabrication or installation defects, and inspection inside a "brick" of structured packing are extremely difficult and may damage the packings. Inspection of the column walls (e.g., for corrosion) can also be difficult and require damaging many packing elements. Inspecting and maintaining random packings is far easier.

Cost. Structured packings typically cost 3 to 10 times more per unit volume than 2-in random packings. However, structured packings are

more efficient and will afford a shorter column. Savings due to the reduced height usually outweigh the additional packing cost. Further, pressure drop per theoretical stage is far lower for structured packing than for random packings (Sec. 8.1.10). In vacuum, this leads to lower reflux, lower operating costs, and smaller column and auxiliaries. Finally, the price per unit volume depends on the quantity ordered, the economic climate, and marketing considerations, and in some cases may be low. Therefore, the only meaningful cost comparison is of the complete designs.

8.1.12 Types of grids

Wooden and plastic grids, similar to those used in cooling towers, have been used in distillation and absorption for decades. The first modern grid was the Glitsch C-grid®, developed in the early 1960s as a means of utilizing sheet metal from which circular valve units (for valve trays) were punched out. Modern grid geometries are designed to promote desirable features, i.e., a high open area, a high capacity, a high resistance to fouling and plugging, and a low pressure drop. The efficiencies of grids are considerably lower than those of both random and structured packings. Grids are primarily used in direct-contact heat transfer, scrubbing, and deentraining services.

Glitsch C-Grid® (Fig. 8.14*a*). This grid is constructed from metal sheets in which 1.5-in holes are punched. The sheet is bent into a multiple V shape, with the holes on the sides of each V. The resulting layer is about 1½ in thick. Each layer is placed horizontally, and with the long sides at 45° to the layer below. C-Grid® has a higher capacity, but a lower efficiency than the Glitsch EF-25A Grid® (below). It is relatively infrequently used, mainly in applications where more capacity is required than EF-25A can offer.

Glitsch EF-25A Grid® (Fig. 8.14*b,c*). This is a seamless structure manufactured in 60 in long × 15 in wide × 2⅛ in high open area panels composed of horizontal, vertical, and slanted members. Adjacent layers of the grid are rotated 45° to produce a crisscross effect, giving it a lattice structure. The Glitsch EF-25A Grid® was introduced in the 1960s, has been popular, and is available in metals and plastics. The Norton Company's Intalox® Grid (in metal) is often considered equivalent to the Glitsch EF-25A Grid®.

Koch Flexigrid® #2 (or Koch High-Capacity Flexigrid®) (Fig. 8.14*d*). This grid is constructed of 60 in long × 16 in wide × 2¾ in high open area panels. The vertical, parallel blades of the grid are held in a fixed rela-

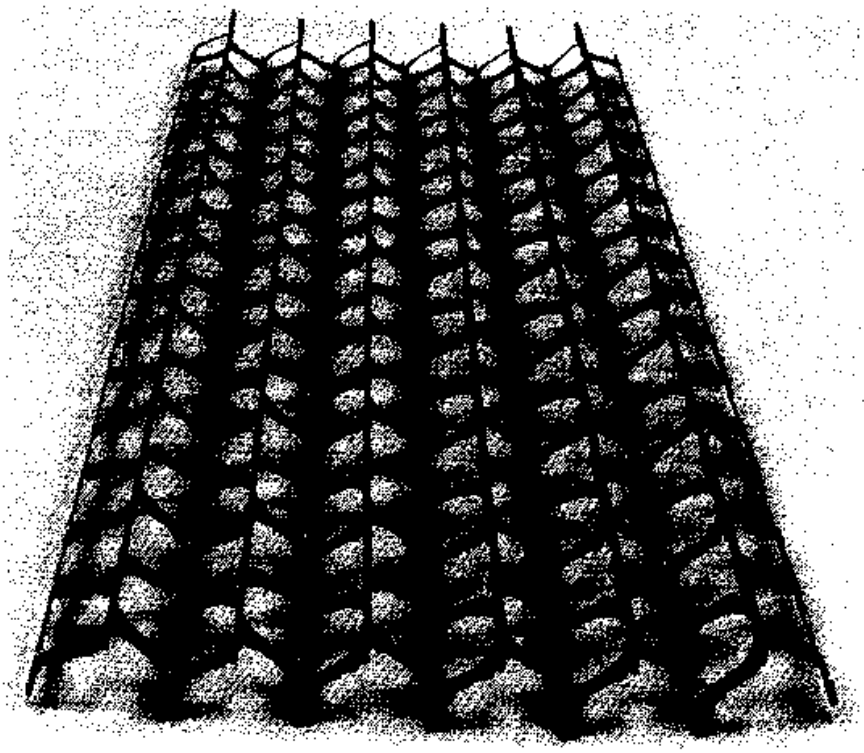

(a)

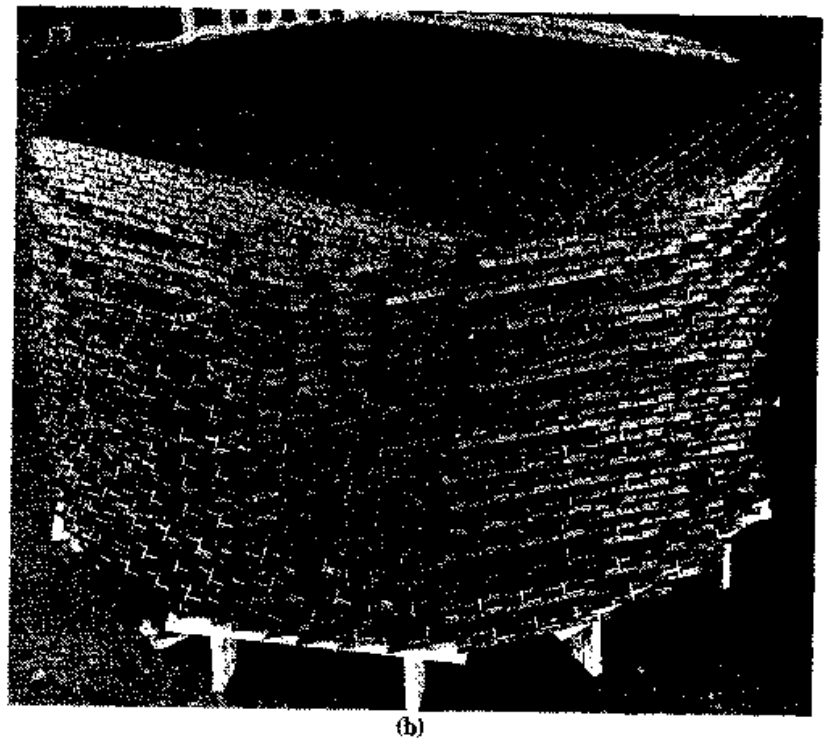

(b)

Figure 8.14 Common grid packings. (*a*) Glitsch C-Grid®; (*b*) Glitsch EF-25A Grid®. (*Parts a and b courtesy of Glitsch Inc.*)

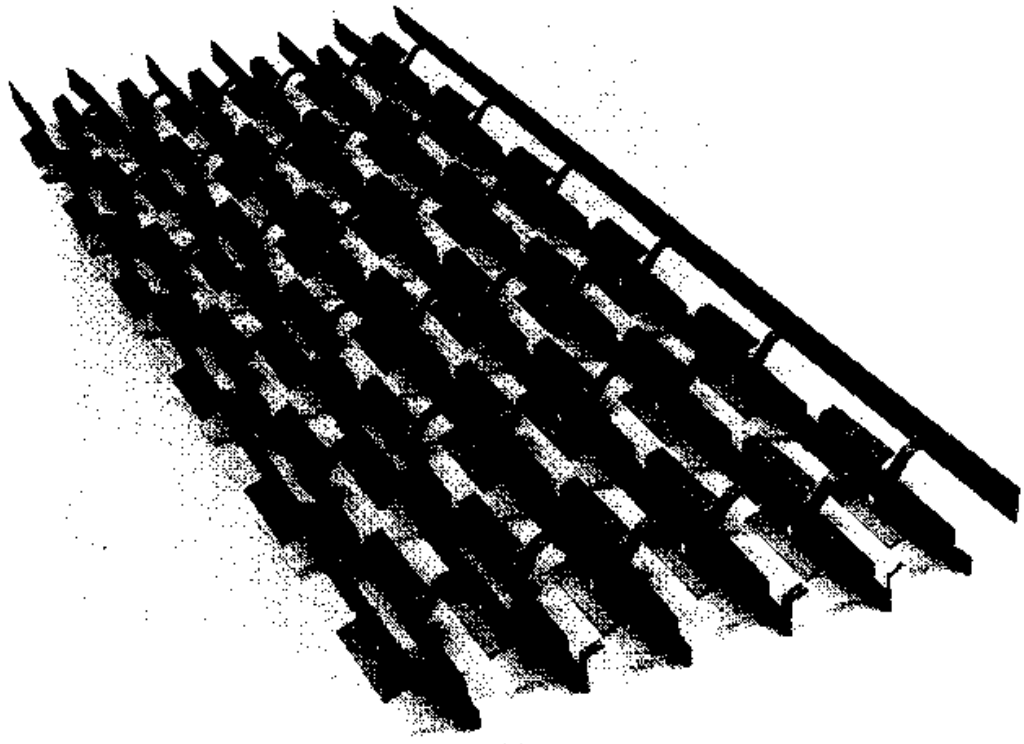

(c)

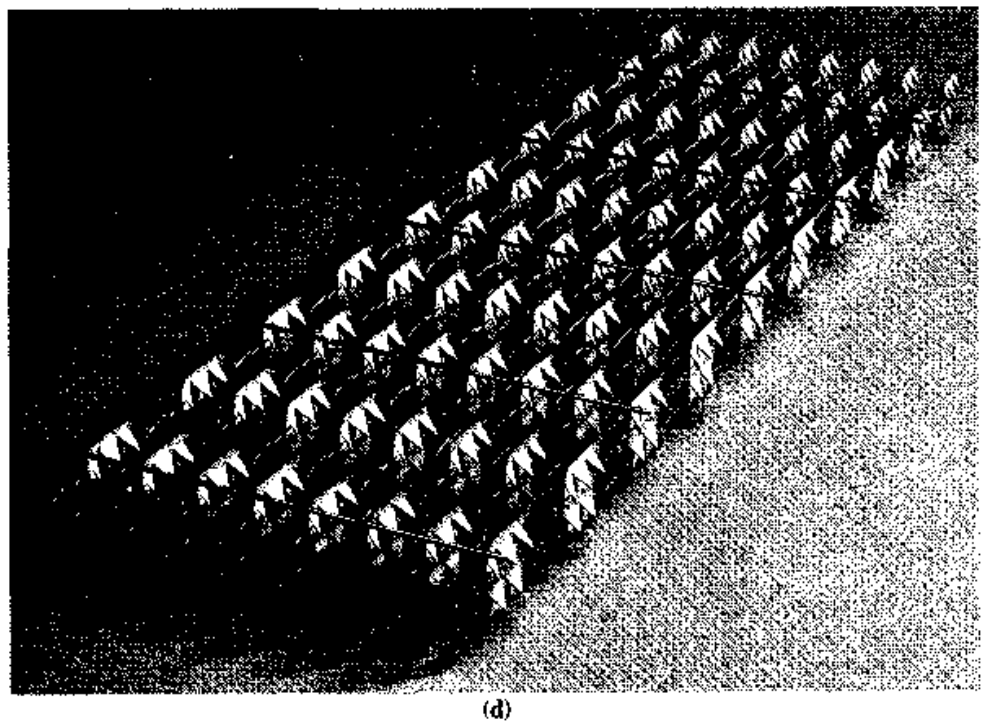

(d)

Figure 8.14 (*Continued*) Common grid packings. (*c*) An element of Glitsch EF-25A Grid®; (*d*) an element of Koch Flexigrid® #2 (*Part c, courtesy of Glitsch Inc. Part d, courtesy of Koch Engineering Company, Inc.*)

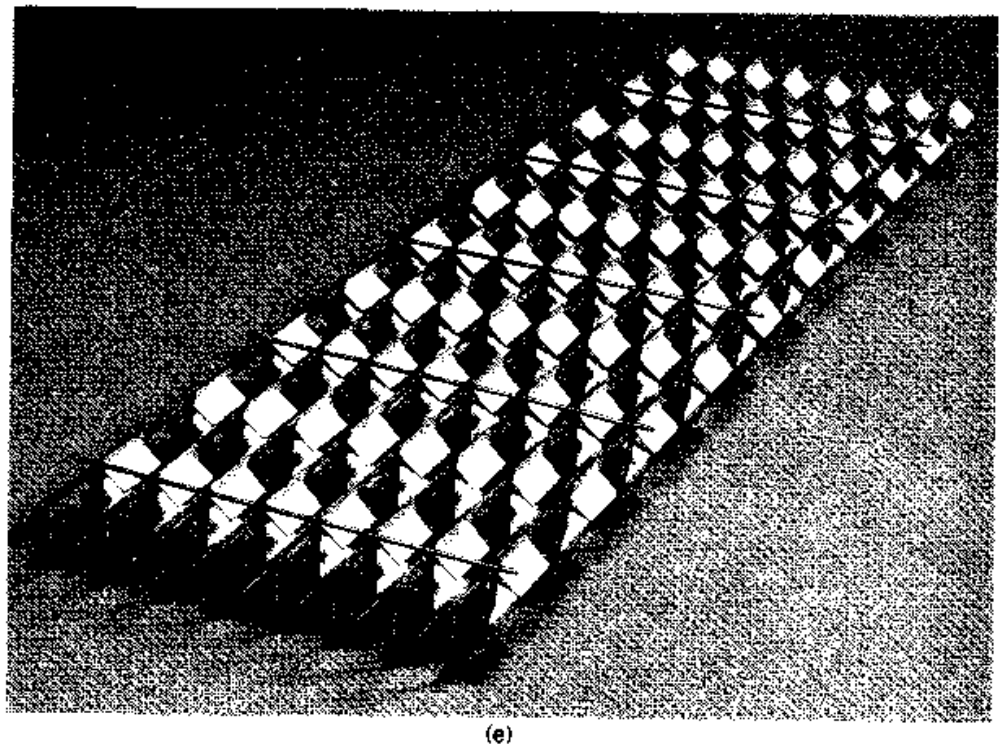

(e)

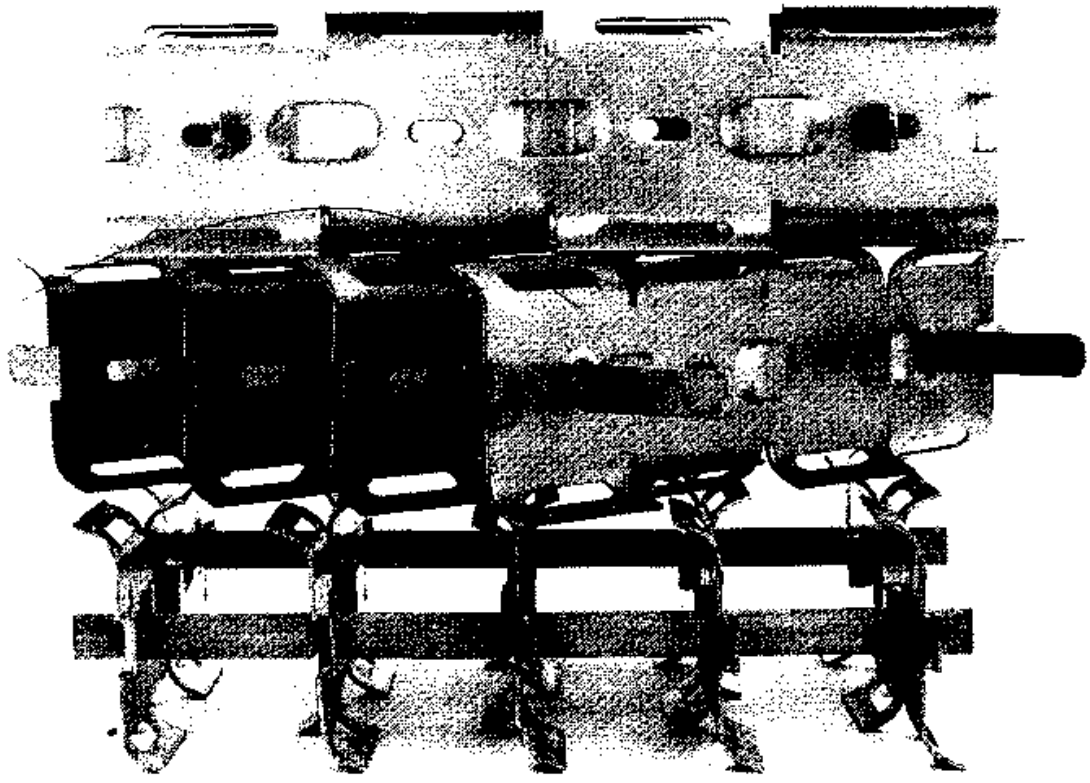

(f)

Figure 8.14 (*Continued*) Common grid packings. (*e*) An element of Koch Flexigrid® #3. (*f*) Three layers of Nutter #3 Snap-Grid™ (*Part e, courtesy of Koch Engineering Company, Inc.; part f, courtesy of Nutter Engineering Corp.*)

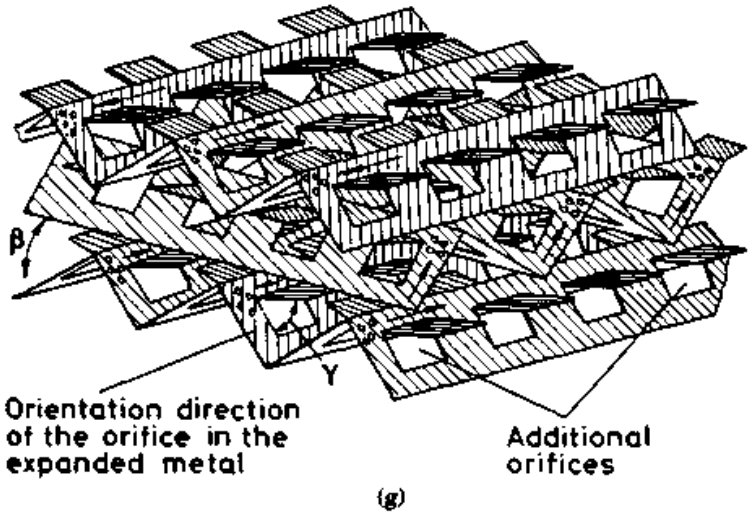

(g)

Figure 8.14 (*Continued*) Common grid packings. (*g*) Perform® Grid. (*Part g from K. Hoppe, J. Keller and L. Krell, Chem. Engnr., February, 1978, p. 110; reprinted courtesy of the Institution of Chemical Engineers, UK.*)

tionship to one another by welded cross members. Each successive layer of grid is rotated by 45° to the previous one. Compared to the EF-25A Grid®, the projections are smaller and angled (Fig. 8.14*d*). This reduces interference to vapor flow but also the area for vapor-liquid contact, giving the grid its higher capacity and lower efficiency. Koch Flexigrid® #2 was introduced in the early 1980s and is available in metals.

Koch Flexigrid® #3 (or Koch High-Efficiency Flexigrid®) (Fig. 8.14*e*). This grid is constructed from panels identical to those of Koch Flexigrid® #2, but the projections are larger and rectangular. This not only makes more area available for vapor-liquid contact and improves the spread of this area, but also increases the resistance to vapor flow. Compared to Flexigrid® #2, Flexigrid® #3 gives higher efficiency at the expense of lower capacity. Koch Flexigrid® #3 was introduced in the 1970s and is available in metals.

Nutter #3 Snap-Grid™ (Fig. 8.14*f*). This grid is constructed from high open area panels composed of spacing bars, I-beam-shaped elements, slotted baffles, and curved tabs. Each panel is at 45° to the panel below. The objective of this intricate design is to maximize vapor-liquid contact and mechanical strength while maintaining a high capacity. The Nutter Snap-Grid™ was introduced in the early 1980s and is available in metals.

Perform® grid (Fig. 8.14*g*). This grid is made of expanded metal components. The direction of orientation of small form-punched orifices

changes both horizontally from one element to the next and vertically from one layer to another. Every layer is rotated at an acute angle β to the layers below. To provide an additional open area, windows are cut in the material, with the flaps projecting out of the material at an acute angle γ. The Perform® grid was introduced in the 1970s and is available in metals from VEB Chemieanlagenbaukombinat Leipzig-Grimma, Germany.

8.1.13 Grid versus other packings

Capacity and efficiency. Capacity data by Glitsch (42) suggest that the Glitsch EF-25A Grid® has a capacity practically identical to CMR® #4. The same source also states that EF-25A has an efficiency two-thirds of that of 2-in Pall® rings in distillation services. Since CMR® #4 has about half the specific surface area as 2-in Pall® rings, it appears comparable to EF-25A Grid® in efficiency as well. Roughly, grids have high capacity and low efficiency, similar to the larger second- and third-generation random packings.

Pressure drop. Due to its high open area and high capacity, grid is one of the lowest-pressure-drop devices. Compared to 2-in Pall® rings, grids typically have a pressure drop three to five times lower; some high-capacity grids have a pressure drop 10 times lower (43).

Wetting. The minimum liquid rate recommended for adequate wetting is about 0.2 to 0.3 gpm/ft^2 (44), although rates down to 0.1 gpm/ft^2 have been successfully used (45,46). These rates are low and are comparable to the minimum wetting rates for corrugated-sheet structured packings (Sec. 8.1.10). Grids therefore can achieve high turndown and perform well at low liquid rates.

Solids. Grids are suitable for solid-containing streams and fouling services. Grid surfaces are designed to be self-draining, avoiding areas where sediment may trap or hot liquid may coke or polymerize. The low pressure drop keeps liquid holdup at a minimum, which reduces the residence time of liquid in the heated zone. The ability of grids to handle solids and minimize fouling is one of their greatest advantages.

Liquid to grids is usually supplied by spray nozzles, and these may plug. As with other distributors, adequate measures are required to prevent plugging, and the grid manufacturer must be supplied with good data on the fouling potential of the service.

Mechanical strength. The lattice structure of grids gives them a mechanical strength advantage compared to random and structured

packings. Close attention is required to the metal thickness of the grid. This usually ranges from 18 to 14 gage; the mechanical strength depends on this thickness. A thinner gage gives a cheaper grid, at the expense of lower strength.

Sensitivity to upsets. The high open area and rugged construction give grids a strong resistance to pressure surges, even greater than that of structured packings. Strong mechanical design and good fastening practices (42,46) must be followed to achieve this resistance.

Corrosion and oxidation. Due to the relatively thick metal, low specific surface area, and rugged construction of grids, their tendency to oxidize is low. Grids tend to degrade to a much lesser degree than either random or structured packings.

Maintenance and troubleshooting. Due to their layered structure, grids are easy to install, remove, inspect, and maintain. Grid cleaning (especially if coked up) may be difficult, often impractical, but even in such cases, it is easier than that of random or structured packings.

Cost. Grids are far less expensive than structured packings, and their volumetric costs are of the same order as those of random packings.

Grid-Ring Combination® (GRC®). In many condensing heat transfer services (such as refinery fractionator pumparound services), the vapor and liquid loads taper as one ascends the bed, due to condensation of vapor. To achieve the high capacity required at the bottom of the bed, the entire bed can be packed with grid alone. A patented improvement (42) that permits shortening of the bed is to use grid near the bottom and to dump random packings on top of the grid. The grid height is designed to condense enough of the vapor so that the remaining vapor and liquid loads do not exceed the allowable capacity of the random packing. The random packings complement the condensation at a higher efficiency than the grid, thus permitting an overall shorter bed to be used.

One alternative and analogous technique is to use structured packings instead of random packings to complete the condensation. Another (47) is to use a "fine" (i.e., high-surface-area, low-capacity) grid instead of the random packings.

8.2 Packing Hydraulics

8.2.1 Pressure drop flow regimes

At low liquid flow rates (region *A-B* in Fig. 8.15), the open cross-sectional area of the packing is about the same as in a dry bed. The

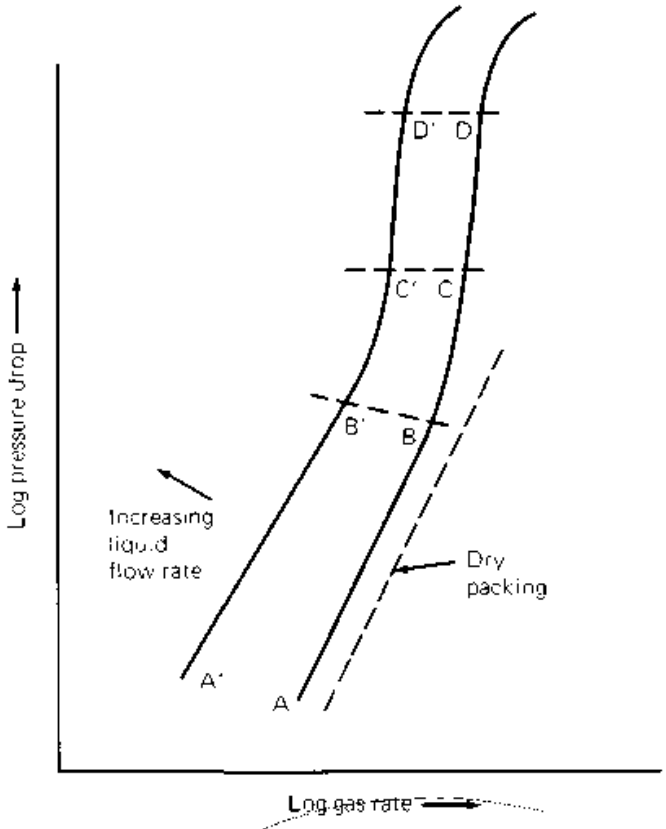

Figure 8.15 Typical pressure drop characteristics of packed towers. (*From H. Z. Kister,* Distillation Operation. *Copyright © by McGraw-Hill, Inc., reprinted by permission.*)

pressure drop is entirely by frictional losses through a series of openings, and therefore is proportional to the square of the gas flow rate. In random packings, the openings are randomly sized and located, and pressure drop is due to expansion, contraction, and changes of direction. In structured packings, the openings are regular and of uniform size, and pressure drop is due to changes in direction.

As liquid rates are raised, the liquid occupies some of the cross-section area, making the openings for gas flow smaller. The pressure drop curve will parallel *A-B* but will be somewhat above it. At high liquid flow rates, the packing voids fill up with frothy liquid. A portion of the energy of the gas is used to support the liquid in the column and pressure drop becomes proportional to the gas rate raised to a power different (usually lower) than 2 (region *A'-B'*). The point where the packing voids fill up, i.e., when tower operation switches from vapor-continuous (normal) to liquid continuous is termed *phase inversion.*

For all liquid flow rates, as gas flow rate is raised, a point is reached when the gas velocity begins to interfere with the free drainage of liquid. Liquid will start to accumulate or "load" the bed, giving this region the name "the loading region." The accumulation of liquid reduces the cross-section area available for gas flow and therefore

accelerates the pressure drop rise. In this region (*B-C* and *B'-C'* in Fig. 8.15) the slope of the curve increases to a power distinctly above 2.

Upon further increases in gas rate, more liquid accumulates, until the liquid surface becomes continuous across the top of the packing. The slope of the curve increases, until it becomes very steep. When this occurs (points *C* and *C'* in Fig. 8.15) the column is flooded.

A stable operating region beyond flooding (above points *D* and *D'*) was discovered (48,49). In this region, the packed column is essentially inverted to a "bubble column." This region is of little significance in industrial practice.

8.2.2 Efficiency flow regimes

Figure 8.16*a* illustrates typical variation in column efficiency as gas rate is raised at a constant *L/V* ratio (i.e., liquid rate increases with the gas rate). To the left of point *A* on Fig. 8.16*a* is the turndown maldistribution region. Upon turndown from normal operating rates, a point is reached where efficiency drops because either the distributor or the packing reaches a turndown limit. Most distributors are designed for turndown ratios of 2 to 4 from their normal design liquid rates. At lower liquid rates, irrigation to the bed is poor, giving poor efficiency. When liquid remains well-distributed in the column upon turndown, point *A* represents the minimum wetting rate of the packing. Below minimum wetting the falling liquid film breaks up, some of the packing surface unwets, and the efficiency drops.

Generally, the minimum wetting rate is at 0.5 to 2 gpm/ft^2 for random packings, and 0.1 to 0.2 gpm/ft^2 for structured packings (Sec. 8.2.15). It follows that point *A* is usually a distributor turndown limit. Regardless of which limit point *A* represents, it is extremely sensitive to maldistribution (Fig. 8.16*b*). When liquid distribution is poor, it will take more liquid to wet the entire bed, and point *A* will shift to the right. If distribution is very poor, point *A* may never be observed, and the curve will have no flat region at all. A V-shaped curve is not uncommon, and is indicative of poor distribution.

Region *A-B* (Fig. 8.16*a*) has turbulent liquid film, good wetting of the packing, good mass transfer, and essentially constant efficiency. This region is ideal for packed column design and operation.

Raising gas velocity past point *B* moves column operation into the loading region. Initially, efficiency improves because of the greater liquid holdup (region *B-E*), but this improvement is short-lived. As the flood point is approached, the efficiency passes through a maximum (point *E*), and then drops (region *E-C*) because of excessive entrainment.

Packed towers are usually designed for region *A-B*. Although region

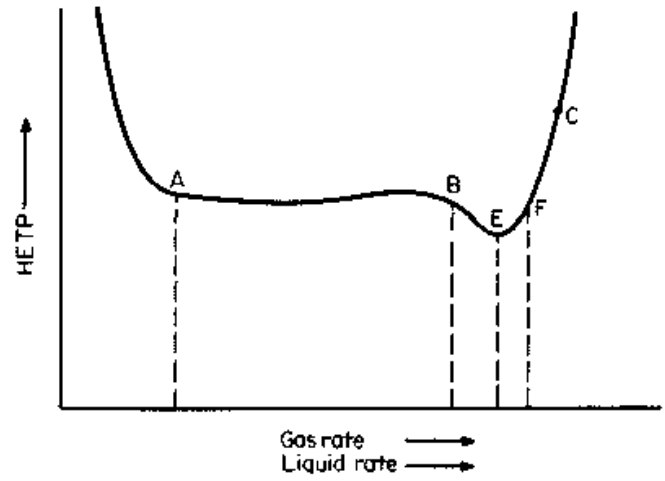

(a)

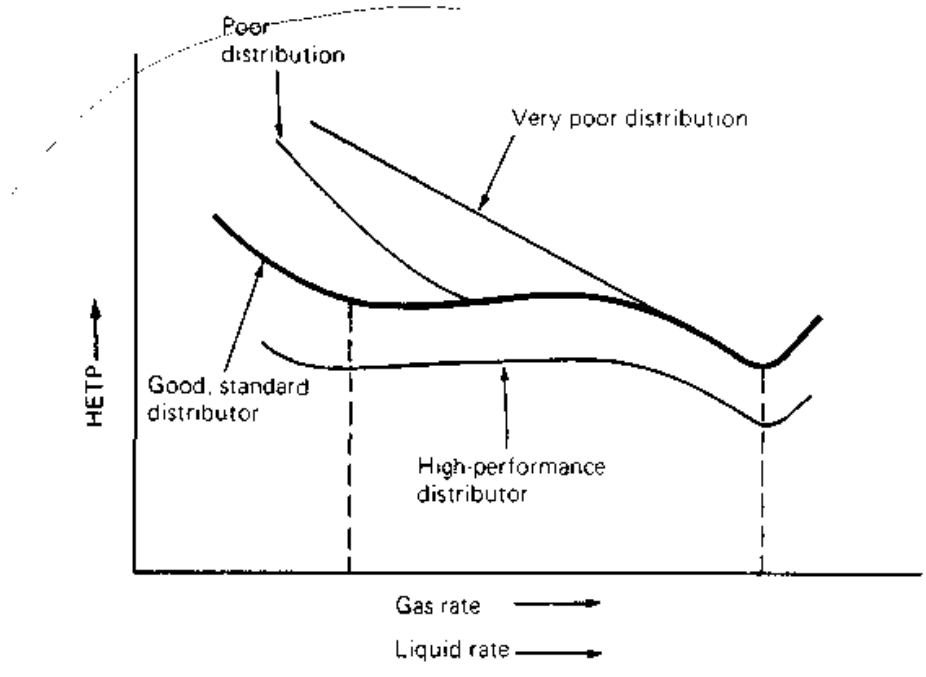

(b)

Figure 8.16 Typical efficiency characteristics of packed towers. (*a*) Typical efficiency characteristics for random packings and for most corrugated-sheet structured packings; (*b*) effect of liquid distribution on the efficiency characteristics of part *a*. (*Part b from H. Z. Kister,* Distillation Operation. *Copyright © by McGraw-Hill, Inc. Reprinted by permission.*)

B-F gives the highest efficiency, it is usually avoided in design because of the proximity of the flood point. In practice, operation is normally stable and design efficiency or better is achieved throughout region *A-F*.

Most wire-mesh and some corrugated-sheet structured packings

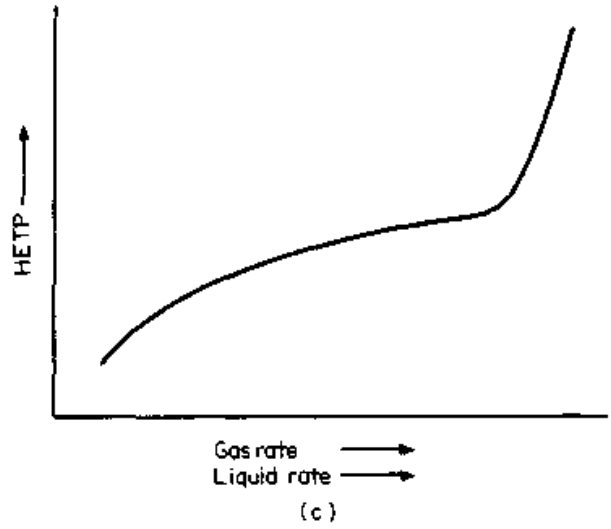

(c)

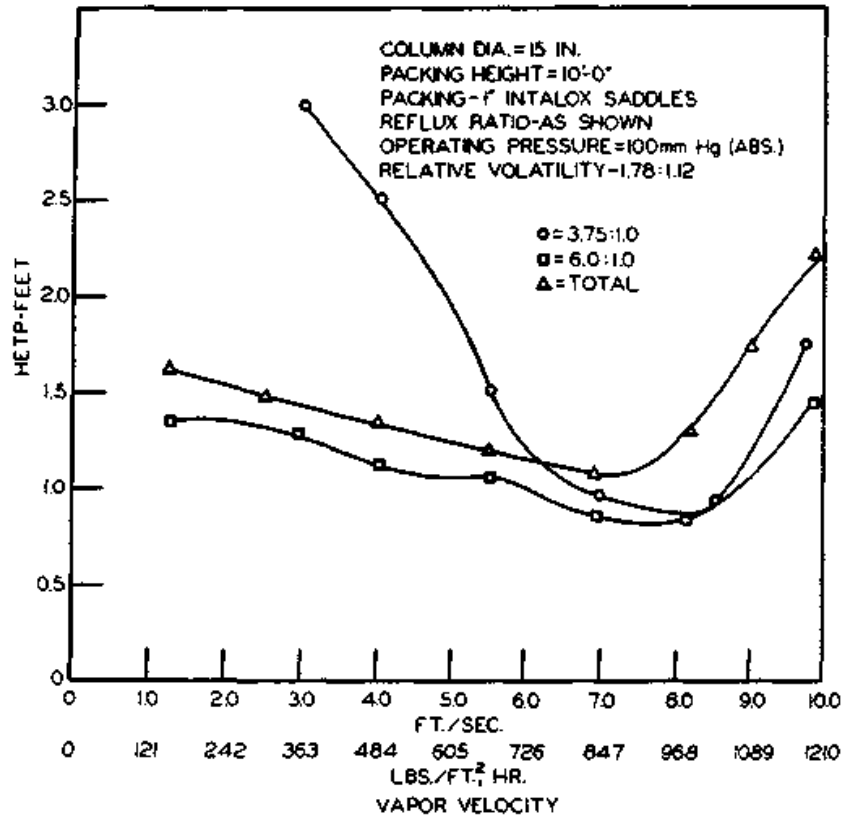

(d)

Figure 8.16 (*Continued*) Typical efficiency characteristics of packed towers. (*c*) Typical efficiency characteristics for wire-mesh structured packings; (*d*) example of efficiency characteristics, measured for random packing, that deviate from those in parts *a* and *c*. (*Part d from J. S. Eckert and L. F. Walter,* Hydrocarb. Proc. & Pet. Ref., February 1964. *Reprinted courtesy of Hydrocarbon Processing.*)

have the efficiency curve of Fig. 8.16*c* rather than 8.16*a*. Here region *A-B* slopes upward, and point *E* is not observed. According to the mass transfer models of Bravo and Fair (50) and of Spiegel and Meier (21), raising vapor and liquid loads enhances the mass transfer coefficient and interfacial area (this improves efficiency) but lowers the gas residence time (this lowers efficiency). In corrugated-sheet packing, these counteracting effects are balanced, and efficiency is independent of loads. On the other hand, surfaces of wire-mesh packings are fully wetted due to their excellent wetting characteristics, making the interfacial area independent of loads. The residence time effect outweighs the mass transfer coefficient effect, giving the efficiency curve of Fig. 8.16c.

An alternative explanation, preferred by the author, is in terms of mechanisms postulated by Kurtz et al. (31*a*). As liquid rate increases, more vapor is entrained down the bed. This drops efficiency. Because structured packings permit far less lateral movement of fluids than random packings, far more vapor will be carried downward. The vapor entrainment will be most detrimental to efficiency when fluid lateral movement is restricted most. This can be expected with narrow flow channels (e.g., wire-mesh structured packings), at high liquid rates and high pressure.

The efficiency curves described above are somewhat idealized. In practice, efficiency curves generally follow the above principles, but may deviate from the patterns shown in Figs. 8.16*a* to *c*. Kunesh (51) states that point *E* in Fig. 8.16*a* is not always observed, and that in many cases the curve between points *B* and *F* is flat. Figure 8.16*d* is an example of experimentally measured curves for a random packing that deviate from Figs. 8.16*a* and *b*. The hydraulics and mass transfer processes taking place in a packed bed are extremely complex and are not well-understood.

Summary. The above discussion identifies the following regimes for packed column operation.

- *The turndown maldistribution regime (region to the left of* A *in Fig. 8.16a, not identified from the pressure drop curves):* Operation in this region is undesirable because of poor efficiency.
- *The preloading regime (regions A-B and A'-B' in Figs. 8.15 and 8.16a):* Most packed towers are designed to operate in this region. Column efficiency is independent of flow rate and column pressure drop uniformly increases with vapor flow rate. An exception is wire-mesh structured packing, where column efficiency declines with an increase in loads (Fig. 8.16c).
- *The loading regime (regions* B-C *and* B'-C' *in Figs. 8.15 and*

8.16a): Liquid replaces vapor as the continuous phase as a column changes from normal to flooded operation. An excellent illustration of this process was given by Harrison and France (52). Most columns can operate in this region and achieve maximum efficiency, but it is not normally used for design. Some instability ("operational flood") may occur at higher rates in this region (53).

- *The flooding regime (above point C and C' in Figs. 8.15 and 8.16a):* This region is characterized by instability, entrainment, and poor efficiency and is therefore avoided.

8.2.3 Flood point: concept and traps

Flood-point definition. In 1966, Silvey and Keller (54) listed 10 different flood point definitions that have been used by different literature sources. A recent survey (59) listed twice that many. As Silvey and Keller pointed out (54) the existence of so many definitions puts into question what constitutes flooding in a packed tower, and at what gas rate it occurs. Symptoms used to identify flood in these definitions include appearance of liquid on top of the bed, excessive entrainment, a sharp rise in pressure drop, a sharp rise in liquid holdup, and a sharp drop in efficiency. An examination of the definitions shows some conflicts in inferring the flood point from even a single symptom. For instance, one definition sets the flood point when "slight splashing" occurs, while another sets it when a higher degree of entrainment ("marked spraying") is experienced. Many definitions use inconcise terms such as "appreciable amounts," or "a very high value," thus leaving room for subjectivity. Other definitions use arbitrary criteria such as "½-in liquid buildup on top of the bed" or a "pressure drop of 2 in of water per foot of packing." Finally, Kunesh (51) points out that flooding is an inherently unstable condition, and that an observer using a single definition consistently may report different results for two experimental runs because of variations of such factors as an increase in boilup and the stability of pressure control.

Based on the above, some designers argued (5,15,57) that the traditional approach of using the flood point as the upper capacity limit of a packed column is best abandoned. They recommended shifting to alternate criteria such as maximum operational capacity or maximum permissible pressure drop. Others (3,37,41,51,58–60) stick with the flood-point criterion while recognizing its limitations. There are strong, practical reasons for retaining the flood point as the prime criterion for the upper capacity limit.

First and foremost, the alternative capacity criteria—namely the maximum operational capacity and the maximum pressure drop—have been demonstrated to be less reliable than the flood point (see Secs. 8.2.4 and 8.2.5). Bolles and Fair (55), MacDougall (58), and

Kister and Gill (60,60*a*) demonstrated that despite differences in definitions, flood-point data compared quite well to correlation predictions. Both Kister and Gill (60,60*a*) and MacDougall (58) show that flood data from various sources (using various definitions) can be correlated to with ±10 to 15 percent accuracy. It was also demonstrated that the flood point can be predicted far more reliably than packing pressure drop (55,58) and maximum operational capacity (60).

Second, flood point data are easy to find, while maximum operational capacity data are less abundant. Generating maximum operational capacity data requires expensive efficiency measurements, while flood-point determination requires far less expensive tests.

Third, maximum operational capacity data are practically nonexistent at high liquid rates. Efficiency measurements are usually performed at or close to total reflux (liquid to vapor mass ratios of about unity) in order to prevent pinching from impairing data accuracy. In order to obtain data at high liquid rates, liquid to vapor mass ratios of the order of 2 to 3 or more are usually required.

Which definition to use? The surveys of Kister and Gill (59,60*a*) suggest that most flood-point definitions describe the point of flooding initiation ("incipient flooding"; point C on Figs. 8.15 and 8.16*a*). There are only three exceptions—"The slope of the pressure drop curve (plotted against gas velocity) goes to infinity"; "the gas velocity at which efficiency goes to zero"; and "The pressure drop reaches 2 in of water per foot of packing." These exceptions describe fully developed flood conditions. The different incipient flooding definitions gave surprisingly little scatter of flood-point data (for a given packing under similar operating conditions). It follows that any definition describing flooding initiation should be satisfactory.

The author believes that due to the variations in the predominant symptom with the system and the packing, the use of multiple symptoms is most appropriate. The author prefers the following definition by Bravo and Fair (50), "A region of rapidly increasing pressure drop with simultaneous loss of mass transfer efficiency. Heavy entrainment is also recognized as a symptom of this region." An almost identical definition was presented earlier by Billet (56).

8.2.4 Maximum operational capacity (MOC): concept and traps

The maximum operational capacity or throughput is defined (15) as the "Maximum vapor rate that provides normal efficiency of a packing" (i.e., point *F* in Fig. 8.16*a*).

The MOC is clear-cut in Fig. 8.16*a*. On the other hand, locating the

MOC in Fig. 8.16*d* is difficult and leaves a lot of room for subjectivity. Further, MOC determination is sensitive to the accuracy of efficiency measurements—factors such as liquid and vapor distribution, sampling procedure, end effects at the top and bottom of the packings, and the availability of a large number of efficiency points near the MOC, where conditions may not be steady-state. For instance, for one set of published experimental data reported by Eckert and Walter (61), MOC increased by about 10 percent due to reducing packed height from 10 to 5 ft.

The MOC is a useful upper-capacity criterion, specifically related to packing efficiency. However, the MOC is far from the panacea for resolving the uncertainties inherent in the flood-point concept, as it substitutes those for new uncertainties.

8.2.5 Pressure drop: Inherent limitations and traps

Pressure drop This is often used to specify packed tower capacity. The application of this criterion, and the interpretation of packing pressure drop data are not trouble-free. Some inherent limitations and traps are

1. In small columns (<3 ft in diameter) pressure drop varies with tower diameter (3,56). With random packings, the smaller the tower diameter, the lower the pressure drop, possibly due to enhancement of wall effects. Since the bulk of the published pressure drop data were obtained in pilot-scale columns, a correlation based on these data will give optimistic predictions for commercial-scale columns. The magnitude of the diameter effect on pressure drop (at fixed operating conditions) varies with packing size and geometry, with no coherent trend. For 2-in metal Pall® rings, Billet (3,62) measured a 20 to 30 percent higher dry pressure drop in a 2 ft 7 in diameter column than in a 9-in diameter column. With ⅝-in Pall® rings, the corresponding difference was only of the order of 5 percent (56). This diameter effect may intensify when column diameter diminishes below 9 in (3,11). With some corrugated structured packings, the reverse effect was observed (3,31,32), e.g., pressure drop about 10 to 20 percent lower in a 3-ft-diameter column than in a 1-ft-diameter column.
2. Dry-packed beds have higher pressure drops than wet-packed beds. Billet (56) and Kister (40) report cases where changing from dry to wet packing increased column capacity by 5 percent and reduced pressure drop by 10 percent. Ludwig (63) reports cases where this pressure drop reduction was 50 to 60 percent. The

packing method is seldom reported by literature sources presenting test data.

3. Packing particles may be nonuniform. Kunesh (51) shows size variation among ceramic saddles of the same nominal size that came out of a single box. Further, for the same nominal packing type and size, there are differences in shape, size, and particle thickness among packings produced by different manufacturing processes. All these have an effect on pressure drop.
4. Pressure drop is a function of vapor and liquid velocities, densities, and physical properties. The velocities and densities vary with changes in compositions along the packed bed. For test systems where these variations are large, pressure drop data may contain significant errors.
5. Pressure drops measured under deep vacuum (<50 mmHg) are affected by the pressure drop and the pressure gradient along the bed. Consider a 10-ft-tall packed bed operating at 20 mmHg at the top with a pressure drop of 0.5 in of water per foot of packing. The pressure at the bottom of this bed will be 29 mmHg. The velocity and pressure drop at the bottom of the bed will be 31 percent lower than at the top. The average pressure drop per foot of bed will be roughly 84 percent of the pressure drop that would have been measured for a very short bed with the same top pressure.
6. Pressure drop measurements in pressure towers include the static head of the vapor. To obtain the actual packing pressure drop, the static head must be subtracted from the pressure drop measurement. At high pressure, the static head is often higher than the packing pressure drop, making the pressure drop a difference between two large numbers. Most pressure drop data are not corrected for static vapor head. Data sources seldom state whether such a correction has been performed. This may lead to serious errors, especially for low-pressure-drop packings, even at pressures as low as atmospheric. For an atmospheric system with a molecular weight of 100, boiling at about 200°F, the static vapor head is about 0.04 in of water per foot of packing. This static head can lead up to a 40 percent error when the measured pressure drop is 0.1 in of water per foot of packing.
7. In some cases (65), it has been observed that nonuniform liquid distribution can lead to lower pressure drop than under uniform distribution. MacDougall (58) postulated that liquid maldistribution can generate gas maldistribution, which in turn will affect pressure drop. MacDougall extended this argument to cast suspicion on pressure drop data measured at liquid rates be-

low the distributor turndown limit. Recent experiments by Sohlo and Kouri (66) and Stoter et al. (67) confirmed that liquid maldistribution can generate gas maldistribution at high gas rates, but not at low gas rates. Combining Sohlo and Kouri's findings with MacDougall's arguments suggest that data obtained at high vapor rates and turned-down liquid rates are likely to give optimistic pressure drops.

8. For ceramic packings, reported pressure drops are for unchipped and unbroken pieces. In practice, breakage and chipping of ceramic packings occur in shipment, when loading packings into the column and during operation. Small pieces and chips of packings reduce the cross-section area and increase pressure drop. This may increase a pressure drop by 15 to 75 percent (63).
9. Plastic and thin-wall metal packings deflect with time and temperature and compress. The problem is aggravated in tall beds and where a plastic approaches its maximum use temperature. The compression raises pressure drops. The rise in pressure drop, however, is generally smaller than that due to ceramics breakage.
10. Pressure drops for foaming systems are higher than for nonfoaming systems (1). Most published pressure drop data are for nonfoaming systems, and will give optimistic estimates when applied to foaming systems. Eckert (1) presents suggestions for extending pressure drop data to foaming systems.

8.2.6 Flood-point prediction

Sherwood-Eckert generalized pressure drop correlation (GPDC). For several decades, the Sherwood-Eckert GPDC chart has been the standard of the industry for predicting flood points and pressure drops. This chart was initially developed by Sherwood et al. (68). Sherwood's chart, later modified by Lobo et al. (69), contained only a single curve that predicted packing flood points. Leva (70) retained the flood-point curve and added a new family of curves onto the chart to predict packing pressure drop. Copigneaux (71) and Eckert (53,72) proposed further modifications. In a later version, Eckert (74) omitted the flood curve from the chart, retained only the pressure drop curves, and performed other minor modifications. Finally, Strigle (15) changed the scales of Eckert's later version from log-log to semilog to make interpolation between adjacent pressure drop curves easier. McNulty and Hsieh (31) detailed the history of modifications to the correlation.

The last popular version of the GPDC chart that contained a flood-point curve was the Eckert correlation (53,72). This version (Fig. 8.17)

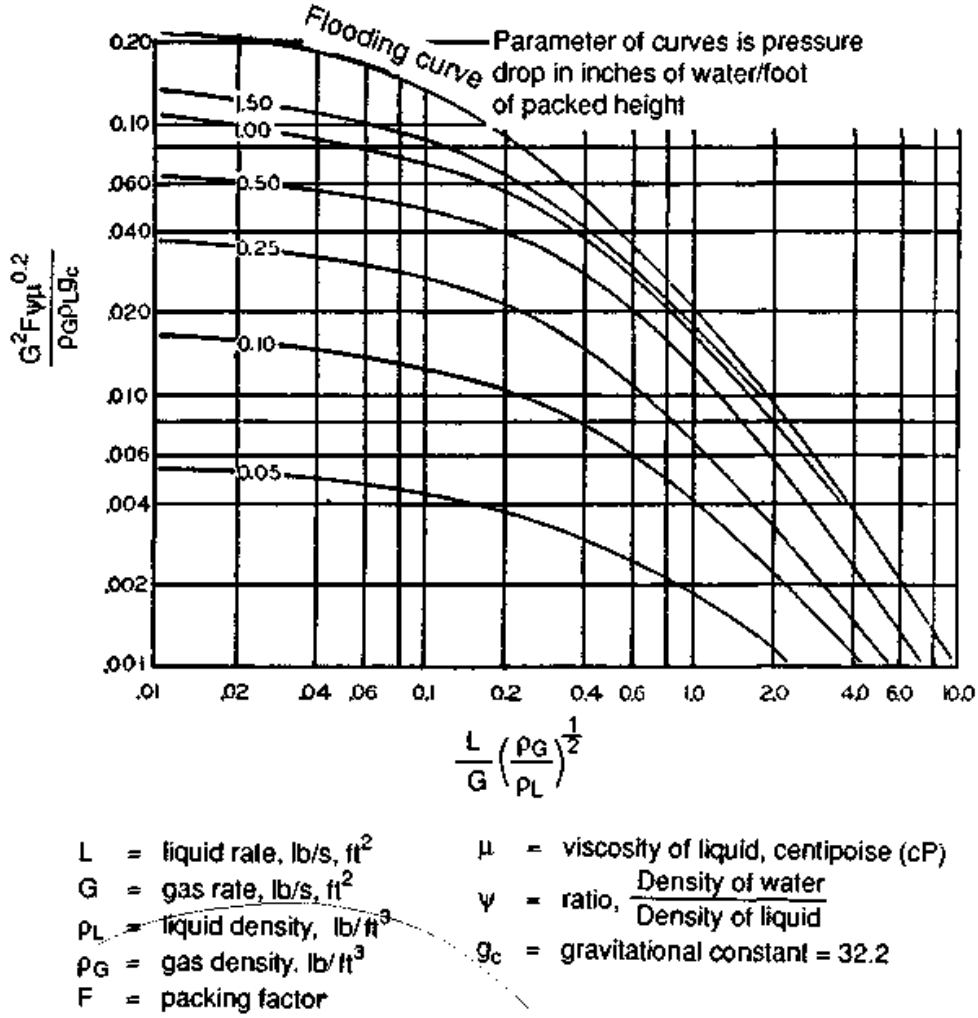

Figure 8.17 The Eckert 1970 version of the GPDC correlation. (From J. S. Eckert, *Chem. Eng. Progr.*, *66*(3), March 1970, p. 39. Reproduced courtesy of the American Institute of Chemical Engineers.)

was the industry's standard for flood-point prediction for random packings (e.g., 14,41,55,58–60).

The GPDC chart ordinate describes the balance between the vapor momentum force, that acts to entrain swarms of liquid droplets, and the gravity force, that resists the upward entrainment. This closely resembles the force balance used by Souders and Brown for entrainment flooding in tray columns (Sec. 6.2.4). A comparison of Eq. (8.22) (which describes the GPDC chart ordinate per a recent version) and Eq. (6.10) depicts the close resemblance. The relevance of this force balance to packed tower flooding was demonstrated recently by the success of the Higee technique (centrifugal distillation) to largely increase column capacity by enhancing the gravity force that resists droplet entrainment.

The GPDC chart abcissa is the flow parameter [Eq. (8.21)], the ratio of liquid kinetic energy to vapor kinetic energy. This parameter has been applied to tray columns (Sec. 6.2.3), but is far more suitable

for describing the influence of liquid rate in a true counter-current contactor like a packed tower.

Silvey and Keller (75) compared predictions from the Eckert correlation to experimental data for ceramic Raschig rings. Agreement was good for rings 1.5 in and smaller, but for 3-in rings the correlation predictions were optimistic.

Bolles and Fair (55) compared flood-point predictions from the Eckert correlation to published experimental data for random packings. Their massive data bank consisted mainly of data for first-generation packings, but also included some data for second-generation packings. For the data compared, Bolles and Fair showed that Eckert's correlation gave reasonable flood-point prediction. Statistically, they showed that if a safety factor of 1.3 was applied to the correlation flood-point predictions, the designer will have 95 percent confidence that the column will not flood.

MacDougall (58) compared flood-point data to predictions from the Eckert correlation for first- and second-generation packings. His study came up with an identical conclusion and an identical safety factor to those derived by Bolles and Fair.

Kister and Gill (60) compared flood-point predictions from the Eckert correlation to published experimental data for random packings. Their massive data bank consisted solely of second- and third-generation packings, 1 in and larger in nominal size. They showed that the Eckert correlation gave grossly optimistic predictions for all but the smaller modern packings. For most larger modern packings, the flood point coincided with the curves for pressure drops of 0.5 to 1.5 in/ft of packing (see Fig. 8.17) rather than with the flood curve. Kister and Gill concluded that the Eckert correlation gives good flood-point predictions only for lower-capacity random packings (packing factors, $F_p > 60$). A corollary is that the Eckert correlation works well for most first-generation packings, for which it was developed, but not for most modern high-capacity packings.

Based on the above reliability studies, the author recommends the Eckert flood correlation (the flood curve on Fig. 8.17) only for random packings whose packing factors F_p exceed 60.

The Kister and Gill correlation. Zenz (76) discovered that packing pressure drop at the flood point decreases as the packing capacity increases. A similar observation was reported by Strigle and Rukovena (15,77) and Maćkowiak (73*b*). Kister and Gill (60) applied this principle to derive a simple flood point correlation

$$\Delta P_{\text{Fl}} = 0.115 F_p^{0.7} \tag{8.1}$$

Equation (8.1) expresses the pressure drop at the flood point as a func-

tion of the packing factor alone. Once this pressure drop is known, the flood velocity can be calculated using one of the standard pressure drop prediction methods (Secs. 8.2.8 and 8.2.9).

Kister and Gill compared flood-point predictions from Eq. (8.1) to their massive data banks for second- and third-generation random packings (60) and for structured packing (60*a*). Pressure drops were calculated using the Kister and Gill GPDC interpolation charts (Sec. 8.2.9). They showed that Eq. (8.1) predicted all the flood points in their data bank to within ±15 percent and most to within ±10 percent.

The flood velocity calculated by the Kister and Gill correlation is tolerant to inaccuracies in flood pressure drop predictions. For instance, an error of 20 percent in the flood pressure drop calculated by Eq. (8.1), at a flood pressure drop of 1 in of water per foot of packing, will only introduce an error of 4 to 8 percent in the flood velocity calculation. This is because of the convergence (or "bunching") of the pressure drop curves for pressure drops in the range of 0.5 to 1.5 in of water per foot of packing (Fig. 8.17). Further, the effect of packing factor on the flood pressure drop acts in an opposite direction to the effect of packing factor on the flood velocity. This makes the flood velocity also insensitive to inaccuracies in the packing factors.

A weak link in the correlation is the packing pressure drop prediction. Inaccurate pressure drop prediction procedures will lead to inaccurate flood-point predictions using this correlation. For best results, the author recommends applying Eq. (8.1) together with pressure drop predictions by interpolation (Sec. 8.2.9).

For high packing factors (F_p > 60), Eq. (8.1) predicts flood pressure drops greater than 2 in of water per foot of packings. In this situation, Eq. (8.1) will give similar predictions to those obtained from the flood curve on the Eckert correlation (Fig. 8.17).

For high-capacity structured packings of unique geometry, such as the Norton Intalox® 2T and the Jaeger MaxPac®, Eq. (8.1) consistently predicts flood points that are 5 to 10 percent low (31*b*,60*a*). Although this is well within the correlation accuracy, it suggests that Eq. (8.1) does not distinguish the unique "high capacity" features of these two structured packings.

Flood prediction by the Billet and Schultes correlation. Billet and Schultes (79,80) modified the GPDC to take liquid holdup into account. The important parameter was left out of earlier versions of the correlation. Its inclusion improves the theoretical validity of the correlation at the expense of greater complexity. Billet and Schultes derived their flood-point correlation from their liquid holdup equation by postulating that at the flood point, a small increase in vapor or liq-

uid velocity effects a near-inifinite change in holdup. The Billet and Schultes (79) correlation is

$$u_{S,\mathrm{Fl}}^2 \frac{\rho_G}{\rho_L} = \frac{2}{0.3048} \frac{(\epsilon - h_{L,\mathrm{Fl}})^3}{\epsilon} \frac{h_{L,\mathrm{Fl}}}{a_p} C_{i,\mathrm{Fl}}{}^2 \left[F_{\mathrm{lv}} \left(\frac{\mu_L}{\mu_v} \right)^{0.2} \right]^{-n_{\mathrm{Fl}}} \tag{8.2}$$

F_{lv} is the flow parameter given by

$$F_{\mathrm{lv}} = \frac{L}{G} \sqrt{\frac{\rho_G}{\rho_L}} \tag{8.3}$$

$C_{i,\mathrm{Fl}}$ and n_{Fl} are given by

$$\left.\begin{aligned} C_{i,\mathrm{Fl}} &= \mathrm{C}_{1,\mathrm{Fl}} \\ n_{\mathrm{Fl}} &= 0.388 \end{aligned}\right\} \text{for } F_{\mathrm{lv}} \le 0.4 \tag{8.4}$$

$$\left.\begin{aligned} C_{i,\mathrm{Fl}} &= \mathrm{C}_{2,\mathrm{Fl}} \\ n_{\mathrm{Fl}} &= 1.416 \end{aligned}\right\} \text{for } F_{\mathrm{lv}} > 0.4 \tag{8.5}$$

a_p, ϵ, $C_{1.\mathrm{Fl}}$ and $C_{2,\mathrm{Fl}}$ are constants obtained from Table 8.2. a_p is the specific surface area and ϵ is the void fraction of the packing. $h_{\mathrm{L,Fl}}$ is the fractional liquid holdup (ft^3 liquid/ft^3 of bed) at the flood point, calculated from

$$h_{L,\mathrm{Fl}}^3 (3h_{L,\mathrm{Fl}} - \epsilon) = 6\epsilon \frac{\mathrm{Re}_L}{\mathrm{Ga}_L} \tag{8.6}$$

This gives a fourth-order equation in $h_{L,\mathrm{Fl}}$. The equation has only one solution of physical significance, given by

$$\frac{\epsilon}{3} \le h_{L,\mathrm{Fl}} \le \epsilon \tag{8.7}$$

The Reynolds number used in Eq. (8.6) is based on the liquid velocity at the flood point. The Reynolds and Galileo numbers Re_L and Ga_L are given by

$$\mathrm{Re}_L = \frac{\rho_L u_L}{0.000672 a_p \mu_L} \tag{8.8}$$

$$\mathrm{Ga}_L = \frac{g \rho_L^2}{(0.000672 \mu_L)^2 a_p^3} \tag{8.9}$$

The Billet and Schultes correlation applies both to random and structured packings, has a good theoretical basis, and was demonstrated (79) to predict a large number of flood data to within ±10 percent. On

TABLE 6.2 Constants for Billet and Schultes Correlation (79–81)

Packing	Nominal size, in	Characteristics			Flood		Load	
		N_p, l/ft^3	a_p, ft^2/ft^3	ϵ, ft^3/ft^3	$C_{1,Fl}$	$C_{2,Fl}$	$C_{1,Lo}$	$C_{2,Lo}$
Metal Random Packings								
Pall® ring	2	176.8	34.3	0.951	1.580		2.725	
	1.4	552.7	47.9	0.946	1.679		2.629	
	1.0	1345.1	65.5	0.942	2.083		2.627	
	⅝	6490.9	112.3	0.933	2.081		2.550	
Hiflow® ring	2	141.6	28.1	0.977	1.626		2.702	
	1	1130.3	60.5	0.962	2.177		2.918	
Bialecki ring	2	177.8	36.9	0.966	1.896	1.627	2.916	3.616
	1.4	514.7	47.2	0.965	1.865	1.883	2.753	3.850
	1.0	1472.5	68.6	0.945	1.856	1.782	2.521	3.412
CMR®	1.5	1720.1	53.3	0.974	1.841		2.697	
	1.0	4487.3	70.9	0.971	1.996		2.703	
	⅝	15,686	103.6	0.951				
Raschig ring	⅝	10,838	177.5	0.917				
Plastic Random Packings								
Pall® ring	2	188.7	31.1	0.926	1.757		2.616	
	2(Grid)				1.886		2.967	
	1.4	472.4	45.2	0.907	1.742		2.654	
	1.0	1481.0	68.6	0.880	2.064	2.252	2.696	4.062
Hiflow® ring	3.5				1.597		2.853	
	2	198.1	36.6	0.924	1.871		2.894	
	2(Super)				1.702		2.866	
	1				1.989		2.842	
Bialecki ring	2				1.540	1.366	2.558	3.221

Plastic random packings (*Continued*)								
Nor-Pac®	2	218.3	29.0	0.949	1.786		2.959	
	1.4	485.5	42.4	0.930	2.242		3.179	
	1	1260.1	54.9	0.927				
	1 Type A				2.656		3.419	
	1 Type B				2.472		3.277	
	1 Type C				2.156		2.990	
	1 10-web				2.083		2.865	
	⅜				2.173		2.893	
	⅝	5486	97.4	0.918	2.406	2.246	2.911	3.881
Intalox® saddle	2				1.548		2.362	
	2(grid)				1.657		2.675	
	1.4				1.600		2.317	
Raiu® Ring	2				1.812		2.843	
Jaeger Tri-Paks®	1¼	339.8	42.5	0.928				
Tellerette®	1¼	1048.8	57.9	0.930				
	1				2.132		2.913	

TABLE 8.2 Constants for Billet and Schultes Correlation (79–81) (*Continued*)

Packing	Nominal size, in	Characteristics			Flood		Load	
		N_p, l/ft^3	a_p, ft^2/ft^3	ϵ, ft^3/ft^3	$C_{1,Fl}$	$C_{2,Fl}$	$C_{1,Lo}$	$C_{2,Lo}$
Ceramic Random Packings								
Pall® ring	2	182.8	36.9	0.770	1.913	1.830	2.846	3.762
Hiflow® ring	3				1.565		2.903	
	2				1.694		2.819	
	1.4				1.667		2.664	
	¾(4 webs)	2873	72.9	0.797	2.410		2.875	
	¾(6 webs)	3126	81.0	0.776				
Raschig ring	2				1.574	1.499	2.482	3.312
	1	1483	61.4	0.640	1.899	1.950	2.454	3.450
	⅝	6230	94.5	0.690				
	¾	24000	150.0	0.570				
Berl saddle	1	1770	72.0	0.725				
	½	15000	133.0	0.660				
Stacked Random Packing								
Pall® ring (ceramic)	2	212.7	42.3	0.670	3.024		3.793	
Impulse packing (ceramic)	2	215.2	31.1	0.830	1.655	1.505	2.664	3.401
	2,N	237.4	34.3	0.816	1.917		3.004	
	2,N,T	235.3	42.1	0.766				
Bialecki packing (metal)	1.4	587.2	53.8	0.960				
	1	2218	101.0	0.940	2.794		3.411	

Structured Packings—Metal								
Gempak®	A2 T-304	—	61.6	0.977	2.099		2.986	
Ralu® pak	250	—			2.558		3.178	
Impulse packing	250	—	76.2	0.975	1.996	1.838	2.610	3.458
Montz B1®	100	—	30.5	0.987	1.911		3.089	
	200	—	61.0	0.978	2.339		3.116	
	300	—	91.4	0.930	2.464	2.034	3.098	3.616
Structured Packings, Plastic								
Mellapak®	250Y	—	76.2	0.960	2.464		3.157	
Montz C2®	200	—			1.973		2.653	
Euroform®	110	—	33.5	0.936	1.975		3.075	

the debit side, the constants required for using the correlation are unavailable for many common packings.

Mersmann's correlation and Maćkowiak's correlation. Mersmann (73) postulated that a thin liquid film forms in the flow channel of the packing. The ratio of film thickness to equivalent packing diameter is a function of the liquid load. Mersmann combined this function with a trickle flow model to yield an expression for dry packing pressure drop at flood as a function of liquid rate. Maćkowiak (73*a*) surveyed sources that followed up and improved on Mersmann's initial model.

Maćkowiak (73*b*) compared predictions from Mersmann's correlation to a massive data bank. He found that Mersmann's correlation gave good prediction for the low-capacity first-generation packings (for which it was derived), but grossly optimistic flood predictions for modern high-capacity random and structured packings. As packing capacity increases, the flood pressure drop did not stay constant, as predicted by the correlation, but became smaller as described earlier. These problems are identical to those reported with the GPDC chart.

Maćkowiak (73*a*,73*b*) derived a new flood correlation. Like the Billet and Schultes correlation, it is based on the drop entrainment model and takes liquid holdup into account. Unlike Billet and Schultes, Maćkowiak uses a different set of premises and expressions. Maćkowiak's correlation applies for both random and structured packings, has a good theoretical basis and was shown (73*a*,73*b*) to predict a large number of flood data to within ±8 percent. On the debit side, the correlation is complex and requires the availability of four constants for each packing. Maćkowiak also states (73*a*) that for high liquid rates, Mersmann's film model is more suitable than his drop model.

Flood prediction by interpolation. GPDC interpolation plots are used to interpolate actual flood data. Data interpolation gives accurate flood-point prediction, but can only be used where sufficient flood point data are available.

Until recently, interpolation using GPDC plots was the only published method for predicting structured packing flood points. Figure 8.18 shows GPDC flood plots by Fair and Bravo (50), Billet (3,50), Spiegel and Meier (21), and Dolan, Hausch, and Petschauer (2,24, 31*e*) for several structured packings. Billet (3,56), Fair (41), and Maćkowiak (73*b*) present GPDC plots also for many random packings. MacDougall (58) checked Billet's plots for Raschig and Pall® rings against data and found them to give good flood predictions.

Chapter 10 presents a compendium of GPDC data interpolation charts for flood, MOC, and pressure drop prediction, both for random and structured packings. When flood data are absent, pressure drop data can be used for approximating the flood point using Eq. (8.1).

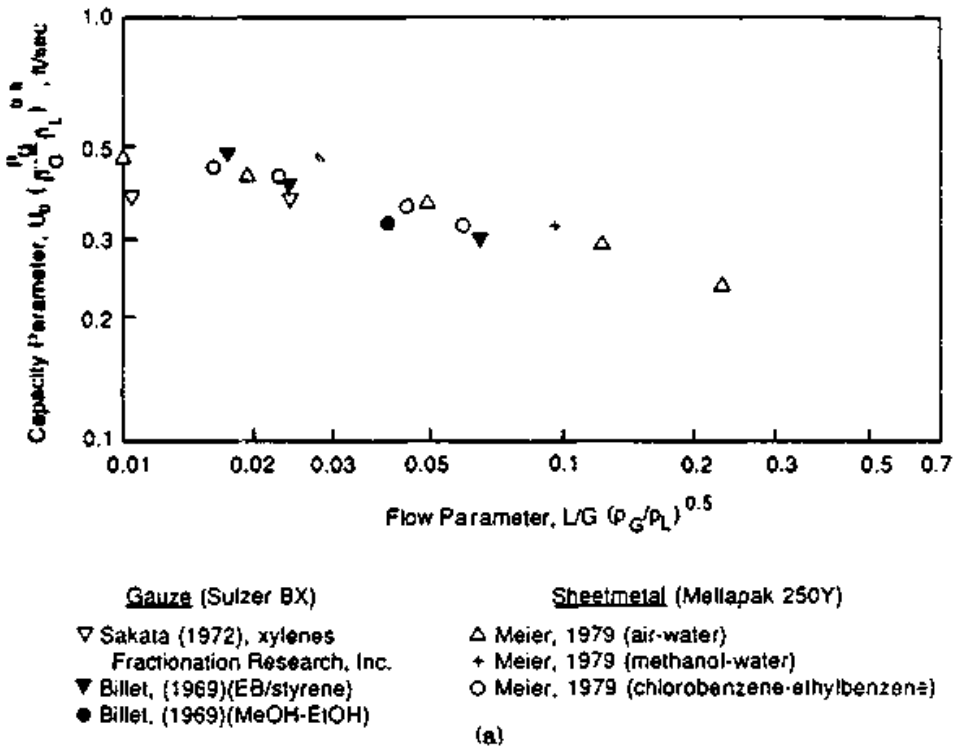

Figure 8.18 GPDC interpolation plots for structured packings flood points. (*a*) The Fair and Bravo plot for Sulzer BX® and Mellapak® 250Y. (*Part a, from J. R. Fair and J. L. Bravo, I. Chem. E. Symp. Ser. No. 104, p. A183, 1987; reprinted courtesy of the Institution of Chemical Engineers (UK).*)

For random and structured packings, all the flood data plotted on the GPDC interpolation charts of Chapter 10 are based only on definitions that describe incipient flooding (Sec. 8.2.3). Unfortunately, for grids, all literature flood data are based on the definition "the gas velocity at which the packing pressure drop reaches 2 in of water per foot of packing." This definition describes "fully developed" rather than "incipient" flood (Sec. 8.2.3). For lack of alternative, those data were plotted on charts 10.8005 to 10.8108. Therefore, for grids only, interpolation of flood data points (charts 10.8005 to 10.8218, four charts only) is likely to yield capacities roughly 10 to 15 percent higher than incipient flooding.

Others. Flood correlations are often available in the manufacturer literature (e.g., 8,31,82) or on manufacturers' computer disks. A flood correlation by Beck (83) was shown by MacDougall (58) to be accurate, but applies only for Pall® and Raschig rings and Berl and Intalox® saddles.

Which method to use. Data interpolation is generally the most accurate and should be preferred whenever flood data are available. Otherwise either if pressure drop data are available or when pressure drop can be reliably predicted, Eq. (8.1) is recommended. When the packing factor F_p exceeds 60, the Eckert correlation, Fig. 8.17 is recommended. At

System		Packing	Type	p_t	a_s	H
				mbar	m	m
Air/Water, 293 K	•	Mellapak	250 Y	1000	0.30	
"	▲	Rolu Pak	250 YC	1000	0.45	1.8
"	⊖	Montz	B1 300	1000	0.22	1.45
"	■		B1 300	1000	0.45	1.7
"	▽		B1 200	1000	0.22	1.4
"	▼		B1 100	1000	0.30	1.4
Chlorobenzene/ Ethylbenzene	◆		B1 300	66.7	0.22	1.4

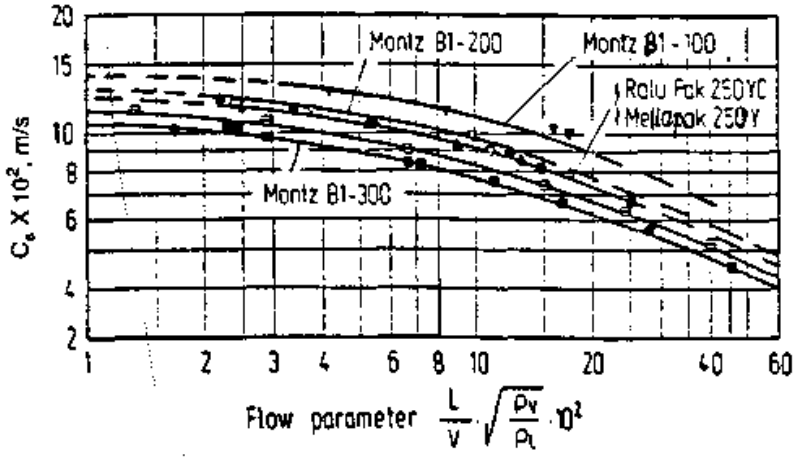

(b)

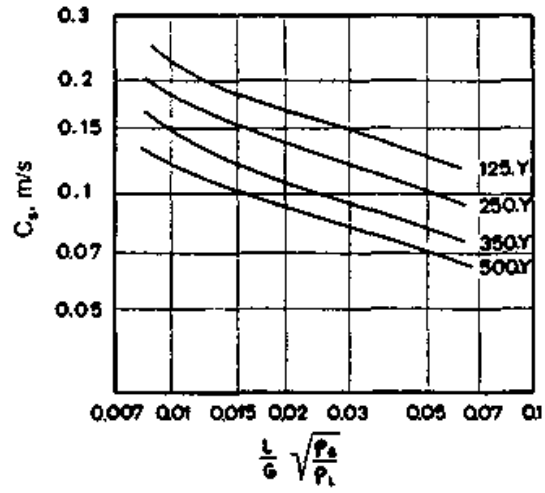

(c)

Figure 8.18 (*Continued*) GPDC interpolation plots for structured packings flood points. (*b*) The Billet plot for several structured packings; (*c*) the Spiegel and Meier plot for Mellapak®. (*Part b from R. Billet,* Packed Column Analysis and Design, *Ruhr University, Bochum, 1989, reprinted courtesy of Ruhr University; part c, from L. Spiegel and W. Meier, I. Chem. E. Symp. Ser. 104, p. A203, 1987; reprinted courtesy of the Institution of Chemical Engineers (UK).*)

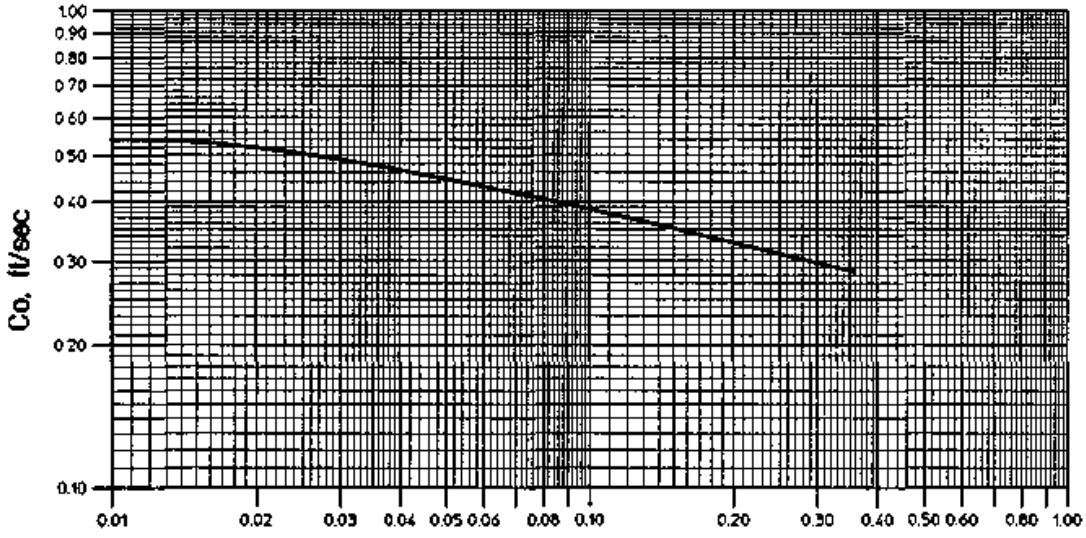

FLOW PARAMETER, X

$$\text{Efficient Capacity, Csc} = \text{Co}\left[\frac{\sigma}{20}\right]^{0.16}\left[\frac{\mu}{0.2}\right]^{-0.11}$$

1) Calculate flow parameter, X
2) Find Co from graph
3) Calculate Csc from equation
4) % efficient capacity = $\frac{Cs}{Csc} \cdot 100$

SUGGESTED LIMITS ON PHYSICAL PROPERTY CORRECTION FACTORS:

$5 \le \sigma \le 73$

$0.07 \le \mu \le 1.1$

NOMENCLATURE

PROPERTY	SYMBOL	BRITISH UNITS	METRIC UNITS	DEFINITIONS
Gas Rate	G	Lbs/ft² sec	KG/M² sec	$X = \frac{L}{G}\frac{\sqrt{\rho_G}}{\sqrt{\rho_L}}$
Liquid Rate	L	Lbs/ft² sec	KG/M² sec	
Gas Density	ρ_G	Lbs/ft³	KG/M³	$Cs = \frac{G}{\sqrt{\rho_G}\sqrt{\rho_L - \rho_G}} = \frac{Fs}{\sqrt{\rho_L - \rho_G}}$
Liquid Density	ρ_L	Lbs/ft³	KG/M³	
Liquid Viscosity	μ	Centipoise	Centipoise	$Fs = \frac{G}{\sqrt{\rho_G}}$
Surface Tension	σ	Dyne/Cm	Dyne/Cm	

(d)

Figure 8.18 (*Continued*) GPDC interpolation plots for structured packings flood points. (*d*) The Dolan, Hausch and Petschauer plot for Intalox® 2T Structured Packing. (*Part d, from G.W. Hausch, P. Quotson, and K. Seeger, "Structured Packing Revamp of a 305 Psig Depropanizer," paper presented at the AIChE Annual meeting, Los Angeles, California, November 1991; reprinted courtesy of the Norton Company.*)

vacuum and low superatmospheric pressures, and when the appropriate constants are available, the Billet and Schultes correlation is also recommended.

8.2.7 Maximum operational capacity (MOC) prediction

MOC correlations for proprietary packings are sometimes available in the manufacturer literature (e.g., 15,30) or on manufacturers' com-

puter disks. The only other published correlation is by Kister and Gill (60,60*a*). This correlation simply states

$$u_{S,\text{MOC}} = 0.95u_{S,\text{Fl}} \tag{8.10}$$

where u_{Fl} is evaluated from Eq. (8.1). This correlation was shown (60,60*a*) to predict practically all published MOC data to within ±20 percent and most published MOC data are within ±15 percent, for both random and structured packings.

For some high-capacity structured packings of unique geometry, such as the Norton Intalox® 2T and the Jaeger MaxPac™, combining Eq. (8.1) with Eq. (8.10) predicts MOCs that are consistently 10 to 15 percent low. Although this is well within the correlation accuracy, it suggests that the correlation does not distinguish the unique high-capacity features of these two structured packings.

8.2.8 Pressure drop prediction by correlation

Limitations of packed-tower pressure drop correlations are systematic rather than random. It has been demonstrated (60) that a correlation that gives excellent statistical fit to experimental data can give poor predictions for many situations commonly encountered in industrial practice. This anomaly originates from a bias in pressure drop data banks toward the air-water system, and from a data shortage for nonaqueous systems at pressure, vacuum, and high and low liquid rates. Further, a correlation may work well for the majority of packing types and poorly for only a few, but the user can rarely tell (without plotting data) whether the packing under consideration is one of the few for which the correlation does not work.

An excellent statistical fit to data is therefore insufficient to render a packing pressure drop correlation suitable for design. In addition to a good fit to data, the correlation limitations must be fully explored. Most published packing pressure drop correlations fail miserably here: their limitations are often unknown, and if known, are seldom reported.

Interpolation of actual experimental data circumvents the systematic correlation limitations, gives reliable and accurate pressure drop prediction, is difficult to computerize, and requires that suitable interpolation charts are available. This section deals with predicting pressure drop by correlation. Section 8.2.9 describes interpolating experimental pressure drop data.

Neither correlation nor interpolation can overcome the limitations inherent in pressure drop *data* (Sec. 8.2.5). It is therefore essential

that the user be aware of these when applying either correlation or interpolation.

The Eckert generalized pressure drop correlation (GPDC) chart. For many decades, the Eckert GPDC chart has been the standard of the industry for random packing pressure drop prediction. Even though it has fallen in popularity in the last couple of decades, this method is still recommended by many recent design publications (1,14,15,17,41). It is based on work by Leva (70), who introduced constant pressure drop curves on the Sherwood flooding chart (Fig. 8.17). Leva's chart was later refined by Eckert (1,53,72,74), Prahl (85), and Strigle et al. (5,15,77). Recent charts by Eckert (74) and Strigle et al. (5,15,77) omit the flooding curve (see Sec. 8.2.6). Figure 8.19*a* and *b* shows the latest (Strigle) versions of the Eckert GPDC chart (15). These two diagrams are identical, except that in Fig. 8.19*b*, Strigle changed the scales from log-log to semilog to make readings between adjacent pressure drop curves easier to obtain.

Both agreement (75,86) and disagreement (87,88) between measured pressure drops and those predicted by the Eckert GPDC have

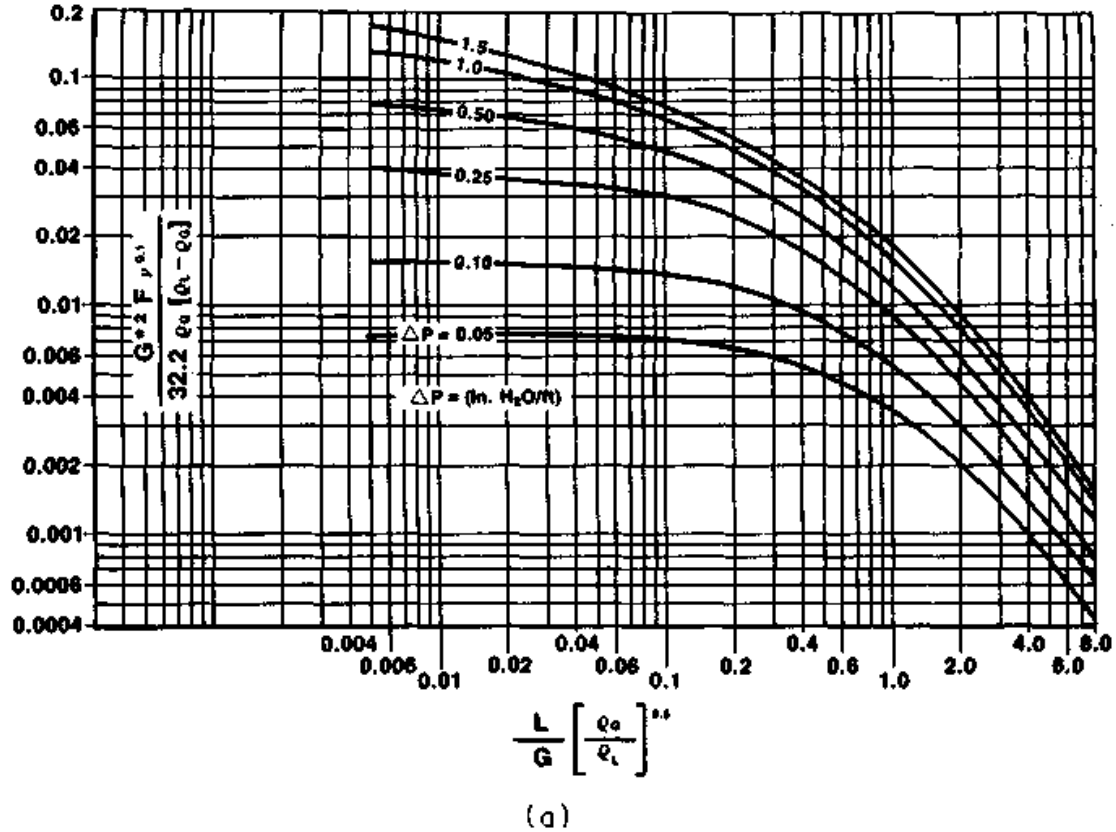

Figure 8.19 The latest version of the GPDC pressure drop correlation. (*a*) The latest log-log version of Eckert's correlation, as presented by Strigle (15). (*Part a from Ralph F. Strigle, Jr.*, Random Packings and Packed Towers. *Copyright © 1987 by Gulf Publishing Company, Houston, Texas. Used with permission. All rights reserved.*)

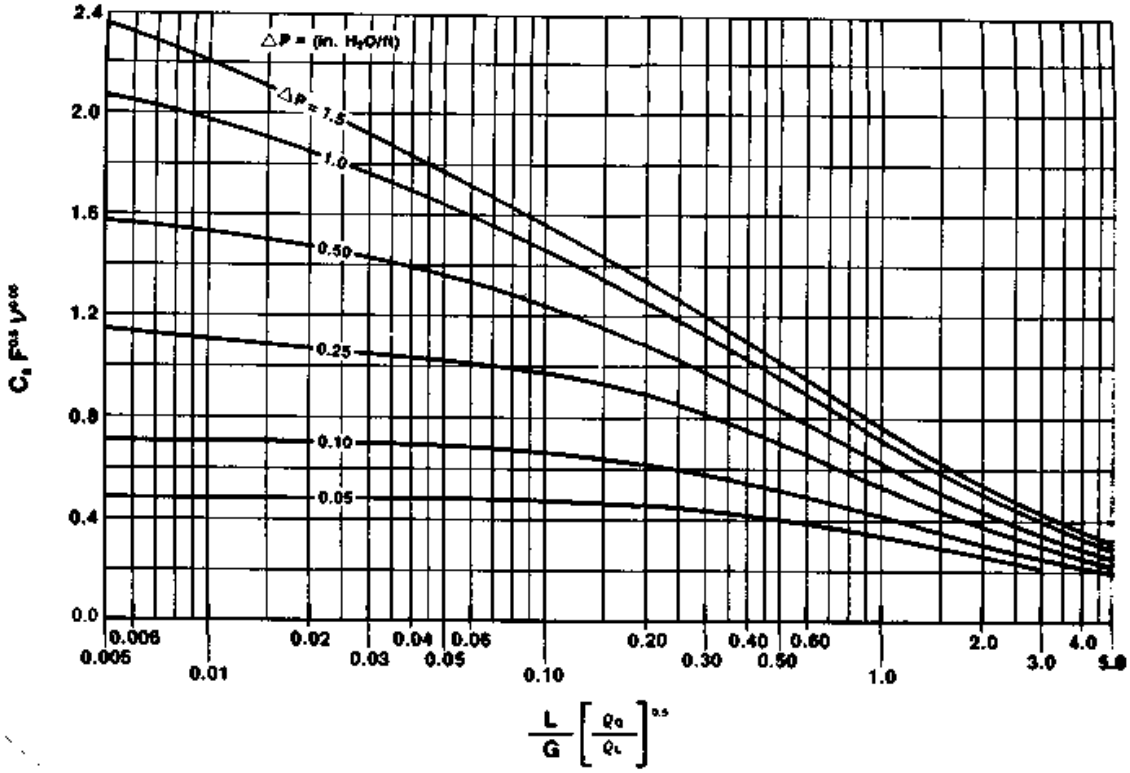

(b)

Figure 8.19 (*Continued*) The latest version of the GPDC pressure drop correlation. (*b*) A version identical to part *a*, but plotted on semilog paper, produced by Strigle (15). (*Part b from Ralph F. Strigle, Jr.*, Random Packings and Packed Towers. *Copyright © 1987 by Gulf Publishing Company, Houston, Texas. Used with permission. All rights reserved.*)

been reported. Bolles and Fair (55) used thousands of published data to show that pressure drops predicted by the Eckert correlation need to be multiplied by a safety factor of 2.2 to 2.5 for 95 percent confidence of success. MacDougall repeated this analysis, but pruned out data in the loading and high-turndown regions, that may have contributed to such a high safety factor, and looked only at Pall® rings. His analysis yielded the same safety factor as Bolles and Fair.

Strigle (15) and Kister and Gill (60) compared predictions from the latest version of the Eckert correlation (Fig. 8.19*a* and *b*) to thousands of random packing pressure drop measurements. The Eckert correlation was shown to give good predictions for most pressure drop data (15,60). It generally works well for the air-water system for flow parameters as low as 0.01 and as high as 1 (60). For nonaqueous systems, it works well for flow parameters of 0.03 to 0.3 (typical of atmospheric distillation).

The Eckert correlation was shown (60) to be optimistic for flow parameters greater than 0.3 (typical of pressure distillation and/or high liquid rate applications). Strigle (15) attributes these optimistic predictions to enhanced liquid frothiness at higher pressure. The en-

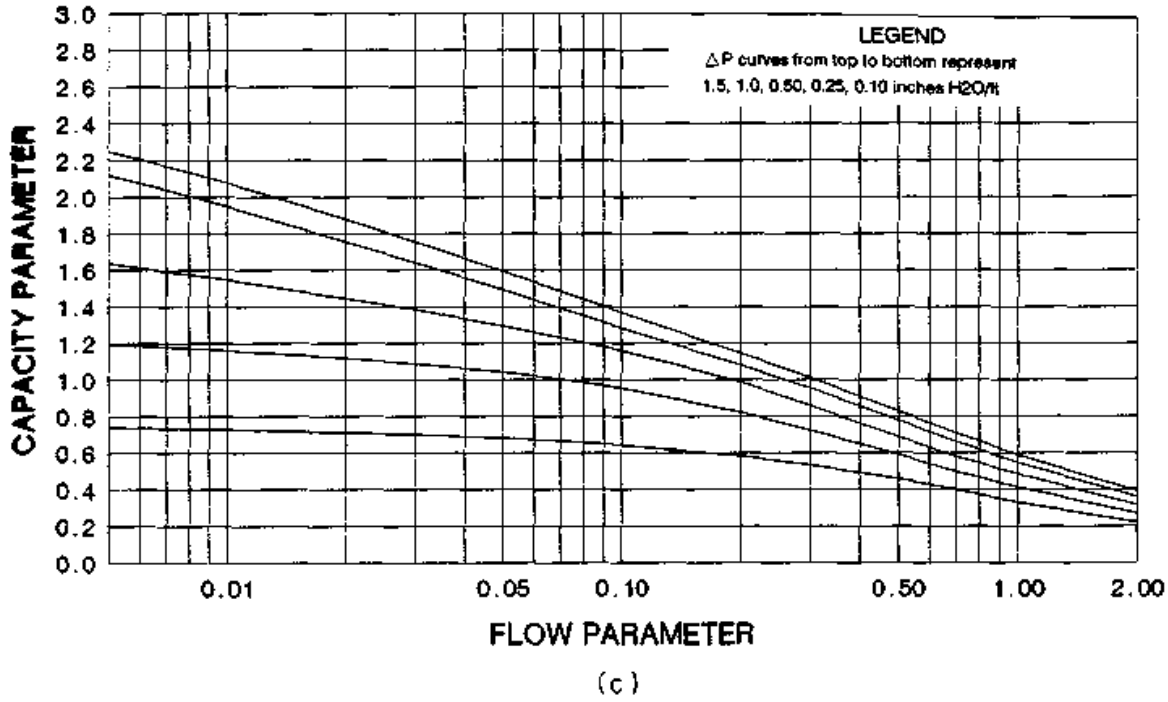

Figure 6.19 (*Continued*) The latest version of the GPDC pressure drop correlation. (*c*) The Kister and Gill GPDC (SP) chart for structured packings only.

hanced frothiness may also be explained by a switch from a vapor- to a liquid-continuous dispersion, which, according to Billet and Schultes (78,79), takes place at a flow parameter of 0.4. It is worth noting that the prediction difficulty at higher flow parameters is not unique to the Eckert correlation, but has also been noticed in other correlations (73*b*,78,79).

For nonaqueous systems, the Eckert correlation is also optimistic for flow parameters lower than 0.03, which are typical of vacuum distillation and/or low liquid rates. Robbins (89) shows that the GPDC correlation use of liquid density and liquid viscosity is invalid at low flow parameters, where liquid properties should have little effect on pressure drop. It is worth noting that according to Robbins, this prediction difficulty is not unique to the Eckert correlation, but will be encountered whenever a correlation predicts a pressure drop dependence on liquid properties at low liquid rates.

Predictions from the Eckert correlation are sensitive to the packing factor (Sec. 8.2.10). Strigle (15) and Kister and Gill (60) found that most packing factors reported in the literature are satisfactory. However, for a few packings, the packing factors gave poor fit to experi-

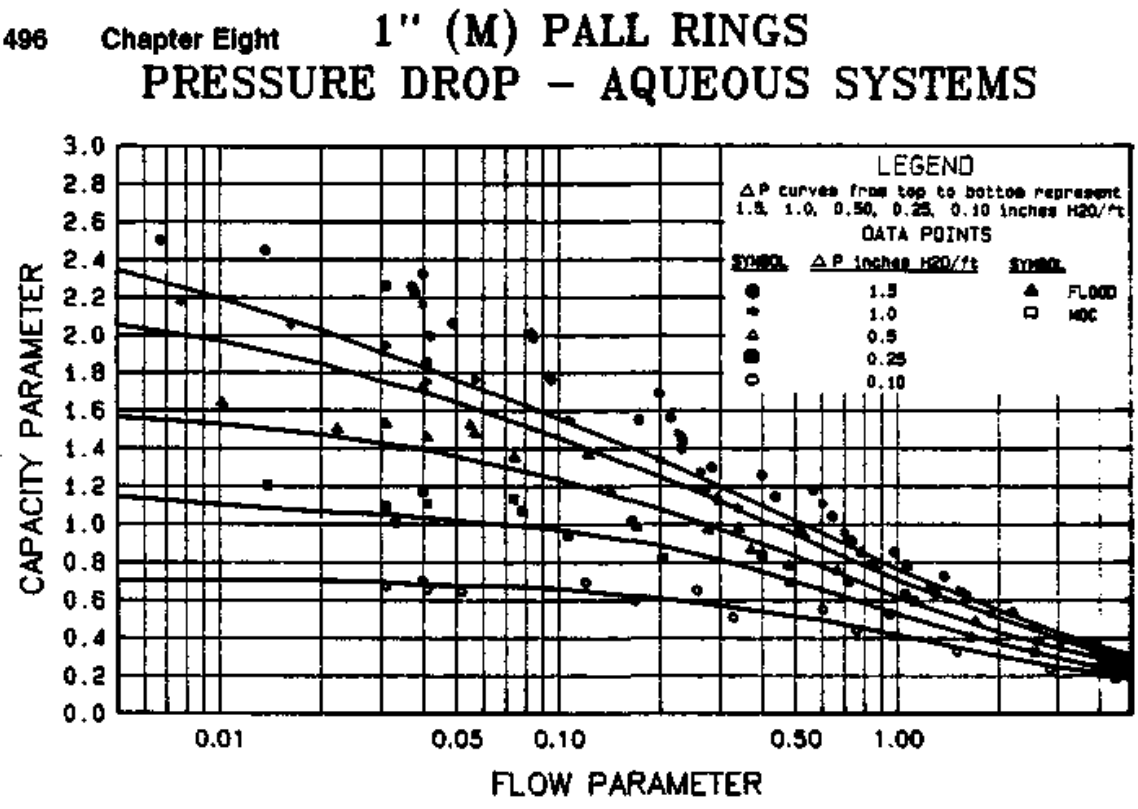

(d)

Figure 8.19 (*Continued*) The latest version of the GPDC pressure drop correlation. (*d*) Superimposing experimental pressure drop data for a given packing generates a GPDC interpolation chart for this packing.

mental pressure drop data (60). Also, for some packings, the dependence of pressure drop on vapor and liquid loads was not adequately predicted by the Eckert correlation (15,60).

The Kister and Gill generalized pressure drop correlation for structured packings [GPDC (SP)] charts. The latter limitation above severely obstructed attempts to apply the Eckert correlation to structured packings. Specifically, in structured packings, pressure drop rise with flow parameter is much steeper than the Eckert GPDC curves predict. The Eckert curves are based on random packing data, and for these, the capacity fall-off and the pressure drop rise with higher flow parameters are much milder than in structured packings (see Sec. 8.1.10).

Kister and Gill (31*b*) modified the Eckert chart curves empirically to fit structured packing data. For structured packings, this modified chart (Fig. 8.19c) was shown (31*b*) to give much better predictions than the Eckert chart. For flow parameters between 0.02 and 0.2 for nonaqueous systems or 0.01 and 1 for air-water, and for packing factors between 6 and 30, Fig. 8.19c was shown (31*b*) to work well for all

structured packings. Packing factors to be used with the GPDC (SP) chart (Fig. 8.19c) are listed in Table 10.1.

Outside the above range, there are regions where Fig. 8.19c gives less reliable predictions of pressure drop. For some structured packings with high (>30) packing factors, the rate of rise of pressure drop with flow parameter or vapor velocity differs from that predicted by Fig. 8.19c. For nonaqueous systems, a region of prediction uncertainty exists at high flow parameters ($F_{lv} > 0.3$).

The Robbins correlation (89). As an alternative to the GPDC, Leva (70) derived an equation for pressure drop. For a dry bed, pressure drop can be calculated from a momentum balance.

$$\Delta P = C_1 \rho_G u_s^2 \tag{8.11}$$

In order to allow for irrigation, Leva modified the dry pressure drop correlation to give

$$\Delta P = C_1 10^{(C_2 u_L)} \rho_G u_s^2 \tag{8.12}$$

Leva's equation applies to gas-continuous operation only (70,84). At very high liquid loads, pressure drop is not proportional to the square of the vapor velocity (Sec. 8.2.1, Fig. 8.15), and Eq. (8.12) does not apply. According to Billet and Schultes (78,79), the transition from gas- to liquid-continuous operation occurs at a flow parameter [Eq. (8.3)] of 0.4.

Robbins points out that with dry beds and at low liquid loads, liquid physical properties have practically no effect on pressure drop. This is correctly predicted by Leva's equation (8.12), but not by the GPDC chart, because the chart uses liquid viscosity and liquid density.

Robbins found that the constant C_1 in Eq. (8.12) correlates directly with the packing factor. This observation permitted him to derive packing factors from dry pressure measurements [applying Eq. (8.12) with $u_L = 0$]. He also found that the constant C_2 in Eq. (8.12) correlates well with the square root of the packing factor and the liquid viscosity to the 0.1 power. These findings permitted Robbins to express the curves shown in Fig. 8.15 in a generalized form, giving the equation

$$\Delta P = C_3 G_f^2 10^{C_4 L_f} + 0.4\left(\frac{L_f}{20{,}000}\right)^{0.1} (C_3 G_f^2 10^{C_4 L_f})^4 \tag{8.13}$$

where

$$C_3 = 7.4 \times 10^{-8} \tag{8.13a}$$

$$C_4 = 2.7 \times 10^{-5} \tag{8.13b}$$

$$G_f = G\left[\frac{0.075}{\rho_G}\right]^{0.5}\left[\frac{F_{pd}}{20}\right]^{0.5} \qquad \text{for } P \le 1.0 \text{ atm} \tag{8.14a}$$

$$G_f = G\left[\frac{0.075}{\rho_G}\right]^{0.5}\left[\frac{F_{pd}}{20}\right]^{0.5} 10^{0.3\rho_G} \qquad \text{for } P > 1 \text{ atm} \tag{8.14b}$$

$$L_f = L\left[\frac{62.4}{\rho_L}\right]\left[\frac{F_{pd}}{20}\right]^{0.5} \mu_L^{0.1} \qquad \text{for } F_{pd} \ge 15 \tag{8.15a}$$

$$L_f = L\left[\frac{62.4}{\rho_L}\right]\left[\frac{20}{F_{pd}}\right]^{0.5} \mu_L^{0.1} \qquad \text{for } F_{pd} < 15 \tag{8.15b}$$

Equation (8.13) states that pressure drop is the sum of two terms. The first term describes the friction loss through the packing, and is the only important term in the preloading regime and when L_f is below 20,000. Under these conditions, the pressure drop is proportional to the square of the gas rate. The second term describes the increase in the slope of the pressure drop with gas rate in the loading regime.

Equation (8.13) applies only for $L_f \le 20{,}000$. Figure 8.20 is a graph of the Robbins correlation that applies for values of L_f both below and above 20,000. When $L_f > 20{,}000$, only Fig. 8.20 should be used, not Eq. (8.13) (89,90).

For some packings with dry-bed packing factors F_{pd} lower than 15, Eq. (8.15*a*) does not accurately represent the liquid rate dependence. Equation (8.15*b*) gives a better preliminary estimate of L_f at these lower packing factors. Due to the approximation involved, L_f jumps up by a factor of about 1.5 when F_{pd} changes from 15 to 14.

The Robbins correlation applies at atmospheric pressure and under vacuum, but not at elevated pressures (90). Equation (8.14*b*) includes a gas density correction term for a preliminary estimate at pressures exceeding atmospheric. Due to the approximation, Eq. (8.14*b*) is unsuitable for design (90). Generally, the Robbins correlation is not recommended for superatmospheric pressures (90).

At very high liquid rates, pressure drop for nonaqueous systems can be considerably higher than with aqueous systems (60). In this very high liquid rate region (flow parameter > 0.3), Robbins's correlation was extensively tested only for aqueous systems. Caution is required.

For a dry packed bed ($L = L_f = 0$) at atmospheric pressure, Eq. (8.13) reduces to

$$\Delta P_d = 0.00375\, C_3\, F_{pd}\, \frac{G^2}{\rho_G} \tag{8.16}$$

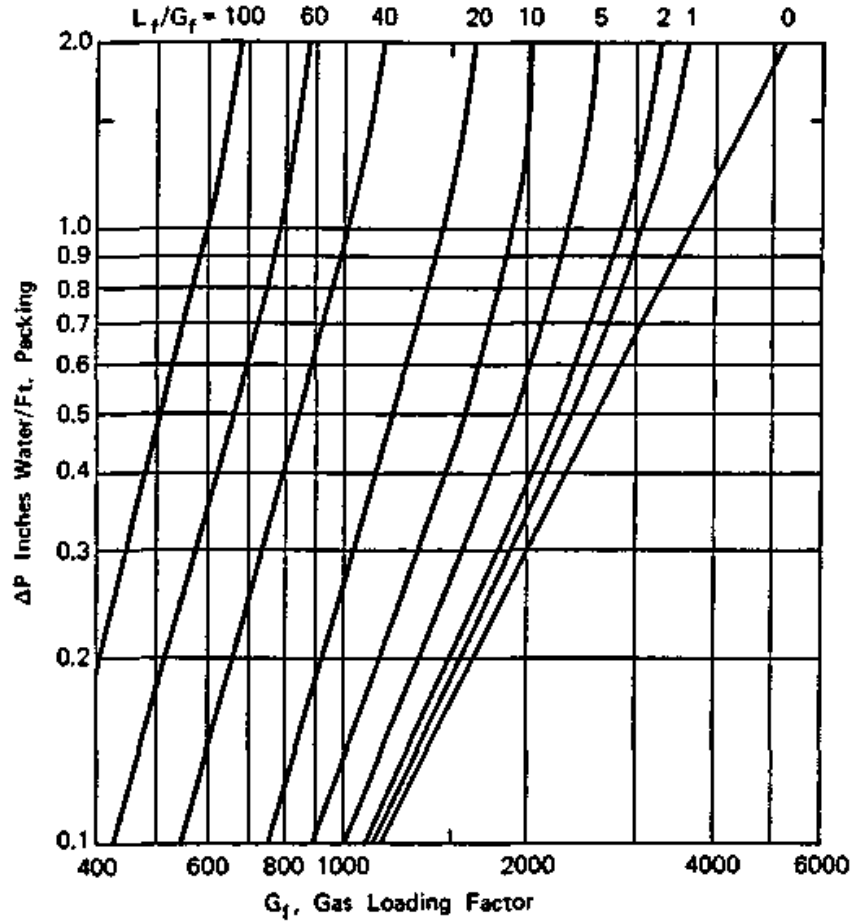

Figure 8.20 The Robbins generalized pressure drop correlation. (*From L. A. Robbins,* Chem. Eng. Progr., *May 1991, p. 87. Reprinted courtesy of the American Institute of Chemical Engineers.*)

Equation (8.16) permits estimating F_{pd} for any packing from dry pressure drop measurements. Table 8.3 gives F_{pd} for various commercial packings. A more comprehensive list is elsewhere (89). The dry packing factors in Table 8.3 are those to be used in Eqs. (8.14) and (8.15).

Theoretical correlations. Two approaches have been used for theoretically modeling packed-tower pressure drop:

1. *The channel model:* This model attributes packed-column pressure drop to the resistance to flow in a multitude of parallel channels. The channels may have bends in them or may have contractions and enlargements. Liquid flows down the walls of the channel, thus consuming some of the available cross-section area. This in turn increases the pressure drop. The channel model has been applied both for random and structured packings (e.g., 3,62,73*b*,78,91,92,92*a*). A popular application of this model is the Bravo et al. (91) correlation for structured-packing pressure drop:

TABLE 8.3 Dry Bed Packing Factors for the Robbins Pressure Drop Correlation (89)

Random Packings

Packing	Material	Data supplier	Size (inches, *or* number, *or* metric number)								
			Inch	⅝	1	1.5	2	2.5	3	3.5	
			No.	0.7	1	1.5	2	2.5	3	3.5	4
			MNo	15	25	40	50	60	70		
Raschig rings (1/16-in wall)	Metal	Norton	Inch		150	84	68				
Pall® rings	Metal	Norton	Inch	80	53	28	24				
Ballast® rings	Metal	Glitsch	Inch		37	30	19			14	
Flexirings®	Metal	Koch	Inch				25				
Hy-Pak®	Metal	Norton	No		40	26	17		13		
Ballast® Plus	Metal	Glitsch	MNo					14			
Chempak®	Metal	Chem-Pro	No		29		17				
Cascade® MiniRings	Metal	Glitsch	No		31		24		13		9.8
Metal Intalox®	Metal	Norton	MNo	51	43	26	17				
Nutter rings®	Metal	Nutter	No	39	27	20	17	15	11		
Pall® rings	Plastic	Norton	Inch	106	55	40	25			12	
Ballast® rings	Plastic	Glitsch	Inch		42	34	20			13	
Cascade® MiniRings	Plastic	Glitsch	No*		28		28		10		
Super Intalox® saddles	Plastic	Norton	No		40		26		14		
Ballast® saddles	Plastic	Glitsch	No		49		23		14		
Levapak®	Plastic	Leva	No				16				
Tri-Packs®	Plastic	Jaeger	Inch				13				
Tellerettes®	Plastic		No		40						
Raschig rings	Ceramic	Norton	Inch		150	80	70				
Berl saddles	Ceramic	Koch	Inch		94	47	31				
Intalox® saddles	Ceramic	Norton	Inch		94	50	37		20		
Super Intalox® saddles	Ceramic	Norton	Inch		62		31				

Structured Packings and Grids (Metal)

Packing	Data supplier	No.		Type (Number)			
		Other		1	2	3	4
Flexipac®	Koch	No	—	32	11	4.5	3.2
Koch-Sulzer BX®	Koch	Other	16				
Monts A-2®	Chem-Pro	Other	23				
Hyperfil®	Chem-Pro	Other	140				
Neo-Kloss®	Chem-Pro	Other	6				
Glitsch Grid® EF25A	Glitsch	Other	5				

*The number is followed by a suffix A; for instance, No. 1 means Cascade® MiniRing No. 1A.

$$\Delta P = \left(0.395 + \frac{214.3}{\mathrm{Re}_G}\right)\left(\frac{\rho_G u_{\mathrm{eff}}^2}{d_{\mathrm{eq}}\, g_c}\right)\frac{1}{(1 - C_5\mathrm{Fr}^{0.5})^5} \tag{8.17}$$

where

$$u_{\mathrm{eff}} = u_S/(\epsilon \sin\theta) \tag{8.18}$$

$$\mathrm{Re}_G = 124\,\frac{d_{\mathrm{eq}}\, u_{\mathrm{eff}}\, \rho_G}{\mu_G} \tag{8.19}$$

$$\mathrm{Fr} = \frac{12\,u_L^2}{d_{eq}\,g} \tag{8.20}$$

Values of θ, d_{eq}, ϵ, and C_5, where available, and the range of data used for deriving the correlation, are listed in Table 8.1. For the Sulzer BX® packing, data from several systems were used in the correlation deviation, but for corrugated-sheet packings, only air-water data were used.

2. *The particle model:* This model attributes pressure drop to friction losses due to drag of a particle. The presence of liquid reduces the void fraction of the bed and also increases the particle dimensions. Ergun (94) applied this model for single-phase flow (e.g., fixed and fluidized beds). Stichlmair et al. (95) successfully extended this model to correlate pressure drop and flood for both random and structured packings. Their correlation is complex and requires some additional validation, but is the most fundamental correlation available.

Which method to use? This question is addressed in the next section.

8.2.9 Pressure drop prediction by interpolation

Interpolation of pressure drop data is more accurate and reliable than correlation prediction. However, it requires that an interpolation chart be available, and is difficult to computerize.

GPDC interpolation. Superimposing experimental data points (for a given packing) on the curves of generalized pressure drop correlation (GPDC) chart (Sec. 8.2.8) converts the GPDC chart into an interpolation chart (for the packing), e.g., Fig. 8.19*d*. Pressure drops are calculated by interpolating the plotted pressure drop data. The correlation curves help guide the interpolation. Chapter 10 contains the entire atlas of interpolation charts and an application procedure.

For random and grid packings (Fig. 8.19*d*, and Charts 10.1002 to 10.3517 and 10.8005 to 10.8205 in Chap. 10), the curves on the interpolation charts are those of the Strigle version of the Eckert GPDC (Fig. 8.19*b*). For structured packings (Charts 10.5001 to 10.6504), the curves on these interpolation charts are those of the Kister and Gill GPDC (SP) (Fig. 8.19c). For all charts (random, structured or grid packings), the abscissa of the correlation is the flow parameter, given by

$$F_{lv} = \frac{L}{G}\left(\frac{\rho_G}{\rho_L}\right)^{0.5} \tag{8.21}$$

For all charts (random, structured, and grid packings), the ordinate of the correlation is the capacity parameter, given by

$$\text{Capacity parameter} = C_S F_p^{0.5} \nu^{0.05} \tag{8.22}$$

In Eq. (8.22), ν is the kinematic viscosity of the liquid. [*Note:* The kinematic viscosity (centistokes) is obtained by dividing the dynamic viscosity (centipoises) by the specific gravity, *not* by the liquid density).] C_S is the C-factor, i.e., the superficial gas velocity corrected for vapor and liquid densities, given by

$$C_S = u_S \sqrt{\frac{\rho_G}{\rho_L - \rho_G}} \tag{8.23}$$

F_p is the packing factor, which is an empirical factor characteristic of the packing size and shape. The packing factor to be used is marked on each GPDC interpolation chart in Chap. 10. Table 10.1 lists the values and sources of these packing factors.

Flood and maximum operational capacity (MOC) data are also plotted on the GPDC interpolation charts, and the charts can be used for interpolating these. Where flood and MOC data are absent, Eqs. (8.1) and (8.10) can be used for inferring flood points and MOCs from pressure drop data on the charts.

The suitability of the GPDC interpolation charts as a basis for interpolation is not accidental. Packing pressure drops correlate extremely well with GPDC coordinates, i.e., the flow parameter and the capacity parameter. The dependence does not always follow the correlation contours, but always appears to exist. Further, the correlation coordinates are essentially a "performance diagram," i.e., a plot of a vapor load against liquid load, a tool commonly used for analyzing column performance.

The conversion of the GPDC into interpolation charts overcomes the multitude of correlation limitations (Sec. 8.2.8). The GPDC interpolation charts readily identify any regions where data veer off the correlation curves and give reliable estimates (by data interpolation) in these regions. Packing factors, often criticized for being inaccurate and inconsistent (Sec. 8.2.10), cease to be critical variables. Inaccuracies in packing factors merely cause data to veer off the curves, and have no effect on the interpolation.

It may be argued that the interpolation procedure breaks down when data are absent. The counter argument is that the GPDC correlation curves are always there to fall back on and get a prediction, but now there is also a tool to warn that there are no data in this region and that uncertainty is involved.

One problem that the GPDC interpolation charts cannot solve is the

inherent *data* limitations (Sec. 8.2.5). Even here these charts help. Table 10.1 lists the source of data and experimental conditions. This information is essential for evaluating and allowing for the uncertainty associated with the inherent data limitations.

A shortcoming of the GPDC interpolation data chart procedure is that it replaces a single correlation chart by an atlas. The interpolation charts consume more storage space in the design manual or on the computer and require a greater updating effort.

Robbins interpolation procedure (89,90). This procedure makes use of pressure drop versus gas rate plots at constant liquid rate for a reference system. For most packing, such plots are available in the manufacturer's literature (e.g., 8,10,12,13,22,24,31,82), usually with air-water as the reference system. The plots look exactly like Fig. 8.15, but contain curves for many liquid rates.

The Robbins correlation [Eq. (8.13) or Fig. 8.20] expresses the pressure drop as a function of G_f and L_f alone. Applying Eq. (8.14*a*) for the reference system gives

$$G_f = G_{\text{ref}}\left(\frac{0.075}{\rho_{G,\text{ref}}}\right)^{0.5}\left(\frac{F_{\text{pd}}}{20}\right)^{0.5} \tag{8.24}$$

Combining Eqs. (8.14*a*) and (8.24) gives

$$G_{\text{ref}} = G\left(\frac{\rho_{G,\text{ref}}}{\rho_G}\right)^{0.5} \tag{8.25}$$

A similar application of Eq. (8.15*a*) gives

$$L_{\text{ref}} = L\left[\frac{\rho_{L,\text{ref}}}{\rho_L}\right]\left[\frac{\mu_L}{\mu_{L,\text{ref}}}\right]^{0.1} \tag{8.26}$$

Equations (8.25) and (8.26) express the vapor and liquid rates for any system in terms of equivalent vapor and liquid loads of the reference system. These equivalent rates, i.e., G_{ref} and L_{ref}, are then used with the reference system plots to obtain the pressure drop. When the reference system is air-water, then $\rho_{G,\text{ref}} = 0.075$ lb/ft^3, $\rho_{L,\text{ref}} = 62.4$ lb/ft^3, and $\mu_{L,\text{ref}} = 1$ cP.

The Robbins interpolation procedure overcomes many of his correlation limitations (Sec. 8.2.8). The packing factor is eliminated and so are any associated inaccuracies (Sec. 8.2.10). The inaccuracy of the liquid rate dependence for low dry packing factors ($F_{\text{pd}} < 15$) is no longer a problem, because experimental data are directly interpolated to establish this dependence. Any inaccuracies in generalizing Fig. 8.20

have no effect on the interpolation procedure. If data are available for a nonaqueous reference system, the Robbins interpolation procedure is suitable also for predicting pressure drop for nonaqueous systems at very high liquid rates (flow parameter > 0.3).

One problem that the Robbins interpolation procedure cannot overcome is predicting pressure drop for elevated pressure systems. Another problem that the Robbins interpolation procedure cannot overcome is the inherent limitations of the pressure drop data (Sec. 8.2.5).

Which method to use. Section 8.2.8 draws attention to the systematic nature of the limitations of packed-tower pressure drop correlations. Due to this systematic nature, the author warns against basing packing pressure drop calculations on any correlations whose limitations are not well known. Section 8.2.8 presents three correlations and elaborates on their limitations and application boundaries. Within their boundaries, these correlations should give reliable predictions. Use of any other correlation is dangerous unless its limitations are explored.

Interpolation of packing pressure drop data is superior in accuracy and reliability, and should always be preferred to correlations. Section 8.2.9 presents two interpolation procedures: The GPDC interpolation charts, and the Robbins interpolation.

The Robbins interpolation procedure can rapidly convert typical manufacturer data into a powerful pressure drop predictor. It requires no special interpolation charts. It is ready for use with any new packing that may crop up. On the other hand, the GPDC interpolation charts bring together data from different sources, test systems, and operating conditions. The GPDC interpolation charts compare the data and check data validity. The author believes that the two interpolation procedures are complementary, and recommends both within their application changes.

8.2.10 Packing factors

Several of the predictive methods above use a "packing factor" to account for the type and size of packing. The packing factor was introduced by Lobo et al. (69) as an approximation for the a_p/ϵ^3 term in the original Sherwood correlation. With the evolution of the general pressure drop correlation (GPDC), the packing factor shifted away from the ratio a_p/ϵ^3 to become an empirical constant that must be experimentally determined for each packing (31). Packing factors are obtained

- By backward calculation from the GPDC correlation, based on average performance of the packing at 0.5, 1.0, and 1.5 in of water pressure drop per foot of packed depth (1). This method proved un-

suitable for the larger second- and third-generation packings that flood at the above range of pressure drop.

- By selecting a factor that gives the best fit of available experimental pressure drop data to the GPDC correlation curves (31*b*,60). This method biases the packing factor toward the regions on the chart for which experimental data exist.
- By inferring packing factors from dry pressure drop measurements, using Eq. (8.16). This method is only suitable for use with the Robbins pressure drop correlation (Sec. 8.2.8). With the GPDC correlation, it biases the packing factor toward the low-liquid-rate region.

Limitations. Additional limitations to the packing factor concept and to its application for pressure drop and flood prediction are

- The packing factor depends on the version of the correlation used. Any changes to correlation curves requires revisions to packing factors.
- With many packings, the rate of change of pressure drop with either flow parameter or capacity factor or both is not adequately predicted by the GPDC correlation (60). For these packings, the packing factor may not give a good data fit.
- Since packing factors are derived from experimental pressure drop data, they are affected by the inherent limitations of the experimental data (Sec. 8.2.5).
- There is confusion as to what are the best packing factors. For instance, Eckert (53,74) gives a packing factor of 20 for 2-in metal Pall® rings; Perry's *Handbook* (14) cites the same factor based on Eckert's work. This packing factor applies both for the early and latest versions of the GPDC correlation (Figs. 8.17 and 8.19*a*,*b*). Strigle (15) recently gave a factor of 27 for the same packing using the same correlation. Kister and Gill (60) show that a packing factor of 27 reflects published experimental data well, yet the packing factor of 20 was used by the industry for two decades. Robbins (89) reports that different manufacturers used different packing factors for the same packing.

Packing factors: to use or not to use? Due to the limitations of the Eckert GPDC (Secs. 8.2.6, 8.2.8) and the problems above, many manufacturers supply no packing factors for their products. This is especially true for structured packings, where the Eckert GPDC curves do not fit experimental data well (30,31,31*b*,60*a*). Unfortunately, this creates a situation where packing capacities are described by a mul-

titude of correlations. Each correlation has its own pitfalls and limitations, and these are often unknown and seldom reported. A designer can at best gain limited experience with each correlation, and this experience becomes rapidly outdated. Keeping track of experiences gained with these correlations becomes a mammoth task. The designer loses feel for their reliability and limitations, and with it, the ability to apply them with confidence.

A major advantage of the "packing factor" approach is that the limitations of both the packing factors and correlations are well-recognized. Further, in distillation, where the liquid to vapor mass ratio is relatively close to unity, the effect of the packing factor limitations is considered relatively small (1,15).

The interpolation procedures in Sec. 8.2.9 completely overcome both the limitations-tracking problem and the packing factor limitations listed above. The Robbins interpolation technique uses no packing factors. Packing factors are used by the GPDC interpolation charts, but only as arbitrary parameters that shift experimental data up or down relative to the chart curves. Any inaccuracies in packing factors are reflected as data deviation from the curves and are accommodated for by the interpolation procedure.

Table 10.1 gives packing factors for use with charts in Chap. 10 and in Fig. 8.19 (i.e., Fig. 8.19*a* or 8.19*b* for random packing; Fig. 8.19*c* for structured packings). Whenever available, those were extracted from Strigle (15) or from the manufacturer's literature. Strigle (15) also has good packing factors for first-generation random packings. Packing factors for use with the Robbins correlation (Sec. 8.2.8) are listed in Table 8.3.

8.2.11 Loading point

The point of transition from the preloading regime to the loading regime is termed the *loading point* (points B or B' on Fig. 8.15). Although early workers proposed that the loading point can be recognized by a sharp change of slope on Fig. 8.15, the present consensus is that the change of slope is gradual, and that no sharp loading point exists in most commercial applications (1,51,52,63,69,76).

The difficulty of defining the flood point (Sec. 8.2.3) extends to the load point. Billet (80) defines the load point where liquid holdup starts increasing with gas velocity. Kunesh (51) defines it as the point beyond which a very small increase in boilup results in a rapid deterioration in efficiency (i.e., point E on Fig. 8.16*a*). Strigle (15) gives two definitions—the *lower loading point,* which is the highest flow rate at which the pressure drop is proportional to the square of the gas flow rate, and the *loading point,* which is the flow rate at which the vapor phase begins to interact with the liquid phase to increase interfacial

area in a packed bed, i.e., point B on Fig. 8.16a. Strigle's and Billet's definitions are similar and are adopted here. Billet (80) shows that the loading point occurs at about 70 percent of the flood point.

Prediction. A rough rule of thumb by Fair et al. (14) suggests that for random packing, the loading point will occur at a packing pressure drop above 0.5 in of water per foot of bed. A correlation by Billet and Schultes (79) is presented below. Considering the uncertainty in defining the loading point, the need for an elaborate correlation may be questioned.

$$u_{s,Lo}^2 \frac{\rho_G}{\rho_L} = \frac{1}{0.3048 a_p}\left[\epsilon\left(\frac{12\mathrm{Re}_L}{\mathrm{Ga}_L}\right)^{1/6} - \left(\frac{12\mathrm{Re}_L}{\mathrm{Ga}_L}\right)^{1/2}\right]^2 C_{i,Lo}^2\left[F_{lv}\left(\frac{\mu_L}{\mu_G}\right)^{0.4}\right]^{-n_{Lo}} \tag{8.27}$$

where

$$\left.\begin{aligned} C_{i,Lo} &= C_{1,Lo} \\ n_{Lo} &= 0.652 \end{aligned}\right\} \text{for } F_{lv} \le 0.4 \tag{8.28a}$$

$$\left.\begin{aligned} C_{i,Lo} &= C_{2,Lo} \\ n_{Lo} &= 1.446 \end{aligned}\right\} \text{for } F_{lv} \ge 0.4 \tag{8.28b}$$

F_{lv}, Re_L, and Ga_L are given by Eqs. (8.3), (8.8), and (8.9), respectively; a_p, ϵ, $C_{1,Lo}$, and $C_{2,Lo}$ are constants for each packing, and are tabulated in Table 8.2. The Reynolds number Re_L is based on the liquid velocity at the load point. The Billet and Schultes correlation predicted most of their load point data within about ±10 percent (79). It applies for both random and structured packings.

8.2.12 Column sizing criteria

Flood point. Packed towers are usually designed to 70 to 80 percent of the flood point velocity (17,55,56,96). This practice provides sufficient margin to allow for uncertainties associated with the flood-point concept (Sec. 8.2.3) and prediction (Sec. 8.2.6) and to keep the design point away from the region at which efficiency rapidly diminishes (just below the flood point).

MOC. Strigle et al. (15,57,97) recommended designing packed towers with a 10 to 20 percent margin from the maximum operational capacity (MOC). Since the MOC is usually about 5 percent below the flood

TABLE 8.4 Maximum Pressure Drops Recommended for Packed Columns with Random Packings

Type of System	Maximum pressure drop, inch water/ft packing	Reference
Atmospheric fractionator	0.50–1.0	63
	0.75–1.0	1,74
	0.5–0.7	17,89
Low- to medium-pressure fractionator	0.75–1.0	63,74,98
	0.5–0.7	17,89
High pressure distillation		
$0.06 < \rho_G/\rho_L < 0.20$ (Note 1)	$0.19F_p^{0.7}(\rho_L/\rho_{H_2O})$	15
$0.20 < \rho_G/\rho_L$ (Note 2)	$0.099F_p^{0.7}(\rho_L/\rho_{H_2O})$	15
Vacuum distillation (Notes 3,4)	0.1–0.25	1,63,98
	0.01–0.05	74
	0.05–0.3	17
	0.05–0.6	89
Foaming materials (Note 5)	0.1–0.25	1,63
Absorbers (Note 5)	0.2–0.6	89
	0.2–0.75	63
	0.25–0.50	74,98
	0.1–0.4	15
Nonfoaming systems absorbers	0.25–0.40	15
Foaming systems absorbers (Note 5)	0.25	15
L/G ratio > 20	Note 6	15

[1]Based on Eq. (8.29)

$$\Delta P = 33\, F_p^{0.5}\, C_S^{2.4}/\sigma \qquad (8.29)$$

[2]Based on Fig. 8.19*a* or *b*.

[3]Because of minimum wetting rate considerations, Ludwig (63) recommends against designing for pressure drops lower than 0.1 in water/ft. Billet (56) also warns against designing packed vacuum towers with too low a pressure drop.

[4]Reasons for the low pressure drop recommended for vacuum systems are prevention of mist and entrainment at the high vapor velocities experienced under vacuum (1), and minimizing bottom temperature, and therefore, material degradation (1,89).

[5]The maximum pressure drop is low because of the high foaming tendency. This is equivalent to incorporating derating factors in tray column design (Sec. 6.2.10). Eckert (1) describes an alternative and better means of derating packed tower designs for foaming systems.

point (Sec. 8.2.7), the Strigle et al. criterion is equivalent to designing at 76 to 86 percent of the flood-point velocity. This criterion is therefore less conservative than the above flood-point criteria.

Pressure drop. Packed towers are designed so that the pressure drop at any point in the tower does not exceed a recommended maximum value. Maximum pressure drop criteria for packed towers are listed in Table 8.4. For vacuum distillation, foaming systems, and where fan horsepower needs to be minimized, the pressure drop criteria frequently set tower diameter.

TABLE 8.4 Maximum Pressure Drops Recommended for Packed Columns with Random Packings (*Continued*)

Type of System	Maximum pressure drop, inch water/ft packing	Reference
Absorbers (Note 5) (Continued)		
Amine absorbers (Note 5)	0.25	15
Hot carbonate absorbers (Note 5)	0.30	15
Chlorine drying (Note 7)	0.10–0.15	15
SO_3 absorption (Note 8)	0.25–0.30	15
Atmospheric	0.2–0.4	17
Pressure (Note 9)	0.5–1.0	17
Regenerators (Note 5)	0.2–0.6	89
	0.2–0.75	63
	0.25–0.50	74,98
	0.15–0.50	15
Inert gas stripping of foaming systems (Note 5)	0.25	15
Steam or reboiled solvent stripping of foaming systems	0.3	15
Amine regenerators (Note 5)	0.3	15
Hot carbonate regenerators	0.4	15
Atmospheric	0.2–0.4	17
Pressure (Note 9)	0.5–1.0	17
Scrubbers (Note 10)	0.25–0.6	15
Using water	0.6	15
Using liquids other than water $\rho_L > 50$ lb/ft^3	0.4	15
Foaming scrubbers	0.35	15

[9]Gas rate should not exceed 85 percent of the rate which gives a pressure drop of 1.5 in water per foot of packing based on Fig. 8.19*a* or *b*.

[7]Refers to chlorine gas drying using sulfuric acid. The reason for the low pressure drop is that chlorine is dried in a number of towers arranged in series. The overall pressure drop desired for the system is low.

[8]Refers to SO_3 absorption in sulfuric acid production. Reason for low pressure drop is to avoid entrainment of acid out of the absorber while allowing for some pressure drop rise due to accumulation of sulfonation products and packing chips in the packed bed.

[9]Presumably nonfoaming services.

[10]Examples include HF, HCl, ammonia, chlorine, sulfur dioxide scrubbers.

Which criteria to use? Some designers (5,15,57,97) abandoned the flood-point criterion in favor of the MOC. The majority (3,17,41,50, 51,55,56,58–60,96) prefer the flood-point criterion. Neither of these criteria is free of limitations (Secs. 8.2.3 and 8.2.4), but those associated with the MOC are far more restrictive. In addition, the ground rule of designing to 70 to 80 percent of flood is much better established than the equivalent rule for MOC.

The maximum pressure drop criterion is used jointly with the flood-point criterion. The column is designed to the more conservative of the two criteria. If MOC is preferred to flood point, the maximum pressure drop criterion is used jointly with the MOC criterion, and the column is designed for the more conservative of the two.

8.2.13 Average pressure drop

For computer calculations, a packed bed can be divided into several intervals. The bed pressure drop is the sum of all the interval pressure drops. Alternatively, the specific pressure drop can be calculated at the top of the bed and at the bottom of the bed. The average specific pressure drop is then calculated from (15)

$$\Delta P = (0.5\Delta P_{top}^{0.5} + 0.5\Delta P_{bot}^{0.5})^2 \tag{8.30}$$

Instead of using Eq. (8.30), the specific pressure drop is sometimes taken as the arithmetic average of ΔP_{top} and ΔP_{bot}. This gives a slightly conservative estimate of the average pressure drop (15).

8.2.14 Liquid holdup

Liquid holdup is the liquid present in the void spaces of the packing. At flooding, essentially all the voids are filled with liquid or froth. Reasonable liquid holdup is necessary for good mass transfer and efficient tower operation, but beyond that, it should be kept low. High holdup increases column pressure drop, the weight of the packing, the support load at the bottom of the packing and tower, and the column drainage time. Most important, when distilling thermally unstable materials, high holdup may lead to excessive product degradation and fouling.

Static holdup is liquid remaining on the packing after it has been fully wetted and drained for a long time. The contribution of static holdup to mass transfer rates is limited (99). Static holdup can be estimated using the relationship of Shulman et al. (100), as recommended (14). Shulman's correlation was derived during the first generation of random packing, but the author is not aware of any updated alternatives.

Operating holdup is the liquid on the packing attributed to dynamic operation and is defined as the difference between total holdup and static holdup (101). Operating holdup contributes to mass transfer, as it provides residence time. Operating holdup can be estimated using Buchanan's correlation (101), as recommended (14). More recent correlations by Billet and Schultes (81), by Maćkowiak (73*b*,92*a*), and by Mersmann and Deixler (92*b*) apply to second- and third-generation random packings as well as some structured packings.

Maćkowiak (73*b*) evaluated liquid holdup predictions from several recent correlations. His evaluation selected a simplified version of the Mersmann and Deixler correlation over alternative methods (92*a*), and demonstrated that it fitted experimental holdup data to within ±20 to 25 percent. This correlation has a sound theoretical basis and can be expressed in a dimensionless form. It has been extensively tested for random packings, but the author has no information on how it works for structured packings. The simplified version of the Mersmann and Deixler correlation (73*b*, 92*a*) is

$$h_L = \frac{1}{12\epsilon}\left(\frac{\mu_L}{\rho_L}\right)^{\frac{1}{6}}(u_L\, a_p)^{0.5} \tag{8.31}$$

Re_L in Eq. (8.32) is obtained from Eq. (8.8). ϵ and a_p are obtained from Table 8.2. Eq. (8.31) is only valid in the preloading regime (i.e., at less than 65 percent of the flood vapor velocity). The range of application of the correlation is

$$400 < \frac{\sigma}{\rho_L}\left(\frac{a_p}{\epsilon}\right)^2 < 18{,}300 \tag{8.32}$$

$$0.15 < \mathrm{Re}_L < 200 \tag{8.33}$$

and

$$\left.\begin{aligned} 17 < a_p &< 130\ \mathrm{ft^2/ft^3} \\ 0.57 < \epsilon &< 0.99 \\ 58 < \rho_L &< 70\ \mathrm{lb/ft^3} \\ 0.6 < \mu_L &< 14\ \mathrm{cP} \end{aligned}\right\} \tag{8.34}$$

The effect of liquid and vapor rates on the operating holdup is shown in Fig. 8.21. In the preloading regime holdup is essentially independent of vapor flow (100,101), but is a strong function of liquid flow rate and packing size. Smaller-size packings and high liquid rates tend to have more holdup.

8.2.15 Minimum wetting rate

The minimum wetting rate (MWR) is the lower stability limit of packings. It is the liquid load below which the falling liquid film breaks up, and the liquid shortage causes dewetting of the packing surface. The area available for mass transfer diminishes, and efficiency drops (Sec. 8.2.2; point *A* on Fig. 8.16*a*).

Schmidt (102) described the MWR in terms of a force balance between wetting and dewetting forces at a dry patch along the path of a falling liquid film. While the gravity and viscous forces resist dewetting, the surface tension and vapor shear forces tend to dewet the falling film. The MWR therefore rises with an increase in surface tension and liquid density, and with a decrease in liquid viscosity. Large packing sizes and poor surface wetting characteristics also contribute to higher MWR. The effect of vapor rate on the MWR becomes important near the loading point, when the shear force becomes significant, and higher vapor rates also increase the MWR.

MacDougall (58) added the surface tension gradient to the list of relevant factors. A system is surface tension positive ($\sigma+$) when surface

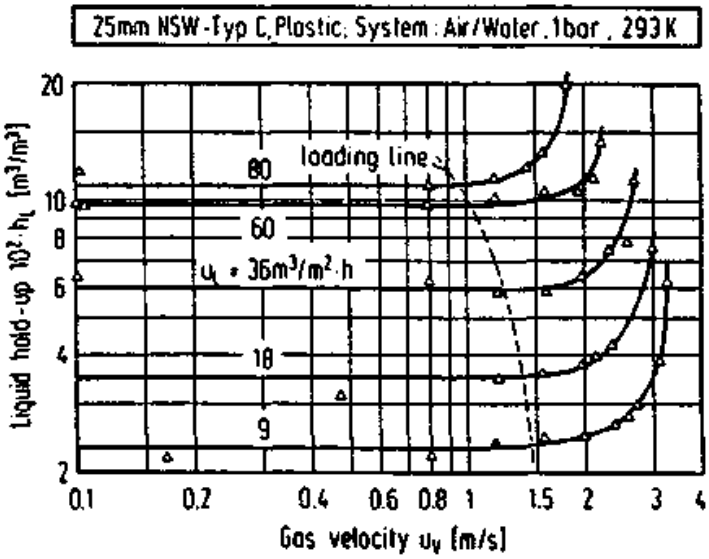

(a)

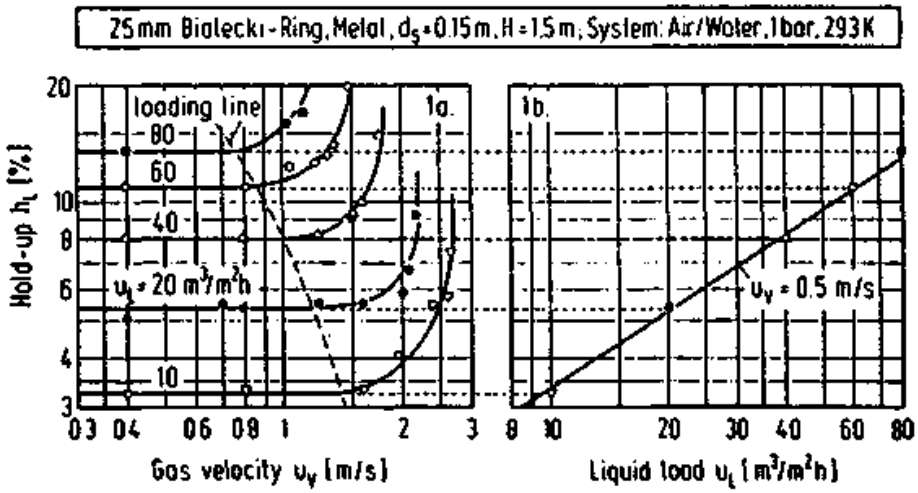

(b)

Figure 8.21 Effect of liquid and vapor rates on the operating holdup of two modern random packings. (*a*) 25-mm Nor-Pac®; (*b*) 25-mm Bialecki rings. [*Part a, from R. Billet and M. Schultes, I. Chem. E. Symp. Ser. 104, p. A159, 1987; part b, from R. Billet and M. Schultes, I. Chem. E. Symp. Ser. 104, p. B255. Both parts reprinted courtesy of the Institution of Chemical Engineers* (UK)].

tension increases as liquid goes down the column, surface tension neg ative ($\sigma-$) when surface tension drops as liquid goes down the colum and surface tension neutral when surface tension does not chang along the column. As outlined earlier (Sec. 6.4.4), the tendency of liquid film to break up is higher for a negative than for a positive sys

tem. MacDougall (58) estimates that for a negative system the MWR is approximately twice as high as for a positive system.

Schmidt (102) observed that flooding and minimum wetting are caused by two different mechanisms. A low-liquid-rate column may therefore flood even when it operates below the MWR. This is most likely to occur in vacuum systems (where liquid rates are low and vapor velocities are high) and in high-surface-tension, low-viscosity systems.

Prediction by correlation. Schmidt (102) developed the following correlation from his fundamental model which describes minimum wetting for random packings.

$$Q_{MW} = 0.3182 \frac{C_L^{2/9} (1 - \cos \phi)^{2/3}}{(1 - T_L)^{0.5} a_p^{0.5}} \tag{8.35}$$

where C_L is the liquid falling film number, and T_L is the shear stress number, given by Eqs. (8.36) and (8.37), respectively.

$$C_L = 1633.6 \frac{\rho_L \sigma^3}{\mu_L^4} \tag{8.36}$$

$$T_L = 0.9 \left(\frac{u_S}{u_{S,Fl}} \right)^{2.8} \tag{8.37}$$

The angle ϕ in Eq. (8.35) is the contact angle, discussed in more detail in Sec. 8.2.16. Contact angles are difficult to estimate; a chart useful for preliminary estimates was presented by Mersmann and Deixler (92*b*). For systems that do not experience underwetting (Sec. 8.2.16), the $(1 - \cos\phi)^{2/3}$ term in Eq. (8.35) can be approximated by assuming $\phi \approx 10°$, giving Eq. (8.38):

$$Q_{MW} = 0.0196 \frac{C_L^{2/9}}{(1 - T_L)^{0.5} a_p^{0.5}} \tag{8.38}$$

Schmidt's correlation is sensitive to the contact angle estimate [both in Eqs. (8.35) and (8.38)]. Table 8.5 lists the range of applicability of Schmidt's correlation. The Schmidt correlation is based on data for Raschig and Pall® rings (102), mainly for positive-surface-tension systems (58).

Prediction by rule of thumb. Popular rules of thumb for minimum wetting rates in random packings are

TABLE 8.5 Range of Applicability of Schmidt's Minimum Wetting Rate Correlation (102)

Pressure, mmHg abs	15–760
Liquid falling film number, C_L	2.44×10^8–6.77×10^{10}
Galileo number, Eq. (8.9)	27,000–36,000,000
L/G	0.5–1.25
Contact angle ϕ, degrees	8–20
Packing material	Ceramic, copper, or stainless steel

- A rule of thumb cited by Ludwig (63)

$$Q_{MW} = 3 \tag{8.39}$$

This rule is conservative; a more realistic range for minimum wetting rates is 0.5 to 2 gpm/ft^2. In some nonaqueous services, liquid rates sometimes as low as 0.1 to 0.25 gpm/ft^2 are successfully handled. This rule applies only where underwetting (Sec. 8.2.16) is not a problem.

- Glitsch's rule of thumb (Table 8.6) for CMR® random packings when the packing surface area exceeds 43 ft^2/ft^3. Both Ludwig (63) and the author like these rules, but they only apply to CMR® #1, #1.5, and #2. To extend these rules to other packings, the author applied Schmidt's model (102). Equation (8.38) gives

$$Q_{MW} \propto a_p^{-0.5} \tag{8.40}$$

The surface area per unit volume is about 75 ft^2/ft^3 for CMR® #1; 57 ft^2/ft^3 for CMR® #1.5, and 45 for CMR® #2. It is conceivable that Glitsch's rules are based on an average value of a_p of about 60. Equation (8.40) will then become

TABLE 8.6 Glitsch's Rule of Thumb for Minimum Wetting (6,63,103)

(Basis: CMR® with a_t > 43 ft^2/ft^3)

Material	Minimum wetting rate, gpm/ft^2
Unglazed ceramic (chemical stoneware)	0.2
Oxidized metal (carbon steel, copper)	0.3
Surface-treated metal (etched stainless steel)	0.4
Glazed ceramic	0.8
Glass	1.0
Bright metal (stainless steel, tantalum, other alloys)	1.2
PVC-CPVC	1.4
Polypropylene	1.6
Fluoropolymers (PTFE type)	2.0

$$Q_{MW} \approx [Q_{MW} \text{ from Table 8.6}] \times (60/a_p)^{0.5} \qquad (8.40a)$$

Experiments by Chuang and Miller (34) confirm good performance of #1 and #2 metallic, surface-treated CMR® and #1 Hy-Pak® at liquid rates of the order of 0.3 to 0.8 gpm/ft^2 with an aqueous system. Their experiments also showed inferior performance when surface treatment was inadequate. This gives support to the metallic values listed in Table 8.6, but emphasizes that "surface-treated" and "oxidized metal" refer to proper conditioning of packing surfaces.

Structured packings. Superior wetting characteristics compared to random packings (Sec. 8.1.10) characterize structured packings. With metal packings, satisfactory performance was reported down to 0.1 gpm/ft^2 in corrugated-sheet structured packings, and down to 0.05 gpm/ft^2 for wire-mesh structured packings.

Reducing minimum wetting rates. Surface treatment of the packing can substantially reduce the MWR (34,63). Techniques of conditioning packing surfaces include oxidizing, sandblasting, and etching. The improvement depends on the technique and its effectiveness. Chuang and Miller (34) tested a metallic random packing with an aqueous system at low liquid rates (about 0.3 gpm/ft^2). They used two alternative techniques for oxidizing the packing surfaces. The packings oxidized with the more effective technique gave a column efficiency twice as high as those oxidized by the less effective technique.

8.2.16 Underwetting

Laboratory- and pilot-scale distillation experiments with systems that exhibit large differences in surface tension along the column showed a sharp drop in efficiency at the high-surface-tension end of the column. Distilling the methanol-water system, Ross, Ponter et al. (36,104) observed high efficiencies at high and moderate methanol concentrations (low surface tension) and low efficiencies at low methanol concentrations (high surface tension). There appeared to be a critical methanol composition below which performance deteriorated rapidly. This was observed with several types and sizes of random packings and one wire-mesh structured packing (Hyperfil®). The poor performance at the low-methanol-concentration end appeared independent of the type and size of packing. Visual observations with disc columns attributed these effects to underwetting.

Underwetting is a packing surface phenomenon, which breaks up liquid film. The tendency of the liquid film to break (the degree of wet-

ting) is expressed by the contact angle (Fig. 8.22). A contact angle of zero indicates perfect wetting; an angle of 180° indicates no wetting. Mersmann and Deixler (92*b*) provide a preliminary chart for estimating contact angles. The contact angle depends both on the surface and the liquid (92*b*,104,105) and is a strong function of composition. In systems with large surface tension gradients, both contact angles and minimum wetting rates may vary rapidly with changes of composition or surface tension (104,105). Liquid viscosity (106,107) and the surface tension gradient (108) may also have an effect. Reference 105 reviews most of the work reported on underwetting. Extensive studies by Ponter et al. (104,105,109) showed that

- The underwetting effects are most significant in aqueous-organic systems, and tend to occur at the high-surface-tension (aqueous) end of the composition range.
- Changing the material and surface roughness of the packing may significantly affect efficiency in systems susceptible to underwetting.
- In systems susceptible to underwetting, column efficiency can be improved under certain conditions (but not always) by the addition of small amounts of surfactants.

Koshy and Rukovena (110,111) extensively experimented with the methanol-water and water-DMF systems using #25 IMTP® packing in a pilot-scale column. They proposed an alternative theory to explain the low efficiencies observed at the water-rich end of the columns. Accordingly, packing efficiency varies with the group λ (= mG'/L'), which is the ratio of the slope of the equilibrium curve to the slope of the operating line. When λ is close to unity, it has little effect on efficiency. As λ deviates from unity (roughly, for values of λ greater than 3 or lower than 0.5 for the systems studied), efficiency drops, sometimes dramatically. Koshy and Rukovena recognize that surface tension gradients may influence the differences in efficiency between widely different systems, but argue that these gradients are not the major cause for efficiency differences observed for a single system.

If the Koshy and Rukovena theory is correct, then only high-relative-volatility systems are likely to be affected by λ, because at

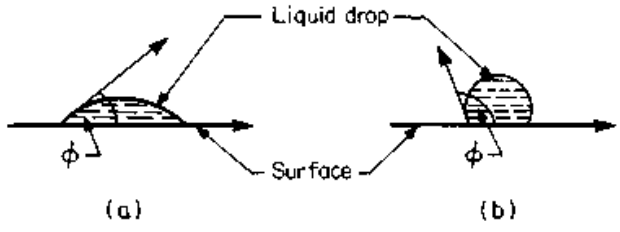

Figure 8.22 Contact angles. (*a*) Acute, good wetting; (*b*) obtuse, poor wetting.

low volatility, λ ranges from ½ to 2. For high-volatility systems, the drop in efficiency will be greatest when a high reflux ratio is used, and is likely to occur near the high-purity end of the column.

The underwetting theory appears to be supported by more evidence compared to the λ theory. The author analyzed Koshy and Rukovena's data (110,111) and believes that all their observations can be explained in terms of the underwetting theory. Further, the analysis showed that Koshy and Rukovena's results were in striking agreement with those of Ross, Ponter et al. (36,104), and even the critical methanol concentration appeared the same.

8.2.17 Minimum vapor rate

When vapor velocity through a packed bed is excessively low, the following adverse effects may be encountered.

1. *Vapor maldistribution:* Packing pressure drop places a resistance in the vapor path that helps spread the vapor radially. If pressure drop is too low, vapor will tend to channel through the bed, leading to poor mass transfer.
2. *Laminar vapor flow:* This will tend to reduce mass transfer.

For these reasons, it is a common practice (15,52,63) to design random packed beds for a pressure drop not smaller than 0.1 in of water per foot of packing. In practice, there are many columns that operate efficiently at a lower pressure drop.

8.3 Comparing Trays and Packings

Almost every separation can be performed either with trays or with packings. The factors discussed below influence the choice between trays and packings. These factors only represent economic pros and cons, and each may be overridden. For instance, column complexity is a factor favoring trays, but gas plant demethanizers that often use one or more interreboilers are traditionally packed.

A couple of trays-versus-packing comparisons have appeared in the recent literature (31*a*,111*a*). These comparisons emphasize capacity, efficiency, and costs. Both are based on several assumptions that the author would strongly challenge. For this reason, the author would not recommend applying conclusions from these comparisons in any design decision. Instead, the author strongly recommends analyzing each design case on its own merits.

An excellent discussion of the pros and cons of trays and packings

was presented by Thibodeaux and Murill (111*b*). This discussion is updated and expanded on below.

8.3.1 Factors favoring packed columns

Vacuum systems. Packing pressure drop is much lower than trays. In a tray tower, the open area of each tray is typically 5 to 10 percent of the column cross-section area. Each tray is analogous to a restriction orifice of an area ratio of 10 to 20 to 1. This gives a high velocity and a high pressure drop. Further, each tray typically holds 1 to 2 inches of clear liquid, through which the vapor must pass, and which incurs further pressure drop. Tray pressure drop is typically of the order of 0.15 psi per theoretical stage. On the other hand, the open area in a packed tower is usually greater than 50 percent of the column cross-section area, and liquid resistance to gas flow is relatively small. This leads to a typical pressure drop of 0.04 psi per theoretical stage with random packings and about half of that with structured packings.

Consider a vacuum column with 10 theoretical stages, operating at 1 psi top pressure. The bottom pressure will be 2.5 psi with trays, but only 1.4 psi with packings. The packed tower will have a much better relative volatility in the lower parts, thus reducing reflux and reboil requirements and bottom temperature. This means less product degradation, more capacity, and smaller energy consumption. This is a major advantage for packings.

Low-pressure-drop applications. By virtue of their low pressure drop compared to trays (above), packings are favored in any application where it is economical to minimize pressure drop. A typical example is an atmospheric or low-pressure column whose overheads are compressed. Every pound per square inch of pressure drop here translates into greater compression ratio requirement and higher compressor capital and energy costs.

Revamps. The pressure drop advantage that packing has over trays is invaluable in vacuum column revamps. By optimizing the revamp design pressure, the pressure drop reduction can be translated into a capacity gain, an energy gain, separation improvement, or various combinations of these benefits.

Packings also offer easy trade-off between capacity and separation. Going to smaller packings converts spare capacity in the tower into separation stages. Larger packings can overcome capacity bottlenecks at the expense of loss in separation. If both of these can be performed in different sections of the same column, and assuming no pinch near the feed, capacity or separation or both can be improved with little

penalty. In other situations, a separation loss due to revamping with larger packings can be compensated by a slight, almost unnoticeable increase in reflux. In tray columns, changing tray spacing will give similar results, but is more difficult to do.

Small-diameter columns. When column diameter is less than 3 ft, it is difficult to access the column from inside in order to install and maintain the trays. "Cartridge" trays are often installed, or an oversized diameter is used. Either option is expensive. Cartridge trays also run into leakage and hold-down problems (40). Packing is normally a cheaper and more desirable alternative.

Corrosive systems. The range of packing materials is wider than that commonly available for trays. Ceramic and plastic packings are cheap and effective. Trays can be manufactured in nonmetals, but packing is usually a cheaper and more desirable alternative.

Foaming (and emulsion). The foaming tendency is greater on trays than with packings due to the higher vapor and liquid velocities and the more violent vapor-liquid contact. The advantage of packings with foaming systems is small, but often appears exaggerated due to poor downcomer sizing practices.

Low liquid holdup. Packings generally have lower liquid holdup than trays. This is often advantageous either for reducing polymerization and degradation or as a safety measure aimed at reducing the inventory of hazardous materials.

Batch distillation. Because of the smaller liquid holdup of packed columns, a higher percentage of the liquid can be recovered as top product.

8.3.2 Factors favoring tray columns

The following factors generally favor trays compared to either random or structured packings:

Solids. Trays can handle solids a lot easier than packed columns. Both gas and liquid velocities are often an order of magnitude higher on a tray than through packings. These high liquid and gas velocities provide a sweeping action that keeps tray openings and perforations clear. Solids tend to accumulate in the voids of packed columns. There are fewer locations where solids can be deposited in a tray column. Further, packed towers need liquid distributors, and plugging in these

has been a common troublespot. Cleaning trays is easier than cleaning random packings, while cleaning structured packings is practically impossible.

High liquid rates. Multipass trays effectively lower the liquid load "seen" by each part of the tray. A similar trick cannot be applied with packed towers; the capacity of packings, especially structured, tends to rapidly fall off at high liquid rates. It is often more economical to handle high liquid rates in tray columns.

Large diameter. Packings are prone to severe maldistribution problems in large-diameter columns. These problems are far less severe in plate columns.

Complex columns. Interreboilers, intercondensers, cooling coils, and side drawoffs are more easily incorporated in tray than in packed columns. In packed columns, every complexity requires additional distribution and/or liquid collection equipment.

Feed composition variation. One way of allowing for design uncertainties and feedstock variation is by installing alternate feed points. In packed columns, every alternate feed point requires expensive distribution equipment.

Performance prediction. There is greater uncertainty in predicting packed column performance. Greater overdesign is often required.

Chemical reaction/absorption. By using high weirs, trays are capable of providing greater residence time for absorption or chemical reaction than packing.

Weight. Tray columns usually weigh less than packed columns. This saves on the cost of foundations, supports, and column shell.

Intermittent operation. When temperature is either lower or higher than atmospheric, intermittent operation repeatedly expands and contracts the shell. This may crush the packings or damage the shell in a packed column, but is easy to accommodate for in tray columns.

Trays versus random packings. The following factors generally favor trays compared to random packings, but usually not compared to structured packings.

Low liquid rates. With the aid of serrated weirs, splash baffles, reverse-flow trays (40), and bubble-cap trays, low liquid rates can be handled better in tray columns. Packed columns suffer from liquid dewetting and maldistribution at low liquid rates.

Turndown. Valve and bubble-cap trays normally give better turndown than packings. Unless very expensive distributors are used, packed tower turndown is usually limited by distributor turndown. With random packings, dewetting may also limit turndown.

Process surges. Random packings are usually more troublesome than trays in services that suffer from frequent process surges (e.g., those caused by slugs of water entering a hot oil column, relief valve lifting, compressor surges, or instability of liquid seal loops). Structured packings are considered to be less troublesome than trays in such services.

Trays versus structured packings. The following factors generally favor trays compared to structured packings, but usually not compared to random packings.

Materials of construction. Due to the thin sheets used in structured packings, their materials of construction need to have better resistance for oxidation or corrosion. For a service in which carbon steel is usually satisfactory with trays, stainless steel may be required with structured packings.

Column wall inspection. With structured packings, it is often difficult to inspect the column wall without damaging the structured packings. Due to their snug fit, structured packings are easily damaged during removal.

Washing and purging. Thorough removal of residual liquid, wash water, air, or process gas trapped in structured packings at startup and shutdown is more difficult than with trays. Inadequate removal of these fluids may be hazardous.

Chapter

9

Packing Efficiency and Scaleup

9.1 Packing Efficiency

9.1.1 The transfer unit concept

Figure 9.1 analyzes a mass transfer element in a packed column. The number of moles per hour flowing into the section is $V'y_1$, and the number of moles per hour flowing out is $V'y_2$. The number of pound moles per hour transferred, N', is given by

$$N' = V'y_2 - V'y_1 = V'\,dy \tag{9.1}$$

Since the volume of the element is $A_T\,dH$ (Fig. 9.1*a*), the number of moles transferred per unit volume over the section is given by (N is in pound-moles per hour per cubic foot)

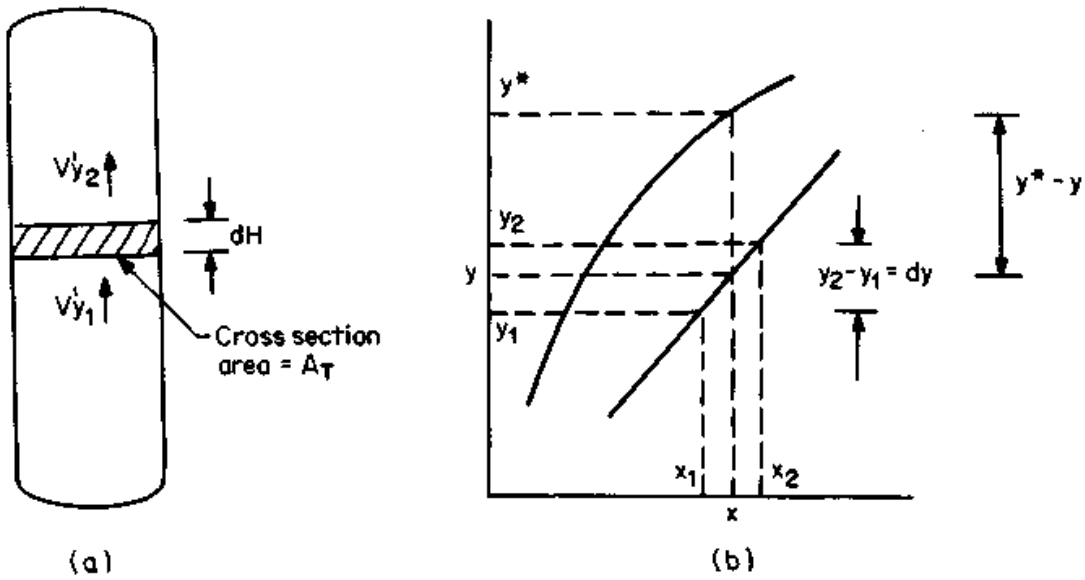

Figure 9.1 Mass transfer in packed columns. (*a*) Differential section; (*b*) driving force diagram.

$$N = (V'y_2 - V'y_1)/(A_T\,dH) \tag{9.2}$$

or

$$N = V'dy/(A_T\,dH) \tag{9.3}$$

The number of moles transferred per unit volume can also be calculated from the mass transfer equation

$$N = k_{OG}\,a_e\,P\,(y^* - y) \tag{9.4}$$

Combining Eqs. (9.3) and (9.4) and rearranging gives

$$\frac{A_T\,k_{OG}\,a_e\,P\,dH}{V'} = \frac{dy}{y^* - y} \tag{9.5}$$

The above applies for a differential section. Integrating over a packed bed H feet tall

$$\frac{A_T\,k_{OG}\,a_e\,P}{V'}\int_0^H dH = \int_{y_{in}}^{y_{out}} \frac{dy}{y^* - y} \tag{9.6}$$

which gives

$$H = \text{HTU} \times \text{NTU} \tag{9.7}$$

where

$$\text{NTU} = \int_{y_{in}}^{y_{out}} \frac{dy}{y^* - y} \tag{9.8}$$

$$\text{HTU} = \frac{V'}{A_T\,k_{OG}\,a_e\,P} \tag{9.9}$$

A more detailed derivation which spells out the assumptions is given elsewhere (87,112,113).

Number of transfer units (NTU). NTU is defined by Eq. (9.8). This is a measure of the difficulty of separation. Figure 9.1*b* illustrates this concept. The NTU relates the change in bulk phase composition to the average driving force.

Height of transfer unit (HTU). The height of a transfer unit is best defined from Eq. (9.7) as the height of packing which gives a change in composition equivalent to one transfer unit. It is therefore a direct measure of column efficiency.

Analogy to tray columns. In concept, the NTU is analogous to the number of theoretical stages in a trayed column. It only depends on the equilibrium and component balance curves (Fig. 9.1*b*) and is unaffected by the mode of contact. The main difference between NTU and number of theoretical stages is that NTU is a measure of the separation difficulty best related to a continuous contactor, while the number of theoretical stages is a measure of separation difficulty more useful for a stage-by-stage contactor. In a similar manner, the HTU is analogous to the inverse of tray efficiency.

9.1.2 The HETP concept

The concept of HETP (height equivalent of a theoretical plate) was introduced to enable comparison of efficiency between packed and plate columns. HETP is defined as

$$\text{HETP} = H/n \tag{9.10}$$

A similar HETP value can be obtained for a plate column if the tray spacing is known

$$\text{HETP (trayed column)} = 100 \times S/E \tag{9.11}$$

Relationship between HTU and HETP. The relationship between HETP and HTU has been shown to be (111,113,114)

$$\text{HETP} = \text{HTU}\,\frac{\ln \lambda}{\lambda - 1} \qquad \text{for } \lambda \neq 1 \tag{9.12}$$

and

$$\text{HETP} = \text{HTU} \qquad \text{for } \lambda = 1$$

where

$$\lambda = mG'/L' \tag{9.13}$$

HETP versus HTU. Packed-height computations can be carried out using either the HTU or the HETP approach. Both approaches should give essentially the same result. The HETP approach is usually preferred because it has the following advantages:

1. The HETP approach is suitable for multicomponent systems, while the HTU approach is difficult to apply for these.
2. The HETP approach can use the stage-by-stage computer programs that are used for multistage calculations.
3. The HTU approach is more complex and more difficult to use, but

appears to achieve no improvement in accuracy when compared with the HETP method.

4. The HETP approach enables easier comparison with plate columns.

The main advantage of the HTU method is that it enables easier analysis in terms of mass transfer coefficients, and therefore it is more suitable for fundamental analysis and model development. The HETP can simply be calculated from the HTU using Eqs. (9.10) and (9.12).

9.1.3 Factors affecting HETP

Packing size and type (Secs. 8.1.2, 8.1.4, and 8.1.10). Generally, packing efficiency increases (HETP decreases) when

- Packing surface area per unit volume increases. Efficiency increases as the particle size decreases (random packing) or as the channel size narrows (structured packing).
- The packing surface is better distributed around a packing element.

Vapor and liquid loads (Fig. 8.16). For constant L/V operation in the preloading regime, generally

- Liquid and vapor loads have little effect on random packings HETP.
- HETP increases with loadings in structured packing. The effect is most pronounced in wire-mesh structured packings, and much less pronounced in corrugated-sheet structured packings. With larger-crimp corrugated-sheet structured packings, HETP is usually practically independent of vapor and liquid loads.

Distribution (Sec. 9.2). Both liquid and vapor maldistribution have a major detrimental effect on packing efficiency.

***L/V* ratio.** Most packed-column efficiency testing has been at total reflux. Some tests for both random (3,61,115) and structured packings (3,32,116) suggest that efficiencies at finite reflux are similar to those at total reflux.

Some tests by Koshy and Rukovena (110,111) with aqueous, high-relative-volatility systems ($\alpha > 2$) gave much lower random packing efficiencies at high and low L/V than close to total reflux. They interpreted the results as an L/V ratio effect; however, underwetting (below) can also explain these data.

Pressure. Generally pressure has little effect on HETP of both random (117,118) and structured (3,32) packing, at least above 1 to 2 psia.

At deep vacuum (< 1 to 2 psia) there are data to suggest that efficiency decreases as pressure is lowered for random packings (117,118), but most of these data can also be explained by poor wetting or maldistribution. For distillation at high pressures (> 200 to 300 psia), there is evidence to suggest that structured-packing efficiency diminishes as pressure is raised (24,31*a*).

Physical properties. Data presented by a number of workers (98,115,119,120) suggest that generally, random packing HETP is relatively insensitive to system properties. A survey of the data in Chap. 11 will lead to a similar conclusion. The data in Chap. 11 also indicate that the insensitivity to system physical properties extends to nonaqueous systems in structured packings. For water-rich systems, structured-packing HETPs tend to be much higher than for nonaqueous systems (Sec. 8.1.10).

Underwetting (Sec. 8.2.16). With aqueous-organic systems, HETP tends to increase at the aqueous end of the column, both with random and structured packings.

Errors in VLE. These affect packing HETP in the same way that they affect tray efficiency (Sec. 7.3.1). The discussions, derivation, and Fig. 7.6 apply equally to tray and packed towers.

Two liquid phases. Harrison (121) presents two case studies: in one, adding water to two water-insoluble organics had no effect on HETP. In another, a key component was soluble in both liquid phases, and HETP was about 50 percent higher than normal. Harrison argues that a second liquid phase leads to lower efficiency only when it impairs diffusion of the key species. On this basis, Harrison expects efficiency loss also when an "inert" liquid or vapor represents a large fraction of the liquid or vapor phase.

Summary. In the preloading regime, packing size, type, and distribution affect HETP. With aqueous-organic systems, HETP may be sensitive to underwetting and composition. HETP of structured packings may also be affected by pressure (at high pressure), and vapor and liquid loads.

9.1.4 HETP predictions—mass transfer models

Three approaches are commonly used for HETP prediction: mass transfer models, rules of thumb, and data interpolation. These ap-

proaches will be discussed in the next three sections, starting with the mass transfer models.

The Bravo and Fair correlation (122). This correlation is based on the two-film model, that assumes resistance to mass transfer in both the vapor and liquid phases. The correlation treats the mass transfer coefficient independently from the interfacial area, and accounts for effects of partial wetting. The correlation is based on extensive commercial and pilot scale efficiency measurements for first generation packings and Pall® rings, and applies to random packings only.

For calculating mass transfer coefficients, the Bravo and Fair correlation uses the relationship by Onda et al. (123).

$$\frac{k_G}{a_p D_G} = 5.23 \mathrm{Re}_G^{0.7}\, \mathrm{Sc}_G^{1/3}\, (a_p D_p)^{-2} \tag{9.14}$$

$$k_L \left(\frac{\rho_L}{0.000672\, g\, \mu_L}\right)^{1/3} = 0.0051 \left(\mathrm{Re}_L \frac{a_p}{a_w}\right)^{2/3} \mathrm{Sc}_L^{-0.5}\, (a_p D_p)^{0.4} \tag{9.15}$$

where

$$\frac{a_w}{a_p} = 1 - \exp\left[-1.45\, \mathrm{Re}_L^{0.1}\, \mathrm{Fr}_L^{-0.05}\, \mathrm{We}_L^{0.2} \left(\frac{\sigma_c}{\sigma}\right)^{0.75}\right] \tag{9.16}$$

σ_c is the critical surface tension, and is 75 dynes/cm for steel, 61 for ceramic, and 33 for polypropylene.

$$\mathrm{Re}_L = \frac{\rho_L u_L}{0.000672\, a_p\, \mu_L} \tag{9.17a}$$

$$\mathrm{Re}_G = \frac{u_S \rho_G}{0.000672\, a_p\, \mu_G} \tag{9.17b}$$

$$\mathrm{Fr}_L = \frac{a_p\, u_L^2}{g} \tag{9.18}$$

$$\mathrm{We}_L = \frac{\rho_L u_L^2}{a_p\, (\sigma/453.23)} \tag{9.19}$$

$$\mathrm{Sc}_L = \frac{0.000672\, \mu_L}{\rho_L D_L} \tag{9.20a}$$

$$\mathrm{Sc}_G = \frac{0.000672\, \mu_G}{\rho_G D_G} \tag{9.20b}$$

The effective mass transfer area is given by

$$a_e = a_p \sigma^{0.5} H^{-0.4} (\mathrm{Ca}_L \, \mathrm{Re}_G)^{0.392} \tag{9.21}$$

where

$$\mathrm{Ca}_L = \frac{0.3048 u_L \, \mu_L}{\sigma} \tag{9.22}$$

The transfer units for each phase are calculated from

$$H_G = u_S/(k_G \, a_e) \tag{9.23a}$$

$$H_L = u_L/(k_L \, a_e) \tag{9.23b}$$

The overall HTU is given by

$$\mathrm{HTU} = H_G + \lambda \, H_L \tag{9.24}$$

where λ is given by Eq. (9.13). HETP can be calculated using Eq. (9.12).

Some data relevant to the application of Bravo and Fair's correlation are tabulated in Table 9.1. Note that the a_p values used in deriving this correlation are slightly different from those used by Billet and Schultes (Table 8.2).

Bravo and Fair (122) statistically analyzed the reliability of their model. They concluded that multiplying an HETP calculated from their model by a safety factor of 1.6 will give 95 percent confidence that the column is not too short. This factor is slightly lower than the Bolles and Fair (55,96) and the Onda et al. (123) correlations. MacDougall (58) repeated the statistical analysis after he rearranged the data bank, and showed that a safety factor of 1.3 is more appropriate, making the Bravo and Fair correlation much better than the others.

The Bravo, Fair et al. correlation for structured packing. Bravo, Rocha, and Fair (124) developed the first published fundamental model for structured-packing efficiency. This model was developed for the Sulzer BX wire-mesh packing, but has recently (25,50) been extended to corrugated-sheet packings.

Like their random-packing efficiency model (above), the Bravo, Fair et al. structured-packing model is based on the two-film theory. The HTU is calculated from the mass transfer coefficients and interfacial areas using Eqs. (9.23) and (9.24). The HETP can be calculated from the HTU using Eqs. (9.12) and (9.13). The mass transfer coefficients are evaluated from

$$\mathrm{Sh}_G = 0.0338 \, \mathrm{Re}_G^{0.8} \, \mathrm{Sc}_G^{0.333} \tag{9.25}$$

TABLE 9.1 Data Base and Range of Application for the Bravo and Fair (122) Random Packing Efficiency Correlation

1. a_p values used in correlation for packings included in data bank

Packing	Material	Size, inches						
		½	⅝	¾	1	1.5	2	3
Raschig rings	Ceramic	112		74	58	37	28	19
Raschig rings	Metal				56	39	29	
Berl saddles	Ceramic				76			
Pall® rings	Metal		104		63		31	

2. Range of variables for test systems

Pressure	1–165 psia
Gas density	0.02–1.8 lb/ft^3
Liquid density	31–62.4 lb/ft^3
Surface tension	6–73 dyne/cm
Relative volatility	1.1–1.9

3. Restrictions placed by Onda et al. (123) on his model. Since Eqs. (9.14) to (9.20) were derived by Onda et al., these restrictions may flow on to the Bravo and Fair correlation

$0.04 < Re_L < 500$

$1.2 \times 10^{-6} < We_L < 0.27$

$2.5 \times 10^{-9} < Fr_L < 0.018$

$0.3 < \sigma_c/\sigma < 2$

and

$$k_L = 2\sqrt{12 D_L u_{L,\text{eff}}/(\pi S)} \tag{9.26}$$

where

$$\text{Sh}_G = \frac{k_G d_{\text{eq}}}{12 D_G} \tag{9.27}$$

$$\text{Re}_G = \frac{d_{\text{eq}} \rho_G (u_{\text{eff}} + u_{L,\text{eff}})}{0.00806\ \mu_G} \tag{9.28}$$

$$u_{L,\text{eff}} = 11.9 \left[\frac{\Gamma^2 g}{\rho_L \mu_L}\right]^{1/3} \tag{9.29}$$

The vapor Schmidt number, Sc_G and the effective gas velocity, u_{eff}, are calculated by Eqs. (9.20*b*) and (8.18), respectively. Values of the channel angle θ and of the packing equivalent diameter, d_{eq} are in Table 8.1. The liquid flow rate Γ is given by

$$\Gamma = \frac{L}{3600\, p} \tag{9.30}$$

The available perimeter p of the packing channels is given by

$$p = 12\left[\frac{4S}{Bh} + \frac{1}{h}\right] \tag{9.31}$$

The flow channel geometry is illustrated in Fig. 8.9, and dimensions S, B, and h (whenever available) are listed in Table 8.1. The effective area of the packing, a_e, is the packing surface area that is wet, i.e.,

$$a_e = \beta a_p \tag{9.32}$$

For wire-mesh structured packings, due to the excellent wetting characteristics of the surface, as well as for corrugated-sheet structured packings at above 85 percent of flood, the packing surface is fully wetted, i.e.,

$$\beta = 1.0 \tag{9.33a}$$

For corrugated-sheet structured packings at less than 85 percent of flood only a portion of the surface is wetted, and this portion is a function of the surface Reynolds number. For design purposes, Bravo et al. recommended estimating the wetted fraction from

$$\beta = 0.50 + 0.58\,(u_S/u_{S,\text{Fl}}) \tag{9.33b}$$

Bravo et al. (124) demonstrate that their correlation gives good predictions of published data for the Koch-Sulzer BX (wire-mesh) packings. For corrugated-sheet structured packings, they state that their effective area equation [Eq. (9.32)] is an oversimplification (25). Surface characteristics influence interfacial area and its rate of change with column loadings (125,125*b*), and these are not accounted for by the simple Eq. (9.33*b*). Interpolating data in Ref. 125*b* can give closer estimates for β. The interfacial area prediction is currently undergoing further study (125,125*a*,125*b*).

Others. For random packings, correlations by Onda et al. (123) and by Bolles and Fair (55,96) were mentioned earlier. Predictions from the Bravo and Fair correlation were shown to be better than from those correlations. A new recent random packing correlation by Bornhutter and Mersmann (126) is the first to account for mass transfer in drops as well as in the liquid film. The authors show experimentally that with large (2 to 3 in) packings, drops often provide more mass transfer surface than the liquid film. A new efficiency correlation that applies both for random and structured packings has just been reported by Billet and Schultes (126*a*). The correlation is based on the two-film model. Although it does not directly account for drop mass transfer, it does so indirectly by accounting for surface tension gradients (these gradients influence drop formation). Initial testing of the correlation against a wide data bank appears very promising (126*a*). An efficiency correlation for Sulzer's BX and Mellapak structured packings was developed by Spiegel and Meier (21). The correlation is based on a model similar to that of Bravo and Fair (25,124), except that it neglects the liquid mass transfer coefficient. Unfortunately, Spiegel and Meier did not fully define some of their constants, making their correlation difficult to apply.

9.1.5 HETP prediction—rules of thumb

Because there are only few variables that significantly affect random-packing HETP (Sec. 9.1.3), and due to the unreliability of even the best mass transfer model, rules of thumb for HETP successfully compete with mass transfer models. It has been the author's experience that rules of thumb for HETP prediction are more accurate and more reliable than mass transfer models. A similar conclusion was reached by Porter and Jenkins (127).

Table 9.2 lists the rules of thumb available in the published literature. Most are based on second- and third-generation random packings and should not be applied to first-generation packings. The majority of rules are in very close agreement with each other. Porter

TABLE 9.2 Published Rules of Thumb for Random-Packing HETP

	Porter & Jenkins (127)	Frank (128)	Chen (98)	Harrison & France (52)	Walas (129)	Rose (130)	Ludwig (63)	Vital (120)	Strigle (15)
1. General									
HETP (ft) =	$< 1.5d_p$					$1.11d_p$	1.5–2		
1-in packing		1.50	1.50	1.50	1.3–1.8				1.2–1.6
1.5-in packing		2.17	2.17	2.17					1.5–2.0
2-in packing		2.92	2.92	3.0	2.5–3.0				1.8–2.5
Note	1,2,4	2,3	4	4	2	4			5
2. Vacuum									
Note		6							7
3. Absorption									
HETP (ft) =		5–6							
4. Small column									
HETP (ft) =		D_T					D_T	D_T	
Note		8					9	8	

Notes

1. For 83% of published Pall® ring data. $< 2d_p$, for 97% of the Pall® ring data.
2. For Pall® rings.
3. For Intalox® saddles.
4. Presumably for modern packings.
5. For IMTP®. See Table 9.3 for restrictions and details.
6. Add 6 inches to values above because of reduced irrigation efficiency.
7. Same as general, but needs correction (see Table 9.3) for high viscosity systems.
8. For column diameter < 2 ft.
9. For column diameter 1–4 ft. for $D_T < 1$ ft, use HETP = 1 ft.

and Jenkins's (127), Frank's (128), Harrison and France's (52), Chen's (98), and Walas's (129) general rules of thumb are practically the same. Strigle's (15) and Rose's (130) general rules of thumb are more optimistic. The author prefers the Porter and Jenkins rule of thumb because it agrees with most other sources, it was successfully tested against an extensive data bank, and it is slightly conservative, and therefore suitable for design.

For small-diameter columns, the rules of thumb presented by Frank (128), Ludwig (63), and Vital et al. (120) are identical. The author believes that for small columns, the more conservative value predicted from either the Porter and Jenkins or the Frank-Ludwig-Vital rule should be selected for design. Summarizing

$$\left.\begin{aligned} &\text{HETP} = 1.5\,d_p && \text{for Pall® rings or similar high-efficiency packing} \\ &\text{HETP} \geq D_T && \text{for } D_T < 2 \text{ ft} \end{aligned}\right\} \quad (9.34)$$

In high-vacuum columns (<2 psia), and where underwetting is a problem, these rules may be optimistic. Further discussion is in Sec. 9.1.3.

Harrison and France (52) presented the only published rule of thumb for structured packings efficiency. This rule states that HETP is 9 in for ¼-inch crimp height, 18 in for 1/2-inch crimp, and 33 in for 1-in crimp. The author found this rule to do well when the crimp angle is 45°, but to be less satisfactory for other angles. Based on data in Chap. 11, the author proposes an alternative rule of thumb.

$$\text{HETP} = \frac{1200}{a_p} + 4 \quad (9.35)$$

Crimp heights and specific surface area are listed in Table 8.1. The 4 in added in Eq. (9.35) gives this rule a conservative bias. Eliminating the 4 from Eq. (9.35) will improve the fit of this rule to data, and for a crimp angle of 45° will make it practically identical to Harrison and France's. However, the author feels that just like in the Porter and Jenkins rule (above), the conservative bias is needed to render the rule suitable for design.

Service-oriented rules of thumb. Strigle (15) proposed a multitude of rules of thumb as a function of the service, column pressure, and physical properties. The author extracted these rules of thumb from Strigle's book and listed them in Table 9.3. These rules are based on the extensive experience of Strigle and the Norton Company.

TABLE 9.3 Strigle's (15) HETP Rules of Thumb

1. Atmospheric distillation (300 mmHg–80 psia)

$$\ln \text{HETP} = n_H - 0.187 \ln \sigma + 0.213 \ln \mu_L \tag{9.36}$$

where n_H is given by the tabulation below

	Packing, in		
	1 (#25)	1½ (#40)	2 (#50)
Pall® ring (Metal)	1.1308	1.3582	1.6584
IMTP® (Metal)	1.1308	1.3185	1.5686
Intalox® (Ceramic)	1.1308	1.3902	1.7233

Basis: Strigle's regression of Norton's, Billet's, and published FRI data.
Restrictions:
1. 4 dyne/cm $< \sigma <$ 36 dyne/cm
2. 0.08 cP $< \mu_L <$ 0.83 cP
3. High-performance distributors
4. $0.6 < \lambda < 1.8$. Outside this range, HETP is likely to be higher

Design: Apply with a safety factor of
20% for easy separations (< 15 theoretical stages)
15% for separations requiring 15–25 theoretical stages
Use precise HETP values for more difficult separations

2. Atmospheric distillation (300 mmHg–80 psia)

IMTP packing size	HETP, ft
#25	1.2–1.6
#40	1.5–2.0
#50	1.8–2.5

Basis: These are typical efficiencies per Strigle's experience.
Restrictions:
1. $\sigma >$ 13 dyne/cm
2. $\mu_L <$ 0.70 cP
3. Applies to paraffins, naphthenes, aromatics, alcohols, and ketones with MW < 100
4. Do not apply to systems with chemical reactions, chemical association, or high-level ionization in the liquid phase
5. $0.6 < \lambda < 1.8$. Outside this range, HETP is likely to be higher

3. Vacuum distillation (< 300 mmHg)
Rule 2 (above) gives typical HETPs for IMTP® packings in vacuum distillation. However, the liquid phase offers more resistance to mass transfer. The HETP increase is correlated as a liquid viscosity correction, as follows:

Liquid viscosity, cP	Relative HETP, %
0.22	100
0.35	110
0.75	130
1.5	150
3.0	175

Note: If reflux is highly subcooled, add one additional theoretical stage to the rectifying section to allow for reflux reheating.

TABLE 9.3 Strigle's (15) HETP Rules of Thumb (*Continued*)

4. Pressure distillation (>80 psia)
   a. For stripping light hydrocarbons from heavier ones, design HETP values are given by

$$\text{HETP} = 4.5 - 0.6 \ln \text{MW}_L + C_6 \tag{9.37}$$

IMTP Size	C_6
#25	− 0.41
#40	0
#50	+ 0.53

Restrictions:
1. $22 < \text{MW}_L < 72$. For aliphatic hydrocarbons with $84 < \text{MW}_L < 114$, HETP will be lower by up to 10% compared to values derived from Eq. (9.37) for $\text{MW}_L = 72$
2. For high methane or hydrogen concentrations, HETP can be up to 30% greater than that predicted by Eq. (9.37)

   b. Design HETP values for fractionations of C_3 and C_4 hydrocarbons at pressures of 320 and 90 psia, respectively,

IMTP size	HETP, ft
#25	1.33–1.50
#40	1.58–1.75
#50	1.92–2.17

Restrictions:
1. Above refer to separation of similar light components (e.g., C_3 splitters, C_4 splitters). A C_2 splitter will have an HETP about 20% higher than a C_3 splitter.
2. The efficiency in the stripping section may be lower (as much as a 10% higher HETP value) than in the rectifying section with the same packing.

9.1.6 HETP predictions—data interpolation

Interpolation of experimental HETP data is the most reliable means of obtaining design HETP values. This is hardly surprising, and can even be anticipated in an area where our understanding of the theory is so poor that rules of thumb can do better than theoretical models. The author feels that it is always best to derive HETP from experimental data, and to check it against a rule of thumb.

Eckert (72), Chen (98), and Vital et al. (120) tabulated experimental HETP data for various random packings. The author extended these tabulations and included data published for structured packings. Chapter 11 presents this collection of published HETP data and a detailed procedure for interpolating such HETP data.

A prerequisite to any interpolation of packing data is thorough familiarity with the factors that affect HETP. These factors are listed in Sec. 9.1.3, and elaborated on in various other sections (which are re-

ferred to in Sec. 9.1.3). Overlooking any of the factors listed can very easily lead both the data interpolation and the resulting design to be grossly incorrect.

9.2 Maldistribution and Its Effects of Packing Efficiency

9.2.1 Effects of liquid maldistribution on HETP: an overview

Maldistribution in packed columns may cause a severe reduction in column efficiency. For 1-in packings, HETP may increase by a factor as high as 2 or 3 due to maldistribution (116,131,132).

Early models (133,134) expressed the effect of liquid maldistribution on packing efficiency in terms of a simple channeling model. A portion of the liquid bypasses the bed, undergoing negligible mass transfer, and then rejoins and contaminates the rest of the liquid. Huber et al. (132,135) and Zuiderweg et al. (136) replaced the simple bypassing by variations in the local L/V ratios (Sec. 9.2.2). The overirrigated parts have a high L/V ratio, the underirrigated parts a low L/V ratio. Regions with low L/V ratios experience pinching (Sec. 2.2.5), and therefore, produce poor separation.

Huber, Yuan, et al. (116,132,135,137) added lateral mixing (Sec. 9.2.3.) to the model. Lateral deflection of liquid by the packing particles tends to homogenize the liquid, thus counteracting the channeling and pinching effect.

A third factor is the nonuniformity of the flow profile through the packing (Sec. 9.2.4). This nonuniformity was observed as far back as 1935 (138) and first modeled by Cihla and Schmidt (139). Hoek (140) combined this factor with the previous two for modeling the effect of maldistribution on packing efficiency.

9.2.2 Effect of maldistribution on local L/V ratio

When maldistribution occurs, some areas in the bed receive more liquid and other areas receive less. This causes variation in the L/V ratio along the bed cross section. The effect of these variations in L/V ratio on column efficiency are best illustrated by an example using the x-y diagram. A similar example, recently presented by McMullan et al. (140a), proved effective for analyzing a troublesome maldistribution case history.

Example 9.1 A packed column is used to achieve the separation described in Example 2.1, Sec. 2.2.4. Due to fouling, some holes in the reflux distributor are

plugged. The blockage pattern is such that one half the column receives 45 percent of the liquid, and the other half receives 55 percent of the liquid (± 5 percent maldistribution). This maldistribution pattern persists throughout the rectifying section. The liquid is redistributed at the feed point, and distribution is perfect below this point.

1. How many stages are required in the rectifying section?
2. To what extent is the rectifying section efficiency reduced due to this maldistribution?

solution

Step 1 Same as step 1 of Example 2.1, Sec. 2.2.4.

Step 2 Same as step 2 of Example 2.1, Sec. 2.2.4.

Step 3 Simulate the rectifying section of the column as two columns operating in parallel. Subscripts 1 and 2 describe the column that receives 55 and 45 percent of the liquid, respectively. The following equations apply:

$$L_1' = 0.55L' \qquad L_1' = 117 \text{ lb-mole/h}$$

$$L_2' = 0.45L' \qquad L_2' = 96 \text{ lb-mole/h}$$

$$V_1' = 0.5V' \qquad V_1' = 142 \text{ lb-mole/h}$$

$$V_2' = 0.5V' \qquad V_2' = 142 \text{ lb-mole/h}$$

$$D_1' = V_1' - L_1' = 142 - 117 = 25 \text{ lb-mole/h}$$

$$D_2' = V_2' - L_2' = 142 - 96 = 46 \text{ lb-mole/h}$$

also

$$D_1'x_{D_1} + D_2'x_{D_2} = D'x_D$$

$$25x_{D_1} + 46x_{D_2} = 71 \times 0.95 = 67.5$$

Step 4 Apply Eq. (2.9) to derive equations for the component balance lines for each of the parallel columns.

Column 1

$$y = \frac{L_1'x}{V_1'} + \frac{D_1'x_{D_1}}{V_1'}$$

or

$$y = \frac{117x}{142} + \frac{25x_{D_1}}{142} = 0.824x + 0.176x_{D_1}$$

Column 2

$$y = \frac{L_2'x}{V_2'} + \frac{D_2'x_{D_2}}{V_2'}$$

or

$$y = \frac{96x}{142} + \frac{46x_{D_2}}{142} = 0.676x + 0.324x_{D_2}$$

Step 5 The solution for x_{D_2} and x_{D_1} must be obtained by trial and error.

Assume

$$x_{D_1} = 0.99$$

Then

$$46x_{D_2} + (0.99)(25) = 67.5 \qquad x_{D_2} = 0.93$$

The solution involves finding x_{D_1} and x_{D_2} such that column 1 and column 2 have an equal number of stages. The bottom section is the same, and has the same component balance line as in Example 2.1.

Figure 9.2 shows x-y diagrams for column 1 and column 2. Solution was obtained on first trial, giving 8 stages in each rectifying section. This compares to five theoretical stages for the case of no maldistribution (Example 2.1). The apparent (measured) efficiency in the rectifying section is $\frac{5}{8}$ = 62.5 percent of the efficiency achievable with a perfectly distributed column.

Effect of changes in local *L/V* ratio on packing efficiency. Example 9.1 illustrates a 40 percent reduction in efficiency resulting from a liquid maldistribution of the order of as little as 5 percent between two halves of a column. A similar analysis of an actual troublesome maldistribution case history (140*a*) also showed that it does not take much maldistribution to cause a major efficiency loss. Example 9.1 also illustrates the following:

1. The reduction in efficiency depends on the relationships between the component balance lines and equilibrium curve of the x-y diagram. This makes it a function of factors such as reflux ratio, product purity, location of the feed point, thermal state of the feed, relative volatility, and shape of the equilibrium curve.
2. Maldistribution can cause localized pinching. The user is encouraged to repeat Example 9.1 for a ±10 percent liquid maldistribution (60/40 instead of 55/45). In this case, the required separation will never be achieved because "column 2" (Fig. 9.2*b*) operates below minimum reflux, which drops the apparent rectifying section efficiency to zero. In practice, the operator will need to increase reflux ratio or accept a lower product purity. Lowering product purity or increasing reflux ratio eliminates the pinch, and the resulting apparent efficiency will return to a value greater than zero.
3. Adequate prediction of the effect of maldistribution on efficiency

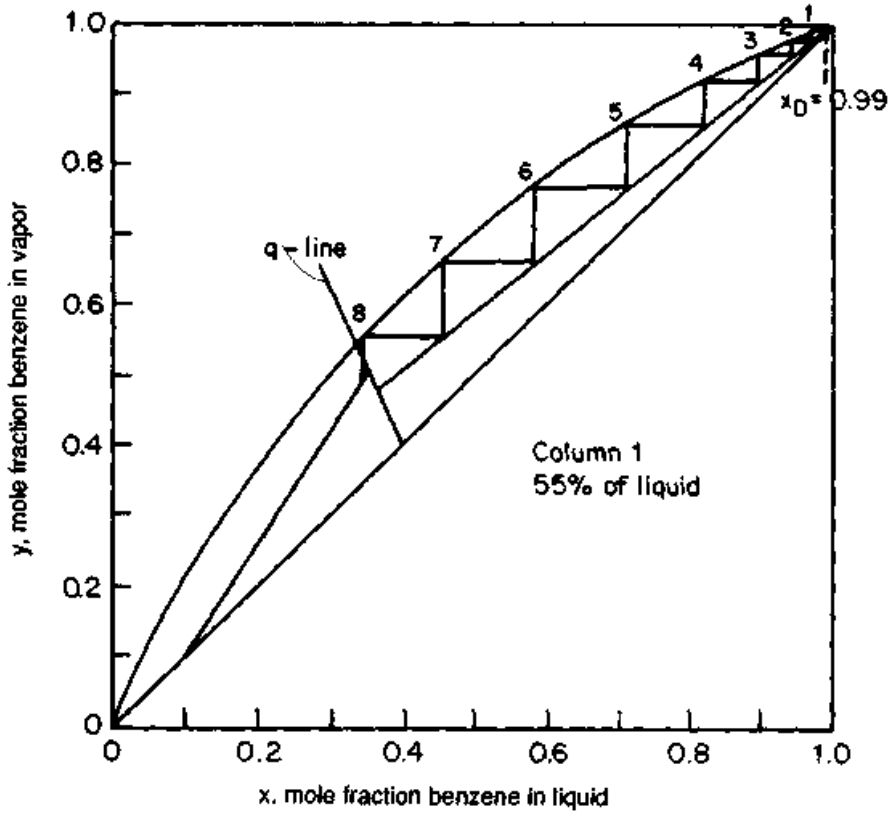

(a)

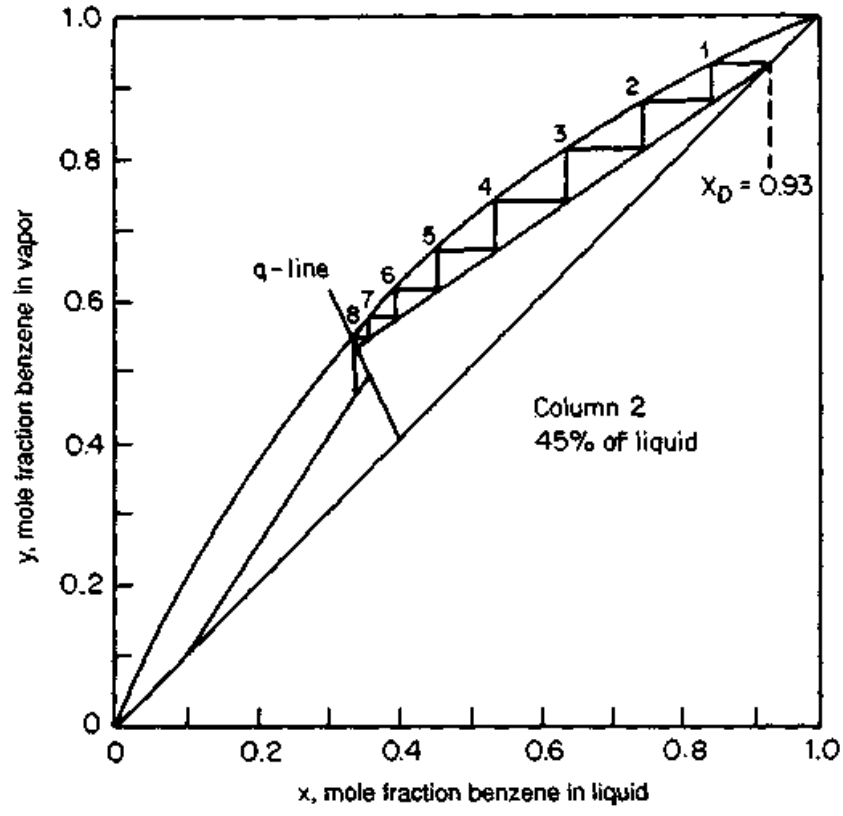

(b)

Figure 9.2 *x-y* diagrams for Example 9.1. (*a*) Column 1; (*b*) column 2.

requires a procedure that knits a maldistribution model together with a stage calculation model. Minimum requirement is a shortcut expression for maldistribution interknitted with a shortcut stage model (e.g., an x-y diagram). Such a procedure will suffer from all the limitations of shortcut stage models (e.g., Sec. 2.2.2). For rigorous computations, a rigorous model for maldistribution must be interknitted with a rigorous stage model (Chap. 4). A proper model would be extremely complex and appears to be many years down the road.

9.2.3 Effect of lateral mixing

Comparison of Fig. 9.2*a* to *b* shows that maldistribution causes changes in composition along the column cross section. At the same height, the mole fraction of the lighter component is highest when the local L/V ratio is highest. For instance, in column 1 of Example 9.1 (55 percent of the liquid), half way up the rectifying section (stage 4) the liquid contains 82 percent benzene while in column 2 (45 percent of the liquid), at the same height, the liquid contains 53 percent benzene (see Fig. 9.2). Lateral mixing, both of vapor and liquid, acts to reduce this composition difference, thus counteracting the reduction of packing efficiency. This lateral mixing is caused by liquid and vapor flow sideways around each packing element.

Huber and Hiltbrunner (135) showed that when the column to packing diameter ratio (D_T/D_p) is smaller than 10, the effect of lateral mixing is so large that only a strong maldistribution can decrease column efficiency (but note also that this range of D_T/D_p is uncommon in practice because of wall effects, Sec. 9.2.4). However, when D_T/D_p is greater than 30, the lateral mixing becomes too small to counteract the influence of maldistribution, and the effect of variations in L/V ratio dominates.

In large-diameter towers and long beds, a redistributor may help correct a maldistributed composition profile. For instance, remixing stage 4 liquid of the two columns in Example 9.1 would have alleviated the pinch. Good redistribution practices are discussed elsewhere (40).

In the presence of maldistribution, efficiency becomes a function of the following parameters.

1. The L/V ratio
2. The D_T/D_p ratio
3. Feed and product compositions
4. Thermal state of the feed and feedpoint location

5. Packing height
6. Relative volatility

The effects of these variables on efficiency in the presence of maldistribution are complex and interactive, as can be expected from Example 9.1. For instance, it has been shown (116,137) that under some feed composition and reflux conditions, efficiency increases with feed composition; under other conditions, the converse occurs. It has also been shown that as L/V was reduced from total reflux, efficiency improved—at least in some cases. Note, however, that the reverse may occur in other columns.

9.2.4 Effect of liquid flow nonuniformity

Early work on liquid flow in a packed bed used a "random-walk" probability model (139,141–144). The spread of liquid from a point source was described by the normal gaussian distribution. In the 1960s, Porter et al. (141–143) developed the rivulet model, postulating that liquid runs down the packing along "preferred paths" or rivulets. The preferred paths take a random route through the packings. Rivulets may be of different sizes, may coalesce (when the path of one runs into another) and may split. Most recent models (67,136,145,146) analyze liquid spread in terms of Albright's concept (145) of interconnected random cells. Liquid and vapor leaving each cell are distributed to the surrounding cells according to some splitting rules. Based on both modeling and experimentation, the following have been established:

1. Liquid profile unevenness is more severe at low liquid flow rates (140,142,147).
2. Liquid flows through the bed in a time-independent stable flow pattern (140,141,148).
3. Both preflooding and repacking the bed influence the stable flow pattern (66,140,141,149). Repacking has a much greater effect than preflooding (141).
4. The liquid reaches a stable profile after a certain height from the top of the bed, assuming good initial liquid irrigation (66,131,140, 147,149).
5. Smaller packings tend to spread the liquid more uniformly than larger packings (140). The liquid spread depends on packing geometry, but not on packing material (140,141). Structured packings generally spread liquid very uniformly (66,140,146). Modern random packing spread the liquid somewhat less uniformly, but more uniformly than first-generation random packings (140).

6. The uniformity of liquid spread in structured packings strongly depends on (67,146) texture of surface, presence and size of perforations, connection of packing elements in packing layers, and presence of wall wipers.
7. Below the loading point, gas velocity has little effect on liquid flow profile (66,67,140).

Hoek (140) measured packed-bed liquid distribution profiles. A typical profile is shown in Fig. 9.3. It shows variation of liquid flows throughout the bed, and a tendency of liquid to flow toward the wall.

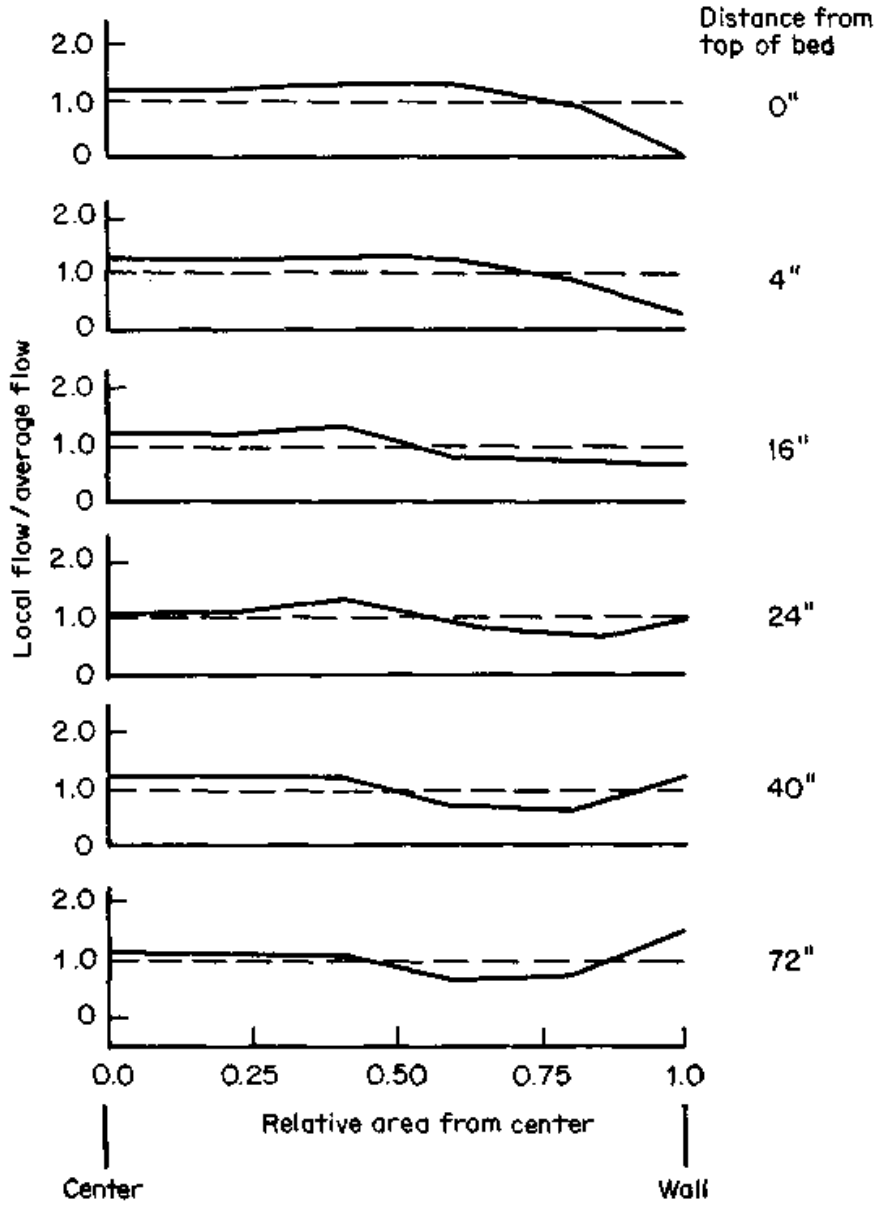

Figure 9.3 Liquid spread profile in a packed column (20-in-ID column, packed with 6 ft of 2-in Pall® rings, water study. *Data from P. J. Hoek, Ph.D. thesis, University of Delft, The Netherlands, 1983.*)

Wall flow (66,67,140,141–149). The tendency of liquid to flow toward the walls of packed columns is a fundamental phenomenon associated with packed-column hydraulics. The development of wall flow is illustrated in Fig. 9.4 using typical measurements by Hoek (140) in a pilot-scale column. The column diameter was 20 in, and the outer distributor nozzle was located about 1.5 in from the wall. In these experiments, "wall flow" was defined as the flow in the outer ring of the column (with an area of 16 percent of the column cross section).

Figure 9.4 shows little wall flow near the top of the bed. This is because the liquid distributor drip points stop short of the wall (the unirrigated ring at the top of the bed was 1 in wide in Hoek's measurements). With increasing depth below the top of the bed, liquid

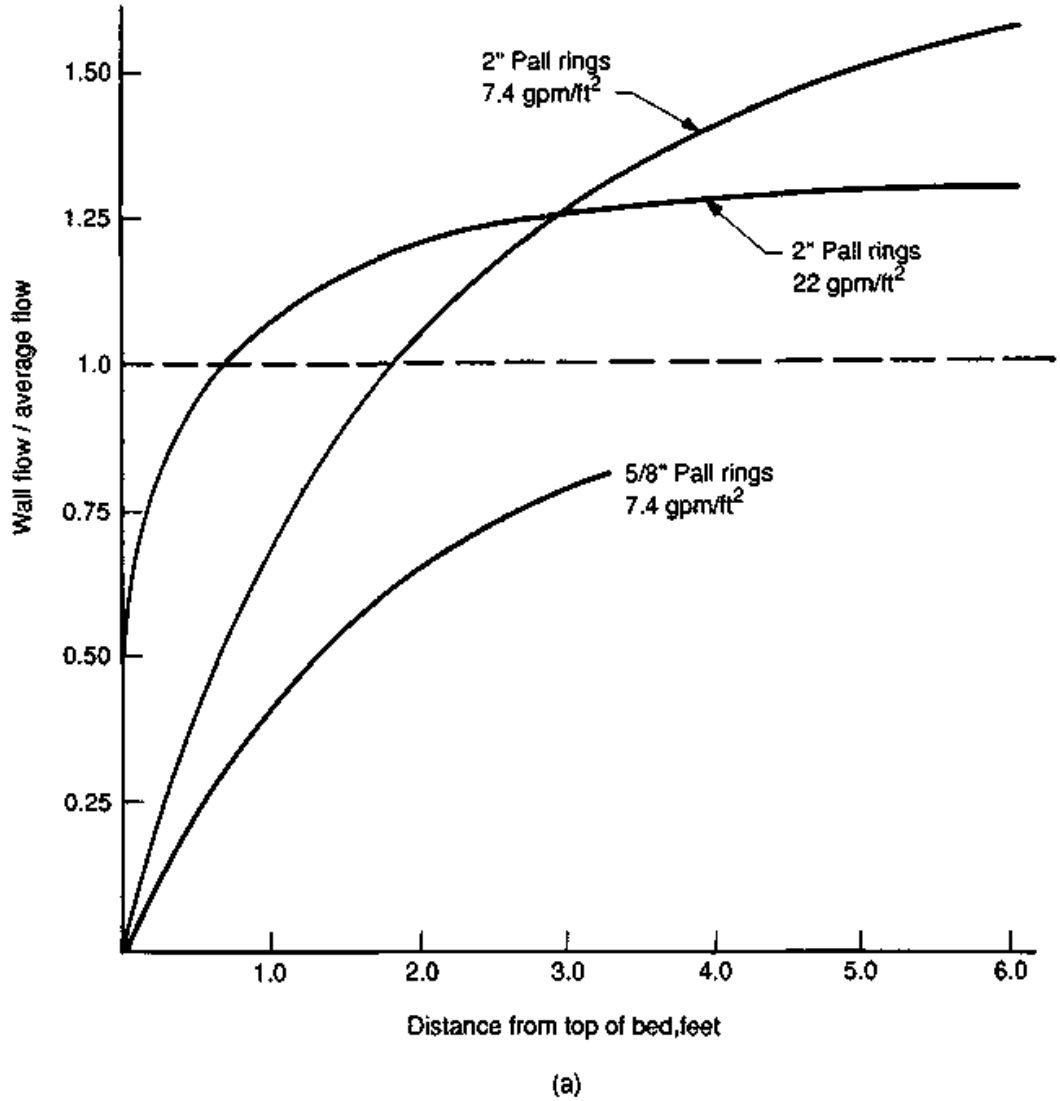

Figure 9.4 Fraction of flow in the wall region of a packed column. (*a*) Effect of liquid rate and packing size. (*20-in-ID column, water study. Data from P. J. Hoek, Ph. D. thesis, University of Delft, The Netherlands, 1983*).

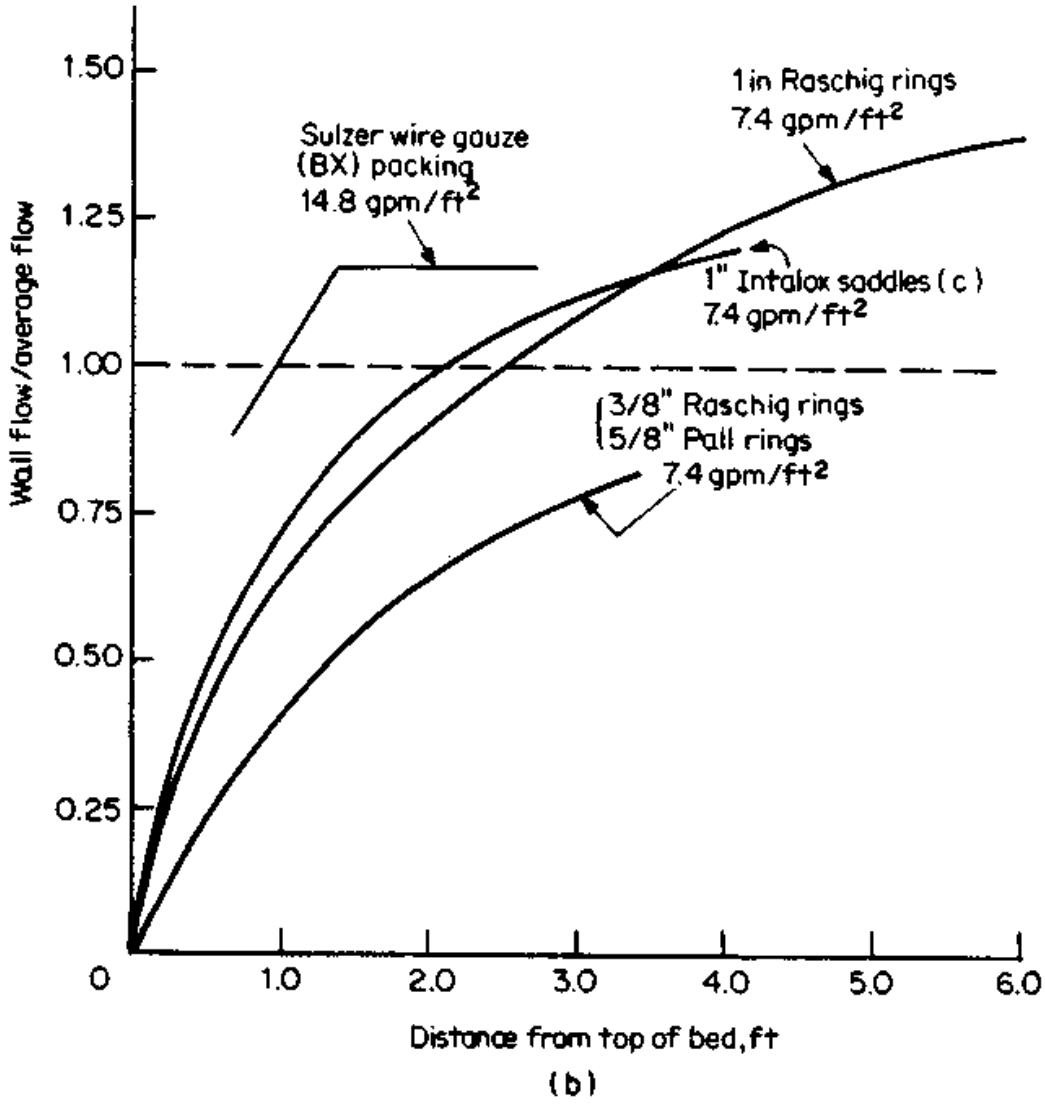

Figure 9-4 (*Continued*) Fraction of flow in the wall region of a packed column. (*b*) Effect of packing type (20-in-ID column, water study. *Data from P. J. Hoek, Ph.D. thesis, University of Delft, The Netherlands, 1983.*)

spreads through the packing and on to the wall. The liquid reaching the wall is partially deflected back into the bed and partially flows down the wall. The wall flow therefore increases until an equilibrium is reached.

Figure 9.4*a* shows that packings that promote uniform liquid spread (Pall® rings; small-diameter packings) also deflect the liquid toward the wall at a slower rate. For these packings, it takes a greater distance into the bed before the wall flow becomes equal to the bed average flow. It follows that for such packings, it is important that the initial distributor irrigates the packing near the column wall (140). Figure 9.4 also shows that wall flow is more of a concern at low than at high liquid flow rates. Other conclusions reached, based on experi-

mental work in laboratory and pilot-scale columns as well as theoretical predictions are

1. In large columns, the amount of liquid flowing down the wall at equilibrium is very small (141,144).
2. In small columns, the proportion of liquid flowing down the wall at equilibrium can be high. It is therefore recommended to design for a ratio of column to packing diameter (D_T/D_p) of at least 10 (1,14,56,141,148).
3. Redistributors and wall wipers counteract the spread of liquid toward the wall. There is uncertainty regarding their effectiveness in keeping the liquid off the walls of randomly packed towers (144). It appears that their main value is in promoting lateral mixing (Sec. 9.2.3). In structured packings, well-designed wall wipers were shown (67) to effectively keep liquid off the wall.
4. The factors affecting the development of wall flow are the same as those that affect the liquid spread. These include height into the bed, packing type, packing size, and liquid flow rate (66,140).

9.2.5 The zone-stage model

Zuiderweg, Kunesh et al. (131,136,150,150*a*) combined the effects of local L/V ratio, lateral mixing, and liquid spread into a single model that describes the effect of liquid maldistribution on packing efficiency. The work leading up to this model was performed at Fractionation Research Inc. (FRI) and at Delft University in The Netherlands. The model is still undergoing development.

The model postulates that in the absence of maldistribution, there is a "basic" (or "true" or "inherent") HETP which is a function of the packing and the system only. This HETP can be inferred from data for small towers, in which lateral mixing is strong enough to compensate for any pinching (Sec. 9.2.3).

The model divides the column axially into a finite number of sections, each section being one "basic" theoretical stage (Fig. 9.5). The length of each section is therefore equal to the "basic" HETP of the packing. Radially, the column is divided into a number of zones, each zone having the width 2 to 3 times the size of a packing particle (Fig. 9.5). Each zone-stage (i.e., each rectangle on Fig. 9.5) is considered to be a region in which liquid and vapor are mixed ideally, and the vapor stream leaving the zone-stage is in equilibrium with the liquid stream leaving the zone-stage.

A fraction K_1 of the liquid stream in every stage flows downward into the next lower stage. The balance (i.e., $1 - K_1$) flows sideways into the adjacent zones and splits according to the ratio of the interfa-

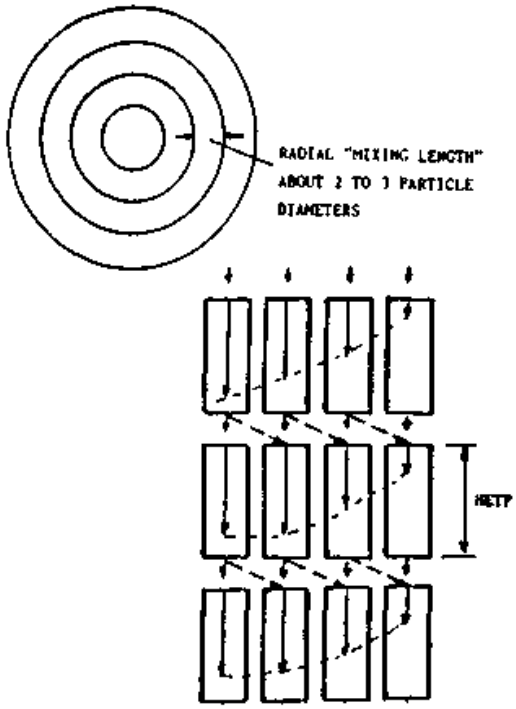

Figure 9.5 The zone-stage model. (*From F. J. Zuiderweg, P. J. Hoek, and L. Lahm, Jr., I. Chem. E. Symp. Ser. 104, p. A217, 1987. Reprinted courtesy of the Institution of Chemical Engineers, UK.*)

cial areas between the zones. The vertical and sideways flows, added in the next lower layer of stages, determine the flow distribution. It was shown (150*a*) that this distribution pattern can be derived from diffusion theory if $K_1 = 2/3$. A higher value of K_1 reflects an increase of flow near the wall.

For a given packing [i.e., inherent liquid spreading characteristics, usually characterized by a *liquid spreading coefficient* (150*b*)], and a fixed number of radial zones, the vertical height needed to achieve a fixed value of K_1 is a dependent variable calculated from the diffusion equation (150*a*,150*b*). This height is generally unequal to the stage height. To bridge the two, the zone-stage model employs an interpolation procedure. Vapor is assumed to be uniformly distributed, although this assumption is not required by the model. Vapor and liquid flow through each zone-stage are constant, with all interzone bulk liquid flow occurring between stages.

Kunesh et al. (131,150*a*) showed good agreement between predictions from the zone-stage model and some experimental data. Zuiderweg et al. (136,150,150*a*) applied the model to explain published efficiency data in terms of maldistribution effects. Zuiderweg et al. (136) also applied the zone-stage model to gain insight into the effect of several variables on efficiency in the presence of maldistribution. Their results are preliminary and require experimental confirmation.

Alternative models. Stichlmair and Stemmer (146,151) model the column as a large number of parallel channels, each operated at a differ-

ent liquid rate and at plug flow. The degree of maldistribution is ex pressed by a *maldistribution number*, which is evaluated from standar deviations of concentration measurements. This maldistribution num ber is used in a chart that converts the pseudo number of transfe units (i.e., plug flow) into an actual number of transfer units (i.e., al lowing for maldistribution).

9.2.6 Empirical prediction of the effects of maldistribution

Moore and Rukovena (152) proposed the empirical correlation in Fig 9.6 to determine the efficiency loss due to liquid maldistribution in packed tower containing Pall® rings or Metal Intalox® packing. Thi correlation was only recently proposed, and more experience with it predictions is required before it can be generally applied with confi dence. Nevertheless, it has been shown (152) to work well for severa case studies (Fig. 9.6), is simple to use, and is valuable at least as preliminary guide.

To quantify the quality of liquid irrigation, the correlation uses th distribution quality rating index. Typical indexes are 10 to 70 percen for most standard commercial distributors; 75 to 90 percent for inter mediate-quality distributors, and over 90 percent for high-performanc distributors. Moore and Rukovena (152) present a method for calcu lating a distribution-quality rating index from distributor geometry This method is spelled out in a companion book (40).

9.2.7 Effect of vapor maldistribution on packing efficiency

Vapor is easier to distribute than liquid, but vapor maldistributio can also be troublesome. The effects of vapor maldistribution hav been investigated far less than those of liquid maldistribution. Th following findings have been reported:

1. Vapor flow through packings tends to be uniform if the initial liq uid and vapor distributions to the packings are uniform (15,66).
2. A nonuniform initial vapor profile is often generated in the colum vapor inlet and vapor redistribution regions (153–157), especiall when inlet velocities are high. Vapor maldistribution was shown t strongly depend (153,154,157) on the geometry of the vapor inle (i.e., whether tangential, radial, etc.). The use of properly designe gas distributors can largely mitigate vapor maldistributio (23,152–157). Commercial vapor distributor designs are discusse elsewhere (23,40,152).
3. Although vapor spreads radially through the packing quite rapidly

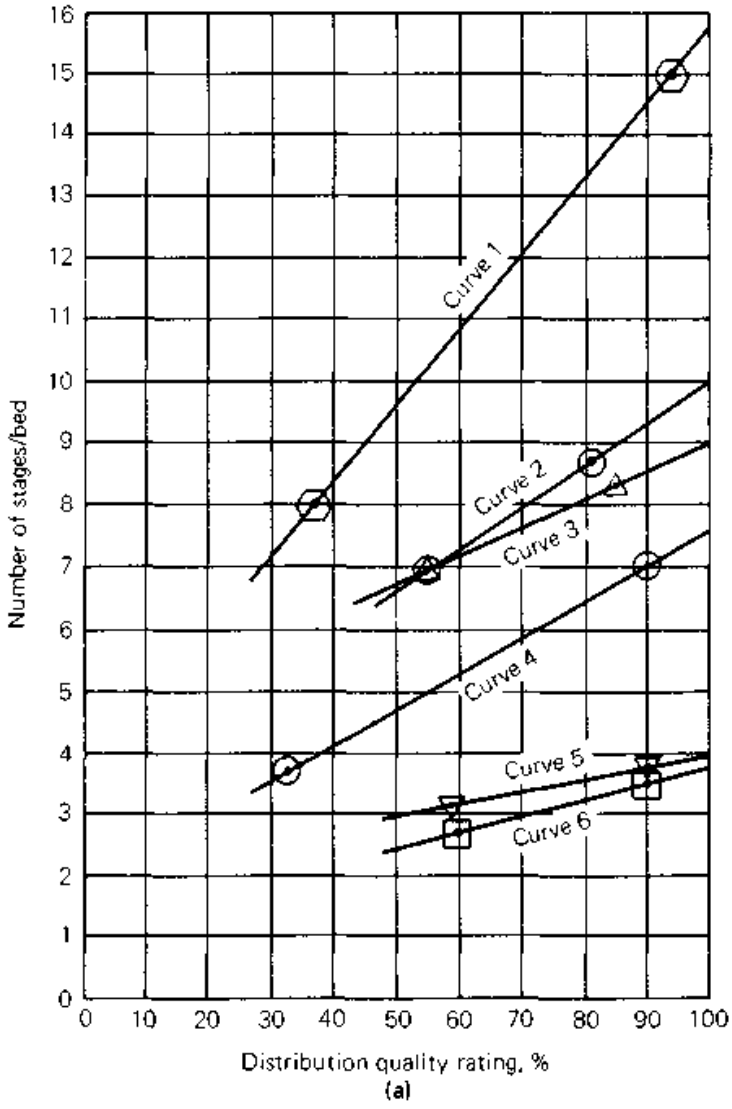

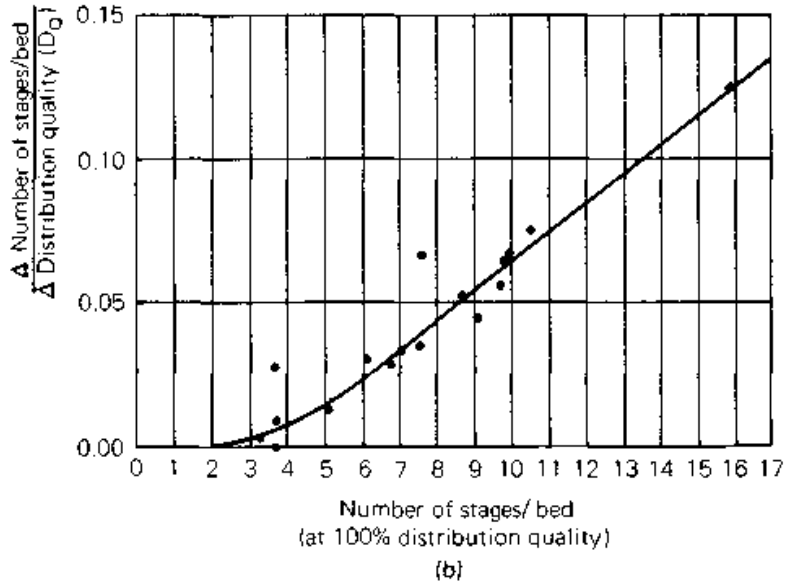

Figure 9.6 Effect of irrigation quality on packing efficiency. (*a*) Case histories demonstrating efficiency enhancement with higher distribution quality rating. (*b*) Correlation of the effect of irrigation quality on packing efficiency. (*From F. Moore and F. Rukovena, Chemical Plants & Processing, Europe edition, August 1987. Reprinted courtesy of Chemical Plants and Processing and of the Norton Co.*)

a nonuniform profile will persist at least for some height, causing pinching similar to that described in Sec. 9.2.2.

4. The packed height through which a nonuniform profile persists is a function of column diameter (156). In pilot-scale columns, vapor maldistribution was found to persist for a bed height of the order of 1 ft (155,157). In large-diameter columns, this maldistribution persists to a much greater height (15,152,154). In a number of 15-ft-diameter absorbers (154), vapor maldistribution persisted through a 50-ft bed; the efficiency was about half that encountered during good vapor distribution.
5. Redistribution of vapor depends on a balance between the vertical and horizontal pressure gradients (157). The horizontal pressure gradient depends on column diameter, and diminishes rapidly as column diameter increases. This explains the strong effect of diameter in item 4 above. Another important factor cited by Porter and Ali (157) is vortex formation. This can cause downward flows of vapor in the bed. Downward flows were actually measured by Kabakov and Rozen (154) and Porter and Ali (157).
6. The maldistribution tendency correlates well with the ratio of packed height to packing size (157). Therefore, smaller sizes of packing require smaller packed depths for distribution to become uniform. However, the more open structure of the larger packings promotes horizontal movement giving further reduction in maldistribution tendency. Stikkelman and Wesselingh (155) demonstrated that the tendency to even out maldistribution increased with the openness of the packing structure.
7. Vapor nonuniformity may be troublesome with those structured packings that permit substantial radial spread only parallel to their sheets (155). The orientation of structured packing sheets usually alters every 8 to 12 in of bed depth, and the changes of orientation mitigate this nonuniformity. However, the disturbance created to the composition profile may linger for a greater depth.
8. Vapor maldistribution may be induced by liquid maldistribution (66) when vapor flows are high. Regions of high liquid holdup impede vapor rise and channel the vapor into the lighter-loaded regions (66). Since liquid tends to accumulate near the wall, vapor will tend to channel through the center.

9.2.8 Implications of maldistribution to packing design practice

This section presents the implications of the maldistribution studies to packing design practice. Implications of maldistribution studies to

distributor design practices are outside the scope of this book and are discussed at length in a companion book (40). Conclusions that pertain to packing design practices are:

1. Three factors appear to set the effect of maldistribution on efficiency (Secs. 9.2.1 to 9.2.4).
   - *The pinching effect.* Local changes in L/V ratio, causing local composition pinches (Sec. 9.2.2).
   - *Lateral mixing effect.* Packing particles deflect both liquid and vapor laterally. This promotes mixing of vapor and liquid and counteracts the pinching effect (Sec. 9.2.3).
   - *Liquid nonuniformity effect.* Liquid flows unevenly through the packing and tends to concentrate at the wall (Sec. 9.2.4).
2. At small tower to packing diameter ratios ($D_T/D_p < 10$), the lateral mixing cancels out the pinching effect, and a greater degree of maldistribution can be tolerated without a serious efficiency loss (3,132,136). At high ratios ($D_T/D_p < 40$), the lateral mixing becomes too small to counteract the pinching effect (132). The effects of maldistribution on efficiency are therefore most severe in large-diameter columns and small-diameter packings.

   A good design practice is to look for a packing size that will give a D_T/D_p between 10 and 40. This is often impractical, and higher ratios are common. When D_T/D_p exceeds 40, there is an incentive to minimize it. When D_T/D_p exceeds 100, avoiding efficiency loss due to maldistribution is extremely difficult (116,137). Ratios exceeding 100 should either be avoided, or a special allowance should be made for loss of efficiency due to maldistribution.
3. Wall flow effects become large when D_T/D_p falls below about 10 (Sec. 9.2.4). Packing diameter should be selected such that D_T/D_p exceeds 10.
4. Columns containing less than five theoretical stages per bed are relatively insensitive to liquid maldistribution. With 10 or more stages per bed, efficiency is extremely sensitive to maldistribution (15,152,158; see Fig. 9.6). Beds consisting of small packings or structured packings, which develop more theoretical stages per bed, are therefore more sensitive to maldistribution than equal-depth beds of larger packings.
5. Maldistribution tends to be a greater problem at low liquid flow rates than at high liquid flow rates (1,66,136). The tendency to pinch and to spread unevenly is generally higher at the lower liquid flow rates.
6. A packed column has reasonable tolerance for a uniform or smooth variation in liquid distribution and for a variation that is totally random (*small-scale maldistribution*). However, the impact

of discontinuities of zonal flow (*large-scale maldistribution*) is much more severe (51,131,136,137,139,158,159).

This is a particularly useful finding. In terms of the maldistribution models, small-scale maldistribution will be evened out by the lateral mixing, and therefore will cause few ill effects. On the other hand, the lateral mixing will either be powerless to rectify a large-scale maldistribution problem, or will take considerable bed length to do so (meanwhile, efficiency will be lost).

Figure 9.7 shows HETPs measured in tests that simulate various types of maldistribution in a 4-ft column containing a 12-ft bed of 1-in Pall® rings (131,160). The *y*-axis is the ratio of measured HETP in the maldistribution tests to the HETP obtained with an excellent distributor.

Figure 9.7*a* shows virtually no loss of efficiency when a distributor uniformly tilts such that the ratio of highest to lowest flow is 1.25 (i.e., a "1.25 tilt"). On the other hand, an 11 percent chordal blank of a level distributor causes packing HETP to rise by 50 percent.

Figure 9.7*b* compares continuous tilts with a ratio of maximum to minimum flow of 1.25 and 1.5 to a situation where one-half of the distributor is passing 25 percent more liquid than the other half. The latter ("zonal") situation causes a much greater rise in HETP than a "uniform" maldistribution with twice as much variation from maximum to minimum.

Figure 9.7*c* shows results of tests in which flows from individual distributor drip points were varied in a gaussian pattern (maximum/mean = 2). When the pattern was randomly assigned, there was no efficiency loss. When the variations above the mean were assigned to a "high zone," and those below the mean to a "low zone," HETP rose by about 20 percent.

7. A packed bed appears to have a "natural distribution," which is an inherent and stable property of the packings (15,131,136, 140,145,158,159). An initial distribution which is better than natural will rapidly degrade to it, and one that is worse will finally achieve it, but sometimes at a slow rate. If the rate is extremely slow, recovery from a maldistributed pattern may not be observed in practice (136,159).
8. In the presence of large-scale maldistribution, packing efficiency decreases as packing height increases (Fig. 9.6; also 15,131, 132,136). This is due to composition nonuniformity generated by pinching and to the development of wall flow. With small packings, the above may occur even in the absence of initial maldistribution (136).

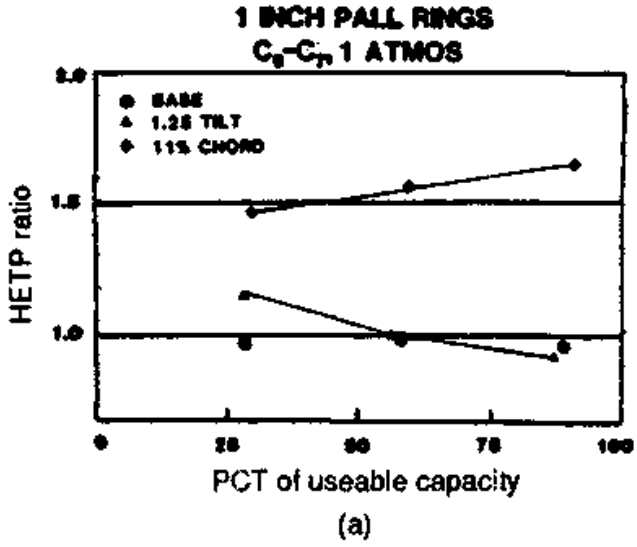

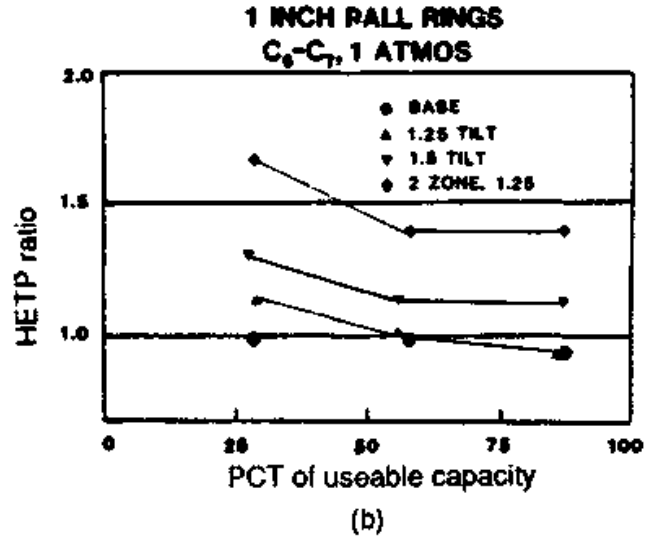

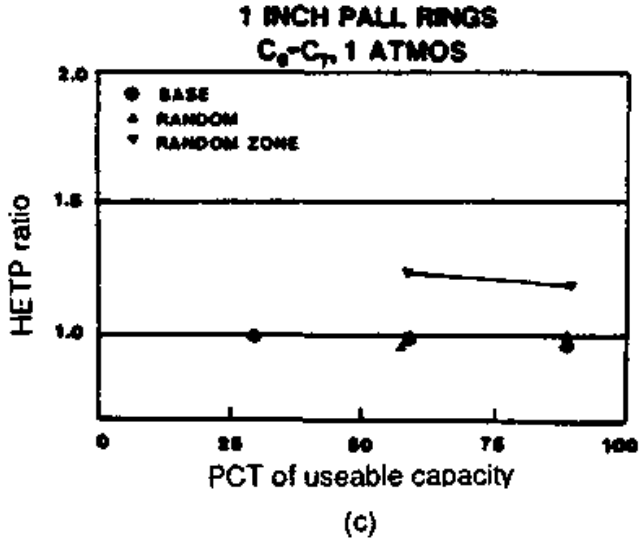

Figure 9.7 Comparing the effects of "small-scale" and "large-scale" maldistribution on packing HETP. (*a*) Comparing the effect of a simulated continuous tilt (max/min flow ratio = 1.25) to the simulated effect of blanking a chordal area equal to 11 percent of the tower area. (*b*) Comparing the effects of simulated continuous tilts (max/min flow ratios 1.25 and 1.5) to the effects of a situation where one-half of the distributor passes 25 percent more liquid to the other half. (*c*) Comparing the effects of random maldistribution to those of zonal maldistribution. (*Reprinted with permission from J. G. Kunesh, L. Lahm, and T. Yanagi, Ind. Eng. Chem. Res., vol. 26, p. 1845, copyright (1987) American Chemical Society.*)

An implication of this observation is that it is important to follow good redistribution practices. If a tall bed is unavoidable, it may be beneficial to attempt using larger packings in it.

9. Liquid maldistribution lowers packing turndown (15,160,161). The two upper "standard distributor" curves in Fig. 8.16*b* represent a progressively lower quality of initial liquid distribution. The diagram shows that packing turndown becomes progressively poorer with greater maldistribution. Figure 9.7*b* provides further illustration of this turndown loss.
10. Vapor distribution can be troublesome, especially in large-diameter columns. This type of maldistribution is best tackled at the source by paying attention to the vapor inlet arrangements. Common commercial vapor distributor designs are discussed elsewhere (23,40,152).

9.3 Packed-Tower Scaleup

9.3.1 Diameter considerations

For random packings there are many reports (3,56,98,136,140*a*,162–167) of an increase in HETP with column diameter, fewer in which column diameter had little effect on HETP (3,56,162,163), and an odd case in which increasing column diameter led to a decrease in HETP (56). Billet and Maćkowiak's (3,62,166) scaleup chart for Pall® rings implies that efficiency decreases as column diameter increases.

For structured packings, tests with the Koch-Sulzer BX and CY wire-mesh packings and with Mellapak 250Y showed no diameter effect on HETP (3,19,32,33). Wu and Chen (167) state that the same applies to Gempak packings. On the other hand, tests with Hyperfil showed an increase in HETP with column diameter (168).

The increase in HETP with column diameter appears to be most pronounced for small column diameters (<1 ft; Refs. 56,164) and with smaller packings (<1 in; Refs. 56,136). It has therefore been recommended that for scaleup purposes, a column at least 1 ft in diameter, and preferably larger, should be used (164).

Practically all sources explain the increase of HETP with column diameter in terms of enhanced maldistribution (3,56,62,136,148,162–164). Pilot columns seldom operate at column to packing diameters ratios (D_T/D_p) larger than 20; under these conditions, lateral mixing effectively counteracts loss of efficiency due to maldistribution pinch (Sec. 9.2.3). On the other hand, industrial-scale columns usually operate at D_T/D_p ratios of 30 to 100; under these conditions, lateral mixing is ineffective for counteracting maldistribution pinch.

In order to increase D_T/D_p, it may appear attractive to perform the

pilot test using a smaller packing size than will be used in the prototype. The measured HETP can then be adjusted for the difference in packing size using a theoretical model or a rule of thumb (Secs. 9.1.4 and 9.1.5). A successful application of this technique was reported for wire-mesh packings (169). In practice, however, the technique of scaling up from data for a smaller packing is seldom used (170). The author also strongly recommends against it. There is a considerable uncertainty in predicting the effect of packing size on HETP. Further, lateral spread (Sec. 9.2.4) is a strong function of packing size, and scaling up its effects is practically impossible.

In small columns, the wetted wall contributes to mass transfer. This problem can be overcome by keeping the ratio of column to packing diameter above 10 (Sec. 9.2.4). For cases where wall effects are significant, Wu and Chen (167) recommend applying the following safety factor.

$$\frac{\text{HETP}_{\text{prototype}}}{\text{HETP}_{\text{pilot}}} = \frac{1}{(1 - A_{\text{wall}}/A_{\text{packing}})} \tag{9.38}$$

The area ratio is given by

$$\frac{A_{\text{wall}}}{A_{\text{packing}}} = \frac{\pi D_T H}{\pi/4\, D_T^2 H\, a_p} = \frac{4}{D_T a_p} \tag{9.39}$$

As column diameter is increased, it becomes more difficult to maintain the number of distributor drip points per unit area (3,40). Also, the fraction of unirrigated area under the top distributor (near the column wall) may vary. These changes can lead to enhancement of maldistribution in the prototype. It was recommended (170) to use the same number of drip points per unit area and to ensure that liquid is distributed to the column wall both in the prototype and in the pilot column.

Packing a pilot column is easier than packing a much larger column. A better packing technique in the pilot column will give better HETP. Billet (56) presents an example in which the opposite occurred, and the larger column achieved a better HETP than the smaller. It is best to pack the pilot column using the same technique that is intended for the prototype.

9.3.2 Height, loading, wetting, and other considerations

Height effects. Experimental data for random packings show that HETP slightly increases with bed depth (3,56,61,98,144). This increase in HETP appears to be more important at low liquid rates

(61,98). Using the zone-stage model (Sec. 9.2.5), Zuiderweg et al. (136) predicted a slight effect of bed depth on HETP for larger packings, but a large effect for smaller packings.

For structured packing, tests with Mellapak 250Y (32) showed no effect of bed height on packing efficiency. Tests by Martin et al. (171) using several structured packings in a 10-ft-tall bed showed that in some cases, the lower part of the bed has a higher HETP than the upper part, while in other cases, HETP was uniform throughout the bed.

The effect of bed depth on packing HETP is attributed to liquid maldistribution (56,136,171). Zuiderweg et al. (136) suggest that the uneven liquid flow generates an uneven concentration profile and localized pinching near the bottom of the beds. The tests by Martin et al. (171) confirm that the problem area is near the bottom. According to the zone-stage model (Sec. 9.2.5), as well as the empirical correlation by Moore and Rukovena (Sec. 9.2.6), the greater the number of stages per bed, the greater is the rise in HETP with bed depth. The presence and extent of maldistribution plays an important role in determining the bed-depth effect (136,140).

As the bed depth increases, end effects (i.e., mass transfer in the region of liquid introduction and in the region where liquid drips from the packing supports) become less important. Such end effects tend to lower the HETP observed in short columns, such as pilot-plant columns.

In summary, bed depth may significantly influence HETP. This adds uncertainty to scaleup. Shallow test beds should be avoided. Most investigators use beds at least 5 ft tall, and often more than 10 ft tall. One suggestion (172) is to test the pilot columns at different heights of packings. The FRI sampling technique (below) can detect maldistribution along the bed height.

Loadings. For many random and corrugated-sheet structured packings, HETP is independent of vapor and liquid loadings (Fig. 8.16*a*). For wire-mesh and many corrugated-sheet structured packings, HETP increases with vapor and liquid loads (Fig. 8.16*c*). For some packings, HETP decreases as vapor and liquid loads increase (Fig. 8.16*d*).

Wu and Chen (167) recommend pilot testing over the entire range between the expected minimum and maximum operating rates, and taking the highest measured HETP as the basis for scaleup. The author concurs. With structured packings, the load effect may be due to liquid rather than vapor loads, and the pilot tests should cover the range of liquid loads (i.e., gpm per square foot of column cross section) that is expected in the prototype.

Wetting. At low liquid rates, the onset of minimum wetting can affect scaleup, particularly with random packings and aqueous systems. The criteria in Sec. 8.2.15 should be examined to check if operation near minimum wetting is likely. If it is, scaleup can be unreliable. The unreliability can be alleviated by pilot-testing at the composition range expected in the prototype, and by using identical packing materials and surface treatment in the pilot tests and in the prototype.

Underwetting (Sec. 8.2.16). At the aqueous end of aqueous-organic columns, underwetting is most significant. Near the onset of underwetting, HETP becomes strongly dependent on composition, packing material and surface roughness, and the presence of surfactants. When underwetting is likely, scaleup can be unreliable. The unreliability can be alleviated by pilot-testing at the composition range expected in the prototype, and by using identical packing materials and surface treatment in the pilot tests and in the prototype.

Preflooding. For one structured packing test with an aqueous system, Billet (3) measured higher efficiency for a preflooded bed compared to a non-preflooded bed. Presumably, the preflooding improved either wetting or distribution. Section 9.2.4 addresses the effect of preflooding on distribution. Billet (3) recommends preflooding the packing both in the prototype and in the pilot column to ensure maximum efficiency.

Sampling. Fractionation Research Inc. (FRI) developed a sampling technique that eliminates the influence of "end effects" and detects a maldistributed composition profile. This technique (75,88,131,160) samples the bed at frequent intervals, typically every 2 ft or so. HETP is determined from a plot of these interbed samples rather than from the top and bottom compositions.

It is imperative that the interbed samplers catch representative samples, which are an average through the bed cross section. Caution is required when the liquid is highly aerated and turbulent (e.g., above 200 psia or above 20 gpm/ft^2). The author highly recommends the FRI sampling technique for all other conditions.

Aging. Billet (3) showed that for some plastic packings in aqueous systems, the efficiency after one week's operation was almost double the efficiency of new packings. Little further change was observed after one week. Billet explains the phenomenon by improved wetting. He recommends that data for plastic packings should only

be used for scaleup after being in operation for an adequately long period.

9.3.3 Packed-tower scaleup: summary and recommendations

In general, the key to a successful scaleup of packed columns is producing identical distribution conditions in the pilot column to those expected in the prototype. Sections 9.2.1 to 9.3.2 show that this is practically impossible to achieve. Packed-column scaleup is therefore often uncertain and sometimes dangerous. For best results, one can only do the best he or she can. Based on Secs. 9.3.1 and 9.3.2, this includes

- Use the same packing type and size in the pilot column as those that will be used in the prototype.
- Use a pilot column at least 1 ft in diameter.
- Use a column to packing diameter ratio of at least 10; alternatively, correct HETP for wall effects using Eq. (9.38).
- In the pilot column distributor, use the same number of drip points per unit area as in the prototype and ensure that liquid is distributed to the wall in the same manner as in the prototype.
- Pack the pilot column using the same packing technique as in the prototype.
- Use a bed at least 5 ft tall, preferably at least 10 ft tall, in the pilot column.
- Use the FRI sampling technique and samplers for calculating pilot column HETP.
- Perform pilot tests over the entire range of vapor and liquid loads between the expected minimum and maximum operating rates. Use the highest measured HETP as the basis for scaleup.
- Be on the watch for wetting and underwetting effects. When these are likely, scaleup can be particularly unreliable.
- When wetting or underwetting effects are likely, pilot-test at the composition range expected in the prototype. Also, use identical materials of construction and surface treatment in the pilot tests and the prototype.
- Compare the pilot HETP under preflooded conditions to the efficiency measured under non-preflooded conditions.
- Ensure plastic packings have been properly aged prior to the pilot test.

Safety factor. Even if the above techniques are followed, some uncertainty still remains. To allow for this uncertainty, it has been recommended (98,120) to add 6 to 12 in to the HETP measured in small-scale columns, and possibly more in vacuum columns operating at low liquid rates. This recommendation has been criticized (163) for being too conservative. An alternative recommendation (167) is to add a 10 to 15 percent safety factor.

9.4 Packed-Column Sizing

9.4.1 Strategy

Most modern packings are proprietary. Optimum column sizing is an interactive process between the user (or the user's representative) and the manufacturer, beginning at an early stage of the design. An effective user-manufacturer interactive procedure is:

1. Survey process factors that may constrain packed-tower design. These include feed solids content, fouling, corrosion, foaming, potential for pressure surges, startup and shutdown procedures, the possibility of pyrophoric deposits and hot oil remaining on packing surfaces at shutdown, and the possibility of precipitation and adverse reactions. These influence the choice of packing and the distributor design.

   Several troublesome experiences resulted from insufficient attention to this guideline (40). These experiences included plugging, premature flooding, poor separation, fires, dislodging of packed beds, severe corrosion, melting of plastic packing, breakage of ceramic packing, loss of capacity, and others.
2. Perform a preliminary packed-tower sizing. It is best to base this step on a packing for which reliable information is available near the expected operating point, e.g., on Pall® rings for random packings. The preliminary design should be rigorous, not shortcut. A column built as per this design must work. The only feature distinguishing this preliminary design from the final design is that at this preliminary point the column may be somewhat oversized, i.e., nonoptimum.

   The preliminary design provides a basis for deciding which manufacturers, which packings, and what packing sizes should be considered. The preliminary diameter and bed height provide a suitable basis for comparing quotes. An "apples-to-apples" comparison of different quotes is extremely difficult when column height and diameter vary.
3. Prepare an inquiry specification with a quote request. This document should communicate to the suppliers information about the

service, the design duty, requirements and constraints, and solicit bids that can readily be compared.

- *Include all data, constraints, or requirements arising from step 1 above.* If uncertain about how fouling, potential for pressure surges, startup and shutdown constraints, etc., affect the packing design, discuss these with the suppliers.
- *Include all relevant process information as well as the preliminary column diameter, bed heights, and spaces between beds.* Request a base quote using the preliminary design. Do not specify packing type and size, but list any constraints such as "we require random packing, 1.5 to 2.5 inch nominal size or equivalent." Request the suppliers to take exception to any details that in their opinion will not work.
- *Request the supplier to prepare an alternate quote for a design that can reduce the column diameter or bed heights.* Specify whether diameter reduction or bed height reduction is more desirable.

4. Once the quotes are received, compile a "short list" of the more attractive bids. Evaluate the alternate quotes by comparing to experimental data, correlation predictions, or sound design criteria. Chapters 10 and 11 contain all the published information the author could find on proprietary packings. Additional information may be available in proprietary data banks. If your data are insufficient to form a judgment, question the supplier's design basis and ask for backup data.

   Often, the evaluation reveals a sound alternate quote with too tight a design. Modify the design to one that you are comfortable with, and request the supplier to revise the alternative quote. The author strongly believes that the user must be confident that the alternate design will perform adequately before accepting it. The confidence must be based on engineering rather than on sales claims alone. Any problems must be discussed with the supplier.
5. Once comfortable with the quoted designs (modified per step 4 above) those quotes should be analyzed economically to determine which one is best.

9.4.2 Column sizing example

Example 9.2 For the depropanizer in Examples 2.4 (Sec. 2.3.1), 3.4 (Sec. 3.2.5), and 6.1 (Sec. 6.5.2), would a packed tower be better than a tray tower? Process loads and physical properties are the same as those in Table 6.10. The service is nonfouling, the streams have a negligible solid content, the corrosive tendency is low, and pressure surges are unlikely.

solution Section 8.3 compares the advantages of packed and trayed towers. A study of the items listed in this section reveals no clear frontrunner. The high tendency to foam will give a slight edge to packings; the high liquid loads and the greater uncertainty in performance prediction will give a slight edge to trays. There is a need to size the column for packings and compare to the trayed tower design (Sec. 6.5.11). The procedure in Sec. 9.4.1 will be used.

STEP 1 CONSIDERATIONS There are no apparent constraints imposed by solid, corrosion, and pressure surge potential. The foaming potential can be inferred from tray column information. Table 6.7 classifies depropanizers as a low-foaming system, and suggests a derating factor of 0.9 for tray columns. Tables 6.4 and 6.5 suggest a somewhat higher foaming tendency, but these specifically address downcomers. It appears that for the current design, the system is best considered low-foaming, with a derating factor of 0.9 as per Table 6.7.

Other considerations in step 1 are the startup–shutdown procedure. The startup sequence usually involves the steps of steaming, purging, and pressuring up prior to feed introduction; the shutdown sequence is the reverse. Of these steps, steaming is a hot-commissioning operation and may constrain the choice of materials of construction. Pyrophoric deposits are unlikely, nor is hot oil on packing surfaces (the heaviest hydrocarbon is in the C_6 range), precipitation and adverse reaction. In summary, the relevant step 2 considerations are foaming and startup–shutdown steaming.

STEP 2 CONSIDERATIONS The next step is to look at the various types of packings. The depropanizer is a high-pressure distillation service. Section 8.1.10 recommends against using structured packings for high pressure distillation. Grids are seldom used for clean distillation services (Sec. 8.1.13). Random packings are therefore clear frontrunners for the depropanizer. With its low corrosion potential, carbon steel is suitable for the packing. Plastic is unlikely to offer any distinct advantages here, and is at a disadvantage because of the steaming step at startups and shutdowns.

As with tray towers (Sec. 6.5.1), the sizing procedure involves a trial-and-error calculation, in which a preliminary design is first set and refined by checking against performance correlations. As with tray towers, the sizing calculations are performed at the points listed in Sec. 6.5.1—i.e., the highest and lowest loaded points in each section of tower. For the depropanizer, the highest loadings are on stages 19 (bottom) and 3 (top) and the lowest are on stages 9 (bottom) and 8 (top), as shown in Table 6.10. These points will be used in the sizing calculation.

9.4.3 Column sizing example: first trial

As per step 2 (Sec. 9.4.1) the preliminary design will use carbon steel Pall® rings. This design can later be refined by working with suppliers on the use of third-generation packings (Step 4). As an initial estimate, it will be assumed that 2-in Pall® rings will be used throughout the column. This assumption will be reviewed later. For this packing, the flood point can be accurately determined by interpolation (Sec. 8.2.6), using Chart 10.1004A. Alternatively, the flood point can be determined using the Kister and Gill correlation [Eq. (8.1)]. The GPDC flood correlation (Fig. 8.17) is not suitable for 2-in Pall® rings.

	Top section	Bottom section	Note
1. Flood point by GPDC interpolation			
G, lb/h ft^2	$121{,}184/A_T$	$129{,}112/A_T$	Table 6.10
L, lb/h ft^2	$85{,}360/A_T$	$185{,}434/A_T$	Table 6.10
ρ_G, lb/ft^3	2.478	3.614	Table 6.10
ρ_L, lb/ft^3	27.944	27.191	Table 6.10
F_{lv}	0.210	0.524	Eq. (8.21)
Capacity parameter	1.29	0.95	Chart 10.1004A
μ_L, cP	0.128	0.113	Table 6.10
ν, cS	0.286	0.259	$62.4\mu_L/\rho_L$
F_p, ft^{-1}	27	27	Chart 10.1004A
$C_{S,Fl}$, ft/s	0.264	0.196	Eq. (8.22)
2. Flood point by the Kister and Gill correlation			
ΔP_{Fl}, in of water per ft	1.16	1.16	Eq. (8.1)
F_{lv}	0.210	0.524	Above
Capacity parameter @ flood	1.27	0.93	Chart 10.1004B
$C_{S,Fl}$, ft/s	0.260	0.192	Eq. (8.22)

Both calculations are in good agreement. Since data interpolation is more accurate than correlation, the values calculated by interpolation will be used in the design.

To calculate a column diameter, the column will be designed for 75 percent of flood as per the criterion in Sec. 8.2.12. In addition, a derating factor of 0.9 will be applied for the calculation as per discussion on foaming in Sec. 9.4.2.

	Top section	Bottom section	Note
C_S, design (nonderated), ft/s	0.198	0.147	$0.75 \times C_{S,Fl}$
C_S, design (derated), ft/s	0.178	0.132	$0.9 \times (C_S$,design)
$\sqrt{\rho_G/(\rho_L - \rho_G)}$	0.312	0.392	
u_S, design (derated), ft/s	0.572	0.337	Eq. (8.23)
CFS	13.584	9.924	Table 6.10
A_T, ft^2	23.75	29.43	CFS/u_S
D_T, ft	5.50	6.12	$\sqrt{\frac{4}{\pi}A_T}$

Diameter calculation using the maximum pressure drop criterion. The maximum pressure drop criterion is used jointly with the flood-point criterion, and the column diameter is set so that it satisfies the more conservative of the two criteria (Sec. 8.2.12). Table 8.4 gives the maximum pressure drop criteria. These are used in the calculation below.

	Top section	Bottom section	Note
ρ_G/ρ_L	0.089	0.133	
ρ_L/ρ_{H_2O}	0.448	0.436	
F_p, ft^{-1}	27	27	Table 10.1
Max ΔP, in of water per ft	0.86	0.83	Table 8.4, Note 1
σ, dyne/cm	3.30	2.84	Table 6.10
$\Delta P_{max}\sigma/(33\sqrt{F_p})$	0.0166	0.0137	Eq. (8.29)
$C_{S,max}$	0.181	0.167	Eq. (8.29)
$u_{S,max}$	0.580	0.426	Eq. (8.23)
A_T	23.42	23.30	CFS/$u_{S,max}$
D_T	5.46	5.45	$\sqrt{\frac{4}{\pi}A_T}$

Note that no derating was used here. The previous flood calculation was derated because of the foaming tendency at high pressure. This is not taken into account in the interpolation, which is based on data at lower pressure. On the other hand, the pressure drop criterion used applies specifically for high-pressure distillations, and should therefore contain any needed derating.

The flood-point and the maximum pressure drop criteria gave comparable tower diameters. The more conservative of the two criteria gives diameters of 5.50 and 6.12 for the top and bottom section of the tower, respectively. As the diameters for the top and bottom sections are not much different, it is attractive to use uniform column diameter. The decision of whether to make the top and bottom section diameters the same is based on the same criterion as for tray columns (Sec. 6.5.3). The preliminary column diameter is the larger for the two column sections, i.e., 6.12 ft. This diameter is normally rounded to the next nearest half foot, but in this example it is rounded only to the next nearest quarter foot. A diameter of 6.12 is far closer to 6 ft than to 6.5 ft. Column diameter is relatively small, and three excessive inches substantially increase the costs. The column is operated at high pressure, and high-pressure shells are expensive. Therefore, the preliminary column diameter is 6 ft 3 in.

Bed height calculation

	Top section	Bottom section	Note
d_p, in	2	2	Sec. 9.4.2
D_T, ft	6.25	6.25	Above
$12D_T/d_p$	38	38	
HETP, ft	3	3	Eq. (9.34)
n	7	11	Table 6.10
Total packed height, ft	21	33	$n \times$ HETP

Comment. The recommended published criteria surveyed by Kister (40) suggest that it is best to redistribute liquid approximately every 20 ft, and to have no more than 10 theoretical stages per bed. Both of these criteria suggest that the bottom section of the tower should have two packed beds with a redistributor in between, while the top section should contain one packed bed.

Substituting 1.5-in Pall® rings for 2-in rings in the bottom section will lower the packed height to 25 ft [Eq. (9.34)], possibly at the price of only a slight increase in tower diameter. This may make it possible to get rid of the redistributor and get away with a single packed bed in the bottom section. Such a design will be in slight violation of the recommended distribution criteria (above), and will also have a higher column to packing diameter ratio. Both factors will render such a design more sensitive to maldistribution. Little is known about how detrimental maldistribution is to multicomponent distillation efficiency at high pressure. The author feels that a relatively small investment (in a redistributor) is justified here in order to keep the design less sensitive to maldistribution. The author would therefore prefer two beds of 2-in Pall® rings in the bottom section.

The flood-point calculations above show that there is some spare capacity in the top section. This can be utilized for reducing the height of the top section by using smaller packings. The number of stages in the top bed, and the lower bed height, will remain well within the above guidelines for good redistribution practice. The bed to packing diameter ratio will increase somewhat; however, going from 2 in to 1.5 in would only increase the ratio by 33 percent, and this should be tolerable.

In summary, the second trial will use the following:

$$D_T = 6.25 \text{ ft}$$

$$d_p = 2 \text{ in in bottom section, } 1.5 \text{ in in top section}$$

9.4.4 Column sizing example: second trial

	Top section	Bottom section	Note
D_T, ft	6.25	6.25	Sec. 9.4.3
d_p, in	1.5	2.0	Sec. 9.4.3
A_T, ft^2	30.68	30.68	$\frac{\pi}{4}D_T^2$
CFS	13.584	9.924	Table 6.10
u_S, design ft/s	0.443	0.324	CFS/A_T
C_S, design ft/s	0.138	0.127	Eq. (8.23)

Flood point calculations Three calculation methods have been considered (Sec. 8.2.6): Interpolation, the Kister and Gill correlation, and the Billet and Schultes correlation. For the top section, interpolation cannot be used because, for 1.5-in Pall® rings, the flood/MOC data are only available for flow parameters of 0.07 and lower (Chart 10.1003). The flow parameter for the top section is 0.210 (Sec. 9.4.3). For the bottom section, the Billet and Schultes correlation cannot be used because the flow parameter is 0.524. At this flow parameter, a value for $C_{2,Fl}$ is required (Eq. 8.5) but is unavailable in Table 8.2.

	Top section	Bottom section	Note
1. *Flood point by GPDC Interpolation*			
$C_{S,Fl}$, ft/s	—	0.196	Sec. 9.4.3
$C_{S,Fl}$ (derated), ft/s	—	0.176	0.9 × $C_{S,Fl}$
% Flood	—	72%	100(C_S, design)/ $C_{S,Fl}$ (derated)
2. *Flood point by the Kister and Gill correlation*			
F_p, ft^{-1}	40	Unchanged from Sec. 9.4.3	Chart 10.1003
ΔP_{Fl}, in water per ft	1.52	↓	Eq. (8.1)
F_{lv}	0.210	↓	Sec. 9.4.3
Capacity parameter @ flood	1.45	↓	Chart 10.1003
ν,cS	0.286	↓	Sec. 9.4.4
$C_{S,Fl}$, ft/s	0.244	↓	Eq. (8.22)
$C_{S,Fl}$, derated	0.220	0.173	0.9 × $C_{S,Fl}$
% Flood	63%	73%	100(C_S, design)/ ($C_{S,Fl}$, derated)
3. *Flood point by Billet and Schultes correlation*			
a_p	47.9	—	Table 8.2
u_L	0.0277	—	$L/(3600\,A_T\rho_L)$
Re_L	187.2	—	Eq. 8.8
Ga_L	30.92×10^6	—	Eq. 8.9
ϵ	0.946	—	Table 8.2
$h_{L,Fl}$	0.316	—	Eq. 8.6
$C_{i,Fl}$	1.679	—	Table 8.2
n_{Fl}	0.388	—	Eq. 8.4
μ_V	0.0090	—	Data
$u_{S,Fl}$	0.736	—	Eq. 8.2
$u_{S,Fl}$ derated	0.662	—	0.9 × $u_{S,Fl}$
% flood	67%		100 (u_S, design/ $u_{S,Fl}$ derated)

Compliance with the maximum pressure drop criterion

	Top section	Bottom section	Note
F_p, ft^{-1}	40	27	Table 10.1
ρ_G/ρ_L	0.089	0.133	Sec. 9.4.3
ρ_L/ρ_{H_2O}	0.448	0.436	Sec. 9.4.3
Max ΔP, in water per ft	1.13	0.83	Table 8.4, note 1
σ, dyne/cm	3.30	2.84	Sec. 9.4.3
ΔP, in water per ft	0.55	0.43	Eq. (8.29)

Bed height calculation

	Top section	Bottom section	Note
$12D_T/d_p$	50	38	
HETP, ft	2.25	3	Eq. (9.34)
n	7	11	Table 6.10
Total packed height, ft	16	33	$n \times$ HETP

Comment. The calculations show that the current design is adequate. Flooding calculations performed using different correlations gave very similar answers. The column is lightly loaded in the top section. It may be tempting to go to an even smaller (1-in) packing in the top section, and save more vertical height. However, such a move is likely to further increase the column to packing diameter ratio to about 75, making the column more sensitive to maldistribution. The author would therefore feel uncomfortable with a further reduction of packing diameter in the top section.

9.4.5 Column sizing example: design checks

The design checks that will be performed in this example are MOC, pressure drop, efficiency data, and minimum wetting. Other checks that are often performed are loading point, liquid holdup, and efficiency from a theoretical correlation. The author excluded these checks because he expects them to serve little purpose in this example. The uncertainty involved in defining and predicting the load point argues against basing a design on this parameter. Liquid holdup is seldom a concern with high-pressure systems. Finally, as was previ-

ously stated (Sec. 9.1.5), theoretical methods of predicting packing efficiency compare unfavorably with the empirical rule of thumb used here (Sec. 9.4.4). Further, high pressure is outside the range of application of most, if not all, the popular theoretical methods (e.g., Table 9.1).

MOC check

	Top section	Bottom section	Note
$C_{S,\mathrm{Fl}}$ (derated), ft/s	0.220	0.176	Sec. 9.4.4
$C_{S,\mathrm{MOC}}$ (derated), ft/s	0.209	0.167	Eq. (8.10)
C_S, design, ft/s	0.138	0.127	Sec. 9.4.4
% MOC	66%	76%	100 C_S, design/ [$C_{S,\mathrm{MOC}}$ (derated)]

This is well in line with the MOC criterion in Sec. 8.2.12.

Average bed pressure drop calculation

Most methods for pressure drop calculation assume the column handles a nonfoaming mixture. Therefore, they do not strictly apply to the high-pressure column in this example, where systems do show a tendency to foam. The only published method that applies for these conditions is Strigle's [15; Eq. (8.29)]. This method was used earlier in this example to check compliance with the maximum pressure drop criterion. Here it is used to calculate the average bed pressure drop.

	Top section	Bottom section	Note
ΔP @ stages 3 and 19, in of water per ft	0.55	0.43	Sec. 9.4.4
Stage 8, 9 calculation:			
ρ_G	2.325	3.017	Table 6.10
ρ_L	30.122	29.029	Table 6.10
CFS	13.060	7.629	Table 6.10
A_T	30.68	30.68	Sec. 9.4.4
u_S	0.426	0.249	CFS/A_T
C_S	0.123	0.085	Eq. (8.23)
σ	4.44	3.40	Table 6.10
F_p	40	27	Sec. 9.4.4
ΔP, in of water per ft	0.31	0.13	Eq. (8.29)
Average ΔP, in of water per ft	0.42	0.26	Eq. (8.30)

Maximum pressure drop by interpolation. Section 8.2.9 states that for high-pressure systems, the GPDC interpolation procedure is the most suitable. This method will be used here.

	Top section	Bottom section	Note
F_{lv}	0.210	0.524	Sec. 9.4.3
C_S, design ft/s	0.138	0.127	Sec. 9.4.4
ν,cS	0.286	0.259	Sec. 9.4.3
F_p, ft^{-1}	40	27	Sec. 9.4.4
Capacity parameter @ design	0.82	0.62	Eq. (8.22)
ΔP @ design, in of water per ft	0.22	0.40	Charts 10.1003 and 10.1004B

Comment. This calculation is based on data for nonfoaming systems. The calculated pressure drop is satisfactory, but the actual pressure drop would be somewhat higher due to the foaming tendency.

Efficiency check. HETP data will be compared with the calculated HETP (Sec. 9.4.4). Table 11.1 is searched for efficiency data on columns in similar service that contain random packings. The following data, extracted from Table 11.1 are relevant:

Service	Pressure, psia	Reflux ratio	Diameter, in	Height, ft	Packing		HETP, in
					Type	Size, in	
Depropanizer, top section	270	0.74	23	16	Pall®(M)	1.5	38
Depropanizer, bottom section	270	0.74	23	24	Pall®(M)	1.5	29
Deethanizer, top section	300	0.42	18	20	Pall®(M)	1.5	35
Deethanizer, bottom section	300	0.24	30	18	Pall®(M)	2.0	40

The calculated HETPs (Sec. 9.4.4) are 27 in for the top section (1.5-in Pall® rings) and 36 in for the bottom section (2-in Pall® rings). Compared to the data, the calculated HETPs appear optimistic.

Could the Table 11.1 data have been measured under mal-

distribution? The ratios of column to packing diameters range from 12 to 15; at these ratios, lateral mixing should have mitigated the pinching effects. The bed heights were low, and did not violate good redistribution practice (except for one case—and this case gave the lowest HETP!). There is no evidence to suggest maldistribution. The data therefore imply that the high HETPs are possibly system-related. These data, therefore, serve as a better basis for HETP in this example than Eq. (9.34).

The Table 11.1 data suggest that the top sections operate at HETPs of the order of 35 to 38 in with 1.5-in Pall® rings. The bottom sections have an HETP of about 29 in with 1.5-in Pall® rings, and 40 in with 2-in Pall® rings. The difference (11 in) is similar to the difference predicted from Eq. (9.34), and therefore, makes sense. It follows that for design purposes, an HETP value of 38 in is a good estimate for the top section of the depropanizer in this example, while an HETP of 40 in is a good estimate for the bottom section. Note that these values are not conservative; they match the available data.

Minimum wetting. As with a tray tower, this turndown check is performed at the lowest loaded stages (8 and 9; see Table 6.10) at turned down conditions. As per Example 6.1, the problem requires turndown to 60 percent of the expected design loads. Therefore, the vapor and liquid loads shown in Table 6.10 for stages 8 and 9 are multiplied by 0.6 for the minimum wetting check.

	Top section	Bottom section	Note
GPM @ design	304	598	Table 6.10 (stages 8 and 9)
GPM @ turndown	182	359	0.6 × GPM
GPM/ft^2 @ turndown	5.9	11.7	

Since these rates are well above 3 gpm/ft^2, the column operates well above minimum wetting [Eq. (8.39)].

Revision to design following checks. The only design revision required following the above checks is for bed heights, due to the change in HETP (see "Efficiency Check" above).

	Top section	Bottom section	Note
d_p, in	1.5	2	Sec. 9.4.4
D_T, ft	6.25	6.25	Sec. 9.4.4
12 D_T/d_p	50	38	
HETP, in	38	40	See "Efficiency Check"
n	7	11	
Total packed height, ft	22.2	36.7	(n × HETP)/12
Packed height, ft (rounded)	22	2 beds, 19 ft each	
Average ΔP, in of water per ft	0.42	0.26	See "Average bed pressure drop calculation" above
Total bed pressure drop, in of water	9.2	9.9	ΔP × (packed height)

Total packing pressure drop = 9.2 + 9.9 = 19.1 in of water = 0.7 psi

9.4.6 Column sizing example: design and performance summary

Design summary

	Top section	Bottom section
Tower diameter, ft	6.25	6.25
No. of packed beds	1	2
Total packed height, ft	22	38
Type of packing	Pall® rings (M)	Pall® rings (M)
Packing size, in	1.5	2.0

Performance summary

	Top section	Bottom section
% Flood	63%	72%
Pressure drop, in of water per ft		
Max, expected	0.55	0.43
Max, allowable	1.13	0.83
Bed average	0.42	0.26
Total bed pressure drop, in of water	9.2	9.9
Design HETP, in	28	40
No. of theoretical stages	7	11

Loads at design point

	Top section	Bottom section
Vapor C_S, ft/s	0.138	0.127
Flow parameter, F_{lv}	0.21	0.52
Liquid, gpm/ft^2	12.4	27.7

9.4.7 Concluding comments on design philosophy

The design proposed in Sec. 9.4.6 was shown to satisfy all the performance criteria, and is optimized for Pall® rings. The next section will speculate how it can be further optimized using third-generation packings.

The example reflects a major difficulty often encountered in packed-tower design: the inability to tell whether a correlation will give a suitable prediction for the service under consideration. For many years, this difficulty was circumvented by grossly oversizing packed towers. With the recent renaissance of packed towers, which was coupled by a fierce competition among the suppliers, the oversizing eroded away. The prediction problem remained. While in the past this problem stayed hidden in an oversized column, it raised its ugly head once the oversizing eroded. The result was a relatively large number of designs failing to meet their performance objectives.

It is important to recognize that working with packed-tower correlations alone is not sufficient for ensuring that a design will work. Data interpolation is far superior to our present correlations, and is the only reliable design tool. When no data are available to interpolate for a given packing in a given service, the designer has only two options: either to grossly oversize the column or to gamble.

The design strategy in Sec. 9.4.1 has been tailored to this state of the art. Chapters 10 and 11 contain all the data that the author could find in the published literature, and present them in a manner that can be readily interpolated.

The above also has strong implications when it comes to selecting a supplier of proprietary packing. Proven track record of a packing in a given service should always be a major consideration, especially when backed by actual performance data. Remember, the availability of good performance data can—and often does—make a difference between success and failure.

9.4.8 Column sizing example: speculation on suppliers' modifications to the preliminary design

As per step 4 in Sec. 9.4.1, the preliminary design in Sec. 9.4.6 will be sent to the suppliers of third-generation packings. The inquiry will request a quote for an alternate design. Below is a speculation on the response of a typical packing supplier. The estimate is based on a typical metallic third-generation packing with a packing factor of 18 in the bottom section and 24 in the top section. All major suppliers market packings that roughly have these packing factors.

Column diameter

	Top section	Bottom section	Note
Packing	1.5-in third-generation	2-in third-generation	
F_p, ft^{-1}	24	18	Premise
ΔP_{flood}, in of water per ft	1.06	0.87	Eq. (8.1)
F_{lv}	0.210	0.524	Sec. 9.4.6
Capacity parameter	1.22	0.80	Chart 10.XXXX
(@ flood; based on different	1.15	0.81	Chart 10.XXXX
packings of the same packing factor)	1.14	0.86	Chart 10.XXXX
Capacity parameter (typical)	1.17	0.82	Average of above
ν, cS	0.286	0.259	Sec. 9.4.3
$C_{S,Fl}$, ft/s	0.254	0.207	Eq. (8.22)
C_S, design (derated), ft/s	0.172	0.140	$0.75 \times 0.9 \times C_{S,Fl}$
$\sqrt{\rho_G/(\rho_L - \rho_G)}$	0.312	0.392	Sec. 9.4.3
u_S, design (derated), ft/s	0.550	0.356	Eq. (8.23)
CFS	13.584	9.924	Table 6.10
A_T	24.70	27.87	CFS/u_S
D_T, ft	5.61	5.96	$\sqrt{(4/\pi)A_T}$
D_T, ft (rounded	6	6	

There is little published information on estimating HETP for third-generation packings in this service. The only published relevant method is that by Strigle (15) for the stripping of light hydrocarbons from heavier ones using IMTP® [Eq. (9.37) in Table 9.3]. The column simulation gives a typical bottom section molecular weight of 58 in the depropanizer. For #50 IMTP®, Eq. (9.37) in Table 9.3 gives

$$\text{HETP} = 4.5 - 0.6 \ln 58 + 0.53 = 2.6 \text{ ft}$$

For argument sake, it will be assumed that this equation applies for

the rectifying section as well. With an average molecular weight of 40 in that section, and assuming #40 IMTP®, Eq. (9.37) from Table 9.3 gives

$$\text{HETP} = 4.5 - 0.6 \ln 40 = 2.3 \text{ ft}$$

Assuming these HETPs apply to the current example, the heights are

Top section

$$2.3 \text{ ft} \times 7 \text{ stages} = 16.1 \text{ ft (say 16 ft)}$$

Bottom section

$$2.6 \text{ ft} \times 11 \text{ stages} = 28.6 \text{ ft (say 30 ft)}$$

Alternate design. Comparison to the preliminary design follows:

	Preliminary design	Alternate design
Packing	Pall® rings	Third-generation random
Diameter, ft	6.25	6.0
Packed height, ft	60	46
Top section	22	16
Bottom section	38	30
Packing size, in		
Top section	1.5	1.5
Bottom section	2.0	2.0

Evaluation of the alternate design. The alternate design is attractive and can save considerable capital compared to the preliminary design, but the user must be convinced that it will work before proceeding with it.

The third-generation packings used are of the same nominal size as the Pall® rings. Looking at Fig. 8.7, this suggests lower packing factors, but much the same packing surface area, and therefore, much the same efficiency as the Pall® rings. Yet, this is not so; the efficiency predicted for the Pall® rings is 23 percent lower than that predicted for the third-generation packing. The difference is associated with the basis of the HETP prediction. The key for acceptance of the alternate quote here is, therefore, being convinced that the supplier's basis for the lower HETP is correct.

Normally, the HETP used by the supplier was derived from tests or experience in similar towers. The user needs to confirm that this ex-

perience was correctly and conservatively translated into the design HETP for the new tower. It may be possible to obtain actual test data from an existing tower; these would provide a very reliable check. Unfortunately, data are often unavailable, and the user needs to troubleshoot the design without them. Asking the right questions is important. Here are some:

- What HETPs were used in the previous designs? What was their basis?
- Were there performance tests that confirmed the design HETPs? Were the performance tests conducted rigorously (see Ref. 40 for good testing practices), or did they simply consist of taking sets of readings?
- Was a sensitivity analysis conducted on the effects of measurement errors on HETP (see Ref. 40)? What variables were the data sensitive to?
- Was the VLE used in the test data analysis the same as the VLE used in the current design? If not, does analyzing the test data using the current VLE lead to higher HETP (see Secs. 7.3.1 and 7.3.6).
- Were the packings (type and size), distributors, and redistributors similar to those that will be used in the current design? If not, how does the design HETP account for the differences?
- Was the column used to derive the data of the same scale (diameter, bed heights) as will be used in the new design? If not, are there any scaleup effects that should be allowed for?
- Are there any differences in operation—such as the nature of the feed mixture, pressure, temperature, etc., that may affect the scaleup of HETP to the new design?

Modification of the alternate design. Once the replies to the above questions are evaluated, a new design basis emerges. This basis is established by closely working with the supplier until an HETP is derived with which both the user and the supplier are comfortable.

9.4.9 Column sizing example: trays or packings?

Example 9.2 asked (Sec. 9.4.2) whether a packed tower would be better than trays for the depropanizer. The design with trays is in Sec. 6.5.11. For the comparison, it is assumed that after evaluation of the alternate design (with third-generation packing; Sec. 9.4.9) it was found to be sound and not too tight.

	Tray tower	Packed tower	Note
Column diameter, ft	6	6	
Top section:			
No. of trays	11		11 trays ↔ 10 spacings
Tray spacing, in	21		
Packed height, ft		16	
Allowance for distributor, ft		2	
Allowance for support or holddown, ft		1	
Total height, ft	17.5	19	
Bottom section:			
No. of trays	18		18 trays ↔ 17 spacings
Tray spacing, in	24		
Packed height, ft		30	
Allowance for distributor, ft		2	
Allowance for redistributor, ft		4	Needs to accommodate a manhole as well
Allowance for support or holddown, ft		2	
Total height, ft	34	38	
Middle section (between top and bottom)			
Height, ft	3.5	4.5	Large enough to accommodate manhole; in packed tower, also vapor distribution device
Height of packed or trayed portion of column, ft	55	61.5	

Comment. In this example, a tray tower is slightly shorter, and otherwise much the same size as a packed tower. In such a case, a tray tower will be preferred both because of the height saving and due to the smaller cost of trays compared to packings plus distributors. Also, the use of a trayed tower in this example will reduce the degree of uncertainty regarding performance prediction.

9.5 Nomenclature (Chapters 8 and 9)

9.5.1 English letters

a_e	Effective interfacial area for gas-liquid contact per unit volume, ft^2/ft^3
a_p	Packing surface area per unit volume, ft^2/ft^3
A_T	Tower cross-sectional area, ft^2
$A_{packing}$	Total effective packing surface area, ft^2
a_w	Wetted surface area of the packing per unit volume, ft^2/ft^3, given by Eq. (9.16)
A_{wall}	Wetted column wall surface area, ft^2

B	Length of base of structured packing flow channel, in
C_1,C_2	Constants in Leva's pressure drop equations, Eqs. (8.11) and (8.12)
C_3,C_4	Constants in the Robbins pressure drop equation, Eq. (8.13); defined by Eqs. (8.13*a*) and (8.13*b*)
C_5	Constant in the Bravo et al. pressure drop correlation. Eq. (8.17), given in Table 8.1
C_6	Constant in Strigle's HETP equation for hydrocarbon stripping, Eq. (9.37)
$C_{1,\mathrm{Fl}},C_{2,\mathrm{Fl}}$	Constants in Billet's flood correlation, Eqs. (8.4) and (8.5), given in Table 8.2
$C_{1,\mathrm{Lo}},C_{2,\mathrm{Lo}}$	Constants in Billet's load-point correlation, Eqs. (8.28*a*) and (8.28*b*), given in Table 8.2
$C_{i,\mathrm{Fl}}$	Constant in Billet's flood correlation, given by Eqs. (8.4) and (8.5)
$C_{i,\mathrm{Lo}}$	Constant in Billet's load-point correlation, given by Eqs. (8.28*a*) and (8.28*b*)
C_L	Liquid falling film number, defined by Eq. (8.36)
C_S	Vapor capacity factor, or *C*-factor, defined by Eq. (8.23), ft/s
Ca_L	Capillary number of the liquid, Eq. (9.22), dimensionless
CFS	Vapor flow rate, ft^3/s
D	Diffusion coefficient for key component, ft^2/s
D'	Distillate flow rate, lb-mole/h
d_a	Outer diameter of packing particle, in
dH	Fractional height element, ft
dy	Difference in mole fraction of the more volatile component across a fractional height element (Eq. 9.1)
d_{eq}	Equivalent diameter of structured-packing flow channel, in, values given in Table 8.1
d_p	Packing diameter, in
D_p	Packing diameter, ft
d_s	Same as D_T
D_T	Tower diameter, ft
E	Efficiency of a tray tower, percent
F,F_p	Packing factor, values listed in Table 10.1, ft^{-1}
F_{lv}	Flow parameter, given by Eqs. (8.3) and (8.21)
F_{pd}	Dry-bed packing factor, values listed in Table 8.3, ft^{-1}
Fr_L	Froude number of the liquid. Given by Eq. (8.20) for the Bravo et al. pressure drop correlation, and by Eq. (9.18) for the Bravo and Fair efficiency correlation, dimensionless
G	Gas flow rate, $\mathrm{lb/h\text{-}ft}^2$ (Only in Fig. 8.17, units are $\mathrm{lb/s\text{-}ft}^2$)

G^*	Gas flow rate, lb/s-ft^2
G'	Gas flow rate, lb-mole/h
G_f	Gas loading factor in the Robbins pressure drop equation, defined by Eq. (8.14), lb/hr-ft^2
g	Acceleration due to gravity, 32.2 ft/sec^2
g_c	Dimensional constant, 32.2 lb-ft/(lbf-s^2)
Ga_L	Galileo number, given by Eq. (8.9)
GPM	Liquid load, gpm
H	Bed height, feet
h	Height of packing particle, in
h	Height of structured packing flow channel (i.e., crimp height), in
H_G	Height of gas transfer unit, ft
H_L	Height of liquid transfer unit, ft
h_L	Liquid holdup, ft^3 liquid/ft^3 bed volume
HETP	Height equivalent of a theoretical stage, ft
HTU	Height of a transfer unit, defined by Eq. (9.9), ft
K_1	Fraction of liquid stream on a stage that flows downward (Sec. 9.2.5)
k_G	Vapor phase mass transfer coefficient, ft/s
k_L	Liquid phase mass transfer coefficient, ft/s
k_{OG}	Overall mass transfer coefficient, based on the gas phase, lb-mole/(h) (ft^2) (atm)
L	Liquid flow rate, lb/h-ft^2 (Only in Fig. 8.17, units are lb/s-ft^2)
L'	Liquid flow rate, lb-mole/h
L_f	Liquid loading factor in the Robbins pressure drop equation, defined by Eq. (8.15), lb/h-ft^2
m	Slope of the equilibrium curve
MOC	Maximum operational capacity, Sec. 8.2.4
MW	Molecular weight
MWR	Minimum wetting rate, Sec. 8.2.15
N	Number of moles transferred per unit volume, lb-mol/h ft^3
N'	Number of moles transferred, lb-mol/h
n	Number of theoretical stages in a packed bed
n_{Fl}	Constant in Billet's flood correlation, given by Eq. (8.4) and (8.5)
n_H	Constant in the Strigle HETP rules of thumb, Eq. 9.36, given in Table 9.3
n_{Lo}	Constant in Billet's load-point correlation, given by Eq. (8.28*a*) and (8.28*b*)

N_p	Number of packing particles per unit volume, values listed in Table 8.2, ft^{-3}
NTU	Number of transfer units, defined by Eq. (9.8)
P	Pressure, atm
p	Available perimeter for liquid flow through structured packing channel, given by Eq. (9.31), ft/ft^2
p_T	Tower top pressure, mbar
ΔP	Packed-bed specific pressure drop, inches water per foot of packed height
Q_{MW}	Minimum wetting rate, gpm/ft^2 of tower cross-section area
Re	Reynolds number. Different forms used for different correlations. Given by Eq. (8.8) for Billet's flood and load correlations, by Eq. (8.19) for the Bravo et al. pressure drop correlation, by Eq. (9.17) for the Bravo and Fair efficiency correlation, and by Eq. (9.28) for the Bravo et al. efficiency correlation. Dimensionless
S	Tray spacing [only in Eq. (9.11)], ft
S	Side length of structured packing flow channel, in
Sc	Schmidt number. Given by Eqs. (9.20). Dimensionless
Sh_G	Vapor phase Sherwood number, given by Eq. (9.27). Dimensionless
T_L	Liquid shear stress number, given by Eq. (8.37)
u_{eff}	Effective gas velocity inside a structured packing flow channel, defined by Eq. (8.18), ft/s
u_L	Liquid superficial velocity, based on the cross-section area of the empty column, ft/s
$u_{L,eff}$	Effective liquid velocity through structured packing channel, defined by Eq. (9.29), ft/s
u_S, u_V	Vapor superficial velocity, based on the cross-section area of the empty column, ft/s
V	Same as G
V'	Vapor flow rate, lb-mole/h
We_L	Weber number of the liquid. Given by Eq. (9.19), dimensionless
x	Fraction of the more volatile component in the liquid
y	Fraction of the more volatile component in vapor
y^*	Equilibrium mole fraction of the more volatile component in the vapor

9.5.2 Greek letters

α	Relative volatility
β	Fraction of structured packing surface that is wetted, given by Eq. (9.33)

Γ	Liquid flow based on perimeter of structured packing channel, given by Eq. (9.30), lb/ft s
ϵ	Fractional bed voidage. Values listed in Tables 8.1 and 8.2
θ	Angle of inclination of the structured packing flow channel from the horizontal. Values listed in Table 8.1, degrees
λ	mG'/L'
μ	Viscosity, cP
ν	Kinematic viscosity, cS
π	3.142...
ρ	Density, lb/ft^3
σ	Surface tension, dyne/cm
σ_c	Critical surface tension, dyne/cm, Sec. 9.1.4
ϕ	Contact angle, shown in Fig. 8.22, degrees
ψ	Ratio of the density of water to the density of the liquid

9.5.3 Subscripts

0,1,2	Different points along the column height
1,2	Denotes the two parallel columns (Sec. 9.2.2 only)
atm	At atmospheric pressure
bot	At the bottom of the packed bed
D	Distillate
d	Dry (i.e., no liquid flow)
Fl	At the flood point
G	Gas
H_2O	Water
in	Entering the packed bed
L	Liquid
Lo	At the loading point
min	Minimum
max	Maximum
MOC	At the maximum operational capacity
out	Leaving the packed bed
pilot	Of pilot column
prototype	Of prototype
ref	For reference system
top	At the top of the packed bed
V	Vapor

9.6 References (Chapters 8 and 9)

1. Eckert, J. S., in P. A. Schweitzer (ed.), *Handbook of Separation Techniques for Chemical Engineers,* McGraw-Hill, New York, 1979.
2. Norton Company, Bulletin SI-72, Akron, Ohio, 1973.
3. Billet, R., *Packed Column Analysis and Design,* Ruhr University, Bochum, 1989.
4. Eckert, J. S., *Chem. Engnr.* (London), Nov., p. 712, 1974.
5. Strigle, R. F., Jr., and K. E. Porter, *I. Chem. E. Symp. Ser.* 56, p. 3.3/19, 1979.
6. Glitsch, Inc., Bulletin 345, Dallas, Texas, 1986.
7. Nutter Engineering Corp., Bulletin N-2, Tulsa, Okla., 1989.
8. Nutter, D. E., *I. Chem. E. Symp. Ser.* 104, A129, 1987.

8*a*. Koch Engineering Company Inc., Bulletin KRP-2, Wichita, Kansas, 1987. (Revised version with HcKp, 1991.)

9. Billet, R., and J. Maćkowiak, *Chemie-Technik 13*(12), p. 37, 1984; *ibid., 14*(4), p. 91, 1985; *ibid., 14*(5), p. 195, 1985.
10. Jaeger Products, Inc., Bulletin No. JTP-600, Spring, Texas.
11. Billet, R., and J. Maćkowiak, *Verfahrenstechnik 16,* p. 67, 1982.
12. Lantec Products, Inc., "Tower Packing Technology Breakthrough from LANTEC," Agoura Hills, California.
13. Leva, M., D. Bhaga, and A. Trickett, *Chem. Engnr.,* Sept. 27, p. 25, 1990.
14. Fair, J. R., D. E. Steinmeyer, W. R. Penney, and B. B. Crocker in R. H. Perry and D. Green (eds.), *Chemical Engineers' Handbook,* 6th ed., McGraw-Hill, New York, 1984.
15. Strigle, R. F., Jr., *Random Packings and Packed Towers,* Gulf Publishing, Houston, Texas, 1987.
16. Horner, G., *Chem. Engnr.,* p. 22, November 1984.
17. Thurgood, D. B., *Chem SA,* p. 487, September 1984.
18. Seidel, R. O., *Experience in the Operation of Activated Hot Potassium Carbonate Acid Gas Removal Plants (U.S.),* Seminar on Raising Productivity in Fertilizer Plants, Baghdad, Iraq, March 23–25, 1978.
19. *Sulzer Technical Review,* 3/1970.
20. ACS, Inc., "High Efficiency Column Packing," design manual, Houston, Texas.
21. Spiegel, L., and W. Meier, *I. Chem. E. Symp. Ser.* 104, p. A203, 1987.
22. Bonilla, J. A., J. Shieh, and P. Wang, paper presented at the National AIChE Meeting, Denver, Colorado, August 24, 1988.
23. Chen, G. K., and K. T. Chuang, *Hydrocarb. Proc. 68*(2), p. 37, 1989.
24. Rukovena, F., Jr., and R. F. Strigle, Jr., paper presented at the National AIChE meeting, Houston, Texas, April, 1989.
25. Fair, J. R., and J. L. Bravo, *Chem. Eng. Prog. 86*(1), p. 19, 1990
26. Jaeger Products, Inc., Product Bulletin 500, 1989, Spring, Texas.

26a. Bravo, J. L. (Jaeger Products Inc.), private communication, February 1991.

27. Nutter Engineering Corp., Bulletin B-1, Tulsa, Oklahoma, 1987.
28. McGlamery, G. G., Ph.D. Thesis, University of Texas at Austin, 1988.
29. Buhlman, U., *Chemie Technik Int.,* p. 49, 1988.
30. Norton Chemical Process Products, Bulletin IS-1, Akron, Ohio, 1988.
31. McNulty, K. J., and C. L. Hsieh, paper presented at the Annual Meeting of the AIChE, Los Angeles, California, Nov. 14–19, 1982.

31*a*. Kurtz, D. P., K. J. McNulty, and R. D. Morgan, *Chem. Eng. Prog. 87*(2), p. 43, 1991.

31*b*. Kister, H. Z., and D. R. Gill, paper to be presented in "Distillation and Absorption," Institution of Chem. Engrs. (UK), Birmingham, September 7–9, 1992.

31*c*. Kean, J. A., H. M. Turner, and B. C. Price, *Hydrocarb. Proc. 70*(4), p. 47, April 1991.

31*d*. Kean, J. A., H. M. Turner, and B. C. Price, paper presented at the AIChE Annual Meeting, Los Angeles, California, November 1991.

31*e*. Hausch, G. W., P. Quotson, and K. Seeger, paper presented at the AIChE annual meeting, Los Angeles, California, November 1991.

32. Meier, W., R. Hunkeler, and D. Stöcker, *I. Chem. E. Symp. Ser.* 56, p. 3.3/1, 1979.
33. Meier, W., and M. Huber, *I. Chem. E. Symp. Ser.* 32, p. 4:31, 1969.

34. Chuang, K. T., and A. I. Miller, *Can. J. Chem. Eng. 66*(6), p. 377, 1988.
35. Chen, G. K., L. Kitterman, and J. Shieh, *Chem. Eng. Prog. 79*(11), p. 49, 1983.
36. Ross, T. K., and B. Haqjoo, in H. Sawistowski (ed.), *Final Report by the ABCM/BCPMA Distillation Panel,* Chem. Ind. Assoc., London, 1964; also Discussion.
37. Spiegel, L., paper presented at the AIChE Annual Meeting, Chicago, Illinois, November 1990.
38. Sulzer Bros. Ltd., *Separation Columns for Distillation and Absorption,* Winterhur, Switzerland, 1986.
39. Nygren, P. G., in P. A. Schweitzer (ed.), *Handbook of Separation Techniques for Chemical Engineers,* McGraw-Hill, New York, 1979.
40. Kister, H. Z., *Distillation Operation,* McGraw-Hill, New York, 1990.
41. Fair, J. R., in R. W. Rousseau (ed.), *Handbook of Separation Process Technology,* Wiley, New York, 1987.
42. Glitsch, Inc., Bulletin 423, Dallas, Texas, 1986.
43. Koch Engineering Company, Inc., Bulletin KFG-2, Wichita, Kansas, 1985.
44. Glitsch, Inc., "Addendum to Bulletin 7070," Dallas, Texas, 1979.
45. Golden, S. W., and M. J. Binkley, *Oil Gas J.,* p. 197, July 30, 1984.
46. NPRA panel discussion, *Oil Gas J.,* August 23, 1965.
47. Kulbe, B., K. Hoppe, and J. Keller, *Int. Chem. Eng. 25*(3), p. 474, 1985.
48. Leung, L. S., B. E. T. Hutton, and D. J. Nicklin, *Ind. Eng. Chem. Fund. 14*(1), p. 63, 1975.
49. Buchanan, J. E., *Ind. Eng. Chem. Fund. 15*(1), p. 87, 1976; Leung, L. S., D. J. Nicklin, and B. E. T. Hutton, *ibid., 15*(1), p. 88, 1976.
50. Fair, J. R., and J. L. Bravo, *I. Chem. E. Symp. Ser.* 104, p. A183, 1987.
51. Kunesh, J. G., *Chem. Eng.,* p. 101, Dec. 7, 1987.
52. Harrison, M. E., and J. J. France, *Chem. Eng.,* p. 121, April 1989.
53. Eckert, J. S., *Chem. Eng. Prog., 66*(3), p. 39, 1970.
54. Silvey, F. C., and G. J. Keller, *Chem. Eng. Prog. 62*(1), p. 68, 1966.
55. Bolles, W. L., and J. R. Fair, *I. Chem. E. Symp. Ser.* 56, p. 3.3/35, 1979.
56. Billet, R., *Distillation Engineering,* Chemical Publishing Co., New York, 1979.
57. Dolan, M. J., and R. F. Strigle, Jr., *Chem. Eng. Prog. 76*(11), p. 78, 1980.
58. MacDougall, L. V., *Chem. SA,* p. 255, October 1985.
59. Kister, H. Z., and D. R. Gill, paper presented at the AIChE Spring Meeting, Orlando, Florida, March 1990.
60. Kister, H. Z., and D. R. Gill, *Chem. Eng. Prog., 87*(2), p. 32, 1991.
60*a*. Kister, H. Z., and D. R. Gill, paper presented at the AIChE Annual Meeting, Los Angeles, California, November 17–22, 1991.
61. Eckert, J. S., and L. F. Walter, *Hydrocarb. Proc. 43*(2), p. 107, 1964.
62. Billet, R., and J. Maćkowiak, *Fette. Seifen. Anstrichmittel* 86, p. 349, 1984.
63. Ludwig, E. E., *Applied Process Design for Chemical and Petrochemical Plants,* vol. 2, 2d ed., Gulf Publishing, Houston, 1979.
64. Drew, J. W., *Chem. Eng.,* Nov. 14, p. 221, 1983.
65. Nutter, D. E. (Nutter Engineering), Private communication, February 1990.
66. Kouri, R. J., and J. J. Sohlo, *I. Chem. E. Symp. Ser.* 104, p. B193, 1987.
67. Stoter, F., Z. Olujić, and J. de Graauw, paper presented at the AIChE Annual Meeting, Chicago, Illinois, November, 1990.
68. Sherwood, T. K., G. H. Shipley, and F. A. L. Holloway, *Ind. Eng. Chem. 30*(7), p. 765, 1938.
69. Lobo, W. E., L. Friend, F. Hashmall, and F. A. Zenz, *Trans. Am. Inst. Chem. Engrs.* 41, p. 693, 1945.
70. Leva, M., *Chem. Eng. Prog. Symp. Ser. 50*(10), p. 51, 1954.
71. Copigneaux, P., *Hydrocarb. Proc. 60*(2), p. 99, 1981.
72. Eckert, J. S., *Chem. Eng. Prog. 59,*(5), p. 76, 1963.
73. Mersmann, A., *Chem. Ing. Tech. 37*(3), p. 218, 1965.
73*a*. Maćkowiak, J., *Chem. Eng. Technol.* 13, p. 184, 1990.
73*b*. Maćkowiak, J., *Fluiddynamik von Kolonnen mit Modernen Füllkörpern und Packungen für Gas/Flüssigkeitssysteme,* Otto Salle Verlag, Frankfurt am Main, und Verlag Sauerländer, Aarau, Frankfurt am Main, 1991.
74. Eckert, J. S., *Chem. Eng.,* p. 70, April 14, 1975.

75. Silvey, F. C., and G. J. Keller, *I. Chem. E. Symp. Ser.* No. 32, p. 4:18, 1969.
76. Zenz, F. A., *Chem. Eng.*, August, p. 176, 1953.
77. Strigle, R. F., Jr., and F. Rukovena, Jr., *Chem. Eng. Progr. 75*(3), p. 86, 1979.
78. Billet, R., and M. Schultes, in *Beiträge zur Verfahrens- und Umwelttechnik*, p. 108, Ruhr Universität Bochum, 1991.
79. Billet, R., and M. Schultes, *I. Chem. E. Symp. Ser.* 104, p. B255, 1987.
80. Billet, R., *I. Chem. E. Symp. Ser.* 104, p. A171, 1987.
81. Billet, R., and M. Schultes, *I. Chem. E. Symp. Ser.* 104, p. A159, 1987.
82. Glitsch, Inc., Bulletin 357, Dallas, Texas, 1989.
83. Beck, R., *Chem. Ing. Techn.*, 44, p. 596, 1972.
84. Leva, M., *Tower Packings and Packed Tower Design*, The U.S. Stoneware Co., Ohio, 1953.
85. Prahl, W. H., *Chem. Eng.*, August 11, p. 89, 1969, and *ibid.*, Nov. 2, p. 109, 1970.
86. Strigle, R. F., and K. Hiramatsu, *Oil Gas J.*, Sept. 26, p. 63, 1983.
87. Van Winkle, M., *Distillation*, McGraw-Hill, New York, 1967.
88. Clay, H. A., J. W. Clark, and B. L. Munro, *Chem. Eng. Prog. 62*(33), p. 51, 1966.
89. Robbins, L. A., *Chem. Eng. Prog.*, May, p. 87, 1991.
90. Robbins, L. A., (Dow Chemical USA), Private communication, September, 1990.
91. Bravo, J. L., J. A. Rocha, and J. R. Fair, *Hydrocarb. Proc. 65*(3), p. 45, 1986.
92. Bemer, G. G., and G. A. J. Kalis, *Trans. Inst. Chem. Engrs.* (London), *56*, p. 200, 1978.
92*a*. Maćkowiak, J., *Chem. Eng. Process*, 29, 93, 1991.
92*b*. Mersmann, A., and A. Deixler, *Chem. Ing. Tech. 58*(1), 19, 1986.
93. Fair, J. R., (The University of Texas at Austin), Private communication, 1986.
94. Ergun, S., *Chem. Eng. Prog. 48*(2), p. 89, 1952.
95. Stichlmair, J., J. L. Bravo, and J. R. Fair, *Gas Sep. Purif. 3*, p. 19, March 1989.
96. Bolles, W. L., and J. R. Fair, *Chem. Eng.*, July 12, p. 109, 1982.
97. Strigle, R. F., Jr., *Chem. Eng. Progr. 81*(4), p. 67, 1985.
98. Chen, G. K., *Chem. Eng.*, p. 40, March 5, 1984.
99. Thoenes and Kramers, *Chem. Eng. Sci.*, 8, p. 271, 1958.
100. Shulman, H. L., C. F. Ullrich, N. Wells, and A. Z. Proulx, *AIChE J.*1, p. 259, 1955.
101. Buchanan, J. E., *Ind. Eng. Chem. Fund*, 6, p. 400, 1967.
102. Schmidt, R., *I. Chem. E. Symp. Ser.* 56, p. 3.1/1, 1979.
103. Glitsch, Inc., Bulletin TP/US/M4, Dallas, Texas, 1983.
104. Ponter, A. B., G. A. Davies, W. Beaton, and T. K. Ross, *Trans. Inst. Chem. Engrs.* (London) *45*, p. T345, 1967.
105. Ponter, A. B., paper presented in the AIChE Meeting, Boston, August 21, 1979.
106. Mangers, R. J., and A. B. Ponter, *Ind. Eng. Chem. Proc. Des. Dev. 19*, 530, 1980.
107. Ponter, A. B., and P. H. Au-Yeung, *Chem. Ing. Tech. 56*(9), p. 701, 1984.
108. Van der Klooster, H. W., and A. A. H. Drinkenburg, *I. Chem. E. Symp. Ser.* 56, p. 2.5/21, 1979.
109. Ponter, A. B., P. Trauffler, and S. Vijayan, *Ind. Eng. Chem. Proc. Des. Dev., 15*(1), p. 196, 1976.
110. Koshy, T. D., and F. Rukovena, Jr., *Hydrocarb. Proc. 65*(5), p. 64, 1986.
111. Koshy, T. D., and F. Rukovena, Jr., paper presented at the Annual Meeting of the AIChE, Los Angeles, California, November 1982.
111*a*. Robinson, K., *Chem. Engnr.*, June 27, p. 23, 1991.
111*b*. Thibodeaux, L. J., and P. W. Murrill, *Chem. Eng.*, July 18, p. 155, 1966.
112. King, C. J., *Separation Processes*, 2d ed., McGraw-Hill, New York, 1980.
113. Sherwood, T. K., R. L. Pigford, and C. R. Wilke, *Mass Transfer*, McGraw-Hill, New York, 1975.
114. Katayama, T., and F. Yoshida, *J. Chem. Eng. Japan 1*(1), p. 42, 1968.
115. Morris, G. A., in P. A. Rottenburg (ed.), *Proceeding of the International Symposium on Distillation*, p. 146, The Institution of Chemical Engineers, London, 1960.
116. Yuan, H. C., and L. Spiegel, *Proceedings of the 2nd World Congress of Chemical Engineering*, Montreal, Canada, Vol. IV, p. 274, October 1981.
117. Kister, H. Z., and I. D. Doig, *Can. J. Chem. Eng. 60*(2), p. 155, 1982.
118. Zelvinskii, Ya. D., A. A. Titov, and V. A. Shalygin, *Khim. Tekhnol. Topl. Masel* 12, p. 10, 1966.

119. Eckert, J. S., E. H. Foote, and L. F. Walter, *Chem. Eng. Prog. 62*(1), p. 59, 1966.
120. Vital, T. J., S. S. Grossel, and P. I. Olsen, *Hydrocarb. Proc. 63*(12), p. 75, 1984.
121. Harrison, M. E., *Chem. Eng. Prog. 86*(11), p. 80, 1990.
122. Bravo, J. L., and J. R. Fair, *Ind. Eng. Chem. Proc. Des. Dev.* 21, p. 162, 1982.
123. Onda, K., H. Takeuchi, and Y. Okumoto, *J. Chem. Eng. Japan 1*(1), p. 56, 1968.
124. Bravo, J. L., J. A. Rocha, and J. R. Fair, *Hydrocarb. Proc. 64*(1), p. 91, 1985.
125. Bravo, J. L., A. A. Patwardhan, and T. F. Edgar, paper presented at the AIChE Spring Meeting, Orlando, Florida, March 1990.
125*a*. Cárdenas, J. C., F. J. Illezcas, B. Garcia, G. Palacios, E. M. Escamilla, and J. A. Rocha, paper presented at the AIChE Annual Meeting, Chicago, Illinois, November, 1990.
125*b*. Bravo,J. L., J. A. Rocha, and J. R. Fair, paper presented at the AIChE annual meeting, Los Angeles, California, November 1991.
126. Bornhütter, K., and A. Mersmann, paper presented at the AIChE Annual Meeting, Chicago, Illinois, November 1990.
126*a*. Billet, R., and M. Schultes, in *Beiträge zur Verfahrens- und Umwelttechnik*, p. 88, Ruhr Universität, Bochum, 1991.
127. Porter, K. E., and J. D. Jenkins, *I. Chem. E. Symp. Ser.* 56, Summary paper, London, 1979.
128. Frank, O., *Chem. Eng.*, March 14, p. 110, 1977.
129. Walas, S. M., *Chem. Eng.*, March 16, p. 75, 1987.
130. Rose, L. M., *Distillation Design in Practice*, Elsevier, Amsterdam, 1985.
131. Kunesh, J. G., L. L. Lahm, and T. Yanagi, *I. Chem. E. Symp. Ser.* 104, p. A233, 1987.
132. Meier, W., and M. Huber, *Chem. Ing. Tech. 39*, p. 797, 1967.
133. Mullin, J. W., *Indust. Chem. Mfr. 33*, p. 408, 1957.
134. Manning, R. E., and M. R. Cannon, *Ind. Eng. Chem. 49*(3), p. 347, 1957.
135. Huber, M., and R. Hiltbrunner, *Chem. Eng. Sci 21*, p. 819, 1966.
136. Zuiderweg, F. J., P. J. Hoek, and L. Lahm, Jr., *I. Chem. E. Symp. Ser.* 104, p. A217, 1987.
137. Yuan, H. C., and L. Spiegel, *Chem. Ing. Tech. 54*, p. 774, 1982.
138. Baker, T., T. H. Chilton, and H. C. Vernon, *Trans. Am. Inst. Chem. Engrs., 31*, p. 296, 1935.
139. Cihla, Z., and O. Schmidt, *Coll. Czech. Chem. Comm. 22*, 896, 1957.
140. Hoek, P. J., Ph.D. Thesis, University of Delft, The Netherlands, 1983.
140*a*. McMullan, B. D., A. E. Ravicz, and S. J. Wei, *Chem. Eng. Prog.*, July, p. 69, 1991.
141. Porter, K. E., *Trans. Inst. Chem. Engrs. (London), 46*, T69, 1968; also Porter, K. E., V. D. Barnett, and J. J. Templeman, *ibid.*, T74; and Porter, K. E., and J. J. Templeman, *ibid.*, T86.
142. Porter, K. E., and G. K. Stephens, *Can. J. Chem. Eng. 47*(6), p. 258, 1969.
143. Porter, K. E., and M. C. Jones, *Trans. Inst. Chem. Eng. (London) 41*, p. 240, 1963.
144. Jameson, G. J., *Trans. Inst. Chem. Engrs. (London), 44*, p. T198, 1966; also *ibid., 45*, p. T74, 1967.
145. Albright, M. A., *Hydrocarb. Proc., 63*(9), 173, 1984.
146. Stichlmair, J., and R. Potthoff, paper presented at the AIChE Annual Meeting, Chicago, Illinois, November, 1990.
147. Leva, M., D. Bhaga, and R. Al Samadi, paper presented at the AIChE Spring National Meeting, Orlando, Florida, March 18–22, 1990.
148. Groenhof, H. C., *Chem. Eng. J. 14*, p. 181, 1977; and *ibid.*, p. 193, 1977.
149. Al Samadi, R. A., C. M. Evans, G. M. Cameron, M. E. Fayed, and M. Leva, paper presented at the AIChE Spring National Meeting, Houston, Texas, April 2–6, 1989.
150. Zuiderweg, F. J., and T. Yanagi, paper presented at the AIChE National Meeting, Houston, April 6–9, 1989.
150*a*. Zuiderweg, F. J., J. G. Kunesh, and D. W. King, paper presented at the AIChE summer meeting, Pittsburgh, Pennsylvania, August 1991.
150*b*. Stikkelman, R. M., Ph. D. thesis, Delft University, The Netherlands, 1989.
151. Stichlmair, J., and A. Stemmer, *I. Chem. E. Symp. Ser.* 104, p. B213, 1987.
152. Moore, F., and F. Rukovena, paper presented at the 36th Canadian Chemical En-

gineering Conference, October 5–8, 1986; same paper published in *Chemical Plants and Processing* (European edition), p. 11, August 1987.
153. Muir, L. A., and C. L. Briens, *Can. J. Chem. Eng.* 64, p. 1027, 1986.
154. Kabakov, M. I., and A. M. Rozen, *Khim Prom,* No. 8, p. 496, 1984; *Soviet Chem. Ind. 16*(8), p. 1059, 1984.
155. Stikkelman, R. M., and J. A. Wesselingh, *I. Chem. E. Symp. Ser. 104,* p. B155, 1987.
156. Porter, K. E., K. A. O'Donnell, and A. A. Zaytoun, *I. Chem. E. Symp. Ser.* 73, p. L28, 1982.
157. Porter, K. E., and Q. H. Ali, "Gas Distribution in Packed Columns," Handout, 1984.
158. Dolan, M. J., and J. Sauter, paper presented at the Annual Technical Meeting of the AIChE, South Texas Section, November 1, 1988.
159. Zuiderweg, F. J., and P. J. Hoek, *I. Chem. E. Symp. Ser.* 104, p. B247, 1987.
160. Kunesh, J. G., L. Lahm, and T. Yanagi, *Ind. Eng. Chem. Res. 26*(9), p. 1845, 1987.
161. Strigle, R. F., Jr., and M. J. Dolan, *Can. Proc. Equip. Control News,* October, 1983.
162. Windebank, C. S. (chairman), Discussion of papers presented in session 4, *I. Chem. E. Symp. Ser.* 32, p. 4:64, 1969.
163. Dolan, M. J., and G. K. Chen, Discussion of paper in Ref. 98, *Chem. Eng.,* p. 5, May 14, 1984.
164. Report of the E.F.C.E. Working Party on Distillation, *Chem. Engnr.* p. CE 21, January/February 1966.
165. McMullan, B. D., A. E. Ravicz, and S. J. Wei, paper presented at the AIChE Annual Meeting, Chicago, Illinois, November, 1990.
166. Billet, R., and J. Maćkowiak, Verfahrenstechnik *17*(4), p. 203, 1983.
167. Wu, K. Y., and G. K. Chen, *I. Chem. E. Symp. Ser.* 104, p. B225, 1987.
168. Nutter Engineering Corp., Chem-Pro Bulletin HY-2, Tulsa, Oklahoma.
169. Hufton, J. R., J. L. Bravo, and J. R. Fair, *Ind. Eng. Chem. Res.* 27, 2096, 1988.
170. Porter, K. E., and M. C. Jones, *I. Chem. E. Symp. Ser.* 104, p. A245, 1987.
171. Martin, C. L., J. L. Bravo, and J. R. Fair, paper presented at the National AIChE Meeting, New Orleans, Louisiana, March 1988.
172. Mottola, A. C., and L. L. Fellinger, *Chem. Eng. Prog. 74*(10), p. 94, 1978.

Chapter

10

Packing Capacity and Pressure Drop GPDC Interpolation Charts Atlas

by Henry Z. Kister

Brown & Root Braun, Alhambra, California

David R. Gill

Simulation Sciences, Inc., Brea, California

Interpolation of experimental flood, pressure drop, and maximum operational capacity (MOC) data is the most reliable and accurate method available for predicting flood, pressure drop, and MOC. As pointed out in Secs. 8.2.6 to 8.2.9, use of correlations to predict these parameters can lead to poor and dangerously optimistic results in many situations frequently encountered in commercial practice.

This chapter presents an atlas of charts for interpolating flood, pressure drop, and MOC. For random and grid packings (Charts 10.1002 to 10.3517 and 10.8005 to 10.8205), the charts are plots of the Eckert generalized pressure drop correlation (GPDC) curves, with experimental data superimposed on them. These plots permit data interpolation

with the aid of the Eckert GPDC. Similarly, for structured packings (Charts 10.5001 to 10.6504), the charts are plots of the Kister and Gill GPDC (SP) (Fig. 8.19c), with experimental data superimposed on them. The principles of the method were described in Secs. 8.2.6 to 8.2.9. A detailed procedure is given in Sec. 10.1, while Sec. 10.2 provides a guide for chart numbers. Table 10.1 lists the sources of all data plotted on the charts.

10.1 Application Guidelines for Using the GPDC Interpolation Charts

Estimating flood and pressure drop using the GPDC interpolation charts involves data interpolation and extrapolation within the framework of the generalized pressure drop correlation (GPDC) chart (Fig. 8.19*b* or *c*). This technique is expected to yield reliable estimates when appropriate data are available in the vicinity of the operating point. The reliability of the estimates will diminish with the extent to which extrapolation is required. Whenever extensive extrapolation is required, the estimates are unreliable, and the calculation is best abandoned.

1. Select the appropriate GPDC interpolation chart for the packing considered.
2. Using the operating conditions or design conditions, and the packing factor listed on the chart, determine the operating point on the interpolation chart.
3. Check if any data are plotted in the vicinity of the operating point. If not, look for the closest region of the diagram that contains data. If this region is remote from the operating point, the calculation is unreliable and is best abandoned (proceed to step 9 below). If the region is close, judiciously extrapolate data near the operating point. Items 4 and 5 below give some guidelines. Bear in mind that you are in an uncertain area. Allow for this uncertainty.
4. Check if data points in the vicinity of the operating point match the correlation. If so, obtain the pressure drop directly from the correlation curves, and go to 6 below. If not, proceed with 5.
5. Draw a curve fitting data points in the vicinity of the operating point. If the data points show a clear trend in this region, it may best be to follow the data points. If no clear trend is shown, it may best be to draw the curve parallel to the correlation curve. Often, a compromise is best. Some engineering judgment may be needed here; a conservative estimate may be best.

6. Compare the nature of the operating system (aqueous or nonaqueous) to the nature of the data points used above. Keep in mind that the aqueous data on the charts are almost entirely air-water data. If the operating system contains less than 50 percent water, it may behave more like a nonaqueous system than an aqueous system. If the nature of the operating system is not the same as that for which the data points are plotted, or if using the extrapolation procedure in step 3 above, proceed to 7 below. Otherwise, proceed to 8 below.
7. Look for a GPDC interpolation chart for a reference packing which has data for a system of the same nature as the operating system at the same operating point. The reference packing must belong to the same packing class (random, structured, or grid) as the packing considered. Attempt to select a reference packing with as similar a packing factor and as similar a geometry as possible. Using data for the reference packing, obtain an estimate of the effect of system nature on pressure drop. If this effect is small, say less than 20 percent, correct the pressure drop estimate for your packing. If the effect is large, say more than 20 percent, the calculation is unreliable and is best abandoned (proceed to step 9 below).

   Keep in mind that if you reached this step, you are in an uncertain region. The uncertainty is even greater if the system nature has a considerable effect on packing pressure drop. Proceed with extreme caution, recognizing that your calculation in this case will at best be only an educated guess. It may pay to consider using the reference packing instead of the one you had in mind because it offers more confidence in the reliability of the performance prediction.
8. Check the range of column diameters and packing depths used to develop the data points in the chart (Table 10.1). Study Secs. 8.2.3 to 8.2.5 that address the inherent limitations of flood and pressure drop data. Make a judicious estimate as to the extent to which scaleup, packing technique, or other factors may influence extension of the data from Table 10.1 to your specific case. The scatter of data around the curves in Fig. 8.19*d* can give some guidelines as to the magnitude of these factors. All data on this diagram were obtained using a single packing (1-in Pall® ring) and almost all using the air-water system, so the scatter does reflect the inherent data limitations. Adjust your estimate accordingly. Engineering judgment is needed here; a conservative estimate may be best. Your calculation is complete; skip step 9.
9. You would only reach this step if the calculation is abandoned. In this case, it would be best to request the manufacturer to provide

data on the packing in the vicinity of the operating point, or to consider some packing for which there is more confidence in the performance prediction.

10.2 A Guide to the GPDC Interpolation Charts

The GPDC (generalized pressure drop correlation) interpolation charts are all numbered in the chapter number (10) followed by a 4-digit suffix. The four digits stand for the following

- First two digits give the packing number. The numbers were allocated as follows:

  10–13 second generation random packings

  20–23 common third generation random packings

  30–35 other third generation random packings

  50 wire-mesh structured packings

  60–65 corrugated sheet structured packings

  80–82 grids

- Third digit gives the packing material. 0 = metal; 1 = plastic; 2 = ceramic.
- Fourth digit is an indicator of the nominal size of the packing. For random packings, it is roughly twice the nominal packing size. For structured packings, it is roughly 8 times the crimp height.

All the charts contain data for pressure drop, flood, and MOC. Small symbols represent data for aqueous systems, while large symbols represent data for nonaqueous systems. In the case of 1- and 2-in metal Pall® rings, due to the large number of data points, each chart was split into three diagrams: a flood data chart, an aqueous pressure drop data chart, and a nonaqueous pressure drop data chart. Similarly, for Mellapak® 250Y, the chart was split into an aqueous chart and a nonaqueous chart each containing flood, MOC, and pressure drop data.

All random packing charts (10.1002 to 10.3517) and grid packing charts (10.8005 to 10.8205) contain the Strigle version of the Eckert GPDC curves (Fig. 8.19*b*). All structured packing charts (10.5001 to 10.6504) contain the Kister and Gill GPDC (SP) curves (Fig. 8.19*c*).

Some unique considerations associated with flood-point definition apply to the grid charts only (10.8005 to 10.8108 only). These are described in Sec. 8.2.6 and should be consulted before interpolating flood data on those charts.

CHART 10.1002A
1" (M) PALL RINGS
FLOOD

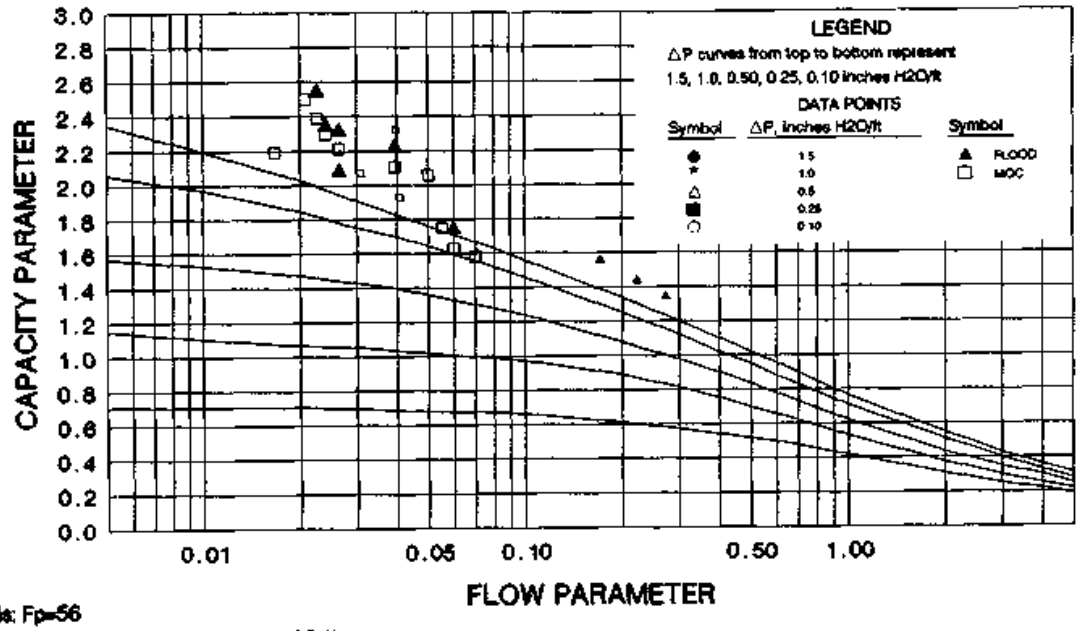

Basis: Fp=56
Pressure drop measured in inches H2O/ft
Large symbols represent non-aqueous data

CHART 10.1002B
1" (M) PALL RINGS
PRESSURE DROP - NON-AQUEOUS SYSTEMS

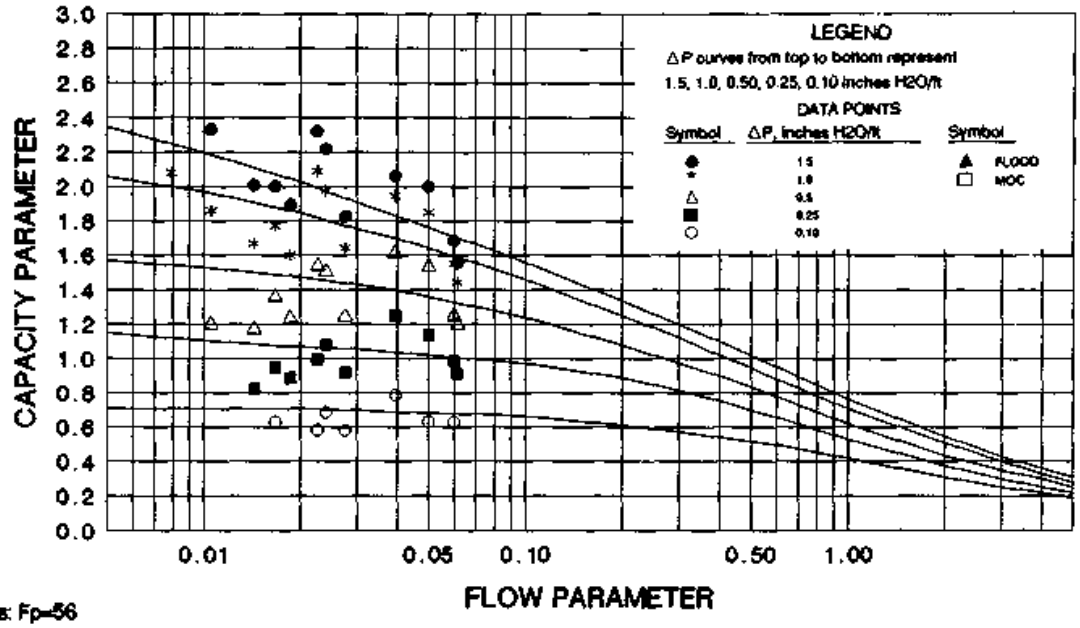

Basis: Fp=56
Pressure drop measured in inches H2O/ft
Large symbols represent non-aqueous data

CHART 10.1002C
1" (M) PALL RINGS
PRESSURE DROP - AQUEOUS SYSTEMS

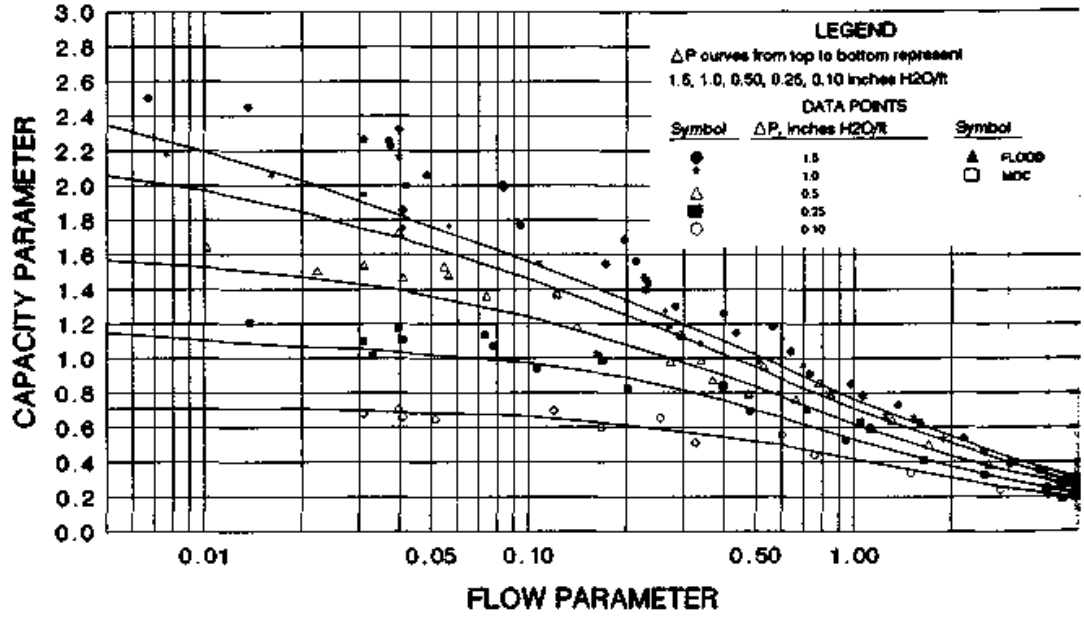

Basis: Fp=56
Pressure drop measured in inches H2O/ft

CHART 10.1003
1.5" (M) PALL RINGS
FLOOD & PRESSURE DROP

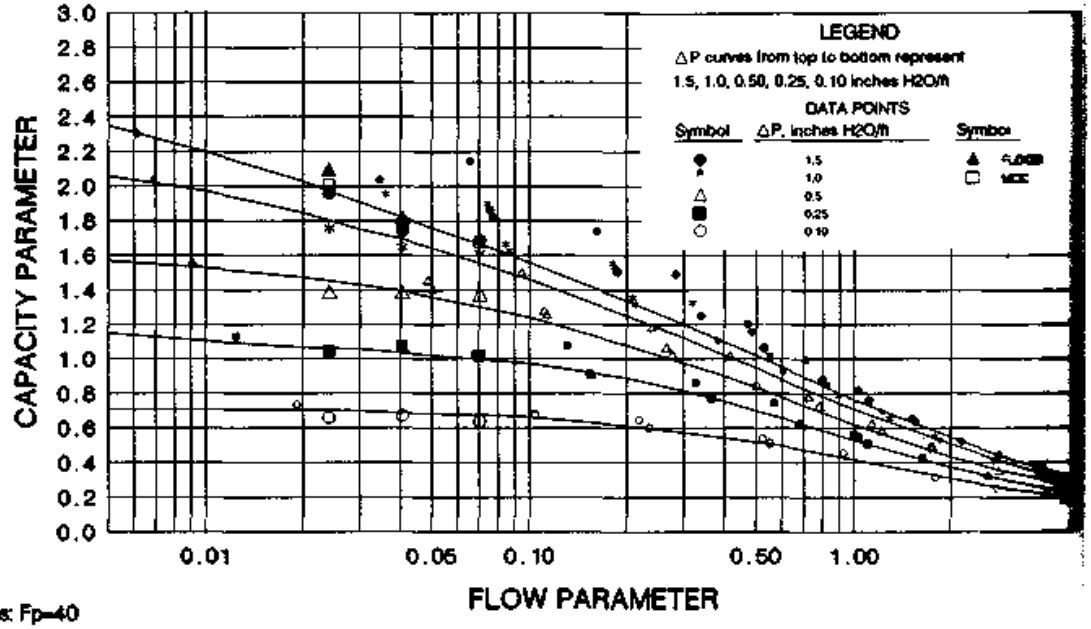

Basis: Fp=40
Pressure drop measured in inches H2O/ft
Large symbols represent non-aqueous data

CHART 10.1004A
2" (M) PALL RINGS
FLOOD

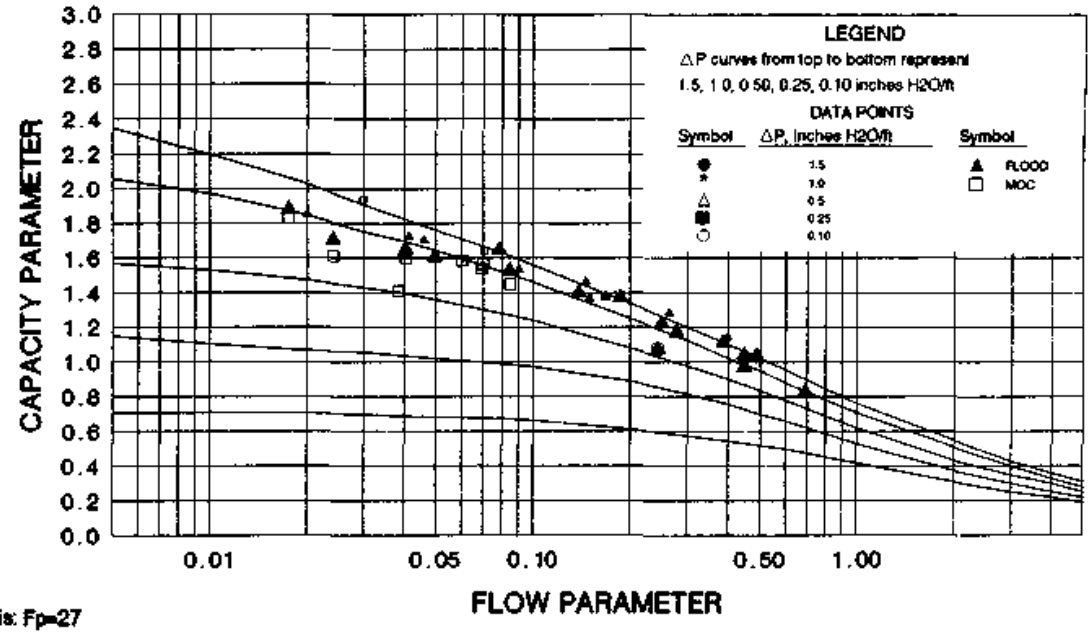

Basis: Fp=27
Pressure drop measured in inches H2O/ft
Large symbols represent non-aqueous data

CHART 10.1004B
2" (M) PALL RINGS
PRESSURE DROP - NON-AQUEOUS SYSTEMS

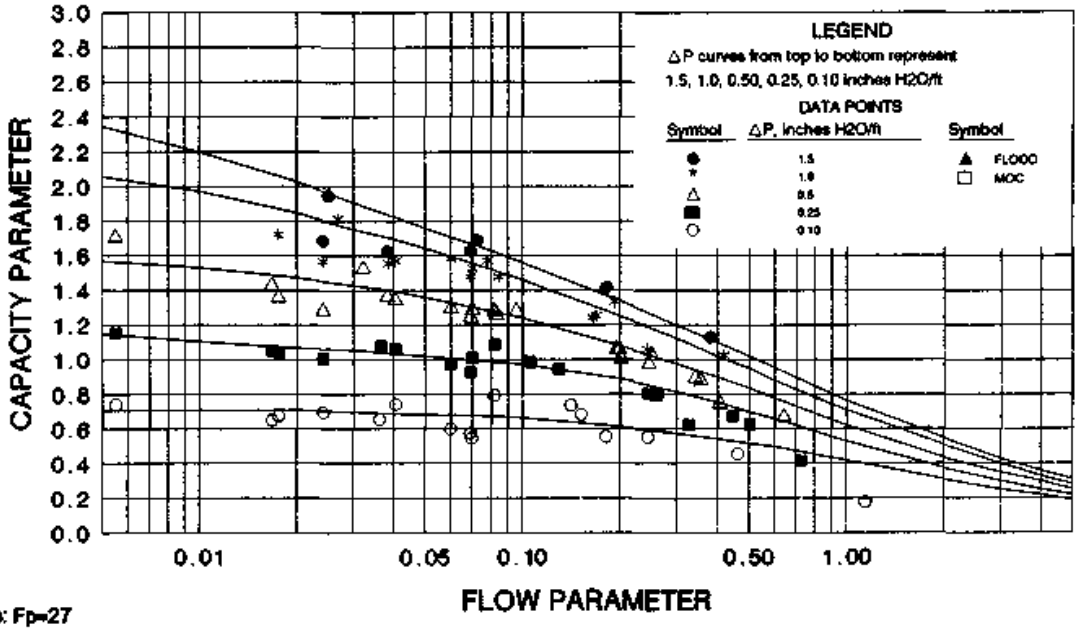

Basis: Fp=27
Pressure drop measured in inches H2O/ft
Large symbols represent non-aqueous data

CHART 10.1004C
2" (M) PALL RINGS
PRESSURE DROP – AQUEOUS SYSTEMS

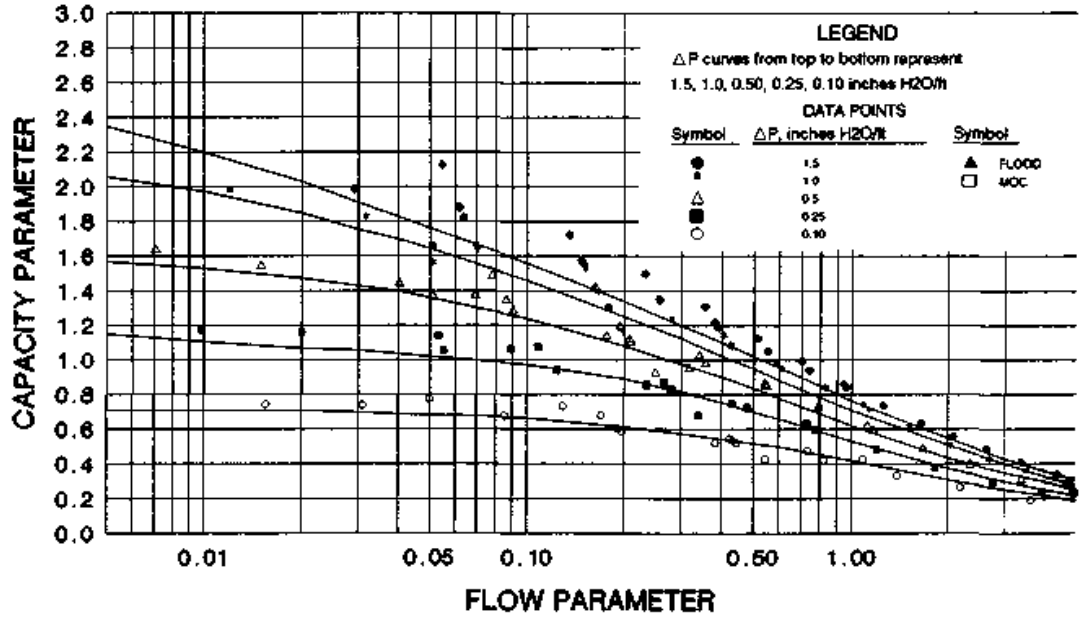

Basis: Fp=27
Pressure drop measured in inches H2O/ft

CHART 10.1007
3.5" (M) PALL RINGS
PRESSURE DROP

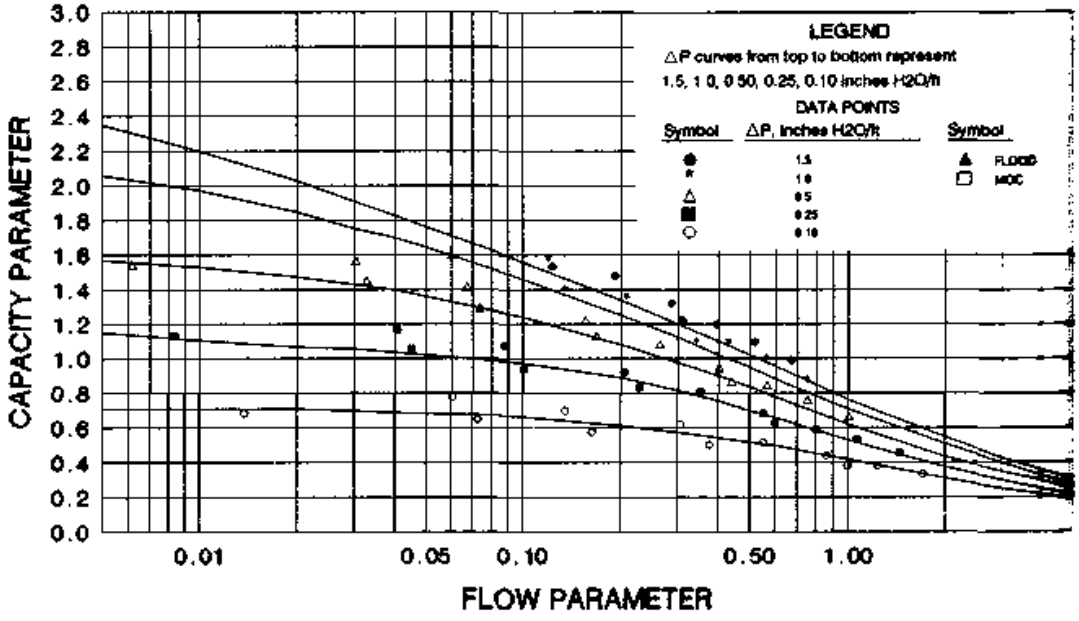

Basis: Fp=18
Pressure drop measured in inches H2O/ft

CHART 10.1012
1" (P) PALL RINGS
PRESSURE DROP

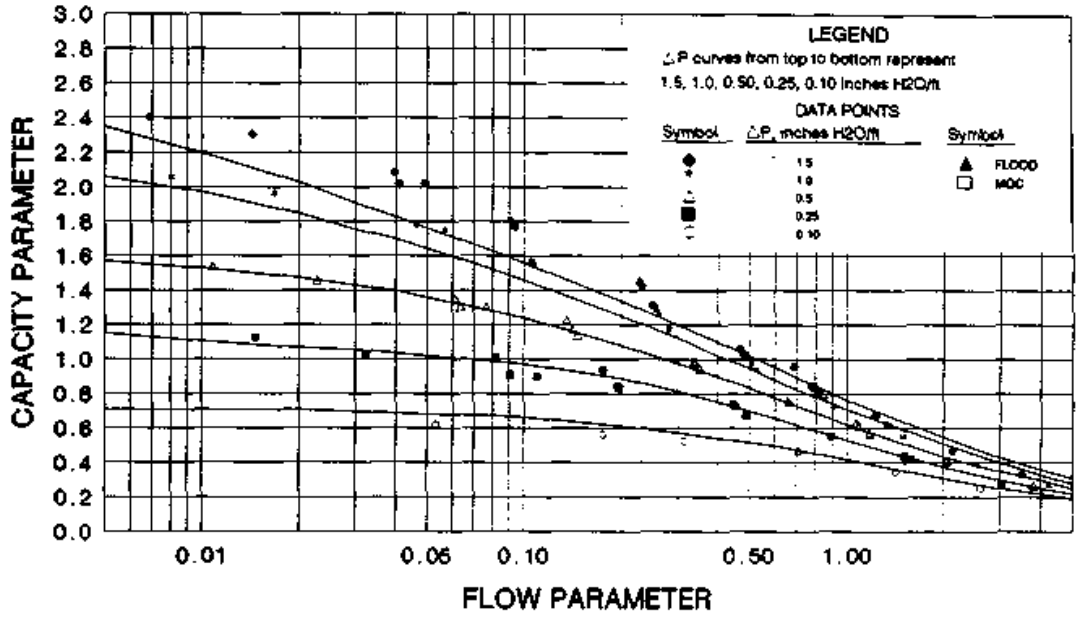

Basis: Fp=55
Pressure drop measured in inches H2O/ft

CHART 10.1013
1.5" (P) PALL RINGS
PRESSURE DROP

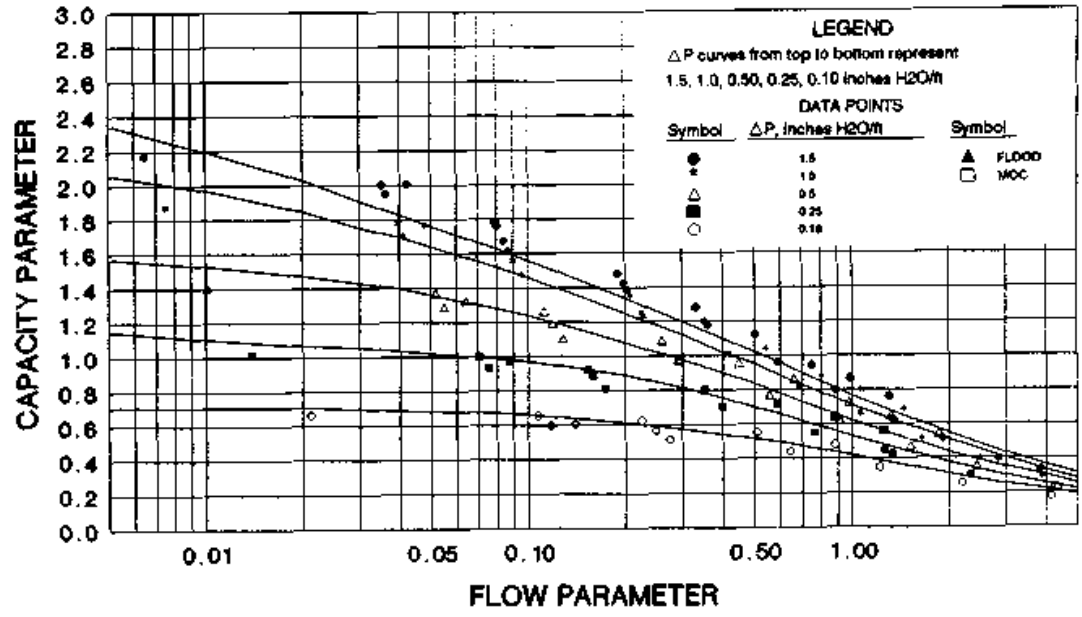

Basis: Fp=40
Pressure drop measured in inches H2O/ft

CHART 10.1014
2" (P) PALL RINGS
PRESSURE DROP

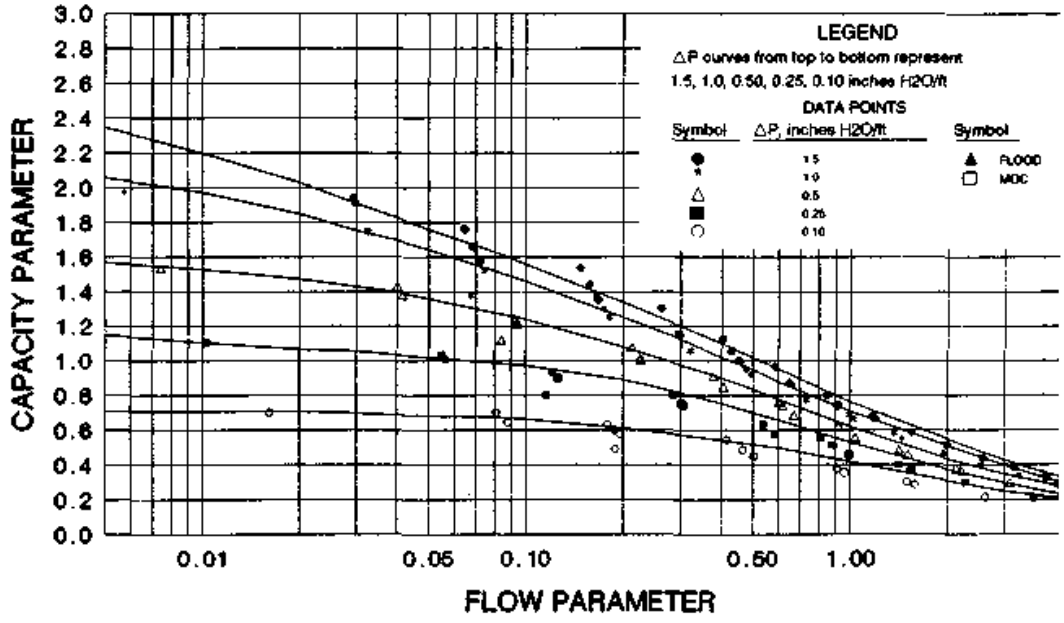

Basis: Fp=26
Pressure drop measured in inches H2O/ft

CHART 10.1017
3.5" (P) PALL RINGS
PRESSURE DROP

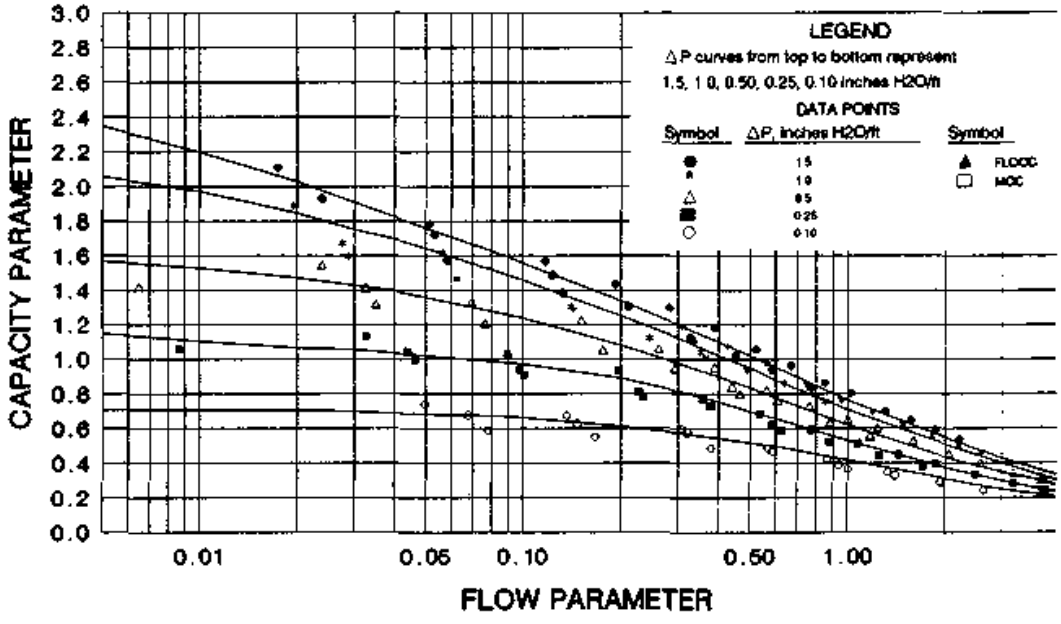

Basis: Fp=17
Pressure drop measured in inches H2O/ft

CHART 10.1022
1" PALL RINGS CERAMIC
FLOOD & PRESSURE DROP

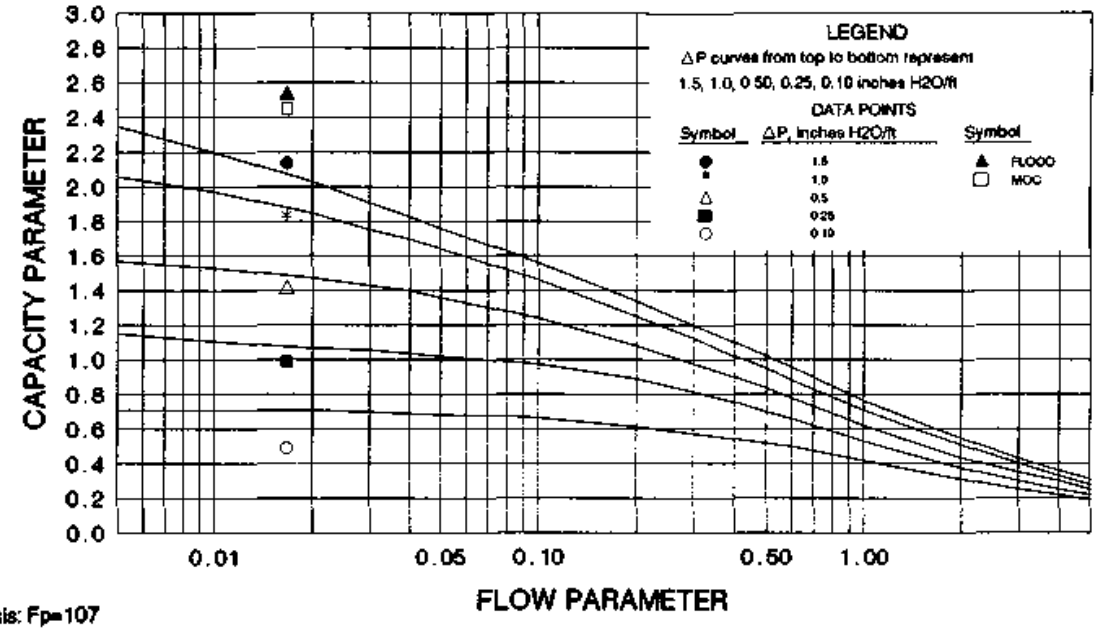

Basis: Fp=107
Pressure drop measured in inches H2O/ft
Large symbols represent non-aqueous data

CHART 10.1024
2" PALL RINGS CERAMIC
PRESSURE DROP

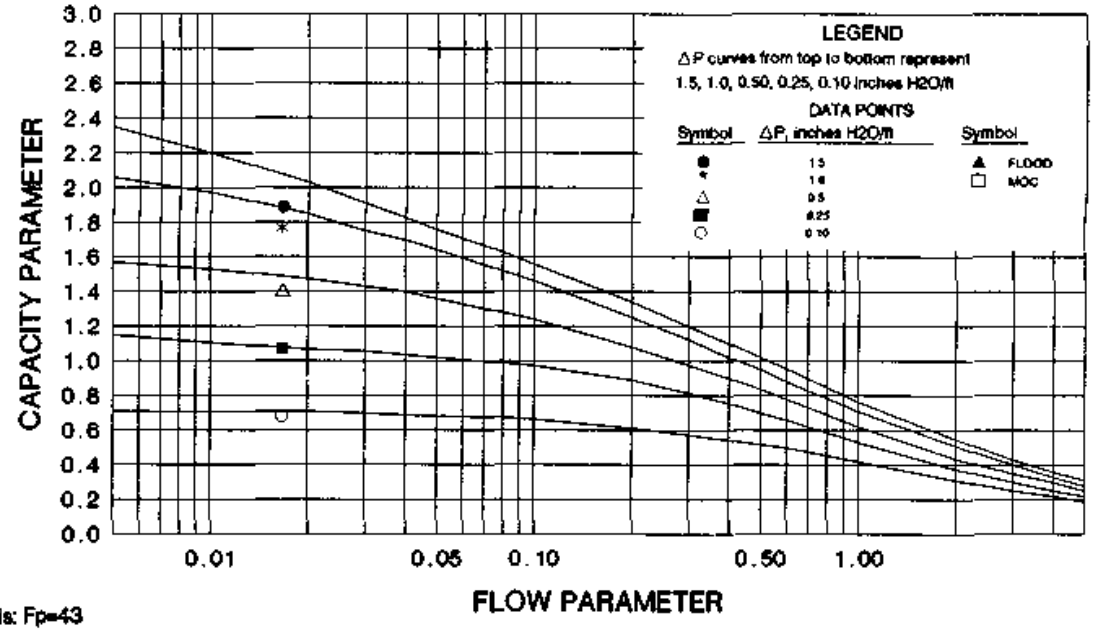

Basis: Fp=43
Pressure drop measured in inches H2O/ft
Large symbols represent non-aqueous data

CHART 10.1112
1"(P) SUPER INTALOX, FLEXI- & BALLAST SADDLES
PRESSURE DROP

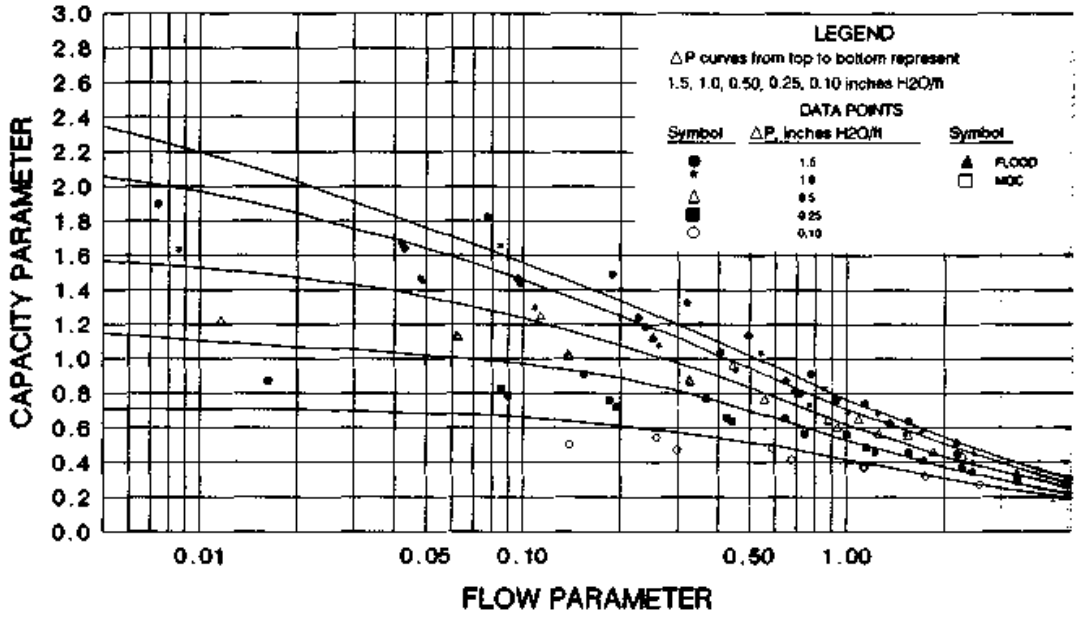

Basis: Fp=40
Pressure drop measured in inches H2O/ft

CHART 10.1114
2"(P) SUPER INTALOX, FLEXI- & BALLAST SADDLES
FLOOD & PRESSURE DROP

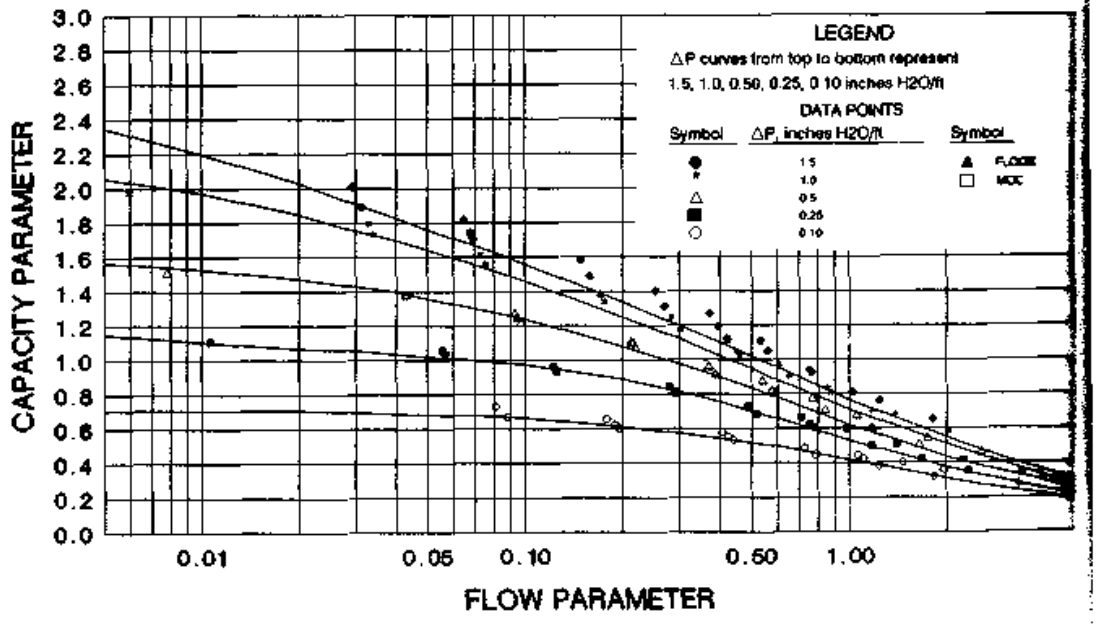

Basis: Fp=28
Pressure drop measured in inches H2O/ft

CHART 10.1116
3"(P) SUPER INTALOX, FLEXI-, & BALLAST SADDLES
PRESSURE DROP

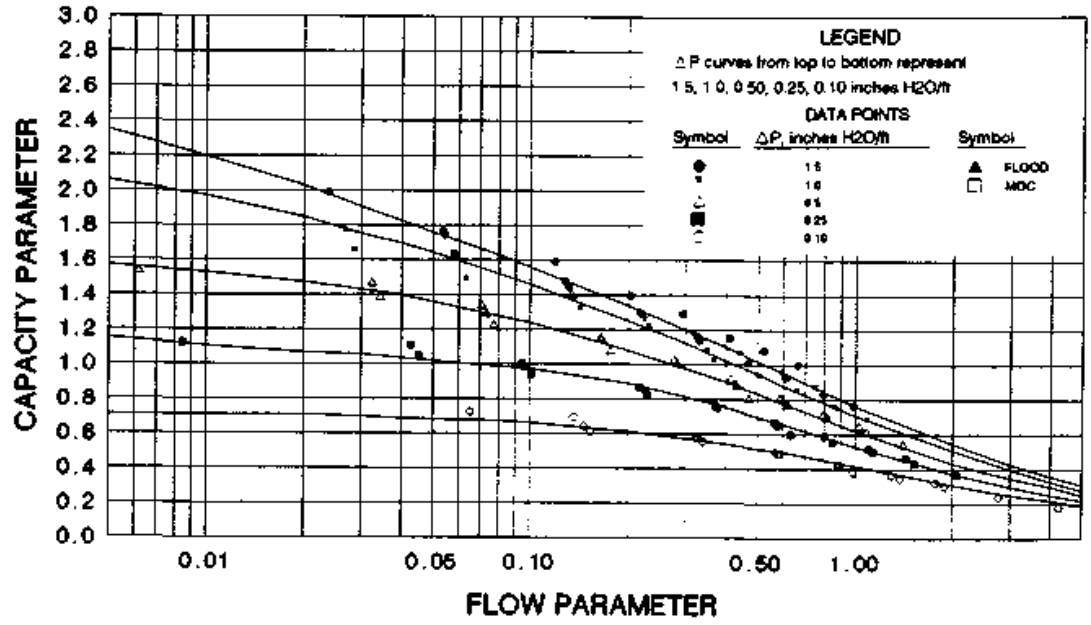

Basis: Fp=18
Pressure drop measured in inches H2O/ft

CHART 10.1122
1" (C) INTALOX & FLEXI- SADDLES
FLOOD & PRESSURE DROP

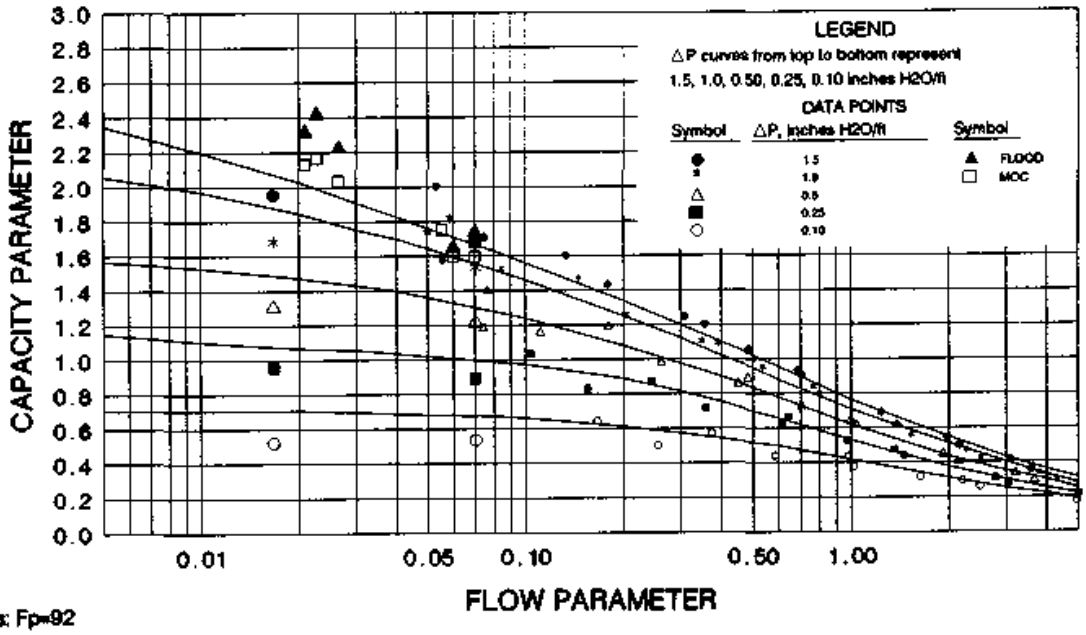

Basis: Fp=92
Pressure drop measured in inches H2O/ft
Large symbols represent non-aqueous data

CHART 10.1123
1.5" (C) INTALOX & FLEXI- SADDLES
FLOOD & PRESSURE DROP

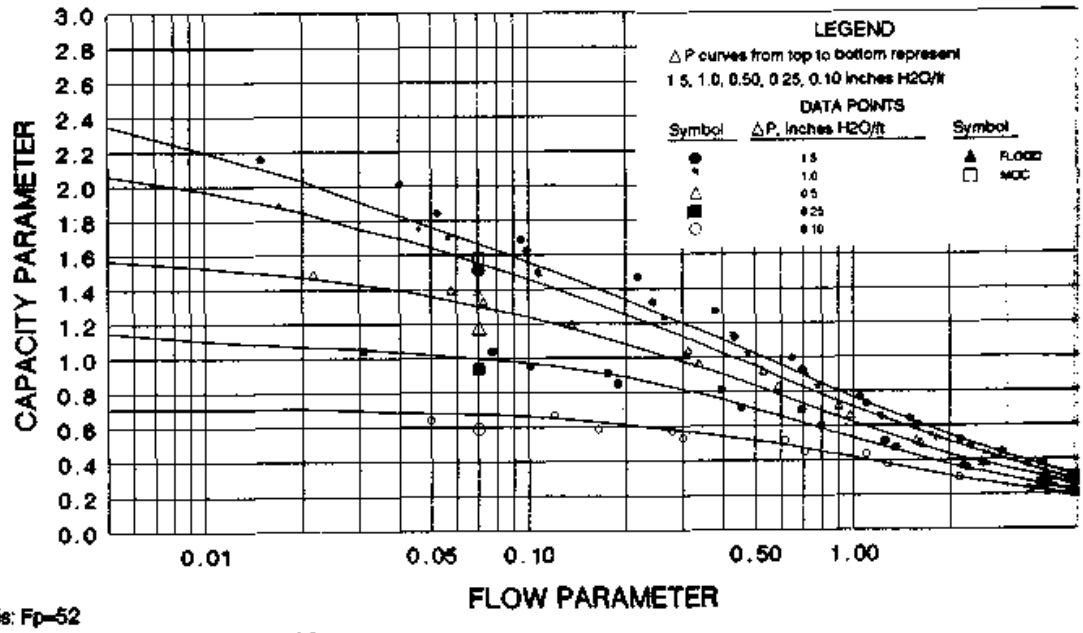

Basis: Fp=52
Pressure drop measured in inches H2O/ft
Large symbols represent non-aqueous data

CHART 10.1124
2" (C) INTALOX & FLEXI- SADDLES
FLOOD & PRESSURE DROP

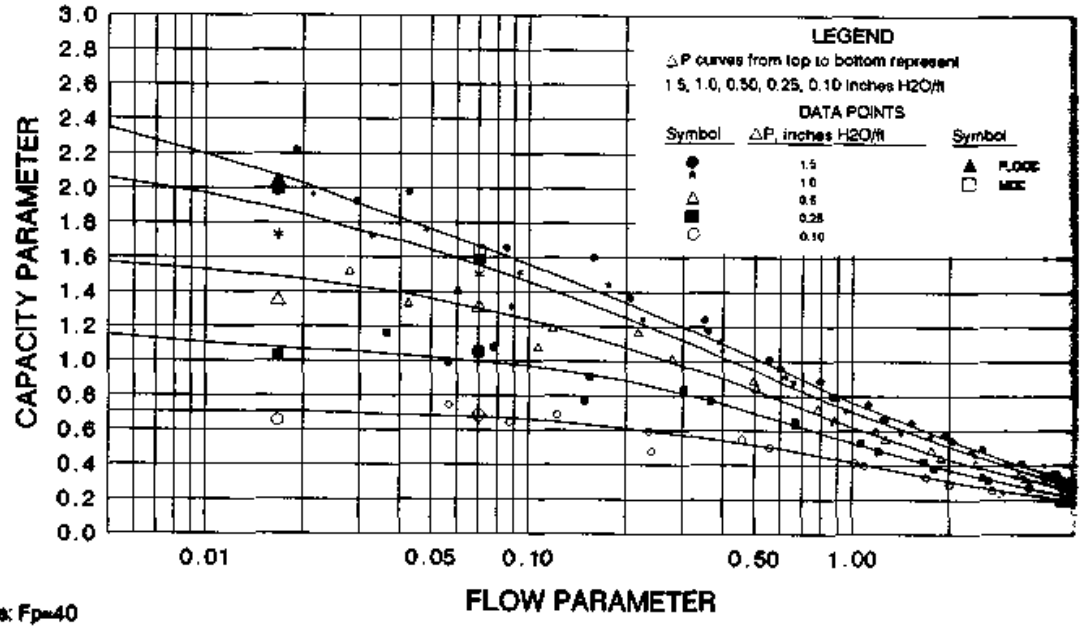

Basis: Fp=40
Pressure drop measured in inches H2O/ft
Large symbols represent non-aqueous data

CHART 10.1126
3" (C) INTALOX & FLEXI- SADDLES
PRESSURE DROP

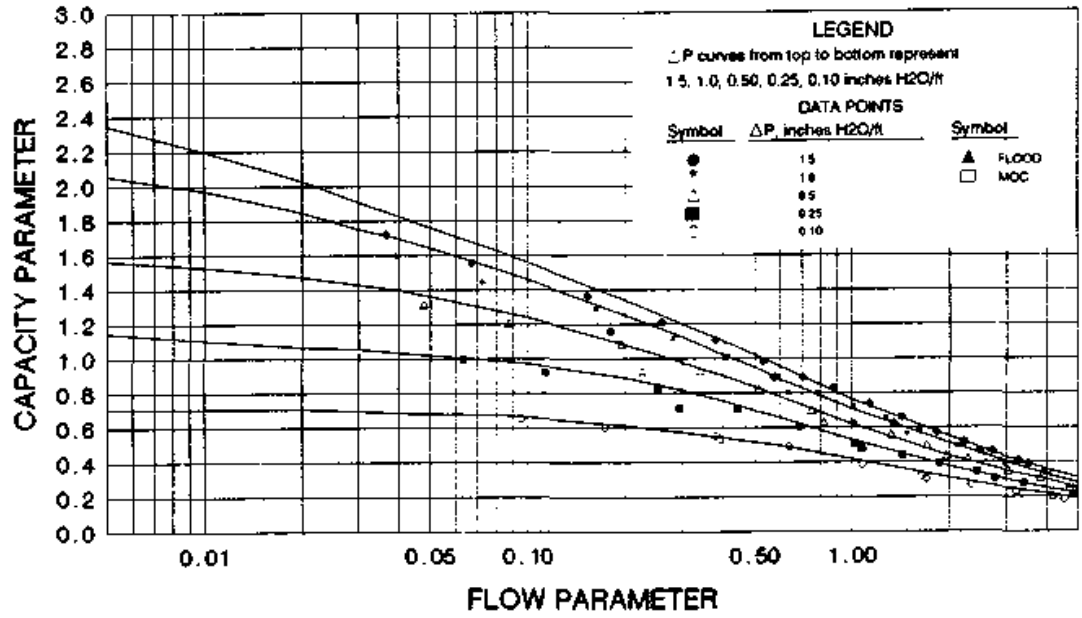

Basis: Fp=22
Pressure drop measured in inches H2O/ft

CHART 10.1322
#1(C) SUPER INTALOX
PRESSURE DROP

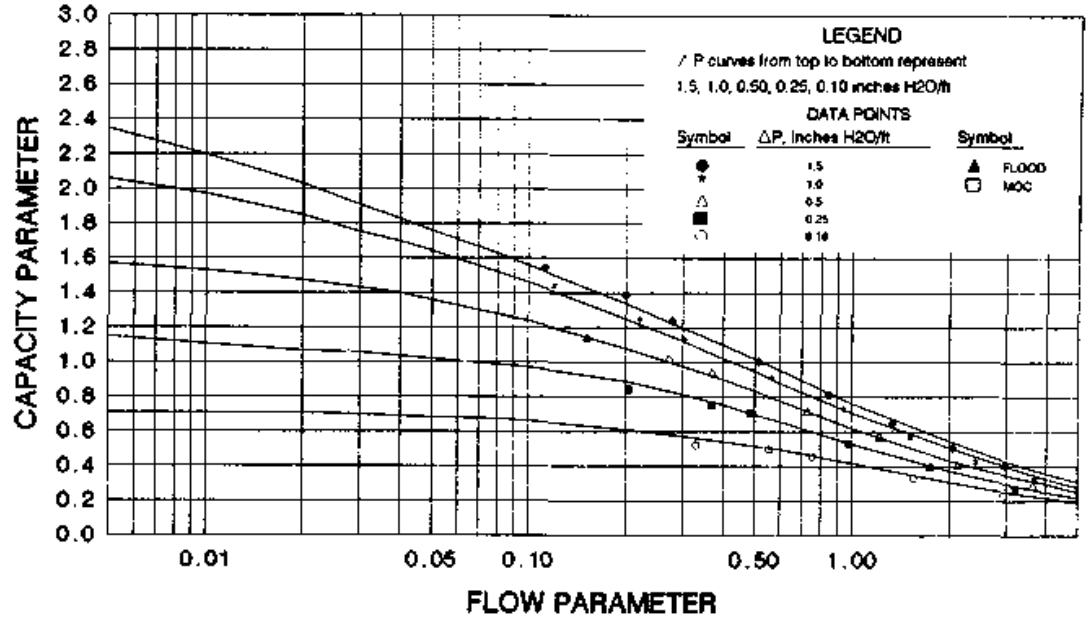

Basis: Fp=60
Pressure drop measured in inches H2O/ft

CHART 10.1324
#2(C) SUPER INTALOX
PRESSURE DROP

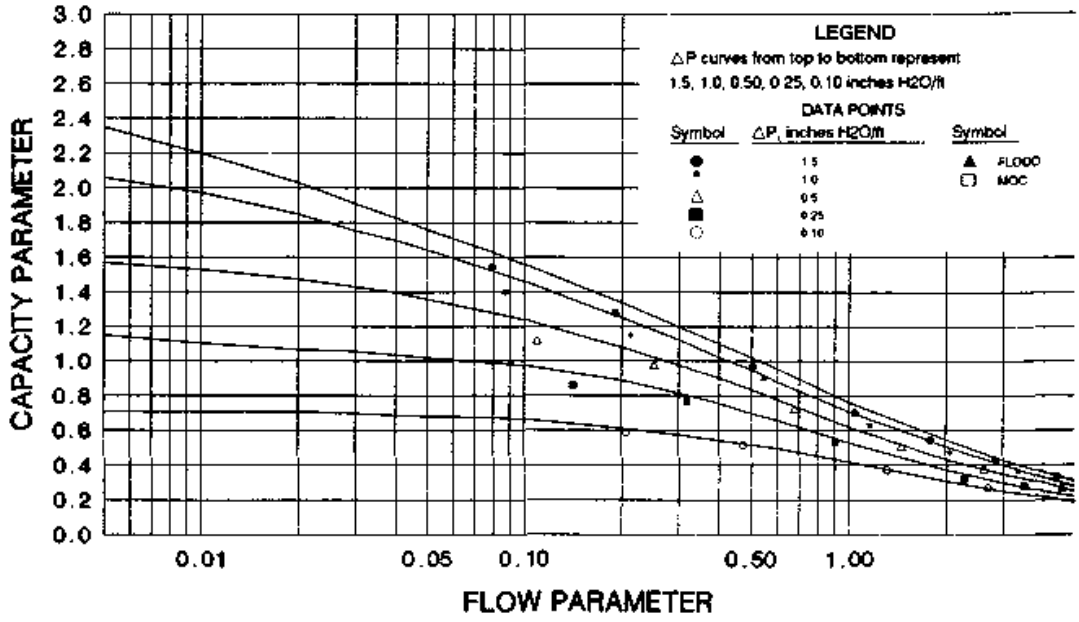

Basis: Fp=30
Pressure drop measured in inches H2O/ft

CHART 10.1203
#1(M) HY-PAK & K-PAC
FLOOD & PRESSURE DROP

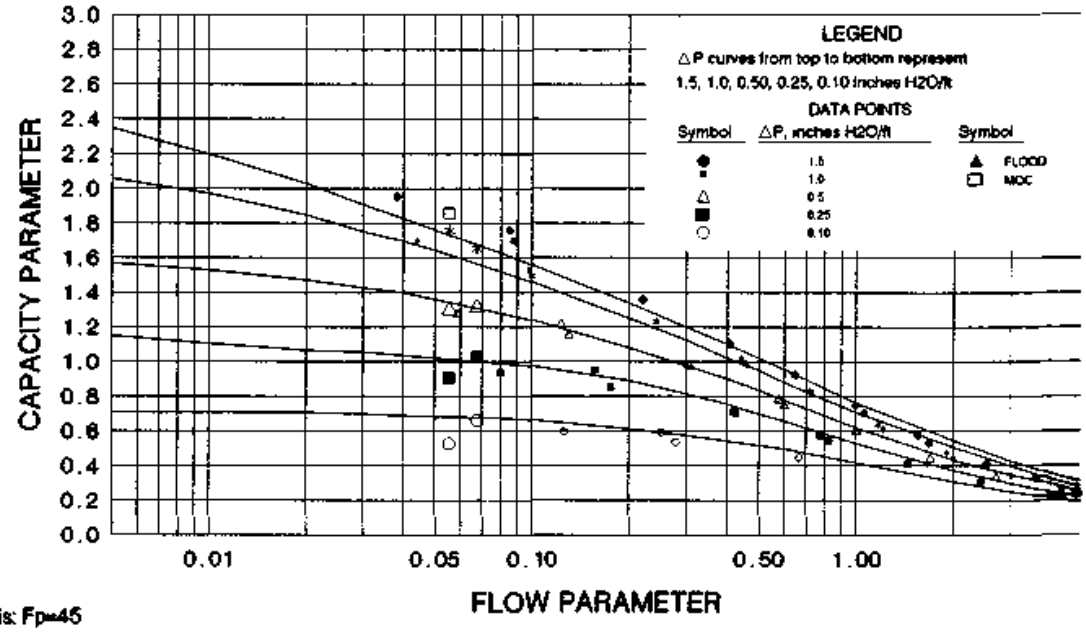

Basis: Fp=45
Pressure drop measured in inches H2O/ft
Large symbols represent non-aqueous data

CHART 10.1204
#1.5 (M) K-PAC
PRESSURE DROP

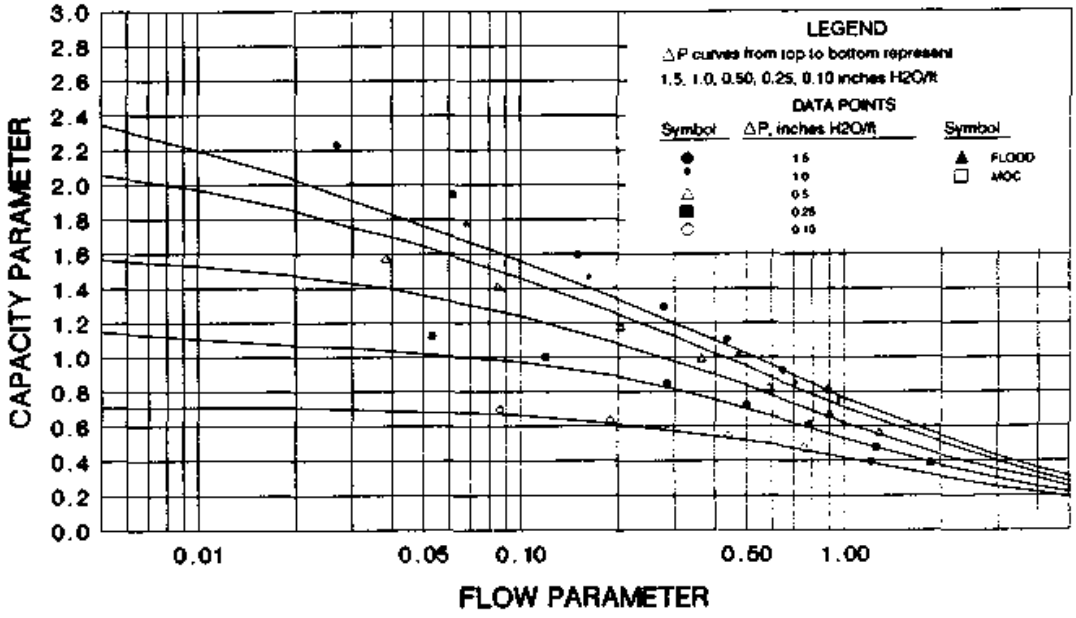

Basis Fp=29
Pressure drop measured in inches H2O/ft

CHART 10.1205
#2(M) HY-PAK, K-PAC & BALLAST +
FLOOD & PRESSURE DROP

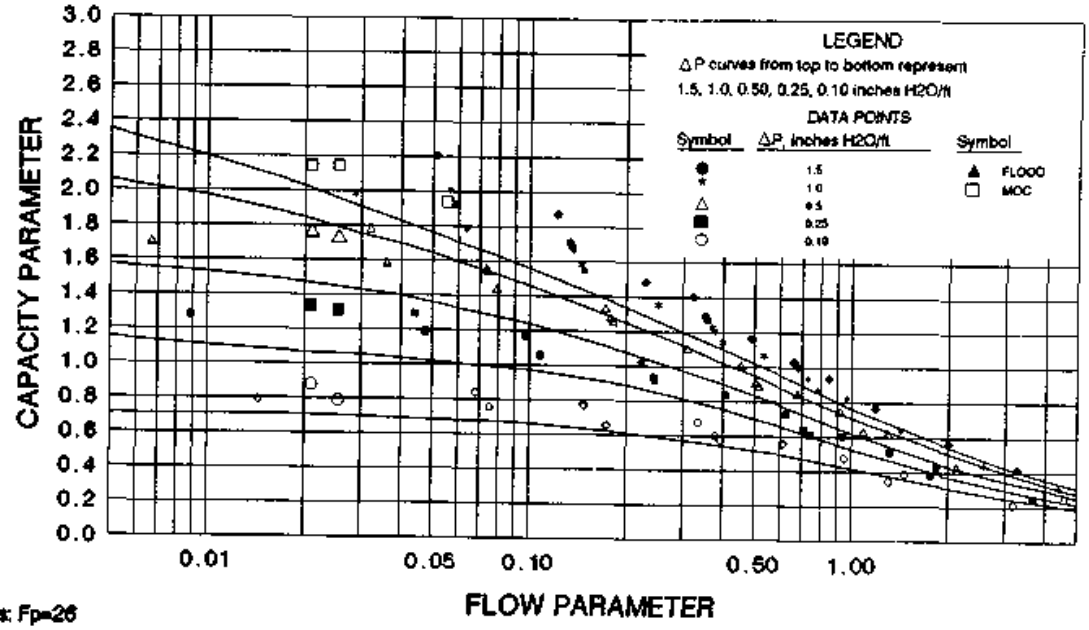

Basis: Fp=26
Pressure drop measured in inches H2O/ft
Large symbols represent non-aqueous data

CHART 10.1207
#3(M) HY-PAK & K-PAC
PRESSURE DROP

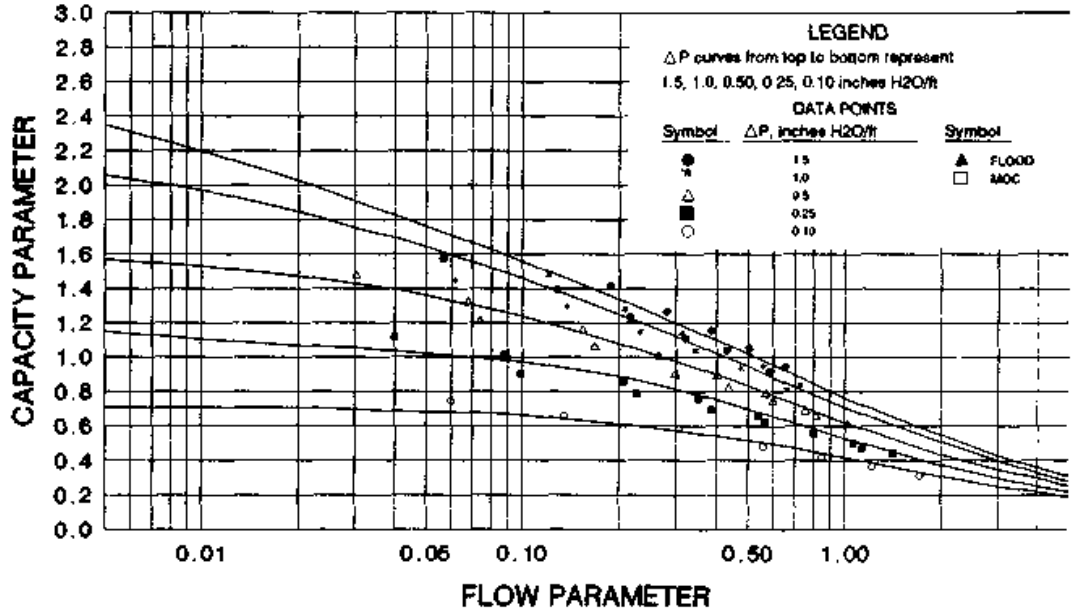

Basis: Fp=16
Pressure drop measured in inches H2O/ft

CHART 10.2002
#25 IMTP
FLOOD & PRESSURE DROP

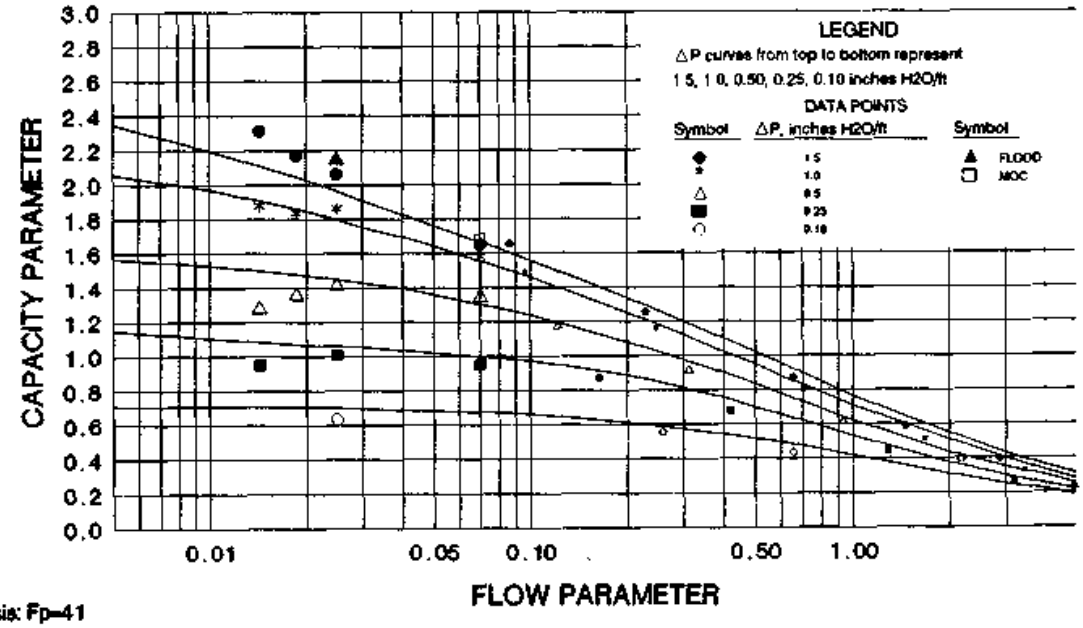

Basis: Fp=41
Pressure drop measured in inches H2O/ft
Large symbols represent non-aqueous data

CHART 10.2003
#40 IMTP
FLOOD & PRESSURE DROP

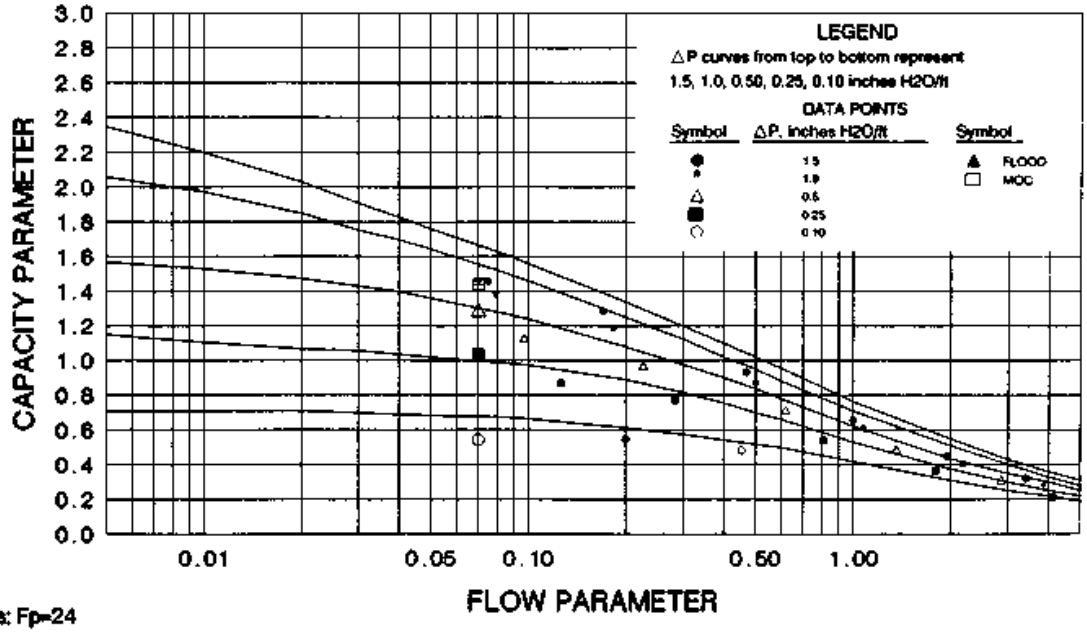

Basis: Fp=24
Pressure drop measured in inches H2O/ft
Large symbols represent non-aqueous data

CHART 10.2004
#50 IMTP
FLOOD & PRESSURE DROP

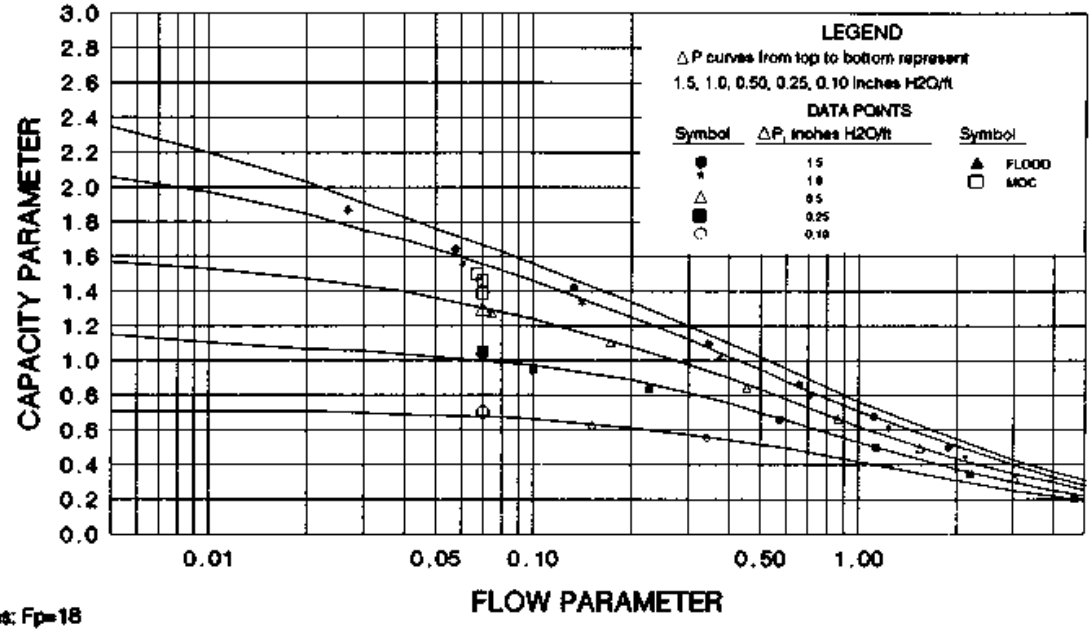

Basis: Fp=18
Pressure drop measured in inches H2O/ft
Large symbols represent non-aqueous data

CHART 10.2006
#70 IMTP
FLOOD & PRESSURE DROP

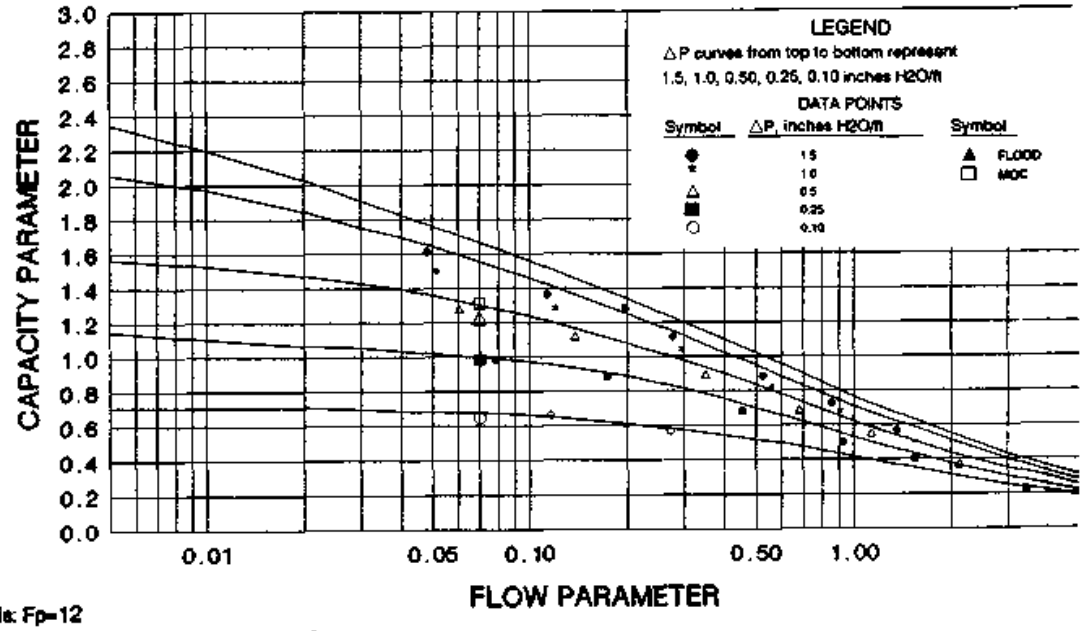

Basis: Fp=12
Pressure drop measured in inches H2O/ft
Large symbols represent non-aqueous data

CHART 10.2101
#1(M) CMR
FLOOD & PRESSURE DROP

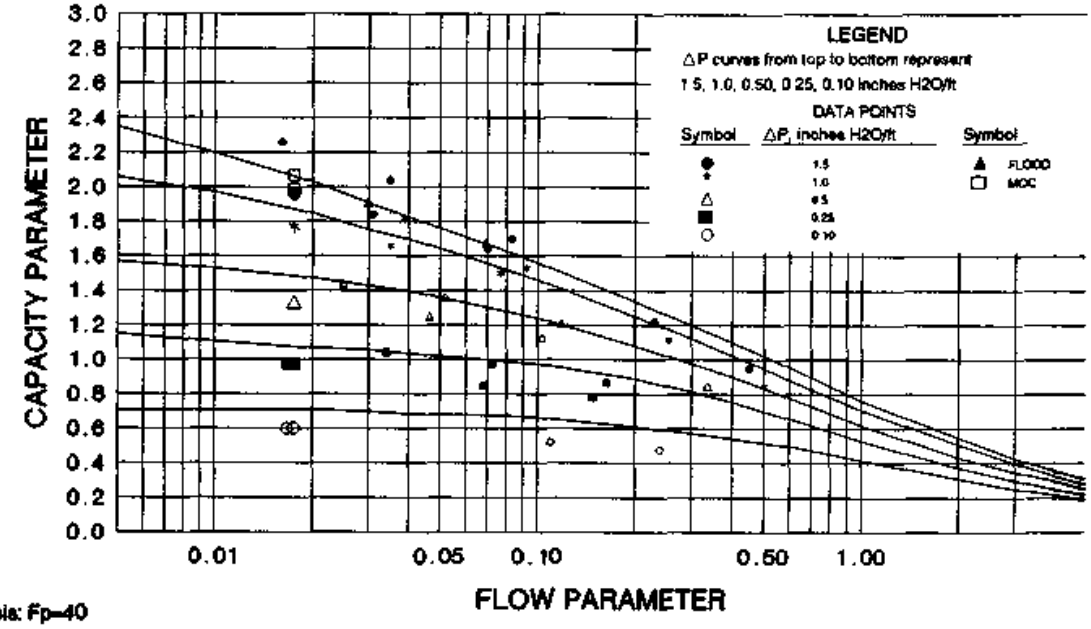

Basis: Fp=40
Pressure drop measured in inches H2O/ft
Large symbols represent non-aqueous data

CHART 10.2102
#1.5(M) CMR
FLOOD & PRESSURE DROP

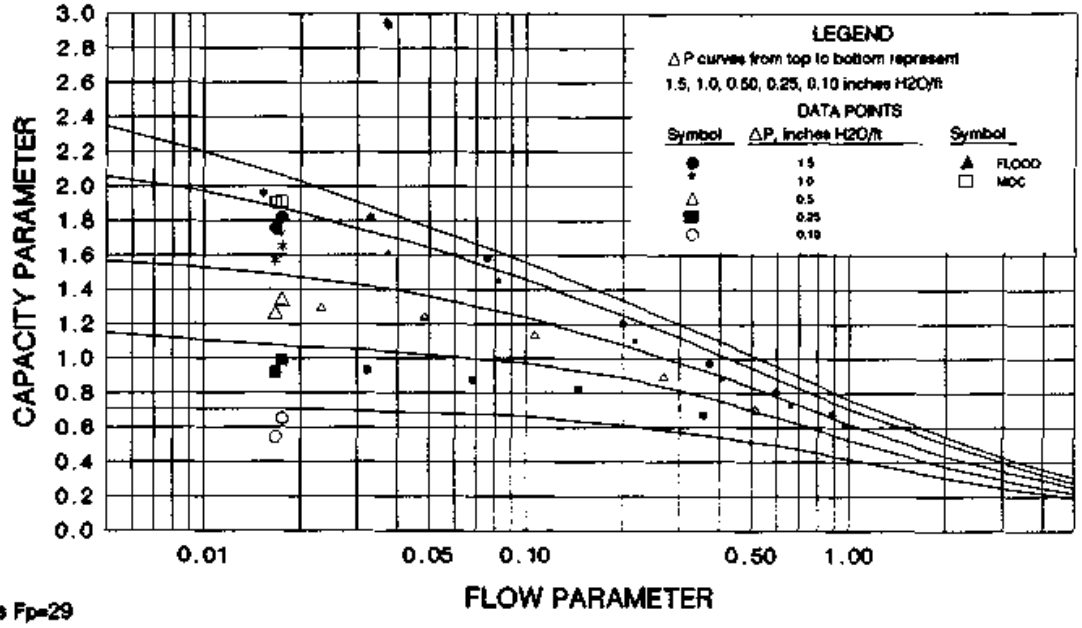

Basis Fp=29
Pressure drop measured in inches H2O/ft
Large symbols represent non-aqueous data

CHART 10.2103
#2(M) CMR
PRESSURE DROP

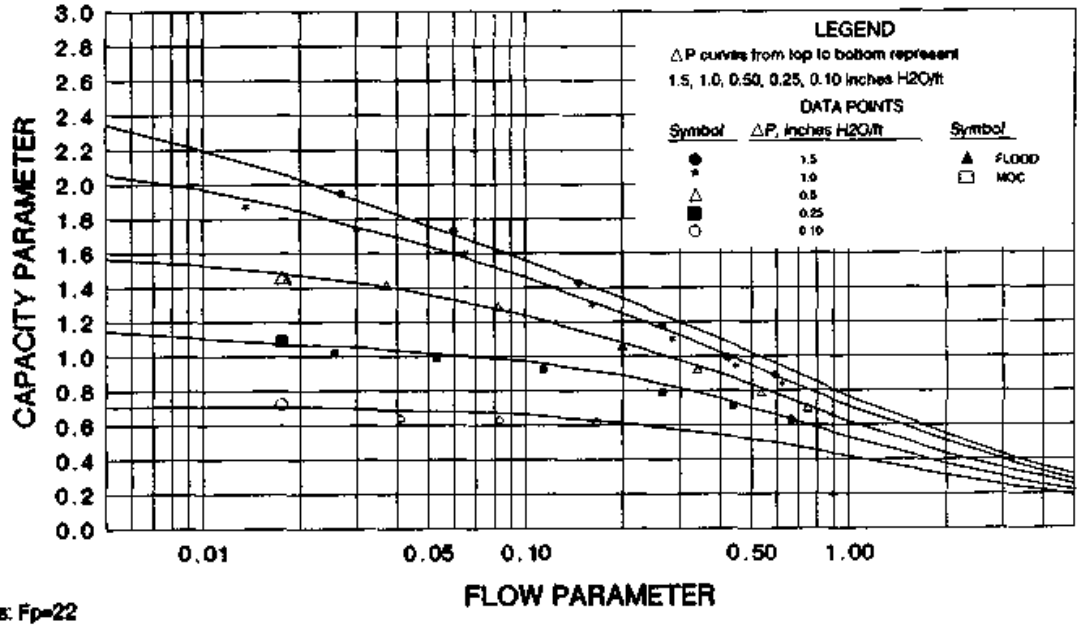

Basis: Fp=22
Pressure drop measured in inches H2O/ft
Large symbols represent non-aqueous data

CHART 10.2104
#2.5(M) CMR
PRESSURE DROP

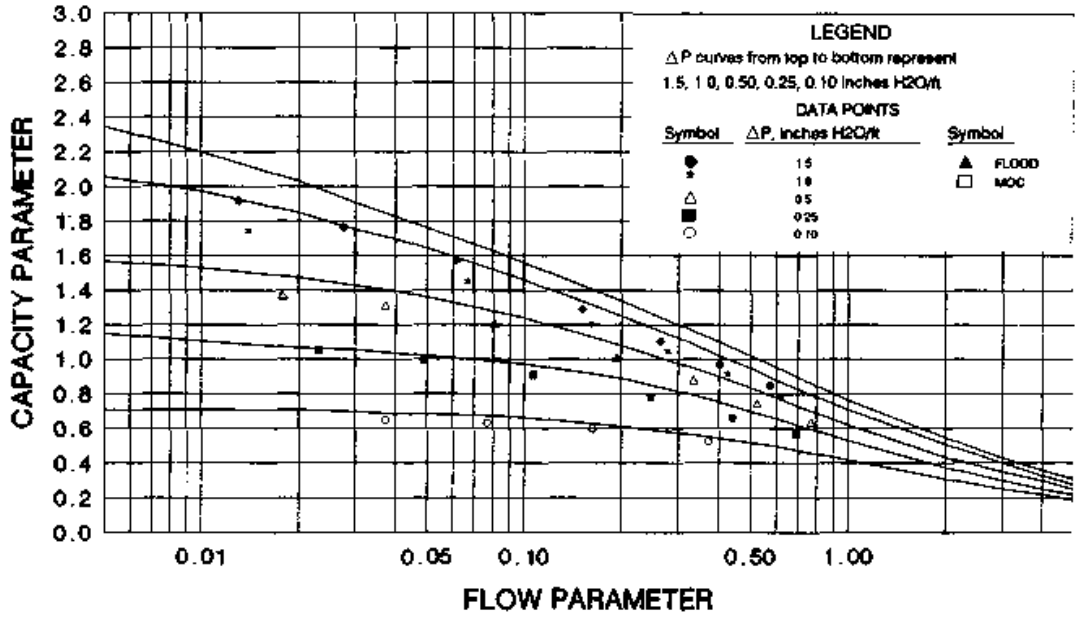

Basis: Fp=19
Pressure drop measured in inches H2O/ft

CHART 10.2105
#3(M) CMR
PRESSURE DROP

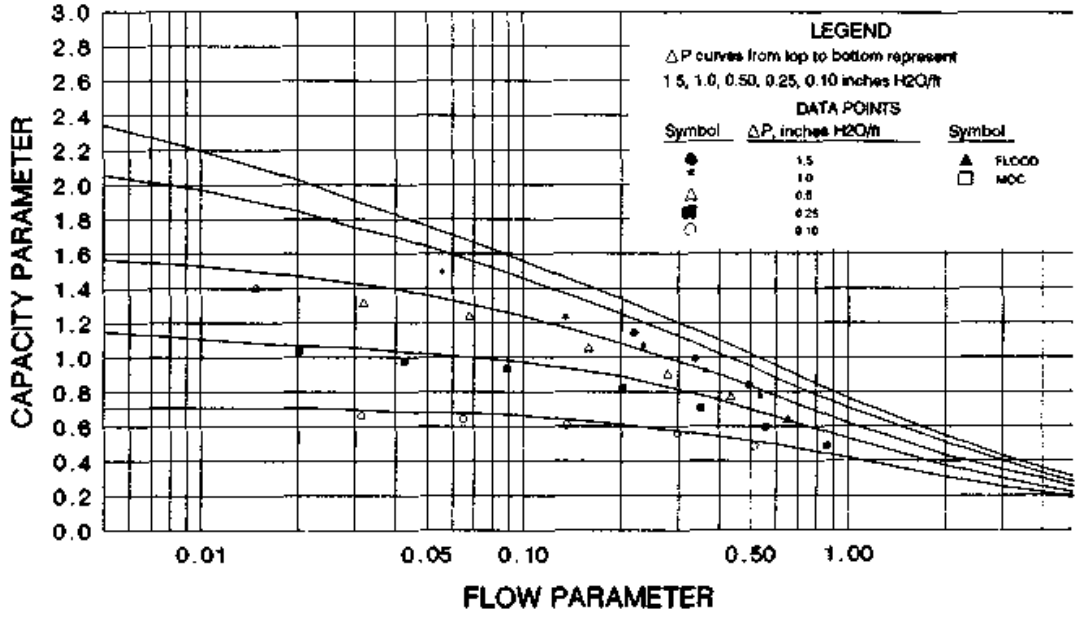

Basis: Fp=14
Pressure drop measured in inches H2O/ft

CHART 10.2106
#4(M) CMR
PRESSURE DROP

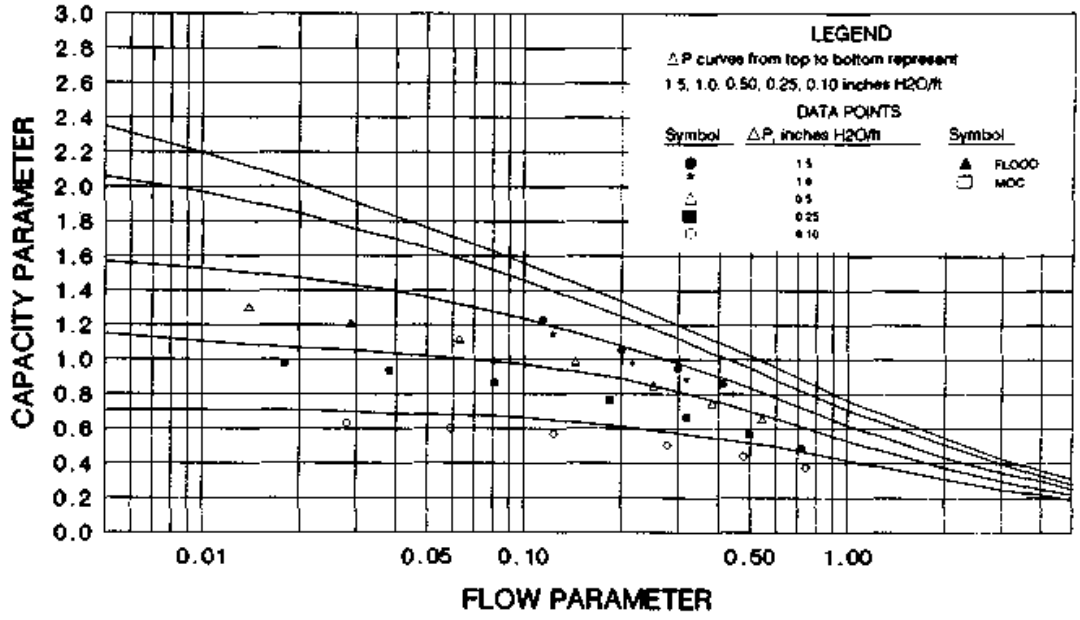

Basis: Fp=10
Pressure drop measured in inches H2O/ft

CHART 10.2111
#1A(P) CMR
PRESSURE DROP

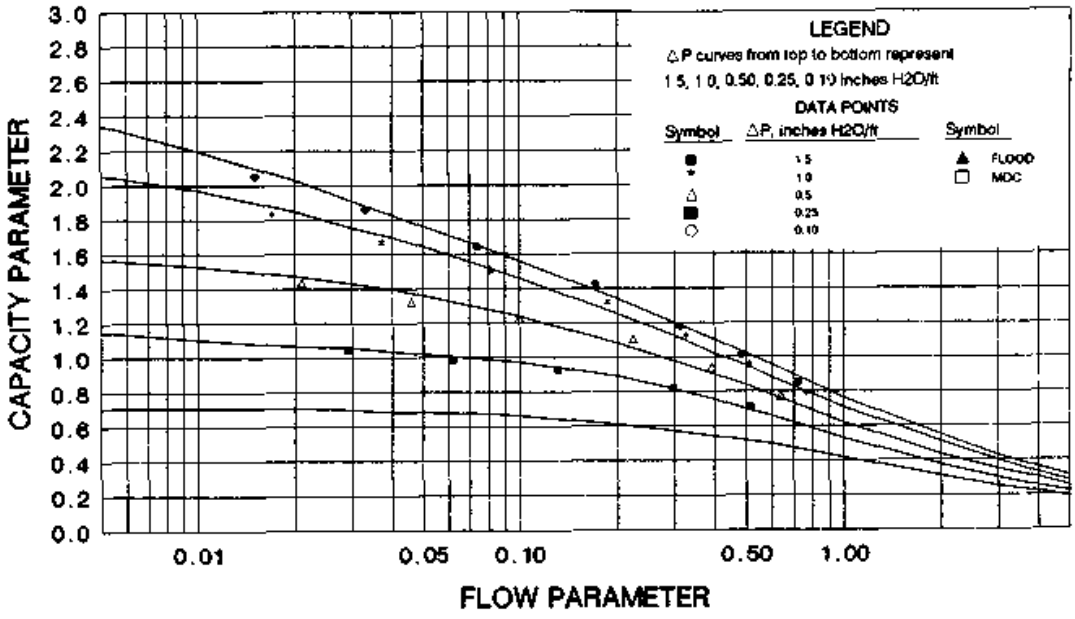

Basis: Fp=30
Pressure drop measured in inches H2O/ft

CHART 10.2113
#2A(P) CMR
PRESSURE DROP

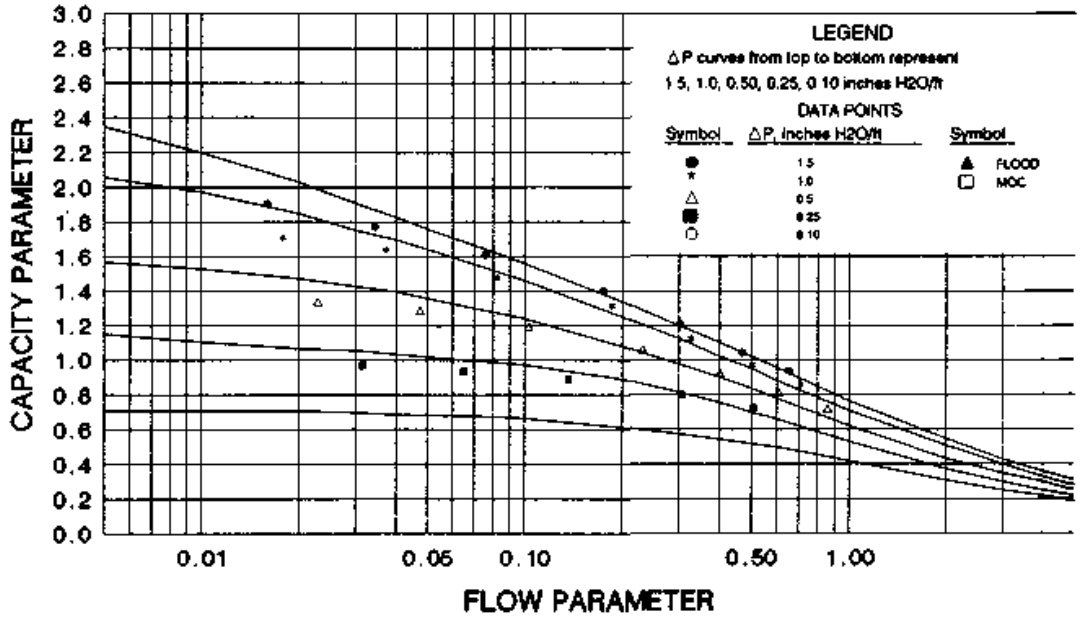

Basis: Fp=30
Pressure drop measured in inches H2O/ft

CHART 10.2115
#3A(P) CMR
PRESSURE DROP

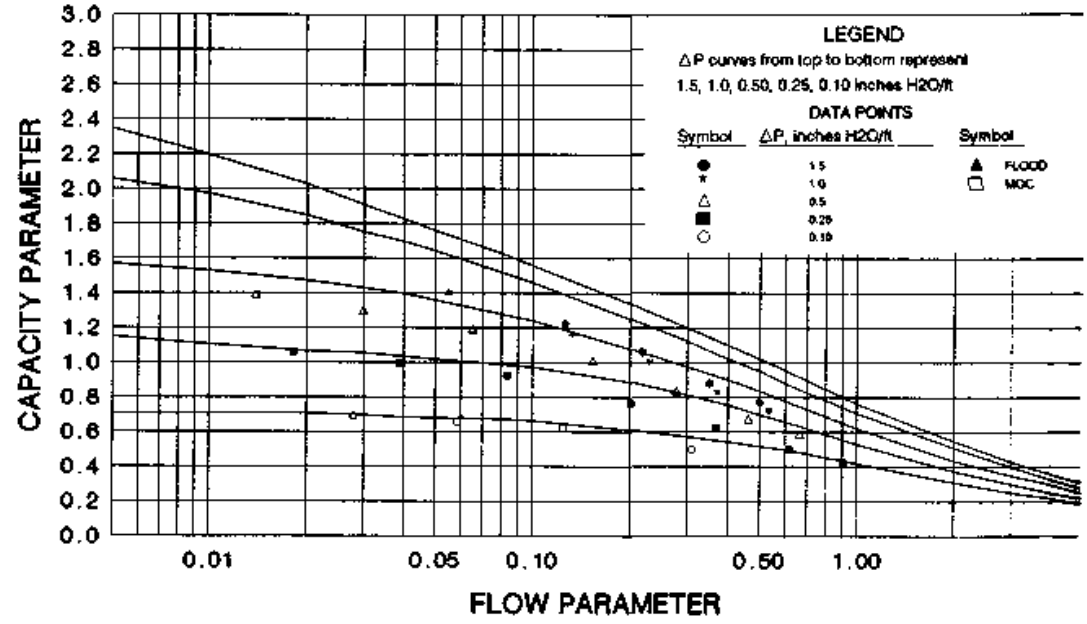

Basis: Fp=12
Pressure drop measured in inches H2O/ft

CHART 10.2202
#1 NUTTER RINGS
PRESSURE DROP

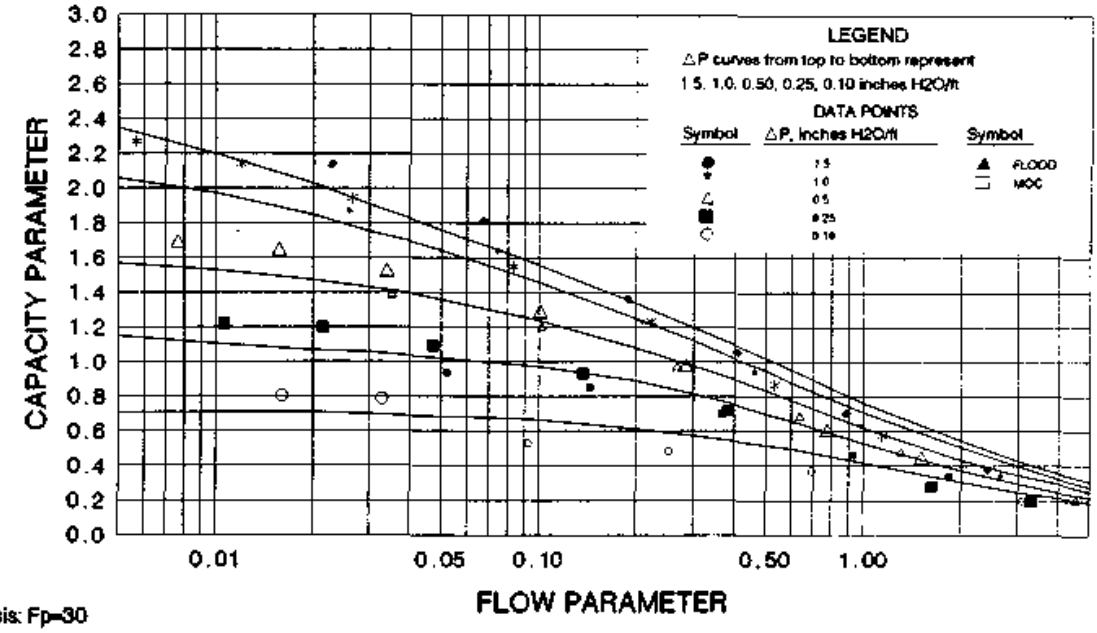

Basis: Fp=30
Pressure drop measured in inches H2O/ft
Large symbols represent non-aqueous data

CHART 10.2203
#1.5 NUTTER RINGS
PRESSURE DROP

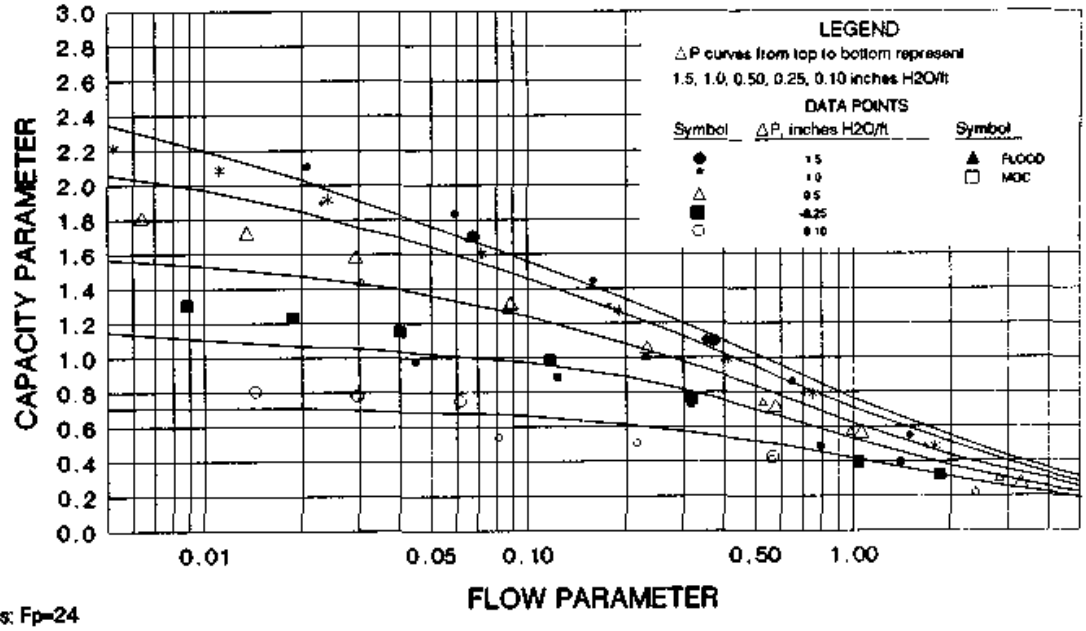

Basis: Fp=24
Pressure drop measured in inches H2O/ft
Large symbols represent non-aqueous data

CHART 10.2204
#2 NUTTER RINGS
FLOOD & PRESSURE DROP

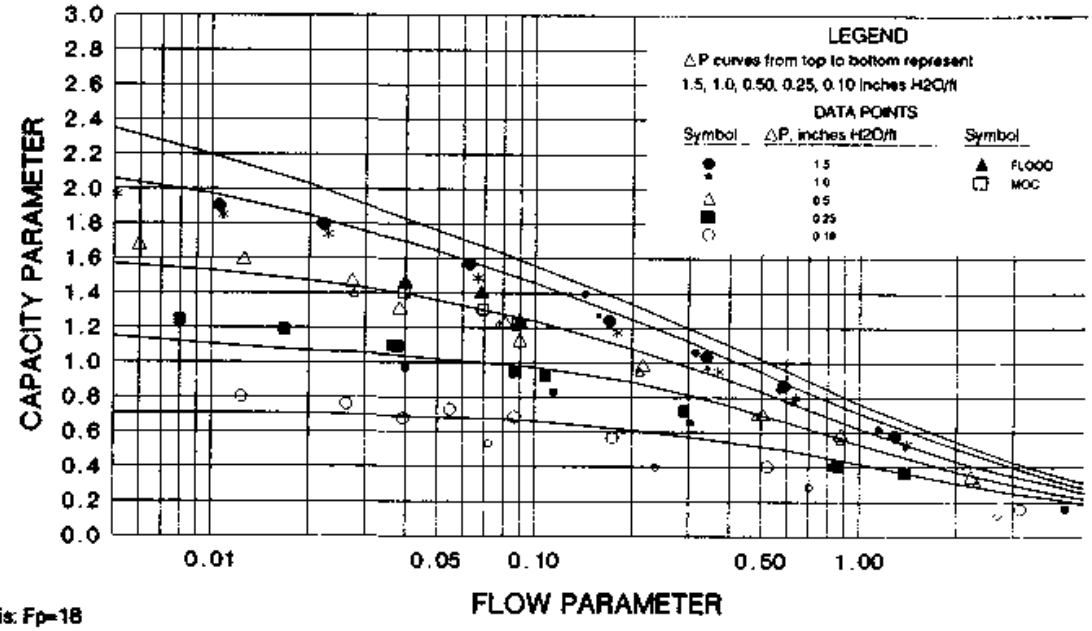

Basis: Fp=18
Pressure drop measured in inches H2O/ft
Large symbols represent non-aqueous data

CHART 10.2304
2" (M) HIFLOW RINGS
FLOOD & PRESSURE DROP

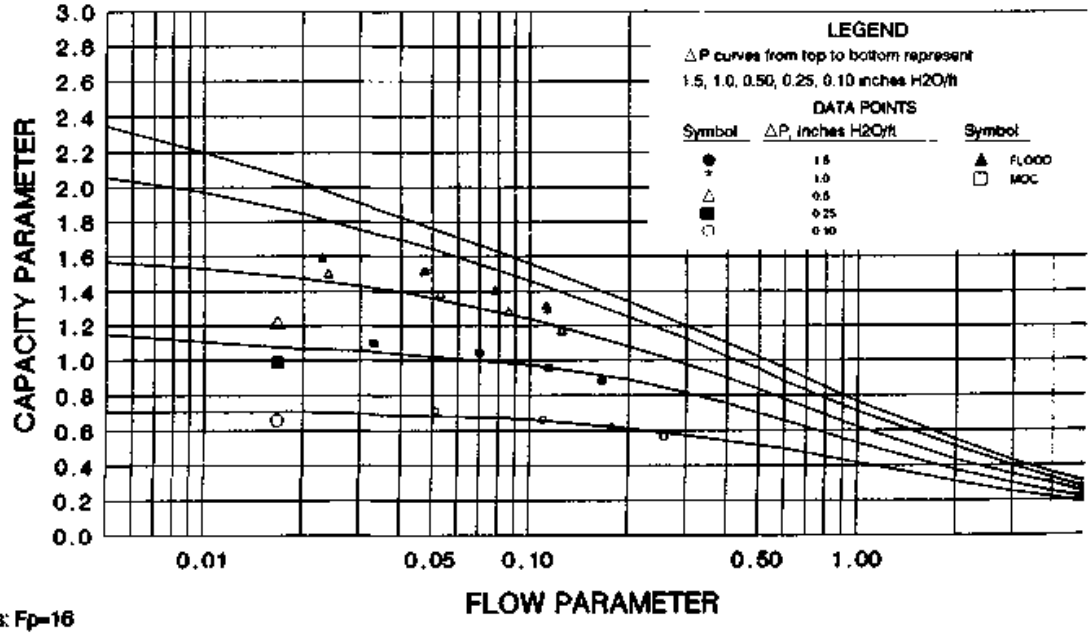

Basis: Fp=16
Pressure drop measured in inches H2O/ft
Large symbols represent non-aqueous data

CHART 10.2312
1"(P) HIFLOW RINGS
FLOOD & PRESSURE DROP

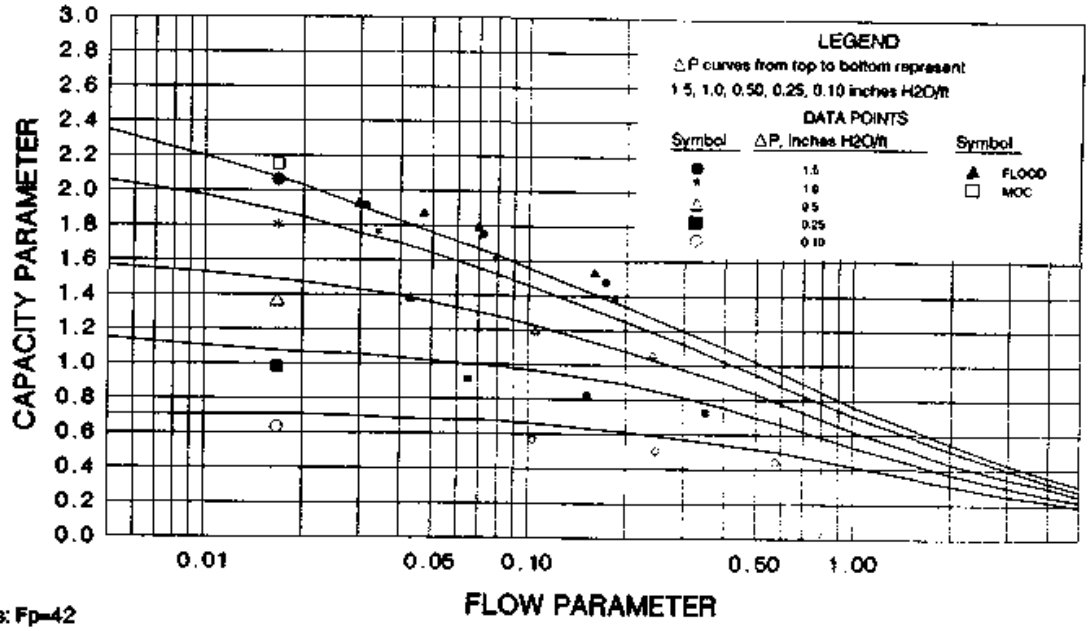

Basis: Fp=42
Pressure drop measured in inches H2O/ft
Large symbols represent non-aqueous data

CHART 10.2314
2"(P) HIFLOW RINGS
FLOOD & PRESSURE DROP

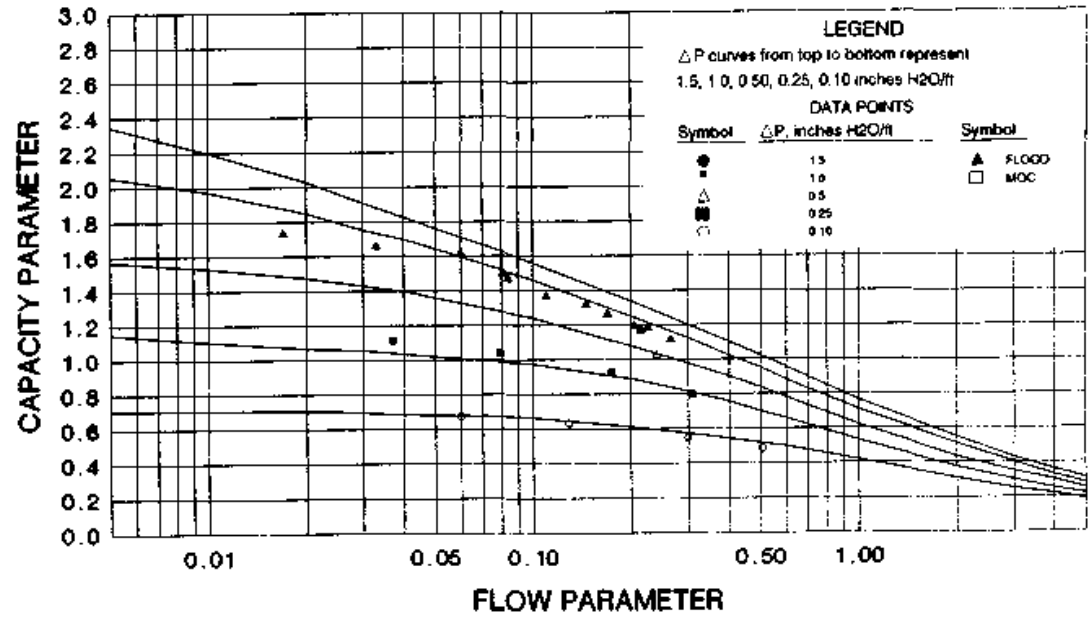

Basis: Fp=20
Pressure drop measured in inches H2O/ft

CHART 10.2317
3.5"(P) HIFLOW RINGS
FLOOD & PRESSURE DROP

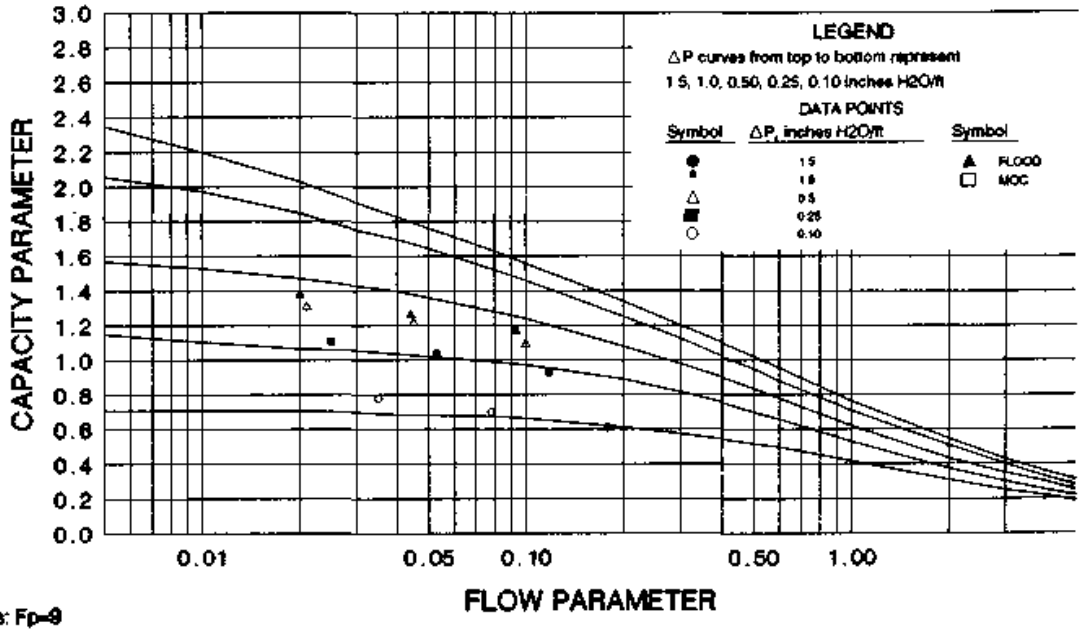

Basis: Fp=9
Pressure drop measured in inches H2O/ft
Large symbols represent non-aqueous data

CHART 10.2323
1.5" (C) HIFLOW RINGS
FLOOD & PRESSURE DROP

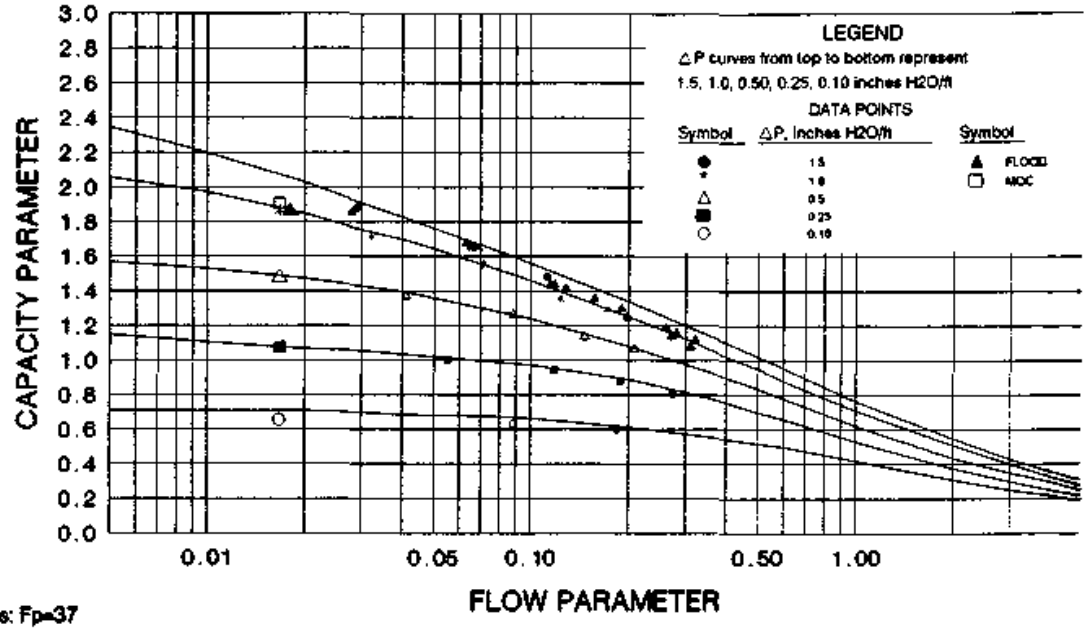

Basis: Fp=37
Pressure drop measured in inches H2O/ft
Large symbols represent non-aqueous data

CHART 10.2324
2" (C) HIFLOW RINGS
FLOOD & PRESSURE DROP

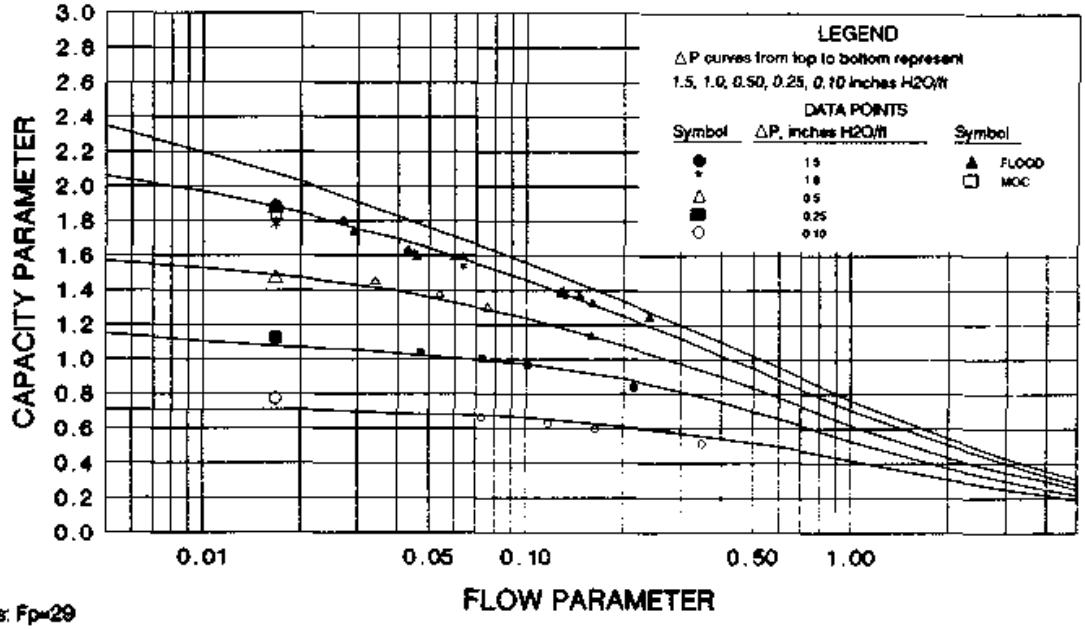

Basis: Fp=29
Pressure drop measured in inches H2O/ft
Large symbols represent non-aqueous data

CHART 10.2326
3" (C) HIFLOW RINGS
FLOOD & PRESSURE DROP

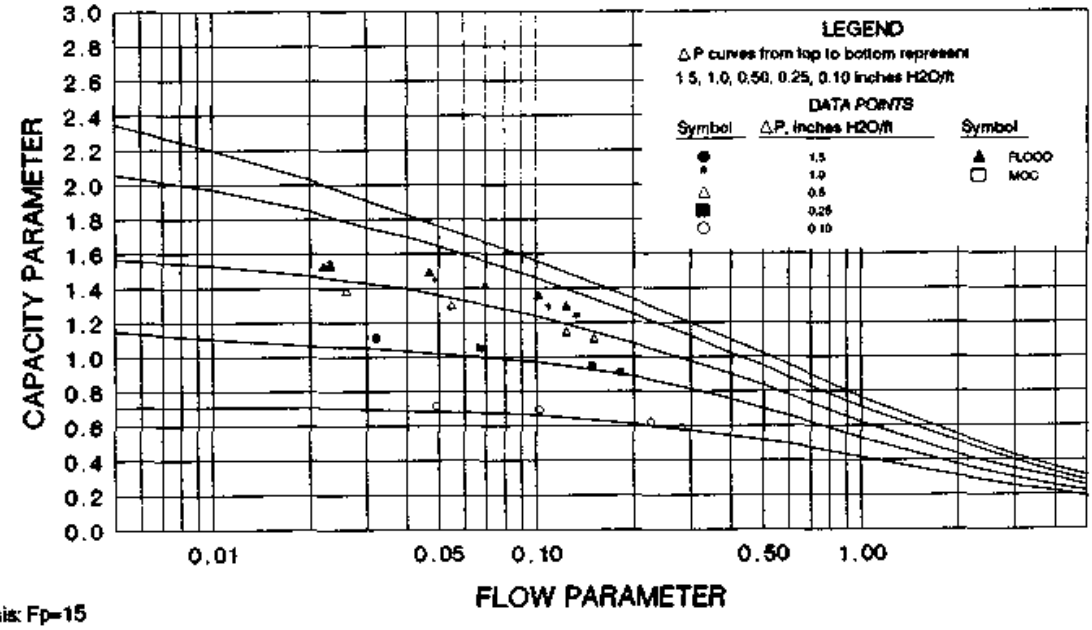

Basis: Fp=15
Pressure drop measured in inches H2O/ft
Large symbols represent non-aqueous data

CHART 10.2402
#1 HcKp
PRESSURE DROP

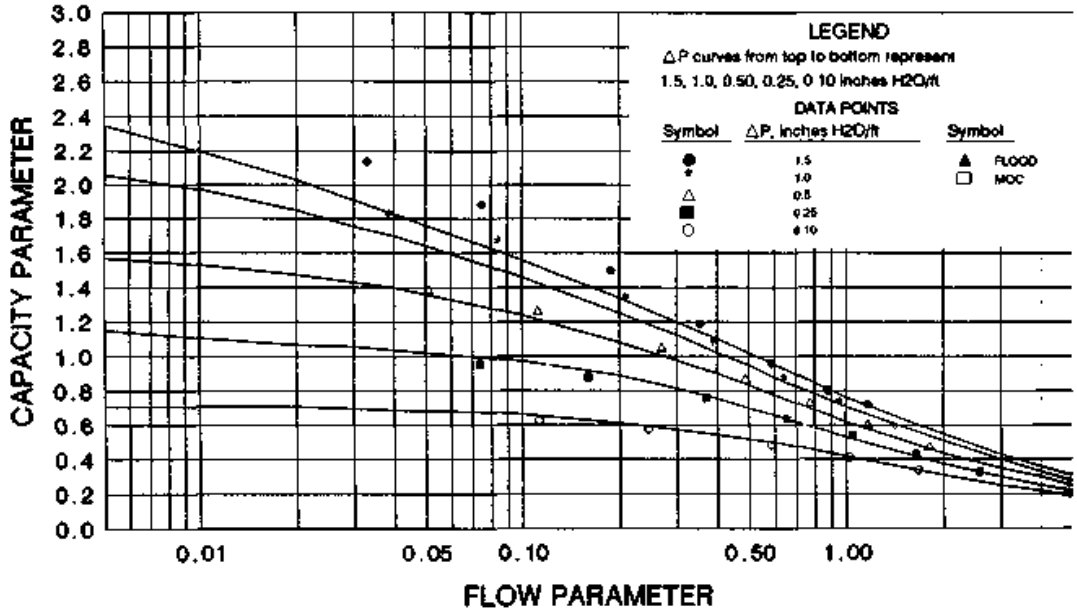

Basis Fp=40
Pressure drop measured in inches H2O/ft

CHART 10.2403
#1.5 HcKp
PRESSURE DROP

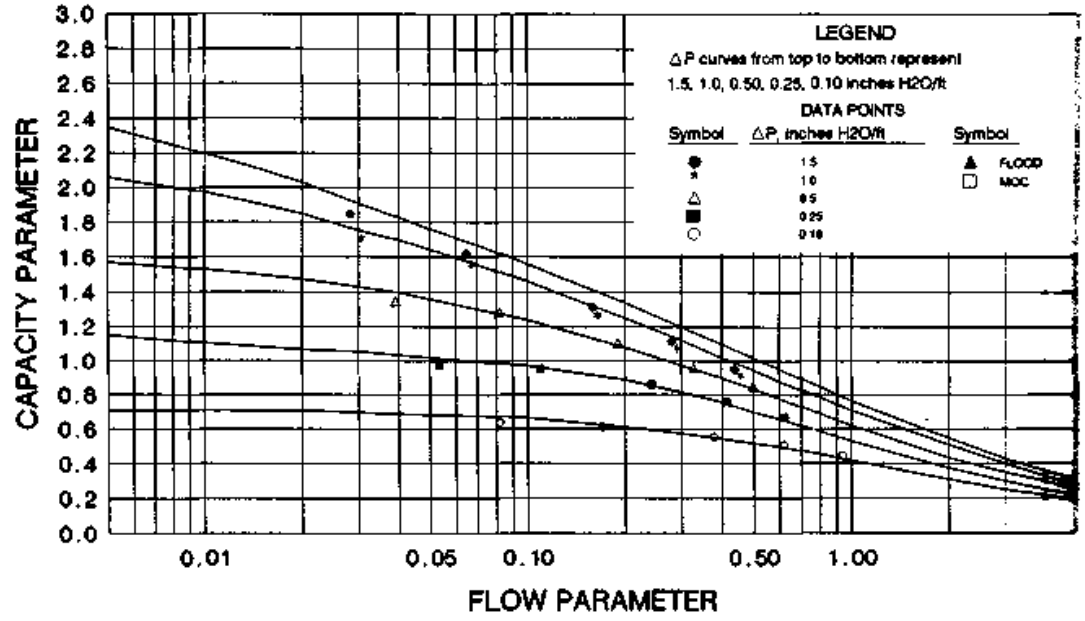

Basis Fp=22
Pressure drop measured in inches H2O/ft

CHART 10.2404
#2 HcKp
PRESSURE DROP

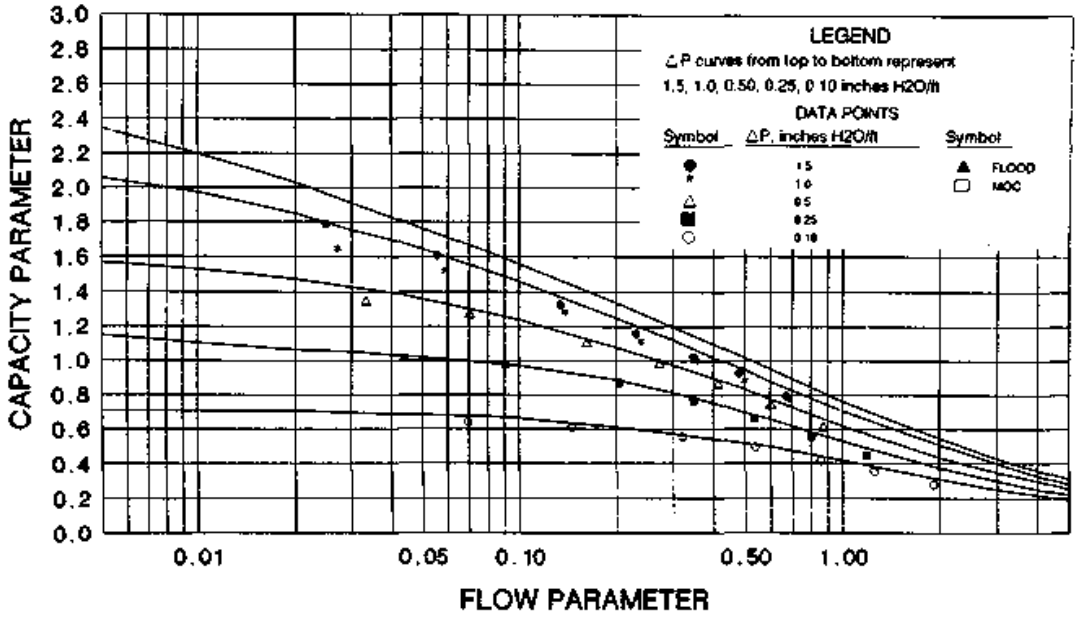

Basis Fp=16
Pressure drop measured in inches H2O/ft

CHART 10.2406
#3 HcKp
PRESSURE DROP

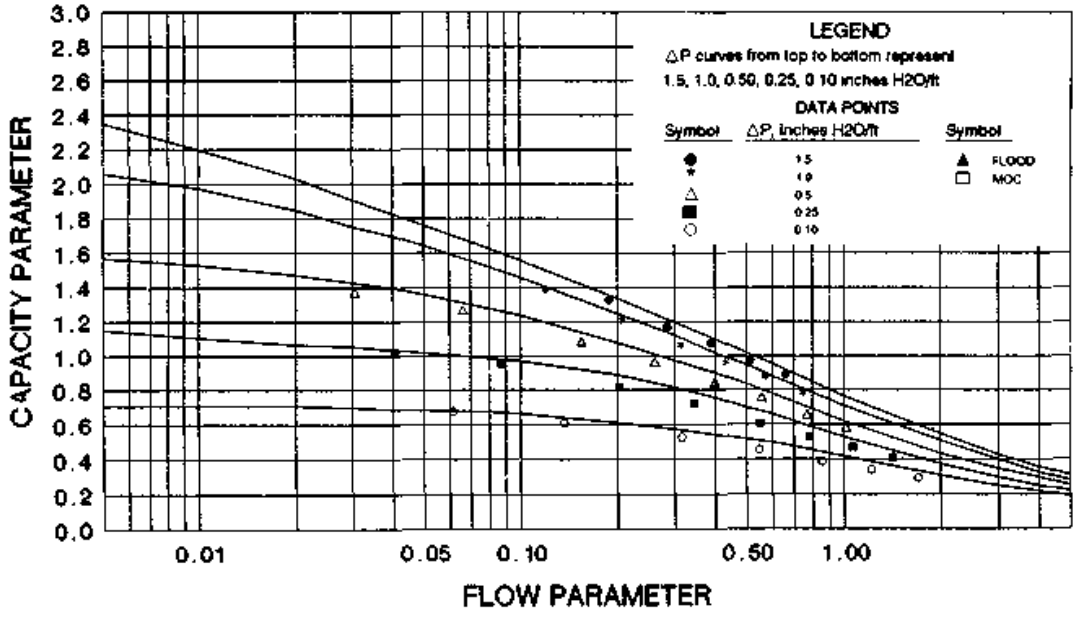

Basis Fp=14
Pressure drop measured in inches H2O/ft

CHART 10.3002
#1 (M) CHEMPAK & LEVAPAK
PRESSURE DROP

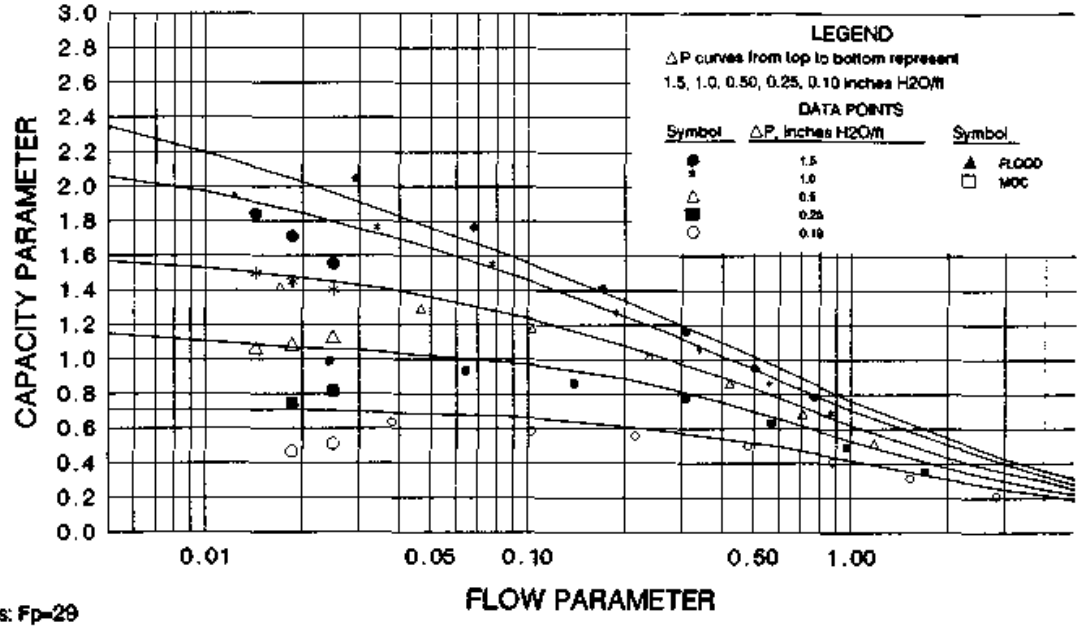

Basis: Fp=29
Pressure drop measured in inches H2O/ft
Large symbols represent non-aqueous data

CHART 10.3004
#2 (M) CHEMPAK
PRESSURE DROP

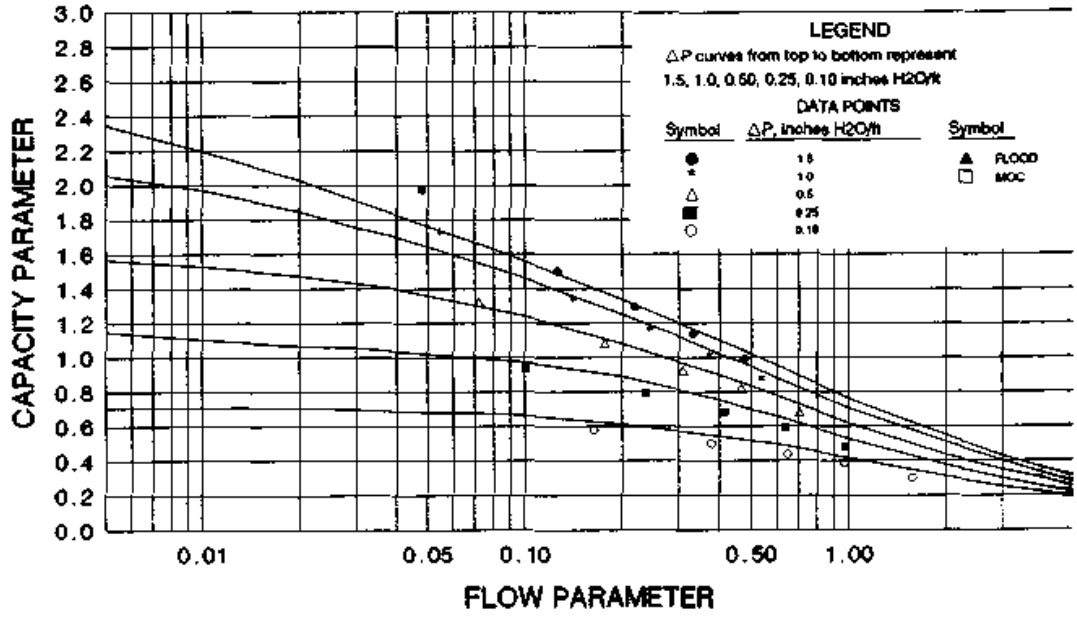

Basis: Fp=18
Pressure drop measured in inches H2O/ft

CHART 10.3104
#1 (2") (M) JAEGER TRIPACKS
FLOOD & PRESSURE DROP

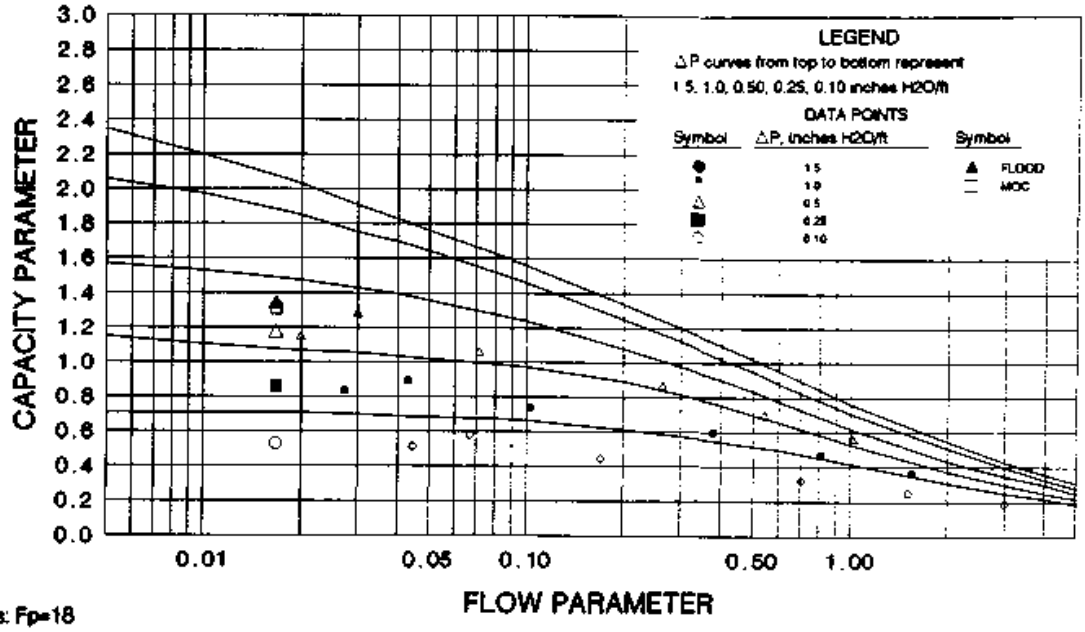

Basis: Fp=18
Pressure drop measured in inches H2O/ft
Large symbols represent non-aqueous data

CHART 10.3106
#2 (3") (M) JAEGER TRIPACKS
PRESSURE DROP

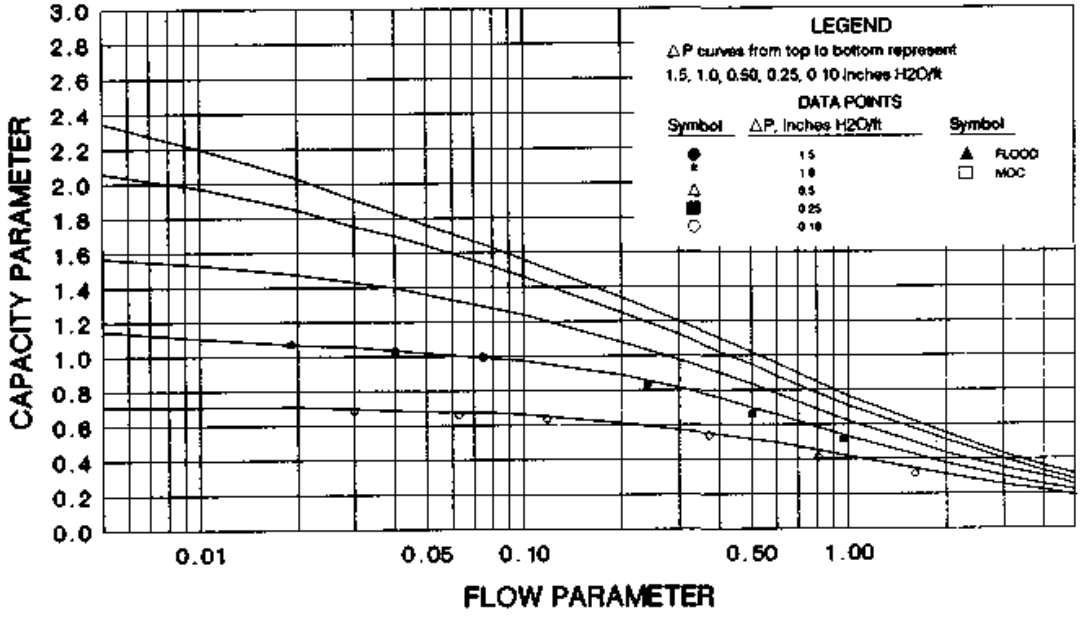

Basis: Fp=14
Pressure drop measured in inches H2O/ft

CHART 10.3114
#1 (2" & 45mm) (P) JAEGER TRIPACKS
FLOOD & PRESSURE DROP

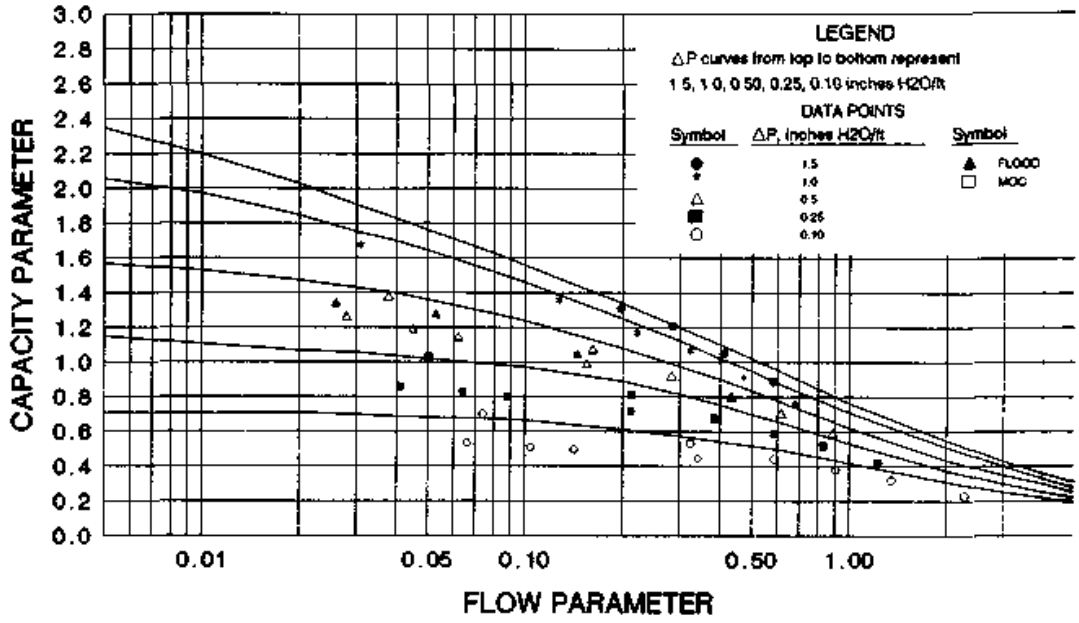

Basis: Fp=15
Pressure drop measured in inches H2O/ft

CHART 10.3116
#2 (3") (P) JAEGER TRIPACKS
PRESSURE DROP

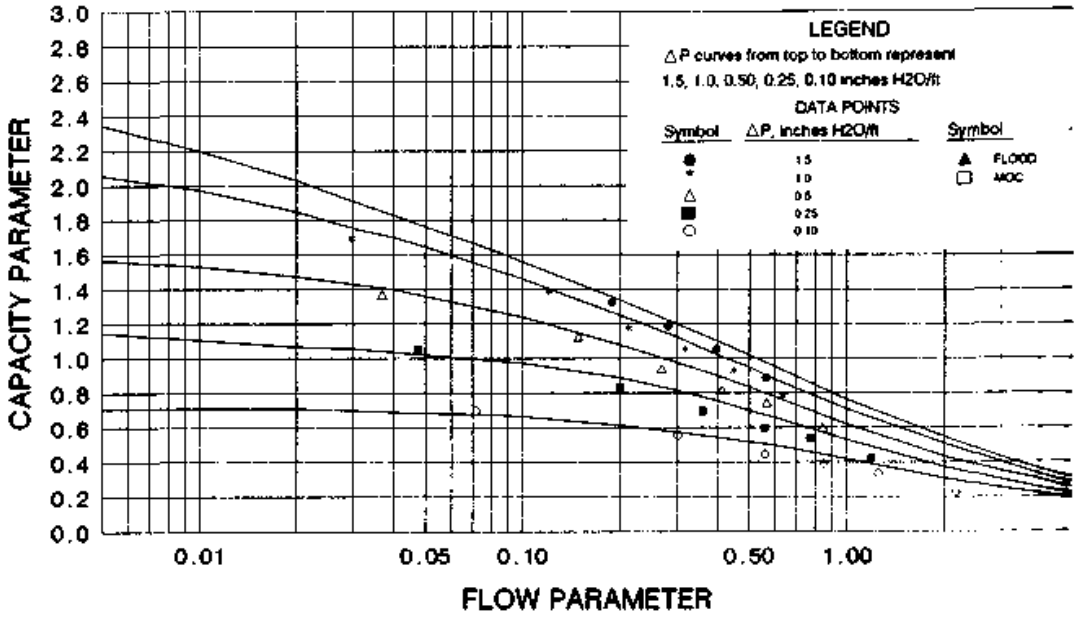

Basis: Fp=14
Pressure drop measured in inches H2O/ft

CHART 10.3212
1" (P) NOR PAC
FLOOD & PRESSURE DROP

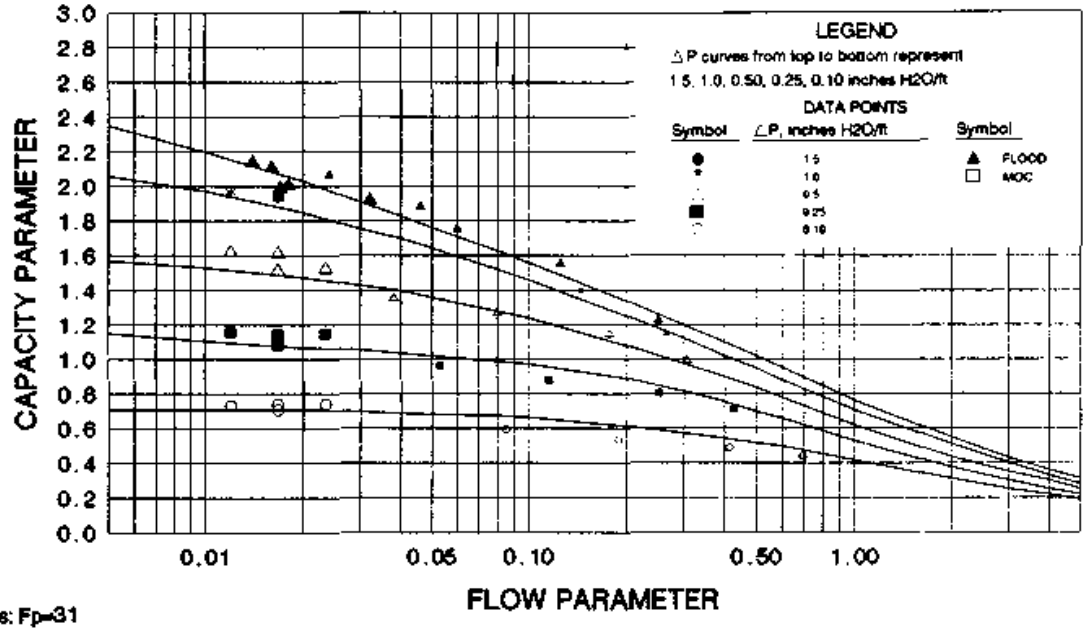

Basis: Fp=31
Pressure drop measured in inches H2O/ft
Large symbols represent non-aqueous data

CHART 10.3213
1.5" (P) NOR PAC
FLOOD & PRESSURE DROP

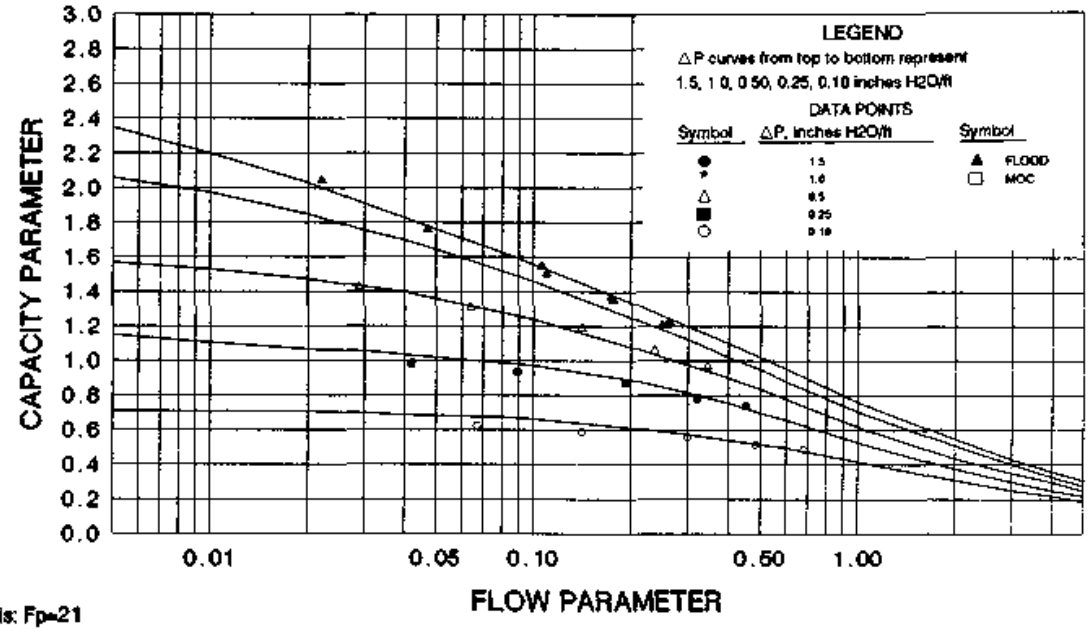

Basis: Fp=21
Pressure drop measured in inches H2O/ft
Large symbols represent non-aqueous data

CHART 10.3214
2" (P) NOR PAC
FLOOD & PRESSURE DROP

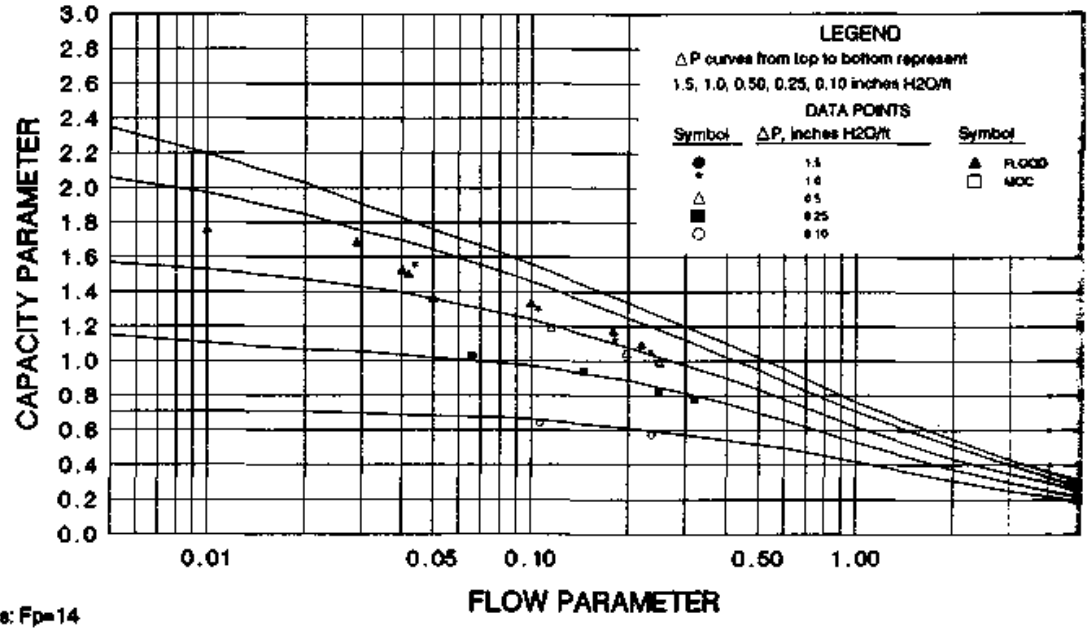

Basis: Fp=14
Pressure drop measured in inches H2O/ft
Large symbols represent non-aqueous data

CHART 10.3316
INTALOX SNOWFLAKE
PRESSURE DROP

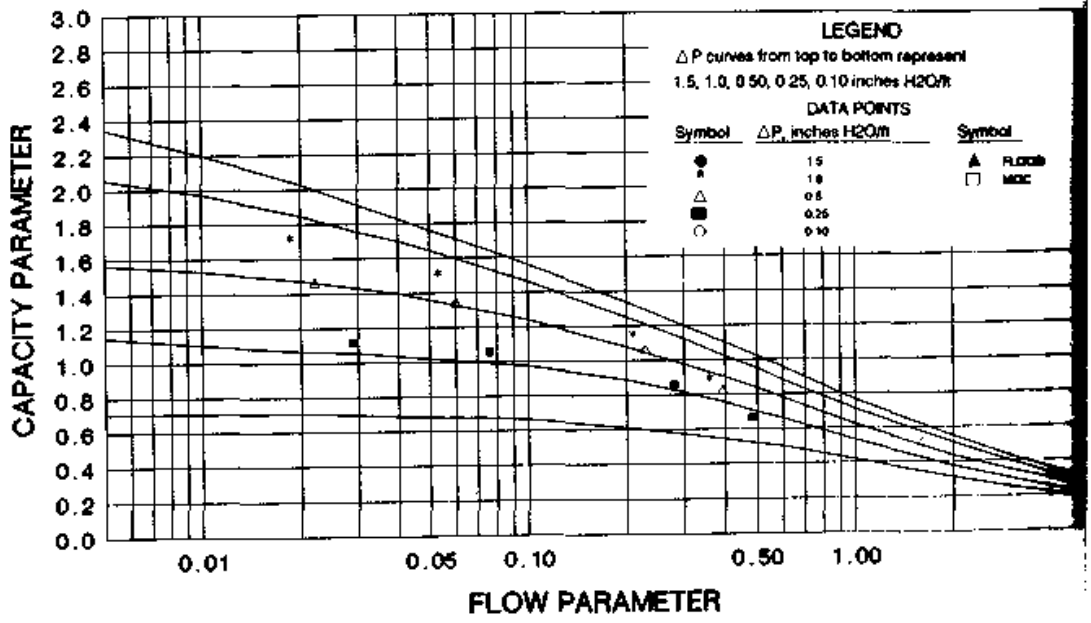

Basis: Fp=13
Pressure drop measured in inches H2O/ft

CHART 10.3417
3.5" (P) LANPAC
PRESSURE DROP

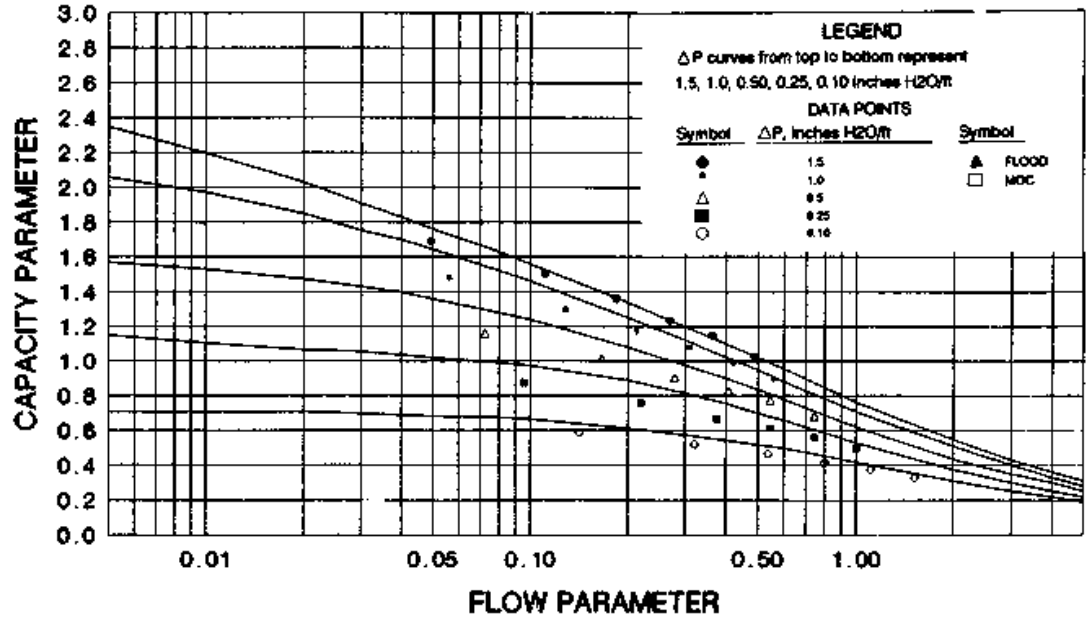

Basis: Fp=14
Pressure drop measured in inches H2O/ft

CHART 10.3517
#3 (3.5") (P) IMPAC
PRESSURE DROP

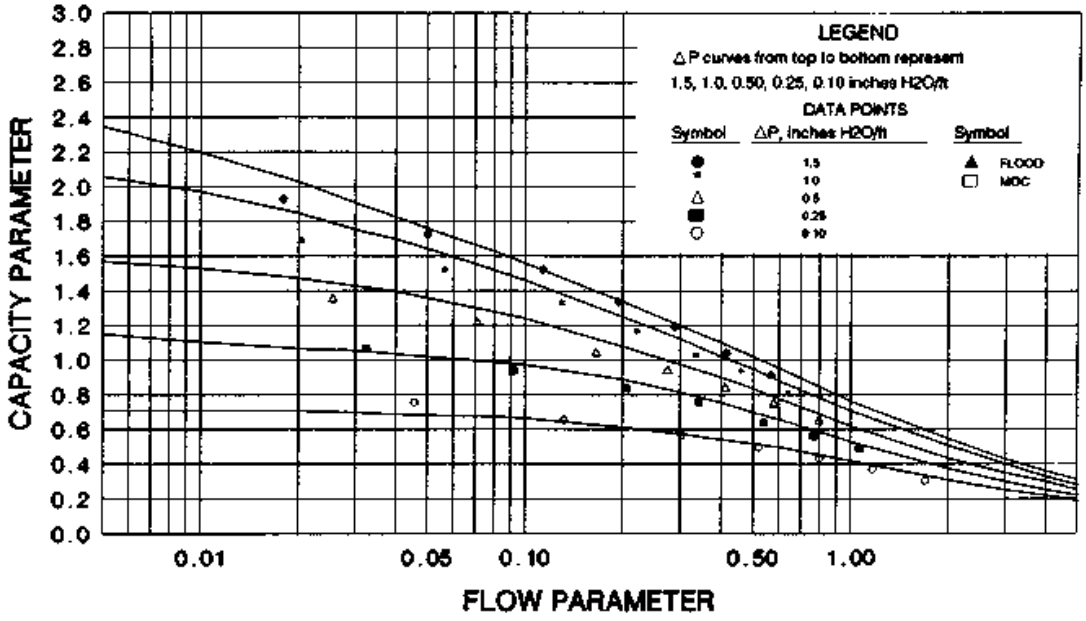

Basis: Fp=15
Pressure drop measured in inches H2O/ft

CHART 10.5001
KOCH - SULZER CY PACKING
FLOOD & PRESSURE DROP

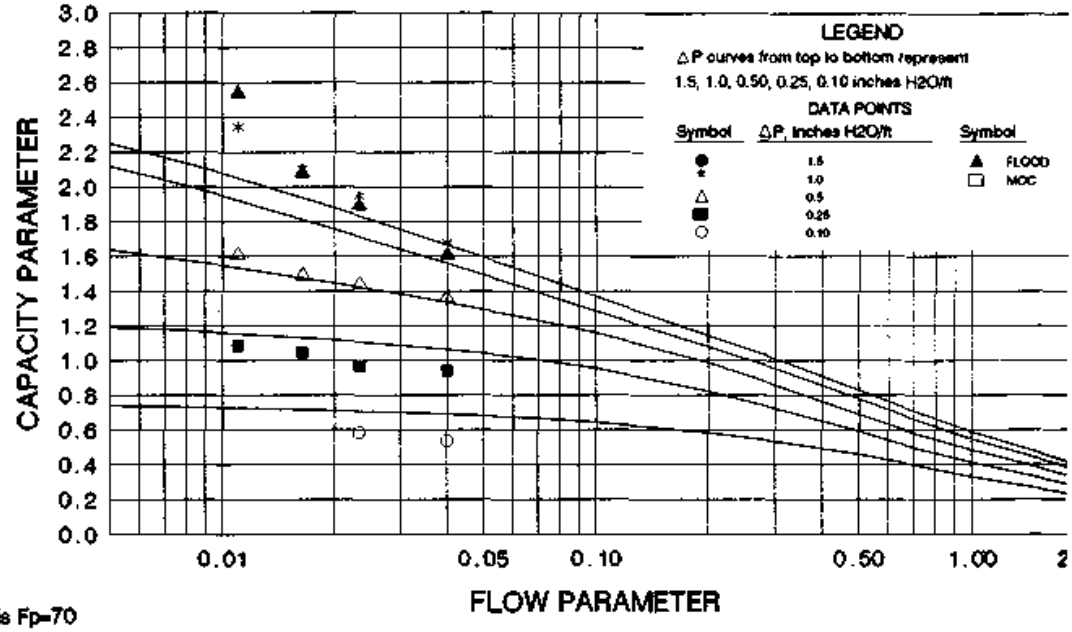

Basis Fp=70
Pressure drop measured in inches H2O/ft
Large symbols represent non-aqueous data

CHART 10.5002
KOCH - SULZER BX PACKING
FLOOD & PRESSURE DROP

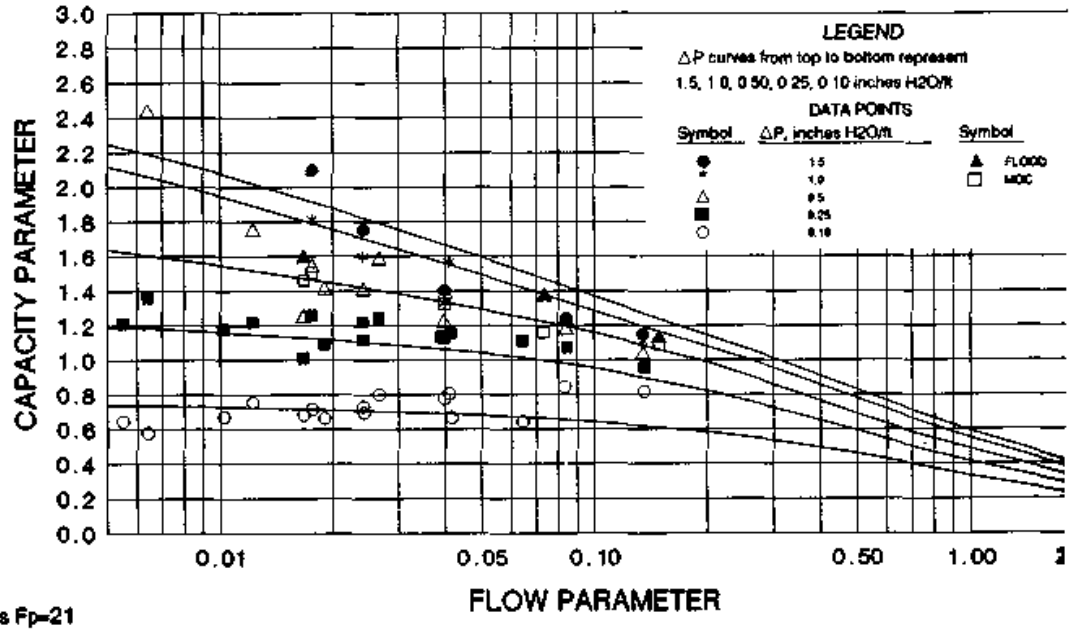

Basis Fp=21
Pressure drop measured in inches H2O/ft
Large symbols represent non-aqueous data

CHART 10.6002
SULZER MELLAPAK 500Y
FLOOD & PRESSURE DROP

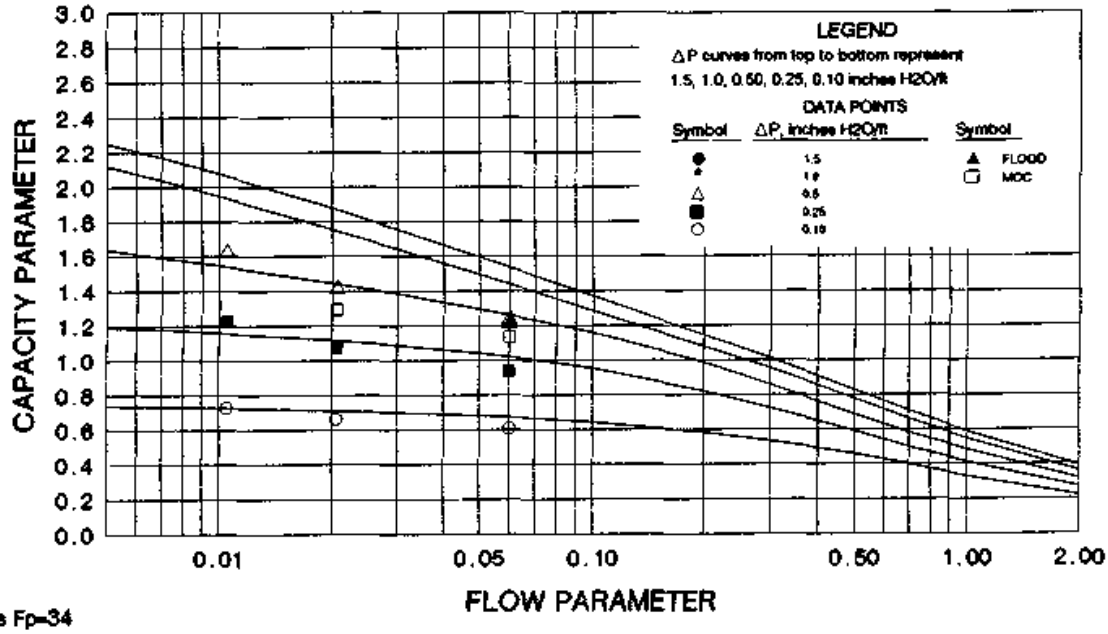

Basis Fp=34
Pressure drop measured in inches H2O/ft
Large symbols represent non-aqueous data

CHART 10.6003
SULZER MELLAPAK 350Y
FLOOD & PRESSURE DROP

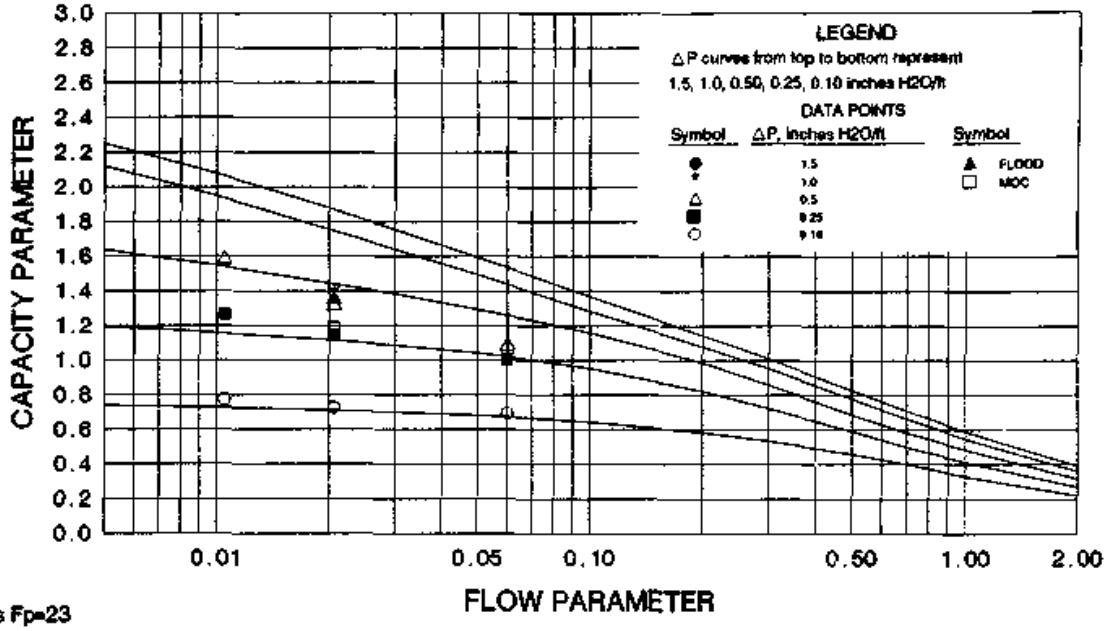

Basis Fp=23
Pressure drop measured in inches H2O/ft
Large symbols represent non-aqueous data

CHART 10.6004A
SULZER MELLAPAK 250Y
FLOOD & PRESSURE DROP – NON-AQUEOUS

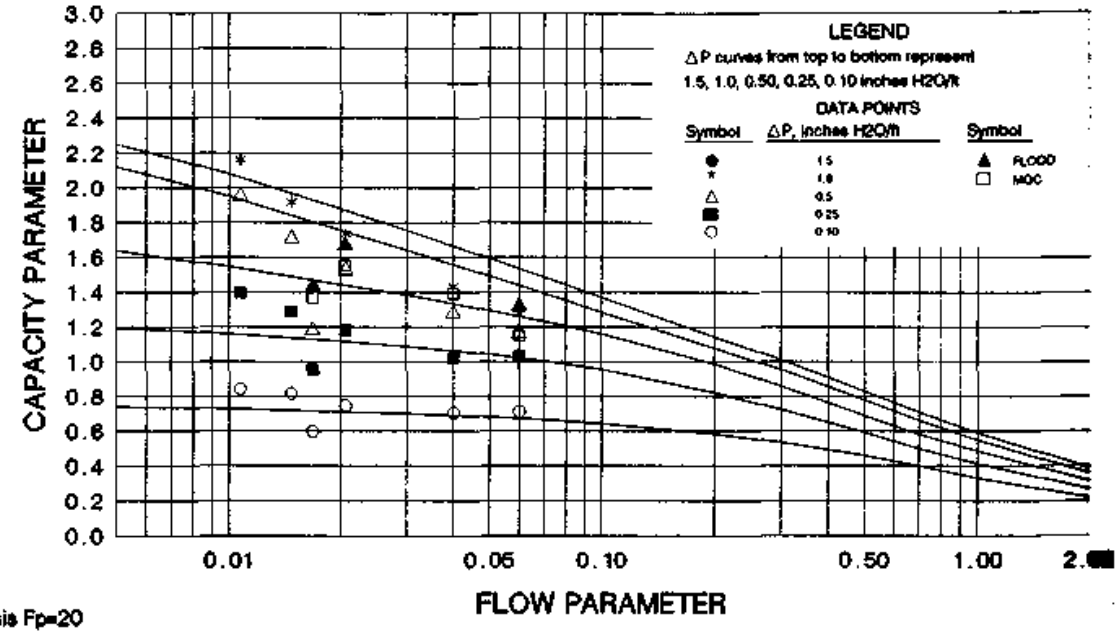

Basis Fp=20
Pressure drop measured in inches H2O/ft
Large symbols represent non-aqueous data

CHART 10.6004B
SULZER MELLAPAK 250Y
FLOOD & PRESSURE DROP – AQUEOUS

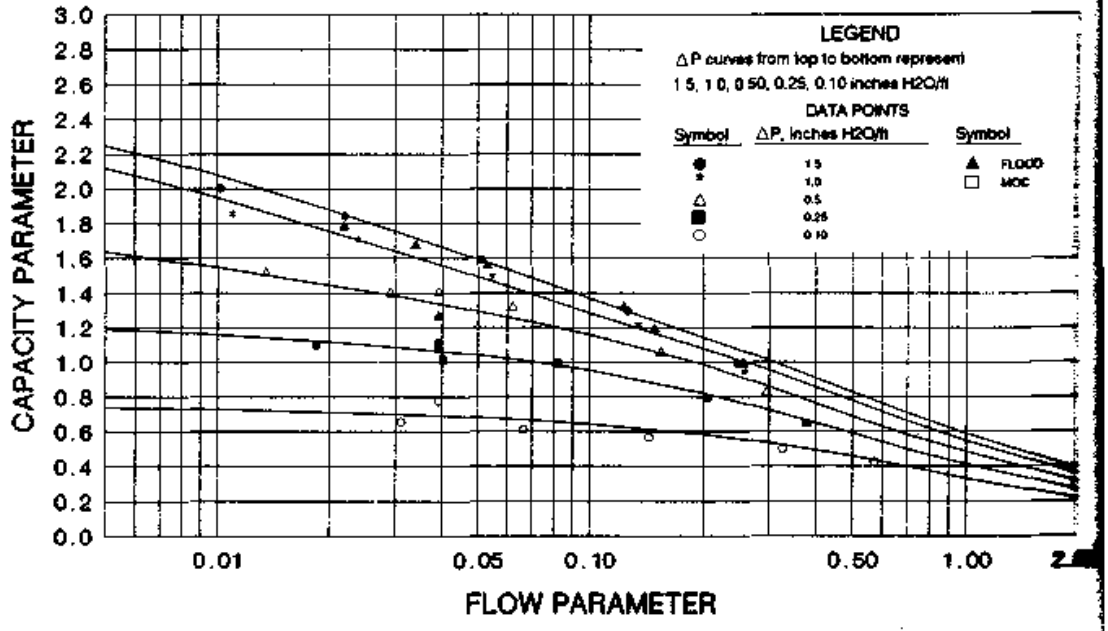

Basis Fp=20
Pressure drop measured in inches H2O/ft

CHART 10.6008
SULZER MELLAPAK 125Y
FLOOD & PRESSURE DROP

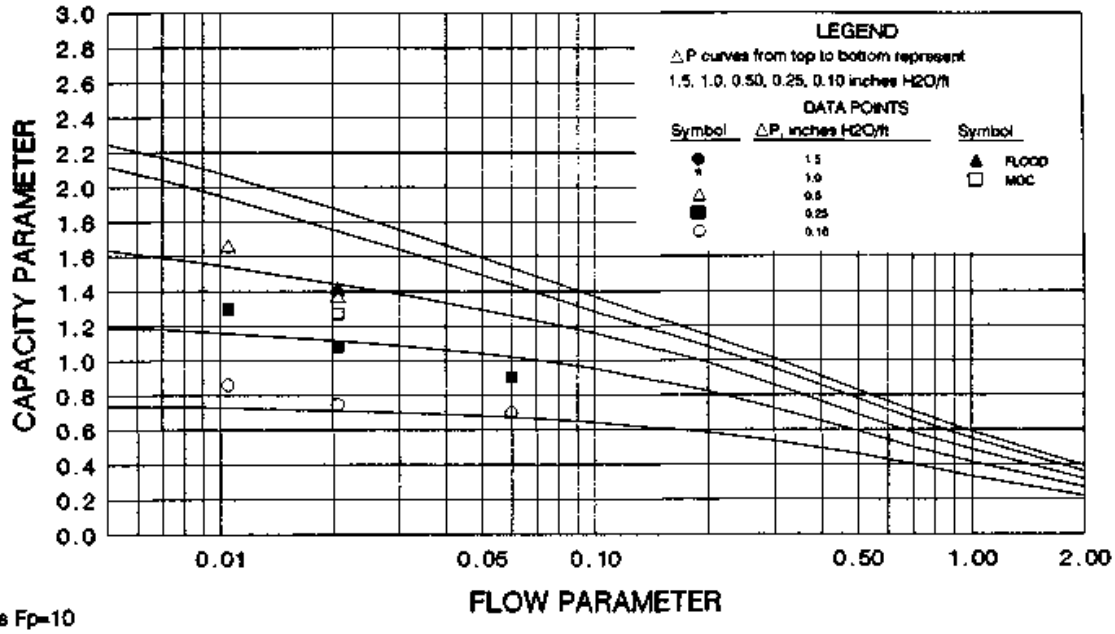

Basis Fp=10
Pressure drop measured in inches H2O/ft
Large symbols represent non-aqueous data

CHART 10.6014
SULZER MELLAPAK 250Y PLASTIC
PRESSURE DROP

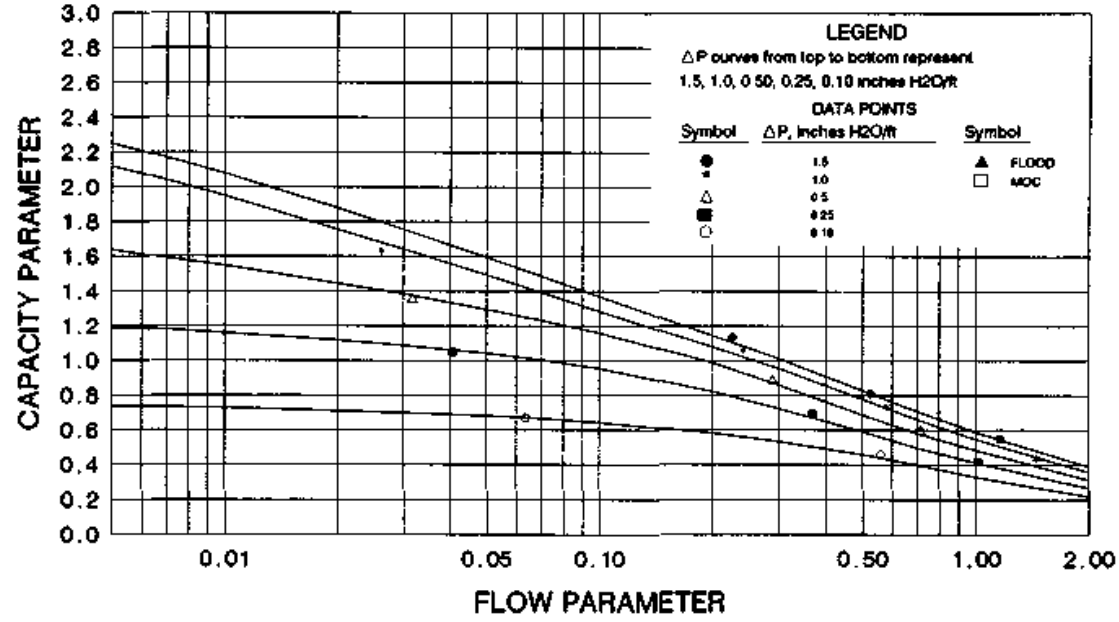

Basis Fp=22
Pressure drop measured in inches H2O/ft

CHART 10.6102
KOCH FLEXIPAC #1
FLOOD & PRESSURE DROP

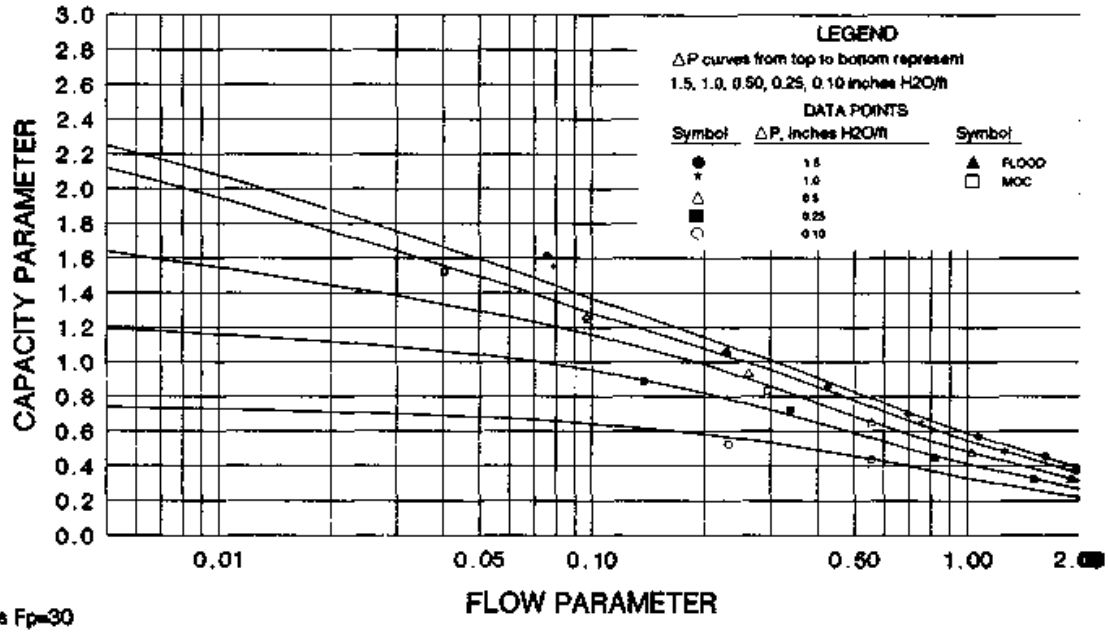

Basis Fp=30
Pressure drop measured in inches H2O/ft
Large symbols represent non-aqueous data

CHART 10.6104
KOCH FLEXIPAC #2
FLOOD & PRESSURE DROP

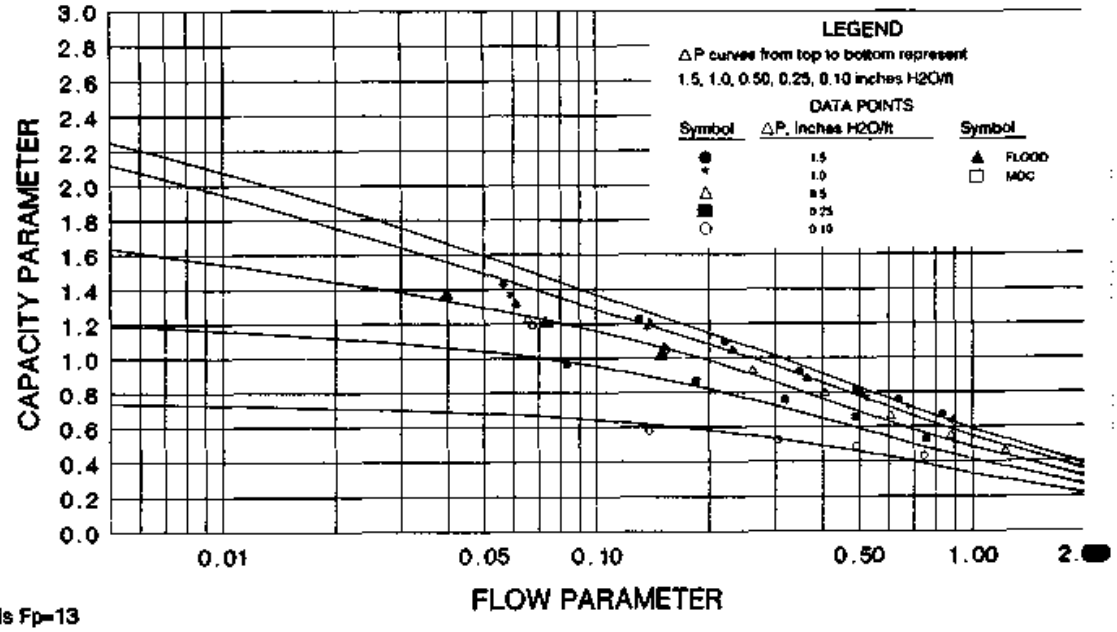

Basis Fp=13
Pressure drop measured in inches H2O/ft
Large symbols represent non-aqueous data

CHART 10.6106
KOCH FLEXIPAC #3
FLOOD & PRESSURE DROP

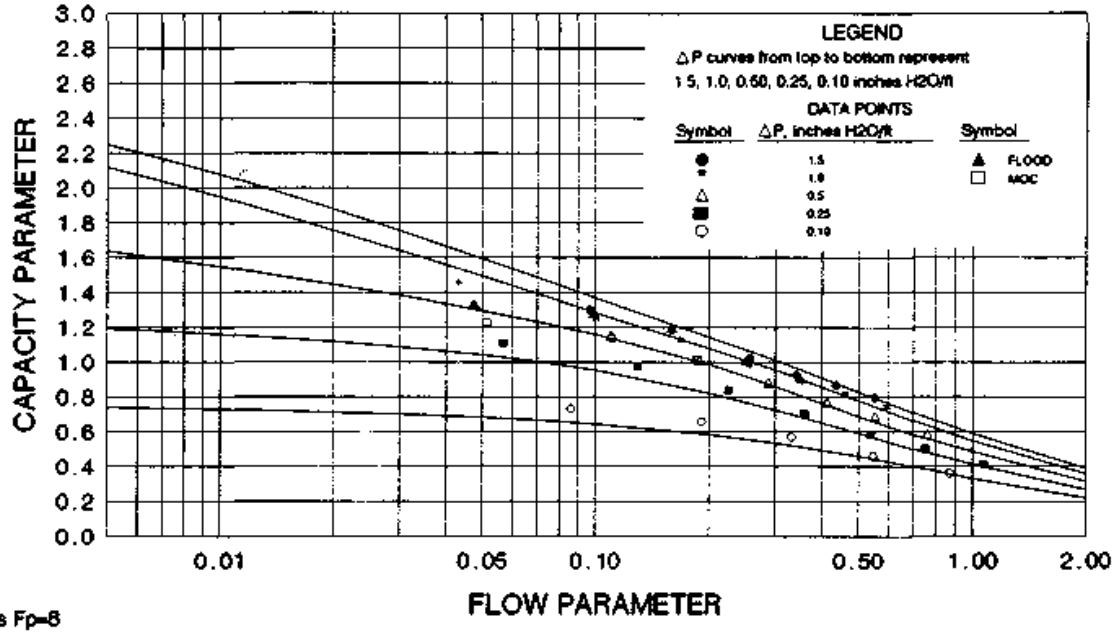

Basis Fp=6
Pressure drop measured in inches H2O/ft
Large symbols represent non-aqueous data

CHART 10.6108
KOCH FLEXIPAC #4
PRESSURE DROP

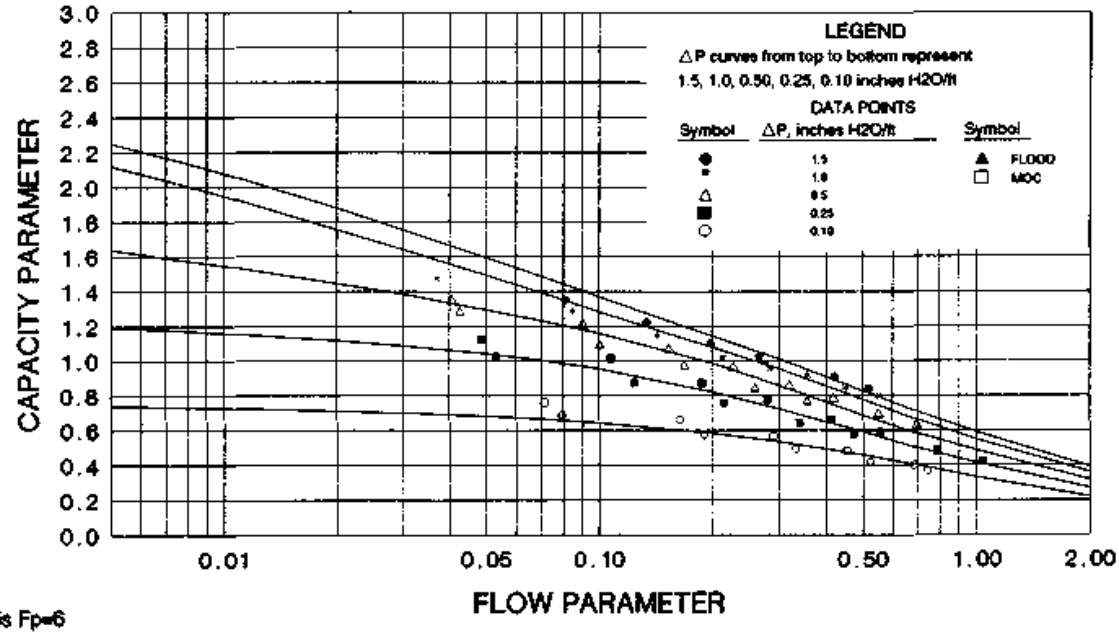

Basis Fp=6
Pressure drop measured in inches H2O/ft
Large symbols represent non-aqueous data

CHART 10.6122
KOCH FLEXERAMIC #28
PRESSURE DROP

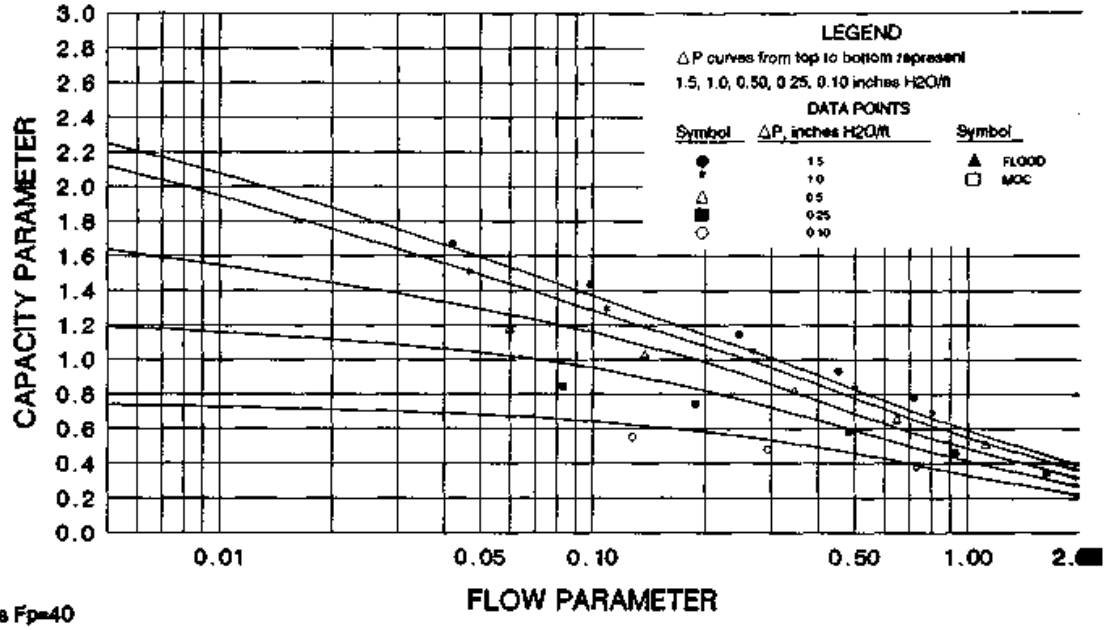

Basis Fp=40
Pressure drop measured in inches H2O/ft
Large symbols represent non-aqueous data

CHART 10.6124
KOCH FLEXERAMIC #48
PRESSURE DROP

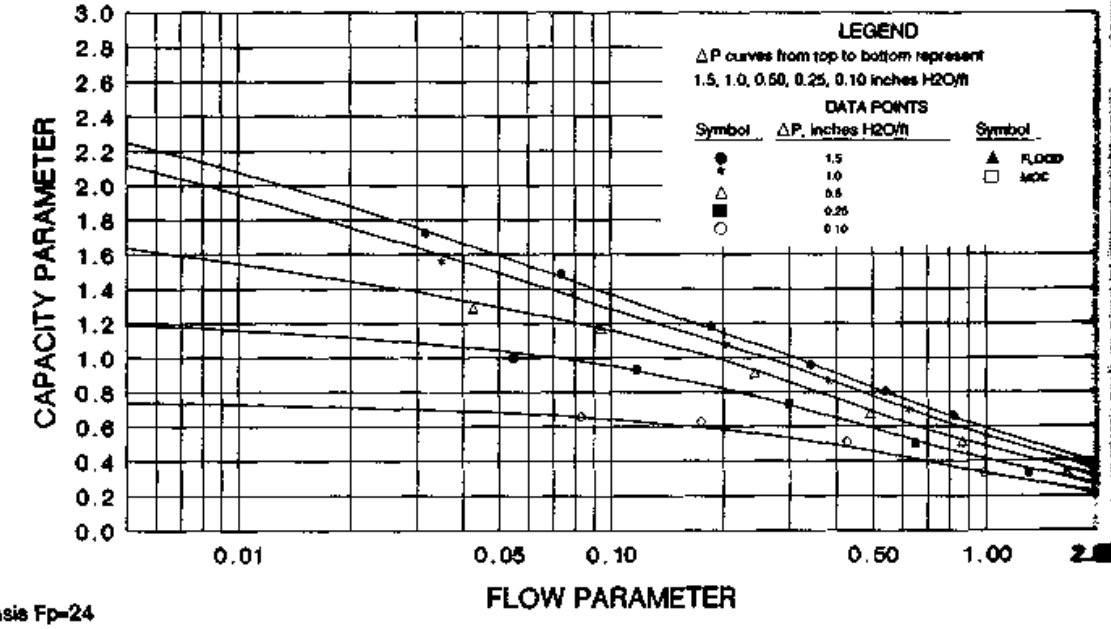

Basis Fp=24
Pressure drop measured in inches H2O/ft
Large symbols represent non-aqueous data

CHART 10.6128
KOCH FLEXERAMIC #88
PRESSURE DROP

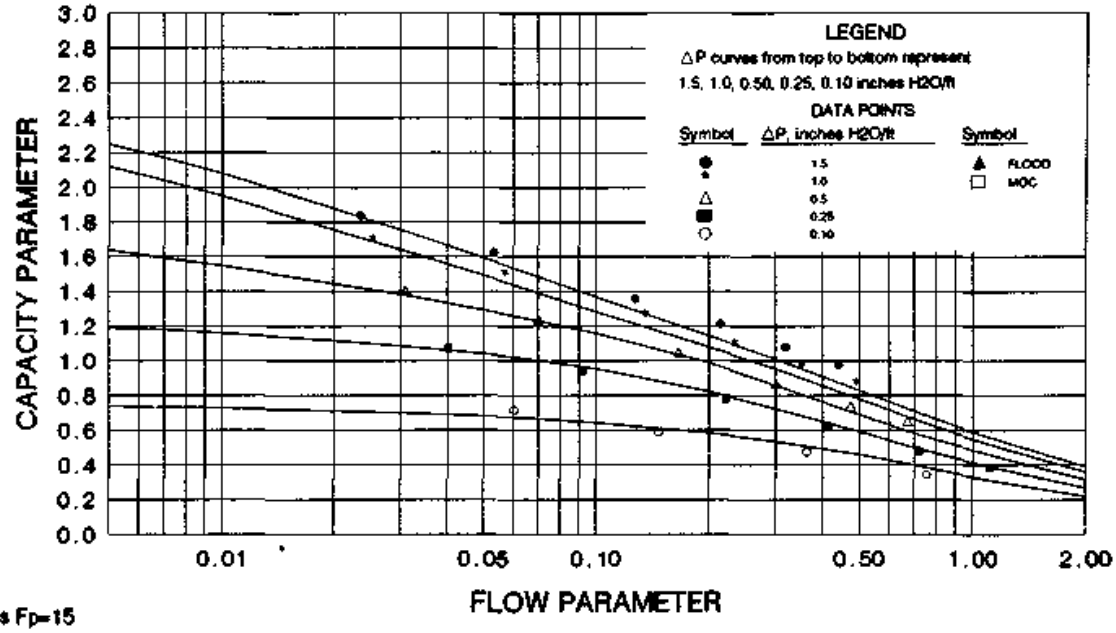

Basis Fp=15
Pressure drop measured in inches H2O/ft
Large symbols represent non-aqueous data

CHART 10.6202
GLITSCH GEMPAK 4A
PRESSURE DROP

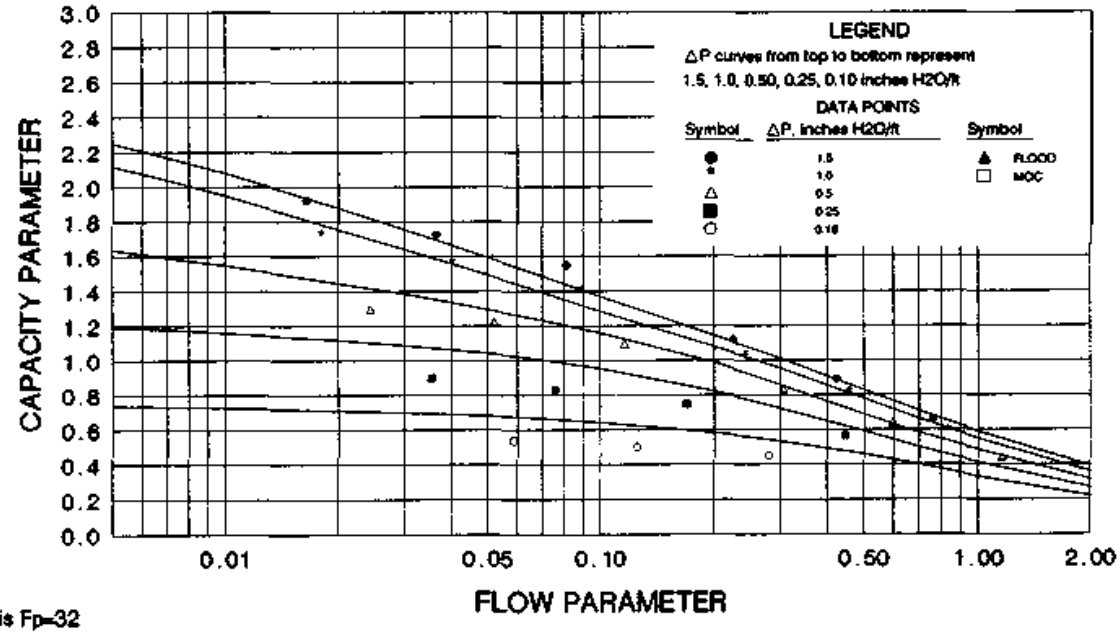

Basis Fp=32
Pressure drop measured in inches H2O/ft
Large symbols represent non-aqueous data

CHART 10.6203
GLITSCH GEMPAK 3A
FLOOD & PRESSURE DROP

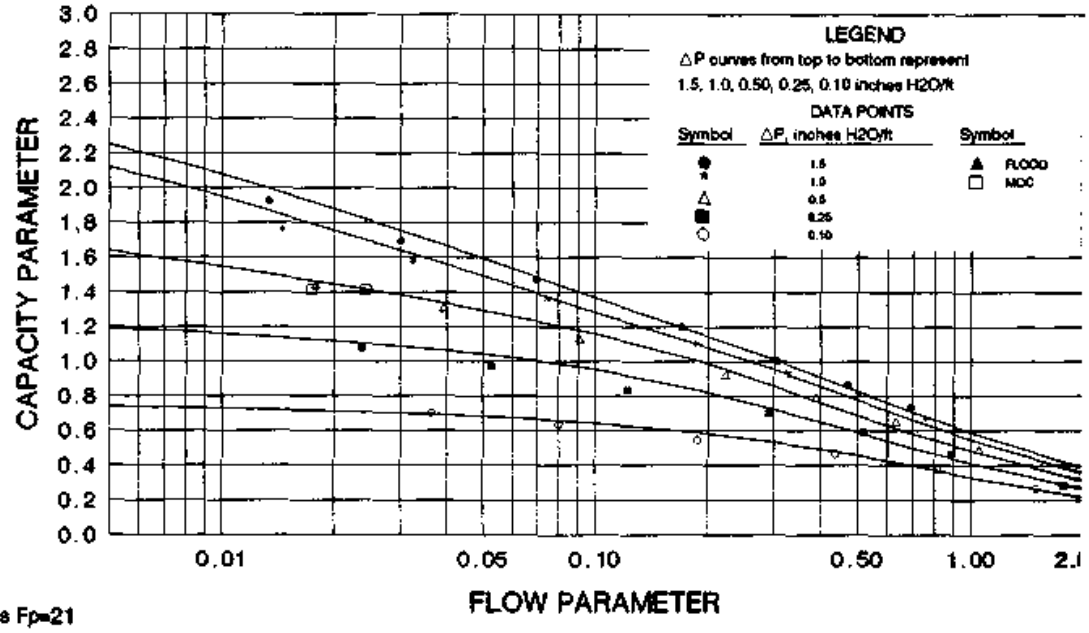

Basis Fp=21
Pressure drop measured in inches H2O/ft
Large symbols represent non-aqueous data

CHART 10.6204
GLITSCH GEMPAK 2A
FLOOD & PRESSURE DROP

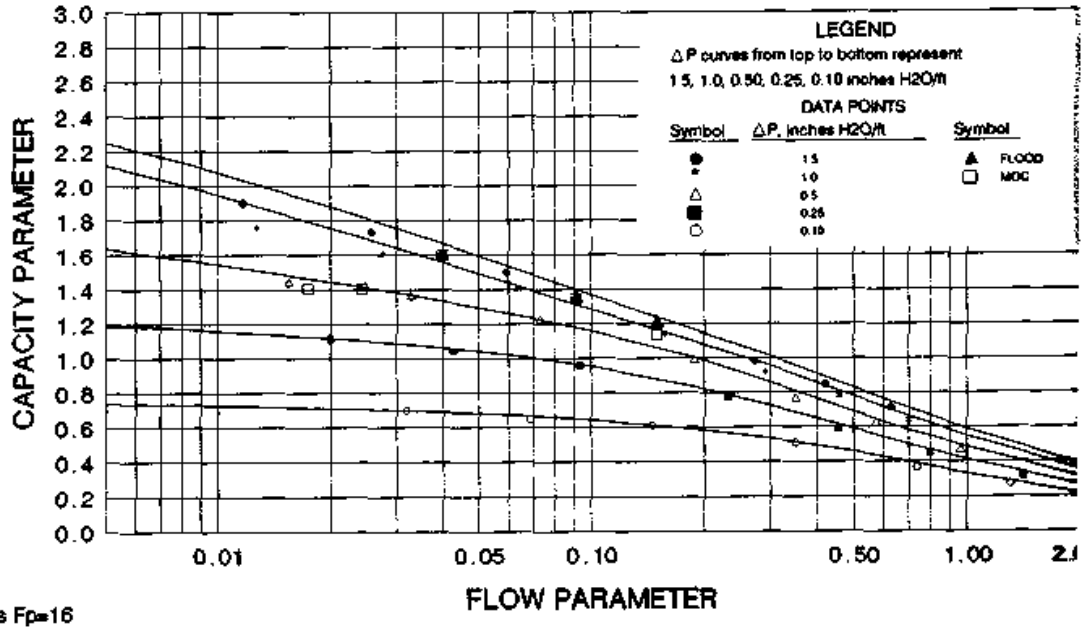

Basis Fp=16
Pressure drop measured in inches H2O/ft
Large symbols represent non-aqueous data

CHART 10.6206
GLITSCH GEMPAK 1.5A
FLOOD & PRESSURE DROP

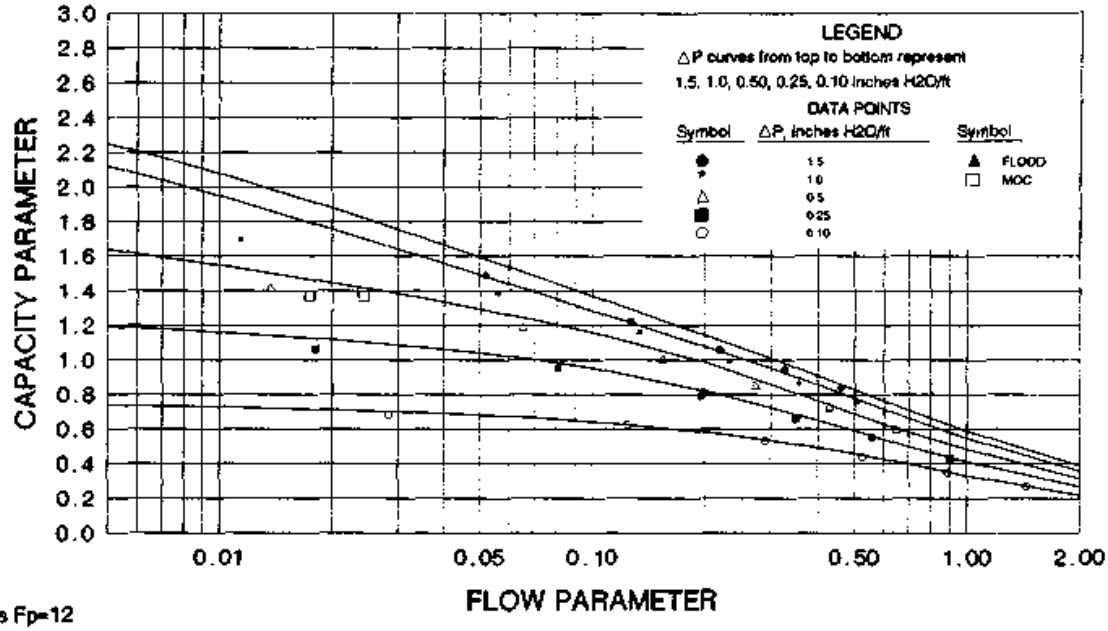

Basis Fp=12
Pressure drop measured in inches H2O/ft
Large symbols represent non-aqueous data

CHART 10.6208
GLITSCH GEMPAK 1A
FLOOD & PRESSURE DROP

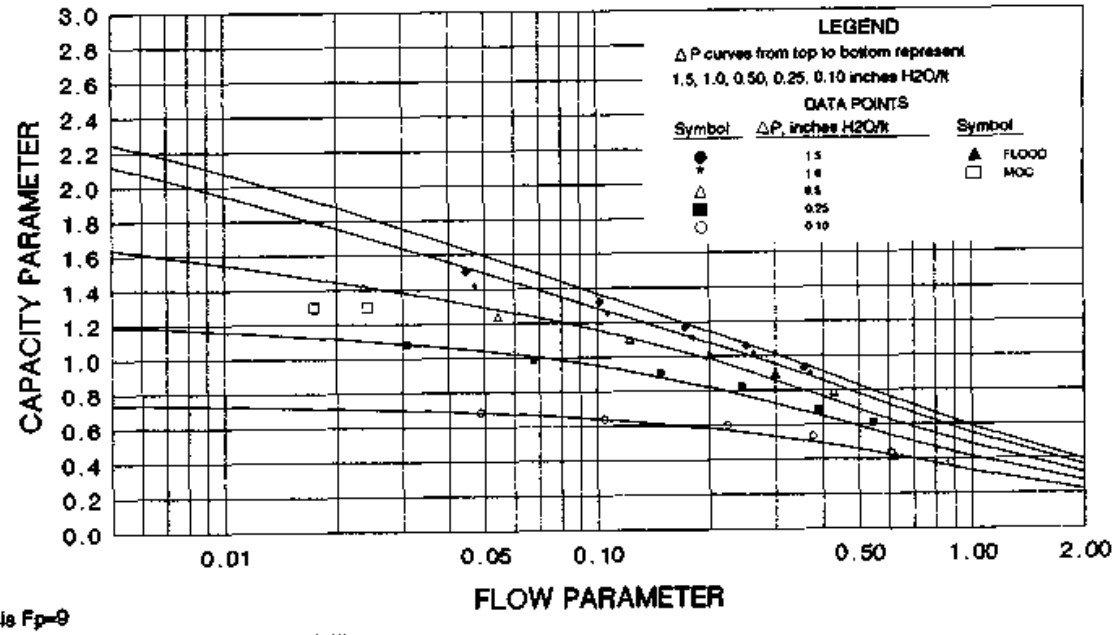

Basis Fp=9
Pressure drop measured in inches H2O/ft
Large symbols represent non-aqueous data

CHART 10.6209
GLITSCH GEMPAK 0.5A
PRESSURE DROP

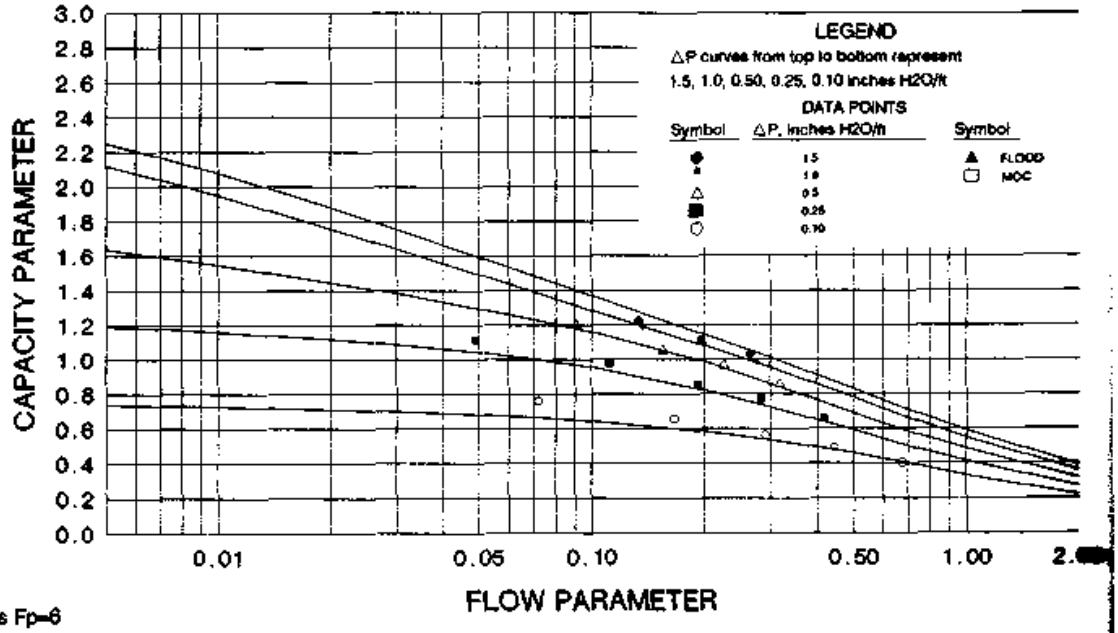

Basis Fp=6
Pressure drop measured in inches H2O/ft
Large symbols represent non-aqueous data

CHART 10.6302
MONTZ B1-300
FLOOD & PRESSURE DROP

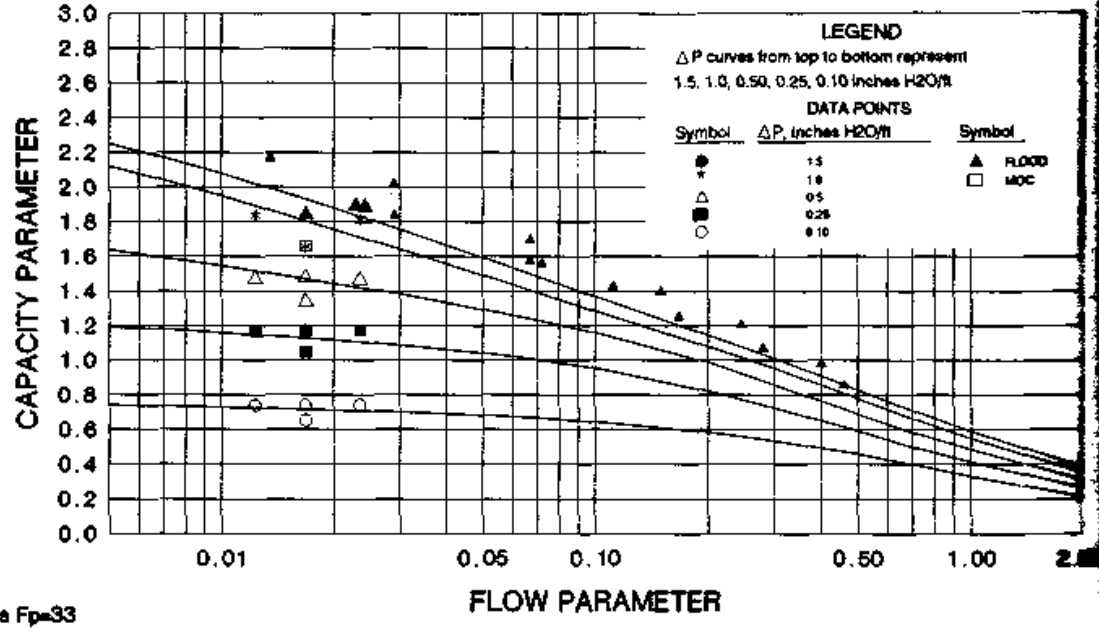

Basis Fp=33
Pressure drop measured in inches H2O/ft
Large symbols represent non-aqueous data

CHART 10.6303
MONTZ B1-250
PRESSURE DROP

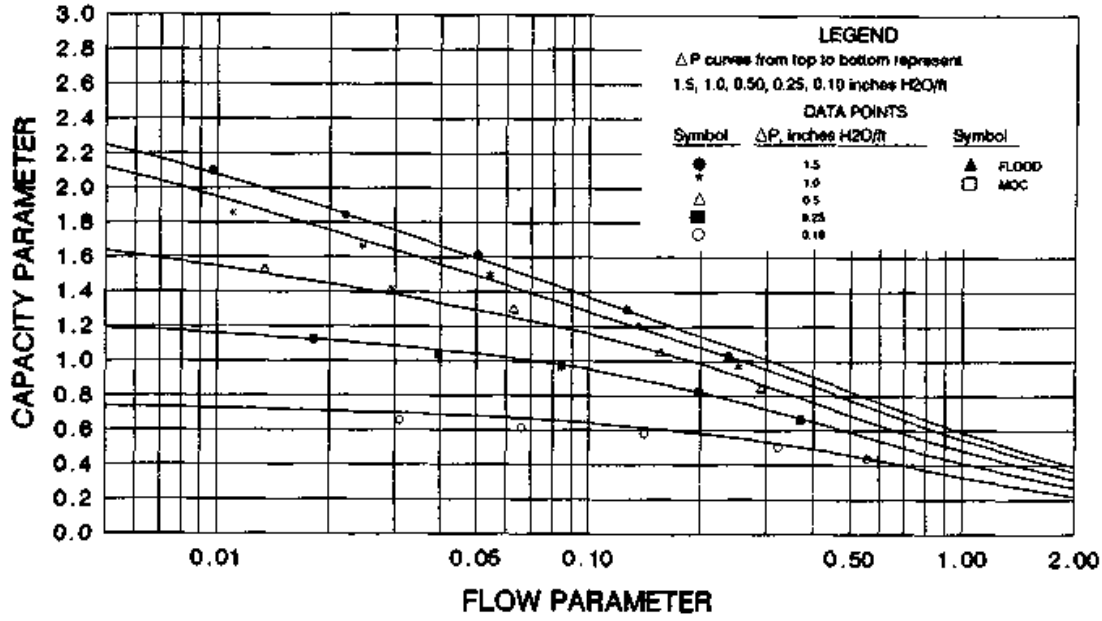

Basis Fp=20
Pressure drop measured in inches H2O/ft

CHART 10.6402
NORTON INTALOX 1T
PRESSURE DROP

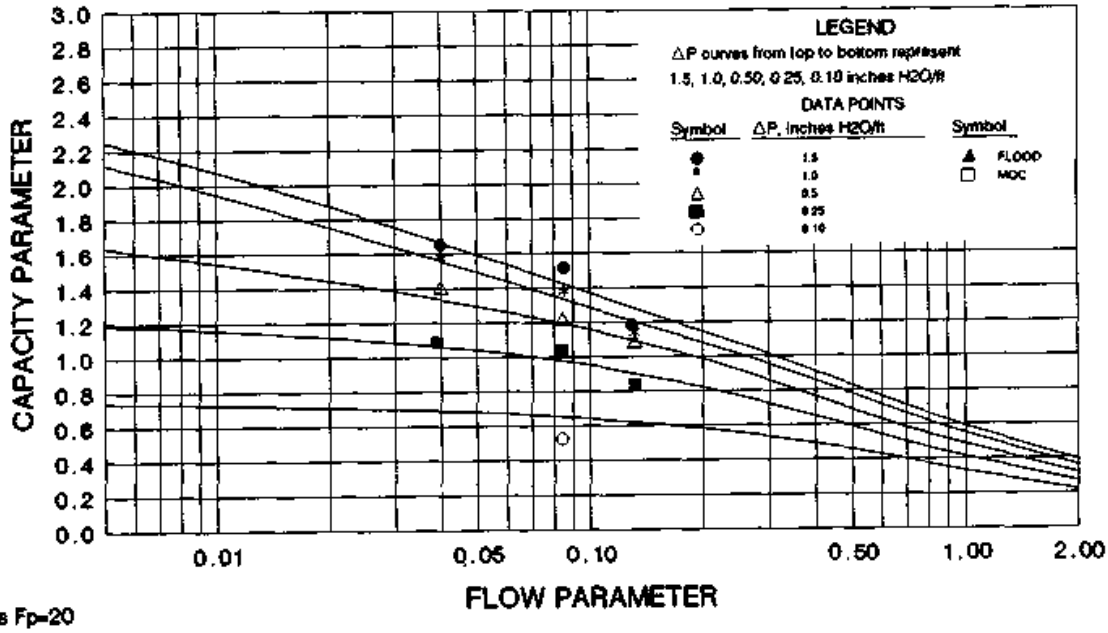

Basis Fp=20
Pressure drop measured in inches H2O/ft
Large symbols represent non-aqueous data

CHART 10.6404
NORTON INTALOX 2T
FLOOD & PRESSURE DROP

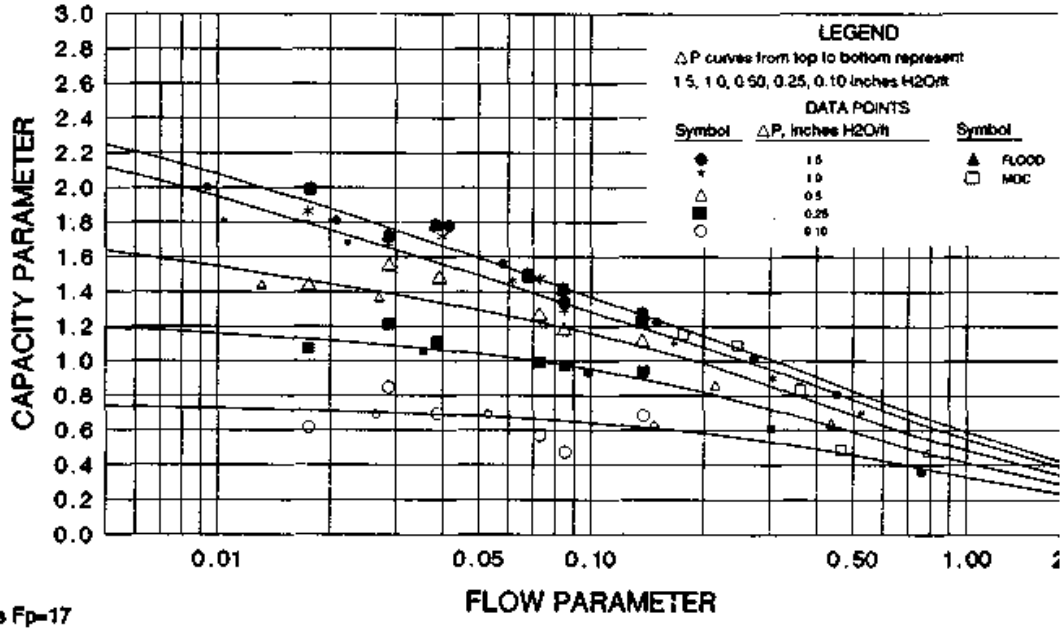

Basis Fp=17
Pressure drop measured in inches H2O/ft
Large symbols represent non-aqueous data

CHART 10.6408
NORTON INTALOX 3T
PRESSURE DROP

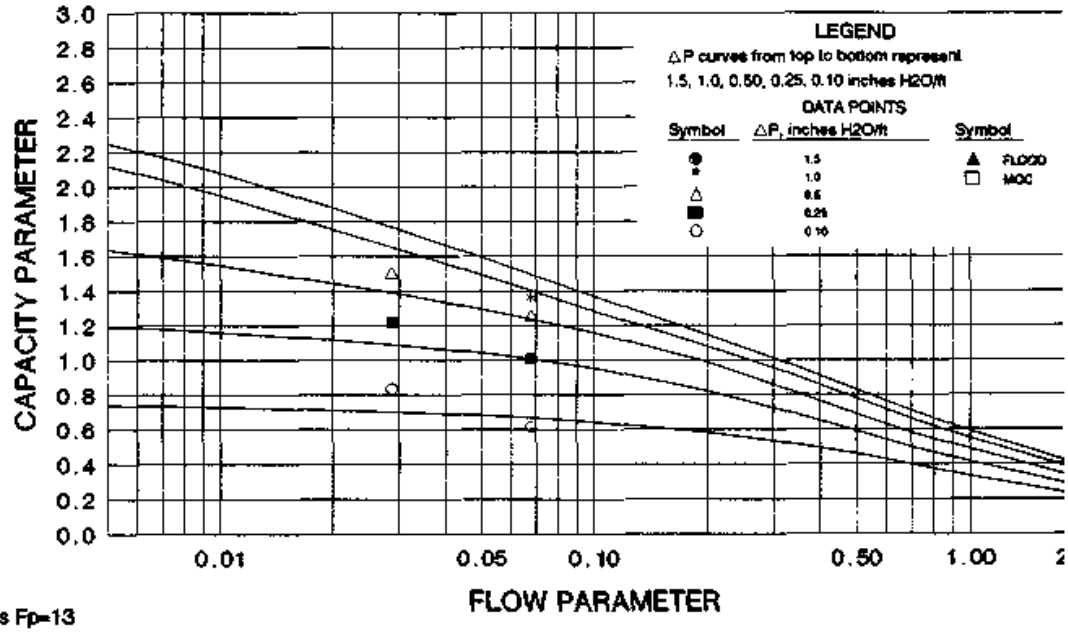

Basis Fp=13
Pressure drop measured in inches H2O/ft
Large symbols represent non-aqueous data

CHART 10.6504
JAEGER MAXPAC
FLOOD & PRESSURE DROP

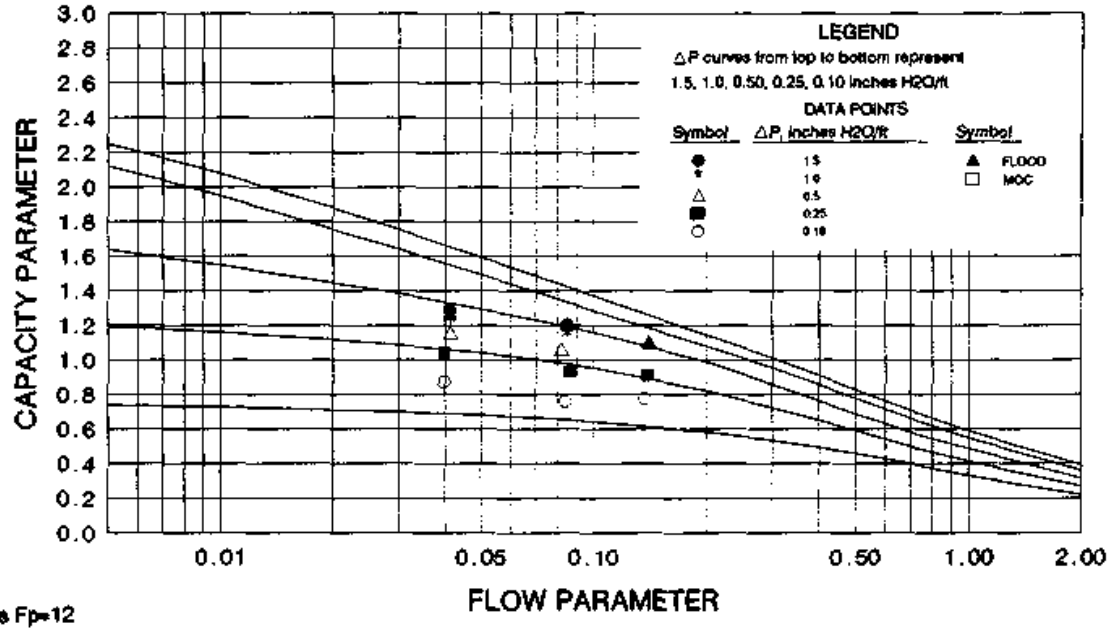

Basis Fp=12
Pressure drop measured in inches H2O/ft
Large symbols represent non-aqueous data

CHART 10.8005
GLITSCH GRID EF-25A
FLOOD & PRESSURE DROP

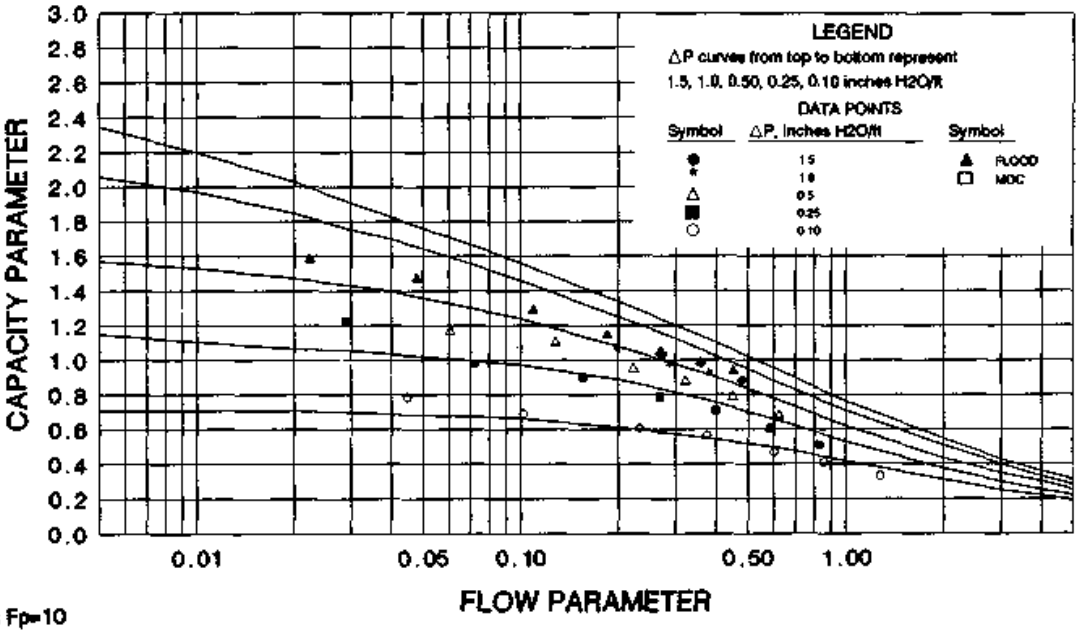

Basis Fp=10
Pressure drop measured in inches H2O/ft
See Sec 8.2.6 before interpolating flood data

CHART 10.8015
GLITSCH GRID EF-25AP
FLOOD & PRESSURE DROP

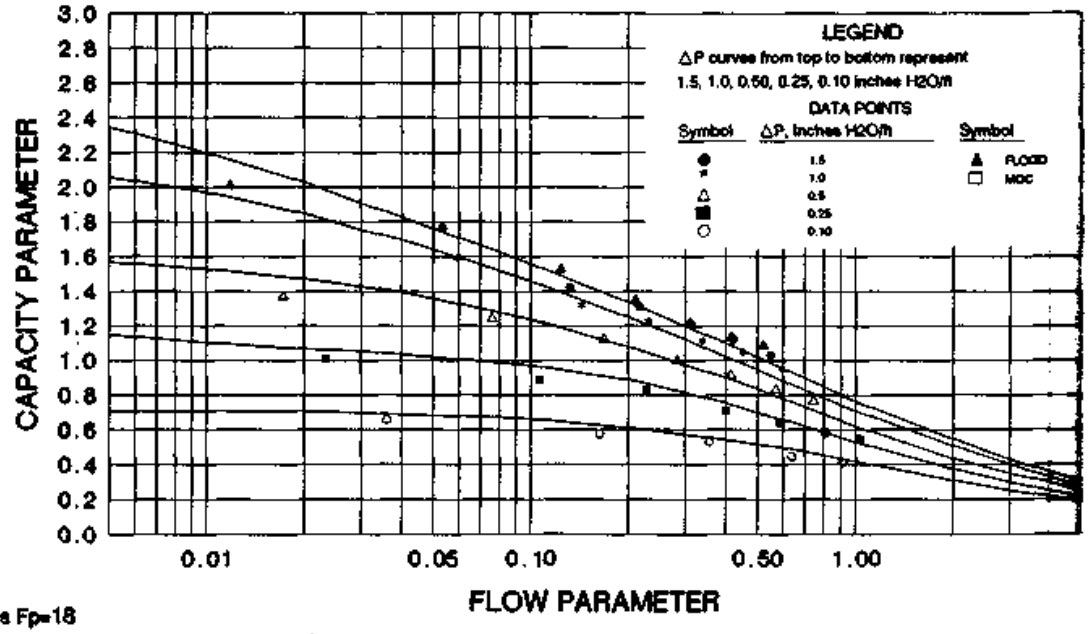

Basis Fp=18
Pressure drop measured in inches H2O/ft
See Sec 8.2.6 before interpolating flood data

CHART 10.8104
KOCH FLEXIGRID #3
FLOOD & PRESSURE DROP

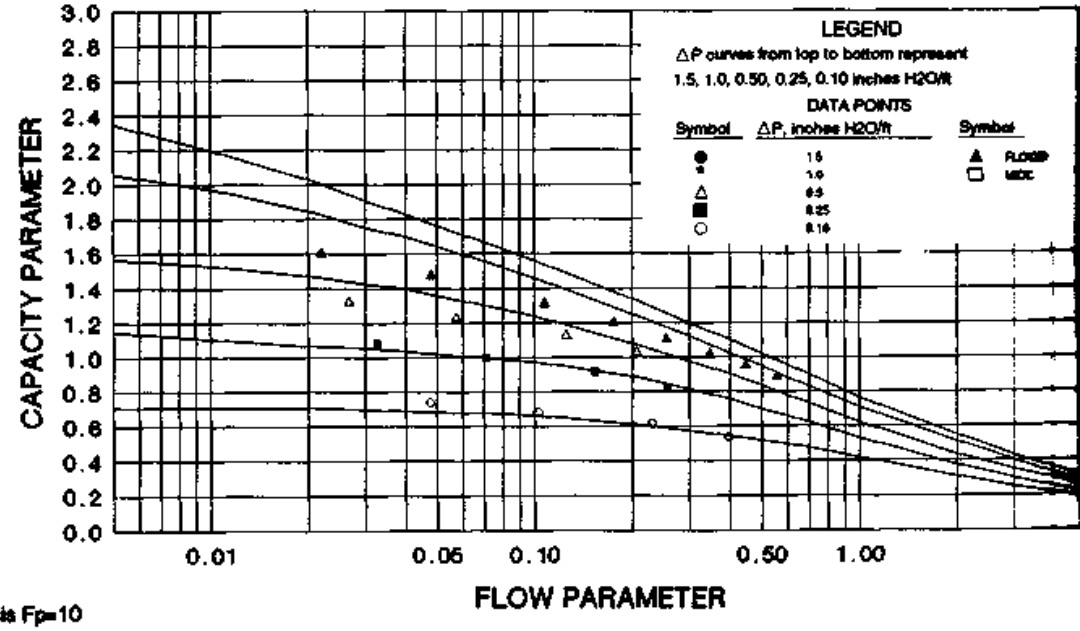

Basis Fp=10
Pressure drop measured in inches H2O/ft
See Sec 8.2.6 before interpolating flood data

CHART 10.8108
KOCH FLEXIGRID #2
FLOOD & PRESSURE DROP

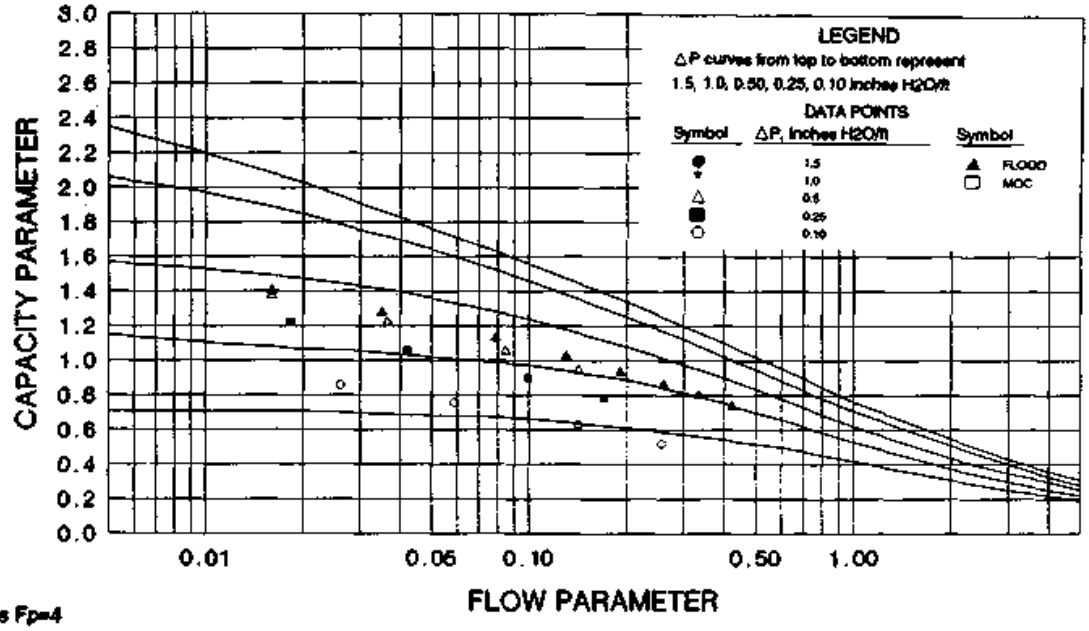

Basis Fp=4
Pressure drop measured in inches H2O/ft
See Sec 8.2.6 before interpolating flood data

CHART 10.8205
NUTTER SNAP GRID #3
FLOOD & PRESSURE DROP

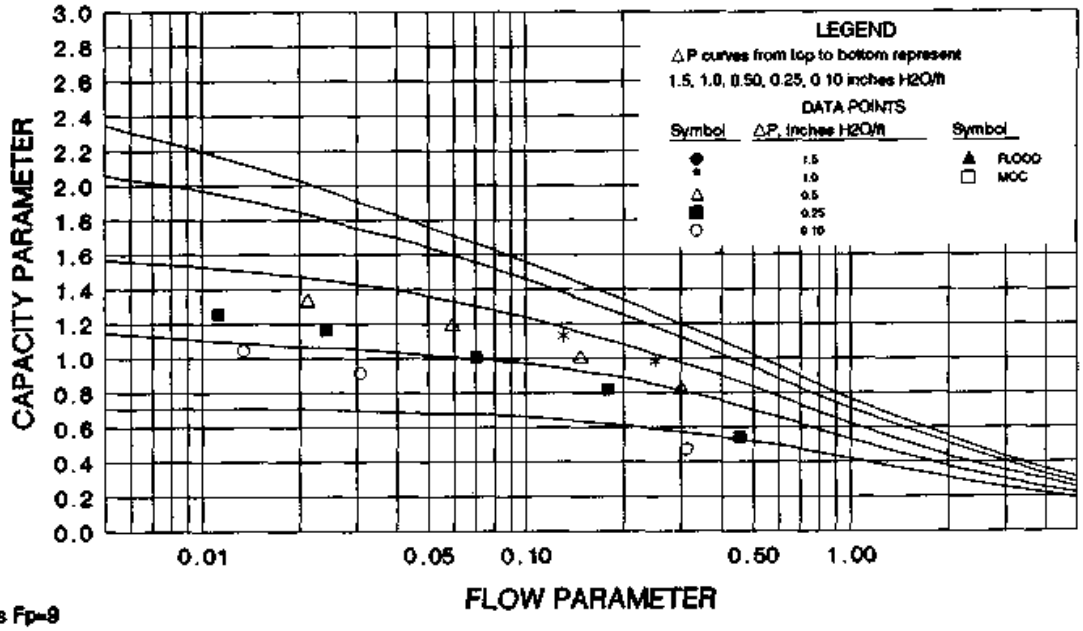

Basis Fp=9
Pressure drop measured in inches H2O/ft
Large symbols represent non-aqueous data

TABLE 10.1 Data Used in Charts

Random Packings

Chart	Packing	F_p	F_p source (ref. number)	Data source (ref. number)	System	Pressure	Flow parameter	Test column: Dia. in	Test column: Packed ht., ft	No. of data points
10.1002A	1" (M) Pall®	56	1	2 (BASF)	Ethylbenzene-styrene	100 mmHg	0.024	20	4	2
				2 (BASF)	Methanol-ethanol	Atm	0.040	20	7	2
				3,4 (Norton)	iC_8-toluene	Atm	0.055–0.070	15	10	4
				3,4 (Norton)	iC_8-toluene	100 mmHg	0.021–0.026	15	10	5
				4 (Norton)	Benzene-toluene	Atm	0.050	15	10	1
				4 (Norton)	Methanol-water	Atm	0.031	15	5	1
				4 (Norton)	IPA-water	Atm	0.041	15	10	1
				4 (Norton)	Acetone-water	Atm	0.040	15	5,10	1
				5 (Bochum Uni)	Chlorobenzene-ethylbenzene	50 mmHg	0.017	9	5	1
				6 (Birmingham Uni)	Cis-trans decalin	100 mmHg	0.027	18	5	1
				2 (BASF)	Air-water	Atm	0.17–0.28	17	5	3
10.1002B	1" (M) Pall®	56	1	2 (BASF)	Ethylbenzene-styrene	100 mmHg	0.024	20	4	5
				2 (BASF)	Methanol-ethanol	Atm	0.040	20	7	5
				4 (Norton)	iC_8-toluene	Atm	0.060	15	10	5
				4 (Norton)	iC_8-toluene	100 mmHg	0.023	15	10	5
				4 (Norton)	Benzene-toluene	Atm	0.050	15	10	5
				4 (Norton)	Methylchloroform-toluene	Atm	0.061	15	5	4
				5 (Bochum Uni)	Chlorobenzene-ethylbenzene	50 mmHg	0.017	9	5	5
				6 (Birmingham Uni)	Cis-trans decalin	100 mmHg	0.028	18	5	5
				6 (Birmingham Uni)	Cis-trans decalin	40 mmHg	0.019	18	5	4
				6 (Birmingham Uni)	Cis-trans decalin	20 mmHg	0.014	18	5	4
				6 (Birmingham Uni)	Cis-trans decalin	10 mmHg	0.011	18	5	3
				6 (Birmingham Uni)	Cis-trans decalin	5 mmHg	0.008	18	5	1

10.1002C	1" (M) Pall®	56	1	7 (Norton)	Air-water	Atm	0.014–5.0	30	10	44
				8 (Glitsch)	Air-water	Atm	0.007–1.1	84	6	20
				9 (Koch)	Air-water	Atm	0.037–2.2	36	2	29
				2 (BASF)	Air-water	Atm	0.17–0.48	17	5	9
				4 (Norton)	Methanol-water	Atm	0.031	15	5	5
				4 (Norton)	IPA-water	Atm	0.041	15	10	5
				4 (Norton)	Acetone-water	Atm	0.040	15	5,10	5
10.1003	1.5" (M) Pall®	40	1	2 (BASF)	Ethylbenzene-styrene	100 mmHg	0.024	20	4	7
				2 (BASF)	Methanol-ethanol	Atm	0.040	20	7	7
				10,11 (Norton)	iC_8-toluene	Atm	0.070	15	10	6
				7 (Norton)	Air-water	Atm	0.063–5.0	30	10	40
				8 (Glitsch)	Air-water	Atm	0.006–1.0	84	6	24
				9 (Koch)	Air-water	Atm	0.036–1.8	36	2	30
10.1004A	2" (M) Pall®	27	1	2 (FRI)	C_6-C_7	260 mmHg	0.038–0.45	48	18	5
				2 (FRI)	C_6-C_7	24 psia	0.050–0.49	48	18	5
				2 (FRI)	IPA-water	Atm	0.050–0.44	48	18	5
				2 (FRI)	iC_4-nC_4	165 psia	0.24–0.69	48	18	4
				2 (BASF)	Methanol-ethanol	Atm	0.040	20	7	2
				2 (BASF)	Ethylbenzene-styrene	100 mmHg	0.024	20	4	2
				2 (BASF)	Ethylbenzene-styrene	50 mmHg	0.016	20	4	2
				12 (Nutter)	Air-Isopar®	Atm	0.078–0.38	30	4	3
				13 (Mitsui)	C_6-C_7	Atm	0.069	20	8	1
				4,11 (Norton)	iC_8-toluene	Atm	0.060–0.070	15	10	2
				5 (Bochum Uni)	Air-water	Atm	0.020–0.15	18	7	4
				14 (Koch)	Air-water	Atm	0.030–0.17	36	2	3
				15 (Glitsch)	Air-water	Atm	0.17	36	4	1

TABLE 10.1 Data Used in Charts (*Continued*)

Random Packings										
								Test column		
Chart	Packing	F_p	F_p source (ref. number)	Data source (ref. number)	System	Pressure	Flow parameter	Dia. in	Packed ht., ft	No. of data points
10.1004B	2" (M) Pall®	27	1	2 (FRI)	C_6-C_7	260 mmHg	0.036–0.45	48	18	13
				2 (FRI)	C_6-C_7	24 psia	0.062–0.50	48	18	13
				2 (FRI)	iC_4-nC_4	165 psia	0.16–1.27	48	18	11
				2 (BASF)	Methanol-ethanol	Atm	0.040	20	4,7	4
				2 (BASF)	Ethylbenzene-styrene	100 mmHg	0.024	20	4	5
				2 (BASF)	Ethylbenzene-styrene	50 mmHg	0.018	20	4	4
				2 (BASF)	Propylene glycol-ethylene glycol	10 mmHg	0.0055	20	4	3
				12 (Nutter)	Air-Isopar[d]	Atm	0.025–0.64	30	4	13
				12 (Mitsui)	C_6-C_7	Atm	0.069	20	8	5
				4,11 (Norton)	iC_8-toluene	Atm	0.060–0.070	15	10,20	8
				5 (Bochum Uni)	Chlorobenzene-ethylbenzene	50 mmHg	0.017	9	5	3
10.1004C	2" (M) Pall®	27	1	7 (Norton)	Air-water	Atm	0.054–5.0	30	10	49
				8 (Glitsch)	Air-water	Atm	0.007–0.73	84	6	22
				14 (Koch)	Air-water	Atm	0.062–1.12	36	2	28
				15 (Glitsch)	Air-water	Atm	0.18–0.54	36	4	5
				12 (Nutter)	Air-water-ammonia	Atm	0.012–0.031	30	4	4
				2 (FRI)	IPA-water	Atm	0.049–0.44	48	18	13
10.1007	3.5" (M) Pall®	18	1	8 (Glitsch)	Air-water	Atm	0.006–1.0	84	6	20
				9 (Koch)	Air-water	Atm	0.030–1.7	36	2	34
10.1012	1" (P) Pall®	55	1	7 (Norton)	Air-water	Atm	0.014–5.0	30	10	39
				8 (Glitsch)	Air-water	Atm	0.007–1.5	84	6	20
				9 (Koch)	Air-water	Atm	0.041–1.3	36	2	20
10.1013	1.5" (P) Pall®	40	1	7 (Norton)	Air-water	Atm	0.042–5.0	30	10	40
				8 (Glitsch)	Air-water	Atm	0.006–1.3	84	6	23
				9 (Koch)	Air-water	Atm	0.035–1.9	36	2	35

10.1014	2" (P) Pall®	26	1	7 (Norton)	Air-water	Atm	0.065–5.0	30	10	45
				8 (Glitsch)	Air-water	Atm	0.006–0.81	84	6	23
				9 (Koch)	Air-water	Atm	0.029–2.1	36	2	35
				5 (Bochum Uni)	Air-water	Atm	0.068–0.19	18	5	4
10.1017	3.5" (P) Pall®	17	1	7 (Norton)	Air-water	Atm	0.017–5.0	30	8	64
				8 (Glitsch)	Air-water	Atm	0.007–1.1	84	6	21
				9 (Koch)	Air-water	Atm	0.024–1.9	36		39
10.1022	1" (C) Pall®	107	16	17 (Bochum Uni)	Chlorobenzene-ethylbenzene	50 mmHg	0.017	9	5	7
10.1024	2" (C) Pall®	43	16	5,17 (Bochum Uni)	Chlorobenzene-ethylbenzene	50 mmHg	0.017	9	5	5
10.1112	1" (P) Super Intalox®, Flexi™ & Ballast™ Saddles	40	1	7,18 (Norton)	Air-water	Atm	0.077–5.0	15	10	37
				8 (Glitsch)	Air-water	Atm	0.007–1.2	84	6	20
				9 (Koch)	Air-water	Atm	0.043–2.5	36	2	34
10.1114	2" (P) Super Intalox®, Flexi™ & Ballast™ Saddles	28	1	7,18 (Norton)	Air-water	Atm	0.064–5.0	30	10	39
				8 (Glitsch)	Air-water	Atm	0.006–1.1	84	6	23
				9 (Koch)	Air-water	Atm	0.029–2.3	36	2	38
10.1116	3" (P) Super Intalox®, Flexi™ & Ballast™ Saddles	18	1	7,18 (Norton)	Air-water	Atm	0.053–4.3	30	10	40
				8 (Glitsch)	Air-water	Atm	0.006–0.98	84	6	20
				9 (Koch)	Air-water	Atm	0.024–1.8	36		39

TABLE 10.1 Data Used in Charts (*Continued*)

Random Packings										
								Test column		
Chart	Packing	F_p	F_p source (ref. number)	Data source (ref. number)	System	Pressure	Flow parameter	Dia. in	Packed ht., ft	No. of data points
10.1122	1" (C) Intalox® & Flexi®-Saddles	92	1	10 (Norton)	iC_8-toluene	Atm	0.070	15	10	6
				3 (Norton)	iC_8-toluene	Atm	0.055–0.070	15	10	5
				3 (Norton)	iC_8-toluene	100 mmHg	0.021–0.026	15	10	6
				17 (Bochum Uni)	Chlorobenzene-ethylbenzene	50 mmHg	0.017	9	5	5
				7 (Norton)	Air-water	Atm	0.075–5.0	30	10	36
				8 (Koch)	Air-water	Atm	0.053–5.0	36		29
				17 (Bochum Uni)	Air-water	Atm	0.050–0.074	12	3	3
10.1123	1½" (C) Intalox® & Flexi®-Saddles	52	1	10,11 (Norton)	iC_8-toluene	Atm	0.070	15	10	6
				7 (Norton)	Air-water	Atm	0.015–5.0	30	10	46
				9 (Koch)	Air-water	Atm	0.040–5.0	36		39
10.1124	2" (C) Intalox® & Flexi®-Saddles	40	1	10,11 (Norton)	iC_8-toluene	Atm	0.070	15	10	6
				5 (Bochum Uni)	Chlorobenzene-ethylbenzene	50 mmHg	0.017	9	5	7
				7 (Norton)	Air-water	Atm	0.030–5.0	30	10	48
				9 (Koch)	Air-water	Atm	0.019–5.0	36		38
				5,17 (Bochum Uni)	Air-water	Atm	0.088–0.24	18	5	4
10.1126	3" (C) Intalox® & Flexi®-Saddles	22	1	7 (Norton)	Air-water	Atm	0.036–5.0	30	10	61
				9 (Koch)	Air-water	Atm	0.18–5.0	36		20
10.1203	#1 (M) Hy-Pak® & K-Pak®	45	1	19 (Norton)	Air-water	Atm	0.085–5.0	30	10	32
				9 (Koch)	Air-water	Atm	0.038–1.9	36	2	25
				19 (Norton)	iC_8-toluene	Atm	0.055–0.067	15	10	9
10.1204	#1.5 (M) K-Pac®	29	1	9 (Koch)	Air-water	Atm	0.028–1.9	36		33

10.1205	#2 (M) Hy-Pak®, K-Pak®, & Ballast Plus®	26	1	19 (Norton)	Air-water	Atm	0.052–5.0	30	10	29
				8 (Glitsch)	Air-water	Atm	0.007–0.70	84	6	21
				9 (Koch)	Air-water	Atm	0.032–1.8	36	2	35
				19 (Norton)	iC_8-toluene	100 mmHg	0.021–0.026	15	10	8
				20 (Norton)	iC_8-toluene	Atm	0.055	15	10	1
10.1207	#3 (M) Hy-Pak® & K-Pak®	16	1	19 (Norton)	Air-water	Atm	0.057–1.1	30	10	24
				9 (Koch)	Air-water	Atm	0.030–1.4	36		34
10.1322	1" (C) Super Intalox® Saddles	60	1	18 (Norton)	Air-water	Atm	0.11–5.0	30	10	34
10.1324	2" (C) Super Intalox® Saddles	30	1	18 (Norton)	Air-water	Atm	0.079–5.0	30	10	28
10.2002	#25 (M) IMTP®	41	1	6 (Birmingham Uni)	Cis-trans decalin	80 mmHg	0.025	18	5	6
				6 (Birmingham Uni)	Cis-trans decalin	40 mmHg	0.019	18	5	3
				6 (Birmingham Uni)	Cis-trans decalin	20 mmHg	0.014	18	5	4
				10,11 (Norton)	iC_8-toluene	Atm	0.070	15	10	5
				21 (Norton)	Air-water	Atm	0.086–5.0	30	10	21
10.2003	#40 IMTP®	24	1	10,11 (Norton)	iC_8-toluene	Atm	0.070	15	10	5
				21 (Norton)	Air-water	Atm	0.075–5.0	30	10	24
10.2004	#50 IMTP®	18	1	11,22 (Norton)	iC_8-toluene	Atm	0.070	15	10	5
				22 (Norton)	C_6-C_7	Atm	0.067	15	10	1
				21 (Norton)	Air-water	Atm	0.057–4.7	30	10	26
10.2006	#70 IMTP®	12	1	21 (Norton)	iC_8-toluene	Atm	0.070	15	10	4
				21 (Norton)	Air-water	Atm	0.049–3.4	30	10	26
10.2101	#1 (M) CMR®	40	23	24 (Glitsch)	o-p Xylenes	50 mmHg	0.018	6	10	1
				5 (Bochum Uni)	p-m Xylenes	50 mmHg	0.018	9	5	6
				5 (Bochum Uni)	Chlorobenzene-ethylbenzene	50 mmHg	0.017	9	5	2
				23 (Glitsch)	Air-water	Atm	0.016–0.50	36	4	17
				5 (Bochum Uni)	Air-water	Atm	0.030–0.24	12	5	12

TABLE 10.1 Data Used in Charts (*Continued*)

Random Packings										
								Test column		
Chart	Packing	F_p	F_p source (ref. number)	Data source (ref. number)	System	Pressure	Flow parameter	Dia. in	Packed ht., feet	No. of data points
10.2102	#1.5 (M) CMR®	29	23	5 (Bochum Uni)	Chlorobenzene-ethylbenzene	50 mmHg	0.017	9	5	6
				5 (Bochum Uni)	p-m Xylenes	50 mmHg	0.018	9	5	6
				23 (Glitsch)	Air-water	Atm	0.015–0.97	36	4	23
10.2103	#2 (M) CMR®	22	23	25 (Glitsch)	Ethylbenzene-styrene	50 mmHg	0.018			3
				23 (Glitsch)	Air-water	Atm	0.014–0.75	36	4	29
10.2104	#2.5 (M) CMR®	19	23	23 (Glitsch)	Air-water	Atm	0.013–0.77	36	4	31
10.2105	#3 (M) CMR®	14	23	23 (Glitsch)	Air-water	Atm	0.015–0.86	36	4	27
10.2106	#4 (M) CMR®	10	23	23 (Glitsch)	Air-water	Atm	0.015–0.85	36	4	28
10.2111	#1A (P) CMR®	30	23	23 (Glitsch)	Air-water	Atm	0.015–0.77	36	4	25
10.2113	#2A (P) CMR®	30	23	23 (Glitsch)	Air-water	Atm	0.016–0.86	36	4	26
10.2115	#3A (P) CMR®	12	23	23 (Glitsch)	Air-water	Atm	0.014–0.91	36	4	27
10.2202	#1 (M) Nutter®	30	This work	12 (Nutter)	Air-Isopar®	Atm	0.006–3.3	30	4	23
				12 (Nutter)	Air-water	Atm	0.023–5.0	30	4	27
10.2203	#1.5 (M) Nutter®	24	This work	12 (Nutter)	Air-Isopar®	Atm	0.005–5.0	30	4	29
				12 (Nutter)	Air-water	Atm	0.021–2.8	30	4	27
10.2204	#2 (M) Nutter®	18	This work	12 (Nutter)	Air-water	Atm	0.021–5.0	30	4	25
				12 (Nutter)	Air-Isopar®	Atm	0.005–5.0	30	4	37
				13 (Mitsui)	C_6-C_7	Atm	0.069	20	8	2
				13 (FRI)	C_6-C_7	260 mmHg	0.039	48	14	6
				13 (FRI)	C_6-C_7	24 psia	0.086–0.091	48	14	6

10.2304	2" (M) Hiflow®	16	This work	5,17 (Bochum Uni)	Chlorobenzene-ethylbenzene	50 mmHg	0.017	9	5	3
				5,17 (Bochum Uni)	Air-water	Atm	0.023–0.26	18	7	18
10.2312	1" (P) Hiflow®	42	This work	5 (Bochum Uni)	Chlorobenzene-ethylbenzene	50 mmHg	0.017	9	5	6
				17 (Bochum Uni)	Air-water	Atm	0.031–0.58	12	3	19
10.2314	2" (P) Hiflow®	20	This work	5,17 (Bochum Uni)	Air-water	Atm	0.017–0.26	12	5	12
				5,17 (Bochum Uni)	Air-water	Atm	0.037–0.51	18	5	9
10.2317	3.5" (P) Hiflow®	9	This work	17 (Bochum Uni)	Air-water	Atm	0.020–0.18	18	7	13
10.2323	1.5" (C) Hiflow®	37	This work	17 (Bochum Uni)	Chlorobenzene-ethylbenzene	50 mmHg	0.017	9	5	6
				17 (Bochum Uni)	Air-water	Atm	0.028–0.32	18	2	14
				17 (Bochum Uni)	Air-water	Atm	0.029–0.27	12	5	18
10.2324	2" (C) Hiflow®	29	This work	5,17 (Bochum Uni)	Chlorobenzene-ethylbenzene	50 mmHg	0.017	9	5	7
				5,17 (Bochum Uni)	Air-water	Atm	0.027–0.35	12	3	26
10.2326	3" (C) Hiflow®	15	This work	17 (Bochum Uni)	Air-water	Atm	0.023–0.28	18	7	22
10.2402	#1 HcKp®	40	This work	9 (Koch)	Air-water	Atm	0.033–2.6	36		33
10.2403	#1.5 HcKp®	22	This work	9 (Koch)	Air-water	Atm	0.028–0.94	36		25
10.2404	#2 HcKp®	16	This work	9 (Koch)	Air-water	Atm	0.025–1.9	36		35
10.2406	#3 HcKp®	14	This work	9 (Koch)	Air-water	Atm	0.031–1.7	36		36
10.3002	#1 (M) Chempak® and Levapak®	29	26	6 (Birmingham Uni)	Cis-trans decalin	20 mmHg	0.014	18	5	3
				6 (Birmingham Uni)	Cis-trans decalin	40 mmHg	0.019	18	5	5
				6 (Birmingham Uni)	Cis-trans decalin	80 mmHg	0.025	18	5	5
				26 (Chem-Pro)	Air-water	Atm	0.012–2.6	14	5	34
10.3004	#2 (M) Chempak®	18	26	26 (Chem-Pro)	Air-water	Atm	0.048–1.6	14	5	25
10.3104	#1 (M) Jaeger Tripacks®	18	27	5,17 (Bochum Uni)	Chlorobenzene-ethylbenzene	50 mmHg	0.017	9	5	5
				5,17 (Bochum Uni)	Air-water	Atm	0.030–0.067	12	4	3
				27 (Jaeger)	Air-water	Atm	0.020–3.0	24	14	15
10.3106	#2 (M) Jaeger Tripacks®	14	27	27 (Jaeger)	Air-water	Atm	0.19–1.6	24	14	12

TABLE 10.1 Data Used in Charts (*Continued*)

Chart	Packing	F_p	F_p source (ref. number)	Data source (ref. number)	System	Pressure	Flow parameter	Test column: Dia. in	Test column: Packed ht., feet	No. of data points
Random Packings										
10.3114	#1 (P) Jaeger Tripacks®	15	27	5,28 (Bochum Uni)	Air-water	Atm	0.026–0.34	12	4	16
				27 (Jaeger)	Air-water	Atm	0.031–0.23	24	14	28
10.3116	#2 (P) Jaeger Tripacks®	14	27	27 (Jaeger)	Air-water	Atm	0.030–0.22	24	14	28
10.3212	1" (P) Nor-Pac®	31	This work	29 (Bochum Uni)	Chlorobenzene-ethylbenzene	25 mmHg	0.013	9	5	5
				5,29 (Bochum Uni)	Chlorobenzene-ethylbenzene	50 mmHg	0.017	9	5	12
				29 (Bochum Uni)	Chlorobenzene-ethylbenzene	100 mmHg	0.023	9	5	3
				29 (Bochum Uni)	Chlorobenzene-ethylbenzene	200 mmHg	0.032	9	5	1
				29 (Bochum Uni)	Air-water	Atm	0.024–0.69	16	5	19
10.3213	1.5" (P) Nor-Pac®	21	This work	29 (Bochum Uni)	Air-water	Atm	0.022–0.68	16	5	24
10.3214	2" (P) Nor-Pac®	14	This work	5,28 (Bochum Uni)	Air-water	Atm	0.010–0.32	12	5	21
10.3316	Intalox® Snowflake®	13	30	30 (Norton)	Air-water	Atm	0.019–0.48	30	10	12
10.3417	3.5" (P) LANPAC®	14	31	31 (Lantec)	Air-water	Atm	0.049–1.5	36		30
10.3517	#3 (P) IMPAC®	15	32	32 (Lantec)	Air-water	Atm	0.018–1.7	36		35
Wire-Mesh Structured Packings										
10.5001	Koch-Sulzer® CY	70	This work	34 (Sulzer)	Chlorobenzene-ethylbenzene	20 mmHg	0.011	20,39	5–11	4
				34 (Sulzer)	Chlorobenzene-ethylbenzene	50 mmHg	0.016	20,39	5–11	4
				34 (Sulzer)	Chlorobenzene-ethylbenzene	100 mmHg	0.023	20,39	5–11	5
				34 (Sulzer)	Chlorobenzene-ethylbenzene	300 mmHg	0.040	20,39	5–11	5

10.5002	Koch-Sulzer® BX	21	This work	34 (Sulzer)	Cis-trans decalin	5 mmHg	0.0064	20,39	6–10	3
				34 (Sulzer)	Cis-trans decalin	20 mmHg	0.012	20,39	6–10	3
				34,35 (Sulzer)	Cis-trans decalin	50 mmHg	0.019	20,39	6–10	3
				34 (Sulzer)	Cis-trans decalin	100 mmHg	0.027	20,39	6–10	3
				36 (FRI)	o-p Xylenes	16 mmHg	0.010	10,39	8	2
				36 (FRI)	o-p Xylenes	100 mmHg	0.024	10,39	8	2
				36 (FRI)	o-p Xylenes	300 mmHg	0.042	10,39	8	2
				36 (FRI)	o-p Xylenes	730 mmHg	0.064	10,39	8	2
				37 (BASF)	Ethylbenzene-styrene	50 mmHg	0.016	20	7	6
				37 (BASF)	Ethylbenzene-styrene	100 mmHg	0.024	20	7	5
				37 (BASF)	1,2 Propylene glycol-ethylene glycol	10 mmHg	0.0055	20	7	2
				37 (BASF)	Methanol-ethanol	Atm	0.040	20	7	6
				5 (Bochum Uni)	Chlorobenzene-ethylbenzene	50 mmHg	0.017	9	4.5	5
				38 (SRP)	C_6-C_7	250 mmHg	0.040	18	10	4
				39 (SRP)	C_6-C_7	Atm	0.073	18	10	2
				38 (SRP)	C_6-C_7	24 psia	0.064	18	10	6
				38,39 (SRP)	C_6-C_7	60 psia	0.14	18	10	7
				Corrugated-Sheet Structured Packings						
10.6002	Mellapak® 500Y	34	This work	40 (Sulzer)	Chlorobenzene-ethylbenzene	19 mmHg	0.011	39	> 8	3
				40 (Sulzer)	Chlorobenzene-ethylbenzene	76 mmHg	0.021	39	> 8	4
				40 (Sulzer)	Chlorobenzene-ethylbenzene	Atm	0.060	39	> 8	5
10.6003	Mellapak® 350Y	23	This work	40 (Sulzer)	Chlorobenzene-ethylbenzene	19 mmHg	0.011	39	> 8	3
				40 (Sulzer)	Chlorobenzene-ethylbenzene	76 mmHg	0.021	39	> 8	6
				40 (Sulzer)	Chlorobenzene-ethylbenzene	Atm	0.060	39	> 8	4
10.6004A	Mellapak® 250Y	20	This work	40,41 (Sulzer)	Chlorobenzene-ethylbenzene	19 mmHg	0.011	39	15	4
				41,42 (Sulzer)	Chlorobenzene-ethylbenzene	38 mmHg	0.015	39	15	4
				40-42 (Sulzer)	Chlorobenzene-ethylbenzene	76 mmHg	0.021	39	15	6
				41,42 (Sulzer)	Chlorobenzene-ethylbenzene	304 mmHg	0.040	39	15	5
				40-42 (Sulzer)	Chlorobenzene-ethylbenzene	Atm	0.060	39	15	6
				5 (Bochum Uni)	Chlorobenzene-ethylbenzene	50 mmHg	0.017	9	5	6

TABLE 10.1 Data Used in Charts (*Continued*)

Corrugated-Sheet Structured Packings (*Continued*)

Chart	Packing	F_p	F_p source (ref. number)	Data source (ref. number)	System	Pressure	Flow parameter	Test column Dia. in	Test column Packed ht., feet	No. of data points
10.6004B	Mellapak® 250Y	20	This work	42 (Sulzer)	Methanol-water	Atm	0.039	39	5	5
				42 (Sulzer)	Air-water	Atm	0.010–0.81	12		25
				5 (Bochum Uni)	Air-water	Atm	0.022–0.26	12		6
10.6008	Mellapak® 125Y	10	This work	40 (Sulzer)	Chlorobenzene-ethylbenzene	19 mmHg	0.011	39	> 8	3
				40 (Sulzer)	Chlorobenzene-ethylbenzene	76 mmHg	0.021	39	> 8	5
				40 (Sulzer)	Chlorobenzene-ethylbenzene	Atm	0.060	39	> 8	2
10.6014	Mellapak® 250Y plastic	22	This work	42*a* (Sulzer)	Air-water	Atm	0.026–2.0			15
10.6102	Flexipac® #1	30	This work	14 (Koch)	Air-water	Atm	0.040–2.0	36	2	26
10.6104	Flexipac® #2	13	This work	43 (SRP)	C_6-C_7	250 mmHg	0.040	18	10	1
				43 (SRP)	C_6-C_7	Atm	0.073	18	10	1
				43 (SRP)	C_6-C_7	60 psia	0.15	18	10	1
				14 (Koch)	Air-water	Atm	0.056–1.2	36	2	37
10.6106	Flexipac® #3	8	This work	14 (Koch)	Air-water	Atm	0.043–1.1	36	2	40
10.6108	Flexipac® #4	6	This work	14 (Koch)	Air-water	Atm	0.041–1.0	36	2	29
				14 (Koch)	Air-water	Atm	0.037–0.74	14		24
10.6122	Flexeramic® #28	40	This work	44 (Koch)	Air-water	Atm	0.042–1.6			23
10.6124	Flexeramic® #48	24	This work	44 (Koch)	Air-water	Atm	0.032–1.7			27
10.6128	Flexeramic® #88	15	This work	44 (Koch)	Air-water	Atm	0.024–1.1			28
10.6202	Gempak® 4A	32	45	46 (Glitsch)	Air-water	Atm	0.016–1.2	36	4	25
10.6203	Gempak® 3A	21	45	46 (Glitsch)	o-p Xylenes	50 mmHg	0.017			1
				46 (Glitsch)	o-p Xylenes	100 mmHg	0.024			1
				46 (Glitsch)	Air-water	Atm	0.013–1.8	36	4	34

10.6204	Gempak® 2A	16	45	46 (Glitsch)	o-p Xylenes	50 mmHg	0.017			1
				46 (Glitsch)	o-p Xylenes	100 mmHg	0.024			1
				39 (SRP)	C_6-C_7	250 mmHg	0.040	18	10	2
				39 (SRP)	C_6-C_7	24 psia	0.091	18	10	2
				39 (SRP)	C_6-C_7	60 psia	0.15	18	10	2
				46 (Glitsch)	Air-water	Atm	0.012–1.4	36	4	34
10.6206	Gempak® 1.5A	12	45	46 (Glitsch)	o-p Xylenes	50 mmHg	0.017			1
				46 (Glitsch)	o-p Xylenes	100 mmHg	0.024			1
				46 (Glitsch)	Air-water	Atm	0.011–1.4	36	4	29
10.6208	Gempak® 1A	9	45	46 (Glitsch)	o-p Xylenes	50 mmHg	0.017			1
				46 (Glitsch)	o-p Xylenes	100 mmHg	0.024			1
				46 (Glitsch)	Air-water	Atm	0.024–0.88	36	4	28
10.6209	Gempak® 0.5A	6	This work	46 (Glitsch)	Air-water	Atm	0.049–0.68	36	4	20
10.6302	Montz B1-300®	33	This work	5 (Bochum Uni)	Chlorobenzene-ethylbenzene	25 mmHg	0.012	9	5	4
				5 (Bochum Uni)	Chlorobenzene-ethylbenzene	50 mmHg	0.017–0.024	9	5	12
				5 (Bochum Uni)	Chlorobenzene-ethylbenzene	100 mmHg	0.022	9	5	4
				5 (Bochum Uni)	Air-water	Atm	0.014–0.40	9	5	6
				5 (Bochum Uni)	Air-water	Atm	0.029–0.46	18	6	7
10.6303	Montz B1-250®	20	This work	47 (Montz)	Air-water	Atm	0.010–0.56			25
10.6402	Norton Intalox® 1T	20	This work	38 (SRP)	C_6-C_7	250 mmHg	0.040	18	10	4
				38 (SRP)	C_6-C_7	24 psia	0.085	18	10	5
				38 (SRP)	C_6-C_7	60 psia	0.13	18	10	4

TABLE 10.1 Data Used in Charts (*Continued*)

Corrugated-Sheet Structured Packings (*Continued*)

Chart	Packing	F_p	F_p source (ref. number)	Data source (ref. number)	System	Pressure	Flow parameter	Test column Dia. in	Test column Packed ht., feet	No. of data points
10.6404	Norton Intalox® 2T	17	This work	48,49 (Norton)	Ethylbenzene-styrene	50 mmHg	0.018	15	9.3	6
				48,49 (Norton)	iC_8-toluene	100 mmHg	0.029	15	9.3	6
				48,49 (Norton)	iC_8-toluene	Atm	0.073	15	9.3	6
				38,39,49 (SRP)	C_6-C_7	250 mmHg	0.039	18	10	7
				39,49 (SRP)	C_6-C_7	Atm	0.068	18	10	2
				38,39,49 (SRP)	C_6-C_7	24 psia	0.085	18	10	7
				38,39,49 (SRP)	C_6-C_7	60 psia	0.14	18	10	7
				49 (FRI)	iC_4-nC_4	100 psia	0.18	48	12	1
				49 (FRI)	iC_4-nC_4	165 psia	0.25	48	12	1
				49 (FRI)	iC_4-nC_4	300 psia	0.36	48	12	1
				49 (FRI)	iC_4-nC_4	400 psia	0.46	48	12	1
				49 (Norton)	Air-water	Atm	0.0094–0.79	15	9.3	26
10.6408	Norton Intalox® 3T	13	This work	48,49 (Norton)	iC_8-toluene	100 mmHg	0.029	15	9.3	3
				48,49 (Norton)	iC_8-toluene	Atm	0.073	15	9.3	4
10.6504	Jaeger MaxPac®	12	This work	38,50 (SRP)	C_6-C_7	250 mmHg	0.040	18	10	7
				38,50 (SRP)	C_6-C_7	24 psia	0.085	18	10	7
				38,50 (SRP)	C_6-C_7	60 psia	0.14	18	10	4
					Grids					
10.8005	Glitsch Grid® EF25A	10	This work	51 (Glitsch)	Air-water	Atm	0.022–1.3			34
10.8015	Glitsch Grid® EF25AP	18	This work	51 (Glitsch)	Air-water	Atm	0.012–1.0			37
10.8104	Koch Flexigrid® #3	10	This work	52 (Koch)	Air-water	Atm	0.022–0.56			20
10.8108	Koch Flexigrid® #2	4	This work	52 (Koch)	Air-water	Atm	0.016–0.42			20
10.8205	Nutter Snap Grid™ #3	9	This work	53 (Nutter)	Air-Isopar®	Atm	0.011–0.45	30		14

10.3 Acknowledgment

About twelve of the GPDC interpolation charts were first published by the authors in *Chem. Eng. Prog.*, February, p. 32, 1991. The kind permission of the American Institute of Chemical Engineers for reprinting these charts is gratefully acknowledged.

The authors are grateful to those who donated invaluable unpublished data to the research that produced the GPDC interpolation charts. Special thanks are due to Dale Nutter, Nutter Engineering; Jose Bravo, Separation Research Program; and George Bonilla and Layton Kitterman, Glitsch Inc.

10.4 References

1. Strigle, R. F., Jr., *Random Packings and Packed Towers*, Gulf Publishing, Houston, 1987.
2. Billet, R., *Chem. Eng. Prog. 63*(9), p. 53, 1967.
3. Eckert, J. S., and L. F. Walter, *Hydrocarb. Proc. & Pet. Ref., 43*(2), p. 107, 1964.
4. Eckert, J. S., E. H. Foote, and L. F. Walter, *Chem. Eng. Prog. 62*(1), p. 59, 1966.
5. Billet, R., *Packed Column Analysis and Design*, Ruhr Universitat Bochum, Germany, 1989.
6. Elsby, K., N. Ashton, and A. Arrowsmith, *I. Chem. E. Symp. Ser.* 104, p. A143, 1987.
7. Norton Company, Bulletin DC-11, Akron, Ohio, 1977.
8. Glitsch, Inc., Bulletin 217, 3d ed., Dallas, Texas, 1975.
9. Koch Engineering Company, Inc., Bulletin KRP-1 and KRP-2, Wichita, Kansas, 1987. (Revised version with HcKp, 1991)
10. Strigle, R. F., Jr., and K. E. Porter, *I. Chem. E. Symp. Ser.* 56, p. 3.3/19, 1979.
11. Strigle, R. F., Jr., and F. Rukovena, Jr., *Chem. Eng. Prog. 75*(3), p. 86, 1979.
12. Nutter Engineering, Division of Patterson-Kelley Co.—HARSCO Corporation, Unpublished data.
13. Nutter, D. E., *I. Chem. E. Symp. Ser.* 104, p. A129, 1987.
14. McNulty, K. J., and C. L. Hsieh, Paper presented at the annual meeting of the AIChE, Los Angeles, California, November 14–19, 1982.
15. Gangriwala, H. A., *I. Chem. E. Symp. Ser.* 104, p. B89, 1987.
16. Jaeger Products Inc., General Catalogue 100, Spring, Texas.
17. Billet, R., and J. Maćkowiak, *Chemie-Technik 13*(12), p. 37, 1984; *ibid. 14*(4), p. 91, 1985; *ibid. 14*(5), p. 195, 1985.
18. Norton Company, Bulletin SI-72, Akron, Ohio, 1973.
19. Norton Company, Bulletin HY-30, Akron, Ohio, 1975.
20. Eckert, J. S., *Chem. Eng.*, April 14, p. 70, 1975.
21. Norton Company, Bulletin IM-82, Akron, Ohio, 1979.
22. Strigle, R. F., Jr., and M. J. Dolan, *Can. Proc. Equip. Control News*, October 1983.
23. Glitsch, Inc., Bulletin 345, Dallas, Texas, 1986.
24. Wu, K. Y., and G. K. Chen, *I. Chem. E. Symp. Ser.* 104, p. B225, 1987.
25. Glitsch, Inc., Bulletin TP/US/M4, Dallas, Texas, 1983.
26. Nutter Engineering Company, Chem-Pro Bulletin 703, Tulsa, Oklahoma, 1977.
27. Jaeger Products Inc., Bulletin JTP-600, Spring, Texas.
28. Billet, R., "Modern plastic packings for more efficient separation processes," paper presented at the Center for Energy Studies, University of Texas, Fall 1985.
29. Billet, R., and J. Maćkowiak, *Verfahrenstechnik* 16, p. 67, 1982.
30. Norton Company, Bulletin GWS-1, Akron, Ohio, 1987.
31. Lantec Products Inc., Technical Bulletin 8T-5, Agoura Hills, California.
32. Lantec Products Inc., "IMPAC," Technical Bulletin, Agoura Hills, California.

33. Leva, M., D. Bhaga, and A. Trickett, *Chem. Engr.* (London), p. 25, September 27, 1990.
34. Meier, W., *Sulzer Tech. Rev.*, No. 3, 1970.
35. Meier, W., and M. Huber, *I. Chem. E. Symp. Ser.* 32, p. 4:31, London, 1969.
36. Bravo, J. L., J. A. Rocha, and J. R. Fair, *Hydrocarb. Proc. 65*(3), p. 45, 1986.
37. Billet, R., *I. Chem. E. Symp. Ser.* 32, p. 4:42, London, 1969.
38. Bravo, J. L., Separation Research Program, private communication, 1990.
39. Martin, C. L., J. L. Bravo, and J. R. Fair, Paper presented at the AIChE National Meeting, New Orleans, Louisiana, March 7, 1988.
40. Spiegel, L., and W. Meier, *I. Chem. E. Symp. Ser.* 104, p. A203, 1987.
41. Meier, W., W. D. Stoecker, and B. Weinstein, *Chem. Eng. Prog. 73*(11), p. 71, 1977.
42. Meier, W., R. Hunkeler, and D. Stöcker, *I. Chem. E. Symp. Ser.* 56, p. 3.3/1, London, 1979.
42*a*. Sulzer Chemtech, "Separation Columns for Distillation and Absorption," Winterthur, Switzerland.
43. Fair, J. R., and J. L. Bravo, *Chem. Eng. Prog. 86*(1), p. 19, 1990.
44. Koch Engineering Company, Inc., Knight Division, Bulletin KCP-1, Akron, Ohio, 1989.
45. Bonilla, J. A., J. Shieh, and P. Wang, Paper presented at the AIChE Summer National Meeting, Denver, Colorado, August 24, 1988.
46. Glitsch, Inc., Bulletin 357, Dallas, 1989.
47. Julius Montz GmbH "Montz-Pak Typ B1" Bulletin, Hilden, Germany.
48. Norton Company, Bulletin IS-1, Akron, Ohio, 1988.
49. Rukovena, F., Jr., and R. F. Strigle, Jr., Paper presented at the AIChE Spring National Meeting, Houston, Texas, April 1989.
50. Jaeger Products, Inc., Product Bulletin 500, Spring, Texas, Dec. 1989.
51. Glitsch, Inc., Bulletin 207, Dallas, Texas, 1985.
52. Koch Engineering Company Inc., Bulletin KFG-2, Wichita, Kansas, 1985.
53. Nutter Engineering, Bulletin SG-1, Tulsa, Oklahoma, 1987.

Chapter

11

Packing Efficiency Data

Currently, interpolation of experimental HETP data is the most reliable means of obtaining packed-tower design HETPs. Due to our poor understanding of packing hydraulics and mass transfer, rules of thumb outperform theoretical models, while data interpolation outperforms both (Secs. 9.1.4 to 9.1.6).

Eckert (6) was first to tabulate HETP data in a format suitable for interpolation. Vital, Grossel, and Olsen (65) recommended such data over predictive methods, subject to availability of data for a system similar to that considered. The author concurs with this recommendation. In this chapter, Eckert's table is updated and largely expanded, and new tables and charts are added for structured packings.

11.1 Random Packings

Table 11.1 contains published efficiency data for random packings. Section 11.1.1 presents a procedure recommended by the author for applying these data. Section 11.1.2 is a legend for the comments in the right-hand column of Table 11.1.

11.1.1 Interpolation procedure

The following steps are recommended.

1. Examine Sec. 9.1.3, and determine what constitutes a system similar to the system under consideration. Then scan Table 11.1, marking all the data for similar systems.
2. Check if sufficient marked data are available for the packing under consideration. If so, use these data and go directly to step 6; it may pay to use steps 3 to 5 as a check. If not, proceed to step 3.
3. Compare HETPs for the marked systems to HETPs of other systems with the same packing. If significantly higher, a system effect

is implied. Estimate the magnitude of this system effect from these data, and allow for it in the design.

4. Compare the HETP for the packing under consideration to the rule of thumb in Eq. (9.34). If different, estimate the magnitude of this packing effect from the data, and allow for it in the design.
5. Predict packing HETP using Eq. (9.34) and adjust its prediction using factors derived in steps 3 and 4 above. Examine the reliability of these factors. The larger the number of data points they are based on, the more reliable they are. Some judgment is required here; the author advocates a conservative approach.
6. Closely examine the considerations in Sec. 9.3.3. Use these to scale up the HETP from the above steps to your column. Pay attention to effects of diameter, height, and wetting. Judgment is required. It may pay to look at the original reference from which the data were derived in order to check whether distribution, data scatter, or test procedure have influenced the data.
7. Compare the value calculated in step 6 against prediction from Eq. (9.34). Select the most conservative, unless there is enough data to verify with confidence that the HETP calculated in step 6 is lower.

11.1.2 Legend for Table 11.1 comments

1. Data show a clear loading region (see Figure 8.16*a*). HETP in the loading region is lower than the listed HETPs.
2. Data show a continuous decline of HETP with higher loads (see Fig. 8.16*b*). This implies maldistribution; at low liquid rate (<2 gpm/ft^2) also a possible wetting problem. The HETPs listed are within a turndown of 1.5 from the apparent loading point.
3. High purity (>95 percent) of nonaqueous component in column overhead.
4. Where two values are shown under column diameter or column height, the first describes the relevant dimension above the feed, the second describes the relevant dimension below the feed.
5. Value reported under reflux ratio is mass vapor to liquid ratio.
6. High purity (>99 percent) distillate product.
7. Low purity (<90 percent) of nonaqueous component in column overhead.
8. Given ring dimensions 35 × 35 mm.

9. Batch distillation data.
10. Value reported under reflux ratio is mass vapor to liquid ratio at the bottom of the column.
11. Given ring dimensions 80 × 80 mm.
12. Data measured with chemically oxidized packing particles made out of phosphor bronze. In this application, much higher HETPs were demonstrated for the same or similar packing that were not specially surface-treated.
13. AEC is short for Atomic Energy of Canada.
14. Pressure cited is at bottom of tower.
15. Original installation experienced plugging, maldistribution, and much higher HETP. Cited HETP was achieved after modifications, but a small degree of plugging and maldistribution remained.
16. Data marked * were not directly supplied by the article, but were estimated by the author from information contained in the article. They may not be accurate, but should be quite reasonable.
17. Separation was performed in two columns in series, each containing three packed beds of 27 to 30 ft in depth. Feed entered below the second bed.
18.

	Mole % methanol in bottom	Mole % water in top	Comment
A	3–65	0.05–0.34	
B	0.1–0.5	5–17	Underwetting in bottom?
C	5–6	5–10	
D	6–7	17–24	
E	30	2.2	Methanol-rich
F	8–13	24–53	Water-rich

19. A large number of tests.
20.

	Mole % water in bottom	Mole % DMF in top	Comment
A	81–83	0.2	Underwettting in top?
B	71–79	0.2–0.9	
C	66	1.5	No underwetting?

21. Measured during first week of operation; may change with aging.

TABLE 11.1 Published Efficiency Data for Random Packings

System	Column diameter in	Packed height, ft	Pressure	Reflux ratio	Liquid rate range, gpm/ft^2 (approx.)	HETP, in	Source	Ref.	Comment (see Sec. 11.1.2)
				⅝-in Pall® rings (M), hydrocarbons					
Isooctane-toluene	15	10	Atm	∞	2.0–4.5	18	Norton	1	
Isooctane-toluene	15	10	Atm	6.0	1.7–4	16	Norton	1	1
Isooctane-toluene	15	10	Atm	3.8	2.0–4	13–16	Norton	1	1,2
o-p xylenes	6	10	50 mmHg	∞	0.9–1.8	14–15	Glitsch	2	1,2
Ethylbenzene-styrene	20	4.9	100 mmHg	∞	1.5–3	11–15	BASF	3–5	2
Ethylbenzene-styrene	31	6.5	100 mmHg	∞	1.7–3	8–13	BASF	3–5	2
				⅝-in Pall® rings (M), organics					
Methanol-ethanol	20	4.9	Atm	∞	2.7–5	10–12	BASF	3,4	1,2
Methanol-ethanol	31	6.6	Atm	∞	2.7–5	10–12	BASF	3,4	1,2
Methanol-ethanol	6	3.3	Atm	∞	1.0–5	8	BASF	3,4	1
				⅝-in Pall® rings (M), aqueous					
Acetone-water	15	9.5	Atm	1.0	1.5–3.5	16	Norton	6	3
				1-in Pall® rings (M), hydrocarbons					
Isooctane-toluene	15	5	Atm	∞	1.0–8	16	Norton	1	1
Isooctane-toluene	15	10	Atm	∞	1.3–7	17	Norton	1,7	1
Isooctane-toluene	15	20	Atm	∞	3–7	21–23	Norton	1	1
Isooctane-toluene	15	5	Atm	6.0	3.5–6	11	Norton	1	1
Isooctane-toluene	15	10	Atm	6.0	1.1–6	13	Norton	1,8	1
Isooctane-toluene	15	20	Atm	6.0	3.5–6	13–18	Norton	1	2
Isooctane-toluene	15	10	Atm	3.8	2.2–6	12	Norton	1	1
Isooctane-toluene	15	10	100 mmHg	∞	1.6–3.5	14	Norton	1	1
Isooctane-toluene	15	10	100 mmHg	6.0	1.6–3.5	10–12	Norton	1,8	2

1-in Pall® rings (M), hydrocarbons (*Continued*)									
Isooctane-toluene	15	10	100 mmHg	3.8	1.5–3	9–14	Norton	1	2
Benzene-toluene	15	10	Atm	∞	1.8–7	16–17	Norton	4	1
Benzene-toluene	15	5	Atm	∞	1.8–7	16–17	Norton	4	1
Benzene-toluene	15	10	Atm	6.0	1.3–7	14	Norton	8	1
Pentane-isopentane	18	9/7.6	Atm	0.9	7	18	Norton	6	4,5
Light naphtha/heavy naphtha	15	10	100 mmHg	1.1	0.8–1.6	24–39	Norton	6	
Light naphtha/heavy naphtha	15	10	100 mmHg	0.6–0.8	0.7–1.7	17	Norton	6	
Cis-trans decalin	18	5	5 mmHg	∞	0.7–0.8	15–16	Birmingham U	9	
Cis-trans decalin	20	3.6	10 mmHg	∞	0.4–0.9	13–17	BASF	10	1,2
Cis-trans decalin	18	5	10 mmHg	∞	0.8–1.6	12–15	Birmingham U	9	2
Cis-trans decalin	18	5	20 mmHg	∞	0.7–2.4	14–16	Birmingham U	9	1
Cis-trans decalin	18	5	40 mmHg	∞	1.0–2.7	14–15	Birmingham U	9	1
Cis-trans decalin	18	5	100 mmHg	∞	1.0–3.5	14	Birmingham U	9	1
Ethylbenzene-styrene	20	6.5	100 mmHg	∞	1.8–3.5	13–19	BASF	3–5	2
Ethylbenzene-styrene	31	6.5	100 mmHg	∞	1.6–3	11–17	BASF	3,5	2
1-in Pall® rings (M), organics									
Methylethyl ketone–toluene	15	9.5	Atm	5.2	2.4–6	12–16	Norton	6	6
Methylethyl ketone–toluene	15	9.5	Atm	3.0	1.7–5	16	Norton	6	
1,1,1 Tricholoroethane-toluene	15	5	Atm	∞	3.5–6	16–17	Norton	8	1
Chlorobenzene-ethylbenzene	6	5.6	25 mmHg	∞	0.7–1.6	25	Bochum Uni	11	1
Chlorobenzene-ethylbenzene	6	5.6	50 mmHg	∞	1.0–2.1	19	Bochum Uni	11	1
Chlorobenzene-ethylbenzene	9	5	50 mmHg	∞	0.5–2.3	16	Bochum Uni	12	1
Chlorobenzene-ethylbenzene	6	5.6	100 mmHg	∞	1.6–2.9	16	Bochum Uni	11	1
Chlorobenzene-ethylbenzene	6	5.6	200 mmHg	∞	1.7–4	15	Bochum Uni	11	1
Methanol-ethanol	20	6.6	Atm	∞	2.7–5	13	BASF	3,4	1
Ethylene glycol–1,2 Propylene glycol	20	3.6	10 mmHg	∞	0.2–0.5	20	BASF	10	1,2

TABLE 11.1 Published Efficiency Data for Random Packings (*Continued*)

System	Column diameter in	Packed height, ft	Pressure	Reflux ratio	Liquid rate range, gpm/ft^2 (approx.)	HETP, in	Source	Ref.	Comment (see Sec. 11.1.2)
1-in Pall® rings (M), aqueous									
Acetone-water	18	15.5/12	Atm	0.6	1.5	14.5	Norton	6	3,4
Acetone-water	15	9.5	Atm	1.0	1.6–4.5	17	Norton	6	3
Acetone-water	15	10	Atm	6.0	1.5–7	11	Norton	8	1,3
Acetone-water	15	5	Atm	6.0	1.5–7	11–13	Norton	8	3
Methanol-water	15	9.5	Atm	1.2	1.2	26	Norton	6	7
Methanol-water	15	5	Atm	6.0	1.4–5	8	Norton	8	3
Ethanol-water	12	6.6	Atm	∞	—	8–10	Karlsruhe Uni	13	
IPA-water	15	15	Atm	6.0	1.5–4.5	13	Norton	8	1,3
1½-in Pall® rings (M), hydrocarbons									
Deethanizer, top section	18	20	300 psia	0.42	~ 40–50	35	Norton	6	5
Depropanizer, top section	23.4	16	270 psia	0.74	~ 20–25	38	Norton	6	5
Depropanizer, bottom section	23.4	24	270 psia	0.74	~ 20–25	29	Norton	6	5
Debutanizer, top section	19.5	12	90 psia	1.6	~ 5	29	Norton	6	
Debutanizer, bottom section	19.5	18	90 psia	1.6	~ 5	24	Norton	6	
Isooctane-toluene	15	10	Atm	∞	3.5–9	21	Norton	7,14	1
Ethylbenzene-styrene	20	6.6	100 mmHg	∞	1.8–3.5	16–19	BASF	3,4	1,2,8
Ethylbenzene-styrene	20	13.0	100 mmHg	∞	1.3–3.5	16–19	BASF	3	1,8
Ethylbenzene-styrene	31	12.3	100 mmHg	∞	2.0–3.5	13–19	BASF	3	2,8
1½-in Pall® rings (M), organics									
Menthones	22	32	Atm	14.3	~ 1	19	Norton	6	9
Tar acid distillation	18	30	100 mmHg	16.6	3	19	Norton	6	9
Cresols	18	30	100 mmHg	2.0	~ 1.5	28	Norton	6	9
Phenol-ortho cresol	18	30	100 mmHg	15.7	3	19	Norton	6	
Fatty acid distillation	30	40	37 mmHg	1.5	~ 1	34	Norton	6	

1½-in Pall® rings (M), organics (*Continued*)									
DMPC, DMPC cresols/DBOC	18	30	20 mmHg	0.1–1	~ 2–4	19	Norton	6	9
Methanol/Ethanol	20	6.6	Atm	∞	2.0–5	15	BASF	3,4	1,8
1½-in Pall® rings (M), aqueous									
Acetone-water	15	9.5	Atm	1.0	3	18	Norton	6	3
Ethylene glycol-water	42	6/10	230 mmHg	0.6	0.6	36	Norton	6	3,4
2-in Pall® rings (M), hydrocarbons									
Isooctane-toluene	15	5	Atm	∞	0.6–10	23–25	Norton	1	1
Isooctane-toluene	15	10	Atm	∞	0.6–10	26–28	Norton	1	1
Isooctane-toluene	15	10	Atm	∞	2.9–10	27–29	Norton	7,14	1
Isooctane-toluene	15	20	Atm	∞	1.5–10	30–32	Norton	1	1
Isooctane-toluene	15	10	Atm	24.0	2.7–9	27–29	Glitsch	15,16	1
Isooctane-toluene	15	5	Atm	6.0	0.4–9	18–21	Norton	1	1
Isooctane-toluene	15	10	Atm	6.0	0.7–9	21–24	Norton	1,8	1
Isooctane-toluene	15	20	Atm	6.0	2.1–8	23–24	Norton	1,8	1
Isooctane-toluene	15	10	Atm	3.8	1.4–8	19–25	Norton	1	2
Isooctane-toluene	15	20	Atm	3.8	2.0–7	23–25	Norton	1	1
Isooctane-toluene	24–42	5	Atm	—	—	24	Glitsch	17	
Isooctane-toluene	24–42	10	Atm	—	—	30	Glitsch	17	
Isooctane-toluene	24–42	20	Atm	—	—	32	Glitsch	17	
Isooctane-toluene	15	10	100 mmHg	6.0	1.5–4	23–28	Norton	18	2
Isooctane-toluene	15	10	100 mmHg	3.8	0.9–4	24–25	Norton	19	
Isooctane-toluene	24–42	5	100 mmHg	—	—	24	Glitsch	17	
Isooctane-toluene	24–42	10	100 mmHg	—	—	26	Glitsch	17	
Isooctane-toluene	24–42	20	100 mmHg	—	—	28	Glitsch	17	
Cyclohexane-n heptane	20	8	Atm	∞	2.2–11	25–28	Nutter	20	
Ethylbenzene-styrene	31	12.3	100 mmHg	∞	1.9–4	20–23	BASF	3	1,2
Ethylbenzene-styrene	31	6.6	100 mmHg	∞	1.7–4	21	BASF	3,5	1
Ethylbenzene-styrene	20	4.4	100 mmHg	∞	0.5–3.5	20–21	BASF	3–5,21	1
Ethylbenzene-styrene	20	6.6	50 mmHg	∞	0.7–3	28	BASF	3–5,21	1

TABLE 11.1 Published Efficiency Data for Random Packings (*Continued*)

System	Column diameter in	Packed height, ft	Pressure	Reflux ratio	Liquid rate range, gpm/ft^2 (approx.)	HETP, in	Source	Ref.	Comment (see Sec. 11.1.2)
2-in Pall® rings (M), hydrocarbons (*Continued*)									
Ethylbenzene-styrene	24–42	10	100 mmHg	—	—	22	Glitsch	17	
Ethylbenzene-styrene	24–42	20	100 mmHg	—	—	26	Glitsch	17	
Cis-trans decalin	20	6.6	10 mmHg	∞	0.5–1.5	30–33	BASF	3,4	
Cis-trans decalin	20	4.4	10 mmHg	∞	0.5–1.5	20–21	BASF	10	
Para-ortho xylenes	24–42	10	100 mmHg	—	—	33	Glitsch	17	
Para-ortho xylenes	24–42	10	50 mmHg	—	—	31	Glitsch	17	
Para-ortho xylenes	24–42	10	16 mmHg	—	—	28	Glitsch	17	
Absorber	36	23	865 psia	1.33	~ 20–25	34	Norton	6	5
LO Top fractionator	36	17	157 psia	3.3	~ 8–10	30	Norton	6	
LO Bottom fractionator	48	17	157 psia	0.53	~ 25–30	34	Norton	6	10
Deethanizer bottom	30	18	300 psia	0.24	~ 60–80	40	Norton	6	10
Gas plant absorber	48	23	900 psia	1.28	~ 10–15	35	Norton	6	5
2-in Pall® rings (M), organics									
1,2 Propylene glycol-Ethylene glycol	20	4.4,6.6	10 mmHg	∞	0.2–0.7	38	BASF	3–5,10,21	
Methanol-ethanol	20	4.4	Atm	∞	1.6–6	19–20	BASF	3–5,21	1
Methanol-ethanol	20	6.6	Atm	∞	1.6–6	20–21	BASF	3,4	1
Methanol-ethanol	20	13.0	Atm	∞	2.4–6	21	BASF	3	1
Chlorobenzene-ethylbenzene	9	4.8	50 mmHg	∞	0.9–2.4	30	Bochum Uni	12,22	1
2-in Pall® rings (M), aqueous									
Acetone-water	24–42	5	Atm	—	—	18	Glitsch	17	
Acetone-water	24–42	10	Atm	—	—	20	Glitsch	17	

2-in Pall® rings (M), aqueous (*Continued*)									
Methanol-water	24–42	10	Atm	—	—	21	Glitsch	17	
IPA-water	24–42	10	Atm	—	—	24	Glitsch	17	
Formic acid-water	36	18/17	Atm	4.2	~ 3–4	30	Norton	6	3,4
3½-in Pall® rings (M), hydrocarbons									
Ethylbenzene-styrene	31	6.6	100 mmHg	∞	0.5–4	29	BASF	3,21	1,11
#1 HY-PAK® (M), hydrocarbons									
Isooctane-toluene	15	10	Atm	24	1.2–7	19	Norton	18	1
Isooctane-toluene	15	10	Atm	3.8	2.3–7	17–18	Norton	18	1
#1 HY-PAK® (M), aqueous									
H_2O–D_2O	12	9.8	100 mmHg	∞	0.7–1.6	19–20	AEC	23	12,13
H_2O–D_2O	12	9.8	200 mmHg	∞	1.0–1.9	19	AEC	23	12,13
H_2O–D_2O	12	9.8	350 mmHg	∞	1.1–1.7	19	AEC	23	12,13
#2 HY-PAK® (M), hydrocarbons									
Isooctane-toluene	15	10	Atm	24	2.7–9	31–33	Glitsch	15,16	1
Isooctane-toluene	15	10	Atm	3.8	0.8–10	24–26	Norton	24	
Isooctane-toluene	15	10	100 mmHg	24	1.1–5	24–29	Norton	18	
Isooctane-toluene	15	10	100 mmHg	6	1.1–4.5	24–29	Norton	18	
Isooctane-toluene	15	10	100 mmHg	3.8	0.4–4	23–26	Norton	19	
Isooctane-toluene	15	10	100 mmHg	3.8	1.0–4	24–29	Norton	18	
#25 IMTP® (M), hydrocarbons									
Isooctane-toluene	15	10	Atm	∞	2.0–8	17	Norton	7,14	1
Isooctane-toluene	15	10	Atm	∞	2.5–9	15	Norton	25	1
Cis-trans decalin	18	5	20 mmHg	∞	0.9–2.6	15–16	Birmingham U	9	1
Cis-trans decalin	18	5	40 mmHg	∞	1.5–3	15	Birmingham U	9	1
Cis-trans decalin	18	5	80 mmHg	∞	0.7–4	14–15	Birmingham U	9	1

TABLE 11.1 Published Efficiency Data for Random Packings (*Continued*)

System	Column diameter in	Packed height, ft	Pressure	Reflux ratio	Liquid rate range, gpm/ft^2 (approx.)	HETP, in	Source	Ref.	Comment (see Sec. 11.1.2)
#25 IMTP® (M), hydrocarbons (*Continued*)									
Ethylbenzene-styrene, bottom section	294	24 Ft 3 Beds	190 mmHg	8–10	3.5	19	Chevron	26	14,15
Isobutane-(1-butene, 2-butene, n-butane)		27–30 Ft 6 Beds	83/86* psia	> 8.0*	—	(16–18)*	Norton	27	16,17
#25 IMTP® (M), organics									
Cyclohexane-cyclohexanol	15	10	70 mmHg	∞	~ 2–8	19–21	Norton	28	
#25 IMTP® (M), aqueous									
Methanol-water	15	10	Atm	∞	3.5–4.5	15–17	Norton	29	18A,19
	15	10	Atm	∞	3.0–4	22–25	Norton	29	18B,19
	15	10	Atm	3–3.5	2.5–2.6	18–21	Norton	29	18C
	15	10	Atm	2	2.2	24–25	Norton	29	18D
	15	10	Atm	1	2.0	10	Norton	29	18E
	15	10	Atm	1	1.7–1.8	29–33	Norton	29	18F
	15	10	Atm	0.55	1.2	41–44	Norton	29	18F
	15	10	Atm	0.27	0.7	68–92	Norton	29	18F
Water-DMF	15	10	Atm	∞	1.8	36–38	Norton	29	20A
	15	10	Atm	4.3	1.5	31–34	Norton	29	20A
	15	10	Atm	0.7–2.3	0.8–1.3	27–30	Norton	29	20B
	15	10	Atm	0.5	0.6	25	Norton	29	20C
#40 IMTP® (M), hydrocarbons									
Isooctane-toluene	15	10	Atm	∞	2.5–9	21	Norton	7,14	1
Isooctane-toluene	15	10	Atm	∞	3.5–10	18	Norton	25	1

#40 IMTP® (M), hydrocarbons (*Continued*)									
Ethylbenzene-styrene	15	10	50 mmHg	∞	1.0–3.5	17–18	Norton	30	1
Ethylbenzene-styrene	36	31	50 mmHg	∞	1.0–3.0	18	Norton	30	1
Ethylbenzene-styrene	354	31	50 mmHg	8–10	1.7	21	Chevron	26	15
#50 IMTP® (M), hydrocarbons									
Isooctane-toluene	15	10	Atm	∞	3.5–11	25	Norton	7,14	1
Isooctane-toluene	15	10	Atm	∞	2.7–11	25–27	Norton	25,31	1
Cyclohexane-n heptane	15	10	Atm	∞	2.2–12	27–29	Norton	31	1
#70 IMTP® (M), hydrocarbons									
Isooctane-toluene	15	10	Atm	∞	2.7–12	37	Norton	25	1
#0 CMR® (M), hydrocarbons									
o-p xylenes	6	10	50 mmHg	∞	0.7–1.4	12–13	Glitsch	2	1
#1 CMR® (M), hydrocarbons									
o-p xylenes	6	10	50 mmHg	∞	1.0–2.5	14–16	Glitsch	2	1,2
p-m xylenes	9	4.9	50 mmHg	∞	0.3–2.3	13–17	Bochum Uni	12	
#1 CMR® (M), aqueous									
D_2O–H_2O	12	9.8	50 mmHg	∞	0.7–1.2	15–18	AEC	23	12,13
D_2O–H_2O	12,20	9.8	100 mmHg	∞	0.6–1.5	15–17	AEC	23	12,13
D_2O–H_2O	30	9.8	100 mmHg	∞	0.3–0.6	17–18	AEC	23	12,13
D_2O–H_2O	12	9.8	200 mmHg	∞	0.7–1.7	16–17	AEC	23	12,13
D_2O–H_2O	20	9.8	200 mmHg	∞	0.8–1.6	16–17	AEC	23	12,13
D_2O–H_2O	30	9.8	200 mmHg	∞	0.7–0.8	17–18	AEC	23	12,13
D_2O–H_2O	12	9.8	350 mmHg	∞	0.7–1.4	17–18	AEC	23	12,13
D_2O–H_2O	20	9.8	350 mmHg	∞	0.7–1.5	17	AEC	23	12,13
D_2O–H_2O	30	9.8	350 mmHg	∞	0.6	18	AEC	23	12,13
D_2O–H_2O	12	9.8	500 mmHg	∞	0.7–3	16–18	AEC	23	12,13

TABLE 11.1 Published Efficiency Data for Random Packings (*Continued*)

System	Column diameter in	Packed height, ft	Pressure	Reflux ratio	Liquid rate range, gpm/ft^2 (approx.)	HETP, in	Source	Ref.	Comment (see Sec. 11.1.2)
#1.5 CMR® (M), hydrocarbons									
p-m xylenes	9	4.9	50 mmHg	∞	0.6–2.7	15–20	Bochum Uni	12	1
#1.5 CMR® (M), organics									
Chlorobenzene-ethylbenzene	9	5	50 mmHg	∞	0.5–2.7	19	Bochum Uni	12	1
#2 CMR® (M), hydrocarbons									
Ethylbenzene-styrene	15	—	50 mmHg	—	—	18–24	Glitsch	15,16	2
#2 CMR® (M), aqueous									
D_2O–H_2O	12	9.8	100 mmHg	∞	0.7–1.5	20–22	AEC	23	12,13
D_2O–H_2O	12	9.8	200 mmHg	∞	1.0–1.6	20–22	AEC	23	12,13
D_2O–H_2O	12	9.8	350 mmHg	∞	1.0–1.7	20–21	AEC	23	12,13
#3 CMR® (M), hydrocarbons									
Isooctane-toluene	15	10	Atm	24	2.7–9	27	Glitsch	15,16	1
#2 Nutter rings® (M), hydrocarbons									
Cyclohexane-n-heptane	20	8	Atm	∞	1.3–11	24–26	Mitsui	20,32	1
Cyclohexane-n-heptane	48	14	260 mmHg	∞	1.2–6	28–30	FRI	20,32	1
Cyclohexane-n-heptane	48	14	24 psia	∞	2.5–12	23–25	FRI	20	1

2-in Hiflow® rings, organics									
Chlorobenzene-ethylbenzene	9	4.8	50 mmHg	∞	0.4–2.3	30	Bochum Uni	22	1
Chlorobenzene-ethylbenzene	9	4.8	50 mmHg	20	0.4–2.0	30	Bochum Uni	12	1
Chlorobenzene-ethylbenzene	9	4.8	50 mmHg	5.7	0.4–1.8	30	Bochum Uni	12	1
Chlorobenzene-ethylbenzene	9	4.8	50 mmHg	2.4	0.3–1.4	30	Bochum Uni	12	1
Chlorobenzene-ethylbenzene	9	4.8	50 mmHg	1.0	0.2–1.0	25	Bochum Uni	12	
#1 Chempak® #1 Levapak® (M), hydrocarbons									
Cis-trans decalin	18	5	20 mmHg	∞	1.0–2.2	16–17	Birmingham U	9	1
Cis-trans decalin	18	5	40 mmHg	∞	0.7–2.8	16–17	Birmingham U	9	1
Cis-trans decalin	18	5	80 mmHg	∞	0.8–3.5	16–17	Birmingham U	9	1
Isooctane-toluene	14	5	Atm	∞	1.2–6	12–13	Leva	32*a*	
#2 Chempak®/#2 Levapak® (M), hydrocarbons									
Isooctane-toluene	14	5	Atm	∞	0.8–6	17–18	Leva	32*a*	
2-in Jaeger Tri-Packs® (M), organics									
Chlorobenzene-ethylbenzene	9	4.8	50 mmHg	∞	0.4–2.4	28	Bochum Uni	12,22	1
1-in Pall® rings (C), organics									
Chlorobenzene-ethylbenzene	9	4.8	50 mmHg	∞	0.4–1.8	10–20	Bochum Uni	33	2
Chlorobenzene-ethylbenzene	9	4.8	50 mmHg	5	1.0	21	Bochum Uni	33	
Chlorobenzene-ethylbenzene	9	4.8	50 mmHg	3.3	0.9	20	Bochum Uni	33	
Chlorobenzene-ethylbenzene	9	4.8	50 mmHg	2.6	0.9	20	Bochum Uni	33	
2-in Pall® rings (C), organics									
Chlorobenzene-ethylbenzene	9	4.9	50 mmHg	∞	0.9–2.7	26	Bochum Uni	12,33	1

TABLE 11.1 Published Efficiency Data for Random Packings (*Continued*)

System	Column diameter in	Packed height, ft	Pressure	Reflux ratio	Liquid rate range, gpm/ft^2 (approx.)	HETP, in	Source	Ref.	Comment (see Sec. 11.1.2)
1-in Intalox® saddles (C), hydrocarbons									
Light naphtha/heavy naphtha	15	10	100 mmHg	0.7–0.8	0.5–1.0	28–32	Norton	6	
Isooctane-toluene	15	10	Atm	∞	1.8–6	17	Norton	7,14	1
Isooctane-toluene	15	10	Atm	∞	0.8–6	16–19	Norton	1	
Isooctane-toluene	15	10	Atm	6.0	1.2–5	14–18	Norton	1	2
Isooctane-toluene	15	10	Atm	3.8	2.0–5	10–16	Norton	1	2
Isooctane-toluene	15	10	100 mmHg	∞	0.8–2.7	13–18	Norton	1	2
Isooctane-toluene	15	10	100 mmHg	6.0	0.4–2.6	10–16	Norton	1	2
Isooctane-toluene	15	10	100 mmHg	3.8	1.2–2.4	11–24	Norton	1	2
1-in Intalox® saddles (C), organics									
Methylethyl ketone-toluene	15	9.5	Atm	5.1	1.2–4	8–11	Norton	6	6
Methylethyl ketone-toluene	15	9.5	Atm	3–3.5	1.1–3.5	11–12	Norton	6	
$CH_3Cl/CH_2Cl_2/CHCl_3/CCl_4$	19	68	Atm	0.44	9	18	Norton	6	5
Methylene light ends	18	44	Atm	0.42	10	18	Norton	6	5
Benzene-chlorobenzene	15	9.5	Atm	1.0	0.8	44	Norton	6	
Chlorobenzene-ethylbenzene	9	4.8	50 mmHg	∞	0.6–1.8	12–19	Bochum Uni	33	2
1-in Intalox® saddles (C), aqueous									
Acetone-water	14	10.5/2.5	Atm	3.1	1.2	18	Norton	6	3,4
Acetone-water	15	9.5	Atm	1.0	1.6–3	19–22	Norton	6	3
Methanol-water	12	18/9	Atm	3.0	2.5	18	Norton	6	3,4

1-in Intalox® saddles (C), aqueous (*Continued*)									
Ethanol-water	12	6.6	Atm	∞	—	12	Karlsruhe Uni	13	1
IPA-water	18	5/6	Atm	0.6	1.0	19	Norton	6	4,7
1½-in Intalox® saddles (C), hydrocarbons									
Isooctane-toluene	15	10	Atm	∞	2.4–7	22–23	Norton	7,14	1
1½-in Intalox® saddles (C), organics									
Methylfuran–methyl tetrahydrofuran	24	24/24	Atm	7.6	4.5	21	Norton	6	4
Benzoic acid–toluene	24	6/15	Atm	0.5	3.0	18	Norton	6	4,10
Benzene-chlorobenzene	15	9.5	Atm	1.0–2.0	1.6–2.5	36–46	Norton	6	6
Benzene-chlorobenzene	72	18/14	100 mmHg	1.0	2.5	42	Norton	6	4,6
Methylene product column	25	45	Atm	7.8	~ 8–10	18	Norton	6	
Chloroform product column	22	90	Atm	High	~ 6–7	18	Norton	6	
1½-in Intalox® saddles (C), aqueous									
Furfural-water	20	6/12	Atm	1.3	~ 1.5	24	Norton	6	4,7
Methyl isobutyl ketone, steam stripping	42	14/14	Atm	0.078	12	48	Norton	6	4,10
2-in Intalox® saddles (C), hydrocarbons									
Isooctane-toluene	15	10	Atm	∞	2.9–9	29–31	Norton	7,14	1
2-in Intalox® saddles (C), organics									
Chlorobenzene-ethylbenzene	9	4.9	50 mmHg	∞	1.3–2.3	16–34	Bochum Uni	12	2
2-in Intalox® saddles (C), aqueous									
Acetone-water	15	9.5	Atm	1.0	1.6	21	Norton	6	
Tall oil–steam	144/96	18/36	Atm	0.020	~ 8	30	Norton	6	3,4,10

TABLE 11.1 Published Efficiency Data for Random Packings (*Continued*)

System	Column diameter in	Packed height, ft	Pressure	Reflux ratio	Liquid rate range, gpm/ft^2 (approx.)	HETP, in	Source	Ref.	Comment (see Sec. 11.1.2)
20-mm Hiflow® rings (C), organics									
Chlorobenzene-ethylbenzene	9	4.8	50 mmHg	∞	0.5–1.6	11–13	Bochum Uni	33	
Chlorobenzene-ethylbenzene	9	4.8	50 mmHg	10	1.3	12	Bochum Uni	33	
Chlorobenzene-ethylbenzene	9	4.8	50 mmHg	5	0.6,1.2	12–13	Bochum Uni	33	
Chlorobenzene-ethylbenzene	9	4.8	50 mmHg	4	0.6	13	Bochum Uni	33	
35-mm Hiflow® rings (C), organics									
Chlorobenzene-ethylbenzene	9	4.8	50 mmHg	∞	0.5–2.4	25	Bochum Uni	33	1
50-mm Hiflow® rings (C), organics									
Chlorobenzene-ethylbenzene	9	4.9	50 mmHg	∞	0.9–2.7	27–28	Bochum Uni	12	1
1-in Pall® rings (P), organics									
Chlorobenzene-ethylbenzene	9	4.9	50 mmHg	∞	0.6–2.1	16	Bochum Uni	12	1
1-in Pall® rings (P), aqueous									
D_2O–H_2O	12	10			< 0.3	31	AEC	23	13
D_2O–H_2O	72	~ 31.5 ft 6 beds			< 0.3	47	AEC	23	13,21
1-in Hiflow® rings (P), organics									
Chlorobenzene-ethylbenzene	9	4.9	50 mmHg	∞	0.5–2.6	14–16	Bochum Uni	12	1
2-in Hiflow® rings (P), organics									
Chlorobenzene-ethylbenzene	9	4.9	50 mmHg	∞	0.6–2.6	26	Bochum Uni	12	1

1-in Nor-Pac® rings, organics									
Chlorobenzene-ethylbenzene	6	5.6	25 mmHg	∞	1.4–2.3	27	Bochum Uni	11,34	1
Chlorobenzene-ethylbenzene	6	5.6	50 mmHg	∞	1.1–3	26	Bochum Uni	11,34	1
Chlorobenzene-ethylbenzene	6	5.6	100 mmHg	∞	1.6–4	25	Bochum Uni	11,34	1
Chlorobenzene-ethylbenzene	6	5.6	200 mmHg	∞	1.3–5	24	Bochum Uni	11,34	1
Chlorobenzene-ethylbenzene	6	5.6	400 mmHg	∞	2.0–5	23	Bochum Uni	11,34	1
Chlorobenzene-ethylbenzene	9	4.9	25 mmHg	∞	0.7–1.8	28	Bochum Uni	11	
Chlorobenzene-ethylbenzene	9	4.9	50 mmHg	∞	0.9–2.7	26–27	Bochum Uni	11	1
Chlorobenzene-ethylbenzene	9	4.9	100 mmHg	∞	1.4–2.7	25	Bochum Uni	11	
Chlorobenzene-ethylbenzene	9	4.9	50 mmHg	∞	0.5–2.7	20	Bochum Uni	34	1

11.2 Structured Packings

11.2.1 Efficiency data plots

Figures 11.1 to 11.10 and Table 11.2 contain published efficiency data for structured packings. Section 11.2.2 presents a procedure recommended by the author for applying these data. Section 11.2.3 is a legend for the comments in the right-hand column of Table 11.2.

Unlike random packings, structured-packing HETP often rises with loads (Fig. 8.16c). HETP is measured at a constant reflux ratio (L/V), usually at total reflux, so that vapor and liquid loads are raised and lowered simultaneously. It is therefore difficult to state whether HETP rises due to the increase in the vapor load or that in the liquid load (Sec. 8.2.1), but there are suggestions (Sec. 8.1.10) that the liquid load plays the prime role.

During scaleup, the user must judge whether the load effect is vapor- or liquid-related, or select the more conservative of those. Consider a service to be designed for a C-factor of 0.2 ft/s and a liquid rate of 15 gpm/ft^2 using the Koch-Sulzer BX® packing. Figure 11.2*a* suggests an HETP between 4 and 7 in, assuming the load effect is vapor-related. Figure 11.2*b* suggests an HETP between 12 and 18 in, assuming the load effect is liquid-related. The author knows of a case where the designer judged the effect to be vapor-related in circumstances similar to that example. The result was a column that did not achieve its separation.

To provide the designer with all the needed information, Figs. 11.1 to 11.10 have HETPs plotted both against the vapor and liquid loads. The liquid load is expressed as gpm/ft^2 of empty column cross-section area. The vapor load is expressed as the C-factor, C_S (ft/s), given by

$$C_S = u_S \sqrt{\frac{\rho_G}{\rho_L - \rho_G}} \tag{11.1}$$

where u_S is the superficial vapor velocity, ft/s, based on the empty column cross-section area, and ρ_G and ρ_L are the vapor and liquid densities, respectively.

11.2.2 Interpolation procedure

The procedure below is based on the axiom that while data interpolation is generally quite reliable, extrapolation seldom is. Extrapolation is best avoided. When unavoidable, it must be performed conservatively and with extreme caution. The following steps are recommended.

1. Examine Secs. 8.1.10 and 9.1.3, and determine what constitutes a system similar to the system under consideration.
2. Look at the data for the packing under consideration. Check whether there is sufficient data for a system similar to yours with the considered packing. If so, proceed to step 3. If not, proceed to step 7.
3. Using the vapor and liquid loads in your design, read test HETPs from parts *a* and *b* of the diagram for the relevant packing. Pick the more conservative of the values you read. If extrapolation is required to obtain the test HETP, your value may be unreliable. If extrapolation is excessive, it is best to terminate the calculation (step 7).
4. Look at data for the packing considered and for similar packings, using Figs. 11.1 to 11.10 and Table 11.2. Pay special attention to column diameter and height effects and to system effects that may be apparent in the data. Also, look for any weird dependencies of HETPs on vapor or liquid rates or any other odd behavior of HETP. All these effects (if they occur) need to be allowed for in the design. Judgment is required, and the author advocates a conservative approach.
5. Examine Sec. 9.3.3, and use its guidelines to scale up the HETP from the test data to your column. Pay attention to the effects of diameter, height, and underwetting. Judgment is required here. It pays to look at the original reference from which the data was extracted in order to check whether distribution, data scatter, or test procedure could have influenced the data.
6. Check that you have not violated any of the criteria recommended in Sec. 8.1.10. Your calculation is now complete; skip step 7.
7. If you reached this step, interpolation of the data in this chapter cannot answer your problem. Check if proprietary data banks or the packing supplier have the data you are missing. If you cannot obtain these data, consider an alternative packing for which HETP can be predicted with confidence for your system.

11.2.3 Legend for Table 11.2 comments

1. At "75 percent of flood."
2. Material is chemically oxidized phosphor bronze.
3. AEC stands for the Atomic Energy of Canada.
4. *C*-factor (Eq. 11.1) of about 0.2 ft/s.

5. EG stands for ethylene glycol; DEG stands for diethylene glycol; TEG stands for triethylene glycol.
6. Where two values are shown under column height, the first describes the packed height above the feed, the second the packed height below the feed.
7. Reflux ratio about 1.0 to 1.5.
8. High purity (>99 percent) of both top and bottom products.
9. Pressure cited is at bottom of tower.
10. Value of bed height is the "total packed height" specified by the source. Presumably, there were a few packed beds.
11. DEA stands for diethanol amine; TEA stands for triethanol amine.
12. Underwetting?
13. No distributor was used, but it was stated (45,46) that with a distributor, the same efficiency is obtained.
14. Obtained with high-surface-area (>600 ft^2/ft^3) Goodloe® packing, not with the standard Goodloe®. Material was copper-bronze (49).
15. Flexipac® data.
16. *C*-factor of about 0.3 ft/s.
17. Concentration range 10 percent methanol at bottom to 98 percent at top.
18. Water content 60 to 99.5 percent; stainless steel packings.
19. This is an isotope exchange system rather than a bona-fide distillation system. Separation is part of the GS process, and runs at molar L/V of 0.5.
20. Naphtha wash section in a fluid catalytic cracker (FCC) main fractionator.
21. Below the feed there are three packed beds.
22. The pressure is the average pressure in this section of column.
23. Atmospheric crude tower, naphtha/light fuel oil (LFO) fractionation section.
24. Atmospheric crude tower, kerosene/gas oil fractionation section.
25. Atmospheric crude tower, naphtha/kerosene fractionation section.
26. Atmospheric crude tower, gas oil/resid fractionation section.
27. Atmospheric crude tower, light fuel oil (LFO)/atmospheric gas oil (AGO) fractionation section.
28. Atmospheric crude tower, stripping section.

29. Based on Norton's analysis of FRI's data.
30. ITdC stands for Instituto Technologico de Celaya, Mexico.
31. Maldistribution? Compare Fig. 8.16*b*.

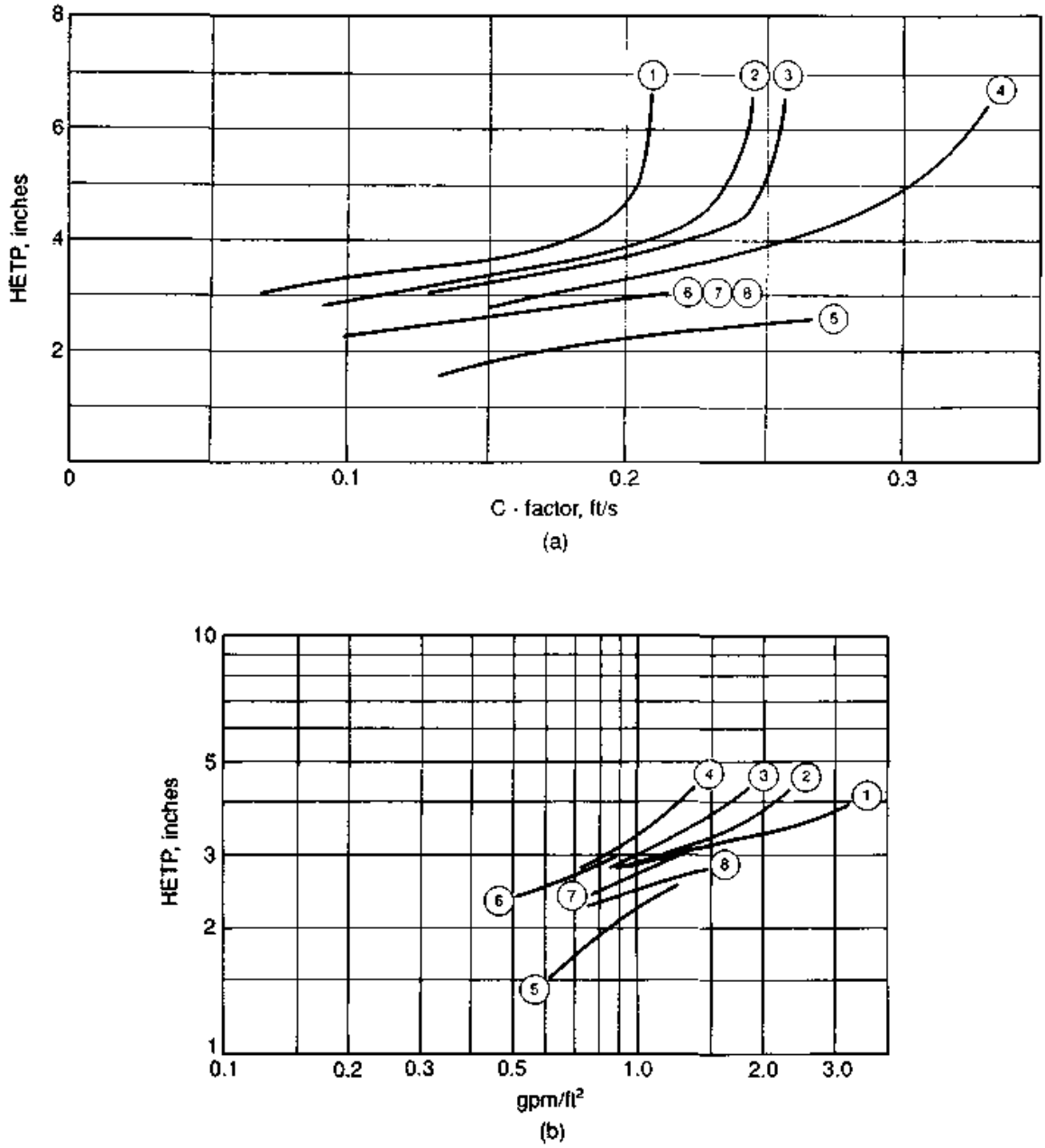

Figure 11.1 Published HETP data for Koch-Sulzer® CY wire-mesh structured packing (see Table 11.2 for curve identification). (*a*) Plotted against vapor load; (*b*) plotted against liquid load.

TABLE 11.2 Published Efficiency Data for Structured Packings

System	Column diameter, in	Packed height, ft	Pressure, mmHg	Figure no.	Curve no.	HETP, in	Source	Ref.	Comment (see Sec. 11.2.3)
Koch-Sulzer® CY wire-mesh structured packing									
Chlorobenzene-ethylbenzene	20,40	5–10	300	11.1	1		Sulzer	35	
Chlorobenzene-ethylbenzene	20,40	5–10	100	11.1	2		Sulzer	35	
Chlorobenzene-ethylbenzene	20,40	5–10	50	11.1	3		Sulzer	35	
Chlorobenzene-ethylbenzene	20,40	5–10	20	11.1	4		Sulzer	35	
Chlorobenzene-ethylbenzene	3–40	5–10	20–300	—	—	3.2–4.5	Sulzer	35	1
Water-D_2O	10	20	120	11.1	5		Sulzer	36	
Water-D_2O	12	10	100	11.1	6		AEC	23	2,3
Water-D_2O	12	10	200	11.1	7		AEC	23	2,3
Water-D_2O	12	10	300	11.1	8		AEC	23	2,3
Koch-Sulzer BX® wire-mesh structured packing									
Ortho-para xylenes	10,40	8.5	Atm	11.2	1		FRI	37	
Ortho-para xylenes	3,10,40	3–8.5	300	11.2	2		FRI	37	
Ortho-para xylenes	3,10,40	3–8.5	100	11.2	3		FRI	37	
Ortho-para xylenes	3,10,40	3–8.5	16	11.2	4		FRI	37	
Cis-trans decalin	20,40	6–10	100	11.2	5		Sulzer	35	
Cis-trans decalin	2.5,4,10,20,40	3–10	50	11.2	6		Sulzer	35,38,39	
Cis-trans decalin	4,20,100	7–10	20	11.2	7		Sulzer	35,39,40	
Cis-trans decalin	3–40	—	7–100	—	—	6–8	Sulzer	39	4
Cis-trans decalin	40	13.5	38	—	—	10.8	Sulzer	41	4
Ethylbenzene-styrene	20	6.5	100	11.2	8		BASF	3,21	
Ethylbenzene-styrene	20	6.5	50	11.2	9		BASF	3,21	
n-Heptane-cyclohexane	18	10	3040	11.2	10		SRP	42	
n-Heptane-cyclohexane	18	10	Atm	11.2	11		SRP	42	
Chlorobenzene-ethylbenzene	8.5	4.5	50	11.2	12		Bochum Uni	12	
Methanol-ethanol	20	6.5	Atm	11.2	13		BASF	3,21	
1,2 Propylene glycol-EG	20	6.5	10	11.2	14		BASF	3,21	5

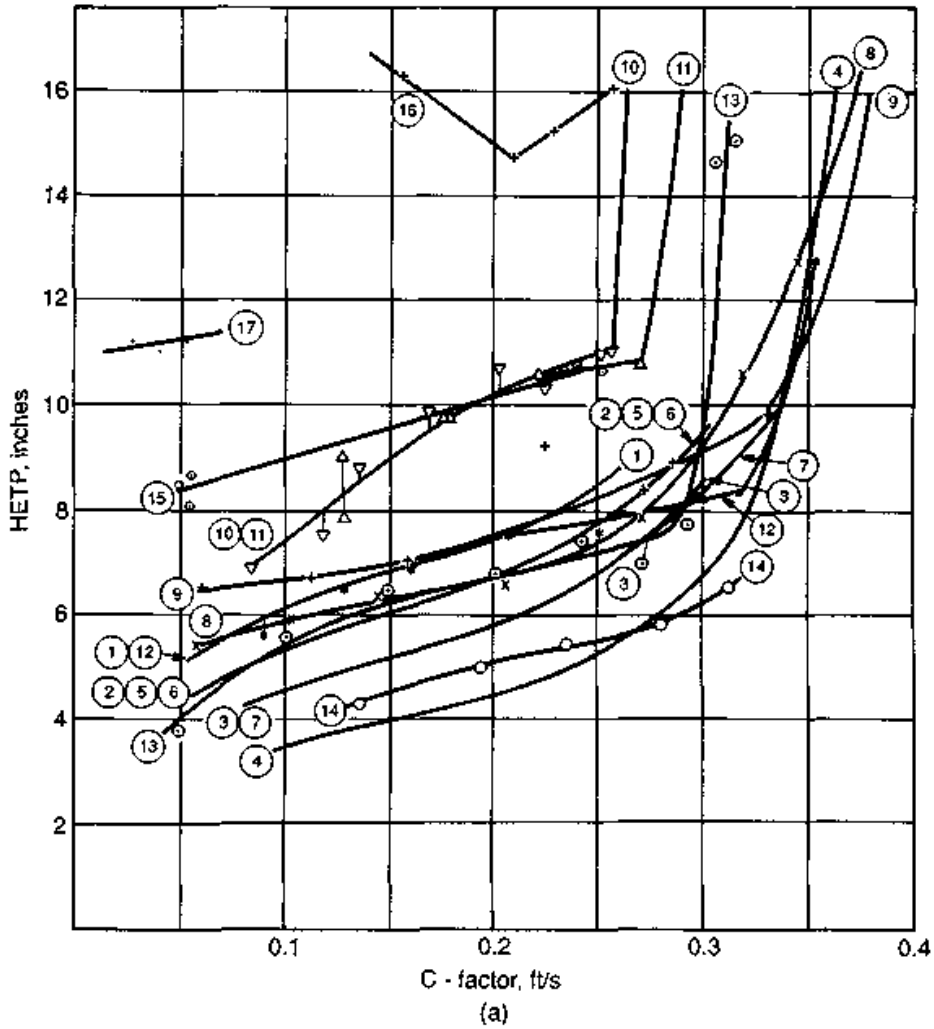

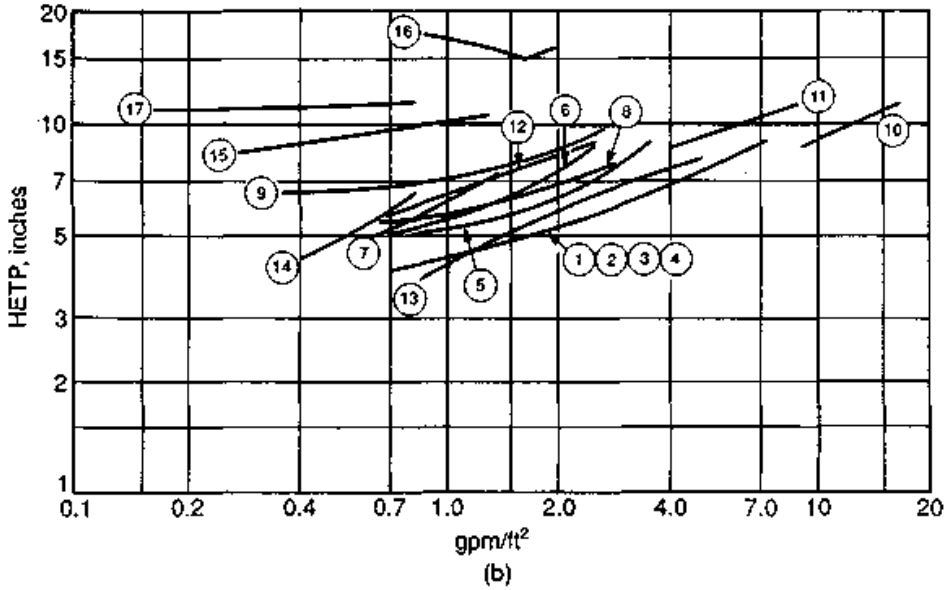

Figure 11.2 Published HETP data for Koch-Sulzer BX® wire-mesh structured packing (see Table 11.2 for curve identification). (*a*) Plotted against vapor load; (*b*) plotted against liquid load.

TABLE 11.2 Published Efficiency Data for Structured Packings (*Continued*)

System	Column diameter, in	Packed height, ft	Pressure, mmHg	Figure no.	Curve no.	HETP, in	Source	Ref.	Comment (see Sec. 11.2.3)
Koch-Sulzer BX® wire-mesh structured packing (*Continued*)									
EG-DEG	4	5	50	11.2	15		Koch	38	5
EG-DEG	—	—	100	11.2	16		Glitsch	43	5
DEG/TEG	4	7.5/7.5	14–17	—	—	9.2	Koch	39	4–8
DEG/TEG	66	3.3/5.5	24	—	—	9.4	Koch	39	4–9
Ortho cresol/2,6 xylenol	—	47	—	—	—	7.6	Koch	39	8,10
DEA/TEA product tower	4	7.5	—	—	—	8.2	Koch	39	4,11
DEA/TEA product tower	48	8.5	15.5–18	—	—	10.4	Koch	39	4,11
DEA/TEA recycle tower	4	7.5	—	—	—	8.4	Koch	39	4,11
DEA/TEA recycle tower	30	8	3.5–6	—	—	11.0	Koch	39	4,11
Methanol-water	6	5	Atm	11.2	17	—	Arkansas U	44	12
Goodloe® wire-mesh structured packing									
Ortho-para xylenes	12	20	100	11.3	1		Glitsch	45	
Ortho-para xylenes	6	10	50	11.3	2		Glitsch	2	
n-Heptane-Methylcyclohexane	4	—	Atm	11.3	3		Imperial Oil	46	13
Benzene-EDC	3	3	Atm	11.3	4		Packed column	47,48	13
Benzene-EDC	4	3	Atm	11.3	5		Packed column	47	13
Water-D_2O	24	10	300	11.3	6		Glitsch	45	14
Water-D_2O	12,20	10	100	11.3	7		AEC	23	2
Water-D_2O	12	10	200	11.3	8		AEC	23	2
Water-D_2O	12	10	300	11.3	9		AEC	23	2
Montz A3-500™ Wire-Mesh Structured Packing									
Chlorobenzene-ethylbenzene	9	5	50	—	—	4–7	Bochum Uni	50	

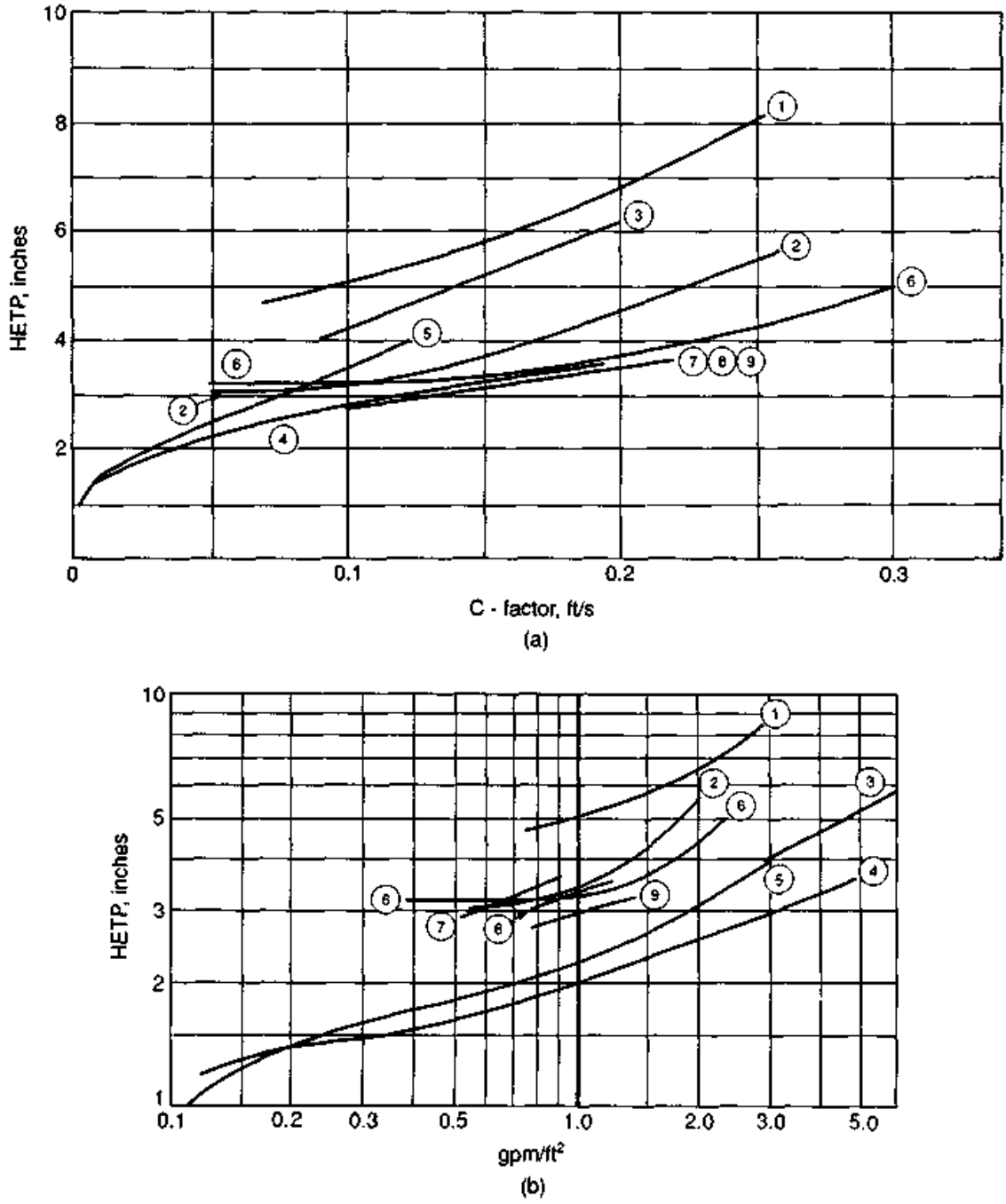

Figure 11.3 Published HETP data for Goodloe® wire-mesh structured packing (see Table 11.2 for curve identification). (*a*) Plotted against vapor load; (*b*) plotted against liquid load.

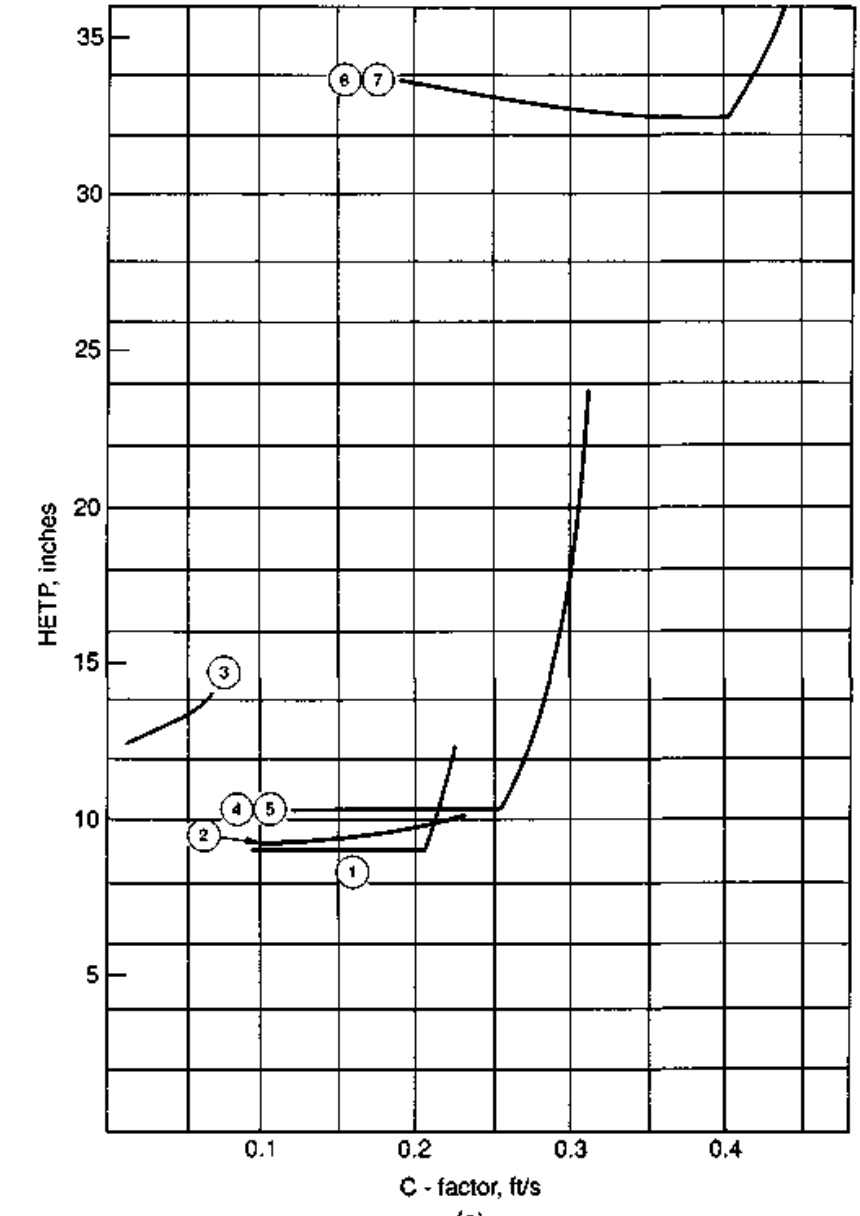

Figure 11.4 Published HETP data for Mellapak® 125Y, 350Y, and 500Y and Flexipac® #1 structured packings (see Table 11.2 for curve identification). (*a*) Plotted against vapor load; (*b*) plotted against liquid load.

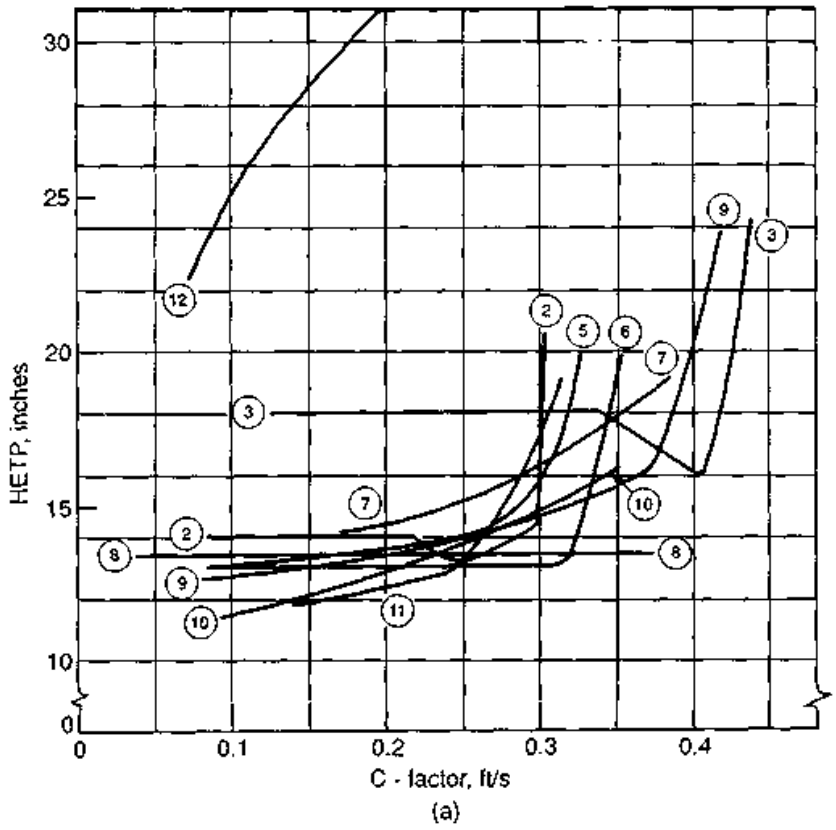

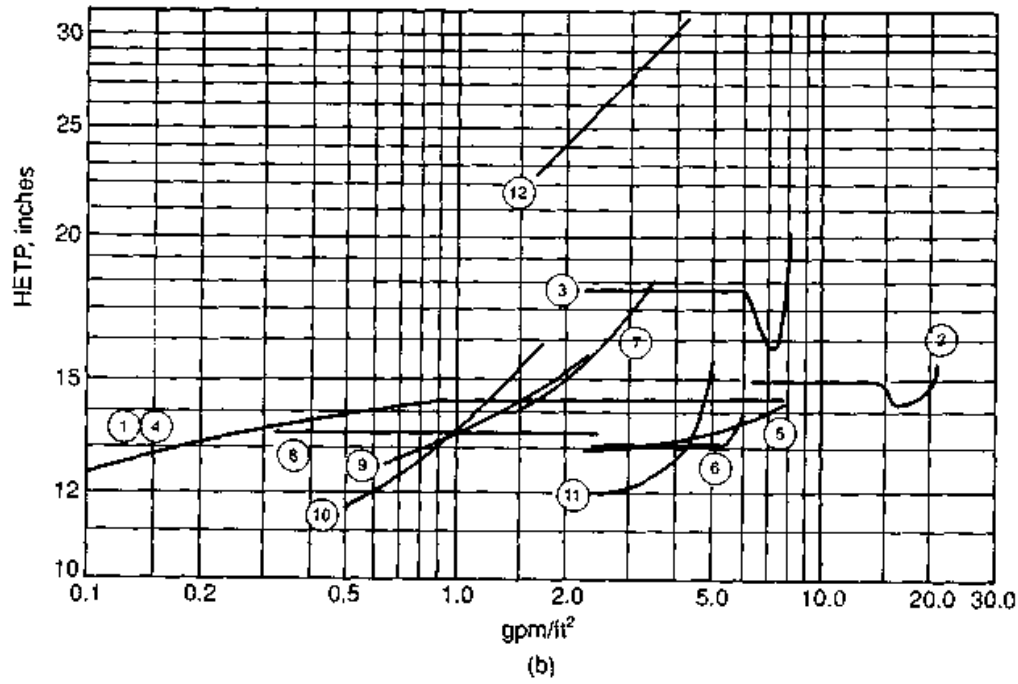

Figure 11.5 Published HETP data for Mellapak® 250Y and Flexipac® #2 structured packings (see Table 11.2 for curve identification). (*a*) Plotted against vapor load; (*b*) plotted against liquid load.

TABLE 11.2 Published Efficiency Data for Structured Packings (*Continued*)

System	Column diameter, in	Packed height, ft	Pressure, mmHg	Figure no.	Curve no.	HETP, in	Source	Ref.	Comment (see Sec. 11.2.3)
Mellapak® CY structured packing									
H_2O–D_2O	12	10	100–300	—	—	8.3	AEC	23	2,3
Mellapak® 500Y/Flexipac® #1 structured packing (Unmarked data signifies Mellapak® data. A star after system, and comment 15, signify Flexipac® data)									
Chlorobenzene-ethylbenzene	40	8–28	Atm	11.4	1		Sulzer	51,52	
Chlorobenzene-ethylbenzene	40	8–28	76	11.4	2		Sulzer	51,52	
Methanol-water*	6	5	Atm	11.4	3		Arkansas U	44	12,15
Mellapak® 350Y structured packing									
Chlorobenzene-ethylbenzene	40	8–28	Atm	11.4	4		Sulzer	51,52	
Chlorobenzene-ethylbenzene	40	8–28	76	11.4	5		Sulzer	51,52	
Chlorobenzene-ethylbenzene	40	18	76	—	—	10.4	Sulzer	53	
Mellapak® 250Y/Flexipac® #2 structured packing (Unmarked data signifies Mellapak® data. A star after system, and comment 15, signify Flexipac® data)									
Cis-trans decalin	40	—	7–Atm	11.5*b*	1		Sulzer	52,53	
Cis-trans decalin	40,47	14.5	304	—	—	14	Sulzer	53	16
Cis-trans decalin	18	14.5	304	—	—	13	Sulzer	53	16
Cis-trans decalin	10	14.5	304	—	—	12	Sulzer	53	16
Cis-trans decalin	8.5	17	76	—	—	13–15	Sulzer	54	16
n-Heptane-cyclohexane*	18	10.5	3100	11.5	2		SRP	42	15
n-Heptane-cyclohexane*	18	10.5	250	11.5	3		SRP	42	15

Mellapak® 250Y/Flexipac® #2 structured packing (Unmarked data signifies Mellapak® data. A star after system, and comment 15, signify Flexipac® data) *(Continued)*									
Chlorobenzene-ethylbenzene	40	—	7–Atm	11.5*b*	4		Sulzer	52,53	
Chlorobenzene-ethylbenzene	40	14.5	Atm	11.5	5		Sulzer	51,52,54,55	
Chlorobenzene-ethylbenzene	10,40	—	304–Atm	—	—	15	Sulzer	54	16
Chlorobenzene-ethylbenzene	40	14.5	304	11.5	6		Sulzer	54,55	
Chlorobenzene-ethylbenzene	40	4–22	304	—	—	16	Sulzer	54	16
Chlorobenzene-ethylbenzene	40,47	14.5	304	—	—	14	Sulzer	53	16
Chlorobenzene-ethylbenzene	18	14.5	304	—	—	13	Sulzer	53	16
Chlorobenzene-ethylbenzene	10	14.5	304	—	—	12	Sulzer	53	16
Chlorobenzene-ethylbenzene	40	14.5	76	11.5	7		Sulzer	51,52,54,55	
Chlorobenzene-ethylbenzene	40	4–22	76	—	—	15	Sulzer	54	16
Chlorobenzene-ethylbenzene	6,10,40	—	38–76	—	—	13–15	Sulzer	54	16
Chlorobenzene-ethylbenzene	8.5	4	50	11.5	8		Bochum Uni	12	
Chlorobenzene-ethylbenzene	40	14.5	38	11.5	9		Sulzer	54,55	
Chlorobenzene-ethylbenzene	40	14.5	19	11.5	10		Sulzer	55	
Methanol-water	40	4.6	Atm	11.5	11		Sulzer	54	17
Water-DMF	—	—	200, Atm	—	—	26–28	Sulzer	54	18
H_2S/HDS-water	12	3.4	315 psia	11.5	12		AEC	56	3,19
Mellapak® 170Y/Flexipak #3 structured packing (Unmarked data signifies Mellapak® data. A star after system, and comment 15, signify Flexipac® data)									
Chlorobenzene-ethylbenzene	40	6–21	76	—	—	21–22	Sulzer	53	
FCC Naphtha wash*	168	—	—	—	—	24	GHR	57	15,20
Mellapak® 125Y structured packing									
Chlorobenzene-ethylbenzene	40	8–28	Atm	11.4	6		Sulzer	51,52	
Chlorobenzene-ethylbenzene	40	8–28	76	11.4	7		Sulzer	51,52	

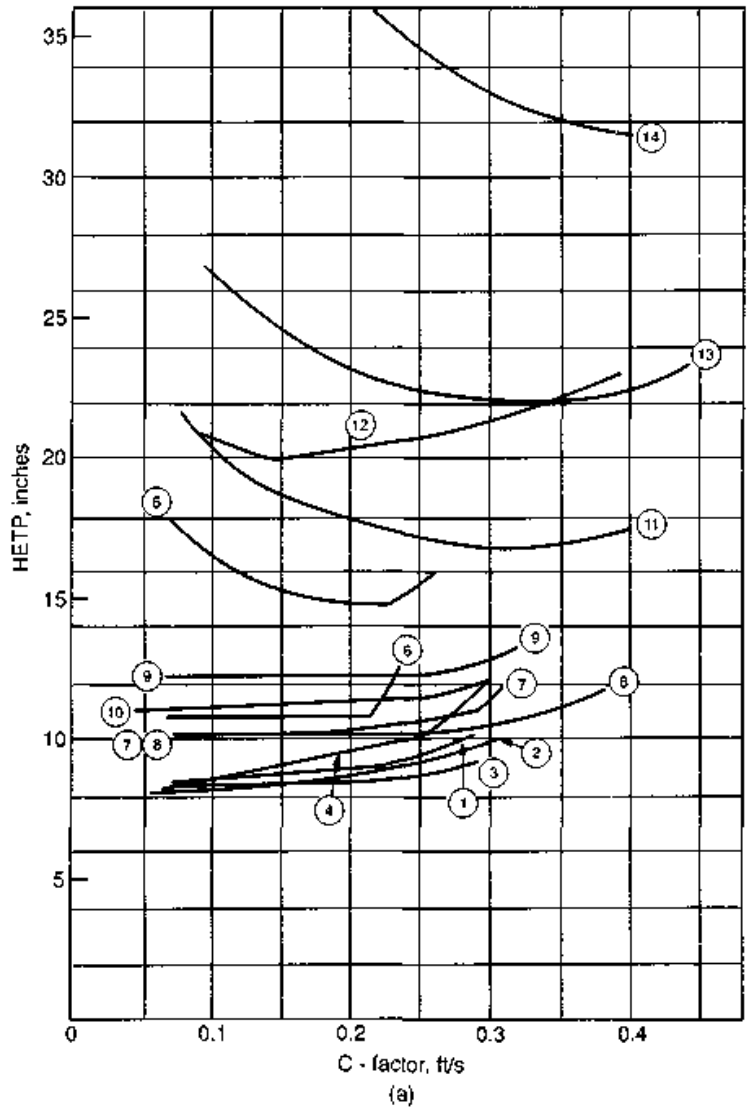

Figure 11.6 Published HETP data for Gempak® 0.5A, 1A, 1.5A, 3A, and 4A structured packings (see Table 11.2 for curve identification). (*a*) Plotted against vapor load; (*b*) plotted against liquid load.

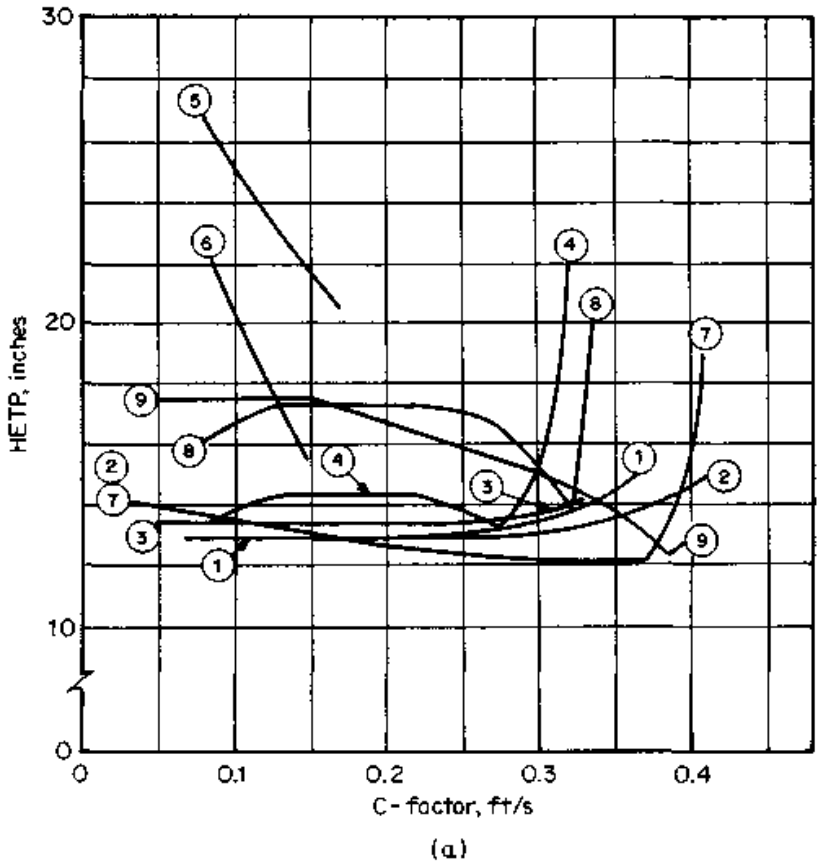

Figure 11.7 Published HETP data for Gempak® 2A and Gempak® 2AT structured packings (see Table 11.2 for curve identification). (*a*) Plotted against vapor load. (*b*) plotted against liquid load.

TABLE 11.2 Published Efficiency Data for Structured Packings (*Continued*)

System	Column diameter, in	Packed height, ft	Pressure, mmHg	Figure no.	Curve no.	HETP, in	Source	Ref.	Comment (see Sec. 11.2.3)
Gempack 4A structured packing									
Para-ortho xylenes	6	10–21	100, Atm	11.6*a*	1		Glitsch	43	
Para-ortho xylenes	—	—	50–100	11.6	2		Glitsch	58	
Para-ortho xylenes	6	10	50	11.6	3		Glitsch	2	
Ethylbenzene-styrene	—	10–20	50	11.6	4		Glitsch	59	
EG-DEG	6	—	100	11.6	5		Glitsch	43	5
Acetone-water	6	—	Atm	11.6	6		Glitsch	43	
Gempak® 3A structured packing									
Para-ortho xylenes	6	10–21	100, Atm	11.6*a*	7		Glitsch	43	
Para-ortho xylenes	—	—	50–100	11.6	8		Glitsch	58	
Para-ortho xylenes	6	10	50	11.6	9		Glitsch	2	
Ethylbenzene-styrene	—	10–20	50	11.6	10		Glitsch	59	
Gempak® 2A structured packing									
Para-ortho xylenes	6	10–21	100, Atm	11.7*a*	1		Glitsch	43	
Para-ortho xylenes	—	—	50–100	11.7	2		Glitsch	58	
Ethylbenzene-styrene	—	10–20	50	11.7	3		Glitsch	59	
Ethylbenzene-styrene	156	34/94	119	—	—	17	Glitsch	60	6,21
n-Heptane-cyclohexane	18	10.5	3100	11.7	4		SRP	42	
n-Heptane-cyclohexane	10	14.5	Atm	11.7	5		ITdC	61*a*	30,31
Methanol-ethanol	10	14.5	Atm	11.7	6		ITdC	61*a*	30,31
Crude naphtha/LFO	174	6.5	1550	—	—	19.5	Glitsch	61	22,23

Gempak® 2AT structured packing									
Para-Meta xylenes	9	5	50	11.7	7		Bochum Uni	12	
n-Heptane-cyclohexane	18	10.5	3100	11.7	8		SRP	42	
Chlorobenzene-ethylbenzene	9	5	50	11.7	9		Bochum Uni	12	
Gempak® 1.5A structured packing									
Para-ortho xylenes	—	—	50–100	11.6	11		Glitsch	58	
Crude kero/GO	156	6.5	1180	—	—	25.5	Glitsch	61	22,24
Crude naphtha/kero	156	12	1125	—	—	28.8	Glitsch	61	22,25
Gempak® 1A structured packing									
Para-ortho xylenes	6	10–21	100, Atm	11.6α	12		Glitsch	43	
Para-ortho xylenes	—	—	50–100	11.6	13		Glitsch	58	
Crude GO/resid	156	4	1220	—	—	25.5	Glitsch	61	22,26
Crude LFO/AGO	174	9	1600	—	—	28.0	Glitsch	61	22,27
Gempak® 0.5A structured packing									
Para-ortho xylenes	—	—	50–100	11.6	14		Glitsch	58	
Crude stripping	—	9	1250	—	—	53	Glitsch	61	22,28

TABLE 11.2 Published Efficiency Data for Structured Packings (*Continued*)

System	Column diameter, in	Packed height, ft	Pressure, mmHg	Figure no.	Curve no.	HETP, in	Source	Ref.	Comment (see Sec. 11.2.3)
Intalox® structured packing 2T									
Isooctane-toluene	15	9.5	Atm	11.8	1		Norton	62,63	
Isooctane-toluene	15	9.5	100 mmHg	11.8	2		Norton	62,63	
Ethylbenzene-styrene	15	9.5	50 mmHg	11.8	3		Norton	62,63	
n-Heptane-cyclohexane	18	10	60 psia	11.8	4		SRP	62,63	
n-Heptane-cyclohexane	18	10	24 psia	11.8	5		SRP	63	
n-Heptane-cyclohexane	18	10	Atm	11.8	6		SRP	62,63	
n-Heptane-cyclohexane	18	10	250 mmHg	11.8	7		SRP	62,63	
Isobutane-n-butane	48	12	100 psia	11.8	8		FRI	63	29
Isobutane-n-butane	48	12	165 psia	11.8	9		FRI	63	29
Isobutane-n-butane	48	12	300 psia	11.8	10		FRI	63	29
Isobutane-n-butane	48	12	400 psia	11.8	11		FRI	63	29
Intalox® structured packing 3T									
Isooctane-toluene	15	9.5	Atm	11.8	12		Norton	62,63	
Isooctane-toluene	15	9.5	100 mmHg	11.8	13		Norton	62,63	

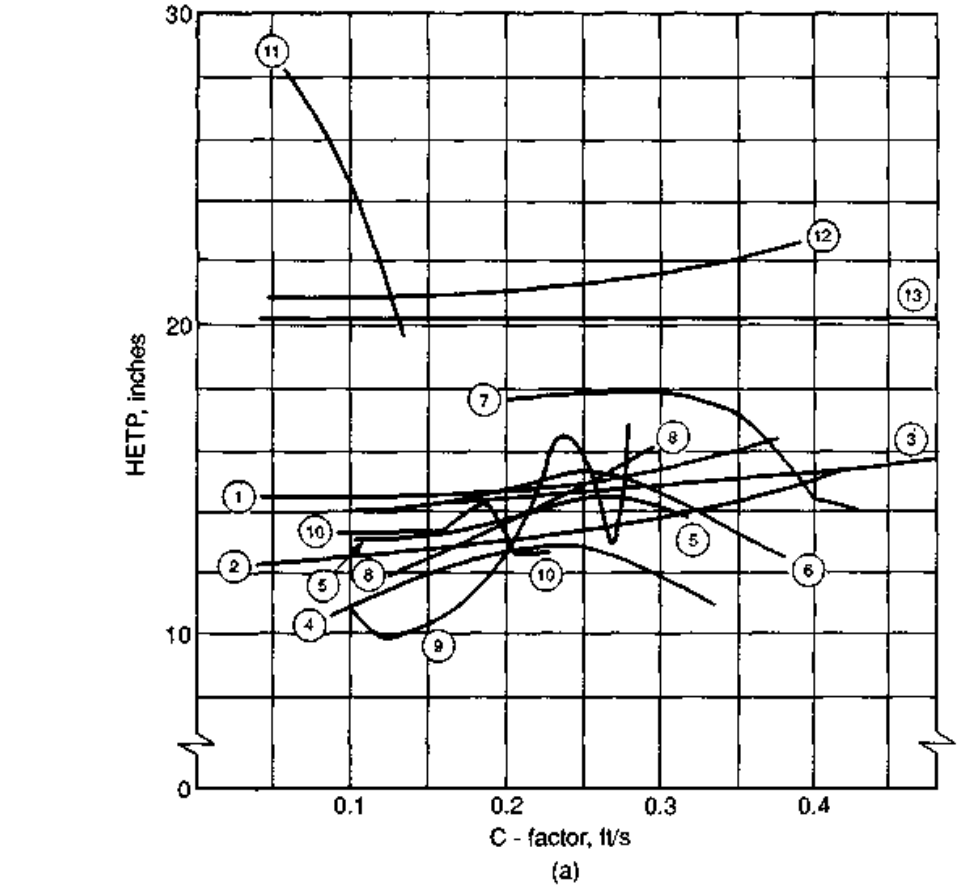

Figure 11.8 Published HETP data for Intalox® structured packing 2T and 3T (see Table 11.2 for curve identification). (*a*) Plotted against vapor load; (*b*) plotted against liquid load.

TABLE 11.2 Published Efficiency Data for Structured Packings (*Continued*)

System	Column diameter, in	Packed height, ft	Pressure, mmHg	Figure no.	Curve no.	HETP, in	Source	Ref.	Comment (see Sec. 11.2.3)
Montz B1-300® structured packing									
Chlorobenzene-ethylbenzene	9	5	100	11.9	1		Bochum Uni	12	
Chlorobenzene-ethylbenzene	9	5	50	11.9	2		Bochum Uni	12,50	
Chlorobenzene-ethylbenzene	9	5	25	11.9	3		Bochum Uni	12	
Montz B1-200® structured packing									
Chlorobenzene-ethylbenzene	9	5	50	11.9	4		Bochum Uni	50	
Max-Pak® structured packing									
n-Heptane-cyclohexane	18	10	3100	11.10	1		SRP	64	
n-Heptane-cyclohexane	18	10	1240	11.10	2		SRP	64	
n-Heptane-cyclohexane	18	10	250	11.10	3		SRP	64	

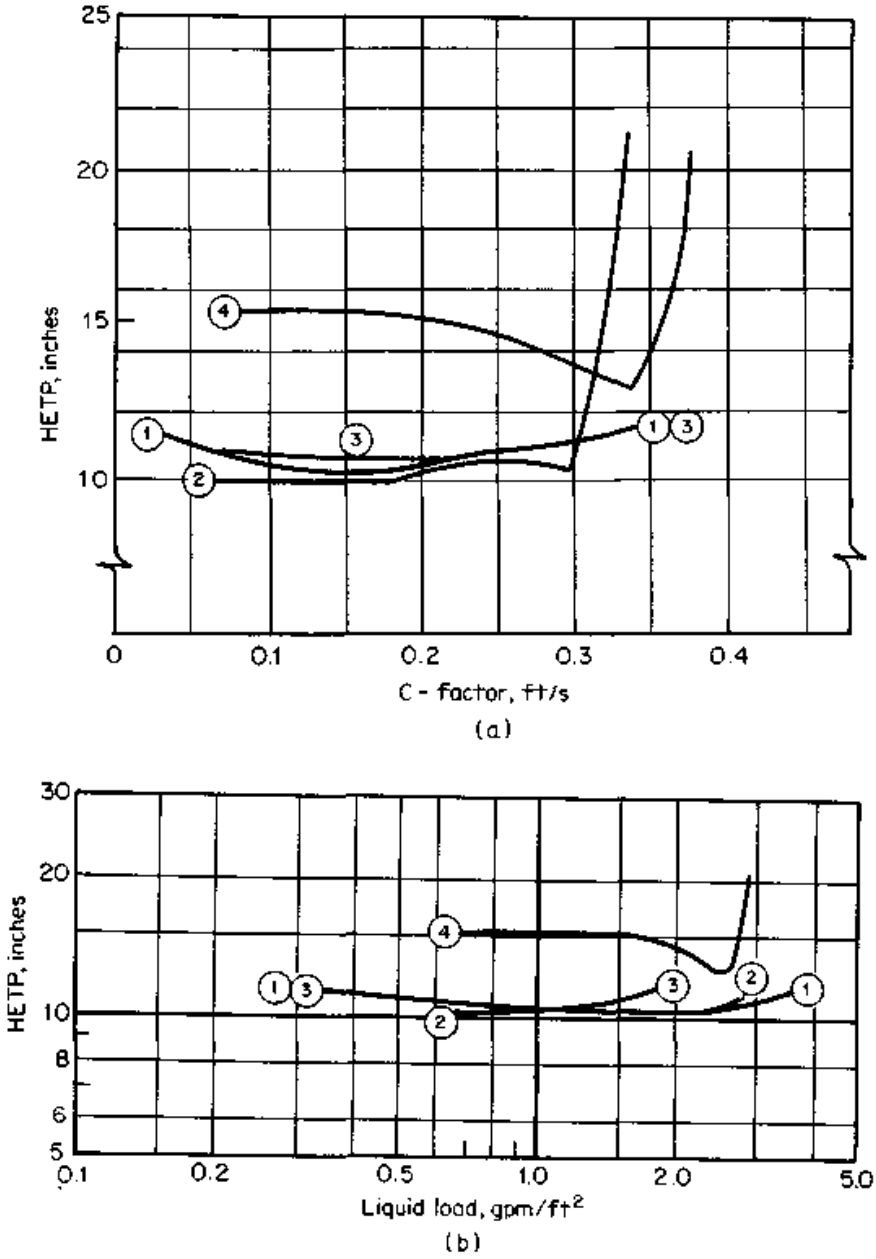

Figure 11.9 Published HETP data for Montz B1-200® and B1-300® structured packings (see Table 11.2 for curve identification). (*a*) Plotted against vapor load; (*b*) plotted against liquid load.

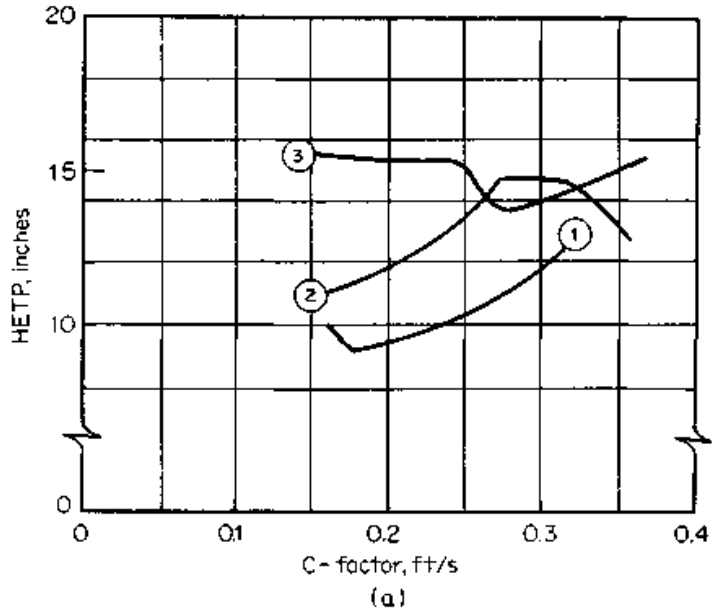

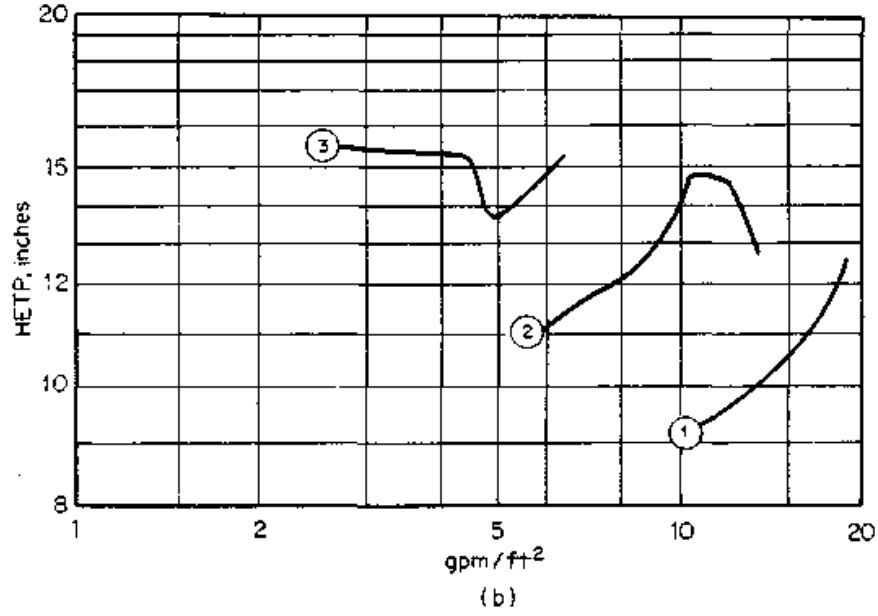

Figure 11.10 Published HETP data for Max-Pak® (see Table 11.2 for curve identification). (*a*) Plotted against vapor load; (*b*) plotted against liquid load.

11.3 References

1. Eckert, J. S., and L. F. Walter, *Hydrocarb. Proc. & Pet. Ref. 43*(2), p. 107, 1964.
2. Wu, K. Y., and G. K. Chen, *I. Chem. E. Symp. Ser.* 104, p. B225, 1987.
3. Billet, R., *Distillation Engineering*, Chemical Publishing Co., New York, 1979.
4. Billet, R., *Chem. Eng. Prog. 63*(9), p. 53, 1967.
5. Billet, R., S. Conrad, and C. M. Grubb, *I. Chem. E. Symp. Ser.* 32, p. 5:111, 1969.
6. Eckert, J. S., *Chem. Eng. Prog. 59*(5), p. 76, 1963.
7. Strigle, R. J., Jr., and F. Rukovena, *Chem. Eng. Prog. 75*(3), p. 86, 1979.
8. Eckert, J. S., E. H. Foote, and L. F. Walter, *Chem. Eng. Prog. 62*(1), p. 59, 1966.
9. Elsby, K., N. Ashton, and A. Arrowsmith, *I. Chem. E. Symp. Ser.* 104, p. A143, 1987.
10. Raichle, L., and R. Billet, *Chem. Ing. Techn. 37*(4), p. 367, 1965.
11. Billet. R., and J. Maćkowiak, *Verfahrenstechnik 16*, p. 67, 1982.
12. Billet, R., *Packed Column Analysis and Design*, Ruhr University, Bochum, Germany, 1989.
13. Kirschbaum, E. *Destillier und Rektifizier Technik*, 4 Aufl., Springer-Verlag, Berlin, 1969.
14. Strigle, R. J., Jr., and K. E. Porter, *I. Chem. E. Symp. Ser.* 56, p. 3.3/19, 1979.
15. Glitsch, Inc., Bulletin TP/US/M4, Dallas, Texas, 1983.
16. Glitsch, Inc., Bulletin 345, Dallas, Texas, 1986.
17. Chen, G. K., *Chem. Eng.*, March 5, p. 40, 1984.
18. Norton Company, Bulletin HY-30, Akron, Ohio, 1975.
19. Eckert, J. S., *Chem. Engr.* (London), Nov., p. 712, 1974.
20. Nutter, D. E., *I. Chem. E. Symp. Ser.* 104, p. A129, 1987.
21. Billet, R., *I. Chem. E. Symp. Ser.* 32, p. 4:42, 1969.
22. Billet, R., and J. Maćkowiak, *Chemie-Technik 14*(4), p. 91, 1985.
23. Chuang, K. T., and A. I. Miller, *Can. J. Chem. Eng. 66*(6), p. 377, 1988.
24. Eckert, J. S., *Chem. Eng.*, April 14, p. 70, 1975.
25. Norton Company, Bulletin IM-82, Akron, Ohio, 1979.
26. McMullan, B. D., A. E. Ravicz, and S. J. Wei, *Chem. Eng. Prog.*, July, p. 69, 1991.
27. Strigle, R. F., Jr., and K. Fukuyo, *Hydrocarb. Proc. 65*(6), p. 47, 1986.
28. Strigle, R. F., Jr., and F. Rukovena, Jr., Proc. 2nd World Congress of Chemical Engineering, Montreal, Canada, Vol. IV, p. 247, October 4–9, 1981.
29. Koshy, T. D., and F. Rukovena, Jr., *Hydrocarb. Proc. 65*(5), p. 64, 1986; and fuller version of this paper, presented at the AIChE Annual Meeting, Los Angeles, California, November 19, 1982.
30. Zanetti, R., *Chem. Eng.*, May 27, p. 22, 1985.
31. Strigle, R. F., Jr., and M. J. Dolan, *Can. Proc. Equip. Control News*, October 1983.
32. Nutter Engineering, Bulletin NR-2, Tulsa, Oklahoma, 1988.
32*a*. Leva, M., *Chem. Eng. Progr. 76*(9), p. 73, 1980.
33. Billet, R., and J. Maćkowiak, *Chemie-Technik 14*(5), p. 195, 1985.
34. Billet, R., *Energieeinsparung bei Thermischen Stofftrennverfahren*, Huthig Verlag, Heidelberg, 1983.
35. Meier, W., *Sulzer Tech Review* No. 3, 1970.
36. Meier, W., and M. Huber, *I. Chem. E. Symp. Ser.* 32, p. 4:31, 1969.
37. Bravo, J. L., J. A. Rocha, and J. R. Fair, *Hydrocarb. Proc. 64*(1), p. 91, 1985.
38. Kuk, M. S., *Chem. Eng. Prog. 75*(5), p. 68, 1979.
39. Lubowicz, R. E., and P. Reich, *Chem. Eng. Prog. 67*(3), p. 59, 1971.
40. Koch Engineering, Bulletin KS-1, Wichita, Kansas.
41. Yuan, H. C., and L. Spiegel, Proc. 2nd World Congress of Chemical Engineering, Montreal, Canada, Vol. IV, p. 274, October 1981.
42. Martin, C. L., J. L. Bravo, and J. R. Fair, Paper presented in the AIChE National Meeting, New Orleans, Louisiana, March 7, 1988.
43. Glitsch, Inc., An addendum to Glitsch Publication No. 40283, Dallas, Texas, 1983.
44. Eldridge, R. B., T. E. Russel, and J. L. Turpin, Paper presented at the AIChE National Meeting, Houston, Texas, April 1989.
45. Glitsch, Inc., Bulletin 254, Dallas, Texas, 1983.
46. Cooke, G. M., *Analyt. Chem. 39*(3), p. 286, 1967.
47. Bragg, L. B., *Ind. Eng. Chem. 49*(7), p. 1062, 1957.

48. Glitsch, Inc., Bulletin 520A, Dallas, Texas, 1981.
49. Chen, G. K. (Glitsch Inc.), Private communication, November, 1983.
50. Nutter Engineering Corp., Bulletin N-1, Tulsa, Oklahoma, 1986.
51. Spiegel, L., and W. Meier, *I. Chem. E. Symp. Ser.* 104, p. A203, 1987.
52. Sulzer Bros. Ltd., *Performance Characteristics, Sulzer Column Packing Mellapak*, Winterthur, Switzerland, 1985.
53. Spiegel, L., Paper presented at the AIChE Annual Meeting, Chicago, Illinois, November 1990.
54. Meier, W., R. Hunkeler, and D. Stoecker, *I. Chem. E. Symp. Ser.* 56, p. 3.3/1, 1979.
55. Meier, W., W. D. Stoecker, and B. Weinstein, *Chem. Eng. Prog. 73*(11), p. 71, 1977.
56. Spagnolo, D. A., and K. T. Chuang, *Can. J. Chem. Eng. 64*, p. 62, February 1986.
57. Lieberman, N. P., *Hydrocarb. Proc. 63*(4), p. 143, 1984.
58. Glitsch, Inc., Bulletin No. 357, Dallas, Texas, 1989.
59. Chen, G. K., and J. Shieh, Paper presented at the AIChE National Meeting, Denver, Colorado, August 28–31, 1983.
60. Chen, G. K., and K. T. Chuang, *Hydrocarb. Proc. 68*(2), p. 37, 1989.
61. Golden, S. W., and S. Costanzo, Paper presented at the AIChE National Meeting, Orlando, Florida, March 1990.
61*a*. Cardenas, J. C., F. J. Illezcas, B. Garcia, G. Palacios, E. M. Escamilla, and J. A. Rocha, Paper presented at the AIChE Annual Meeting, Chicago, Illinois, November 1990.
62. Norton Company, Bulletin IS-1, Akron, Ohio, 1988.
63. Rukovena, F., Jr., and R. F. Strigle, Jr., Paper presented at the AIChE National Meeting, Houston, Texas, April 1989.
64. Jaeger Products Inc., Product Bulletin 500, Spring, Texas, 1989.
65. Vital, T. J., S. S. Grossel, and P. I. Olsen, *Hydrocarb. Proc. 63*(12), p. 75, 1984.

Name Index

This index includes names of authors, packings, computer simulators, and the like. The most significant page references appear in boldface type.

Subject Index

This subject index omits names of authors, packings, computer simulators, and the like, which appear in the preceding name index. The most significant page references appear in boldface type.

Chemical Engineering

State-of-the-art methods for achieving optimal design of distillation processes

DISTILLATION DESIGN

Distillation Design provides complete, up-to-date coverage of the principles and practical aspects of designing this important industrial process for the food, chemical, pharmaceutical, petrochemical, petroleum refining, gas, and alcohol industries.

This definitive sourcebook examines process and equipment design procedures, discusses the limitations of the various design methods, and provides nuts-and-bolts solutions to help you design trouble-free systems. The book also presents worked-out examples of typical design problems, as well as guidelines for using computer programs in design.

Engineers will find detailed information on key fractionation concepts ... column process design and shortcut calculations ... tray design and operation ... tray efficiency ... packing design and operation ... packing efficiency and scaleup ... packing capacity and pressure drop ... and much more.

Essential for troubleshooting and diagnosing design malfunctions, *Distillation Design* offers design, process, and project engineers expert solutions to design and longer-term plant problems.

Photograph by T. Linck / Superstock, Inc.

ISBN 0-07-034909-6

90000

9 780070 349094

McGraw-Hill, Inc.
Serving the Need for Knowledge
1221 Avenue of the Americas
New York, NY 10020